NAFEMS

NAFEMS DACH CONFERENCE

PROCEEDINGS

Inhaltsübersicht der Fachbeiträge nach Sessions sortiert ab Seite 12

SPONSOREN

Platin

HEXAGON

PSEVEN TECOSIM

Gold

BETA SIMULATION SOLUTIONS

CADFEM

cenit

DASSAULT SYSTEMES

em engineering methods AG

PIDTec.

rescale

SCALE IT-Solutions for CAE

Silber

ESTECO

FEMFAT software :BY MAGNA POWERTRAIN

gns

GNS Systems IT Services for Engineering

SIDACT GmbH

TECHNIA PART OF ADDNODE GROUP

Medienpartner: DIGITAL ENGINEERING MAGAZIN

www.nafems.org/dach24

ISBN 978-1-83979-232-8

The NAFEMS World Congress 2025 in Salzburg, Austria, will bring the global engineering simulation community together from 19-22 May 2025.

We'll be pushing the technology forward creating a cross-industry, cross-technology exchange of ideas, best practice, and information like never before, whilst getting down to the business of what we all strive for; making simulation ever better and ever more accessible.

Simulation is now right at the forefront of the product design process - and we're bringing it right to the top of your agenda with three days of outstanding simulation content, delivered by experts and thought-leaders from the community, ushering in the next generation of simulation.

We want you

The community wants to hear your story, your experience, and your message. Every major software vendor, industrial user, industry guru, and technology expert will be part of it - and you belong with them.

Be part of something truly special - submit your 300-600 word abstract - the call for papers submission form opens soon!

Join us!

Impressum

The conference is organized by NAFEMS Deutschland, Österreich, Schweiz GmbH
Griesstr. 20, 85567 Grafing, Germany, Phone: +49 176 217 984 01, Fax: +49 3 22 11 08 99 13 41
E-mail: info@nafems.de. www.nafems.org

ISBN 978-1-83979-232-8
First published: 2024, Order Reference NRC24Dach

:em engineering methods

Femfat by Magna Powertrain

Scapos

4RealSim

GNS

Scale

BETA CAE Systems

GNS Systems

Sidact

Cadfem

Hexagon

SustainedBizz

CAIQ

ihf Ingenieurgesellschaft

Technia

Cascate

Intes

Tecosim/pSeven

Cenit

NAFEMS

Total Materia

Dassault Systémes

Noesis Solutions

VMAP Standards

DHCAE

PDTec

WIN-Verlag

Esteco

Rescale

HEXAGON

Hexagon is a global leader in digital reality solutions, combining sensor, software and autonomous technologies. We are putting data to work to boost efficiency, productivity, quality and safety across industrial, manufacturing, infrastructure, public sector, and mobility applications.

Our technologies are shaping production and people related ecosystems to become increasingly connected and autonomous – ensuring a scalable, sustainable future. Hexagon's Manufacturing Intelligence division provides solutions that use data from design and engineering, production and metrology to make manufacturing smarter. For more information, visit hexagon.com/mi.

Hexagon (Nasdaq Stockholm: HEXA B) has approximately 24,000 employees in 50 countries and net sales of approximately 5.2bn EUR.

Learn more at hexagon.com and follow us @HexagonAB.

Hexagon ist ein weltweit führender Anbieter von Sensor-, Software- und autonomen Lösungen, die in Form einer „digital Reality" effizient miteinander verbunden werden. Wir nutzen Daten, um die Effizienz, Produktivität, Qualität und Sicherheit von Anwendungen in der Industrie und der Produktion sowie in den Bereichen Infrastruktur, Mobilität und im öffentlichen Sektor zu steigern.

Mit unseren Technologien gestalten wir zunehmend stärker vernetzte und autonome Ökosysteme in der Fertigung sowie für den Menschen und sorgen so für Skalierbarkeit und Nachhaltigkeit in der Zukunft. Der Geschäftsbereich Manufacturing Intelligence von Hexagon nutzt Daten aus Design und Engineering, Fertigung und Messtechnik als Basis für innovative Lösungsansätze zur Optimierung von Fertigungsprozessen. Weiter Informationen finden Sie auf hexagon.com/mi.

Hexagon (Nasdaq Stockholm: HEXA B) beschäftigt ca. 24.000 Mitarbeiter in 50 Ländern und erzielt einen Nettoumsatz von etwa 5,2 Mrd. EUR.

Erfahren Sie mehr unter hexagon.com. Folgen Sie uns auch auf @HexagonAB.

www.hexagon.com

TECOSIM

pSeven SAS

pSeven SAS is an independent software editor in the market of PIDO (Process Integration & Design Optimization) tools and collaborative engineering environments. The flagship products are pSeven and pSeven Enterprise. pSeven is a desktop application for integration and automation of various CAD/CAE and other engineering tools, design optimization and predictive modeling based on ML/AI. pSeven Enterprise is a cloud-native low-code platform developed to automate engineering process at scale and to build/deploy/manage Hybrid Digital Twins.

Our mission is to deliver the efficient and flexible software solutions to help our customers to:

- Ensure process quality using automated workflows.
- Decrease product design time thanks to the integration and orchestration of their engineering software toolchain.
- Enhance product performance with multidisciplinary design optimization and predictive models.

Nowadays, pSeven solutions are used for process integration, workflow automation and design exploration worldwide. Leaders in aerospace, automotive and other industries have implemented pSeven products in the design processes to boost their engineering capabilities and improve their products globally.

TECOSIM Group

With around 650 employees, TECOSIM is a highly capable partner for development processes and a world-leading specialist in computer-aided engineering (CAE). The internationally active group has its headquarters in Wiesbaden, Germany, and has four further branches in Germany as well as locations in the UK, India, Japan, Romania and the US. TECOSIM support customers in the transportation, energy, health and industrial sectors. Its engineers work on challenging tasks in simulation, design, construction, electronics and software development. Virtual benchmarking methods based on digital twins and the provision of engineering specialists complete the services the Company offers. TECOSIM is reseller of pSeven and responsible for sales and first-level user support for innovative software solutions pSeven and pSeven Enterprise in the German-speaking countries.

As a driver of innovation, TECOSIM uses trend-setting methods and provides comprehensive consultation services – from initial concepts through to all-in-one solutions ready for series production.

www.tecosim.com/de/services/

BETA CAE Systems transformed CAE by introducing revolutionary automation software tools and practices into Simulation and Analysis processes more than 30 years ago.

Committed to our mission to enable engineers to deliver results of high value, we continue to offer state-of-the-art, high-performance software and best-in-class services. Our simulation solutions liberate low risk and high Return-On-Investment innovation.

The ground-breaking technology, the excellent services and our high standards of business ethics are the three pillars on which BETA was founded and grows since then.

Our passion for engineering, our drive for excellence, and our loyalty to customers and partners, are the key ingredients of our success. We first established our reputation in the Automotive sector and now we are proud of the deployment of our software also in the Aerospace, Defence, Biomechanics, Electronics, Energy, and other industries. Our solutions exceed their requirements in all the simulation disciplines, and allow for the development of the right product, for the right market, at the right time.

www.beta-cae.com

CADFEM - EMPOWERING DIGITAL ENGINEERING

Better performing and more sustainable. Digital engineering involves tapping the full potential of technical creativity, precise data models, and clever workflows. This ensures that a good idea results in an excellent product – for manufacturers, customers, and the environment.

Simulations are a pivotal technology for this. From initial brainstorming, variant comparisons, concept development, and material selection to aspects such as manufacturability, operation, and recycling, simulation quickly, transparently, and reliably provides answers to countless physical questions from the entire life cycle of products and processes.

The name CADFEM has been synonymous with simulation since 1985 and has been supporting companies, researchers, and universities in the successful use of Ansys and other simulation products ever since. This is made possible by the CADFEM team of over 450 employees worldwide. Through training offers, support, project work, contract calculations, and IT services, they ensure a seamless implementation of the simulation software.

Moreover, data management solutions, automation, workflows, and customization by CADFEM make simulation an integral part of highly efficient, tailor-made digital engineering.

www.cadfem.net / www.cadfemgroup.com

CENIT empowers sustainable digitalization. With a broad solutions and services portfolio, CENIT enables clients to optimize their horizontal and vertical business processes. Our solutions are based on innovative technologies in: product lifecycle management, the digital factory and enterprise information management. With interdisciplinary knowledge of the processes involved and their considerable expertise in the field, CENIT consultants provide customers with end-to-end advice to ensure that solutions are implemented with an understanding of the entire value chain.

With a holistic approach and based on trusted partnerships, CENIT takes responsibility for solutions on behalf of our clients. From the initial consultation to the introduction of innovative IT solutions, right through to ensuring a cost-effective operation. The CENIT team adapts to each client, taking a practical approach, which enables measurable operational optimizations. CENIT has been helping prestigious customers in key industries to gain competitive advantages for over 30 years.

CENIT has nearly 900 employees worldwide who work with customers from: automotive, aerospace, industrial equipment, tool and mold manufacturing, financial services, and trade and consumer products industries.

www.cenit.com

Unsere 3DEXPERIENCE® Plattform bildet die Grundlage unserer in 12 Branchen eingesetzten Anwendungen und bietet ein breites Portfolio von Branchenlösungen.

Dassault Systèmes, die 3DEXPERIENCE® Company, stellt Unternehmen und Anwendern „virtuelle Universen" zur Verfügung und rückt somit nachhaltige Innovationen in greifbare Nähe. Die weltweit führenden Lösungen setzen neue Maßstäbe bei Konstruktion, Produktion und Service von Produkten.

Die Lösungen zur Zusammenarbeit von Dassault Systèmes fördern soziale Innovation und erweitern die Möglichkeiten, mithilfe der virtuellen Welt das reale Leben zu verbessern.

Die Gruppe bietet einen Mehrwert für über 210.000 Kunden jeder Größe in allen Branchen und in über 140 Ländern. Weitere Informationen erhalten Sie unter www.3ds.com. Besuchen Sie uns:

3DS.com/simulia

:em AG develops innovative methods and software solutions for engineering. As an integrator of IT systems, :em AG has a comprehensive cross-industry portfolio. True to the vision "We deliver the digital future for engineering." :em AG supports the practical implementation of the digital transformation at its customers with a broad range of services and software applications.

For this purpose, :em's team designs digitalization strategies and roadmaps and supports the realization of model-based, digital development. With its software product ReqMan®, and a broad consulting portfolio with topics such as Digital Twin (DT), Enterprise Architecture Management (EAM), Product Lifecycle Management (PLM), Application Lifecycle Management (ALM), Model Based Systems Engineering (MBSE), Cooperation and Requirements Management as well as Model Based Definition, :em AG supports customers from the industries Mobility & Transportation, Mechanical and Plant Engineering, Aerospace Engineering, Electrical Engineering and Information Technology as well as Medical Engineering and Life Science.

www.em.ag

We support our customers with leading engineering, process, and data management solutions, tightly integrated into a global development organization for virtual product development and as a result promoting innovation and success.

- More than 20 years of experience and know-how
- The PDTec AG is active in the market since 1998.
- The PDTec AG supports you in the optimization of process chains in the product life cycle and has as integrator of IT systems in the product development process a comprehensive range of cross-industry products and services.

Extensive portfolio

- Collaborative Engineering
- Solutions for internal collaboration in product development
- Solutions for external cooperation in product development
- Integration of product, process and simulation data throughout the product lifecycle.
- Consistent and continuous management of product, process, and simulation data throughout the product lifecycle.

The PDTec AG with its divisions PDM and SDM is your partner for a holistic-oriented development process, introduction, adaptation, and application of methods and systems for information processing. The PDTec AG offers first-class services and well-engineered standard software for integrating data, processes, and systems.

The employees of the PDTec AG have detailed knowledge of industry-specific processes with many years of project experience.

- We rely on the latest and best technologies.
- We guarantee practical and sustainable solutions within the shortest time.

www.pdtec.com

Rescale's AI-powered cloud high performance computing (HPC) platform makes accelerating innovation possible for any organization. Innovators use Rescale to provide R&D teams the world's largest library of fully managed software applications and performance-driven computing architectures, robust data security, intelligent controls, and a seamless AI-driven experience.

Leveraged by a majority of Fortune 500 companies to accelerate time to market, Rescale has been recognized by Gartner as a Cool Vendor for Cloud Infrastructure, by Deloitte as a Technology Fast 500 company, and by the World Economic Forum as a Global Innovator Unicorn. Learn more at rescale.com.

www.rescale.com

IT-Solutions for CAE

SCALE offers software solutions and IT services for process and simulation data management in the automotive and other industry sectors. Our core product, SCALE.sdm, is designed to orchestrate the holistic management of simulation and test data within the realm of virtual product development.

In addition to software solutions, our services span software development for process and data management, finite element method development, and numerical optimization for the functional design of vehicle components.

SCALE serves as a development partner for leading automotive companies and actively participates in research projects focused on Machine Learning and Artificial Intelligence applications in the automotive industry. Collaborating with top universities and institutes in Germany, we strive for innovation, creativity, and excellence in all our endeavors.

The team at SCALE comprises a blend of experienced CAE engineers and computer scientists dedicated to delivering cutting-edge solutions.

www.scale.net

ESTECO is an independent software provider, highly specialized in numerical optimization and simulation data management with a sound scientific foundation and a flexible approach to customer needs. Our technology brings modularity, ease of use, standardization, and innovation to the engineering design process. With 20 years' experience, the company supports leading organizations in designing the products of the future, today. ESTECO smart engineering suite brings enterprise-wide solutions for design optimization, simulation data management and process integration and automation with the aim of helping companies excel across this innovation journey and accomplish the shift to agile product development. Over 300 international organizations – including Cummins, Embraer, FIAT, Ford Motor Company, JLR, Honda, Toyota, Whirlpool, VOLVO - have chosen ESTECO to consolidate specialized expertise, streamline teamwork and boost product development across a wide spectrum of industrial sectors. Founded in 1999, the company is headquartered in Trieste (Italy), with offices in Michigan (USA), Pune (India) and an international network of channel partners.

www.esteco.com

The Magna Powertrain Engineering Center in St. Valentin is a globally recognized development partner for vehicle engineering, alternative propulsion systems, application software and a full range of testing services.

Its own software product FEMFAT (Finite Element Method Fatigue) is the globally leading software for finite element based fatigue life prediction. It increases the reliability and robustness of components in the automotive industry as well as in machinery & plant construction. Based on stresses from finite element analysis, FEMFAT delivers analysis results such as fatigue life or damage as well as safety factors. This enables the identification of lightweight design potentials and potential weak spots already at an early product development phase.

www.femfat.magna.com

Founded in 1994, gns mbH has quickly established itself as a dynamic company created by a group of experts in engineering analyses.

Today, gns mbH is at the forefront of innovation, offering services such as mesh generation for complex shell and solid structures, analyses using state-of-the-art finite element and boundary element codes, and the development of customized software tools such as user interfaces and graphical post-processors.

With a strong focus on advanced commercial software products such as ANIMATOR4, GENERATOR4 and OPENFORM, gns mbH develops and supports solutions specifically tailored to the needs of its most demanding customers and the most complex engineering challenges in the industry.

Recently, gns mbH has demonstrated its innovative strength by starting to develop FEA models of honeycomb crash barriers used in the automotive industry. This underlines gns mbH's commitment to remain at the forefront of technological development.

www.gns-mbh.com

GNS Systems - IT Services for Engineering

GNS Systems offers innovative IT services for virtual product development.

Our portfolio includes customised services in the areas of high performance computing, technical data management, software engineering and systems & application management. We use state-of-the-art methods and technologies - from cloud computing to data management & analytics, deep learning & artificial intelligence and virtual reality. In these areas we plan, implement and operate complex systems and application infrastructures - either on-prem, hybrid or in the cloud. Our agile, cross-functional teams work both nationally and internationally for well-known companies in the automotive, aerospace and mechanical and plant engineering industries. Thanks to our many years of experience, we offer our customers comprehensive, detailed consulting and proven implementation.

www.gns-systems.de

SIDACT is a spin-off of Fraunhofer based in Germany founded in August 2012. SIDACT markets, supports and further develops FEMZIP and DIFFCRASH since January 1st, 2013. FEMZIP and DIFFCRASH were developed by members of the Numerical Software department of the Fraunhofer Institute SCAI since 2002. Six patents are exclusively licensed by SIDACT from Fraunhofer for engineering applications protecting the kernel technologies of its products. Six scientists from Fraunhofer joined SIDACT and work for support and further developments of the SIDACT products. We like to use advanced math in software products or tailored applications to improve the usability of numerical simulations and gaining further insights from vast amount of numerical simulation results. Today's customers of SIDACT are car manufactures from Europe, US, India, China, South Korea and Japan. SIDACT products are supported by local distributors in all of these regions. In 2016 Sidact GmbH was awarded with the seal of approval „Innovative through research" by the Stifterverband für Deutsche Wissenschaft.

www.sidact.com

Wir bei TECHNIA machen Ihnen den Weg frei für Ihre Innovation, Kreativität und Rentabilität. Wir kombinieren branchenführende Product Lifecycle Management Tools mit Fachwissen, damit Sie den Weg von der Produktidee bis zur Implementierung entspannt beschreiten können. Mit über 30 Jahren Branchenerfahrung, 6000 Kunden weltweit und erstklassigem PLM-Wissen arbeiten wir Hand in Hand mit Ihrem Unternehmen zusammen, um Ihnen ein außergewöhnliches PLM-Erlebnis zu bieten. Mit 33 Niederlassungen auf der ganzen Welt sind wir bei Ihnen vor Ort - sowohl als globaler branchenübergreifender Implementierungspartner und Premiumserviceanbieter, aber auch als lokaler Partner. SIMULIA - Realistische Simulation: Mit Hilfe der Simulation können Produkteigenschaften und deren Verhalten bereits sehr früh in der Entwicklungsphase kostengünstig untersucht werden. Das Produktspektrum von SIMULIA umfasst: CATIA Analysis, SIMULIA Abaqus, Tosca, fe-safe, SIMULIA Isight, SIMPOE, SIMPACK sowie Simulation Lifecycle Management. Wollen Sie mehr erfahren über TECHNIA oder unsere Simulationslösungen, dann nehmen Sie gerne Kontakt mit uns auf: Telefon: +49 721 97043 - 16, E-Mail: info-center@technia.de

www.technia.de

1-P KEYNOTE-VORTRÄGE

2-A AI/ML 1

2-B SPDM 1

2-C CFD 1

2-D MULTIPHYSIK 1

2-E VMAP 1

3-P KEYNOTE-VORTRÄGE

4-A AI/ML 3

4-B SPDM 2

4-C AI/ML 2 / CFD 2

4-D FATIGUE-FAILURE-DURABILITY 1

4-E METHODEN 1

5-A AI/ML 4

5-B SPDM 3

5-C AI/ML - 5 / CFD 3

5-D OPTIMIERUNG 1

5-E AUTOMATION

6-A AI/ML 6

6-B SPDM 4

6-C MBSE - SIM. CREDIBILITY - VVUQ

6-D MATERIAL

6-E CFD 4

7-A AI/ML 7

7-B OPTIMIZATION 2

7-C CFD 5

7-D MULTIPHYSIK 2

7-E SPDM 5

8-A AI/ML 8

8-B DIGITAL TWINS - DEMOKRATISIERUNG

8-C CFD 6

8-D METHODEN 2

8-E SPDM 6

9-A AI/ML 9

9-B PROZESSE - HPC

9-C FATIGUE-FAILURE-DURABILITY 2

9-D MEHRKÖRPERSIMULATION MKS

PSE

Professional Simulation Engineer

It's Time
to Get Certified

nafems.org/pse

The Science and Engineering of the James Webb Space Telescope

Michael T. Menzel

JWST Mission Systems Engineer

NASA

The James Webb Space Telescope (JWST), launched on December 25, 2021, is NASA's successor mission to the Hubble Space Telescope.JWST has been designed and developed to observe "first light" objects in the nascent universe, the evolution of galaxies over cosmic history, star birth within our own galaxy, planet formation and evolution both in our solar system and in solar systems around other stars and to make detailed observations of some of the recently discovered exoplanets.

The JWST telescope has an aperture greater than 6 meters in diameter, and along with its compliment of science instruments must be cooled to cryogenic temperatures below 50K.It is operated at the Sun-Earth L2 point to keep thermal sources such as the Sun and Earth in the same general direction so that their radiation can be shielded by a "tennis court sized" sunshield, allowing the payload to attain these temperatures passively.

The observatory is now well into its first year of science operations, producing magnificent images and science data that is already reshaping our understanding of the early universe.This presentation will give an overview ofJWST science, its system design and challenges and the way integrated systems analysis was performed to address them.The presentation will then discuss the science observations and data collected to date.

Digitalisierung der Entwicklung

Gerd Rapin

Leiter Methodenentwicklung – Mechatronik & Mehrkörper-Simulationen (MKS)

Volkswagen

KI in der FEM-Simulation: Beschleunigte Optimierung von Kunststoffschnapphaken-Designs in der Automobilindustrie

Florian Dirisamer (Digital Physics AI GmbH)

1 Zusammenfassung

Im Mittelpunkt der Produktentwicklung in der Automobilindustrie steht die kontinuierliche Optimierung von Komponenten, insbesondere von Kunststoffbauteilen, um Ziele wie Leichtbau, Haltbarkeit, Kosteneffizienz und Zuverlässigkeit zu erreichen. Die Einführung von künstlicher Intelligenz (KI) in diesen Prozess markiert eine revolutionäre Veränderung, insbesondere durch den Einsatz neuronaler Netze. Diese Technologien ermöglichen es, aus einer Vielzahl von Daten zu lernen und das Verhalten von Materialien und Komponenten unter verschiedenen Belastungen mit hoher Präzision vorherzusagen. Der Einsatz von KI in der Finite-Elemente-Methode (FEM) führt zu einer drastischen Reduktion der für Simulationen erforderlichen Zeit. Anstatt Tage oder Wochen mit der Durchführung komplexer Simulationen zu verbringen, können trainierte Systeme Ergebnisse in Minuten oder sogar Sekunden liefern. Dies ermöglicht eine viel schnellere Iteration von Designvarianten, was die Entwicklungszyklen verkürzt und die Markteinführungszeit beschleunigt. Der Einsatz von KI ermöglicht auch eine tiefgehende Analyse und Optimierung von Designs, ohne dass ein exponentieller Anstieg der Rechenressourcen erforderlich ist. Dies führt zur Entwicklung leichterer, kostengünstigerer und leistungsfähigerer Komponenten mit längerer Lebensdauer, was in der Automobilindustrie, wo jedes Gramm zählt, von entscheidender Bedeutung ist. Um die praktische Anwendung und die Vorteile dieser technologischen Fortschritte zu veranschaulichen, wird die Präsentation eine Fallstudie zur Optimierung von Kunststoffschnapphaken vorstellen. Wir werden demonstrieren, wie der Einsatz von KI-unterstützten FEM-Simulationen nicht nur die Entwicklungsprozesse beschleunigen, sondern auch deren Qualität verbessern kann. Wir werden die technischen Herausforderungen darlegen, die angewandten Lösungen präsentieren und die erzielten Verbesserungen diskutieren. Diese Fallstudie zeigt, wie KI-Technologien innovative Entwicklungen in der Automobilindustrie vorantreiben und neue Möglichkeiten für die Produktentwicklung eröffnen.

2 Motivation

Die Integration von Künstlicher Intelligenz (KI) hat zu tiefgreifenden Veränderungen in verschiedenen Branchen geführt, und auch das computerunterstützte Engineering (CAE) erfährt einen bedeutenden Einfluss. Dieser Artikel untersucht das Potenzial von KI in der Finite-Elemente-Methode (FEM), mit besonderem Fokus auf die Optimierung der Systemeffizienz und die Bewältigung von Herausforderungen, die durch inverse Probleme und Black-Box-Komponenten entstehen. Innovative Ansätze werden hervorgehoben, um zu zeigen, wie KI genutzt werden kann, um FEM-Simulationen effizienter und handhabbarer zu machen, insbesondere im Umgang mit inversen Problemen oder Black-Box-Komponenten. Die Optimierung der Effizienz ist von größter Bedeutung in der technischen Entwicklung, da sie direkt zu Zeit- und Ressourceneinsparung führt. Durch den Einsatz von KI-Techniken wie maschinellem Lernen und Optimierungsalgorithmen können FEM-Simulationen beschleunigt werden, ohne an Genauigkeit einzubüßen.

3 Methode

Hier wird eine Fallstudie aus dem Bereich der Finite-Elemente-Methode (FEM) vorgestellt, die neben der Strömungsmechanik (CFD) eine der am häufigsten verwendeten Methoden in der Ingenieurssimulation ist. In der Regel sind Simulationen in diesem Umfeld zeitaufwendig und dauern oft mehrere Stunden für einen einzelnen Designpunkt. Darüber hinaus stellt die Bestimmung sinnvoller Randbedingungen (BC) eine besondere Herausforderung dar, da eine Vielzahl von Geometrien, Materialparametern, Randbedingungen sowie Produktionsinformationen und Maschineneinstellungen einen erheblichen Einfluss auf die Verformungseigenschaften und Versagensarten haben, wie z. B. kein versagen, zu hohe Biegespannung, zu hohe Kerbspannung usw. Die schematische Komponente für diese Präsentation ist in Fig. 1 dargestellt.

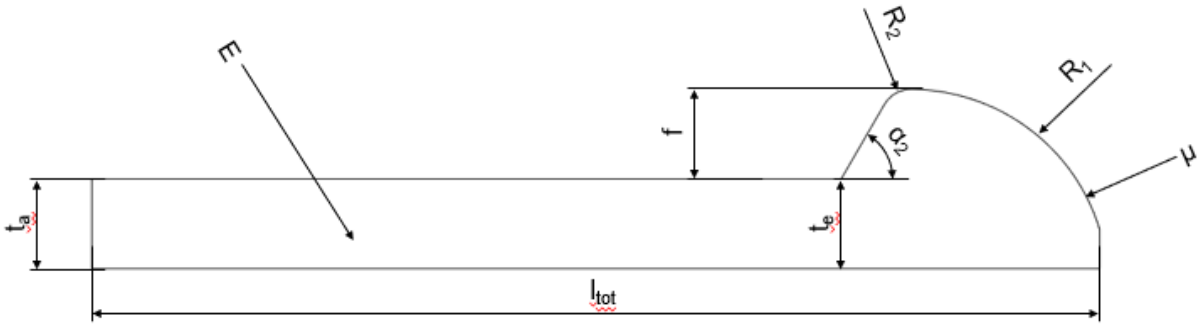

Fig. 1
Eine schematische Komponente, die die Anwendbarkeit von KI-Vorhersagen in FEM-Simulationen veranschaulicht.

Die Simulationsergebnisse für eine Kombination aus Geometrie- und Materialparametern sowie Randbedingungen, einschließlich der simulierten Verformungen und Spannungen, werden mittels FEM simuliert. Außerdem werden die Versagensarten durch die Bewertung des Verformungs- und Spannungsverhaltens bestimmt. Ein einzelnes Simulationsergebnis für den Kunststoffschnapphaken ist in Fig. 2 dargestellt.

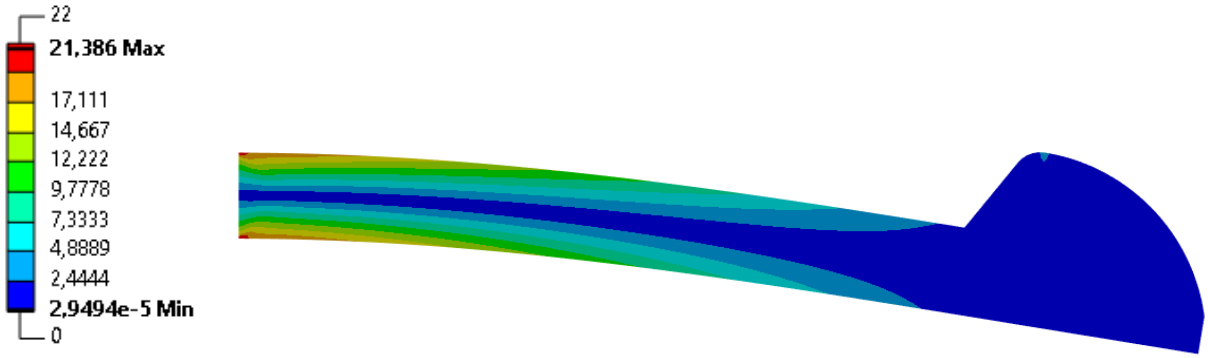

Fig. 2
Ein schematisches Ergebnis einer untersuchten Geometrie, Materialparameter und Randbedingungskombination.

Durch die Nutzung Künstlicher Intelligenz (KI) werden Simulationen beschleunigt, und inverse Problemformulierungen können effizient gelöst werden, da dies die Ableitung von Geometrie, Materialien und Randbedingungen basierend auf gewünschten maximalen Spannungen und Versagensarten ermöglicht. Maschinelles Lernen (ML) wird eingesetzt, um Simulationsdaten zu nutzen und komplexe Zusammenhänge zwischen Eingangsparametern und gewünschten Ausgangsvariablen zu erfassen. Fig. 3 zeigt die verwendeten Parameter zusammen mit ihren entsprechenden Grenzen und Verwendungsbereichen. Es zeigt auch, welche Parameter als Randbedingungen (Eingangsparameter) in der Simulation festgelegt sind und welche Parameter als Ergebnisse (Ausgangsparameter) der Simulation bewertet werden. Darüber hinaus können beim ML Ausgangsparameter aus der Simulation als Eingangsparameter für das ML-modell verwendet werden, um eine inverse Vorhersage von ursprünglichen Eingangsparametern durchzuführen. Eingangsparameter für das KI-Training können in diesem Fall beispielsweise die maximale Spannung, der Versagensmodus und einige vordefinierte Geometrie- und Materialparameter sein, während Ausgangsvariablen beispielsweise ein fehlender Geometrieparameter sein könnten. Das trainierte KI-Modell ermöglicht schnelle Vorhersagen und die Lösung inverser Probleme zur Bestimmung optimaler Parameter basierend auf dem gewünschten Verhalten, ohne einen Optimierungsalgorithmus und zahlreiche Simulationen durchführen zu müssen.

Category	Parameter		Limits		Unit	Sim*	AI-P**
Geometry	Total length	l_{tot}	1	50	mm	I	I
	Deflection	f	1	5	mm	I	I
	Joining radius factor	f_{R1}	2,2	3	1	I	I
	Rounding radius factor	f_{R2}	0,22	0,33	1	I	I
	Joining partner radius factor	f_{RF}	0,09	0,2	1	I	I
	Release Angle	α_2	30	90	°	I	I
	Radius	R	0	10	mm	I	I
	Cantilever thickness beginning	t_a	1	10	mm	I	I
	Cantilever thickness end	t_e	1	10	mm	I	I
	Snap arm width	b	1	20	mm	I	I
Material model	Young's Modulus	E	500	100 000	MPa	I	I
BC	Coefficient of friction	μ	0,1	1	1	I	I
BC	Max. Stress	σ_{max}	1 Parameter		MPa	O	O
	Failure Type	F	7 Categories		-	-	O

Fig. 3
Darstellung der untersuchten Geometrie, Materialparameter und Randbedingungen mit den jeweiligen Grenzwerten.

Der vorgestellte Ansatz kombiniert physikalische Simulationen mit KI, um Zeitersparnis in Simulationen zu erreichen und optimierte Randbedingungen zu bestimmen. Dabei wird die Vorhersagegenauigkeit beibehalten und die Effizienz von FEM-Simulationen gesteigert. Durch die inverse Vorhersage mithilfe von KI können Probleme schnell gelöst werden, die anderweitig oft nur als Optimierungsprobleme ohne KI gelöst werden würden, bei denen in diesem Fall eine große Anzahl von Simulationen mit angepassten Randbedingungen zu einer schrittweisen Annäherung der gewünschten Geometrie führt. Dies ist jedoch sehr zeitaufwendig und ressourcenintensiv, was durch KI erheblich verkürzt und reduziert werden kann. Dies ist besonders bedeutsam, wenn tatsächliche Maschinenmessdaten und zugehörige Komponentenfertigung anstelle von Simulationsdaten verwendet werden, da dies die Anzahl der mit unterschiedlichen Parametersätzen herzustellenden Komponenten erheblich reduziert und durch KI optimiert werden kann. Dies führt zu erheblichen Zeit-, Ressourcen- und Kosteneinsparungen und fördert die Nachhaltigkeit.

4 Ergebnisse

Basierend auf der maximalen Spannung und dem Versagensmodus bei der inversen Vorhersage wurde die erforderliche Länge des Kunststoff-Schnapphakens mithilfe von KI vorhergesagt. Es wurde eine vergleichende Simulation mit dem zuvor unbekannten Parametersatz durchgeführt, um die maximale Spannung und den Versagensmodus zu bewerten. Diese Ergebnisse wurden dann verglichen, wobei eine Übereinstimmung von über 95% zwischen der gewünschten maximalen Spannung und der simulierten maximalen Spannung erzielt wurde (Abb. 4).

Da die Länge des Schnapphakens aus den definierten Parametersätzen der Geometrie, der Materialparameter und der Randbedingungen der vorherigen Simulationen ermittelt wurde, war keine zusätzliche Simulation für weitere Analysen der maximalen Spannung erforderlich. Durch die Nutzung des Trainings der KI durch Umstrukturierung des bestehenden Datensatzes konnten die Zeit- und Ressourcenanforderungen erheblich reduziert werden.

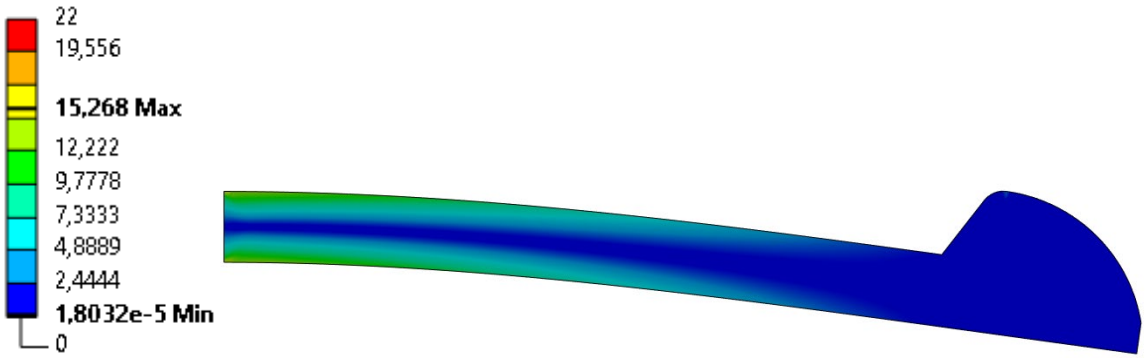

Fig. 4
Ein schematisches Ergebnis einer untersuchten Geometrie-, Materialeigenschafts- und Randbedingungskombination.

5 Zusammenfassung

Das Ziel des Papers ist es, ein umfassendes Verständnis für die Auswirkungen von KI in FEM- und CFD-Simulationen zu vermitteln, insbesondere bei der Optimierung der Systemeffizienz und dem effektiven Umgang mit inversen Problemen und Black-Box-Komponenten. Durch den Einsatz von KI-Techniken können Ingenieure neue Wege zur Effizienzoptimierung erschließen und sicherstellen, dass komplexe Komponenten verwaltet werden können. Diese Fortschritte ermöglichen das Design sichererer, innovativerer und effizienterer Systeme, was zu Fortschritten in verschiedenen Branchen beiträgt.

Es wird gezeigt, dass die Ermittlung der erforderlichen Prozess- und Maschinenparameter für die gewünschte Bauteilqualität durch die inverse Lösung einer Aufgabe durch KI ohne die Lösung eines Optimierungsproblems machbar ist. Dies reduziert die Entwicklungszeit sowie den Materialeinsatz und den Ressourcenverbrauch erheblich. Darüber hinaus kann durch die Umstellung der Aufgabenstellung auf direkte Vorhersage die maximale Spannung in einem Bauteil ohne zusätzliche Simulationen und Berechnungen abgeleitet werden. Diese Vorhersagen von Geometrie- und Materialparameter sowie Randbedingungsparametern können je nach Datenverfügbarkeit mit hoher Genauigkeit realisiert werden.

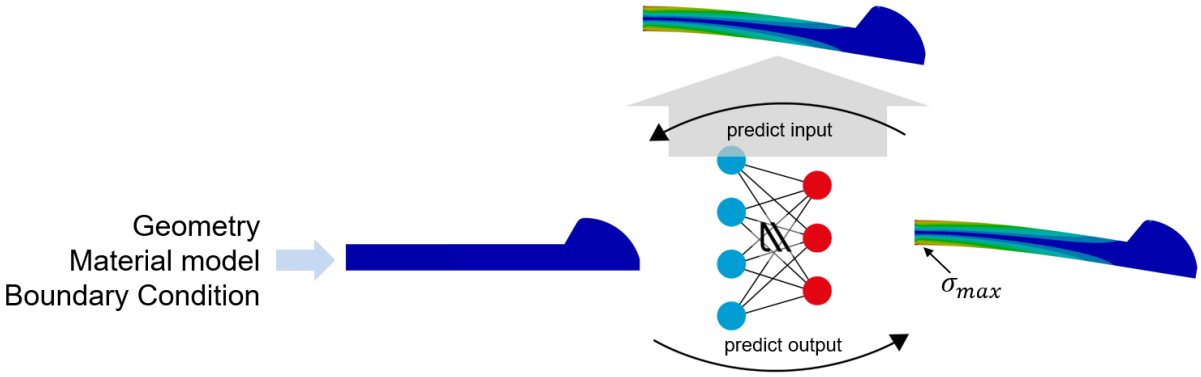

Fig. 5
Die Visualisierung der Vorhersage von Ausgabeparametern (Vorhersage der Ausgabe) und der inversen Vorhersage von Eingabeparametern (Vorhersage der Eingabe) mithilfe von KI kann am Beispiel eines Kunststoffschnapphakens erfolgen.

Boosting Simulation & Testing Tasks by Integrating AI/ML in SPDM

Alexander Köppe (PDTec AG) , Simon Mayer (sustainedBIZZ GmbH)

1 Summary

Integrating the use of neuronal networks into the workflow of engineers as a way of optimization and knowledge sharing.

1.1 The Idea

Running simulations typically requires specialized expertise. Assuming that increased design complexity leads to a proportional rise in the number of simulations and tests required, the development process must become more efficient to manage this growth. Enhancing efficiency could reduce the need to expand human resources, especially in a challenging labor market.

We present an approach that utilizes small neural networks, trained by non-AI experts, for narrowly scoped use cases. By enabling this capability for everyone involved in the process, we could achieve a significant impact, providing a new and safe way to share knowledge. In addition, it will be possible to carry out tasks outside the specialist area to a certain extent.

1.2 Example Process

Our baseline is a simplified CAE process where a designer creates geometries that are then analyzed by a simulation engineer or tested as prototypes.
In each iteration loop, all roles involved must process every design to determine if it meets the requirements.

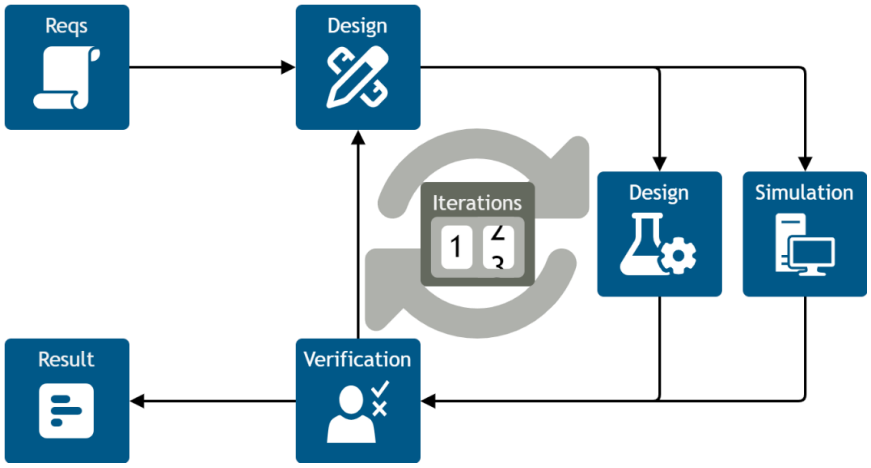

Figure 1:

Example Process without ML

By modifying this process to allow designers to verify their designs using a trained model, we can reduce the number of iterations by eliminating unsuitable candidates early. Additionally, this approach can guide designers to optimize efficiently by predicting optimal design parameters from the start.

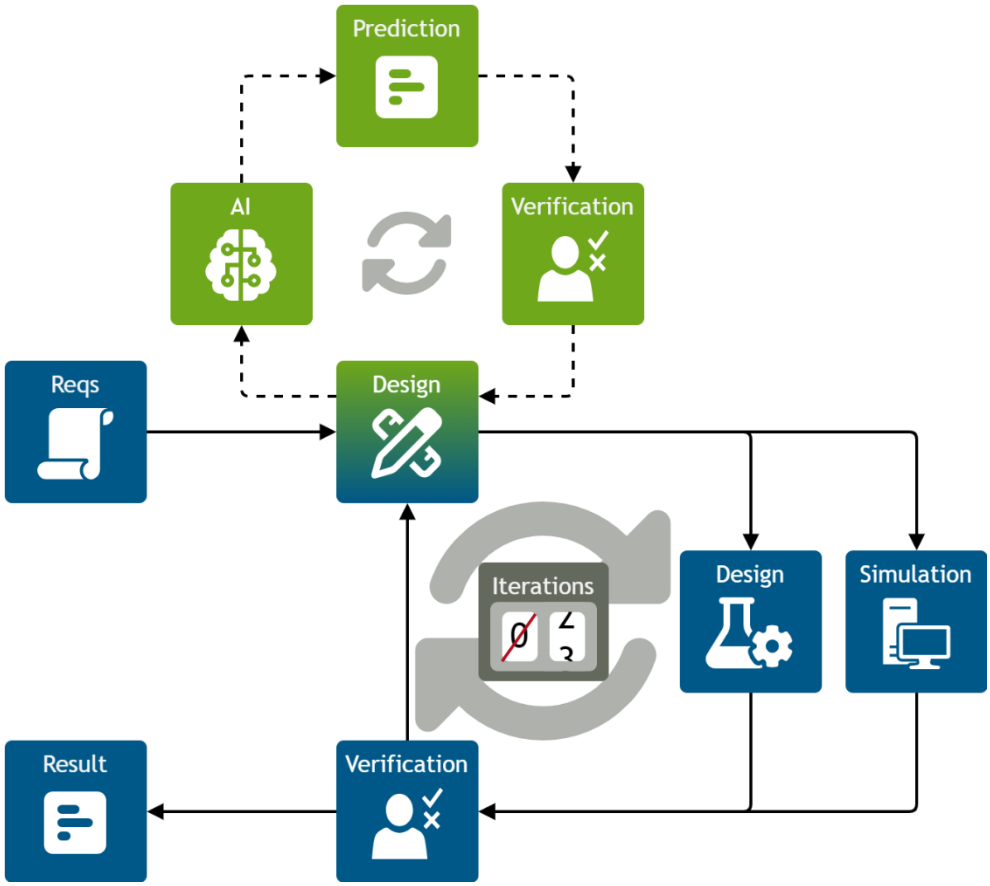

Figure 2:

Example Process with ML

This approach can also be beneficial for simulation engineers. It may reduce the need for simulations by eliminating candidates likely to fail and providing high-confidence predictions for candidates. These predictions can then be analyzed in a more targeted manner.

This approach to using machine learning creates a novel method for sharing knowledge among teams, or even across the entire enterprise if necessary. It empowers individuals to work more autonomously, enabling them to make decisions beyond their field to advance their tasks. This leads to reduced overhead from time spent in meetings, emails, or waiting for responses to blocking questions. Final decisions remain in the hands of the respective experts.

2 Analysis

In scenarios where machine learning is a daily tool, it must be easy to use for both training and prediction. Additionally, having readily accessible training data at all times is essential.

There are two major aspects to consider. First, to make machine learning accessible to everyone, we need a robust application that supports no-code training and offers complete automation when necessary. The same applies to using trained models for predictions. Second, it is essential to have readily available training data at all times.

To maximize availability, the application should run on any type of desktop hardware. It should also be capable of running as a service on dedicated hardware.

3 Solution

Considering the aspects of our analysis, we conclude that instead of focusing on training large-scale neural networks for general applications, we should train small to tiny neural networks tailored to solve very specific problems.

Training small-scale neural networks allows for training on entry-level hardware in a reasonable amount of time. It also reduces the amount of necessary training data to achieve a sufficient level of confidence. Additionally, if training fails for any reason, the impact is minimal since the efforts are kept low.

Since these neural networks are designed to address very specific problems, it becomes necessary to have many of them, with one for each problem. This necessitates an efficient system for storing and sharing the networks to maximize their utility and prevent them from getting lost.

3.1 Machine Learning Application

In general, model training is conducted by machine learning experts. However, smaller neural networks can be managed by a largely automated process, finding appropriate models automatically in exchange for training time. This allows efficient training even for users with limited knowledge of machine learning. Additionally, a guided workflow to preprocess and rate training data before training further improves the success rate.
Combining these features in a no-code application is key to enabling users to utilize machine learning as a daily tool.

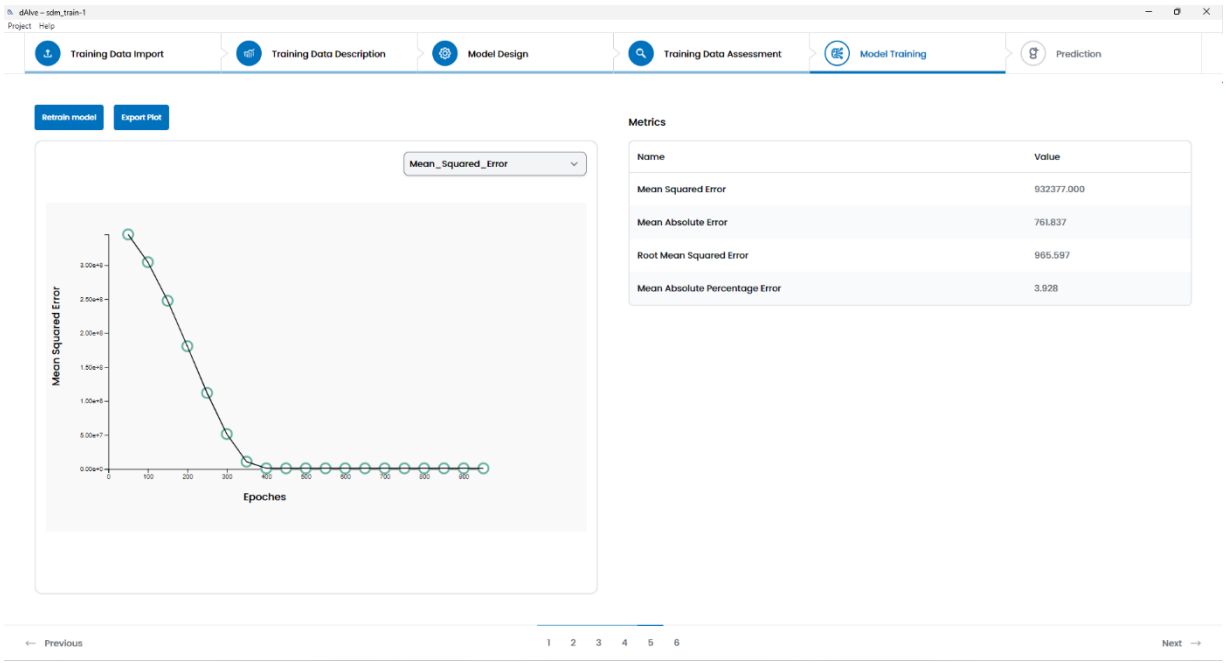

Figure 3:

Training of a Model using No-Code Application

3.2 Prediction

Just as training must be as effortless as possible, using those trained models should be easy as well. This can be achieved by integrating training and prediction capabilities into the same application, with support for the same input data types used during training, here CSV files. This ensures that models shared with colleagues can be easily utilized whenever needed, with minimal overhead.

3.3 Data Management

As mentioned in the analysis, providing training data and storing the models after training is essential in this scenario, given the large number of models in use. It is necessary to track which training data led to which model and what predictions have been made using each model. Additionally, having a shared library of ready-to-use models to choose from can be very convenient.

These requirements can be met using a simulation data management application, which serves as both a database for training data and a platform for sharing models.

If a simulation data management application is already in use, there is an opportunity to process this data for feeding into a machine learning process. It is also convenient to immediately store data that may be used as training input in the appropriate format. Having a large database of existing simulations is crucial for users to start with a reasonable amount of training data. Furthermore, it enables the continuous improvement of the database by adding more data over time.

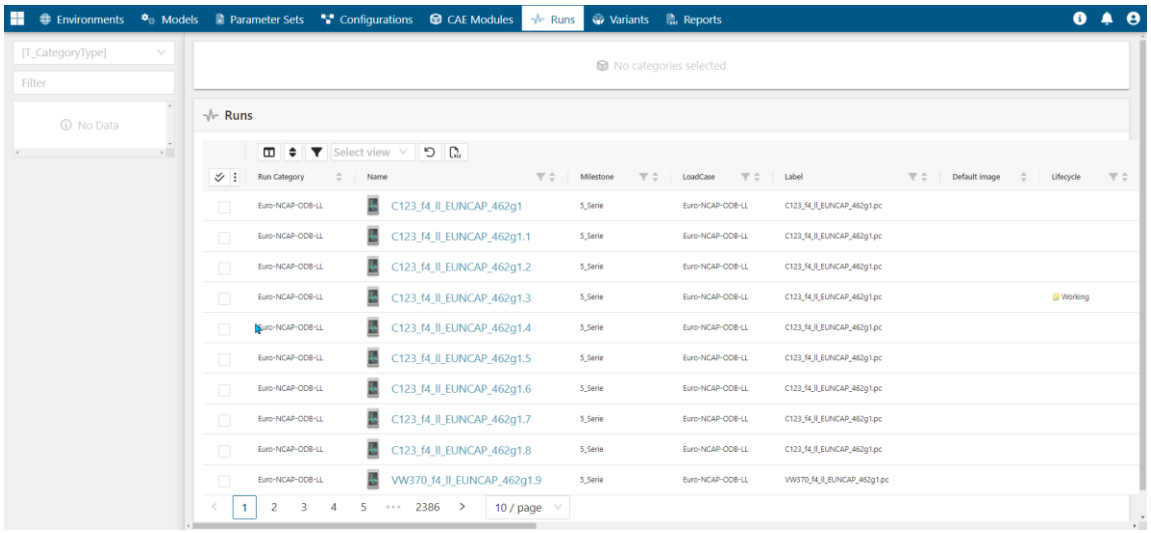

Figure 4:
Simulation Date Management Application

4 Conclusion

Bringing together data management applications and machine learning tools appears to be a promising approach. Since users often need to handle and process large amounts of data upfront, it makes sense to integrate machine learning capabilities directly into data management applications to alleviate the user's efforts. By allowing applications to automatically exchange data in the background using predefined data formats or APIs, the integration becomes seamless.

The better the integration, the faster and more effortless training can be initiated. With lower upfront efforts, users are more likely to benefit from using these tools, making it economically effective.

Vom Wunschergebnis zur Lösung – mittels Machine Learning in Minuten zum CAD-Konzeptentscheid

Michael Probst (CAIQ GmbH), Julian Klein (CAIQ GmbH), Raphael Sigloch (AUDI AG) (

1 Summary

Unter den bekannten Herausforderungen ist es eine Notwendigkeit, sehr frühzeitig die richtigen Designentscheidungen zu treffen. Klassische 3D-Smulationen als Grundlage sind sehr geeignet, aber beanspruchen ihre Zeit. Der Ansatz, über Machine Learning (ML) Modelle für Echtzeitprognosen eines Systemverhaltens zu generieren, bietet sich an.

Mittels geeigneter Technologie werden hinreichend viele Designvarianten erzeugt und simuliert, um den Designraum möglichst vollständig abzubilden. Mittels der auf die Ergebnisse hin trainierten ML-Modelle können schnell Parameter gesetzt und erfolgreiche Experimente gefunden werden. Die Besonderheit besteht darin, dass auf Basis der gesetzten „Wunschergebnisse“ (Masse, Material, ...) die Eingabegrößen gefunden werden, die diese Vorgaben erfüllen.

2 Motivation

Das klassische „Ping-Pong“ zwischen Konstruktion und Simulation ist insbesondere für die Frühe Phase des Entwicklungsprozesses nicht mehr zeitgemäß. Der altbekannte Zeit- und Kostendruck erfordert in zunehmendem Maße den Einsatz von Datentechnologien („KI“) für sehr schnelle Antworten auf prinzipielle Designfragen.

Damit diese Technologien sinnvoll und erfolgreich in den Prozess integriert werden können, ist eine ebenso umfangreiche wie valide Datenbasis erforderlich, die es normalerweise erst zu erstellen gilt. Für die Abbildung des Designraums bieten reine Simulations-basierte Verfahren schon gute Optionen wie Morphing, allerdings ist hierbei die Auswahl an möglichen Designparametern stark eingeschränkt und die Modellparametrisierung mitunter sehr komplex.

Zudem sollten in der frühen Phase möglichst viele und auch valide Designmöglichkeiten sehr schnell evaluiert werden können, um auf dieser Basis den optimale Parametersatz bzgl. der Anforderungen zu finden. Für frühzeitige, schnelle und valide Designentscheidungen ist es aber ebenso wichtig, das bestehende Knowhow der Konstrukteure bereits in die Datenentstehung einfließen zu lassen. Dadurch kann vermieden werden, unnötige Schleifen z. B. wegen vernachlässigter Fertigungsrestriktionen zu drehen.

3 Vorgehen

Es geht also darum, unter Einbeziehung des Konstruktionsknowhows und der Simulationsexpertise eine valide Datengrundlage für in unserem Fall Machine Learning zu erzeugen. Heutige CAD-Systeme bieten hervorragende Möglichkeiten, parametrisierte CAD-Modelle aufzubauen und davon Variationen abzuleiten. Da es nun aber um sehr viele – tausende – von Modellen geht, scheidet Handarbeit vollständig aus. Unserer Erfahrung nach ist insbesondere im weit verbreiteten CATIA V5 eine besondere Herausforderung, Update-stabile, parametrisierte Modelle mit entsprechenden Parameterabhängigkeiten zu erzeugen. Die Fehlerrate (nicht update-fähige Modelle) kann je nach Kom-

plexität des Modells bis zu 50% erreichen. Eine darauf basierende Parameterstudie (Design of Experiments, kurz DoE) würde also bis zu 50% des Lösungsraumes garnicht abbilden.

Um dieses Problem zu lösen, bedienen wir uns der Technologie des Fast Concept Modeller (FCM), der in CATIA V5 als zusätzliche Workbench integriert werden kann und ermöglicht, 100% Updatestabile CAD-Modelle zu erzeugen. Hinzu kommt, dass wir mit dem FCM auch alle für die Simulation erforderlichen Informationen bereits in CATIA verankern und als Parameter steuern können. Beispiele sind Verbindungstechnik, Solvereinstellungen, Materialkarten oder auch Netztopologieparameter.

Die Technologie des FCM erlaubt darüber hinaus, zwischen den jeweiligen Designparametern logische und mathematische Beziehungen zu definieren, die beispielsweise Abhängigkeiten unter Parametern (Abstand) oder von Designelementen (Fläche) definieren. Das Aktivieren oder Deaktivieren eines Bauteils ist ebenso möglich wie das Steuern der Anzahl von Designelementen wie Sicken, Rippen oder Schottblechen und deren geometrischer Beschreibung.

All diese Möglichkeiten helfen dabei, im CAD-Modell die möglichen Designparameter und Abhängigkeiten vollständig abzubilden und auf Knopfdruck beliebig viele Parametervariationen zu erstellen. Somit ist es vollautomatisiert möglich, >10.000 CAD-Modelle aufzubauen und an den Folgeprozess zu übergeben.

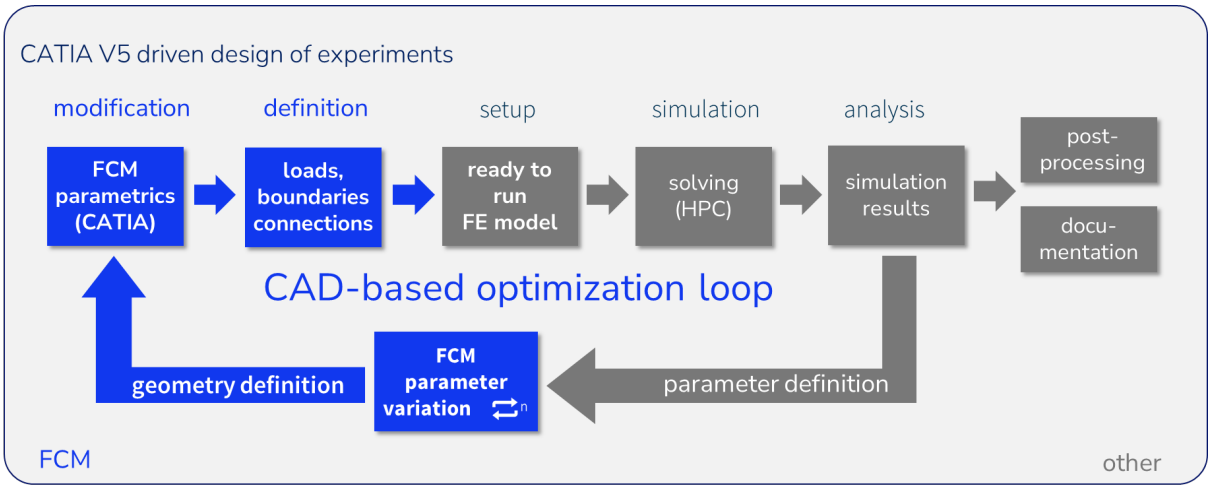

Fig. 1
Klassischer DoE- oder Optimierungsprozess, erweitert um CAD und gesteuert aus CATIA V5

Das CAD-Modell wird anschließend mit all den für die Simulation inhärenten Informationen an einen Preprozessor (Ansa, Hypermesh) übergeben. Mittels Automatisierungen wird das jeweilige FEM-Modell vollautomatisch erstellt und anschließend an einen Rechenserver weitergegeben.

Erfahrungsgemäß ist nach dem Solving noch der Prozessschritt der Auswertung auf dem Rechenserver erforderlich, da die gewünschten Informationen selten direkt vorliegen. Weitere Automatisierungen werden also erstellt, um aus den Rechenergebnissen die gewünschten Informationen, beispielsweise Integrale, zu erzeugen.

Der Vorteil ist, dass uns nun die Ergebnisgrößen mit direktem Bezug zu allen Eingangsparametern (Geometrieparameter, Material, Wanddicken, etc.) vorliegen.

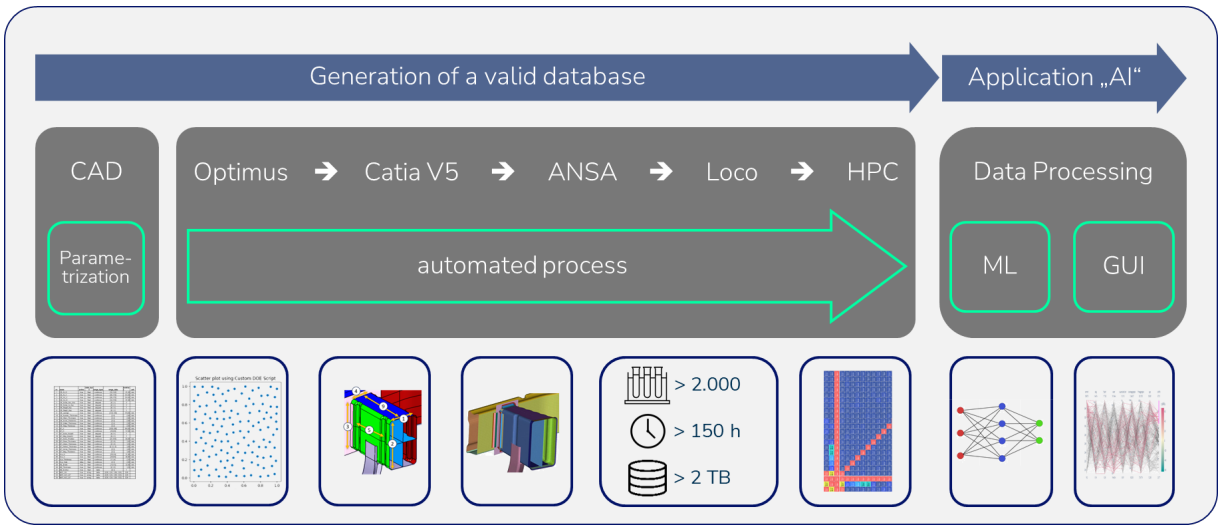

Fig. 2
automatisierter Prozess: Sampling, DoE, Modellerstellung, Simulation, Auswertung mit anschließendem Training der ML-Modelle

Die verwendeten Input-Parametervektoren mit den zugehörigen Ergebnisvektoren werden anschließend für das Training Ergebnis-spezifischer ML-Modelle verwendet. Hierbei ist zu beachten, dass genügend Test- und Validierungsdaten außen vor gelassen werden, um die Modellqualität zu gewährleisten. Die Verwendung von mindestens 20% der Daten zur Validierung hat sich als günstig erwiesen, kann aber je nach Problem auch größer ausfallen.

Die Anwendung der ML-Modelle für unseren Use Case (siehe unten) erfordert wiederum eine Applikation, die bei CAIQ im Haus entwickelt wurde. Mittels dieser App können die trainierten Modelle eingelesen und die Trainingsdaten so direkt weiter verwertet werden.

Allerdings sind hierbei die Eingabe- und Ausgabevektoren sehr umfangreich und nicht für jede Fragestellung zielführend. Üblicherweise grenzt der Bearbeiter hier beide Vektorfelder stark ein, um das spezifische Problem zu lösen.

Die App ermöglicht, dass mit eingegrenzten Inputvektoren (kleinere Ranges, oder Festsetzung) auf den ML-Modellen neue DoE mit >10.000 Experimenten durchgeführt werden können, um so den Lösungsraum nochmals deutlich feiner abzuscannen. Mittels Paralleler Koordinaten Darstellung können dann geeignete Ergebnisvektoren identifiziert und die zugehörigen Inputparameter identifiziert und extrahiert werden. Dies ist innerhalb von wenigen Minuten erledigt und der Entwickler hat eine erste Möglichkeit, mit den Ergebnissen weiterzuarbeiten.

4 Anwendung

Use Case Crash Management System (CMS) bei optimaler Bauraumausnutzung im Ergebniskorridor:

Das ausgewählte Beispiel (Fig. 3, 3a) zeigt, die Variabilität. Neben den klassischen kontinuierlichen Parametern stehen auch Sprunggrößen (Anzahl von Designelementen wie Rippen, Schottbleche), Tabellen (Material) oder Ein-Aus-Schalter zur Verfügung (Prallplatte).

In diesem Beispiel wurden als Basis für die DoE ca. 2.300 3D-Simulationen durchgeführt, wobei das Problem bewusst so gewählt wurde, dass die Simulationen inkl. der Auswerteberechnungen über ein Wochenende durchlaufen (HPC bei Audi).

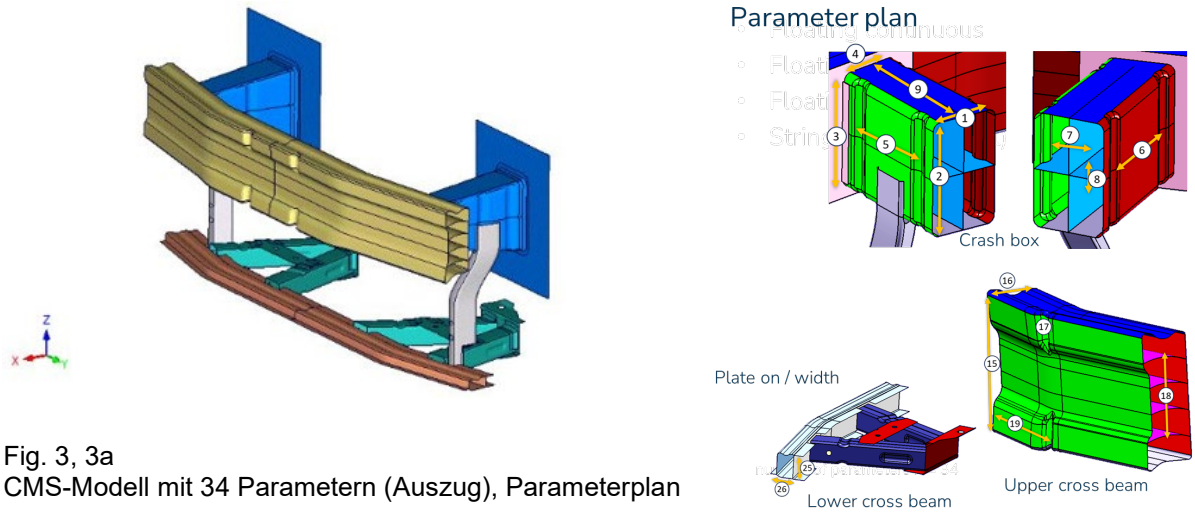

Fig. 3, 3a
CMS-Modell mit 34 Parametern (Auszug), Parameterplan

Ein klassischer Anwendungsfall ist die Veränderung des Bauraumes. Im dargestellten Fall (Fig. 4) hat die bis dato gültige Version des CMS eine Länge von 180mm, eine Masse von 9,63 kg (Zielwert <10kg) und ein Kraftniveau von 160 kN (Zielwert<200kN).

Wenn sich nun der Bauraum wie dargestellt auf 160 mm verkürzt und dennoch die Zielvorgaben hinsichtlich Energieaufnahme, Gewicht und Intrusionstiefe eingehalten werden sollen, führt das zu einem höheren Kraftniveau wegen des kürzeren Verformungsweges. Es kann nun sehr schnell auf Basis der Simulationen oder auf Basis von weiteren DoEs auf den angelernten Modellen eine Parameterkonstellation gefunden werden, die die Kernanforderungen erfüllt (Fig. 4 untere Kurve).

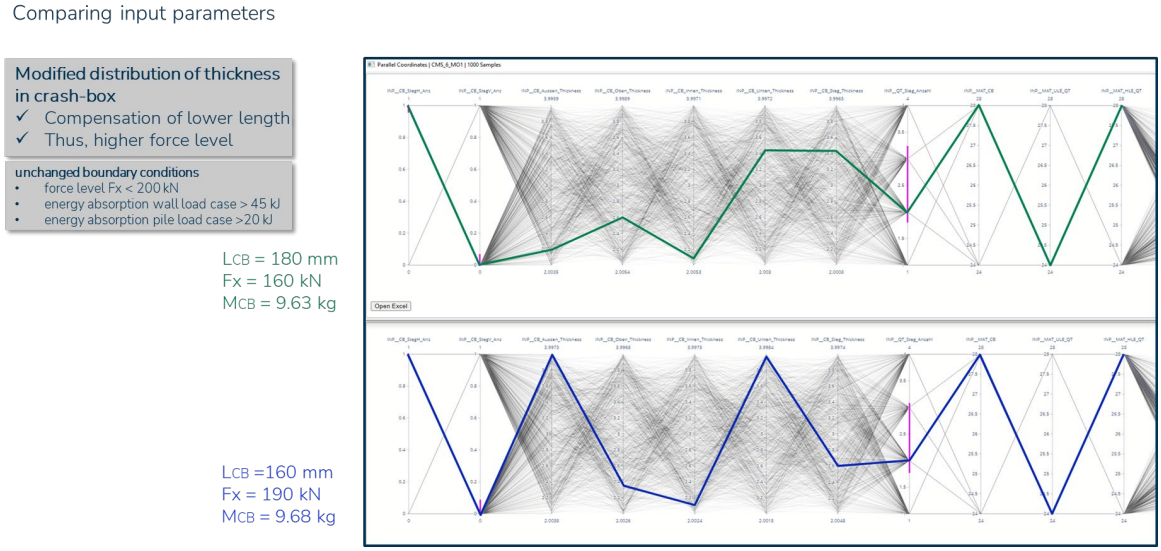

Fig. 4

Fallbeispiel Bauraumverkürzung von 180mm auf 160 mm mit erfolgreichem Parametervektor

Es ist eine Möglichkeit, an den Eingabe-Parametern (Schieberegler in der App) „herumzuspielen“, bis ein passendes Ergebnis herauskommt. Dies kann sich aber mühselig gestalten und nicht notwendigerweise zum besten Ergebnis führen.

Daher ist die Anwendung erweitert worden um die Möglichkeit, den Ergebnisvektor ebenfalls nach Bedarf einzugrenzen. Auf Basis der ML-Modelle können unter Verwendung dieser Eingabe- und Ausgaberäume neue DoE-Reihen durchgeführt werden, die sukzessive den Spielraum einengen und somit zu einem neuen Optimum führen.

Wenn über die Iterationen die Anzahl der möglichen Eingabevektoren bei Erfüllung der Ergebnisvektoren genügend eingeschränkt ist, lässt sich die Matrix der erfolgreichen Eingabevektoren per Knopfdruck exportieren und in CATIA einlesen.

In CATIA werden wiederum vollautomatisch die CAD-Files erzeugt, die in Simulationsmodelle umgesetzt und simuliert werden können. Mit diesen 3D-Simulationen werden abschließend die Ergebnisse aus den ML-Modellen qualifiziert.

Fig. 5

Basierend auf eingegrenzten Ergebnisvektoren (rot) gefundene Inputparameter (blau), die die Anforderungen erfüllen.

5 Conclusions

Insbesondere in der Frühen Phase haben konzeptionell-konstruktive Richtungsentscheidungen einen großen Hebel hinsichtlich nachfolgenden Aufwänden und Kosten. Die Kopplung von CAD-basierten DoE mit Simulation und Machine Learning bietet einen hocheffizienten Ansatz, in nahezu Echtzeit Varianten durchzuspielen und Richtungsentscheidungen abzuleiten.

Die Voraussetzung hierfür, nämlich die vollständige Abbildung des Designraums in der Modellierung, ist durch die update-stabile Technologie (CATIA V5 mit dem FCM) gegeben.

Mit der vollständigen Automatisierung der Teilschritte werden 1000e Simulationen durchgeführt und ausgewertet. Dies als Basis erlaubt eine rekursive, vom Wunschergebnis her ansetzende, iterative Vorgehensweise, um in kürzester Zeit eine erfolgreiche Parameterkonstellation zu finden.

Der abschließende 3D-Kontrolllauf dient dazu, das Ergebnis zu verifizieren und das Produktverhalten unter den Lastbedingungen genau zu analysieren.

Mit dem vorbereitenden Aufwand der DoE und der ML-Modellierung und des Trainings können nun z. B. generische Modelle erzeugt werden und simulationsbasierte Designentscheidungen innerhalb von Minuten getroffen werden.

6 References

[1] Aachener Karosserietage, “App based behaviour prediction for car body structures”, Markus Sandfort (Audi) und Michael Probst (CAIQ), 20.09.2023

KI-Expertensysteme in der Produktentwicklung als Chance für die Konservierung von wertvollem Expertenwissen und nachhaltigerer Ressourcenplanung (Forschungsprojekt EP 4.0)

Dr.-Ing. Dirk Rensink (SEGULA Technologies)

Dipl.-Ing. Lars-Christian Bütow (:em AG)

Mareike Keil (M.Sc.) (:em AG)

1 Motivation

System Design und Optimierung der Produktentwicklung sind vor allem in der Automotiv-Branche stark abhängig von Expertenwissen, welches durch zunehmenden Fachkräftemangel immer wertvoller wird. Viele Unternehmen lassen zudem im Hinblick auf Kostenersparnis und Ressourcenengpass möglichst viele Aufgaben von kostengünstigeren und daher meist unerfahreneren Ingenieuren erledigen. Daher müssen Seniorexperten ihre realen, praktischen Erfahrungen an die jungen Entwicklungsingenieure übermitteln können. Dies gewährleistet die Wettbewerbsfähigkeit der Hersteller und Zulieferer und sichert die Qualität der Ergebnisse. Des Weiteren resultieren die zunehmende Digitalisierung und Globalisierung in einer immer größeren Datenmenge, die während der Produktentwicklung erzeugt wird. Jedoch liegen diese Daten meist an verschiedenen Orten in unterschiedlichen und zum Teil nur in menschenlesbaren Formaten vor. Diese distributive Verwaltung der Daten, sowie die Arbeitsweise auf Distanz haben zur Folge, dass keine konsolidierten Daten vorliegen und somit kein Single-Point-Of-Truth (SPOT) existiert.

Das Forschungsprojekt „Entwicklungsplattform 4.0“, welches in diesem Vortrag präsentiert wird, widmet sich den oben aufgeführten Herausforderungen. Innerhalb dieses Projekts wird ein KI-Expertensystem aufgebaut, das u.a. Test- und Simulationsdaten miteinander verknüpft und hierdurch einen SPOT schafft.

In diesem Beitrag wird zunächst auf KI-Expertensysteme sowie deren Nutzung allgemein eingegangen. Anschließend erfolgt eine kurze Vorstellung des Forschungsprojekts „Entwicklungsplattform 4.0“ sowie die Präsentation der Wissensdatenbank und des WikiBots, die der Konservierung und Bereitstellung des Expertenwissens dienen. Zum Schluss werden noch zukünftige Potenziale und Entwicklungsmöglichkeiten hervorgehoben.

2 KI-Expertensysteme

KI-Expertensysteme stellen eine spezielle Art von Künstlicher Intelligenz (KI) dar, die mit dem Ziel entwickelt wurden, menschenähnliche Entscheidungen auf einem bestimmten Fachgebiet zu treffen und komplexe Probleme zu lösen [1]. Sowohl die Entscheidungsfindung als auch die Problemlösung dieser Systeme basieren auf einer Kombination von Daten, Algorithmen und menschlichem Fachwissen. Im Wesentlichen versuchen sie entsprechend, das Wissen, die Erfahrung und die Entscheidungsprozesse eines menschlichen Experten zu modellieren, zu interpretieren und nachzuahmen.

KI-Expertensysteme bestehen im Allgemeinen aus nachfolgenden Komponenten (siehe Figur 1):

- **Wissensbasis (Knowledge Base):** Enthält das Fachwissen von Experten, welches in Form von Regeln, Heuristiken und Fallbeispielen gespeichert ist und dient als Referenz für die Entscheidungsfindung.
- **Inferenzmaschine (Inference Machine):** Verwendet das Wissen aus der Wissensbasis sowie Algorithmen, um Schlussfolgerungen zu ziehen bzw. Probleme zu lösen.
- **Interaktive Benutzerschnittstelle (User Interface):** Ermöglicht die Interaktion zwischen Nutzer und System.
- **Erklärungskomponente:** Erklärt dem Anwender die Schlussfolgerung, z.B. anhand der zugrundeliegenden Regeln.
- **Wissenserwerbskomponente:** Extrahiert das Fachwissen von menschlichen Experten und bereitet es so auf, dass es vom Expertensystem genutzt werden kann.

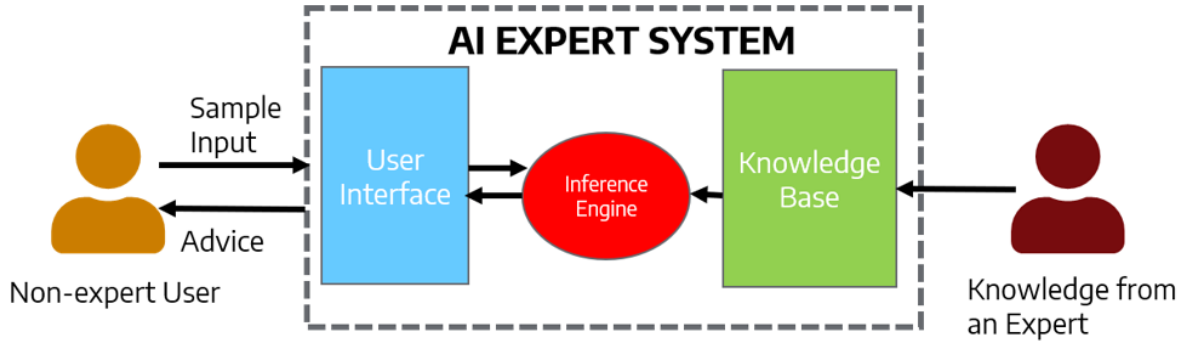

Figur 1: Aufbau eines KI-Expertensystems

Angemerkt sei hier, dass die Unterscheidung zwischen regelbasierten und selbstlernenden KI-Expertensystemen vorteilhaft ist. Diese beiden Formen weisen grundlegend verschiedene Ansätzen zur Problemlösung und zur Informationsverarbeitung auf. Während regelbasierte Expertensysteme explizite Regeln für die Entscheidungsfindung und Problemlösung verwenden, die von menschlichen Experten erstellt werden, basieren selbstlernende Expertensysteme auf Algorithmen des maschinellen Lernens, um aus Daten zu lernen und ihre Leistung im Laufe der Zeit zu verbessern. Sie kommen ohne explizite Regeln von menschlichen Experten aus. Die Regeln bei regelbasierten Expertensystemen werden in Form von "Wenn-Dann"-Anweisungen definiert, die angeben, welche Aktion in Abhängigkeit von bestimmten Bedingungen ausgeführt werden soll. Regelbasierte Expertensysteme gelten als transparent und nachvollziehbar, da die Entscheidungslogik durch die expliziten Regeln klar definiert ist. Selbstlernende Expertensysteme hingegen analysieren große Mengen von Daten, identifizieren Muster und treffen Entscheidungen auf Basis dieser Muster. Sie gelten daher als flexibel und können sich an veränderte Umstände und neue Daten anpassen. Aufgrund ihrer komplexen internen Strukturen sind sie allerdings undurchsichtiger als regelbasierte Expertensysteme.

Ein bekanntes Beispiel für ein regelbasiertes KI-Expertensystem ist das Deep Blue-System von IBM [2], das für das Schachspielen entwickelt wurde. Deep Blue setzte eine Vielzahl von Techniken ein, darunter speziell entwickelte Hardware, um Schachzüge zu berechnen und Entscheidungen zu treffen, die denen eines menschlichen Schachgroßmeisters ähneln. Hierdurch gelang es Deep Blue den damals amtierenden Schachweltmeister Garry Kasparov zu besiegen. Da Deep Blue auf vordefinierten Strategien und Algorithmen basierte und das System nicht in der Lage war, aus neuen Informationen zu lernen, zählt es zu den regelbasierten KI-Expertensystemen.

Ein Beispiel für ein selbstlernendes KI-Expertensystem ist das von Google DeepMind (früher DeepMind Technologies) entwickelte Computerprogramm AlphaGo, welches den amtierenden Weltmeister Lee Sedol geschlagen hat. AlphaGo verwendet nicht das Wissen von Experten bzw. von diesen definierte Regeln als Wissensbasis, sondern maschinelles Lernen und tiefe neuronale Netze, um auf Basis von großen Datenmengen und Mustererkennung in Spielzügen das Spiel Go zu erlernen. Daher zählt es zu den selbstlernenden KI-Expertensystemen.

KI-Expertensysteme kommen in vielen Bereichen wie Medizin und Produktentwicklung zum Einsatz. In der Medizin werden sie z.B. zur Diagnose von Krankheiten verwendet [3] und in der Fertigung z.B. für die Qualitätskontrolle und Prozessoptimierung [4].

3 Konservierung von Expertenwissen

3.1 Entwicklungsplattform 4.0

Das durch den BMWK-geförderte Forschungsprojekt „Entwicklungsplattform 4.0" beschäftigt sich neben einer Verbesserung der Effizienz und Qualität in der Produktentwicklung auch mit einer umfassenden Unterstützung von Junior-Ingenieuren sowie mit der Erhaltung und Bereitstellung von (Simulation und Test) Senior-Expertenwissen. Diese ambitionierten Ziele werden durch eine Vernetzung der Simulations- und Testdatenmanagement Welt und der damit verbundenen Ressourceneinsparung erreicht sowie durch den Einsatz eines WikiBots, um den Anwendern einen benutzerfreundlichen und zielführenden Zugriff auf wertvolles Expertenwissen zu bieten [5].

Um entsprechende Wissensquellen dem Wikibot zur Verfügung zu stellen, wurde neben der Wissensdatenbank (siehe 3.2) auch ein Prozessbegleiter implementiert. In diesem werden alle (wertvollen) Informationen aus den einzelnen Phases des Simulationprozesses gespeichert (siehe Figur 2).

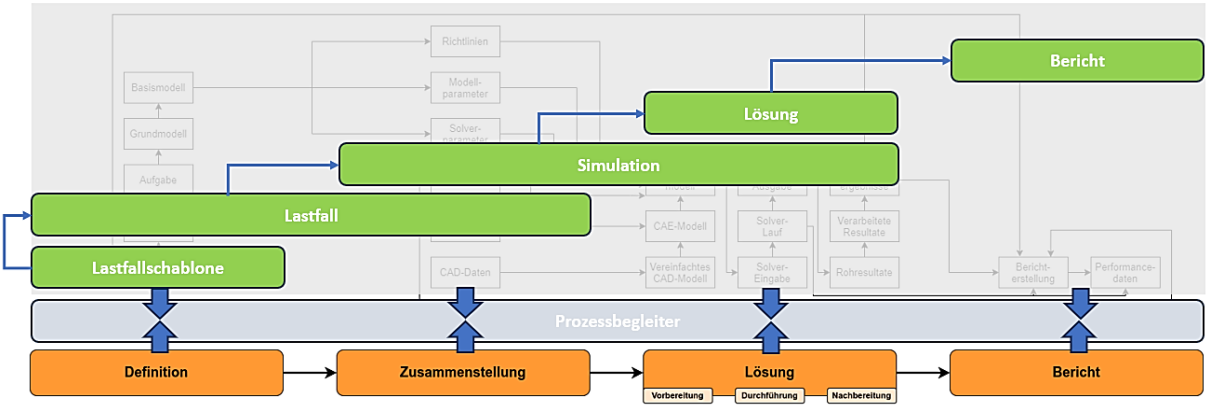

Figur 2: Einbettung des Prozessbegleiters in den Simulationsprozess

Figur 3 zeigt, welche Artefakte in welcher Phase relevant sind und gibt damit auch eine Übersicht über die im Prozessbegleiter hinterlegten Informationen.

Die Phasen *Definition*, *Zusammenstellung*, *Lösung* und *Bericht* sind dabei wie folgt zu verstehen:

- **Definition:** Definition der Aufgabe mit einer möglichst genauen Beschreibung der Inhalte und der zu berichtende Ergebnisse
- **Zusammenstellung**: Sammlung aller zur Aufgabenstellung notwendigen Daten
- **Lösung:** Lösung der Aufgabenstellung
- **Bericht:** Erstellung des Berichts, Reflexion für das Qualitätsmanagement

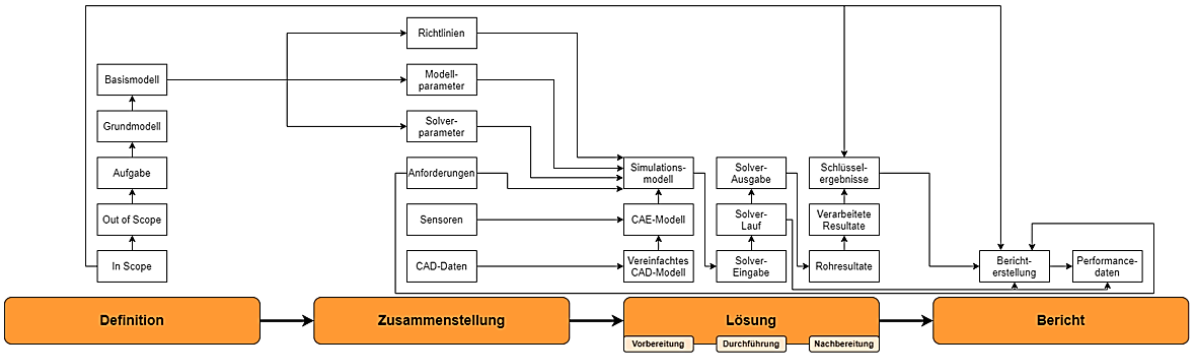

Figur 3: Artefakte innerhalb der Phasen des Simulationsprozesses

3.2 Wissensdatenbank und WikiBot

Die Implementierung einer Wissensdatenbank und eines WikiBots und die damit verbundene Konservierung von Expertenwissen sowie dessen zur Verfügungstellung führen zukünftig zu einer Effizienzsteigerung und Entwicklungszeitverkürzung. Durch den Aufbau einer Wissensdatenbank und die Nutzung des WikiBots, können Junior-Ingenieure auf Erfahrungswerte von Senior-Ingenieuren zu jeder Zeit zugreifen und ihr Wissen erweitern sowie Aufgaben zielführender und schneller erledigen. Zudem wird das Risiko von fehlerhaften bzw. unvollständigen Parametersätzen und Einstellungen bei Tests und Simulationen reduziert. Darüber hinaus wird die Anzahl der Tests und Simulationen minimiert, wenn auf entsprechende Erfahrungswerte zugegriffen werden kann.

Um die aufgeführten Vorteile zu erreichen, erfassen Senior-Ingenieure ihr Wissen über Simulationen und Tests in einem betriebsinternen Expertensystem – der Entwicklungsplattform 4.0. Diese Plattform kann durch Junior-Ingenieure genutzt und ggf. eigenständig nach erfolgter Freigabe durch das Qualitätsmanagement ergänzt werden. Die Erfassung erfolgt hierbei in einer lokalen Wissensdatenbank, so dass die Daten und die wertvoll gesammelten Erfahrungswerte nicht unerwünscht verbreitet werden können und der Cyberschutz gewährleistet ist.

Der schnelle Zugriff auf dieses Wissen wird durch einen lokalen WikiBot ermöglicht. An jeder Stelle im Expertensystem hat der Anwender die Möglichkeit den WikiBot aufzurufen und seine Frage zu stellen

(siehe Figur 4). Darüber hinaus existiert eine eigene WikiBot-Seite im System, in dem ähnlich zu ChatGPT alte Anfragen gespeichert werden (siehe Figur 5).

Der WikiBot filtert basierend auf der Anfrage des Anwenders die Wissensdatenbank nach den gewünschten Informationen, stellt diese dem Nutzer zur Verfügung und interpretiert die Ergebnisse ggf. Dies verkürzt den Arbeitsprozess ungemein, da der für die Aufgabe zuständige Ingenieur nicht viele verschiedene Datenbanken nach den Informationen selbst durchsuchen und nicht passende Ansprechpartner identifizieren und auf deren Rückmeldung warten muss.

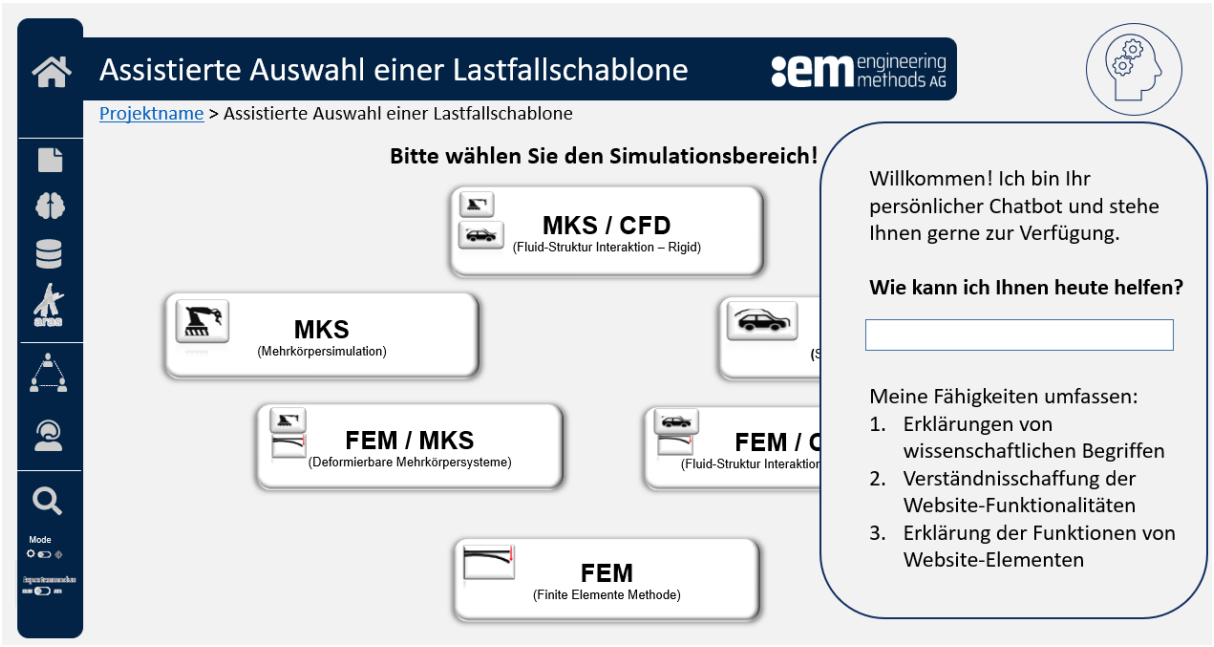

Figur 4: Zugriff auf den WikiBot zu jeder Zeit im System

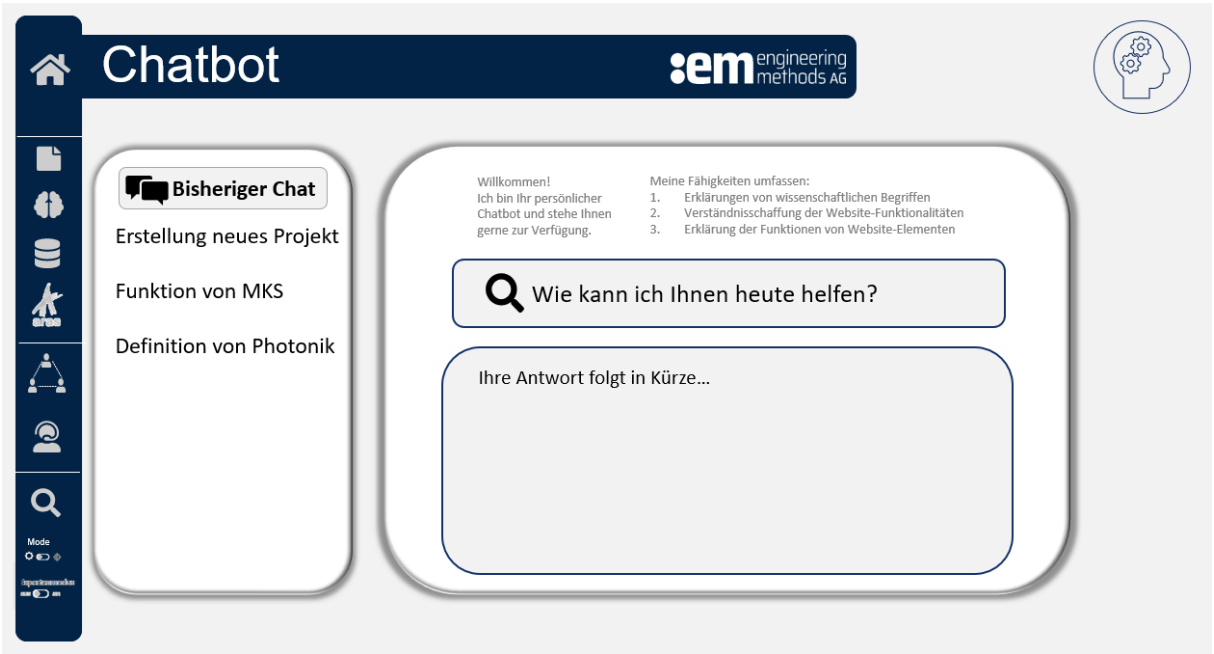

Figur 5: WikiBot Übersichtsseite mit gespeicherten Anfragen

4 Zusammenfassung und Ausblick

Aufgrund des demografischen Wandels können wertvolles Expertenwissen und gemachte Erfahrungswerte nicht mehr ausreichend in den Unternehmen weitergegeben werden und gehen damit verloren. Um den nachfolgenden Generationen dennoch eine Möglichkeit zu bieten, zukünftig von diesem Wissen zu profitieren, wird im Rahmen des Forschungsprojekts „Entwicklungsplattform 4.0“ ein KI-Expertensystem aufgebaut, dass das Fachwissen konserviert und für berechtigte Personen zugänglich macht. Hierfür wird eine Wissensdatenbank implementiert, in der unter anderem

Erfahrungswerte gespeichert sind. Um eine zielführende und schnelle Bereitstellung der Daten zu gewährleisten, werden die Anwender durch einen WikiBot unterstützt. Dieser durchsucht zielgerichtet die Wissensdatenbank nach passenden Informationen, die der Beantwortung der gestellten Frage des Nutzers entsprechen, stellt diese übersichtlich aufbereitet zur Verfügung und interpretiert diese.

Zukünftig soll es möglich sein, dass der WikiBot zudem aus alten Projekten lernt und somit dem Anwender potenzielle Projektverzögerungen aufzeigen und entsprechende Handlungsempfehlungen geben kann.

5 Danksagung

Dieses Forschungs- und Entwicklungsprojekt wird durch das Bundesministerium für Wirtschaft und Klimaschutz (BMWK) im Rahmen des Verbundprojekts „Aufbau einer Entwicklungsplattform 4.0 – EP 4.0“ gefördert (Förderkennzeichen 19I21020A) und zudem unterstützt durch den TÜV Rheinland Consulting GmbH, Projektträger Bodengebundene Verkehrstechnologien (PT BVt) mit der Vereinbarung № 19 I 21020A (June 02, 2021). Dafür danken wir dem BMWK und dem TÜV Rheinland.

Träger:	BMWK
Fachprogramm:	Neue Fahrzeug- und Systemtechnologien
Schwerpunkt:	Künstliche Intelligenz als Schlüsseltechnologie für das Fahrzeug der Zukunft
Beteiligte Partner:	SEGULA Technologies, FKFS, :em AG, Fraunhofer IESE (UB)
Projektbeginn:	01.06.2021
Projektdauer:	3,5 Jahre

6 Literaturverzeichnis

[1] Myers, W. (1986). Introduction to expert systems. *IEEE Intelligent Systems*, *1*(01), 100-109.

[2] Hsu, F. H. (2002). *Behind Deep Blue: Building the computer that defeated the world chess champion*. Princeton University Press.

[3] Alugubelli, R. (2016). Exploratory study of artificial intelligence in healthcare. *International Journal of Innovations in Engineering Research and Technology*, *3*(1), 1-10.

[4] Pierre, K., Haneberg, A. G., Kwak, S., Peters, K. R., Hochhegger, B., Sananmuang, T., ... & Forghani, R. (2023, April). Applications of artificial intelligence in the radiology roundtrip: process streamlining, workflow optimization, and beyond. In *Seminars in Roentgenology* (Vol. 58, No. 2, pp. 158-169). WB Saunders.

[5] Vorhabensbeschreibung “Entwicklungsplattform 4.0”. Konsortialteam des Forschungsprojekts (2021)

On the introduction of cloud-based SPDM in multidisciplinary simulation teams

Michael Göttlinger (Hilti Entwicklungsgesellschaft mbH)

1 Abstract

Dealing with highly individualized simulation processes is a significant challenge when implementing a simulation data management system and must be taken into account when choosing a solution and refining the implementation concept. In this regard, we present our situation and the solution approach developed by separating uniform administrative processes and workflow-specific tasks. The presentation further shows important aspects in the decision-making process for a system solution, describes learnings on the various dimensions in the project and provides insight into our experience with cloud-based implementation.

2 Introduction & Motivation

The digitalization of development processes is an essential step in order to meet the demand for shorter development times, a constantly growing product portfolio and ultimately the vision of the fully virtual prototype. Furthermore, modern AI-based algorithms rely on carefully managed and precise data structures.
The systematic management of simulation data and processes provides an important building block here and, in its initial steps, faces the challenge of having to be integrated into PLM structures that have evolved over decades. For small and medium-sized simulation teams in particular, the task of combining their usually diverse and highly individualized calculation processes in a central SPDM solution and managing the complexity of system implementation seems enormous.

3 Overcoming complexity with highly individualized Simulation Workflows

Doing research on available contents, the majority of contributions and experience reports concentrate on gaining efficiency in model preparation and automation of recurring modeling steps, e.g., automated mesh generation and input deck assembly. But especially smaller in size, but no less powerful computational engineering departments usually still cover a wide range of disciplines, thus leading to a high diversity in their workflows. In combination with a large and heterogenous product portfolio, this leads to a high degree of individualization which reveals, to openly address the bare facts, low degree of automation, a limited expected scalability together with high implementation effort for a centralized simulation data management solution. But there are still significant advantages to be gained, when all data is organized in a feature-rich repository, which automatically connects every piece of information to its context and provides an extensive API to connect to existing and future systems within the company. This prepares you well for handling connected workflows in the System Simulation environment, contributes to the digitalization of the development processes and enables you to further optimize reliability and response times. In addition, all business-critical information meets today's essential data security requirements and protects your knowledge from potential loss.

Our implementation concept is designed to achieve homogenization and individualization at the same time. We introduce a two-layered concept of task organization, uniform processes for the administrative work and adapted process templates for the individual modeling workflows. The admin work includes task and project management activities, handling of supporting data like general information or field results and provides a “digital notebook” for the engineers. The workflow templates are designed with high involvement of the process owners (key users) and allow configuration to individual requirements. In many cases, we rely on case-related bulk importer, which retain the “local” working style of the users and are able to lift the entire task into the SPDM. This data import process realizes automated typecasting, attribute extraction and assignment, as well as the interconnection of every information and file according to the process configuration. This “soft” integration of the software tools involved, which form an end-to-end workflow, is significantly less complex than the deep integration of authoring tools using its offering programming interfaces. Together with the separation of task administration and actual simulation business, this significantly reduces the effort required to integrate new simulation processes.

4 Requirements assessment, Stakeholder engagement and Decision making

Finding ourselves in the situation outlined above, the starting point was a comprehensive model-based analysis of our processes and interfaces. Using a model-based approach, our core simulation processes were recorded, including the software in use, data input and generation, required infrastructure and interaction with partners across departments as well as in external collaboration. Special attention was paid to steps that are of particular importance to the engineers as well as elements that have so far been painful and obstructive. The consolidation and evaluation of these records was considerably simplified by this process model, as an inverse mapping of typified and linked information resulted in a uniform process structure and summarized our technical requirements for an SPDM system. In order to achieve this result in the traditional way on the flipchart, almost unfulfillable conditions are placed on the availability of the participants in terms of location and time, which may likely lead to fragmented information and poor alignment. Figure 1 schematically shows the procedure from process mapping to aggregating the required SPDM functionality, which then provided the basis for contacting solution providers and finally nominating our partner for the proof-of-concept phase.

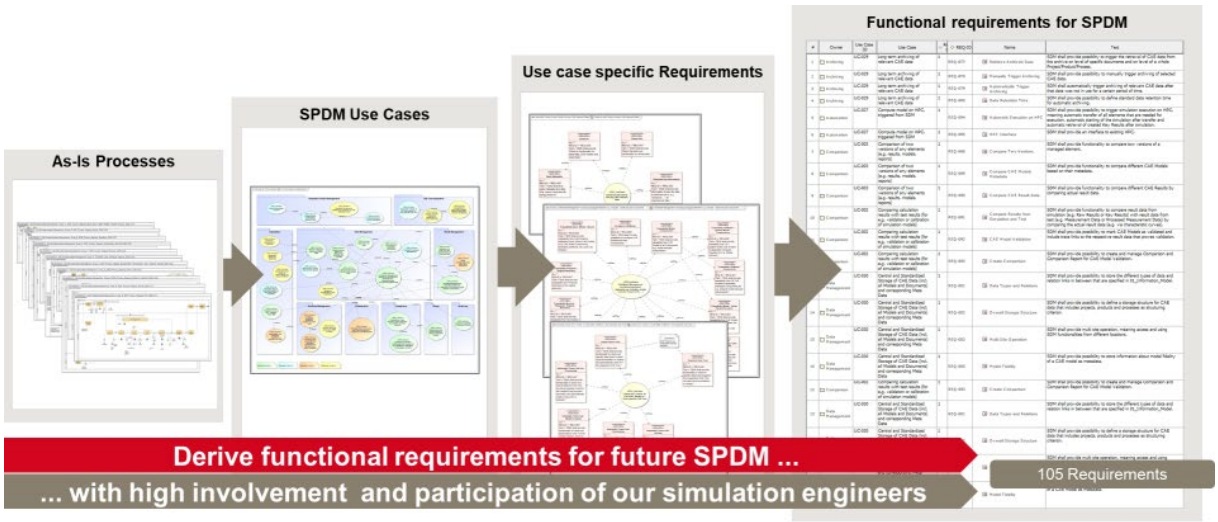

Figure 1: Process to derive functional requirements for SPDM solution using a model-based approach

In addition to identifying technical requirements, it is essential to coordinate with all stakeholders involved in the system implementation at an early stage. Apart from procurement and legal interests, functional interfaces have to be considered, like PLM and testing facilities. But most importantly, various IT disciplines have a distinct interest in the overall project. Especially IT security is an effort which has to be considered and may certainly be managed as possible “showstopper” of the entire initiative.

5 SPDM Deployment using Cloud infrastructure

Adding on the last statement, we jointly developed a concept to realize the deployment of our SPDM environment in the (public) Cloud. With this decision, we build on pre-approved infrastructure taking advantage of numerous built-in benefits, such as seamless integration to modern and secure authentication mechanism (SSO incl. MFA) and existing backup solutions. Furthermore, the application proxy functionality provides external service partners with convenient access to the system without the need to distribute company-owned devices. This setup comes with a multi-level security framework to protect against unauthorized access. The ability to flexibly adapt computing performance and storage size as well as to establish proximity to other systems in the cloud is self-explanatory. It should be noted that this concept has a disadvantage in terms of the connection to the HPC infrastructure. In many situations this service still exists traditionally on self-hosted or externally provided hardware, so with us. As we observe the more relevant export of data from the SPDM to the HPC as comparatively small in size, we do not expect any restrictions in functionality and performance.

In conclusion, an SPDM setup in the Cloud can further lower the entry barrier, especially if no company-owned data center infrastructure is available. Ultimately, the effort required to maintain the infrastructure, software and hardware, is significantly reduced.

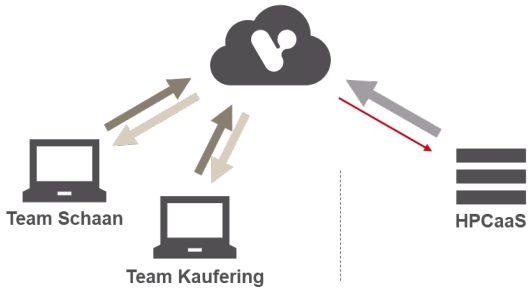

Figure 2: Cloud-deployment concept for SPDM with major data streams involved

6 Learnings to share

The most critical point when starting an SPDM project is to early focus on possible showstoppers, which may not necessarily deal with the actual use and functionality. IT enterprise architecture and security approval is an effort, as several roles and processes are involved. Furthermore, the timely alignment with procurement and legal before starting the proof-of-concept ensures a smooth transition to the targeted deployment project.
It is worth mentioning that in the implementation project phase, the results of the early requirements project do not necessarily represent an implementation-ready specification and further detailing of the individual use case definitions is necessary. Also, the communication between simulation experts and data management specialist must grow to create a mutual understanding of the SPDM system and simulation processes, as well as for the different terminology involved.
At the stage where you are aiming for commitment from the management of your organization, I would personally concentrate on highlighting the *enablers* of an SPDM system rather than investing too much time in ROI scenarios.

7 Acknowledgment

We would like to expressly thank our partners at Hexagon and :engineering methods for their excellent collaboration on the project, adding their experience and passion to considerably contribute to a successful launch of our SPDM system.

SPDM-centric systems connection for seamless end-to-end simulation data management

Irene Makropoulou (BETA CAE Systems)

1 Introduction

In today's rapidly evolving engineering landscape, effective management of simulation processes and associated data is paramount for ensuring product quality, reducing time-to-market and enhancing competitiveness. Therefore, Simulation Process and Data Management (SPDM) systems are at the focal point of the strategy, guiding and shaping how simulation workflows are orchestrated and how simulation data is managed.

With their inbuilt solutions for version control, data lifecycle management, data access control and data search, SPDM systems ensure that internal and external users of these systems get access to the right data promptly and hassle-free, and that data are traceable along the complete digital thread. However, as data are produced and consumed by other systems and software applications, the seamless integration of the SPDM system within the complete CAE environment is a key enabler for the efficient coordination of simulation processes, as the ease of data exchanges across diverse systems, tools and stakeholders determines the extent at which simulation processes can be standardized and automated, the effort required for their deployment and maintenance, and last but not least, the security of data overall.

2 An SPDM-centric CAE environment

In an SPDM-centric CAE environment, the SPDM system has the role of a digital hub that facilitates data handling in context and ensures the use of the right software application for every needed data transformation, taking also care of the good housekeeping of process byproducts.

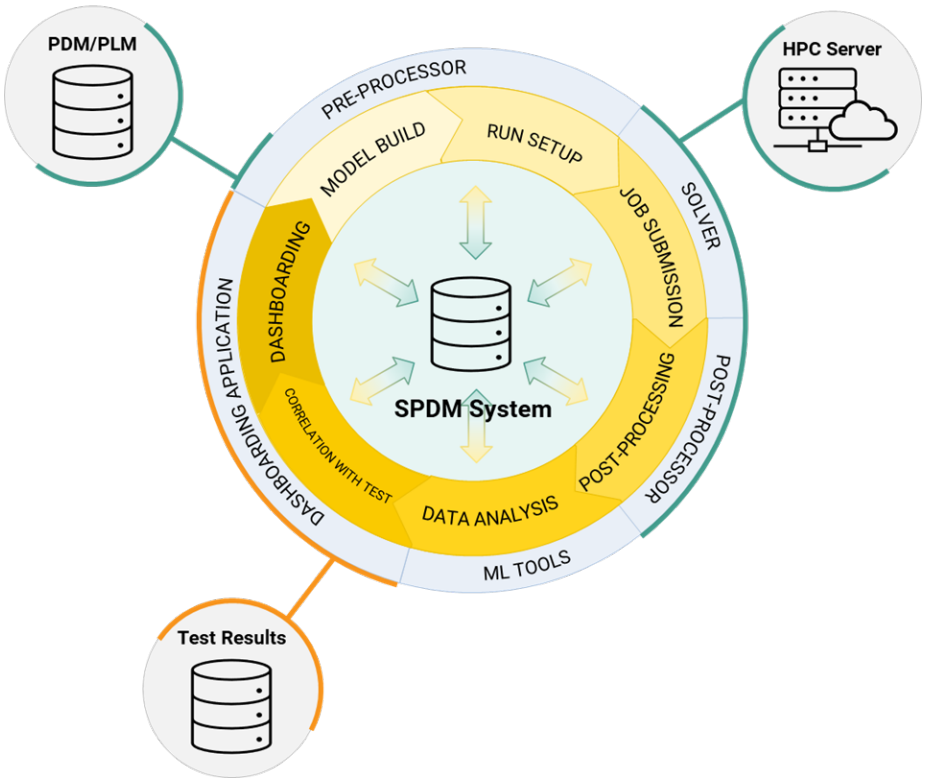

Fig. 1. Schematic representation of an SPDM-centric CAE environment

Fig. 1 above shows a schematic representation of such CAE environment. In the process layer (yellow), CAE activities start with model build and run set-up and advance to submission of the simulation job to the solver and post-processing. Produced data may be used for further data analysis and simulation results may need to be correlated with test. Finally, quick assessment of the system performance is made with the aid of dashboards. The same process steps are relevant for both 3D and 0D/1D simulations.

In the applications layer (blue), model build and run-set-up are managed within the pre-processor, job submission to the solver and post-processing are more often handled in the HPC systems, either located on-premises or cloud-based, data analysis is conducted by Machine Learning tools and correlation with test results as well as overall results presentation is made within the dashboarding applications.

In this environment all primary CAE functions are orchestrated by the SPDM system, data flows seamlessly from the data storage to the applications and vice-versa and the connection to key peripheral systems is implemented with either inbuilt functionality of the SPDM system or via key CAE applications.

3 Systems connection

In the paragraphs below, the key connections of the SPDM system towards peripheral systems and applications are explored through real-world case studies. The core components of the example CAE environment are shown in Fig. 2. In this environment:

- The SPDM system is BETA's SPDRM, with its desktop client, KOMVOS
- The PDM system is Siemens PLM Teamcenter
- The HPC server is managed by Slurm
- The dashboarding application is BETA's web app, ANSERS
- Data analysis is performed with BETA's ML Toolkit add-on
- Test results are stored in an ASAM-ODS server
- ANSA and META are the primary pre- and post-processing tools, used in conjunction with other special pre-processors and custom Python post-processing scripts

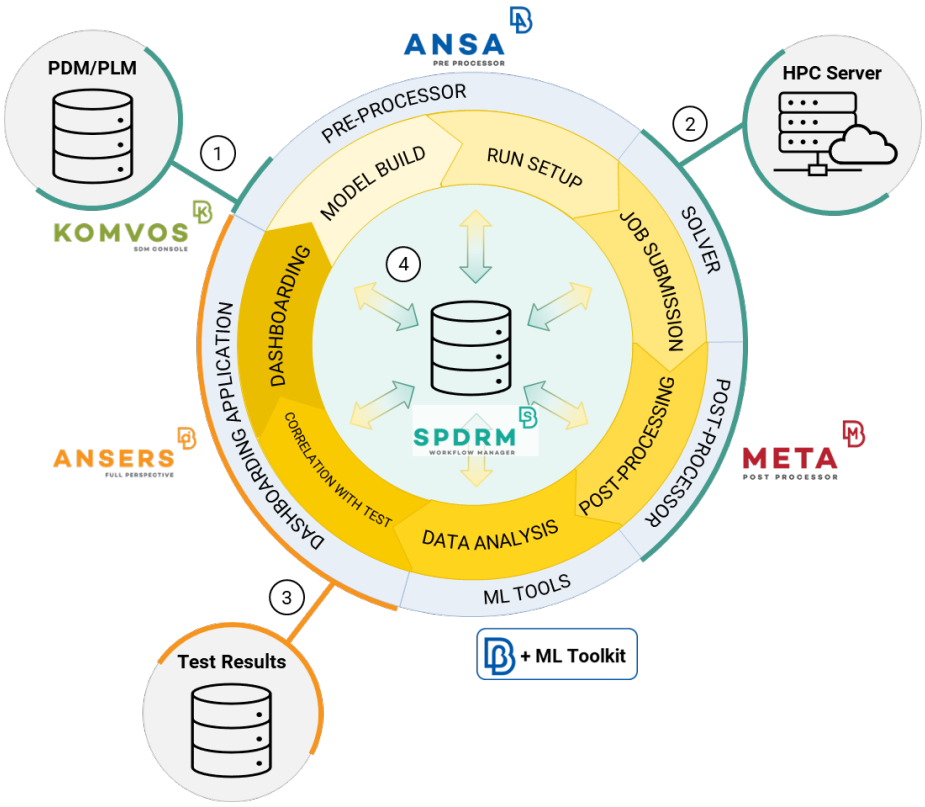

Fig. 2. Example CAE environment

3.1 Case 1: SPDM system to PDM/PLM

The connection of SPDRM to Teamcenter is implemented with the aid of the PLMXML importer available out-of-the-box in the SPDRM desktop client, KOMVOS. Through this interface, users can quickly and efficiently read product structures in the SPDM system and create sub-assemblies that will be used as input to simulation activities down the road. In this process, the metadata defined on parts and groups, of the product structure, as well as positioning and variant conditions information -when available- are also read and kept in the SPDM system, allowing the detection of library and carry-over parts and commonalities between structures. KOMVOS is able to visualize (Fig.3) the model in the embedded JT viewer, and also orchestrate the CAD files translation process by utilizing ANSA workers in the background, ensuring that multi-positioned parts are handled only once and library and carry-over parts are reused.

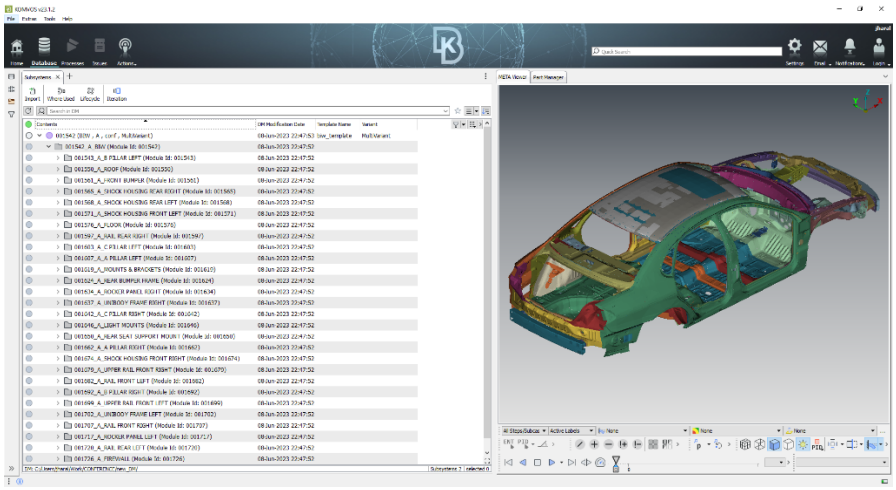

Fig. 3. PLMXML tree and JT files preview in KOMVOS

A challenge encountered often in the PDM/PLM-SPDM interface is that the initial structure of the model in the PDM system (CAD structure) may not facilitate the CAE function-driven organization of the simulation model (CAE structure). KOMVOS meets this challenge with its support of Simulation Model and Subsystem Templates, which are advanced filters captured in xml files that are used to populate CAE Subsystems by cherry picking branches of the complete CAD structure. In this way, the CAE structure of the complete Simulation Model can be managed right at the moment the CAD data enter the SPDM system, in a consistent manner (Fig. 4)

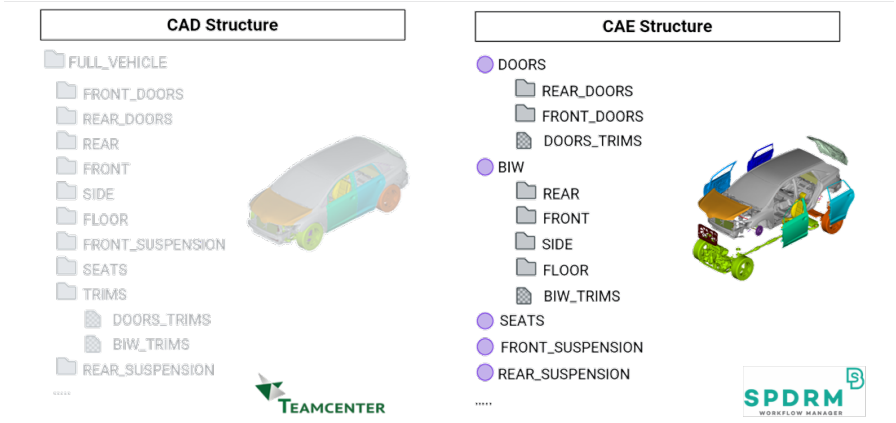

Fig. 4. CAD-to-CAE structure mapping in KOMVOS

3.2 Case 2: SPDM system to the HPC server

The connection of the SPDM system to the HPC server enables the direct submission of jobs to the solver through the SPDM environment and the monitoring of their status. In SPDRM, this connection is

implemented through the HPC Submission process template (Fig.5), that manages the submission of each simulation, from the data export to the storage of the processed results back to the SPDM system.

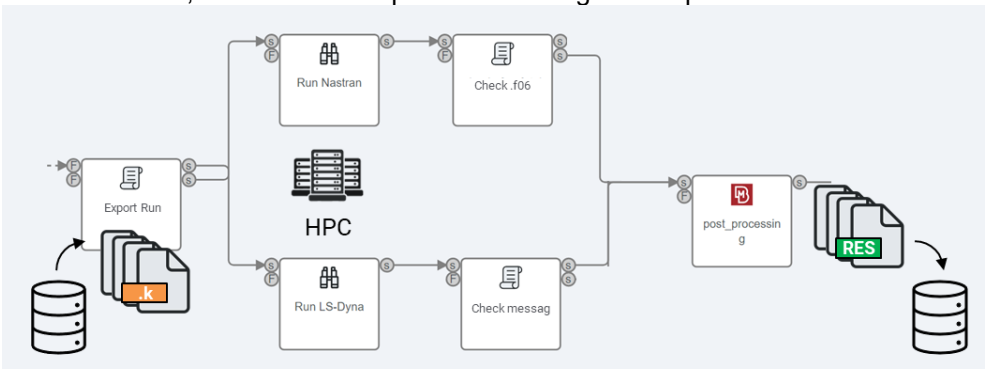

Fig. 5. HPC Submission Process Template

This process template is a visual representation of the automatic process executed by the system every time a Simulation Run is submitted to the HPC. The job submission command is issued through the Observer Nodes labeled „Run Nastran“ and “Run LS-Dyna“ (for submission to Nastran and LS-Dyna solvers respectively), that execute a Python script. Right after the execution of the command, the system gets in „waiting“ mode, for some signal of job completion from the HPC system. The mapping of Slurm job statuses to job completion signals is available out-of-the-box and enables the SPDM system to know if the job is still in queue, if it is running, if it is finished normally or if some error has occurred. Each user can review the status of submitted jobs in the „Submitted Jobs“ list but also in association with the submitted data.

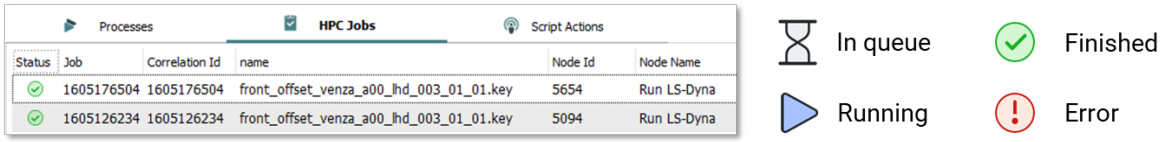

Fig. 6. Submitted Jobs list and legend of possible job status categories

3.3 Case 3: SPDM system to the Test Results database

The connection of the SPDM system to the Test Results database is needed in all instances when simulation data needs to be compared with test data. In cases where the SPDM system embeds a results viewer, the possibility of the client application to connect to both the data sources of simulation results and test data is a key enabler for correlation studies.

In this case study, the SPDRM desktop client, KOMVOS, comes with a built-in interface for connection to ASAM-ODS servers, that enables browsing and visualization of test data. Similar and even more enhanced possibilities are given through the dashboarding web application ANSERS, where 2d plots and other types of *dashlets* are pre-configured to display both simulation and test data, with any required transformation on test data automatically applied.

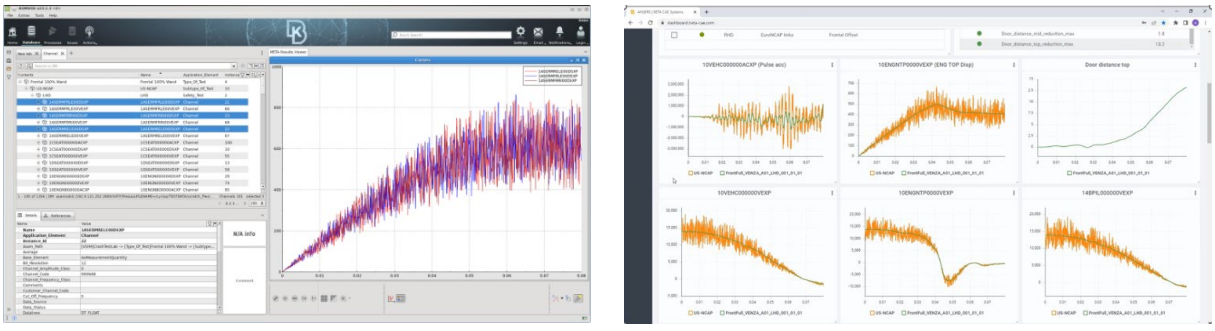

Fig. 7. 2d plots combining simulation results and test data in KOMVOS (left) and ANSERS (right)

3.4 Case 4: SPDM system to the CAE applications

CAE applications need a connection to the SPDM system in order to read data stored in the data vault or write data in the data vault in an easy way. Usually, data needs to be exported from the SPDM system to the file system, from where they are manually ported to the different applications. Following a similar course, to upload data back to the data vault, some „data import“ process is triggered in the SPDM system, where the user is prompted to add the required metadata for the proper classification of the incoming package. This approach is not ideal, as data circulates through the organization out-of-context, and information security may be compromised. Additionally, this handling may not even be possible for complex data sets that represent a collection of data objects, interrelated to one another.

SPDRM supports two alternatives for its connection to CAE applications:

- Direct connection, for applications that include a direct interface to SPDRM
- Indirect connection via the SPDRM client, KOMVOS, for applications that do not include a direct interface to SPDRM

3.4.1 Direct connection to CAE applications

CAE applications that include a direct interface to SPDRM can search for data in the SPDRM vault directly through their graphical user interface or script API. Data can be downloaded in the applications so that it is edited, and then be saved back to SPDRM as an updated version. This direct interface is built using SPDRM’s REST API.

All BETA Suite Applications (ANSA, META, KOMVOS) have a direct connection to SPDRM, out-of-the-box. Additionally, BETA’s dashboarding web application, ANSERS, has a direct connection built-in.

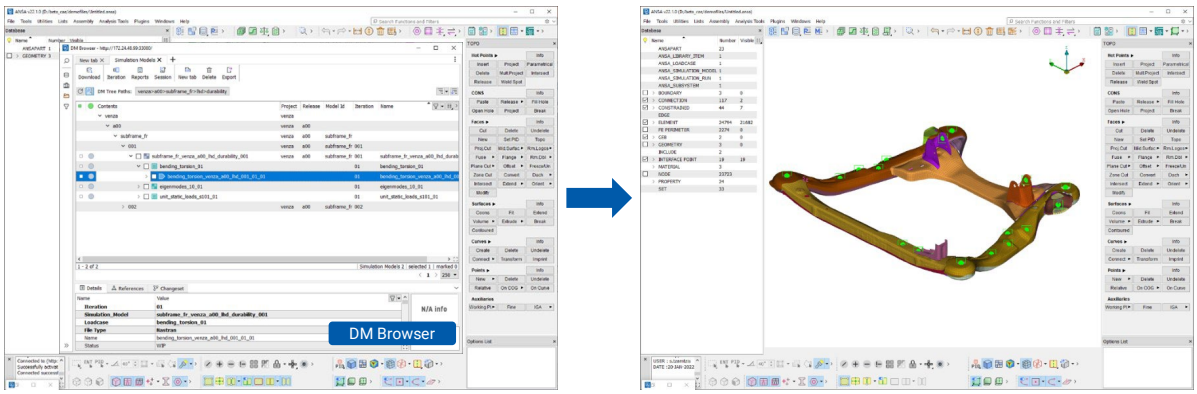

Fig. 7. Search and Download SPDRM data in the ANSA session

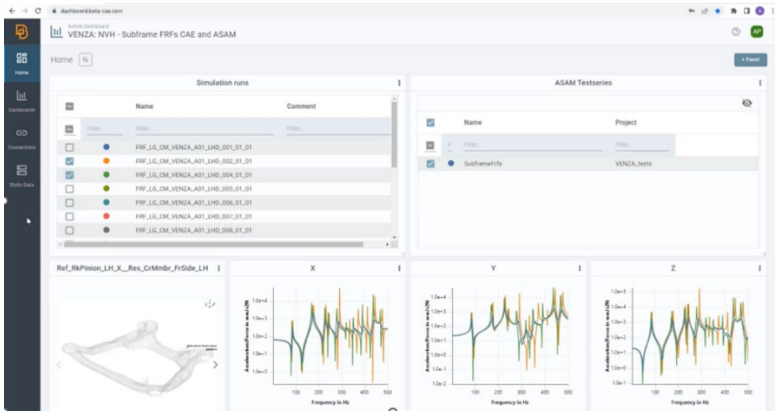

Fig. 8. ANSERS dashboard displaying results stored in SPDRM

3.4.2 Indirect connection to CAE applications

CAE applications that do not include a direct interface to SPDRM are registered as file editors and are proposed when editing data through KOMVOS, based on the file extension (Fig. 9).

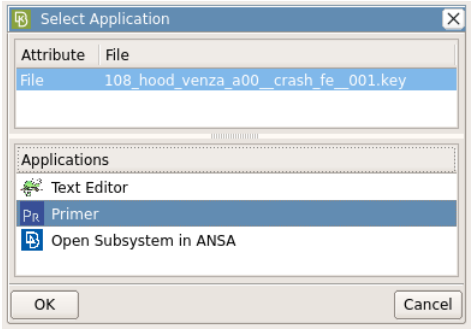

Fig. 9. Applications registered as editors of .key files

When an application is selected, it is directly opened and the selected data is loaded. Making any modification, saving the file and closing the application will lead to the file being re-imported in SPDRM, as a new version of the source data.

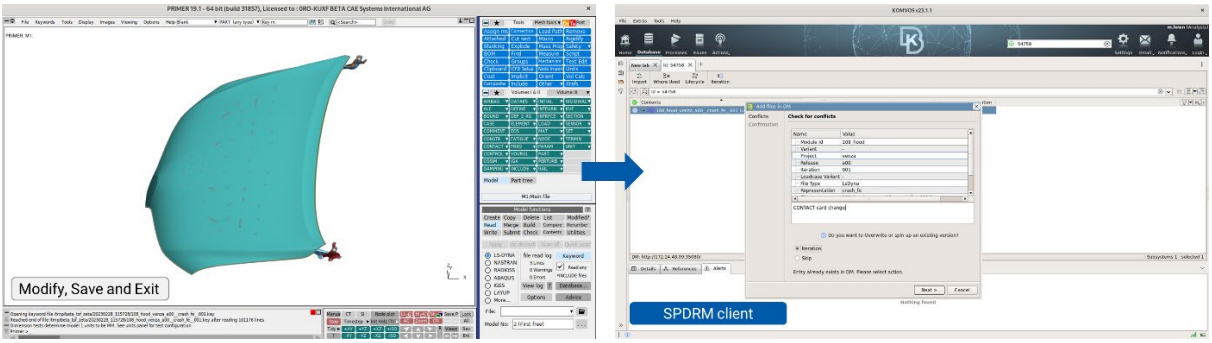

Fig. 10. Editing data in CAE applications with no direct interface to the SPDM system

4 Conclusions

With the seamless integration of the SPDM system within the complete CAE environment being a key enabler for the efficient coordination of simulation processes, this work highlights the benefits of adopting an SPDM-centric approach for the connection of different systems using four case-studies from real world applications.

These examples attempted to demonstrate that only powered by the SPDM system, it is possible to establish effective and efficient connections with the most critical systems and applications related to CAE and simulation engineering.

This approach contributes to shaping a strategic mindset where SPDM systems are not just peripheral tools but fundamental components driving effective simulation data management practices, ultimately leading to improved productivity, quality, and innovation in engineering design and development processes.

Datenintegration als Erfolgsfaktor für die Automobilindustrie: Vier Praxis-Beispiele für eine einheitliche Daten- und Prozessintegration sowie optimierte Arbeitsprozesse

Andreas Nicklaß (GNS Systems GmbH)

Die zunehmend datenbasierte Produktentwicklung, die Einführung von XiL-Simulation und ein stärkerer Fokus auf Systems Engineering macht die Automobilindustrie deutlich digitaler, datengetriebener und auch komplexer. Daten avancieren hierbei zum Treiber großer technologischer Innovationen, denn unter dem Druck des Marktes und immer kürzerer und schnellerer Entwicklungszyklen reagieren Automobilunternehmen mit stark vernetzten Entwicklungs- und Produktionsprozessen. Deren Effizienz hängt wesentlich von der Möglichkeit einer globalen Datennutzung ab.

Eine einheitliche Plattform für das Datenmanagement geht die derzeitigen Herausforderungen im Umgang mit (Engineering-)Daten - unter anderem Datenspeicherung und -management, optimaler Datenzugriff, Rückverfolgbarkeit - zukunftsorientiert an. Das dahinterstehende Datenmanagement erfüllt alle Anforderungen, indem die Plattform als cleverer "Information Hub" verteilte Datensilos aufbricht und die interdisziplinäre Datendurchgängigkeit unterstützt. Die Integration KI-basierter Analysen der Datensätze steigern zudem die Effizienz. Als Cloud-basierte Lösung adressiert die Plattform zudem alle Aspekte der Kostenreduktion, Zuverlässigkeit und Flexibilität: Maximale Automatisierung und der Einsatz einer CI/CD-Pipeline beschleunigen die Entwicklungsprozesse und fördern eine schnellere Time-to-Market von Innovationen.

Ausgehend von diesem Konzept einer ganzheitlichen Datenplattform hat GNS Systems optimal an konkrete Kundenbedürfnisse angepasste Lösungen für die Daten- und Prozessintegration entworfen und implementiert. Anhand vier konkreter Anwendungsfälle aus der Automobilindustrie skizziert der Vortrag eine Lösung, die neben dem Datenmanagement auch alle Methoden, Prozesse und Werkzeuge umfasst, die für die Simulation und Berechnung neuer innovativer Produkte wichtig sind, nämlich Daten aus unterschiedlichsten Quellen und Prozessen zusammenzuführen und effizient zu verarbeiten.

Das erste Praxisbeispiel zeigt, wie es ein einheitliches Datenmanagement entlang des gesamten Produktentwicklungsprozesses erlaubt, auch große, heterogene Datenmengen schnell zu verarbeiten, zu speichern und für die Entwicklung neuer Fahrzeugmodelle zu analysieren. Beim zweiten Praxisbeispiel liegt der Fokus auf dem Cloud-Konzept für die Entwicklungsumgebung. Der barrierefreie Zugriff auf Tools und integrierte Entwicklungs- sowie Softwareumgebungen über eine angepasste Lösung für die Daten- und Prozessintegration unterstützt das Unternehmen dabei, die simulationsgetriebene, virtuelle Produktentwicklung signifikant zu beschleunigen. Praxisbeispiel drei stellt die Interoperabilität, also die Verwaltung und Orchestrierung von Daten weltweit verteilter Teams in den Mittelpunkt - konkret sind das beispielsweise Daten aus einer Strukturanalyse aus Europa, aus einer Crash-Analyse in Asien sowie einer Fußgängeraufprall-Analyse in Nordamerika. Der nahtlose Zugriff und die gemeinsame Nutzung der Daten über global verteilte Standorte hinweg trug maßgeblich zu einer Effizienzsteigerung im Produktentwicklungsprozess bei. Das letzte Praxisbeispiel steht im Kontext des autonomen Fahrens. Das Entwickeln neuer Fahrfunktionen ohne einen umfangreichen Datensatz ist schlicht nicht möglich. Der Vortrag zeigt eine angewandte Lösung für die Daten- und Prozessintegration, die effiziente Orchestrierung von Informationen für die Entwicklung autonomer Fahrsysteme über einen falloptimierten Zugriff auf global verteilte Daten realisiert.

Unser Ansatz eines einzigen Datenraums verbindet Lösungen für die Daten- und Prozessintegration mit verschiedenen Tools und Solvern für die Produktentwicklung. Unternehmen profitieren von einem einheitlichen Ökosystem, das die Komplexität hochgradig verteilter Datenlandschaften meistert, indem große Datenmengen aus verschiedenen Quellen auf nachhaltige Weise gestreamt, verarbeitet, gespeichert sowie analysiert werden. Die benötigte Zeit zwischen Entwicklung, Test und Implementierung verkürzt sich so erheblich. Die Fähigkeit, hochkomplexe Szenarien in kürzester Zeit zu simulieren und zu validieren, fördert entsprechend datengestützte Entscheidungen und treibt Produktinnovationen voran. [1] Saw F., Fritsch T.: "Title", John Wiley & Sons, 1995

Einführung und Nutzen eines zentralen Simulationsdatenmanagementsystems bei Dieffenbacher

Dr. Dino Magagnato (Dieffenbacher), Christian Stelzer (CADFEM)

1 Abstract

Die Simulationsdaten werden heute in den typischerweise von jedem Berechnungsingenieur eigenständig verwaltet. Eine zweite Ablage erfolgt häufig durch Konstrukteure, Entwicklungsingenieure und teilweise auch Gruppen- oder Abteilungsleiter. Dies führt dazu, dass Daten doppelt gehalten werden. Sollten diese in jeglicher Form verändert werden, ist sicherzustellen, dass sie konsistent und einheitlich bei allen Ablegern bleiben.

Eine solche Verwaltungsstruktur ist zwar in der Realität umsetzbar, jedoch mühselig und aufwendig zur Konsistenzerhaltung. Besonders, wenn im Laufe eines Projekts viele Varianten entstanden sind. Da die Kommunikation untereinander und der Freigabeprozess der Berechnung oftmals über E-Mails erfolgen, ist eine sehr aufmerksame Ablage der Daten notwendig.

Wird eine solche Verwaltungsmethode verwendet, muss viel wertvolle Ingenieurszeit investiert werden. Die angewandte Methodik dahinter ist in vielen Fällen schwer nachzuvollziehen, was wiederum den internen Wissensaufbau und -Erhalt im Simulationsteam erschwert.

Rechtssicherheit ist bei derartigen Projekten ebenfalls von großer Bedeutung, da die Berechnungen und Auslegungen über längeren Zeitraum nachzuweisen sind. Der Berechnungsingenieur trägt auch die Verantwortung, die Risiken im Blick zu haben und abzuschätzen. Man muss also jederzeit in der Lage sein den Gedankenpfad zu Entscheidungen von Varianten und Berechnungen sowie bestimmte Designentscheidungen nachvollziehen zu können.

Dieser Beitrag ist ein Bericht über unsere Praxiserfahrungen bei Dieffenbacher GmbH seit der Einführung eines Simulationsprozess- und datenmanagementsystems (SPDM). Hierbei zeigen wir eine Reise, die wir seit dem Proof of Concept bis zu unserer aktuelleren Konfiguration gemacht haben. Anhand eines Anwendungsbeispiels wird der Workflow bei Dieffenbacher dargestellt.

Als Lösung zu den zuvor erwähnten Schwierigkeiten wurde bei Dieffenbacher das SPDM Ansys Minerva eingeführt, das von Konstrukteuren, Berechnungsingenieuren und Führungskräften genutzt wird. Hierbei bleiben die Daten konsistent, auch bei jeder Änderung auf Seiten der Geometrie und Anforderungen. Der Weg von der ersten Anfrage über die Varianten, Zwischenergebnisse und dem finalen Bericht wird aufgezeichnet und ist jederzeit auffindbar und nachvollziehbar.

Die Argumentation bei den Budgetgebern für so eine Lösung kann letztlich nur über die Darstellung des Nutzens für die Firma und dem dafür notwendigen Aufwand erfolgen. Risiko und Rechtssicherheit sind für Projekte sicherlich wichtig, diese sind jedoch schwer zu quantifizieren (z.B. in Euro/Jahr). Die Zeitersparnis ist im Gegensatz dazu viel einfacher abzuschätzen. Bei einer informellen Umfrage von Dieffenbacher GmbH wurden Zeiten für verschiedene Verwaltungstätigkeiten bei den Simulationsprojekten abgefragt und daraus ermittelt, welches Einsparpotential denkbar ist. Das Resultat zeigt, dass sich die Investition für die Beschaffung und Einführung bereits innerhalb kurzer Zeit amortisiert.

Bei Dieffenbacher GmbH fand eine Erweiterung der Beschreibung des Simulationsprozesses, um eine wichtige Komponente für wiederkehrende Aufgaben statt, nämlich die Dieffenbacher Toolbox. Da die Beauftragung der Simulationsprojekte direkt in Minerva erfolgt, stehen eine ganze Reihe von Eingangsgrößen vom Beauftragenden gleich als Parameter zur Verfügung. Somit kann nun nicht nur der Berechnungsauftrag gestartet, sondern viele dieser Daten können gleich automatisiert in das Berechnungsmodell eingebaut werden.

Die Pilotphase dauerte von Februar 2023 bis April 2023. Inzwischen ist Ansys Minerva über ein Jahr produktiv im Einsatz.

Die wichtigsten Erkenntnisse aus der bisherigen Einführung sind:

Die größte Herausforderung ist es die bestehenden Prozesse aufzunehmen, in der neuen Struktur schlank und effektiv zu gliedern und alle Beteiligten unter einen Hut zu bringen.
Durch die Einführung von Minerva fällt auf, dass der E-Mail-Verkehr zu den Projekten abgenommen hat. Die Kollegen, die auf die automatisierten Workflows der Dieffenbacher Toolbox aufsetzen, haben große Zeitgewinne. Durch den Freigabeprozess haben die Ingenieure das sichere Gefühl, die wesentlichen Aspekte bedacht zu haben. Dem Thema der Rechtssicherheit wird durch die Nachvollziehbarkeit begegnet.

Einführung und Nutzen eines Simulationsdatenmanagements bei Dieffenbacher

Dr. Dino Magagnato, Dieffenbacher
Christian Stelzer, CADFEM

NAFEMS DACH Konferenz 2024: Konferenz für Berechnung & Simulation im Engineering, 10. – 12. Juni 2024, Bamberg, D

AGENDA

1. Über Dieffenbacher

2. Unsere Produktentwicklung

3. Einführung eines SPDM Systems

4. Nutzen für Dieffenbacher

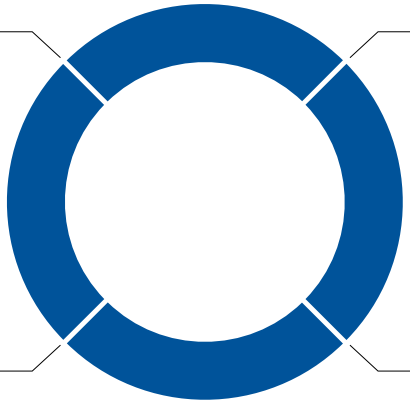

UNSERE GESCHÄFTSBEREICHE

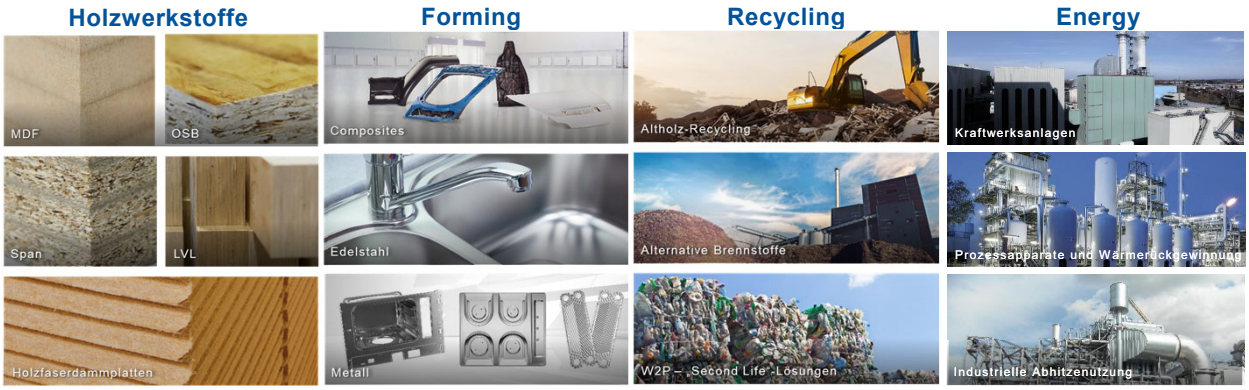

UNSERE LÖSUNGEN

Pressensysteme und komplette Produktionsanlagen für die Holz-, Umform- und Recyclingindustrie.

Kraftwerksanlagen, Abhitze-Systeme und Prozessapparate mit Wärmerückgewinnung für die chemische und petrochemische Industrie.

HOLZWERKSTOFFE

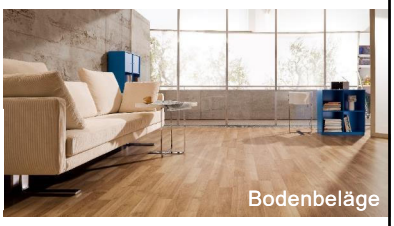

PRODUKTE – HIGHLIGHTS

AGENDA

1. Über Dieffenbacher

2. Unsere Produktentwicklung

3. Einführung eines SPDM Systems

4. Nutzen für Dieffenbacher

ENTWICKLUNGSPROZESS

Status Quo 2021

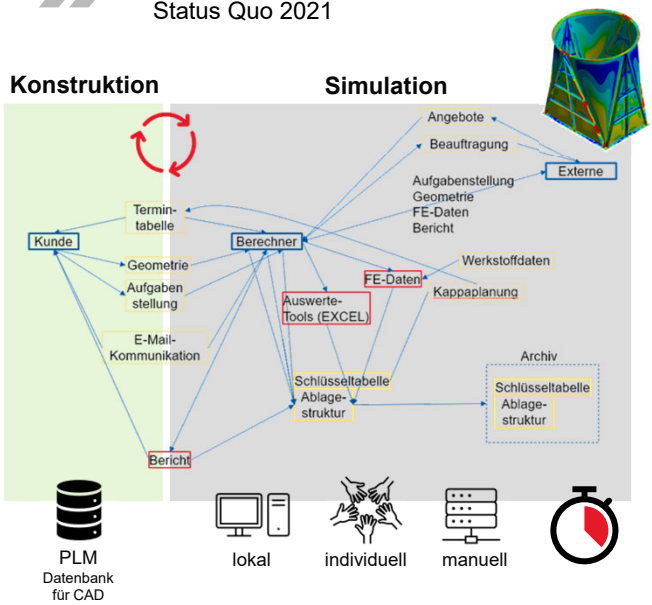

- Daten sind in Ordnerstruktur abgelegt und werden mit Excel-Listen verwaltet und geplant
- Für Berechnung relevante Daten sind über eine Vielzahl von Dokumenten verteilt
- Daten liegen in den Dokumenten teils doppelt vor
- Strukturen werden in Leverkusen und Eppingen teils doppelt vorgehalten
- Abstimmung erfolgt per E-Mail
- Optimierungspotenzial bei Freigabe- und Revisionierung-Prozess

TREIBER FÜR DAS PROJEKT

- Doppelte Datenhaushaltung bedeutet **Aufwand**
  - **Konsistenz** muss manuell sichergestellt werden
  - Bei Änderungen aufwändig und **unsicher**
- Fehlende digitale **Nachvollziehbarkeit**
  - Nachweis der **korrekten Auslegung** nach längerer Zeit sehr aufwändig

Initiale Abschätzung Aufwand/Nutzen

- Thema Risiko schwer bewertbar
- Thema Aufwand für Datenhandling gut bewertbar
  - ➢ Einfache Abfrage von Aufwänden für Datenverwaltung per E-Mail
  - ➢ Ergebnis: Investition und Aufwand für die Implementierung rechnet sich für uns bereits innerhalb des ersten Jahres

ANFORDERUNGEN

SOLL Zustand

AGENDA

1. Über Dieffenbacher

2. Unsere Produktentwicklung

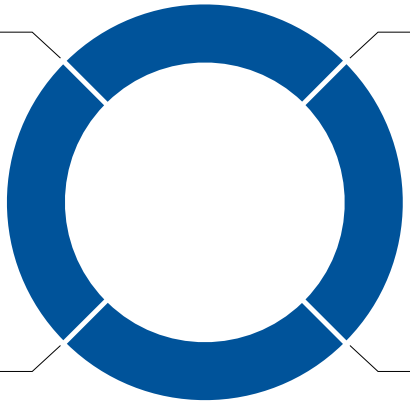

3. Einführung eines SPDM Systems

4. Nutzen für Dieffenbacher

CS0

START UNSERER REISE

- Ausgangssituation
  - Simulationsteam nutzt Ansys Mechanical
  - Automatisierung manueller Schritte in Mechanical
    → Dieffenbacher Toolbox
  - **Manuelle Verwaltung** der Simulationsaktivitäten und Simulationsdaten **durch jeden Berechner**
  - Vertrauensvolle Zusammenarbeit mit CADFEM seit vielen Jahren
- Diskussion ähnlicher Problemstellungen auf CADFEM ANSYS Conference 2021
- **Evaluierung von Ansys Minerva in Zusammenarbeit mit CADFEM**

DIEFFENBACHER CADFEM

ÜBERBLICK ÜBER DIE PROJEKTPHASEN

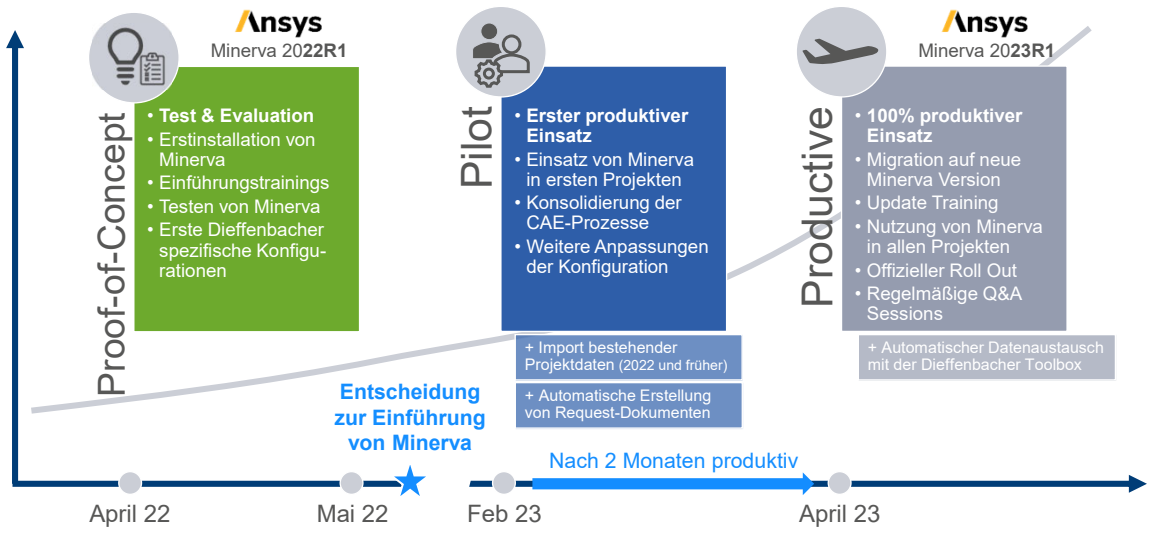

VOM PROOF-OF-CONCEPT ZUM BEST PRACTICE

- **Evaluation von Ansys Minerva**
  - in 4 Wochen
  - auf bestehender Hardware in der Dieffenbacher IT Umgebung

Erwartungshaltung ausgehend von der IST Situation

- **Entwicklungsprozess**
  - Beteiligte Personen und Perspektiven:
    - Designer (Auftraggeber)
    - Simulation Manager
    - CAE-Analyst
    - IT
  - Jeder reflektiert seinen eigenen Arbeitsprozess (**Silo**)
  - Internes Alignment für einen gemeinsamen Arbeitsprozess (**Plattform**)

Vom Silo zur gemeinsamen Plattform

CS0

PROZESS FÜR EINEN SIMULATIONSAUFTRAG

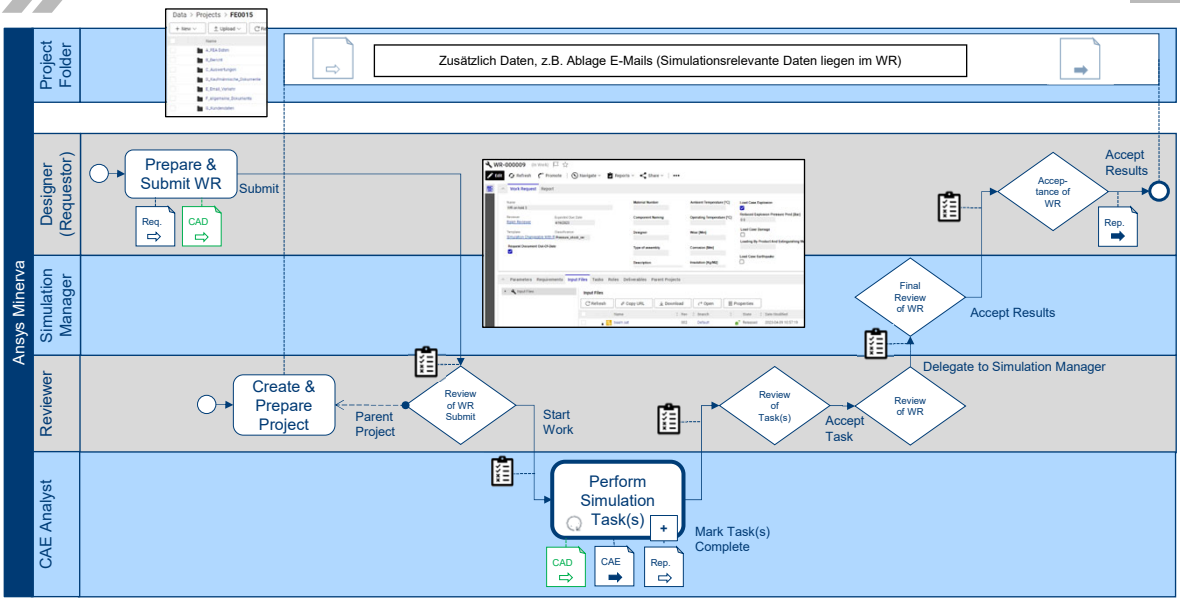

PROZESS FÜR EINEN SIMULATIONSAUFTRAG

Vom Simulationsauftrag bis zur Berichtsprüfung

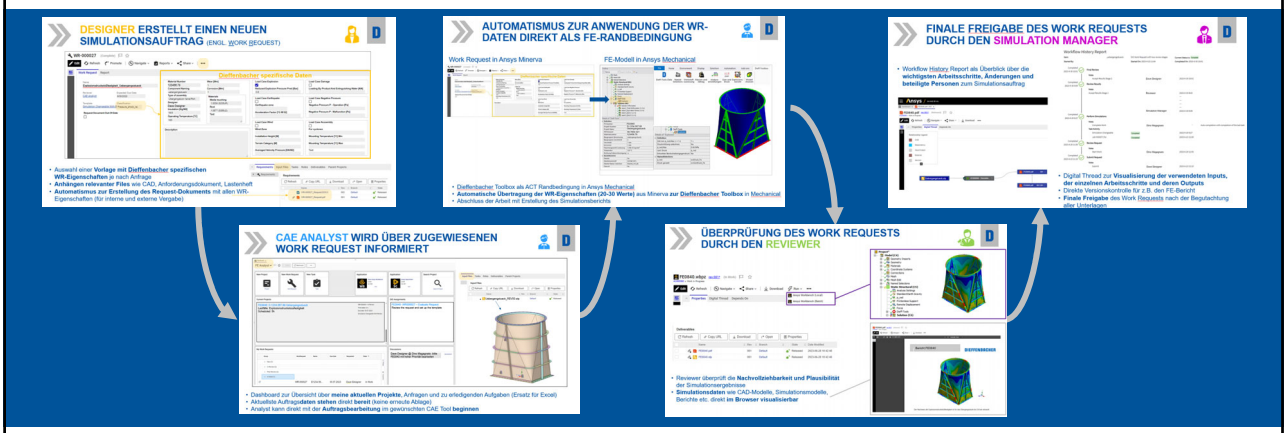

Nutzung von Minerva über den Web-Browser

DESIGNER ERSTELLT EINEN NEUEN SIMULATIONSAUFTRAG (ENGL. WORK REQUEST)

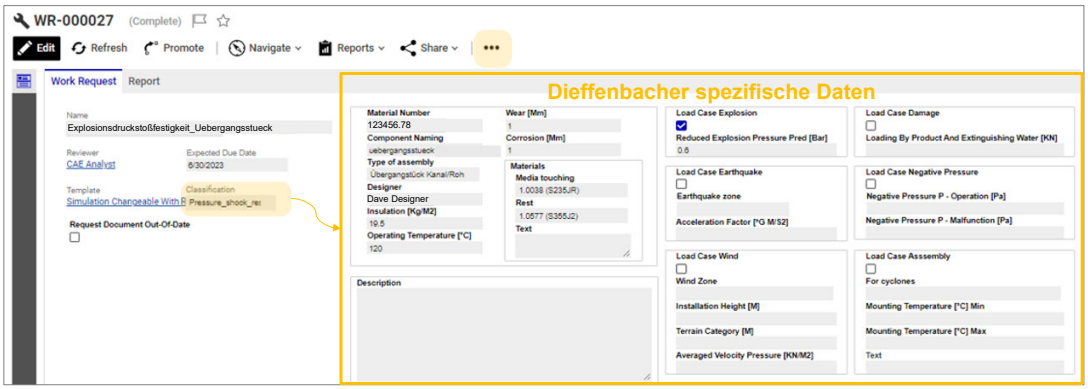

- Auswahl einer **Vorlage mit Dieffenbacher spezifischen WR-Eigenschaften** je nach Anfrage
- **Anhängen relevanter Files** wie CAD, Anforderungsdokument, Lastenheft
- **Automatismus zur Erstellung des Request-Dokuments** mit allen WR-Eigenschaften (für interne und externe Vergabe)

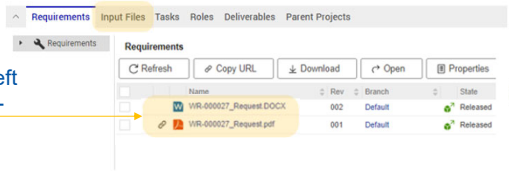

CAE ANALYST WIRD ÜBER ZUGEWIESENEN WORK REQUEST INFORMIERT

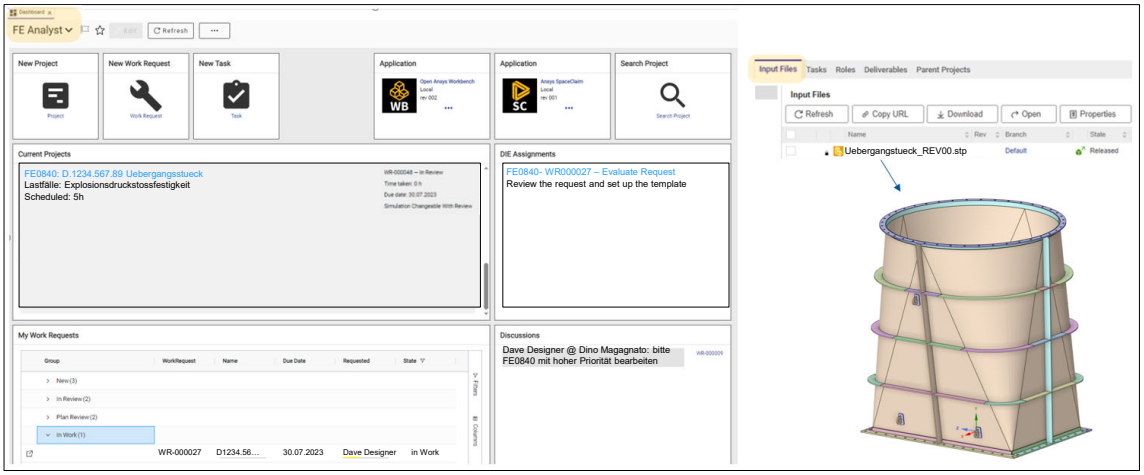

- Dashboard zur Übersicht über **meine aktuellen Projekte**, Anfragen und zu erledigenden Aufgaben (Ersatz für Excel)
- Aktuellste Auftrags**daten stehen** direkt **bereit** (keine erneute Ablage)
- Analyst kann direkt mit der **Auftragsbearbeitung** im gewünschten CAE Tool **beginnen**

AUTOMATISMUS ZUR ANWENDUNG DER WR-DATEN DIREKT ALS FE-RANDBEDINGUNG

Work Request in Ansys Minerva

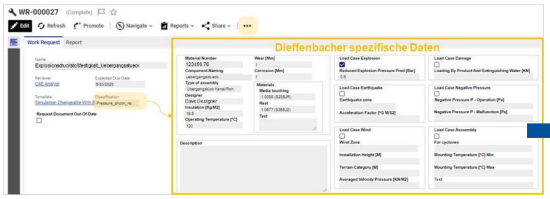

FE-Modell in Ansys Mechanical

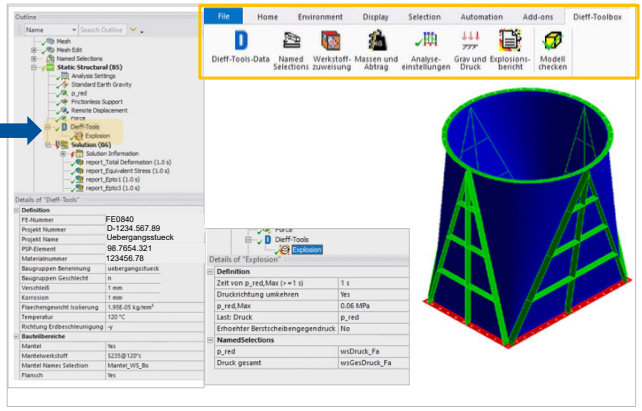

- Dieffenbacher Toolbox als ACT Randbedingung in Ansys Mechanical
- **Automatische Übertragung der WR-Eigenschaften (20-30 Werte)** aus Minerva **zur Dieffenbacher Toolbox** in Mechanical
- Abschluss der Arbeit mit Erstellung des Simulationsberichts

ÜBERPRÜFUNG DES WORK REQUESTS DURCH DEN REVIEWER

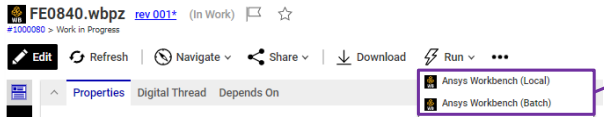

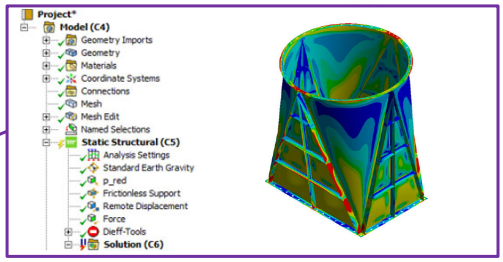

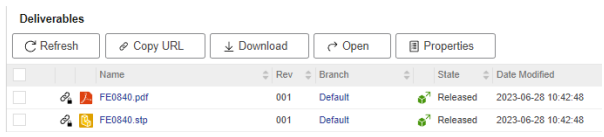

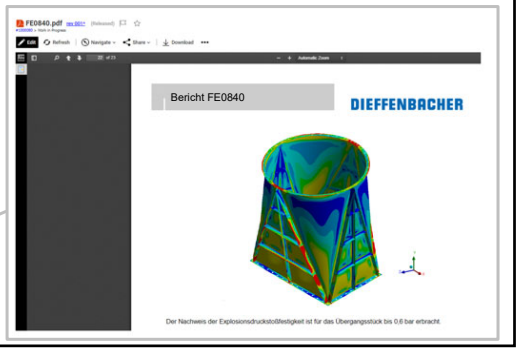

- Reviewer überprüft die **Nachvollziehbarkeit und Plausibilität** der Simulationsergebnisse
- **Simulationsdaten** wie CAD-Modelle, Simulationsmodelle, Berichte etc. direkt **im Browser visualisierbar**

FINALE FREIGABE DES WORK REQUESTS DURCH DEN SIMULATION MANAGER

D

- Workflow History Report als Überblick über die **wichtigsten Arbeitsschritte, Änderungen und beteiligte Personen** zum Simulationsauftrag

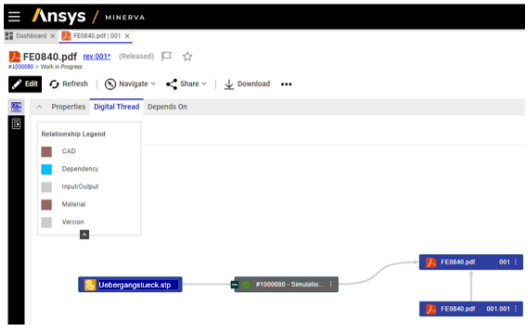

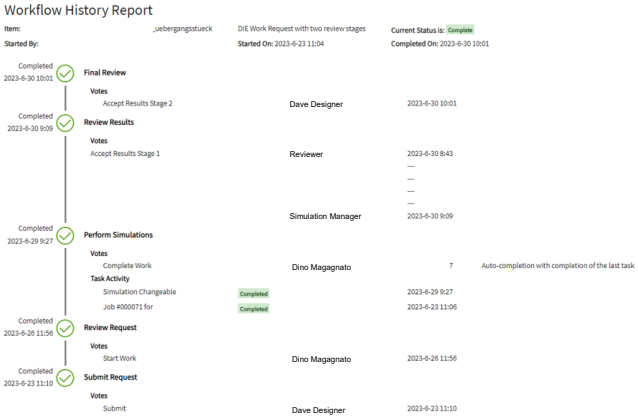

- Digital Thread zur **Visualisierung der verwendeten Inputs, der einzelnen Arbeitsschritte und deren Outputs**
- Direkte Versionskontrolle für z.B. den FE-Bericht
- **Finale Freigabe** des Work Requests nach der Begutachtung aller Unterlagen

VERWALTUNG UND ADMINISTRATION VON ANSYS MINERVA DURCH IT ADMIN

D

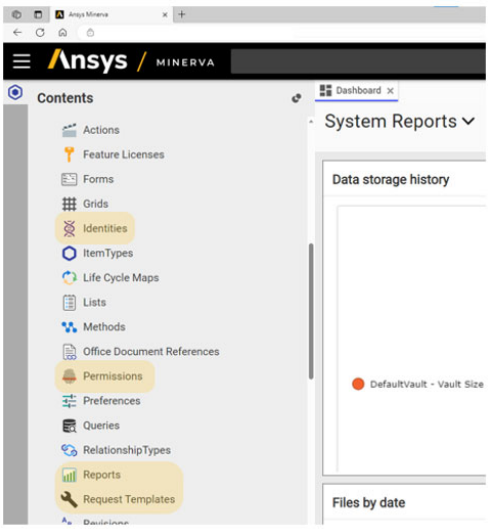

D Thomas Schmetzer
CAD-/PLM-Administrator

FEEDBACK

- Installation von Ansys Minerva **innerhalb 1 Tages**
- **Single Sign-On** sodass Nutzung des Windows Logins zur Anmeldung in Minerva und gleichzeitig Einhaltung der Dieffenbacher Passwort Policy
- Einfache **Verwaltung der User**, Gruppen und **Berechtigungen**
- **Automatisierter Import** der Bestandsdaten aus dem Filesystem (2022 und früher)
- Einspielen von **Minerva-Konfigurationen** mit Unterstützung von CADFEM. Sehr gut vorbereitet und dokumentiert
- **Schnelle Lösungsfindung** durch kompetente Ansprechpartner und regelmäßigen Austausch **mit CADFEM**

AGENDA

1. Über Dieffenbacher

2. Unsere Produktentwicklung

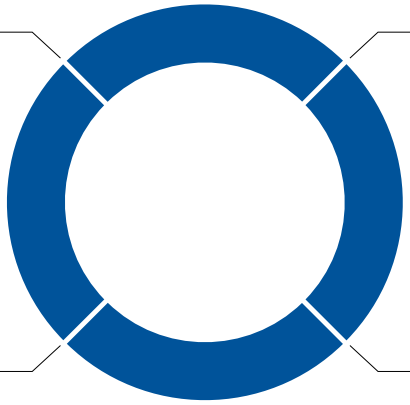

3. Einführung eines SPDM Systems

4. Nutzen für Dieffenbacher

NUTZEN DES SPDM SYSTEMS FÜR DIEFFENBACHER

Dino Magagnato
Projektleiter SPDM

- ✓ Investition und Aufwand rechnet sich für uns bereits im ersten Jahr
- ✓ Große Zeitersparnisse
  - bei Standard-FE-Berechnungen
  - durch Automatisierung → schnelles Return of Investment
- ✓ Datensichere Langzeitarchivierung von FE-Projekten
  - Einfache Suche und Wiederverwendung früherer Projekte
- ✓ Bessere Kommunikation zwischen Berechnern, Konstrukteuren und Führungskräften
- ✓ Einfachere Planung und Überblick über die Simulationsprojekte


NOW LET’S MOVE TOGETHER
FORWARD
DIEFFENBACHER
MOVE FORWARD. TOGETHER.

Ensure IP splash- and jet-water protection with highly automated SPH simulation

Kai Häberle (Alfred Kärcher SE & Co.KG)

Benjamin Legrady (DIVE Solutions GmbH)

1 Introduction

In almost every product of Kärcher water is moved by some electrically driven mechanism. Consequently, it cannot be guaranteed that the product will not come into contact with water during the application. The housing is usually not watertight due to openings for cooling, connectors, or maintenance. Thus, water might enter the device and contact electrical parts. To prevent the user from such harm, countermeasures must be made in the product's design to ensure splash- and jet-water protection. The norm DIN EN 60529 [1] defines against what kind of test scenarios the device must be protected. These so-called IPX tests represent situations in real life and reach from vertical dropping water, to splashing water from a hemisphere to high-pressure jets that are passed over the whole device. Valid IPX splash- and jet-water tests must be conducted with prototypes close to the mature phase or even with series parts. Hence, issues are discovered in a late stage of the development process, which leads to time-consuming and costly revisions of the design.
This paper discusses the novel workflow for the simulation of IPX4 splash water tests. We numerically validate the water tightness in an early CAD design stage. IPX4 tests are highly standardized tasks that repeatedly occur in Kärcher's design cycle. IPX4 testing therefore lends itself to a virtual test strategy. The simulation of splash water tests has become possible through the progress in SPH simulation software. Compared to classic CFD methods, mesh-free modeling enables the simulation of moving open boundaries, free stream flow, and moving solids in a large domain while capturing small-scale capillary force-driven flows in tight gaps [2]. Furthermore, a local refinement method [3] significantly reduces the simulation effort and facilitates focusing on critical parts of the device. However, as an application, IPX4 testing remains largely undiscussed in the SPH literature. The present study uses the commercial SPH code provided by Dive Solutions. It demonstrates how simulation, pre- and post-processing for IPX4 tests are fully automated and integrated into Kärcher's development process using a Python API. The paper therefore highlights an efficient workflow in industrial design. The automated evaluation of the wetting on the critical components, the visualization of the flow paths, and pre-defined views of the solution save further person-hours. Additionally, these results provide more insights compared to the experimental testing and, thus, make a faster decision possible. We close with a discussion of future potential for improvement and an assessment of the automatability of other IPX testing classes within an SPH framework.

2 IPX Water Protection Tests

The norm DIN EN 60529 [1] defines protection classes of housings for electrical devices. These include the protection of persons from touching dangerous parts inside the housing, the protection of the device against solid foreign particles, and the protection of the device against damage by water leaking into the housing. A naming convention is defined where the letters IP, which stands for ingress protection rating, are followed by two numbers. The first number relates to the protection class against solid particles and

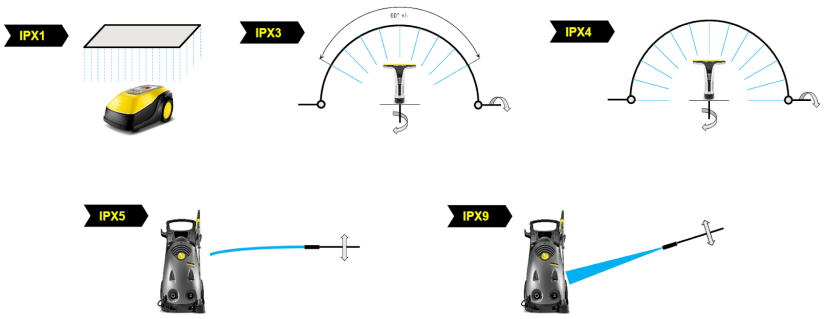

Figure 1 Schematic overview of five selected IPX water protection classes that are important for Kärcher.

the second number defines the water leakage protection class. Since this work is only interested in water leakage, an X will replace the first number.
The water leakage classes reach from droplets, splash water, and jet spray to high-pressure jets and submerge. For Kärcher the classes illustrated in Fig. 1 are of interest. Out of them, the IPX4 splash water test will be discussed in more detail in the following.

2.1 IPX4 Test Case in Detail

The IPX4 class represents the protection against splash water from all directions [1]. The test rig consists of a pipe in the form of a semicircular arch which is equipped with several nozzles, cf. Fig. 2. The latter have an opening diameter of 0.4 mm and are positioned at 50 mm distance on the arch. The arch is swivel-mounted and rotates ±180° concerning the vertical. Different arch diameters from 200 to 1600 mm ensure that the distance between the device and the nozzles is less than 200 mm. The device is positioned on a turntable rotating around the vertical axis. Each nozzle is exposed to 0.07 l/min and the total test duration is 10 min.

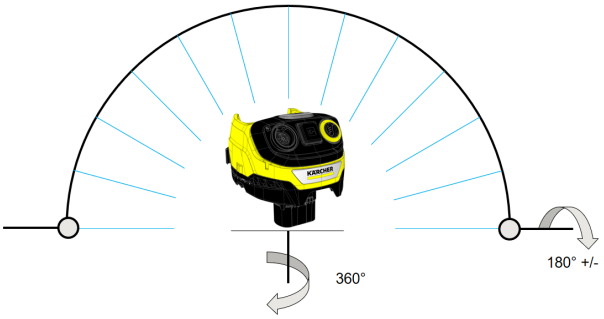

Figure 2 Illustrative depiction of the test rig for the IPX4 case.

3 SPH in Detail

3.1 Governing Equations of Fluid Mechanics in the Weakly Compressible SPH Formalism

Fundamental to the SPH method is the spatially discrete representation of a continuum with so-called particles. These collocation points, which move along their trajectories, inherit the physical properties of the continuum. At these points, a weighted interpolation, i.e. the kernel function w, is used to determine its properties based on its distance from adjacent particles and their physical quantities ϕ. As the interpolation radius may extend beyond the presence of fluid, e.g. at walls, a renormalization factor γ is introduced to account for the missing content and ensure at least zeroth order consistency [4].
The described interpolation reads:

$$\phi(x_p) = \frac{1}{\gamma(x_p)} \int w(x_p - x)\phi(x)\, dV, \tag{1}$$

$$\gamma(x_p) = \int w(x_p - x)\, dV. \tag{2}$$

Here, the Wendland kernel of the fifth order is used as a weighting function. Using the derivative of the kernel, the SPH formalism allows for an approximation of spatial derivatives, which is crucial for solving partial differential equations numerically.
The concept is illustrated in Fig. 3. Specific care has to be taken for the consideration of boundary handling. Consider the lower green particle at position x_p then, with its kernel function w, the kernel interpolation of a derivative for an arbitrary quantity ϕ will have a volume integral contribution ($\int \ldots$ dV) and a boundary integral contribution ($\oint \ldots$ dB). The first comes from within the fluid, i.e. the contribution from the surrounding particles and the latter stems from the kernel overlapping with the wall. Here $\boldsymbol{n}$ is the inward-pointing surface normal. To ease readability, the renormalization term is ignored. Integration by parts yields [6]:

$$\nabla\phi(x_p) = \int \nabla w(x_p - x)\phi(x)\, dV - \oint \nabla w(x_p - x)\phi(x)\boldsymbol{n}(x)\, dB. \tag{3}$$

In the current work, a weakly compressible modeling approach is utilized allowing for small density changes, i.e. less than 1% to model incompressible fluid behavior. An equation of state links the pressure and density of the fluid.

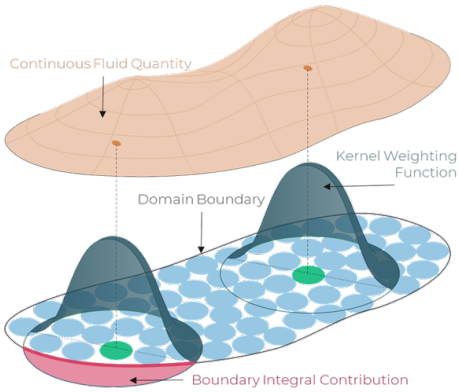

Figure 3 3D visualization of the SPH interpolation within the fluid (right) and with domain boundary contribution (left) [5].

For the governing equations of fluid mechanics, incompressibility is considered for the derivation of the momentum equation. Contrarily, the continuity equation is solved in its compressible form to account for the density changes introduced by the modeling approach. Here, the equation of state proposed by [7] and [8] is used. This yields the governing equations for weakly compressible SPH in the Lagrangian formulation:

Particle Advection: $$\frac{d\boldsymbol{x}}{dt} = \boldsymbol{v}, \quad (4)$$

Continuity Equation: $$\frac{d\rho}{dt} = -\rho\nabla \cdot \boldsymbol{v}, \quad (5)$$

Momentum Equation: $$\frac{d\boldsymbol{v}}{dt} = -\frac{1}{\rho}\nabla p + \frac{1}{\rho}\nabla \cdot (\mu(\nabla \otimes \boldsymbol{v}) + (\nabla \otimes \boldsymbol{v})^T)) + \boldsymbol{g}, \quad (6)$$

Equation of State: $$p = \frac{(\rho_0 c_0^2)}{\gamma}(\frac{\rho}{\rho_0})^\gamma + p_{0,} \quad (7)$$

with the position of the particles $\boldsymbol{x}$, velocity $\boldsymbol{v}$, time t, density ρ, pressure p, dynamic viscosity μ, gravity $\boldsymbol{g}$, background pressure p_0, artificial speed of sound c_0, reference density ρ_0 and exponent γ, which is set to 7.0 for water [8].

The equations are discretized using the SPH formalism. The temporal derivatives are discretized with a Runge-Kutta 4 alike [9] scheme, separating the acoustic and advective time steps for faster computation [10]. To improve numerical stability and the quality of the pressure field, an additional diffusive term is added to the continuity equation [11]. To ensure a regular particle distribution while avoiding unintended particle clumping, a particle shifting technique is applied [12]. This improves the interpolation quality of the scheme [13] while maintaining the overall volume of simulated fluid. The utilized method is inspired by [14] and [15]. In this work, no turbulence model is utilized.

3.2 Modeling Fluid-Wall Interaction with SPH

In Sabrowski et al. [16], different boundary-condition approaches are discussed. This work uses a segment-based mesh representation to treat boundary conditions [17]. This approach was chosen as it allows for a very accurate and native representation of computer-aided design (CAD) geometries in the SPH method and ensures to account for the boundary contribution of the SPH interpolation.

3.3 Modeling of Open Boundaries with SPH

Open Boundaries are considered simulation domain interfaces that allow for both, in- and outflow of fluid. In this work, a so-called semi-analytical boundary framework [18] is applied that uses a segment-based mesh representation of the open boundary interface. Either velocity or pressure boundary conditions are prescribed on the boundaries according to the desired inflow or outflow situations. Particles grow or shrink continuously on these interfaces e.g. specified support points and are released into the fluid domain or removed from the fluid domain when they gain or undercut a certain mass. Their properties are not only defined by the set boundary conditions but take the inner fluid state as well as the states of the open boundary and walls into account.

3.4 Modeling of Surface Tension with SPH

On a molecular level, two molecules of the same phase experience different attracting or repelling force magnitudes dependent on the distance between them. For short-range, the electrons of the molecules cause a strong repellent force, for intermediate-range, intermolecular forces like Van-der-Waals forces cause an intermolecular attraction. For the bulk, repellent and attractive forces equal out showing no resulting force. On the molecular level, the magnitude of each force represents the cohesion of this bond.

However, at the phase interface between two different fluids, the difference in intermolecular forces creates a net force perpendicular to the interface. The macroscopic result is an inward-directed force

that is characterized by the so-called surface tension σ describing a tensile force per length acting tangentially to the contact surface. As a consequence, the surface is curved and the pressure within a droplet is larger than the atmospheric pressure [19], [20].
Of course, this effect is not only present between fluids but also between two fluids and a solid along the contacting line of the three media. For the stationary situation, a so-called static contact angle θ is formed that is representative of the triple between fluids and a solid.
Including these effects in the equations is typically done by adding a force $\boldsymbol{F}_S$ to the momentum equation:
Modified Momentum Equation:

$$\frac{d\boldsymbol{v}}{dt} = -\frac{1}{\rho}\nabla \mathrm{p} + \frac{1}{\rho}\nabla \cdot (\mu(\nabla \otimes \boldsymbol{v}) + (\nabla \otimes \boldsymbol{v})^T)) + \boldsymbol{g} + \frac{1}{\rho}\boldsymbol{F}_S. \quad (8)$$

For reliable predictions of flow behavior that includes capillary-driven flow the continuum surface-force model is chosen. This model exploits the macroscopic values behavior of the surface tension by assuming a direct proportional behavior between surface tension coefficient and surface tension force with surface curvature κ along the local surface normal $\boldsymbol{n}$

$$\boldsymbol{F}_S = \sigma\kappa\boldsymbol{n}. \quad (9)$$

Brackbill [21] formulated this approach for a grid-based multiphase approach. It was consecutively adapted for the SPH single-phase formalism and refined in Vergnaud et al. [2], as well as in Bierwisch [22]. The static contact angle is eventually set as a material value of the surface normal along the triple line between the fluids-solid contact line.

3.5 Modeling of Refined Areas with SPH

Refined areas refer to using different spatial numerical resolutions depending on certain criteria. The perfect particle-based solver adapts the particle size to be fine enough in areas of interest and as coarse as possible in others to get the result at the lowest computational time without introducing numerical errors and without sacrificing physical insights. The naïve approach to letting particles interact with one another does immediately violate the conditions, such as:

- Larger particles have larger kernel sizes than smaller particles, thus, the large particle interacts with the small particle while the small does not interact with the large one. This would violate Newton's third law, i.e. action would not equal reaction.
- Compensating for this caveat by enlarging the smaller kernel radius leads to a larger particle neighbor count, thus, the computational performance gained by having fewer particles is diminished by accounting for more particle interactions.

The model idea that is used in this paper for the SPH code consists of small layers that coexist on top of the coarser domain to avoid overlapping of the kernels [17]. Here, the coarse particles enter the region of interest and, in the so-called buffer layer of the fine particles, are split into finer particles. Fluid properties are interpolated into this layer by SPH formalism from coarse to fine particles ensuring information coupling of fine and coarse regions. Afterward, the flow equations are solved on the fine particles and coarse particles are passively advected. Once the fine particles leave the buffer zone, the flow equations are solved by the re-activated coarse particles, and the fine ones are deleted. This ensures mass conservation for the coarse layer.

3.6 Python API

The cloud-native simulation suite of Dive Solutions comes with an additional possibility to leverage scripting in Python. Their software development kit (SDK) fisherman provides the fundament to use the representational state transfer (REST) application programming interface (API) to exchange information between the user's machine and the platform based on secured data transmissions including e.g. authentication measures. This allows for the efficient creation of openings and motions according to e.g. the conditions defined in the IPX4 class reducing the simulation setup-time to seconds.

Figure 4 Illustration of a Kärcher WD6 wet and dry vacuum cleaner head, with a depiction of the main electrical parts.

4 Simulation of the IPX4 Test Case

The functionality of the simulation process is illustrated based on a wet and dry vacuum cleaner shown in Fig. 4. The head of the vacuum cleaner incorporates all electrical parts and thus, it suffices to apply the IPX4 test just on the head. Critical parts that should be kept dry are the switch, the power socket, the printed circuit board (PCB), and the blower motor.

4.1 Preprocessing

The preprocessing can be kept to a minimum due to the application of a custom-fit Python API script for the model preparation to simulate the IPX4 test case. What remains to be done manually is the conversion of the CAD data into single or multiple STL (Standard Tessellation Language) files. Previously it was explained that a segment-based mesh representation is used to account for the fluid-wall interaction. Therefore, it is important to defeature small curvatures to ensure a minimal number of elements to reduce the simulation costs. A further reduction can be achieved by merging the various parts into as few as possible STL files to avoid the double representation of solid-solid contact areas. Finally, the device has to be positioned such that the origin of the coordinate system is located centrally on the bottom of the device with the gravity vector showing in negative z-direction. Then, the geometry data can be imported into the Python API script to create the model.

4.2 Python API Automation

In the next step, the STL files are loaded by the Python script. According to the size of the device, the script automatically chooses the right size of the spraying arch. Furthermore, the user only has to define the name of the project, the particle diameter for the discretization, the total simulation time, and regions for local particle refinement.

4.3 Simulation Run

The simulation can either be started directly by the Python API or by the browser-based GUI of Dive Solutions. It runs on a cloud-native HPC cluster on, at the time of writing, an AMD EPYC™ 7V73X as the largest computing instance.

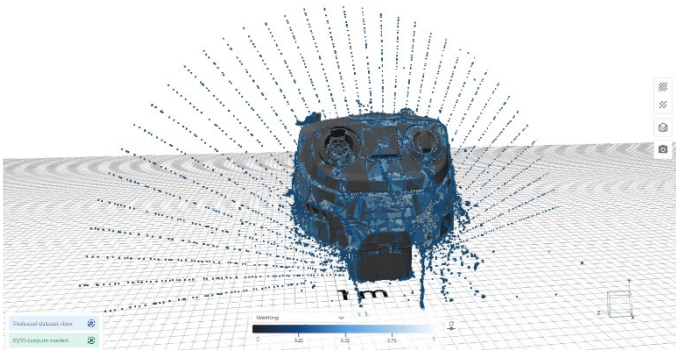

Figure 5 Display of the particle distribution and evaluation of the wetting on the surfaces directly in the web interface of Dive Solutions.

4.4 Post Processing

A first and intermediate check of the simulation results can be done on the web interface of Dive Solutions while the simulation is still running. Among the various possible options, the visualization of the particle distribution and the immediate evaluation of the wetting are the most important choices for IPX4 simulations. Therewith, a quick verification of the settings, e.g. positioning, particle size, and refinement areas, could be achieved. However, Fig. 5 also shows that the wetting is calculated on the coarse STL mesh, which only gives a rough estimate of the water distribution.
Opening the result data in the open-source software ParaView allows for a more detailed evaluation. A predefined procedure calculates the wetting on a refined STL mesh using the so-called Shepard-Summation [23]. These results are then time-averaged over the whole simulation, cf. Fig. 6 (left). Furthermore, it is possible to determine and visualize the flow path throughout the device as depicted in Fig. 6 (right). This helps greatly to understand the movement of the water and to deduce countermeasures.
These steps can also be predefined in the Python API for an automated export if desired. For a quick estimate, if the test has failed, the wetting could be graded into a simple pass and fail category by automatically evaluating the wetting on critical parts and defining a Shepard-Summation value of 0.5 as failed.

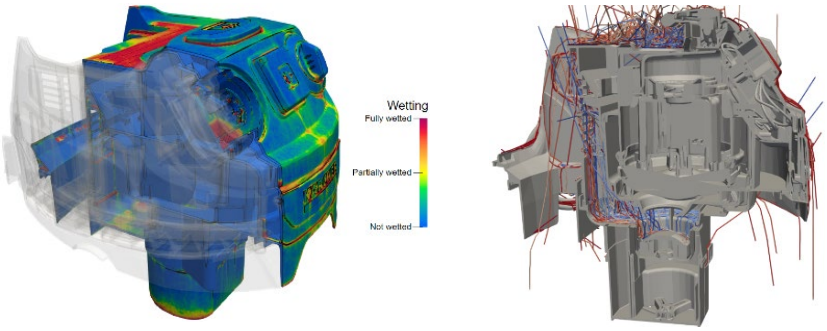

Figure 6 Detailed view of the wetting (left) and the flow paths (right).

4.5 Focus on Capillarity

Capillarity is one major effect that could cause leakage issues. Capillary forces are driven by the surface tension, which has been already discussed before in Section 3.4. It was also explained that for the current use case and a SPH single-phase description, it is best to use a continuum surface force to model the surface tension. In order to correctly calculate these forces a sufficiently fine discretization of the smallest channels has to be ensured. Dive recommends ten particles across the width of the channel for a high-accuracy evaluation. Of course, it is impossible to simulate the whole device and spraying setup with such a discretization, even when applying local refinement techniques. Therefore, the idea is to identify water accumulations close to critical regions, e.g. the switch, which could be a gateway for the water to reach the electronics. A subsequent simulation focuses on the critical region and uses a finer resolution depending on the channel width that exists in this region. The water can be either applied by defining a water volume that represents the identified accumulation or by having a constant water spray onto the region.

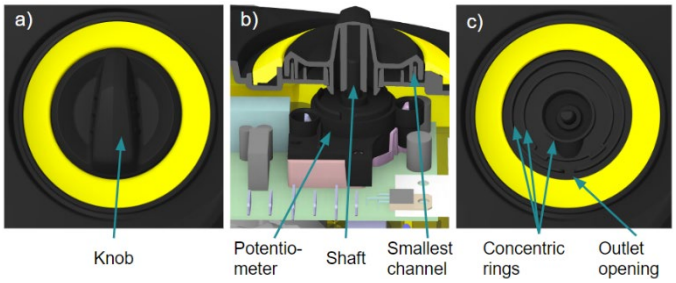

Figure 7 Detailed illustration of the switch of the Kärcher WD6. The knob in a) is directly connected via a shaft with the potentiometer, where the latter is mounted on the PCB, see b). To prevent water intrusions a kind of labyrinth is defined by concentric retention walls on the knob and housing, compare b) and c).

In the current case the switch of the vacuum cleaner, cf. Fig. 7, was of special interest and here the second boundary condition with a constant water spray was chosen. The question was if water reaches the shaft which connects the knob with the potentiometer on the PCB (printed circuit board). This should be prevented by concentrical retention walls both on the knob and the housing around the shaft.
After running both the test and the simulation the black knob of the switch was removed to compare the water wetting beneath it. In Fig. 8 the direct comparison clearly shows similar water distributions in the outer most grove and also in the second grove close to the outlet openings (see close-up pictures in Fig. 8). In both cases, the areas closer to the shaft remained dry.

4.6 Comparison of SPH Simulation and Testing

Especially the evaluation of the simulation results reveals the additional value gained by the simulation compared to the testing. The foremost reason is of course, that the testing can only be done reasonably with prototypes close to the series-production status, whereas the simulation only depends on the CAD data. Then there is the testing procedure. The IPX4 test run itself is also highly automated and is finished after 10 min.
The problematic and error-prone part is the evaluation afterward. As shown in the top row of Fig. 9, the device has to be dried after the test run on the outer surfaces. This is done to prevent water that remains on the outside from getting into the device when disassembling it. During the latter, part by part is carefully removed without shaking the device to not falsify the results. Then water entrapments are searched, especially on critical parts and it is tried to determine the flow paths of the water.

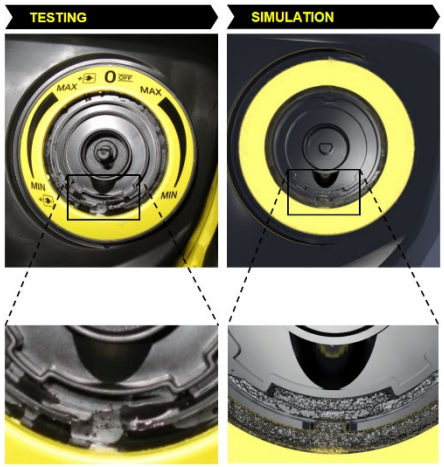

Figure 8 Testing and simulation results of the IPX4 test at the switch. The lower close-up pictures show the comparison of water accumulations between the retention walls.

With the new simulation method, the evaluation of the IPX4 case becomes much faster, less error-prone and it provides more information, cf. lower row of Fig. 9. After the simulation the wetting of all surfaces and the flow paths are automatically determined. Hence, one can get a clear understanding of where water entered and on which way it reached its destination. This helps enormously in finding solutions to prevent leakages.

5 Future Potential and Improvements

The presented method can be easily adapted to the IPX3 case, since it only requires a change in the placement of the nozzles on the spray arch and a reduction of the angular movement.
Furthermore, the method is currently expanded to the IPX5 test case. There, a single, more massive water jet pointing at the device from a three-meter distance and directed over the whole surface. Often,

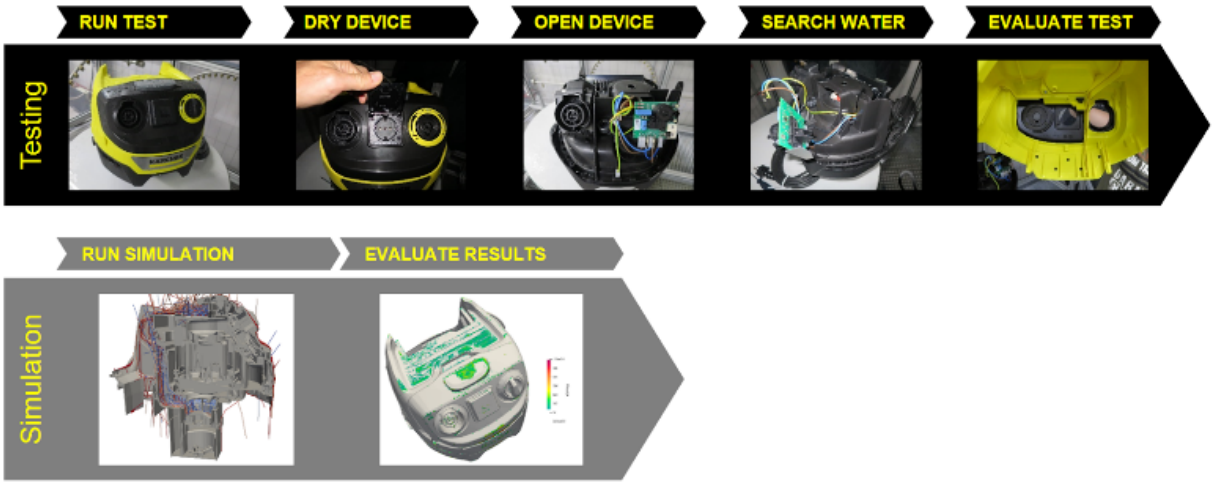

Figure 9 Confrontation of the evaluation procedure of the IPX4 test against the post processing steps after simulation.

this test is not conducted by an automated testing assembly but by a person holding the nozzle and aiming at the device. This could lead to varying results if different persons conduct the test. By defining an automated simulation process it is intended to improve the repeatability of the IPX5 test.
An unresolved issue so far is the influence of deformed surfaces due to warpage from the molding process or due to deformations during the assembly of the device on the IPX4 test. These deformations create openings at the contact surfaces between two adjacent parts. Since the geometry for the simulation is directly based on the original CAD data these openings cannot be captured by the current simulation method.
A first workaround would be to identify water accumulations on contact surfaces that are close to critical regions with the existing simulation method. Then one could take special care on warpage and assembly deformations at these points. One could also introduce an artificial opening between the parts where the accumulation of water was found and run the simulation again to investigate the movement of the water if it enters there.

In the second possibility, first, a molding process simulation of the parts would be conducted. The warpage of the parts would be determined and saved as new CAD data. The latter would then be applied in a structural mechanics simulation for the assembly of the parts. This would again result in a newly deformed geometry set, which finally could be applied to the IPX4 simulation. This is a much more complex procedure, which probably is only reasonable on special occasions, e.g. where warpage influences are expected from the beginning. Furthermore, this procedure already requires a lot of detailed information regarding the molding process and the assembly of the parts, which are usually only available in a later stage of the development process.

6 References

[1] Degrees of protection provided by enclosures (IP Code) (IEC 60529:1989 + A1:1999 + A2:2013); German version EN 60529:1991 + A1:2000 + A2:2013.

[2] Vergnaud, A. “Améliorations de la précision et de la modélisation de la tension de surface au sein de la méthode SPH, et simulations de cas d'amerrissage d'urgence d'helicoptères”, Doctoral dissertation, École centrale de Nantes, 2022.

[3] Chiron, L., Oger, G., De Leffe, M., & Le Touzé, D., “Analysis and improvements of Adaptive Particle Refinement (APR) through CPU time, accuracy and robustness considerations” Journal of Computational Physics, 354, pp. 552-575, 2018.

[4] Kulasegaram, S. et al., 2004, “A variational formulation based contact algorithm for rigid boundaries in 2D SPH applications,” Computational Mechanics 33(4), pp. 316-325.

[5] Legrady, B., 2024, “Particle-Based CFD Study of Lubrication in Power Transmission Systems Using Local Refinement Techniques,” Power Transmission Engineering, 2, pp. 36-49.

[6] Leroy, A., 2014, “A new incompressible SPH model: towards industrial applications,” Ph.D. thesis, Université Paris-Est.

[7] Adami, S., Hu, X. Y., Adams, N. A., 2012, “A generalized wall boundary condition for smoothed particle hydrodynamics,” Journal of Computational Physics 231, pp. 7057-7075.

[8] Cole, H. R., 1948, Underwater Explosions, Princeton. New Jersey: Princeton University Press.

[9] Antuono, M. et al., 2012, “Numerical diffusive terms in weakly-compressible SPH schemes,” Computer Physics Communications 183(12), pp. 2570-2580.

[10] Zhang, C., Rezavand, M., and Hu, X., 2020, “Dual-criteria time stepping for weakly compressible smoothed particle hydrodynamics,” Journal of Computational Physics 404, pp.109-135.

[11] Mayrhofer, C. et al., 2012, “Study of differential operators in the context of the semi-analytical wall boundary conditions,” Proceedings of the 7th International SPHERIC Workshop, pp. 149-156.

[12] Lind, S. J. et al., 2012, “Incompressible smoothed particle hydrodynamics for free-surface flows: A generalised diffusion-based algorithm for stability and validations for impulsive flows and propagating waves,” Journal of Computational Physics 231, pp. 1499–1523.

[13] Oger, G., et al., 2016, “SPH accuracy improvement through the combination of a quasi-Lagrangian shifting transport velocity and consistent ALE formalisms,” Journal of Computational Physics 313, pp. 76-98.

[14] Michel, J. et al., 2021, “Considerations on Particle Shifting Technique for SPH schemes,“ Proceedings of the 15th International SPHERIC Workshop, pp. 30-37.

[15] Lyu, H. G. and Sun, P. N., 2022, “Further enhancement of the particle shifting technique. Toward better volume conservation and particle distribution in SPH simulations of violent free-surface flows,” Applied Mathematical Modelling 101, pp. 214-238.

[16] Sabrowski, P., Beck, L., Wybranietz, T., 2019, “Modern WCSPH in industrial multiphase application considering complex moving boundaries,” Proceedings of the 14th SPHERIC International Workshop, Exeter, June 25-27, pp. 266-273.

[17] Chiron, L., et al., 2019, “Fast and accurate SPH modelling of 3D complex wall boundaries in viscous and non-viscous flows,” Computer Physics Communications 234, pp. 93-111.

[18] C. Kassiotis, D. Violeau, and M. Ferrand. Semi-Analytical Conditions for Open Boundaries in Smoothed Particle Hydrodynamics. Proceedings of the 8th International SPHERIC Workshop, pages 28–35, 2013.

[19] M. V. Berry. The molecular mechanism of surface tension. Physics Education, 6(2), 1971.

[20] A. Marchand, J. H. Weijs, J. H. Snoeijer, and B. Andreotti. Why is surface tension a force parallel to the interface? American Journal of Physics, 79(10), 2011.

[21] J.U. Brackbill, D.B. Kothe, and C. Zemach. A continuum method for modeling surface tension. Journal of Computational Physics, 100(2), 1992.

[22] Bierwisch. C., “Consistent Thermo-Capillarity and Thermal Boundary Conditions for Single-Phase Smoothed Particle Hydrodynamics. Materials”, 14:4530, 2021.

[23] Shepard, D. (1968): A Two-Dimensional Interpolation Function for Irregularly-Spaced Data. In: Proceedings of the 1968 23rd ACM national conference on, S. 517–524. ACM Press, New York, USA.

Simulation of Electric Engine Oil Cooling with Smoothed Particle Hydrodynamics (SPH)

Felix Pause, Malwine Fischer, Georg Mensah (dive solutions GmbH)

1 Summary

As the automotive industry is shifting towards electrification, the design of electric engines is key for optimizing vehicle performance. Balancing increased power and longevity with compactness and simplicity necessitates the use of sophisticated cooling strategies to maintain optimal operating temperatures. Various simulation methods have been explored in the past, ranging from traditional Volume of Fluid (VOF) techniques to particle-based approaches.
Smoothed Particle Hydrodynamics (SPH) has gained traction in drivetrain engineering, particularly for gearbox lubrication, due to its ability to accurately model free surface and multiphase flows, as well as its efficacy in handling complex geometries and moving components. Consequently, SPH is increasingly applied in the design of electric engines.
This presentation presents findings from simulations of a simplified, actively cooled electric engine employing SPH. The results are validated against experimental data, demonstrating the method's efficacy in predicting oil dynamics and heat transfer.

2 Experimental Reference and Simulation Setup

The simulations shown in this publication are based on the experimental work conducted by Davin et al. [1] as a benchmark. Davin et al. investigated a 40kW radial flux machine equipped with 12 coils and examined different cooling configurations. Here, we focus on investigating a setup utilizing 5 inlets to distribute oil onto the coil windings Since the experimental setup is symmetrical, our simulation model encompasses only half of the domain, with symmetry boundary conditions applied to the center plane. The set-up is illustrated in Figure 1.

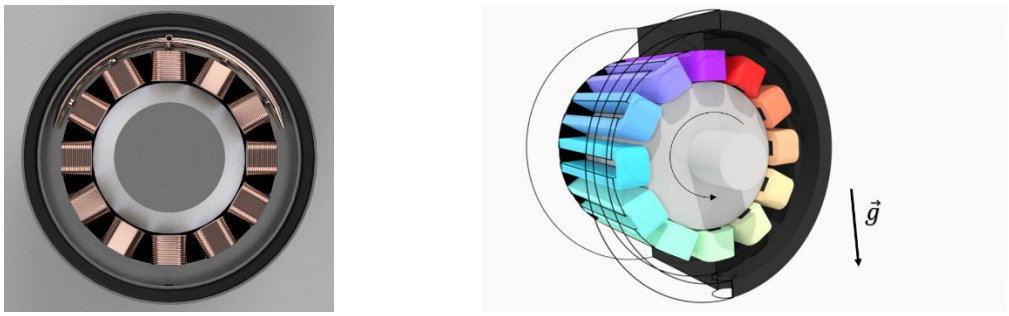

Fig 1. Simulation setup used for the investigation. Green arrows indicate position of oil injection.

Two parameters have been varied to validate the method against the experimental references: the inlet mass flows and the inlet temperature of the coolant. Since the properties of the coolant oil were not reported in the original work, some assumptions had to be made. The viscosity was given at 50 and 75°C. Therefore, the following exponential law was used to interpolate between these two points and account for the influence of reduced viscosity with increasing temperature:

$$\nu(T) = \nu_{50°C} \cdot \exp\left(\log\left(\frac{\nu_{75°C}}{\nu_{50°C}}\right) \cdot \frac{T-50}{75-50}\right).$$

The density, thermal conductivity, specific heat capacity, surface tension coefficient and contact angles were not reported. Thus, typical values for coolant oils were used to set them.
The following table summarizes the configurations used to generate the experimental results:

Property	Value
Rotor Speed	2750 RPM
Inlet Volume Flow Rate	110 l/h, 220 l/h, 368 l/h
Inlet Temperature	50°C, 75°C
Viscosity at 50 °C	30E-6 m²/s

Viscosity at 75 °C	12E-6 m²/s
Oil Density	930 Kg/m³
Surface Tension Coefficient	0.03 m/N
Contact Angle	30°
Coil Temperature	110°C
All other Surfaces	Adiabatic

3 Results and Conclusions

For each of the six operating points, the heat flow rates on the coils are obtained and compared with the experimental results.

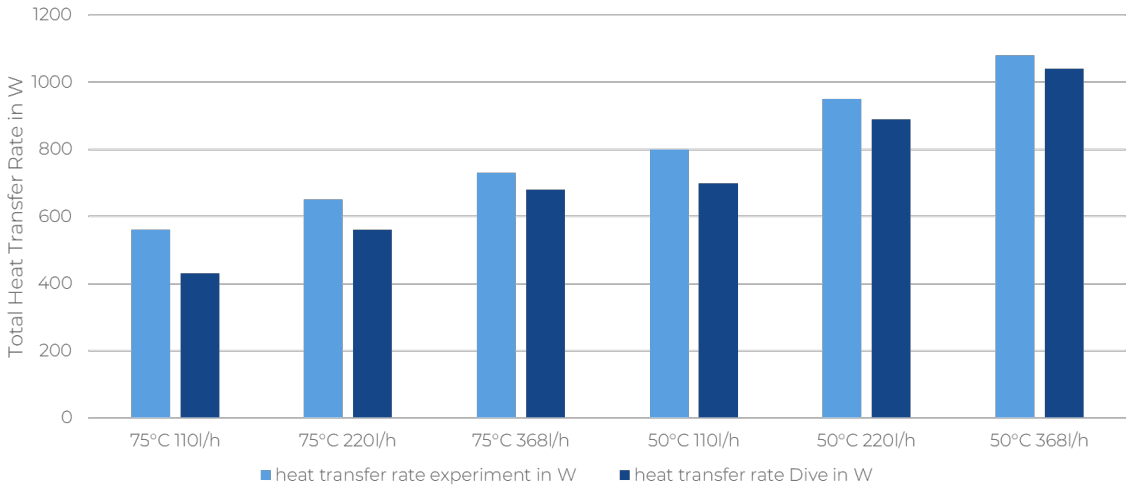

The simulation generally follows the experimental trend of increasing heat transfer rates with increasing volume flow rates and decreasing inlet temperatures. Moreover, a 77% to 96% match with experimental reference is found for the 6 operating points. Given the accuracy of an experiment and the assumptions made, this indicates that the simulation can capture the complex multiphase flow present in the electric engine. The method can therefore be used to test different design variations. In Figure 2, a snapshot of oil distribution predicted by the simulation is given. Here, the oil flow could be optimized by changing nozzle position or design, ensuring that all coils are adequately cooled.

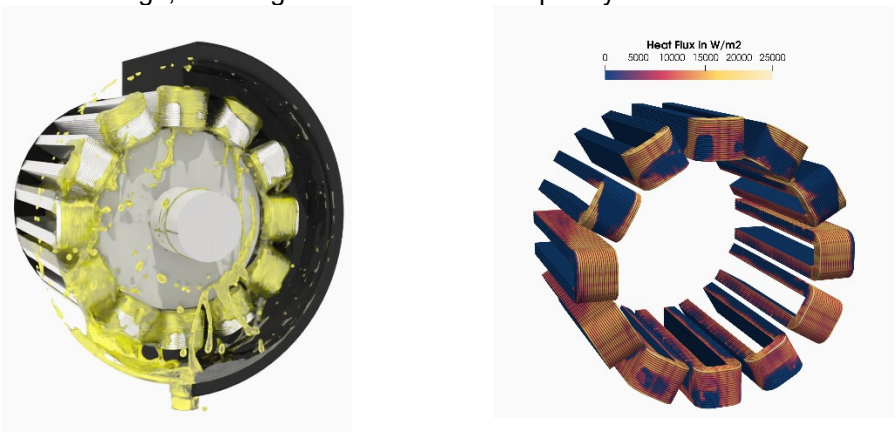

Fig 2. Oil distribution and time-averaged heat fluxes at 368 l/h and 75°C

4 References

[1] Davin et al., “Experimental study of oil cooling systems for electric motors”, Applied Thermal Engineering 75 (2015) 1-13

SIMULATION OF ELECTRIC ENGINE OIL COOLING WITH SMOOTHED PARTICLE HYDRODYNAMICS (SPH)

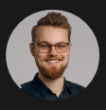

Felix Pause (CPO & Founder)
dive solutions GmbH, Berlin

SCHAEFFLER MAHLE ZF FEV KÄRCHER
weg B/S/H/ FENDT Sumitomo Drive Technologies DANA KESSLER·CO

i. **INTRO: OVERVIEW DIVE & SPH**
ii. **ELECTRIC ENGINE CASE**
iii. **SIMULATION RESULTS**
iv. **TAKEAWAYS & OUTLOOK**

DIVE: REMOVING ALL LIMITATIONS IN THE CFD PROCESS

Meshing-free CFD

- In-house SPH solver
- No meshing → reduced turnaround times
- No calibration → predictable results

Cloud-native CAE platform

- HPC out of the box, up-to-date with newest hardware gen.
- Automatic versioning & data management of simulations
- Parallelized simulation and data analysis
- Empower design engineers with CFD

SPH development started 2014 in industrial research projects

Today, Dive is an established partner for enterprises in various industries

Strong partners in industry and academia

SMOOTHED PARTICLE HYDRODYNAMICS (SPH) SOLVES THE LANGRANGIAN FORMULATION OF THE NAVIER-STOKES-EQUATIONS

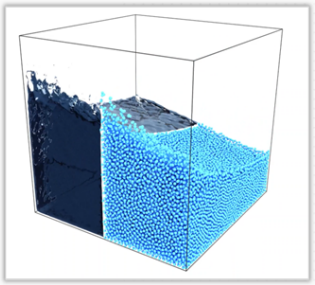

Mass conservation

$$\frac{\mathrm{d}\rho}{\mathrm{d}t} = -\rho \nabla \cdot \boldsymbol{v}$$

Momentum conservation

$$\frac{\mathrm{d}\boldsymbol{v}}{\mathrm{d}t} = -\frac{1}{\rho}\nabla p + \frac{\eta}{\rho}\Delta \boldsymbol{v} + \boldsymbol{g}$$

$$\rho_a \sum_b m_b \left(\frac{p_a}{{\rho_a}^2} + \frac{p_b}{{\rho_b}^2}\right) \nabla w_h(\boldsymbol{r}_{ab})$$

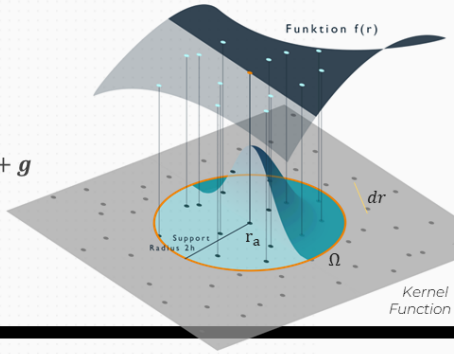

The lagrangian nature of the method **intrinsically captures interfaces** (walls, phases) this creates **advantages over classic Eularian/VOF-style** approaches

Reduced preprocessing time & simplified automation

Droplets are preserved

Drastic speedups for cases with high geometric complexity

SPH'S MODELING CAPABILITIES, ACCURACY AND EFFICIENCY HAVE BEEN CONTINOUSLY EXPANDED IN RECENT YEARS

Free Surface and Multiphase Fluid Dynamics

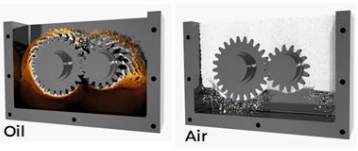

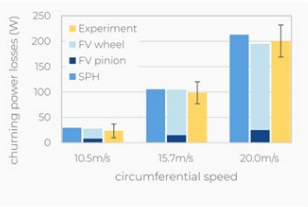

Stanic et al., Tribology International, 2018

Surface Tension Driven Flows

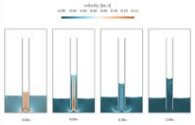

Capillary Effects

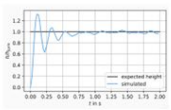

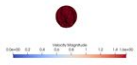

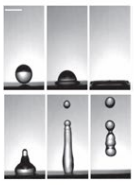

Droplet Impact & Formation

A. Vergnaud, 2022
C. Bierwisch et al., Materials, 2021

Heat Transfer

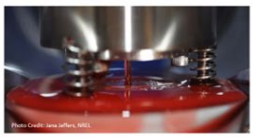

Impact of Surface Shape on Heat Transfer

Bennion & Gilberto, InterPACK, 2015
Mensah et al., Spheric, 2023,

INCREASING ADOPTION ACROSS INDUSTRIES

DRIVETRAIN

Planetary Gearbox

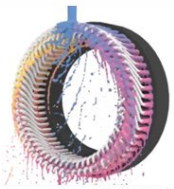

Electric Engine

Bearings

Sealings

MANUFACTURING

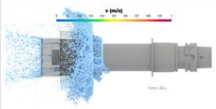

Honing

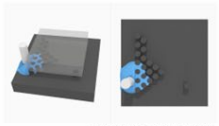

Microchip Glue Underfill

AUTOMOTIVE

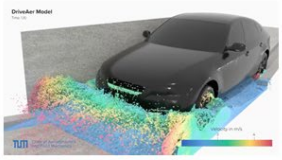

Water Wading

CLEANING

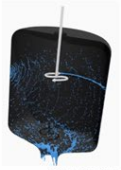

Tank Cleaning

Washers

AND MANY MORE ...

Dive NAFEMS

i. INTRO: OVERVIEW DIVE & SPH
ii. ELECTRIC ENGINE CASE
iii. SIMULATION RESULTS
iv. TAKEAWAYS & OUTLOOK

ELECTRIC ENGINE DESIGN CHALLENGES

Goals Increasing Power, Reducing Size
Constraints Managing Temperatures and System Complexity

→ Evaluation of different cooling concepts

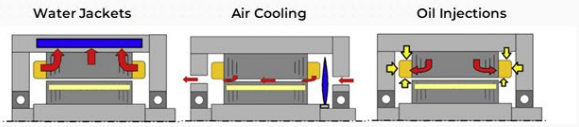

Davin et al., "Experimental study of oil cooling systems for electric motors", Applied Thermal Engineering 75 (2015) 1-13

EXPERIMENTAL REFERENCE

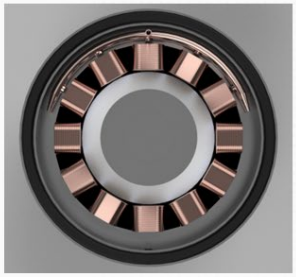

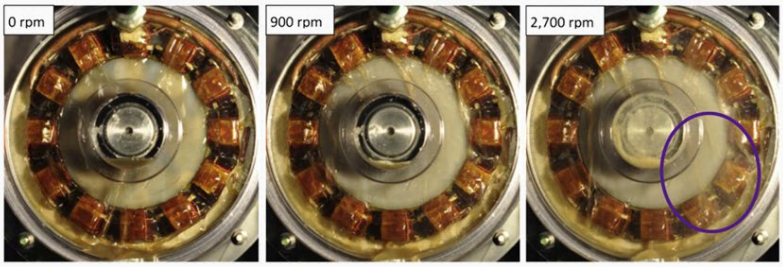

Reference Case

Davin et al., "Experimental study of oil cooling systems for electric motors", Applied Thermal Engineering 75 (2015) 1-13

- Simplified geometry
- industrial conditions
- Broad range of validations done

CFD Challenges

- Multiphase flow
- High rotational speeds, long cycle times
- Heat Transfer in films

Dive NAFEMS

i. **INTRO: OVERVIEW DIVE & SPH**
ii. **ELECTRIC ENGINE CASE**
iii. **SIMULATION RESULTS**
iv. **TAKEAWAYS & OUTLOOK**

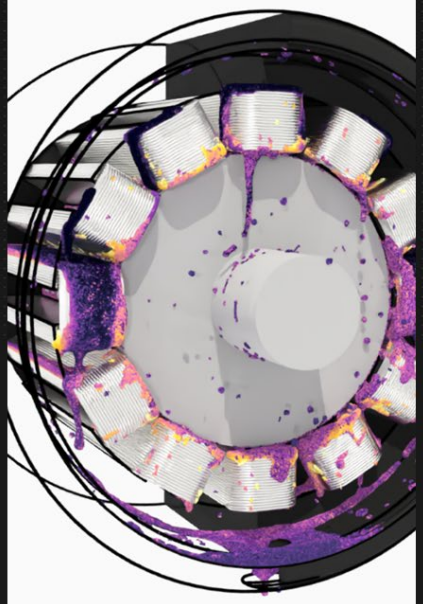

SIMULATION SETUP

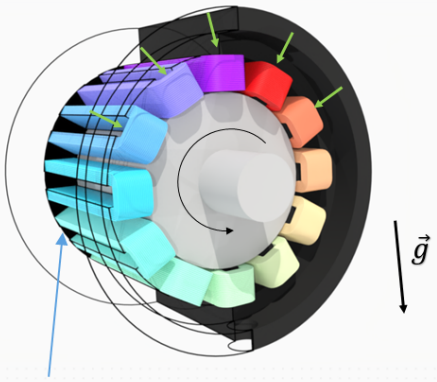

symmetry boundary condition

Property	Configuration
Rotational Speed	2750 rpm
Inlet Volume Flow Rate	110 l/h, 220 l/h, 368 l/h
Viscosity	Temperature dependent
Inlet Temperature	50°C, 75°C
Coil Temperature	110°C
All other Surfaces	Adiabatic
Density	930 Kg/m³
Surface Tension Coefficient	0.03 m/N
Contact Angle	30°
Particle diameter	0.6 mm

RESULTS FOR 368 L/H, 75°C

Simulated for 5 seconds (1/4 video playback speed)

Oil Distribution *Temperature Field*

EVOLUTION OF THE HEAT TRANSFER

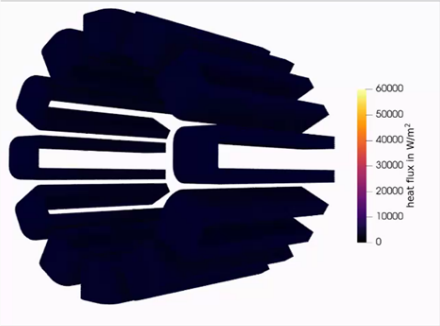

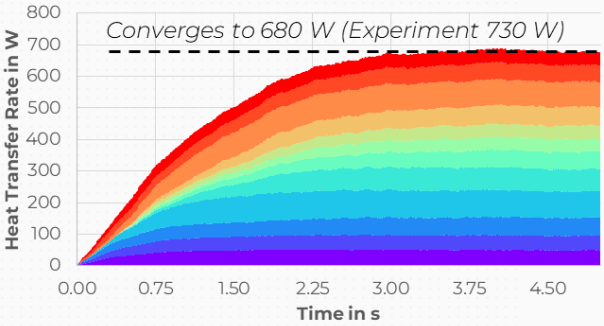

HEAT TRANSFER DISTRIBUTION

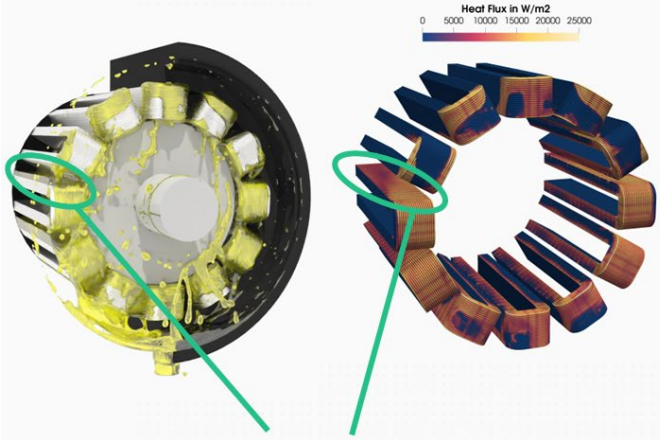

Gravity driven agglomeration of oil leads to increase in heat transfer on coils 4 and 10

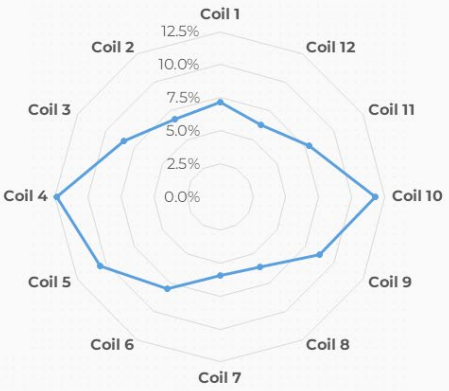

Left	Right	Top	Bottom
coil 2-6	*coil 8-12*	*coil 11-3*	*coil 5-9*
46%	**41%**	**39%**	**37%**
Rotor Spin		*Gravity*	

TOTAL HEAT TRANSFER RATES IN OTHER OPERATING POINTS

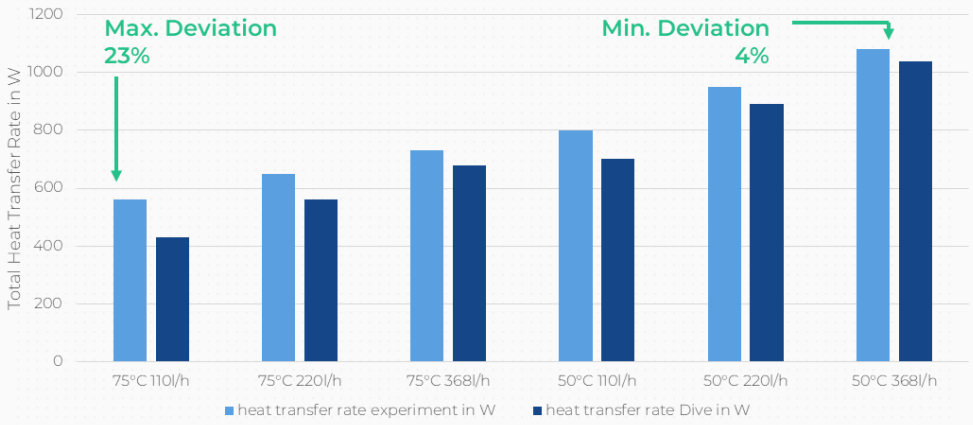

Dive NAFEMS

i. INTRO: OVERVIEW DIVE & SPH
ii. ELECTRIC ENGINE CASE
iii. SIMULATION RESULTS
iv. TAKEAWAYS & OUTLOOK

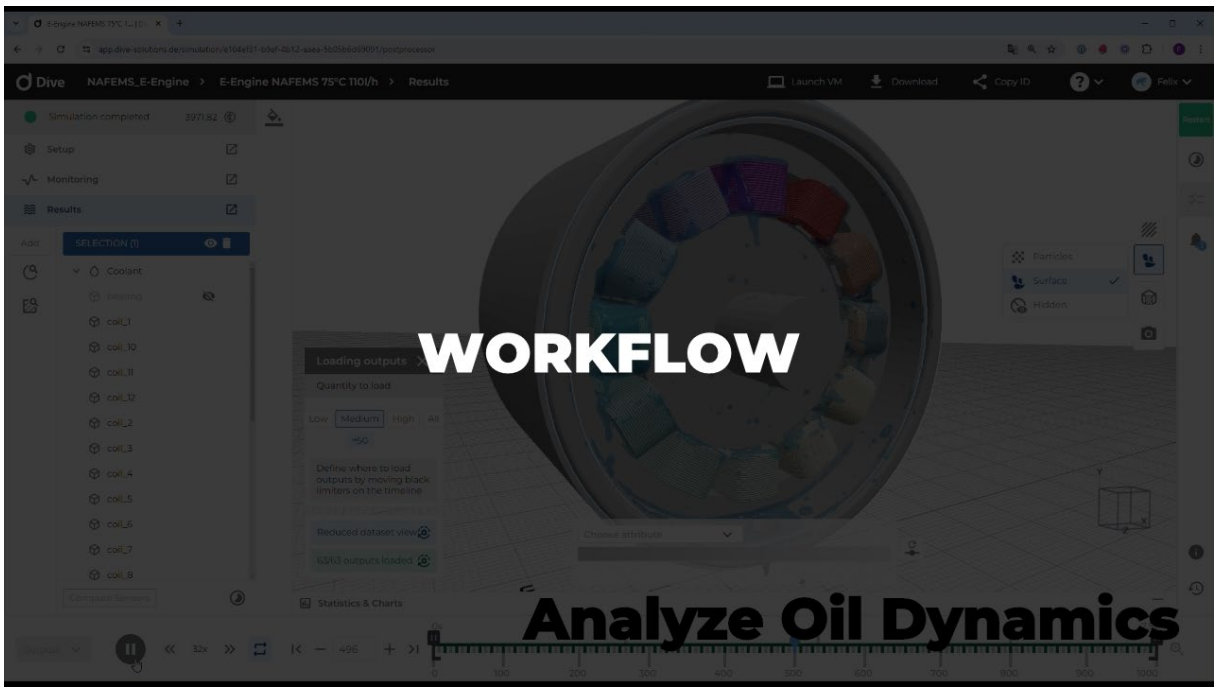

CONCLUSION

- **SPH is widely applied and extensively validated** in different sectors and applications
  - Reliable prediction of complex multiphase flows in drivetrain, automotive, manufacturing and more
- **Heat Transfer accurately predicted** in the electric engine case
  - 4-23 % deviation
- **High computational efficiency, low preprocessing effort**
  - 1-2 d computing time, initial setup time ~1-3 hrs, additional effort per operating point <5 min
- **Cloud parallelization of simulation and data analysis** allow **rapid design space exploration**
  - E.g. change nozzle type (flat, conic), positions (dripping, shaft), inlet conditions (temperature, volume flow rate) or other design changes
  - Here, 6 operating points were run in parallel. Total turnaround time was 3 days (including pre and postprocessing). More operating points do not significantly change turnaround time.

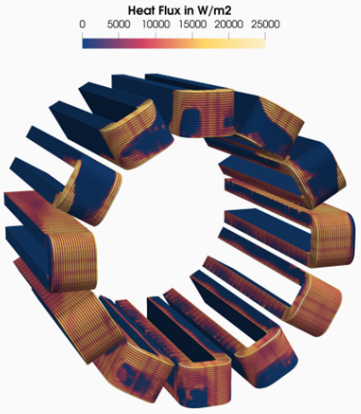

ENJOY ENGINEERING

We believe that engineers should be able to focus on delivering great products. We take care of everything else.

Presented by: Felix Pause – Founder & CPO

pause@dive-solutions.de

Dive

dive solutions GmbH
Mollstraße 30-32, 10249 Berlin
info@dive-solutions.de

Einfluss von innovativen Leichtbaumaßnahmen eines permanenterregten Synchronmotors auf die simulative Ermittlung der Temperaturentwicklung seiner Komponenten.

Dewald, A.; Kern, J.; Bause, K.; Ott, S.

Elektrische Traktionsmotoren sind zur Einhaltung der geplanten Mobilitätswende unumgänglich. Neben der Etablierung nachhaltiger Antriebskonzepte muss die energetische Effizienz dieser Antriebe gewährleistet und kontinuierlich verbessert werden. Zur Erhöhung des Gesamtwirkungsgrades wird die Gesamtmasse der Systemkomponente Motor mithilfe innovativer Leichtbaumaßnahmen optimiert.

Dazu werden im Vorhaben des FedeRo Projekts die Komponenten mit dem größten Gewichtsanteil, dazu zählen das Blechpaket, der Rotor und die Wuchtscheiben, möglichst masseeffizient optimiert. Der Rotor wurde bereits als Polygonhohlwelle ausgelegt, sodass der Pressverband zwischen Welle und Nabe Vorteile in der Dimensionierung der Verbindung erwirkt. Aus Gründen mechanischer und thermischer Festigkeit dürfen die Komponentenmassen nicht beliebig reduziert werden. Besonders im Bereich des Thermomanagements ist die Wärmekapazität linear von der Masse der Komponenten abhängig, wodurch rückwirkend die Temperaturen zunehmen. Gefährdend für den Elektromotor werden diese Temperaturen ab 135°C. Hier steigt die Gefahr der permanenten Entmagnetisierung und damit die Gefahr der Reduktion des Gesamtwirkungsgrades.

Diese Veröffentlichung untersucht den simulativen Einfluss der iterativ designoptimierten Komponenten des Elektromotors auf die Maximaltemperaturen im Motor. Mithilfe der Kombination von CFD und CHT Simulationsmethoden in der Umgebung ANSYS Fluent wird ein vorab elektromagnetisch simuliertes Verlustkennfeld thermisch auf das Rotorblechpaket projiziert. Die Materialien werden mittels reeller Wärmeübergangskoeffizienten thermisch verknüpft. Reguliert wird das System aktiv durch eine Rotorinnenkühlung, die eine Durchströmung der Rotorhohlwelle ermöglicht. Im Kühlkreislauf wird neben der Wärmeleistung eine zirkuläre Strömung durch die Rotation des Rotors induziert. Untersucht wurden die Rotordrehzahlen bei 3000 und 13100 U/min.

Ziel der Untersuchung ist den thermischen Einfluss der aktuellen Designänderung auf die vorherige Iteration innerhalb des Simulationsmodells festzustellen. Somit können thermische Effekte vorhersehbar reproduziert und für die Evaluierung reeller Gestaltgebung zu Hilfe genommen werden.

Innovative Leichtbaumaßnahmen an einer permanenterregten Synchronmaschine – Simulationsbasierte Einflussanalyse auf das thermische Verhalten

Dewald A.; Kern J.; Bause, K.; Ott, S.

Motivation der Untersuchung

- Zunehmende Elektrifizierung in Deutschland
- Zur erreichung der Klimaziele 2035 ist die Elektrifizierung notwendig
- Großes Potential in der Gewichtsreduktion von Motorkomponenten [1]

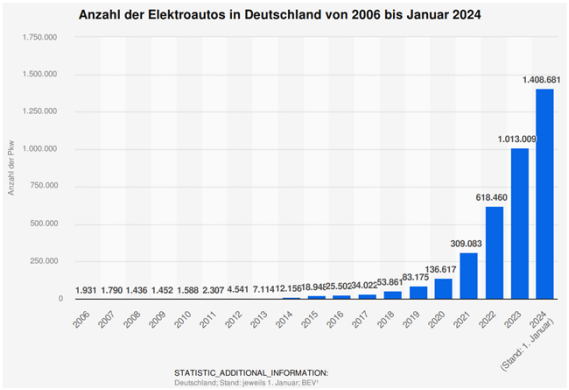

[2]

Steigerung der Effizienz im elektrischen Antriebsstrangs gewünscht

NAFEMS DACH Konferenz 2024: Konferenz für Berechnung & Simulation im Engineering, 10. – 12. Juni 2024, Bamberg, D

Dimensionen des Referenzmotors

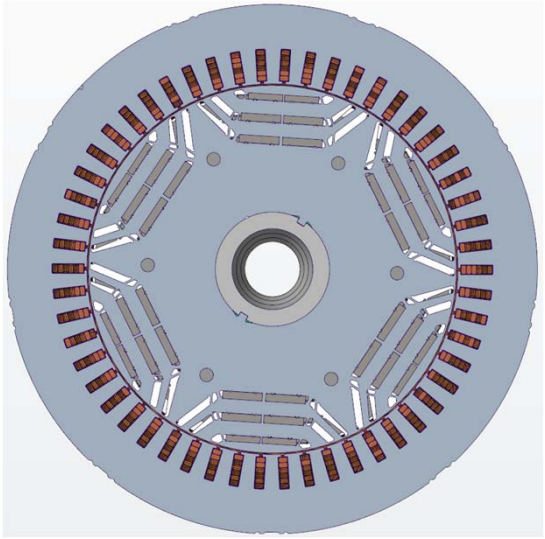

- Achsantrieb für PKW BEV Vorderachse

• Peak Leistung:	160 kW
• Dauerleistung:	117 kW
• Rotordurchmesser außen:	175 mm
• Rotordurchmesser innen:	55 mm
• Statordurchmesser außen:	255 mm
• Statordurchmesser innen:	179 mm
• Motorlänge:	134 mm

Massenverteilung Referenzmotor

- Hauptbaugruppen im Traktionsmotor bilden
  - Rotor
  - Stator
- Untersuchte Komponente
  - Rotor

Massenaufteilung des Rotors:

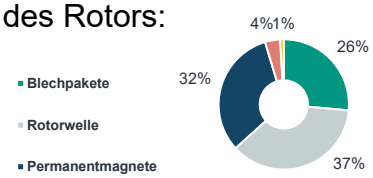

Traktionsmotor

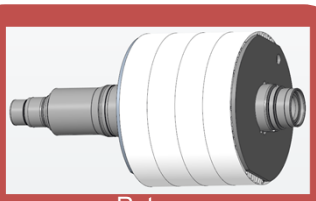

Rotor

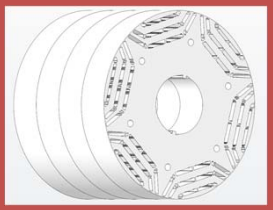

Blechpakete 26%

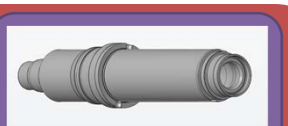

Rotorwelle 37%

Permanentmagnete 32%

Leichtbaumaßnahmen der Rotorwelle

- Gestaltänderung der Rotorwelle zum Polygon
  - Sorgt für Reduktion der Fügekräfte
  - Geringere Pressverbandauslegung notwendig
  - Besseres mechanisches Hochdrehzahlverhalten
  - Weniger Eigenspannungen im Produktionsprozess

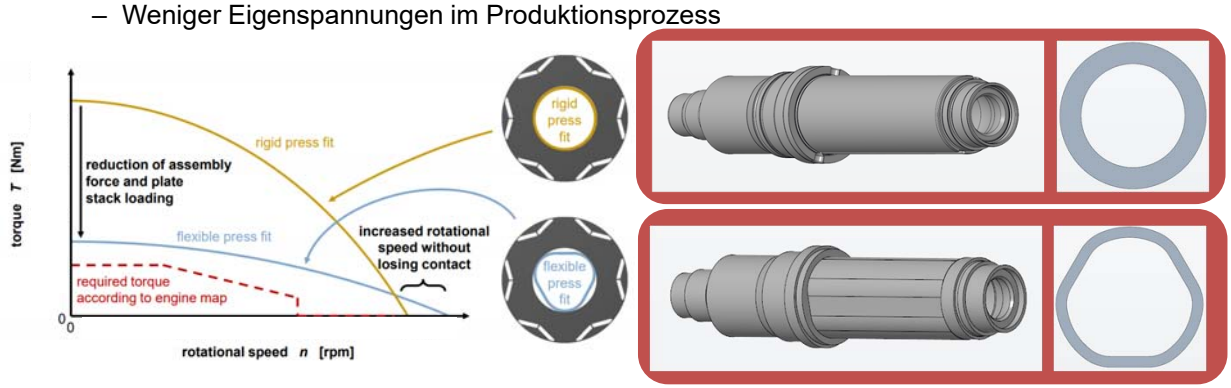

Designiterationen

Optimierte Rotorgeometrie durch Iterieren des Rotordesigns

- Die Erste Iteration sieht die Gestaltänderung der Rotorwelle zum Polygon vor
- Reduktion der Masse im Bereich der Welle-Naben-Verbindung von 47%
  - Wandstärke Referenzsystem: 8 mm
  - Nach Designiteration: 4 mm

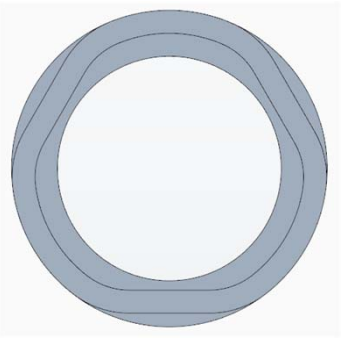

Thermische Betrachtung des Systems

- Trockenlaufender E-Motor
- Antriebsverluste als Wärme frei
- Wärmeabfuhr erfolgt effektiv im Inneren des Rotors
- Kühlsystem
  - Durchlaufkühlung durch Rotorwelle
  - Wasser-Glykol-Lösung
  - 75°C Konditionierungstemperatur

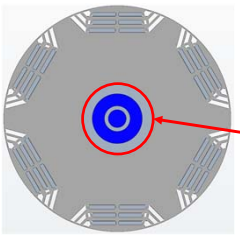

Verfügbare Fläche des Rotors zur Wärmeabfuhr

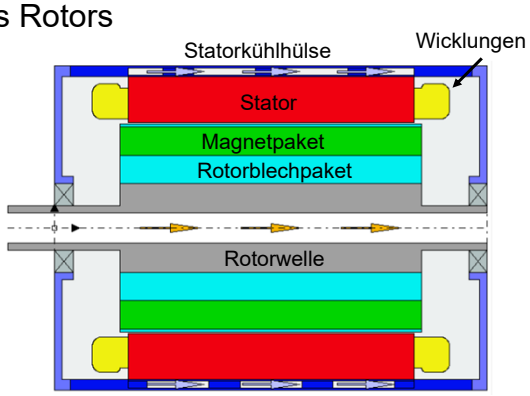

[3]

Thermische Problemstellung

- Gestaltänderung der Rotorwelle zum Polygon:
  → Signifikante Verringerung der Kontaktflächen
  → Verschlechterung der Wärmeübertragung wird vermutet

Außendurchmesser jeweils gleich

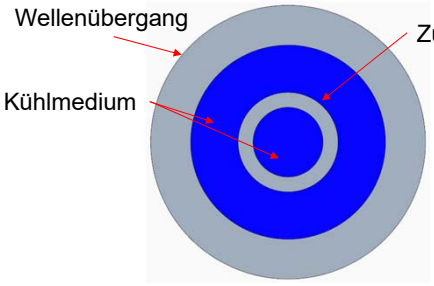

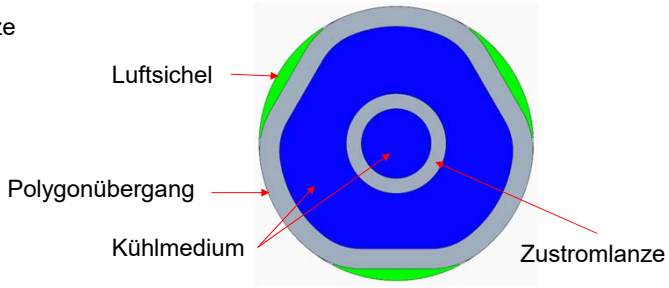

Die effektive Wärmeübertragungsfläche reduziert sich maßgeblich

Bedeutung der Temperatur

- Thermische Begrenzung el. Maschinen:
  - Zersetzungstemperatur der Isoliermaterialien
  - Curietemperatur der Permanentmagnete

- Was ist die Curie Temperatur?

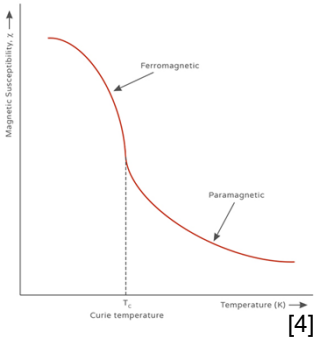

[4]

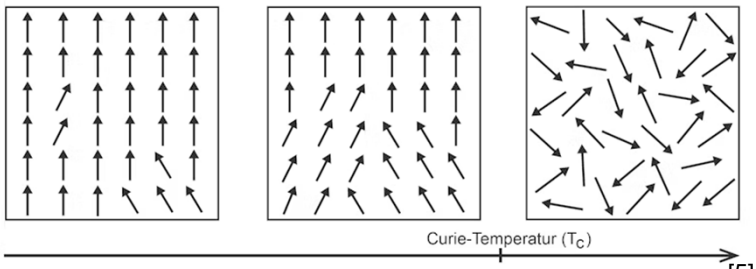

[5]

Bei 140°C permanente Demagnetisierung der Magnete!

Festlegen des Versuchsplans

- Thermische Betrachtung von:
  - Anfahrt: $n_A = 23\%\ n_{Max}$; $M_A = 63\%\ M_{max}$
  - Feldschwäche: $n_F = n_{max}$; $M_F = 13\%\ M_{max}$

- Verlustleistungsverteilung abhängig vom Betriebspunkt
  - Kupferverluste abh. von Statorstrom
  - Eisenverluste abh. von E-Feld Drehfrequenz
  - Mech. Verluste abh. von Drehzahl

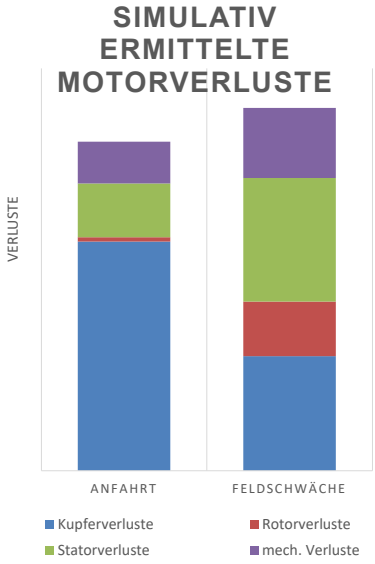

Thermische Untersuchung

- ANSYS – Fluent
- Das Referenzsystem wird nur 2D untersucht

2D - Untersuchungen

- Ziele:
  - Referenzsystem abbilden
  - Initiale Temperaturabschätzung
  - Vereinfachung des 3D – Systems
  - Ersatzmodellierung:

  → Statorübergang

  → Magnetluftkavitäten

3D - Untersuchungen

- Ziele:
  - Temperaturverlauf des Rotorquerschnitts mit Fokus der Temperatur im Magnet sowie Kühlwasser
  - Strömungsanalyse der Rotorinnenkühlung
  - Vergleich der Betriebspunkte

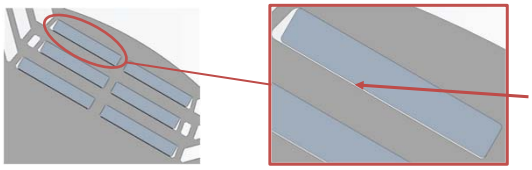

Ablauf der 2D-Simualtionen

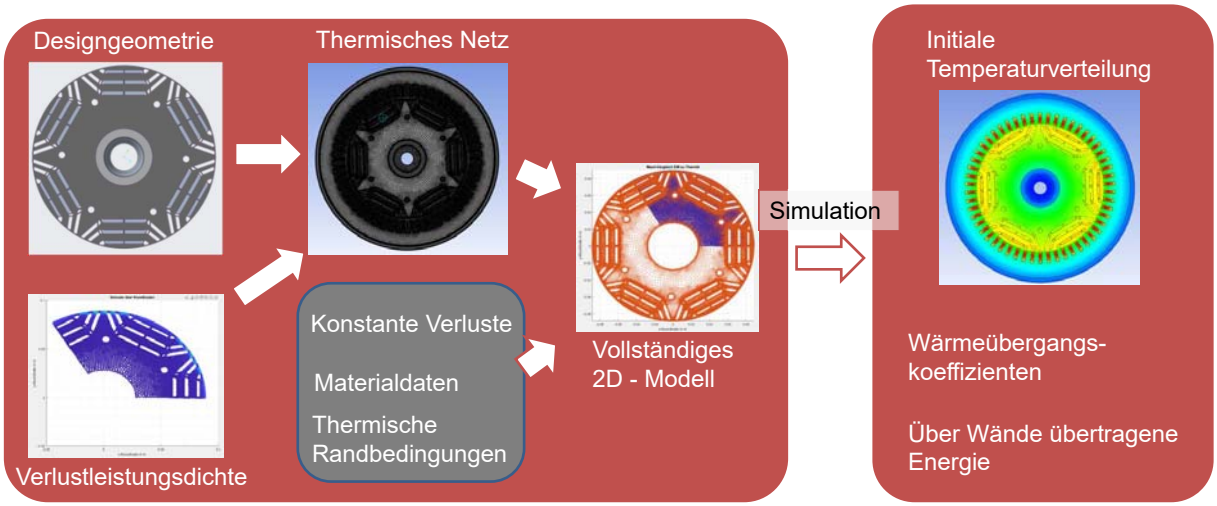

Ablauf der 3D-Simulationen

2D - Ergebnisse
- Mittlere Verlustleistungsdichten
- Wärmeübergangskoeffizienten

Weitere Eingangsgrößen
- Axiale Kühlmittelführung
- Einbringen der Lagerstellen und Gleitringdichtung
- Darstellung der Verzahnung als Fläche
- Ein- und Ausflussbedingungen

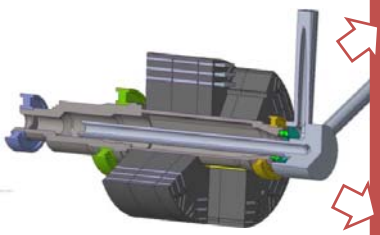

Temperaturverläufe

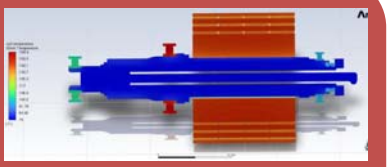

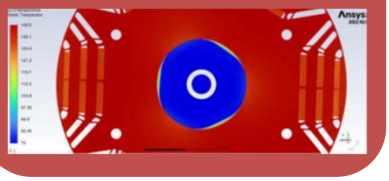

Strömungsgeschwindigkeiten

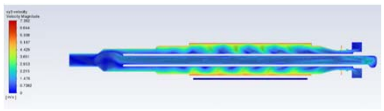

Druckverläufe

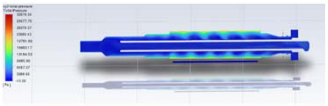

Ergebnis Anfahren

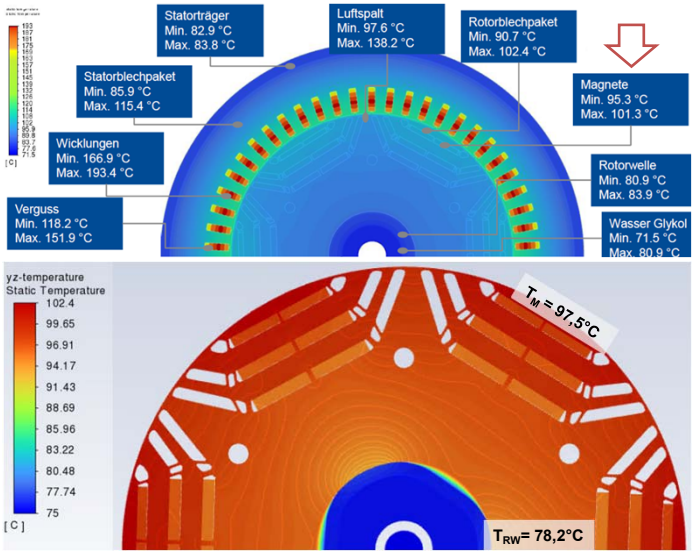

Anfahrts Betriebspunkt:
n_A = 23% n_{Max}; M_A = 63% M_{max}

- Die Luftsicheln im Polygon sorgen für eine leicht höhere Temperatur in den Magneten
- Einfluss des Polygons auf Magnettemperatur während Anfahrt vernachlässigbar
- Grund sind geringe Eisenverluste im Rotor (rot)

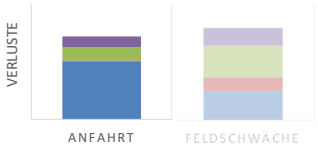

Ergebnis Hochdrehzahl

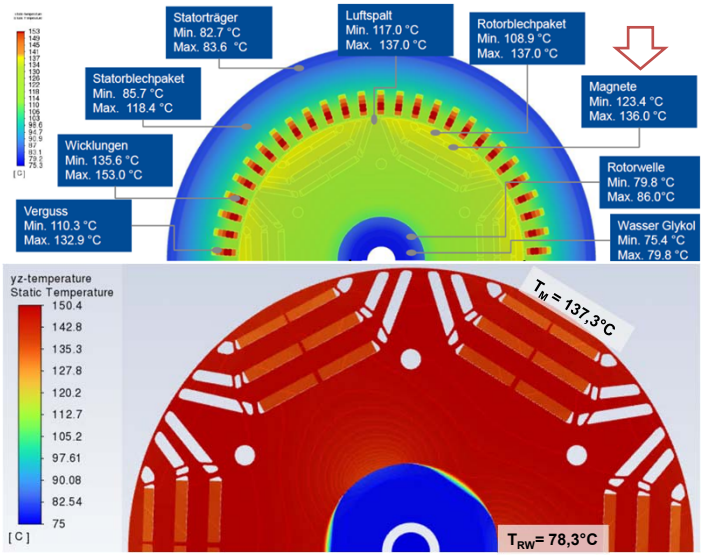

Feldschwäche Betriebspunkt:
$n_F = n_{max}$; M_F = 13% M_{max}

- Die Polygonform sorgt für hohe Temperaturgradienten zwischen Welle und Rotorblech
- Die mittlere Magnettemperatur steigt deutlicher als beim Referenzsystem
- Steigenden Rotorverluste (rot), in der Magnetumgebung

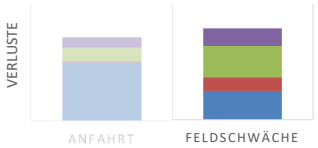

Ergebnis Kühlsystem mit Polygonwelle

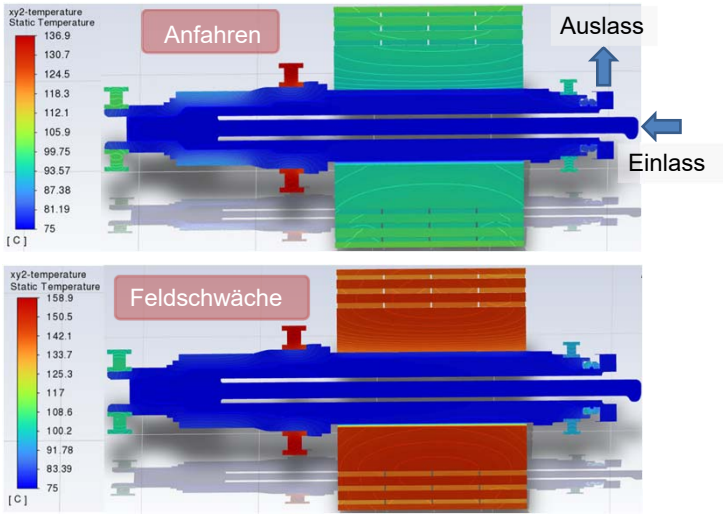

- Rotorverluste
  - Anfahrt: 38 W
  - Feldschwäche: 475 W
- Max. Kühlleistungen
  - Anfahrt: - 398 W
  - Feldschwäche: - 503 W

- Wärmeabfuhr stagniert mit höheren Verlusten
- Förderung des Fluids nicht das Problem
- Temperatur der Rotorwelle in beiden Betrieben bei 78°C

- Geringer konvektiver Übergang Problematisch

Fazit und Ausblick

- In beiden Betriebspunkten, Magnete unter T_C = 140°C
  - Bei Polygon im Feldschwächebereich grenzwertig (T_M = 137,5°C)
- Polygonform thermisch vernachlässigbar im Anfahrbereich
- Negativer Einfluss der Polygonform auf Temperatur im Feldschwächebereich
- Erkenntnisse fließen in weitere Iterationen ein
  - Darunter Hochdrehzahlauslegung
- Ermöglichen des Vergleichs der Designiterationen in 3D untereinander

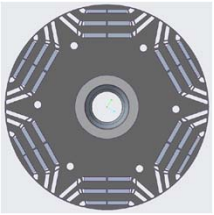

Referenzmaschine

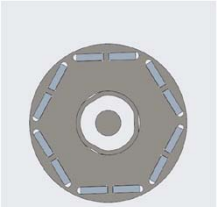

Designvorschlag

Vielen Dank für Ihre Aufmerksamkeit

NAFEMS DACH Konferenz 2024: Konferenz für Berechnung & Simulation im Engineering, 10. – 12. Juni 2024, Bamberg, D

Dieses Projekt wird vom Bundesministerium für Wirtschaft und Klimaschutz (BMWK) aufgrund eines Beschlusses des Deutschen Bundestages gefördert.

Bundesministerium für Wirtschaft und Klimaschutz

Referenzen

[1] https://doi.org/10.1515/zwf-2022-1103
[2] https://de.statista.com/statistik/daten/studie/265995/umfrage/anzahl-der-elektroautos-in-deutschland/
[3] 10.1109/ICEMS.2019.8922026
[4] https://www.sciencefacts.net/curie-temperature.html
[5] https://www.supermagnete.de/magnetismus/curietemperatur

NAFEMS DACH Konferenz 2024: Konferenz für Berechnung & Simulation im Engineering, 10. – 12. Juni 2024, Bamberg, D

Kontaktdaten

- **Anton Dewald**

- Mail: anton.dewald@kit.edu
- Tel.: +49 721 608 – 44798
- Karlsruher Institut für Technologie
- **IPEK – Institut für Produktentwicklung**

Integrated 1D and 3D Workflow for EV Battery System Development

C. Chang[1], C. Stromberger[2], H. Li[1], A. Colleoni[2], V. Lebrun[2], S. Kandasamy[1], F. Gandhi[1], Dr. F. Hesse[1]

[1]Dassault Systèmes SIMULIA
[2]Dassault Systèmes CATIA

Summary:

With the growing market for electric vehicles comes a need for quick and accurate simulation of the thermal behavior of electric vehicle battery systems. This battery system development with a focus on thermal performance can be done using full 3D computational fluid dynamics simulations with conjugate heat transfer applied to the 3D battery module and cold plate geometries using Dassault Systèmes' **3D**Experience Platform's Fluid Dynamics Engineer role. However, for early conceptual design, where many design iterations need to be tested, this can become prohibitively expensive. There is also a need for quick and accurate battery modelling when integrated into larger 1D systems of the vehicle. This talk, therefore, discusses the correlation of the thermal behavior of 3D battery model systems with numerically cheaper 1D battery models developed using the Dymola Modelica library. Examples of the good correlation achieved between the 3D and 1D models are presented through a canonical liquid cooled battery pack with uniform loading and, subsequently, the battery pack with a load cycle based on the EPA Urban Dynamometer Driving Schedule.

Keywords: Electric vehicle battery systems, Computational fluid dynamics, Reduced-order models

1 Introduction

The advent of the electric vehicle market brings with it numerous challenges for battery system development. For one, there is a significant proliferation of battery and cooling designs. This means there are many designs to choose from, but limited (prior) test data to understand which battery and cooling design to choose. Additionally, there is a high pressure to reduce development time (i.e. time-to-market) as well as the battery development cost. Furthermore, a holistic design approach is sought after, where the full vehicle thermal design is accounted for. More specifically, cooling/heating of both the battery and cabin must be considered as well as an efficient design is needed for extended battery range.

The objective of this blog post is to describe a fast, accurate and automated calibration workflow to accelerate battery conceptual design, component scaling, and performance trade-off analysis. This is achieved through an integrated 1D and 3D model correlation workflow for battery conceptual design. The user will not need to rely on past test data or correlation, can quickly evaluate and choose between designs, can perform drive cycle / full vehicle thermal system analysis, and can iterate and improve when more design detail is revealed. A pictorial representation of this process is illustrated in figure 1. First, a 3D simulation of the battery system is performed. The data is then used to calibrate a 0D/1D model, which enables an accelerated analysis of the battery system to be performed. One, therefore, has an ideal setting to iterate over many battery system designs in a short time, ultimately being able to then choose the optimal battery system and cooling design for the intended application. Subsequently, one returns to the higher fidelity 3D simulation world to validate the 0D/1D battery and cooling model, thereby closing the design loop illustrated in figure 1. The remainder of this blog post is organized into a methodology description that is subseqeuntly folllowed by a description of a use-case and a concluding statement.

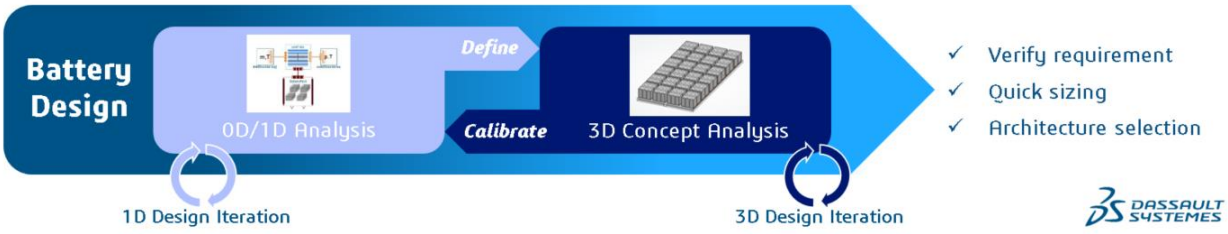

Fig. 1: Representation of the integrated 1D and 3D workflow for EV battery system development

2 Methodology

To begin, one starts with a battery cell level correlation. Specifically, one creates a 3D battery cell parametric model and characterizes / correlates a 1D battery cell parametric model from the Dymola Modelica library. This correlation work is then carried over to the battery module / pack level where, again, a 3D representation of the battery module and cold plate is used to characterize / correlate a 1D representation of the battery module and cold plate system from the Dymola Modelica library.

The Dymola Modelica library that is used to create the 0D/1D battery and cooling system representation offers a plethora of tunable parameters. At the battery cell level, one is able to discretize the thermal capacity, and parametrize thermal properties, either directly or calculated based on geometry and material data (see figure 2a). Meanwhile, on the battery module level, the individual cell behavior is maintained, but now thermal interactions between the cells and environment is accounted for as well (see figure 2b). At the battery pack level, one reuses battery module models and also considers additional housing and interfaces (see figure 2c). Moving on, the liquid cooling cold plate model (see figure 3) offers variable flow geometry with vectorized fluid channel for the independent modelling of parallel fluid channels and solid wall element discretization. It also enables a 2D wall dynamic thermal capacitance grid with 3D thermal inertia of the heat exchanger core to be accounted for. Overall, the parameterization of the cold plate correlates to the actual design data in terms of dimensions, material properties, and number of channels.

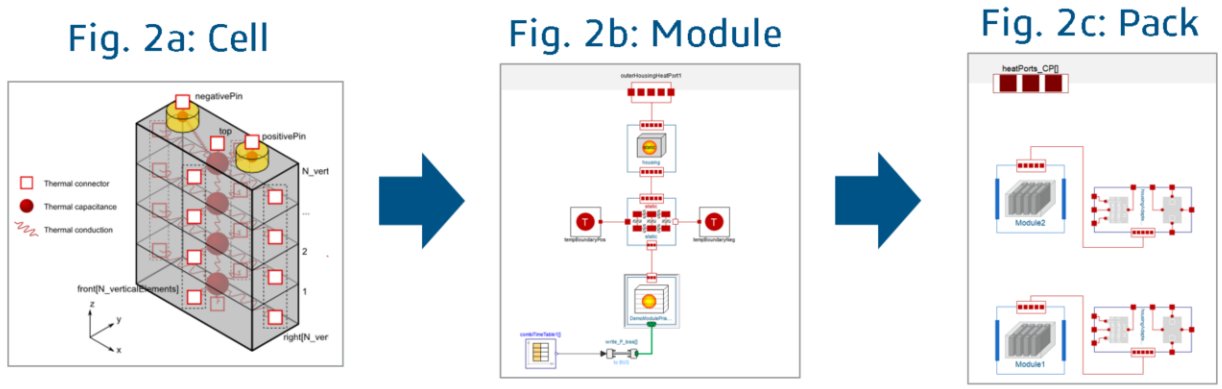

Fig. 2: Dymola Modelica library representations of (a) a battery cell, (b) a battery module, and (c) a battery pack

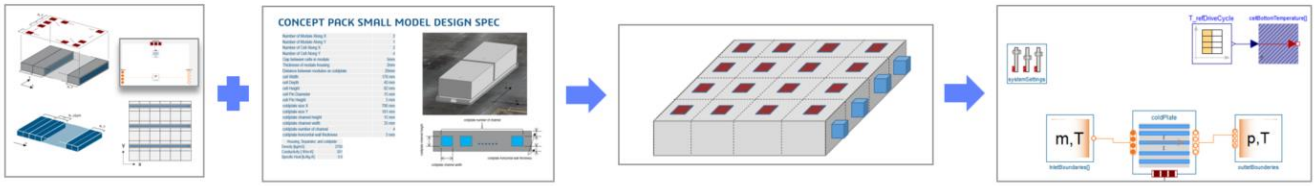

Fig. 3: Dymola Modelica library representation of a cooling plate and its channels

Having described the 0D/1D Dymola Modelica representation of the battery system and cooling pattern, the 3D model must now be described. The 3D representation of the battery system and cooling geometry is parametric (see figure 4a-4b). It has continuous parameters for the cell dimensions, housing, terminals, channel design and more. Meanwhile, discrete parameters account for the number of cells, modules and cold plate cooling channels. This parametric model is purposely made robust to implement it in an automatic workflow. Furthermore, for the computational fluid dynamics (CFD) and conjugate heat transfer (CHT) analysis, the **3D**Experience Platform based FMK Reynolds-Averaged Navier-Stokes (RANS) solver is used. The solid domain is solved for using a finite element model (FEM). There is automatic contact detection for solid-to-solid contact and fluid-to-solid contact interfaces. Also, there is automatic fluid domain detection and sealing.

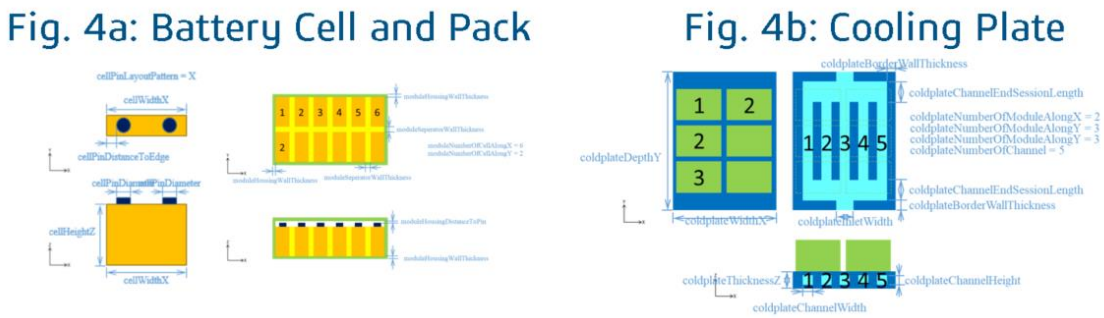

Fig. 4: Parameterized (a) battery cell and pack, and (b) cooling plate geometries

With both the 0D/1D and 3D battery system and cooling plate representations discussed, the subsequent step is to clarify the correlation methodology. Specifically, one wishes to correlate the 0D/1D model behavior with the 3D model as a reference. The strategy entails correlating the solid and fluid domains separately for better efficiency. Reason being, fluid convection behavior is non-linear (as made clear by the non-linear convection term in the Navier-Stokes equations), while solid conduction is linear in behavior (as made evident by the linear heat diffusion equation). For fluid convection, one therefore correlates flow dependent thermal convection behavior. With solid conduction, a two-step process is adopted: steady-state results are correlated by tuning the conduction path, while transient results are correlated by tuning the thermal mass distribution. The correlation workflow outlined above is automated. Dymola simulations and Python optimization routines are used for the parameter correlation. The optimization algorithm itself consists of the differential evolution method with a population of 10 and iterations up to 1000, where the final design is refined using the gradient method to minimize the prediction error with respect to the 3D result.

3 Sample Results

To illustrate the use of this 3D to 0D/1D correlation workflow for battery system development, validation is performed using an electric vehicle (EV) duty cycle where the lightweight vehicle battery load is taken from the United States Environmental Protection Agency (EPA) Urban Dynamometer Driving Schedule (UDDS) to represent typical city driving conditions. The associated vehicle speed and battery load are depicted in figure 5. For a battery pack consisting of two battery modules each with eight battery cells, the best and worst temperature comparison between the 3D and 0D/1D result is shown in figure 6. At best, the battery temperature delta is as low as 0.10°C, while in the worst case the battery temperature delta is as high as 0.26°C.

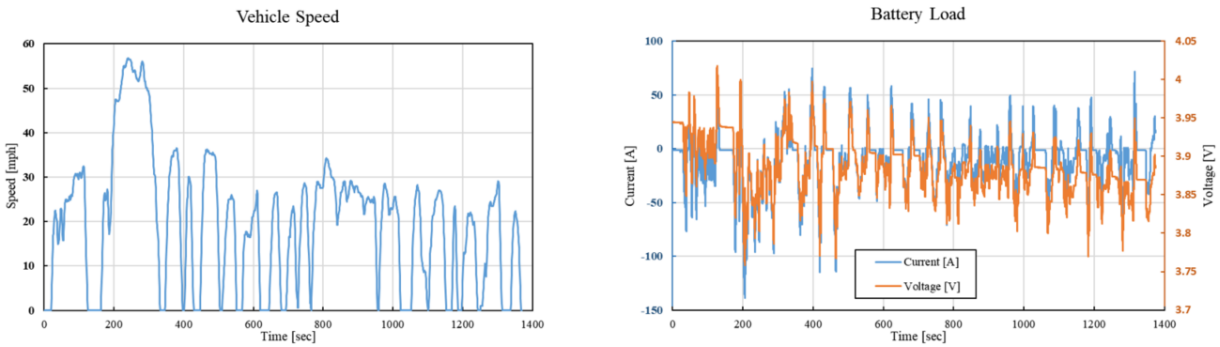

Fig. 5: EPA UDDS vehicle speed and accompanying battery load

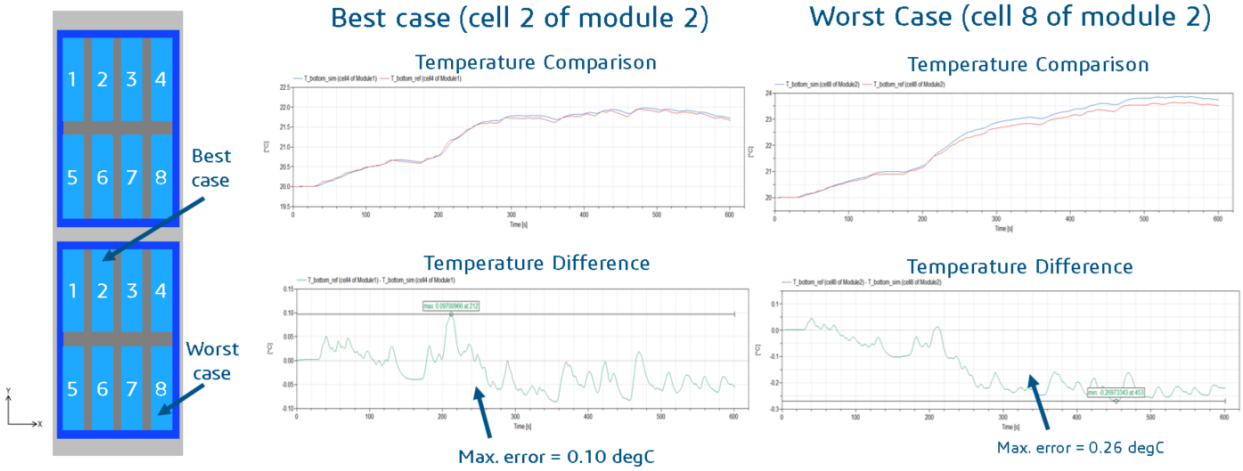

Fig. 6: Comparison between 3D and 0D/1D temperature results for a battery system running with the UDDS cycle

4 Conclusion

In summary, an integrated 0D/1D and 3D correlation workflow for EV battery system development has been presented. It has been shown that, even for a highly dynamic and realistic load cycle, good accuracy can be obtained when the 0D/1D model has been appropriately tuned based on the 3D battery system results. This means that for future battery system development work, the 0D/1D model can be used to provide high fidelity analysis even without a prior physical model. The presented workflow also represents a Dassualt Systèmes example of MODSIM, integrated modelling and simulation, and, thereby, is a proponent of Dassault Systemès' long-term strategy of breaking silos between designers and simulation engineers while accelerating the product development cycle.

Der Weg zur globalen elektromagnetischen Feldsimulation in Hörgeräten

T. Fischer, S. Lensing, O. Nipp

WS Audiology
Henri-Dunant-Str. 100
91058 Erlangen, Deutschland

1 Einleitung

Moderne Hörgeräte sind fortschrittliche Hörcomputer und sind seit langem schon in der modernen vernetzten Welt gut eingebunden. Aufgrund seiner Größe und der vorherrschenden Integrationskomplexität eines Hörgerätes ist die elektromagnetische Feldsimulation vor allem für die Integration von Funksystemen ein notwendiges und unverzichtbares Handwerkszeug.

So kann die Antennenperformance am Kopf wie auch die Störeinkopplung von internen getakteten Komponenten in die Funksysteme nur mit Hilfe von Simulationen abgeschätzt werden. Die Simulation trägt außerdem dazu bei, die Anzahl an Iterationszyklen zu verringern oder bereits in ersten Hardwareaufbauten gute Ergebnisse zu erzielen.

In diesem Artikel sollen aber nicht nur die Vorteile der Simulation und der Reifegrad der einzelnen Simulationsverfahren hervorgehoben werden, sondern auch die Möglichkeiten, die sich einer Firma bieten, Simulation nachhaltig einzuführen, z.B. durch personelle Organisation oder Prozesse.

2 Der Aufbau von Hörgeräten

Heutzutage bieten Hörgeräte wesentlich mehr als die klassische Hörverstärkung mittels Mikrofone und einem integrierten Lautsprecher. In Abbildung 1 wird der prinzipielle Aufbau gezeigt.

2.1 Mechanischer Aufbau

Das Gerät besteht aus zwei Mikrofonen, einem Stecker für einen externen Lautsprecher (receiver in canal, RIC), einem Lithium-Ionen (Li-Ion) Akkumulator und einem galvanischen Ladekontakt.

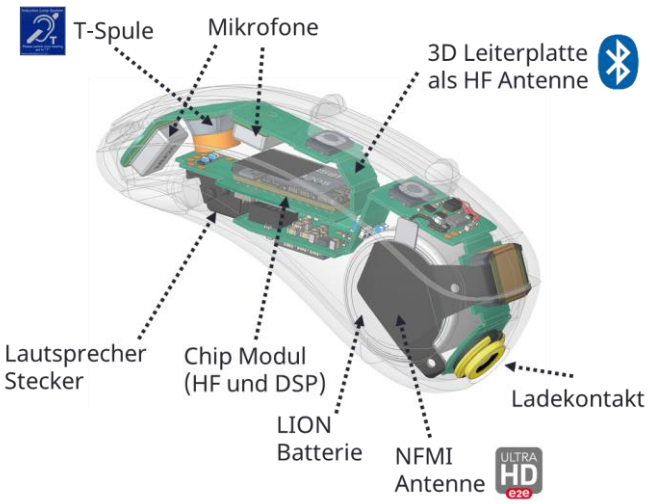

Abbildung 1: Aufbau eines modernen Hörgeräts

Die Leiterplatte ist flexibel und 4-lagig mit einer Dicke von 200um aufgebaut, wobei sie sehr komplex um mehrere Achsen in dem Gehäuse gefaltet wird. Die integrierten Schaltungen sind auf dem Chip-Modul untergebracht und beinhalten eigenentwickelte Integrierte Schaltungen (ICs), Signalprozessoren (DSPs) sowie den Bluetooth Chip, der die Hochfrequenz (HF) Antenne ansteuert.

Die HF Antenne ist dabei nicht als eigene Komponente aufgebaut, sondern durch eine geeignete Unterteilung der vorhandenen Kupferflächen auf der Leiterplatte als Dipol realisiert. Die Near Field Magnetic Induction (NFMI) Antenne besteht aus einem kleinen Kern und verbundenen magnetischen Folien. Die Tele (T)- Spule stellt ebenfalls eine Stabkernantenne dar.

2.2 Funktion der Funksysteme

Bei diesem Hörgerät gilt es drei verschiedene Funksysteme auf engstem Raum zu integrieren (siehe Tabelle 1). Das T-Spulen System nutzt dabei die Magnetfelder von Telefonlautsprechern oder Induktionsschleifen an speziell ausgezeichneten Plätzen und leitet dieses magnetische Signal elektrisch in den Signalpfad weiter. Das NFMI System vernetzt die Hörgeräte untereinander. Die Integration des Bluetooth Systems stellt den höchsten Aufwand dar, da Wellenausbreitung und vielfältige Kopplungseffekte berücksichtigt werden müssen.

Tabelle 1: Übersicht der Funksysteme

Funksystem	Frequenz	Art	Funktion
T-Spule	Akustisch	Magnetisch Induktiv	- Magnetfeldaufnahme von Telefonlautsprecher - Magnetfeldaufnahme von spez. Infrastruktur
NFMI	3,28 MHz oder 10,6 MHz	Magnetisch Induktiv	- Kopplung u.a. der Lautstärke zwischen Hörgeräten - Austausch von Audiosignalen zwischen Hörgeräten zur binauralen Signalverarbeitung
Bluetooth	2450 MHz	Wellenausbreitung	- Steuerung des Hörgeräts über APPs - Musikhören über Smartphone - Telefonieren über Smartphone

3 Elektromagnetische Simulation von Hörgeräten

Im Jahr 2004 hat der WSA Vorgänger Siemens Audiologische Technik GmbH mit der Hörgerätelinie ACURIS das erste NFMI Funksystem für die Vernetzung von Hörgeräten auf den Markt gebracht. Auch wenn die Datenraten sehr überschaubar waren, wurde hier bereits elektromagnetische Feldsimulation in FEKO zur Bestimmung der Antennenparameter und optimaler Einbauorte genutzt. Heutzutage wird bei WSA hauptsächlich die Simulia CST Studio Suite eingesetzt.

3.1 Gebogene mehrlagige Leiterplatten

Wie in Abbildung 1 gezeigt, ist die dünne Leiterplatte mehrfach um verschiedene Achsen gebogen. Viele Programme zur Entwicklung von Leiterplatten arbeiten nur in zwei Dimensionen und können gebogene Modelle nicht geeignet exportieren.

Deswegen muss bei WSA für die Modellierung in CST Studio Suite die Leiterplatte noch gebogen werden. Lange Zeit wurde dafür ein aufwändiger Prozess eingesetzt, der die Hürde zur Nutzung der Simulation extrem hoch angesetzt und Simulation parallel zum eigentlichen Entwicklungsprozess erschwert hat [1]. Seit 2020 ist es jedoch möglich, die automatische Biegung der Leiterplatte direkt beim Import durchzuführen. Die Simulationsanwender können nun schnell eine modellierbare Leiterplatte mit allen Einzelheiten und korrekten elektrischen Netznamen erzeugen (siehe Abbildung 2). Dies bedeutete einen großen Schritt in die Richtung, Simulationen parallel zur Designphase der Leiterplatten einzusetzen.

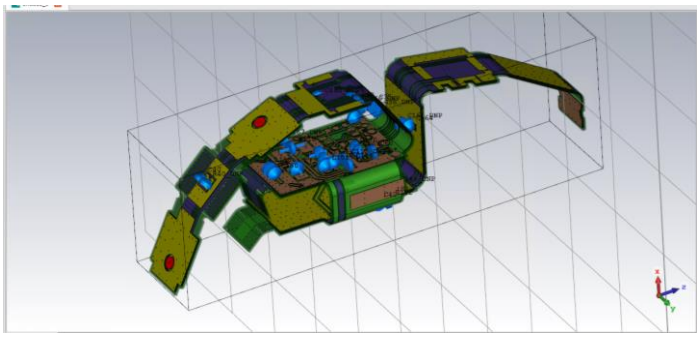

Abbildung 2: Eine Leiterplatte des Hörgeräts direkt nach dem Import inklusive automatischer Biegung

Die Modelle können damit problemlos mit einem tetrahedralen Netz vernetzt und im Frequenzbereich simuliert werden. Simulationen in Zeitbereich erfordern dagegen ein hexahedrales Netz, also die Zerlegung in rechteckige Blöcke und können nicht alle Details auflösen. Hier muss also die Leiterplatte noch vereinfacht werden.

3.1.1 Simulation der magnetischen Antennen (T-Spule, NFMI)

Für die Simulation der magnetischen Antennen ist keine Leiterplatte erforderlich, außer der Einbauort nimmt Einfluss auf die Antennenparameter L (Induktivität), ESR (Äquivalenter Serienwiderstand) und A_e (Äquivalente magnetischer Fläche). Für die T-Spule müssen diese Parameter im akustischen Frequenzbereich, z.B. 5 kHz bestimmt werden, für die NFMI Antennen bei Frequenzen von 3,28 MHz oder 10,6 MHz.

Wichtig für beide Antennen ist die Modellierung der Kernmaterialien mit der richtigen magnetischen Permeabilität, die entweder vom Hersteller im Datenblatt vorliegt oder iterativ durch Parameterstudien bestimmt werden muss. Die Kopplung des Stabkerns der NFMI Antenne wird durch weich-magnetische Folien an den Seitenfläche der Batterie noch verstärkt.

Zur Modellierung der Windungen wird jeweils ein spezielles Dünndraht Modell verwendet, welches nicht extra vernetzt werden muss. Da die T-Spule mehr als 10000 Windungen umfasst, werden die Windungen hier außerdem durch ein äquivalentes Windungsmodell mit je einer Lage außen und innen mit wenigen Windungen ersetzt (siehe Abbildung 3a). Beide Maßnahmen helfen, Simulationszeit zu sparen. In Abbildung 3b sind die Feldlinien der NFMI Antenne gezeigt, wodurch sehr gut die Wirkung der weich-magnetischen Folien zur Erhöhung der Antennenperformance erkennbar wird.

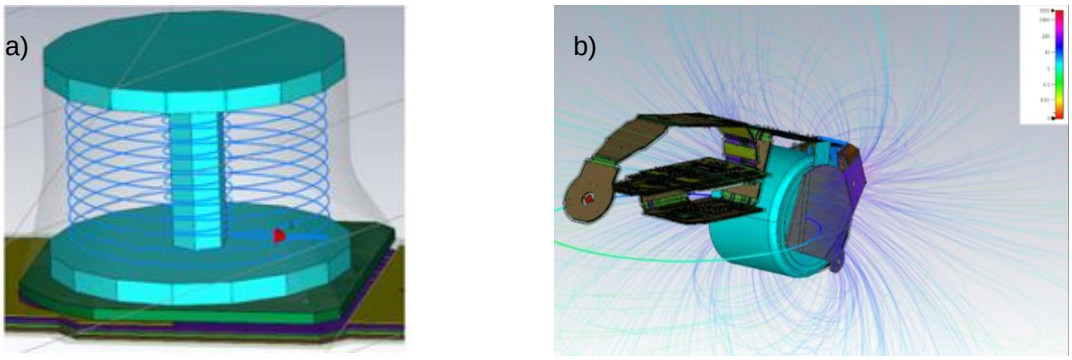

Abbildung 3: Modell der T-Spule (a) und Simulation der NFMI Antenne (b)

3.1.2 Simulationen der HF Antennen

Moderne Hörsysteme sollen möglichst klein und unsichtbar sein, was im Gegensatz zu den Größenanforderung einer klassischen HF Antenne bei einer Betriebsfrequenz von 2,45 GHz steht. Zur Veranschaulichung soll hier auf einen einfachen λ/2 Dipol verwiesen werden, der im gewünschten Band eine Gesamtlänge von 12,5 cm einnimmt. Dieser Platz ist bei weitem im Hörgerät nicht vorhanden, was die Entwicklung einer solchen Antenne sehr herausfordernd macht.

In Abbildung 4a ist die Tragesituation zwischen Kopf und Ohr gezeigt, welche erheblichen Einfluss auf die Funktion der Antenne hat. Metallische Komponenten innerhalb des Hörgeräts sowie das Hörgerätegehäuse nehmen ebenfalls Einfluss auf die Antennenparameter Abstrahleffizienz, Bandbreite und Körperwellenausbreitung. Nur über die genaue Kenntnis von einschränkenden Effekten können die Miniaturantennen für die Integration in ein Hörgerät optimiert werden. In Abbildung 4b ist die Vernetzung mittels eines tetrahedralen Netzes gezeigt. Das Fernfelddiagramm in Abbildung 4c bestimmt, wie gut die Antenne rund um den Kopf abstrahlt. Daraus lässt sich die Abstrahleffizienz bestimmen.

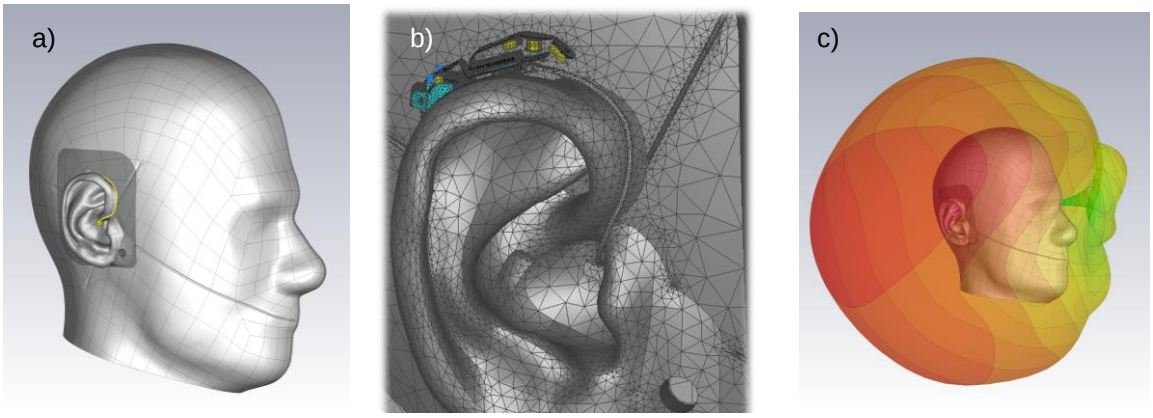

Abbildung 4: Darstellung der Simulationsumgebung (a), vernetztes Modell (b), Fernfelddiagramm (c)

3.2 Simulation der Elektromagnetischen Verträglichkeit

Ein wichtiger Punkt bei der Integration der Funksysteme in Hörgeräte ist es, Störeinkopplungen in die Funksysteme zu vermeiden. Egal ob diese intern vom Hörgerät selbst erzeugt werden oder durch externe Einflüsse vorgegeben werden, wie z.B. bei der Elektrostatischen Aufladung (ESD) oder bei vorgegebenen externe Störfelder von Smartphones oder anderen Funksystemen (EMS).

3.2.1 Interne Störeinkopplung in die Funksysteme

Interne Störungen im Hörgerät sind oft unvermeidlich und werden beispielsweise durch getaktete Mikroprozessoren oder Spannungsversorgungs-Komponenten verursacht. Die genaue Modellierung der Störquellen erfordert tiefes Expertenwissen, zum einen in der verbauten internen Elektronik, zum anderen in deren richtiger Modellierung und Simulation.

Der physikalische Vorgang lässt sich sehr einfach mit der Störeinkopplung in die T-Spule beschreiben (siehe Abbildung 5). Der Strom, der im externen Lautsprecher das Schallsignal erzeugt, muss über Zuleitungen auf der Leiterplatte und den Stecker geführt werden. Der Strom erzeugt ein Magnetfeld, welches in die T-Spule einkoppelt. Geeignete Leitungsführungen können in diesem Fall die Einkopplung minimieren.

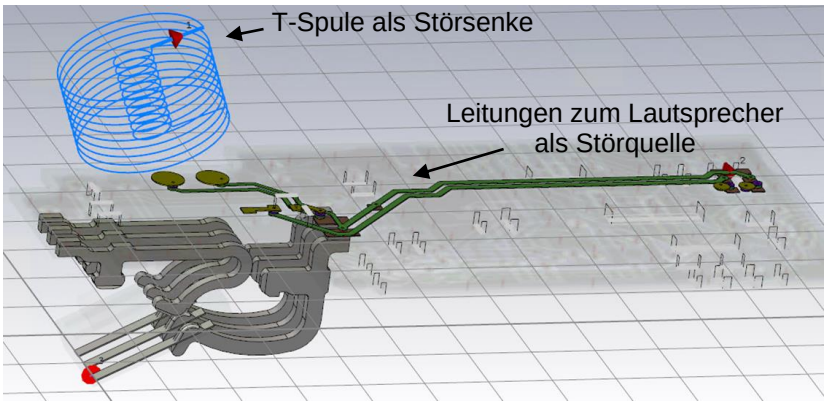

Abbildung 5: Simulation der Störeinkopplung durch Ströme in der Lautsprecherleitung

Auch wenn bei der Simulation von Störeinkopplungen in die NFMI Antenne magnetische Kopplungen ebenfalls den dominierenden Effekt darstellen, spielt das Dielektrikum der Leiterplatte und ebenfalls die Verteilungsnetze der ICs eine Rolle und müssen bei der Nachbildung der Störquelle meistens mit berücksichtigt werden. Abbildung 6a zeigt eine Einkopplung verursacht durch eine unsachgemäß verlegte Leitung / platzierte Kondensatoren der Spannungsversorgung.

Den höchsten Aufwand stellt die Simulation der Störeinkopplung bei HF Antennen dar. Hier muss das Gehäuse und die Umgebung des Hörgeräts am Ohr ebenfalls mit modelliert und simuliert werden, sowie die Leiterplatte mit allen Details vorliegen. Weiterhin ist gerade die Modellbildung der Störquellen aufgrund oft unbekannter Parameter der verwendeten ICs in diesem Frequenzbereich sehr schwierig. Stattdessen kann aber auch auf einen reziproken Ansatz zurückgegriffen werden [2]. Abbildung 6b zeigt das elektrische Feld bei Antennenanregung. Bereiche mit niedriger Feldstärke (blau oder grün) eigenen sich hier besonders für ICs, die als potenzielle Störquellen agieren.

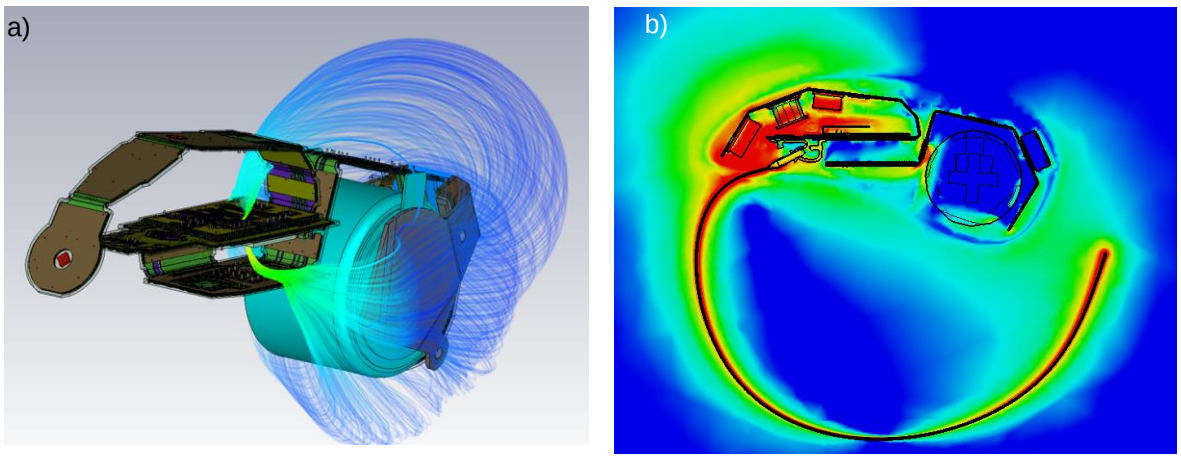

Abbildung 6: Störeinkopplung in die NFMI Antenne (a) und Bluetooth Antenne (b)

3.2.2 Externe Störeinkopplung

Hörgeräte unterliegen als Medizinprodukt, aber auch wegen den verbauten Funksystemen einer Vielzahl von Normen zur Prüfung der Robustheit im Bereich ESD oder EMS, z.B. EN 301 489. Simulationen in diesem Bereich sind absolute Experten-Simulationen und außerdem nicht immer durch lineare Simulationen darstellbar. Beispielweise wird bei der Messung mit einem ESD Puls als Messgröße nur festgehalten, ob sich relevante Systemparameter im Hörgerät ändern oder ein Neustart stattfindet. In der Simulation kann die Ausbreitung der Störung sehr gut simuliert werden, die Korrelation mit den Messungen stellt aber einen sehr komplexen nichtlinearen Vorgang dar.

3.3 Betrachtung der Komplexität

Es lassen sich zwei einfache Aussagen treffen. Mit steigendem Frequenzbereich steigt die Anzahl an relevanten Komponenten zur Simulation an, gleichzeitig muss aber auch die Vernetzung immer feiner durchgeführt werden, was den Rechenaufwand ebenfalls steigen lässt. Antennen Simulationen sind gut beherrschbar und zeigen einen hohen Reifegrad. Bei Störeinkopplungen hingegen kann die Störquelle u.a. nur sehr komplex modellierbar sein und nicht immer eine unmittelbare Verifikation durch Messungen ermöglichen. Gerade letztere Simulationen sind noch Experten-Simulationen.

4 Organisation und Infrastruktur der Simulationen

Die Organisation und die Infrastruktur ist bei WSA historisch gewachsen und hat sich sowohl der Leistungsfähigkeit der Werkzeuge als auch einer globalen Arbeitsweise gut angepasst.

4.1 Infrastruktur

Es kommen an den drei Standorten in Singapur, Lynge (Dänemark) und Erlangen (Deutschland) jeweils ein lokaler Verbund von Simulationsservern zum Einsatz. Dies bietet insgesamt den besten Kosten-Nutzen Faktor für eine 24-7 Simulation, wobei auf unterschiedliche Zeitzonen keine Rücksicht genommen werden muss.

In Erlangen beispielsweise befinden sich Server spezialisiert auf Modellierung, Simulationen im Frequenzbereich und im Zeitbereich. Insgesamt stehen 144 Kerne, 2,5 TB RAM und sechs NVIDIA Tesla Beschleunigerkarten zur Verfügung.

Modellierung und Parametrisierung wird an jedem Standort über einen Remote Desktop Zugriff auf die Server durchgeführt, wobei handelsübliche Bürocomputer verwendet werden. Zur Simulation wird die Funktion verteiltes Rechnen verwendet, d.h. die Simulationen werden lokal in eine Warteschlange gestellt und nacheinander abgearbeitet.

Global nur einmal verfügbar ist die von WSA erstellte Bibliothek, welche Komponenten wie die T-Spulen, NFMI Antennen, IC Störmodelle u.vm. enthält. Alle Komponenten unterliegen einer Versionierung und beinhalten eine Dokumentation. In diese Bibliothek werden nur Modelle eingepflegt, welche durch Messungen gut und mehrfach verifiziert sind.

4.2 Personelle Organisation

Wie bei vielen Unternehmen hat auch bei WSA die elektromagnetische Simulation sehr einfach begonnen. Nach einigen Evaluierungen wurde ein kommerzielles Simulationwerkzeug beschafft und ein Simulationsexperte benannt. Die Zunahme der Simulationen als auch der Wunsch nach Simulations-Demokratisierung hat zum Rollenmodell in Abbildung 7 geführt.

Abbildung 7: Rollenmodell der Simulationsanwender

Die unterste Stufe zeigt „Simulations User“, die Basiswissen in der Simulation aufgebaut haben und in anderen Bereichen Experten sind. Sie werden bei dem Review der Simulationsergebnisse von den „Simulations Experten“ unterstützt, welche in einem oder mehreren Simulationsbereichen Experten sind. Die oberste Stufe stellen die „Simulations Key Experten“ dar, welche pro Standort nur einmal existieren und einen gewissen Anteil ihrer Arbeitszeit für Simulationen und Networking innerhalb und außerhalb von WSA aufbringen sollen. Nach diesem Modell arbeiten mittlerweile 20 Anwender an allen drei Standorten mit steigender Tendenz.

4.3 Prozesse

Auch wenn die Simulation mittlerweile entwicklungsbegleitend erfolgt, kann das vorrangige Ziel, Iterationszyklen zu verringern nicht uneingeschränkt erreicht werden, da auch andere Disziplinen bedient werden müssen wie z.B. Aufbautechnik, Chipentwicklung, Prototypenstudien u.v.m.

Die elektromagnetische Feldsimulation führt jedoch mittlerweile zu mehr zielgerichteten Varianten und guten Ergebnissen schon in der ersten Iteration. Im ersten Hörgerät einer neuen Plattform dient die Simulation vor allem dazu, neue Effekte zu verstehen, durch Messungen zu verifizieren und neue Modelle für die Bibliothek zu generieren. In der vorgelagerten Architekturphase geht es um generelle Machbarkeit und Platzierung von Komponenten. Bei allen nachgelagerten Hörgeräten einer neuen Plattform dient die Simulation zur Vorhersage von Problemen und Performance. Abgeleitete Geräte sind kleine Modifikationen im Vergleich des bereits existierenden Originalgeräts, hier wird die Simulation nur bei Bedarf und zum Verstehen von Problemen eingesetzt. Der Prozess ist vereinfacht in Tabelle 2 dargestellt und hilft, einen guten Kosten-Nutzen Faktor einzuhalten.

Tabelle 2: Einfache Darstellung des Simulationsprozesses

Beschreibung	Architektur-Phase	Erstes Hörgerät neue Plattform	Spezielle Formfaktoren	Abgeleitete Geräte
Häufigkeit	Bei Bedarf	Immer	Zielgerichtet	Bei Bedarf
Aufwand Modellierung	Mittel	Hoch	Niedrig / Mittel	Niedrig
Rolle	Experte	(Key) Experte	User / Experte	User / Experte
Nutzen	Hoch	Mittel / Hoch	Hoch	Mittel
Tätigkeiten	- Machbarkeit - Platzierbarkeit	- Modellgenerierung für Bibliothek - Verstehen von Problemen und Performance	- Vorhersage von Problemen und Performance	- Verstehen von Problemen

5 Zusammenfassung und Ausblick

In diesem Artikel wurde gezeigt, dass Hörgeräte ein vielfältiges Innenleben besitzen, welcher die Entwicklung der Antennen für die verschiedenen Funksysteme und deren Integration sehr herausfordernd macht.

Die elektromagnetische Feldsimulation ist ein sehr gutes Werkzeug, die Herausforderungen zu verringern oder Komponenten zu entwerfen, die schwerlich oder nicht zielgerichtet ohne Simulation entwickelt hätten werden können.

Es wurde gezeigt, dass die Antennensimulationen gut beherrschbar sind und dass die Simulation von Störeinkopplung immer noch ein Expertengebiet darstellt. Prozesse, Infrastruktur und Rollen sind so angepasst, das größtmögliche Kosten-Nutzen Verhältnis zu erreichen und die Simulation auf längere Sicht nachhaltig zu betreiben.

Vor allem die Simulation von externen Störeinkopplungen steckt bei WSA noch in den Anfängen und wird momentan mit zahlreichen internen und externen Forschungsprojekten weiter ausgebaut.

6 Literatur

[1] Fischer T.: “Handling of complex bended multilayer PCB structures”, CST Usergroup Meeting 2015, Darmstadt

[2] Mantzke A., Leone M., Fischer T.: „Efficient analysis and reduction of magnetic near-field-coupling in mixed-signal PCBs via the reciprocity principle”, IEEE International Symposium on Electromagnetic Compatibility (EMC) 2015, Dresden

EMV-Schirmung und Thermik - Auf der Suche nach der besten Lösung

Jochen Kinzig (Cenit AG)

1 Einleitung

Elektrische Geräte müssen gesetzliche oder auch vom Kunden vorgegebene Anforderungen an die elektromagnetische Verträglichkeit (EMV) erfüllen. Häufig wird ein geschirmtes Gehäuse verwendet, um die Abstrahlung von Störungen zu reduzieren. Ein vollständig geschlossenes Gehäuse wäre hinsichtlich der elektromagnetischen Abschirmung optimal, würde aber zu einem Wärmestau im Gerät führen, da sich die elektronischen Bauteile durch die Verlustleistung erwärmen. Lüftungsöffnungen schaffen hier Abhilfe, wirken sich aber negativ auf die elektromagnetische Abschirmung (sog. Schirmdämpfung) aus. Dieser Zielkonflikt kann nur durch die gemeinsame Betrachtung beider Fragestellungen aufgelöst werden. Nicht nur die EMV-Abschirmung, sondern auch die thermische Kühlung müssen gleichzeitig analysiert werden. Eine parametrische Studie gibt einen tiefen Einblick in die beeinflussenden Parameter und hilft dem Entwickler, die beste Lösung zu finden. Zu diesem Zweck werden Design of Experiments- und Metamodell-Techniken eingesetzt, um eine Designraumerkundung in wirtschaftlich vertretbarer Zeit zu ermöglichen. Dieser Workflow wird für ein Beispielgerät mit EMV-Abschirmung und integriertem Lüfter exemplarisch dargestellt. Es wird gezeigt, wie mit einer interaktiven Designraumerkundung eine Lösung gefunden werden kann und was die Vorteile dieser Vorgehensweise gegenüber einer automatischen Mehrzieloptimierung sind.

2 Allgemeine Anforderungen an ein Schirmgehäuse

Beim sogenannten Common Mode fließen Ströme an einem differenziellen Paar gleichzeitig auf beiden Leiterbahnen in dieselbe Richtung. Damit der Stromkreis geschlossen bleibt, fließen die Ströme über das Schirmgehäuse zurück zur Quelle. Bei höheren Frequenzen wird dies immer in der Nähe des Hin-Strompfades passieren, damit die Induktivität und damit die Impedanz möglichst niedrig bleibt. Treten auf diesem Rückstrompfad aufgrund von Öffnungen im Gehäuse Impedanzsprünge auf, entstehen abgestrahlte Störungen, d.h. die Schirmwirkung des Gehäuses sinkt. Wenn es dennoch erforderlich ist, Öffnungen im Rückstrompfad vorzusehen, sollten diese so gestaltet werden, dass die Impedanz möglichst wenig erhöht wird. So kann es beispielsweise sein, dass sich ein langer Spalt nur wenig auf die Schirmdämpfung auswirkt, wenn er nahezu parallel zur Rückstromrichtung liegt. Dahingegen kann bereits ein kurzer Spalt problematisch sein, wenn dieser quer zur Stromrichtung liegt. In Abschnitt 5.2 wird verdeutlicht, wie groß die Auswirkung einer ungünstigen Spaltausrichtung sein kann.

3 Simulation des Schirmgehäuses

Die Methode der Designraumerkundung wird an dem in Abb. 1 gezeigten Gehäuse vorgestellt. Im Innern des Gehäuses befindet sich eine Platine mit elektronischen Komponenten. Im Gehäusedeckel sind Lüftungsschlitze vorgesehen mit einem aktiven Lüfter, angebracht an der Unterseite der Lüftungsschlitze. Der Spalt zwischen Gehäuse und Gehäusedeckel wird in diesem Modell vernachlässigt, um das Augenmerk gezielt auf den Einfluss der Gestaltung der Lüftungsschlitze zu legen. In der Realität wird ein solcher Spalt immer vorhanden sein (z.B. Dichtungsmaterial oder Aluminiumoxid-Schicht) und er spielt eine sehr große Rolle, da er quer zur Rückstromrichtung liegt. Für eine gute Schirmdämpfung muss durch geeignete Schrauben und sonstige Kontaktierungsmaßnahmen ein niederimpedanter Strompfad sichergestellt werden [1]. Dies soll hier aber nicht näher betrachtet werden. Das Gehäuse wird hinsichtlich EMV (Schirmdämpfung) und Thermik untersucht. Für die Schirmdämpfung wird ein differenzielles Leiterpaar im Common Mode angeregt. Im Abstand von 3m in alle Richtungen (kugelförmige Anordnung der Messstellen) werden die E-Felder ausgewertet. Diese Berechnung wird einmal mit Gehäuse und einmal ohne Gehäuse durchgeführt. Aus dem Verhältnis der berechneten E-Felder wird die Schirmdämpfung ermittelt. In der dafür verwendeten Software CST Studio Suite gibt es hierzu fertige Makros, die vom Anwender zur Auswertung genutzt werden können. Für die thermische Berechnung wird im vorliegenden Fall der in CST Studio Suite integrierte CHT Solver genutzt, mit dem auch die durch den Lüfter erzeugte Luftströmung simuliert werden kann. In Abb. 2 sind die Ergebnisse der beiden Berechnungsdisziplinen gezeigt. Es zeigt sich, dass für die dargestellte Konfiguration die erlaubten Grenzwerte nicht eingehalten werden. Die Schirmdämpfung liegt deutlich unterhalb der geforderten 40dB und die max. Temperatur überschreitet die erlaubten 150°C.

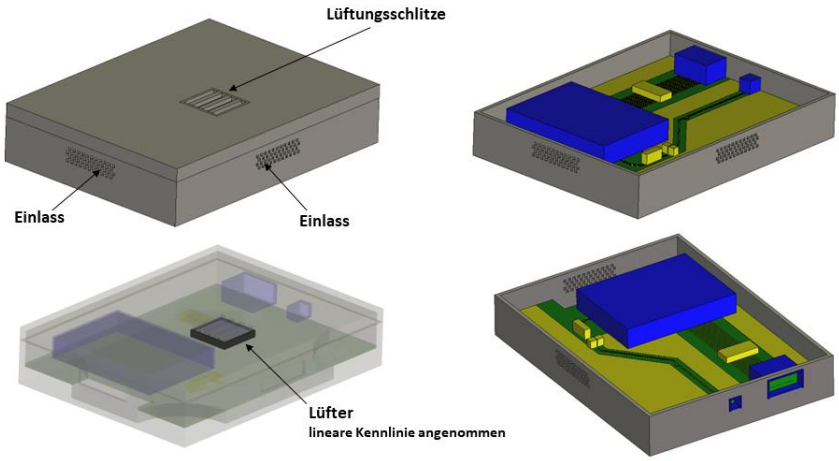

Abb. 1
Beispielmodell: Platine in einem Aluminiumgehäuse.

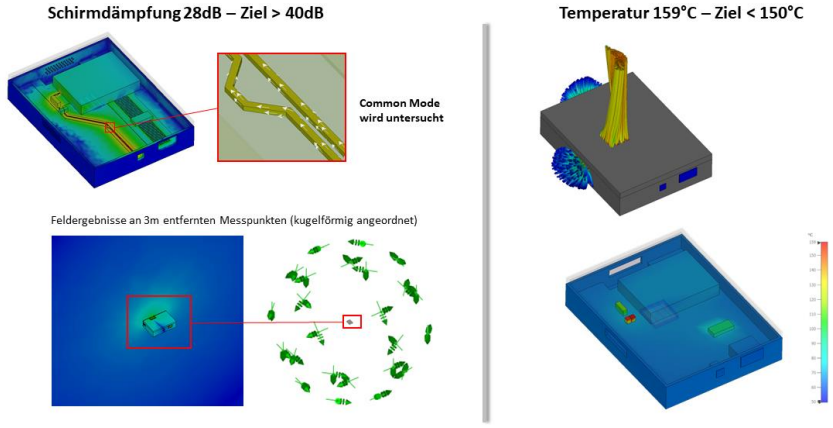

Abb. 2
Schirmdämpfung (links) verfehlt die Anforderung deutlich und Temperatur (rechts) liegt ebenfalls über der maximal erlaubten Temperatur

4 Optimierung der Schirmdämpfung und des Kühlungsverhaltens

4.1 Prinzipielle Vorgehensweise bei der Optimierung

Für die Mehrzieloptimierung wird die Software Isight verwendet, mit der die Design-Parameter (Design Variablen) automatisiert verändert und anschließend die Simulationen gestartet werden. Im vorliegenden Fall wird mit zwei Design Variablen begonnen, der x- und der y-Position des Lüfters und der zugehörigen Öffnungen (Richtungsdefinitionen s. Abb. 7). Die Schirmdämpfungsberechnung läuft mit ca. 10 Minuten Rechenzeit vergleichsweise schnell. Die thermische Berechnung benötigt aufgrund der Luftströmung allerdings mehr als 4 Stunden. Da bei einer Mehrzieloptimierung, je nach Algorithmus, mehr als 100 Optimierungsiterationen nötig sein können, wird hier nicht direkt auf den Ergebnissen der 3D-Berechnungen optimiert, sondern ein Zwischenschritt eingeführt, die Erstellung sogenannter Metamodelle. Metamodelle sind mathematische Ersatzmodelle, die auf Basis von Berechnungs- oder Versuchsergebnissen erstellt werden. Für das vorliegende Beispiel werden die Parameter in einer DoE mit dem Latin Hypercube Sampling verteilt. Mit diesen Parametern werden die 3D-Simulationsmodelle berechnet. Die DoE erstellt die Eingangsparameter mit dem Ziel, dass mit möglichst wenig Berechnungen eine gute Vorhersage im Parameterraum möglich ist. Die Metamodelle werden mit „Elliptical Basis Functions“ erstellt. Da Metamodelle sehr schnell rechnen, kann die Optimierung mit Hilfe von globalen Verfahren erfolgen, die üblicherweise viele Iterationen benötigen, aber auch lokale Optima sehr zuverlässig finden. Als Optimierungsalgorithmus wird hier AMGA (Archive-Based Micro Genetic Algorithm) verwendet [2], der sehr gut für Mehrzieloptimierungen geeignet ist.

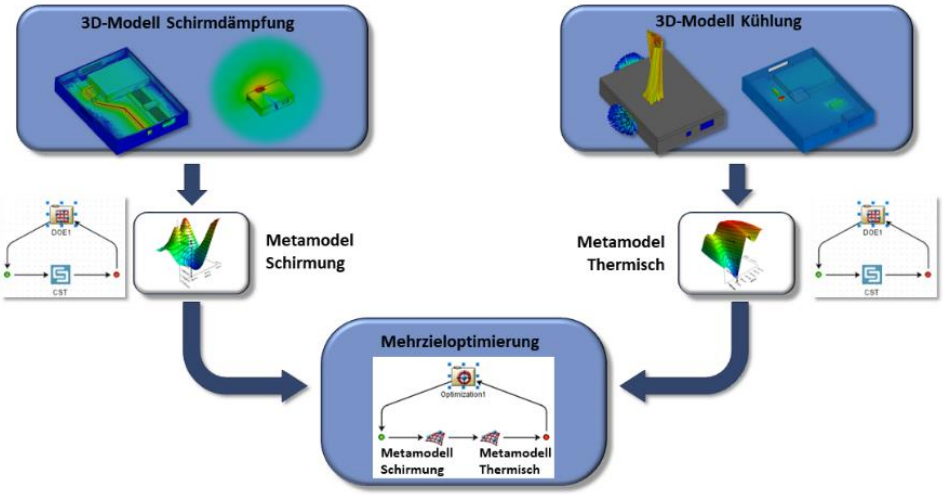

Abb. 3
Metamodelle als Zwischenstufe ermöglichen eine Mehrzieloptimierung mit vielen Iterationen

4.2 Designraumerkundung als Alternative zur Mehrzieloptimierung

Metamodelle bieten neben der Nutzung bei der automatischen Mehrzieloptimierung eine weitere, sehr attraktive Anwendungsmöglichkeit. Dies wird im Folgenden als Designraumerkundung bezeichnet. Die Idee ist, Metamodelle als interaktives Vorhersagemodell zu nutzen. Abb. 5 zeigt das Temperatur-Metamodell unseres Gehäuses mit zwei Eingangsparametern. Im 2D-Farbbild ist die maximale Temperatur im Gehäuse dargestellt, abhängig von der x- und der y-Position des Lüfters.
Kommen weitere Parameter hinzu, können diese beispielsweise mit Schiebereglern variiert werden und das 2D-Farbbild ändert sich interaktiv. Der Anwender kann auf diese Weise in Echtzeit untersuchen, welchen Einfluss eine Parameteränderung auf das Ergebnis hat. Die automatische Mehrzieloptimierung liefert demgegenüber nur die beste Lösung. Der Vorteil der Designraumerkundung ist also, dass der Nutzer mit Hilfe von Metamodellen Zusammenhänge besser verstehen kann und somit schnell einen tieferen Einblick in sein Produkt erhält. Selbstverständlich bedeutet eine solche Designraumerkundung etwas mehr manuellen Aufwand als eine automatische Optimierung. Wird der große Nutzen des Erkenntnisgewinns gegenübergestellt, ist dieser Mehraufwand häufig gerechtfertigt.

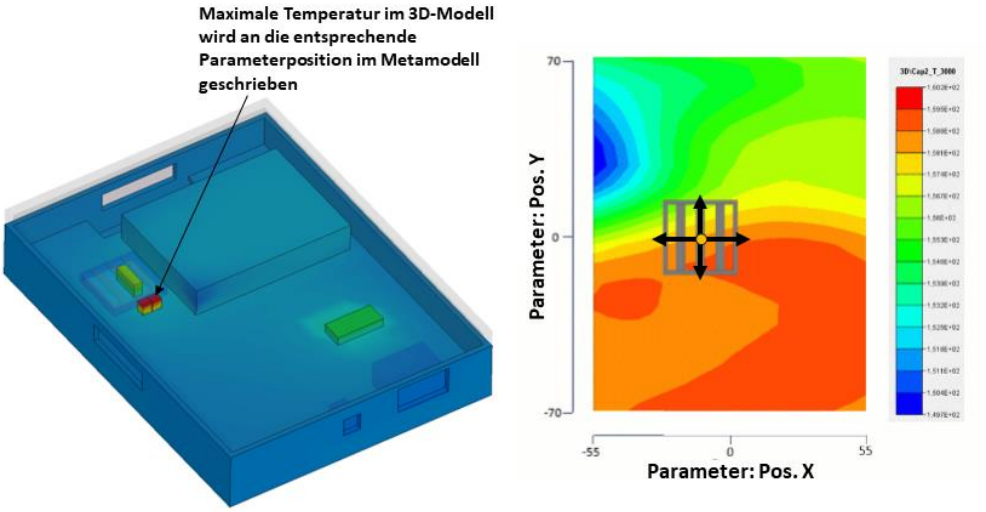

Abb. 4
Darstellung eines Metamodells mit zwei Parametern, am Beispiel der maximalen Bauteiltemperatur. Bei mehr als zwei Parametern können die restlichen Parameter z.B. über Schieberegler eingestellt werden und die 2D-Darstellung ändert sich interaktiv.

5 Vergleich der Ergebnisse aus Mehrzieloptimierung und Designraumerkundung

5.1 Ergebnisse mit 2 Parametern

Um die Stärken der Designraumerkundung zu veranschaulichen, wird für das Beispielgehäuse die beste Lösung sowohl mit einer automatischen Mehrzieloptimierung als auch mit Hilfe einer Designraumerkundung gesucht. Abb. 5 zeigt das Ergebnis der Designraumerkundung. Das Metamodell für die Temperatur (links im Bild) zeigt, dass es nur einen kleinen Bereich gibt, in dem der Lüfter liegen muss. Das Metamodell für die Schirmdämpfung (rechts im Bild) zeigt einen großen Bereich, der bei entsprechender Positionierung des Lüfters die Anforderungen an die Schirmdämpfung nicht erfüllt. Leider liegt der Bereich, in dem der Lüfter liegen muss, um die Temperaturanforderung zu erfüllen, mitten in dem Bereich, der aus EMV-Sicht zu vermeiden ist. Es gibt hier also einen klaren Zielkonflikt, der offensichtlich nicht mit nur zwei Design Variablen zu lösen ist. Die Mehrzieloptimierung zeigt übrigens das gleiche Ergebnis. In Abb. 6 ist die Paretokurve zu sehen, also die Kurve, entlang der alle optimalen Ergebnisse für beide Ziele liegen. Keine dieser optimalen Lösungen liegt innerhalb des Zielbereichs (Schirmdämpfung>40dB, Temperatur<150°C).

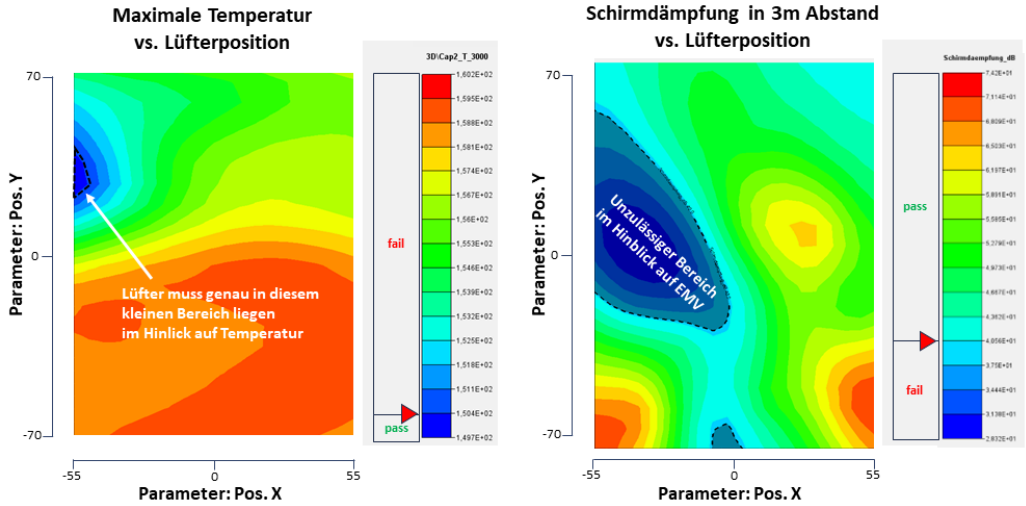

Abb. 5
Zielkonflikt: Um die max. zulässige Temperatur nicht zu überschreiten, müssen die Lüftungsöffnungen in einem Bereich liegen, in dem sie die Schirmdämpfung unzulässig herabsetzen würden.

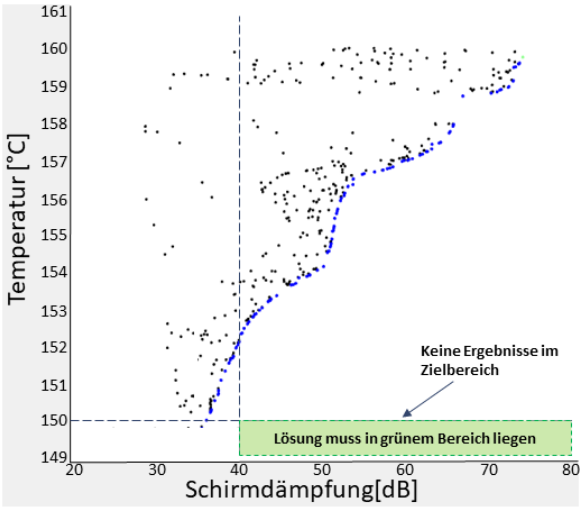

Abb. 6
Eine Paretokurve (blaue Punkte) stellt die besten, möglichen Lösungen dar. Die Paretokurve liegt komplett außerhalb des Zielbereichs. Der Zielkonflikt ist also auch in der Mehrzieloptimierung zu sehen.

5.2 Ergebnisse mit 3 Parametern

Um den Zielkonflikt zu lösen, müssen demnach zusätzliche Design Variablen eingeführt werden. Positiv ist hierbei zu erwähnen, dass die vorhandenen Daten, die mit zwei Parametern erstellt wurden, wiederverwendet werden können, um ein Metamodell mit zusätzlichen Parametern zu erstellen. Die Metamodelle können also im Laufe der Zeit mit Daten gefüttert werden und „wachsen“. Im gezeigten Beispiel wird ein zusätzlicher Parameter eingeführt, die Rotation der Lüftungsschlitze (in Abb. 7 „Rot. Z“ genannt). Wie bereits vorher erwähnt, gibt es die Möglichkeit, den Designraum mit Schiebereglern interaktiv zu erkunden, falls mehr als zwei Parameter verwendet werden. Abb. 8 zeigt die 2D-Farbdarstellung des Schirmdämpfungs-Metamodells für drei Winkelpositionen. Als Zielbereich ist der Bereich eingezeichnet, in dem der Lüfter liegen muss, um eine möglichst niedrige Temperatur zu erreichen. Bei einem Winkel von +60° wird eine Schirmdämpfung von 60dB erreicht, wenn die Lüftungsschlitze im Zielbereich liegen. Hier kann also sowohl die Temperaturanforderung erfüllt werden als auch die Schirmung. Bei einer entgegengesetzten Verdrehung von -60° wiederum wird die Schirmung noch schlechter als im Ausgangszustand.

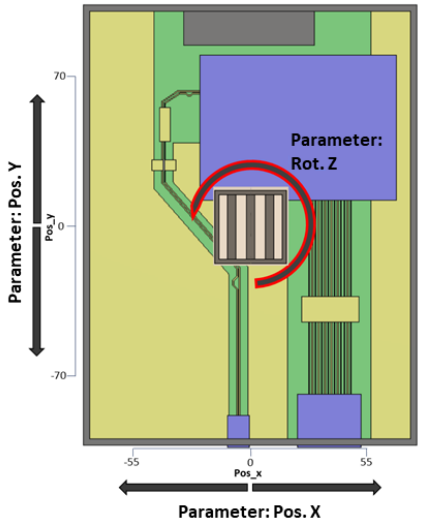

Abb. 7
Zur Auflösung des Zielkonflikts werden die Metamodelle um einen dritten Parameter ergänzt – die Rotation der Lüftungsschlitze

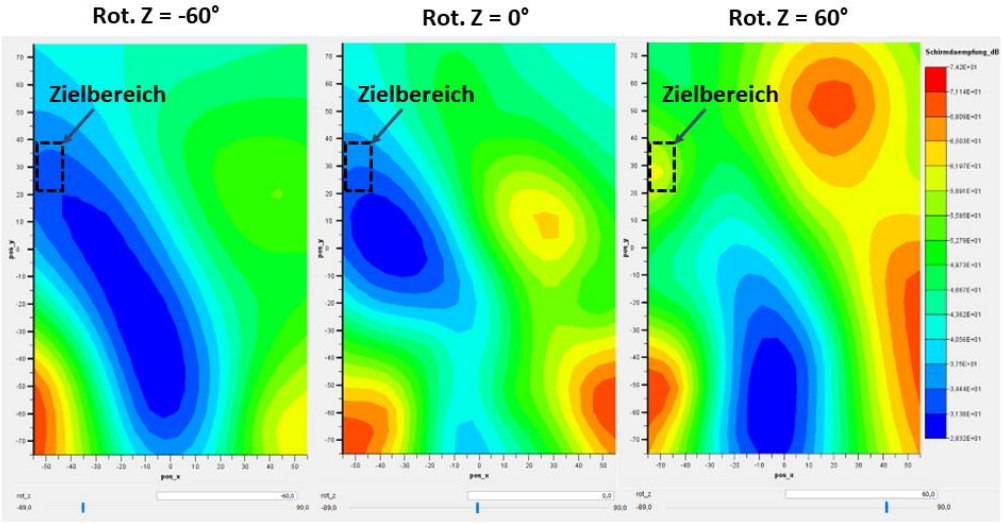

Abb. 8
Die Designraumerkundung zeigt eine mögliche Lösung für einen Rotationswinkel von +60° und eine erhebliche Verschlechterung in negativer Drehrichtung.

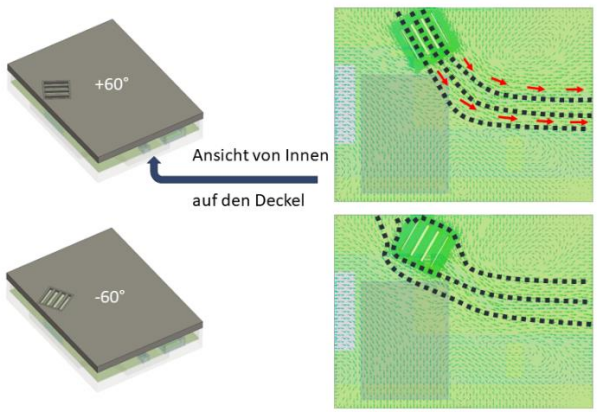

Abb. 9
Physikalische Erklärung: Bei einem Winkel von +60° wird der Rückstrompfad nur minimal gestört, während die Lüftungsschlitze bei -60° nahezu senkrecht zum Rückstrompfad stehen und somit eine deutliche Erhöhung der Induktivität verursachen.

Die Designraumerkundung zeigt also, dass die Verdrehung in positive Richtung erfolgen muss, auch ohne, dass der physikalische Grund verstanden sein muss. Wird nun für diese beiden Winkel der Rückstrompfad betrachtet (s. Abb. 9), folgt die physikalische Erklärung. Es ist die bereits in Abschnitt 2 erläuterte Impedanz, die für eine Verdrehung um 60° minimal wird, da die Lüftungsschlitze exakt parallel zum Rückstrompfad liegen.

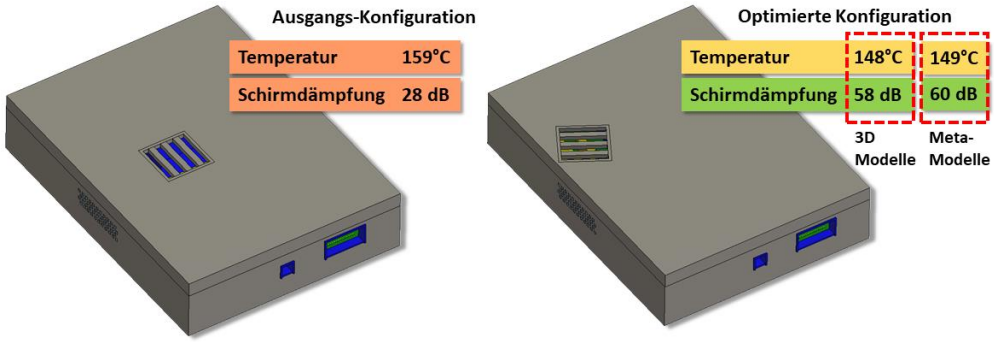

Abb. 10
Durch die Verdrehung der Lüftungsschlitze konnte die Schirmdämpfung erheblich vergrößert werden, sodass die Lüftungsschlitze in den sensiblen Bereich positioniert werden konnten, um die Temperatur zu minimieren. Die Vorhersage der Metamodelle liegt nahe an den 3D-Simulationsergebnissen.

6 Zusammenfassung

Die Methode der Designraumerkundung ist eine Alternative zur automatischen Mehrzieloptimierung. Mit beiden Methoden können vergleichbare Ergebnisse erzielt werden. Der Unterschied liegt im Weg zur besten Lösung. Während die Mehrzieloptimierung automatisch die besten Lösungen liefert, gewinnt der Anwender bei der Designraumerkundung wertvolle Erkenntnisse über wichtige Zusammenhänge und kann so ein tieferes Verständnis für sein Produkt schaffen. Auch wenn die Designraumerkundung etwas mehr manuellen Aufwand bedeutet, überwiegt häufig der Nutzen durch gesteigerten Erkenntnisgewinn.

7 Literatur

[1] Kühn, Michael; Messer, Marcel; Weigel, Robert: Einfluss der Kontaktierung auf die Schirmdämpfung von Gehäusen. In: emv : Internationale Fachmesse und Kongress für Elektromagnetische Verträglichkeit, Düsseldorf, 2018, S. 151-157

[2] Tiwari, Santosh; Koch Patrick; Fadel, Georges; Deb, Kalyan: AMGA: An archive-based micro genetic algorithm for multi-objective optimization. In: Genetic and Evolutionary Computation Conference, GECCO 2008, Proceedings, Atlanta, GA, USA, July 12-16, 2008, S. 729-736

A multi-physics simulation framework for Maxwell's equations

Thomas Rüberg, Lars Kielhorn, Jürgen Zechner (TAILSIT GmbH, Graz, Austria).

1 Summary

TAILSIT has a long standing experience in integrating three-dimensional Finite Element (FEM) and Boundary Element (BEM) methods to address electromagnetic problems [1]. This methodology leverages the advantages of FEM for volumetric electromagnetic simulations and BEM for modeling exterior domains, resulting in a comprehensive solution framework that is perfectly suited for the simulation of multi-physics phenomena.
Because the exterior, unbounded air region is excluded from the numerical model, the coupling of FEM-BEM techniques offers a powerful framework for analyzing electromagnetic interactions within complex geometries while considering their impact on mechanical systems.

Prominent examples for multi-physical problems in conjunction with electromagnetic phenomena are structural deformations induced by electromagnetic forces, thermo-mechanical coupling in electro-magnetostrictive materials, and magnetohydrodynamics. To this date, only very few commercial products are available that allow for a seamless integration of mechanical and electromagnetic solvers.

TAILSIT aims to overcome this lack of available coupling tools by providing a flexible, and yet easy-to-use framework to accomplish such kinds of multi-physical problems. We achieve this by using preCICE [2], an open-source coupling library for multi-physics simulations. preCICE offers a well-defined API for exchanging data between a wide range of very different numerical solvers. In this talk we will present a preCICE adapter for our FEM-BEM coupling code.

Through numerical experiments and validation against analytical solutions, the efficiency and accuracy of the proposed approach is demonstrated across a range of scenarios (see for example Fig. 1). This work contributes to advancing the understanding and simulation capabilities of multi-physics phenomena involving electromagnetic interactions, paving the way for enhanced design and optimization of electromechanical systems in diverse engineering applications.

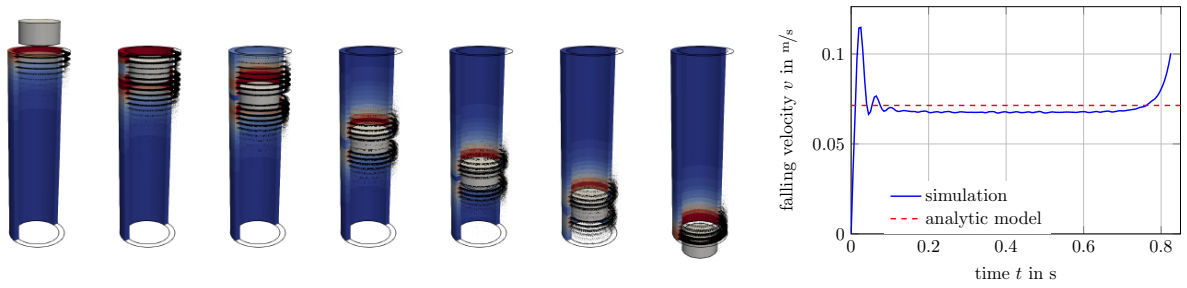

Fig. 1: Simulation of a magnet falling through a copper pipe: snapshots with induced currents (left), falling velocity (right)

2 References

[1] T. Rüberg, L. Kielhorn, and J. Zechner. Electromagnetic devices with moving parts — simulation with FEM/BEM coupling. Mathematics, 9(15):1804, 2021.
[2] G. Chourdakis, K. Davis, B. Rodenberg, M. Schulte, F. Simonis, B. Uekermann et al. preCICE v2: A sustainable and user-friendly coupling library. Open Res Europe 2022, 2 :51

Collaborating with CAE-processes and -data across several brands of the VW-group

R. Luijkx (AUDI AG)

M. Thiele (SCALE GmbH)

1 Summary

Today, virtual product development is essential in vehicle projects, in order to keep costs down. However, managing CAE-related work across a large automotive group with several brands becomes a challenge. It is therefore important to establish means for effective collaboration on CAE-data, CAE-methods and CAE-processes, and it makes sense to organize simulation data in such a way that common components such as materials, impactors, barriers and dummies, as well as certain process-scripts or simulation-methods in general, can be shared across the group's various brands. To this end, libraries of common CAE-models and all types of process-scripts are created and maintained by a small number of experts to be used by all CAE users across the different group brands and partners. To ensure that this also works regardless of the location of the CAE engineers, and to enable effective collaboration, a dedicated IT-solution is required to exchange data between all locations within the group and with its various partners.

Within the VW-Group, simulation data management has already been used for many years to control CAE-processes and data management. In the past, however, the CAE-methods and processes have been different for each of the group's brands, and the sharing of common CAE-models has been limited. Overcoming these limitations to the benefits of collaborative CAE-model development has been a challenge in recent years.

This presentation addresses how to organize the collaboration within the domain of crash and structural stiffness analysis between many CAE-engineers across different locations. The focus is on how data can be structured and exchanged, how CAE-processes can be standardized such that they are applicable for everyone and ultimately how all the data and results can be prepared for storage in the different data management systems of the respective brands. In addition to collaboration between the engineers of the different group brands, we'll also focus on how OEMs and their external partners and suppliers can work together effectively.

Collaborating with CAE-processes and -data across several brands of the VW-group

NAFEMS DACH Konferenz 2024:
Konferenz für Berechnung & Simulation im Engineering
10. – 12. Juni 2024, Bamberg, Germany

R. Luijkx (AUDI AG), M. Thiele (SCALE GmbH)

Agenda

01 **Motivation**
Where do we come from? & Why using data management for crash simulation?

02 **Collaboration**
Teamwork in a heterogeneous environment with hundreds of engineers on the same projects.

03 **Data structures**
How to organize data for effective collaboration?

04 **System integration**
CAE-Tools, HPC, Archiving of simulation results

05 **Summary & Outlook**
CAViT, …

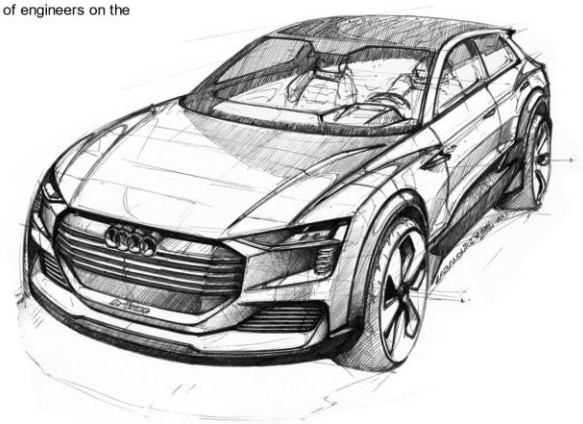

Motivation

rising dimensions of complexity

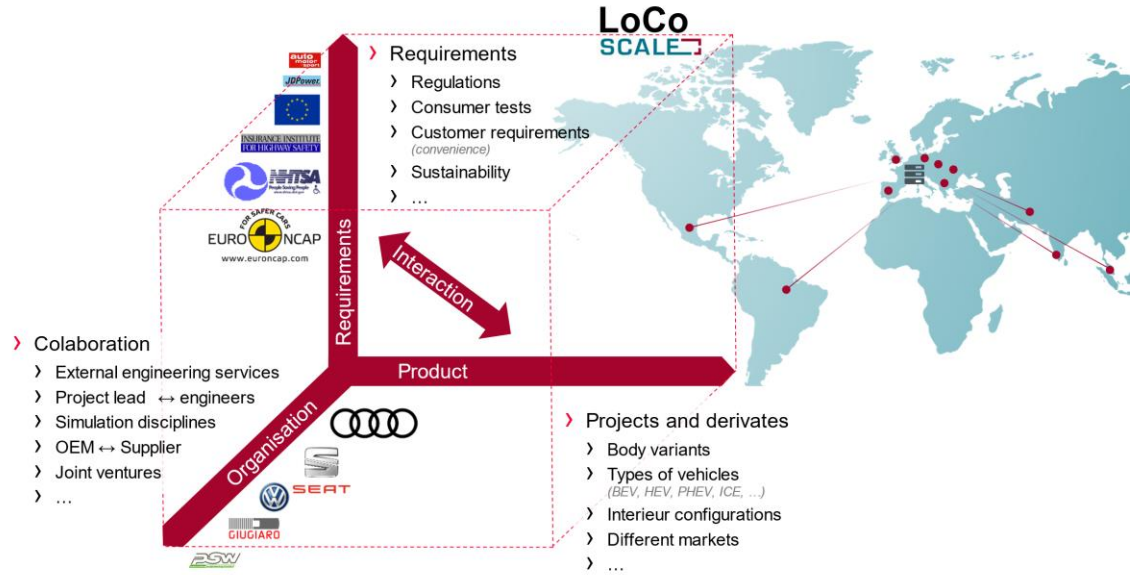

Motivation

increasing complexity of simulation models

- Increasing level of detail for models
  - More elements
  - More components
    (sub models)
  - More details

2017 Audi D5

Elementkantenlänge: Ø 5 mm
Elementanzahl: 6.000.000

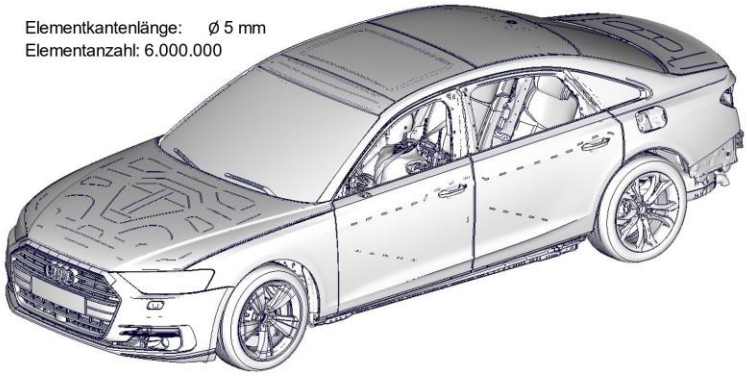

Motivation

collaboration with other brands and external partners

- CAE isindispensable in vehicle development
- Engineers need to collaborate across many sites
- Several brands throughout the VW -Group sharing CAE-Models and Methods
  - material libraries
  - barriers , impactors , dummy models
  - Standardized solver control cards
  - Scripts, tools and process chains
- Engineering service suppliers and partners are integrated
  - Some partners work with VDI clients *(remote desktop)*
  - Some partners synchronize the CAE -Data
  - Some strategic partners use their own servers to synchronize data for larger teams

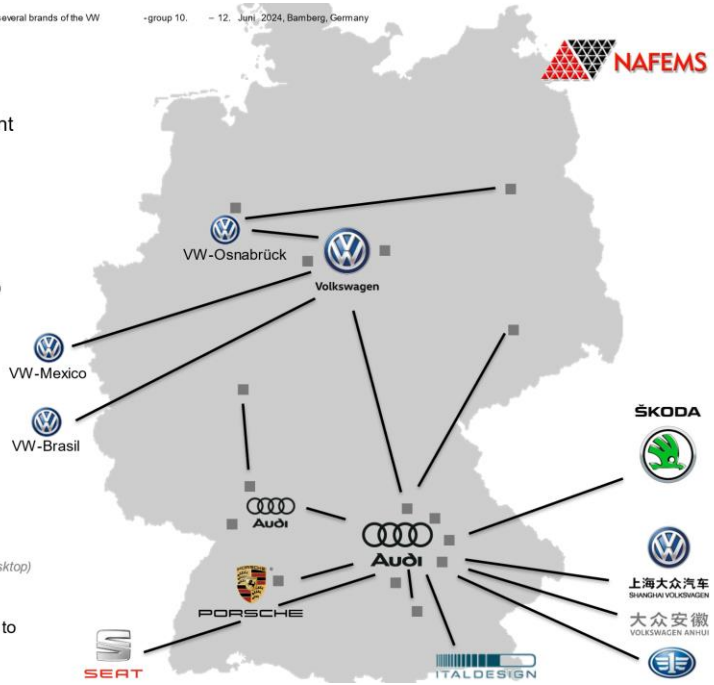

Motivation

usage of LoCo within VW-Group

NAFEMS

- ~1100 users during last 365 days
- Data since 02-2011
  - ~7.8 million assembled simulations
  - ~2.8 million component-versions
  - ~800 thousand pool-versions
  - ~60TB of simulation input data
- Simulation Disciplines *(~23 different disciplines)*
  - Structural crash *(PAMCRASH, LS-DYNA)*
  - Occupant safety *(PAMCRASH, LS-DYNA)*
  - Interieur head impact *(PAMCRASH)*
  - Pedestrian safety *(PAMCRASH)*
  - Seat systems *(PAMCRASH)*
  - NVH *(NASTRAN, Abaqus)*
  - Multi Body Dynamics *(ADAMS)*
  - ...

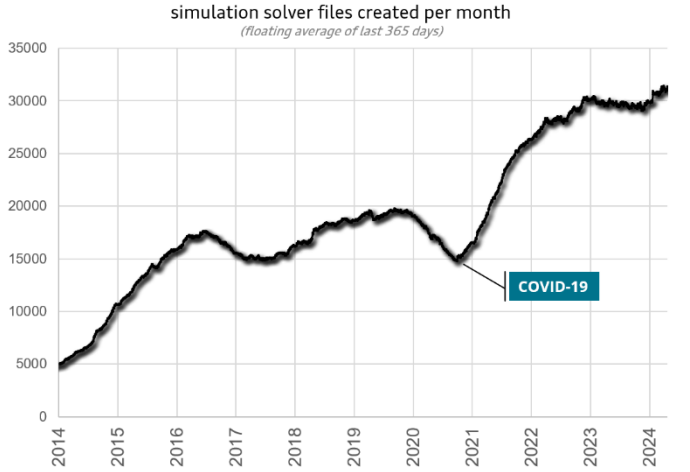

Collaboration

Teamwork with many engineers

- **Traceability** by Version control
  - Each change automatically documented
  - Completely traceable history
  - Versions are unique
    (can be used for identification and communication)
- Data synchronized between CAE engineers
  - Each change instantly available for everyone
  - No handling of files in file system
    (no manual up - and download of data)
- Live Mode
  - Collaboration in across the world in real time
  - Simultaneous working on different components in one model
  - Each change is instantly propagated to the team
  - Automatic locking of files being worked on

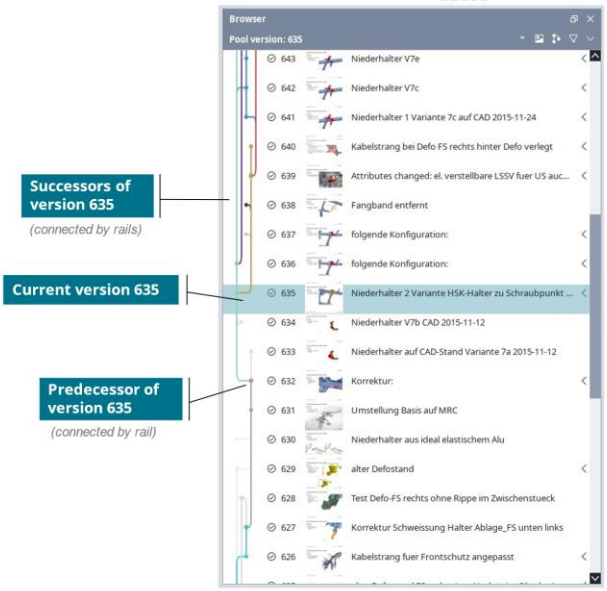

Collaboration

Teamwork with many engineers

- **Traceability** by Version control
  - Each change automatically documented
  - Completely traceable history
  - Versions are unique
    (can be used for identification and communication)
- Data synchronized between CAE engineers
  - Each change instantly available for everyone
  - No handling of files in file system
    (no manual up - and download of data)
- Live Mode
  - Collaboration in across the world in real time
  - Simultaneous working on different components in one model
  - Each change is instantly propagated to the team
  - Automatic locking of files being worked on

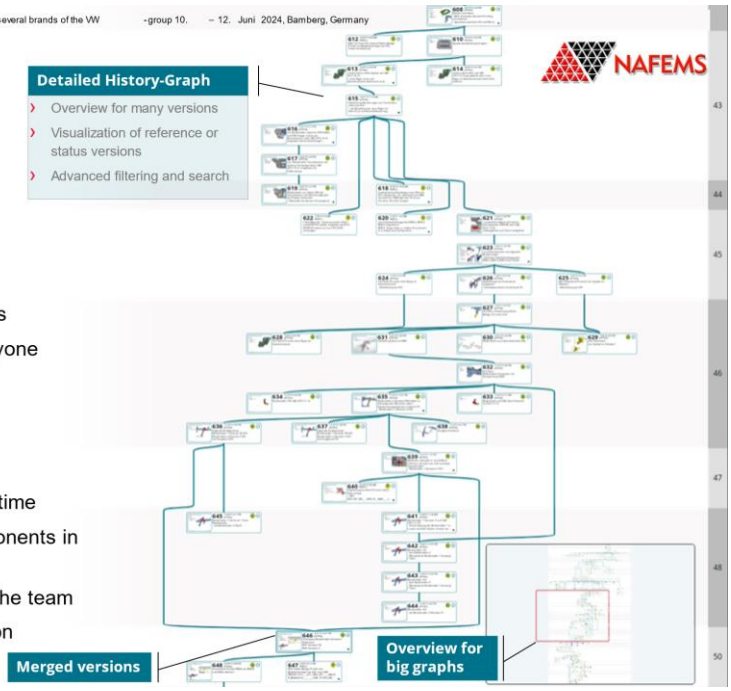

Data structures

project structure with shared data

- Data shared across multiple brands
  - Organized in library pools
  - Can be mounted by any project
- Standardization
  - Assures comparability between projects
  - Reduces errors
- Democratization / knowledge transfer
  - Experts prepare models and methods
  - Every CAE-engineer can access and use the provided libraries

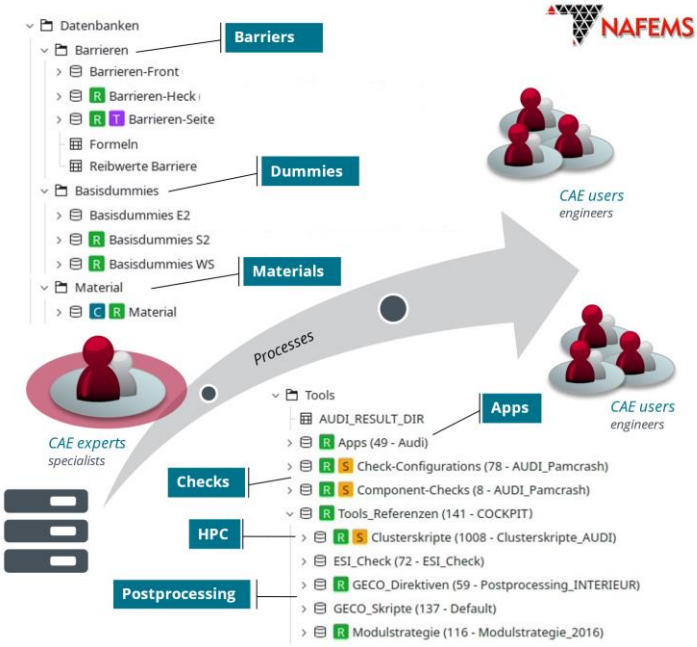

Data structures

automatic creation of many load cases from many components

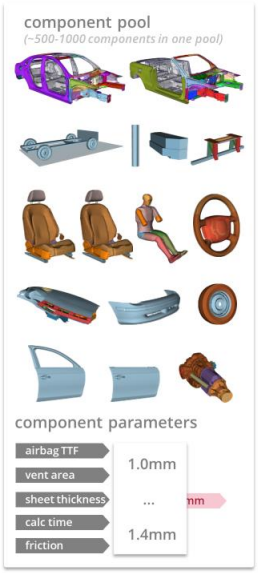

Assembly of multiple load cases and derivates

(~200-300 run-configurations for one vehicle derivate)

Setup of optimizations and DOEs

- Parameters and optimization goals are defined
- Assembly of vast amounts of simulations

System integration

tools and scripts

NAFEMS

CAE– Preprocessing Tools

- Open directly on local workstation
  (no cumbersome up - and download of files)
- Data automatically synchronized
- Use native applications on desktop
- Python scripting API
- Apps managed by key-users

Solver Disciplines

- Flexible setup and Configuration
  (completely manageable by advanced users)
- User-scripts for pre- and post-processing
- Python templates for assembly

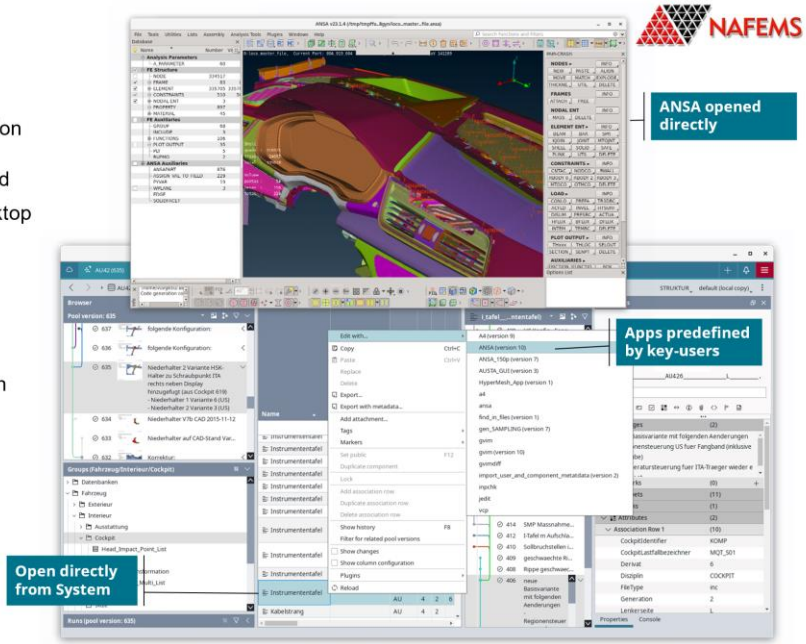

System integration

model quality assurance through checks

NAFEMS

- Errors need to be detected as early as possible!
- Checks can be implemented for:
  (implementation as scripts maintained within the system)
  - Individual files
  - Simulation runs

Files

- Can be executed directly after each edit
- On the local desktop or through the HPC
- For a single file only or in the context of a simulation
  (e.g. datacheck of single file)

Simulation runs

- Run during job submit before solving phase starts
- Results are displayed in LoCo
- Reports of checks *(e.g. PDF)*

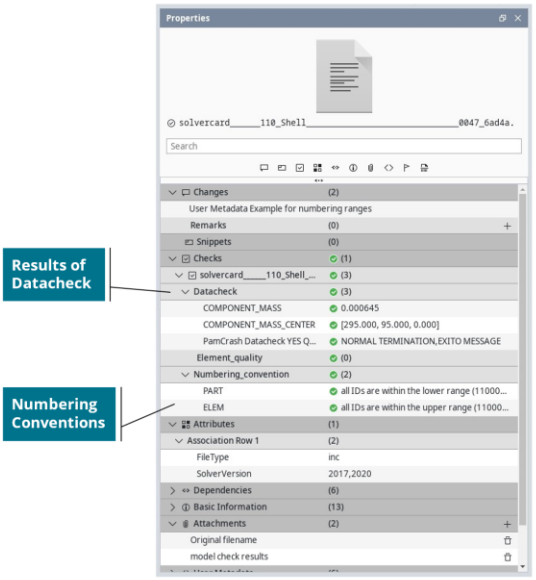

System integration

submission of simulation jobs to HPC systems

- Job submission
  - Directly from desktop client
  - Solver and queuing parameters
- Queuing system
  - Starting and killing of jobs
  - Multiple different HPC systems on different locations with different queuing systems can be integrated
- Progress feedback
  - API for creating feedback for every process
  - HPC scripts can provide progress feedback independent of server infrastructure
  - Progress feedback for complex simulation jobs
    (helps users in case simulation jobs are running into problems)

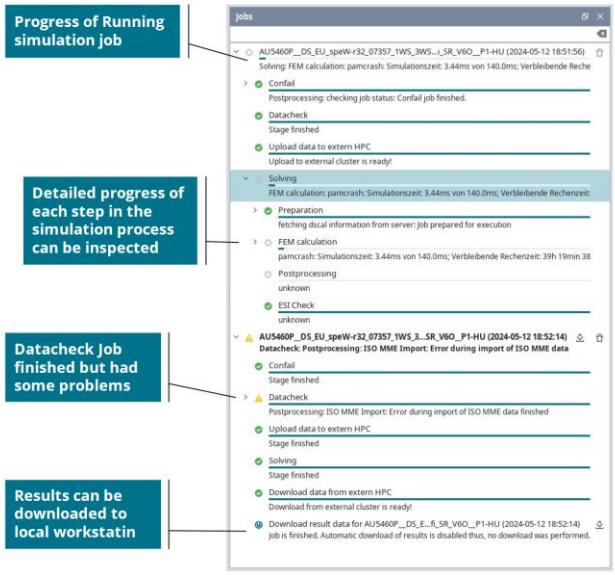

Summary & Outlook

Summary

- Increasing demand for CAE
- SDM essential
  - Collaborating with many engineers
  - Enforcing standardization
- Usability and performance are the most important factors

Outlook

- Further performance optimization
- Tight integration with Results
  (CAVIT\|SCALE.result)
- Cloud
- Machine Learning
  - Event Detection
  - Data Analysis
  - …

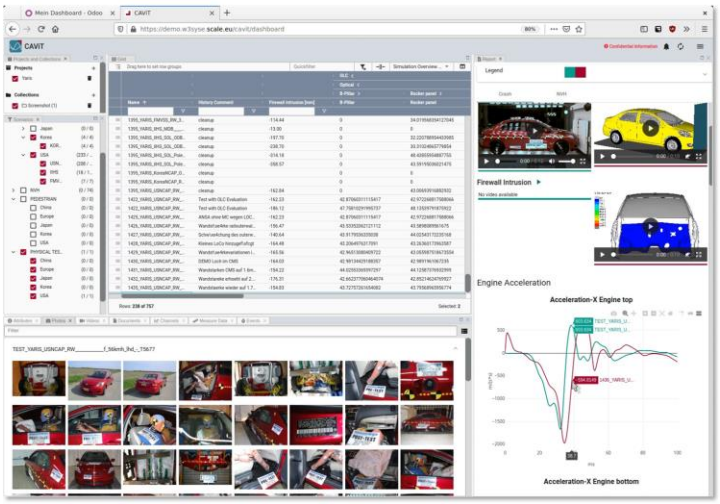


Collaborating with CAE -processes and -data across several brands of the VW -group 10. – 12. Juni 2024, Bamberg, Germany
RITTWAGE
Thank you !

Key Role "Mindset": Data Management & AI in Porsche's Development

Maximilian Rabus

Dr.Ing. h.c. F. Porsche AG

1 Introduction

Since the release of ChatGPT on November 30, 2022, artificial intelligence has been on everyone's lips. On this day, the enormous possibilities that AI offers were first experienced by individuals without technical expertise. Pre-trained models, as in the case of ChatGPT, also offer numerous potentials for companies. A significant advantage of using these models is that no own expertise in model building and no large resources or own data bases for model training are required. However, available pre-trained models cannot solve all problems. Especially in product and vehicle development, creating own models – so-called train-from-scratch models – is often much more effective. Besides expertise in model building and operation, the underlying data base is primarily a crucial prerequisite for the efficient use of the data-driven model.

Therefore, the keynote by Maximilian Rabus (Data Domain Manager in the Department “Data-Driven Development” at Dr. Ing. h.c. F. Porsche AG) focuses on the role of the necessary mindset in data management in the context of AI. Reliable and quickly available data is an important factor for efficient development and business success. To master today's challenges, intelligent, high-performance, and at the same time stable IT solutions are indispensable. However, technical solutions alone are not enough: employees must have the right mindset to use all data effectively.

It is precisely this pillar that Rabus places at the center, asking what each employee can contribute to a successful data culture. Porsche’s methodological approach aims to strategically expand IT solutions with suitable capabilities while at the same time focusing on the mindset of all involved regarding data management.

2 Mindsets for a Successful Data Culture

2.1 Mindset "Data as Products": An Analogy to Online Shopping

As an example, Rabus highlights a typical data provisioning and usage process. In development, enormous amounts of data are generated. The problem is that users have different requirements for the data, leading to high effort for the data creator to customize the data. Data provisioning often occurs through various channels like email, Teams, or departmental hard drives. Once the data reaches the user, it must be extensively managed and processed before it can be used effectively. In the worst case, the same pre- and processing steps are redundantly carried out by different users, showing that the entire process is associated with a lot of effort and non-value-adding steps.

To enable employees to focus on the essentials when dealing with data, Porsche's approach is to establish the so-called "Data Mesh". At the core of this data mesh approach is the mindset of thinking of data as products. Rabus explains this using an analogy to online shopping. An online platform connects customers and merchants, enabling easy and intuitive product search, listing all products clearly, allowing providers a very large customer reach, and offering an uncomplicated ordering and support process. Customers appreciate the wide selection and the central and simple search, receiving detailed product descriptions and reviews. Merchants are responsible for product quality, providing high-quality product descriptions, and ensuring availability and deliverability for optimal customer satisfaction.

The focus of the analogy is on the merchant: The merchant wants to market his product – for this, he feels particularly responsible for the quality of his product and an optimal product description to generate the highest possible customer satisfaction.

Rabus emphasizes that exactly this merchant mindset is valuable in the context of data management and how essential it is that the data provider – in analoigy to the merchant – feels responsible for his (data) product. A data provisioning and usage process can drastically change with this mindset. The provider is responsible for creating a standardized data product, listed and described in the so-called data catalog, and handles pre- and processing steps to provide users with an optimal (data) product. The provider defines and provides a product once, which can then be consumed by all users through standardized interfaces. Since individual preprocessing steps are eliminated for the user, the user can directly focus on his development activities. This simultaneously ensures scalability, as new users or use cases can directly work with the standardized data products without additional effort.

Thinking of data as a product is the foundation for efficient data usage and scalability. Standardization and adoption of explicit responsibility by the data provider are key for an efficient data management.

2.2 Mindset "Decentralized Data Management": Not One Tool for Everything, but a Connected System Landscape for a Seamless Experience

Rabus also addresses the widespread paradigm of centralization: one data model, one database, one tool as a comprehensive solution for the entire management of all existing data in a company. He explains the disadvantages of the long-pursued paradigm of a central IT solution that was supposed to replace all existing systems for data management. This includes the loss of individual capabilities, which would inevitably result from unconditional harmonization. Besides compromising available capabilities and enormous efforts for simultaneous process harmonization, this approach especially reduces flexibility and adaptation speed.

Using the example of a smartphone, where individual apps are connected to provide a seamless experience, he argues for a decentralized data management concept. Such a decentralized concept has the advantage that individual tools and platforms can have their own data management concepts, which prove optimal for the respective use case – depending on the available capabilities. Fundamentally, the tools and platforms are not isolated but form an IT system landscape. Data exchange takes place via the described standardized data products. When successfully implemented, the user does not experience unnecessary system boundaries or breaks but perceives a system landscape where all tools (with their individual capabilities) lead to an optimal result.

As a practical example, Rabus cites the cross-analysis of measurement and simulation data at Porsche. Porsche's Data Analytics Tool "KVM" obtains relevant information "on demand" as data products from respective source systems, such as simulation data from "CAE-PDM" and test data from "Cluu", without managing all data permanently in the analytics system.

2.3 Mindset "Connect Skills": AI & Domain Experts in Development Departments

Rabus presents insights into Porsche’s organizational development in the context of simulation to draw conclusions on possible AI developments.

Early successes in virtual simulation at Porsche were achieved around 1978 with some specialists in different development areas. The topic was new, and the pioneers faced challenges, like fighting against reservations – as is the case today with AI. Virtual simulation ultimately established itself and quickly became an important tool in development, especially due to the need for ever shorter development cycles. To leverage synergies, all simulation experts at Porsche were consolidated into one department in the 1990s – a centralized simulation department for all development areas. The demand for virtual simulation continued to rise. For this reason, the first decentralization was carried out around 2005: one simulation department per development area. This brought engineers and simulation experts closer, enhancing collaboration. Nevertheless, it became clear that the "physical" and "virtual" worlds had to grow together even closer. For this reason, further decentralization was carried out a few years ago. Today, simulation experts are an integral part of each development team. The advantage is crystallizing that immediate interlocking and intensive exchange without departmental boundaries provide the optimal conditions for efficient development.

Rabus sees a similar path in the context of AI. Some experts started around 2015 as pioneers in the development departments. As with the pioneers in the simulation environment, there were concerns and reservations about the new technology. To leverage synergies, Porsche centralized the experts as part of a restructuring in 2022. Today, there is a specialized department that centralizes and bundles AI activities for the entire development.

Rabus questions what the future holds for Porsche. Will we go through the same development as with simulation – a decentralization into all specialist areas? In his view, the greatest added value arises when AI and domain experts work directly interlocked on a problem. Intensive exchange is a prerequisite for the successful use of AI: Only when domain and AI knowledge pull together, do the full possibilities of AI unfold optimally. For this reason, he considers the further decentralization of AI expertise into all development areas as a great potential for even more efficient use of data-driven methods.

Once again, the suitable mindset of all involved is the key to success: openness to new technology and the motivation to combine and complement skills from different areas to develop the best result together – as a team – even if that means doing things differently or in a new way than before.

2.4 "Data Driven Mindset": Making Data-Driven Development Decisions

Finally, Rabus emphasizes another decisive mindset in decision-making.

In development, countless decisions are made every day. Often, we decide based on individual experiences. Not always does the subjective impression align with the opinion or desire of our customers. As William Edwards Deming said, “In God we trust. All others must bring data.” This means that data can bring a significant advantage to development decisions. Instead of making decisions purely based on experience, it is often helpful to also include suitable data. This data-driven mindset can help, among other things, to significantly reduce uncertainties in the decision-making process and develop even better products. Data-driven decisions require the necessary data basis, which should always be defined early and consistently gathered throughout development.

3 Conclusions

In conclusion, the effective use of AI and data management in Porsche's development hinges on adopting the right mindsets. The "Data as Products" mindset emphasizes the importance of treating data like a merchant treats their products, ensuring high quality, clear descriptions, and easy accessibility. The "Decentralized Data Management" mindset advocates for a connected system landscape, allowing various tools to work together seamlessly rather than relying on a single, centralized solution. The "Connect Skills" mindset highlights the necessity of integrating AI and domain experts within development teams to foster collaboration and enhance problem-solving capabilities. Finally, the "Data Driven Mindset" underlines the importance of making decisions based on data rather than intuition alone, reducing uncertainties and leading to better products. These mindsets collectively drive efficient data utilization, foster innovation, and ultimately contribute to Porsche's success in a data-driven world.

PORSCHE

The power of artificial intelligence is so incredible that it will change society in profound ways.

Bill Gates
(Founder of Microsoft)

From 2035, there will no longer be a job that has nothing to do with artificial intelligence. Every activity that involves analyzing large data sets and drawing conclusions from them will be checked: Can't AI do this faster and with fewer errors?"

Hubertus Heil
(Federal Minister of Labor)

In the next ten years, the upheavals triggered by AI will be the most important factor for change in all industries.

If we don't keep pace with the changes of the AI age, we will be displaced."

Daniel Zhang
(Ex-CEO Alibaba)

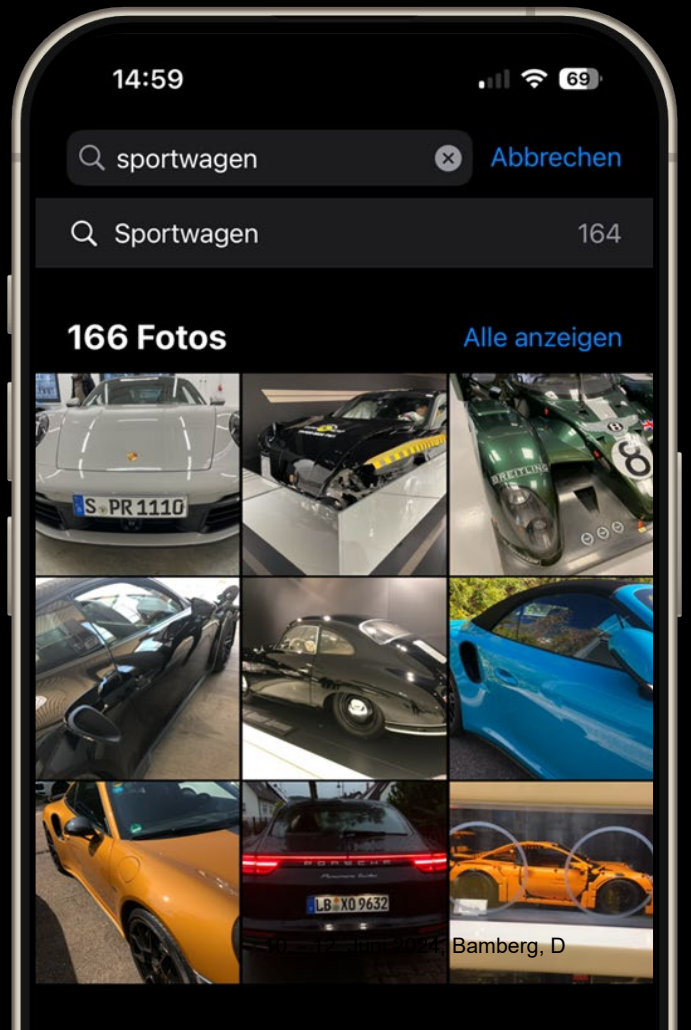

Key Role „Mindset“

Data Management and AI in Porsche's Development

November 30, 2022

Pretrained Models

... e.g. Language Processing, image recognition, ...

+

Key for success: Data Management!

Train-From-Scratch Models

... e.g. Occupant load prediction, outlier detection, noise detection, ...

Data Provision via Individual Data Sets

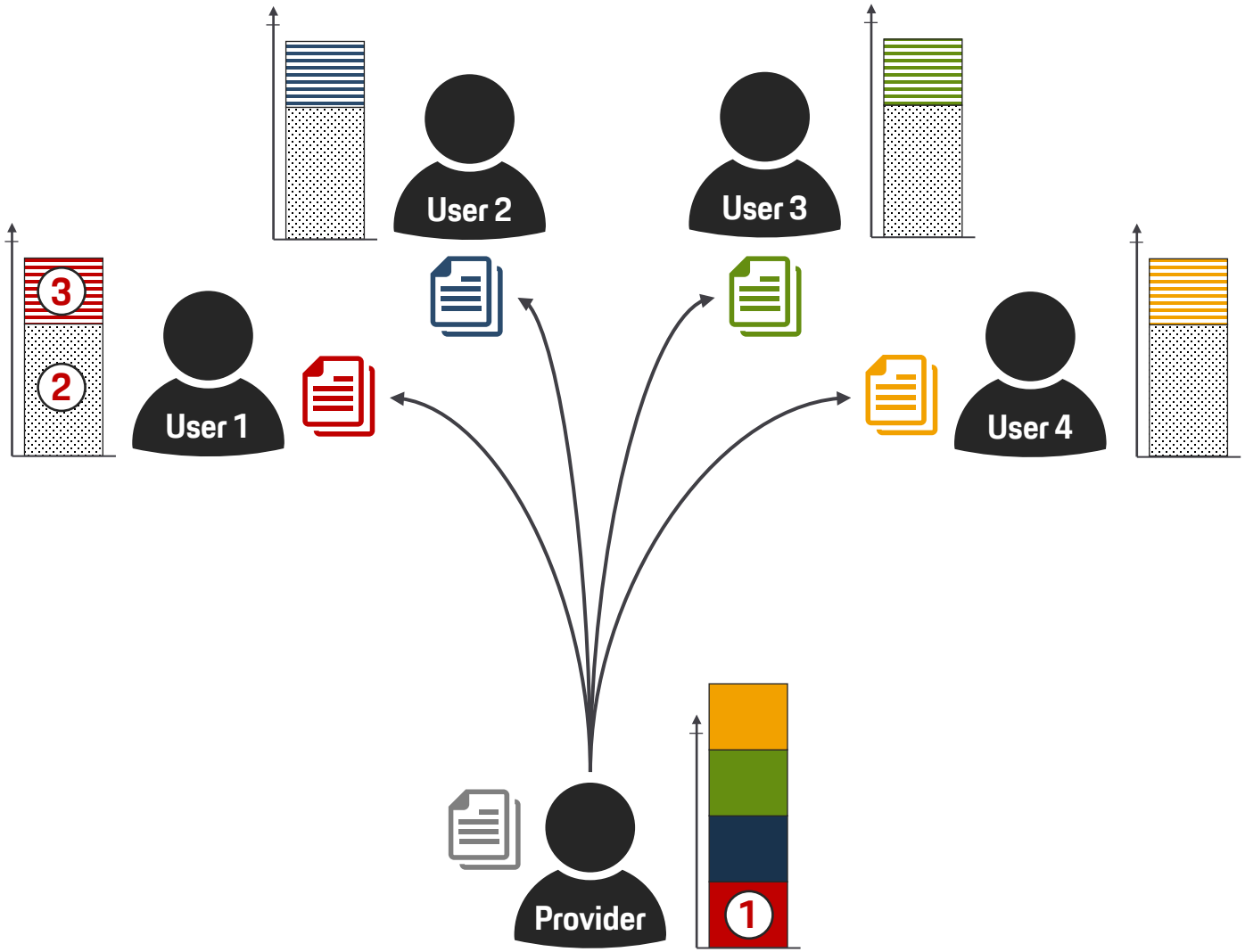

1 | Data Provision

Creation and provisioning of individual data sets leads to high manual effort for data producer

2 | Data Management & Engineering

High effort of storing, managing and processing individual data sets for data user

3 | Data Usage

Each usage of data needs lots of tedious data management in advance

» **Individual data sets prevent scaleability!**
New mindset necessary: data product thinking!

Data Mesh & Online Shopping Platform | Where is the connection?!

Producer

Focus on providing product to market:
Responsible for product quality and description!

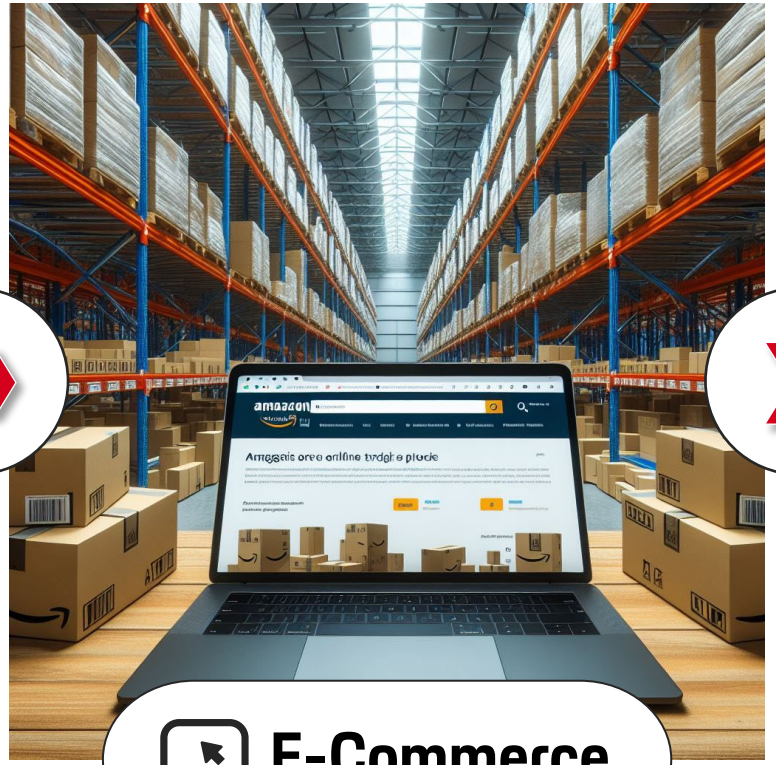

E-Commerce

Focus on connection:
Lists all products and enables efficient search & order process!

Customers

Appreciates easy shopping process:
Happy about large selection of well described products with high quality!

Data Mesh & Online Shopping Platform | Where is the connection?!

Provider

Focus on providing product to market:
Responsible for product quality and description!

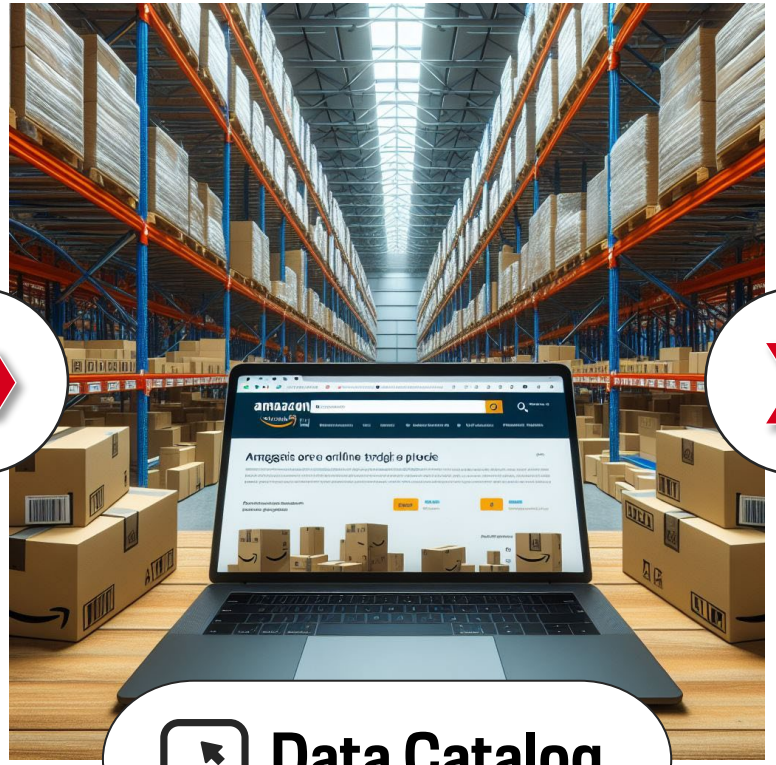

Data Catalog

Focus on connection:
Lists all products and enables efficient search & order process!

Users

Appreciates easy shopping process:
Happy about large selection of well described products with high quality!

Data Provision via Data Products

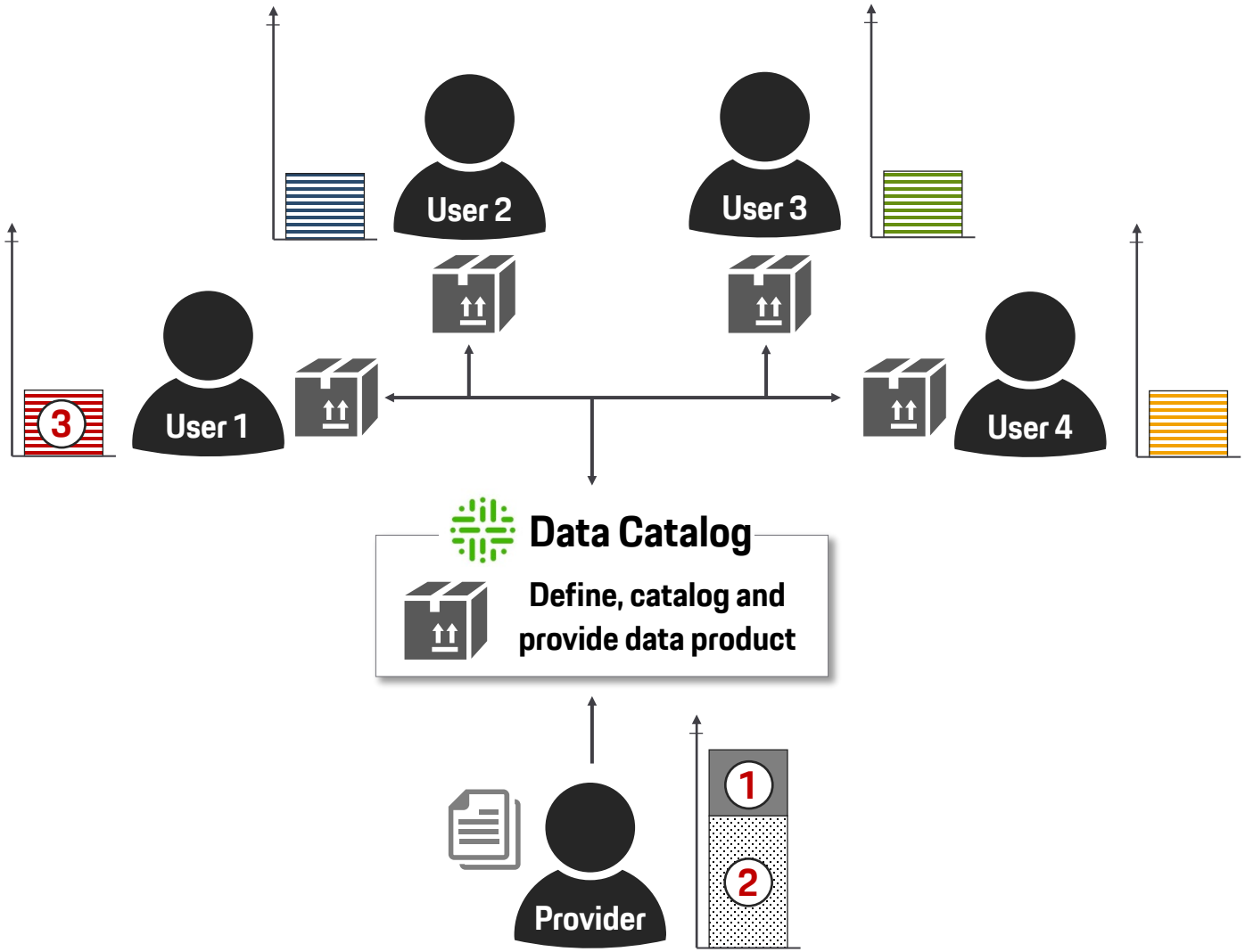

1 | Data Provision

Definition, creation and provisioning of standardized data products via data catalog by data producer

2 | Data Management & Engineering

Standardized data engineering done by the producer for direct consumability by users

3 | Data Usage

Direct usability of data products enables users to focus on their main responsibility

Data Products enable scaleability!
Standardization & clear responsibilities are key!

Image created with Microsoft Copilot Designer

Image created with Microsoft Copilot Designer

Image created with Microsoft Copilot Designer

Image created with Microsoft Copilot Designer

Image created with Microsoft Copilot Designer

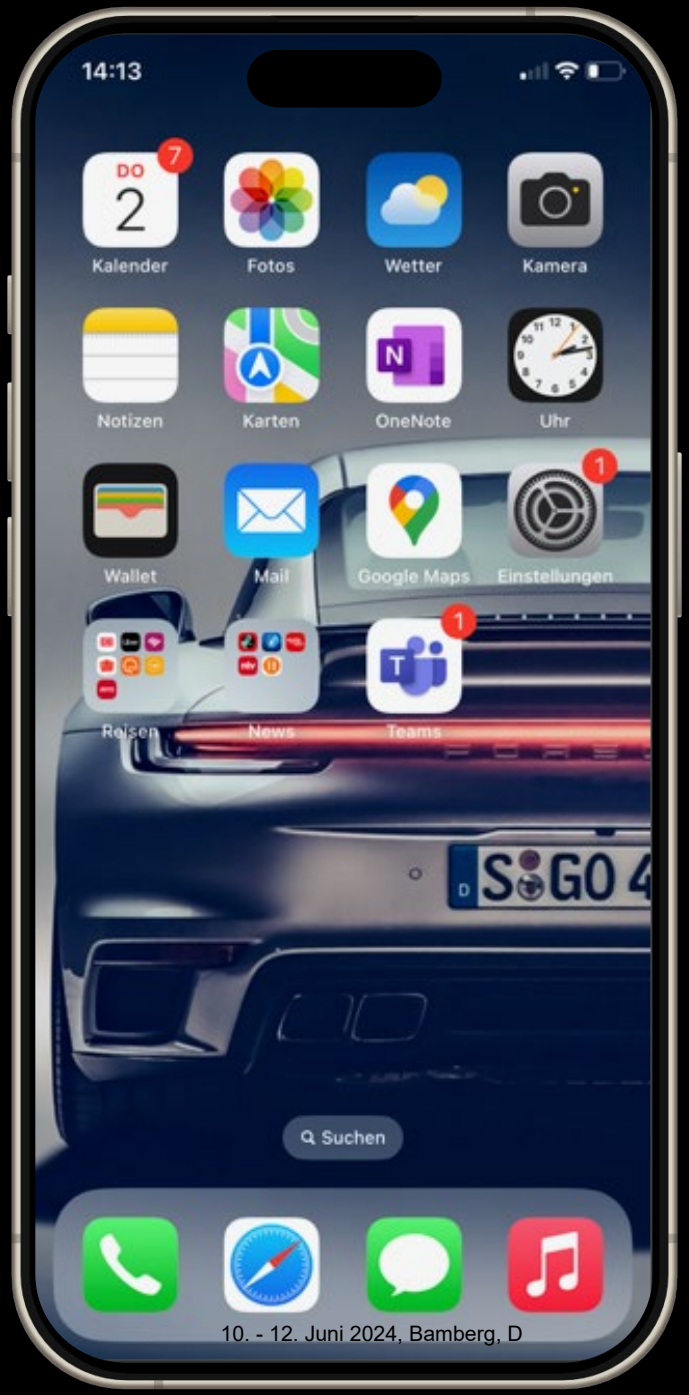

Image created with Microsoft Copilot Designer

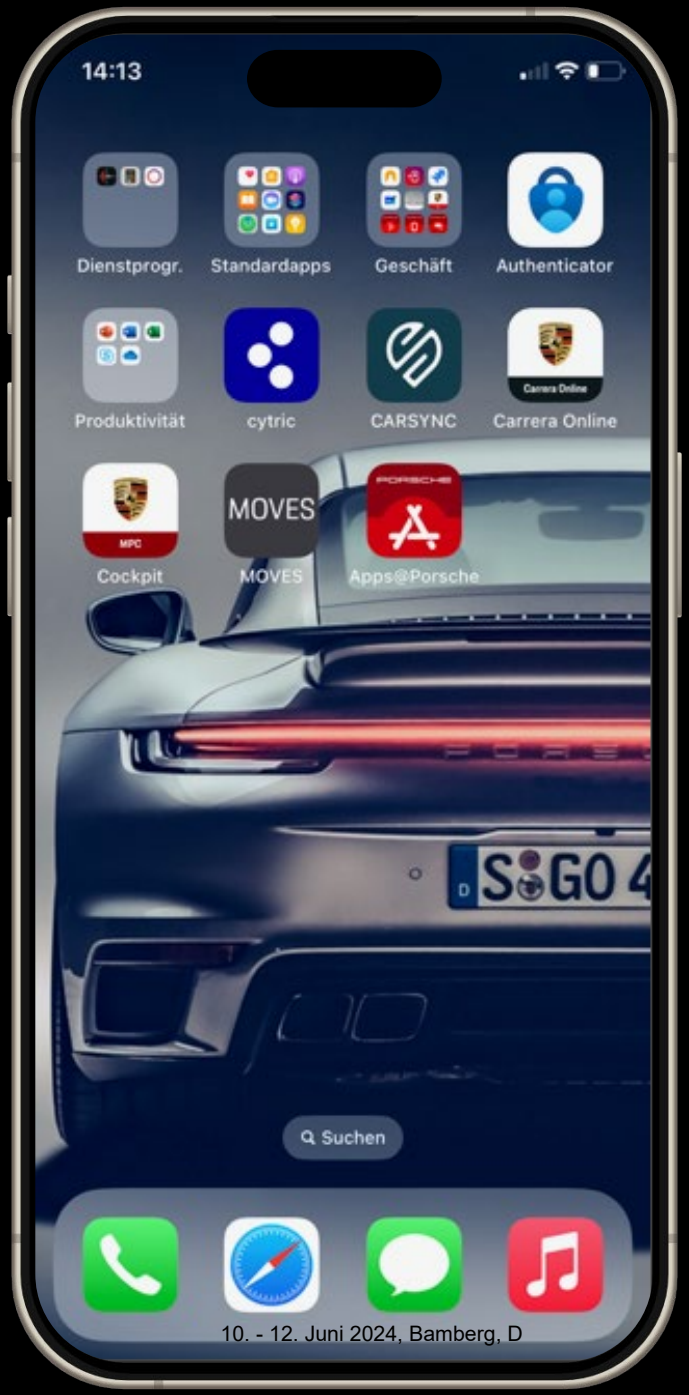

Image created with Microsoft Copilot Designer

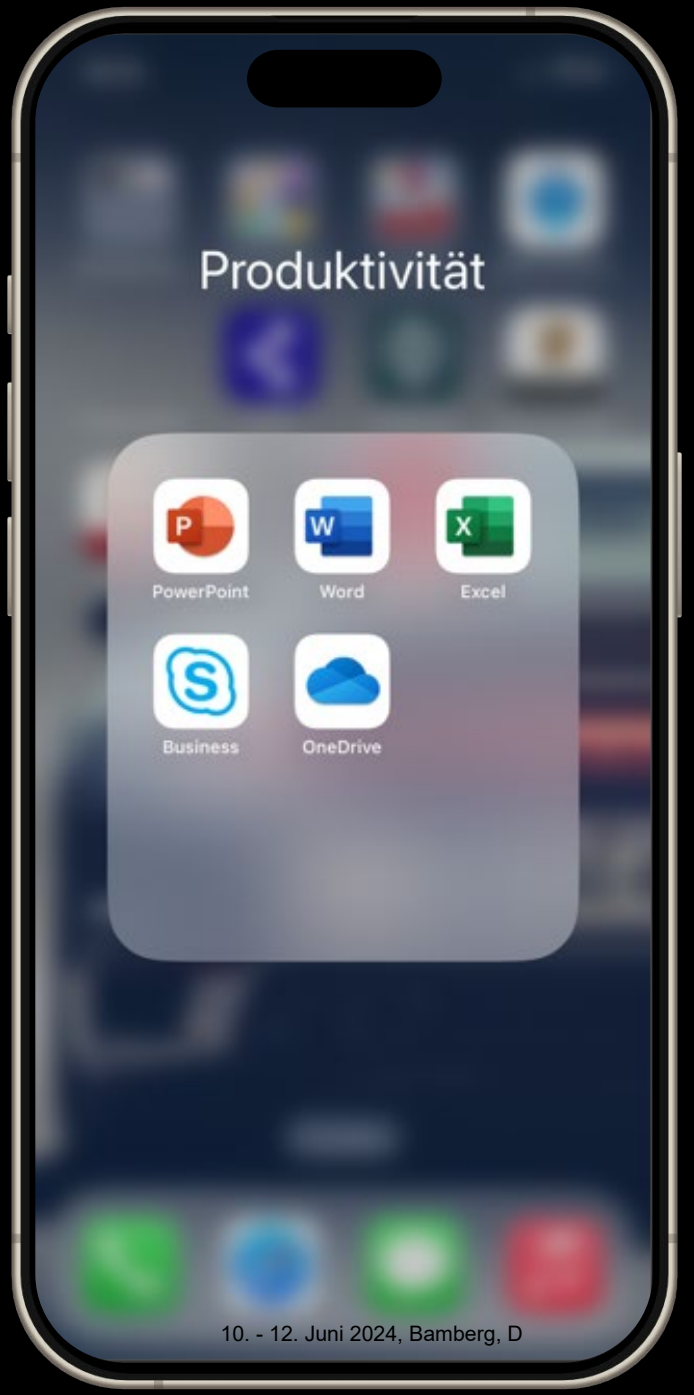

Image created with Microsoft Copilot Designer

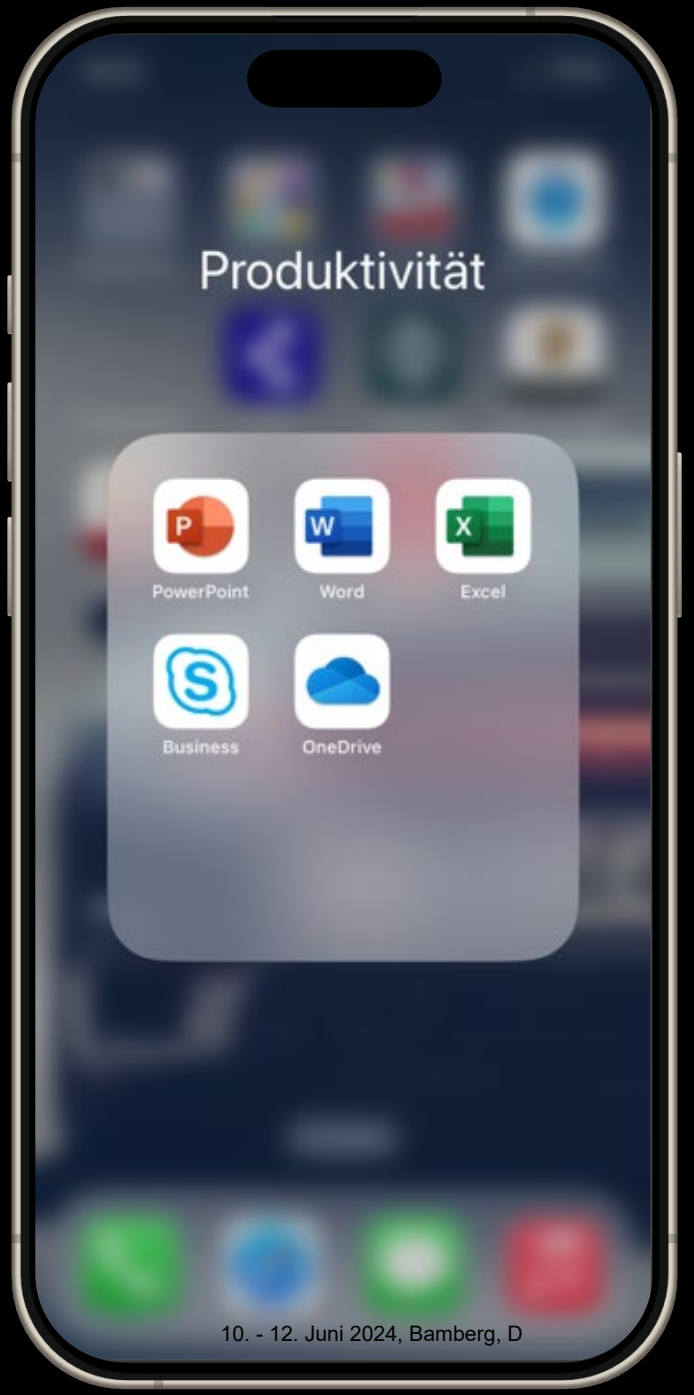

Image created with Microsoft Copilot Designer

Tool landscape instead of centralization: Decentralized data management

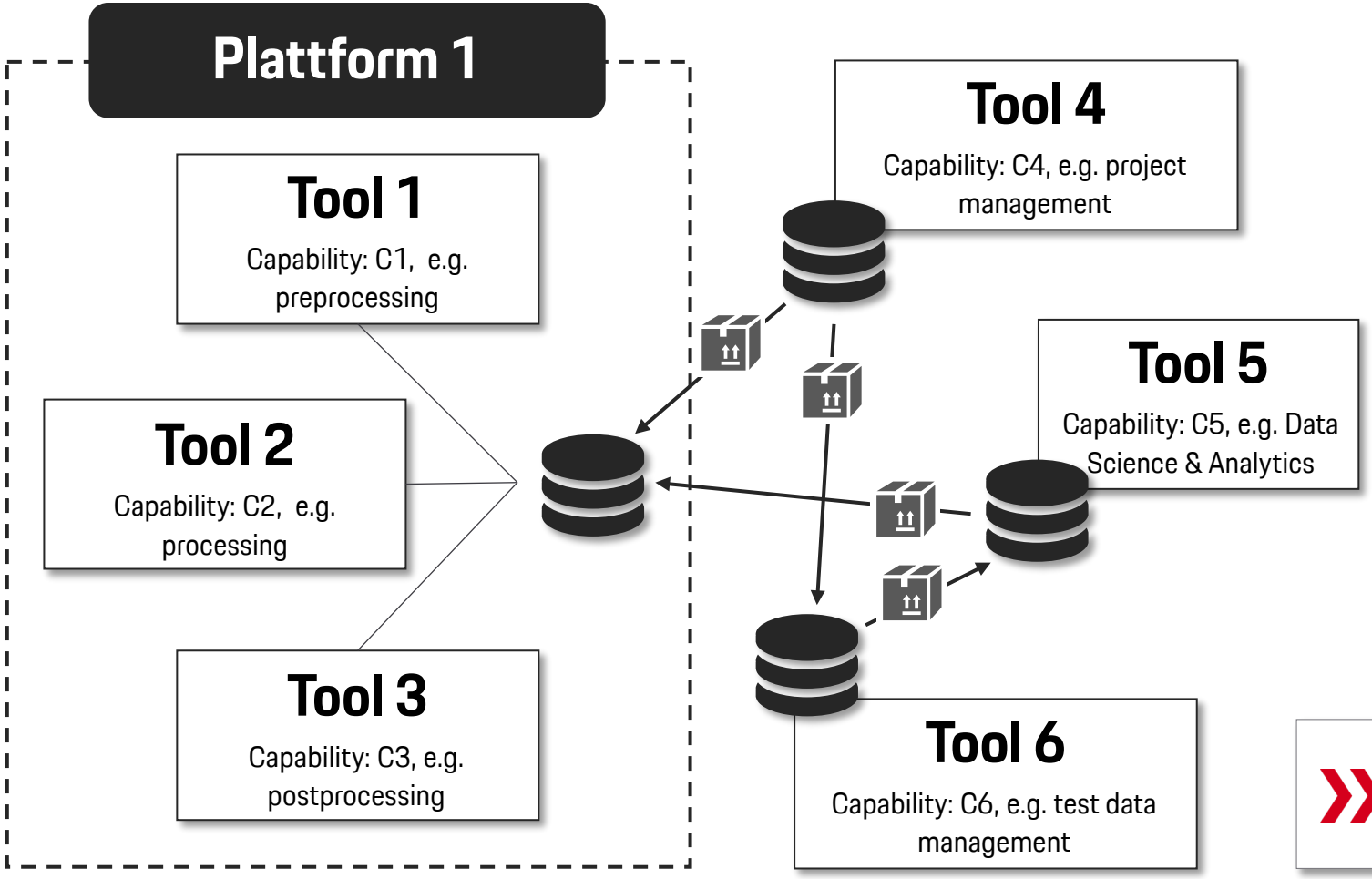

1 | Tools with Different Capabilities

Avoiding bottlenecks by developing different tools with specialized capabilities

2 | Decentralized Data Management

No efforts for harmonization or centralized data storage

3 | Data Products for Data Exchange

Provision of standardized data products, which can be found and are described in data catalog

» **Decentralized data management & exchange of data products enable scalability!**

Tool landscape instead of centralization: Decentralized data management

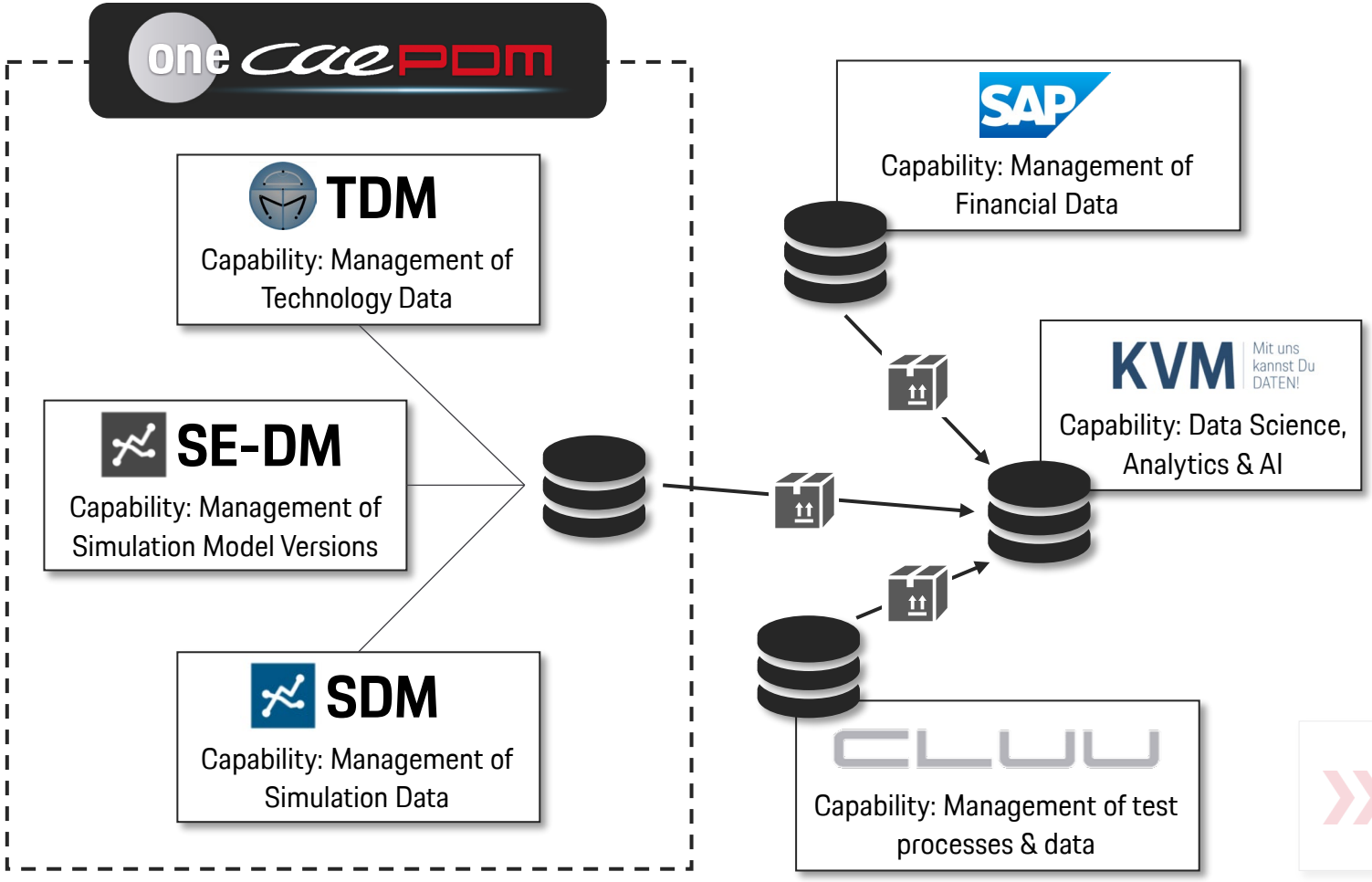

1 | Tools with Different Capabilities

Avoiding bottlenecks by developing different tools with specialized capabilities

2 | Decentralized Data Management

No efforts for harmonization or centralized data storage

3 | Data Products for Data Exchange

Provision of standardized data products, which can be found and are described in data catalog

» **Decentralized data management & exchange of data products enable scalability!**

Organizational evolution in the context of Simulation & AI at Porsche

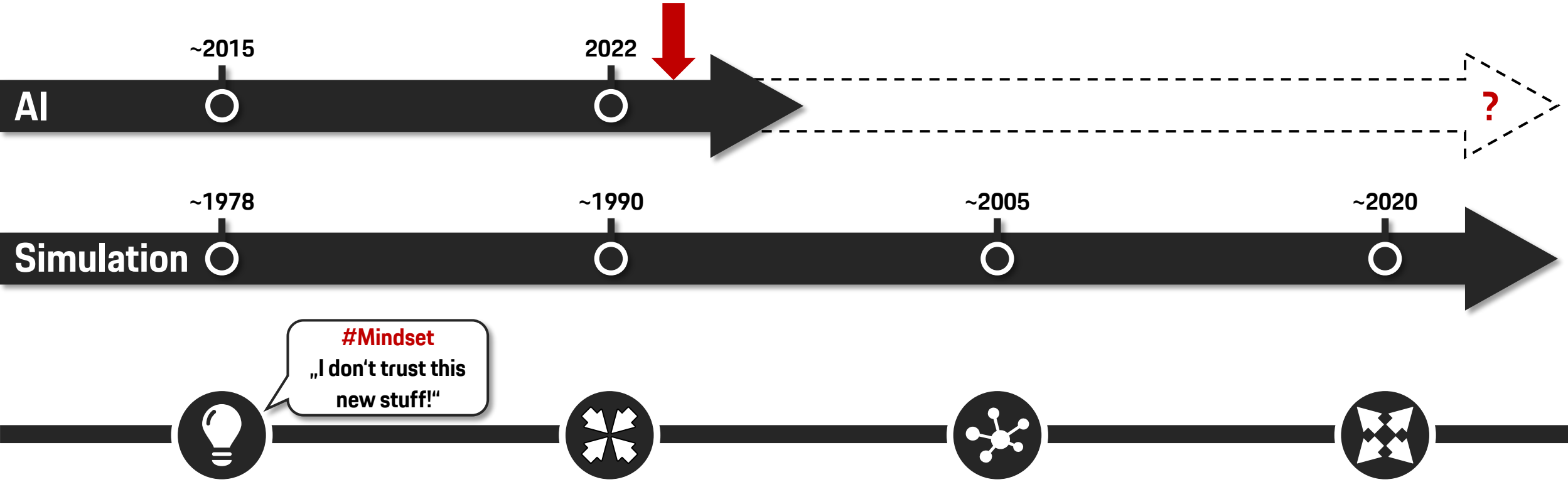

1 | Pioneers

Early specialists and experts in individual business units across the development

2 | Centralization

Consolidation of experts into one single business unit for the whole development

3 | Decentralization #1

Distribution of experts into several business units across the development

4 | Decentralization #2

Integration of experts into (almost) every business unit in the development

Why do we need Data & AI experts in every business unit?

"All my decisions are based on and evaluated by data!"

#DataDrivenMindset

"I know what customers need: My decisions are based on my personal experience & expectations"

» "In God we trust. All others must bring data"
Dr. W. E. Deming

Thank you for your attention.
Are there any questions?

Maximilian Rabus

Special thanks to ...

Zukunft gestalten: Wie KI und ML die Arbeitsweise in CAE beeinflussen werden

Astrid Walle

Data Science & Simulation Expert

Siemens Energy

The integration of Machine Learning (ML) and Artificial Intelligence (AI) is significantly impacting various domains within Computer-Aided Engineering (CAE), catalyzing advancements across simulation, optimization, and design methodologies.

Enhanced turbulence models, powered by AI, offer improved simulation accuracy for complex fluid dynamics. The development of surrogate models for scalars and fields from simulation data is streamlining design cycles, enabling rapid prototyping, optimization and the evaluation of manufacturing deviations.

Real-time digital twins, supported by these models, are becoming feasible, providing live operational insights and predictive analytics for systems across diverse industries. Generative design is revolutionizing geometry creation by automatically generating structures based on performance criteria, surpassing traditional parameter-based methods.

Collectively, these innovations in ML and AI are not only refining existing CAE techniques but are also unlocking new capabilities, leading to more efficient, sustainable, and creative engineering solutions.

Connected Engineering and Bio-Inspired Product Development

Christian Hamm

Leiter Bereich Bionischer Leichtbau und Funktionelle Morphologie

Alfred-Wegener-Institut Helmholtz-Zentrum für Polar- und Meeresforschung

Die Leistungsprofile neu zu entwickelnder Produkte sind sehr anspruchsvoll und werden ständig erweitert: sie sollen (multi-) funktional, ressourceneffizient produziert, klima- und umweltfreundlich sowie wirtschaftlich herstellbar sein. Weitere Aspekte sind zuverlässige Lieferketten und ein ansprechendes Design.

Biologische Strukturen besitzen solche Eigenschaften in hohem Maße, da sie über Jahrmillionen durch die Evolution an vielfältige Umweltfaktoren angepasst sind. So sind z.B. die Silikatschalen der Kieselalgen sehr leicht, permeabel und mechanisch widerstandsfähig, aufgrund der genutzten Materialien mit wenig Energieaufwand herstellbar sowie umweltfreundlich. Die Strukturen der Kieselalgen sind außerdem als ausgesprochen ästhetisch bekannt.

Entscheidend für die effektive Entwicklung anspruchsvoller Produkte, die all diese Aspekte optimal kombinieren, ist die Möglichkeit, den Entwicklungsprozess mit Lastenheften, Designkonzepten, Varianten und Optimierungsprozessen sowie Bewertungen wie Belastbarkeit, Preis und CO2-Footprint schnell und zuverlässig zu gestalten. In unseren Projekten setzen wir dafür „Connected Engineering“ ein. In dieser Präsentation wird diese Prozessautomatisierung anhand von Fallbeispielen für bio-inspirierte Produktentwicklung vorgestellt.

Vernetzung der Test- und Simulationswelt in einem PLM-System zur Förderung einer nachhaltigeren Entwicklung (Forschungsprojekt EP 4.0)

Dipl.-Ing. Lars-Christian Bütow (:em AG)

Mareike Keil (M.Sc.) (:em AG)

Robert Kircher (B. Sc.) (:em AG)

1 Motivation

Viele Hersteller, insbesondere in der Automobilbranche, setzen heutzutage neben etablierten Testverfahren vermehrt auf Simulationen in der Produktentwicklung. Dieser Trend führt zunächst zu einer doppelten Dokumentationsarbeit und erhöht somit die Arbeitslast. Zudem steigt die Komplexität des Datenmanagements aufgrund der Nutzung unterschiedlicher Ablageorte für diese Simulations- und Testdaten. Trotz dieser anfänglichen Herausforderungen können optimal implementierte Simulationsmodelle jedoch die Anzahl der physischen Tests elementar reduzieren.

Für eine zielführende Umsetzung dieser Art von Ressourcenreduktion ist es jedoch entscheidend, dass die Planung der Tests und Simulationen verknüpft erfolgt und nicht unabhängig voneinander stattfindet. Insbesondere im Hinblick darauf, dass eine kostenoptimierte Durchführung von CAE-Berechnungen und Tests einen entscheidenden Wettbewerbsvorteil in der technischen Dienstleistung darstellt. Daher kann eine verknüpfte Test- und Simulationswelt maßgeblich zum wirtschaftlichen Erfolg eines Unternehmens beitragen.

Ein zusätzlicher Nutzen entsteht, wenn die in Relation gesetzten Daten als Trainingsgrundlage für ein KI-Modell dienen. Mithilfe eines solchen Modells können Projekte, die auf dem Vergleich von Test und Simulation basieren, kostengünstig als Dienstleistung angeboten werden. Ein Beispiel hierfür wäre die Untersuchung des Crash-Verhaltens von Fahrzeugen.

Das erfolgreiche Management von Simulations- und Testdaten in einem PLM-System bildet zudem die Basis eines Assistenzsystems im Rahmen des BMWK-geförderten Forschungsprojekts „Entwicklungsplattform 4.0”.

In diesem Beitrag wird daher zunächst auf die Vorteile der hybriden Validierung und Verifizierung sowie der verknüpften Test- und Simulationswelt eingegangen. Zum Abschluss erfolgt ein Überblick über das erstellte neutrale Datenmodell sowie die Anpassung des PLM-Systems ARAS, um diese Verknüpfung technisch umzusetzen und somit die Effizienz und Qualität der Entwicklungsprozesse weiter zu verbessern.

2 Hybride Validierung & Verifizierung

Die hybride Validierung und Verifizierung steht im Mittelpunkt eines umfassenden Ansatzes zur Gewährleistung der Qualität und Zuverlässigkeit von Produkten oder Systemen. Durch die Integration verschiedener Validierungs- und Verifizierungstechniken wird eine breite Abdeckung der Produktmerkmale und -funktionen erreicht. Diese umfassende Prüfung ermöglicht es, potenzielle Probleme zu identifizieren und anzugehen, bevor sie sich zu größeren Schwierigkeiten entwickeln.
Die Flexibilität hybrider Ansätze ist ein weiterer Schlüsselvorteil. Sie ermöglichen eine anpassungsfähige Herangehensweise, die spezifischen Anforderungen und Eigenschaften eines jeden Produkts oder Systems gerecht wird. Tools wie ReqMan können beispielsweise dabei helfen, Kundenanforderungen angemessen herunterzubrechen oder zu splitten, um eine effektive Prüfung sicherzustellen.

Durch die Kombination mehrerer Validierungs- und Verifizierungstechniken können Schwachstellen und Fehler präziser identifiziert werden. Dies führt zu einer insgesamt höheren Qualität des Endprodukts oder -systems, da potenzielle Mängel frühzeitig erkannt und behoben werden können.

Ein weiterer Vorteil liegt in der Risikominderung. Die Nutzung verschiedener Techniken zur Validierung und Verifizierung ermöglicht es, verschiedene Blickwinkel und Herangehensweisen einzubeziehen, was wiederum dabei hilft, potenzielle Risiken frühzeitig zu erkennen und zu mindern.

Die Effizienz des Validierungs- und Verifizierungsprozesses wird durch hybride Ansätze ebenfalls gesteigert. Indem die Stärken verschiedener Techniken genutzt werden, können Probleme schneller identifiziert und gelöst werden, was letztendlich zu einer beschleunigten Markteinführung des Produkts führt.

Eine gründliche Validierung und Verifizierung trägt nicht nur zur Verbesserung der Produktqualität bei, sondern führt auch zu einer insgesamt verbesserten Benutzererfahrung. Durch die frühzeitige Erkennung und Behebung potenzieller Probleme oder Mängel werden Kundenbedürfnisse besser erfüllt.

Die Kombination verschiedener Ansätze zur Validierung und Verifizierung trägt schließlich dazu bei, die Gesamtzuverlässigkeit des Produkts oder Systems zu erhöhen, da eine Vielzahl potenzieller Schwachstellen adressiert wird. Dies führt zu einer gesteigerten Kundenzufriedenheit und einer stärkeren Positionierung im Markt.

Insgesamt bietet die hybride Validierung und Verifizierung eine robuste und effektive Methode, um die Qualität und Zuverlässigkeit von Produkten und Systemen sicherzustellen. Durch die Integration verschiedener Techniken können die Vorteile jedes Ansatzes maximiert werden, was letztendlich zu einem erfolgreichen Produkt oder System führt.

3 Vernetzung Simulations- und Testwelt

Die Verknüpfung von Test- und Simulationsumgebungen bietet eine Vielzahl von Vorteilen, die die Effizienz und Qualität der Produktentwicklung maßgeblich beeinflussen. Ein herausragender Aspekt ist die Kosteneffizienz, da Simulationen die Notwendigkeit teurer physischer Prototypen und Testausrüstungen drastisch reduzieren können. Insbesondere bei komplexen und kostenintensiven Testverfahren führt dies zu erheblichen Kosteneinsparungen, die den Entwicklungsprozess ökonomisch optimieren.

Darüber hinaus ermöglichen Simulationen eine erhebliche Beschleunigung des Testprozesses im Vergleich zu physischen Prototypen. Die schnelle Durchführung von Tests verkürzt die Time-to-Market für neue Produkte oder Systeme erheblich, was wiederum die Wettbewerbsfähigkeit des Unternehmens steigert und einen früheren Zugang zu neuen Marktchancen ermöglicht.

Die Kombination von Simulationen und physischen Tests eröffnet auch die Möglichkeit einer umfassenderen Testabdeckung. Während Simulationen bestimmte Szenarien leicht reproduzieren können, bieten physische Tests oft eine realistischere Validierung. Durch die synergetische Verknüpfung beider Ansätze können daher mehr Testfälle abgedeckt werden, was die Zuverlässigkeit der Testergebnisse verbessert und potenzielle Risiken minimiert.

Die Flexibilität von Simulationen ermöglicht es, Testbedingungen zu variieren und verschiedene Szenarien schnell zu modellieren. Dies erlaubt eine agile und iterative Testmethodik, die es Entwicklern ermöglicht, verschiedene Designoptionen effektiv zu evaluieren und zu optimieren, um die Anforderungen und Erwartungen der Kunden optimal zu erfüllen.

Des Weiteren tragen Simulationen dazu bei, potenzielle Probleme frühzeitig im Entwicklungsprozess zu identifizieren und zu beheben, was das Risiko von Fehlern oder unerwarteten Problemen in späteren Entwicklungsphasen minimiert. Durch die frühzeitige Erkennung und Behebung von Problemen wird die Produktqualität insgesamt verbessert und die Kosten für spätere Fehlerkorrekturen gesenkt.

Die Verknüpfung von Test- und Simulationsdaten ermöglicht es, wertvolle Erkenntnisse über das Verhalten des Produkts oder Systems zu gewinnen. Diese Erkenntnisse können genutzt werden, um zukünftige Designs zu verbessern, die Leistung weiter zu optimieren und Innovationen voranzutreiben. Insgesamt bietet die Verknüpfung von Test- und Simulationsumgebungen eine leistungsfähige Methode, um die Produktentwicklung zu beschleunigen, Kosten zu senken und die Qualität zu verbessern. Durch die synergistische Integration verschiedener Test- und Simulationsmethoden können Unternehmen ihre Wettbewerbsfähigkeit stärken und innovative Lösungen schneller auf den Markt bringen.

4 Vorgehen im Forschungsprojekt „Entwicklungsplattform 4.0“

4.1 Allgemeine Informationen

Im Rahmen des Forschungsprojekts „Entwicklungsplattform 4.0" wird nicht nur eine Verbesserung der Effizienz und Qualität in der Produktentwicklung angestrebt, sondern auch eine umfassende Unterstützung für unerfahrene Ingenieure sowie die Konservierung und Zugänglichmachung des Wissens erfahrener Fachkräfte. Diese ambitionierten Ziele werden durch die bereits erwähnte Ressourceneinsparung im Bereich der Simulationen und Tests erreicht, wobei eine strukturierte und vernetzte Ablage bis auf die Parameterebene eine zentrale Rolle spielt [1].

Besonders bedeutend ist dabei die Parameterebene, da zahlreiche kostengünstige Simulationen dazu genutzt werden können, Tests zu definieren und kritische Bereiche bzw. Parameter vorab zu identifizieren. Auf diese Weise kann eine beträchtliche Einsparung finanzieller Ressourcen durch die Reduzierung physischer Tests erreicht werden. Derzeit erfolgt diese Effizienzsteigerung jedoch hauptsächlich durch die Erfahrung von langjährigen Mitarbeitern, die über das notwendige Fachwissen verfügen.

Um eine wettbewerbsfördernde hybride Validierung und Verifizierung zu ermöglichen, ist eine vernetzte Planung von Tests und Simulationen in einem PLM-System unerlässlich. Zu diesem Zweck wurde im Rahmen des Forschungsprojekts zunächst ein neutrales Datenmodell entwickelt, das sich auf die strukturierte Vernetzung von Simulations- und Testdaten konzentriert. Dieses Datenmodell wurde in das vorhandene PLM-System ARAS integriert und um fehlende Elemente erweitert (siehe 4.2), um eine nahtlose Verbindung zwischen Simulationen und Tests zu gewährleisten.

Zusätzlich wurde ein Testdatenmanagement neu konzipiert und die Relationen zwischen den Simulations- und Testdaten klar definiert (siehe 4.3). Durch diese Maßnahmen wird eine transparente und konsistente Dokumentation der hybriden Validierung und Verifizierung in einem System gewährleistet. Diese nachvollziehbare und durchgängige Verknüpfung trägt dazu bei, dass das gesammelte Wissen und die Ergebnisse der Entwicklungsarbeit effizient genutzt werden können und einen nachhaltigen Beitrag zur kontinuierlichen Verbesserung der Entwicklungsprozesse leisten.

4.2 Neutrales Datenmodell

Das definierte neutrale Datenmodell enthält alle Standard-Objekttypen eines PLM-Systems und umfasst insgesamt 70 verschiedene Datentypen. Mit dem Ziel, die Simulations- und Testwelt miteinander zu verknüpfen, wurde bei der Erstellung des neutralen Datenmodells und der Definition der Objekttypen der Fokus in erster Linie auf mehrere Simulations- und Test-Objekttypen sowie auf deren Relationen gelegt (siehe Figur 1). So gehört zu einem Auftrag beispielsweise immer eine Simulationsaufgabe (Simulation Task) und ein physikalischer Test (Physical Test), zu denen wiederum immer Reports, Ergebnisse und Parametersätze (Input Parameter) gehören.
Mit diesem Datenmodell ist der Vergleich von Test und Simulation bis auf die Parameterebene dokumentierbar.

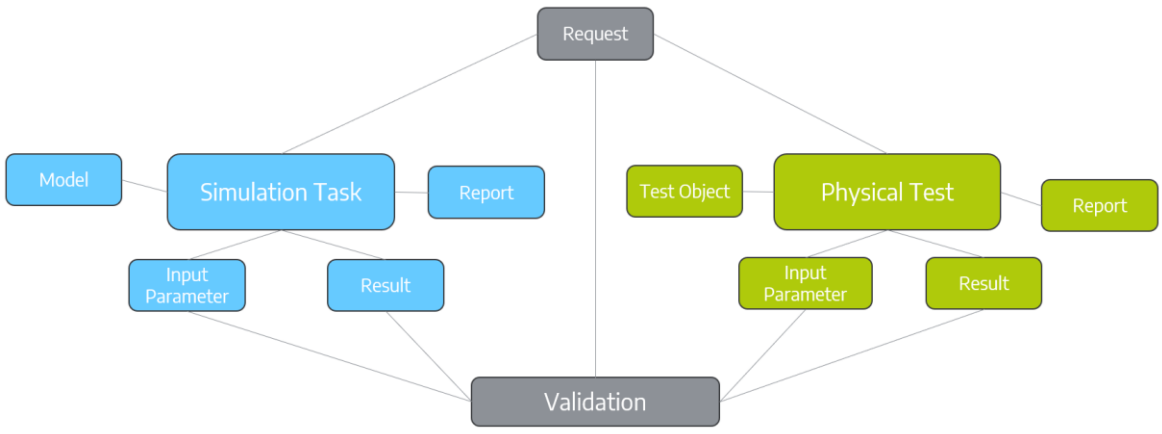

Figur 1: Schematischer Auszug aus dem Datenmodell, der die Simulations-Objekttypen (blau) und die Test-Objekttypen (grün) zeigt

Für Simulation und Test wurden die in Tabelle 1 gelisteten Attribute definiert. Bei „Behavior“ kann z.B. angegeben werden, ob das Verhalten „incompressible“ oder „compressible“ ist.

Tabelle 1: Übersicht der definierten Attribute für Simulation und Test

Attribute Simulation	Attribute Test
Behavior	Classification
Changed By	Created On
Input Data	Description
Method	ID
Project	Input Data
Simulated by	Method
Simulation Method	Owner
Status	Project
Status 12	Constraints
Type of Physics	Responsible Engineer
Physics Nature	Result – successful or not
Complexity	Status
Time Dependency	Type
	Target Parameter
	Time Dependency

4.3 Anpassung ARAS

Im PLM-System ARAS können sowohl die Lastfälle als auch die Simulationsmodelle mit entsprechenden Informationen und Parametern hinterlegt werden. Über die Modellnummern können diese dann verknüpft werden. Um die Verknüpfung zu erzielen, die ebenfalls die Art der Beziehung zeigt, wurden in ARAS sowohl für die Simulationen als auch für die Tests Relationen definiert. Diese sind inkl. Beschreibung der Tabelle 2 zu entnehmen. Figur 2 zeigt die Umsetzung in ARAS.

Tabelle 2: Relationen für Simulation und Test im PLM-System ARAS

Relationen Simulation	Beschreibung / Beispiele
sm_Task DesignRepresentation	Verbindet die Simulation mit CAD Daten
sm_Task Document	Verbindet die Simulation mit taskrelevanten Dokumenten, welche nicht explizit als Input oder Output gelistet werden sollen
sm_Task InputArtifact	Verbindet die Simulation mit Elementen, welche Einfluss auf die Simulation nehmen. Zum Beispiel Parametersätze, Materialdaten, Skripte, u.v.m.
sm_Task OutputArtifact	Verbindet die Simulation mit allen Elementen, welche bei der Simulation anfallen.
sm_Task SimulationModel	Verbindet die Simulation mit dem Simulationsmodell (CFD, FEA, 1D, 3D Modell).
sm_Task Guidelines	Verbindet die Simulation mit Hilfen, Methoden und Anleitungen, welche bei der Simulation befolgt wurden oder geholfen haben

Relationen Test	Beschreibung / Beispiele
tm_em_Guidelines	Verbindet den Test mit Hilfen, Methoden und Anleitungen, welche bei dem Test befolgt wurden oder geholfen haben
tm_em_Planning	Verbindet den Test mit Testressourcen wie Prüfständen, deren Belegung und dem Skilllevel der Bediener
tm_em_Report	Verbindet den Test mit Ergebnisreport
tm_em_Run	Verbindet den Test mit einem oder mehreren individuellen Testläufen mit ihren Ergebnis Daten (Rohdaten, Messchriebe und Ähnliches)
tm_em_TestObject	Verbindet den Test mit den Daten des physischen Testobjekts

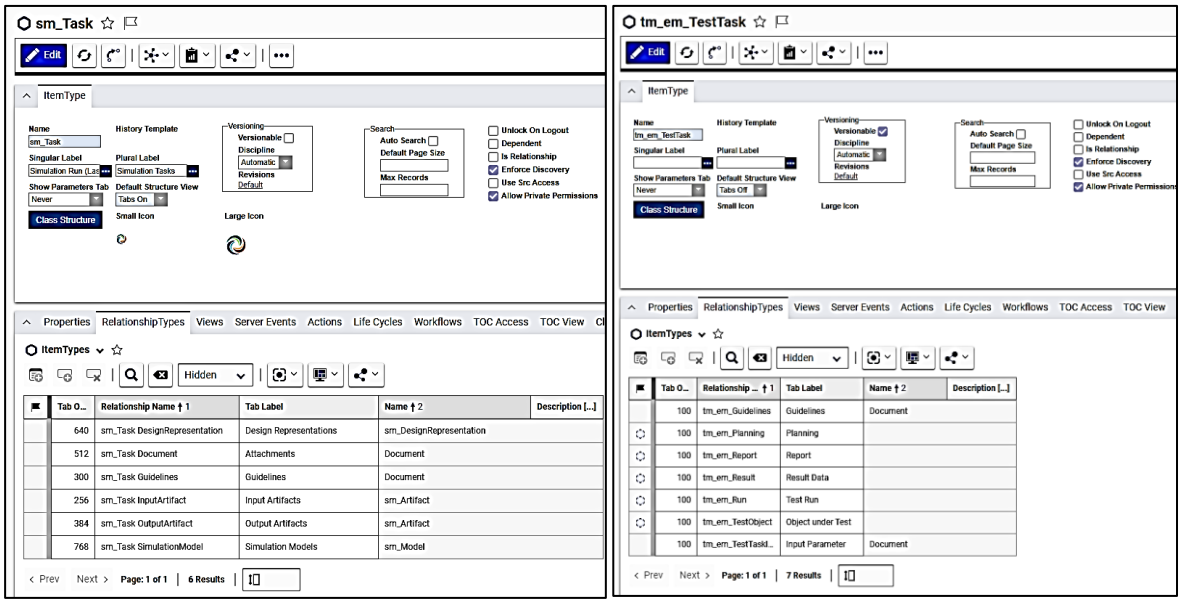

Figur 2: Relationen der Simulation (links) und Relationen des Tests (rechts) im PLM-System ARAS

Durch die angelegten Relationen können sowohl die Simulationen als auch die Tests mit allen notwendigen Informationen verknüpft und bei den entsprechenden Lastfällen hinterlegt werden. Wird also ein Lastfall im PLM-System ARAS aufgerufen, so erhält der Anwender eine Übersicht über alle damit verbundenen Simulationen und Tests sowie dazugehörigen Informationen, z.B. CAD-Daten.

Diese vernetzte Welt dient dann als Basis für ein KI-Modell, welches anhand dieser Daten dem Nutzer eine Handlungsempfehlung hinsichtlich durchzuführender Simulationen und Tests liefert. Hierfür werden zu dem aktuellen Lastfall ähnliche bzw. passende Lastfälle in der Datenbank gefiltert und die dort durchgeführten Simulationen und Tests bewertet. Diese Informationen werden vom KI-Modell interpretiert und es erfolgt ein Vorschlag, welche Simulationen bzw. Tests durchgeführt werden sollten, um das Projekt erfolgreich abzuschließen.

5 Zusammenfassung und Ausblick

Die Integration und Verknüpfung der Simulations- und Testumgebungen innerhalb eines PLM-Systems stellen einen bedeutenden Schritt dar, um die Wettbewerbsfähigkeit von Unternehmen zu stärken. Diese nahtlose Verbindung ermöglicht eine hybride Validierung und Verifizierung, die einen wesentlichen Beitrag zum wirtschaftlichen Erfolg von Unternehmen leisten kann. Durch die Zusammenführung von Test- und Simulationsdaten ergeben sich eine Vielzahl von Vorteilen, darunter Kosteneffizienz, Zeitersparnis, Risikominderung, umfassende Testabdeckung, verbesserte Produktqualität, sowie erhöhte Flexibilität und Wissensgewinn.

Insbesondere die Vernetzung von Simulations- und Testdaten dient als Grundlage für die Entwicklung und das Trainieren von KI-Modellen. Diese Modelle können genutzt werden, um Projekte, die auf dem Vergleich von Simulation und Test basieren, kostengünstig als Dienstleistung anzubieten. Durch die Verwendung von KI-gestützten Analysen und Vorhersagen können Unternehmen ihre Entwicklungsprozesse optimieren und ihre Leistung auf dem Markt verbessern.

Des Weiteren bildet das erfolgreiche Management von Simulations- und Testdaten in einem PLM-System die Grundlage für ein Assistenzsystem im Rahmen des Forschungsprojekts „Entwicklungsplattform 4.0". Dieses Projekt zielt darauf ab, unerfahrene Ingenieure und Nicht-Experten bei ihrer täglichen Arbeit zu unterstützen und das wertvolle Fachwissen erfahrener Mitarbeiter zu konservieren und zugänglich zu machen. Durch die Integration von verknüpften Simulations- und Testdaten in dieses Assistenzsystem wird die Effizienz und Qualität der Arbeit weiter gesteigert, was letztendlich zu einem nachhaltigen Erfolg des Unternehmens beiträgt.

Insgesamt ermöglicht die nahtlose Vernetzung von Simulations- und Testumgebungen in einem PLM-System eine effektive Nutzung von Ressourcen, eine Verbesserung der Prozesseffizienz und eine Steigerung der Wettbewerbsfähigkeit. Diese integrative Herangehensweise unterstützt Unternehmen dabei, sich in einem dynamischen Marktumfeld zu behaupten und ihre Position zu festigen.

6 Danksagung

Dieses Forschungs- und Entwicklungsprojekt wird durch das Bundesministerium für Wirtschaft und Klimaschutz (BMWK) im Rahmen des Verbundprojekts „Aufbau einer Entwicklungsplattform 4.0 – EP 4.0“ gefördert (Förderkennzeichen 19I21020A) und zudem unterstützt durch den TÜV Rheinland Consulting GmbH, Projektträger Bodengebundene Verkehrstechnologien (PT BVt) mit der Vereinbarung № 19 I 21020A (June 02, 2021). Dafür danken wir dem BMWK und dem TÜV Rheinland.

Träger:	BMWK
Fachprogramm:	Neue Fahrzeug- und Systemtechnologien
Schwerpunkt:	Künstliche Intelligenz als Schlüsseltechnologie für das Fahrzeug der Zukunft
Beteiligte Partner:	SEGULA Technologies, FKFS, :em AG, Fraunhofer IESE (UB)
Projektbeginn:	01.06.2021
Projektdauer:	3,5 Jahre

7 Literaturverzeichnis

[1] Vorhabensbeschreibung “Entwicklungsplattform 4.0”. Konsortialteam des Forschungsprojekts (2021)

Scale and democratize Reduced Order Modeling techniques within an SPDM framework

M. Turchetto, A. Viola (ESTECO SpA, Italy)

T. Gloesslein (ESTECO Software Gmbh, Germany)

1 Abstract

Physics-based simulations such as Computational Fluid Dynamics (CFD), require a lot of computational power, memory, and storage. This typically requires a lot of time and that's why the use of CFD is restricted to the design cycle and pre-production phases. The ideal scenario is to employ CFD during the conceptual design phase, allowing you to get a precise understanding of how a product performs under various conditions before moving into more expensive stages of product development. To make it happen, there is an increasing trend towards leveraging simulation data to train mathematical models with Machine Learning (ML) techniques to overcome some of the challenges of physics-based simulation methods. In particular, ML methods coupled with Reduced Order Modeling (ROM) offers a powerful approach to deal with complex, high-dimensional problems that are typically associated with 3D CAE simulations. It reduces the complexity of a full-order numerical model while preserving its essential behavior.

Despite all of their benefits, data-driven modeling approaches like ROM are still not widely adopted for a number of reasons. These include but are not limited to the difficulty of storing, versioning and tracing data for the ROM training without an SPDM framework in place. Also, ROM training requires a lot of expertise to fine-tune the ROM and integrate it in an automated design loop. This makes it challenging to extend the usage of ROM-based tools to design engineers and other stakeholders.

What if you could rely on a Simulation Process and Data Management (SPDM) framework to store and re-use data to train reduced order models, and make them usable by a wider audience of engineers? Considering a common fluid dynamic problem like the analysis of the flow field past airfoils with different shapes, we demonstrate how an SPDM framework can be beneficial to manage all the data associated with the simulations and ROM training while allowing for them to be easily interrogated by non-experts to simulate new accurate designs in a fraction of the time.

2 Case study: Democratizing physics-based and data-driven modeling/analysis of flow past airfoils within a collaborative SPDM framework

CFD simulations are a cornerstone for aerodynamic design, but their complexity requires expertise and great computational resources. This simplified case study introduces a new collaborative approach which combines the use of an SPDM framework with ROM techniques to achieve rapid performance assessments of an airfoil's design performance. We envision a scenario where two kinds of engineers are involved:

- Simulation expert who is responsible for creating CFD results, training the ROM with that data and making it available to others for fast design predictions
- Designer who typically has a strong understanding of design principles without an in-depth background in CFD would perform ROM-based predictions by using a simplified application (already trained and validated by the subject matter expert)

Performing an airfoil's external aerodynamics simulation is a complex task that demands a deep understanding of mesh structuring and creation, fluid dynamics, computational methods, and specific characteristics of the airfoil. The goal of such a simulation is to accurately predict the airfoil's performance under various conditions, providing valuable insights for the design and optimization of wing structures. But, several factors contribute to the complexity of airfoil simulations. Proficiency with

specialized simulation software and a deep understanding of fluid dynamics principles are essential for obtaining accurate and useful results. And, the computational resources needed to run these simulations can be substantial, particularly for complex or unsteady flow conditions. In this scenario, machine learning methods coupled with ROMs provide a pragmatic solution to the challenges posed by the high computational demands of full-scale 3D CAE simulations. By enabling the construction of accurate, significantly less resource-intensive surrogate models, ROMs allow for quicker, more cost-effective analyses in the field of CAE.

The ROM approach is ideally suited for solving complex, high-dimensional problems associated with 3D CAE simulations. It reduces the complexity of a full-order numerical model while maintaining its essential characteristics. With ROM, you are getting a comprehensive model of your problem, in this use case the entire flow field around the airfoil, rather than a quantity of interest as with standard Response Surface Models (RSM). It employs a non-intrusive mathematical technique called Proper Orthogonal Decomposition (POD) to encode the solution space and reduce its dimensionality.

ROMs represent a low-cost surrogate for the full-order model, but remain explainable by encapsulating the relevant core features and behaviors of the original problem through the POD. As a result, quasi-real-time evaluations of physical phenomena can be carried out, exploiting the information provided by a carefully selected or in some cases pre-existing set of design solutions.

The first step towards training ROMs is to build CAE datasets to assess the external aerodynamic performance of the airfoil with process automation and design optimization software like modeFRONTIER. By integrating the open source CFD solver OpenFOAM into the simulation workflow, the simulation expert can apply design of experiments (DOE) algorithms to generate a small training dataset that explores the input variable designs pace like the angle of attack of the airfoil and its shape for the aircraft aerodynamic assessment. At the end of this phase, the simulation expert can analyze the airfoil design dataset(s) by training a ROM which employs a mathematical technique called Proper Orthogonal Decomposition (POD) and a regression model (Radial Basis Function, Gaussian Processes or Neural Network).

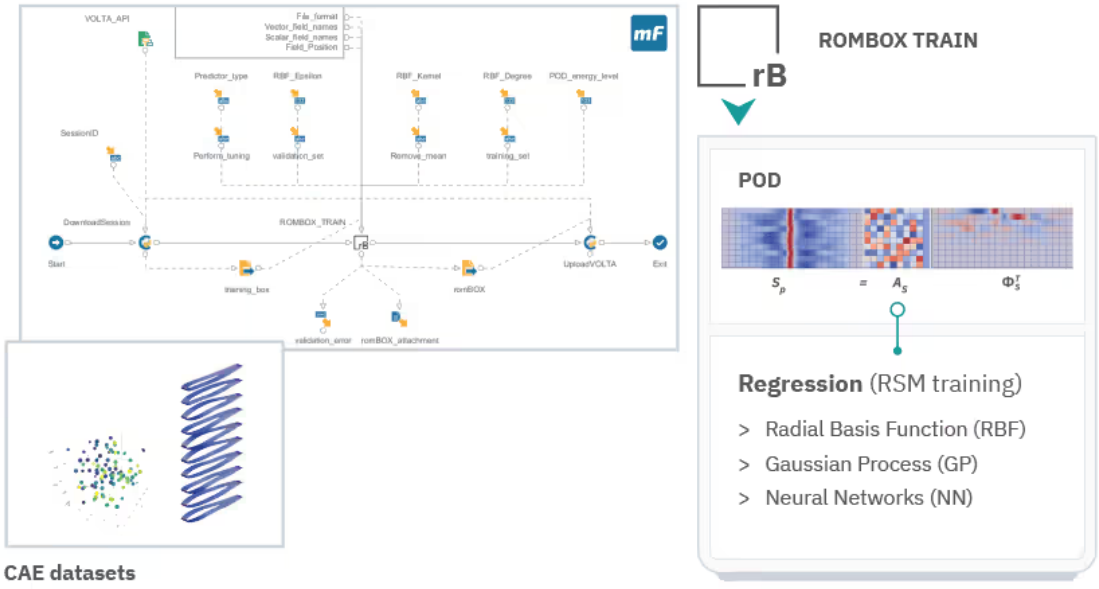

Figure 1

ROM methodology: Proper Orthogonal Decomposition (POD) + regression model

The simulation expert can use the trained reduced order model for predictions by executing ROM-based fluid dynamics analysis through a simulation workflow that exposes the geometrical parameters that were originally used to explore the design space. This workflow can then be made available to a non-

simulation expert like a design engineer within an SPDM framework like ESTECO VOLTA to quickly predict the aerodynamic behavior, similarly as in the case of directly using CFD simulations.

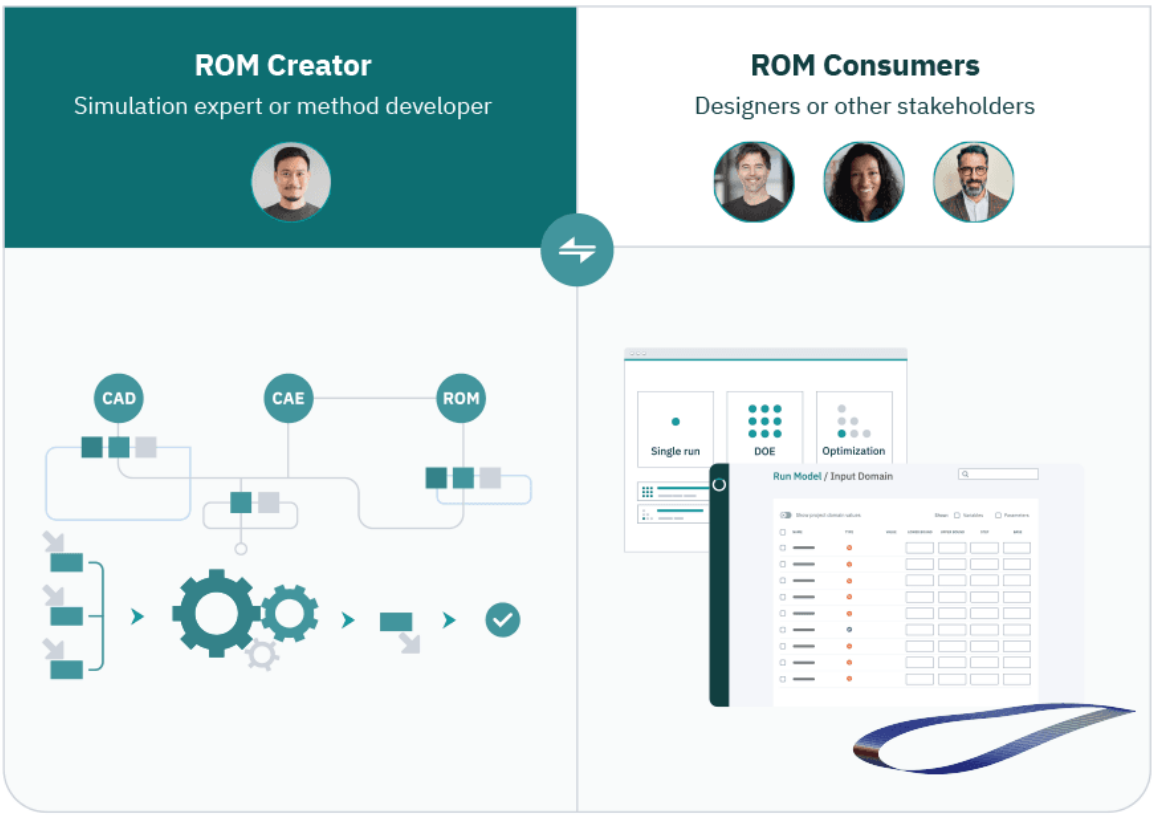

Figure 2

An SPDM system for different ROM users

By using this approach, all numerical models can be managed rationally and everything applicable that has been evaluated before can be used to train and validate ROMs. These models can be easily interrogated by non-simulation experts from a simplified web interface to make these methodologies more accessible across the development process. As a result, they can evaluate hundreds of new designs nearly instantly and determine whether they satisfy specific KPIs.

3 Conclusions

Unlike complex and time-consuming CFD simulations, the execution of ROM-based simulations from a web-based SPDM framework enables non-coding engineers to obtain rapid predictions of an airfoil's aerodynamic performance for various design configurations. This facilitates iterative design exploration and decision-making from early on in the development and design process, allowing designers to focus on the most promising design variations while minimizing their reliance on the expert's time.

4 References

[1] Battaglia L., Carlini F., Clarich A., Russo R.: "an uncertainty quantification method based on proper orthogonal decomposition and polynomial chaos expansion", AeroBest 2023, 2023

Raising the treasure of SPDMs –

How data compression and automatized event detection support engineers

D. Borsotto, V. Krishnappa, S. Müller, F. Natter, T. Roth, K. Schreiner, H. Talaat, C.-A. Thole, T. Weinert

SIDACT GmbH, Germany

1 Introduction

To cope up with the ever growing amount of simulation runs being performed, tools and techniques are needed to store the huge amount of simulation data and to make use of data being stored. While current Simulation Data Management systems allows managing and accessing datasets and would facilitate putting this into action for analysis, the demand on bandwidth and storage increases.
Even with SPDMs, the users usually only had tools and time to make rather straight forward model to model comparisons, between current model versions and their immediate predecessors. To take analysis capabilities and model development a leap forward, it is necessary to also make use of whole model development branches to learn from the gathered simulation information. With the availability of such tools, the value of past simulation data increases.
This gives rise to two challenges. The first challenge is to implement an efficient storage mechanism keeping as many simulation results as possible. This challenge can be met by data compression. It has proven in many application fields that specialized compression tools like FEMZIP [1] for simulation results outperforms general compression tools like Winzip [2].
The second challenge is to introduce a tool capable of analyzing Terabytes of simulation result files and supporting the engineer in his task of creating crashworthiness design.
Model order reduction allows building a database meeting the second challenge. Continuously being fed with new simulation runs, a database makes it in reasonable time possible to automatically detect unknown behavior in the most recent simulation runs compared to all predecessors at a time. To achieve this, the database does not only need to store and detect every new deformation pattern, but in addition needs to handle geometric changes and being able to detect local effects.
Such databases allow to automatically detecting anomalies within the crash deformation behavior, pinpointing exactly to the location in space and time where the model is showing unknown or unwanted deformation patterns. While in daily work the engineer often only has time to compare single simulations with each other, this approach shows how to compare the current simulation with hundreds of predecessors at a time.

2 Benchmark Data set

In this paper, we investigate our strategies on the LS-DYNA™ [3] model of the Chevrolet Silverado modeling a frontal crash. It is provided free of charge by the National Highway Traffic Safety Administration (NHTSA), see [4]. The model consists of 929.181 elements, 682 parts divided into 34 1D elements, 567 2D elements and 81 3D elements. The model was simulated 50 times with sheet thickness variations without geometric changes. 152 time steps with a sampling rate of 1ms were written out. Thus, the temporal resolution is twice as high in comparison to simulation results, which are generated nowadays by automobile manufacturers. On the other hand, the number of elements is smaller by a factor of 5. The uncompressed size is for the array of simulation results is 452.7 GB.

3 Data Compression

For our compression approach, we follow three ideas.
The first strategy is motivated by the Rate-Distortion theory [5]. Loosely speaking, it says „The greater the permissible reconstruction error, the higher the compression rate." Since numerically simulated data contains numerical and modelling errors anyways, a lossy compression seems reasonable.
The second idea is to remove as many dependencies in the data as possible by predicting values with already processed values. We perform this step to improve the statistical properties for compression.

The third strategy is to apply an asymmetric compression with spending more time for compression than for decompression. Since the compression can be performed directly on an HPC system with high CPU performance for a simulation that usually need several hours up to days to complete, it is reasonable, if the on-the-fly decompression, e.g. when loading the data set into a postprocessor, is accelerated.
In the following section, we address the main components of our proposed compression strategy. We focus on the lossy compression of numerically simulated floating point data since it is generally dominating the size of simulation results.
The main steps of the proposed compression strategy are:

1. Quantization
2. Prediction
3. Encoding

In the quantization step, we map a floating point number to an integer, considering a user specified precision, the so-called quantum q. Hereby, we divide the floating point number f by the quantum q and round it to the next integer number i:

$$i = round\left(\frac{f}{q}\right).$$

This procedure is called absolute quantization [2]. At time of decompression, the original floating point value f can be reconstructed by

$$\tilde{f} = i \cdot q.$$

With the quantization, we introduce a loss in precision for the floating point value f bounded by the reconstruction error

$$e_f = \left|f - \tilde{f}\right| \leq \frac{q}{2}.$$

After quantization, the resulting integer values can be predicted exploiting the knowledge regarding the finite element model used to simulate the data. The main idea is to eliminate redundancies in time and space and between similar simulation results. This reduces the entropy of data sets which can be utilized by several encoders, e.g. entropy encoders [4].
In the last compression stage, we encode the residuals of prediction. If the data was predicted well, the range of different numbers will be much smaller than the number of all possible values in the 32 Bit range. Therefore, we can provide shorter bit representations for frequently occurring values. This leads to the application of an entropy encoder like Huffman coding or arithmetic coding [6] or specialized mesh-based encoders, like the induced Markov chain encoder [7].

The applications of the compression strategies for the use cases of compression of single simulation results and compression of an array of simulation results follow.

3.1 FEMZIP

Data compression has become an integral part of today's computer-aided engineering (CAE). Almost 20 years ago, our data compression approach was presented [8] and has since established itself as a unique compression tool on the market. The ability to return to the original d3plot output format eliminates a lock-in effect, allowing companies to remove FEMZIP from their processes without leaving any residue.
As part of a new development of FEMZIP-L, the compression and decompression algorithms have been parallelized to achieve significantly faster processing times. For the compression of a model, the runtime could be reduced from about 100 seconds for FEMZIP-L 13.02 with the compression option "-L4" to just under 40 seconds. For loading all post values into GNS Animator [9], the runtime could be accelerated from 143 seconds for FEMZIP-L 13.02 to 131 seconds for FEMZIP-L 15.
The compression efficiency is very high for the Silverado datasets, since post values that are not needed for the analysis are stored very imprecisely. These include the velocities and accelerations as node variables and the shell history element variables. Using the precisions as in [10], a compression ratio of 63.9 on average over all simulation results can be achieved, so that the data set can be reduced from an initial size of 452.7 GB to only 7.1 GB.

3.2 SDMZIP

In this section we investigate how similarities between simulation models can be exploited to improve compression compared to FEMZIP compression. For this purpose, we consider the Predictive Principal Component Analysis (PPCA) method [10, 11, 12], which is the core of the SDMZIP compression tool [13].
The compression is performed as follows. First, all available simulation models are decomposed into components and the geometry of the models is stored in a database (db). Subsequently, the time-dependent post values for each part (PID) are extracted from all result files and PCA [14] is applied to the respective data matrices. Here, the data matrix is first centered by subtracting the mean value of the row sum from each column. Subsequently, a singular value decomposition (SVD) is applied. The results of the SVD act as a dimension reduction method, where only the leading left-hand singular vectors (principal components) and right-hand singular vectors (coefficients), as well as the corresponding singular values, are further processed. For this purpose, the principal components are stored in the database and the coefficients in a simulation-specific file (ssf). The difference between PPCA and other methods using PCA for compression is that the reconstruction, i.e. the multiplication of the principal components with the singular values and the coefficients is used as a prediction for the data matrix. The error of the prediction is stored in the ssf-file. Thus, a given accuracy is maintained during decompression. The number of singular values and thus the dimension of the reduction is determined by an optimization procedure with regard to the compression rate to be achieved.
If all 50 LS-DYNA results of the Silverado model are already available for the proposed offline step, a compressed size of 1.4 GB for all simulation results can be achieved using the identical precisions as for FEMZIP-L, see Section 3.1. This is a factor of 5.1 more efficient compression than FEMZIP-L and a compression ratio of 326.4 is achieved, which means that the size has been shrunk to significantly less than 0.5% of the original size.
Usually, not all simulation results are available in an SPDM system, but they are calculated and added gradually during the development process. For this purpose, the Online procedure of the PPCA was developed. In this procedure, the data matrices for the post values of one part are predicted with the principal components already in the db file. If the crash behaviour of the newly added result is similar, the prediction error is small. If a new crash behavior occurs or new components are added, this data is written to a database update file (udb). With this procedure, the event space is learned little by little. Therefore, the compression rate for the Online use case, where one simulation result is added after the other, is worse than in the Offline case with a total compression rate of 235.3. However, the achieved compression rate is higher by a factor of 3.7 compared to FEMZIP-L and the compressed size is less than 0.5% of the original size as in the Offline case.

4 Model Order Reduction

With the data compression tools already presented, it is possible to hold a large number of models. But it is necessary to make a profit out of the data treasure. For this purpose we apply model order reduction (MOR) to compare new simulation results not only against single data sets but against a whole development tree. With this strategy, all simulations undertaken remain valuable and engineers benefit all the more from the work of their colleagues.
In the remainder of this section, we describe the implementation of MOR in the tool FEMALYST. First, data sets, should they have geometric changes, are mapped to each other. This achieves that models with geometric adjustments can also be compared. The comparison between the simulation results is then carried out in the FEMALYST Event Detection. For this purpose, individual simulation results are usually added to the database in an initialization phase. All subsequent results are then compared with the database. The comparison is based on the node positions as well as on the post values. Using the FEMALYST Event Score, the behavior in the simulation is evaluated for each component and if it behaves unexpectedly, it is marked as an anomaly.
In the following, we will go into more detail about the process and the techniques used and conclude this section with a short evaluation.

4.1 Geometric Mapping

One of the main challenges in making simulation results comparable over a complete development tree is the handling of geometric changes. We address this challenge with a geometric mapping. The user has the possibility to specify part ID (PID) ranges before starting the FEMALYST analysis. Within the PID ranges, the grid entities are mapped using a nearest neighbor method. For the elements, the topology of the finite element mesh is also taken into account. For strong geometric changes, there is the possibility to influence the mapping in such a way that the number of grid entities that are mapped

to an element or node is limited. With these strategies it is possible to make models with geometric changes comparable.

4.2 FEMALYST Event Detection

The techniques being developed focus both on the possibility to automatically spot unknown behaviour in new simulation runs, as well as being able to track known behaviour which engineers flag as being important. It allows detecting new behaviour/events within the current simulation compared to all predecessors and automatically raises this to the engineer.
The basic idea is similar to that of the Online procedure of SDMZIP, see Section 3.2. Using dimensionality reduction, in this case Principal Component Analysis (PCA) [14], a low-dimensional database is built. When a new dataset is added, it is examined how well the new dataset fits into the event space of the already processed datasets. If the data set is similar, a representation is well possible and no event is raised. If the behavior in individual components or subcomponents differs substantially from the previously learned event space, an event is raised and this is communicated to the user. Since event detection runs automatically as a batch process in the workflow, the user does not have to take any action and is warned that the crash behavior has changed even before opening the model in a postprocessor.

4.2.1 FEMALYST Event Score

The before mentioned detection of new events is based on a PCA related outlier score computation. This results in an event score in the range from [0;2] for every part and time-step, defining how much of an unknown behaviour this event represents. This also gives feedback to the engineer right away about how strong the outlier is, depending on the value of the event score. A score below 1 represents known behaviour, while scores above 1 represents unknown behaviour. The higher the FEMALYST score, the stronger the outlier.
With respect to the challenge of analysing crash structures it is mandatory to not only highlight complete parts which are conspicuous, but also the local segment of the part which showed the behaviour, which is why internally parts are being split into fragments, see Fig. 1, to also support a high geometrical resolution and detect local events. Additionally, next to the geometry also all post-values, as e.g. strains and stresses, as well as failure are being analysed.
To not only detect single part differences the event computation incorporates an event clustering. Based on the neighbourhood and the propagation of the deformation, parts are clustered together, forming events which also represent the propagation over time and space. Especially with respect to finding possible root causes for the deviation, this allows to get a first idea about the causal chain.

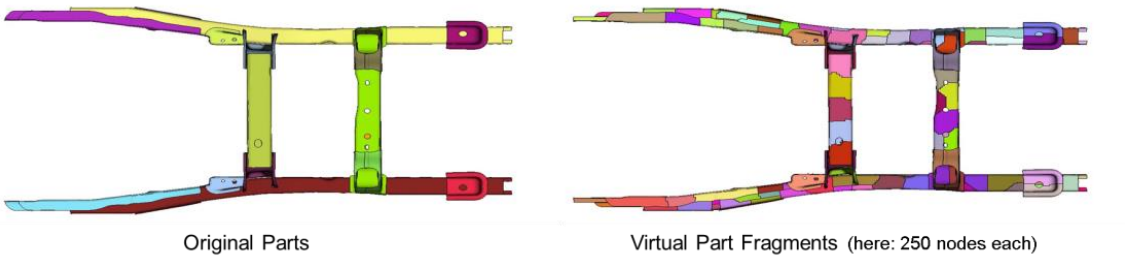

Fig. 1
Decomposition of parts to detect local events. Geometry taken from the example case: Chevrolet Silverado [4]

4.2.2 Tracking Events

As part of the process, the newly learned behavior is added to the database and is considered already known for future simulations. Since this can also include an unwanted behavior, the so-called tracked events were introduced, which offer the possibility to warn or inform the engineer when a certain behavior occurs.
Moreover, there are behaviors (desired/undesired) which the Engineer vividly remembers but cannot recall. In such situations, FEMALYST can act as a “search engine” for searching events of interest in the database. Such a search can reveal the simulations which show a behavior similar to the event searched and could also spot time-shifted behaviors. Event searches are computationally inexpensive and can be performed interactively, thanks to the precise characterization and representation of behavioral patterns in the database.

4.3 Evaluation

A detailed robustness analysis [16] [17] of a set of simulation runs from the Chevrolet Silverado [4], based up on thickness variations in the range of [-3;3] % , showed a clear bifurcation. While for some simulation runs the break-booster hooked up to the suspension, being pushed into the firewall, for others there was no such hook-up. Therefore, the test scenario shown here consists of a set of simulation runs with similar behavior of no hook-up and a newly analyzed simulation containing the hook-up, see Fig. 2.

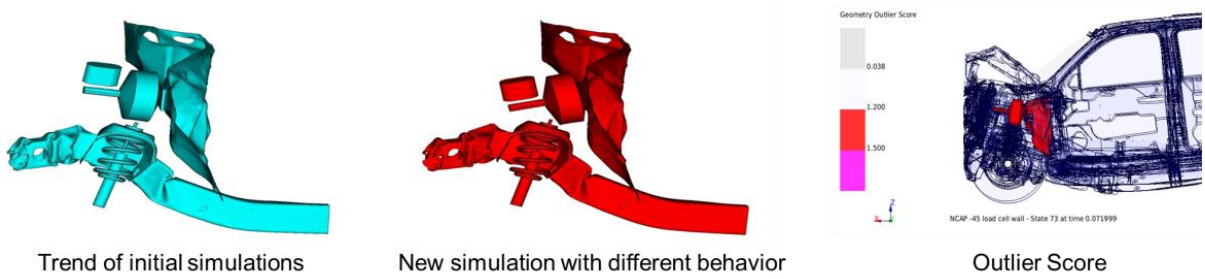

Fig. 2
Detection of different deformation patterns in a crash scenario. The outlier score automatically detects and highlights the area with new behavior

As seen in Fig. 2, the break booster and the firewall have outlier scores above 1.2 and are clearly marked as events.

5 Summary

SPDM systems make it possible to store simulation results in a structured way and to provide them with meta-information. By using efficient data compression, which focuses on compression efficiency as well as on the speed of decompression, SPDM systems become significantly more powerful, since more simulation results can be stored and processed faster. In addition, there is the possibility to apply novel compression algorithms, which on the one hand promise higher compression algorithms, and on the other hand provide the basis for automated analysis of new simulation results. This automated analysis supports the engineer by marking anomalies and evaluating them with the help of the FEMALYST Event score. With this, the engineer can already make statements as to whether a crash-relevant adjustment was successful, even before he opens the model in the postprocessor. On the one hand, this accelerates the development and, on the other hand, it relieves the engineer, since the complete model no longer has to be analysed and unexpected side effects are automatically reported.

6 Literature

[1] SIDACT GmbH, FEMZIP, https://www.sidact.de/femzip (accessed 05/03/2024).
[2] Corel Corporation, Winzip, https://winzip.com (accessed 05/03/2024).
[3] ANSYS Inc., “ANSYS LS-DYNA”, https://www.ansys.com/de-de/products/structures/ansys-ls-dyna (accessed 05/03/2024).
[4] NHTSA, Chevrolet Silverado, https://www.nhtsa.gov/sites/nhtsa.gov/files/mass-reduction-feasibility-2014-silverado.zip (accessed 05/03/2024).
[5] T. M. Cover and J. A. Thomas, Elements of information theory. Hoboken, N.J.: Wiley-Interscience, 2006.
[6] D. Salomon, Data Compression: The Complete Reference, Springer-Verlag New York, Inc., Secaucus, NJ, 2006.
[7] S. Müller, “Induced markov chains for the encoding of graph-based data”, In Signal Processing and Information Technology (ISSPIT), 2014 IEEE International Symposium, pp. 143–148.
[8] C.-A. Thole, Compression of LS-DYNA Simulation Results using FEMZIP, presented at the 5th European LS-DYNA User Conference, Birmingham, 2005.
[9] GNS, “Animator”, https://www.gns-mbh.com/products/animator4/ (accessed 05/03/2024).
[10] S. Müller, “Compression of an array of similar crash test simulation results“, Logos Verlag, Berlin, 2022.

[11] S. Mertler, S. Müller, C.-A. Thole, “Predictive principal component analysis as a data compression core in a simulation data management system”. In Data Compression Conference (DCC), 2015, pp. 173–182.
[12] S. Mertler, S. Müller, C.-A. Thole, “EP2924585A1 Method for compressing observations of a plurality of test procedures“, EP Patent, 2015.
[13] SIDACT GmbH, SDMZIP, https://www.sidact.de/sdmzip (accessed 05/03/2024).
[14] J. Lee, M. Verleysen, “Nonlinear dimensionality reduction”. Springer, New York, 2007.
[15] SIDACT GmbH, FEMALYST, https://www.sidact.de/femalyst (accessed 05/03/2024).
[16] D. Borsotto, R. Strickstrock, C. A. Thole, Robustness analysis - Significant reduction of scatter occurrence, presented at NAFEMS Seminar: Optimization and Robust Design, March 23-24, 2015.
[17] SIDACT GmbH, DIFFCRASH, https://www.sidact.de/diffcrash (accessed 05/03/2024).

KI in CFD-Simulationen: Neuronale Netzwerke optimieren atmosphärische Wassergeneratoren zur Reduktion des Energiebedarfs

Florian Dirisamer (Digital Physics AI GmbH)

1 Zusammenfassung

Atmosphärische Wassergeneratoren (AWGs) gewinnen Wasser aus der Luft durch Kondensation, was besonders in trockenen Gebieten viel Energie erfordert. Ihre Energieeffizienz ist daher entscheidend für Nachhaltigkeit und Wirtschaftlichkeit, besonders in Regionen mit schlechter Energieversorgung, wie abgelegenen oder katastrophengeplagten Gebieten. Um die Energieeffizienz zu erhöhen, konzentriert sich die Forschung auf die Reduktion des Strömungswiderstands durch Optimierung der Leitungsquerschnitte und Umlenkungen. Das Paper verwendet eine gekoppelte Berechnung aus künstlicher Intelligenz (KI) und CFD-Simulation (Computational Fluid Dynamics) zur energie- und ressourcenschonenden Optimierung. Ein maschinelles Lernmodell (ML) beschleunigt die Simulationen und erzeugt neue Ergebnisse effizient. Simulationen zeigen, dass Umlenkbleche den Druckverlust verringern und die Strömungshomogenität verbessern, was den Wassergewinnungsprozess effizienter macht. Allerdings verursachen Umlenkbleche zusätzliche Produktionskosten, weshalb Wirtschaftlichkeitsbetrachtungen notwendig sind. Insgesamt kombiniert der Ansatz physikalische Simulationen mit KI, was erhebliche Zeit- und Ressourceneinsparungen ermöglicht und die Effizienz und Nachhaltigkeit der AWGs verbessert.

2 Motivation

Die Energieeffizienz atmosphärischer Wassergeneratoren (AWGs) (Fig. 1) ist von entscheidender Bedeutung, da sie die Nachhaltigkeit und Wirtschaftlichkeit dieser innovativen Technologie maßgeblich beeinflusst. AWGs, die Wasser aus der Luft gewinnen, indem sie die Feuchtigkeit kondensieren, benötigen beträchtliche Energiemengen – besonders in trockenen Gebieten mit niedriger Luftfeuchtigkeit, wo der Kondensationsprozess besonders energieaufwendig ist. Eine hohe Energieeffizienz bedeutet, dass weniger Energie benötigt wird, um die gleiche Menge Wasser zu erzeugen.

AWGs werden häufig in Regionen eingesetzt, die über eine schlechte Energieversorgung verfügen. Dazu gehören trockene und Wüstenregionen, abgelegene und isolierte Gebiete, Katastrophengebiete sowie Regionen mit verschmutztem oder kontaminiertem Wasser. In diesen Gebieten rückt die Energieeffizienz weiter in den Vordergrund. Um den notwendigen Energiebedarf zu decken, wird häufig auf Solarmodule zurückgegriffen, was die verfügbare Energiemenge stark einschränkt.

Da bei den Hauptkomponenten zur Wassergewinnung nur begrenzt Energie eingespart werden kann, konzentriert sich dieses Paper auf die Reduktion des Strömungswiderstands. Es untersucht die Optimierung der Leitungsquerschnitte und insbesondere der Umlenkungen im gesamten AWG, um die Energieeffizienz zu verbessern. Diese Optimierungen könnten entscheidend dazu beitragen, die Technologie effizienter und nachhaltiger zu machen, sodass sie auch unter herausfordernden Bedingungen zuverlässig und wirtschaftlich arbeiten kann.

Um auch bei der Entwicklung der optimierten Umlenkungen und den damit verbunden Simulationsaufgaben Energie- und Ressourcenschonend umzugehen, wird auf eine gekoppelte KI-CFD-Simulation zurückgegriffen, in welcher die Basiswerte für unterschiedliche Betriebspunkte durch wenige CFD-Simulationen ermittelt werden. Anschließend wird das Eingangs-Ausgangsverhalten der CFD-Simulation durch ein ML-Modell zurückgegriffen, welches nach der Erstellung des Modells innerhalb kürzester Zeit und äußerst ressourcenschonend neue Simulationsergebnisse erzeugen kann. Somit lassen sich die Umlenkungen des Luftstroms im AWG optimieren und der Energiebedarf senken.

Fig. 1

Beispielhafte Darstellung eines atmosphärischen Wassergenerators zur Gewinnung von Trinkwasser [1]

Methode

Hier wird eine Anwendung aus dem Bereich der Strömungsmechanik (CFD) vorgestellt, die neben der Finite-Elemente-Methode (FEM) eine der am häufigsten verwendeten Methoden in der Ingenieurssimulation ist. In der Regel sind Simulationen in diesem Umfeld äußerst zeitaufwendig und dauern oft mehrere Stunden oder auch Tage für einen einzelnen Designpunkt. Darüber hinaus stellt die Bestimmung sinnvoller Randbedingungen (BC) eine besondere Herausforderung dar, da eine Vielzahl an Geometrie und Materialparametern, sowie Randbedingungen und weiterer Eigenschaften einen erheblichen Einfluss auf den Druckverlust und die Strömungshomogenität im Auslass haben. Ein reduzierter Druckverlust führt zu einem reduzierten Energiebedarf im Lüfter, wohingegen eine verbesserte Strömungshomogenität im Auslass eine gleichmäßige Anströmung eines Wärmetauschers und somit eine erhöhte Effizienz in der Wassergewinnung erzielt. Die schematische Komponente für diese Präsentation ist in Fig. 2 dargestellt.

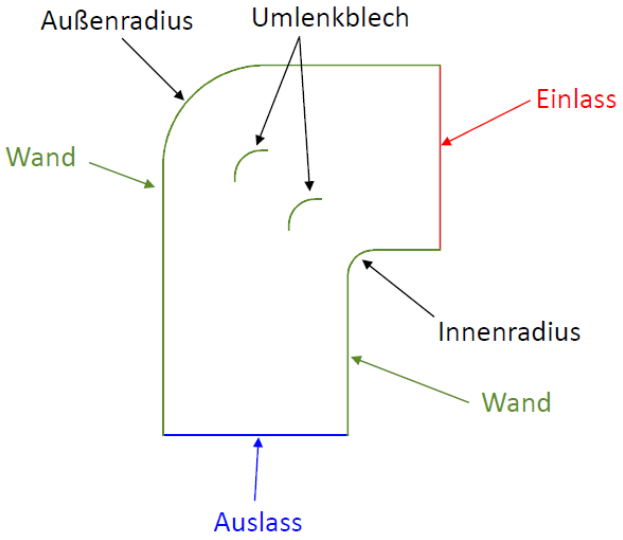

Fig. 2
Die Grundgeometrie der Struktur mit beschrifteten Komponenten, welche in unterschiedlichen Konfigurationen durch CFD-Simulationen ermittelt wurde

Die Simulationsergebnisse für eine Kombination aus Geometrieparametern sowie Randbedingungen, werden mittels CFD simuliert und der Druckverlust, sowie die Strömungsgeschwindigkeiten ermittelt. Aus diesen Strömungsgeschwindigkeiten bzw. insbesondere der Verteilung der Strömungsgeschwindigkeiten am Auslass kann die Strömungshomogenität ermittelt werden. Ein einzelnes Simulationsergebnis für die Struktur ist in Fig. 2 dargestellt.

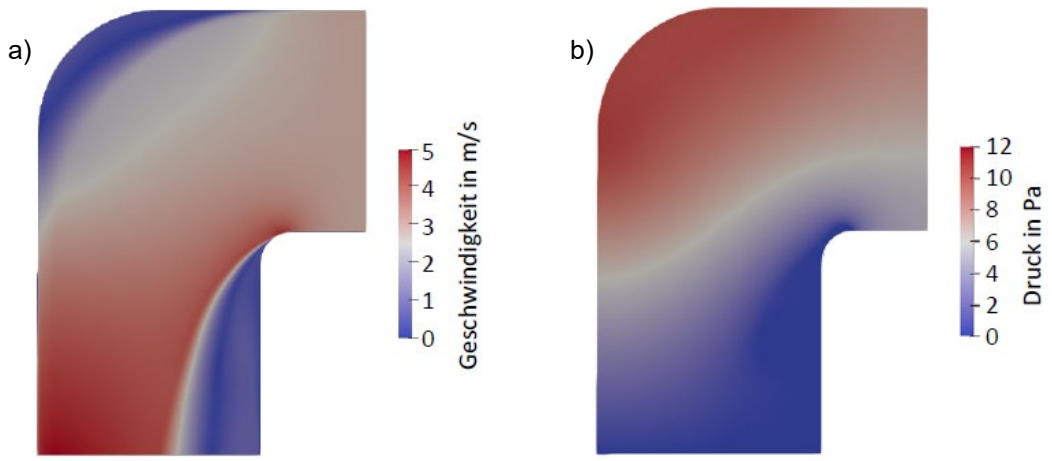

Fig. 3
Ein schematisches Simulationsergebnis einer untersuchten Geometrie- und Randbedingungskombination
a) die ermittelte Strömungsgeschwindigkeitsverteilung
b) der ermittelte Druckverlust

Durch die Nutzung von ML können die Simulationen deutlich beschleunigt werden, da anstelle von Differenzialgleichungen, welche in der Regel bei CFD- und FEM-Simulationen gelöst werden und zumeist sehr Zeit- und Rechenintensiv sind, auf Matrixoperation zurückgegriffen wird, welche nach einem durchgeführten Training sehr rasch ermittelt werden kann. Beim Training wird die Eingangs- und Ausgangsstruktur der Simulation für unterschiedliche Betriebspunkte verwendet, um die Gewichtungen der einzelnen Stränge des ML-modells zu ermitteln. Dadurch lassen sich anschließend neue Vorhersagen unbekannter Parametersets innerhalb weniger Millisekunden durchführen. Die verwendeten Parameter mit den zugehörigen Wertegrenzen sind in Fig. 4 dargestellt.

Kategorie	Parameter		Wertegrenzen		Einheit	Sim*	KI-P**
Randbedingung	Strömungsgeschwindigkeit	$\dot{V}$	13 000	18 000	m^3/h	I	I
Geometrie	Außenradius	R_A	0	1 000	mm	I	I
	Innenradius	R_I	0	100	mm	I	I
	Anzahl Umlenkbleche	n_U	0	14	1	I	I
Randbedingung	Druckverlust	p_V	1 Parameter		Pa	O	O
	Strömungshomogenität	H	1 Parameter		1	O	O

Fig. 4

Darstellung der untersuchten Geometrieparameter und Randbedingungen mit den jeweiligen Wertegrenzen

Der vorgestellte Ansatz kombiniert physikalische Simulationen mit KI, um Zeitersparnis in Simulationen zu erreichen und Randbedingungen zu ermitteln. Dabei wird die Vorhersagegenauigkeit beibehalten und die Effizienz von CFD-Simulationen gesteigert. Durch die Vorhersage mithilfe von KI können Probleme schnell gelöst werden, die anderweitig oft nur zeitaufwendig ohne KI gelöst werden. Diese Methode wird insbesondere bedeutsam, wenn tatsächliche Maschinenmessdaten und zugehörige Komponentenfertigung anstelle von Simulationsdaten verwendet werden, da dies die Anzahl der mit unterschiedlichen Parametersätzen herzustellenden Komponenten erheblich reduziert und durch KI optimiert werden kann. Dies führt zu erheblichen Zeit-, Ressourcen- und Kosteneinsparungen und fördert die Nachhaltigkeit.

3 Ergebnisse

Basierend auf den simulierten Parametersets werden durch die Vorhersage die Ergebnisse weiterer nicht simulierte Sets ermittelt und diese können anschließend in die Grafik mit aufgenommen werden. Aufgrund von vergleichenden Simulationen, welche ins Training nicht mit aufgenommen wurden, konnte die Vorhersage des ML-System verifiziert werden und eine Vorhersagegenauigkeit von >95% konnte erzielt werden. Ein, durch das ML-Modell vorhergesagtes Ergebnis für unterschiedliche Innenradius- und Außenradiuskombinationen insbesondere auch mit Umlenkungsblechen ist in Fig. 5 visualisiert. Es zeigt sich hierbei, dass bei einer Verwendung von Umlenkblechen der Druckverlust in der Rohrleitung deutlich reduziert werden kann.

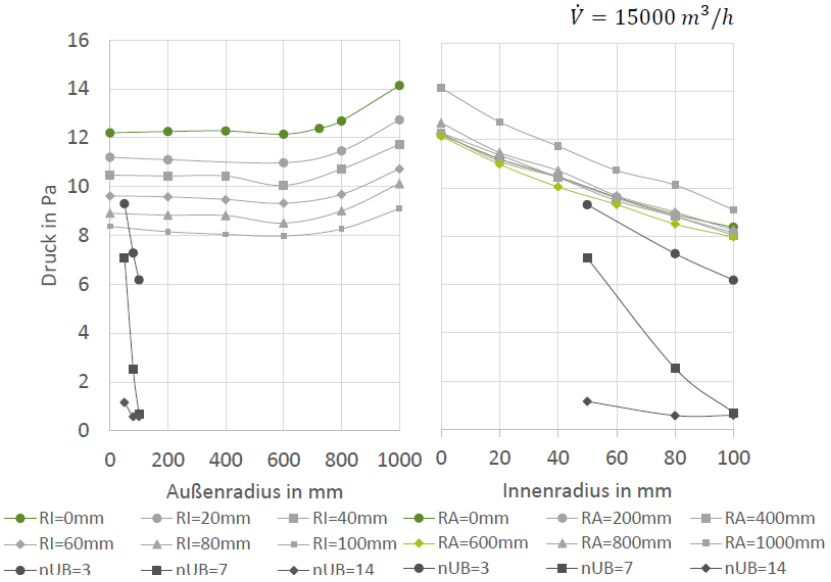

Fig. 5

Beispielhafte Vorhersageergebnisse unterschiedlicher Geometriekombinationen bei einem Luftvolumenstrom von 15 000 m³/h

Ebenso hat sich herausgestellt, dass die Verwendung von Umlenkblechen eine deutlich verbesserte Strömungshomogenität im Auslassbereich mit sich bringt (Fig. 6). Da dies jedoch Produktionsbedingt zu einem erheblichen Mehraufwand führt und somit Mehrkosten verursacht, müssen im Nachgang Wirtschaftlichkeitsbetrachtungen durchgeführt werden, um die tatsächliche Verwendung von Umlenkungsblechen durchzuführen.

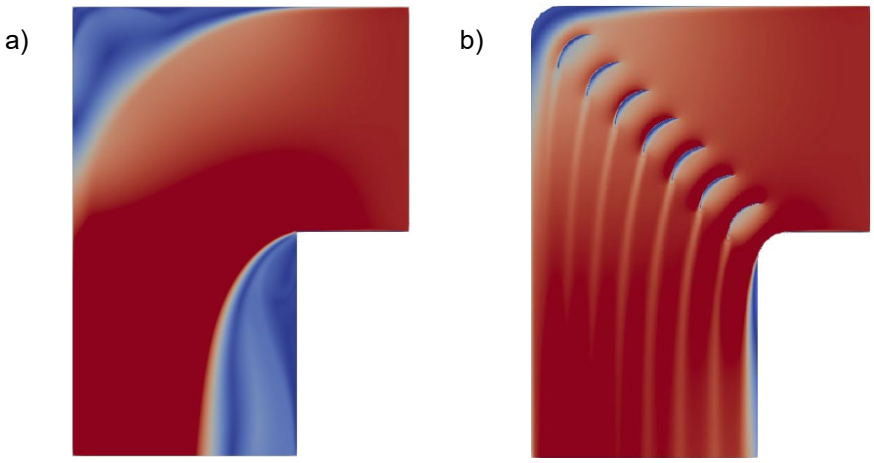

Fig. 6

Darstellung von Simulationsergebnissen a) ohne Umlenkungsbleche und b) mit Umlenkungsblechen

ML-basiertes Auslegungstool für Leistungselektronikkühler auf Basis von CFD-Simulationsdaten

Arnulf Sehlinger, Dominik Plein, Hendrik Plooij, Sebastian Spring (Tplus Engineering GmbH)

1 Summary

Der Beitrag untersucht den Einsatz von Methoden des maschinellen Lernens auf Basis von 3D-CFD-Simulationsdaten. Mithilfe vollautomatisierter CFD-Simulationen wird ein Parameterraum für Geometrien eines Leistungselektronikkühlers untersucht. Die Ergebnisse werden anschließend verwendet, um mithilfe trainierter Modelle integrale Größen sowie lokale Verteilungen vorherzusagen.

2 Einleitung

Anwendungen basierend auf den verschiedenen Möglichkeiten der künstlichen Intelligenz halten in so gut wie allen Bereichen des Alltags Einzug. In den Ingenieursanwendungen bieten sich hier ebenfalls vielfältige neuartige Möglichkeiten.
In unserem Beitrag möchten wir ein ML-basiertes Auslegungstool als Ersatz für ein korrelationsbasiertes oder anderweitiges 1D-Auslegungsverfahren vorstellen. Dabei stammen sämtliche Trainingsdaten für das maschinelle Lernen von automatisierten 3D-CFD-Simulationen. Mithilfe dieser Simulationen wird ein zuvor definierter Parameterraum systematisch analysiert. Anschließend wird ein Modell trainiert, welches eine Vorhersage relevanter Parameter oder Leistungsgrößen erlaubt.
Die Motivation ist hierbei, dass durch die Verwendung von detaillierten CFD-Simulationen als Grundlage für das Modelltraining eine höhere Genauigkeit in der Vorhersage erreicht werden kann, als dies mit klassischen Auslegungsmethoden basierend auf Korrelationen oder sonstigen empirischen Berechnungsverfahren möglich ist. Zudem wird in unserem Beispiel der Parameterraum bewusst sehr groß gewählt, wie es bei den klassischen Verfahren unüblich ist. Neben der Vorhersage integraler Größen werden auch lokale Verteilungen mithilfe von Bilderkennungsverfahren vorhergesagt.

3 Erstellung von Trainingsdaten

Die Trainingsdaten für das maschinelle Lernen werden mithilfe von CFD-Simulationen generiert. Die Simulationsdaten werden dabei vollständig automatisiert erstellt. Im vorliegenden Fall basiert der komplette automatisierte Workflow ausschließlich auf Open Source Software.
Als Beispielanwendung für die hier vorgestellte Methodik wird ein Kühler für Elektronikmodule gewählt. Eine etablierte und weit verbreitete Kühlerbauart für derartige Anwendungen sind Kanäle mit Pin Fin Strukturen.

3.1 Geometrieerstellung

Da die Simulation einer kompletten Kühlergeometrie mit vielen kleinen Strukturen sehr aufwändig ist, wird im Folgenden eine repräsentative Einheitszelle verwendet. In den CFD-Simulationen wird dies durch Verwendung entsprechender periodischer Randbedingungen realisiert. Ein beispielhaftes Simulationsmodell für eine Einheitszelle eines Pin Fin Kühlers zeigt Abbildung 1.

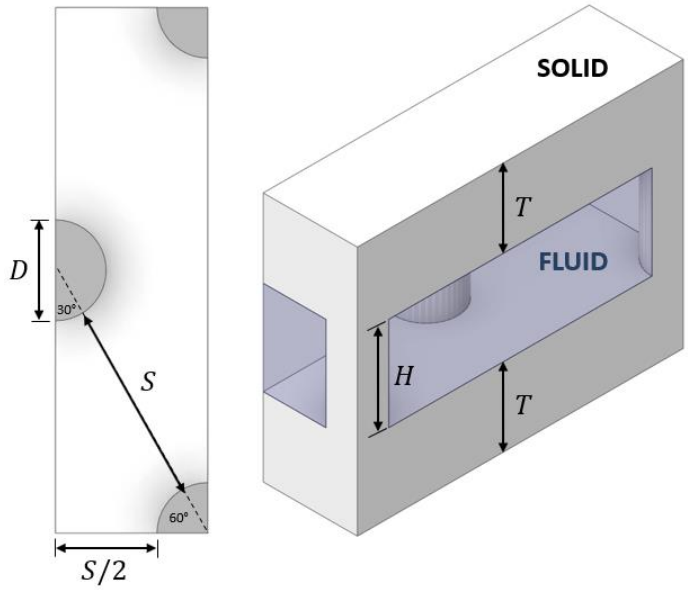

Abbildung 1: Repräsentatives Design der Pin Fin Kühler Einheitszelle

Für die parametrisierte und voll automatisierte Geometrieerstellung wird die CAD-Software pythonOCC [1] verwendet. Diese bietet den Vorteil einer sehr flexiblen Modellgestaltung durch direkte Programmierung bzw. durch Skripten der einzelnen Konstruktionsschritte sowie einer schnellen Programmausführung.
Das CAD-Modell für die Simulationen besteht aus einem Fluidmodell und dem Festkörper der Pin Fins. Insgesamt beeinflussen drei Parameter die Konstruktion des Modells, diese sind der Durchmesser D, die Höhe H und der Abstand S.

3.2 Vernetzung

Für die Vernetzung werden snappyHexMesh oder cfMesh aus dem Open Source CFD-Software-Paket OpenFOAM® [2] ausgewählt. Nach umfangreichen Tests konnte eine effiziente, robuste und qualitativ hochwertige Vernetzungsstrategie aufgebaut werden. Die mit snappyHexMesh erstellten Gitter weisen grundsätzlich konforme Interfaces zwischen Fluid und Solid, die mit cfMesh erstellten verwenden nicht-konforme Interfaces. Bei beiden Vernetzern wird auf eine möglichst feine Wandauflösung zur Abbildung des Wärmeübergangs durch den Einsatz von Prismen- / Wandschichten geachtet.

3.3 CFD-Simulation

Für die Bewertung der verschiedenen Kühlergeometrien werden 3D-CFD-Simulationen der jeweiligen Einheitszellen durchgeführt. Die Wärmeleitung in den Bauteilen wird berücksichtigt, sodass alle Simulationen als CHT-Simulationen durchgeführt werden. Als CFD-Löser wird der Löser chtMultiRegionSimpleFoam von OpenFOAM verwendet.
Die Strömung der Flüssigkühlung ist bei den Abmessungen des Parameterraums überwiegend turbulent, für die Simulationen wird deshalb das SST-Turbulenzmodell ausgewählt.
Als thermische Randbedingung wird ein konstanter Wandwärmestrom auf einer Seite der Kanalwand aufgeprägt. Um das Modell der Einheitszelle verwenden zu können, werden entsprechende Anpassungen am Setup vorgenommen. Zum einen wird über einen Quellterm in den Impulserhaltungs-gleichungen der gewünschte Massenstrom eingestellt. Zum anderen wird für das Kühlmedium ein Zielwert für die Bulk-Temperatur vorgegeben, der über einen Regler und einen Quellterm in der Energieerhaltungsgleichung erreicht wird. Bei der einseitig beheizten Kühlerstruktur wird somit sichergestellt, dass sich das Fluid bei Verwendung des periodischen Modellansatzes nicht unbegrenzt aufheizt.
Darüber hinaus werden in OpenFOAM zusätzliche Funktionen implementiert, welche die Stabilität der relevanten Zielgrößen automatisiert bewerten und den Abbruch der Simulationen steuern.

3.4 Prozess-Steuerung

Die Trainingsdaten für das maschinelle Lernen werden mithilfe des eigens erstellten vollautomatisierten Workflows zur CFD-Simulation der Kühlergeometrien generiert. Der schematische Ablauf der gesamten Prozesskette ist in Abbildung 2 dargestellt.

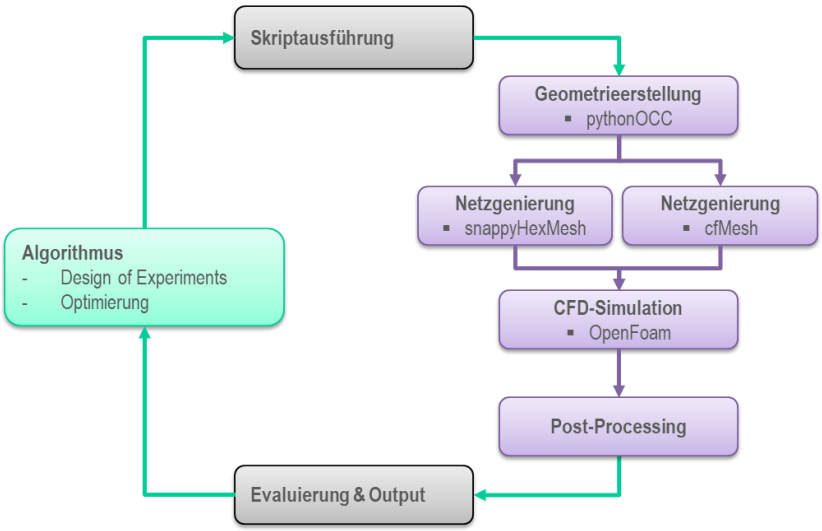

Abbildung 2: Vollautomatisierter Workflow für die Datengenerierung mittels CFD-Simulation.

Für die Steuerung des Workflows wurde die Open Source Software Dakota [3] ausgewählt. Das verwendete Design of Experiments (DoE) ermöglicht es, durch systematische Planung und statistische Auswertung einen definierten Parameterraum möglichst effizient zu untersuchen. Dabei ist das gewählte Sampling in Form der Latin Hypercube Sampling (LHS) Methode von Vorteil, da hiermit die Anzahl der Designs bzw. CFD-Simulationen beliebig gewählt werden kann.

4 Ergebnisse

Von der statistischen Versuchsplanung „Design of Experiments“ wurden insgesamt 8.000 Designs in Form von CFD-Simulationen angefordert. Dabei wurde der Parameterraum bewusst sehr groß definiert, um die Anforderung an die Modellbildung mittels maschinellen Lernens hochzusetzen. Mithilfe des oben beschriebenen Workflows wurden ca. 6.500 Designs erfolgreich mit CFD-Simulationen berechnet.

4.1 Vorhersage integraler Kenngrößen

Für eine Anwendung als 1D-Auslegungstool werden mithilfe des maschinellen Lernens integrale Größen trainiert. Für den Kühler sind dies Druckverlust und Kühlleistung, letztere in dimensionsloser Form als Nußelt-Zahl. Nach Tests mit verschiedenen Regressionsverfahren wurden die besten Ergebnisse mit einem zweischichtigen neuronalen Netz mit jeweils 64 Neuronen erreicht. Die Ergebnisse zeigt Abbildung 3. Dort wird die Vorhersage des neuronalen Netzes mit CFD-Ergebnissen verglichen, wobei diese Simulationsergebnisse nicht Bestandteil der Trainingsdaten waren.
Im Vergleich der Ergebnisse lässt sich eine recht gute Übereinstimmung zwischen der Vorhersage durch das trainierte neuronale Netz und den CFD-Daten erkennen. Der prozentuale Mittelwert der Differenz (mean absolute percentage error, MAPE) liegt hier bei ca. 9%. Somit eignet sich der Ansatz grundsätzlich als Alternative zu alternativen 1D-Berechnungsverfahren.

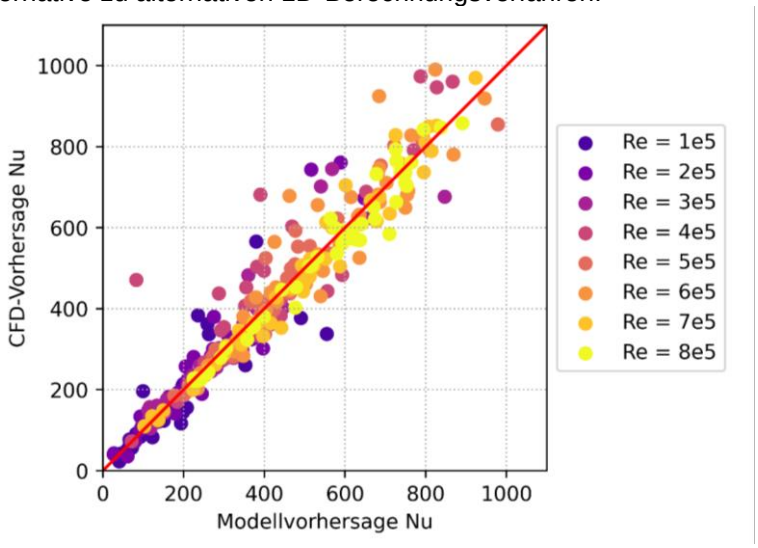

Abbildung 3: Gegenüberstellung Vorhersage neuronales Netz und CFD-Ergebnis (Testdaten).

4.2 Vorhersage lokaler Verteilungen

In einem nächsten Schritt wird die Vorhersage lokaler Größen trainiert. Im Fall des Pin Fin Kühlers wird hierfür die Temperaturverteilung auf der heißen Seite verwendet. Das Ziel ist dabei zu untersuchen, inwieweit die Temperaturverteilung trainiert und durch das ML-basierte Modell vorhergesagt werden kann.
Für die technische Umsetzung wird ebenfalls auf ein mehrschichtiges neuronales Netz zurückgegriffen. Als Eingangsgrößen dienen insgesamt vier Skalare: Reynoldszahl sowie die geometrischen Größen Durchmesser, Abstand und Höhe. Als Ausgabe wird für das Training die Temperaturverteilung auf der heißen Wandseite dem neuronalen Netz in Form einer Abbildung vorgelegt. In dieser Abbildung hat jeder Pixel einen Farbwert im RGB-Farbraum und besitzt somit drei Werte für Rot, Grün und Blau. Aufgrund dessen werden drei neuronale Netze für die Primärfarben trainiert.
Mit dieser Methode wird die Temperaturverteilung sehr gut vorhergesagt. Ein Vergleich zwischen einer Temperaturverteilung aus der CFD-Simulation (oben) und der Vorhersage des neuronalen Netzes (unten) ist in Abbildung 4 gezeigt.

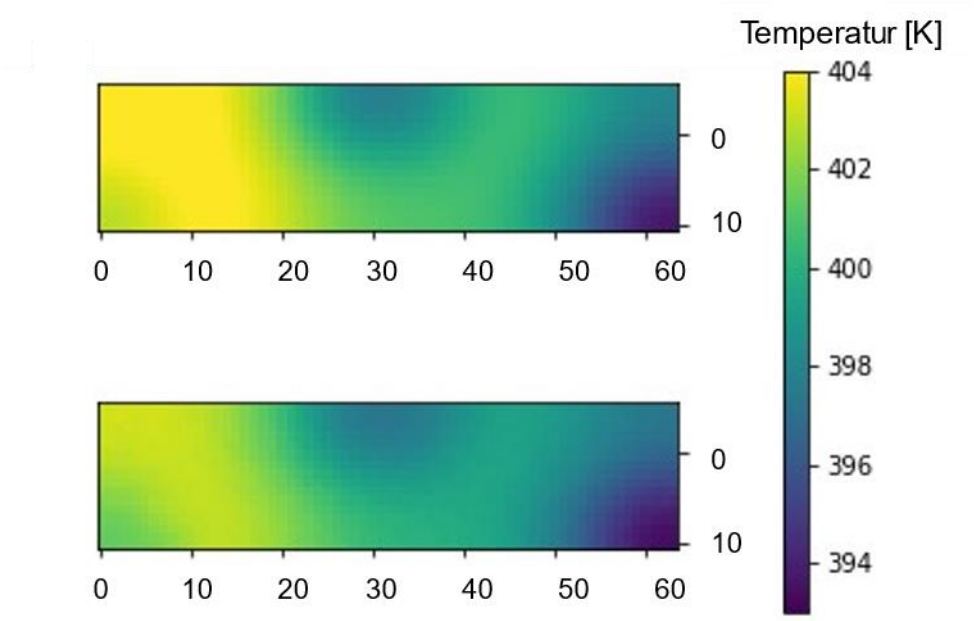

Abbildung 4: Beispielhafter Vergleich zwischen Ausgabebild für das Training (oben) und vom neuronalen Netz vorhergesagte Temperaturfeld (unten).

In der unmittelbaren Nähe der zylindrischen Pin Fins weichen die Temperaturwerte ab, hier befinden sich auch die größten Gradienten im Temperaturfeld. Insgesamt ist es für die Vorhersage von lokalen Temperaturen jedoch ein recht gutes Ergebnis.

5 Zusammenfassung

In unserem Beitrag haben wir die Möglichkeiten des maschinellen Lernens auf Basis von CFD-Simulationsergebnissen untersucht. Für den Anwendungsfall eines Pin-Fin-Kühlers für Leistungselektronik wurden automatisierte CFD-Simulationen zur Bewertung eines groß definierten Parameterraums aufgebaut. Die Prozesskette verwendet dabei ausschließlich Open Source Software. Der so erstellte Datensatz diente als Training für die Modelle des maschinellen Lernens. Mithilfe neuronaler Netze wurde zunächst die Vorhersage integraler Größen trainiert. Dabei zeigte sich eine gute Übereinstimmung, sodass ein derartiges ML-basiertes Tool anstelle alternativer 1D-Auslegungs- und Berechnungsverfahren verwendet werden kann. Weiterhin wurde die Vorhersage lokaler Temperaturverteilungen getestet. Dabei zeigte sich ebenfalls eine sehr gute Übereinstimmung in der Vorhersage, was einen klaren Mehrwert gegenüber klassischen Auslegungsverfahren bedeutet.
Nach den vielversprechenden ersten Erkenntnissen ist geplant, die bisherigen Untersuchungen um weitere Einflussfaktoren wie bspw. Kühlmedium oder Material zu erweitern. Darüber hinaus ist der die Erweiterung um weitere Kühlergeometrien geplant.

6 Literatur

[1] Python Wrapper für OpenCASCADE: https://github.com/tpaviot/pythonocc

[2] https://openfoam.com This offering is not approved or endorsed by OpenCFD Limited, producer and distributor of the OpenFOAM software via www.openfoam.com, and owner of the OPENFOAM® and OpenCFD® trade marks.

[3] Dakota v. 6.15, Open Source Software von Sandia National Laboratories zur Optimierung und Unsicherheitsbestimmung: https://dakota.sandia.gov/

7 Acknowledgement

This project has received funding from the Key Digital Technologies Joint Undertaking (KDT JU) under Grant Agreement No 101007237. The JU receives support from the European Union's Horizon 2020 research and innovation programme and Germany, France, Italy, Sweden, Austria, Czech Republic, Spain.

Fully Transient Vehicle Crash Predictions powered by SimAI

Srikanth Adya, Pierre Yser (Ansys)

1 Summary

Deep learning methods have had a significant impact on simulation data in the recent past. SimAI is a deep learning-based AI platform that has shown to be very effective in approximating the behavior of fluid flow applications, especially fully developed steady state flows simulated by CFD solvers. The underlying neural networks in SimAI are very versatile and can be easily extended to structural applications as well. This study aims at demonstrating the applicability of SimAI for highly non-linear transient structural simulations like automotive crash. We use a sled model to simulate a frontal impact of the vehicle with a flat rigid-wall. Multiple training samples are generated by changing the thicknesses of several parts. This dataset is used to train a SimAI model and the resulting model can predict the full field vehicle deformation and the rigid-wall force signals within 10% relative error throughout the transient event. SimAI is many orders of magnitude faster in predicting the system behavior than direct numerical simulation and hence can be very effective in evaluating designs upfront in the design development process.

2 Introduction

With shrinking automotive development timelines, CAE has been a very integral part of vehicle design process in the past couple of decades. Vehicle safety is one of the most critical parts of this process. With new safety regulations being added in multiple regions every year, virtual analysis has become a reliable tool to access a vehicle‘s crash and safety performance virtually, without having to rely too much on costly physical testing. LS-DYNA is one such tool that has become an industry standard when it comes to building high fidelity crash models. Over the years, the complexity of these models have grown exponentially with details like, airbags, dummies, restraint systems, spotwelds, adhesives, material failures etc. being captured to improve the predictivity of the model. While this has resulted in improving our confidence in CAE predictions and in turn reduction in the number of physical tests, its has also made the models much larger and thus increasing the need for large compute resources to solve these models. Off late, it‘s not uncommon to see full vehicle models with 40 to 50 million elements requiring about 25 to 30 hours to solve a complete crash event on about 700 to 1000 CPUs on a modern-day high-performance compute cluster.

Apart from the compute overhead, there is also a significant preprocessing cost involved in generating these models. Typically, once a new car design is available, it takes anywhere between two to three months to clean the CAD, mesh it, add all the necessary connections and materials, debug for any errors and establish a baseline performance. Usually, during the early concept phase of the design, the geometry is not fully mature. Parts and subsystems are borrowed from legacy programs and plugged into the new design. Since these components were not designed to be in the new vehicle, most often than not, a lot of time is spent in clearing geometric intersections and penetrations between neighbouring parts. These penetrations, if not cleared, would result in poor model predictions and numerical instabilities in the model that would cost a lot of time and effort during the design evaluations. And even if good clean geometry is available, most often, the CAE model fails to keep up with all the design changes and tends to lag the design iterations. Consequently, only few designs are ever thoroughly evaluated.

Hence, there is a need for a solution where a designer, who is not an expert in Finite Element method, can quickly evaluate multiple designs and make an informed decision on the best option. Traditionally, optimization tools have tried to fill this need by parameterizing CAE models and building meta-models and response surfaces that can be used to predict the behaviour of a new design. But these meta-models rely heavily on parameterized input. It is easy to parameterize variables like part gauges and material properties but parameterizing the geometry is a challenge. Changing geometries needs to be done in conjunctions with a CAD tool or a morphing tool and this is usually a time-consuming process. Also, the response surfaces that are generated are usually only capable of predicting a scalar response like, the peak acceleration at a point in the model, maximum intrusion at a point in the vehicle or an injury measure on the dummy. Some of the newer tools also try to predict a signal instead of just a scalar, but even then, the useful information that can be extracted from these meta-

models are restricted to a very specific region of interest in the vehicle. If the design change has an influence anywhere else in the model, the meta-model would fail to highlight it.

Hence there is a need for a tool that can quickly but accurately predict the full 3D response of a new design. With advances in machine learning methods, it is now possible to learn from lots of existing data and make inferences on unknown designs. SimAI is an Ansys tool that takes advantage of this technology and builds AI models that are trained on simulation data. In this paper, we discuss the technology being used as well as its application in vehicle crash performance predictions.

3 SimAI Technology

SimAI is a novel deep learning method which employs Implicit Geometric Deep Learning to approximate solutions for highly coupled non-linear partial differential equations. SimAI does not solve partial differential equations directly but learns the full 3D information from traditional solvers like LS-DYNA and quickly infers new solutions for efficient design iterations. SimAI thus combines a unique multi-scale implicit graph neural network architecture with physical priors (integral coefficients computed from local values, equivariance …) to deliver AI models for any type of physics [1][2].

SimAI is delivered on a cloud platform that enables anyone to create AI models, store them as a library of models and to run inferences on these models to get high fidelity predictions for specific workflows. This platform is accessible through a webapp and through a Software Development Kit (SDK) allowing for agile workflow and process automation.

4 Numerical Model Description

SimAI can generate a reduced order model of both parametric and non-parametric data. In this section, three separate studies are described. In the first case, we generate an AI model for a Tube crush model. This model has geometric variations that will be described in Section 4.1. In Section 4.2

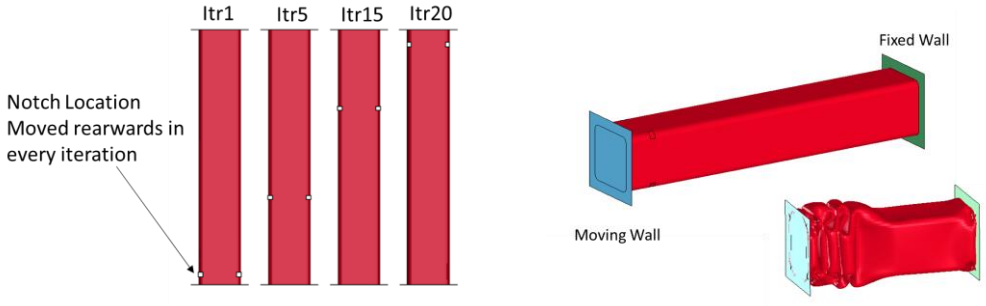

Fig 1. Tube with Notches

we extend this study to make the geometric variations a bit more pronounced by changing the cross-section of the tube. Finally in Section 4.3, we look at a sled model representing a Bumper Impact scenario. In this case, the part thicknesses are parameterized, and the AI model is generated to predict the behaviour of the sled for any thickness value within the training dataset.

4.1 Tube Crush

4.1.1 Tubes with Notches

This dataset consists of a series of 20 rectangular tubes with notches as shown in Fig 1. Geometric variability is introduced in the model by moving the location of the notch rearwards in each design. One of the ends of the tube is constrained by an immovable rigid wall. The other end is in contact with a movable rigid wall which is prescribed an initial velocity of 10m/s. The material of the tube is assumed to be steel with a density of 7.8e-6, young's modulus of 210.0, yield strength 0.4 and tangent modulus of 2.0. The model uses kN, kg, ms and mm for unit system. The above image shows how the tube folds on itself when the rigid wall pushes against the tube.

4.1.2 Tubes with varying cross-section

In this dataset, the geometry variation is a little more pronounced by changing the cross-section of the tubes. Three different cross-sections, rectangular, circular and conical, were generated. Within each of these, tubes with three different dimensions were created as shown in the Table 1 and Fig 2. As in the first case, one end of the tube is resting against a fixed rigid-wall. The other end is in contact with a

moving rigid-wall with an imposed initial velocity of 10m/s. The material properties are same as that used in the previous case.

Cross-section	Set 1	Set 2	Set 3
Conical	50mm front dia	60mm front dia	70mm front dia
Circular	50mm	60mm	70mm
Rectangular	40mmx50mm	50mmx50mm	50mmx60mm

Table: 1. Tube Geometric Variations

Fig 2: Different geometries of the Tube Crush model.

4.2 Bumper Impact Model

In this use-case, a simplified vehicle model is used to model a Bumper Impact load case[6]. The vehicle is impacting a flat rigid-wall at 15.6m/s. The model is cut at the firewall in the longitudinal axis of the vehicle and at the centre of the bumper in the transverse axis. All the edge nodes at the trimmed plane in the x-z plane is imposed a symmetric boundary condition by containing in Y translation and X and Z rotations. The edge nodes in the longitudinal direction are all extra-noded to a part inertia at the CG of the vehicle. This part has the vehicle mass and inertia lumped on it.

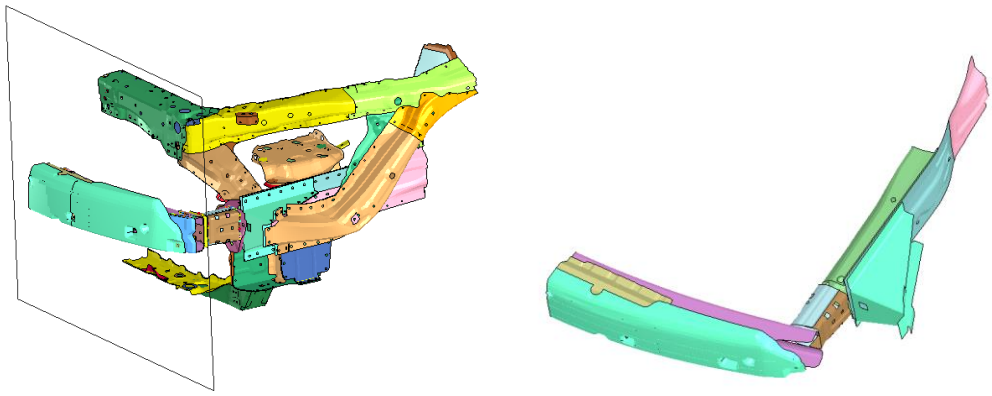

Fig 3: Bumper crush model. Part thickness of the highlighted parts varied.

98 different designs were generated for this case by sampling the part thickness within the min and max bounds. Fig 4. shows a typical crushed state of the bumper along with the rigid-wall force time histories across all the designs.

5 SimAI data Preparation and Model Training

In order to predict a transient response, we need to extract the output field of interest at frequent timesteps. The input data for SimAI needs to contain both the input geometry and the operating/boundary conditions. In our case, the boundary conditions are any thickness changes for the parts as well as the time at which the output response has been extracted. The boundary conditions are fed as a json file. For the tube crush cases, there is no part thickness variation. Hence the json file will only have time as a parameter. For the bumper impact case, along with time, the thicknesses of the seven parts that were changed are also included. Fig 5. shows a typical boundary condition file.

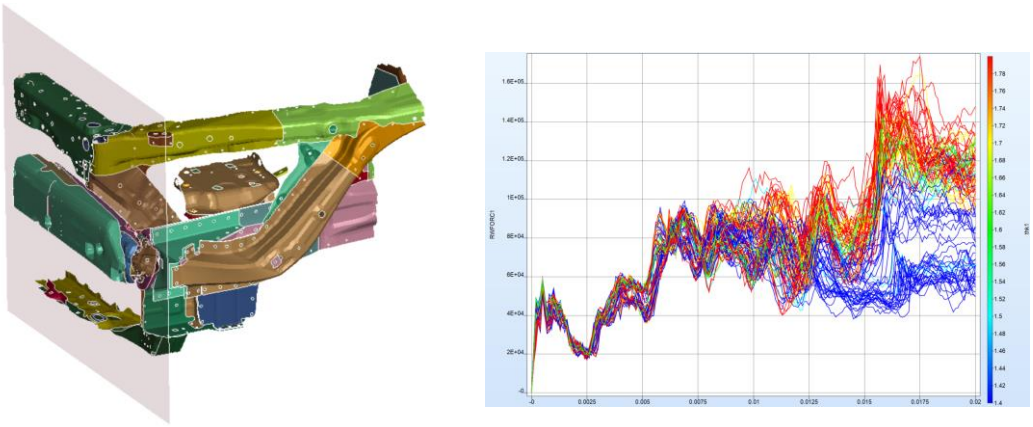

Fig 4: Bumper deformed state and rigid-wall time history plots


```
{
    "thk1": 1.4,
    "thk2": 1.5,
    "thk3": 2.2,
    "thk4": 1.6,
    "thk5": 1.7999999999999998,
    "thk6": 1.9,
    "thk7": 7.5,
    "Time": 0.0009996660519391298
}
```


Fig 5: Boundary condition json file for bumper impact case consisting of thickness parameters and time

Geometry is written out in .vtp or .vtu file formats. vtp holds the surface (shell element) data and vtu holds the volume(solid element) data in them. This file consists of the nodal coordinates , element connectivity along with any nodal or elemental outputs that can be used as inputs or outputs to the model. In the case of the tube crush models the .vtp file includes the undeformed shape and the displacement field at a given timestep. For the Bumper Impact case, we also include the rigid-wall force at a given time as a constant value on all the elements of the model. This is later used as an output variable for the AI model to predict the rigid-wall force at a give time. To read the raw d3plot files and convert them to .vtp and .vtu format, pyDPF was used [4]. Fig 6. shows a sample vtp file for the tube crush and the bumper model.

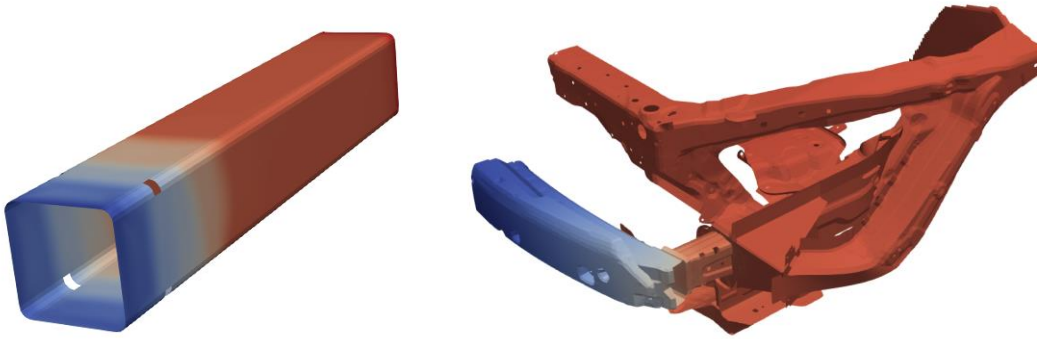

Fig 6: vtp files with displacement field on the nodes

For the Tube crush model with 20 different iterations and 22 states per iteration, extracting vtp for every state would result in a total dataset size of 440 data points. Similarly for the Bumper impact model, with 98 design points and 21 states per design point, we get a total of 2058 data points to train on. Once the input data is thus prepared, it is uploaded to SimAI platform. This can be done manually by dragging and dropping the dataset on the SimAI web interface or using a python SDK called pySimAI[5]. SimAI is currently available as a cloud based solution and is hosted on AWS with all the necessary data security considerations. Once the data is uploaded the dataset within each project is then divided automatically by SimAI into three subset as training set, validation set and the test set

- Training set is used to train the model
- Validation set is used to tune the model architecture
- Test set is used to test the trained model. It is used to give an unbiased estimation of the kernel performance on new cases

5.1 Model configuration

The next step after the data is uploaded is Model Configuration. This involves identify the inputs and the output for the AI model along with the boundary conditions. For the Tube Crush use cases, the inputs for the model are the geometry and the time step. Geometry is extracted from the uploaded .vtp file and the time is read from the boundary condition json file. UX, UY and UZ are the output parameters that the model is trained to predict.

For the Bumper Impact use case, along with time, the part thicknesses defined in the json file are also used as inputs. Also, along with the displacements UX,UY and UZ, rwforc (rigid-wall force) is also defined as an output quantity. The model is now expected to learn the relationship between the geometry and the boundary conditions to the nodal displacements and the rigid-wall force at any given time. Fig 7. shows the model configuration for the Bumper Impact model.

An integral global coefficient called rigidwall_force is also defined for the Bumper model. This acts as a scalar quantity to compare between the solver and the predicted model and helps in accessing the accuracy of the model. The global coefficient is defined as

$$\frac{\int_S (rwforc)}{\int_S (1)}$$

This just means that the constant rigidwall force that was defined on all the elements in the vtp file is summed up and is divided by the total surface area of the model, thus returning a scalar output.

The desired precision of the model is also selected in the model configuration. The precision level directly affect the time required to train the model. A model with accuracy set to Precise takes anywhwere upto 2 days to train. Very Precise takes upto a week to train.

6 Results Discussion

All three model were trained on Tensor Core GPUs on SimAI with a accuracy level of Precise. In the following sections we will discuss the model accuracy as well as some observations on these models.

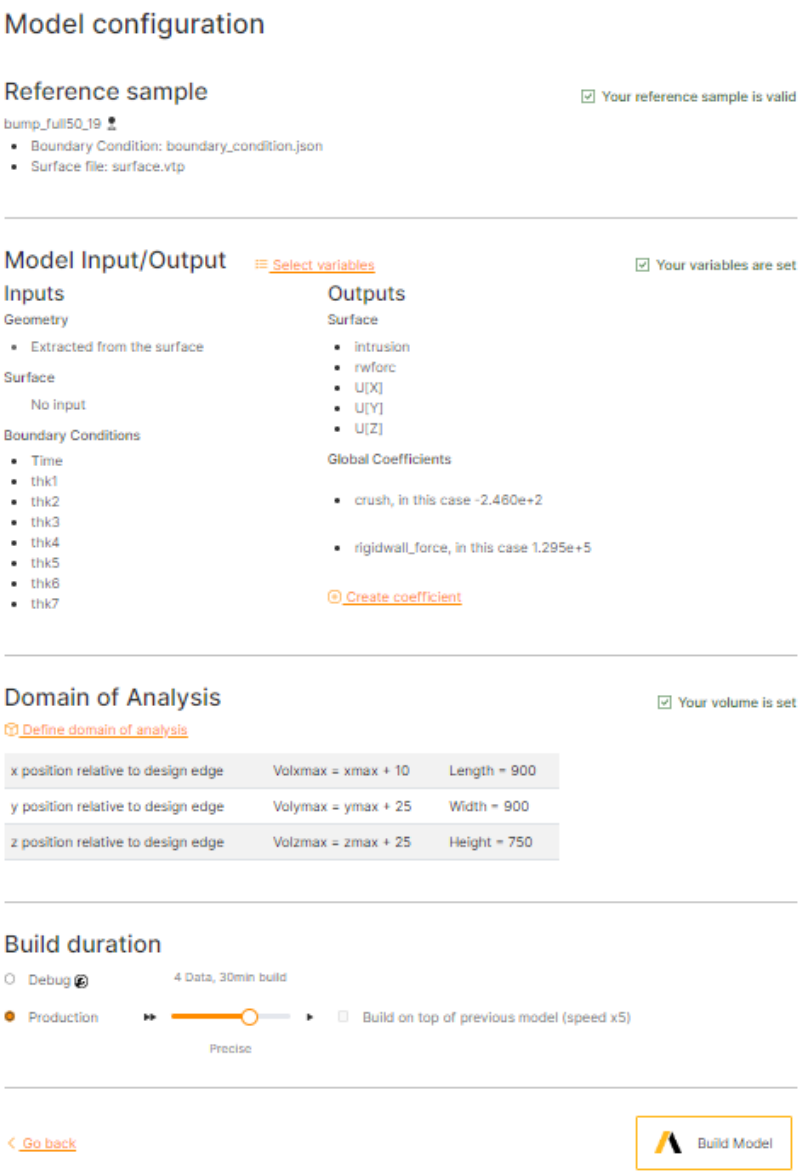

Fig 7: model configuration for Bumper Impact model

Test geometry 81

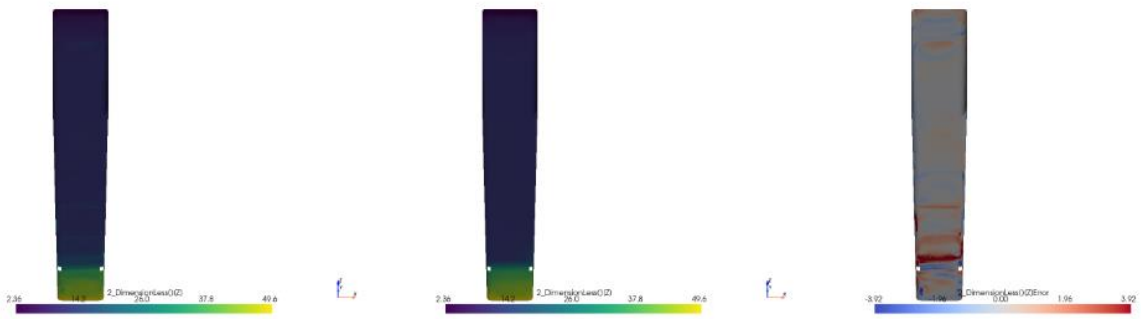

(a) SimAI prediction (b) Solver target (c) Difference

Fig 8: Surface field UZ predicted by SimAI, the solver target and the difference between them

6.1 Tube crush

6.1.1 Tube with Notches

This model took about 12hrs to train to the desired level of accuracy. Once the training is done, a model evaluation report is generated. The model evaluation report compares the SimAI prediction with the Solver prediction and highlights the regions where there are differences as shown in Fig 8. It can also be seen from the Fig 9. that SimAI has managed to learn the relationship between the location of the notch on the tube and the crush pattern of the tube. SimAI accurately predicts the buckling of the tube to be at the location where the notch exists. As can be seen, the AI model has learnt that the buckling of the crush tube occurs where the notch is and hence the tube buckles in the front for the top model corresponding to the notch being in the front. Similarly, the tube buckles at the rear end in the bottom model corresponding to the notch being at the rear end in this case. Model also predicts well for any other location of the notch along the length of the tube.

6.1.2 Model prediction limit

Now that the model behaves well on different geometries within the design space, one more evaluation was done to see how well the model can generalize on a significantly different geometry. In this case, the model was asked to predict the crush on a Tube with a considerably long notch compared to all other samples in the training data. SimAI model predicted a similar crush patter to the previous cases whereas the solver output is significantly different. Fig 10. shows the comparison of SimAI prediction to solver output for this long notch case. The buckling of the model at the mid-section due to the long notch is not predicted by SimAI. This is because SimAI does not solve for any physics equations but infers the full 3D information from the training dataset. Since no such example existed in the training dataset, SimAI could not predict the true behaviour for the model.

6.1.3 Retraining the model with the new design

The model was then retrained by adding the long-notch example into the training dataset. As before, the d3plots for this new case had 20 states. Each state along with the corresponding displacement field was extracted as a vtp file and uploaded to SimAI. The retrained model is now capable of predicting the behaviour of the long-notch more accurately. The model predicts the base case of small-notch and also generalizes to the long-notch as can be seen in Fig 11.

6.1.4 Tubes with varying cross-section

The AI model in this case was trained on different cross-sectional tubes along with changing dimensions. For this case, the model was able to generalize well based on the input geometry. The crush pattern predicted by SimAI for a given shape and dimension agrees well with the solver predictions as shown in Fig 12.

6.2 Bumper Impact

The aim of this load case was to predict both the deformed shape as well as the rigid-wall force for a given geometry. This model took about 21hrs to train on NVIDIA A10G Tensor Core GPU. Fig 12. shows the trend plot for the global coefficient “rigidwall_force”. The X-axis is the SimAI prediction for a give design at a given timestep. Y-axis is the corresponding Solver value for the same design at the same time step. A perfect AI model would have all the points on the diagonal meaning a 100% accuracy. But that would also indicate that the model is overfitting to the training data and might not generalize well. As seen in the Fig 13. SimAI model has most of the predictions within 10% error band. The model evaluation report also generates a difference plot of the displacement field prediction. Fig 14. highlights the areas where the SimAI prediction is deviating from the solver.

The SimAI model can be used to make multiple predictions on a new geometry at different timesteps. Each of these predictions will predict a displacement field which can be overlayed on the undeformed geometry to produce the deformed shape. These different states can be then stitched together to generate the time varying displacement field for the entire crash event. Fig 15. compares the deformed shape between SimAI and Solver at a given timestep by overlaying them on each other and is found to be reasonably accurate.

Finally, each prediction also generates the global coefficient “rigidwall_force”. Fig 16. compares the rigid-wall force predictions between Solver and SimAI. Again, the AI model predictions compare reasonably well with the Solver.

The predictions made on the AI models are orders of magnitude faster than the Solver. Each of these timestep predictions take less than a second for rigid-wall force prediction and about 10s to predict the entire displacement field and downloading the model. Predictions can also be made at any time within the lower and upper bounds of the time within the dataset. Thus, the SimAI predictions can be of much finer sampling compared to the Solver.

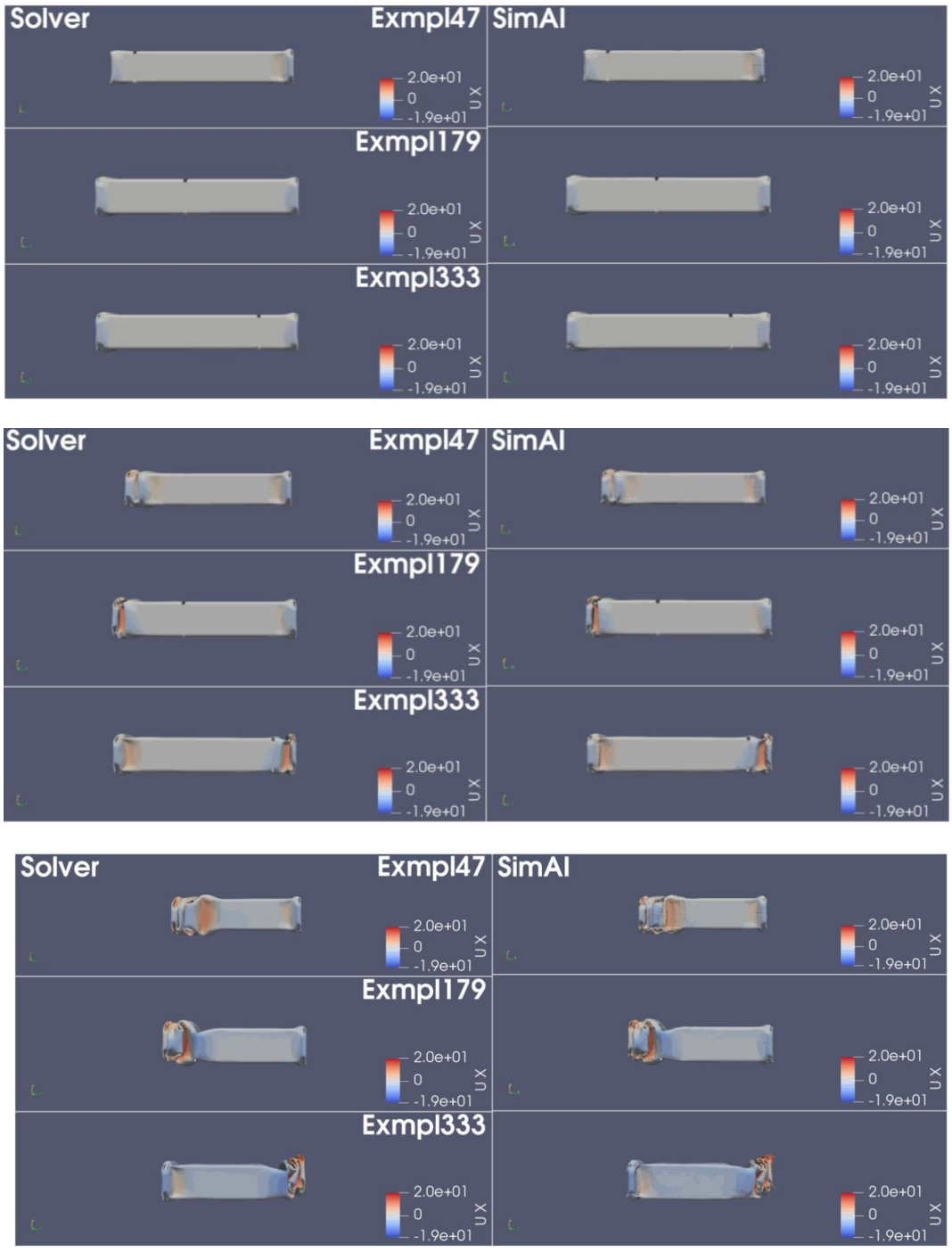

Fig 9: Crush behaviour at different timesteps similar between SimAI and Solver

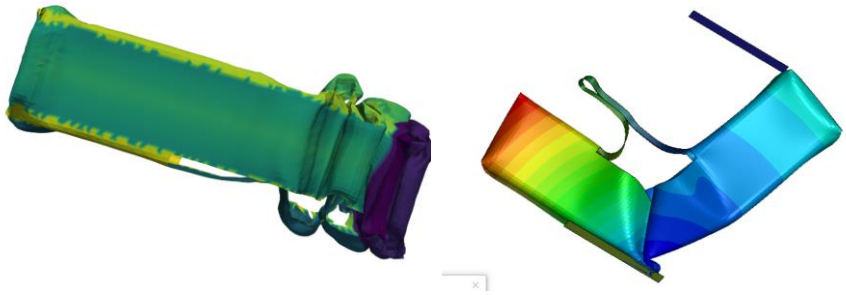

Fig 10: Crush behavior SimAI vs Solver long notch

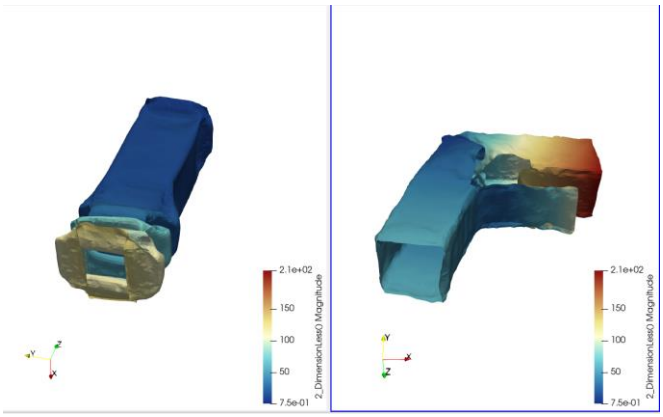

Fig 11: Retrained model with the long-notch sample added to training set.
Model now predicts both cases reasonable accurately

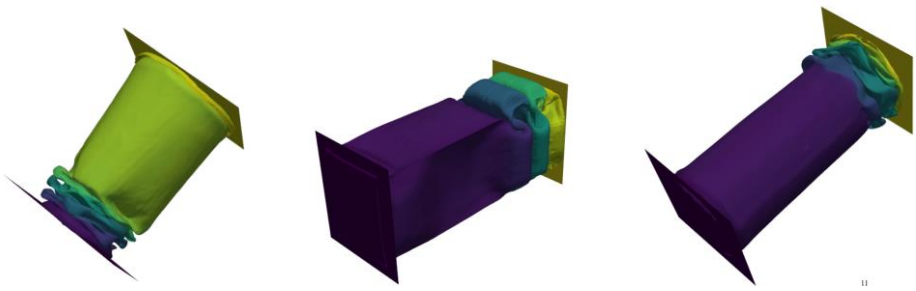

Fig 12: SimAI predictions for differently shaped crush tubes

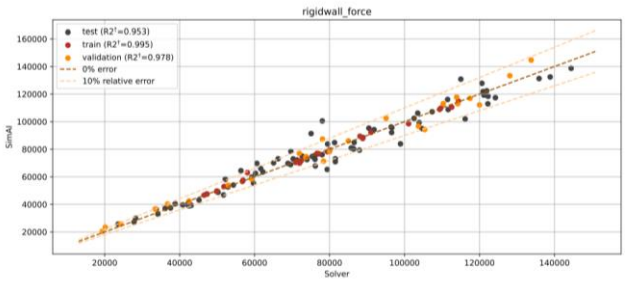

Fig 13: SimAI trend plot for rigidwall_foce

3.4.1 Test geometry 96

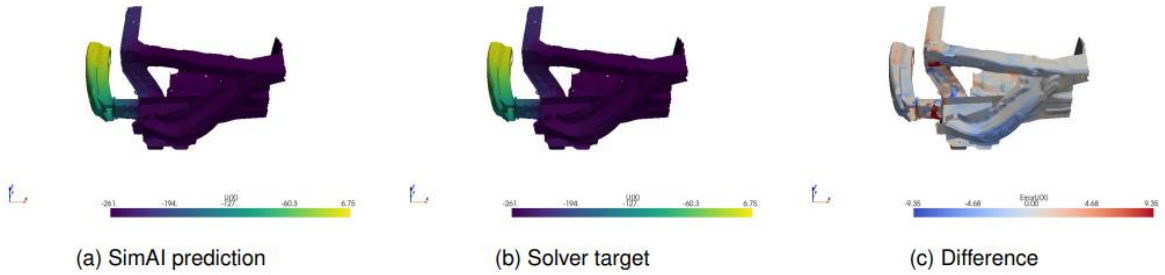

Fig 14: Difference plot for UX displacement field

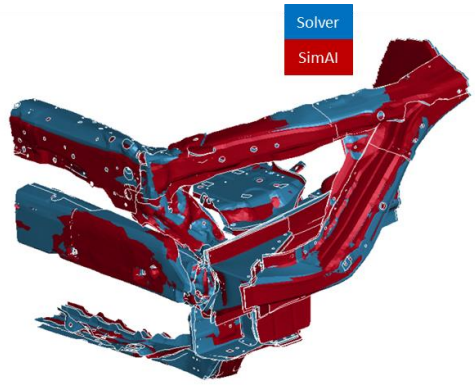

Fig 15: Comparison of the deformed shape between Solver and SimAI

7 Conclusions

The above set of use cases demonstrate the applicability of Deep Learning technology for generating AI models for structural applications by learning the physical behaviour from past LSDYNA simulations. The models can predict both the final deformed state as well as any other intermediate states, thus making it possible to have one single AI model for the transient non-linear event.

The ability of the model to learn the geometric variations between different designs without having to parameterize the geometry makes it very useful for quickly analysing new designs. The study highlights the effectiveness of the AI models as well as its limitations with regards to the model generalization, on completely different geometry than the ones the model was trained on.

The AI-simulation process is very simple and fast to deliver full field responses on surfaces and volumes. Once the model is trained, non-CAE engineers can use the trained model to make predictions on new designs. The predictions can be made on CAD (stl files) directly, thus avoiding the need for meshing the CAD.

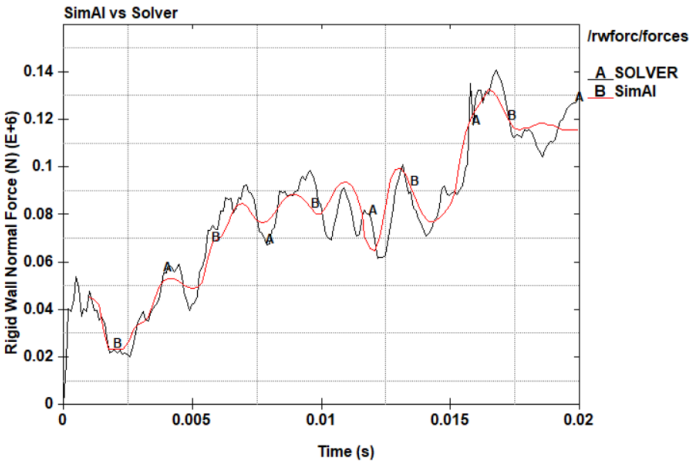

Fig 16: Comparison of rigidwall_force prediction between Solver and SimAI

8 References

[1] J. Verriere et. Al, “How to accelerate car aerodynamic design thanks to Deep Learning Physics
[2] Dr. J Verrier et. al, “Deep Learning Physics for hydrodynamic of trading vessels
[3] LS-DYNA Keyword User Manual – https://lsdyna.ansys.com/manuals/
[4] https://dpf.docs.pyansys.com/version/0.12/getting_started/index.html
[5] https://simai.docs.pyansys.com/version/stable/
[6] https://www.nhtsa.gov/document/honda-accord-lsdyna-zip

Superelement Welds Concept for Fatigue Evaluation

Christos Tegos (BETA CAE Systems)

1 Summary

Spot weld cracks play a significant role in fatigue failure. Consequently, the durability of structures is highly dependent on the accurate modeling of spot welds. In the automotive industry, various methods, such as nominal stress or force-based approaches, have been employed for spot weld fatigue analysis. Nevertheless, incorporating local stress directly yields more precise results. However, this method is based on very fine meshes for the detailed examination of local notch stress leading to significant computational effort. To address this challenge, the superelement approach is introduced. This method involves generating the superelement welds, positioning them to the assembly model, recovering stress components of the notch and finally calculating fatigue damage. A constant radius of the weld describes the notch geometry and von-Mises stress is used as the fatigue criterion.

This study involves the analysis of a rear body of a car with spot welds, providing a comprehensive description of the entire process and the challenges encountered. Comparisons between the superelement welds and those with detailed geometry are also presented to evaluate the method and highlight its advantages.

2 Assembly model

A rear body of a car containing a total of 1113 connections is subjected to two forces perpendicular to the towers. The target of this case study is to model the spot welds with Nastran superelements, retrieve the stress tensor from the notch from every spot weld and apply a time history in order to calculate fatigue life.

Fig. 1
a) Spot welds of the model, b) Applied forces, c) Boundary conditions

3 Process

Fig. 2 illustrates both the entire process and the associated software.

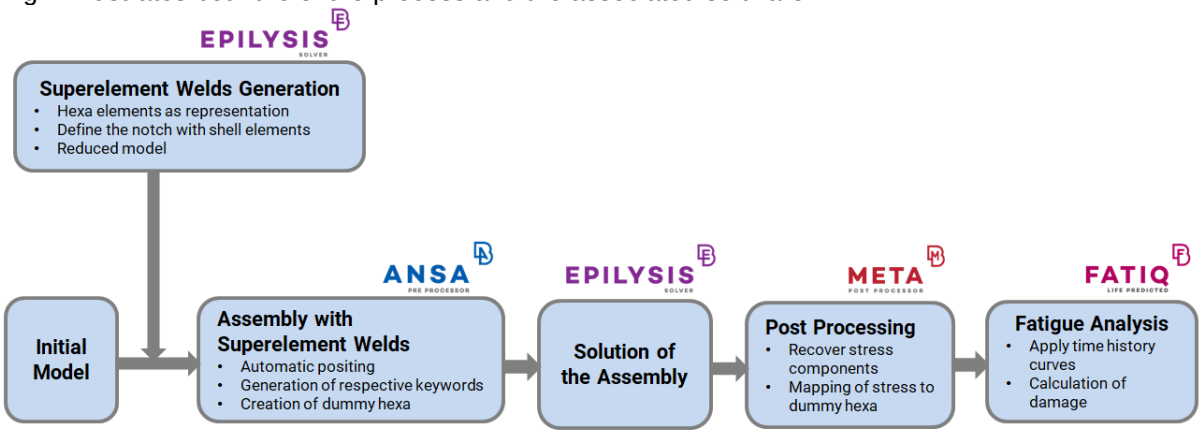

Fig. 2
Workflow

3.1 Superelement Welds Generation

Fig. 3 shows the initial spot weld model that will be replaced with a reduced matrix, comprising 6328 hexa solid elements divided into two blocks. Positioned in the middle of the upper and lower blocks is a notch with a specific radius. The outer nodes of each block are connected together with 96 RBE2 elements and their master nodes are connected with 8 R-Spline elements. A 4-node representation for each block is used, meaning that 8 nodes are the interface nodes where the reduced model (superelement) will be connected to the rest of the model with RBE3 elements.

The stress of interest is the stress that is developed on the notch. To obtain the stress tensor so that it can be used as input in fatigue analysis, 180 additional shell elements with minimal thickness are defined (1e-4 mm).

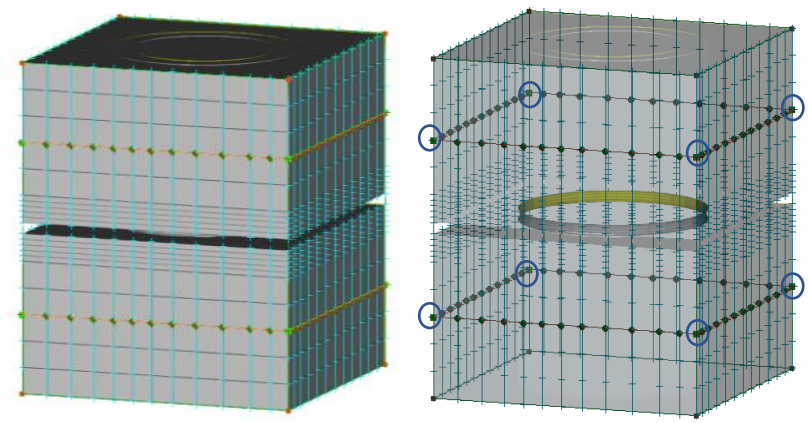

Fig. 3
Spot weld model. The interface nodes and the shell elements of the notch are showed on the right.

3.2 Assembly with Superelement Welds

The assembly creation involves the automatic positioning of the superelement welds on the model by generating the respective Nastran keywords using specific criteria in the ANSA pre-processor. Apparently, superelement welds of different geometrical features should be defined according to the thickness of the connected parts. To achieve this, they are specified accordingly in the table, depicted in Fig. 4.

Functions | Thickness to Diameter Map | Available FE Rep | FE Rep Ref. Library | Partial Realization | Robscan | Superelement

Superelement Defined By: op2 file

Superelement File mapping

4-node Representation | 8-node Representation

Diameter	t1	t2	t3	t4	op2 file	superelement id	diagonal1
4.	0.47	2.			/home/SuperelementWeld_Generatio...	85	
4.	0.7	0.83			/home/SuperelementWeld_Generatio...	66	
4.	0.7	1.6			/home/SuperelementWeld_Generatio...	81	
4.	0.7	1.72			/home/SuperelementWeld_Generatio...	62	
4.	0.7	1.73			/home/SuperelementWeld_Generatio...	82	
4.	0.7	1.9			/home/SuperelementWeld_Generatio...	47	
4.	0.8	0.83			/home/SuperelementWeld_Generatio...	27	
4.	0.8	0.93			/home/SuperelementWeld_Generatio...	30	
4.	0.8	1.			/home/SuperelementWeld_Generatio...	28	
4.	0.8	1.2			/home/SuperelementWeld_Generatio...	29	
4.	0.8	1.7			/home/SuperelementWeld_Generatio...	26	
4.	0.8	1.735			/home/SuperelementWeld_Generatio...	31	
4.	0.83	1.			/home/SuperelementWeld_Generatio...	64	
4.	0.83	1.2			/home/SuperelementWeld_Generatio...	65	
4.	0.83	1.7			/home/SuperelementWeld_Generatio...	35	
4.	0.83	1.73			/home/SuperelementWeld_Generatio...	67	
4.	0.83	1.735			/home/SuperelementWeld_Generatio...	68	
4.	0.83	1.9			/home/SuperelementWeld_Generatio...	45	

total 61 | visible 61

Fig.4
Table where an op2 file (superelement) is assigned per thickness group.

In order to extract the maximum stress that occurs on the notch for each weld, a dummy hexahedral element is also created. This element serves as a reference point for mapping the maximum stress. To prevent any additional stiffness in the analysis, this hexahedral element is assigned a very low Young's Modulus (1e-9 MPa).

The same process is repeated with the initial spot weld geometry (detailed representation). At the end, in order to evaluate the method, the results of the two methods are compared.

3.3 Post Proccesing and Fatigue Analysis

To proceed with fatigue analysis, it is necessary to retrieve the stress tensor from the shell elements of the notch for each spot weld. This is achieved by mapping the stress tensor, as well as the von-Mises stress, onto the hexahedral element in the META post-processor, as illustrated in Fig. 5.

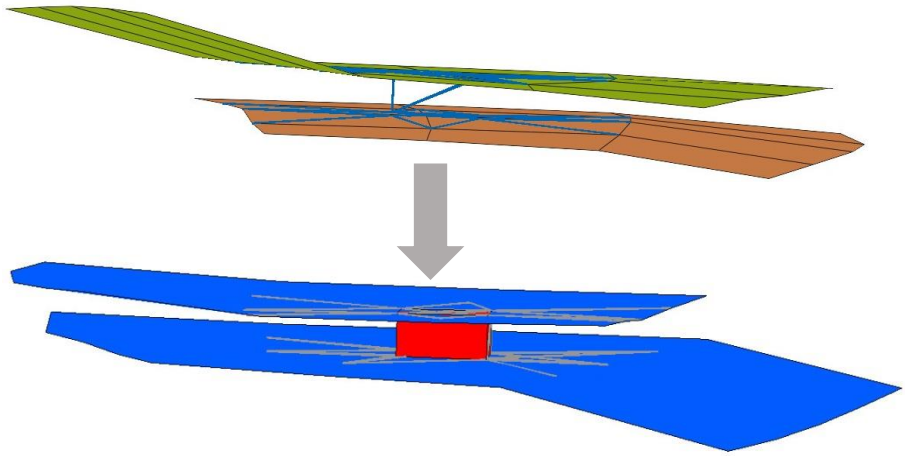

Fig. 5
Mapping of the stress tensor from superelement weld onto the hexahedral element.

The Epilysis solver is used to solve the two static (SOL 101) assembly models, where the welds are represented as superelement and detailed representation respectively. Fatigue analysis is conducted in the FATIQ software, utilizing stress tensor recovered from the META post-processor as input. Time-dependent curves are employed to generate transient stress signals through linear superposition, with von-Mises stress serving as the fatigue criterion. Damage calculation is carried out by applying Miner's rule to cycles extracted through the Rainflow counting algorithm.

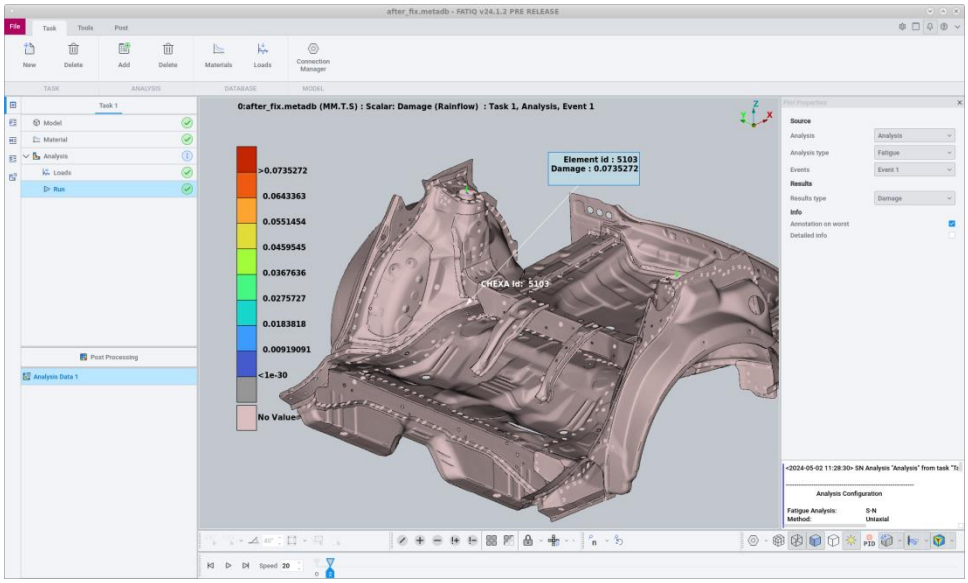

Fig. 6
Fatigue analysis

4 Results and Comparison

Table 1 displays the five spot welds with the highest von-Mises stress values located on the notch, from the two assembly models with the superelement and the detailed representation welds respectively, Fig.7. Notably, the top five spot welds with the highest values of two models agree and as is evident, the percentage differences fall within an acceptable range. The differences in fatigue damage percentage also adhere to the same pattern.

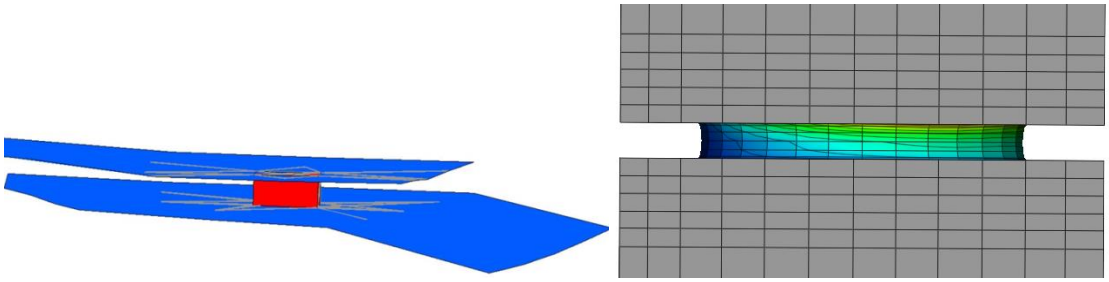

Fig.7
Post-processing of von-Mises stress on the notch of superelement and detailed representation weld model

Weld_ID	Superelement	Detailed_Representation	Difference (%)
5103	379.45	362	**4.59**
3960	296.90	310.6	**4.41**
8775	280.54	274.8	**2.09**
10017	278.61	284.4	**2.04**
5094	244.23	225.6	**8.26**

Table 1
Maximum von-Mises notch stress of the top five spot welds of the two models

In terms of solution time, the total time for both models are presented in Table 2. It is apparent that the utilization of a superelement representation greatly diminishes solution time in contrast to the detailed representation model. This contrast is further pronounced due to the fact that the superelement model employs a single CPU, whereas the alternative model uses eight.

	SOL101 with Superelement welds (1CPU)	SOL101 with Detailed Representation welds (8CPUs)
Time	23mins 7sec	3h 8mins 57sec

5 Conclusions

The entire CAE process, beginning from generating the reduced matrices of the detailed weld geometry to concluding with fatigue analysis using retrieved notch stress, has been presented. Calculating notch stress directly from spot welds by representing them as superelements is a method that yields precise results, significantly reduces solution time and improves overall model handling. This approach empowers the detailed modeling of welds and can similarly be applied to seam welds.

Vorteile durch die Integration der Lebensdaueranalyse in den FEM-Solver

M. Klein, E. Heinemeyer, INTES GmbH

1 Kurzfassung

Als wichtige Ergänzung zur Festigkeitsberechnung mit Finiten Elementen hat sich die Lebensdaueranalyse auf Basis einer Spannungsberechnung im industriellen Einsatz etabliert. Die Ergebnisse der Lebensdaueranalyse werden zur Auslegung von Bauteilen und Baugruppen im Leichtbau genutzt.
An den Simulationsprozess stellt die Ergänzung der Lebensdaueranalyse zusätzliche Anforderungen. Der Austausch großer Datenmengen zwischen verschiedenen Programmen und sogar zwischen Rechenservern verhindert gute Performance und einfache Handhabung. Überwunden werden müssen unterschiedliche Schnittstellenformate, wechselnde Zuordnung einzelner Daten sowie unterschiedlicher Modellbeschreibungen oder Namensräume. Der Datentransfer und die fehlerfreie Nutzung dieses Verfahrens liegt in der Verantwortung des Anwenders und ist nicht Bestandteil der einzelnen Programme und wird deshalb zumeist nicht anforderungsgemäß gewartet. Neben dem Datenhandling müssen für den Gesamtsimulationsprozess auch die unterschiedlichen Release-Zeiträume der beteiligten Software berücksichtigt werden.
Die vollständige Integration der Lebensdauerlebensdaueranalyse in einen allgemeinen FEM-Löser wird als Lösung vorgestellt. Beide Analyseteile, die klassische Spannungsanalyse und die Lebensdaueranalyse, basieren auf einem gemeinsamen Datenmodell. Dadurch ist die Dateneffizienz gewährleistet (große Datenmengen bleiben intern, doppeltes Datenhandling wird vermieden) und der Import/Export oder die Archivierung von Zwischenergebnissen ist nicht mehr notwendig.
Bisher ungenutzte Ergebnisse, die schon vorliegen und nicht zusätzlich berechnet werden müssen, können einfach genutzt werden. Beispielsweise Spannungsgradienten, liegen in optimaler Qualität direkt innerhalb der FEM-Software auf Basis des ursprünglichen FEM-Modells vor. Dadurch kann die Qualität der Ergebnisse gesteigert werden. Zusätzlich profitiert die integrierte Lebensdaueranalyse deutlich in der Performance durch den Wegfall des Datenaustauschs und die HPC-Ausrichtung der FEM-Software.
Durch den reduzierte Datenaustausch werden neue Analyseklassen ermöglicht. Die Spannungsergebnisse aus großen Modellen in Kombination mit vielen Analyseschritten übersteigen häufig die Speicherkapazitäten und verhindern dadurch eine Lebensdaueranalyse vollständig oder ermöglichen nur eine geringe Genauigkeit. Durch die softwaretechnische Integration müssen die vollständigen Spannungsergebnisse aller Berechnungsschritte nicht mehr gespeichert werden, sondern werden direkt („on-the-fly“) von der Lebensdaueranalyse in jedem Berechnungsschritt verwendet und anschließend sofort wieder gelöscht. Durch diese deutliche Prozessverbesserung können neue Klassen von Modellgrößen und deutlich mehr Ergebnisschritte berücksichtigt werden. Die Ergebnisse sind dann viel genauer.
Der Fokus des Vortrags liegt auf der Prozessvereinfachung und der Reduzierung der Rechenzeit für Beispiele aus der industriellen Praxis.

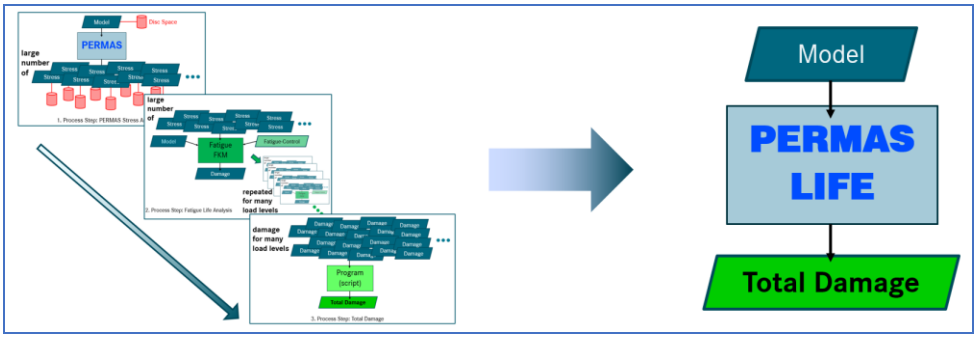

Vom klassischen manuellen 3-Schritte-Prozess zum effizienten integrierten Prozess

2 Referenzen

[1] Alexander Berndt, Jens Michy, Daimler Truck AG, Markus Ast, Eric Heinemeyer, Michael Klein, INTES GmbH, Reduktion der Prozesskomplexität durch Integration der Lebensdauerberechnung in die FEM-Simulation, VDI SIMVEC, 22. – 23. November 2022

[2] Alexander Berndt, Jens Michy, Daimler Truck AG, Michael Klein, INTES GmbH, Integrated Fatigue Lifetime Prediction of a Differential Case, PERMAS Web Conference, 29. Juni – 7. Juli 2022

[3] Jakob Häckh, Steinbeis Transferzentrum, Andreas Schünemann, INTES GmbH, Integrierte Lebensdaueranalyse in PERMAS – Entwicklungsvorschau –, PERMAS Tech Meeting, 22. April 2021

[4] Prof. Dr.-Ing. G. Willmerding, Dipl.-Ing. (FH) Jakob Häckh, Steinbeis Transferzentrum, Fatigue Life estimation using winLIFE and PERMAS, PERMAS Technologietag, 11. April 2019

Vorteile durch die Integration der Lebensdaueranalyse in den FEM-Solver

M. Klein, INTES
E. Heinemeyer, INTES

NAFEMS DACH Konferenz 2024: Konferenz für Berechnung & Simulation im Engineering, 10. – 12. Juni 2024, Bamberg, D

INTES
INTES Ingenieurgesellschaft für technische Software mbH

INTES
INTES GmbH
Breitwiesenstr. 28
D-70565 Stuttgart
Phone +49-711-78499-0
Fax +49-711-78499-10
E-mail: info@intes.de
http://www.intes.de

Privately held and independent Finite Element Technology company since 1984 located in Stuttgart, Paris, Tokyo and Ann Arbor.

Developing and marketing of the FE analysis software PERMAS with graphical user interfaces VisPER and PCGen.

Unified software for thermo-mechanics, vibro-acoustics, and optimization.

High-level specialists with many years of experience form a powerful team. High performance solvers and functional innovations account for the team's success.

Inhalt

- Motivation
- Stand der Technik des aktuellen Prozesses in der Industrie
- Beschreibung des vorhandenen Prozesses, Schritt für Schritt
- Lösung: neuer Simulationsprozess durch Integrations der Lebensdauerberechnung in den FEM-Solver
- Neuer Prozess: Beschreibung und Beispiele
- Zusammenfassung und Ausblick

Motivation

Die Lebensdauerberechnung ist Teil des virtuellen Entwicklungsprozesses von Einzelteilen bis hin zu kompletten Baugruppen. Merkmale der Entwicklungsanforderungen: viele Varianten, mathematische Optimierung erwünscht.

Die Vorhersage der Lebensdauer ist sehr wichtig, aber es ist ein zusätzlicher Schritt mit zusätzlicher Software, zusätzlichen Schnittstellen und hohem Bedarf an Speicherplatz (Spannungstensoren)!

Die Herausforderungen sind:

- Schnittstellen zwischen verschiedenen Softwaren,
- Zwischenspeichern der Ergebnisse auf der Festplatte,
- Lange Rechenzeiten,
- Mehrere zuständige Hotlines,
- Prozess durch proprietäre Skripte oder manuelles Kopieren/Ausführen,
- Endnutzer, der für den Prozess und seine Wartung verantwortlich ist,
- Die Lebensdauerberechnung hat keinen Zugriff auf das interne Wissen/die Ergebnisse der FEM.

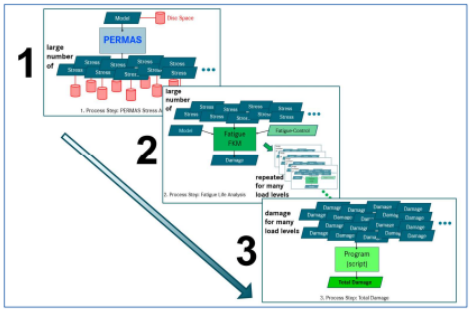

Mehrere Schritte, mehrere Softwaren, mehrere Skripte – Prozess mit umfangreicher Dateiverwaltung

Motivation

Deutliche Verbesserungen sind möglich:

- Prozesskette vereinfachen, Komplexität reduzieren
  - Reduzieren der Anzahl der Dateiformate
  - Reduzieren der (manuelle) Fehlerquellen
  - Reduzieren der Datenzwischenspeicherung/des belegten Speicherplatzes
  - Reduzieren der Anzahl verantwortlicher Softwareanbieter
  - Prozesswartung erforderlich
- Beschleunigung der virtuellen Produktentwicklung
  - Reduktion der Laufzeiten
- Technologievorsprung realisieren
  - Neue innovative Möglichkeiten
  - Erhöhen der Ergebnisgenauigkeit

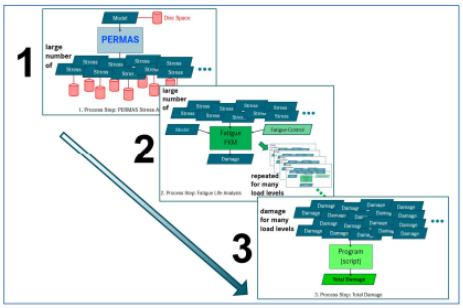

Mehrere Schritte, mehrere Softwaren, mehrere Skripte – Prozess mit umfangreicher Dateiverwaltung

Schwerpunkt dieser Präsentation:
Verbesserungen des Ermüdungsprozesses für industrielle Anwendungen!

State-of-the-Art Industrieller Prozess

- Beispiel eines industriellen Prozesses: Gesamtschädigung einer Strukturbaugruppe (Differential).
- Viele Lastfälle (Schritte) einer nichtlinearen (einschließlich Kontakt) statischen Analyse beschreiben die wiederkehrende Beanspruchung.
- Berücksichtigt werden Spannungen für unterschiedliche Belastungsniveaus.
- Fixe Belastungen aus der Montage werden korrekt berücksichtigt (keine Belastungsniveaus).
- Der Gesamtschaden ergibt sich aus der unterschiedlichen Anzahl der Schadenswiederholungen bei unterschiedlichen Belastungsniveaus.
- Dies erfordert mehrere Schritte (in diesem industriellen Fall 3 Schritte) mit unterschiedlicher Software und Datenübertragung über Dateien und Schnittstellen.
- Beschreibung und Analyse der 3 Schritte.

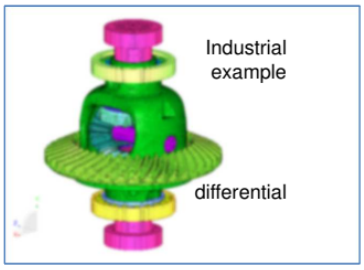

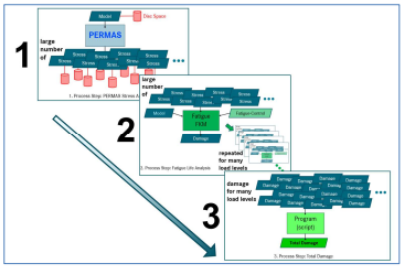

Klassischer Process mit 3 Schritten

1. Schritt

State-of-the-Art Industrieprozess
(vereinfachter Ausschnitt)

Aufgabe: 41 Spannungsergebnisdateien (eine für jeden Analyseschritt) für die weitere Verarbeitung vorbereiten:

- Auf Oberflächenknoten reduziert.
- Gradienten noch möglich?
- Für Gradienten sind weitere Ergebnisse erforderlich.
- Effizienz und Qualität hängen von den Schnittstellen und der Festplatten-I/O-Geschwindigkeit ab.

(Bemerkungen:

- Das Hauptzahnrad hat 41 Zähne.
- Zahl ist oft eine Primzahl.)

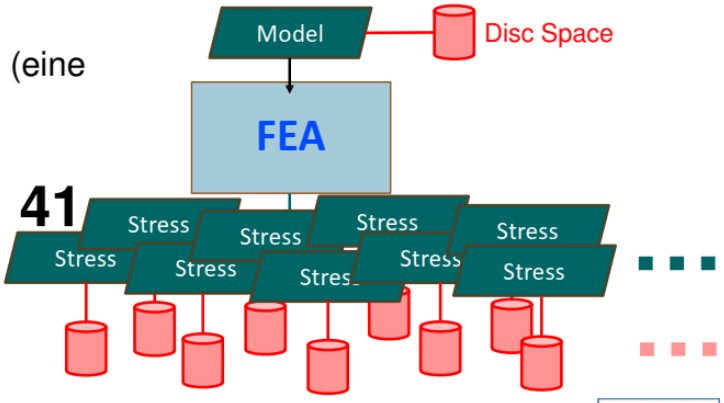

Processschritt: Spannungsanalyse

2. Schritt

State-of-the-Art Industrieprozess
(vereinfachter Ausschnitt)

Aufgabe: Erstelle 70 einzelne Dateien mit der Schädigung für 70 Lastniveaus durch 70 Lebensdaueranalysen basierend jeweils auf den 41 Spannungsdateien.

- 70 Lebensdaueranalysen
- Wiederholtes Lesen des Modells und der Spannungsergebnisse.
- Sehr viele Lese- und Schreibvorgänge.
- Aufwändiges Datenmanagement.

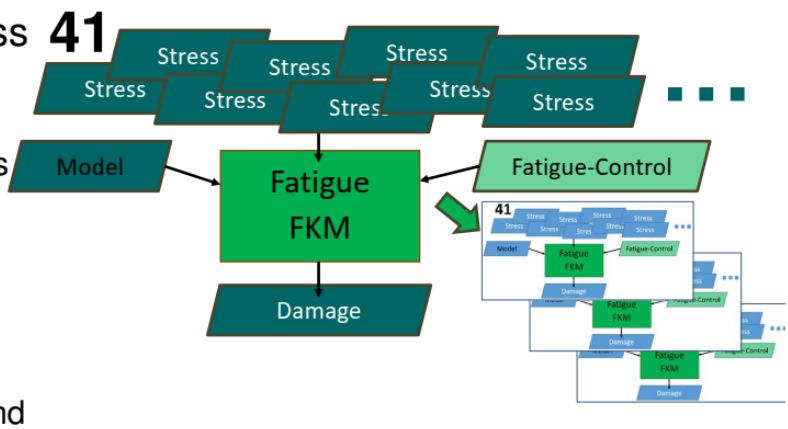

70

Prozessschritt: 70 Lebensdaueranalysen

3. Schritt

State-of-the-Art Industrieprozess
(vereinfachter Ausschnitt)

Aufgabe: Nutze individuelle (Ortsabhängige) Nutzungsprofile durch Wiederholungsanzahl der verschiedenen Lastniveaus.

- Lese 70 Dateien mit Schädigungsergebnissen
- Kombination der Einzelschädigungen durch ein proprietäres Programmskript.
- Individuelle Lastspielanzahl für die 70 Belastungsstufen berücksichtigen.
- Gesamtschädigung berechnen.
- Gesamtschadensdatei schreiben.

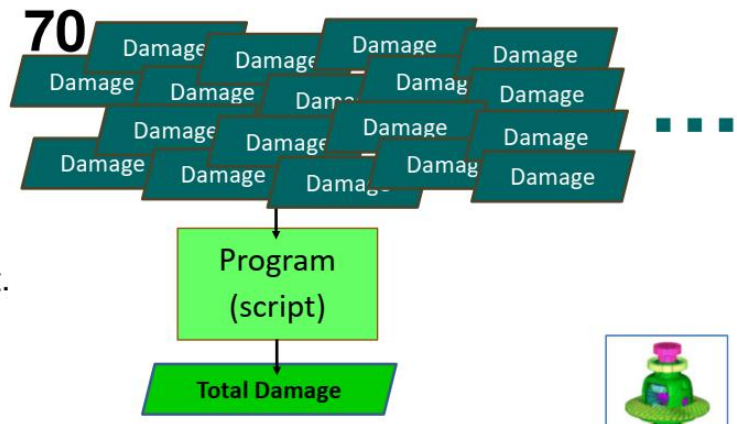

Prozessschritt: Gesamtschädigung

Bisheriger Berechnungsprozess

Drei aufwändige Schritte:

1. PERMAS Spannungsberechnung
2. 70 Lebensdauerberechnungen
3. Kombination der Einzelschädigungen

Prozesscharakteristik:

- Während des gesamten Prozesses werden sehr viele Daten geschrieben und gelesen.
- Die Datenmenge limitiert die Modellgröße (Genauigkeit).
- Die Datenorganisation geschieht manuell und deshalb Fehleranfällig.
- Schnittstellen sind zusätzliche Fehlerursachen.

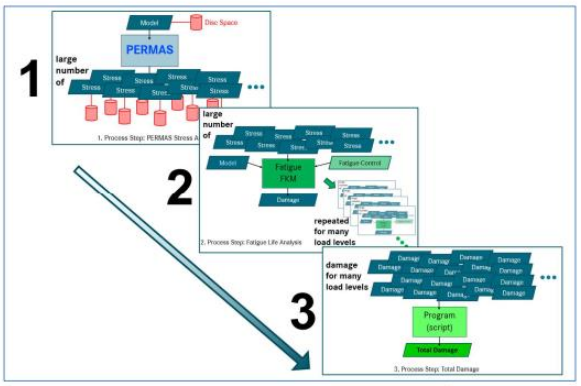

Bisheriger Berechnungsprozess mit 3 Schritten

Lösungsansatz

Lösung: Neuer integrierter Prozess!

Integration der Lebensdauerberechnung in die FE-Software für Spannungsberechnungen.

(Integration = völlige Neuentwicklung der Lebensdauerberechnung in der FE-Software-Infrastruktur, keine internen Schnittstellen, ein Code, eine gemeinsame Datenbasis)

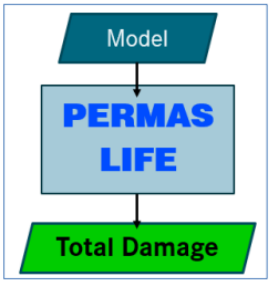

Neuer integrierter Prozess

Drei deutliche Verbesserungen durch Integration:

1. Prozessvereinfachung (und Standardisierung)
2. Genauigkeit
3. Dateneffizienz

1. Prozessvereinfachung

Drei deutliche Verbesserungen durch Integration:

1. **Prozessvereinfachung** (und Standardisierung)
   - z.B. Knotenspannungen intern verfügbar
   - Lebensdauer ist „nur“ ein weiterer Berechnungsschritt
   - Alle Analyseschritte erfolgen in einer gewarteten Software
   - High-Performance Software Infrastruktur:
     - Erfahrung im Umgang mit großen Datenmengen
     - Durchgängige Parallelisierung vorhanden
     - Spezialisten für HPC
   - Lebensdaueranalyse profitiert deutlich von der Softwarebasis
   - Daten-Caching auf die Festplatten ersatzlos aus dem Prozess gestrichen (nicht mehr notwendig)

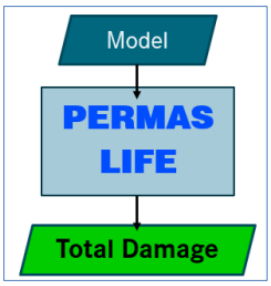

Neuer integrierter Prozess

➜ Die Organisation (Definition) des Gesamtprozesses erfolgt in einer gewarteten Software

2. Genauigkeit

Drei deutliche Verbesserungen durch Integration:

1. Prozessvereinfachung (und Standardisierung)
2. **Genauigkeit**
   - Deutlich größere Modell (feiner vernetzt, mehr Freiheitsgrade) trotzdem verkürzte Rechenzeit und weniger Daten
   - Spannungen in interner Genauigkeit (mehr Stellen)
   - Spannungen im Innern, zusätzlich zur Oberfläche, ohne zusätzlichen Datentransfer
   - Genaue Spannungsgradienten
     - Genaue Normalenrichtung (Oberflächennormale)
     - Gradienten berücksichtigen Elementansatzfunktionen

   ➜ genauere Lebensdauerberechnung

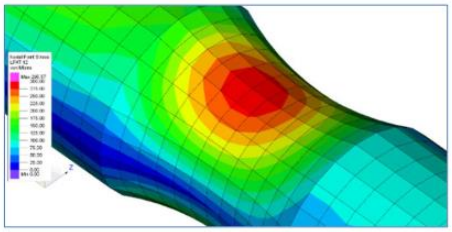

Stress results

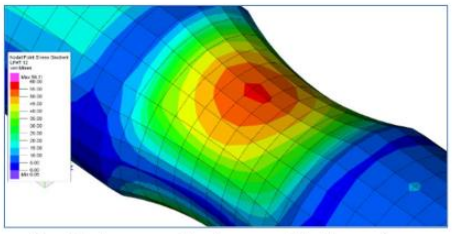

Nodal stress gradients normal to the surface

3. Dateneffizienz

Drei deutliche Verbesserungen durch Integration:

1. Prozessvereinfachung (und Standardisierung)
2. Genauigkeit
3. **Dateneffizienz**
   - Spannungsdaten und Lebensdauerergebnisse in der Gleichen Datenbasis
   - „On-the-fly“: Berechnungen ohne Zwischenspeichern:
     - Anstatt alle Zwischenergebnisse wie Spannungsdaten, einschließlich Gradienten, auf Vorrat zu speichern, bis sie später zur Berechnung von Schädigungsergebnissen verwendet werden, ermöglicht der integrierte Ansatz die schrittweise Berechnung des Endergebnisses und die sofortige Freigabe der Zwischenergebnisse (Löschen).
   - Viel schneller, kein Festplattenspeicher, keine manuelle Verwaltung der Daten (kopieren, sichern, …)

   ➜ **Deutlich größere (vorher nicht rechenbare) Modelle möglich**

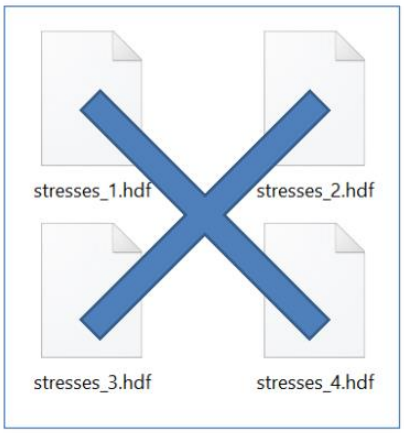

Spannungsdaten nicht in Dateien auf Festplatten

1. Industrielles Beispiel

- Komplexer industrieller Prozess in einem Rechenlauf
- Prozessorganisation vollständig in der FE-Software:
  - Erstellung der Zeitschritte mit Lastkollektiven
  - Individuelle Schädigungsergebnisse für unterschiedliche Belastungsstufen
  - (Genaue Spannungsgradienten)
  - Kombinations der Schädigungsniveaus mit der jeweiligen individuellen Wiederholungsanzahl
  - Export der Gesamtschädigung
- **Schnelle Berechnungszeit: 22 min auf 18 Cores**
  - Spannungsanalyse mit 44 Lastschritten
  - 70 Lebensdaueranalysen
  - Gesamtschädigung basierend auf der Wiederholungsanzahl der Schädigungen auf verschiedenen Lastniveaus
- Prozess ist einfach Übertragbar auf neue Varianten
  - Gekapselte Prozessorganisation unabhängig von den Modelldaten

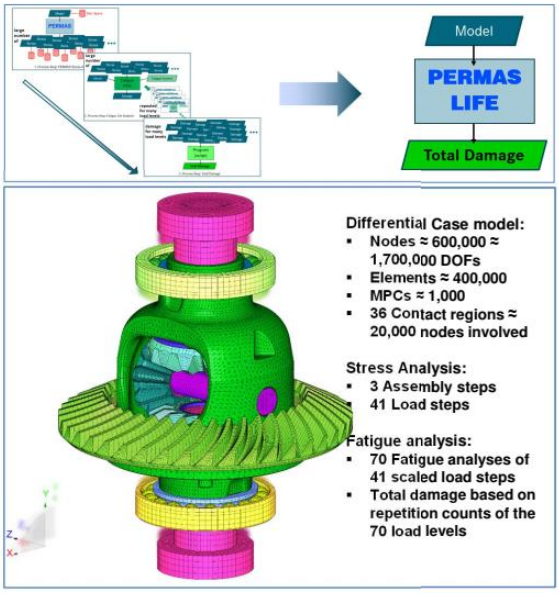

2. Industrielles Beispiel

Vorhersage der Seitenträgerlebensdauer als Teil eines vollständigen LKW-Fahrgestell-FE-Modells

7.900.000	Knoten
5.700.000	Elemente
82.000	Fatigue-Knoten an Volumenelementen
54.000	Fatigue-Knotenpaare an Schalenelementen
515	Eigenmoden
174.000	Zeitschritte
von 16	Schlechtwegteststrecken

Schnelle Berechnungszeit: 3 h 12 min auf 28 Cores

- Modelleinlesen und Konsolidierung
- Modalanalyse
- Transiente Dynamik
- Lebensdauerberechnung
- Ergebnisausgabe

Courtesy of Daimler Truck

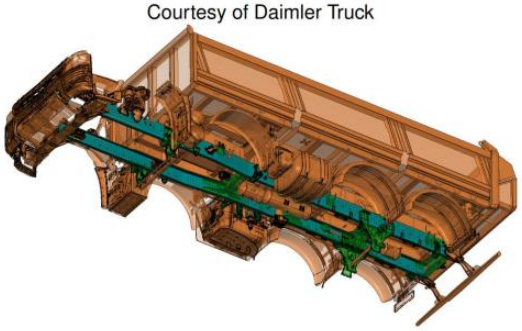

Damage Max(Top,Bottom)

Stand der Implementierung

- Vollständig integrierte Lebensdauerberechnung direkt in FE-Software (PERMAS)
- „High-cycle Fatigue“ (Langzeitbelastung, typ. >1000 Zyklen)
- Multi-axialer Spannungszustand auf Strukturoberflächen (FKM 7.0 und mehr)
- Für alle Volumen- und Schalenelemente
- Klassische Knotenspannungen oder hochgenaue Spannungen und Gradienten
- Mehrere Wöhlerkurven für jedes Material, Oberflächenhärte und -rauheit, Stützfaktor, Mittelspannungskorrektur, Neuber-Korrektur
- Lasten:
  - Collectives: Von Lasten oder Moden (wie Differentialbeispiel)
  - Timeline: Amplitudenzeitfunktionen für Lasten oder Moden
  - Timehistory: Teile aus dem Last-/Zeitverlauf der Primäranalyse (wie Truck-Beispiel)

Zusammenfassung und Ausblick

- Die neue integrierte Lebensdauerberechnung verbessert den Prozess um Größenordnungen.
- Spannungsberechnung und Lebensdauerberechnung sind in einer Software integriert und erfordern keine Schnittstellen.
- Die Genauigkeit wurde gesteigert.
- Die Laufzeiten und der Speicherbedarf wurden deutlich reduziert.
- Grundlegende Technologie und Infrastruktur für die Lebensdauerberechnung sind in der FE-Software PERMAS entwickelt.
- Dies ist der perfekte Ausgangspunkt für Funktionserweiterungen, wie z. B. die Erweiterung um weitere Ermüdungsansätze, Sampling, Optimierung mit Schädigung als Zielfunktion oder Restriktion (integrierte Optimierung ist schon vorhanden!).

Vielen Dank für Ihr Interesse!
Möchten Sie unsere Lebensdaueranalyse testen?
Sprechen Sie mich gerne an!
per E-Mail an klein@INTES.de

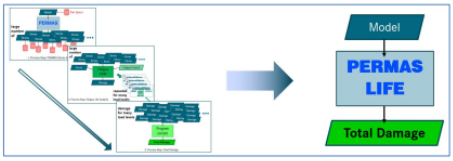

Vom klassischen manuellen 3-Schritte-Prozess zum effizienten integrierten Prozess

NAFEMS DACH Konferenz 2024: Konferenz für Berechnung & Simulation im Engineering, 10. – 12. Juni 2024, Bamberg, D

Enhanced Low Cycle Fatigue Analysis

Gerhard Spindelberger, Axel Werkhausen (MAGNA Powertrain, Engineering Center Steyr)

1 Summary

This paper explores the application of enhanced low cycle fatigue analysis with FEMFAT to address the challenge of predicting plastic deformation in materials subjected to stresses that exceed their yield strength. Mathematical models, such as the von Mises yield criterion and strain hardening models, have been traditionally used to estimate the plastic deformation of metals. However, considering material non-linearity in finite element analysis (FEA) significantly increases analysis time, making it impractical for many engineering applications.
To overcome this problem, this paper proposes the use of PLAST methods in FEMFAT for estimating elasto-plastic stresses. The PLAST methods involve two main components: fitting a kinematic hardening model to the initial branch of the stress-strain curve and employing stress rearrangement methods based on the Neuber method or the equivalent strain energy density (ESED) method. Additionally, the influence of load peak sequence on damage results will be discussed.
A case study focusing on the plates of a rotor in an electric motor is presented to demonstrate the effectiveness of the FEMFAT PLAST approach. The results of the case study show that the new PLAST approach can achieve comparable results to elastoplastic FE analysis while significantly reducing analysis time. Furthermore, the paper discusses how the sequence of load peaks influences the resulting damage predictions, providing valuable insights for engineers in designing fatigue-resistant components.

2 Introduction

In many engineering applications, the stresses experienced by materials can exceed their yield strength, resulting in plastic deformation. The accurate prediction of this plastic deformation is crucial for assessing the structural integrity and fatigue life of components. Mathematical models, such as the von Mises yield criterion and strain hardening models, have been widely used to estimate the plastic deformation of metals. Hardening models describe the behavior of materials under load over the yield point. The hardening process in materials can occur through the expansion or translation of the yield surface. This concept is fundamental in understanding the behavior of materials under plastic deformation. The two primary types of hardening mechanisms based on the nature of yield surface changes are isotropic hardening and kinematic hardening.

2.1 Isotropic and kinematic hardening

Isotropic hardening refers to the expansion of the yield surface in all directions uniformly. In this case, the size of the yield surface increases as plastic deformation progresses. Isotropic hardening is commonly observed in materials that undergo uniform plastic deformation, such as mild steels. As the material experiences more plastic deformation, the yield surface expands – the yield stress increases, indicating a higher resistance to further deformation.

On the other hand, kinematic hardening involves the translation of the yield surface while maintaining its size. This type of hardening is associated with materials that exhibit non-uniform plastic deformation, such as certain types of metals and alloys. As the material undergoes plastic deformation, the yield surface shifts, indicating a change in the material's ability to accommodate further deformation. Kinematic hardening is often characterized by a Bauschinger effect, where the material's yield strength decreases after reverse loading.

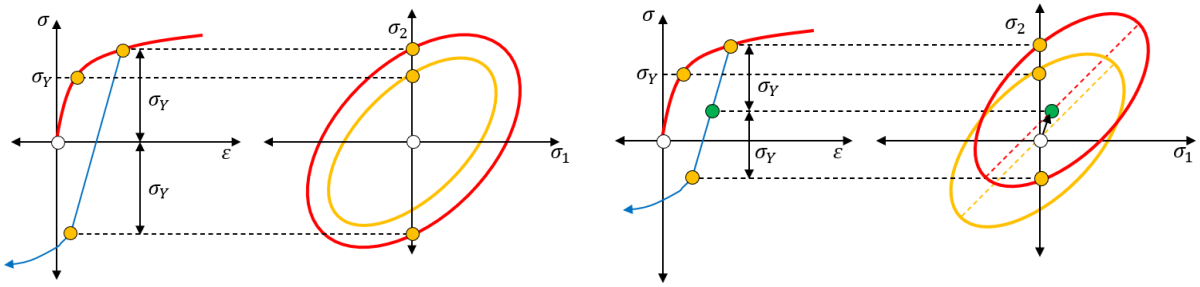

Fig. 1: Yield surface for isotropic hardening (left) and kinematic hardening (right)

However, incorporating material non-linearity in finite element analysis (FEA) can significantly increase computational time and complexity. This poses a challenge for engineers who need to perform efficient and reliable low cycle fatigue analysis.

3 New PLAST method

To address the problem of increased analysis time due to material non-linearity, the use of PLAST methods in FEMFAT for estimating elasto-plastic stresses was proposed. The PLAST methods offer an alternative approach that reduces computational time while maintaining accuracy. The two major components of the FEMFAT PLAST approach are as follows:

1. Fitting a kinematic hardening model to the initial branch of the stress-strain curve: The kinematic hardening model captures the material's behavior during cyclic loading and provides a more accurate representation of the stress-strain response, especially in the plastic range. By fitting this model to the initial branch of the stress-strain curve, the PLAST method accounts for the material's hardening behavior.
2. Stress rearrangement according to Neuber or ESED method: Stress rearrangement methods are employed to account for the redistribution of stresses due to cyclic loading. The Neuber method and the ESED method are commonly used approaches for stress rearrangement. These methods ensure that the elasto-plastic stresses are appropriately distributed, leading to more accurate fatigue life predictions.

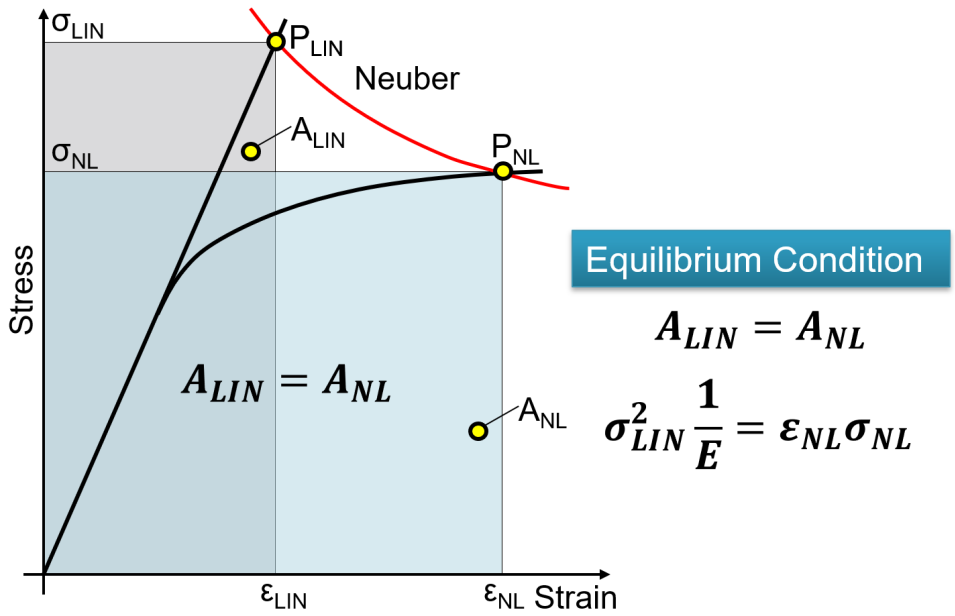

Fig. 2: Stress rearrangement according to Neuber

Procedure of the new PLAST method:

1. Computation of Material Parameters: For each material pair (C_i, γ_i), an optimization process is conducted to determine the values that minimize the error to the cyclic stabilized stress-strain curve. These parameters are specific to the material being analyzed and are crucial for accurately predicting its behavior under cyclic loading. The Ramberg-Osgood parameters K' and n', which define the cyclic stabilized data, serve as reference values for the optimization process.

2. Kinematic Hardening Model: In the cutting plane, the equivalent stress history is rearranged using the kinematic hardening model. This model utilizes the optimized parameters obtained in step 1 for each sample of the load time history. The kinematic hardening model considers the material's response to cyclic loading, accounting for the accumulation and redistribution of plastic deformation.
3. Rainflow Counting: The rearranged stress history obtained from the kinematic hardening model undergoes rainflow counting.

4 Benefits and Case Study:

The advantage of the FEMFAT PLAST approach is to avoid the need for computationally expensive elastoplastic FE analysis. Engineers can significantly reduce analysis time without compromising the reliability of their predictions.
To demonstrate the effectiveness of the FEMFAT PLAST approach, a case study focusing on the plates of a rotor in an electric motor is presented. The case study compares the results obtained using the new PLAST approach with those obtained from an elastoplastic FE analysis. The findings show that the PLAST approach yields similar results to the elastoplastic FE analysis while significantly reducing analysis time.

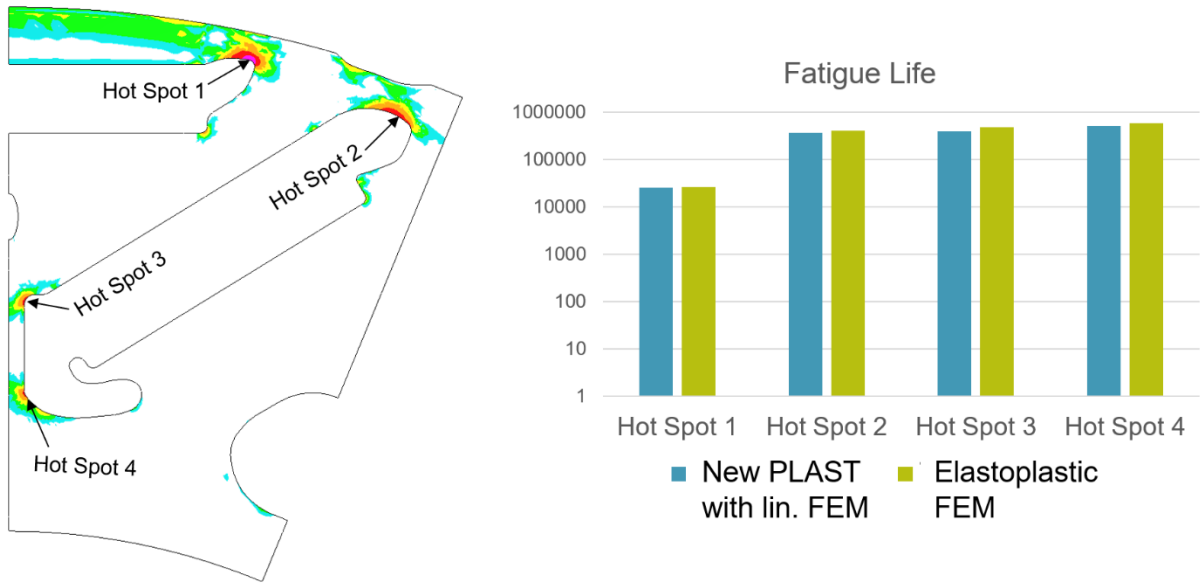

Fig. 3: Comparable fatigue life results for new PLAST with linear FEM and elastoplastic FEM

In Fig. 3 the fatigue results between the new PLAST approach with linear FEM and elastoplastic FEM are very similar. But the total analysis time (FEM + fatigue analysis) of the new method is about 25 times faster!

Additionally, it was discussed how the sequence of load peaks influences the resulting damage predictions. To illustrate the sequence influence, two signals with same rainflow matrix are investigated. The second signal was generated by just flipping the first signal.

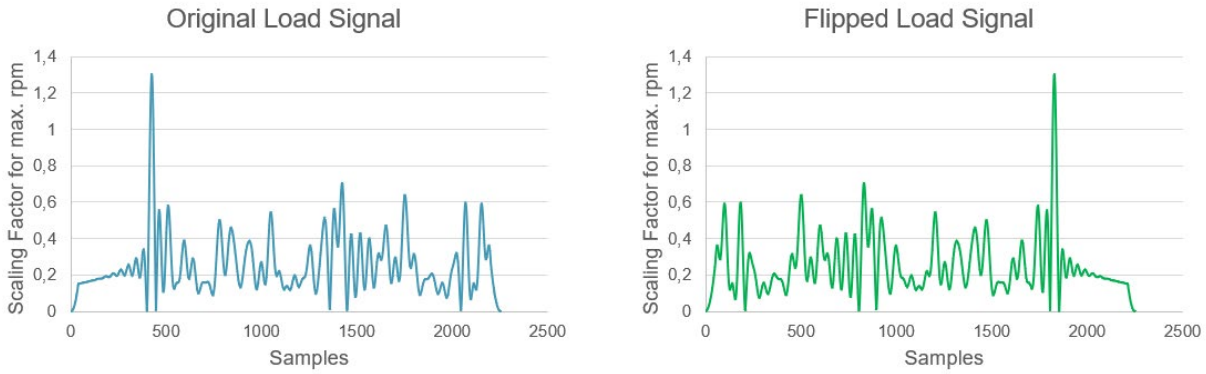

Fig. 4: original signal (right) and flipped signal (left) to study the sequence influence

Both signals were analyzed with the old and new FEMFAT plast method. Both signals provide the same rainflow matrix, thus the old method provides the same damage, independent if the high load peak is at the beginning or at the end of the signal.
In contrast, the new methods demonstrate, that the stress peak at the beginning leads to plastic hardening, thus reducing the damage of the subsequent cycles.

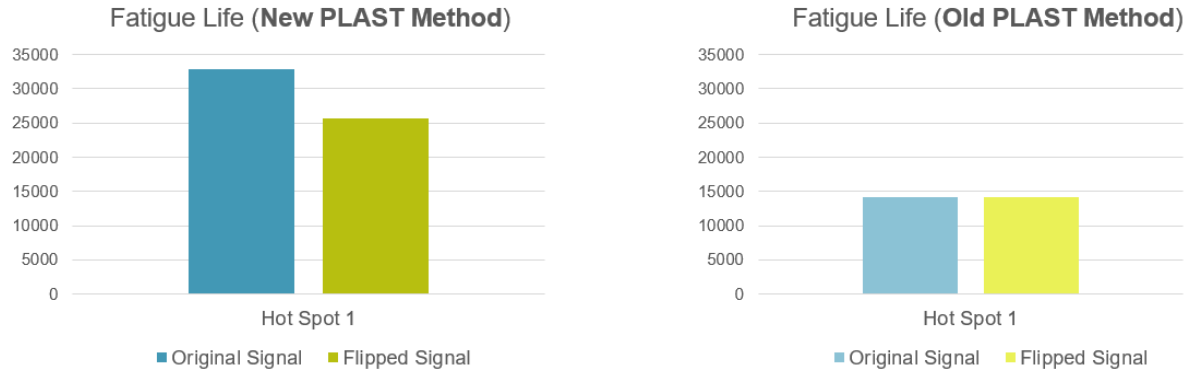

Fig. 5: original signal (right) and flipped signal (left) to study the sequence influence

5 Conclusions

In conclusion, the enhanced low cycle fatigue analysis with the new FEMFAT PLAST method offers a practical and efficient solution for engineers to accurately predict the fatigue life of components subjected to high-stress applications.
By incorporating kinematic hardening in multiaxial fatigue analysis, the influence of the sequence of high load peaks can be predicted with high accuracy even for long time histories.

Enhanced AK-IS / AK-MCS Algorithm for Efficient and Accurate Reliability and Sensitivity Analysis

Patrick Wurm, Alexander Rabofsky
(Magna Steyr Fahrzeugtechnik GmbH & Co KG, Graz)

1 Introduction

In the development of vehicle structure durability, the failure probability, i.e. the likelihood of a vehicle failing within the required fatigue lifetime, is an important metric for assessing the reliability and performance of the vehicle. The calculation of this metric in practical problems is often challenging due to the presence of the numerous random variables that impact the vehicle's performance. The calculation typically necessitates a significant number of model evaluations, which can be infeasible for computationally expensive models. Therefore, there is a pressing need to develop new methods and techniques that can effectively minimize the required number of model evaluations while still accurately estimating the failure probability. Additionally, it is crucial to identify and prioritize the random variables that have the most significant impact on the failure probability. This can be achieved by calculating the sensitivities of the failure probability with respect to the random variables. By understanding and prioritizing the most influential random variables, engineers can make targeted design decisions to lower the failure probability.

To address these challenges, Magna presents an efficient reliability method for calculating the failure probability and its sensitivities in this article. While initially developed for vehicle models, this method is applicable across various domains. Our approach builds upon the widely recognized AK-IS/AK-MCS algorithm[1][2], which falls under the umbrella of active learning techniques in machine learning. By leveraging a Kriging metamodel, the AK-IS/AK-MCS algorithm in its original formulation already has a good degree of efficiency. To further improve the efficiency of the algorithm and to extract the failure probability sensitivities, three modifications have been made. (1) It has been observed that the original convergence criterion of the algorithm tends to be overconservative in practical applications. To overcome this limitation, a more effective criterion has been applied, resulting in further enhancements to computational efficiency. (2) We propose to select the optimal hyperparameters for the Kriging metamodel through cross-validation, as opposed to relying on a default set of parameters. This methodology ensures that the hyperparameters are specifically tailored to the unique characteristics of the problem at hand, thereby optimizing the overall accuracy and adaptability of the algorithm. (3) A post-processing step has been added to determine the failure probability sensitivities as an additional result set, using the well-established score function approach[3]. To demonstrate the effectiveness and relevance of our method, three examples are presented. Through these examples, we showcase the application of our method and highlight its potential in improving reliability calculations for structural durability in various domains.

The subsequent sections will provide a detailed explanation of the methodology, present the results and discussions, and conclude with a summary of the main findings and potential future research directions.

2 Method

2.1 AK-IS/AK-MCS algorithm

The AK-MCS (Active learning Kriging-based Monte Carlo Simulation) algorithm[1] is a reliability analysis technique used to estimate the failure probability of a system with computationally expensive numerical models. By leveraging a set of N_{MCS} candidate samples, the AK-MCS algorithm constructs a Kriging metamodel[4] that approximates the behavior of the numerical model. The Kriging metamodel not only provides predictions of the true behavior of the numerical model at each sample, but also quantifies the associated uncertainty through the Kriging standard deviation. Through an active learning process, the algorithm iteratively selects the most informative sample for evaluation, with a focus on critical areas in the design space. The active learning process terminates once the convergence criteria are satisfied. The failure probability P_f is subsequently calculated using Monte Carlo sampling,

$$P_f \approx \frac{1}{N_{MCS}} \sum_{i=1}^{N_{MCS}} I_F^i, \tag{1}$$

utilizing the Kriging predictions obtained from all candidate samples in the last (converged) model state. In this formula, I_F denotes the failure counter ($I_F^i = 1$ if failure is predicted at sample i, 0 otherwise).

The AK-IS (Active learning Kriging-based Importance Sampling) algorithm[2] is an enhanced version of AK-MCS, specifically designed for analyzing problems with low failure probabilities. The AK-IS algorithm consists of two distinct steps. In the first step, the first-order reliability method (FORM)[5] algorithm is employed to identify the most probable failure point (MPP). Subsequently, in the second step, a set of N_{IS} candidate samples is generated in the vicinity of the MPP. Similar to AK-MCS, an active learning process is then executed until the convergence criterion is met. Finally, utilizing the last (converged) model state, the failure probability P_f is computed using Importance Sampling

$$P_f \approx \frac{1}{N_{IS}} \sum_{i=1}^{N_{IS}} I_F^i \frac{f^i}{f_h^i}, \tag{2}$$

where f^i is the joint Gaussian probability density function over the random variables and f_h is the auxiliary density function which accounts for the biased sampling distribution around the MPP.

2.2 Convergence criterion

Both AK-IS and AK-MCS originally use the same convergence criterion

$$\min\left(\frac{\mu^i}{\sigma^i}\right) \geq 2. \tag{3}$$

In this criterion, μ^i represents the Kriging prediction and σ^i denotes the Kriging standard deviation of sample i. The criterion implies that convergence is reached once the sample with the highest level of uncertainty exhibits at least a probability of approximately 97.7% for accurate classification (failure vs. no failure)[2]. However, our research findings indicate that this convergence criterion tends to be overly conservative when applied in practical scenarios (see Section 3). The criterion's overconservative nature is likely a result of its exclusive focus on the most uncertain sample.

We have applied a more effective convergence criterion[6] that relates the overall probability of misclassification P_m to the estimated failure probability P_f

$$\frac{P_m}{P_f} < \eta \quad (\text{e.g. } \eta = 2\%). \tag{4}$$

If the probability of misclassification is only a small fraction of the probability of failure, we can safely assume that the algorithm has converged. This convergence criterion does not solely rely on the sample with the highest uncertainty to determine convergence, but takes all samples into account.

2.3 Kriging hyperparameters

Another characteristic that both AK-IS and AK-MCS originally share is that they use a default set of hyperparameters for the Kriging metamodel (ordinary Kriging together with an anisotropic squared-exponential function as the correlation model)[1][2]. To enhance the accuracy and adaptability of the algorithm, we propose a novel approach of selecting the hyperparameters through a cross-validation process. This process utilizes all the samples evaluated so far at the current state of the active learning process and splits these samples in a train-test split with a ratio of 75:25. Various combinations of the hyperparameters are applied to the training samples and evaluated against the test samples. The Kriging metamodel is then updated with the most accurate combination of Kriging type and correlation model, determined by minimizing the mean squared error (MSE). This tailored selection of hyperparameters ensures that the Kriging metamodel is specifically optimized for the unique characteristics of the problem at hand.

2.4 Failure probability sensitivities

In their original formulation, both AK-IS and AK-MCS algorithms do not offer the capability to compute the sensitivities of the failure probability with respect to the random variables. However, these sensitivities play a crucial role in facilitating targeted design decisions to minimize the failure probability. To address this limitation, we have introduced a post-processing step that enables the calculation of sensitivities using the well-established score function approach[3]. A major advantage of this approach is that the calculation of sensitivities does not require any additional model evaluations, making it very

fast and cost-effective. This enhancement allows for a more comprehensive analysis of the system's behavior and empowers practitioners to make informed decisions regarding design improvements. The sensitivities s are calculated as [7][8]

$$s_{d_k} \approx \frac{1}{N_{MCS}} \sum_{i=1}^{N_{MCS}} I_F^i \frac{\partial log f^i}{\partial d_k} \text{ and} \tag{5}$$

$$s_{d_k} \approx \frac{1}{N_{IS}} \sum_{i=1}^{N_{IS}} I_F^i \frac{\partial log f^i}{\partial d_k} \frac{f^i}{f_h^i} \tag{6}$$

for AK-MCS and AK-IS, respectively. In these formulas, d denotes either the mean value or the standard deviation of random variable k.

3 Results and Discussion

The AK-IS/AK-MCS algorithm with the three proposed modifications has been applied to various problems. We will here present results from three examples, a cantilever beam with a point load and piecewise constant cross-sections (example A), and two real-world applications in vehicle models (examples B & C). In example A, failure occurs when the stress in the beam exceeds the allowable stress. In examples B & C, failure potentially occurs near the bolted joints, due to fatigue damage induced by the required bridging of a gap arising from the manufacturing process. For example B, the specific analysis centered around the fastening of the lower control arm to a subframe. As for example C, the analysis focused on the fastening of the steering crossbeam to the vehicle frame. Due to confidentiality reasons, the detailed representation of the numerical finite element models used in examples B and C cannot be disclosed. However, Fig. 1 provides schematic diagrams of the three examples. It is worth mentioning that the finite element models for examples B and C consist of approximately 250,000 elements, covering a significantly larger area than what is illustrated in the schematic diagrams.

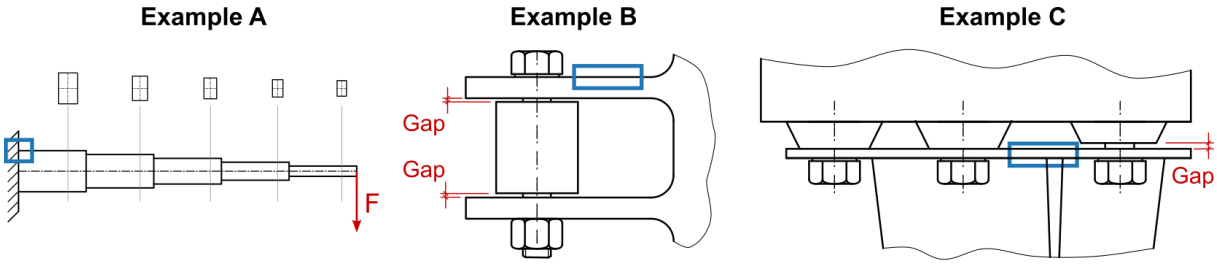

Fig. 1
Schematic diagrams of the three examples. Marked in blue are the critical areas where failure potentially occurs.

Tab. 1 presents the key results from Example A. The results demonstrate that the original AK-IS algorithm requires significantly fewer model evaluations compared to traditional Monte Carlo or Importance Sampling methods for determining the probability of failure. By applying the proposed modifications, we could further reduce the required number of model evaluations by a significant amount, with no loss in precision in the prediction of the failure probability.

Method	Number of Model Evaluations	Failure Probability P_f
MCS	5 x 10^7	1.18 x 10^{-4}
IS	5 x 10^5	1.21 x 10^{-4}
AK-IS ORIGINAL	39 + 146	1.19 x 10^{-4}
AK-IS HP	39 + 85	1.18 x 10^{-4}
AK-IS CC	39 + 7	1.20 x 10^{-4}
AK-IS HP+CC	39 + 5	1.19 x 10^{-4}

Tab. 1
Results from example A. The efficiency of different reliability analysis methods is compared. “MCS” and “IS” denotes Monte Carlo and Importance Sampling, respectively. The AK-IS algorithm is compared in different variants. The “ORIGINAL” variant represents the original implementation as described in the literature[2]. In the variant “HP”, the Kriging hyperparameters are selected through cross-validation as outlined in Section 2.3. The “CC” variant incorporates the more effective convergence criterion as outlined in Section 2.2. Lastly, the “HP+CC” is a combination of both. For AK-IS the number of model evaluations is split into evaluations in step 1 (FORM) + evaluations in the active learning process.

Similar results are observed in example B as depicted in Tab. 2 and Fig. 2. Fig. 3 illustrates the failure probability sensitivities of the set of four random variables studied in example B. These sensitivities reveal that, in this particular example, variations in the standard deviation of the random variables have minimal impact on the failure probability compared to variations in their mean values. The results indicate that reducing the mean value of the random variable "Load Scaling Factor" is the most effective approach for decreasing the failure probability. The next most effective measure is to reduce the mean value of the random variable "Gap Size."

Method	Number of Model Evaluations	Failure Probability P_f
AK-IS ORIGINAL	60 + 108 (not converged)	1.42 x 10^{-1}
AK-IS HP + CC	60 + 43	1.40 x 10^{-1}

Tab. 2
Results from example B. The AK-IS algorithm is compared in the two variants “ORIGINAL” and “HP+CC”. For AK-IS the number of model evaluations is split into evaluations in step 1 (FORM) + evaluations in the active learning process. Due to computational limitations, the variant “ORIGINAL” had to be stopped before the original convergence (Eq. 3) criterion was satisfied.

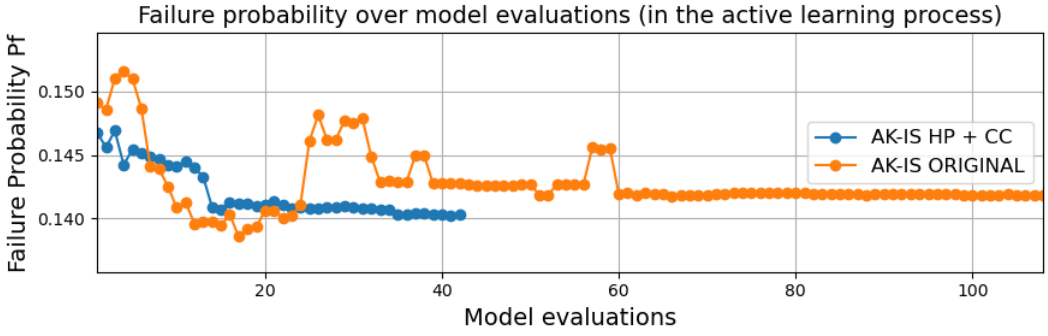

Fig. 2
Failure probability over the model evaluations for example B. The AK-IS algorithm is compared in the two variants “ORIGINAL” and “HP+CC”. Due to computational limitations, the variant “ORIGINAL” had to be stopped before the original convergence (Eq. 3) criterion was satisfied.

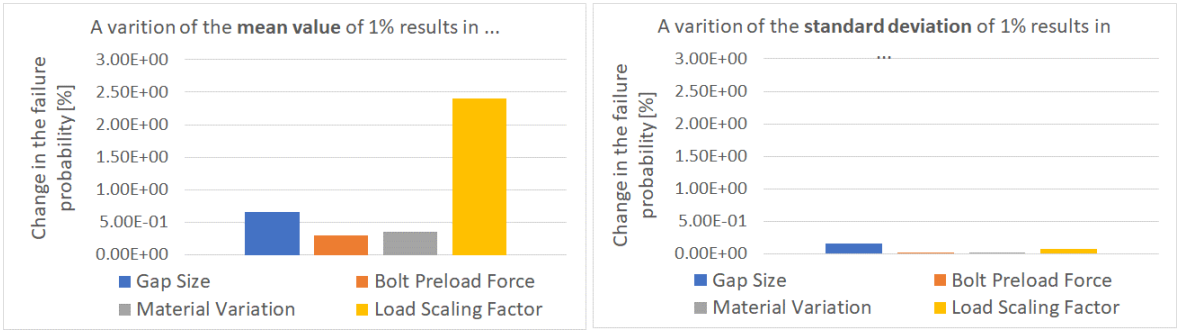

Fig. 3
Failure probability sensitivities for example B.

In example C, a similar sensitivity analysis to that in example B revealed that two specific random variables, namely "Gap Size" and "Wall thickness," have a significant impact on the failure probability. Based on this insight, the design space of these two random variables was further investigated using a grid-based approach. Fig. 4 shows the results of this investigation, where the fatigue damage value is plotted against the two random variables. These results provided valuable insights for making an optimal design decision.

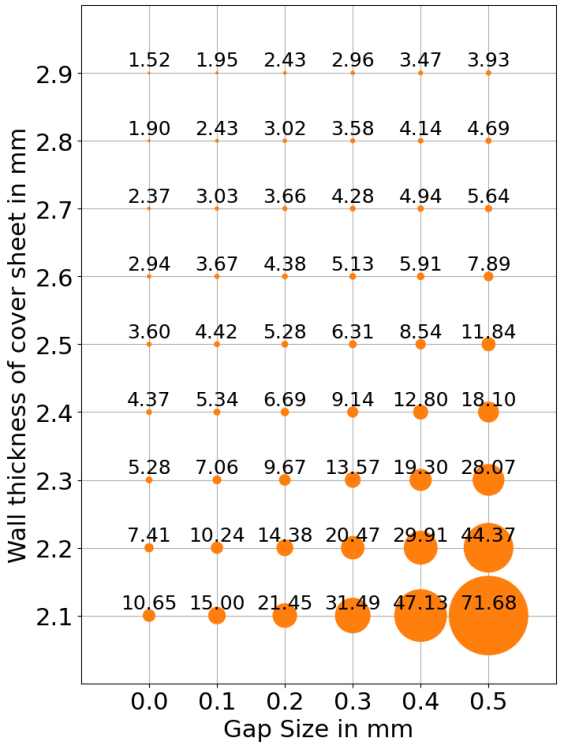

Fig. 4
Fatigue damage over two random variables from a grid-based investigation in example C.

4 Conclusions

In this study, Magna has presented an efficient reliability method for calculating the failure probability and its associated sensitivities in the context of vehicle structural durability and beyond. The objective was to address the challenge of impracticality in performing a large number of model evaluations for complex models, while ensuring accuracy and relevance in the reliability calculations.

Through several enhancements to the AK-IS/AK-MCS algorithm, we have achieved significant improvements. By applying a more effective convergence criterion, the number of model evaluations required for reliability calculations has been minimized. Additionally, the selection of appropriate hyperparameters for the Kriging metamodel through cross-validation has ensured accuracy in the results. The inclusion of a post-processing step to determine the sensitivities of the failure probability

using the score function approach has provided valuable insights into the impact of individual random variables on the failure probability.

The application of our method to three examples has demonstrated its effectiveness and relevance. Future research directions may include further refinement and validation of the method, as well as its application to other domains beyond vehicle structural durability.

5 References

[1] Echard B., Gayton N., and Lemaire M., "*AK-MCS: An active learning reliability method combining Kriging and Monte Carlo Simulation*", Structural Safety, vol. 33, pp. 145-154, 2011.

[2] Echard B., Gayton N., Lemaire M., and Relun N., "*A combined Importance Sampling and Kriging reliability method for small failure probabilities with time-demanding numerical models*", Reliability Engineering and System Safety, vol. 111, pp. 232-240, 2013.

[3] Rubinstein, R., "*The score function approach for sensitivity analysis of computer simulation models*", Mathematics and Computers in Sumulation, vol. 28, pp. 351-379, 1986

[4] Kleijnen J., "*Kriging Metamodeling in Simulation: A Review*", European Journal of Operational Research, vol. 192, pp. 707-716, 2007

[5] Cizelj L., Mavko B., and Riesch-Oppermann H., "*Application of first and second order reliability methods in the safety assessment of cracked steam generator tubing*", Nuclear Engineering and Design, vol. 147, pp. 359-368, 1994

[6] Sun Z., Wang J., Li R., Tong C., "*LIF: A new Kriging based learning function and its application to structural reliability analysis*", Reliability Engineering and System Safety, vol. 157, pp. 152-165, 2017

[7] Dubourg, V., "*Adaptive surrogate models for reliability analysis and reliability-based design optimization*", PHD Thesis, Blaise Pascal University, 2011

[8] Lombardo S. S., and Cadini F. and Cammi A., "*Impact of uncertainties on the safety performances of the LBE-XADS concept nuclear reactor*", Nuclear Engineering and Design, vol. 341, pp. 16-24, 2019

Preplanning of an experimental modal analysis with impulse hammer by using a simulation model

Dr. Michael Mahler (Siemens Industry Software GmbH: michael.baeuerle-mahler@siemens.com ; Institut für Akustik und Bauphysik Universität Stuttgart: michael.mahler@iabp.uni-stuttgart.de)

Theresa Müller, M. Sc. (Institut für Akustik und Bauphysik Universität Stuttgart)

Prof. Dr.-Ing. Philip Leistner (Institut für Akustik und Bauphysik Universität Stuttgart; Fraunhofer Institut für Bauphysik)

Abstract

The evaluation of dynamic behavior-based physics of structures is becoming increasingly important. For example, durability, non-linear and structural as well as vibro-acoustic and(response) behavior are based on material-specific properties. This investigation focuses on the acoustic performance of timber elements. Nevertheless, the methodology used can also be applied to other domains. Timber construction is becoming progressively more important in urban areas. However, the acoustic vibration properties of timber structures are challenging to predict. An early analysis of the building behavior with regard to the standards is required to provide support during the concept and design phase as well as to reduce development and rework costs. Thus, an overall goal is to improve the simulation of (standard) test scenarios with wooden materials in a building framework. This requires good and high-quality input data for the simulation models. For this purpose, an approach for improving the simulation input data via the experimental modal analysis using an impulse hammer is investigated. The excitation and measurement positions will be optimized in advance to improve the quality of the test results quality and to predict the maximum possible optimization opportunity. For such test preparation, a response dynamics simulation including correlation and optimization techniques will be presented and applied on various wood species. Parameter adjustments of the relevant material properties are derived from the investigation and used for the acoustic simulation. The process, the experiences and the potential of such an approach are discussed.

Keywords: modal analysis, impulse hammer, vibration, correlation, Simcenter, FEM, timber

1 Introduction

As a result of the increasing demand for sustainable building methods and constructions, the number of timber buildings in timber construction in urban areas is on the rise [1]. Due to its mechanical properties, timber is an excellent building and construction material enabling the substitution of energy-intensive materials (e. g. concrete). Therefore, its use offers great potential for realizing sustainable construction solutions [2, 3]. Numerous building materials made of wood have become established as a further development of traditional use, such as in timber-frame houses. In addition to solid wood, these also include materials made from composite timber, veneers or lamellas that are bonded together using high pressure and adhesive. This results in high-performance timber materials with an extensive range of applications. In multistory buildings, for example, laminated veneer lumber (LVL) or cross-laminated timber (CLT) made of beech or spruce are suitable for bearing high loads and realizing large spans [4].

For this reason, timber construction represents an essential component for sustainable, climate-friendly construction, in order to reduce greenhouse gas emissions and to contribute to achieve the climate targets that have been set [2, 3]. Modern timber structures, e.g. made of cross-laminated timber, are suitable for industrial prefabrication, resulting in high quality components. Consequently, precise pre-planning is an indispensable part of the construction process [4].

However, early planning stages of buildings require a comprehensive evaluation of the building system behavior. It is particularly important to ensure compliance with standards during the conceptual and design stages of the project, examined in Chapter 2. An early analysis of building behavior with respect to the required standards is essential to support the concept and design phase and thus reduce development and rework costs. The aim objective is to improve the simulation of (standard) test scenarios with wooden materials in a building, presented in Chapter 3. Analyzing systems and coordinating standard performance in a concept and design phase is a challenge. Often the behavior of components is not known or the evaluation is not possible with sufficient accuracy at such an early phase. Thus, an approach for evaluating the behavior of components in a test approach with a dynamic-acoustic focus is propagated in Chapter 4 supplemented by the description of the preparation of the roving hammer test.

The effectiveness of the test case approach depends on various investigations, including those relating to sensors, actuators and devices. These technologies and components are not only cost intensive but also have restrictions. A previous optimization of these components as well as the entire test process is

therefore essential to improve the test quality. Chapter 5 outlines an approach for the preparation and optimization of the test case and the final Chapter details the application of the pre-evaluation within an academic use case. This provides insights into the experience and potential of the process presented and concludes with a comprehensive summary.

2 The research project framework

In contrast to buildings constructed from solid materials such as concrete or masonry, however, lightweight timber constructions pose a particular challenge for architects and planners due to their lower mass and stiffness. Especially with regard to acoustic quality, increased sound transmission in the low-frequency range can impair user comfort, a property that is often associated with lightweight timber constructions [5, 6]. Conventional solutions and improvement strategies are derived from experience with solid construction and usually involve increasing mass to dampen sound-induced vibrations [7].

However, there is a lack of suitable design tools that enable early prediction of compliance with sound insulation standards [6]. In addition, there remain barely any planning tools that holistically consider both the acoustic and structural properties of buildings. Incorporating a thorough vibration analysis into building design has the potential to not only refine the design process, but also improve the overall structural robustness of the building. Such advances emphasize the need for an interdisciplinary approach to address the relationship between acoustic performance and structural integrity.

Such interdisciplinary planning approaches are investigated within the research project Cluster of Excellence IntCDC (Integrative Computational Design and Construction for Architecture) at the University of Stuttgart [8]. The aim is to establish co-design methods that integrate architectural, structural and building physics criteria in feedback with innovative manufacturing and construction techniques. This results in timber construction systems that overcome the typical limitations of multi-storey timber buildings. Using digital technologies, new methods are available to modernize the design concepts of architecture and construction. These methods enable the early consideration of dynamic load-bearing behavior from both an acoustic and structural point of view and complement architectural and manufacturing considerations. [9]

Acoustic comfort is of great significance in timber buildings in consideration of the high potential for disturbance caused by low-frequency impact sound transmission. Studies at the Fraunhofer Institute for Building Physics IBP have shown noise pollution, especially from walking neighbors in multi-story buildings, is one of the most important sources of annoyance [5]. In comparison, wooden ceilings were rated significantly worse than concrete ceilings in terms of nuisance caused by noise from neighbors [5].

Low-frequency vibrations are also relevant to the load-bearing structure and are addressed within the serviceability limit state by using Eurocode 5 [10]. The serviceability limit state comprises the threshold values that influence the functionality of a structure or its load-bearing components under typical conditions of use. The vibration analysis often proves to be the limiting factor during the design process [11].

Structural vibrations in buildings are caused by a variety of factors. Figure 1 provides an overview of the frequency-dependent influences in residential construction in both the structural and acoustic frameworks. Even with sufficient stability, undesirable phenomena such as sound radiation can occur [11].

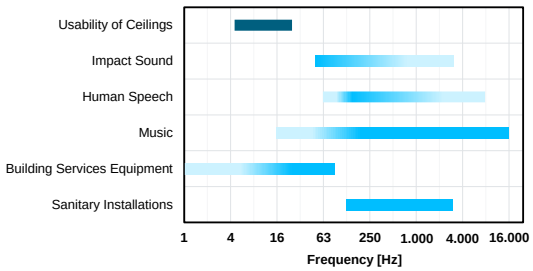

Figure 1. Overview of the frequency ranges of typical impacts in residential construction [12]

In order to achieve desired system behavior in structural vibrations and to comply with acoustic standards, the construction sector has integrated these standards into its praxis. In addition, system standard test cases are defined by regulations set by government and industry. However, such standard test cases require upper-engineered systems for testing purposes. Early prediction of system behavior can be facilitated by simulation technologies. Effective simulation, by contrast, depends on the accurate description of components and their behavior. Thus, there is an urgent need for improvements in describing and evaluating component behavior with high precision. This underlines the importance of conducting component tests to evaluate behavior and developing simulation models to predict component behavior. Simulations can be used to predict component behavior which can optimize component testing and potentially increase the testing quality.

The collaboration between industry and research with the aim of advancing the use of digital tools for the analysis and prediction of acoustically relevant vibration behavior is a key aspect. A partnership between the Institute for Acoustics and Building Physics of the University of Stuttgart and the Siemens Industry Software GmbH has been established as part of this work (Figure 2). Siemens Digital Industries Software has played a central role in providing

simulation tools, implementation assistance and project support.

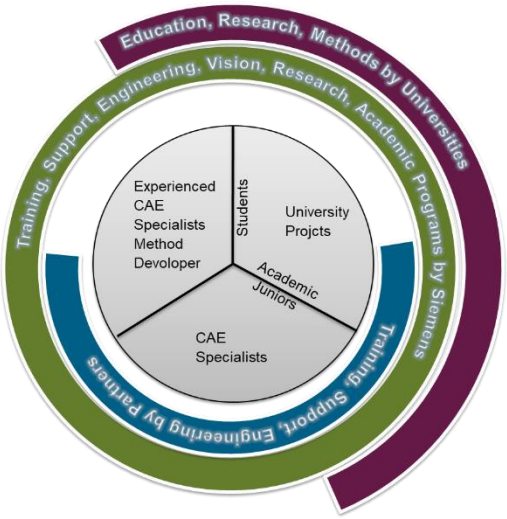

Figure 2. Partner framework concept

3 Consideration of transfer functions in acoustic measurement technology

The DIN EN ISO 10140 [13] describes methods for test bench measurements of the sound insulation of building components, such as airborne and impact sound insulation. When measuring the standard impact sound level, the separating floor is excited with the usual tapping machine within the building acoustics frequency range. Typically, the weighted standard impact sound level is mainly influenced by exceedances in the low one-third octave frequency bands and is often further increased by taking the spectrum adaptation term $C_{I,50\text{-}2500}$ into account [14]. Since both the structural properties of the components and the eigenmodes of the separating floor as well as the receiving room have an influence [14], the consideration of transfer function becomes more prominent in both measurement and calculation processes.

The acoustic behavior of components can be described by the transfer function H (Frequency Response Function – FRF). This function describes the relationship between the excitation and the resulting response (e.g. acceleration, velocity or sound pressure level). In order to describe the transmission properties of a structure, it is essential to record both the excitation (e.g. force) and the response behavior (e.g. acceleration, velocity, deviation). Sensors such as force or acceleration transducers are used to measure and evaluate excitation exerted on the structure. The response caused by the excitation can be measured at the designated response location using acceleration sensors, whereby it is also possible to measure the sonic speed or acceleration. [15]

Laboratory-scale tests require special materials, test environments and equipment, all of which are associated with costs. To reduce costs, it should be feasible to evaluate components and systems at the concept and design stage of building development. Predicting behavior through simulation is ideal for this purpose. However, the lack of suitable planning tools has already been pointed out. Consequently, we will present firstly a standardized method to assess the behavior of building components and secondly an approach to refine the results prior to implementation. The following chapter deals with the roving hammer test for evaluating the behavior of building components.

4 The test case roving impuls hammer vs. roving accelerometer

With the roving hammer test it is possible to determine the mode shapes of a structure. [16] states that the roving hammer test is a common method of modal testing, and some basic knowledge and limitations of the roving hammer test are presented. The roving hammer test requires a hammer to excite the structure and accelerometers that measure the movement of the structure (Figure 3). The roving hammer impacts at least one point on the structure in a single direction, usually in the normal direction of the point of impact. This means that the excitation occurs in a single degree of freedom (DOF). The measurement via the acceleration sensor is carried out at least at one point and in one direction. However, there exist accelerometers and technologies that can measure in multiple directions and at multiple locations, allowing measurement in multiple DOFs.

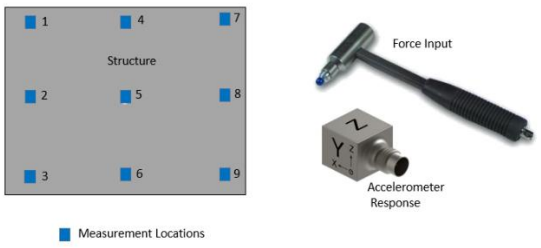

Figure 3. Modal Test Setup [17]

In this context, [16] describes the ongoing process: By attaching the accelerometer to a single degree of freedom (DOF) and loading the structure at as many DOFs as desired, the inherent shape of the structure is determined. This statement holds true because structures can exhibit multiple eigenmodes during the reaction [16]. Rarely can all relevant mode shapes be measured with a single accelerometer. In addition, a single accelerator sensor is often insufficient to accurately represent the motion associated with an eigenmode and make the motion of the structure comprehensible. Usually, multiple accelerator sensors are required to capture the mode shapes over the relevant frequency range.

However, there is often a lack of accelerator sensors and measurement channels, as these are only available limited and are costly. In contrast, the

excitation of the hammer can easily be administered over different areas in a sequential manner. The hammer offers the possibility of exciting the structure at multiple locations with less investment (Figure 4).

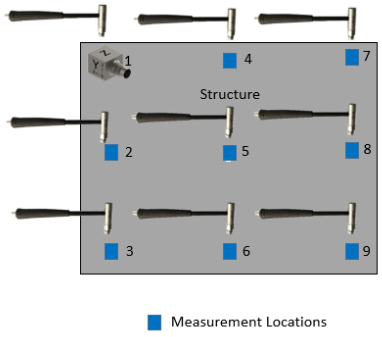

Figure 4. Roving Hammer [17]

Further, the choice of location is critical as placing the accelerometer or the excitation at a junction point of the mode shape may result in limited movement measurement. Consequently, the mode shape may not be accurately represented. In [17] and Figure 5, for example, two mode shapes of the same structure can be seen. To evaluate the left mode shape, the accelerometer must be placed in the middle of the plate to obtain the maximum amplitude, whereas placing the accelerator sensor at the same position for the mode shape on the right will not provide amplitude results. Thus, a sensitive and careful selection of the location is essential.

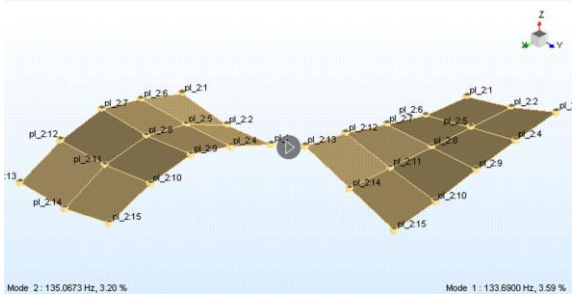

Figure 5. Mode Shape Example [17]

An alternative method to the roving impact hammer test is the roving accelerometer test. In [18] the application of the roving accelerometer approach is described. In this approach, the structure is impacted with an instrumented impact hammer at a fixed location while a tri-axial accelerometer is moved sequentially from point 1 to point 19 for 19 measurements. Thus, the main difference between the roving accelerometer test to the roving impact hammer test is that the impact hammer remains in one location while the accelerometer will be roving from location to location. The concept of the roving accelerometer test is visualized in Figure 6. Further details on the differences between the two approaches are presented in [17].

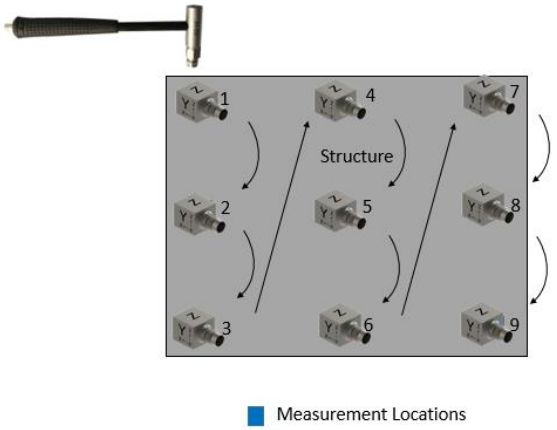

Figure 6. Roving accelerometer [17]

Both approaches can be simulated to compare test cases with simulation models using Siemens Simcenter 3D [19], particularly Simcenter 3D Correlation [20] which serves as the basis for the test pre-simulation discussed in the following chapter.

5 Simulation to prepare the test case

A simulation should be carried out in preparation for the roving hammer test. The software suite from Siemens Industry Software supports the user in determining the impact and sensor positions. In particular, a 'Pre-Test Roving Impact Hammer / Roving Accelerometer Wizard' assists to determine the locations for the roving hammer test locations. A CAD model of the test-object is then created. This can also be done with the Simcenter 3D software suite, including a CAD modeler.

The CAD model is used to further create an FEM simulation model to determine the eigenfrequency of the test object. Thus, both the simulation as well as the roving impact hammer or roving accelerometer test are used to identify the eigenfrequencies of the object. However, different approaches are used or the determination. In Siemens Simcenter 3D Structures [21], the FEM simulation of eigenfrequencies includes pre-processing (e.g. meshing and discretization of the CAD model, parameterization of the simulation model and solver settings), solving (with the included SC Nastran solver) and post-processing (review of the frequencies and mode shapes).

As part of this investigation, a normal mode analysis is performed as an independent solution within SOL103 of the Simcenter Nastran [22] solver.

The determined eigenfrequencies and mode shape form the basis for starting the 'Roving Impact Hammer Pre-Test Wizard' (requiring a manual execution of the provided automation routines) which can also be used for roving accelerometer pre-tests. The Wizard helps identify appropriate impact and sensor locations based on simulation mode shapes as shown in Figure 7. The various steps of the wizard can be seen on the left side of the figure and must be

worked through chronologically. The individual steps are explained in the following.

The first step is to define a name for better data-management of the automated simulation model creation.

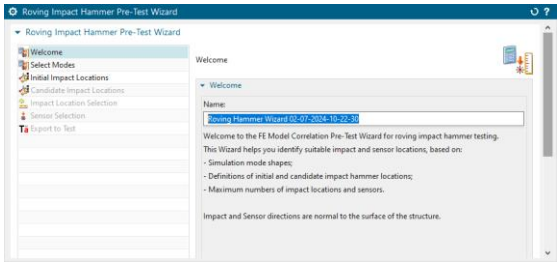

Figure 7. Roving Impact Hammer Pre-Test Wizard [19]

Within the wizard, the modal solution can be selected as the basis for the determination of suitable impact and sensor locations in the second ‘Select Modes’ step. At least one modal solution should be chosen.

Typically, there are initially predefined locations for executions with the impact hammer. The nodes associated with these locations can be selected as initial impact locations in a third step of the wizard. In minimum one initial impact location should be selected.

Further impact locations can be defined in the fourth step, ‘Candidate Impact Locations’, of the wizard. Typically, more than the required impact locations are selected. The selection of the possible impact points leads to a larger number of candidates for further impacts. However, the wizard should help to reduce the number of impacts and focus on a relevant number. For example, there may be ideal areas, such as surfaces, for hammer impacts. Not every point on these areas is relevant, but any point could serve as a candidate for an impact. It is beneficial to reduce the number of impact location candidates by considering the distances between impact locations to avoid executing sites that are close together or almost overlapping. The selection and reduction of impact location candidates can be done in this fourth step ‘Candidate Impact Locations’ of the wizard.

During the application of the wizard, an initial simulation model is generated as add-on to the modal simulation. The Siemens Simcenter 3D Correlation [23] and Siemens Simcenter 3D Pre-Test technologies are used to create this additional simulation model. With these technologies and the data defined in the wizard, a simulation model is created that includes the initial impact and the impact candidates.

After starting the fifth step of the wizard, ‘Impact Location Selection’, the simulation model can be executed after a maximum number of impact locations has been specified and ‘Impact Location Selection’ has been selected. The execution of the add-on simulation model establishes a correlation between the modal simulation model and a pseudo test model containing the initial impact and the candidate impact locations. This correlation process also generates a MAC matrix and a list of impact locations sorted by the impact locations after the relevance determination.

Figure 8. Simulation Tree [19]

The goal is to evaluate the relevance determination by minimizing the deviation between pseudo test and simulation. This can be observed in the MAC matrix, where a reduction in off-diagonal MAC values indicates an improved correlation. Each impact location is assigned an individual off-diagonal MAC value using two approaches:

In the first approach, the selection of impact locations is stopped after reaching a ‘maximum number of impact locations’ (defined in the fifth step of the wizard). The initial impact locations are prioritized, followed by the sorted impact location candidates. In the second approach, the selection of impact locations is stopped after achieving a maximum off-diagonal MAC values, predefined in the wizard as 0.2.

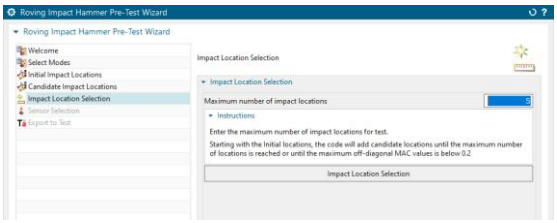

Figure 9. Impact Location Selection within the Wizard [19]

A similar method is used in the sixth step of the wizard, ‘Sensor Selection’. In this step, the ‘Candidate Impact Locations’, excluding the previously selected impact locations, are evaluated and sorted based on their weighted average Drive Point Residue [24] values. The locations with the highest rankings are chosen as sensor locations up to the maximum number of sensors specified in step six of the wizard. It should be noted that the sensors are recognized as unidirectional, oriented in the normal direction of the element surface.

In the final seventh step of the wizard, the option to ‘Export to Test’ is available. This export can be performed for Siemens test technologies or via the universal file format that allows a general approach for other test technologies. In this step, a predefined test model is created based on predefined and optimized impact and sensor locations.

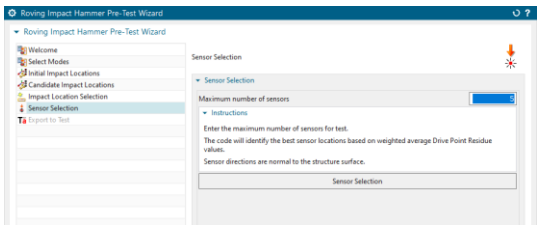

Figure 10. Sensor Selection within the Wizard [19]

It should be noted that the exciter and the sensor locations are interchangeable. This interchangeability makes it easier to implement a roving accelerometer test.

6 Application of the pre-evaluation

The application of a roving hammer test is used in the pre-testing phase of to evaluate the behavior of wooden materials. Due to the uncertainty of wood properties and scattering material values, this pre-testing serves two main objectives:

First, gaining a deeper understanding of the material properties of wood, especially with regard to variability. And second, to gain experience in the preparation of experimental modal tests through the use of simulation models.

To achieve these goals, a simple experimental setup is used and currently under investigation. For the test setup, multiple boards made of different types of wood are employed. These boards measure 2 m in length and are positioned horizontally to allow dynamic movement, with a translational constraint on both ends. The constraint is realized with a half-round wooden bar on top and bottom fixed with clamps.

The locations of the acceleration sensors and the positions of the hammer impacts were evaluated using Simcenter 3D [19]. The optimal implementation of this approach requires some time, especially in determining the ideal testing equipment. Initially, a preliminary evaluation was carried out in which the use of four tri-axial accelerometers was considered. The use of muti-axial sensors is common in testing departments. In this context, it should be noted that the measuring amplifier accommodates a corresponding number of channels for multi-axis acceleration sensors, which leads to a tripling of the required number of channels.

However, the simulation model shows that the use of four multi-axis acceleration sensors did not yield a satisfactory MAC matrix for comparing measurement and simulation data. Further investigations into the virtual evaluation of test scenarios showed that significantly better MAC matrix results can be achieved by using nine single-axis accelerometers with pre-optimized positions.

Based on these findings, an extensive series of measurements is currently being carried out on the basis of the pre-optimized measurement setup. The implementation of material optimization for the use of wood as a material in simulation models is planned as part of the further work of this cooperation. Knowledge of the material parameters and variability will enable more accurate prediction models for the vibration behavior.

7 Conclusion

In summary, the use of the ‘Pre-Test Roving Impact Hammer/ Roving Accelerometer Wizard’ within the Siemens Simcenter 3D Software Suite offers numerous advantages, especially in the area of pre-testing. This approach enables better planning of measurements and ensures that the sensor and impact positions are optimized in advance. This offers the potential to make the entire testing process more efficient. In addition, pre-testing improves the reproducibility of results as the setup is configured and standardized in advance. This leads to greater confidence in the reliability and consistency of the test data obtained. By pre-assessing the maximum quality of the MAC correlation between the simulation model and test model, pre-testing also enables better prediction of results. In addition, a wireframe connecting the locations can be automatically generated for the test and all relevant information can be compiled in an input deck for the test equipment simplifying the set-up process and reducing the potential for errors. Overall, pre-testing with Siemens Simcenter 3D contributes to a more efficient and reliable testing process, which will be further evaluated as the project progresses.

8 References

[1] H. Svatoš-Ražnjević, L. Orozco and A. Menges, "Advanced Timber Construction Industry: A Review of 350 Multi-Storey Timber Projects from 2000–2021," *buildings,* 2022.

[2] O. Bucklin, R. Di Bari, F. Amtsberg and A. Menges, "Environmental Impact of a Mono-Material Timber Building Envelope with Enhanced Energy Performance," *Sustainability,* 2022.

[3] J. L. Skullestad, R. A. Bohne and J. Lohne, "High-rise Timber Buildings as a Climate Change Mitigation Measure – A Comparative LCA of Structural System Alternatives," *Energy Procedia,* 2016.

[4] A. Pech, M. Aichholzer, M. Doubek, B. Höfferl, K. Hollinsky, A. Passer, M. Teibinger and R. Woschitz, Holz im Hochbau - Theorie und Praxis, Birkhäuser, 2016.

[5] M. Späh, A. Liebl and P. Leistner, "Acoustics in wooden buildings - Measurements in the Laboratory and in Single Family Houses," 2014.

[6] M. Caniato, F. Bettarello, A. Ferluga, L. Marsich, C. Schmid and P. Fausti, "Acoustic of lightweight timber buildings: A review," *Renewable and Sustainable Energy Reviews,* pp. 585-596, 2017.

[7] M. Kohrmann, R. Völtl, G. Müller, U. Schanda and M. Buchschmid, "Abschlussbericht zum AiF Forschungsvorhaben "VibWood": Planungshilfen zur schall- und schwingungstechnischen Beschreibung von Holzdecken und zur Bewertung und Dimensionierung von angepassten Schwingungsschutzsystemen," 2014.

[8] A. Menges, J. Knippers, P. Leistner, H. Garrecht and S. Aicher, "Co-Design of Multi-Storey Timber Building Systems for Building Stock Extension," [Online]. Available: https://www.intcdc.uni-stuttgart.de/research/research-projects/rp-3-2/. [Accessed 04 27 2024].

[9] T. Müller and P. Leistner, "Integrative Ansätze zur Körperschallentkopplung im mehrgeschossigen Holzbau," in *DEGA (Hg.) 2023 – Fortschritte der Akustik*, 2023.

[10] DIN German Institute for Standardization, Ed., *Eurocode 5: Design of timber structures - Part 1-1: General - Common rules and rules for buildings; German version EN 1995-1-1:2004 + AC:2006 + A1:2008,* Berlin: Beuth Verlag GmbH, 2010.

[11] P. Hamm, "Schwingungsnachweise von Holzdecken auf Unterzügen," in *10. Europäischer Kongress EBH*, 2017.

[12] A. Nolte, *Integrative Ansätze zur Vermeidung von Schallübertragung im modernen Holzbau,* Stuttgart, 2022.

[13] DIN German Institute for Standardization, Ed., *Acoustics - Laboratory measurement of sound insulation of building elements - Part 1: Application rules for specific products (ISO 10140-1:2021); German version EN ISO 10140-1:2021,* Berlin: Beuth Verlag GmbH, 2021.

[14] F. Schöpfer and U. Schanda, "Analyse der tieffrequenten Trittschallübertragung mittels Übertragungsfunktionen," in *Fortschritte der Akustik - DAGA 2021*, Wien, 2021.

[15] M. Möser, Messtechnik der Akustik, Berlin; Heidelberg: Springer, 2010.

[16] B. J. Schwarz and M. H. Richardson, "Experimental modal analysis," *CSI Reliability week ,* vol. 35, no. 1, pp. 1-12, 1999.

[17] Siemens, "Modal Tips: Roving Hammer versus Roving Accelerometer," Siemens, [Online]. Available: https://community.sw.siemens.com/s/article/modal-tips-roving-hammer-versus-roving-accelerometer. [Accessed 23 01 2024].

[18] Shin Yee Khoo, Yee Cheng Lian, Zhi Chao Ong, Zubaidah Ismail and Siamak Noroozi, "Feasibility study of performing experimental modal analysis with oblique impact testing using various oblique impact directions," *Alexandria Engineering Journal,* vol. 59, pp. 457-473, 2020.

[19] Siemens Industry Software Inc., *Simcenter 3D.*

[20] Siemens Industry Software Inc., "Correlating Simulation & Modal Test Results with Simcenter 3D," Siemens, 29 04 2019. [Online]. Available: https://community.sw.siemens.com/s/article/correlating-simulation-modal-test-results-with-simcenter-3d. [Accessed 07 02 2024].

[21] Siemens Industry Software Inc., "Simcenter 3D for structural simulation," 2023. [Online]. Available: https://static.sw.cdn.siemens.com/siemens-disw-assets/public/1D06sSm7Pdej7B04khlFOj/de-DE/simcenter-3d-for-structural-simulation-sg-ebook-77929-d11.pdf. [Accessed 07 02 2024].

[22] Siemens Product Lifecycle Management Software Inc., Basic Dynamic Analysis User's Guide, Plano: Siemens Product Lifecycle Management Software Inc., 2014.

[23] Siemens Digital Industries Software, "Simcenter 3D for structural dynamics simulation," 2023. [Online]. Available: https://static.sw.cdn.siemens.com/siemens-disw-assets/public/2w2HxTC4C8JJ6ATdKOIOMH/de-DE/simcenter-3d-for-structural-dynamics-simulation-sg-77918-d24.pdf. [Accessed 07 02 2024].

[24] Gerwin Pasch, Stefan Wischmann, Pascal Drichel, Georg Jacobs and Joerg Berroth, "Enhanced method for optimum driving point identification for modal testing," *Journal of Vibration and Control,* vol. 29, no. 7-8, pp. 1472-1483, 2023.

OFPL: A Solver-Independent Description Language for the Simulation of Forming Processes

Koutaiba Kassem, Dirk Sihling, gns mbH

1 Introduction

Digital prototyping has become an indispensable tool in product design, it allows to avoid development risks und to shorten the time-to-market span. It offers industrial designers and manufacturers the ability to virtually explore the complete process of product development before it is physically realized. Digital prototyping can be used in the early phase of a new product design and validation as well as in optimizing functionality, energy efficiency and cost of an existing product, all of this virtually and assisted by appropriate simulation software and user-friendly graphical user interfaces (GUI).
A great number of software products suitable for numerical simulation of forming processes are available on the market. Some of them, for example **Abaqus** and **LS-Dyna**, are multi-purpose applications, covering among many others a large variety of forming processes, and some of them, e.g., **OpenForm**, **PamStamp** and **AutoForm**, are special-purpose applications focused on some specific forming processes like those for sheet metals.
Introducing or even switching to new forming simulation software can be a challenging problem and might involve a lot of costs and effort. Even for experienced users, setting up a sufficiently accurate description of a forming process considering the nomenclature of a new simulation software product is not always an easy task. This is exactly where a standardized and solver-independent process description is needed.
An **O**pen **F**orming **P**rocess **L**anguage (**OFPL**)[1,2,3] was developed and will be presented in this paper.

2 Motivation

The Open Forming Process Language (OFPL) is a metalanguage allowing:

- a solver-independent description of forming processes for numerical simulation.
- the use of different simulation products in combination with only a single graphical user-interface (GUI): the input of the user is translated first to a somehow “normalized” process language, the OFPL.
- to convert one and the same OFPL process definition into different solver-specific input decks using easy to implement converters and considering company-internal simulation know-how. Such converters can be developed independently from a GUI and could be run in batch mode.

OFPL is a straightforward and self-explanatory metalanguage. Currently available for the simulation of sheet metal forming processes, it can be easily extended to cover **f**urther processes.

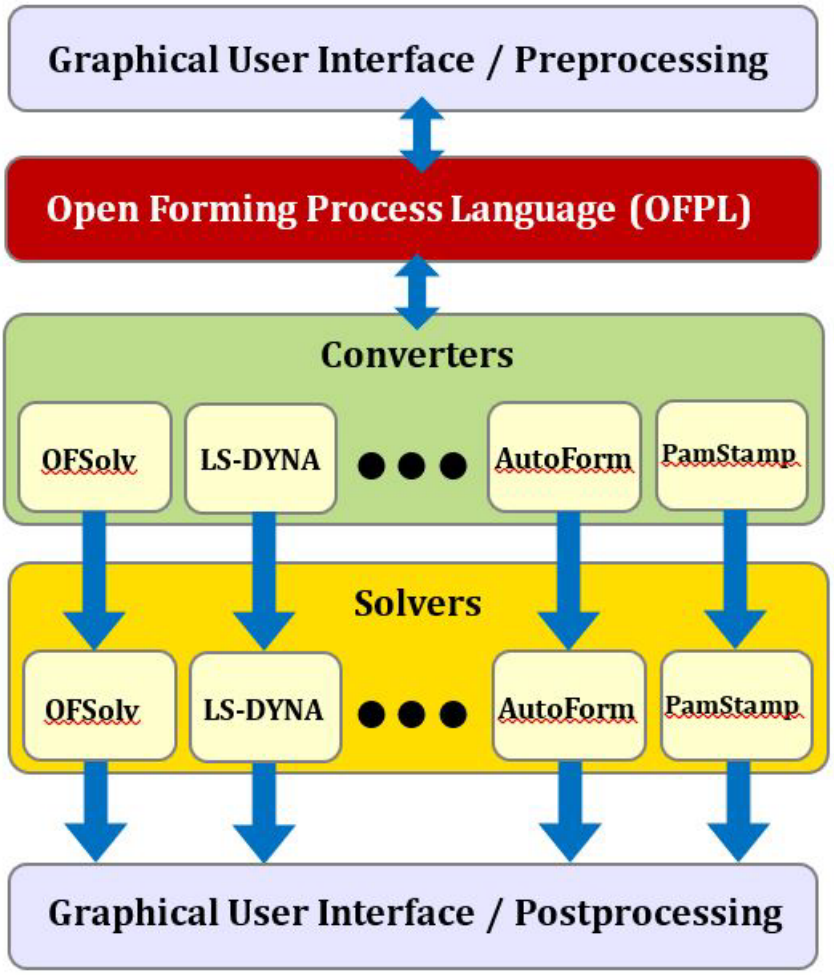

Figure 1: OFPL in a numerical simulation workflow

Figure 1 shows a basic scheme for a numerical simulation workflow using the OFPL metalanguage:

- The forming process is defined once, preferably in an appropriate GUI, independently of the solver(s) used to carry-out the simulation. This user-interface then also takes care of translating the process definition created by the user into the OFPL language.
- Depending on the in-house solvers available, the same OFPL description of the forming process can be converted to the specific requirements of the different solvers and taking existing user experiences and knowledge into account.
- Any modification of the parameters describing the forming process is only defined once in the OFPL description of this process, a further advantage of the OFPL when using it in product optimization loops.

3 Description

The description of a forming process in OFPL requires two kinds of input data stored in separate blocks:
a) The first block of data includes a general description of the process like the name of the project, type of the process, the global unit- and coordinate-system in which the process is described and the path to the files to be used. Information about material and tribological properties of the items involved are also defined here (see Figure 2a).
b) Several blocks each one defining an operation (OP) of the process. In such an operation block both the geometries of tools and work pieces involved in the current operation as well as the different tool activities each one in a separate sub-block (SUB) are defined (see Figure 2b).
An example for such an OFPL description of a deep drawing process consisting of one Operation and two sub-operations is shown in Figure 2 and Figure 3:

```
#============================================================================
#                            OFPL Project
#============================================================================

*GLOBAL_INFO_TYPE:FORMING_PROJECT
*GLOBAL_INFO_OFPL_VERSION:1.0
*GLOBAL_INFO_FILEVERSION:OpenForm v2.22dev99290
*GLOBAL_INFO_DATE:2024-04-24;Mi;Apr;13:41:28
*GLOBAL_INFO_UNITSYSTEM:mm.t.s.C
*GLOBAL_INFO_DATATYPE_FILEDATA:LS-DYNA
*GLOBAL_INFO_GLOBAL_COID:0,0,0;1,0,0;1,1,0
*GLOBAL_INFO_GLOBAL_FORMING_COID:0,0,0;1,0,0;1,1,0
*GLOBAL_INFO_GRAVITY_GLOBAL_FORMING_COID:-3

*GLOBAL_INFO_MATERIAL1_NAME:22MnB5
*GLOBAL_INFO_MATERIAL1_BLANKTHICKNESS:1
*GLOBAL_INFO_MATERIAL1_MATERIALTYPE:
*GLOBAL_INFO_MATERIAL1_ROLLING_DIRECTION:0
*GLOBAL_INFO_MATERIAL1_SURFACEDESCRIPTION:DIESIDE,1
*GLOBAL_INFO_MATERIAL1_FRICTION_SCALING:1
*GLOBAL_DATA_PROJECT_NAME_PROJECT:SquareCup
*GLOBAL_DATA_PROJECT_NAME_PROJECTFILE:SquareCup.ofpl
*GLOBAL_DATA_PROJECT_PATH:C:\Users\Kassem\Downloads
*GLOBAL_DATA_PROJECT_SIMULATIONTYPE:Standard

*GLOBAL_DATA_PROJECT_MATERIAL1_MATERIALFILE_PATH:SquareCup.ofpl_geo\Materials
*GLOBAL_DATA_PROJECT_MATERIAL1_MATERIALFILE_NAME:22MnB5_080.mat
*GLOBAL_DATA_PROJECT_MATERIAL1_MATERIALFILE_FRICTION_PATH:SquareCup.ofpl_geo\Materials
*GLOBAL_DATA_PROJECT_MATERIAL1_MATERIALFILE_FRICTION_NAME:22MnB5_080.mat
*GLOBAL_DATA_SURFACE_OFFSETDESCRIPTION_TYPE:Real
*GLOBAL_DATA_RATIO_ELEMENTLENGTH2THICKNESS:1
*GLOBAL_DATA_FINISHED_PART_COORDINATE:0;0;0
```

Figure 1: OFPL general Project Description

- in the “OFPL Project” block some general information regarding the current forming process are defined using the corresponding “*GLOBAL_INFO” keywords, in addition names and paths to the appropriate material, friction and geometry files are defined using the related “*GLOBAL_DATA” keywords.
- in the “OPERATION xx” block the references to all the tools and parts involved in this process operation are defined. In addition, the activities of each tool during this operation are defined, each action in a separate sub-operation: Figure 3 shows that the forming process consists of a single operation named “OP20”, the tools involved in OP20 are a BINDER-type tool named “BLECHHALTER”, a DIE-type tool named “MATRIZE” and a PUNCH-type tool named “STEMPEL”. The deformable blank is named “PLATINE”.

The forming operation “OP20” is performed in two sub-operations:

- SUB1 describes a force-controlled closing step of TOOL1 (BLECHHALTER) by applying a load of -1.0E+05 [N] while TOOL2 (MATRIZE) is active and stationary.
- SUB2 describes a displacement-controlled closing step of TOOL3 (STEMPEL) by applying a tool travel of -100 [mm] while TOOL1 and TOOL2 are active and loaded respectively stationary.

```
#=============================================
# OPERATION 1
#=============================================
*OP1_NAME:OP20

*OP1_TOOL1_NAME:BLECHHALTER
*OP1_TOOL1_DATA_NAME:OP20_BLECHHALTER.k
*OP1_TOOL1_DATA_PATH:SquareCup.ofpl_geo\OP20
*OP1_TOOL1_TYPE:BINDER
*OP1_TOOL1_SURFACEDESCRIPTION:DIESIDE
*OP1_TOOL1_LOCAL_COID:0,0,0;1,0,0;0,1,0

*OP1_TOOL2_NAME:MATRIZE
*OP1_TOOL2_DATA_NAME:OP20_MATRIZE.k
*OP1_TOOL2_DATA_PATH:SquareCup.ofpl_geo\OP20
*OP1_TOOL2_TYPE:DIE
*OP1_TOOL2_SURFACEDESCRIPTION:PUNCHSIDE
*OP1_TOOL2_LOCAL_COID:0,0,0;1,0,0;0,1,0

*OP1_TOOL3_NAME:STEMPEL
*OP1_TOOL3_DATA_NAME:OP20_STEMPEL.k
*OP1_TOOL3_DATA_PATH:SquareCup.ofpl_geo\OP20
*OP1_TOOL3_TYPE:PUNCH
*OP1_TOOL3_SURFACEDESCRIPTION:DIESIDE
*OP1_TOOL3_LOCAL_COID:0,0,0;1,0,0;0,1,0

*OP1_PART1_NAME:PLATINE
*OP1_PART1_DATA_NAME:PLATINE.k
*OP1_PART1_DATA_PATH:SquareCup.ofpl_geo\Blank
*OP1_PART1_MATERIAL:MATERIAL1
*OP1_PART1_SYMMETRY:None
```

```
#====================
# SUB 1
#====================
*OP1_SUB1_NAME:Closing BLECHHALTER 10t
*OP1_SUB1_TYPE:CLOS
*OP1_SUB1_GRAVITY_STATUS:0

*OP1_SUB1_PART1_DATA_REFINEMENTLEVEL1:1

*OP1_SUB1_TOOL1_STATUS:ACTIVE
*OP1_SUB1_TOOL1_CONSTRAINTS:1;1;0;1;1;1
*OP1_SUB1_TOOL1_LOAD_FORCE:-1;1E+05;1;-1000;1000
*OP1_SUB1_TOOL1_POSITIONING:1;PART1

*OP1_SUB1_TOOL2_STATUS:ACTIVE
*OP1_SUB1_TOOL2_CONSTRAINTS:1;1;1;1;1;1
*OP1_SUB1_TOOL2_POSITIONING:1;PART1

#====================
# SUB 2
#====================
*OP1_SUB2_NAME:Closing STEMPEL
*OP1_SUB2_TYPE:CLOS
*OP1_SUB2_GRAVITY_STATUS:0

*OP1_SUB2_PART1_DATA_REFINEMENTLEVEL1:1

*OP1_SUB2_TOOL1_STATUS:ACTIVE
*OP1_SUB2_TOOL1_CONSTRAINTS:1;1;0;1;1;1
*OP1_SUB2_TOOL1_LOAD_FORCE:-1;1E+05;1;-1000;1000
*OP1_SUB2_TOOL1_POSITIONING:0;PART1

*OP1_SUB2_TOOL2_STATUS:ACTIVE
*OP1_SUB2_TOOL2_CONSTRAINTS:1;1;1;1;1;1
*OP1_SUB2_TOOL2_POSITIONING:0;PART1

*OP1_SUB2_TOOL3_STATUS:ACTIVE
*OP1_SUB2_TOOL3_CONSTRAINTS:1;1;0;1;1;1
*OP1_SUB2_TOOL3_LOAD_DISPLACEMENT:-1;1;0;100
*OP1_SUB2_TOOL3_POSITIONING:0;PART1
```

Figure 2: OFPL Description of a Forming Process

4 OFPL in a forming simulation environment

With the **O**pen **F**orming **P**rocess **L**anguage (**OFPL**) a metalanguage is established, that allows a solver-independent definition of forming processes, that in turn is used to create the input decks needed to run numerical simulation of that process. It marks a separating layer between the mechanical description of a forming process and the numerical requirements of the simulation solver. With the help of converter tools, the **OFPL** process definition is then translated to fit with the input decks of the different solver.

Figure 4 shows an example layout of how to explore the potential of the Open Forming Process Language in combination with a graphical user-interface (GUI) to create a powerful tool that allows the engineer to setup the input decks for different simulation solvers in a very elegant way. The graphically guided Process Definition is made by using appropriate icons representing the different items involved in the forming process (e.g., Tools, Parts, Beads, etc.) and by combining them into templates representing the operations and sub-operations of the process. The set-up of the Mechanical Parameters i.e., the definition of the mechanical properties of every process item (e.g., friction coefficient, load, displacement, etc.) can be done for every operation and sub-operation at an appropriate input table. For this process definition an OFPL description is generated and could be exported for later use. Even the set-up of the solver-dependent Numerical Parameters can be a part of this GUI: a set of best-practice values could be defined as default for every targeted solver and of course are modifiable to account for the available knowledge of experienced users.

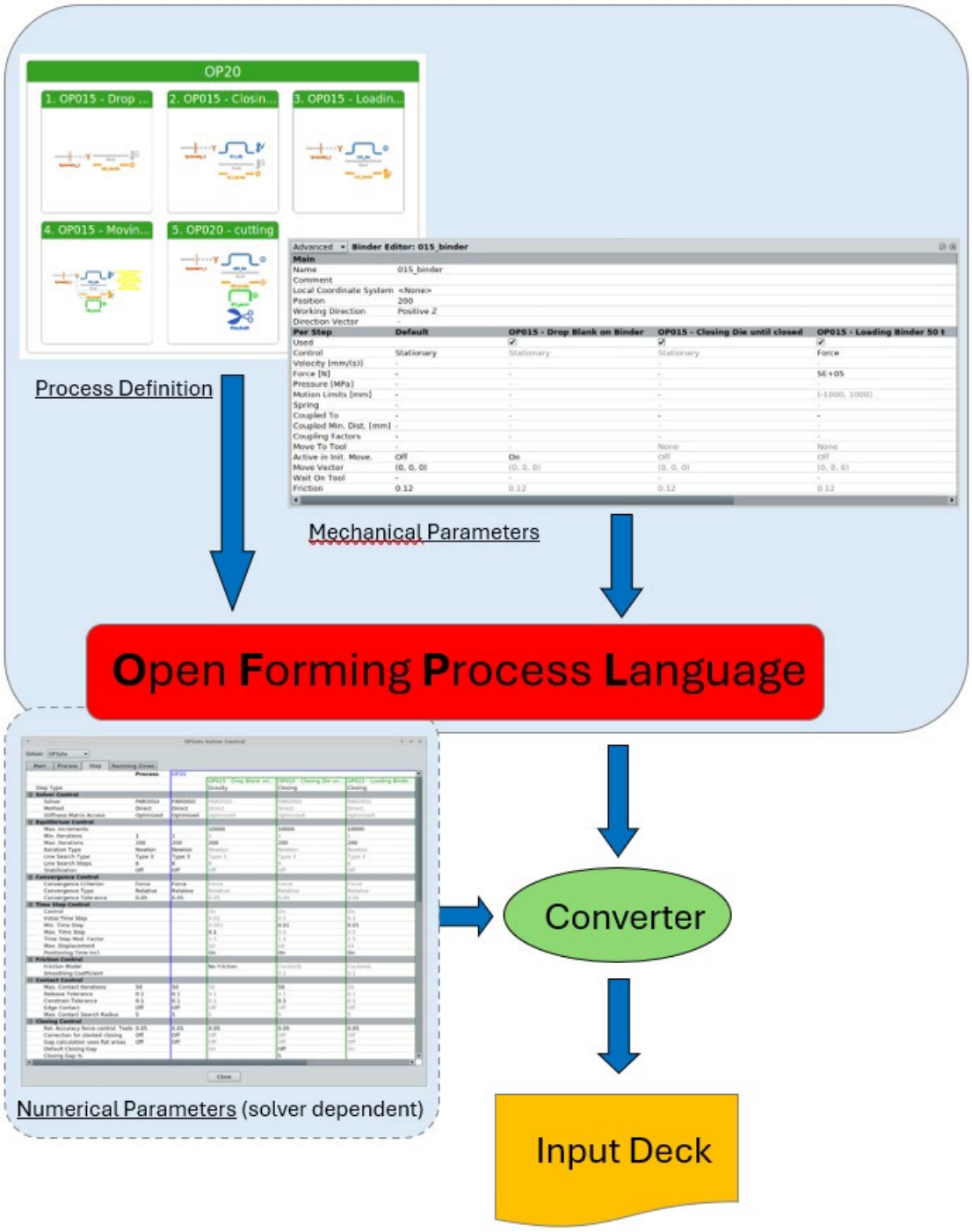

Figure 3: set-up of input decks with OFPL

5 Conclusion

With the **O**pen **F**orming **P**rocess **L**anguage (**OFPL**) a metalanguage is established, that allows a solver-independent definition of forming processes, that in turn is used to create the input decks needed to run numerical simulation of that process. It marks a separating layer between the mechanical description of a forming process and the numerical requirements of the simulation solver. With the help of converter tools, the **OFPL** process definition is then translated to fit with the input decks of the different solver.

6 References

[1] https://www.dynalook.com/conferences/11th-european-ls-dyna-conference/process-metal-forming/forming-simulation-meta-language-and-input-decks/view
[2]https://www.dynamore.de/de/download/papers/dynamore/de/download/papers/forum11/forum11/presentation/04-fleischer-bmw.pdf
[3] https://www.dynamore.de/en/downloads/papers/dynamore/de/download/papers/2016-ls-dyna-forum/Papers%202016/montag-10.10.16/process-sheet-metal-forming-1/umformsimulationen-schnittstellen-und-prozesse

CAE Results Animations, Images and Sounds in AI/ML

Cornelia Thieme (Hexagon)

1 Summary

Today it's standard that machine learning in CAE predicts values and curves from parameters. This presentation shows what can be done beyond number values. Machine learning for industrial applications can also work with full CAE result files, images, 3D geometry files or sound files. The paper gives some practical examples and hints about the settings for a successful prediction.

2 Introduction

Machine Learning (ML) is revolutionizing CAE by predicting the results of CAE analyses from various parameters with high accuracy. ML algorithms help to understand complex relationships between input parameters and results. Instead of an FEM analysis which can run for several hours, ML can predict the result in a few seconds. Engineers save time and can virtually test many more variations in the model, look at robustness and outliers and optimize the parameters.

Typically result values or curves are predicted from parameters. The presentation shows what can be done beyond number values. How can we predict animations (result files of CAE solvers), how can we extract information from images, step, stl or sound files so that the info from these files can be used as parameters?

3 Animations (CAE Result Files)

It is often interesting to predict the results of the whole model, to get an overall impression of the model behaviour due to parameter changes. The CAE results are usually in binary format, which is more efficient than ascii with respect to file size. The binary result files of the CAE solvers are supported by different postprocessors.

The MSC Nastran hdf5 format for example is well documented and accessible by scripting, and is supported by the machine learning software Odyssee. Each value in the hdf5 can be accessed. If a hdf5 result file exists for each of the variants in the learning base, Odyssee can interpolate between them and create a new hdf5 file with the predicted results. The hdf5 structure has characteristic differences for the different analysis types like linear, nonlinear, frequency response, and for the different element and result types – it requires development effort by the software provider to support all of these smoothly.

Beside MSC Nastran hdf5, Odyssee supports also LS-Dyna d3plot format, EnSight generic fluid format and others. This allows to predict animations of full 3D car crashes or CFD analyses.

The following example shows the prediction of the deformation of a seal. The purpose of the analysis is to examine the deflections created during the closing of a door. The seal is made of rubber (hyperelastic material properties). The door is considered very stiff relative to the rubber seal and is modeled as a rigid contact body. The rigid contact body is controlled by a velocity in negative x and y direction (vx and vy).

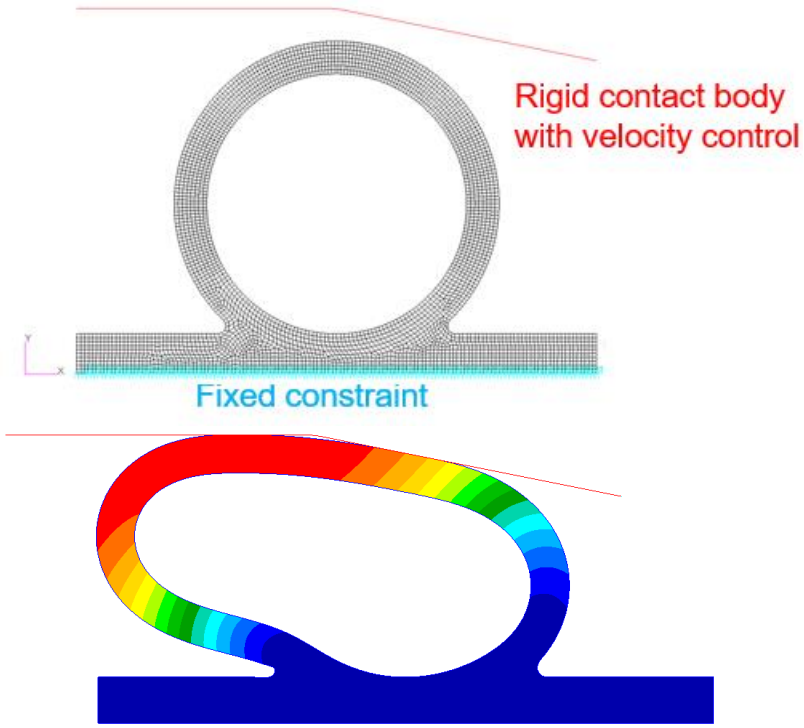

Fig. 1
Seal FEM model with boundary conditions and a typical displacement result

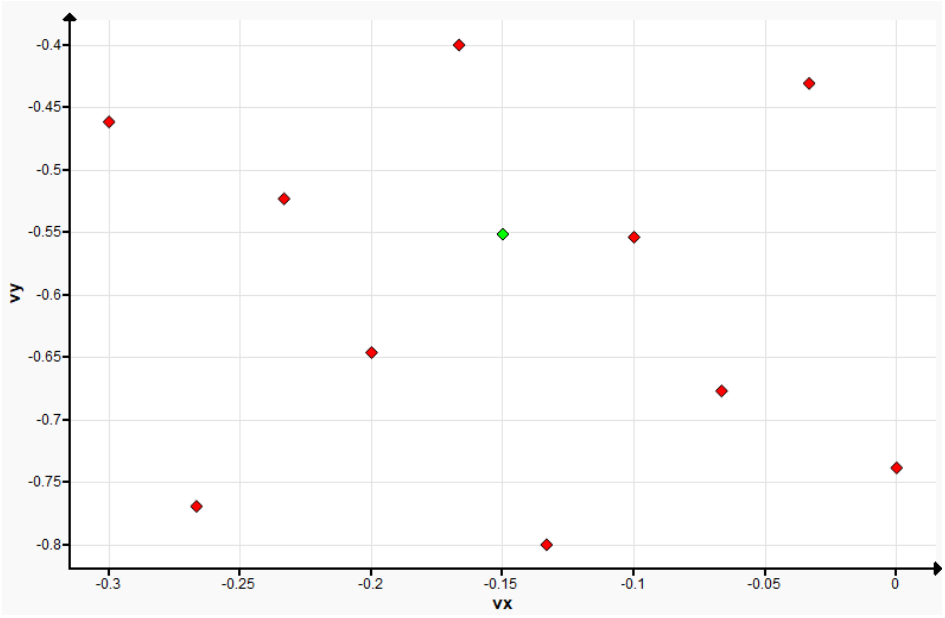

Fig. 2
DOE consisting of 10 parameter combinations of vx and vy. The seal deformation is to be predicted for the green point (vx = -0.15, vy = -0.5)

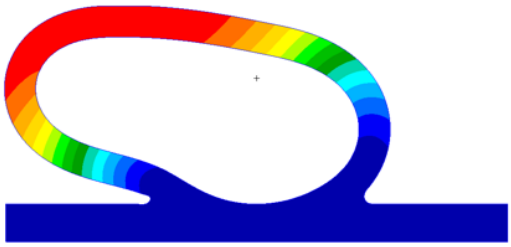

vx = -0.3, vy = -0.461538

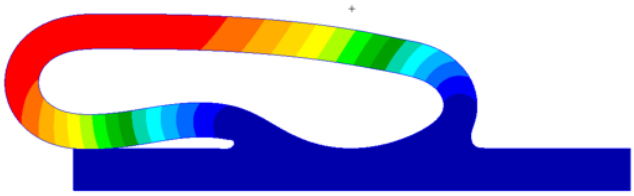

vx = -0.266667, vy = -0.769231

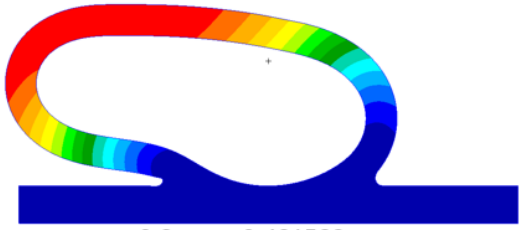

vx = -0.3, vy = -0.461538

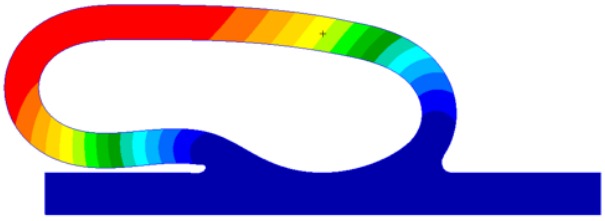

vx = -0.2, vy = -0.646154

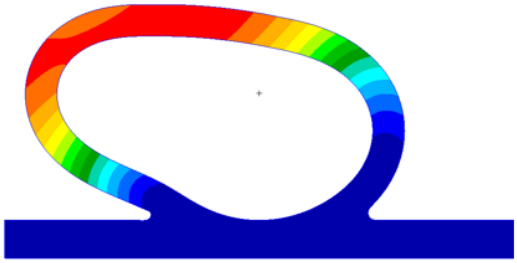

vx = -0.166667, vy = -0.4

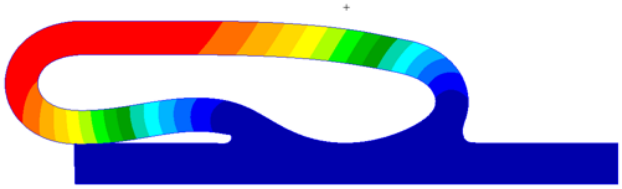

vx = -0.133333, vy = -0.8

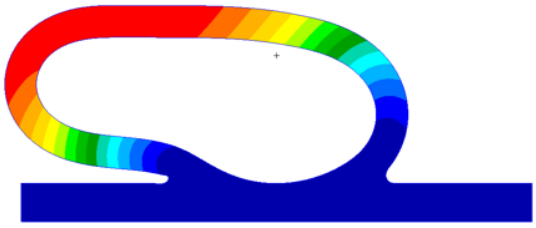

vx = -0.1, vy = -0.553846

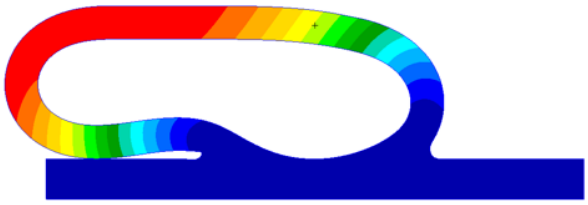

vx = -0.0666667, vy = -0.676923

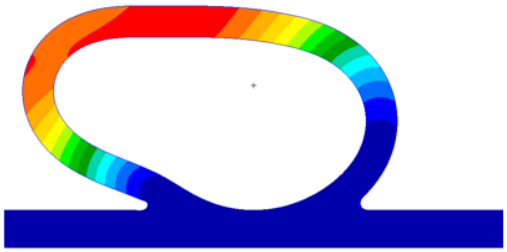

vx = -0.0333333, vy= -0.430769

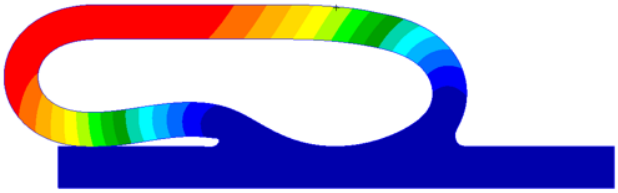

vx = 0, vy = -0.738462

Fig. 3
Results of the 10 variants in the learning base

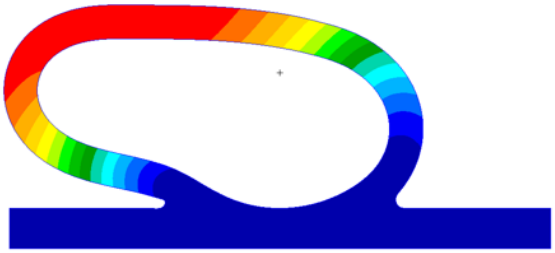

vx = -0.15, vy = -0.5
Prediction

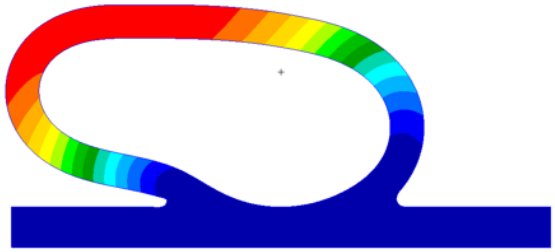

vx = -0.15, vy = -0.5
FEM Result

Fig. 4
Prediction versus FEM result

Fig. 3 shows the 10 results in the learning base. Fig. 4 shows the prediction of the deformation at vx = -0.15, vy = -0.5 vs an FEM result for verification. The prediction is very similar to the FEM result.

The result plots show the true scale deformation, the deformation is also shown as a fringe plot. The small black plus sign marks the origin of the model and is therefore a good reference point for the deformation.

The considerations for prediction of animations are similar to those for predicting values and curves. A well distributed DOE is needed, though Odyssee does not require a high number of samples as an input. Inverse distance, proper orthogonal decomposition (POD), adaptive radial basis function (ARBF), Kriging and other methods can be used. If you are doing cross-validation to find the best prediction method, you would typically do it on values or curves representative for the whole model. In the example, the default method was used: POD for ROM creation and ARBF for interpolation.

The seal analysis is run in 10 time steps. The result for each of these time steps is also predicted by Odyssee, so that a full results animation can be shown, instead of just the images for the final time step shown here in the paper.

4 Images

There are already numerous machine learning applications where results are predicted from images. From X-ray or CT scan interpretation to sorting parts or recognizing faulty parts. Also, wherever the geometry variants are easier to describe by an image than by numeric parameters – e.g. free-form surfaces, sheet metal with beads - image recognition can be useful.

In the first step, Odyssee extracts the information from the images and transforms it into a matrix. In the second step, the matrix is interpolated, just like a parameter file. This is an efficient solution for industrial applications with standardized images. Numerous image extraction algorithms like pixel counting, grey feature indicators or canny filter are available.

In these applications, the images are the input. The output are values, curves, name tags, binary variables which are predicted from the images. How can we also predict images as the output? If the images have been represented by matrices and a new matrix has been predicted, this new matrix cannot always be converted back to an image.

A simple negative example is pixel counting: counting the black pixels in an image can in some cases be sufficient to represent the characteristics of the image compared to other images in the learning base. But if the number of black pixels is the only information you have about an image, it’s not possible to reconstruct the exact image – there are infinite possibilities how the image could look like.

If an image shall be predicted, the right image extraction algorithms must be chosen so that the matrix can be converted back to an image.

5 3D Geometry Files

3D geometry files are used as an input to predict for example the manufacturing time. Also, deformations or other results which you would get from a test or CAE analysis could be predicted directly from the 3D geometry. If a learning base of similar 3D geometry files and results is available, the designer can use them to make more informed decisions just from the CAD model – without test, CAE analysis or prototype.

Odyssee supports step files and stl files. The algorithm extracts characteristic values like edgeloop number, complexity index or volume. If the geometry is complex, it can help to create also images of the geometry in different views and interpret these images, and / or extract additional information from the geometry. All this information can be combined in one learning base. Material values or other non-geometric parameters can also be added to the same learning base. Everything that has a considerable influence on the result should be added.

6 Sound Files

The prediction of sound is often covered by predicting a frequency response curve where the high peaks correspond to loud noise. But it can also be interesting to predict the exact noise. Or to predict damage, identify the reason of a noise, or optimize the sound. Examples could be recognizing bird calls, recognizing cars from their sound, monitoring industrial equipment for failure.

The following example is about different types of mechanical breakdown of a car. Imagine your car makes a strange noise and you want to know what it is. The learning base is made up of mechanical sounds with faults (wav format) and the type of associated breakdown (name tags). When a new sound comes up, the type of associated breakdown shall be predicted. A clustering algorithm is used. An interpolation algorithm would not make sense here, as the predicted name tags are categorial values which cannot be interpolated.

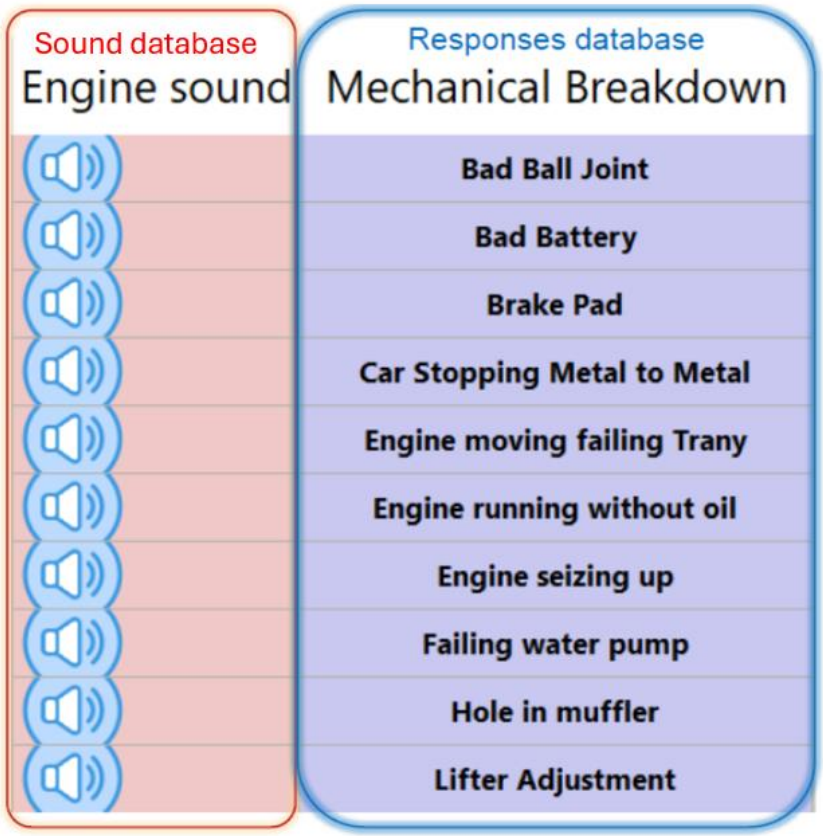

Fig. 5
Part of learning base

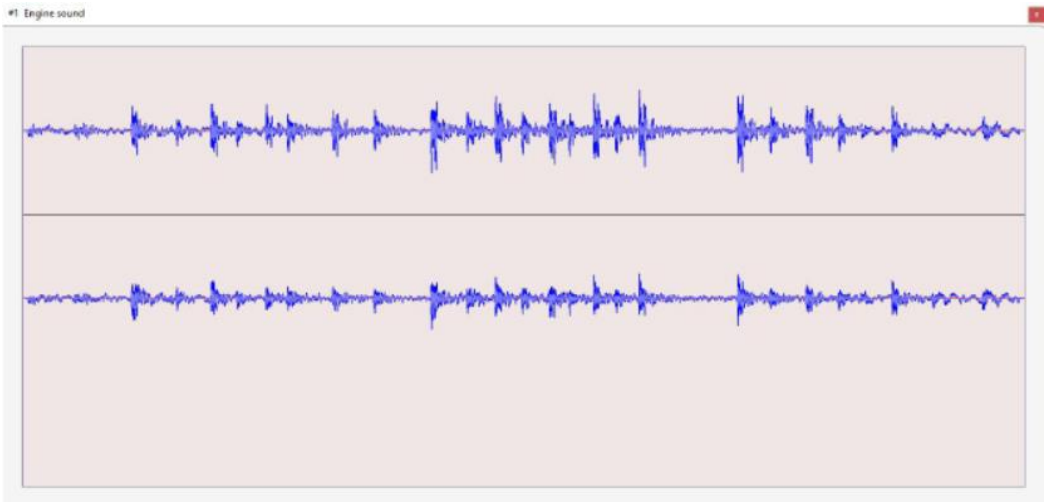

Fig. 6
Example of mechanical sound file in Odyssee

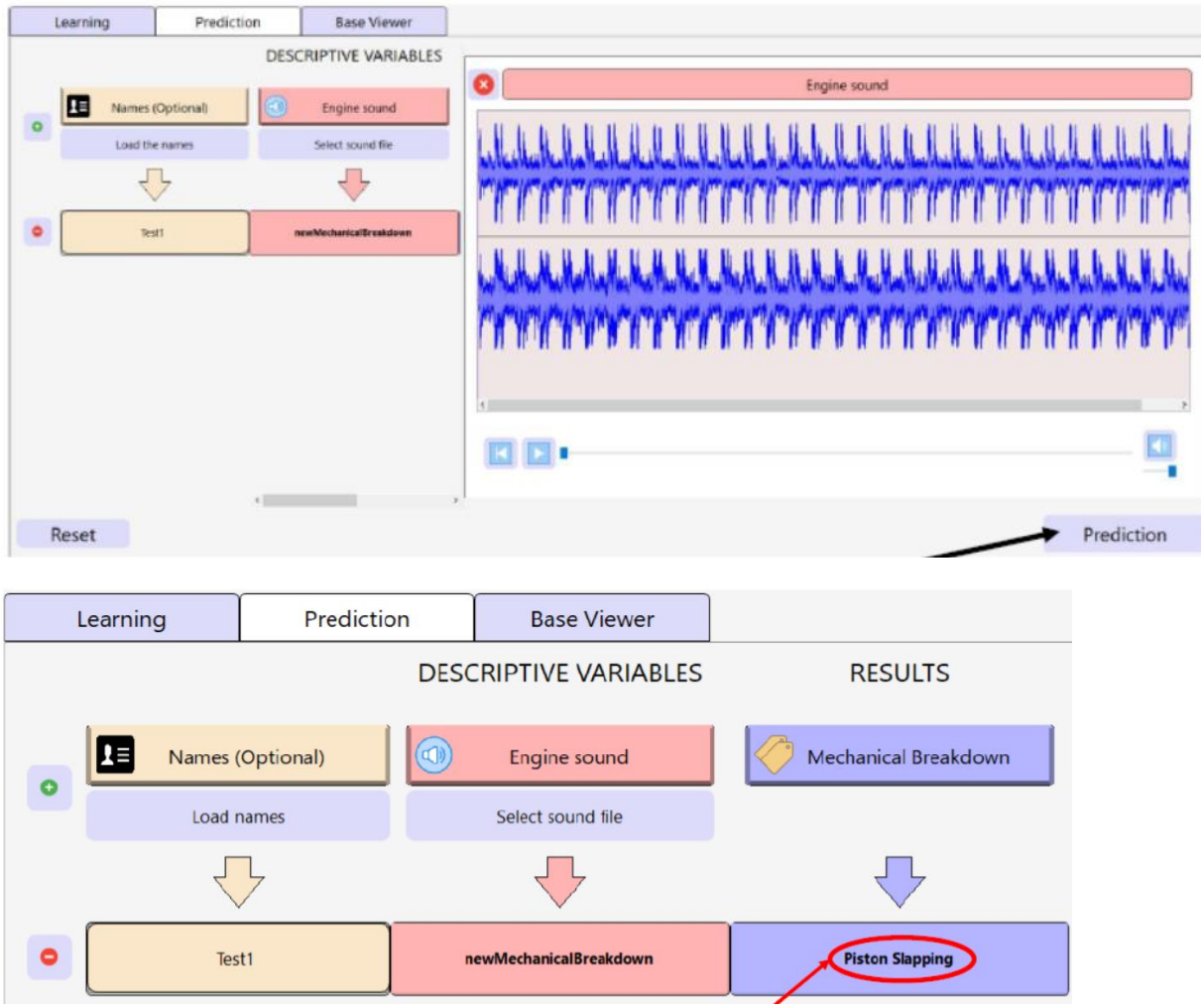

Fig. 7
Loading a new sound file in Odyssee and predicting the type of mechanical breakdown for this sound: piston slapping

7 Conclusions

Beyond values and curves, machine learning for industrial applications can also work with full CAE result files, images, 3D geometry files or sound files. The paper gives some practical hints about the settings for a successful prediction.

8 References

[1] Odyssee 2024.1.1 Documentation

Effizientes probabilistisches maschinelles Lernen für den Ingenieursalltag

Kevin Cremanns (PI Probaligence GmbH)

Marold Moosrainer, Thomas Iberer (CADFEM Germany GmbH)

1 Kurzfassung

Die zunehmende Integration künstlicher Intelligenz (KI) in verschiedene Bereiche macht auch vor dem Ingenieurwesen nicht halt, wo sie sich als unverzichtbares Werkzeug etabliert. In diesem Kontext präsentieren CADFEM und PI Probaligence eine probabilistische Machine-Learning-Lösung, die eine breite Palette von Ingenieursaufgaben effizient unterstützen kann.

Die Lösung ist darauf spezialisiert, mit minimalen Datenpunkten auszukommen und benötigt keine Cloudanbindung. Der Betrieb auf lokaler handelsüblicher Hardware ist ein zentraler Aspekt. Dies macht sie zu einem äußerst nützlichen Instrument für Ingenieure, die mit knappen Ressourcen arbeiten müssen. Die Art der verwertbaren Daten ist vielfältig und reicht von der Verarbeitung numerischer Werte und akustischer Signale bis hin zur Analyse komplexer Entitäten wie transienter FEM/CFD-Simulationen oder 3D-Materialeigenschaften. Genauso umfangreich sind die Anwendungsmöglichkeiten. Sowohl die Erstellung eines digitalen Zwillings als auch die effiziente Versuchsplanung und Optimierung sind mögliche Einsatzszenarien. Der Algorithmus erlaubt die sinnvolle Koppelung echter Versuchsdaten und Simulationen als gemeinsame Datenquelle, um das Training effektiv zu beschleunigen. Die Vorhersage von nicht-parametrischen, sich ändernden Geometrien sowie Anwendungen im Bereich der Echtzeitsteuerung von Produktionsanlagen sind weitere Anwendungsbeispiele.

2 Herausforderungen in der Nutzung von KI im Ingenieurswesen

Ingenieure stehen vor einer Vielzahl von Herausforderungen beim Einsatz von künstlicher Intelligenz (KI) sowohl im Bereich von Simulationen als auch in realen Versuchen. Einer der zentralen Aspekte ist die Gewährleistung der Genauigkeit und Zuverlässigkeit der Ergebnisse. In Simulationen müssen Ingenieure sicherstellen, dass die von KI-Modellen generierten Vorhersagen den physikalischen Gesetzen und den realen Bedingungen entsprechen. Hierbei kann die Komplexität der Modelle und die Notwendigkeit einer sorgfältigen Validierung eine Hürde darstellen.

Im Bereich der realen Versuche stehen Ingenieure vor der Herausforderung, KI-Algorithmen in komplexe experimentelle Umgebungen zu integrieren. Dies erfordert oft die Entwicklung spezieller Sensoren und Datenerfassungssysteme, um die benötigten Daten für die KI-Modelle bereitzustellen. Zudem müssen Ingenieure sicherstellen, dass die KI-Algorithmen in Echtzeit arbeiten können, um schnelle Entscheidungen während des Versuchsprozesses zu treffen.

Ein weiteres wichtiges Anliegen ist die Interpretierbarkeit der Ergebnisse. Ingenieure müssen in der Lage sein, die Entscheidungen und Vorhersagen von KI-Modellen zu verstehen und zu erklären, um das Vertrauen in die Technologie zu stärken und die Akzeptanz in der Ingenieurpraxis zu fördern. Dies kann insbesondere bei komplexen KI-Modellen wie bei tiefen neuronalen Netzen [1] nicht einfach sein.

Die Bewältigung dieser Herausforderungen erfordert typischerweise eine enge Zusammenarbeit zwischen Ingenieuren, KI-Experten und anderen Fachleuten, um die Potenziale von KI voll auszuschöpfen und gleichzeitig die Sicherheit und Zuverlässigkeit von Ingenieurprozessen zu gewährleisten.

3 Auswahl der geeigneten KI-Verfahren

Für Nicht-KI-Experten kann die Auswahl der richtigen Algorithmen für eine bestimmte Problemstellung ebenfalls eine große Herausforderung darstellen. Einer der Hauptgründe dafür ist die Vielzahl an verfügbaren KI-Techniken und Algorithmen, die sich ständig weiterentwickeln. Ohne ein tiefes

Verständnis der Funktionsweise und der Vor- und Nachteile der verschiedenen Algorithmen kann es schwierig sein, den am besten geeigneter Ansatz auszuwählen.

Ein weiteres Problem ist die Komplexität des Hyperparameter-Tunings, insbesondere bei neuronalen Netzen. Hyperparameter sind Parameter, die vor dem eigentlichen Trainingsprozess festgelegt werden müssen und die die Leistung und das Verhalten des Modells stark beeinflussen können. Dazu gehören beispielsweise die Lernrate, die Anzahl der Ebenen und Neuronen in einem neuronalen Netzwerk sowie die Auswahl der Aktivierungsfunktionen. Das Finden der optimalen Werte für diese Hyperparameter erfordert oft eine umfangreiche Suche und eine Vielzahl von Berechnungen, die sowohl rechenintensiv als auch zeitaufwändig sein können.

Um diese Herausforderungen zu bewältigen, können Nicht-KI-Experten auf Werkzeuge und Plattformen zurückgreifen, die Automatisierung und vereinfachte Schnittstellen für die Modellentwicklung und das Hyperparameter-Tuning bieten, sog. Auto-ML Lösungen, die meist in der Cloud angeboten werden. Ein möglicher Nachteil dieser Lösungen ist, dass Sie nur sehr kostenintensiv betrieben werden können und die Daten das eigene Unternehmen verlassen, falls die Cloudlösung nicht selbst betrieben wird. Darüber hinaus ist es hilfreich, mit Experten zusammenzuarbeiten, um bei der Auswahl und Konfiguration von KI-Algorithmen und -Modellen Unterstützung zu erhalten und sicherzustellen, dass die gewählten Ansätze die Anforderungen der spezifischen Problemstellung erfüllen.

4 Deep Infinite Mixture Gaussian Process (DIM-GP)

Das Verfahren Deep Infinite Mixture Gaussian Process (DIM-GP) ist ein Verfahren (siehe Abbildung 1), welches bei den zuvor genannten Herausforderungen den Ingenieur auf mehreren Arten unterstützen kann. Dieses Modell stellt eine Erweiterung des klassischen Gauss-Prozess-Approximationsmodells [2] dar. Im klassischen Gauss-Prozess wird die Kovarianzmatrix des Zufallsfeldtermes als konstant (stationär) im Bereich der Eingangsparameter angenommen. Die Korrelation zweier Datenpunkte hängt dabei nur von dem Abstand beider Punkte ab. Im DIM-GP-Modell wird diese Kovarianzmatrix als ortsabhängig (nicht stationär) definiert, d.h. die Freiheitsgrade des Modells ändern sich abhängig vom Punkt der Vorhersage. Darüber hinaus wird auch eine optimale Kombination verschiedener Kovarianzfunktionen über ein Neuronales Netzwerk automatisch ermittelt. Dieses automatische „Kernel-Engineering“ erlaubt es sich überlagernde physikalische Effekte besser abzubilden als mit einer einzelnen Kovarianzfunktion. Details zum Approximationsmodell sind in [3] zu finden.

Ebenfalls wird auch das erlernbare Rauschen in dem Modell durch ein neuronales Netz abhängig vom Punkt der Vorhersage ermittelt. Dies erlaubt es auch Datensätze zu verarbeiten, dessen Datenpunkte unterschiedlich starkes Rauschen aufweisen. Wenn das Modell erlernt, hat in welchen Designbereichen das Rauschen besonders groß bzw. klein ist kann dies genutzt werden, um nach besonders robusten Designs zu suchen z.B. im Rahmen einer Optimierung.

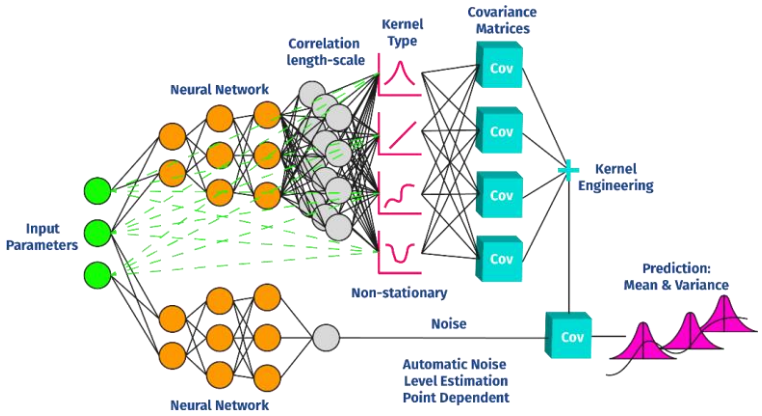

Abbildung 1: Prinzipdarstellung der nicht stationären DIM-GP Approximation der Kovarianzmatrix und das Rauschtermes eines Gauss-Prozesses [1]

DIM-GP wurde mit dem Ziel entwickelt, ein einfach anzuwendendes Verfahren zu sein für das kein KI-Experten Wissen notwendig ist. Es gibt keine Hyperparameter, die einzustellen sind und es lässt sich für eine Vielzahl unterschiedlichster Datentypen und Anwendungen nutzen, so dass nur ein einziger Algorithmus erlernt werden muss. Dadurch soll es ein Werkzeug sein, welches von Domainexperten aus nicht KI-Bereichen einfach und effektiv eingesetzt werden kann.

4.1 Verwertbare Datentypen:

Ingenieure sind tagtäglich mit einer breiten Palette von Daten verschiedenster Formate und Typen konfrontiert, die sie in ihren Arbeitsprozessen verarbeiten müssen. Diese Daten reichen von einfachen skalaren Größen, die beispielsweise Geometrien beschreiben, bis hin zu komplexen Signalen, Feldgrößen und Ergebnissen aus numerischen Simulationen wie Computational Fluid Dynamics (CFD) und Finite-Elemente-Analysen (FEM).

Skalare Größen sind fundamental für die Beschreibung von Geometrien und physikalischen Eigenschaften von Materialien oder Strukturen. Sie können beispielsweise die Abmessungen eines Bauteils, die Dichte eines Materials oder die Temperatur an einem bestimmten Punkt darstellen. Diese Daten werden oft als Ausgangspunkt für weitere Analysen und Simulationen verwendet.

Signale und Feldgrößen sind eine weitere wichtige Datenkategorie, mit der Ingenieure arbeiten. Signale können beispielsweise Sensormessungen oder Steuersignale sein, die in Echtzeit erfasst und verarbeitet werden müssen. Feldgrößen beschreiben die Verteilung physikalischer Größen über einen Raum, wie beispielsweise elektrische Felder, magnetische Felder oder Temperaturverteilungen. Die Analyse und Verarbeitung von Signalen und Feldgrößen ermöglicht es Ingenieuren, komplexe Systeme zu verstehen und zu steuern.

Numerische Simulationen wie CFD und FEM liefern Ingenieuren detaillierte Einblicke in das Verhalten von Strukturen und Systemen unter verschiedenen Bedingungen. Die Ergebnisse dieser Simulationen umfassen oft eine Vielzahl von Daten, darunter Knotenergebnisse, die die physikalischen Größen an diskreten Punkten im Modell beschreiben. Diese Daten können sowohl 2D- als auch 3D-Darstellungen umfassen und können stationäre oder transiente Phänomene darstellen.

Die Vielfalt und Komplexität der Daten, mit denen Ingenieure konfrontiert sind, erfordert fortschrittliche Techniken und Werkzeuge zur Datenverarbeitung, -analyse und -interpretation. Darüber hinaus müssen Ingenieure in der Lage sein, Daten aus verschiedenen Quellen zu integrieren und zu kombinieren, um ein umfassendes Verständnis der Systeme zu entwickeln, an denen sie arbeiten. Durch den effektiven Umgang mit diesen unterschiedlichen Daten können Ingenieure fundierte Entscheidungen treffen und innovative Lösungen für komplexe technische Herausforderungen entwickeln.

Diese Vielfalt an Datenformaten stellt ebenfalls eine Herausforderung für das maschinelle Lernen dar. Nicht jeder Algorithmus kann mit allen Formen der Daten umgehen. DIM-GP hingegen erlaubt es mit allen Formen und Dimensionen von Daten umgehen zu können, solange diese nummerisch sind. Skalare, Signale, Felder, nicht parametrische Geometrien, Knotenergebnisse von stationären oder instationären FEM / CFD Ergebnissen, aber auch Bilder sind sowohl als Eingangs- als auch als Ausgangsinformation möglich (siehe Abbildung 4).

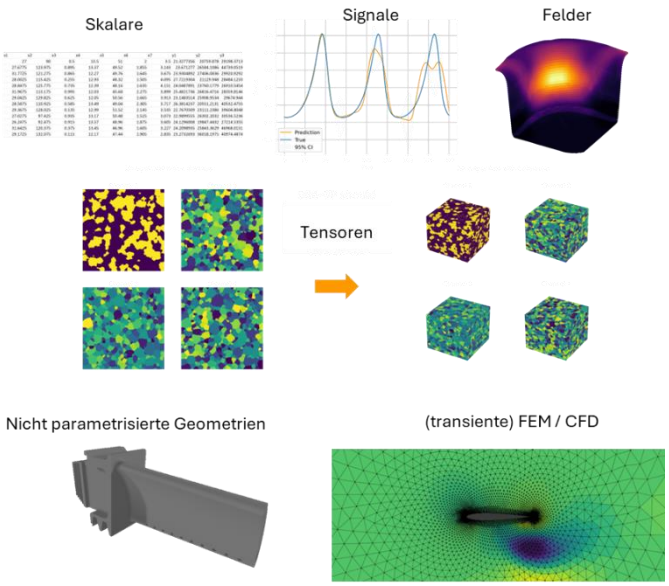

Abbildung 2: Verwertbare Datentypen

4.2 Vereinigung von Simulations- und Versuchsdaten

Der Einsatz von Multi-Fidelity-Ansätzen [4] im maschinellen Lernen bietet eine Vielzahl von Vorteilen, insbesondere im Bereich der schnelleren Generierung von Simulationsdaten und der effektiven Kalibrierung von Simulationsmodellen.

Eine der Hauptanwendungen von Multi-Fidelity im maschinellen Lernen besteht darin, die Effizienz der Simulationsdatenerzeugung zu erhöhen. Dies wird erreicht, indem sowohl grobe als auch feine Netze verwendet werden bei der Generierung der Trainingsdaten, um die Vorhersagegenauigkeit der ML-Modelle zu verbessern. Grobe Netze können schneller simuliert werden liefern aber ungenaue Ergebnisse, während feine Netze detailliertere Ergebnisse liefern, aber mehr Ressourcen benötigen. Durch die Kombination beider Ergebnissquellen kann ein Großteil der Trainingsdaten schnell und effizient generiert werden und nur ein kleiner Teil muss durch ein feines Netz simuliert werden. In Abbildung 5 ist dies schematisch dargestellt.

Ein weiterer wichtiger Anwendungsfall von Multi-Fidelity ist die Simulationskalibrierung, bei der Versuchsdaten (High-Fidelity) mit Simulationsdaten (Low-Fidelity) kombiniert werden, um das Modell an die Realität anzupassen. Oft ist es schwierig, Simulationsmodelle so zu kalibrieren, dass sie die Versuchsergebnisse exakt widerspiegeln. Durch den Einsatz von Multi-Fidelity-Ansätzen ist dies jedoch nicht zwingend erforderlich. Das ML-Modell kann lernen, die Qualität der Versuchsdaten vorherzusagen und den verbleibenden Fehler auszugleichen. Dies ermöglicht es Ingenieuren, Simulationen basierend auf weniger präzisen Modellen durchzuführen, ohne die Vorhersagequalität zu beeinträchtigen.

Ein bedeutender Vorteil dieser Methode besteht darin, dass sie den Entwicklungsprozess beschleunigt und die Kosten senkt, indem sie den Bedarf an aufwändigen Versuchen reduziert und die Rechenzeit für komplexe Simulationen verringert. Darüber hinaus ermöglicht es Ingenieuren, sich auf die wichtigen Aspekte der Problemlösung zu konzentrieren, anstatt sich mit der Feinabstimmung von Simulationsmodellen zu beschäftigen.

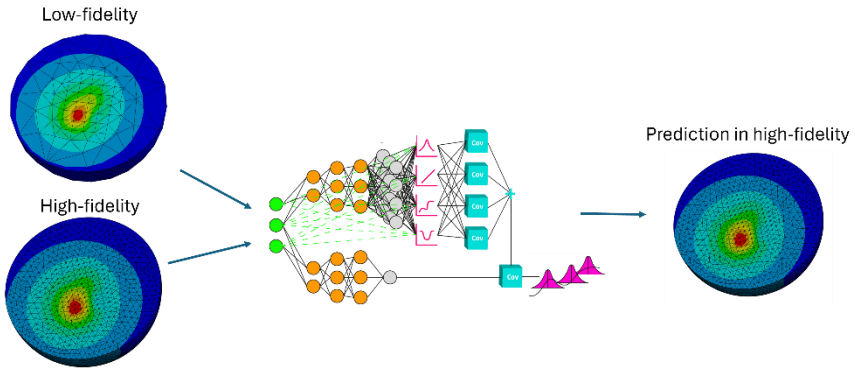

Abbildung 3: Multi-fidelity DIM-GP

5 Datengenerierung und Versuchsplanung

Bayesian Optimization [5] bietet eine leistungsstarke Methode zur Optimierung von komplexen Systemen und zur Generierung hochgenauer digitaler Zwillinge mit reduzierter Unsicherheit. Im Vergleich zur klassischen Versuchsplanung bietet Bayesian Optimization eine höhere Sample-Effizienz, was besonders vorteilhaft ist, wenn die Evaluierung der Zielfunktion sehr zeit- oder ressourcenintensiv ist, wie es bei aufwändigen Finite-Elemente-Analysen (FEM), Computational Fluid Dynamics (CFD) Simulationen oder teuren realen Versuchen der Fall ist.

Ein entscheidender Vorteil der Bayesian Optimization liegt in ihrer Fähigkeit, ein adaptives Modell der Zielfunktion aufzubauen, das während des Optimierungsprozesses ständig aktualisiert wird. Durch die Integration von Unsicherheitsmaßen in dieses Modell ermöglicht Bayesian Optimization eine effiziente Erkundung des Suchraums, um schnell zu vielversprechenden Bereichen zu gelangen, und gleichzeitig eine gezielte Ausbeutung dieser Bereiche zur Verbesserung der Zielfunktion.

Für die Optimierung bedeutet dies, dass Bayesian Optimization mit vergleichsweise weniger Evaluierungen der Zielfunktion auskommt, um gute Lösungen zu finden. Dies ist besonders nützlich bei langwierigen und ressourcenintensiven Simulationen oder Versuchen, da weniger Zeit und Ressourcen für die Exploration des Suchraums benötigt werden. Durch die effiziente Nutzung der verfügbaren Ressourcen kann die Zeit bis zur Entwicklung optimaler Designs erheblich verkürzt werden.

Darüber hinaus ermöglicht die Verwendung von Bayesian Optimization auch die Generierung von hochgenauen digitalen Zwillingen durch die Reduzierung der Unsicherheit in den Modellen. Indem Unsicherheitsmaße in den Optimierungsprozess integriert werden, können Ingenieure nicht nur die besten Designoptionen identifizieren, sondern auch das Verständnis und die Vorhersagefähigkeit ihrer Modelle verbessern. Dies ist besonders wichtig in Bereichen, in denen eine hohe Genauigkeit und Zuverlässigkeit erforderlich sind, wie beispielsweise bei der Entwicklung von Sicherheitssystemen oder auch Lebensdauervorhersagen.

Die Bayesian Optimization Methode lässt sich mit der Multi-Fidelity Modellierung verbinden, so dass der Algorithmus nicht nur vorschlägt welches Design als nächstes berechnet werden soll, sondern auch in welcher Qualitätsstufe. Dies erlaubt es mit maximaler Effizienz die Trainingsdaten und oder Optimierungsdesigns vorschlagen zu lassen.

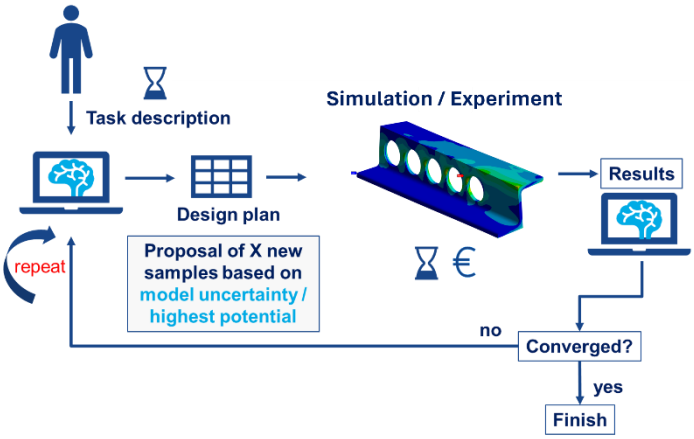

Abbildung 4: Schematische Darstellung der Bayesian Optimization

6 Anwendungsbeispiel

Die Vorteilhafte Verknüpfung der Bayesian Optimization und der Multi-fidelity Modellierung soll im Folgenden Anhand eines Akustikbeispiels gezeigt werden. In diesem Beispiel wird eine Platte mit Rippen zur Versteifung in einem halbkugelförmigen Luftbereich simuliert, um den Fernfeld-Schallleistungspegel zu bestimmen (siehe Abbildung 7). Die Geometrie ist parametrisiert und soll optimiert werden, um die maximale Lautstärke zu minimieren. Ebenfalls ist die Vernetzungsgüte parametrisiert so, dass für den Multi-fidelity Ansatz unterschiedliche Netze verwendet werden können. Die unterschiedlichen Netze wurden bereits in Abbildung 5 dargestellt.

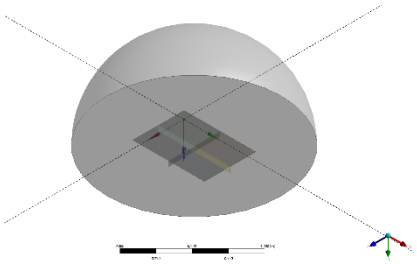

Abbildung 5: Platte mit Versteifungen, die an einem halbkugelförmigen Luftbereich befestigt ist

In Abbildung 8 ist der Fernfeld-Schallleistungspegel des Referenzdesign dargestellt. Dort beträgt das aktuelle Maximum ca. 74 Dezibel. Zur Optimierung wurden insgesamt ein Budget von 30 Simulationen zur Verfügung gestellt.

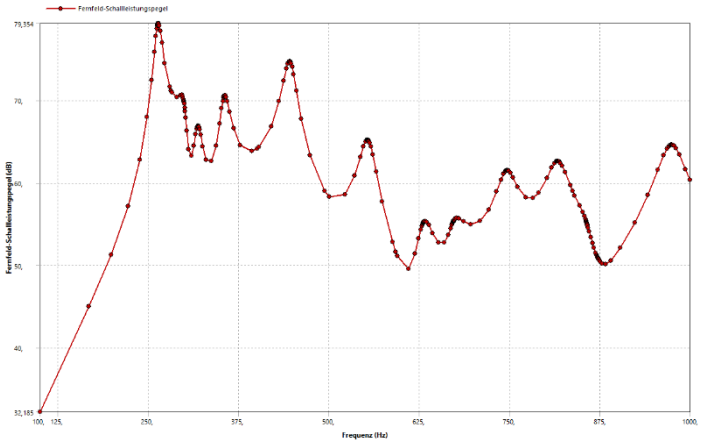

Abbildung 6: Fernfeld-Schallleistungspegel des Referenzdesign. Maximum bei ca. 80 Dezibel.

Die Ergebnisse der Optimierung sind in den Abbildungen 9 und 10 dargestellt. In Abbildung 9 ist der Verlauf der adaptiven Designs dargestellt. Jeder rote Punkt stellt eine High-fidelity Rechnung dar. Die grünen Punkte die Low-fidelity Rechnung. Das linke Bild stellt den gleichen Optimierungsverlauf wie das rechte Bild dar, nur dass nur High-fidelity Simulationen angenommen wurden. Insgesamt wurden im Multi-fidelity Ansatz nur 9 High-fidelity Berechnungen verwendet. Die Zeitersparnis, die sich daraus ergibt, ist in Tabelle 1 dargestellt. Die Ergebnisse zeigen, dass der Multi-fidelity Ansatz ca. **413%** schneller ist. Ebenfalls konnte maximale Lautstärke auf von 79 Dezibel auf ca. 43 Dezibel gesenkt werden (siehe Abbildung 10).

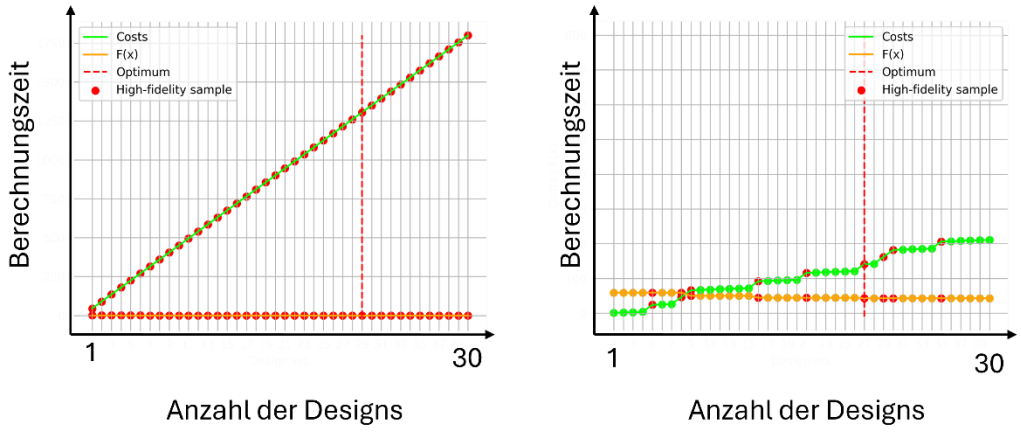

Abbildung 7: Verlauf der Bayesian Optimization und Designauswahl. Links nur High-fidelity und rechts Multi-fidelity.

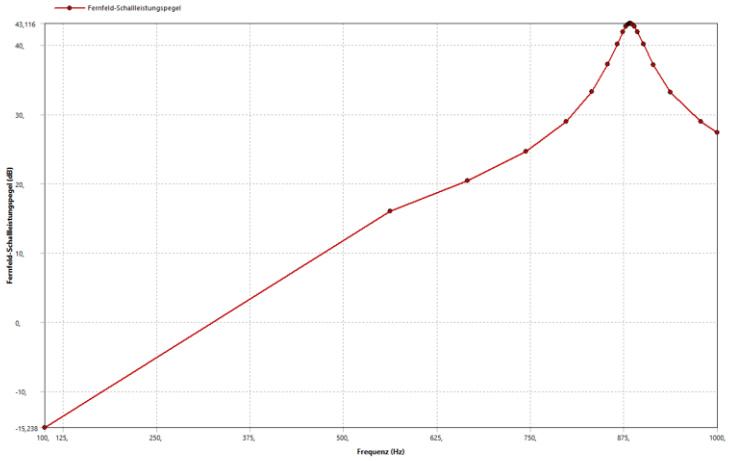

Abbildung 8: Fernfeld-Schallleistungspegel des optimierten Designs. Maximum bei ca. 43 Dezibel.

Ansatz	**Zeitaufwand**
Reine High-fidelity Optimierung	1800 Minuten
Multi-fidelity Optimierung	436 Minuten

Tabelle 1: Vergleich der benötigten Simulationszeit reine High-fidelity Simulationen gegenüber Multi-Fidelity.

7 Zusammenfassung

Ingenieure stehen vor zahlreichen Herausforderungen bei der Anwendung von künstlicher Intelligenz (KI) in Simulationen und realen Versuchen. Diese umfassen die Sicherstellung von Genauigkeit und Zuverlässigkeit der Ergebnisse sowie die Interpretierbarkeit der KI-Vorhersagen. Die Auswahl geeigneter KI-Verfahren und die Bewältigung von Hyperparameter-Tuning sind weitere Herausforderungen. Das Verfahren Deep Infinite Mixture Gaussian Process (DIM-GP) bietet Unterstützung bei diesen Problemen. Es kann beliebige Datenformate verarbeiten und lässt sich auf eine Vielzahl von Anwendungen nutzen, wo typischerweise verschiedene Verfahren benötigt werden. Dies erspart es dem Nutzer sich in verschiedene Verfahren einzuarbeiten.

Die Vereinigung von Simulations- und Versuchsdaten durch Multi-Fidelity-Ansätze ermöglicht eine effiziente Generierung von Simulationsdaten und eine Kalibrierung von Simulationsmodellen. Bayesian Optimization bietet eine leistungsstarke Methode zur Optimierung komplexer Systeme und zur Generierung hochgenauer digitaler Zwillinge mit reduzierter Unsicherheit. Die Verbindung von Bayesian Optimization und Multi-Fidelity-Modellierung ermöglicht eine noch effizientere Optimierung wie das hier vorgestellte Beispiel zeigt.

8 Referenzen

[1] Goodfellow, Ian, Yoshua Bengio, and Aaron Courville. *Deep learning*. MIT press, 2016.

[2] Williams, Christopher KI, and Carl Edward Rasmussen. *Gaussian processes for machine learning*. Vol. 2. No. 3. Cambridge, MA: MIT press, 2006.

[3] Cremanns, Kevin. *Probabilistic Machine Learning for Pattern Recognition and Design Exploration*, Dissertation, RWTH Aachen, 2021.

[4] Kandasamy, Kirthevasan, et al. "Multi-fidelity bayesian optimisation with continuous approximations." *International conference on machine learning*. PMLR, 2017.

[5] Snoek, Jasper, Hugo Larochelle, and Ryan P. Adams. "Practical bayesian optimization of machine learning algorithms." *Advances in neural information processing systems* 25 (2012).

Transformative Evolution: The Journey of AI/ML in Computer-Aided Engineering Optimization

David Schneider (Ansys)

1 Introduction

Historically, CAE practitioners faced numerous challenges, including lengthy simulation times, limited computational resources, and the complexity of accurately modeling physical phenomena. These challenges often led to bottlenecks in product development cycles and increased costs. In recent times, the complexity of engineering problems has only intensified, necessitating more sophisticated and efficient tools to manage the growing scale and intricacy of simulations. The integration of Artificial Intelligence (AI) and Machine Learning (ML) within Computer-Aided Engineering (CAE) can be a game-changer.
This document examines the historical development, current applications, and future trajectory of AI/ML in CAE. It highlights the significant strides made in parametric studies, response surfaces, optimization methods, and other techniques leading to unprecedented levels of efficiency and accuracy in engineering simulations. The benefits these technologies have brought to engineers, such as time savings, deeper insights, and the unlocking of new potentials will be highlighted.

2 Historical Perspective

The genesis of AI/ML in CAE can be traced back to the early days of computational design, where rudimentary algorithms laid the groundwork for today's sophisticated systems. The evolution of statistical methods in CAE has been equally impactful, with techniques such as the Taguchi method and Response Surface Methodology (RSM) enhancing the robustness of simulations and optimizations [1].

The last 25 years have witnessed significant advances in CAE, such as the development of multi-fidelity models, surrogate-based optimization, the integration of cloud computing and many others. These innovations have expanded the boundaries of what's possible in simulation and design [1].

Advancements in Computer-Aided Engineering (CAE) have revolutionized the landscape of engineering simulations. Through the development of sophisticated numerical methods, engineers are now equipped to tackle complex three-dimensional physics problems with unprecedented speed and ease. The accuracy and robustness of results have significantly improved, thanks to the implementation of Finite Element Analysis (FEA), Finite Volume Methods (FVM), and Finite Difference Time Domain (FDTD) techniques. These methods have not only enhanced solver efficiency but also augmented the dynamic visualization capabilities, thereby elevating the overall user experience.

However, the journey towards perfection in simulation is ongoing, and several challenges persist. At the heart of simulation lies a delicate balance between four critical aspects:

1. Accuracy of results
2. Speed of obtaining results
3. User-friendliness of the workflow
4. Robustness of the workflow

Consider the process of mesh generation, a fundamental component of multiphysics solutions. It's a well-acknowledged fact that employing coarser meshes can expedite the simulation process, yet this comes at the cost of diminished accuracy. In a similar vein, workflows that prioritize ease of use often resort to simpler meshes, which, while reducing complexity, can also compromise accuracy. Moreover, such simplifications may lead to additional complications, such as non-convergence of the simulation, ultimately undermining the robustness of the workflow [2].

3 AI/ML in CAE

As we embark on the exploration of Computer-Aided Engineering (CAE) in the modern era, it is imperative to recognize the transformative role of Artificial Intelligence (AI) and Machine Learning (ML). We will delve into techniques and forms where AI/ML not only coexists with traditional engineering practices but actively reshapes them. From predictive analytics to intelligent automation, AI/ML has become an indispensable facet of CAE, offering unprecedented capabilities in design, analysis, and optimization. We will uncover the layers of complexity and the elegance of simplicity that these technologies bring to the forefront of engineering innovation. Join us in discovering how AI/ML is intricately woven into the fabric of CAE, propelling the field towards a future where the synergy between human intellect and machine intelligence reaches new heights of collaborative creativity and efficiency.

3.1 Parametric studies: Design of Experiments and Response Surface Methods

Parametric studies have been revolutionized by AI/ML, enabling engineers to automate the exploration of design variables and their interactions. This automation has led to significant time savings, allowing engineers to focus on higher-level design strategies. AI/ML-driven parametric studies have also provided deeper insights into system behaviors, uncovering relationships between variables that were previously undiscovered. The ability to rapidly iterate over a wide range of parameters has unlocked new potentials in design optimization and product development.

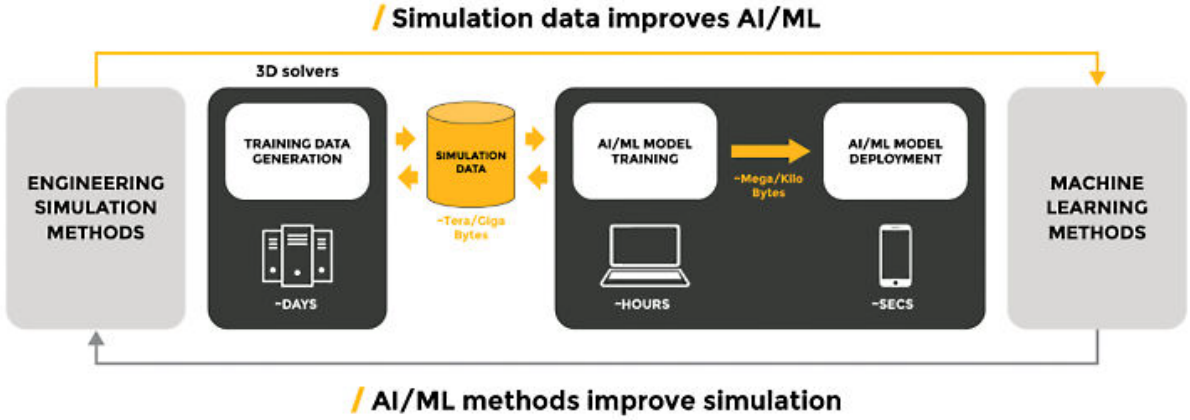

Design of Experiments (DOE), a systematic method to determine the relationship between factors affecting a process and the output of that process, has been revolutionized by AI/ML, enabling more efficient exploration of design spaces and optimization of processes. AI-driven DOE approaches can now autonomously identify optimal experimental designs, reducing the need for human intervention and accelerating the innovation cycle.

Response Surface Methods (RSM), traditionally used for developing an approximate model of the response of interest, is now supercharged with ML algorithms to create more accurate and predictive models. These surrogate models, powered by AI, can predict outcomes with high precision, allowing engineers to simulate various scenarios rapidly and with less computational cost. The synergy between RSM and AI/ML has also facilitated the creation of 'digital twins', virtual replicas of physical systems that can predict the performance and maintenance needs of their real-world counterparts.

3.2 Parametric studies: Sensitivity Analysis & Optimization

Sensitivity Analysis, which assesses how different input variations affect outputs, has been transformed by ML to provide deeper insights into model behavior. ML algorithms enhance Sensitivity Analysis by quantifying the impact of uncertainties, leading to more robust and reliable CAE models. This integration allows for the identification of critical parameters that significantly influence model outputs, guiding engineers towards more focused and effective design modifications.

The realm of Computer-Aided Engineering (CAE) has witnessed a significant surge in the efficacy of optimization methods, thanks to the advent of AI-driven algorithms. These sophisticated algorithms have granted engineers the prowess to traverse intricate design landscapes, pinpointing the most

advantageous solutions with remarkable alacrity. The acceleration afforded by these cutting-edge optimization techniques has been monumental, effectively compressing product development timelines and propelling rapid market entry. Furthermore, the amalgamation of AI/ML technologies has unlocked new horizons of optimization, ushering in an era of innovation and heightened competitiveness in product offerings.

The recent advancements in hybrid optimizers have further enriched this landscape. By amalgamating the strengths of various optimization techniques, hybrid optimizers have emerged as powerful tools that adapt and evolve, ensuring optimal performance across diverse scenarios. These hybrid systems are adept at handling the multifaceted nature of engineering problems, seamlessly integrating different methodologies to overcome the limitations of standalone approaches.

Moreover, the development of self-adapting approaches has introduced a dynamic element to Optimization in CAE. These self-adapting systems are designed to learn from their environment, continuously refining their strategies to better cope with the complexities of the design process. They adjust their parameters in real-time, responding to changes with a level of agility and precision that traditional methods cannot match. This evolution towards intelligent, self-regulating systems marks a pivotal shift in CAE, where the convergence of AI/ML with optimization methods is not just enhancing existing processes but also forging new pathways for discovery and efficiency.

The convergence of AI/ML with parametric studies has led to a paradigm shift in CAE. Engineers can now leverage AI to automate complex simulations, interpret large datasets, and make data-driven decisions with greater confidence. AI/ML-driven parametric studies have also provided deeper insights into system behaviors, uncovering relationships between variables that were previously undiscovered. The ability to rapidly iterate over a wide range of parameters has unlocked new potentials in design optimization and product development. The result is a more streamlined, efficient, and innovative engineering design process that can adapt to rapidly changing technological landscapes. As AI/ML continues to evolve, its role in enhancing parametric studies within CAE is poised to grow, promising even more sophisticated tools and methodologies for the engineers of tomorrow.

3.3 Generative Design

Generative Design employs advanced AI algorithms and ML models to autonomously generate a spectrum of design alternatives, all within the confines of specified performance parameters and physical constraints. It facilitates an extensive exploration of the design space, yielding solutions that are both highly optimized and inherently innovative solutions that might remain undiscovered through conventional engineering approaches.

This technique represents a substantial advancement in design capabilities, empowering engineers with a robust computational tool to automate intricate design processes and amplify creative potential. AI and ML algorithms serve as the driving force behind this method, rapidly iterating through design permutations to identify the most efficient and effective solutions. They simulate various material properties, load conditions, and geometric configurations, converging on designs that meet predefined criteria while pushing the boundaries of innovation.

Generative Design is not merely about automating the design process; it's about redefining the process itself. It enables the creation of complex, lightweight structures that can only be fabricated through modern manufacturing techniques such as additive manufacturing (3D printing). The AI-driven process iteratively improves upon each design, learning from each iteration to optimize for weight, strength, material usage, and manufacturability.

In essence, Generative Design in CAE is a paradigm shift from traditional design methodologies. It leverages the computational intelligence of AI/ML to perform tasks ranging from topology optimization to material selection, from load analysis to thermal management. The result is a harmonious blend of form and function, where each design is not just a static entity but a dynamic solution, continually evolving until it reaches the pinnacle of engineering perfection.

3.4 Improvement in Solver technology and User Experience

The trajectory of solver technology is one of ongoing evolution, propelled by the continuous integration of AI/ML. While significant strides have been made, leading to more efficient and self-adapting solver

settings, this journey is far from complete. Modern solvers equipped with AI-enhanced algorithms represent the current pinnacle of this evolution, offering a glimpse into a future where simulations are faster, more accurate, and increasingly autonomous.

The incorporation of AI into solver technology has not only accelerated the simulation process but has also enhanced the accuracy of results. AI algorithms are designed to learn from previous simulations, enabling them to predict and adjust to complex variables with greater effectiveness. This has been particularly beneficial in handling non-linear and multi-physics problems, where traditional solvers might struggle without extensive human intervention [3].

These AI-infused algorithms are at the forefront of optimizing performance, minimizing the necessity for manual tuning, and heralding a new phase of time efficiency and improved outcomes for complex engineering challenges. Yet, the landscape is still shifting, with research and development persistently pushing the boundaries of what these intelligent systems can achieve. The potential for further advancements suggests that the solvers of tomorrow will be even more adept, capable of learning and adapting in ways that we are only beginning to conceptualize.

These improvements in solver technology represent a paradigm shift in CAE. Engineers can now expect to tackle more complex engineering challenges with increased confidence, knowing that the solvers at their disposal are not just tools, but intelligent partners in the design and analysis process. The result is a significant enhancement in the capability to solve intricate engineering problems, paving the way for more innovative and competitive products in the marketplace.

As the development of solver technologies progresses, we can anticipate a continued enhancement of their capabilities. The integration of AI and ML is not a static endpoint but a dynamic process, with each iteration bringing forth new possibilities and challenges. The solvers that we rely on today are merely the precursors to more sophisticated systems that will emerge as this technological evolution unfolds. The future of CAE is one of perpetual innovation, where solver technology grows ever more integral to solving the intricate puzzles of engineering design and analysis.

3.5 Role of LLM’s

The integration of Large Language Models (LLMs) is an ongoing process, with these models increasingly becoming indispensable tools for engineers. LLMs like ChatGPT have shown remarkable potential in interpreting complex instructions and offering guidance on simulation setup, troubleshooting, and optimization. Their ability to understand and process natural language has made them a significant asset in streamlining the CAE workflow.

However, the evolution of LLMs within CAE is a continuous journey. As these models are trained on vast datasets and improved algorithms, their proficiency in assisting with engineering tasks is expected to grow. The current capabilities of LLMs to facilitate communication between engineers and computational systems are just the beginning. Future developments are anticipated to enhance their understanding of context, technical jargon, and the subtleties of engineering challenges.

By leveraging advanced natural language processing, LLMs are set to become even more integrated into the CAE environment, making it not only more accessible but also more intuitive for engineers. The promise of LLMs lies in their potential to evolve alongside the engineering field, adapting to new technologies and methodologies, and providing a more interactive and responsive user experience.

LLMs have already made significant inroads as assistants in CAE, their full potential is yet to be realized. The ongoing advancements in AI and ML will continue to refine and expand the capabilities of LLMs, ensuring that they remain a growing and evolving resource for engineers in the years to come.

3.6 Openness

The integration of APIs (e.g. Python) has opened up CAE to a broader research community, enabling the rapid testing and deployment of AI/ML innovations within CAE environments. Researchers can now easily connect their own developments with CAE platforms, fostering a collaborative ecosystem where new tools and methods can be integrated seamlessly into existing workflows.

Thanks to the seamless connectivity provided by Python and other APIs, Researchers can now swiftly test and implement their AI/ML advancements. This has created a fertile ground, where the rapid integration of new tools and methods into existing workflows is not just possible but actively encouraged.

This integration is crucial for the advancement of AI/ML within CAE, as it allows for the continuous flow of fresh ideas and cutting-edge technologies into the engineering mainstream. It enables the research community to push the boundaries of current engineering capabilities and paves the way for future developments that could revolutionize the way we approach design, analysis, and optimization in engineering.

In summary, the incorporation of Python and APIs into CAE is not merely a convenience – it is a cornerstone that supports the ongoing advancement of AI/ML technologies in engineering. It is the key that unlocks new possibilities, enabling the engineering community to leverage the power of AI/ML to its fullest extent and drive forward the next wave of engineering innovation.

4 Conclusion

The rising adoption of AI/ML in CAE can be attributed to the persistent challenges faced by practitioners in the past and present. Traditional CAE methodologies often struggled with the computational complexity of multi-dimensional parameter spaces, leading to suboptimal designs and prolonged development cycles. However, AI/ML offers a paradigm shift by enabling efficient exploration of these spaces, thereby mitigating computational bottlenecks and empowering engineers to make informed decisions swiftly. Moreover, the democratization of AI/ML tools and the increasing availability of high-performance computing resources have further catalyzed the integration of AI/ML into CAE workflows, driving innovation and unlocking new frontiers in engineering simulation.

In the realm of Computer-Aided Engineering (CAE), the integration of Artificial Intelligence (AI), Machine Learning (ML), and statistical methods has revolutionized parametric studies, response surface modeling, and optimization techniques. Historically, CAE primarily relied on deterministic approaches, limiting the exploration of complex design spaces. However, the advent of AI/ML has ushered in a new era, enabling practitioners to efficiently navigate intricate parameter landscapes and uncover optimal solutions. Today, AI/ML algorithms are widely employed to analyze vast datasets generated by simulations, extract patterns, and construct predictive models of system behavior.

Today AI/ML techniques play a pivotal role in accelerating solvers and automating the tedious process of finding optimal settings for generative design. By leveraging ML algorithms, engineers can efficiently explore design variations, reducing the computational burden and expediting the product development cycle. Additionally, Language Model-based systems like ChatGPT offer invaluable assistance to users by providing intuitive interfaces for setting up simulations, thereby democratizing access to CAE tools and expertise.

The openness to Python and other APIs has further facilitated the integration of AI/ML research into CAE workflows. Researchers can seamlessly connect AI/ML algorithms with existing CAE software, fostering innovation and enabling the development of tailored solutions for specific engineering challenges. This interoperability not only enhances the accessibility of AI/ML techniques but also encourages interdisciplinary collaboration, leading to novel advancements in CAE methodologies.

The past 25 years have set the stage for a future where AI/ML will continue to transform CAE, unlocking new dimensions of innovation and design excellence.

This extended abstract is the product of a collaboration between human insight and artificial intelligence. Authored with the assistance of AI, it serves as a compelling example of how AI can bolster the efficiency of engineers navigating complex and demanding environments. While this abstract marks a milestone, it is merely a precursor to the ongoing journey of AI-enhanced engineering.

5 References

[1] Francisco J. Montáns, Elías Cueto & Klaus-Jürgen Bathe, Machine Learning in Computer Aided Engineering

[2] Prith Banerjee, How AI and ML are changing simulation, https://www.ansys.com/blog/how-ai-and-ml-are-changing-simulation

[3] Thomas Most, Johannes Will, Jonas Rotermund, Lars Gräning, Artificial Intelligence and Machine Learning Applied in Computer Aided Engineering, https://www.ansys.com/content/dam/resource-center/case-study/artificial-intelligence-machine-learning-applied-computer-aided-engineering.pdf

Removing the Data Science Barriers to Deep Learning Surrogates

Andy Fine (Fine Physics LLC)

Hoss Habib (Key Ward)

1 Summary

The convergence of Artificial Intelligence (AI) and engineering disciplines heralds a transformative potential for optimizing design processes, enhancing analytical methodologies, and advancing simulation technologies.
Despite these prospects, the integration of AI into engineering practices is impeded by significant challenges, primarily stemming from the handling of vast, unstructured engineering datasets and the inherent interdisciplinary gap between engineering and data science expertise.
This paper introduces an automated, engineering-focused framework, designed to bridge this divide by facilitating the efficient preparation and utilization of engineering data for AI applications.
Leveraging advanced algorithms for data sorting and preprocessing, the tool enables the seamless conversion of heterogeneous engineering data into AI-ready formats, addressing compatibility issues across various software tools and file formats prevalent in engineering workflows.
Furthermore, the framework incorporates intuitive, no-code analytics and AI training tools tailored for engineers, alongside comprehensive guidelines and validation checks for data scientists, thereby ensuring the generation of coherent, high-quality datasets for AI modeling.
The efficacy of the framework is demonstrated through a case study within the OpenFOAM community, highlighting its capabilities in significantly reducing the time and expertise required to prepare engineering simulation data for deep learning applications.
The results underscore the potential to not only streamline the AI integration process but also to foster a synergistic collaboration between engineering and data science disciplines, thus dramatically accelerating the adoption of AI technologies in engineering practices.

2 Challenges in engineering AI applications

Data scientists and associated tools are required in deep learning but can come at a high cost with no guarantee of a successful outcome. Engineers are not always data scientists, nor data scientists are not always engineers.
Moreover, the challenges in the current market lie in the difficulty of building an optimal data set for AI. Engineering data comes in many forms and from various sources, which makes it challenging to collect, unify and create coherent data sets for AI. AI models require a specific uniformity of data set. The majority of engineering managers and teams find that their existing data is not sorted in an appropriate way, not compatible and therefore does not work for AI applications. This is a significant obstacle to building the foundation of an AI model.

Here, it is important to mention that such difficulties are a subject to realize when or after conducting a first AI approach.

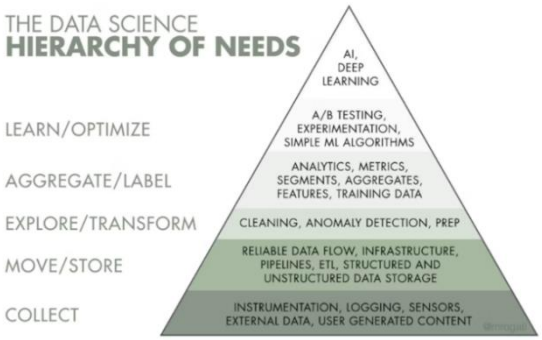

Fig. 1: The Data Science Hierarchy of Needs

Use Case
In this paper, we want to show the automated journey from data source until having the data clean and ready to be used for training an AI surrogate model.

AI Model Description
We will prepare data for an Open-source repository AI model for engineering applications (e.g. PointNet)

Dataset Description
We will use a dataset of a Wing-Body from the NASA Common Research Model.

1. 3D CAD Model: NASA Common Research Model
   a. Open-Source – The NASA Common Research Model (CRM) consists of contemporary supercritical transonic wing and a fuselage that is representative of a widebody commercial transport aircraft. The CRM is designed for a cruise Mach number of M_∞ = 0.85 and a corresponding design lift coefficient of CL=0.5
   b. The NASA Common Research Model (CRM) has enabled many formal and informal international cooperative activities and has enabled aeronautical researches and engineers in industry, government, and academia to work together across organizational and international borders sharing results on relevant problems for the benefit of all
2. The following parameters were varied:
   a. Wing Camber, Sweep, Twist angle, Wing tip displacement, Tip Chord
   b. Total of 320 variations
   c. Table below provides information about the CFD simulations

CFD Simulations	320
CFD Solver	OpenFOAM
Solver Type	rhoSimpleFOAM, turbulent k-epsilon compressible steady state
Cell count	12.5Milion
Mean flow velocity	0.3 Ma

Table 1: Summary of the CFD simulations

Data Processing Steps from RAW Data to AI-Ready Data sets

This diagram explains the data processing steps as well as the preparation steps for the PointNet AI model.

The main problem in the industry is the starting point to prepare these OpenFOAM simulations into an AI-readable format with high quality data for the PointNet AI model.
The PointNet AI model was defined by describing the input of the AI model as the Point Cloud and the Surface normal. While the Output of the AI model was to predict the drag and lift forces as a set of scalar values. Here is to mention that AI models required high memory of GPU/CPU during the training.

We developed an approach to tackle this process more seamlessly.

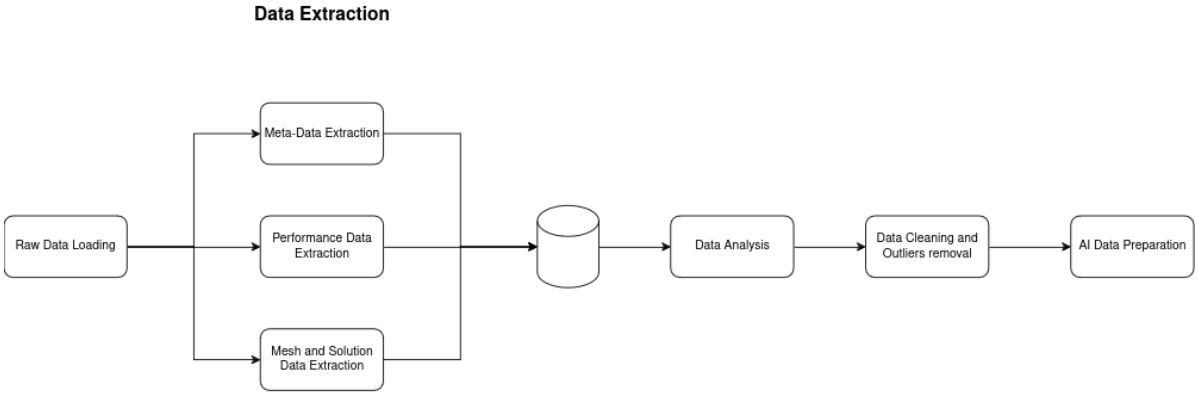

Fig. 2: Key Ward Approach to data processing and data preparation towards the AI model

The following steps were conducted:

1. Data Extraction

The meta data consisted of mathematical models, numerical parameters and the boundary and initial conditions of the OpenFOAM simulations

While the performance data consists of all monitoring and post processing values setup for the simulations. The mesh and result data were also captured as MultiBlock objects saved in a binary format.

2. Data Analysis

To ensure that the data is free from outliers, the data needed to be analyed. Outliers in the data can have a negative impact on the performance of the ai model. Outliers can be caused bay variety of reasons, such as not converged simulations, poor or simulation setup.

a. We used the automated outliers detection developed internally.

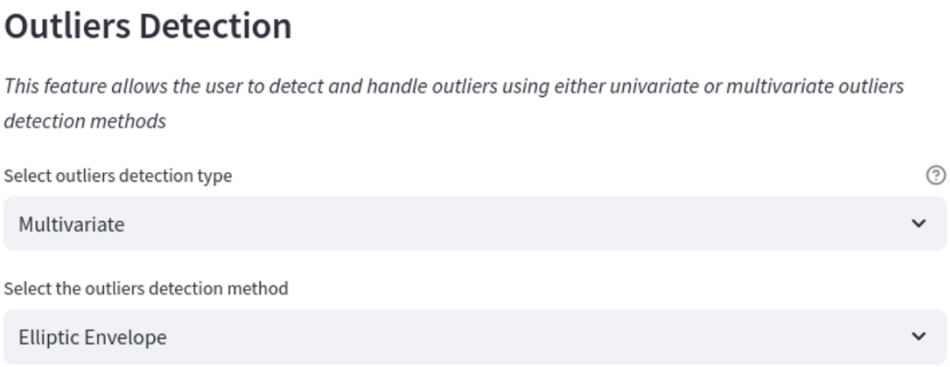

Fig. 3: Key Ward Approach to data processing and data preparation towards the AI model

b. 16 outliers in the existing and were automatically detected and removed
c. Additionally, data points with negative lift force were filtered out.

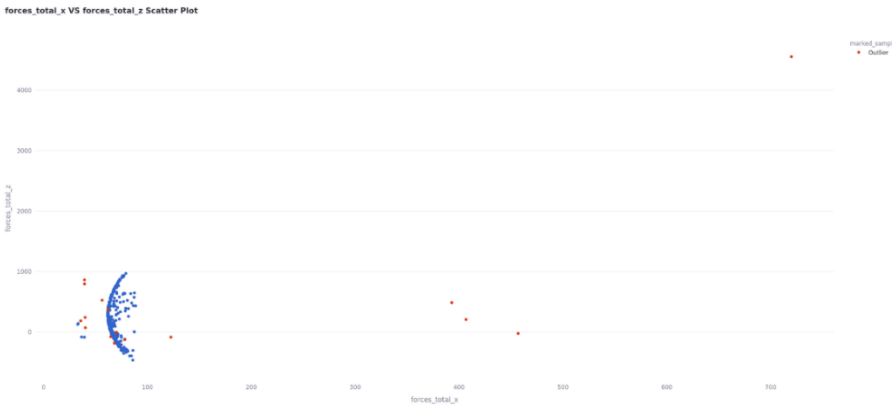

Fig. 4: Outlier Detection

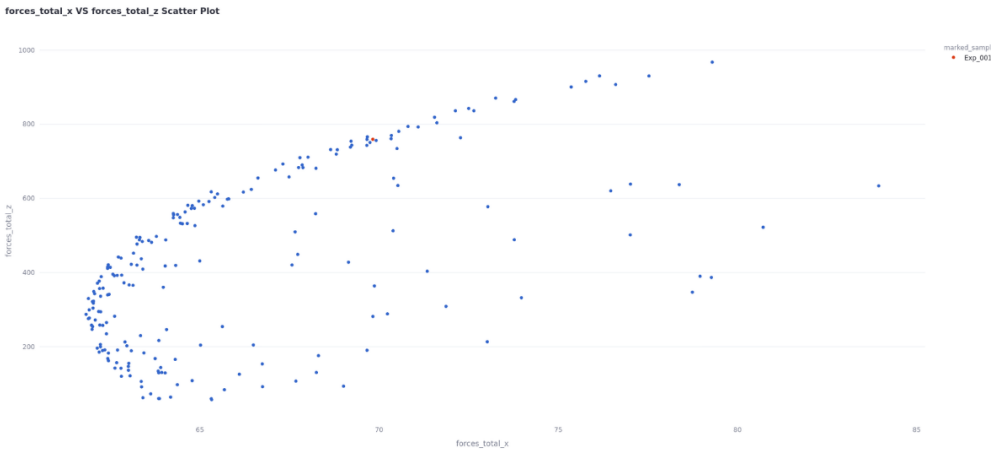

Fig. 5: Data distribution after outlier detection

	Step 1: Data Extraction (sec/data point)	Step 2: Data Analysis	Step 3: Data Cleaning and outliers removal	Step 4 Data Preparation
General approach	Creating data loading & data extraction scripts for OpenFOAM. 2-3 weeks maintenance of code& updates for each case	Microsoft Excel/other tools, not user friendly	Hours to days+time needed to adapt the scripts for new cases	setting up the processing scripts takes days to weeks. Deployment to work on cloud can take days as well. Maintenance of Code & Updates for each case;
Key Ward's approach	40 s/data point on a single core	- no-code plots, just import the data - Automatically generate a comprehensive data analysis report	automated outlier detection & removal done in minutes	Setting up the process takes 5 minutes, processing takes 336 s/data point. Cloud solution - scalable to accommodate bigger models.

Table 2: Key Ward Approach to data processing and data preparation towards the AI model

As a next step, we set up the preparation for the AI model in a way to give engineers the freedom to choose the input and output of the AI model. Moreover, we decimated the surface mesh to allow faster GPU computing for the AI PointNet model. As a last step, a binary file containing the full training data set as input point cloud and ouput lift and drag forces was exported.

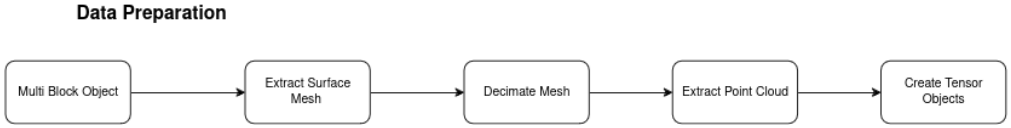

Fig. 6: Data Preparation steps taken

As follow up steps, we imported this file to the PointNet AI model were we could utilize the AI model for design exploration ensuring that the AI model is giving accurate results.

3 Conclusions

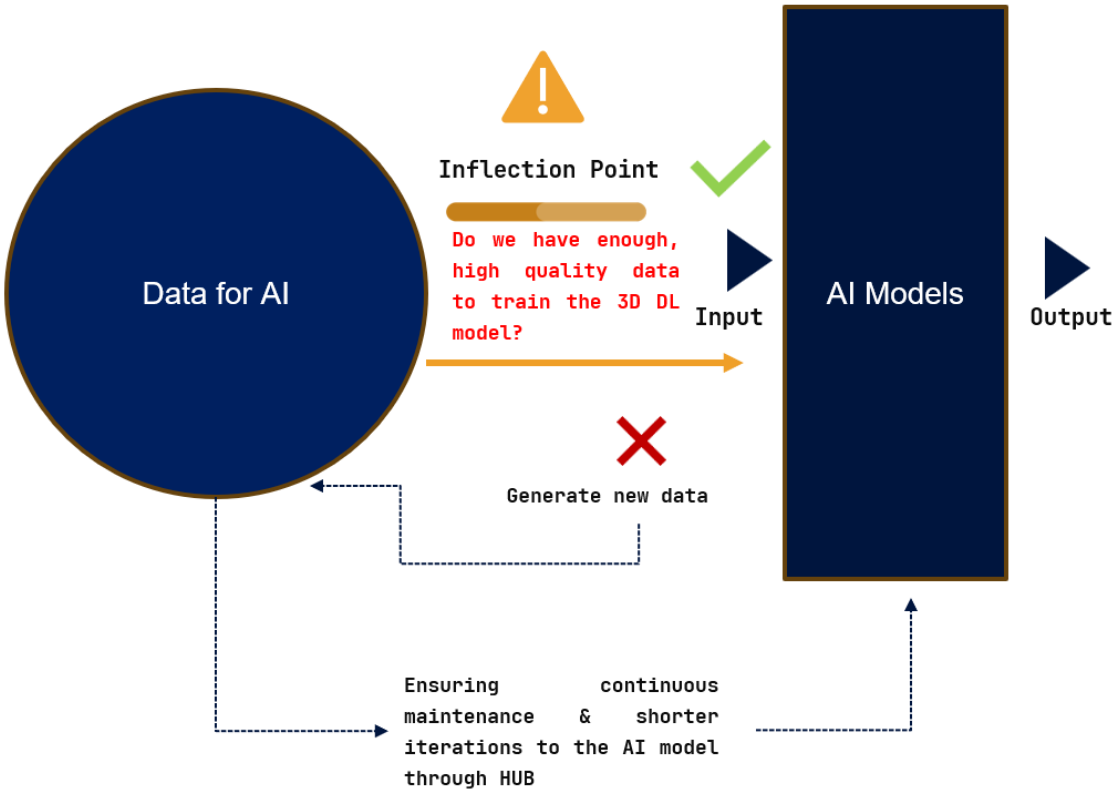

Fig. 7: Risk Mitigation process towards building 3d deep learning surrogates

This research showcases the profound capabilities of automated data preparation systems in engineering, utilizing the NASA Common Research Model (CRM) and the OpenFOAM CFD solver to illustrate this potential. By simplifying the traditionally complex data preparation process, these systems enable engineers without deep learning expertise to adopt and benefit from AI-driven methodologies.

Our process, as detailed in Table 2, demonstrates that such automated tools can considerably reduce the time and expertise required to transform raw, heterogeneous engineering data into coherent, AI-ready formats. This accelerates the initial data evaluation process, enabling a quicker determination of a dataset's suitability for training deep learning models.

Incorporating these automation tools into the MLOPS process addresses significant technical challenges and aligns AI objectives with engineering needs. This strategic integration helps mitigate the risks associated with the adoption and development of deep learning models, and empirical evidence from the study underscores the potential for a significant return on investment. These returns manifest as enhanced efficiencies in product development and reductions in operational costs.

Furthermore, this study provides a reality check on the potential of AI integration into traditional engineering workflows, which is critical in an era where reducing product development time and costs is paramount. The tools empower engineers to leverage complex data effectively, fostering an environment where technical skills and domain expertise converge to innovate and resolve industry challenges.

In conclusion, the movement towards automated, AI-ready data tools represents a significant evolutionary step in engineering practices. This shift not only streamlines existing processes but also sets the stage for sustained innovation and competitive advantage across the engineering sector. Through this pragmatic and holistic integration of AI technologies, the engineering community is better positioned to meet the demands of modern product development and achieve substantial operational improvements.

Addressing challenges in the BiW model build-up process in AUDI AG

Dipl.-Ing. Dipl.-Wirt.Ing. Athanasios Fassas
(BETA CAE Systems, Greece);

Dipl.-Ing. Richard Lindner
(AUDI AG,Germany);

MEng Stamatis Karastamatiadis
(BETA CAE Systems, Greece)

Abstract

The buildup of BiW simulation models brings up several challenges, which the engineering team must overcome. The presented workflow includes the necessary steps, starting from a CAD geometry file to the generation of a meshed BiW model, ready to be used for all the required engineering analysis disciplines, e.g. Crash, NVH, Durability etc. The challenges emerging and how these are addressed are highlighted. Starting the process, we should consider that the “design files” do not always include all the necessary information, and sometimes the provided information is wrong. Furthermore, in most cases, these files are not available at the same time, which increases the complexity of the process and the probability to introduce errors while working on the model. Users working on the model preparation often do not use the same settings, in some cases, not even the same software. All this leads to a lack of robustness. Of course, during the development phase of the BiW model, several parts get a design update and need to be inspected. Which of them includes critical geometrical changes? Is any model affected by this update? Crucial questions arise that every user must deal with, and to have them answered, appropriate workflow and software tools are needed. Among the most challenging issues are storing, browsing, querying, and updating the data. To automate the BiW model-build process, the employment of an SDM-System is essential. An effortless, trouble-free, continuous, and direct communication with such a system ensures the best quality of the process. This presentation reveals how AUDI AG has set up a workflow that supports the user throughout the process, ensures the usage of the same settings for all users, prevents the generation of errors in each step, and monitors the entire process. The software streamlines the process, communicates with the user, and informs him, in a user-friendly way, about the parts of the model that are not processed each time. Specially developed software functionality supports the user during the model update. This highlights all the changes between the different versions of the part, not only at the attributes level but at the geometrical level as well. During the workflow, all processed data are stored in the SDM system. This way, the data are available for all users to work on them and set up the upcoming necessary simulation analysis scenarios. This well-established solution, through a user-friendly interface, ensures the automated and robust browsing, viewing, and updating of the data.

1. The challenges during the process

The BIW model build-up process starts with downloading the model structure from the PDM System. In most cases, this structure holds a lot of unnecessary information. The user has to identify this unneeded information and remove it. While importing the model structure, several checks run and exclude any unwanted parts. In addition, reading the model in a user-

friendly environment by providing the option to view the model in an embedded viewer supports the user in getting the correct decisions.

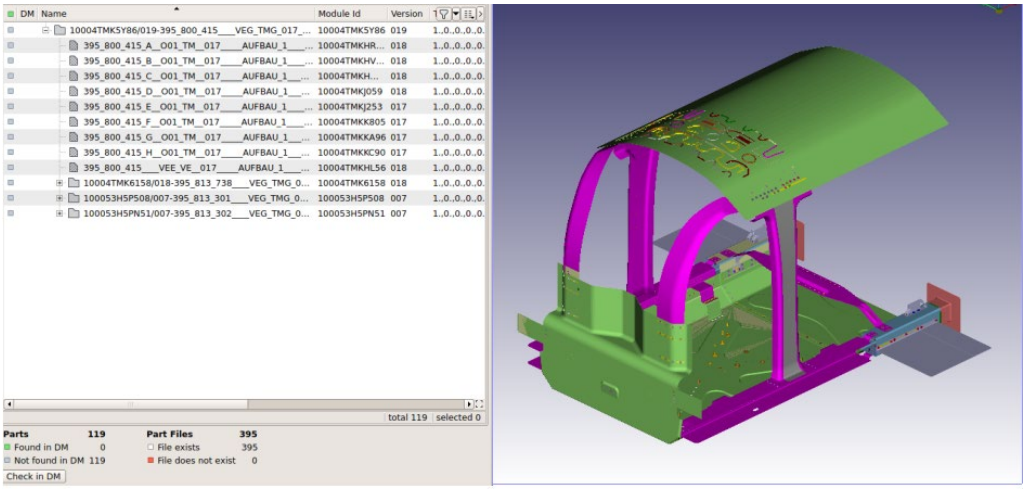

Figure 1: Viewing and browsing the model structure.

After importing the correct structure into the working environment, we can start the model build-up process. It includes several steps, from translating the CAD data to discipline-oriented representations.

The execution of each step includes several automated modifications, such as identifying and excluding parts that do not fulfill the needed criteria to run through an individual process action. In addition, parts that have geometrical errors are fixed automatically. In each step, the user gets information about the status of each component. Color mode helps to identify all those parts that need manual inspection, while information messages guide the user on what to do.

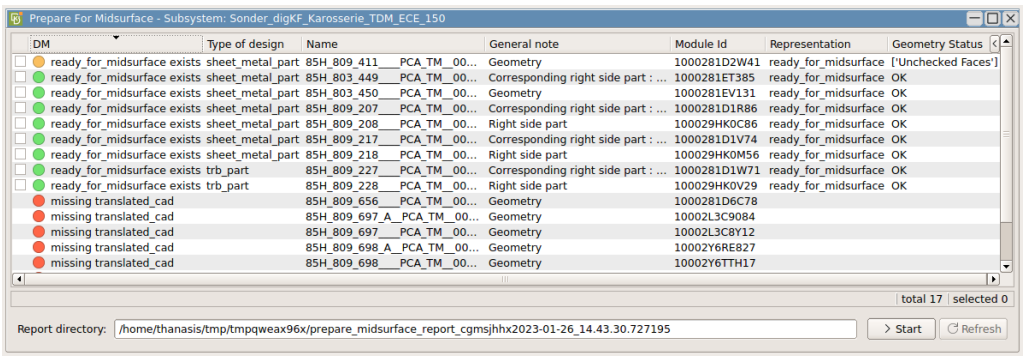

Figure 2: Communication with the user

After the execution of each step, the result is saved in a Data Management System. Having all our parts in an SDM system enables their re-usage in different model configurations without the need to process them twice. Furthermore we can follow their lifecycle during the whole process. Comparison tools assist the user in finding the differences between the various versions of the same part, not only on geometry but on attributes level as well. Problematic parts can be easily found in the Data Management System and opened in the pre-processor for further treatment.

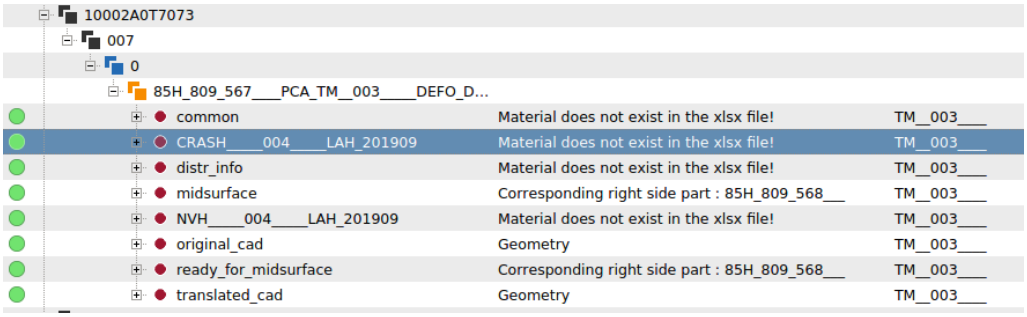

Figure 3: Browsing the parts in the Data Management System

The embedded user provides further assistance to the user. Any attribute value can be used to color the model accordingly. This way, we obtain quick and easy useful information about the model. Similarly, any part isolated on the viewer can be opened in the pre-processor for further treatment.

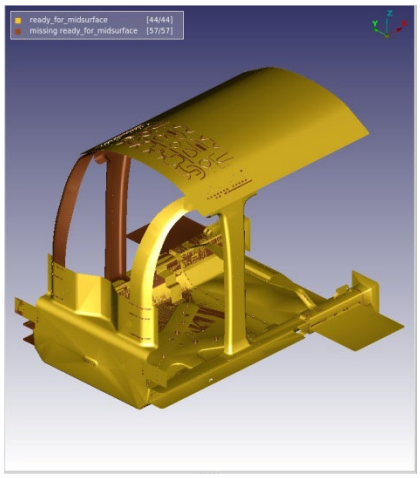

Figure 4: Identify problematic parts in the viewer

A very demanding task is creating the connection entities. All the needed information to create these connection entities is stored in external files. The action for creating the required connection entities, reads these files and stores the result under the correct part in the model structure. Several checks are executed that identify any problematic entity. This information is stored as a user attribute and communicated to the user.

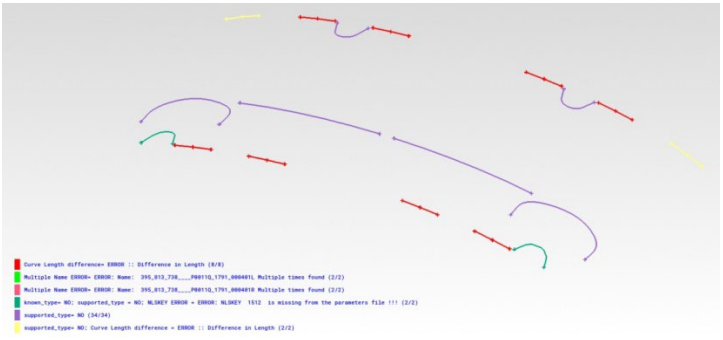

Figure 5: Getting the connection overview of the model

2. Benefits of the automated model process

Using the developed process for the model build-up, AUDI engineers gained a great benefit. All the users working on the same project use the same functionality with the same settings and parameters. The identification of any possible error happens automatically and the provided user interface guides the user to fix them. The result data are stored without any user interaction under the proper position in the Data Management System. In each step of the process, the needed representation of each part is automatically found in the Data Management System and loaded to execute the current action.

Universal Data Space: Verwaltung der datengetriebenen Produktentwicklung mit einer einheitlichen Umgebung für Engineering Daten

Dr.-Ing. Sebastian Fink, Christopher Woll

GNS Systems GmbH, Braunschweig, Germany

1 Einleitung

Die digitale Transformation bietet Unternehmen aller Branchen enorme Chancen – und stellt sie gleichzeitig vor große Herausforderungen. Dennoch lässt sich festhalten, dass bei der überwiegenden Mehrheit der Unternehmen die digitale Transformation 2023 voll im Gange ist, in Teilen sogar schon abgeschlossen, hält die Studie „CIO Agenda 2024“ [1] fest. Mehr als 87 Prozent der Befragten hätten demnach eine Digitalisierungs-Roadmap formuliert, und bei knapp 40 Prozent betrifft dies auch das Gros aller wichtigen Unternehmensprozesse, formuliert die von der Lufthansa Industry Solutions GmbH & Co. KG unterstützte Untersuchung weiter. Ein wichtiger Schlüssel in den fortschreitenden Transformationsprozessen wird auch in den kommenden Jahren die intelligente Aufbereitung und Nutzung der immer größer werdenden Datenmengen sein. So schätzt das international tätige Marktforschungs- und Beratungsunternehmens IDC [2], dass die weltweite Datenmenge bis 2027 auf bis zu 284 ZByte ansteigt. Insbesondere für den Geschäftserfolg ist es daher entscheidend, wie gut Unternehmen aller Branchen in der Lage sind, ihre Daten strategisch zu nutzen. Unternehmen verbessern ihre Wettbewerbsposition durch eine effizientere und intelligentere Nutzung der vorhandenen Daten, durch eine gezieltere Erhebung neuer Daten und durch die Anwendung von fortschrittlichen intelligenten Auswertungsmethoden, vgl. die Lünendonk Studie „Von Datensilos zu Datenströmen“ [3] aus 2022. Das Ziel sollte es daher sein, Daten aus unterschiedlichsten Quellen und Prozessen zusammenzubringen und effizient zu verarbeiten, um diese effektiv nutzen zu können. War Datenmanagement früher ein Prozess, der vornehmlich im Hintergrund stattfand, geht es heute vielmehr darum, Daten für BI und Analytics nutzbar zu machen, wie es zum Beispiel in dem Artikel von BARC "Data Management Survey 23“ [4] ausgeführt wird: Die fachliche und technische Relevanz des Datenmanagements nehme stetig zu und damit gleichzeitig auch die Relevanz des Datenmanagements in der Unternehmensstrategie. Daten sind zu einem strategischen Vermögenswert geworden, der als wirtschaftsrelevantes Gut effizient gepflegt werden sollte.

Unternehmen geht es bereits heute darum auf Grundlage solider Daten bessere Entscheidungen zu treffen, Geschäftsprozesse effizienter zu gestalten oder neue Geschäftsmodelle zu entwickeln. Auch die stärker geforderten Ansätze zur Nachhaltigkeit werden von intelligent erhobenen Daten partizipieren. Mit dem Wandel zu einer datengetriebenen Unternehmenskultur steigen jedoch auch die Anforderungen an das Datenmanagement: Im Vordergrund stehen hier beispielsweise die Transparenz durch eindeutige Datenklassifikationen, nachvollziehbare Datenflüsse und stringente Reporting-Konzepte. Weiterhin notwendig ist die Sicherstellung einer hohen Datenqualität durch entsprechende Kontrollmechanismen und klar geregelte Verantwortlichkeiten und Prozesse, resümiert Lünendonk in fachlicher Zusammenarbeit mit KPMG [3]. Als umfassende und flexible Lösung für die Verwaltung von Daten setzt der Universal Data Space genau dort an, denn mit ihm wird eine nahtlose Datenorchestrierung im Unternehmen ermöglicht. Dieser gleichmäßig leistungsstarke sowie skalierbare Ansatz ermöglicht es, große Datenmengen vollumfänglich zu verarbeiten und sichert einen einfachen Zugriff auf Daten über verschiedene Standorte und Anwendungen hinweg.

2 Status der datengetriebenen Produktentwicklung

Die datengetriebene Produktentwicklung ist eine logische Konsequenz der fortschreitenden Transformation. Sie implementiert eine neue Denkweise in Bezug auf die Daten und erlaubt Agilität in Form von kontinuierlichen Releases (CI/CD), wie in der Veröffentlichung „The data-driven Enterprise of 2025“ [5] von McKinsey nachzulesen ist. Seit einigen Jahren lässt sich beobachten, dass Daten zum Treiber großer technologischer Innovationen avancieren. Denn unter dem Druck des Marktes sowie immer kürzerer und schnellerer Entwicklungszyklen reagieren produzierende Unternehmen mit stark vernetzten Entwicklungs- und Produktionsprozessen, deren Effizienz von der Möglichkeit einer

weltweiten Datennutzung abhängt. So ist zum Beispiel das Entwickeln neuer Fahrfunktionen im Kontext des autonomen Fahrens ohne einen umfangreichen Datensatz schlicht nicht möglich.

Die Produktentwicklung wird entsprechend deutlich digitaler, datengetriebener und auch komplexer. Die effiziente Analyse und Auswertung großer heterogener Datensätze, zum Beispiel mithilfe von geeigneten KI-Methoden, macht es heute schon möglich Muster und Gesetzmäßigkeiten zu erkennen. Darauf aufbauend lassen sich Lösungen für optimierte Prozesse und Abläufe in der Entwicklung und anschließenden Serienproduktion identifizieren. Der datengesteuerte Ansatz liefert dem Entwickler daher die notwendige Basis, um umfangreiche Daten aus einer Vielzahl von Quellen effizient zu nutzen. Datensätze müssen ihr „Aschenputtel-Image“ [6] ablegen und aus der passiven Rolle der reinen Archivierung herauskommen. Denn einen Datenschatz anzuhäufen und nicht zu nutzen, ist in höchstem Maße fahrlässig. So hält McKinsey & Company in einer Studie zur Consumer Electronics Show in Las Vegas 2021 [7] fest, dass die Nutzung von Daten allein aus dem Auto den Mobilitätsunternehmen des gesamten Ökosystems (Autoherstellern, Zulieferern und Serviceanbietern bis hin zu Versicherungen, Infrastruktur- und Tech-Unternehmen) pro Fahrzeug im Schnitt jährlich bis zu 310 US-Dollar zusätzlichen Umsatz erbringen könnte.

Unternehmen stehen also vor der Herausforderung, ihre Datenschätze zu heben und mithilfe der richtigen Datenstrategie Mehrwerte zu generieren. Damit die zukünftige Analyse von Daten zu validen Ergebnissen führt, umfasst eine tragfähige Datenstrategie im besten Fall sowohl die Modernisierung des bestehenden Datenbestandes als auch die Integration neuer Datenquellen. Ins Zentrum der Aktivitäten rückt daher eine einheitliche Datenumgebung. Sie löst nicht nur die bereits genannten Herausforderungen im Umgang mit den immer größer werdenden Datenmengen. Sie bildet auch eine solide Basis, um diesen neuen Anforderungen im Engineering, immer kürzeren Entwicklungszyklen und volatilen Märkten zukunftsorientiert zu begegnen. Entwicklungsingenieure setzen bereits heute für ihre Anwendungen einen uneingeschränkten Zugriff auf sämtliche Daten, einen barrierefreien Zugriff auf Tools und integrierte Entwicklungs- sowie Softwareumgebungen voraus. Darüber hinaus gelten neue Entwicklungen in der Speicherung, Verarbeitung und Verwaltung großer Datenmengen, insbesondere das Cloud- beziehungsweise Edge-Computing, als Katalysatoren für die datengetriebene Wertschöpfung und fördern die Entstehung von daten- und cloudbasierten Ökosystemen, vgl. [8]. Bei den zentralen Zukunftstrends bilden Softwarelösungen, Daten und Plattformen das Zentrum der zukünftige Wertschöpfung.

3 Universal Data Space - Vernetzte Datenumgebung und optimierte Arbeitsprozesse

Mit der integrierten Datenplattform Universal Data Space im Engineering verfolgt GNS Systems einen ganzheitlichen Ansatz zur Verwaltung, Verarbeitung und zum Austausch von Daten. Mit dem entwickelten Ansatz werden Datensilos, Insellösungen sowie Redundanzen aufgebrochen und ein durchgängiger Zugriff auf die wachsende Zahl von Datentypen und Systemen angeboten. Die Lösung erlaubt es, große Datenmengen zu streamen, schnell zu verarbeiten, zu speichern und für die Entwicklung neuer Fahrzeugmodelle zu analysieren. Ebenfalls wird mittels individuell konfigurierbaren Policies ein dedizierter Datenzugriff ermöglicht. Die Verantwortlichkeit für einen optimalen und sicheren Betrieb obliegt hierbei dem Data-Governance-Team.

Über die Plattform können Unternehmen Daten in der Cloud mit Ressourcen On-Prem kombinieren, verarbeiten und für Analysen im Rahmen von Big Data vorbereiten beziehungsweise nutzen. Gemäß der policy-basierten Bereitstellung, Übertragung und Zugriffsrechteverwaltung von global hochgeladenen Daten wird ein optimaler Datenfluss zu jedem Zeitpunkt im Entwicklungsprozess sichergestellt. Ganz gleich ob in Datengaragen, an unterschiedlichen Entwicklungs- oder Produktionsstandorten – der Universal Data Space sichert einen nahtlosen Zugriff und eine gemeinsame Nutzung der Daten über verschiedene Anwendungen hinweg.

3.1 Nahtlosen Datenfluss erlauben

Ganz im Zeichen des Digital Thread lassen sich Daten über den gesamten Lebenszyklus eines Produkts nachverfolgen. Ermöglicht wird dies über die Archivierung von sicherheitsrelevanten Daten und Anwendungen mindestens 10 Jahre nach End of Life (EoL). Die Chance, große Datenmengen aus zugehörigen Anwendungen und Komponenten effizient zu nutzen, ist daher ein entscheidender Vorteil, um im Labyrinth von Daten aus unterschiedlichen Quellen und Formate den Entwicklungsprozess zu optimieren und für zukünftige Fahrzeuggenerationen weiterzuentwickeln. Die Schnelligkeit, Agilität und Effizienz in der Produktentwicklung erhöhen sich mithilfe des Universal Data Spaces signifikant.

Hiermit werden auch schon die wesentlichen Merkmale des Universal Data Spaces deutlich: Der Universal Data Space ermöglicht die Erfassung, Verteilung und Verwaltung großer, unstrukturierter

Datenmengen. Er sichert hierbei stets die Datenqualität, wahrt die Informationsintegrität und beachtet bestehende Rechtsvorgaben. Als lernende Plattform trägt der Universal Data Space daher zur kontinuierlichen Optimierung der Speicher- und Berechnungszuweisungen über den Produktlebenszyklus, die Lieferkette und die nutzerspezifische Datennutzung bei, vgl. Abbildung 1.

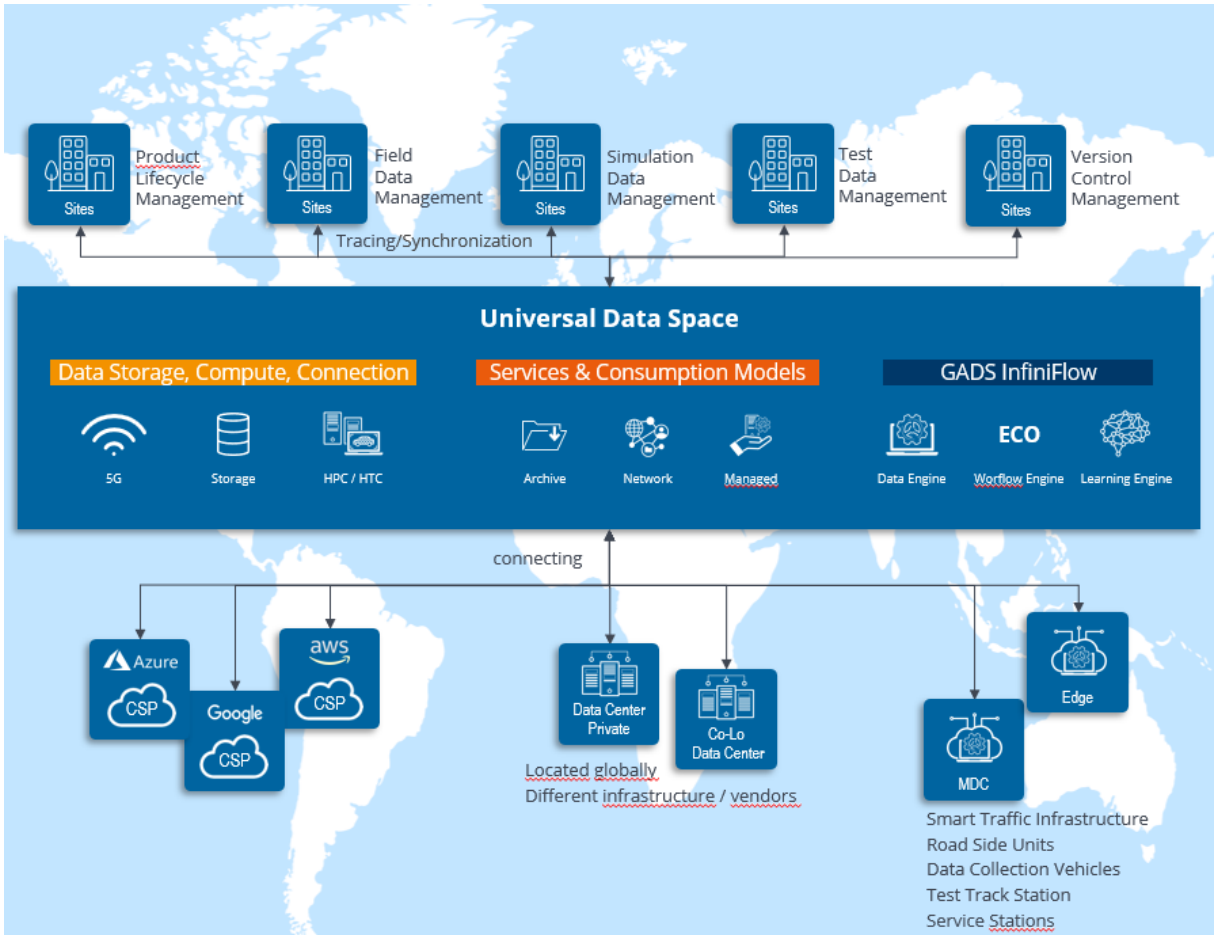

Fig. 1

Die Motivation hinter dem Universal Data Space: Die domänen- und firmenübergreifende Nachverfolgbarkeit der Daten muss im Kontext der individuell vergebenen Daten-IP sowie rechtlicher Vorgaben sichergestellt werden. Gelöst wird die Daten-Orchestrierung mittels einer flexibel konfigurierbaren Richtlinie (policy) sowie einem optimalen Datenfluss.

3.2 Workflows mit konsistenten Daten unterstützen

Die von Anwendung zu Anwendung individuell optimierte Datenhaltung, -berechnung und -übertragung gerade global verteilter Daten stellt einen großen Benefit für den Anwender dar. Dies ist ein wesentlicher Faktor für robuste, effiziente und effektive Daten-Workflows. Die Verknüpfung von Daten, Informationen und Anwendungen über die einheitliche, konsistente Datenplattform bringt dem Anwender einen erheblichen Mehrwert. Die Plattform ermöglicht beispielsweise dem Entwicklungsingenieur weltweit den Zugriff auf Daten mit domänenspezifischen, intelligenten semantischen Datenmodellen. Daten unterschiedlicher Standorte wie zum Beispiel aus einer Strukturanalyse am Hauptsitz in Deutschland, aus einer High-Speed Crash-Analyse in Japan sowie einer Low-Speed Crash-Analyse in einem Safety-Center in Schweden können wie exemplarisch in Abbildung 2 dargestellt über den Universal Data Space einfach verwaltet und orchestriert werden.

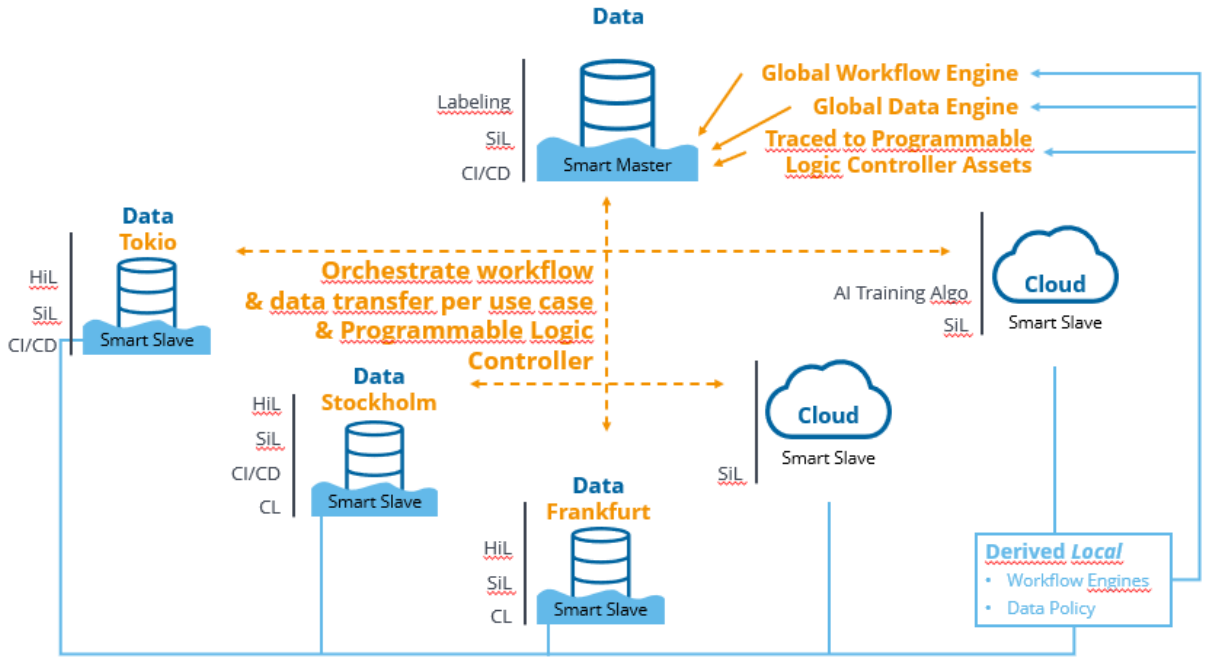

Fig. 2
Der Prozess- und Workflow des Universal Data Spaces: Durch die Anbindung verschiedener Systeme (zum Beispiel verschiedene Prüfstände) über eine einheitliche, konsistente Datenplattform werden Datentransparenz, Datenredundanz und -demokratisierung sowie das Datenmanagement erleichtert. Die Plattform ermöglicht es entsprechend weltweit auf die Daten zuzugreifen. Realisiert wird dies über ein domänenspezifisches, intelligentes semantisches Datenmodell.

Neben dem oben genannten Beispiel für die Anwendung des Universal Data Spaces in der CAE-Umgebung stellt ein zweites Beispiel das autonome Fahren in den F, wo der Universal Data Space ebenfalls einen großen Nutzen generieren könnte.

Hintergrund ist hier die Tatsache, dass Milliarden von Kilometern gefahren werden müssen, um bewerten zu können, ob das autonom fahrende Auto so sicher ist wie das vom Menschen gesteuerte. Der enorme Datensatz, der hierzu notwendig ist, muss zuerst einmal generiert und anschließend aufbereitet werden. Genau hier kommt der vorgestellte Ansatz zum Tragen, denn mittels des Tools können die Daten global über Edge, Core oder Cloud hochgeladen, gespeichert, gesucht sowie weiterverarbeitetet werden. Sobald die Daten hochgeladen und gemäß den vorab definierten Richtlinien aufbereitet wurden, können verschiedene Gruppen wie Entwicklungsingenieure, Datenwissenschaftler oder Forscher weitere Analysen und / oder Visualisierungen mit den aufbereiteten Daten durchführen.

Die hier aufgezeigten Möglichkeiten, Daten vielfältig zu verwenden, tragen zu einer Effizienzsteigerung im Entwicklungsprozess bei. Entwickler erhalten mit diesem zentralisierten Datenmanagement-Tool die notwendige Basis, um komplexe Datenzusammenhänge für die Umsetzung von Innovationen über Systemgrenzen hinweg zu nutzen. Die systemübergreifende, globale Suche nach Daten sowie die Identifizierung und Berücksichtigung von Datenbeziehungen beschleunigen Workflows in der Produktentwicklung signifikant.

3.3 Organisationsspezifische Regeln schaffen maximale Datentransparenz

Mit seinem einheitlichen Plattformansatz verbindet der Universal Data Space die Prozesse, indem er den Gap zwischen Kommunikation, Orchestrierung und Compliance schließt. Hierfür unterstützt der Universal Data Space verschiedene Speichertypen. So können die Daten hochgeladen, verschoben oder von verschiedenen Quellen beziehungsweise Zielen heruntergeladen werden. Insbesondere für die Entwicklung autonomer Fahrzeuge bilden benutzerdefinierte Richtlinien ein starkes Instrument, das dem Entwickler maximale Flexibilität und Effizienz bietet. Mehrere Anwendungen können die gleichen benutzerdefinierten Policies verwenden. Gleichzeitig kann eine Anwendung Aktionen mehrerer benutzerdefinierter Policies ausführen, wie es in Abbildung 3 schematisch aufgezeigt wird.

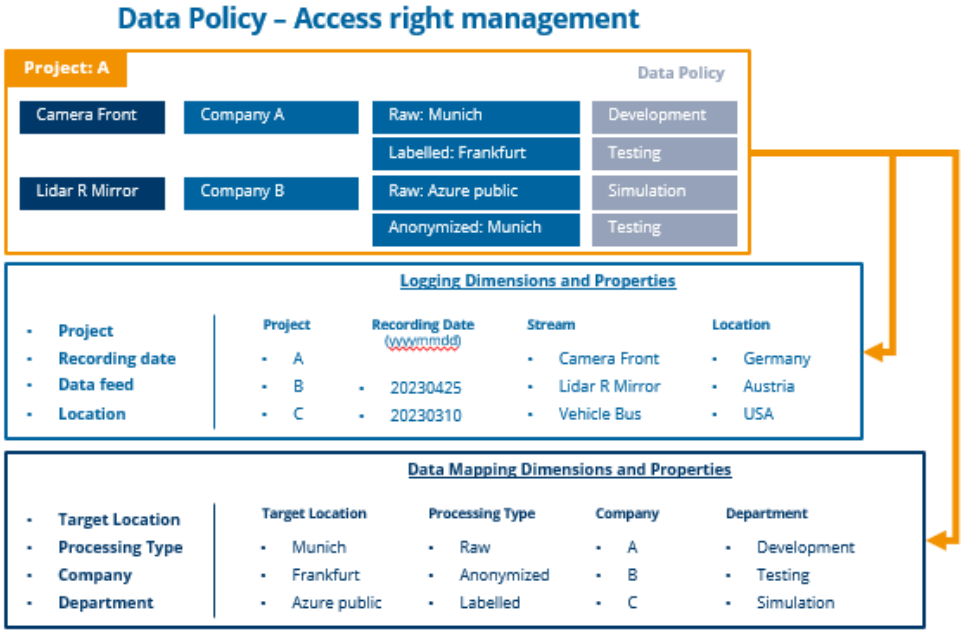

Fig. 3
Benutzerdefinierte Richtlinien und Universal Data Space: Die Speicherung, Übertragung und Verwaltung von Zugriffsrechten sämtlicher hochgeladener Daten ist zu jeder Zeit rechtskonform und entspricht den höchsten Anforderungen der Automobilindustrie. Durch den falloptimierten Zugriff auf globale Daten ist es zudem einfach, Datenintegritätsprüfungen durchzuführen und zuverlässige Ergebnisse, zum Beispiel im Kontext des autonomen Fahrens, zu erhalten.

Das funktioniert wie folgt: Bereits während des Hochladens der Daten erhalten diese ihre Tags. Diese Tags stellen sicher, dass die Daten innerhalb des Systems zum Beispiel mittels Filterung wieder gefunden werden. Die Suche beispielsweise nach einer CAD-Datei, die Teil des Fahrgestells ist, gestaltet sich einfach über die Stichworte CAD und der entsprechenden Fahrgestellkomponente. Tags dienen jedoch auch dazu, die Daten mit der ausgewählten Richtlinie zu kombinieren, damit diese konform der Data Flow Definition ausgeführt werden können. Die Data Flow Definition enthält somit alle relevanten Metadaten, um die Ausführung vieler verschiedener Aufgaben in der Fahrzeugentwicklung zu ermöglichen. Die Gesamtheit der Data Flow Definitionen bildet die Datenrichtlinie ab, die den gesamten Prozessablauf definiert.

In der Praxis gestaltet sich das folgendermaßen: Eine Richtlinie enthält beispielsweise eine Data Flow Definition mit der Aktion "Verschieben". Sobald die Daten hochgeladen wurden, führt die ausgewählte Data Flow Definition mit der Aktion "Verschieben" gemäß der entsprechenden Richtlinie die Aktion aus. Die Daten werden dann an den zuvor festgelegten Zielort verschoben. Dies schafft maximale Datentransparenz. Die Verwaltung der Datenflüsse wird für den Anwender einfacher, da sich die Verweise innerhalt der verschiedenen Daten übersichtlicher gestaltet. Der Einsatz eines Data Product Owners mit einem Frontend hilft dem Anwender den Datenfluss zu überwachen und gemäß den definierten Richtlinien zu steuern.

3.4 Universal Data Space unterstützt die Produktqualität

In der Praxis der Automobilindustrie basiert die Fahrzeugentwicklung auf einer standardisierten Architektur in einem flexiblen Fertigungskontext, so dass für Millionen von Fahrzeugen dieselben Basisteile verwendet werden können. Systeme zur Rückverfolgbarkeit der einzelnen Bauteile über alle Stufen des Fertigungsprozesses hinweg ermöglichen optimierte Lieferketten und kürzere Durchlaufzeiten. Dieses Prinzip lässt sich auch auf den Universal Data Space übertragen: Die enge Vernetzung von Daten über die Plattform ermöglicht eine höhere Transparenz der Datenflüsse. Unternehmen können so Produktionslinien besser überwachen und vergleichen. Zugleich erhalten sie über die einheitliche Datenbasis wichtige Informationen, um herauszufinden, welche Produktionsschritte länger dauern als erwartet und warum. Die hohe Datenintegrität ist somit ein ausschlaggebender Faktor, um Prozesse in der Produktentwicklung zu beschleunigen und zu optimieren. Die Automatisierung der Prozesse in der virtuellen Produktentwicklung moderner Fahrzeuge trägt zusätzlich zur Reduzierung

von Entwicklungszeiten und -kosten bei. Maximale Standardisierung - von der Versionskontrolle über optimal skalierbare Rechenkapazitäten bis hin zu automatisierten Integrationstestsystemen - sichert die Qualität der virtuellen Fahrzeugentwicklung maßgeblich. Eine mögliche Integration KI-basierter Analysen der Datensätze steigert zusätzlich die Effizienz, da sie wertvolle Informationen und Muster erkennen, die gewinnbringend genutzt werden können.

4 Fazit

Schon heute existieren in Unternehmen riesige Datenmengen. Künftig werden es noch erheblich mehr sein. Datengetriebene Unternehmen werden mit ihren Produkten und Diensten zahlreiche Märkte dominieren beziehungsweise neue erschließen. Um eine effiziente Datenanalyse im Unternehmen und über dessen Grenzen hinaus aufbauen zu können, ist eine klare Strategie erforderlich. Diese muss nicht nur interne Datenquellen umfassen, sondern auch externe Informationen berücksichtigen. Der Zugriff auf sämtliche Daten muss eindeutigen Standards unterliegen. Dadurch wird nicht nur ein möglichst homogener Zugang für alle Beteiligten sichergestellt, sondern auch eine optimale Kontrolle der Daten im Hinblick auf Sicherheit, Governance und Compliance.

Eine einheitliche Datenumgebung bietet Entwicklern eine kohärente Strategie, die die Herausforderungen im Umgang mit Daten (zum Beispiel Datenhaltung und -verwaltung, optimaler Datenzugriff, Rückverfolgbarkeit) in einem zukunftsorientierten Ansatz bewältigt. Der dahinterstehende Ansatz eines einzigen Datenraums verbindet verschiedene Tools miteinander, gewährleistet die Rückverfolgbarkeit von Prozessen und erhöht das Vertrauen in den digitalen Datenschatz.

Der Universal Data Space erfasst die spezifizierten Metadaten der Prozesse und orchestriert sie über verschiedene Standorte hinweg, indem individuell definierbare Policies befolgt werden. Entwickler in der Industrie profitieren von der enormen Prozesssicherheit und hohen Flexibilität, die ein einziges System zur Verwaltung der Daten bietet. Es schafft eine effiziente Umgebung für Informationen und stellt eine einheitliche Schnittstelle für das Abrufen von Daten bereit. Das verschlankt den Prozess, der die Daten aus einem physischen System mit Anwendungen zusammenführt, die solche Daten nutzen. Das Resultat ist ein optimierter datengetriebener Entwicklungsprozess. Der Universal Data Space schafft die Grundlage, um an Themen wie zum Beispiel Data Analytics, Smart Data und Predictive Analytics aber auch an die Felder künstliche Intelligenz und Maschinenlernen anzuknüpfen.

5 Referenzen

[1] CIO, CSO und COMPUTERWOCHE: CIO-Agenda 2024, Februar 2024

[2] Statista: Volumen der jährlich generierten/replizierten digitalen Datenmenge weltweit von 2010 bis 2022 und Prognose bis 2027 unter https://de.statista.com/statistik/daten/studie/267974/umfrage/prognose-zum-weltweit-generierten-datenvolumen/; Quelle: IDC (01.09.2023)

[3] Lünendonk/KPMG: Von Datensilos zu Datenströmen - Der Wandel von Banken und Versicherungen zu datengetriebenen Unternehmen, Mindelheim, 2022

[4] BARC: The Data Management Survey 23, 2022

[5] MC Kinsey: The data-driven enterprise of 2025, Januar 2022 unterhttps://www.mckinsey.com/business-functions/quantumblack/our-insights/the-data-driven-enterprise-of-2025 (31.08.2022)

[6] CIO/CSO/Computerwoche: Data-Driven Enterprise 2023, 2023

[7] McKinsey: Der ungenutzte Datenschatz: Durch Fahrdaten jährlich mehrere Hundert US-Dollar Wertpotential pro Auto möglich; Pressemitteilung zur Consumer Electronics Show in Las Vegas 2021 unter https://www.mckinsey.de/news/presse/2021-01-10-car-data (01.09.2023)

[8] e-mobil BW GmbH – Landesagentur für neue Mobilitätslösungen und Automotive Baden-Württemberg: Digitalisierung in der Mobilitätswirtschaft - Erfolgsfaktoren der Daten- und Plattformökonomie, Stuttgart, Februar 2023

The Way to SPDM: Benefits, Introduction Methodology and Experiences from 20 Years of SPDM Projects

Dr. Sebastian Schweigert-Recksiek, Dr. Marcus Krastel, Dirk Meier

:em engineering methods AG

1 Introduction

The functional validation of development stages in all phases of product development in the form of simulations and calculations is becoming increasingly important and represents an important step in ensuring product quality. This applies in particular to the development of complex, mechatronic products.

Many companies are becoming aware of the potential offered by cross-domain, integrated simulation data management and greater integration of simulation data into PDM/PLM processes and tools. The advantages of SPDM systems such as traceability and audit security, time savings when searching for and managing data are often undisputed and a functioning simulation data management system is considered to be one of the prerequisites for future topics such as digital twins and big data analytics. However, the introduction of such a data management system for managing data from calculation and simulation poses a number of challenges that require a systematic approach, a high degree of thoroughness when gathering requirements, and the strong involvement of key users and stakeholders.

In this contribution, we condense the experience from 20 years in SDM consultancy to highlight the benefits companies can gain via SPDM (cf. Figure 1) and sketch a walk-through of a typical SPDM selection and introduction projects. This includes a proven methodology for requirements elicitation, capability assessment, IT architecture considerations, vendor selection, POC conduction, and roll-out preparation – all of which in a model-based manner.

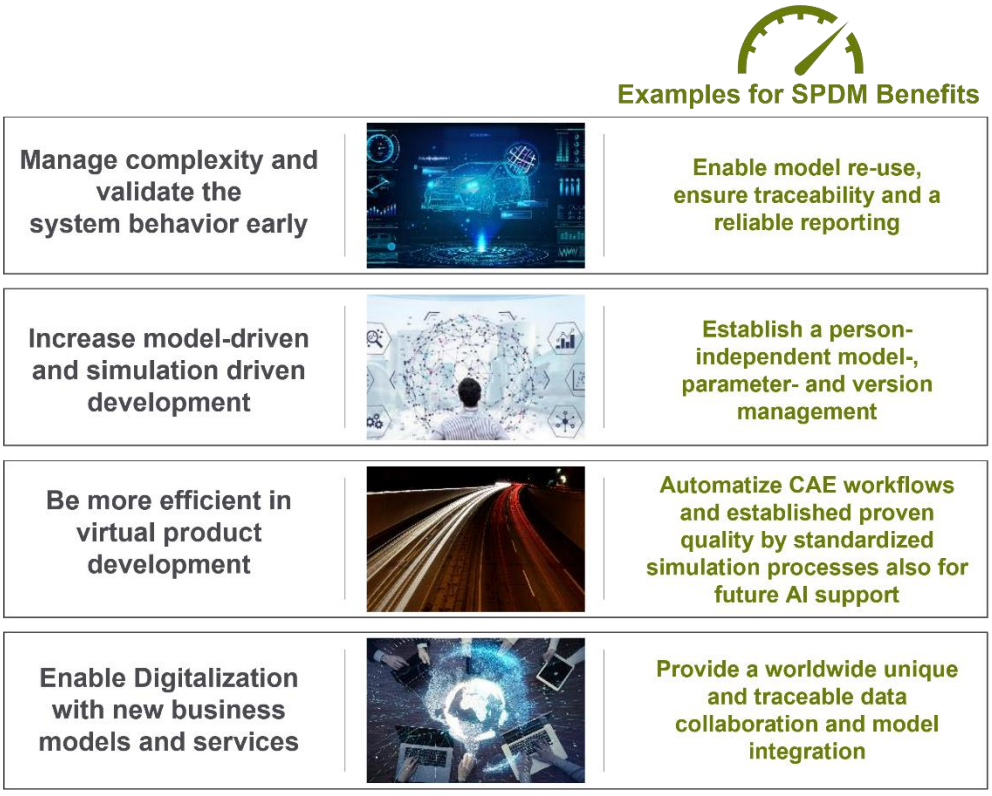

Figure 1 Current Challenges in Digital Engineering – and how SPDM Can Help to Overcome them

2 Benefits of SPDM Systems

The implementation and usage of an SPDM system creates various synergies and benefits in the product development. We distinguish between company-wide benefits and day-to-day benefits for the simulation engineers [1].

2.1 Company-Wide Benefits

Simulation Data Management offers benefits across company functions:

- **Traceability:** SPDM enables audit transparency, allowing for seamless tracking of simulation data throughout processes.
- **Enhanced Security:** SPDM protects against data breaches, ensuring the confidentiality and integrity of sensitive information.
- **Compliance Assurance:** SPDM ensures adherence to standards such as rights and roles, ASPICE, TISAX, etc., facilitating regulatory compliance.
- **Efficiency Optimization:** SPDM streamlines processes and automation, enhancing operational efficiency by enabling the reuse of models, standardization, and avoiding unnecessary simulations.
- **Democratization of Simulation:** SPDM provides widely accessible workflows, democratizing simulation processes and making them available across teams and departments.
- **Foundation for Digitalization:** SPDM lays the groundwork for future digital initiatives such as Digital Twins, data analyses, and alignment of simulation and testing.

2.2 Benefits for Simulation Engineers

In the daily work of the simulation engineers the following benefits can arise:

- **Global Data Access:** SPDM facilitates rapid collaboration by providing fast worldwide data access, overcoming bandwidth limitations.
- **Simplified Data Utilization:** SPDM enables easy access and reuse of resources such as models, reports, and parameters, streamlining workflows.
- **Enhanced Collaboration:** SPDM fosters seamless teamwork across locations through shared data access and real-time notifications.
- **Automation Potential:** SPDM empowers teams to automate routine tasks, allowing them to focus on expert activities and innovation.
- **Improved Model Quality:** SPDM aligns simulation with physical tests, enabling simulation teams to achieve higher-quality models with greater accuracy and reliability.

3 Overview of typical SPDM Capabilities

SPDM includes all Methods, Processes and Tools that are important for the simulation and calculation as well as the activities and interfaces which are necessary to integrate CAE in the overall product development process. Figure 2 gives an overview of the capabilities of SPDM.

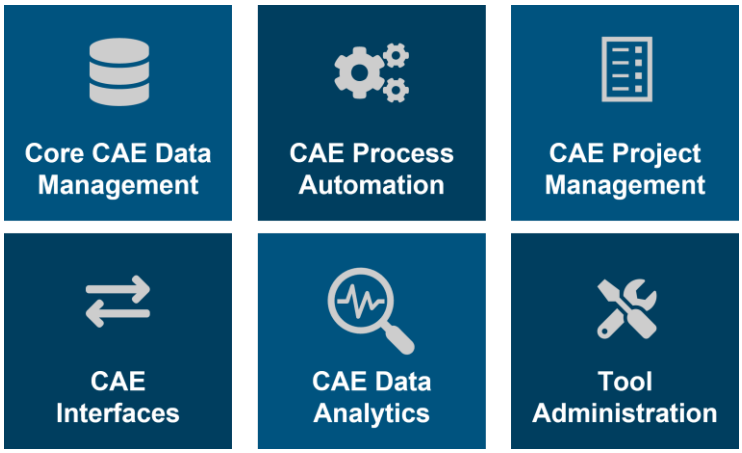

Figure 2 Overview of SPDM Capabilities

In the SPDM context, there are six main capabilities, which are necessary for the successful usage of SPDM:

- **Core CAE Data Management:** Description of the PDM Core Functionality, e.g handling of data, documents inclusive versioning libraries/ templates.
- **CAE Process Automation:** Includes elements for the automation of the simulation processes.
- **CAE Project Management:** Deals with topics of which related to project management, e.g. Task/ Request Management and Resource Planning.
- **CAE Interfaces:** Integration of different tools into the SPDM environment. Each tool integration can be implemented in different stages/levels. From simple integration to complete, automated integration.
- **CAE Data Analytics:** Supports the Simulation Engineers in the analytics of their simulations. For example in the search of metadata, result comparison or in the management of the results.
- **Tool Administration:** Describes different topics in the administration of the SPDM environment, for example the rights and roles management or the customization of the data model.

4 IT Architecture Alternatives for SPDM Solutions

For the successful integration of an SPDM solution in the existing brownfield of a company, a suitable IT architecture in is necessary. Both horizontal (between different domain-specific data management solutions) and vertical integration (e.g. to the engineering applications) are of importance.
In Figure 3, different examples and possibilities for IT architectures are displayed.

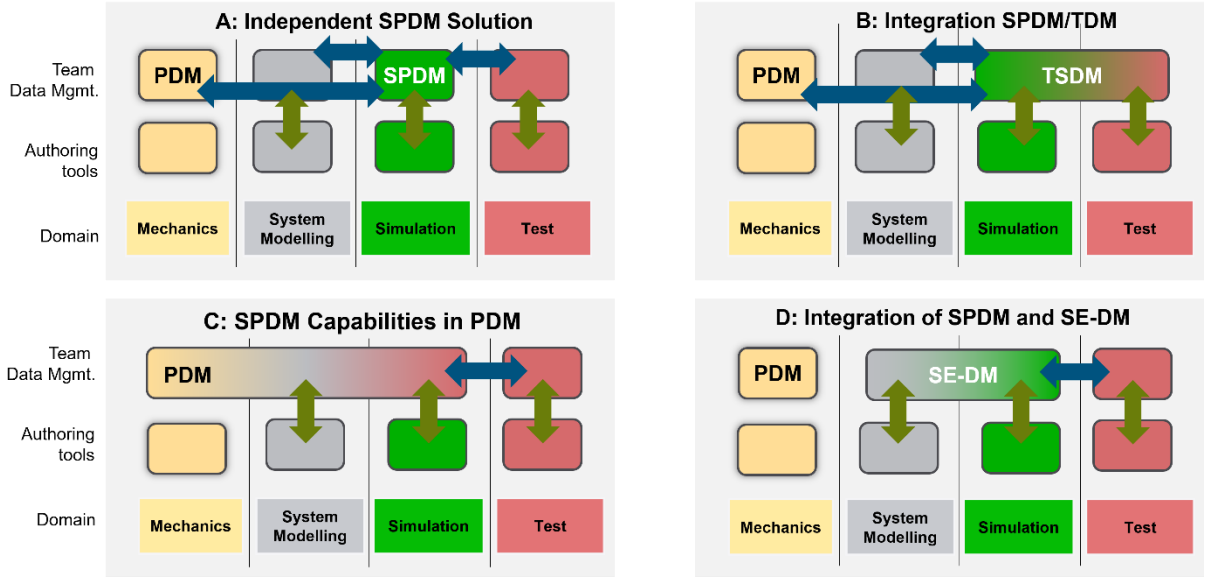

Figure 3 Alternative IT Architectures

- **A: Independent SPDM-tool:** Stand-alone SPDM solution with interfaces for horizontal and vertical integration
- **B: Integration SPDM/TDM:** combined solution for the management of simulation data and test data
- **C: PDM provides SPDM functions:** integration of SPDM capabilities (cf. section 3) into the product data management solution
- **D: Integration with SE:** combined solution for the management of simulation data and systems engineering data

5 Standard Procedure for SPDM Selection using the :em AG Methodology for model-based IT architectures (MBITA®)

Building on 20 years of experience in SPDM projects, the :em AG has developed a standard procedure for the selection and introduction of SPDM systems and has applied this approach successfully at many customers over the years. The procedure is subdivided into ten steps and is supported by the :em methodology of model-based IT architectures (MBITA®, cf. section 6).

When starting a project, the ten standard steps are specifically adapted to the situation of the customer. This adaptation and the definition of the process scope is carried out in the project kick-off. In the next steps, stakeholder workshops and interviews for identification of potentials, benefits, the SPDM and simulation target picture, analysis of use cases and IT environment (including necessary interfaces) are conducted. Depending on the customer's preferences, these analyses can be carried out online or in onsite workshops. After these workshops, the first analysis phase is completed, followed by an evaluation and processing of the findings. Requirements are derived and prioritized. The requirements are clustered into technical requirements, IT requirements, and commercial requirements. With the next steps, a rough plan for the implementation is defined and a business concept is developed.

These steps are followed by an SPDM tool benchmark and the tool decision, which leads to a proof of concept (PoC) with the selected tool. The project is concluded with a pilot project and/or a rollout implementation. Alternatively, the capability analysis in step 7 can also result in finding that sufficient capabilities are already available in the current IT landscape and no additional dedicated SPDM system has to be acquired. Instead of the tool selection in steps 8 and 9, enabling already existing tools can be in focus.

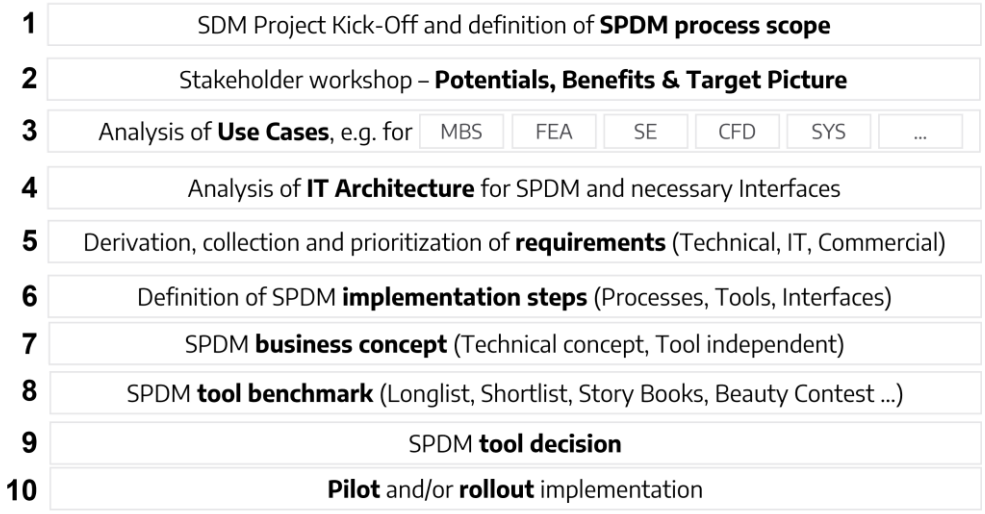

Figure 4 Methodology and Project Approach in a SPDM Project [2]

6 The MBITA methodology for Model-Based IT Architectures

The MBITA® methodology (Model-Based IT Architectures), a registered trademark of :em AG, brings the IT systems in question into a comprehensive end-to-end process context. With a model-based approach that can be used in a variety of IT solutions, MBITA® reduces complexity, avoids costly redundancies and prepares companies for efficient and targeted digitalization.

MBITA® is part of every SPDM selection project of the :em AG. In the beginning of the projects, the as-is processes and their activities, the relevant IT systems, information objects, pain points, capabilities, and the current data storages are documented with MBITA®. The methodology closes the loop (see Figure 5) from the analysis of the as-is processes to to-be use cases and requirements for the future IT landscape, which in turn will lead to new to be activities in the processes. It thereby provides traceability throughout the entire project - from the first interview to the final roll-out requirements for the future SPDM system.

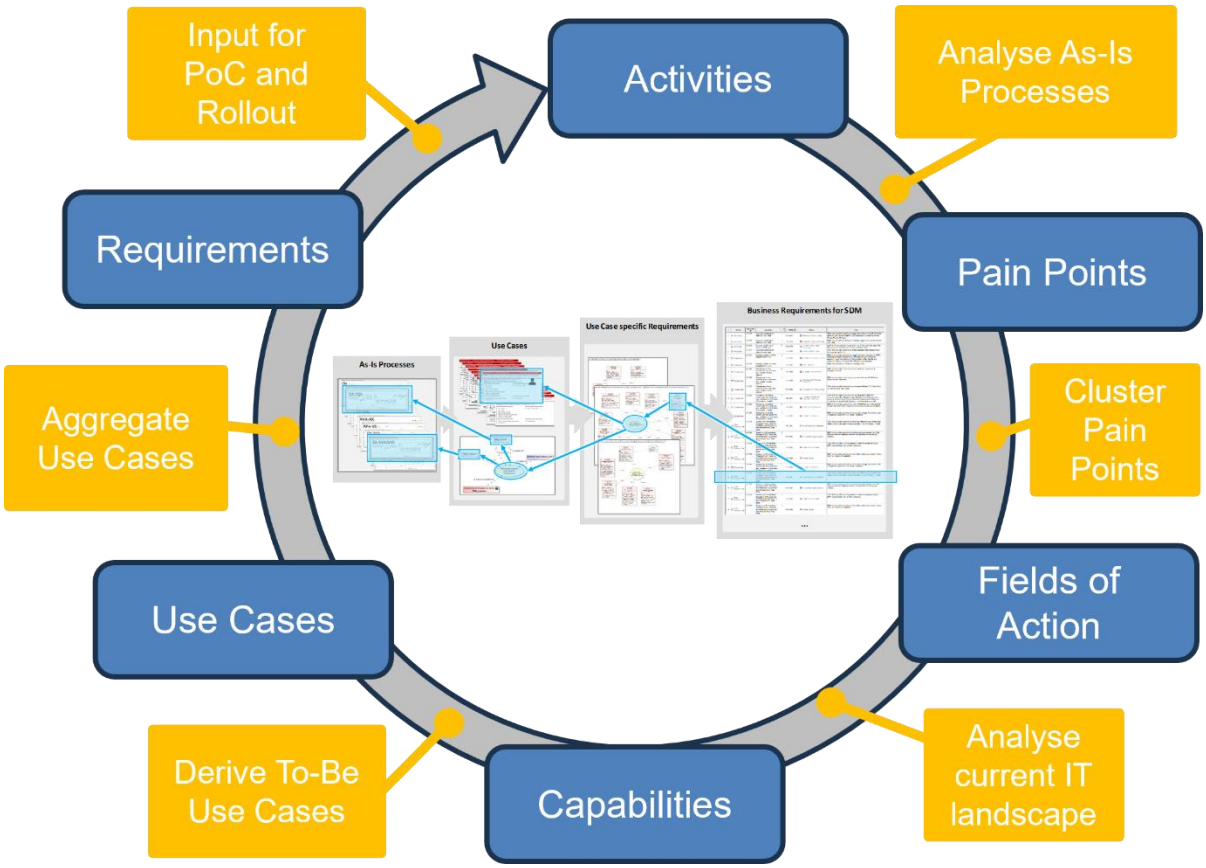

Figure 5 Model-Based approach with the MBITA® Methodology [8]

7 Lessons Learned from 20 years of SPDM Consultancy

In the last 20 years various points for improving the developed standard procedure were documented and various aspects were summarised as do's and don't's:

- **Do's:**
  - An SPDM solution selection should be accompanied by a **capability analysis**. SPDM needs to be integrated into the IT landscape (interface to PLM, ERP, PDM, etc.)
  - **Allocate resources** ahead of time – after vendor selection and POCs, significant efforts for roll-out and maintenance are to be expected.
- **Dont's:**
  - Don't judge a book by its cover – demos and vendor presentations can only give an indication. The full potential of an SPDM solution can only be assessed in **POCs** due to its integrative nature.

Furthermore, five factors have crystallised which contribute to the success of an SPDM evaluation project:

- Clear SPDM vision oriented to the company´s business strategy
- Clear SPDM concept understandable for the business departments
- Clean communication and involvement of stakeholders at all levels and Top management commitment
- Committed and willing employees and trustworthy (external) partners
- Accept that SPDM OOTB (Out of the Box) is an illusion and use this know-how early in the project

8 Examples for SPDM Projects in different Industries

The insights named above ground on trustful partnerships and successful SPDM projects over two decades for example in the automotive industry, manufacturing machines, or in the construction equipment. Table 1 lists some examples of SPDM projects.

Table 1 - Examples for SPDM Projects of the :em AG

Company	Focus Points of the Projects	Reference
Magna Powertrain	From Analysis of processes - to the rollout of an SPDM system	[2]
ZF	Simulation as a Service – SE-DM as a Basis for CAE- und AD-Simulations	[3]
BOSCH Rexroth	Management of Simulation Data within PLM	[4]
Brose	SDM as a building block for digitalization along the development process	[5]
Hilti	Systematic SPDM System selection, PoC Planning and realization	[6]
Bosch	Connecting SPDM capabilities of Teamcenter and Optislang	[7]

Building on this experience in successful projects, we are looking forward to the next 20 years of introducing SPDM at our customers.

9 References

[1] Krastel, M.: “And Yet! The Benefit and Efficiency Gain Through SPDM Can Be Quantified and the ROI is Quickly Achieved”. NAFEMS World Congress 2021.

[2] Schweigert-Recksiek, S., Riener, H., Koch, P., Meier, D., Daners, A., & Krastel, M.: “Handling the Complexity of Tool Selection Processes–Simulation Data Management in the Automotive Supplier Industry”. In DS 121: Proceedings of the 24th International DSM Conference (DSM 2022), Eindhoven, The Netherlands, October, 11-13, 2022 (pp. 88-97).

[3] Moraw, J.: “Simulation as a Service – SE-DM as a Basis for CAE and AD-Simulations at ZF”. Engineering Process Day (EPD) :em AG, Böblingen, 2019.

[4] Haas, U.: “Management of Simulation Data within PLM@DC”. Engineering Process Day (EPD) :em AG, Darmstadt, 2021

[5] Merklein, A.: “SDM as a building block for digitalization along the development process”. Engineering Process Day (EPD) :em AG, Böblingen & Tupy, M. SDM Roundtable, Darmstadt, 2019.

[6] Göttlinger, M.: „Zur Einführung von Cloud-basiertem SPDM in multidisziplinären Simulationsteams“. Engineering Process Day (EPD) :em AG, Darmstadt, 2024

[7] Brunk, M.: SDM @ BOSCH: TC UND OPTISLANG. SDM Roundtable, ;em AG, Darmstadt, 2019.

[8] Fischer, M., Schoft, K.: “Implementation of a Test Data Management (TDM) System at Brose for Realization of Hybrid Validation”. NAFEMS, Bamberg, 2021.

Leveraging Business Process Management for CAE-based Product Development

Kay Schmidt (Cummins Deutschland GmbH)

Tobias Gloesslein (ESTECO Software GmbH)

1 Summary

This abstract delves into the application of Business Process Management (BPM) technology to a simulation-based swirl atomizer development process at Cummins Emission Solutions, showcasing its potential impact on complex engineering design workflows. The envisioned approach facilitates simulations with multiple levels of fidelity through a managed process while involving actors/stakeholders with different roles and backgrounds with the goal of making traceable and well-informed design decisions.

The previously presented vision of the development process shown in Fig. 1 kicks off with an analytical model for early optimization, then progresses through 3D Computational Fluid Dynamics (CFD) analyses and experimental testing while concurrently exploring the robustness of chosen design alternatives [1]. For this application BPM emerges as a pivotal technology for practical implementation, ensuring an incremental enhancement of certainty, model fidelity, and design maturity while democratizing the process for all stakeholders. This democratization is also seen with the use of simulation as a whole with respect to the product development process through the application of a BPM workflow and Multi-disciplinary Design Optimization (MDO) [2]. Compared to the traditional use of simulation in these processes, this vision allows for simulation based development to happen from the early stages. This is also enabled by automated Computer-Aided Engineering (CAE) processes that are tightly integrated into the business process model and its execution as part of this application.

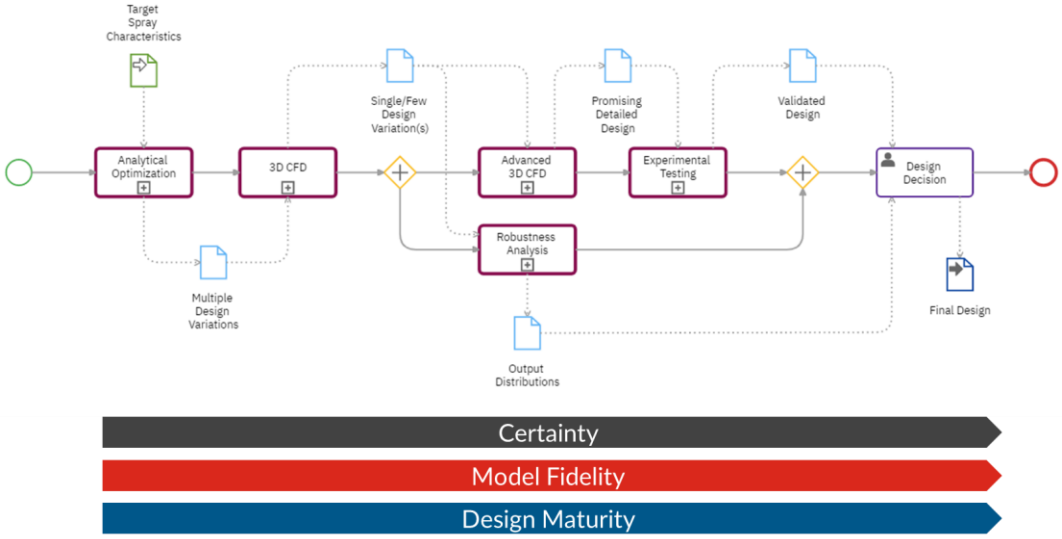

Fig. 1
High level overview of business process vision for CAE-based swirl atomizer development [1]

2 Benefits of BPM in CAE

Four main benefits have been identified through the application of BPM in this context during an initial implementation:

2.1 Process Management

BPM adds structure into the engineering design process or any other modeled process for that matter by automatically facilitating a seamless handover between tasks and the respective data, ensuring its advancement without unnecessary delays. The data (text, files, scripts, models, etc.) is stored in an accessible way, promoting transparency and efficiency (eliminating the search for relevant data) while respecting access control.
At the same time BPM can be used to enforce a modeled process flow. This is useful for actors within that process by removing any uncertainty of whether they are working by the process as intended and the need of having to figure this out in the traditional way – which is only a distraction. From the perspective of the process manager this is also an improvement as they can spend less time monitoring whether the process is being followed.

2.2 Task Assignment

Through BPM, tasks are defined during the modeling of a process and assigned to team members when the necessary information/data is available (preceding tasks are complete/dependencies fulfilled) during the execution of the model. This systematic approach ensures that actors/team members advance in the process once all necessary information is documented, promoting accuracy and reducing errors.

2.3 Traceability

BPM provides real-time visibility into the status of a project and tasks, enhancing transparency across the development process. For this application all relevant data is centralized (stored or linked to) within ESTECO VOLTA, a platform for digital engineering and simulation management, where the business process workflow is created and executed, streamlining data retrieval, allowing for full traceability of data and processes, and creating a collaborative environment. Through the tight integration of automated simulation processes and human tasks within the business process layer traceability can be ensured and streamlined independently of the data source.

2.4 Version Control

BPM ensures that team members consistently use the correct version of methods and models. Subject Matter Experts (SME) can easily update and maintain their methods, eliminating the use of outdated versions by other actors in the process. The association of results with specific versions of methods or automated simulation processes is clearly visible, enhancing accuracy and reliability.

3 Case Study: Swirl Atomizer

When developing a new swirl atomizer there is a multitude of different goals like a target mass flow rate, spray angles, droplet sizes and more. Developing these swirl atomizers for a system like the one shown in *Fig. 2* involves many different actors, especially when pursuing a CAE-based development strategy. From this perspective it (at the very least) includes design engineers, project managers, simulation engineers and test engineers.

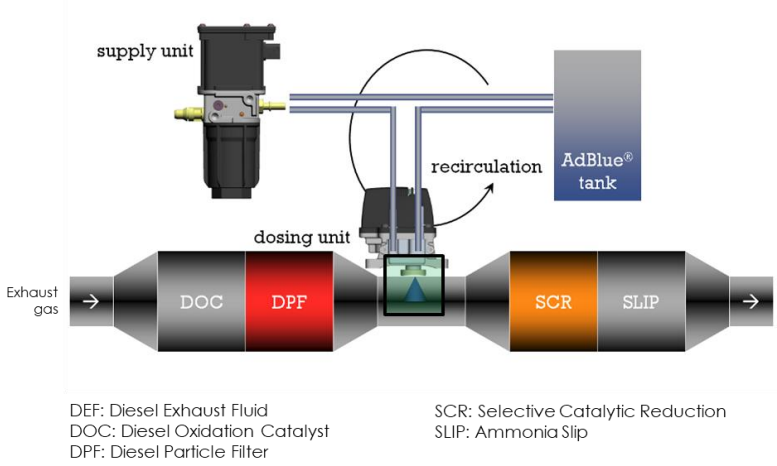

Fig. 2
Schematic of UL2.2 SCR-Dosing System with urea spray and swirl atomizer boxed in green

The same approach can be applied to a wide variety of product development processes and is mostly product independent. The specific models, simulation methodologies, requirements and goals change,

but the overall process will be similar when pursuing simulation based product development. In any of these cases all actors get involved at different and often multiple points of the development process. Each time they require some data/information to carry out a task that will in turn produce new data/information that is required elsewhere. For the sake of efficiency it is crucial that participants within this process have the right information made available to them at the right time. This avoids using the wrong inputs to complete a task and takes away the traditionally large amounts of time that are required to compile all of the necessary data. Creating an executable business process model that not only maps out the process flow (tasks), but also the flow of data between tasks accomplishes exactly that.

3.1 Creating the Business Process Model

Following the ideas behind 2.1 and 2.2 a business process model based on the BPMN 2.0 standard was created in the VOLTA Modeler for the conceptualized simulation based product development process of a swirl atomizer [3]. In its first iteration this process focuses on two aspects of the vision shown in *Fig. 1*, the analytical optimization as well as the first set of 3D CFD simulations. The process model is to be expanded to include the other parts shown in this vision (analysis of robustness and integration of physical testing) as a next step. The modeled part of the business process includes the definition of swirl atomizer requirements and optimization strategies. The post-processing of simulation results including the selection of the most promising candidates (design variations) with their subsequent automated validation is also modeled. In this application all of the simulations with their corresponding strategies wrapped around them are fully automated through simulation processes/workflows. These workflows are embedded into the business process through VOLTA Service Tasks as shown in the schematic representation of this in *Fig. 3*.

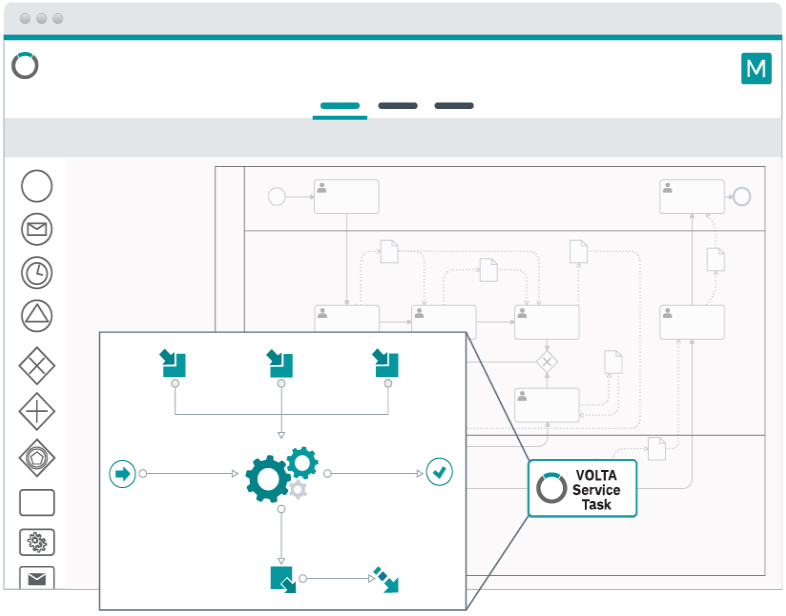

Fig. 3
Schematic of business process modeler showing the use of a service task to embed a simulation process automation within a business process model

Through this implementation a SME can ensure that the right methodologies and models are used at their respective points throughout the process. This also ensures traceability and version control as per 2.3 and 2.4, respectively. As soon as all of the preceding tasks have been completed and the necessary information has been collected, simulation processes like the analytical optimization of the swirl atomizer geometry are automatically started using inputs from the business process layer. In this case, the design engineer can define different targets like the mass flow rate in a so called human task which are then automatically passed to the service which uses this information in its optimization. Setting this business process model and the simulation process models up in this way allows for the repeatability of the process as a whole. At the same time it removes tedious and error prone tasks while allowing the different actors to focus on their area of expertise. In addition to these tasks, additional ones have been added to include approval processes and to verify information at different stages throughout the process. This is a useful mechanism to ensure that any necessary approvals

were given, certain stakeholders are made aware and to allow for technical advisors and SMEs to interject as necessary (all to avoid unnecessary iterations/repetitions).

Modeling the business process has shown to be beneficial on its own by allowing for the identification of inefficiencies and by producing a human readable process model that helps with the bigger picture understanding. However, for this application its execution and management is at least as useful as the model itself.

3.2 Executing the Business Process Model

After the modeling of the process it is exported to the respective business project as a new version. From here any number of instances (sequential and in parallel) of this project can be executed. Each instance of the process (running or completed) reflects an independent swirl atomizer development process. Individual human tasks are then assigned to actors or teams within the scope of the project. As all of the tasks that another depends upon are completed, it automatically gets started and any data that is defined as an input to this task is automatically passed to it. An overview of all of the running and completed tasks is used to abstract the complexity of the bigger picture process for the individual stakeholders involved. An example of this for an intermediate state of the swirl atomizer process is shown in the Kanban board style view in Fig. 4.

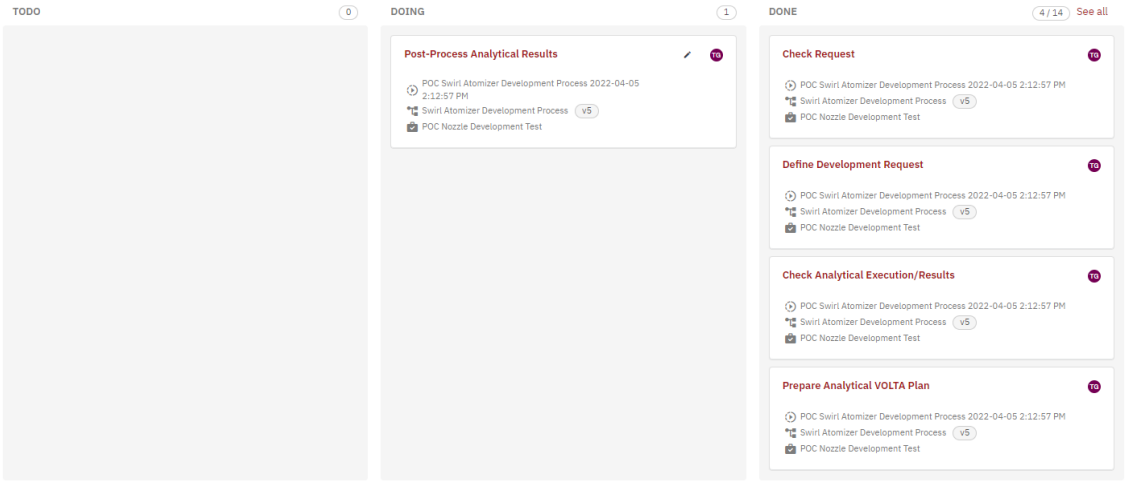

Fig. 4
Kanban board style overview of the completed and active tasks of an instance of the swirl atomizer development process divided into “Todo”, “Doing” and “Done” columns

With respect to this specific use case an actor defines the requirements for a new swirl atomizer as part of a request which is then automatically passed to another actor who assesses it. Once approved another or one of the past actors receives the requirements and generates an optimization strategy for the analytical simulation method. Once this is completed the strategy is automatically executed over the simulation process via the service task. The results of this analysis are then fed back into the business process where one or more of the actors post-process them. This approach goes on until the process has been completed and can involve multiple iterations of parts of it. Throughout all of this, the necessary data for each task is automatically supplied to the respective actor(s) and the process flow is ensured. Actors do not have to question whether they are following the process as they are directly interacting with it as per its automated flow. During or after the execution all of this data flow and process history can be viewed. This level of traceability allows for easier knowledge transfer, can help with troubleshooting down the line and can result in the identification of inefficiencies in the process/model.

4 Conclusions

These and the benefits mentioned in Chapter 0 are already seen to extend beyond the use-case of the development of a swirl atomizer, showcasing the versatility of BPM in enhancing various business processes. Whether in simulation-intensive applications or broader business contexts, the integration of BPM in this manner provides a systematic, transparent, and efficient approach while offering a framework for easier collaboration and traceable decision-making across different types of workflows. This requires not only the capability of modeling such processes, but also the ability of executing them in an environment that allows for their management as well as that of any related processes and data

in a traceable way. At the same time the combination and use of BPM, MDO and even generally simulation process automation throughout the development process further democratizes simulation. The business process workflow generated for the swirl atomizer use-case was already tested, but is yet to be applied to a new development project.

5 References

[1] Gloesslein T., Schmidt K., Haghighi R.: “Development and Democratization of Simulation-Based Swirl Atomizer Development Processes”, NAFEMS Regional Conference Americas, 2022

[2] Schmidt K.: “A personal experience to drive democratization in your product development environment”, Simulation Leadership Forum, 2024

[3] Object Management Group (OMG): “About the Business Process Model and Notation Specification Version 2.0.2”, https://www.omg.org/spec/BPMN/2.0.2/About-BPMN, 2024

[4] Turchetto M., Viola A.: "The Impact of Business Process Modeling in the Context of SPDM Environment: A Human-In-The-Loop Approach for Design Optimization and Business Decision Making", NAFEMS World Congress, 2023

Unsupervised physics-informed deep learning of the flow around an airfoil using a mixed-variable network

Jan Hauke Harmening, Franz-Josef Peitzmann (Westphalian University), Ould el Moctar (University Duisburg-Essen)

1 Summary

Physics-informed deep learning has emerged as an efficient technique for predicting flow fields by training networks to satisfy the underlying equations. However, successful applications of unsupervised learning to complex flow scenarios at high Reynolds numbers remain limited. In this study, we explore a novel unsupervised learning approach to predict the 2.5-dimensional flow field around an airfoil. Through the integration of a mixed-variable network and a vector potential function, the resulting optimization problem featured increased prediction accuracy and speed. The trained network successfully captured essential flow features, including the high gradient boundary layers and the wake of the airfoil. The model was trained to solve the Reynolds-averaged Navier-Stokes equations considering Prandtl's mixing length model. We conducted a sensitivity analysis on the network architecture and quantity of training points. Validation against CFD simulations exhibited a favorable agreement with the reference data, considering that no labeled training data were provided during training. Comparisons with a traditional network architecture showed a superior performance of the proposed mixed-variable vector potential function approach. The study demonstrates the potential of physics-informed deep learning for simulating complex fluid dynamics and offers an avenue for surrogate modeling with a minimum of simulations or measurements.

2 Introduction

Deep learning is a powerful method to yield surrogate models of complex functions. In computational physics, deep learning can be used to teach neural networks correlations between parameters such as lift of an airfoil depending on variables such as angle of attack. Trained models can be used in optimization processes, for real-time steering algorithms, and to gain an enhanced understanding of a system, among others. To train these networks, however, large datasets are necessary that either need to be simulated or measured. Hence, more sophisticated methods are desirable that feature minimal requirements for labeled training data.

Recently, physics-informed deep learning has emerged as an efficient technique for predicting solution fields [1,2]. Using the physics-informed approach, a network is trained to predict spatial or spatio-temporal fields (such as velocity and pressure fields) by penalizing violation of the governing equations (such as the Navier-Stokes equations) with a corresponding loss that is minimized during the training process. As the correct solution of the governing equations does not need to be known a priori, the method can be understood as an unsupervised deep learning approach. Consequently, requirements for sizes of labeled datasets are minimal.

In the field of fluid dynamics, the unsupervised approach was successfully applied in several studies that covered laminar flows at low Reynolds numbers [3-5]. At high Reynolds numbers, emerging turbulence, high gradient boundary layers, and the dominance of the nonlinear convective terms of the Navier-Stokes equations make training of neural networks more challenging. Reynolds-averaging in combination with turbulence modeling is a popular method to eliminate temporal dependencies and the small-scale turbulent structures and, thus, simplify the problem. To promote the training success, additional labeled data can be introduced into the training routine, rendering it semi-unsupervised. In fact, a majority of studies that applied physics-informed neural networks (PINNs) at elevated Reynolds numbers utilized labeled data [6-8] while truly unsupervised approaches remain sparse [9]. In the present work, we contribute to the question of unsupervised physics-informed deep learning methods by applying a novel mixed-variable approach in combination with a vector potential function that has shown great potential in 2-dimensional cases [10,11]. The scope of our study was to explore methods that might be used to generate surrogate models with minimal efforts for simulations or measurements.

3 Method

3.1 Geometry and Flow Field

The physics-informed deep learning method was applied to the flow around the DU99W350 airfoil at an angle of attack of 5°. The airfoil had a chord length c of 1 m and a span s of 2 m and was situated inside a channel. The corresponding 2.5-dimensional flow was subject to a Reynolds number of 2×10^5 and featured a stagnation region at the leading edge, developing high gradient boundary layers, a low-pressure high-velocity suction side on the airfoil, as well as a small wake at the downwind half of the airfoil.

3.2 Governing Equations

The described flow field is governed by the continuity equation as well as the incompressible Reynolds-averaged Naver-Stokes (RANS) equations that read as:

$$\frac{\partial \bar{u}_i}{\partial x_i} = 0 \qquad \text{and} \qquad \bar{u}_j \frac{\partial \bar{u}_i}{\partial x_j} = -\frac{1}{\rho}\frac{\partial \bar{p}}{\partial x_i} + \mu_{res}\frac{\partial^2 \bar{u}_i}{\partial x_j \partial x_j} \tag{1}$$

Here, $\bar{u}_i$ and $\bar{p}$ are the Reynolds-averaged velocity components and pressure, x_i are the spatial dimensions, ρ is the constant fluid density, and μ_{res} represents a resulting dynamic viscosity. The resulting viscosity is computed as the sum $\mu_{res} = \mu + \mu_t$ of the constant fluid viscosity μ and a turbulent viscosity μ_t that is used to model the effects of the turbulent eddies on the mean flow.

3.3 Physics-informed Deep Learning Method

In the present study, we used Prandtl's mixing length model to calculate μ_t. Several turbulence models, including more sophisticated models such as the k-ω model were evaluated in a preliminary study. The other tested models were subject to stability issues during the training process, resulting in unusable predictions. Hence, the simple yet robust mixing model was selected here. Using the mixing length model, the turbulent viscosity was computed as:

$$\mu_t = l_m^2\sqrt{G}, \qquad G = 2\bar{S}_{ij}\bar{S}_{ij}, \qquad \bar{S}_{ij} = \frac{1}{2}\left(\frac{\partial \bar{u}_i}{\partial x_j} + \frac{\partial \bar{u}_j}{\partial x_i}\right), \qquad \text{and} \qquad l_m = \min\left(\kappa d, 0.09 d_{max}\right) \tag{2}$$

Here, l_m is the mixing length, $\sqrt{G}$ is the magnitude of the mean rate of strain tensor, $\bar{S}_{ij}$ are the strain components, $\kappa \approx 0.4$ is the von Kármán constant, d is the wall distance and d_{max} is a characteristic turbulent length scale, here calculated as $d_{max} = V/A$ with $A = 2cs$.

In this work, two different PINNs were compared. The first type is a traditional PINN, that is trained to solve the governing equations (1) and (2). The traditional neural network reads as:

$$NN_\theta(x, y, z, d_s) = (u, v, w, p) \tag{3}$$

where NN is the neural network, θ are the trainable parameters (weights and biases) of the network, x, y, and z are the coordinates, d_s is the scaled wall distance, and u, v, w, and p are the velocity components and the pressure. The scaled wall distance was calculated as:

$$d_s = \frac{1}{d + 1000} \approx 0.001 \tag{4}$$

The second type is a mixed-variable vector potential function (m-v-vpf) network. For this network, the governing equations are re-organized using the stress tensor σ_{ij}:

$$\bar{u}_j \frac{\partial \bar{u}_i}{\partial x_j} = -\frac{1}{\rho}\frac{\partial \sigma_{ij}}{\partial x_j}, \qquad \sigma_{ij} = -p\delta_{ij} + \mu_{res}\left(\frac{\partial \bar{u}_i}{\partial x_j} + \frac{\partial \bar{u}_j}{\partial x_i}\right), \qquad \text{and} \qquad p = -\frac{1}{2}\sigma_{ii} \tag{5}$$

Here, δ_{ij} is the Kronecker delta. The mixed-variable network was trained to not only predict the velocity and pressure field but also the stress components σ_{ij} that must satisfy equations (5) and (2). The purpose of this architecture is to eliminate the second order derivatives of the network outputs in equation (1) and to reduce the computationally costly total number of derivations required for every evaluation of the losses.

Moreover, a vector potential function ψ was applied to further simplify the optimization problem. The velocity components can be calculated from the vector potential function using the cross product:

$$\begin{pmatrix} u \\ v \\ w \end{pmatrix} = \nabla \times \begin{pmatrix} \psi_1 \\ \psi_2 \\ \psi_2 \end{pmatrix} \tag{6}$$

Here, ∇ is the Nabla operator, and ψ_1, ψ_2, and ψ_3 are the vector potential function components. Using the vector potential function, the continuity equation in (1) is automatically satisfied as $\nabla \cdot u = \nabla \cdot (\nabla \times \psi) = 0$. The corresponding vector potential function mixed-variable neural network reads as:

$$NN_\theta(x, y, z, d_s) = \left(\psi_1, \psi_2, \psi_3, p, \sigma_{xx}, \sigma_{yy}, \sigma_{zz}, \sigma_{xy} = \sigma_{yx}, \sigma_{xz} = \sigma_{zx}, \sigma_{yz} = \sigma_{zy}\right) \tag{7}$$

To train the neural networks, a composed loss function was built from the loss $\mathcal{L}_b$ corresponding to the boundary conditions and the loss $\mathcal{L}_e$ corresponding to the governing equations. The mean square losses $\mathcal{L}_b$ and $\mathcal{L}_e$ read as:

$$\mathcal{L}_b = \frac{1}{N_b} \sum_{n=1}^{N_b} \left| U_b^n - \widetilde{U}_b^n \right|^2 \qquad \text{and} \qquad \mathcal{L}_e = \sum_{k=1}^{3} \frac{1}{N_e} \sum_{n=1}^{N_e} |\varepsilon_k^n|^2 \tag{8}$$

where N_b and N_e are the numbers of training points on the boundaries and inside the domain, U_b^n are the given velocity values at point n_b and ε_k^n are the residuals of the k-th governing equation at point n_e. During the training, the parameters of the network are optimized to yield minimal losses. In case of a first derivative optimization algorithm such as Adams, the governing equations are then solved in an iterative procedure by updating the networks' parameters using $\theta := \theta - \eta \nabla \mathcal{L}(\theta)$, with η as the learning rate.

3.4 Network Architecture and Training Procedure

Fully connected feed-forward networks featuring tanh activation functions were used as NN_θ. The network parameters were initialized using the glorot uniform initialization. In the first step of the training, the Adam optimizer was deployed with an initial learning rate η of 0.001. The learning rate was reduced by a factor of 0.9 every 2,000 iterations for a total of 100,000 iterations. Afterwards, the L-BFGS optimizer was deployed. For the airfoil surface, a no slip boundary condition was defined. At the lateral planes in spanwise direction, the plane-normal velocity was restrained to zero. At the inlet face as well as the upper and lower walls, an axial velocity of 1 m/s was prescribed in the chord direction of the foil and the other velocity components were set to zero. At the outlet, a zero spanwise velocity component was prescribed. The training was conducted using the TensorFlow-based Python library DeepXDE [12] on a 16 GB NVIDIA Quadro RTX 5000.

To evaluate the network's size and shape, a sensitivity analysis was conducted using the m-v-vpf network. Furthermore, a sensitivity analysis concerning the number of training points N_b and N_e was carried out. Tab. 1 lists the evaluated network architectures and quantities of training points. The table also contains the computed overall mean squared error (MSE) of the predicted axial velocity field when compared to a reference CFD simulation.

Tab. 1: Parameters and results of the sensitivity analysis

Label	Layers	Neurons	Parameters	N_b	N_e	Purpose	MSE
N40L24	24	40	38,280	17,500	35,000	Reference	8.2×10^{-3}
N45L27	27	45	54,450	17,500	35,000	Network size	9.2×10^{-3}
N35L21	21	35	25,690	17,500	35,000	Network size	12.3×10^{-3}
N64L10	10	64	38,336	17,500	35,000	Network shape	14.1×10^{-3}
N33L34	34	33	37,488	17,500	35,000	Network shape	13.0×10^{-3}
N40L24	24	40	38,280	21,000	40,000	Training points	8.6×10^{-3}
N40L24	24	40	38,280	14,000	30,000	Training points	10.0×10^{-3}

The results of the sensitivity analyses emphasize the suitability of the N40L24 model when applied with 35,000 points inside the volume and 17,500 points distributed on the boundaries. Firstly, changing the shape of the network to a deeper and narrower shape or to a wider but shallower shape led to a deterioration in

accuracy. Secondly, reducing the size of the network correlated with a decreased accuracy while increasing the number of trainable parameters was also accompanied by a moderate decrease in accuracy. Thirdly, reducing the quantity of training points correlated with a decrease in accuracy while a further increase in the number of training points also slightly increased the MSE. While more training points and a larger network could potentially further improve the performance of the model, this also increases graphic memory consumption as well as overall training time. However, for the present study, the size of the problem was limited by the 16 GB graphic memory of the hardware.

3.5 Reference Data

The predictions of the trained models were compared with numerical simulations. The simulations were carried out using the finite volume solver STAR-CCM+ and the stationary incompressible RANS equations (1) were solved. As the PINNs need to compete with state-of-the-art computational models, the low Reynolds k-ω SST turbulence model of Menter [15] was selected for the reference computations. The domain was meshed using the trimmed cell mesher and featured 15 prism layers on the airfoil surface. All y^+ values were below 0.5. A grid sensitivity analysis was conducted using a grid refinement factor of 1.5 to assure the grid size independence of the reference solution.

4 Results and Discussion

The traditional model failed to capture the velocity and pressure field accurately, as shown in Fig. 1. The high velocity regions on the upper and lower sides of the airfoil were elongated in streamwise direction and separated from the airfoil by large shear layers. Furthermore, the pressure of the stagnation region was overestimated and the lower pressure regions on the airfoil were underestimated.

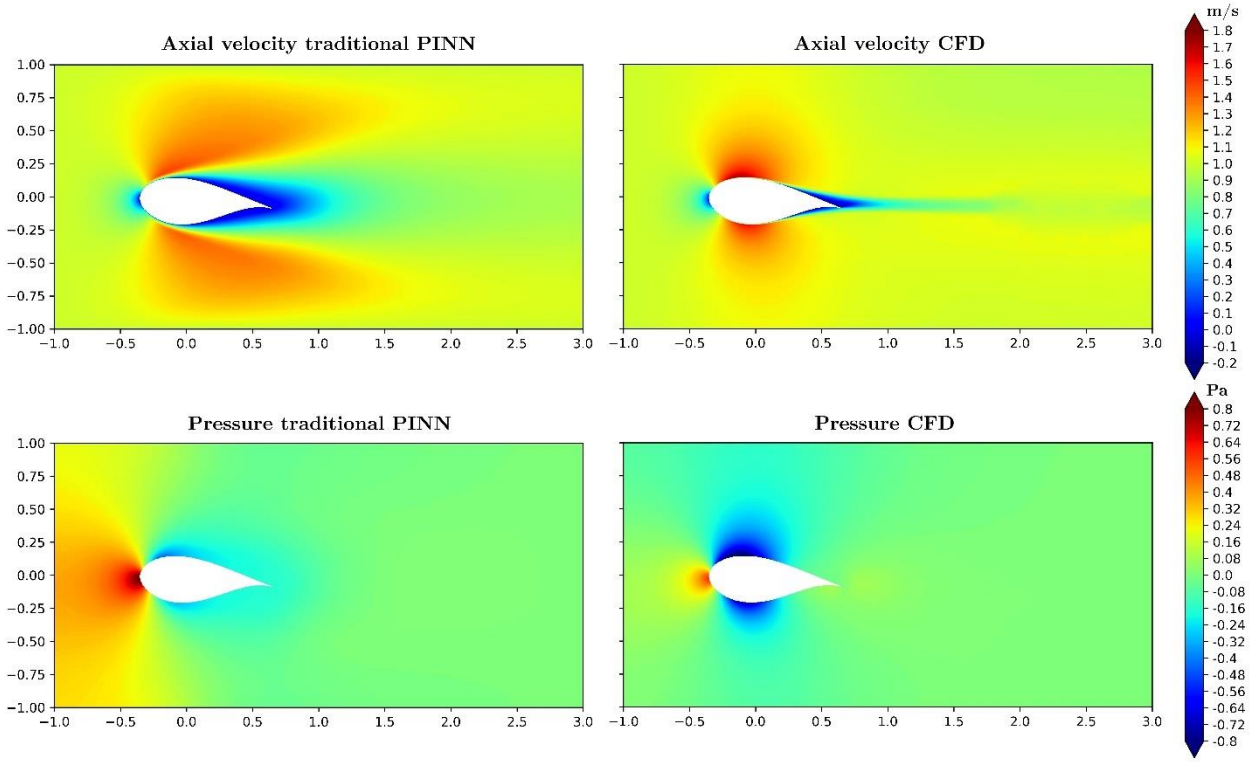

Fig. 1: Comparison of axial velocities (top) and pressure (bottom) around the DU99W350 airfoil as obtained by the traditional PINN (left) and the reference simulations (right).

The axial velocity field and the pressure field were well captured by the m-v-vpf network, as seen in Fig. 2. The model predicted the low velocity and high pressures of the stagnation region, high gradient boundary layers, the low pressure and high velocity region on the suction side as well as the wake of the airfoil

originating from the upper side as well as from the lower side. In comparison with the reference field, the size of the stagnation region as well as the airfoil wake were overestimated, and the boundary layer gradients as well as the high velocity regions were underestimated.

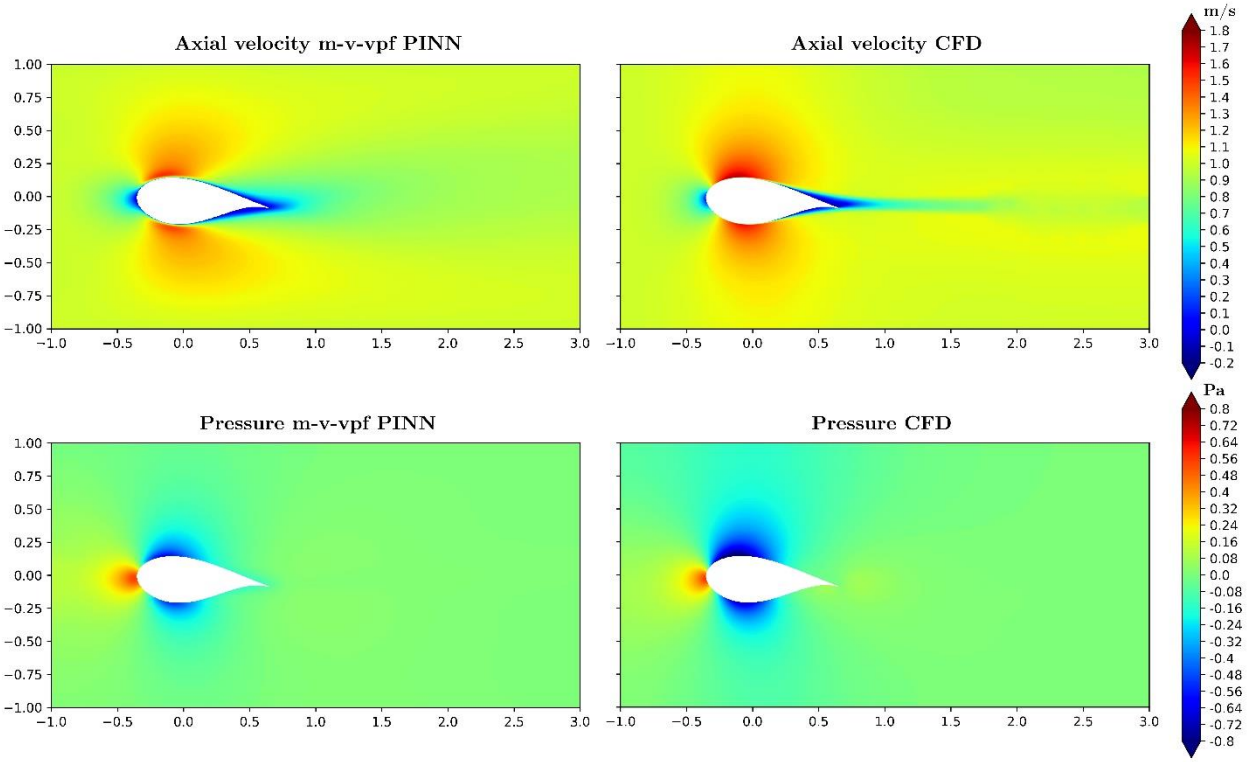

Fig. 2: Comparison of axial velocities (top) and pressure (bottom) around the DU99W350 airfoil as obtained by the mixed-variable PINN (left) and the reference simulations (right).

Fig. 3 exhibits the boundary layer profiles obtained by the three models on the suction side of the airfoil. As also visible in Fig. 1, the traditional PINN failed to capture the steep boundary layer. The m-v-vpf PINN provided a significantly improved prediction, capturing a high gradient, the velocity overshoot of the developing boundary layer, as well as the decline of the axial velocity for increasing distances from the surface. However, the boundary layer gradient as well as the magnitude of the velocity overshoot were still underestimated.

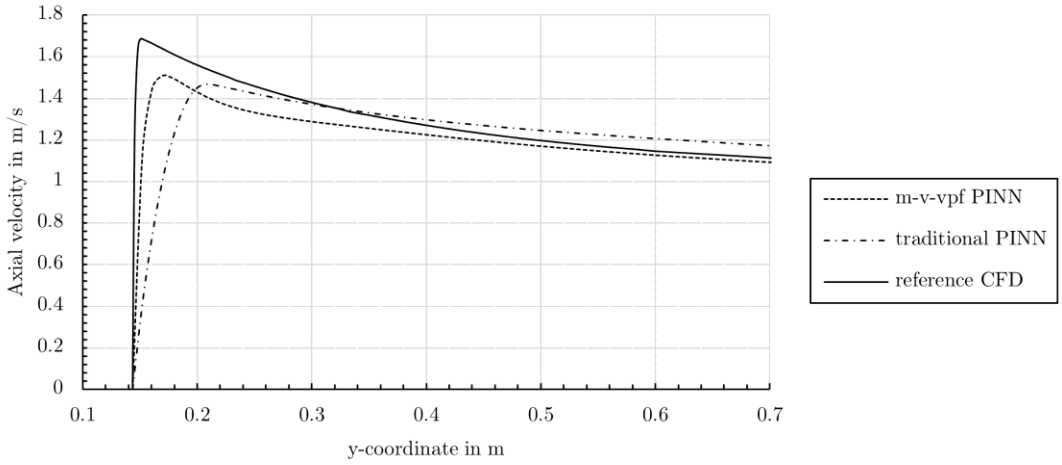

Fig. 3: Boundary layer on the airfoils' suction side at $0.25 \cdot c$ as obtained by the mixed-variable vector potential function (m-v-vpf) PINN, the traditional PINN, and the reference CFD computation.

The results of the present study emphasize the superiority of the mixed-variable vector potential function approach. In agreement with our findings, the traditional PINN method has also been shown to be unreliable in other studies [10,11]. The deviations between the PINNs and the reference CFD solution can be attributed to approximation errors, training or optimization errors, and turbulence modeling differences. The results of the sensitivity analysis do not suggest that qualitative improvements of the predictions can be expected when altering the network architecture or the number of training points. The excellent results of Harmening et al. [14], who used labeled training data, emphasize that the reference flow field can be modeled by much smaller networks and, hence, the contribution of the approximation error can be expected to be minimal. The prediction of the boundary layer could be improved by introducing a damping function. The turbulence modeling differences could be eliminated by incorporating the k-ω SST turbulence model into the governing equations. However, as the k-ω model exhibited stability issues during the preliminary tests, more advanced and stable deep learning methods are required to apply it. This also pertains to further reductions of the training error. There is a growing number of advanced methodological physics-informed deep learning studies and promising methods that could be applied to improve the performance comprise adaptive loss weighting methods [15,16], convolutional neural networks [17-20], curriculum or transfer learning [21], distributed PINNs [2], and network architecture optimizations [23], among others.

In general, *considering that no labeled reference data were provided during training*, there was a favorable agreement between the m-v-vpf PINN predictions and the reference simulations. The PINN was able to learn the structure of the flow and provided smooth and sensible velocity and pressure fields. Hence, the unsupervised method explored here could be used for qualitative comparative objectives. Highly accurate quantitative predictions can be obtained by using a semi-unsupervised approach and adding labeled training data from simulations or measurements [14].

5 Conclusions

In the present work, we applied unsupervised physics-informed deep learning to the 2.5-dimensional Reynolds-averaged flow around an airfoil at an elevated Reynolds number and compared the results of a traditional PINN to a mixed-variable PINN. The main findings of the study are:

- The mixed-variable PINN outperformed the traditional PINN. The traditional PINN did not capture the flow field accurately.
- The mixed-variable PINN captured the stagnation region, the high gradient boundary layers, the high- and low-pressure zones, as well as the wake of the airfoil and provided smooth and sensible flow fields.
- Prandtl's mixed length turbulence model showed to be a robust and reliable model for physics-informed deep learning.
- The mixed-variable PINN could predict the flow field accurately without provision of labeled data during training. Hence, the study offers an avenue for surrogate modeling of Reynolds-averaged flows with a minimum of training data.

6 References

[1] Lagaris I. E., Likas A., and Fotiadis D. I.: "Artificial neural networks for solving ordinary and partial differential equations", IEEE Transactions on Neural Networks, 1998 9(5), pp. 987-1000

[2] Raissi M., Perdikaris P., and Karniadakis G. E.: "Physics-informed neural networks: A deep learning framework for solving forward and inverse problems involving nonlinear partial differential equations", Journal of Computational physics, 2019 378, pp. 686-707

[3] Raissi M., Yazdani A., and Karniadakis G. E.: "Hidden fluid mechanics: Learning velocity and pressure fields from flow visualizations", Science, 2020 367(6481), pp. 1026-1030

[4] Sun L., Gao H., Pan S., and Wang J. X.: "Surrogate modeling for fluid flows based on physics-constrained deep learning without simulation data", Computer Methods in Applied Mechanics and Engineering, 2020 361, 112732

[5] Jin X., Cai S., Li H., and Karniadakis G. E.: "NSFnets (Navier-Stokes flow nets): Physics-informed neural networks for the incompressible Navier-Stokes equations", Journal of Computational Physics, 2021 426, 109951

[6] Eivazi H., Tahani M., Schlatter P., and Vinuesa R.: “Physics-informed neural networks for solving Reynolds-averaged Navier–Stokes equations”, Physics of Fluids, 2022 34(7)
[7] Pioch F., Harmening J. H., Müller A. M., Peitzmann F. J., Schramm D., and el Moctar O.: “Turbulence modeling for physics-informed neural networks: Comparison of different RANS models for the backward-facing step flow”, Fluids, 2023 8(2), 43
[8] Xu H., Zhang W., and Wang Y.: “Explore missing flow dynamics by physics-informed deep learning: The parameterized governing systems”, Physics of Fluids, 2021 33(9)
[9] Hennigh O., Narasimhan S., Nabian M. A., Subramaniam A., Tangsali K., Fang Z., and Choudhry S.: “NVIDIA SimNet™: An AI-accelerated multi-physics simulation framework”, International conference on computational science”, Springer International Publishing, 2021, pp. 447-461
[10] Rao C., Sun H., and Liu Y.: “Physics-informed deep learning for incompressible laminar flows”, Theoretical and Applied Mechanics Letters, 2020 10(3), pp. 207-212
[11] Harmening J. H., Peitzmann F. J., and el Moctar O.: “Effect of network architecture on physics-informed deep learning of the Reynolds-averaged turbulent flow field around cylinders without training data”, Frontiers in Physics, 2024 12
[12] Lu L., Meng X., Mao Z., and Karniadakis G. E.: “DeepXDE: A deep learning library for solving differential equations”, SIAM review, 2021 63(1), pp. 208-228
[13] Menter F.R: “Two-equation eddy-viscosity turbulence models for engineering applications”, AIAA J., 1994 32, pp. 1598–1605
[14] Harmening J. H., Pioch F., Fuhrig L., Peitzmann F. J., Schramm D., and el Moctar O.: “Data Assisted Training of a Physics-Informed Neural Network to Predict the Reynolds-Averaged Turbulent Flow Field around a Stalled Airfoil under Variable Angles of Attack”, Preprint, 2023
[15] Xiang Z., Peng W., Liu X., and Yao W.: “Self-adaptive loss balanced physics-informed neural networks”, Neurocomputing, 2022 496, pp. 11-34
[16] Li S. and Feng, X: “Dynamic weight strategy of physics-informed neural networks for the 2d Navier–Stokes equations”, Entropy, 2022 24(9), 1254
[17] Kim Y., Choi Y., Widemann D., and Zohdi T.: “A fast and accurate physics-informed neural network reduced order model with shallow masked autoencoder”, Journal of Computational Physics, 2022 451, 110841
[18] Wandel N., Weinmann M., and Klein R.: “Teaching the incompressible Navier–Stokes equations to fast neural surrogate models in three dimensions”, Physics of Fluids, 2021 33(4)
[19] Wang R., Kashinath K., Mustafa M., Albert A., and Yu R.: “Towards physics-informed deep learning for turbulent flow prediction”, Proceedings of the 26th ACM SIGKDD international conference on knowledge discovery & data mining, 2020, pp. 1457-1466
[20] Zhu Y., Zabaras N., Koutsourelakis P. S., and Perdikaris P.: “Physics-constrained deep learning for high-dimensional surrogate modeling and uncertainty quantification without labeled data”, Journal of Computational Physics, 2019 394, pp. 56-81
[21] Krishnapriyan A., Gholami A., Zhe S., Kirby R., and Mahoney M. W.: “Characterizing possible failure modes in physics-informed neural networks”, Advances in Neural Information Processing Systems, 2021 34, pp. 26548-26560
[22] Dwivedi V., Parashar N., and Srinivasan B.: “Distributed physics informed neural network for data-efficient solution to partial differential equations”, Preprint, 2019
[23] Wang Y. and Zhong L.: “NAS-PINN: neural architecture search-guided physics-informed neural network for solving PDEs”, Journal of Computational Physics, 2024 496, 112603

Kopplung von CFD mit datengetriebenen Modellen: Sorption von Wasserstoff

Prof. Dr. Georg Klepp (iFE, Technische Hochschule Ostwestfalen-Lippe)

Abstract

Die Speicherung von Energie in der Form von Wasserstoff und die Verwendung von Wasserstoff als Kraftstoff für Fahrzeuge erfordert eine effiziente und effektive Speichertechnologie. Eine Alternative zur Speicherung des Wasserstoffs bei sehr tiefen Temperaturen oder sehr hohen Drücken ist die Speicherung über Physisorption in hochporösen Medien wie Aktivkohle und metallorganischen Gittern oder auch über Chemisorption, wenn zusätzlich eine chemische Bindung auftritt, wie z.B. in Metallhydriden. Dabei sind die Tanks mit einem geeigneten Sorbens gefüllt, wodurch die im Tankvolumen gespeicherte Wasserstoffmenge bei gleichem Druck und bei gleicher Temperatur höher ist als im Tank ohne Sorbens. Aufgrund der Sorptionswärme und ggf. der Reaktionsenthalpie kann es zu einer erheblichen Ungleichverteilung der Temperaturen und der Wasserstoffkonzentrationen im Tank kommen. Dies kann die Speicherkapazität sowie die maximalen Mengenströme bei der Be- und Entladung reduzieren. Um die Speicherkapazität solcher Sorptionstanks zu optimieren und ggf. eine zusätzliche Temperierung auszulegen, werden Simulationsrechnungen durchgeführt.
Die Strömung im Tank wird durch die Gleichung der Massenerhaltung, den Navier-Stokes Gleichungen und der Gleichung der Energieerhaltung beschrieben, wie sie in einem CFD Programm umgesetzt sind. In den Erhaltungsgleichungen sind zusätzlich Quellterme implementiert, die die adsorbierte Phase und die damit verbundene Wärme beschreiben. Diese Quellterme ergeben sich aus der Massen- und Energiebilanz des adsorbierten Wasserstoffs in einem Kontrollvolumen, wobei der Gleichgewichtszustand durch eine geeignete Adsorptionsisotherme (nach Dubinin-Astakhov) beschrieben wird.
Dieses physikalische Modell führt zu einem hohen rechnerischen Aufwand, insbesondere bei komplexen dreidimensionalen Geometrien oder bei der Verwendung von Gasgemischen. Eine rechnerisch weniger aufwändige Alternative ist die Verwendung datengetriebener Modelle, die mit Hilfe maschinellen Lernens (ML) erstellt werden. Dazu wird hier ein hybrider Ansatz gewählt: Die physikalische Modellierung der Strömungsvorgänge wird mit der datengetriebenen Modellierung des Sorptionsvorgangs gekoppelt. Mit dem physikalischen Adsorptionsmodell werden Datensätze generiert, die zum Training der ML-Modelle dienen. Dabei werden unterschiedliche Ansätze des maschinellen Lernens verwendet und der Aufwand bei der Erstellung sowie die Genauigkeit der Vorhersage verglichen. Als besonders geeignet haben sich neuronale Netze mit einer geringen Anzahl von Schichten sowie die Gauss Prozess Regression erwiesen.
Der vorteilhafteste ML Ansatz wird verwendet, um die entsprechenden Quellterme im CFD-Modell zu berechnen. Dadurch wird eine rechnerisch vorteilhafte Formulierung des Problems erreicht. Dieses hybride Modell wird verwendet, um die Be- und Entladung von Aktivkohletanks mit Wasserstoff zu simulieren. Dadurch kann die Druck- und Temperaturverteilung im Tank, die Menge des gespeicherten Wasserstoffs bzw. die Menge des freigesetzten Wasserstoffs bestimmt werden und somit die maßgeblichen Betriebsbedingungen und –parameter identifiziert werden.
Diese erfolgreiche Kopplung eines CFD-Modells mit einem ML-Modell kann als Ausgangspunkt zur Beschreibung weiterer Prozesse dienen. Besonders vorteilhaft ist diese Kopplung bei komplexen, physikalisch unterschiedlichen Prozessen mit unterschiedlichen Ort- und Zeitskalen.

Kopplung von CFD mit datengetriebenen Modellen: Sorption von Wasserstoff

Georg Klepp
iFE, TH OWL, Lemgo

Wasserstoff als Energiespeicher

Stoffliche Speicherung als Wasserstoff
+ hohe gravimetrische Energiedichte
- niedrige volumetrische Energiedichte

Saisonaler Energiespeicher
- Windkraftanlagen
- Haushalte

Kraftstoffe
- Schwerlastverkehr
- Schienefahrzeuge

ICCHMT 2023. :Klepp: Hydrogen Sorption Tank, 203

NAFEMS DACH Konferenz 2024: Konferenz für Berechnung & Simulation im Engineering, 10. – 12. Juni 2024, Bamberg, D

Energiedichte Wasserstoffspeicher

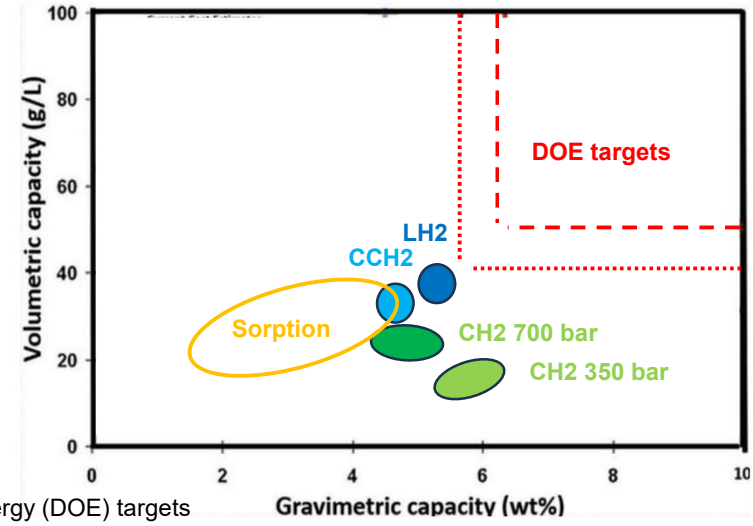

Department of Energy (DOE) targets

Speicherung durch Adsorption

Physisorption

- Adhesion der H_2 Moleküle an Adsorbentoberfläche
- Erhöhte Dichte der adsorbierten Phase (H_2)
- Exotherm

Speicherung durch Adsorption

Materialien mit großer (innener) Oberfläche

Aktivkohle

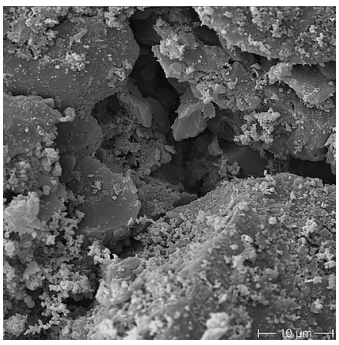

Metallorganische Gitter (MOF)

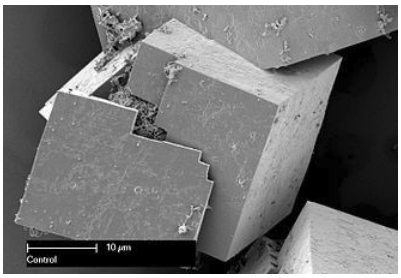

ECRES 2023, 226. Klepp: Adsorbed Gas Storage Digital Twin

Speicherung durch Adsorption

Aktivkohlespeicher

TRL 3

TRL 6

TRL9

ECRES 2023, 226. Klepp: Adsorbed Gas Storage Digital Twin

NAFEMS DACH Konferenz 2024: Konferenz für Berechnung & Simulation im Engineering, 10. – 12. Juni 2024, Bamberg, D

Speicherung durch Adsorption

Wasserstoff in Aktivkohle gespeichert
Gesamtmenge und adsorbierte Phase

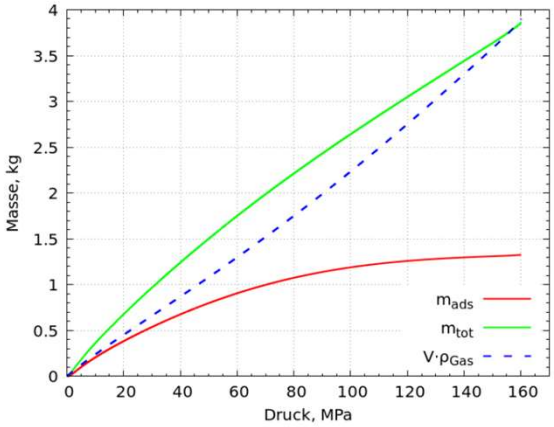

Tank mit 33 Liter Aktivkohle bei 20 °C.

Modellierung

Materialen mit hoher Adsorptionswärme und geringer Porosität
- Inhomogene Verteilung
- Erwärmung / Abkühlung

Physikalische Modellierung
- Koppeln der transiente Strömung in porösen Medien mit Sorptionsmodell
- Aufwändige Implementierung und Berechnung

Alternativer Modellierungsansatz

Gekoppeltes hybrides Modell

- CFD: Transiente Strömung in porösen Medien
- Maschinelles Lernen (ML): Adsorption
  - Implementierung über Quellterme
  - Geringerer numerischer Aufwand als physikalische Modellierung

Strömung

Modellgleichungen für die Strömung im Tank :

- Strömung in porösem Medium
- Massenbilanz mit Quellterm für die adsorbierte Phase
- Energiebilanz mit Quellterm für Adsorptionswärme
- Wärmetransport an Tankoberfläche (über Randbedingung)

Quellterme aus dem Adsorptionsmodell
Numerische Lösung mit openFoam11.

Adsorption

Modellgleichungen für die Adsorption in einem Finiten Volumen:

- Massenbilanz
- Energiebilanz
- Dubinin-Astakhov Adsorptionsisotherme
- Reaktionskinetik
- Zustandsgleichung

Lösung des Gleichungssystems mit Euler-vorwärts Verfahren
Generieren des Datensatzes für das Maschinelle Lernen

Maschinelles Lernen

Datensatz:

- Training und Validierung: 4494 Punkte (5fach kreuzvalidiert)
- Testen: 1498 Punkte

Eingabegrößen	Ausgabegrößen
Druck 1 -150 bar Temperatur 250 – 30 K	Massenstrom adsorbiert 0,1 - 300 (g/s) / kg

ICCHMT 2023. :Klepp: Hydrogen Sorption Tank, 203

Maschinelles Lernen

Training und Validierung

ML method	Neurales Netz 1 x 5 Neuronen	Gauss Prozess Regression Exponentielle Ansatzfunktion
RMSE (Validierung)	1006 e-6	97,3 e-6
R^2 (Validierung)	1.00	1.00
Vorhersage (obj./s)	290.000	55.000
Training Zeit (s)	9,79	54,78

RMSE Wurzel der mittleren Fehlerquadratsumme
R^2 Bestimmtheitsmaß

Maschinelles Lernen

Testdatensatz: Vorhergesagte und vorgegebene Werts

	Neuronales Netzwerk	Gauss Prozess Regression Exponential
RMSE (Test)	5.02e-3	1.78e-3
R^2 (Test)	1.00	1.00

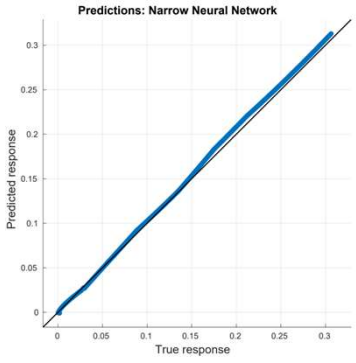

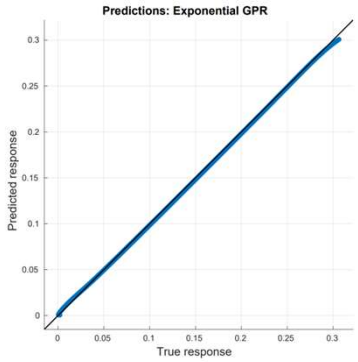

Ergebnisse

Vergleich physikalisches Adsorptionsmodell und ML Adsorptionsmodell (R^2=0,99 RMSE=0,003).
Beladung eines zylindrischen 33 Liter Aktivkohle Tanks mit 0,3 g/s Wasserstoff

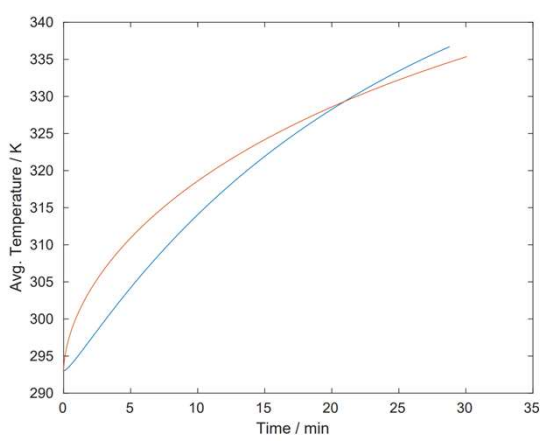

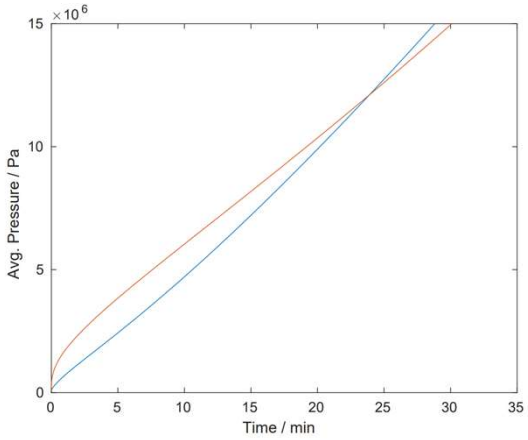

Ergebnisse

Einfluss des Adsorbens (Porosität und Adsorptionswärme)
Beladung eines zylindrischen 196 Liter Aktivkohletanks mit 20,4 Liter/Sekunde Wasserstoff

Ergebnisse

Entwicklung eines ML-Modells für Wasserstoff-Adsorption in Aktivkohle.

Implementierung eines ML-Modells zur Beschreibung der Adsorptionswärme und –massenströme in einem CFD-Modell.

Berechnung der Be- und Entladung von Adsorptionstanks mit Wasserstoff.

Ausblick

Optimierung der Tankgeometrie

- beliebige (unsymmetrische) Tankgeometrien
- Sorbens als Schüttung oder Monolith mit Strömungskanälen
- Temperierung des Tanks

Weiterentwicklung des ML-Modells

- Unterschiedliche Sorbentien (MOF, Metallhydride)
- Unterschiedliche Gase / Gasmischungen

ICCHMT 2023. :Klepp: Hydrogen Sorption Tank, 203

NAFEMS DACH Konferenz 2024: Konferenz für Berechnung & Simulation im Engineering, 10. – 12. Juni 2024, Bamberg, D

Vielen Dank !

Prof. Dr. Georg Klepp
georg.klepp@th-owl.de

CFD Simulations in Manufacturing – Cloud, AI/ML, GPUs – Lessons Learned, and Recommendations

Wolfgang Gentzsch

(Simr, Formerly UberCloud)

High Performance Computing (HPC) in the Cloud is now becoming more and more popular, for all kinds of complex engineering simulation workflows, recently including AI/ML. The reason? Over the last 10 years, access and use of powerful CFD cloud resources became more and more automated and self-service, many of the previous cloud roadblocks have been removed by standard high-performance cloud technologies, and thus HPC as a Service in many different forms is now in every engineer's reach. But beside all the cloud benefits there are still real hurdles to overcome.

In our presentation, we will explain these remaining hurdles and how to resolve them. We will discuss major benefits of using cloud, GPUs, and AI/ML for decision makers, IT experts, and simulation engineers and their managers. Finally, we will demonstrate the wide applicability of Cloud HPC with the aid of several engineering use cases from the automotive, mining, lightning, healthcare device, and construction industries. These manufacturers have been using the cloud now for two to four years, and we will present a summary of their lessons learned and recommendations to provide guidance for manufacturers who are planning to move to the cloud in the next few years.

Engineers have long suffered from inadequate systems and software. Industrial surveys show that about 60% of engineers feel that hardware resources are inadequate for their work. Often, they have to simplify models to fit in current hardware limits thus losing accuracy of their results. In addition, buying your own HPC system comes with even more challenges, such as long procurement cycles; high Total Cost of Ownership (TCO); scalable software; erratic system usage; fast aging of inhouse servers; and the need for trained HPC system experts.

But with the rise of cloud computing its easier than ever to get access to powerful compute with bare metal performance, efficient storage, and low-latency networking. More and more organizations are turning to HPC-based cloud computing due to additional business value coming from increased flexibility and scalability from practically unlimited, on-demand compute and storage capacity that can be provisioned only if needed. The productivity of the simulation team grows thanks to the ability of running more projects in the same time or running more complex simulations without big investments. Compute intensive tasks such as parametric sweeps, multiphysics simulations and large-scale optimization studies to evaluate many design options become possible.

The other benefits include the possibility to increase accuracy of their models by removing memory and CPU limitations so engineers can use more detailed models, access heterogeneous architectures such as GPUs, InfiniBand, large memory, latest processors, etc. Finally, reduce engineering and licensing expenses by reducing computation time.

However, running complex engineering workloads in the cloud is not easy. The engineering team needs the cloud-specific know-how, the integration with existing on premises infrastructure to ensure the security and compliance, hands-on-experience with high performant architectures, on-boarding the complex applications to the cluster, optimizing the software licensing cost for the cloud, efficiently transfer large datasets. All components of compute, storage and visualization should be optimally integrated with on premises infrastructure into a single system.

The Cloud Platform implemented for Freudenberg is addressing these challenges by providing engineers a turn-key scalable engineering platform with automatically integrated compute, storage and networking optimized for a specific CAE software, enabling engineers to significantly reduce IT overhead and modernize their IT infrastructure. The platform provides access to latest hardware optimized for specific application, high-resolution engineering workstations for pre- and post-processing and interactive simulation, scalable HPC and automated update process without downtime, with minimal IT overhead and possibility to autoscale the cluster with tailored hardware for each specific job.

Rapid Aerodynamic Development using CFD and Machine Learning

Dr. F. Hesse[1], J. Higgins[1], F. Gandhi[1], Dr. J. Bi[1], Dr. V. Oancea[1],
Dr. J. Iseler[1], H. Motiwala[1], Dr. V. Jambhekar[1]

[1]Dassault Systèmes SIMULIA

Summary

The vehicle market is evolving rapidly. New players are entering the market, the drive for vehicle electrification is ongoing, many variants of a vehicle are investigated prior to freezing the design, and sustainability is a major topic. In this context, vehicle aerodynamics is ever more crucial. It directly impacts the vehicle range and plays a major role in meeting regulation targets. Vehicle manufacturers must also keep in mind the need for a shorter time-to-market, where one must design faster and not permit late-stage redesign. This all means that a faster assessment of vehicle aerodynamics is imperative. In the past and present, computational fluid dynamics (CFD) has opened the door to virtual aerodynamic testing, allowing manufacturers to test their vehicle shapes before developing a costly and time-intensive prototype that then needs to be experimented on using a wind tunnel. While high-fidelity CFD, such as the PowerFLOW software offered by Dassault Systèmes (3DS), will remain an integral part of the aerodynamic development process of major OEMs, the growth of machine learning (ML) and continual improvement of its algorithms has opened doors to speed-up computational aerodynamics. The current work illustrates how aerodynamic data obtained from the 3DS CFD PowerFLOW software combined with data-driven methods can enable car manufacturers to obtain clean 3D contour plots of the vehicle's surface X-force distribution, the associated integrated vehicle drag force and more within several minutes on a single GPU (after training of the ML model). This represents a significant reduction in computational cost and time, as running a high-fidelity aerodynamics CFD simulation requires several hundred CPUs and a couple of hours. More importantly, the error between the ML predicted drag force and the true PowerFLOW value is not larger than 3%. The geometry investigated is a 3DS electric concept car with varying wheel spoke number and width.

Keywords: Aerodynamics, Computational fluid dynamics, Machine learning, Deep neural networks

1 Introduction

The use of the term digital twin is becoming more and more widespread. It represents a concept in which a digital replica of an object, or even a living being, is created to better understand, engineer, and optimize the real-life twin. So far, in the realm of vehicle aerodynamics, low-fidelity and high-fidelity computational fluid dynamics (CFD) software has been used to predict and improve the aerodynamic behavior (e.g. drag, lift, and yaw characteristics) of the car, thereby bypassing the need for costly physical prototypes until the very final stages of the vehicle design cycle. However, a proper digital twin of a vehicle should be able to illustrate the effect of geometry changes in near real-time, which, so far, using conventional computing architectures is not possible. Quantum computing, a very nascent technology, may solve this, but, for now, the only option is to resort to fast surrogate machine learning (ML) models. These models have learned from past aerodynamic data to predict the new aerodynamic performance of vehicle shapes that were not seen during the ML model training phase. This prediction speed-up solves the global problem of an increasing need for a shorter time-to-market in an ever-more competitive market landscape, where there is a drive for vehicle electrification and there are stricter sustainability regulations as well (see figure 1).

Fig. 1: The need for ML model based surrogates in CFD

The idea is to embed the trained ML model(s) in the design stage such that the degree of fidelity that was previously only possible at the detailed design stage is now possible during the conceptual design phase as well, providing conceptual vehicle designers more aerodynamic insight into their proposed vehicle shapes and preventing fewer late-stage design failures (see figure 2). Specifically, the goal of this work is to demonstrate that ML can be used as a surrogate model to reduce the use of CPUhrs intensive PowerFLOW CFD simulations for aerodynamic drag prediction, while significantly accelerating the compute time from several hours to merely several minutes.

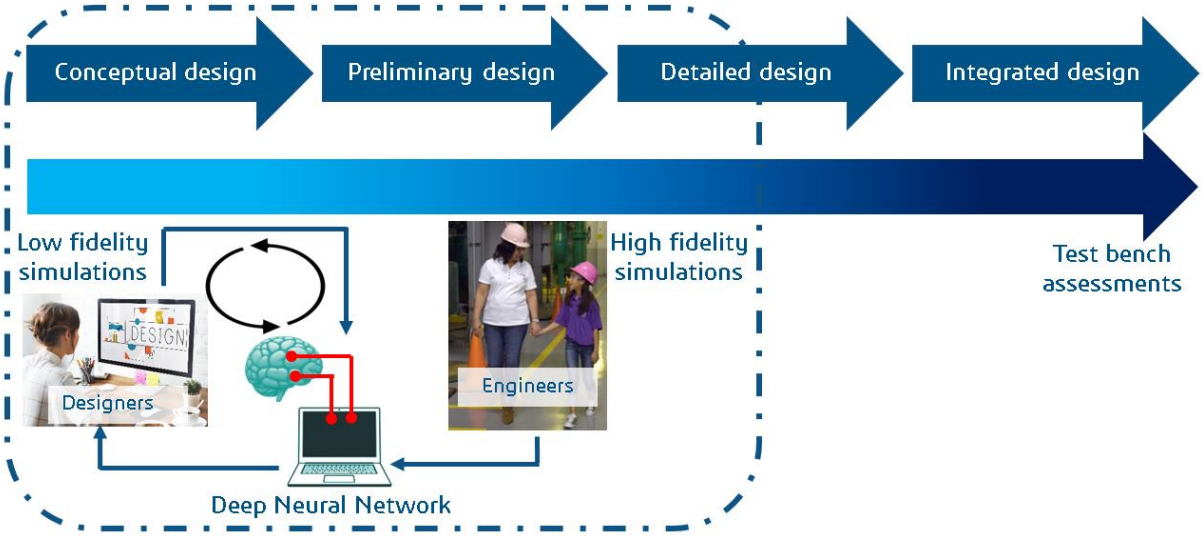

Fig. 2: How ML models are embedded into the aerodynamic development workflow

2 Methodology

As a use-case, the following optimization study is analyzed: a design-of-experiment (DOE), where the tire spoke number and spoke width of the Dassault Systèmes (3DS) E-car geometry (see figure 3) are varied, with the optimization goal being the identification of the lowest vehicle drag configuration. In figure 4, the DOE design space is depicted. Red squares represent the simulation sets that are used to train the ML models, green circles are the validation data points used in the ML training process to observe ML model convergence, and the blue triangles represent the blind test sets that will be used to see how well the ML models generalize to unseen vehicle geometries. The design space extremes are illustrated in figure 5.

Fig. 3: 3DS E-car geometry

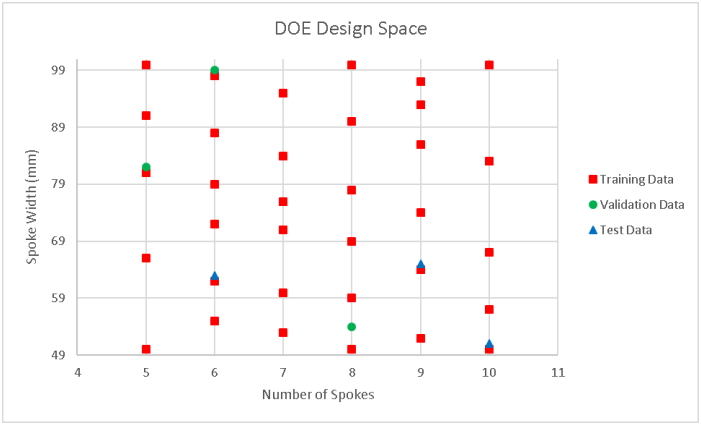

Fig. 4: DOE design space

Spoke #	Spoke Width (mm)
5	50

Spoke #	Spoke Width (mm)
5	100

Spoke #	Spoke Width (mm)
10	50

Spoke #	Spoke Width (mm)
10	100

Fig. 5: Design space extremes

The study can be broken down into two segments: the CFD portion and the ML model part. During the CFD phase, 40 high-fidelity simulations are prepared in PowerDELTA, set-up in PowerCASE,run with PowerFLOW and some results are subsequently visualized in PowerVIZ as a sanity check that the data is reasonable. Each simulation takes about 6 hours and requires up to 300 CPU cores. Sample aerodynamic result visualizations are depicted in figure 6. For this study, the critical surface field representation is the surface X-force distribution. Once the CFD data is collected, 36 simulation points

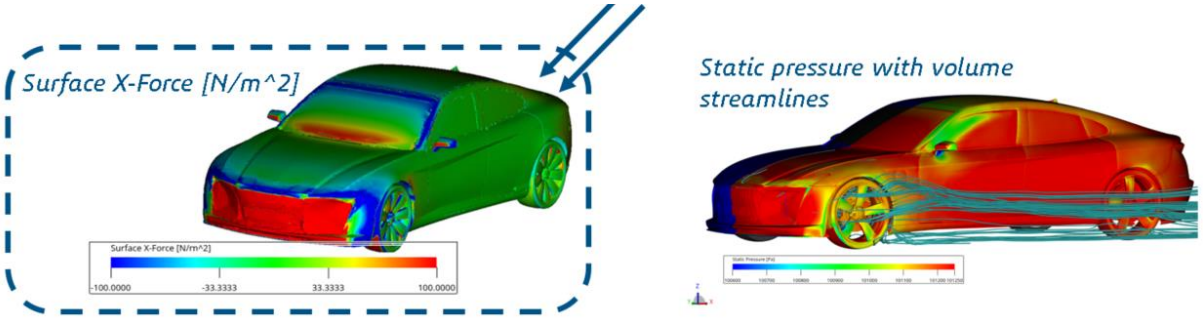

Fig. 6: Flow and surface field representations from the PowerFLOW simulation – the one of interest for this study is the surface X-force distribution

are used to train deep learning neural network models that are written in Python with 3 simulation points used as validation points. A schematic of the feed-forward neural network models applied is depicted in figure 7. The input layer of the neural network models is fed with x-, y-, and z-coordinate

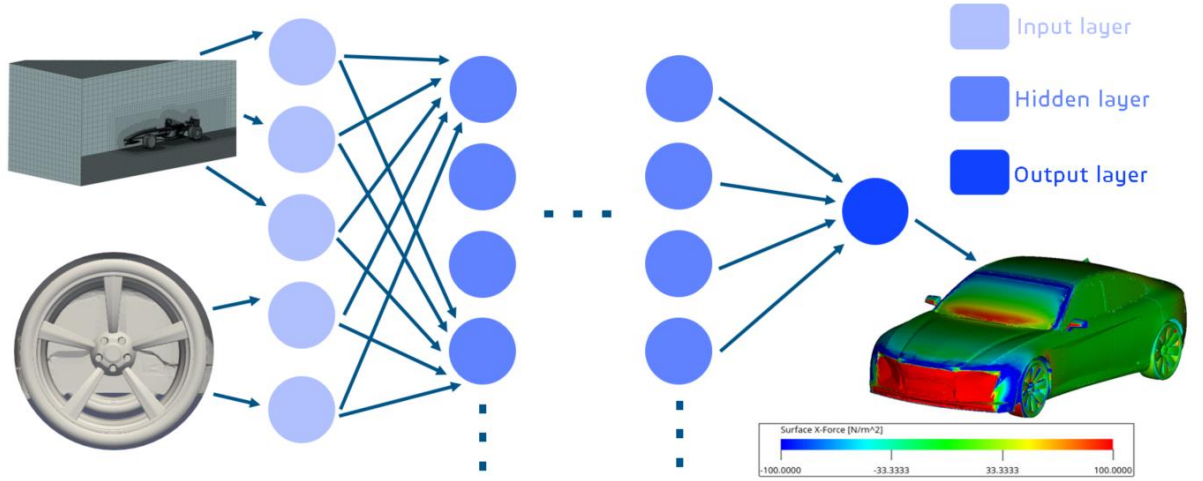

Fig. 7: Schematic of the deep learning neural network models used in this external vehicle aerodynamics DOE study

data, as well as the spoke number and spoke width. This information is then propagated through the hidden layers of the neural network and, finally, at the output layer one obtains the surface X-force distribution of the vehicle. Training the neural network models takes approximately 3 days on a Windows workstation with a single GPU card. Meanwhile, the inference step, where the surface X-force distribution for vehicle geometries not seen during the neural network model training phase is predicted, merely takes several minutes.

3 Results

Before assessing the predictive capabilities of the trained ML models, it is imperative to check that the models are not under-fitting nor over-fitting the training data. This is done by looking at the mean-square-error (MSE) of the models as a function of training epoch. Two sample plots are provided in figure 8. Evidently, the MSE decreases almost monotonically and stays low as well, illustrating that the models should generalize well when exposed to unseen vehicle geometries. Furthermore, the MSE has an order of magnitude of $O(10^{-3})$, which is reasonable as well.

Now, one can look at the ML models predictive capabilities. For the blind test points, table 1 shows the drag force deltas between the true PowerFLOW results and the ML model outcomes and, more importantly, the percentage error. Evidently, the percentage error is well below 2% for all three test

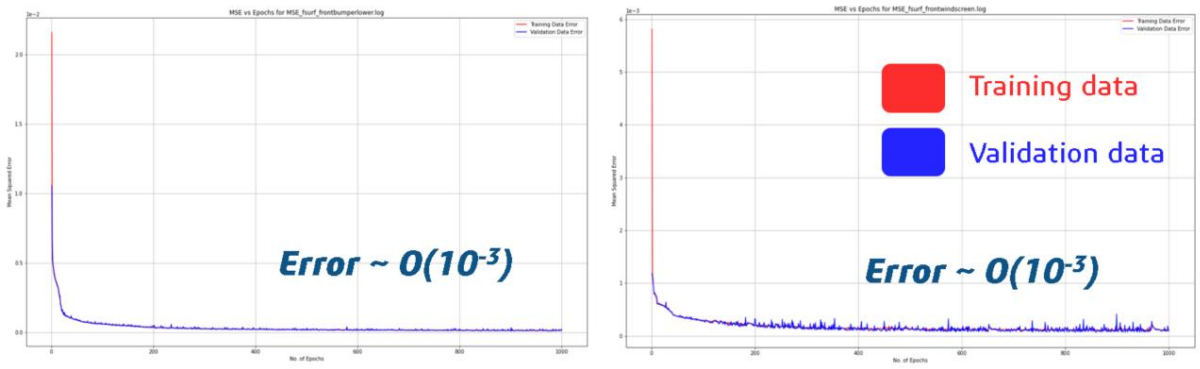

Fig. 8: Sample MSE plots

cases, which is a very good outcome. Beyond that, the trained ML models were applied to all simulation points: training points, validation points, and test points. The associated accuracy of the predications is depicted in figure 9. Here too, one can clearly see that the error lies within the 2% error bound. It is also interesting to note that there is a bias in the ML model results; the ML models consistently over-predict the integrated drag force. Having looked at the integrated drag force, surface X-force distribution plots provide further insight into the predictive capabilities of the ML models. Figure 10 shows these surface contour plots from different angles and viewpoints for run 37 (similar plots are obtained for all other runs). It is quite clear to see that there is almost no difference between the true PowerFLOW results and the ML predicted results. This substantiates the claim that the ML models are good surrogates for expensive high-fidelity PowerFLOW aerodynamic simulations.

Run #*	Spoke #	Spoke Width (mm)	PF Drag Force (N)	ML Drag Force (N)	Drag Force Dif. (N)**	Percent Error (%)***
37	9	65	382.8	388.6	-5.8	-1.5
38	10	51	383.4	386.2	-2.8	-0.7
39	6	63	386.6	388.2	-1.6	-0.4

*Index starts at 0
**Difference = (PF Result) – (ML Result)
*** % Error = (Difference) / (PF Result) x 100%

Table 1: True PowerFLOW drag force vs. ML model predictions for the test points

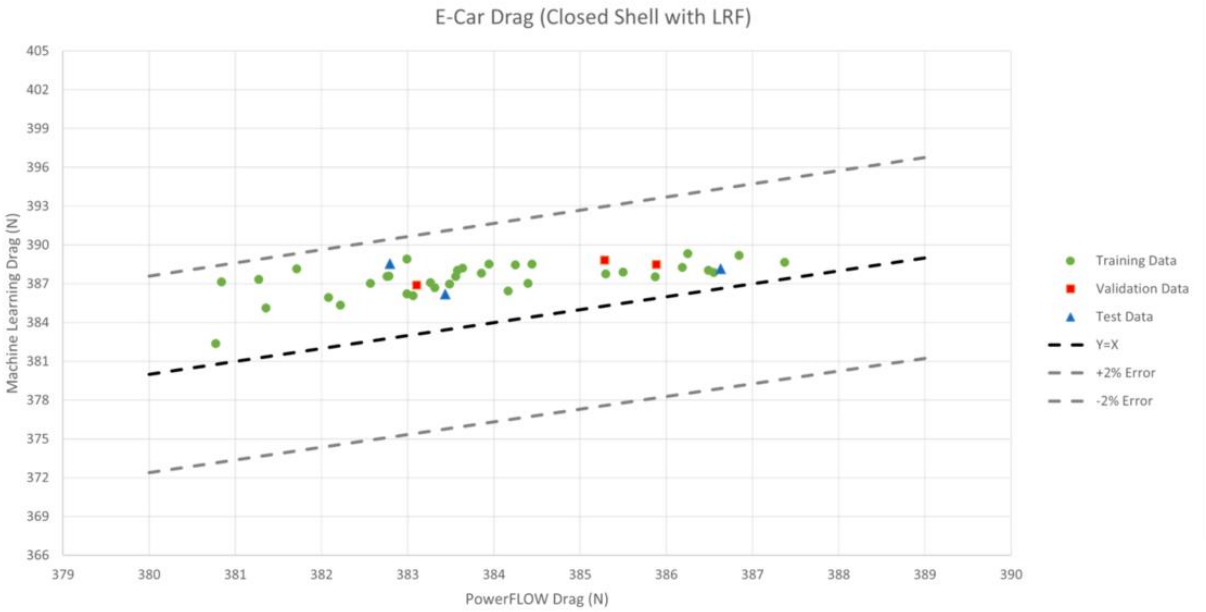

Fig. 9: Overall predictive capability assessment of the ML models

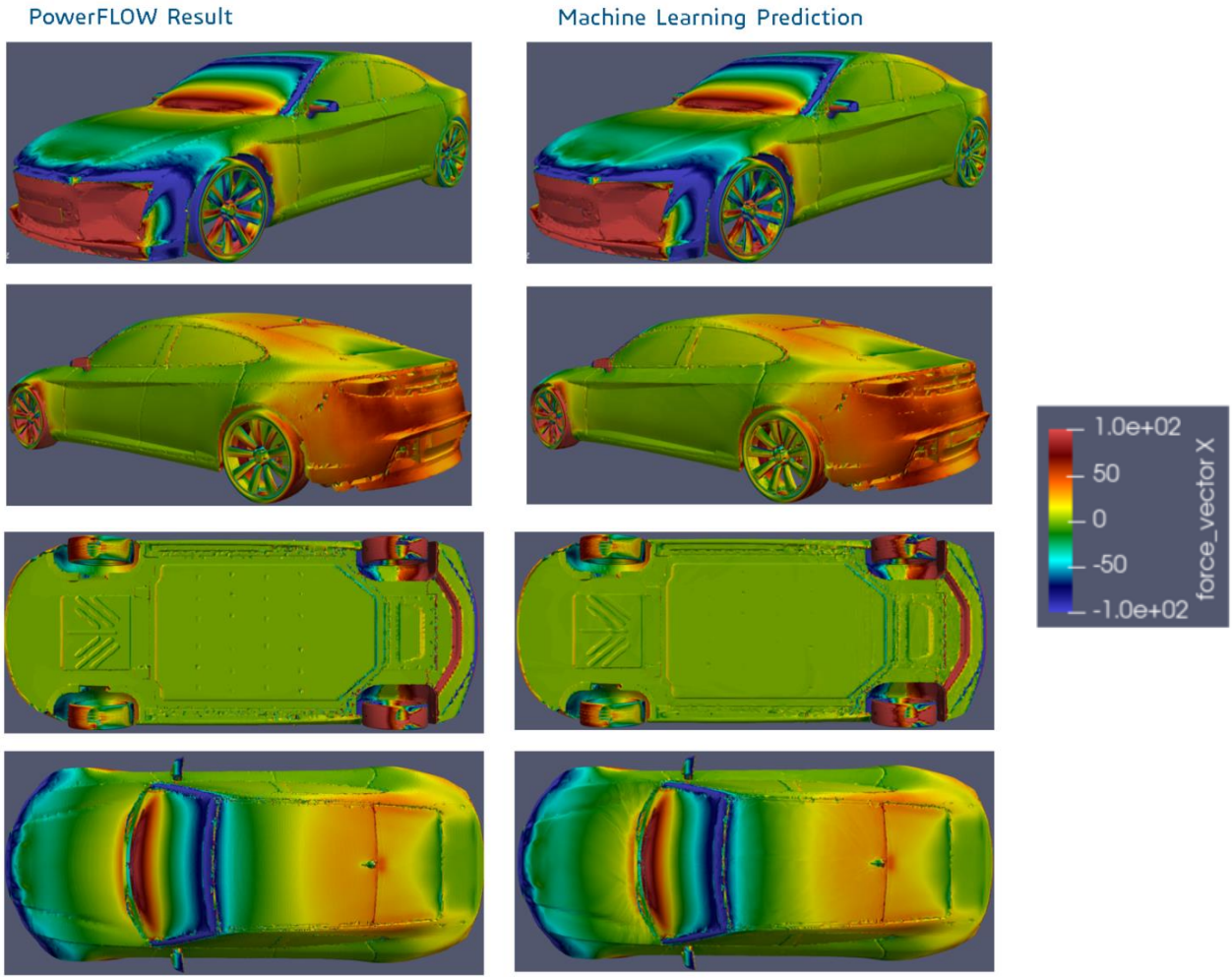

Fig. 10: PowerFLOW result vs. ML result for surface X-force distribution of run 37

4 Conclusion

Overall, a multi-model machine learning approach based on simple feed-forward artificial neural networks has been validated for the use of external aerodynamic drag force prediction of clay-model like vehicles. Once the ML model(s) have been trained on a single GPU for ~ 3 days, inferences (i.e. predictions) of drag force for unseen vehicle geometries takes ~2 minutes as opposed to running a CPUhr intensive high-fidelity PowerFLOW simulation that takes ~6 hours on up to 300 CPU cores. Importantly, the percentage error between the true CFD PowerFLOW data and the ML model predictions of integrated drag force lies at less than 2%.

5 Future Work

A number of avenues for future work exist. One still needs to tune the ML model hyperparameters to accelerate the ML model training and inference steps, while decreasing the ML model output error. It is also imperative that one extend the ML model predictive capabilities to allow good predictions of open-grill vehicle geometries with engine bay components. Furthermore, one also needs to build ML models to allow prediction of fluid volume velocity, thereby allowing the identification of separation lines around the vehicle. Finally, one could also envision the construction of generative AI models that create a new/optimized vehicle geometry with minimal separation lines and, therefore, close to zero low pressure drag enhancing wake regions.

Neuentwicklungen in der Form- und Sickenoptimierung

Dr.-Ing. Michael Scherer, Prof. Dr.-Ing. Ralf Meske

(Tenneco)

Tenneco konnte den Entwicklungsprozess von Leichtbaukolben für Otto- und Dieselmotoren durch den Einsatz einer sensitivitätsbasierten Formoptimierung in den letzten 12 Jahren signifikant beschleunigen und ist mittlerweile in der Lage, innerhalb kürzester Zeit betriebsfeste Kolbendesigns auch für höchste motorische Anforderungen zu berechnen. Hierzu wurde die Inhouse-Software FMShape entwickelt.
Die klassische Entwurfsmethodik ist geprägt durch Iterationen, die auf der erfahrungsbasierten Designänderung in der Konstruktion und der anschließenden Beurteilung der Festigkeit in der Berechnung basieren. Bei Anwendung der Formoptimierung wird die Oberfläche des FE-Modells eines Designentwurfs in der Berechnung iterativ verändert und dann – nachdem nachgewiesen wurde, dass die Verbesserung hinreichend ist – durch die Konstruktion nachgebildet.
Ziel der Formoptimierung ist oft die Verbesserung der Festigkeit durch Abbau von Spannungskonzentrationen. Im Vergleich zur Topologieoptimierung, sind die Geometrieänderungen in der Formoptimierung typischerweise lokal und klein im Verhältnis zu den Gesamtabmessungen eines Bauteils. Nimmt man den Durchmesser eines Kolbens als Bezugsmaß, so liegen die von FMShape vorgenommenen relativen Designänderungen in der Größenordnung von 1 bis 4%. Die mit FMShape erzielte relative Spannungsreduktion liegt im Bereich von 10 bis 40%. Verbesserungen in dieser Größenordnung sind signifikant, da bei den in der Kolbenentwicklung verwendeten zeitfesten Aluminiumwerkstoffen eine Spannungsreduktion von ca. 15% zu einer Verlängerung der Lebensdauer um den Faktor 10 führt.
Im Verlauf der Formoptimierung eines Bauteils ist es sinnvoll, die Fertigbarkeit zu gewährleisten, um die Rückführung der optimierten Geometrie in ein (im Hinblick auf die Fertigung zulässiges) CAD-Modell zu erleichtern. In der Optimierung mit FMShape geschieht dies durch den Einsatz von geometrischen Nebenbedingungen, sogenannten Fertigungsrestriktionen, die in jeder Iteration möglichst exakt eingehalten werden, z.B. Nebenbedingungen, die die Entformbarkeit eines Kolbens, der in einem Gießprozess hergestellt wird, gewährleisten.
Seit kurzem können mit FMShape auch Sickenoptimierungen von Schalenstrukturen durchgeführt werden. Diese neue Funktionalität wurde 2023 hinzugefügt mit dem Ziel, Geschäftsbereiche innerhalb von Tenneco unterstützen zu können, die Sickenoptimierungen in ihrem Entwicklungsprozess nutzen, um das NVH-Verhalten ihrer Bauteile zu verbessern. Das Besondere an der Sickenoptimierung mit FMShape ist eine neuartige Nebenbedingung, mit der der Grad der Versickung einer Schalenstruktur gesteuert werden kann. Die Anwendung dieser Nebenbedingung begünstigt die Entstehung klarer Sickenstrukturen, verbessert damit die Rückführbarkeit der Optimierungsergebnisse in die CAD-Geometrie und erhöht so die Effektivität und Akzeptanz der Methodik innerhalb des Entwicklungsprozesses.
Im Rahmen des Vortrages wird die Methodik der Form- und Sickenoptimierung mit FMShape dargestellt und die Funktionalität des Systems anhand zahlreicher Anwendungsbeispiele erläutert.

Topology Optimization of Continua Considering Stress Characteristics

Nils Wagner, Shyam Suresh, Christian Wulf (INTES GmbH)

1 Summary

A variable density, stress constrained topology optimization based on SIMP and a p-norm aggregated global element stress measure is used herein. The aim of optimization is to achieve maximum material savings by utilizing the structure at its load limit. The challenges are manifold. The number of active stress constraints increases with uniform loading. Furthermore, the optimization problem as such is ill-posed and requires a regularization of the stress constraints. The idea is based on replacing the huge number of element stress constraints with a single stress constraint. This problem is solved by approximating the non-smooth max operator by a continuously differentiable function, such as the p-norm or the Kreisselmeier-Steinhauser function. To prevent trivial solutions, the stresses are penalized to finally obtain a clear 0/1 distribution of the fill levels at the end of the optimization. The methodology is demonstrated using selected examples from the literature. PERMAS is used to solve the topology optimization problems, whereas optimization-relevant data is generated in VisPER via the so-called Topo Wizard. Using the Design Wizard, the hull can be smoothed, a quad layout generated, CAD-compatible splines fitted and exported as a step file.

2 Introduction

The interest in considering stress constraints in topology optimization began at the end of the 1990s. Truss structures were analyzed first [1,3], followed by two- [4, 5, 6, 11, 23, 24, 26, 27, 28, 31, 35] and three-dimensional structures [7, 9, 10, 28, 34, 35]. A very prominent and frequently analyzed example is the L-shaped beam in 2D [6, 7, 14, 23, 25, 27, 29, 30, 31, 32, 33] and 3D [9, 28. 30]. In addition to a simple load case, multiple load cases are considered in Le's work [15] and the design space is also divided into several design elements.
In contrast to the comparatively simple weight and compliance optimizations, the consideration of stress constraints requires significantly more know-how so that the analysis can be carried out numerically efficiently. Various optimization problems are formulated in this context. These include minimizing the maximum element stress subjected to a volume constraint or minimizing the weight or volume and a constraint for the maximum element stress in the design space. Another problem class minimizes compliance under a volume constraint and a global stress constraint. Contact problems with stress constraints are discussed in [13]. Stress constrained topology optimization with design-dependent loads are considered in [17]. In the meantime, additional constraints such as the consideration of natural frequencies [16] and buckling factors [22] are available in the literature. In the optimization loop, generalized eigenvalue problems are therefore solved in addition to a static analysis, which further increases the numerical effort. Dynamic stress constraints from a transient dynamic analysis are now also the subject of current research [19, 20, 21].

3 Stress constraints

The main difficulty in considering stress constraints is to reduce the number of constraints from n, where n is the number of finite elements of the model, to a single constraint for the element stress. There are two main formulations for this in the literature, which can be based either on the p-norm or the Kreisselmeier-Steinhauser function [33]. Both functions are available in PERMAS [36] as library functions, whereby the p-norm [18, 30] is used by default. A stress penalization is used to circumvent the stress singularity problem [30].

4 Topology optimization

Topology optimization aims to seek the best distribution of materials within the design domain so that the resulting structure maximizes its performance. Stress topology optimization can be divided into the stress minimization problem and the stress-constrained problem.
Two different scenarios play a role in practice. When developing prototypes, a CAD model may not yet be available. In this case, one starts directly with a finite element model. In this case, the user can benefit from the Topo Wizard in VisPER [37] to create the data relevant for topology optimization in a machine-

generated manner. The user is guided through the entire process step by step. It is advisable to keep this data in a separate file, as modifications are usually made during optimization.

5 CAD2CAD process

Ideally, a CAD model is already available. In this case, the CAD model is imported in VisPER. The widely used step format is currently supported. After surface meshing, volume meshing takes place.
An internal reference is created between the imported geometry and the finite element model. This makes it possible to distinguish between functional and free-form surfaces. The result of the topology optimization is then smoothed using an iso-surface approach. The identification of unchanged parts to be reused is based on a link between the CAD geometry of the design space with the FE model, that is directly established during meshing and maintained during the entire process chain. This is an important aspect to preserve functional surfaces and hence to reduce manufacturing costs. The creation of the new parametric CAD surfaces starts with the quadrangulation of their triangulation. This 'quad-layout" [2, 29] should produce a minimum number of patches. The resulting quadrangular patches, that are well adapted to geometry, mostly consistently connected and modest in number, then serve to fit spline surfaces. This is achieved by solving an optimization problem of the global parametrization, using so called cross fields [8].

6 Examples

6.1 2D L-shaped Beam

The L-shaped beam (Fig. 1, L=100 mm, t=1mm) with severe stress concentration at the re-entrant corner will also be used here as an introductory example. The design domain is discretized with 100 x 100 elements where the upper 60 x 60 elements are removed. The material properties are Young's modulus, E=2.1 10^5 [N/mm^2], Poisson ratio ν=0.3, density ρ = 7.8 10^{-9} [t/mm^3]. The vertical load F= 500 [N] is distributed over four neighborhood elements to relax stress concentration at the loading region. The initial values of design variables are set to be 0.5. The weight of the structure shall be optimized with respect to a von-Mises stress limit σ = 450 [N/mm^2]. A minimum member size of 2 mm is used herein. Fig. 2 illustrates the result of the topology optimization with a clear separation between solid and void material. Since the optimization seeks a fully stressed design corresponding to the current maximum stress, the re-entrant corner can be successfully trimmed to an arc, as shown in Fig. 2.

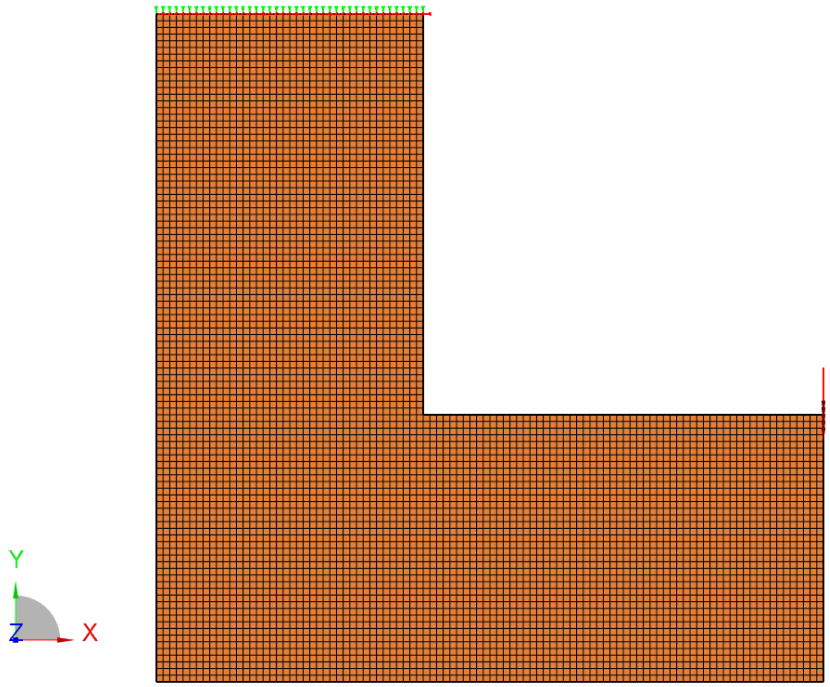

Fig. 1
L-shaped beam

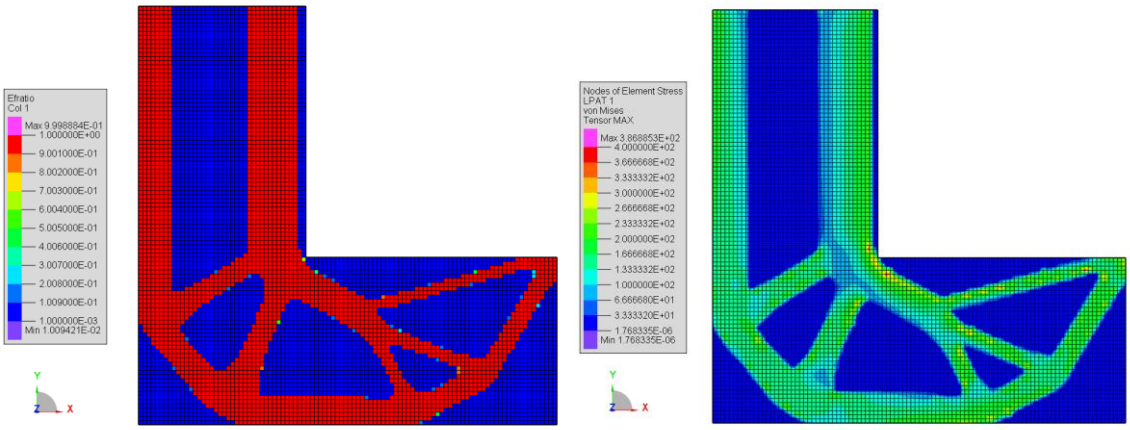

Fig. 2
L-shaped beam left: densities (red: solid, blue: void) right: stress distribution

6.2 3D example

The example (Fig. 3) is adapted from Gu [12]. A linear hexahedral element is adopted to discretize the design domain. The dimensions of the structure are set to be length L=100 [mm], height H=50 [mm], width B=5 [mm], and the element size is set to 1 [mm]. The allowable maximum element stress is 355 N/mm^2, whereas the material properties are defined as E=2.1 10^5 N/mm^2, ν = 0.3, ρ = 7.85 10^{-9} [t/mm^3]. A compliance minimization subjected to a global stress constraint σ_v = 355 [N/mm^2] and a volume fraction $V(\mathbf{x})/V_0$ = 0.5 is used here, where $\mathbf{x}$ is the elemental density vector and V_0 denotes the initial design volume. Convergence is achieved after 71 iterations. The color code adopted here displays elements with x_i = 0 in blue and elements with x_i=1 in red. Intermediate densities no longer exist at the end of the optimization (Fig. 4), as desired.

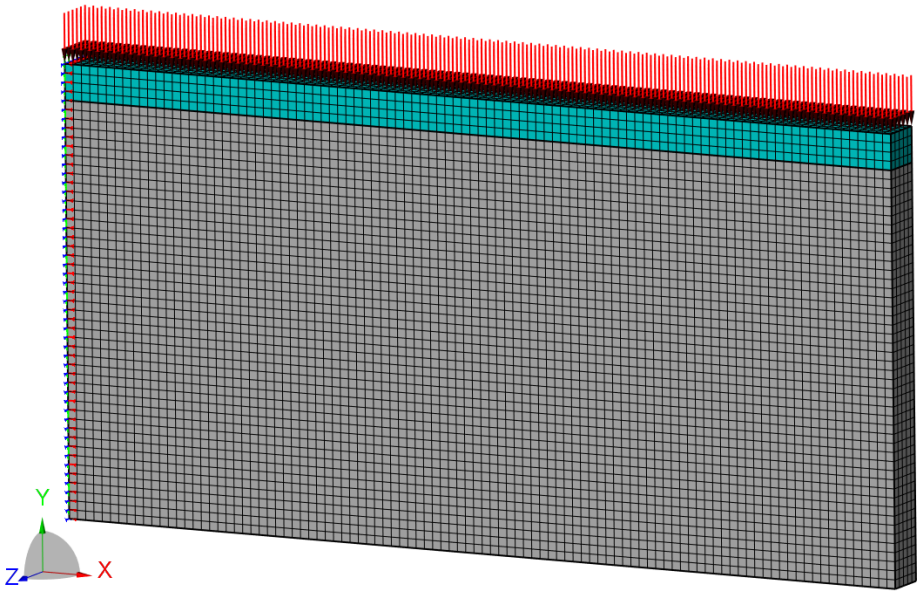

Fig. 3
Cantilever beam subjected to a pressure load. The top 4 element layers are a non-design space.

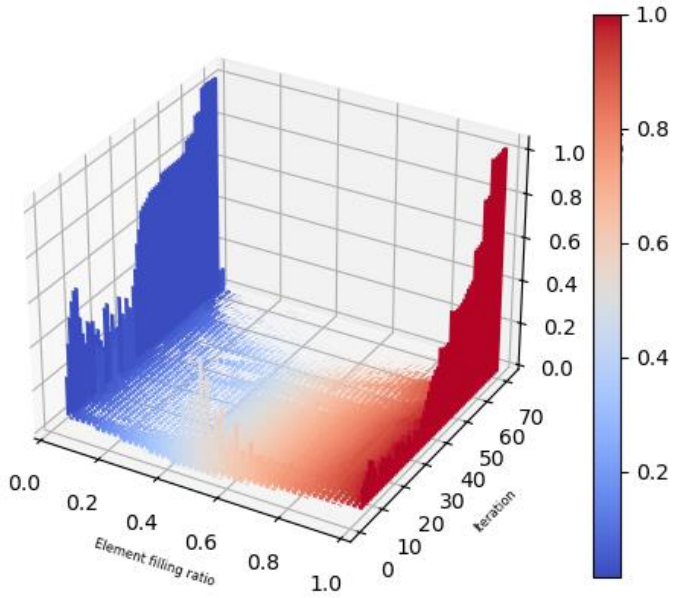

Fig. 4
Cantilever beam: element density distribution (red: solid, blue: void)

The Design Wizard in VisPER is then used to further process the results of the topology optimization, at the end of which the geometry of the optimized structure can be exported as a real CAD file in step format [38].

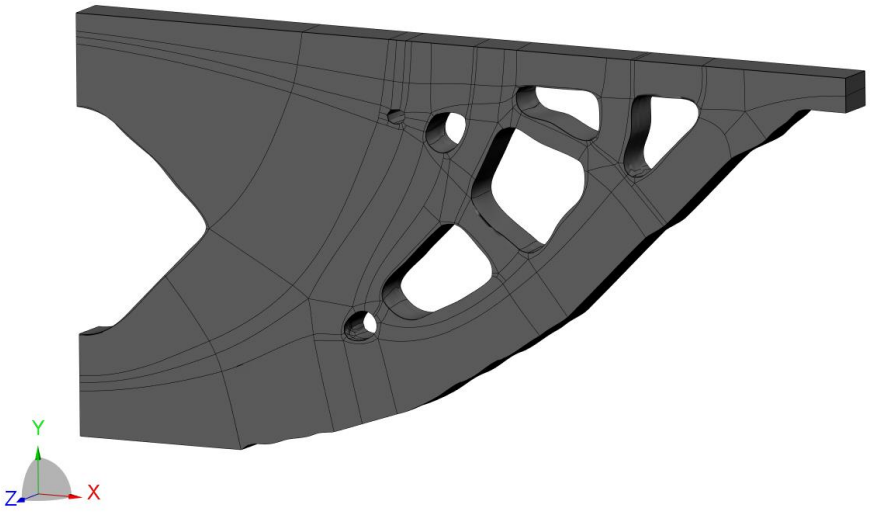

Fig. 5
Quad layout

The export of a real CAD geometry (Fig. 5) represents a significant improvement compared to the previously available stl [39] description (Fig. 6).

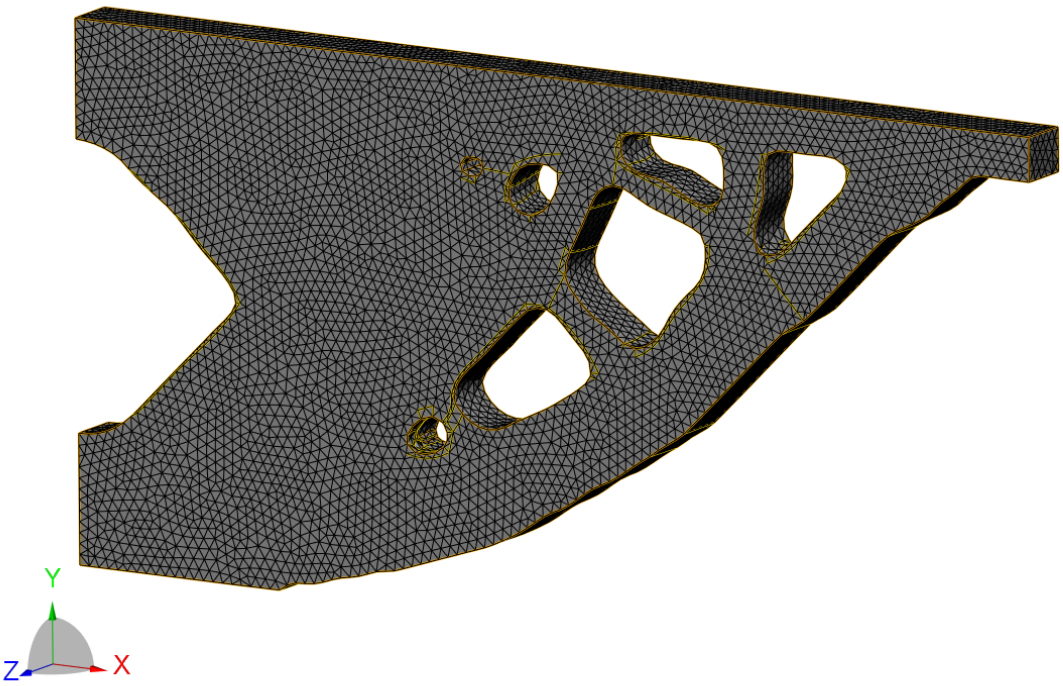

Fig. 6
Unstructured, triangulated surface mesh in stl format

7 Conclusions

Unconstrained compliance minimization problems tend to ignore stress concentration points, leading to an angular shape, which could result in the phenomenon of high stress concentrations, leading to a final design that all too often fails to meet real engineering requirements. Therefore, manual adjustments or shape optimization are used as a subsequent step. The newly available design constraint ($DCONSTRAINT MAXMISES) enables the consideration of stress constraints in topology optimization within PERMAS. However, stress-constrained topology optimization needs more iterations than a classical compliance minimization due to the high nonlinearity of the stress constraint.
The key ingredients, namely the linkage of a FE model with its underlying CAD geometry and the surface parameterization, whose generation is a challenge on its own, are discussed here. The integration of all methods and algorithms in one consistent simulation workflow, has been done for the FE solver PERMAS respectively its graphical user interface VisPER. It is verified by means of some comprehensive and practical examples. These not only demonstrate the complete embedding of topology optimization into a 'CAD to CAD' generative design process, but also that the resulting parameterization of the optimized part is ideally suited for a subsequent parametric shape optimization in a future extension. This is due to the fact, that the parameterization is based on simulation results and hence represents a coarsening of the most important design parameters for a parametric shape optimization. This generative design workflow may be incorporated in each CAD environment that is able to process step format. The basic technology to create a parametric model from a tessellated surface is a generally applicable tool. This is targeted to ease up the usage of simulation-based design and therefore as a contribution to democratization of the use of FEM in the design of components.

8 References

[1] Bruggi, M.: "*On an alternative approach to stress constraints relaxation in topology optimization*", Struct. Multidisc. Optim (2008), Vol. 36, pp. 125—141, https://doi.org/10.1007/s00158-007-0203-6

[2] Campen M., Bommes D., Kobbelt L.: “*Dual loops Meshing: Quality Quad Layouts on Manifolds*”, ACM Transactions on Graphics 31 (4) (2012), pp. 110:1—110:11, https://doi.org/10.1145/2185520.2185606
[3] Cheng G., Jiang Z.:”*Study on topology optimization with stress constraints*”, Engineering Optimization, Vol. 20 (1992), pp. 129—148, https://doi.org/10.1080/03052159208941276
[4] Duysinx P., Bendsoe M. P.: “*Topology optimization of continuum structures with local stress constraints*”, Int. J. Numer. Meth. Engng., Vol. 43, pp. 1453—1478 (1998), https://doi.org/10.1002/(SICI)1097-0207(19981230)43:8%3C1453::AID-NME480%3E3.0.CO;2-2
[5] Duysinx P., Sigmund O.: “*New developments in handling stress constraints in optimal material distribution*”, 7th AIAA/USAF/NASA/ISSMO Symposium on Multidisciplinary Analysis and Optimization 02 September 1998 - 04 September 1998 St. Louis,MO,U.S.A. https://doi.org/10.2514/6.1998-4906
[6] Fan Z., Xia L., Lai W., Xia Q., Shi T.:”*Evolutionary topology optimization of continuum structures with stress constraints*”, Struct. Multidisc. Optim., Vol. 59, pp. 647—658, (2019), https://doi.org/10.1007/s00158-018-2090-4
[7] Fernandes P., Ferrer A., Goncalves P., Parente M., Pinto N., Correira N.: “*Stress-constrained Topology Optimization for Commercial Software; A Python Implementation for ABAQUS”*, Applied Sciences, 2023, Vol. 13, https://doi.org/10.3390/app132312916
[8] Fischer R., Wulf C., Wagner N.: “*Generative Design – Topology Optimization from CAD to CAD*”, NAFEMS World Congress (2023), Tampa, Florida
[9] Fiuk, G., Mrzyglod, M. W.: ”*Numerical benchmarks for topology optimization of structures with stress constraints*”, Bulletin of the Polish Academy of Sciences, Technical Sciences, Vol. 69, 2022, http://dx.doi.org/10.24425/bpasts.2021.139317
[10] Giraldo-Londoño O., Paulino G. H.: “*A unified approach for topology optimization with local stress constraints considering various failure criteria: von Mises, Drucker–Prager, Tresca, Mohr–Coulomb, Bresler–Pister and Willam–Warnke”,* https://doi.org/10.1098/rspa.2019.0861
[11] Granlund G, Wallin M., Tortorelli D., Watts, S.: “*Stress-constrained topology optimization of structures subjected to nonproportional loading*”, Int. J. Numer. Methods Engng. https://doi.org/10.1002/nme.7230
[12] Gu J., Gui T., Yuan Q., Qu J., Wang, Y.: “*Topology optimization method for local relative displacement difference minimization considering stress constraint”*, Engineering Structures, 204 (2024) 117595, https://doi.org/10.1016/j.engstruct.2024.117595
[13] Han Y., Xu B., Duan, Z., Huang, X.: ”*Stress-based topology optimization of continuum structures for the elastic contact problem with friction*”, Struct. Multidisc. Optim., Vol. 65, (2022), https://doi.org/10.1007/s00158-022-03169-1
[14] Huang X., Li W., Nabaki K., Yan X.: “*Reformulation for stress topology optimization of continuum structures by floating projection*”, Computer Methods in Applied Mechanics and Engineering, Vol. 423 (2024), https://doi.org/10.1016/j.cma.2024.116870
[15] Le C., Norato J., Bruns T., Ha C., Tortorelli D.: “*Stress-based topology optimization for continua*”, Struct. Multidisc. Optim, (2009), pp. 605—620, https://doi.org/10.1007/s00158-009-0440-y
[16] Leader M. K., Chin T. W., Kennedy G. J.: “*High Resolution Topology Optimization with Stress and Frequency Constraints”*, AIAA Aviation Forum, 2018, Atlanta, Georgia, https://doi.org/10.2514/1.J057777
[17] Lee E., James K.A., Martins J.R.R.A.:“*Stress-constrained topology optimization with design-dependent loading*”, Struct. Multidisc. Optim., Vol. 46, pp. 647—661, (2012), https://doi.org/10.1007/s00158-012-0780-x
[18] Lee K., Ahn K., Yoo J.: ”*A novel P-norm correction method for lightweight topology optimization under maximum stress constraints*”, Computers & Structures, Vol. 171, pp. 18—30, (2016), https://doi.org/10.1016/j.compstruc.2016.04.005
[19] Li Y., Chang T., Kong W., Wu F., Kong, X.: “*Topological Optimization of Bi-Directional Progressive Structures with Dynamic Stress Constraints under Aperiodic Load”*, Applied Sciences 2024, Vol. 14, http://dx.doi.org/10.3390/app14010322
[20] Long K., Wang, X., Liu H.:”*Stress-constrained topology optimization of continuum structures subjected to harmonic force excitation using sequential quadratic programming*”, Struct. Multidisc. Optim,, Vol. 59, pp. 1747—1759, (2019), https://doi.org/10.1007/s00158-018-2159-0
[21] Luo Y., Kang Z.: “*Topology optimization of continuum structures with Drucker-Prager yield stress constraints*”, Computers and Structures, Vol. 90-91, pp. 65—75, (2012) https://doi.org/10.1016/j.compstruc.2011.10.008

[22] Mitjana F., Cafieri S., Bugarin F., Segonds S., Castanie F., Duysinx P.:"*Topological gradient in structural optimization under stress and buckling constraints*", Applied Mathematics and Computation, Vol. 409, (2021) https://doi.org/10.1016/j.amc.2021.126032
[23] Nabaki, K., Shen, J., Huang, X.:"*Stress minimization of structures based on bidirectional evolutionary procedure*", Journal of Strutural Engineering, Vol. 145(2), (2019), https://doi.org/10.1061/(ASCE)ST.1943-541X.0002264
[24] Oh, M.K., Lee D. S., Yoo J.:"*Stress constrained topology optimization simultaneously considering the uncertainty of load positions*", Int. J. Numer. Methods Eng, Vol. 123 , pp. 339—365, (2021), https://doi.org/10.1002/nme.6858
[25] París J., Navarrina F., Colominas I., Casteleiro M.: "*Topology optimization of continuum structures with local and global stress constraints*", Struct. Multidisc. Optim (2009), Vol. 39, pp. 419—437, https://doi.org/10.1007/s00158-008-0336-2
[26] París J., Navarrina F., Colominas I., Casteleiro M.: "*Block aggregation of stress constraints in topology optimization of structures"*, Advances in Engineering Software 41 (2010) pp. 433–441, https://doi.org/10.1016/j.advengsoft.2009.03.006
[27] Rong J. H., Xiao T. T., Yu L. H., Rong X. P., Xie, Y. J.; "*Continuum structural topological optimizations with stress constraints based on an active constraint technique",* Int. J. Numer. Meth. Engng. 2016; 108:326–360, https://doi.org/10.1002/nme.5234
[28] Senhora F. V., Giraldo-Londono O., Menezes I. F. M., Paulino, G. H.: "*Topology optimization with local stress constraints: a stress aggregation-free approach*", Struct. Multidisc. Optim., Vol. 62, pp. 1639—1668, (2020), https://doi.org/10.1007/s00158-020-02573-9
[29] Shepherd K. M., Hiemstra R. R., Hughes T. J. R.:"*The quad layout immersion: A mathematically equivalent representation of a surface quadrilateral layout*", Computer Methods in Applied Mechanics and Engineering, Vol. 417, (2023), https://doi.org/10.1016/j.cma.2023.116445
[30] Xiao M., Ma J., Lu D., Raghavan, B., Zhang, W.: "*Stress-constrained topology optimization using approximate reanalysis with on-the-fly reduced order modeling*", Adv. Model. And Simul. In Eng. Sci. (2022) Vol. 9,17, https://doi.org/10.1186/s40323-022-00231-x
[31] Yang D., Liu H., Zhang W., Li S.: "*Stress-constrained topology optimization based on maximum stress measures*", Computers and Structures, Vol. 198 (2018), pp. 23—39, https://doi.org/10.1016/j.compstruc.2018.01.008
[32] Wang, M. Y., Li L.: "*Shape equilibrium constraint: a strategy for stress-constrained structural topology optimization*", Struct. Multidisc. Optim. (2013), Vol. 47, pp. 335—352, https://doi.org/10.1007/s00158-012-0846-9
[33] Wang M. Y., Luo Y.: "*An enhanced aggregation method for stress-constrained topology optimization problems*", 10th World Congress on Structural and Multidisciplinary Opimization, May 19-24, 2013, Orlando, Florida, USA
[34] Wu Y., Qiu W., Xia L., Li W., Feng K.: "*Design of an aircraft engine bracket using stress-constrained bi-drectional evolutionary structural optimization method*", Struct. Multidisc. Optim., Vol. 64, pp. 4147—4159 (2021), https://doi.org/10.1007/s00158-021-03040-9
[35] Zhang, H.-Z., He, Q.-C., Chen, Z.-D., Yin, B.: "*Stress-based topology optimization using BESO method with incremental structural nonlinear analysis", http://dx.doi.org/10.21203/rs.3.rs-3594940/v1*
[36] PERMAS V20 (2024) https://www.intes.de
[37] VisPER V20 (2024) https://www.intes.de
[38] https://en.wikipedia.org/wiki/ISO_10303-21
[39] https://en.wikipedia.org/wiki/STL_(file_format)

Topologieoptimierung des Querschnitts von crashbelasteten Profilen am Beispiel des seitlichen Batterieschutzes eines Audi Q8 e-tron

Dr.-Ing. Dominik Schneider, Simon Link, Florian Beyer, Gerrit Schmidt (iNDUVOS GmbH)

1 Einleitung

Optimierungsmethoden haben einen breiten Einzug in den Entwicklungsprozess von Fahrzeugstrukturen gefunden. Sie reduzieren beispielsweise das Bauteilgewicht, die Kosten und den Energieverbrauch in der Herstellung und im Fahrbetrieb drastisch. Der Einsatz von gängigen Topologieoptimierungsverfahren scheitert in Crashanwendungen an den komplexen, zeitabhängigen, nichtlinearen mechanischen Prozessen, dem großen Simulationsaufwand und den nicht ausreichend berücksichtigten Fertigungsanforderungen. Dies hat zur Folge, dass die Auslegung von crashbelasteten Fahrzeugstrukturen oft mit langen Entwicklungszeiten, hohen Kosten und nicht ausgeschöpften Verbesserungspotenzialen einhergehen. Eine neue Lösungsplattform für Optimierungen in diesen Szenarien ist iNDUVOS – Profile, eine Software für die Strukturoptimierung von crashbelasteten Profilstrukturen, die die Herstellbarkeit über Verfahren der Massenfertigung wie Strangpressen und Rollprofilieren gewährleisten kann. Der aktuelle Anwendungsfokus liegt auf seitlich belasteten Strangpressprofilen wie Schwellern und Profile zum Batterieschutz. Solche Strukturen schützen die Insassen, Passanten oder kritische Komponenten in einem Unfall. In dem folgenden Beitrag wird zuerst das Verfahren allgemein erklärt. Danach wird ein Anwendungsbeispiel vorgestellt, in dem die Masse der Profile, welche die Batterie in einem seitlichen Pfahlaufprall schützen, bei sonst gleichbleibender Performance um 8,6 % gesenkt werden konnte. Die grundlegende Methode der Software basiert auf der Graphen- und Heuristikbasierten Topologieoptimierung, die an der Bergischen Universität Wuppertal entwickelt wurde (Ortmann 2013, Ortmann 2021).

2 Methodik

iNDUVOS – Profile ist eine maßgeschneiderte Lösung für die Querschnittsoptimierung von crashbelasteten Profilstrukturen. Zusammengefasst setzt die Software mehrere Algorithmen ein, um die Crashsimulationen von Profilstrukturen zu analysieren und im Anschluss geometrische Verbesserungen vorzunehmen, indem Wände in den Profilquerschnitt eingebracht oder aus diesem entfernt werden. Die Methode arbeitet iterativ und verbessert die Geometrien somit sukzessive über mehrere Iterationen. Während des Prozesses werden verschiedene externe Programme angesteuert, die Simulationsmodelle erstellen, simulieren und optimieren können. Deren Einsatz wird in dem folgenden Kapitel erläutert.

2.1 Eingangsdaten

Um Optimierungen mit iNDUVOS-Profile durchführen zu können, werden einige Ausgangsdaten benötigt. Als erstes muss ein Optimierungsproblem definiert werden. Dazu gehört die Information welches Ziel erreicht werden soll und welche funktionellen Restriktionen einzuhalten sind. Als Strukturantworten können alle Größen gewählt werden, die aus dem Simulationsmodell extrahiert werden können. Oft verwendete Zielgrößen und Restriktionen sind:

- Masse
- Verschiebungen / Intrusionen
- Kontaktkräfte
- Energien
- Plastische Deformation
- Spannungen

Da die Methode über interne Algorithmen für jeden Entwurf die Herstellbarkeit überprüft, müssen auch hierfür zulässige Grenzwerte angegeben werden. In Abb. 1 wird darum ein beispielhafter Profilquerschnitt mit einer Auswahl der möglichen Parameter dargestellt, die festgelegt werden können, um die Herstellbarkeit im Strangpressverfahren zu gewährleisten.

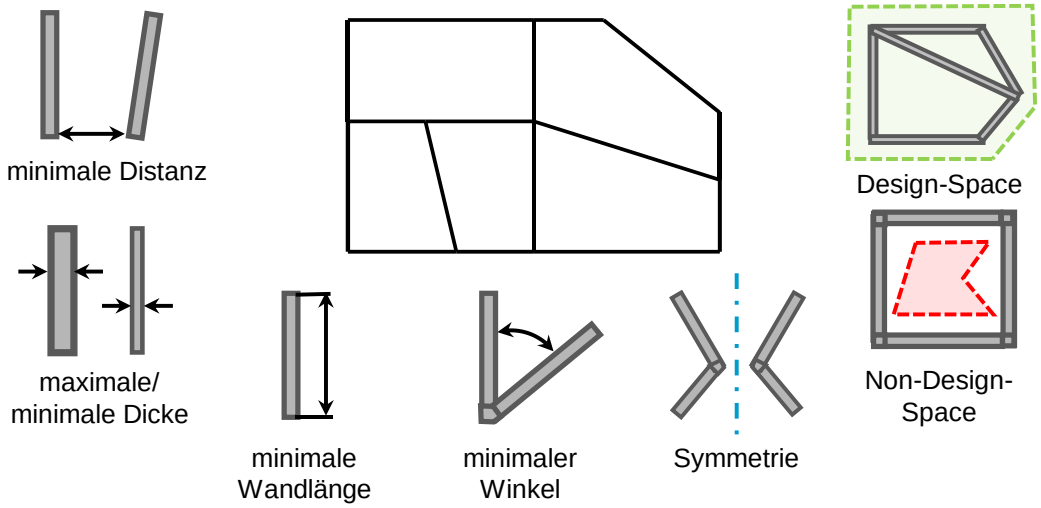

Abbildung 1: Ansicht eines Profilquerschnitts mit Auswahl möglicher definierbarer Fertigungsrestriktionen

Als nächstes wird eine Simulationsmodell benötigt. Neben lang rechnenden Gesamtfahrzeugmodellen können auch kleinere Modelle verwendet werden, die aus Teilstrukturen eines Fahrzeugs aufgebaut werden. Die Modelle müssen so aufbereitet sein, dass die zu optimierenden Profilstrukturen als eigenes Include (Input Deck) durch iNDUVOS-Profile erzeugt werden können und damit in das restliche Modell eingebunden werden. Löcher, Aussparungen und Schnittkanten an den Profilenden können über Verschnittvolumen in Form einer Step-Datei in den Prozess übergeben werden. Als Ausgangsbasis für die Optimierung können ein oder mehrere Startentwürfe vom Anwender vorgegeben werden. In der Regel wird mit einer Profilstruktur ohne innere Wände gestartet, um im Optimierungsverlauf die größte Freiheit zu haben, die bestmöglichen Entwürfe zu finden.

2.2 Ablauf

Basierend auf dem Ausgangsentwurf werden in der ersten Iteration der Optimierung mehrere Simulationen durchgeführt, in denen die Wandstärken des Profils variiert werden, um dieses optimal auf das vorgegebene Optimierungsproblem einzustellen.
In der nächsten Iteration werden die Ergebnisse der Crashsimulationen von internen Algorithmen analysiert. Die Algorithmen basieren auf Expertenwissen von Ingenieuren und identifizieren strukturelle Schwachstellen des Profils während des Crashvorgangs Die verschiedenen Algorithmen identifizieren so unter anderem stark beulende Wände oder Bereiche mit nur geringen Energieabsorptionen. Jeder der Algorithmen verwendet speziell abgestimmte Regeln, um geometrische Veränderungen vorzunehmen, mit dem Ziel das identifizierte Verhalten zu verbessern. Um den Einfluss der Änderung bewerten zu können, wird für jeden Entwurf wieder eine kleine Wandstärkendimensionierung mit mehreren Simulationen durchgeführt. Für die Dimensionierungen können dabei verschiedene Strategien festgelegt werden, die sich in der Stützstellenauswahl und der Art der eingesetzten Metamodelle unterscheiden. Die Entwürfe aller Algorithmen konkurrieren innerhalb einer Iteration miteinander und am Ende werden nur die besten Entwürfe in die nächste Iteration übergeben. Die genaue Anzahl kann vom Anwender festgelegt werden. Danach beginnt der Prozess erneut, sodass die Algorithmen wieder von allen Entwürfen die Simulationsdaten analysieren und neue konkurrierende Entwürfe erzeugen. Der Prozess geht so lange weiter, bis ein Abbruchkriterium erreicht wird. Dies kann unter anderem eine maximale Iterationsanzahl sein oder eine ausbleibende Verbesserung zwischen den Iterationen. Am Ende der Optimierung kann mit dem besten Entwurf noch eine detaillierte Formoptimierung durchgeführt werden, um die Performance der Struktur noch weiter zu verbessern, wenn durch die topologischen Änderungen keine Verbesserung mehr erzielt werden konnte.

3 Anwendungsbeispiel Batterieschutz

Um das volle Potential des Verfahrens aufzuzeigen, wird im Folgenden eine Optimierung vorgestellt. Als Anwendungsbeispiel wird die Batterie eines Audi Q8 e-tron in einem seitlichen Pfahlaufprall gewählt. Das Modell wurde auf der Basis eines LS-DYNA Gesamtfahrzeugmodells des Audi Q8 e-tron aufgebaut, welches durch die Firma *Caresoft Global* bereitgestellt wurde und in einer technischen Fallstudie durch *Alumobility* angepasst wurde. Um den Simulationsaufwand für diese Studie zu reduzieren, wurde nur das Batteriemodul aus dem Modell extrahiert und damit der seitliche Pfahlaufprall modelliert. Die

Geschwindigkeit des Pfahls beträgt 32,5 km/h und seine Masse wurde mit 1200 kg so gewählt, dass die Deformation möglichst nahe an die Deformation im Gesamtfahrzeugmodell herankommt. Das so gewählte Simulationsmodell rechnet auf einem Hochleistungsrechencluster mit 32 CPUs ca. 1,5 Stunden. In Abb. 2 ist das Ausgangsmodell sowie das isolierte Modell des Batteriemoduls abgebildet.

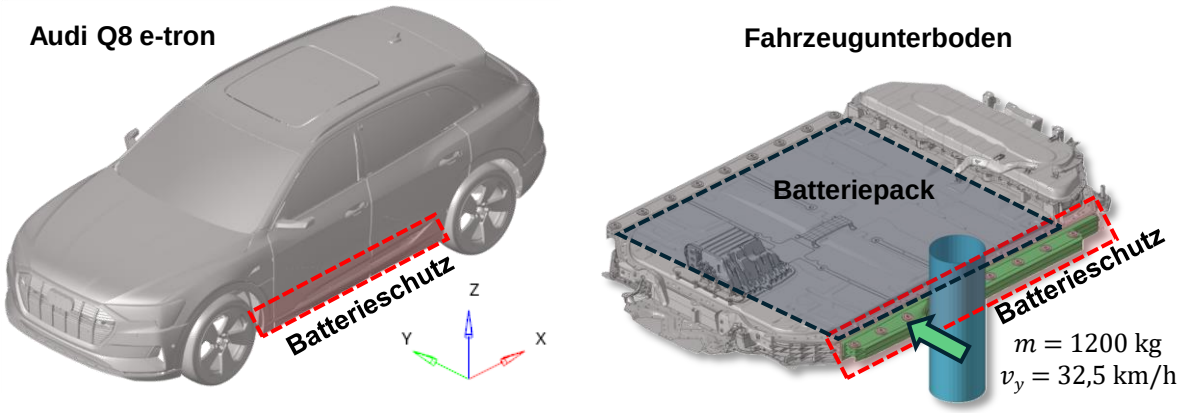

Abbildung 2: Modell des Audi Q8 e-tron (links) und abgeleitetes Modell des Batteriemoduls im seitlichen Pfahlaufprall (rechts)

Das Optimierungsziel ist die Masse zu reduzieren, ohne bei den sonstigen Struktureigenschaften schlechter zu werden. Darum werden die Werte des aktuell eingesetzten Referenzentwurfs als Restriktionen verwendet. So darf die Intrusion des Pfahls nicht größer als 97 mm werden, die Kontaktkraft zwischen Pfahl und dem Batteriemodul muss unter 610 kN bleiben und ein minimaler Abstand von mehr als 7 mm zwischen den Batteriezellen und einem angrenzenden Blech muss eingehalten werden, um eine Beschädigung der Zellen zu verhindern. Der Abstand wird an den 15 in Abb. 3 markierten Finite Elemente Knoten überprüft.

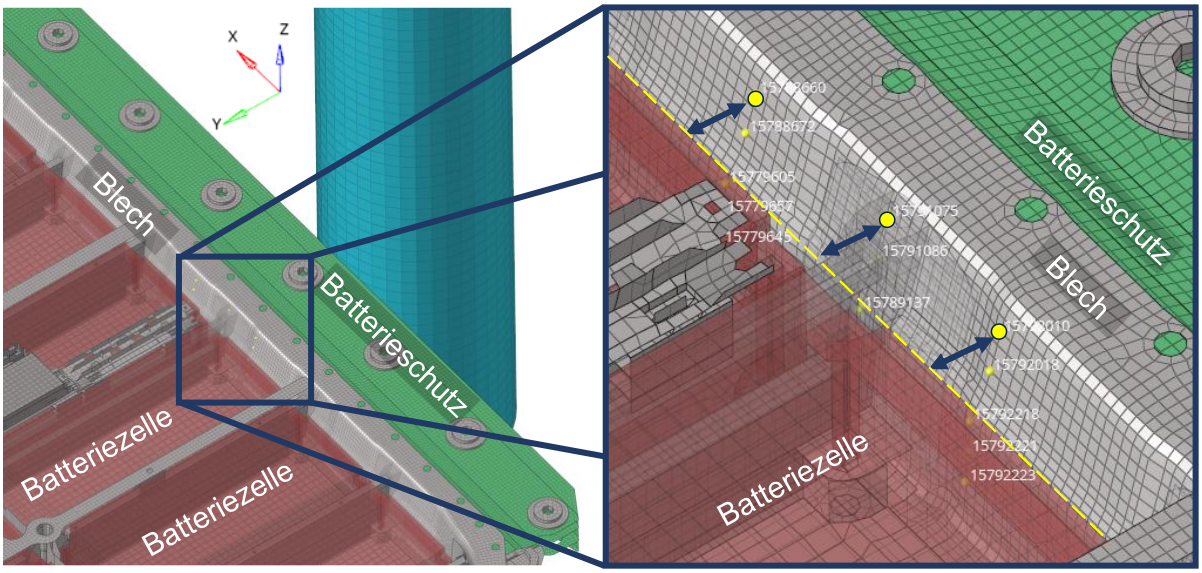

Abbildung 3: Restriktion zur Einhaltung eines Mindestabstands zwischen den Batteriezellen und dem angrenzenden Blech, gemessen an 15 Knoten (zwei Knoten in der Mitte sind verdeckt)

Wie in Abb. 4 nachvollzogen werden kann, startet die Optimierung mit einer Dickendimensionierung des Startentwurfs, in der sechs Simulationen verwendet werden. In der folgenden Iteration werden basierend auf diesem Startentwurf durch die verschiedenen Algorithmen insgesamt sieben verschiedene konkurrierende Entwürfe generiert, die wiederum mit kleinen Dickendimensionierungen bewertet werden. Ab jetzt werden jeweils die fünf besten Entwürfe mit in die nächste Iteration genommen. So werden in den folgenden Iterationen jeweils 37-50 Entwürfe erzeugt, bis in Iteration 11 das vorläufige Abbruchkriterium erreicht wird, da die Topologieänderungen in dieser Iteration keine

weitere Verbesserung erreichen können. In Iteration 12 wird zum Abschluss noch eine detaillierte Dickenoptimierung mit 121 Simulationen durchgeführt, in der 8 Variablen freigegeben sind.

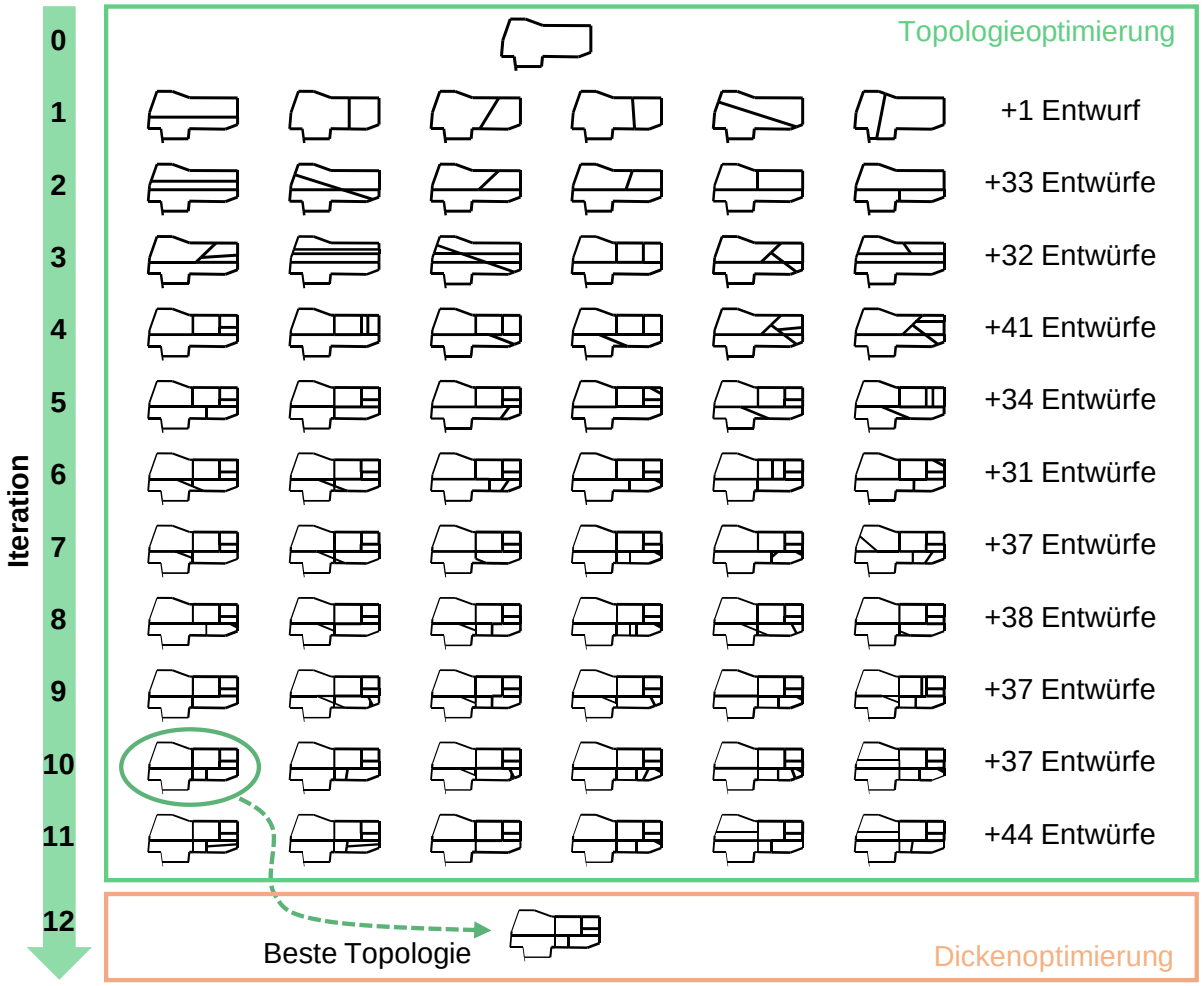

Abbildung 4: Historie mit dem Optimierungsablauf und einer Auswahl der besten Profilquerschnitte der jeweiligen Iteration

In Tabelle 1 wird das optimierte Profil mit dem Referenzentwurf verglichen. Durch die Optimierung konnte die Masse um 8,6 % reduziert werden, wobei alle definierten Restriktionen eingehalten wurden. Die auftretende Maximalkraft konnte durch das verbesserte Deformationsverhalten gleichzeitig um 7,7 % gesenkt werden. Die Fertigungsrestriktionen werden erfüllt, so dass das Profil im Strangpressverfahren hergestellt werden kann. Abb. 5 zeigt die Kraft-Weg-Kurven des besten Entwurfs der Optimierung und der Referenz. Eine Visualisierung der internen Geometriebeschreibung der beiden Querschnitte sowie die zugehörigen Deformationen sind in Abb. 6 in der Schnittansicht dargestellt. Insgesamt wurden in der Optimierung 367 verschiedene Entwürfe durch die Algorithmen erzeugt und mit insgesamt 1173 Simulationen bewertet.

Tabelle 1: Vergleich der Werte des Referenzentwurfs mit dem optimierten Entwurf

Wert	**Referenz**	**Optimiert**
Masse [kg]	17,07	15,6
Pfahleindringung [mm] <=97	96,4	97,0
Max. Kraft [kN] <=610	608	561
Min. Distanz Batteriezellen [mm] >=7	7,2	7,2
Entwicklungszeit insgesamt	ca. 2 Monate	5-7 Tage

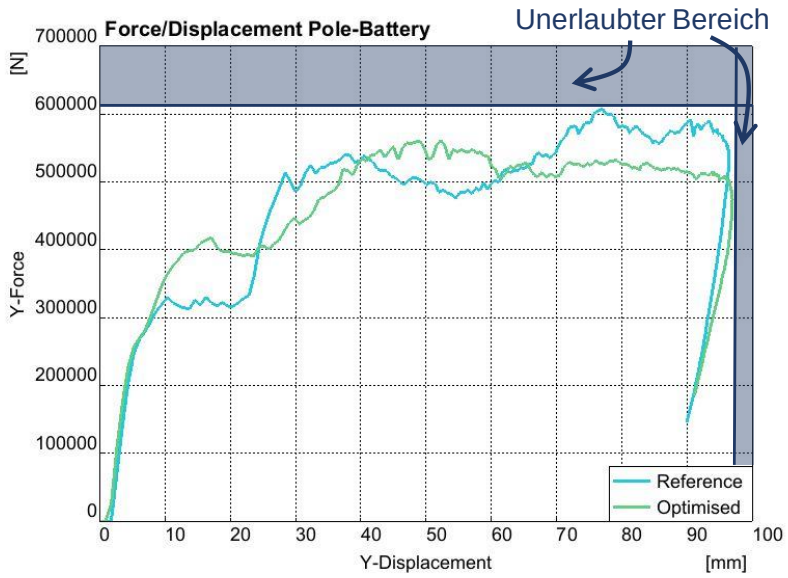

Abbildung 5: Kraft-Weg-Kurve des Referenzentwurfs (blau) und des optimierten Entwurfs (grün)

4 Zusammenfassung

Während einer Optimierung mit iNDUVOS - Profile werden in der Regel 100-400 geometrisch verschiedene Entwürfe generiert, die je nach gewählten Optimierungseinstellungen mit insgesamt 300-1200 Simulationen pro verwendeten Lastfall bewertet werden. Die breitgefächerte, aber gezielte Abtastung des Entwurfsraums führt zu dem großen Verbesserungspotential, das auch in dem Anwendungsbeispiel gezeigt werden konnte. In der automatisch ablaufenden Optimierung konnte die Masse des Batterieschutzes im Audi Q8 e-tron innerhalb einer Woche um 8,6 % reduziert werden. Bezogen auf die 230.000 in Serie produzierten Fahrzeuge ergibt sich neben der verkürzten Entwicklungszeit eine mögliche Materialeinsparung von 690 Tonnen Aluminium mit einem Materialgegenwert von mehr als 2,4 Millionen Euro.
Die Anzahl der durchgeführten Simulationen kann durch verschiedene Optionen reduziert werden, wie die Anzahl der Entwürfe, die in die nächste Iteration überführt werden oder die Deaktivierung einzelner Algorithmen zur Topologieänderung. Dadurch kann das erreichbare Verbesserungspotential jedoch sinken. Der aktuelle Entwicklungsfokus liegt neben der Erweiterung für weitere Anwendungsfelder auf der Reduzierung der benötigten Simulationen. Zusammenfassend können mit iNDUVOS-Profile in kürzerer Zeit sichere und leichtere Profilstrukturen ausgelegt werden, die bereits die Herstellbarkeit berücksichtigen.

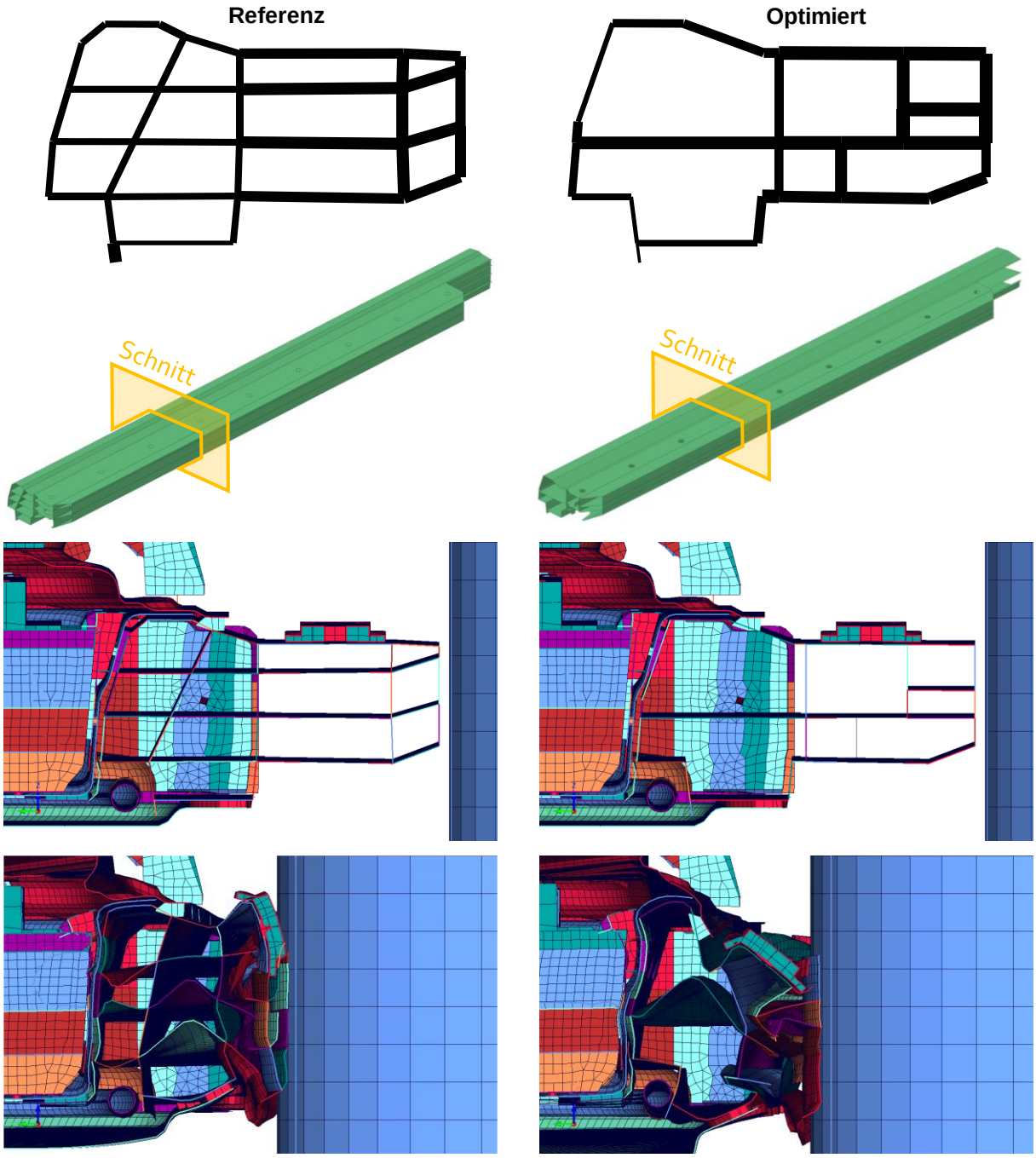

Abbildung 6: Von oben nach unten jeweils Querschnittsansicht, isometrische Profilansicht, undeformierte Schnittansicht und deformierte Schnittansicht des Referenzentwurfs (links) und des optimierten Entwurfs (rechts)

5 Literaturverzeichnis

Ortmann, C., Schumacher, A. (2013): "Graph and heuristic based topology optimization of crash loaded structures", Structural and Multidisciplinary Optimization (2013) 47:839–854

Ortmann, C., Sperber, J., Schneider, D., Link, S., Schumacher, A. (2021): “Crashworthiness design of cross-sections with the Graph and Heuristic based Topology Optimization incorporating competing designs”, Structural and Multidisciplinary Optimization (2021) 64:1063-1077

Design of cooling components through the combination of implicit modeling and topology optimization

Dr. Lieven Vervecken (Diabatix), Sarah da Silva Andrade (Diabatix), Niels Verdijck (Diabatix), Ine Vandebeek (Diabatix)

1 Summary

While topology optimization allows to optimally distribute material within a design domain to achieve the best performance, implicit modeling facilitates the automated and precise generation of complex geometries directly from computational data. By combining both, typical implicit triply periodic minimal structures such as gyroids, and pin/fin structures can be further improved by leveraging the power of topology optimization. This paper investigates and demonstrates the significant advancement that can be achieved by combining both in the context of thermal management, focusing on a case study involving the design of a double-sided power inverter cooling system.

2 Introduction

In the context of thermal management, particularly for high-performance computing systems, the design of cooling components plays a crucial role in system performance and longevity. Traditional methods often fall short in optimizing both the geometric complexity and the material efficiency required for advanced cooling solutions. Implicit modeling and topology optimization emerge as robust tools, offering significant improvements over conventional thermal design processes.

3 Methodology

3.1 Implicit Modeling

Implicit modeling forms the first phase of our design process. This technique allows for the generation of complex geometries that are computationally defined by implicit surfaces without the need for explicit boundary representations. In our approach, we employ implicit functions to design intricate triply periodic minimal surfaces (TPMS) and pin/fin structures. For a detailed exposition of this approach, refer to our publication presented at Therminic 2023 [1].

3.2 Topology Optimization

A multi-objective, multi-constraint genetic algorithm is employed to design the base geometry for the case studies with two primary objectives: increase thermal efficiency and simultaneously mitigate pressure drop. This algorithm systematically adjusts the geometric parameters of the TPMS and pin/fin structures. The topology optimization framework allows for a methodical exploration of the design space, leading to iterative refinement and, ultimately, configurations that adeptly balance thermal performance with flow resistance. Computational fluid dynamics (CFD), evaluated using Diabatix's ColdStream platform [2], is used to evaluate the heat sink's respective thermal dissipations and associated pressure drops during the optimization.

The following flowchart (Fig. 1) illustrates the two possible scenarios for the optimization process. The first scenario involves pure topology optimization, beginning with an empty design region. The second scenario corresponds to the combination of implicit modeling and topology optimization, as described in the methodology herein.

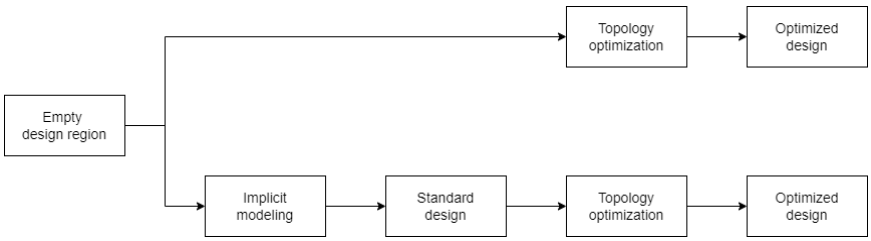

Fig. 1
Flowchart depicting the two possible scenarios for the optimization process

4 Case study: Double-sided power inverter

The practical application of these combined methodologies is demonstrated through the development of a liquid cooling system for a double-sided power inverter.

The double-sided power inverter has two heat sources, located at the top and bottom respectively. The chips emit a total heat of 4002W. Aluminum is used for the housing and heat sink, and the cooling system uses a 40/60 mix of water and glycol as the coolant. The pressure loss has a target of 6kPa. The design domain is highlighted in Fig. 2, consisting of two regions: the bottom and the top. Pins/fins are generated within the design region, with the optimization targets of temperature minimization and temperature variance minimization.

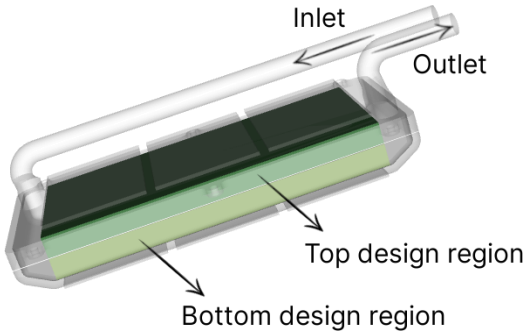

Fig. 2
Double-sided power inverter. The inlet and outlet are highlighted, as well as both design regions

The implicit modeling simulation resulted in two pins heatsinks shown in Fig. 3. This heat sink is used as the initialization to be further improved using topology optimization. The optimization process uses the same targets established in the previous step for implicit modeling. For the current study, the topology optimization algorithm is only allowed to add material to the initial heat sink. The resulting heat sink is shown in Fig. 4a. To help in the visualization, the fluid region corresponding to this heat sink is shown in Fig. 4b, and the temperature field of the chips and copper heat spreads is displayed in Fig. 4c.

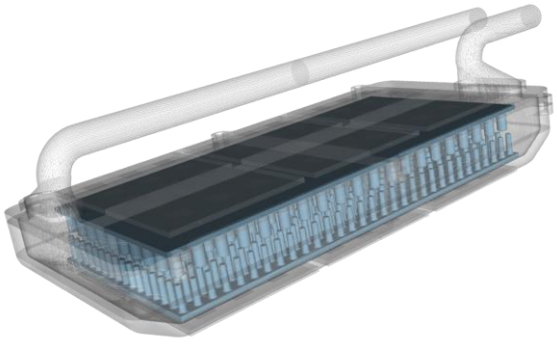

Fig. 3
Heat sinks for the double-sided power inverter after the implicit modelling simulation

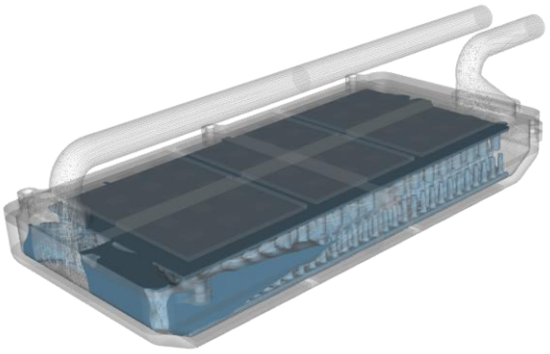

Fig. 4a
Heat sinks for the double-sided power inverter after the topology optimization

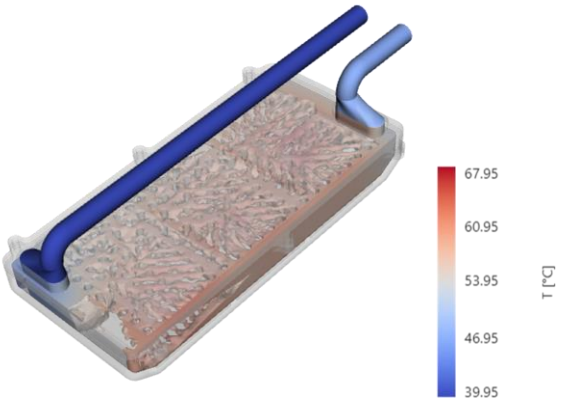

Fig. 4b
Fluid representation of the heat sink after the topology optimization with the temperature field

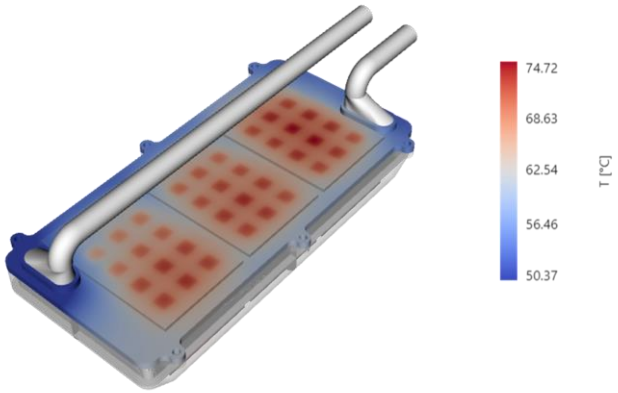

Fig. 4c
Temperature field of the chips and copper heat spreaders

The simulation results for the cooling system reveal a maximum chip temperature of 74.72°C. The observed pressure drop across the system is 2187.7 Pa.

To establish a baseline for comparison, this study contrasts the current case with a scenario where no initial design was provided. In this control case, the design process was initiated from an empty space (similar to Fig. 2), while keeping the geometrical configurations and operational parameters consistent. Fig. 5 depicts the fluid region as it appears in this reference scenario. The CFD simulation shows a peak temperature of 74.80°C for the chips. The pressure drop of the system is 2753.15 Pa.

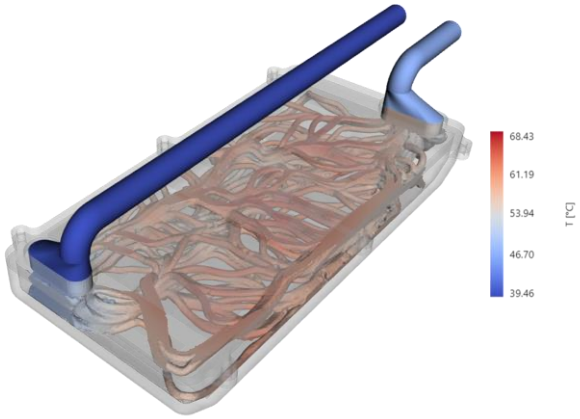

Fig. 5
Control case - Optimization without an initial design

An overview of the results can be found in Fig. 6.

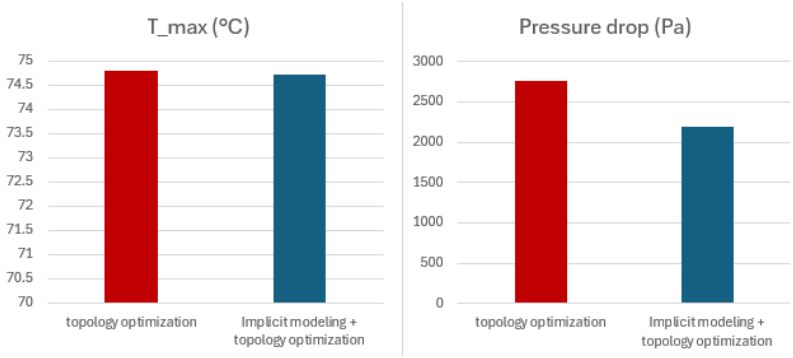

Fig. 6
Overview of the results for maximum temperature of the chip (T_max) and pressure drop for the control case (topology optimization) and the case under study (implicitly modeling + topology optimization).

5 Discussion

This study contrasts two design scenarios of a double-sided power inverter: one with an initial design and one without, referred to as a control case. Notably, the maximum temperature of the heat source in both designs is nearly equivalent, with the current case exhibiting a mere 2% increase. This similarity in thermal performance suggests that the initial design modifications do not significantly impact the thermal peak of the inverter. More striking, however, is the reduction in pressure drop observed in the current case, which is 21% lower than that in the control case. This substantial decrease in pressure drop indicates a more streamlined flow path or improved channel design, which can significantly enhance the overall thermal management system by reducing flow resistance, thereby potentially improving the efficiency and longevity of the power inverter.

We highlight the substantial time savings achieved through the combination of implicit modeling and topology optimization in the design of cooling systems for double-sided power inverters. Compared to the topology optimization-only approach, which starts with an empty design state, inserting an initial design facilitates a more efficient and streamlined design process. This dual approach not only accelerates the development cycle but also enhances the potential for achieving superior performance and innovation in thermal management solutions.

6 Conclusion

The combined use of implicit modeling and topology optimization offers a powerful design strategy for thermal management systems in various sectors, including computing, automotive, and aerospace. This methodology not only enhances the performance and efficiency of cooling components but also contributes to more sustainable manufacturing practices by minimizing material waste.

7 References

[1] Vandebeek, I., Andrade, S.D.S., Sovani, Y. and Vervecken, L., 2023, September. Definition of a Common Parameter Set for Heterogeneous Heat Sink Shapes. In *2023 29th International Workshop on Thermal Investigations of ICs and Systems (THERMINIC)* (pp. 1-4). IEEE.

[2] ColdStream by Diabatix, coldstream.diabatix.com

Quick and Reliable Simulation Process Automation A Critical Driver for Reducing Product Development Time and Cost

B. Webster, PhD, K. Peters
(Novus Nexus, Inc, USA);

M. Felice
(virsolTech Engineering Consulting, LLC, USA)

Abstract

The wide-ranging use of simulations throughout all phases of product development is becoming increasingly important in meeting the growing challenges of global competition. Simulation not only helps to develop competitive products faster but also provides a considerable cost advantage by reducing the number of necessary prototypes and related physical testing.

However, to realize all the achievable benefits of simulation, it needs to be performed systematically, consistently, and efficiently. In an optimal scenario, simulation is directly available to a broader group of users, not just simulation specialists, with designers and analysts collaborating closely.

Automated simulation processes for analysts, designers, and product developers are essential for realizing this systematic and efficient use of simulation. Historically, such broader use of automated processes often fails due to the task's difficulty. Automation via common approaches like scripting (Python, etc.) quickly results in a prohibitive effort for implementation and upkeep, especially when complex or vastly differing geometries are involved. Not only is the initial setup complex here, but extensions or modifications down the line can become exceedingly complicated, too often resulting in a complete rebuild of the processes.

Therefore, new approaches are needed to overcome the current challenges and secure a fuller range of simulation benefits, enabling fast, easy, and robust process automation. This presentation explores how a combination of simulation-specific “no-code” tools (based on abstract modeling) and universal "low-code" tools can drastically simplify automation, even and especially when complex products are involved. The impact of systematically automated simulation processes on the overall development cycle is also analyzed.

Advantages of this approach to automation include the ability for non-CAE specialists to initiate reliable simulations, the relief for analysts from unproductive routine work, the preservation of simulation knowledge, and the continuous use of best practices for future simulations.

1. The challenge of automating simulation processes

The web portal Digital Engineering 247 interviewed several industry veterans for an analysis [1] of how simulation can be improved and made accessible to a broader user group. They named the automation of simulation processes as the most critical factor for broader use. At the same time, it was pointed out that it is often too difficult to automate reliably and with reasonable effort using standard tools.

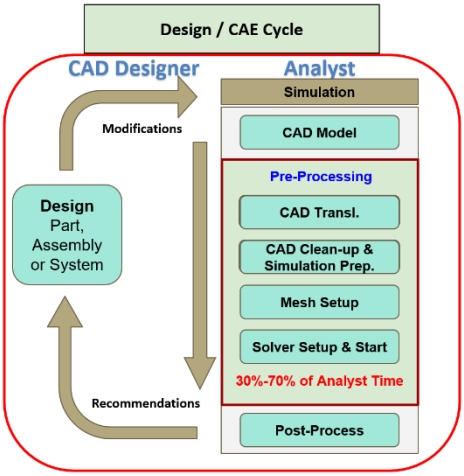

Figure 1 Traditional simulation process starting with CAD model

Under these conditions, it is no surprise that, to this day, it is mainly large companies carrying out vast numbers of similar simulations that implement and benefit from the advantages of simulation process automation. However, new technologies intended to automate simulation processes from the start now allow companies of any size to automate easily and benefit from more systematic, efficient, and dependable simulations.

a. Simulation setup based on specific geometry instances

Common preprocessors require a particular geometry to which all simulation parameters are applied, e.g., material data, loads, specifications for mesh generation, etc.; this is appropriate for analysts who work interactively with the preprocessor; they see the current model to be simulated with all the details and can take them into account accordingly.

However, this procedure is less suitable for automatic processes. The programming (scripts) must anticipate what geometry variations could occur to be able to add the simulation parameters in the correct places. Also, it is often impossible to know all variations in advance, especially in the case of complex geometries. Hence, this approach frequently fails due to a lack of robustness.

Automation using common preprocessors may be feasible with reasonable effort for varying CAD models that only change within foreseeable limits. However, the situation quickly becomes unwieldy when CAD model geometries vary greatly or are very complex.

The dependency on explicit existing geometries explains why automating simulation processes is often challenging. But how can these challenges be overcome?

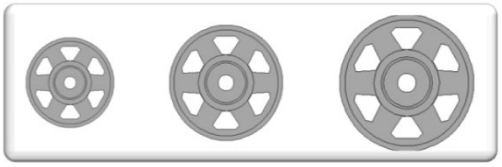

Figure 2: geometries with foreseeable changes

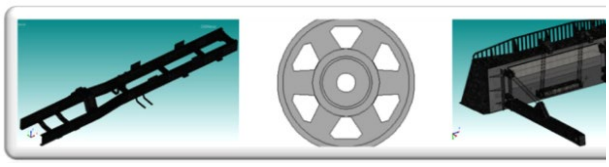

Figure 3: geometries with unforeseeable changes

b. Geometry-independent specification of the simulation

A proven way to overcome geometry dependency and reliably automate even for the most complex CAD models is by employing geometry-independent simulation templates that can be reused for any geometry. These templates, so-called "abstract models," use classes (3D, 2D, 1D) as placeholders for varying CAD instances. To enable such an approach, CAD models to be analyzed are supplemented with text attributes. This allows a preprocessor based on this abstract modeling approach to attach all simulation parameters to the correct solids, surfaces, etc., and automatically generate the files necessary for the solver, including the mesh. To start the automated CAD-to-Solver process, all one

needs is a batch command that specifies which CAD model is to be combined with which abstract model and in which folder the generated solver files are to be stored.

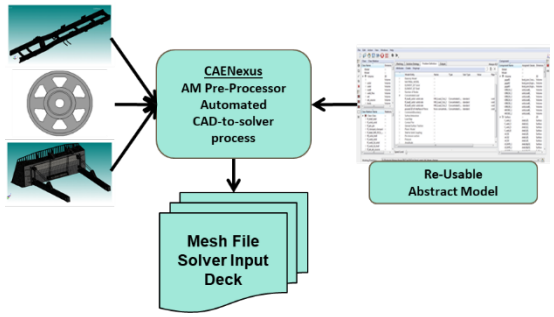

Figure 4: Automatic CAD-to-Solver process for arbitrary geometries

Abstract modeling enables simulation automation by configuring an appropriate template (CAD-to-solver) in less than an hour. Configuring and automatically creating reports by defining their content in the abstract models is also possible.

2. Automation of simulation processes - efficiency through no/low-code tools

Universal low-code tools allow developers to quickly create software applications by configuring user interfaces and workflows. This significantly reduces the programming and scripting that would otherwise be required. Functionality configured in a browser-based GUI, for example, is easier to understand and modify than that implemented through programming. But the name "Low-Code Tools" gives it away: programs, scripts, macros, etc., are still necessary to address the SW applications involved, to process data, etc.

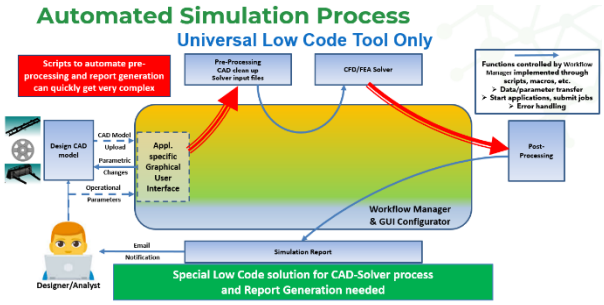

Figure 5: Automation with universal low-code tool

If one automates simulation processes using universal low-code tools only, batch commands for starting the solver, for example, can be implemented relatively quickly. The tool only needs to know where to put the input files and mesh and where to put the results.

On the other hand, a script for preparing the geometry and creating all the solver input files can quickly become very complex and inflexible. The same applies to report generation.

A preprocessor working with abstract modeling can automate the CAD-to-solver process (and reporting) by simply configuring an abstract model. It operates like a no-code simulation automation processor and replaces programming with configuration.

So, suppose one combines a universal low-code with a simulation-specific no-code tool. In that case, end-to-end automation becomes practicable even for complex simulation processes, as the required programming effort is drastically reduced. Figure 6 shows the changed approach with the problematic programming aspects

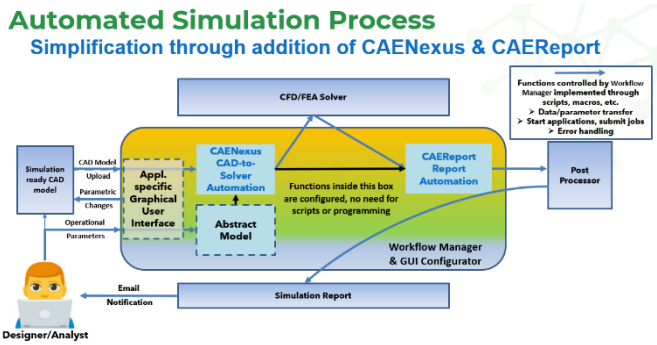

Figure 6: Simplified automation by combining no/low-code tools

avoided. An essential difference in the process with abstract models is that CAD models are prepared for simulation, resulting in a better CAD-to-simulation process and natural path to simulation-driven design.

3. Automation effort and benefits

So far, we have examined automation from a general value perspective and explained why traditional approaches may not deliver the desired benefits. In this chapter, we try to quantify the efficiency gains and required implementation effort. We have chosen two use cases: an FEA use case (ICE Propulsion System for durability) to analyze automation benefits and a CFD use case (automotive HVAC system) to analyze implementation effort applying the no/low code approach.

a. Automation benefits

The following efforts (Figure 7) were estimated based on prior experience using simulation for automotive use cases. They represent ROM numbers for non-automated simulations but are considered accurate enough to quantify efficiency gains through automated simulation. They could vary depending on the specific tools and simulation environment available.

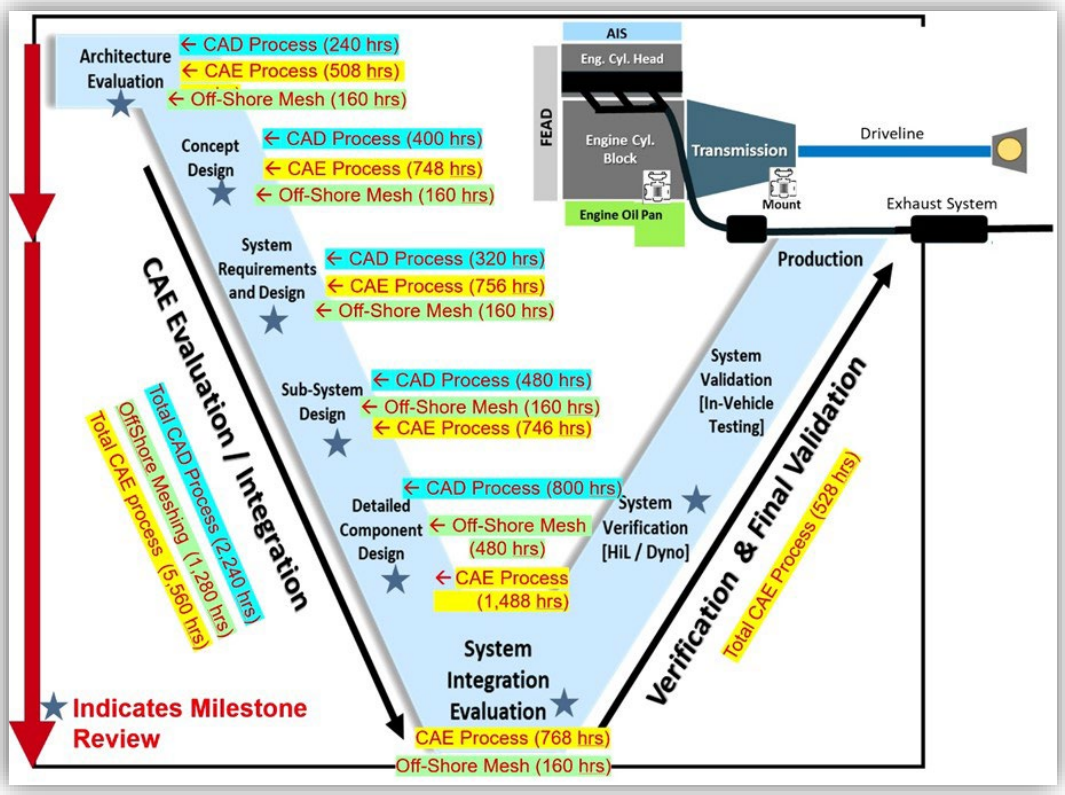

Figure 7: Estimated effort for ICE propulsion system

Automated simulation processes with an appropriate CAD to CAE strategy and report generation can drastically reduce the analyst's effort to execute simulations.

The following table shows the expected reduction for the CAE activities and the resulting efficiency gains.

		Direct CAE Work	Decision support mtgs., project management, …	Total Time
Standard Process	Total global CAE	5,455	1,385	6,840
Automated Process	Total global CAE	555	1,016	1,571
Efficiency Gain		**9.8**	**1.4**	**4.4**

Table 1: CAE efficiency gains through automation

As one can see, automation can heavily impact the actual CAE work. It also impacts meetings due to the consistent simulation process of consistently delivering comparable results. Automatic reports, ideally in the form of 3D digital CAE Reports containing actionable simulation insights, also help to accelerate design decisions.

Now that we have seen the potential for significant efficiency gains once automation is available, let's examine what it takes to get there.

b. Implementation effort

Users of an abstract model-based automation processor can implement simulation automation across various processes (CFD and FEA). Using their own unique no-code automation processor and a universal low-code tool, Novus Nexus has created CFD and FEA automated processes as proof of concept and to capture the necessary effort for the implementation. These existing processes can be quickly converted to address different customer requirements as part of pilot projects (CFD and FEA).

Adding a universal low-code app to automated CAD-to-solver and report generation processes allows easy creation of end-to-end simulations for non-analysts, including browser-based, application-specific user interfaces and notifications when reports are ready.

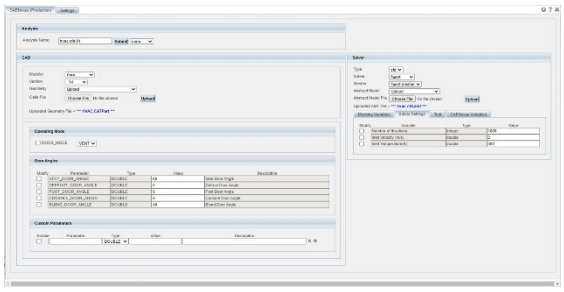

Figure 8: GUI HVAC system CFD simulations

The example shown here addresses automatic CFD simulations used by designers to validate automotive air conditioning systems (HVAC systems).

The user interface in the example shown above offers fewer options than applications currently used by customers. However, due to the configuration options, the effort for such extended interactions usually only takes a few additional hours or days.

Table 2 shows the net times for creating the automated HVAC POC process. It is assumed that specific requirements have already been defined, such as what GUI interactions to provide, clarifying the simulation procedure (best practices), and determining the CAD parameters or boundary conditions the process can change.

Task	HVAC System
CAD preparation - Text Strings	
First model	1 h
Model Variations	0 - 20 min
Abstract Model configuration	
Pre-Processing	8 h
Report	8 h
Universal Low Code Tool actions	
GUI configuration	8 h
Workflow	12 h
System Tests	8 h
Total effort	5 - 6 days

Note: The abstract model for the HVAC system was created from scratch.

Table 2: Implementation effort HVAC automation

4. Conclusions

The above examples show that the automation of simulation processes using no/low-code tools can be implemented efficiently, economically, and reliably, even for complex products. The return on investment is apparent when the implementation requires only hundreds of hours to save many thousands during the production phase.

No/low-code implementations will provide the approach needed to overcome the biggest challenges in automation: CAD-to-solver processes and report generation. They offer a new, easier way to benefit from simulation's advantages. Democratization, relieving analysts of unproductive routine work, continuous use of best practices, and preservation of simulation knowledge make product development more efficient, increasing manufacturers' competitiveness.

5. References

[1] Albright, B., (2019) "*Democratization of Simulation Software*," Digital Engineering, https://www.digitalengineering247.com/article/the-path-to-simulation/

[2] Bertone, Francesca; Webster, Bruce, (2022) "*Fast and Easy Simulation Automation Accelerates Innovation at PAX Scientific for US Navy and Others*," Revolution In Simulation, https://revolutioninsimulation.org/webinar/fast-and-easy-simulation-automation-accelerates-innovation-at-pax-scientific-for-us-navy-and-others

[3] Evans, Davis; Patil, Amol; Patil, Santosh; Peters, Karlheinz; Webster, Bruce (2020) *"Abstract Modeling – Robust Automation of CFD Processes Made Easy,"* NAFEMS Article https://www.nafems.org/publications/resource_center/c_jun_20_americas_250/

Automatisierung von CAE-Prozessen

Dr. André Backes (TECOSIM GmbH)

1 Einleitung

Seit Jahrzehnten werden einzelne Bausteine im Prozess der virtuellen Produktentwicklung Schritt für Schritt automatisiert und dadurch effizienter in der Bearbeitung. Dabei geht es einerseits um Arbeitsschritte im Modell-Aufbau, andererseits um die Auswertung von Simulations-Ergebnissen. Für eine weitere Automatisierung des gesamten Entwicklungsprozesses ist ein tieferes, multidisziplinäres Gesamt-Verständnis des Systems notwendig.

Die TECOSIM GmbH hat seit diesem Jahr eine Kooperation mit dem französischen Software-Hersteller pSeven zur Vermarktung und technischem Support für die Kunden der gleichnamigen Software pSeven in der DACH-Region. Die Software pSeven ermöglicht die Abbildung eines CAE-Prozesses, wobei verschiedene Komponenten zu einem einzigen automatisierten Workflow verknüpft werden können. Die Zusammenführung verschiedener CAE-Disziplinen ermöglicht auf diese Weise ein interdisziplinäres Systemverständnis und damit letztlich eine multidisziplinäre Optimierung im Rahmen der virtuellen Produktentwicklung. Der gesamte Entwicklungsprozess kann damit erheblich beschleunigt werden. Die automatisierte Parameter-Variation ermöglicht in einem weiteren Schritt das Generieren von Metamodellen, entweder für einzelne CAE-Disziplinen oder auch für das Gesamtsystem. Mit solchen Metamodellen kann die Rechenzeit einzelner CAE-Berechnungen enorm reduziert werden, was die Durchführung einer Parameter-Optimierung für sehr komplexe Systeme letztlich erst möglich macht. Die Software pSeven kann für kleinere Workflows als Desktop-Anwendung zum Einsatz kommen, die Cloud-basierte Software-Variante pSeven Enterprise ermöglich schließlich die Skalierung auf große interdisziplinäre Prozesse zur Bearbeitung im gesamten Entwicklungsteam.

2 CAE Prozess

Die Softtware pSeven ermöglicht im ersten Schritt die Definition eines automatischen Prozesses mit Hilfe einzelner Prozess-Bausteine.

Als Beispiel betrachten wir hier die Koppelpunktsteifigkeit im linken Domlager für die Rohkarosserie des Mercedes A180. Ein FEM-Modell dieser Rohkarosserie befindet sich im TECOSIM-Portfolio der Virtuellen Benchmark-Modelle.

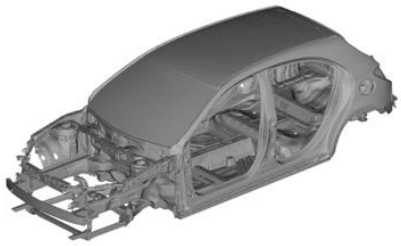

Benchmark-Modell Mercedes A180

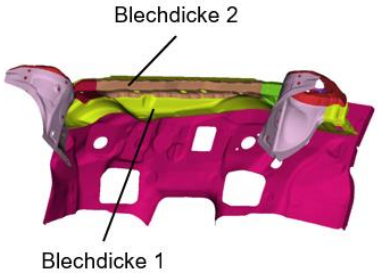

Parameter-Variation

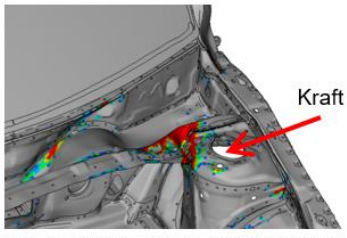

Statische Koppelpunkt-Steifigkeit in y
Domlager vorne links
Spannungs-Plot

Das unten abgebildete Diagramm beschreibt den automatisierten Prozess. Input-Parameter sind die Blechdicken zweier Bauteile der Struktur zwischen den Domlagern. Der nächste Block generiert das zugehörige FEM-Modell. Genauer gesagt werden hier mit Hilfe eines Python-Skriptes die zugehörigen PSHELL-Karten für das Nastran-Modell generiert. Der Nastran-Solver liefert u.a. zwei Dateien, aus einer wird die Masse des Modells ausgelesen, aus der anderen werden die statischen Verschiebungen extrahiert. Ein weiteres Python-Skript berechnet Steifigkeiten aus den Verschiebungen, diese werden an den Output-Block übergeben.

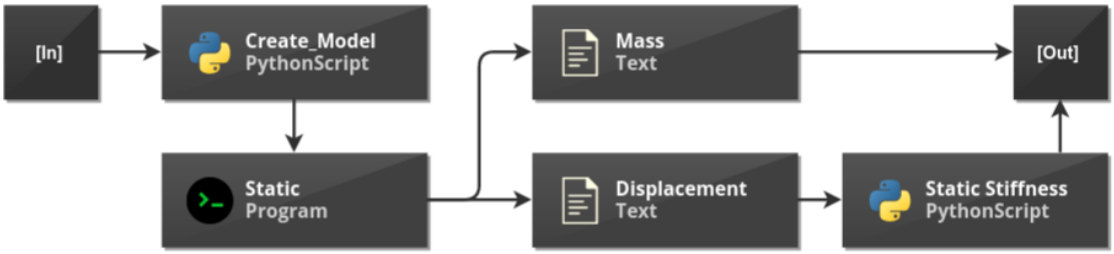

Prozess-Diagramm der Software pSeven

Auf diese Weise liefert der implementierte Prozess zu beliebigen Input-Parametern automatisch die zugehörigen Output-Parameter. Im nächsten Schritt geht es nun darum, dieses Systemverhalten (Input → Output) durch gezielte Variation der Parameter besser zu verstehen.

3 Parameter-Variation

Der abgebildete Prozess ermöglicht nun eine automatische Analyse des Parameter-Raumes durch systematische Variation der definierten Parameter. Die unten abgebildeten Diagramme zeigen eine zugehörige Korrelations-Analyse basierend auf 40 Datenpunkten im Parameter-Raum. Die Software pSeven kann mit Hilfe der sogenannten Smart-Selection-Option die Methode zur Auswahl der Datenpunkte automatisch sinnvoll wählen (z.B. Latin-Hypercube-Sampling).

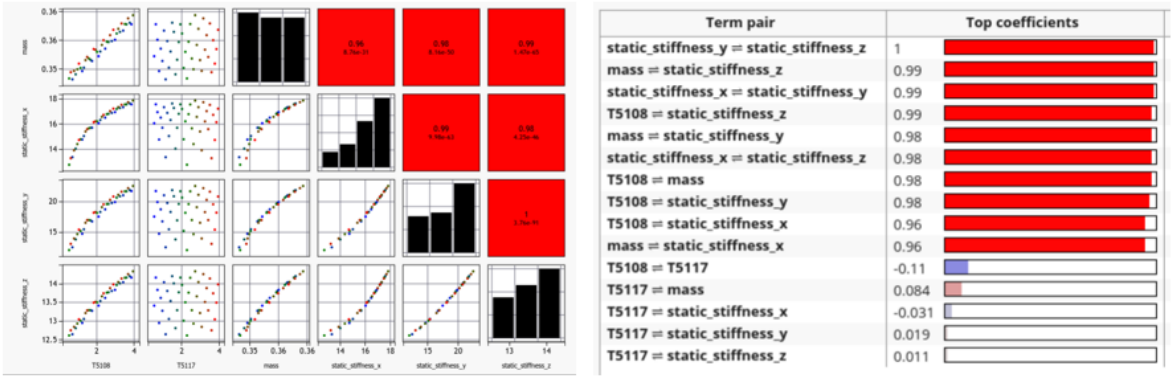

Term pair	Top coefficients
static_stiffness_y = static_stiffness_z	1
mass = static_stiffness_z	0.99
static_stiffness_x = static_stiffness_y	0.99
T5108 = static_stiffness_z	0.99
mass = static_stiffness_y	0.98
static_stiffness_x = static_stiffness_z	0.98
T5108 = mass	0.98
T5108 = static_stiffness_y	0.98
T5108 = static_stiffness_x	0.96
mass = static_stiffness_x	0.96
T5108 = T5117	-0.11
T5117 = mass	0.084
T5117 = static_stiffness_x	-0.031
T5117 = static_stiffness_y	0.019
T5117 = static_stiffness_z	0.011

Korrelations-Analyse der betrachteten Größen

Es zeigt sich, dass die statische Steifigkeit in allen drei Raum-Richtungen im Wesentlichen durch Blechdicke 1 getrieben wird. Unten stehendes Diagramm zeigt einen deutlichen (nichtlinearen) Zusammenhang zwischen Blechdicke 1 und der statischen Steifigkeit in x.

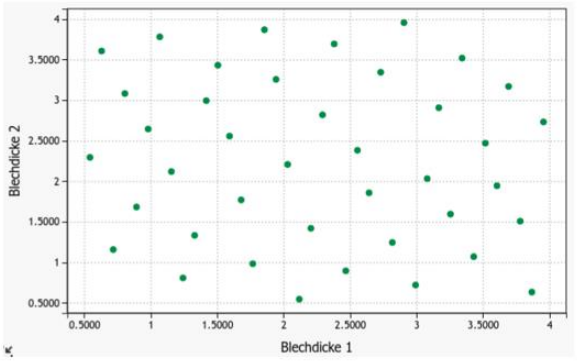

40 Datenpunkte im Parameter-Raum

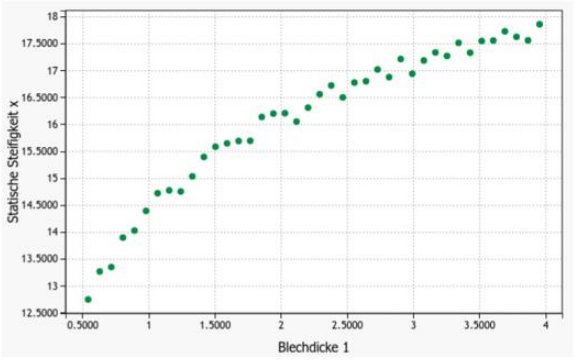

Korrelation Blechdicke 1 / Statische Steifigkeit x

Diese identifizierten Korrelationen können im nächsten Schritt für eine effiziente Parameter-Optimierung verwendet werden.

4 Meta-Modell und Optimierung

Die Software pSeven ermöglicht nun die Generierung eines Meta-Modells auf Basis der vorliegenden Datenpunkte. Dabei kann auch hier die Methode zur Generierung des Meta-Modells durch die Smart-Selection-Option automatisiert sinnvoll gewählt werden. Die unten stehende Abbildung visualisiert den Zusammenhang zwischen den beiden Blechdicken-Parametern und der statischen Steifigkeit in x.
Die Genauigkeit des Meta-Modells hängt im Allgemeinen stark von der Nichtlinearität und der Anzahl der vorliegenden Datenpunkte ab. pSeven bietet hier die Möglichkeit einer Bewertung des Meta-Modells durch Aufteilung der vorliegenden Daten in Trainings- und Test-Daten.

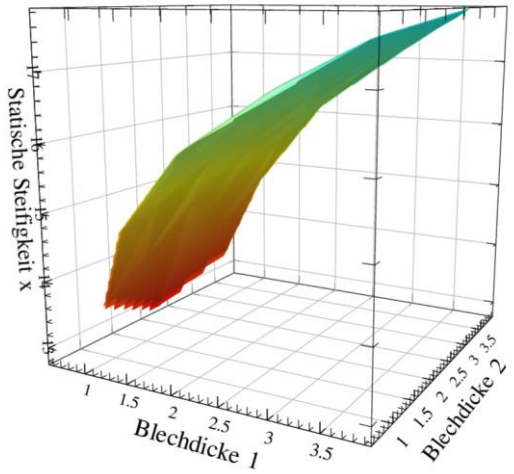

Visualisierung Meta-Modell basierend auf 40 Datenpunkten

Ein solches Meta-Modell liefert zu gegebenen Parametern im Allgemeinen einen sehr viel schnelleren Zugriff auf das Simulationsergebnis als die ursprüngliche Simulation. Das ermöglicht sehr effiziente Analysen des Systemverhaltens, eine sehr effiziente Optimierung der Parameter und insgesamt ein besseres Verständnis des Gesamtsystems.

Die Software pSeven kann Optimierungsaufgaben sowohl mit dem ursprünglichen Simulationsmodell als auch auf dem Meta-Modell lösen. Hier stehen einige effiziente Optimierungsverfahren zur Verfügung, auch hier kann die Methode durch die Smart-Selection-Option automatisch sinnvoll gewählt werden.

5 Nächste Schritte: Multidisziplinäre Optimierung

Eine weitere Stärke in der Prozess-Automatisierung mit pSeven liegt nun darin, dass der bestehende Prozess durch weitere Komponenten aus anderen Disziplinen ergänzt werden kann.
In unserem Beispiel ist die Betrachtung der statischen Koppelpunkt-Steifigkeit nur der erste Schritt. Für das parametrisierte Modell können im automatisierten Prozess zum Beispiel zusätzlich die dynamische Koppelpunkt-Steifigkeit und die Äquivalente abgestrahlte Schall-Leitung (ERP) der Panel-Komponenten berechnet werden.
Entsprechend kann nach einer erneuten zugehörigen Parameter-Studie ein Meta-Modell erstellt werden, aus dem man ein multidisziplinäres System-Verständnis gewinnen kann. Dieses Meta-Modell ermöglicht dann schließlich auch eine effiziente multidisziplinäre Parameter-Optimierung.
Im Sinne einer durch Leichtbau getriebenen Entwicklung wäre in unserem Fall das Optimierungsziel die Bestimmung von Blechdicken mit minimaler zugehöriger Bauteil-Masse unter Berücksichtigung aller Zielwerte aus den Einzel-Disziplinen.

From automatic event detection to automatic cause correlation

Nouran Abdelhady, Dominik Borsotto, Vinay Krishnappa, Stefan Mertler,

Kirill Schreiner, Clemens-August Thole

(SIDACT GmbH)

1 Summary

Reaching and fulfilling several design and crash criteria during the development process is what makes the engineer adapt and redesign the simulation model over and over again. Ideally resulting in new simulation runs with in best case improved performance, matching the intention of the applied changes. For the more demanding case of unforeseen results which do not necessarily fit to the expectations of the actual changes, methods and a workflow are being introduced here, which allow to identify the root cause of this behavior.

In a first instance every new simulation run is being added into an analysis database, which is continuously being used to compare new simulations against. Previous studies have already shown that this process can assist the engineer in automatically highlighting new behavior and pin pointing the engineer to the regions of interest. Rather than only highlighting the new behavior now a second phase is being triggered additionally.

In this second phase the previously detected event is being isolated and analyzed against the gathered data of the development history. The analysis methods used are based up on the Principal Component Analysis, a reduced order modelling technique. This allows not only identifying structures in the data but also correlating deformation patterns against each other. Especially the latter one is of interest for an automated process, as it allows automatically detecting and suggesting possible root causes to the engineer. As an outcome of this process the engineer receives a list of correlating parts, so that he can focus on deriving a better engineering solution to achieve a deterministic behavior, rather than searching for the root cause of the event.

To provide additional information about the type of cause, as for example failure or buckling, the identified parts are also forwarded to a classification prototype. This type of classification shall assist the engineer in deriving a possible design adaptation.

2 Event Detection

In a vehicle product development cycle, numerical simulations have vastly enhanced efficiency and pace of evaluating evolving designs over the course of development. One of the several challenges that remain in such a process is to be able to accurately and easily spot unwanted behaviors as a consequence of design changes, which other-wise is a laborious and time-intensive process and moreover many a times, important behaviors accidentally go unnoticed.

2.1 Femalyst

Femalyst addresses this issue by automatically flagging newly found behaviors termed as Events for every new simulation that is imported into its database. This is achieved through characterizing and learning deformation patters by employing principal component analysis, a popular unsupervised machine learning technique. Femalyst is able to extract and store rich insights in its database from simulation runs at a fraction of disk space, in comparison with original runs. In addition, the tool enables the Engineer to seamlessly search for similar deformation patters across all the runs in the database in an interactive manner.

2.2 Process and Technology

Simulation runs can be imported into the database in succession. The necessary data is extracted from the simulation run during the import, processed and stored in a dedicated Femalyst database. In the analysis stage the simulation is analyzed against all its predecessors for unknown behaviors or outliers and assigned a score for each part (or segment of part. See *Part Fragmentation*) and state.
By looking at the outlier score that ranges from [0,2], one can judge the degree of outlierness of the event, 2 indicating a strong outlier, while 0 indicating a known event or an inlier. In addition to assigning a score, Femalyst **clusters** several sub-part events into a bigger meaningful clusters based on the neighborhood and other measures which could potentially help the Engineer in identifying and understanding the causal chain of the event and its propagation over time and space. Such an analysis is not just performed on geometry but also on other post-values. Thus highlighting and bringing Engineer's attention to outlier-like patterns in stresses, strains etc.

The tool also addresses two major challenges that arise while analyzing a set of simulations in the entire development branch through *Geometry mapping* and *Part fragmentation*

2.3 Part Fragmentation

In order to not lose identification of local effects, the bigger parts are fragmented into smaller sub-parts to facilitate analysis on smaller regions, thus being more sensitive to tiny local behavioral patterns. The granularity of such fragmentation is user- configurable as per the need.

2.4 Geometry Mapping

One of the major challenges is to condition the data across simulations in the entire development branch where, several changes to the model are inescapable. Geometry mapping helps overcome this challenge. Mapping helps identifying geometry entities with each other in-space despite several inevitable changes in the model such as design alterations, re-meshing, addition of new parts, changes in the part ID etc. This helps in conditioning the data from across simulations in order to extract any possible insight and take them on board for analysis. A sophisticated node and element

3 Root Cause Detection

Depending on the event, the crash deviance does not always fit to the engineers expectation, based up on the changes applied to the model beforehand and might even pop up at regions out of scope. While this is one of the benefits of an automatic event detection, which does not focus on a limited area within the model, questions are prompted about the cause of this event.

3.1 PCA

To identify the possible causes for scatter in crash simulation results the Principal Component Analysis (PCA) has been introduced in the past and shown to be an effective method to analyze datasets by means of robustness and identification of root causes for scatter occurrence [1].

According to [3], principle component analysis (PCA) was introduced by Pearson in the context of biological phenomena [4] and by Karhunen in the context of stochastic processes [5].

In [6], PCA was applied to full crash simulation results. Let (p,) be the displacements of simulation run i out of n simulation runs at node p and time t. If $\bar{X}$ (p,t) is the mean of all simulation runs, the covariance matrix C can be defined as

$$C := [c_{ij}]_{1 \le i,j \le n} \quad \text{and} \quad c_{ij} := < X_i - \bar{X}, X_j - \bar{X} >_2$$

The eigenvectors v_i of C form a new basis (principle components) and the λ_i (square roots of the eigenvalues of C) provide a measure for the importance of each component.

If this method is applied to crash simulation results, n^2 scalar products between the simulations runs of length $3 * \#P * \#T$ have to be computed ($\#P$ number of points, $\#T$ number of time steps.)

From

$$\hat{X}(a) := \sum_{i=1}^{n} a_i X_i \quad ,$$

follows that

$$\lambda_i = \left\| \hat{X}(v) \right\|_2 \quad .$$

The $\hat{X}(v_i)$ show the major trends of the differences between the simulation results. The coefficients of the eigenvectors v_i correspond to the contribution of $\hat{X}(v_i)$ to $X_i - \bar{X}_i$ and can be used for cluster analysis and correlation with input parameters. If input parameters have been changed between the different simulation runs, the correlation analysis will indicate how certain trends can be avoided or increased by changing these inputs (e.g. thicknesses of parts) (c.f.[2], Chapter 2.4] for the properties of PCA analysis in general).

Principle Component Analysis is a mathematical method which determines mathematical trends in contrast to physical trends. To be more specific: λ, the square of the maximal eigenvalue of C, can be determined by

$$\lambda = \left(max_v \left\| \hat{X}(v) \right\| \middle| \|v\| = 1 \right)$$

and therefore will be in general a mixture out of several physical effects, like buckling. For further insights please refer to [1].

To now find root causes of scatter occurrence a process is iteratively conducted by the engineer, including the interactive selection of the area of interest and its possible causes. During this process the principle variation modes of the scatter definition are computed using PCA, as described above. The correlation of the scatter modes to a possible source definition is evaluated using a tailored DPCA approach [1]. During such a process the engineer can freely choose the parts, as well as node-sets of interest, which is why the process has always been user driven and not fully automated in the past.

Given the fact that for a robustness analysis as described in this manuscript a set of 30 or more simulation runs is analysed, the use of a dimensional reduction method is beneficial. In our case the Principal Component Analysis is used to easier extract the essence of the crash behaviour for sets of simulations.

3.2 Part Fragmentation

The above mentioned PCA/DPCA analysis allows detecting any and all behaviours of a possible cause which are correlated to the behaviour of the target area of interest. To automate such a process, it is important to have an alternative to the engineer's interactive selection of local sets of nodes, to isolate distinct scatter sources. For this purpose, a part fragmentation algorithm was implemented. To detect effects on/of fragments rather than a whole part, parts are automatically split up during the initial simulation import.

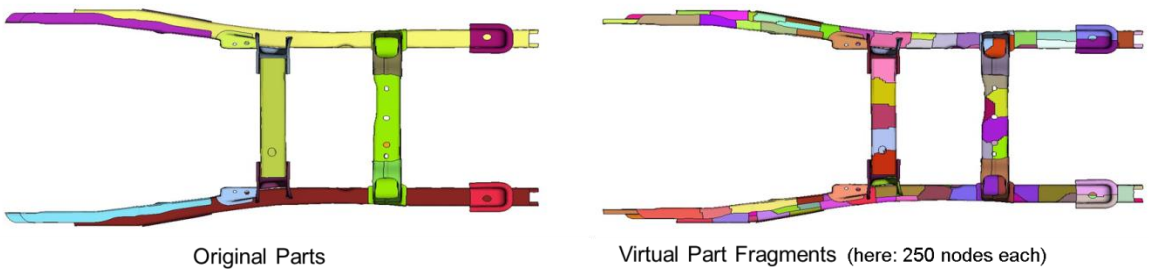

Fig.1: Automatic part fragmentation

3.3 Automation

The iterative detection of a deviation's scatter cause, described in 4.1, is error prone, and would require expert user knowledge and experience. To automate the scatter source detection process, the correlation of a deviation definition to every other fragment behaviour in the full domain at every time step is computed. The relative correlation is visualized to readily identify the biggest cause for the identified scatter.
The relevant source modes are automatically adapted for each source definition. Source modes that are less than a certain threshold of the principle source mode are neglected.
Correlation noise is automatically filtered out. High correlation against source definitions which have negligible scatter is unwanted behaviour, i.e. false negative. To filter correlation noise, the DPCA analysis of a source definition is only computed if the principle mode is above a certain threshold.

4 Test Scenario

A detailed robustness analysis [8] [9] of a set of simulation runs from the Chevrolet Silverado [7], based up on thickness variations in the range of [-3;3] % , showed a clear bifurcation. While for some simulation runs the break-booster hooked up to the suspension, being pushed into the dashboard, for others there was no such hook-up. Therefore the test scenario shown here consists of a set of simulation runs with similar behavior of no hook-up and a newly analyzed simulation containing the hook-up.

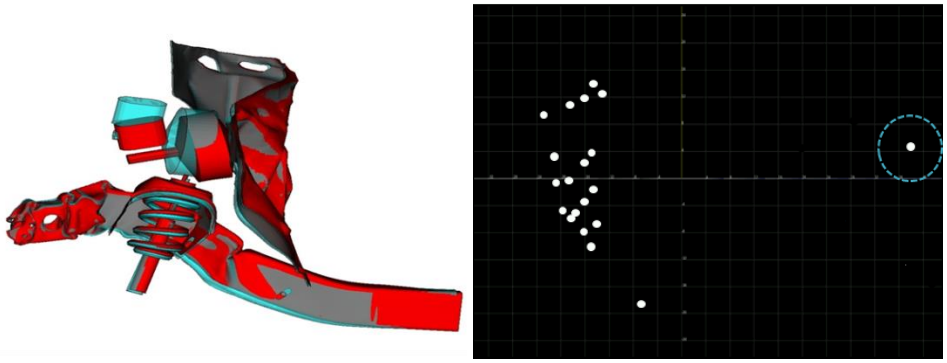

Fig.2: Comparison of hook-up event vs no hook up (previous simulations)

4.1 Automatic Event Detection

Incrementally adding the simulations to the analysis database, the simulation with the hook-up behavior throws a major event at the break booster. The fringe plot shows the outlier score computed for the complete simulation and indicates a different behavior, starting at 62 [ms]. Next to automatically getting the part which is showing a different behavior it also indicates when it starts to differ from previous simulation runs.

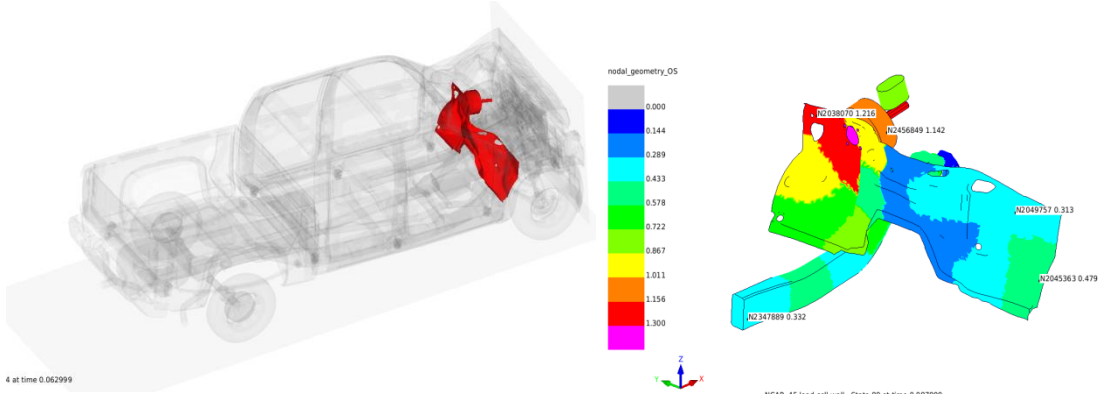

Fig.3: Event detection outlier score

4.2 Automatic Cause Identification

Based up on the results with respect to the event being detected at the dashboard/break booster, the dashboard has been forwarded to automatically identify the root cause of the hook-up. Next to obviously also highlighting the break-booster as a cause for the dashboard variation, additionally a fragment of the rail is being identified with a significant correlation, see Fig. 4.

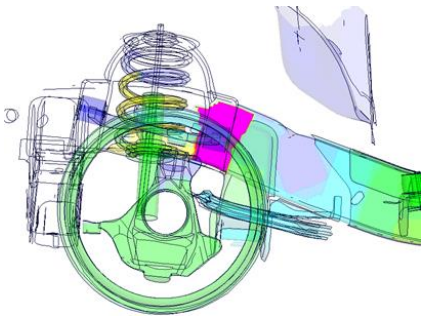

Fig.4: Automatic cause detection

While in previous studies [3] the same region could also be identified as a cause for the scatter, this process for the first time successfully combines the complete automatable chain from event detection to root cause analysis.

5 Search

Femalyst allows the user to search certain behaviour observed in a particular simulation to see if a similar behaviour occurs in other simulations in an interactive manner. A similarity score is computed for their chunk counterparts in all simulations, a sample plot of which is shown in Fig.5. A clear separation of curves, each corresponding to a simulation, in the plot is a consequence of two different behaviours observed for the firewall in these simulations.

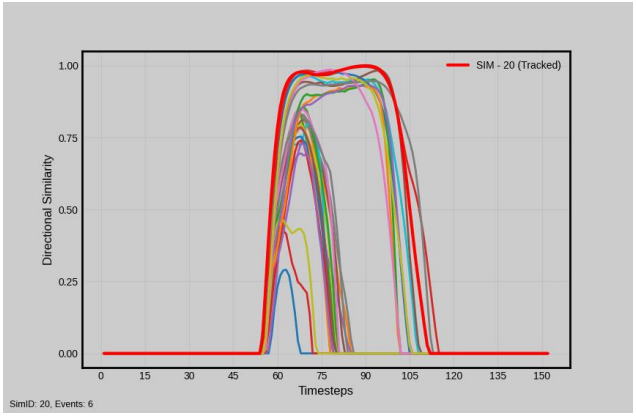

Fig.5: Search results of FemAlyst for similar deformation behavior

6 Conclusions

While in the past PCA based analysis allowed to identify root causes for variation in simulation results, the new modules and workflow described here allow for an automated analysis of simulation results. This automated process detects new behavior, called events, and determines correlated parts throughout the car to identify the cause, which allows for a faster reaction to counteract in case of unwanted behavior.

7 References

[1] C. A. Thole, D. Borsotto, L. Jansen: “Use of Data Reduction Methods for Robust Optimization”, 14th int. LS-DYNA User Conference, June 12-14, 2016

[2] Thole C.A., Nikitina Lialia, Nikitin Igor, Clees T.: “Advanced Mode Analysis for Crash Simulation Results”, 9. LS-DYNA Forum, Bamberg, 2010

[3] Lee M., Verleysen J.: „Nonlinear Dimension Reduction“, Information Science and Statistics, Springer Science+Business Media,2007

[4] Pearson K.: “On lines and planes of closest fit to systems of points in space”, philosophical Magazine,1901,2:559-572

[5] Karhunen K: "Zur Spektraltheorie stochastischer Prozesse", Ann. Acad. Sci. Fennicae, 1946, 34

[6] Ackermann S., Gaul L., Hanss M., Hambrecht T.: „Principal component analysis for detection of globally important input parameters in nonlinear finite element analysis“, In Optimisation and Stochastic Days 5.0 dynardo-dynamic software & engineering, Weimar, 2008

[7] NHTSA, Chevrolet Silverado,https://www.nhtsa.gov/staticfiles/rulemaking/pdf/cafe/Mass-Reduction-Feasibility-2014-Silverado.zip (accessed 01/25/2023)

[8] C. A. Thole, D. Borsotto, R. Strickstrock: “Robustness analysis – Significant reduction of scatter occurrence”, NAFEMS Seminar: Optimization and Robust Design, March 23-24, 2015

[9] SIDACT GmbH, DIFFCRASH, https://www.sidact.com/diffcrash, accessed Jan. 25, 2023

Automated construction of compressor performance maps

Nina MOËLLO (pSeven SAS)

1 Summary

As part of a project with an aircraft turbine manufacturer, the proposed paper focuses on an innovative solution for building and democratizing the use of automated engineering workflows at scale based on the history of compressor performance maps evaluation.

The compressor map allows to easily review and analyse its efficiency, pressure ratio and surge limit across the operating range. Its construction is based on a set of standard CFD simulations. However, combining these simulations to reconstruct the map requires custom logic, including automatic refinement and additional evaluations to explore specific areas of the map. The complex logic behind it remains a fixed and repetitive process. Only domain experts can support and are allowed to alter it.

Democratization becomes a must as there is a large proportion of non-experts who need to use the described methodology frequently. To achieve this, the engineering process behind it must be assembled in a simple form to remain accessible. In addition, multiple competitive runs from different users and massive heavy CFD evaluations require a powerful resource management process.

The paper shows how compressor performance map construction can be scaled with a single author and multiple users, and efficiently managed through user interfaces and applications. The same process can be applied to typical late-stage and even inter-project design changes. Efficiency gains through reduced effort in repetitive tasks and centralized management of the methodology are emphasized.

Key words: automation, compressor map, CAE, CAD, engineering process, resource management.

2 Introduction

Compressor performance map, also known as a compressor characteristic map or just compressor map, is a graphical representation of the performance of a compressor. It is typically presented as a two-dimensional graph with the mass flow on the horizontal axis and the pressure ratio (ratio of the outlet pressure to the inlet pressure of the compressor) on the vertical axis.

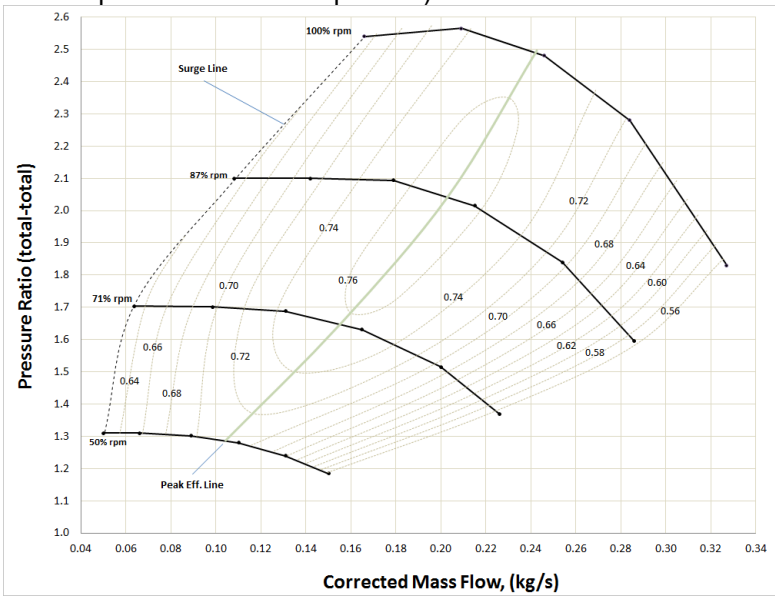

Fig 1. Example of a compressor performance map

When the stages form a gas turbine, the range of possible operating conditions depends on the equilibrium of the gas turbine as a whole. The equilibrium points can also be plotted on the

compressor map to form the operating line. Sometimes it may be necessary to calculate intersection points of the selected branches with the operating line.
The surge limit is the point at which the compressor is unable to maintain stable flow and begins to surge or stall. It is shown as a line on the compressor map, and represents the upper limit of the compressor's operating range. Surge points can only be determined approximately, therefore, depending on the required tolerance, further refinement may be required after the map is constructed.
A compressor map is an important tool for designers and engineers who work with compressors, as it allows them to analyse and optimize the compressor's performance under different operating conditions.
One way to build a compressor map is to run a series of CFD simulations. In this case, each point of the map corresponds to a single simulation and high quality of surge line is ensured by manual iteration over multiple values of the boundary conditions. Obviously, such approach requires a lot of manual work of a simulation engineer. Moreover, multiple parameters may change during the design phase: geometry of the blades, control program (dependency between the orientation of the blades and the rotational velocity), CFD simulation model, etc. Thus, it may be necessary to reconstruct the map several times as the design parameters change.
In this article, we will show how the process of a compressor map construction can be automated and what are the benefits of this approach.

3 Process of compressor performance map construction

Construction begins by building geometric models of the blades of each stage in a CAD software. These models are then imported into an existing project of mesh generator to create the new mesh. The process repeats for each new branch as the blade orientation angle depends on rotational velocity of the branch.
After that, a series of CFD simulations is carried out using the newly generated mesh. Each branch is constructed by incrementing the value of the boundary conditions until the solution becomes numerically unstable (i.e., the surge limit is reached). Once this cycle is complete, one may further refine the surge boundary or compute intersections with the operating line.
The construction process requires manual data transfer between several applications. The process therefore requires constant attention from the simulation engineer. You cannot just run a simulation and pick up the results when it is finished, at least without a proper automation tool.

4 Automating the process

The process of the compressor map construction can be captured in the form of a workflow which consists of three main blocks:

- Block “Main driver” controls the calculation cycle of the branches and intersections.
- Composite block “Single branch” calculates one branch of the compressor map (for single rotation speed).
- Composite block “Single point” calculates the intersection of the operating line with one branch of the compressor map.

Workflow construction has been facilitated by the use of special blocks. These blocks provide a seamless connection to engineering applications (NX, Numeca, Ansys CFX). Such blocks can be developed for any type of software that supports batch execution.

At the start of the workflow all the files needed for performance map construction must be placed in the «Files» folder on the Explorer panel according to the pre-agreed rules. After the workflow is completed successfully, all the produced files can be found on the same Explorer panel.

5 Conclusion

The main benefit is the increased efficiency and time savings. This is achieved by automating repetitive manual operations such as building geometry models, mesh generation, post-processing of the results and data exchange between different software. This approach can be applied to a wide range of tasks that can be standardised and need mass reuse.
The next level of automation can be achieved by developing a special user interface (UI). With such UI the workflow could be used as a Web App. This approach would give the ability to conduct a study to an ordinary user who is not familiar with the case by simplifying the process of providing input data and configuring the task to construct the performance map. The user needs only to prepare the input data.

Automated construction of compressor performance map

Nina MOËLLO
pSeven SAS
nina.moello@pseven.io

About us

We develop software tools for machine learning, optimization, collaborative engineering and low-code automation.

Worldwide sales through a network of resellers

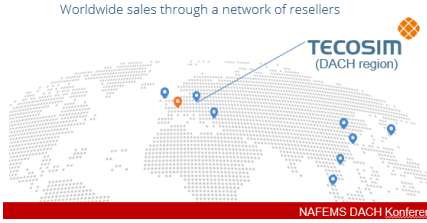

1. **Compressor performance map**
   - Definition
   - Construction
   - Challenges
2. **Automation enabler**
   - Low code platform
   - Collaborative engineering
   - Architecture and accessibility
3. **Process automation**
   - Compressor map workflow
   - Custom block library for capitalization
   - Easy file management
   - Share and democratize
4. **Conclusion**

Compressor performance map Definition

Graphical representation of the compressor performance.

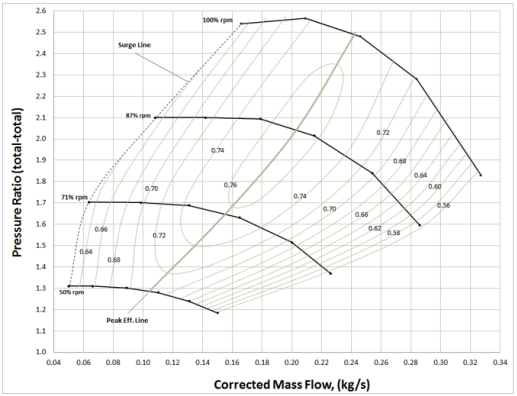

Efficiency	Contour lines
Pressure ratio	Series of branches for each speed
Equilibrium points	Intersection point of the selected branches with the operating lines
Surge limit	Approximated upper limit of the compressor's operating range

Allow designers to analyze and optimize the compressor's performance under different operating conditions.

NAFEMS DACH Konferenz 2024: Konferenz für Berechnung & Simulation im Engineering, 10. – 12. Juni 2024, Bamberg, D

Compressor performance map Construction

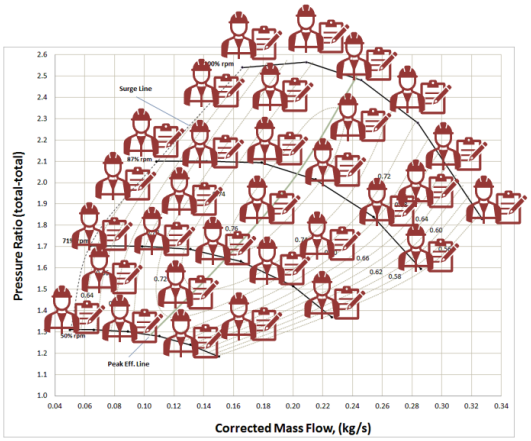

One point	⟺	One CFD simulation, based on several software
High quality of surge line	⟺	Manual iterations over multiple values of the boundary conditions
Parameters changing during design phase (geometry, control program, simulation model, boundaries, etc)	⟺	Reconstruction of the map

Compressor performance map Construction

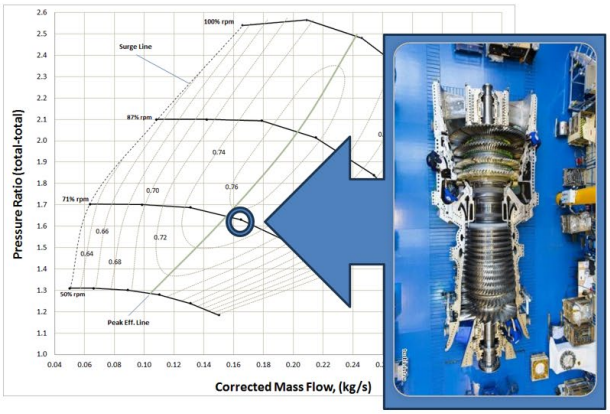

NAFEMS DACH Konferenz 2024: Konferenz für Berechnung & Simulation im Engineering, 10. – 12. Juni 2024, Bamberg, D

Compressor performance map Construction

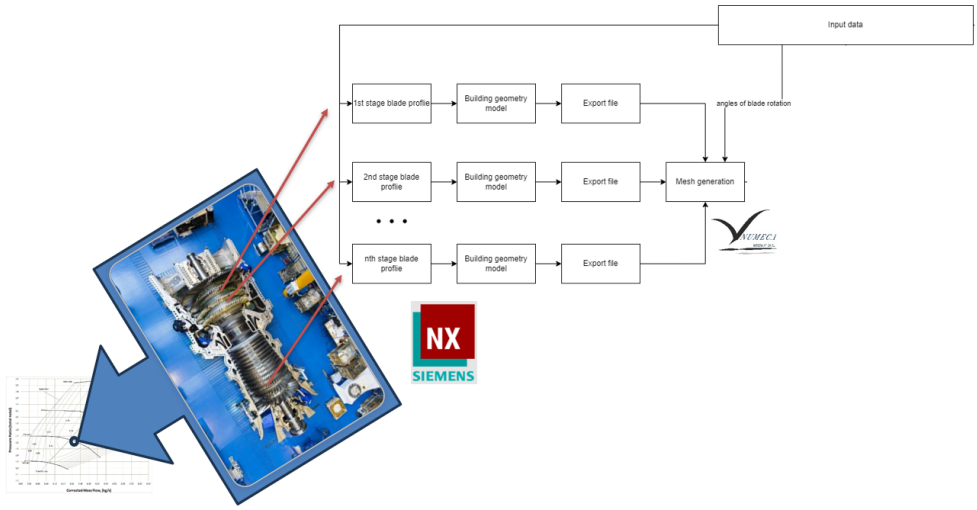

Compressor performance map Construction

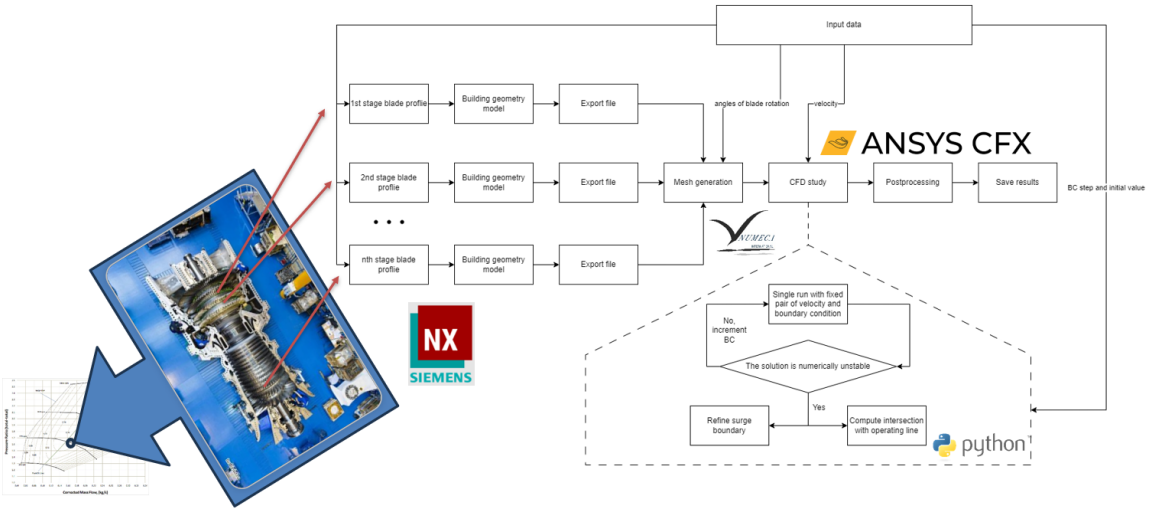

Compressor performance map Challenges

- Many iterations to build one performance map
- Manual data transfer between the applications
- Several different tools to manage for one simulation
- Multiple parameters may change during the design phase
- The entire process is to be done for each compressor

How to alleviate the engineer's heavy task with automation ?

Automation enabler Low-code approach

- Collaborative workflow engine:
  - Visual representation of executable processes
  - Multi-level (nested) workflows
  - Everything is done in the cloud → No need to move files
  - Reusable workflows and blocks for different cases
- Low-code approach:

- Faster implementation and development of Minimal Viable Products

- Logic is always open for inspection and revision

- Flexible depth and order of automation

Accelerate development

Visual representation of executable processes

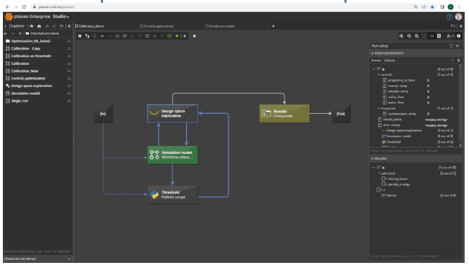

Nested workflows

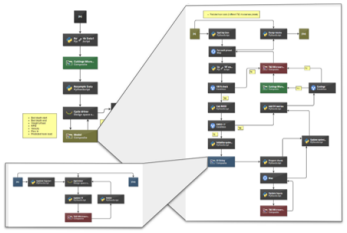

Automation enabler
Collaborative engineering

- Centralized architecture enabling collaboration:
  - Multi-user environment : small group of experienced people to construct the workflows and huge community of engineers to use them.
  - Co-authoring in real-time
  - Centralized & customizable blocks/connectors library
  - Workflow sharing and aggregation
- Integration with other collaborative environments:
  - SPDM, PLM etc.

Co-authoring

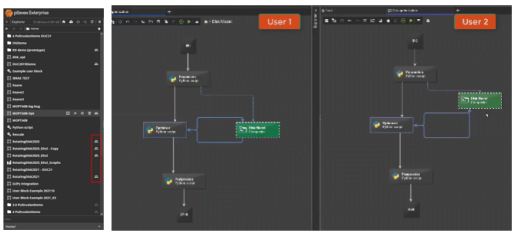

Reuse blocks (3rd party software connector)

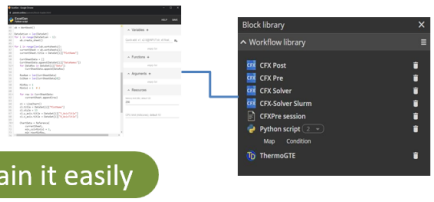

Workflow sharing by reference/link

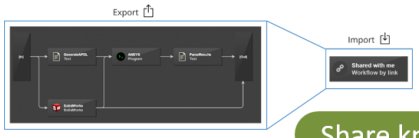

Share knowledge and maintain it easily

Automation enabler
Architecture and accessibility

- Cloud-native architecture:
  - One installation to support
  - Thin client is enough
- Runs in a predefined and well-controlled IT environment:
  - On-premises (Kubernetes)
  - Private cloud (AWS, Digital Ocean, Azure, Huawei Cloud etc.)

aws DigitalOcean Tencent Cloud HUAWEI HUAWEI CLOUD

- Web interface accessible from any browser and any device:
- Execution supports distributed heterogeneous environments (Windows, Linux, HPC)

Access from anywhere, at scale

- Management:
  - Many users can run many resource-intensive workflows at the same time
  - Transparent handling of computing resources

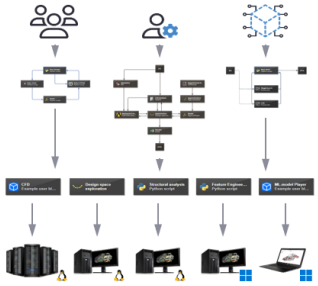

- Managed and scheduled resources

Process automation
Compressor map workflow

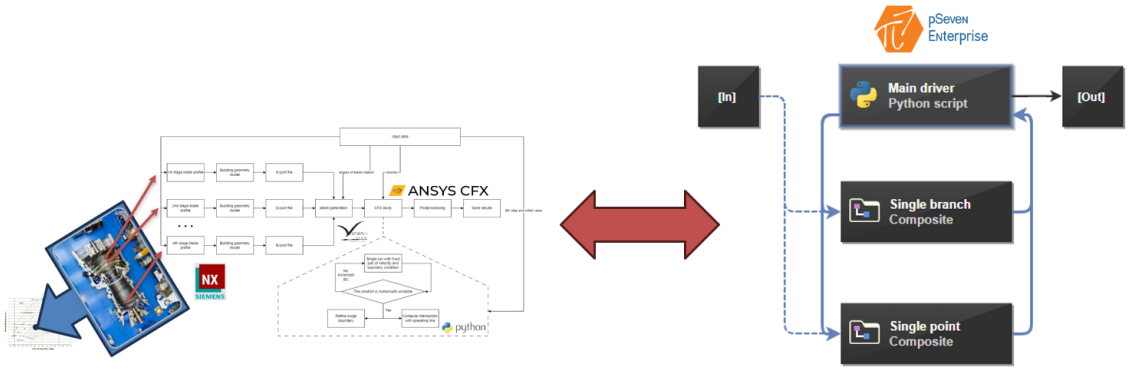

The process of the compressor map construction is captured in the form of a workflow where the first block controls the calculation cycle of the branches and intersections.

Process automation
Compressor map workflow

Single point calculates the intersection of the operating line with one branch of the compressor map.

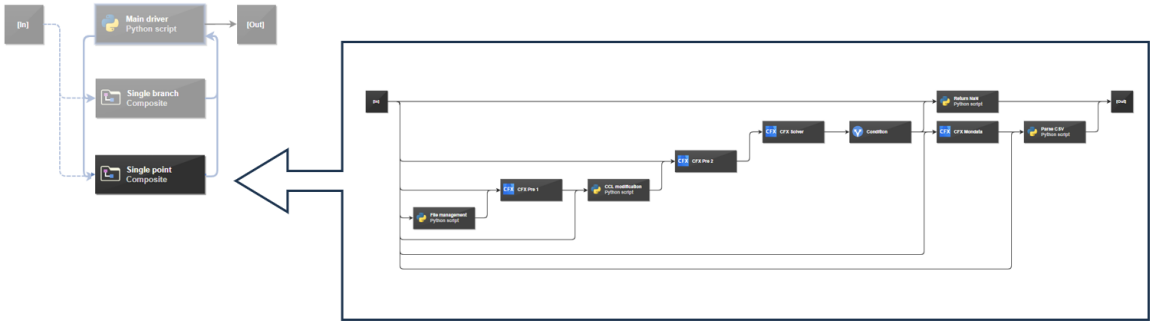

NAFEMS DACH Konferenz 2024: Konferenz für Berechnung & Simulation im Engineering, 10. – 12. Juni 2024, Bamberg, D

Process automation
Compressor map workflow

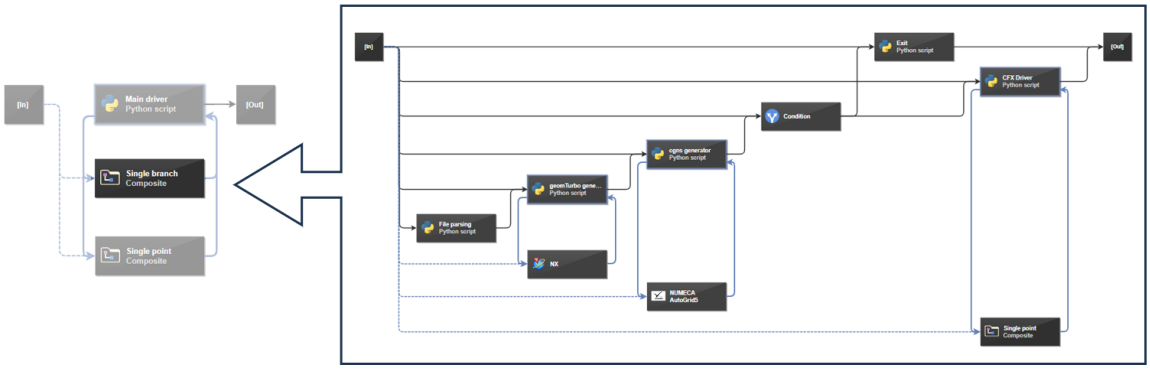

Single branch subworkflow calculates one branch of the compressor map (for single rotation speed).

Process automation
Custom block library for capitalization

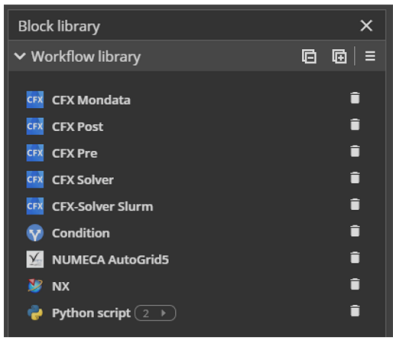

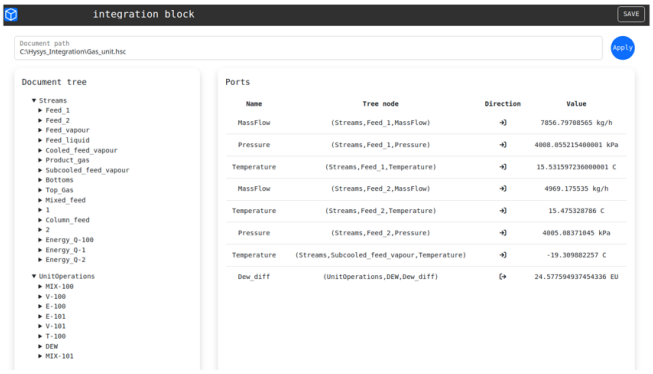

Each block has its own interface which is customized and easily shared with all the users to ensure capitalization of the method and process.

Process automation
File management

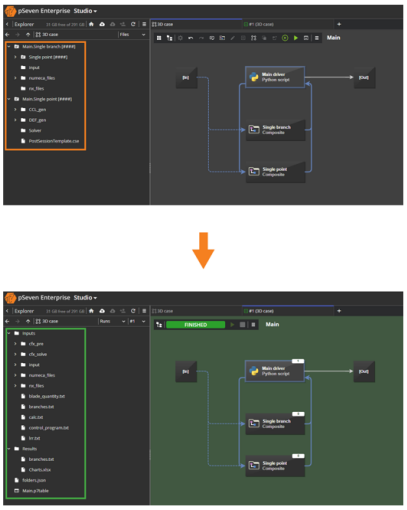

- At the start of the workflow, a dedicated Explorer panel stores the files needed for performance map construction.
- After the workflow is completed successfully, all the produced files are found on the same Explorer panel.

No manual file transfer is required. Everything is managed automatically reducing the risk of user error.

Process automation
Share and democratize

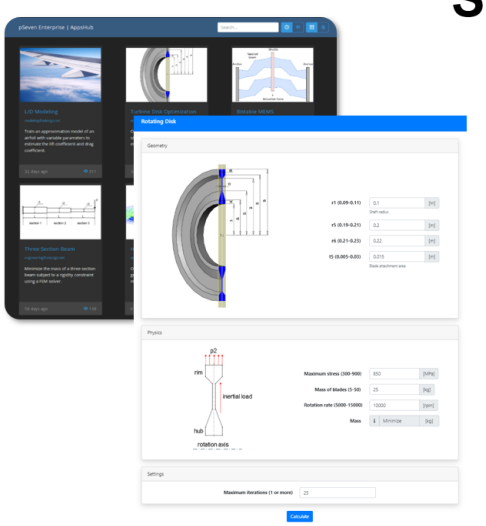

- ✓ Once the workflow is robust and stable, a web application is created (no-code process)
- ✓ A basic UI is provided by default to store the workflow as an application in the App library.
- ✓ The UI can be customized to bring the advanced method to citizen users, and enable exploring post-processed results (plots, tables, pictures, reports…).

Deliver automated workflow as a Web App

Conclusion

Automate repetitive tasks

- Manual operations captured and formalized in a workflow, including the data exchange.
- Robust cycle contributing to reduce rework.
- Generic process valid across the whole line of compressors.

Capture and transfer knowledge

- Multiuser environment, with several levels of abstraction (workflow, application).
- Low-code approach to share, reuse and maintain knowledge easily. Less impacted by company turnover.
- Easier and less costly maintenance.

In a flexible environment

- Multidisciplinary tools integrated for better interactions.
- Several computations on different machines executed from a single point.
- File explorer available.

Engineering cycle (model preparation and simulation) reduced up to 6 times.

Synergizing Data Analysis and Machine Learning with Simulation Data Management

Thiele, M., Liebscher, M., Leichsenring, F. (SCALE GmbH)

Abdelhandy, N., Borsotto, D. (SIDACT GmbH)

Kracker, D. (Porsche AG)

1 Summary

Employing a simulation data management system ensures a comprehensive archive of all conducted simulations within a specified timeframe. This encompasses crucial simulation metadata such as load cases, solver versions, and components, along with the simulation output comprising raw data and derived key-results. Centralizing and organizing this data in a uniform structure facilitates seamless data analysis and knowledge extraction across numerous simulations.
The utilization of open machine learning libraries and third-party solutions enhances the extraction of insights from the stored data, enabling the identification of patterns and trends essential for making data-driven decisions.
This presentation will illustrate the workflow for setting up simulation data and conducting simulations to generate key results necessary for data analysis. Additionally, it will showcase the integration of third-party solutions, such as Femalyst from SIDACT or our proprietary Data Analysis Add-On, through the scalable Add-on concept of SCALE.result.
By adopting this Add-On approach, SIDACT and other entities can seamlessly integrate their technology as third-party tools into existing simulation data management systems, leveraging proprietary front and back-end components while gaining access to simulation data.

Synergizing Data Analysis and Machine Learning with Simulation Data Management

Thiele, M., Liebscher, M. [1], Leichsenring, F. [1]
Abdelhady, N. [2], Borsotto, D. [2]
Kracker, D. [3]

[1] SCALE GmbH
[2] SIDACT GmbH
[3] Porsche AG

NAFEMS DACH Konferenz 2024: Konferenz für Berechnung & Simulation im Engineering , 10. – 12. Juni 2024, Bamberg, D

Agenda

Motivation

Automatization

Integration of 3rd party Data Analysis add-on in an SDM system

- Example of DOE study
- Example of Event Detection

Outlook

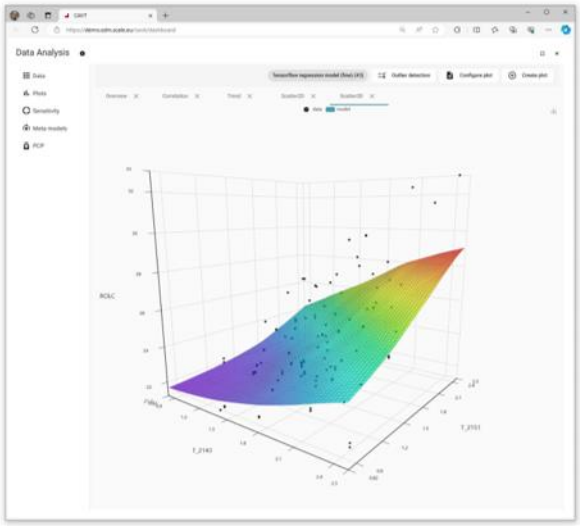

Motivation

Large data sets available in SDM systems

- Huge number of simulations every day
- Some OEMs with > 1.5 Million simulations per year
  (just crash domain only)
- Data stored at central place

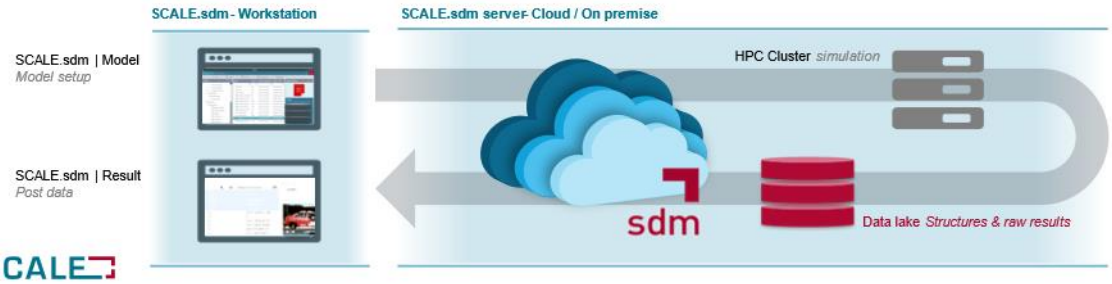

SCALE

Motivation

Advanced ML/AI Methods:

- often custom / proprietary
- SDM provides standard methods
- Domain-specific methods required
  (specific methodologies are often required but not part of standard software or implementations)
- ML/AI Methods custom developed
  (in-house, proprietary or even open -source based)

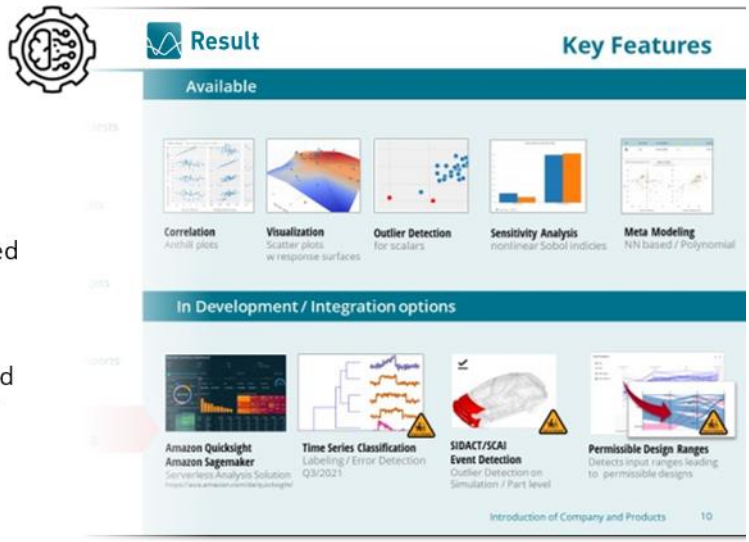

SCALE

Motivation

Problem

- Application of AI/ML methodologies implies scanning large data sets
- Implementation close to data required vs. custom implementation

Solution @ SCALE.sdm

- Add-on concept available
- Distribution of own code to **backend** and **frontend** side in SCALE.sdm possible
- Full structured access to data within server environment

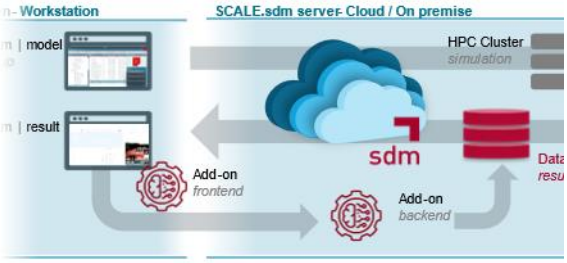

SCALE

Setup of DOE - Porsche 911 Example

Loadcase USNCAP Rigid Wall

- Vehicle Speed 56 km/h
- 100% frontal

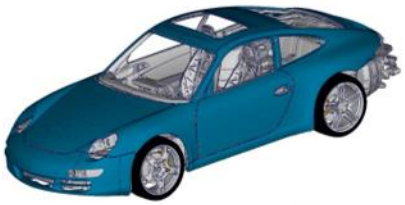

Design of experiments

- sheet metal thickness of **38** parts

  `[0.8,2.5];[1.5,5.0] mm`
- **60** simulation runs

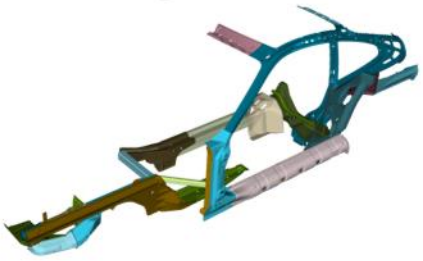

SCALE

The model has been provided by Dr. Ing. h.c. F. Porsche AG which is greatefully acknowledged.

Setup of Simulation Model and DOE in SDM-System

Model

- Multiple load cases in SDM-System

Parameterization

- LS-DYNA parameters
- Placeholder in .key files

DOE

- Samplings can be created directly in SDM -System
- Simulation runs created automatically

SCALE

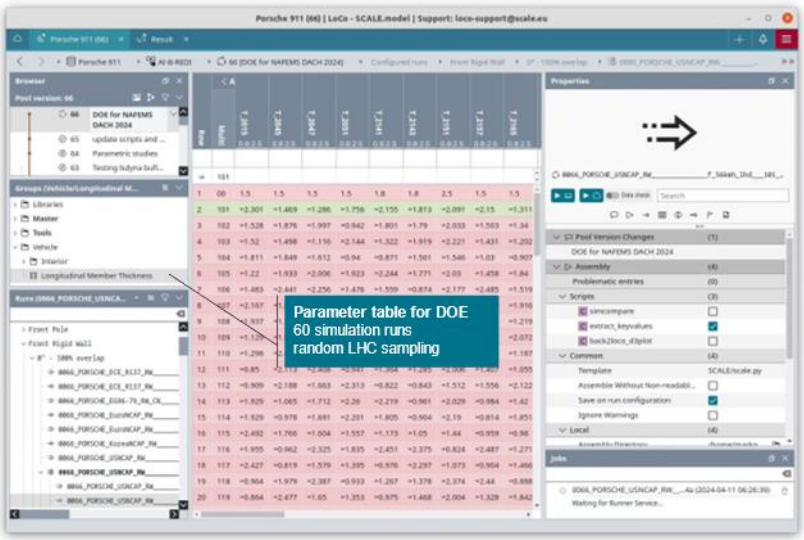

Simulation flow in SDM-System for DOE and event detection

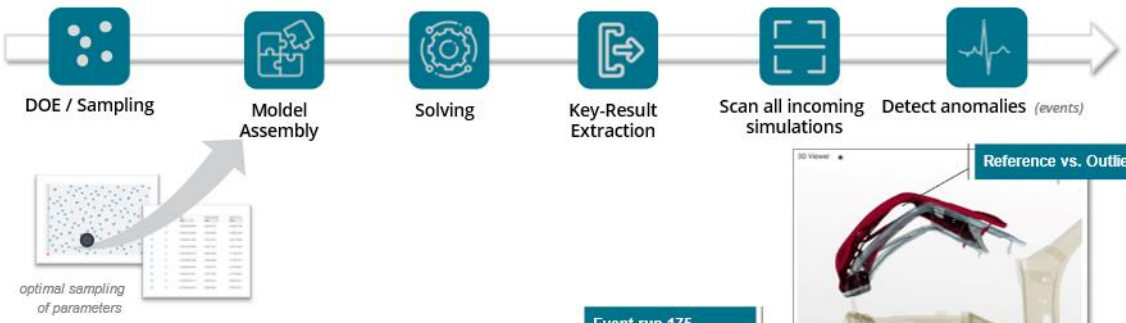

SCALE

Visualization in Result — Porsche 911 Example

CAT & CAE
Compare simulation and physical tests

Evaluation
Visualize and evaluate all key results

Assess Results
Assess with respect to project targets

Reporting
Comprehensive and interactive reports

Data Analysis
Machine Learning and Data Mining

SCALE

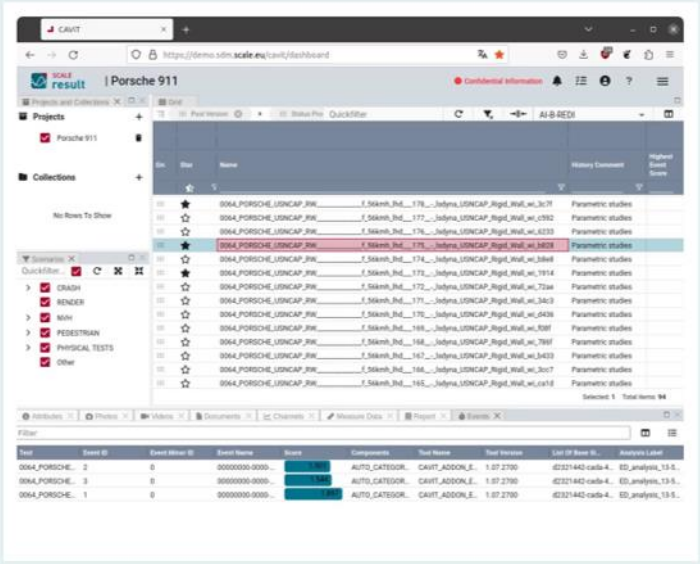

Example SCALE Data Analysis Add-on

Add-on running in web browser

- Basic functionalities
- All data in SDM-System can be used

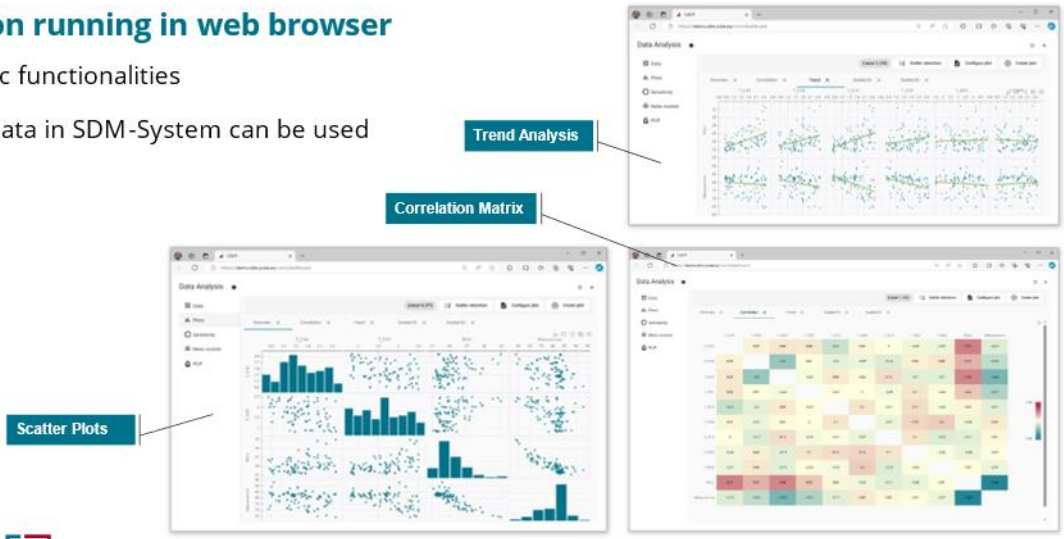

SCALE

Example SCALE Data Analysis Add-on

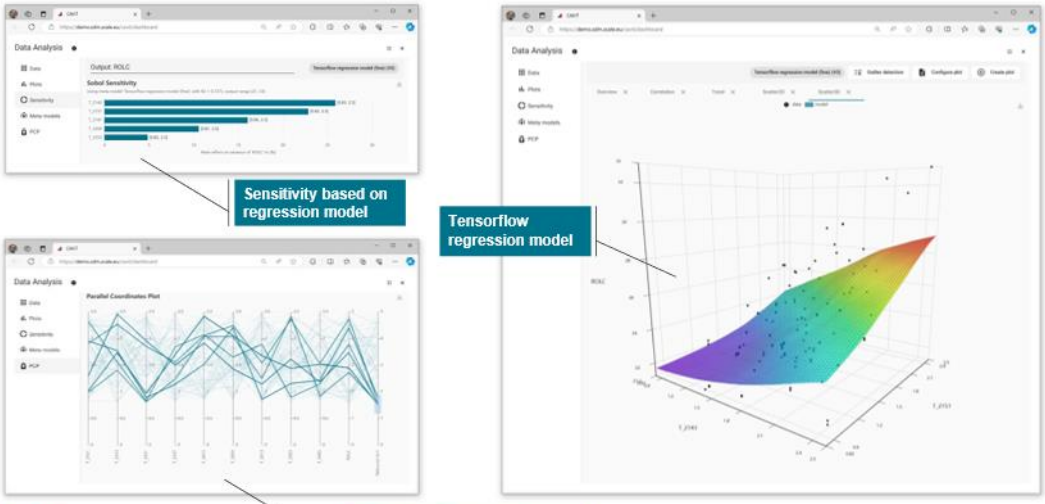

SCALE

Example SIDACT Event Detection: ML-based anomalie detection

What is an event?

- Unknown/unwanted behavior
- anomalies in field variables

Event properties

- Location/Parts
- Outlier Score
- Event type

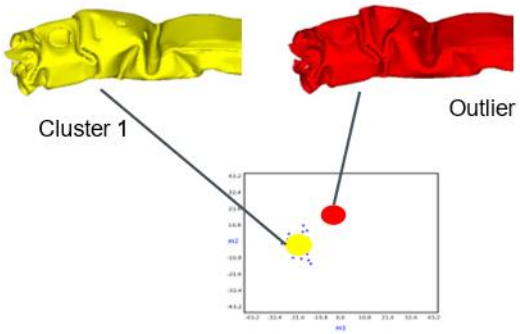

Basic workflow

SCALE

SIDACT GmbH

Example SIDACT Event Detection: ML based anomalie detection

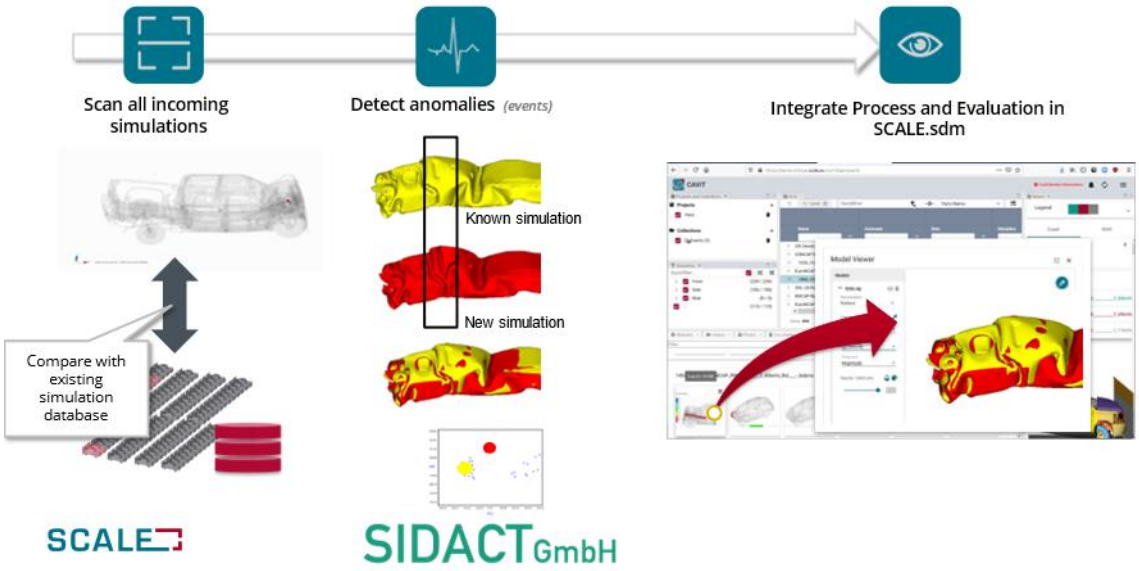

Visualization in Result

Porsche 911 Example

- **CAT & CAE**
  Compare simulation and physical tests
- **Evaluation**
  Visualize and evaluate all key results
- **Assess Results**
  Assess with respect to project targets
- **Reporting**
  Comprehensive and interactive reports
- **Data Analysis**
  Machine Learning and Data Mining

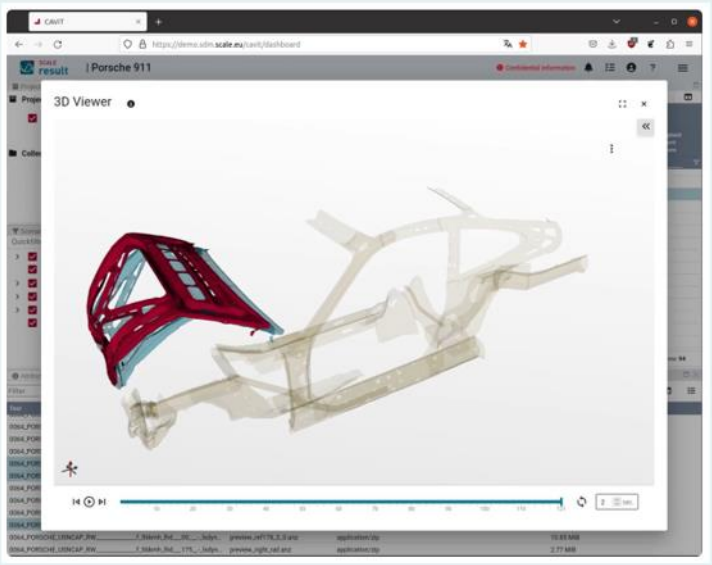

SCALE

SIDACT Event Detection Add-on

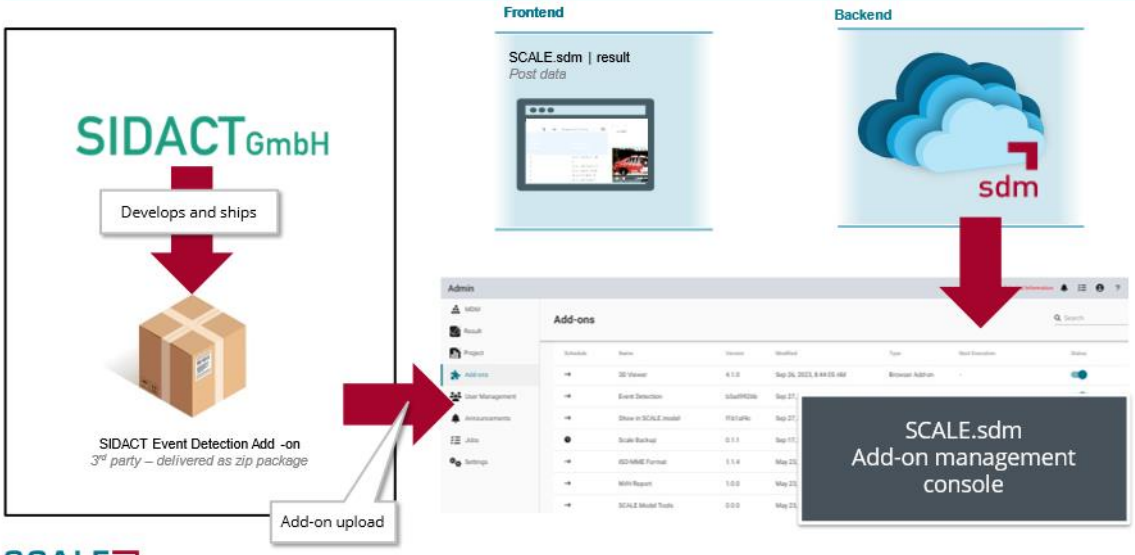

SCALE

Summary

- SDM systems provide structured data sets
- Application of AI/ML methodologies implies scanning large data sets
- Often domain-specific custom ML methods
  (specific methodologies are often required but not part of standard software or implementations)
- Add-on concept enables custom ML-methods and UI extensions in SDM systems
- Example Application: Event Detection by SIDACT

CAT & CAE
Compare simulation and physical tests

Data Analysis
Machine Learning and Data Mining

Event Detection
Anomaly detection by SIDACT GmbH

SCALE

Machine Learning to Empower Engineering Organizations: Technology & Applications

P. Mc Grath, Dr. Pierre Baqué, Kosmas Kritikos, Thomas Von Tschammer

(Neural Concept)

1. Introduction

To tackle new challenges, engineers need radically new capabilities, including more effective ways to harness our computational resources.

Because of their historical origin, simulation tools are not well adapted to design optimization in fast-paced production and design environments. It is extremely hard for design teams to leverage insights provided by advanced simulations and by the specialized teams who develop them. Deep Learning technologies can be used to integrate knowledge from simulation and design optimization tools in the workflow of the design engineers, instead of delegating this task to separate expert teams.

2. Summary

In this talk, we explain how recent algorithms based on Geometric Deep Learning, allow shortcutting any simulation chain through a predictive model that outputs post processed simulation results and optimization suggestions, right from the CAD design. These models are being used in engineering companies to simplify processes and to emulate the expertise of simulation engineers in the hands of product or design engineers early in the development process. Thus, the number of iterations between teams are reduced while accelerating the design activities.

We will also present recent developments and application examples in Geometry Generative Design tools, which can be combined with the predictive models, as well as real use cases of these technologies, enabling optimization within a fragment of the time necessary with traditional simulation techniques.

non-exhaustive list of possible applications:

- heat exchanger design (cfd simulations)
- durability (FEA simulations, transient and static)
- external aerodynamics (cfd simulations)
- internal flows (cfd simulations, turbomachinery, pipes, etc.)
- PCB drop tests (transient fea simulations)
- process simulations (warpage prediction for injection molding, stamping, etc.)

3. IGBT Cooling for power-electronics

Managing peak temperature is crucial in power electronics applications. Designing within these specific Reynolds regimes can be challenging due to the lack of widespread expertise and the intuitive nature required. Additionally, each new design must be tailored to meet unique packaging and boundary condition constraints.

Neural Concept offers a fully automated end-to-end solution that minimizes the need for human intervention. This workflow enables the optimization of designs to meet new constraints in less than 2 hours. A key outcome is that designs produced by the company are typically 10 to 15% more efficient than those created using traditional processes. Moreover, these optimized designs achieve better performance in terms of multiple objectives, including pressure drop and thermal efficiency.

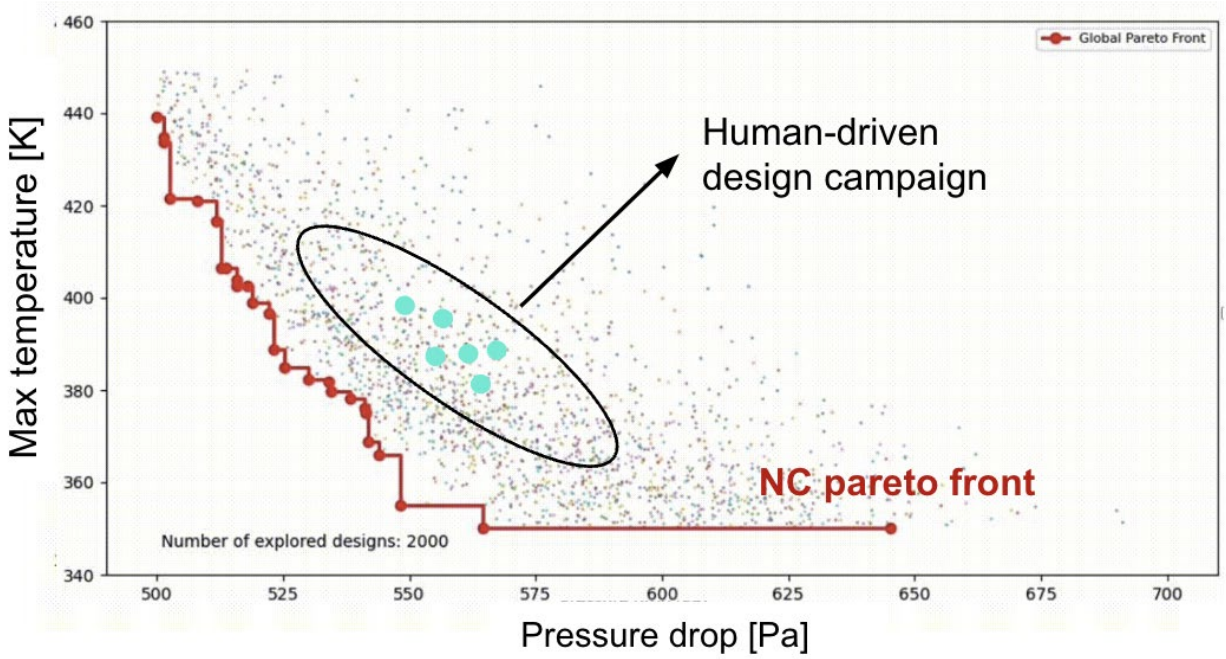

Fig. 1: Results of the optimization campaign: 2000 designs explored in <1h

4. Cold plates

Neural Concept employs physics-informed models for advanced thermal management of EV batteries. Using CAD files that outline the design zone, battery position, and constraints, Neural Concept can generate multiple 3D design outputs, including the Pareto front and physics performance. This approach explores 10,000 designs within a 6-hour cycle, achieving a remarkable 50% reduction in pressure drop.

Design Modules for Pipe Areas (2D, No Spigots): Neural Concept (NC) produces innovative designs that optimize mass-flow distribution, ensure uniform temperature across the system, and minimize pressure drop. The process is streamlined as follows:

- CAD Envelope Provision: Define the design area including inlet/outlet positions, outer boundaries, and restricted zones.
- Manufacturing Constraints Specification: Examples include setting the maximum membrane diameter, minimum wall width, and the smallest allowable radius for dimples or wall ends.
- Design Hyperparameters Adjustment: Control optimization parameters such as the richness of the design space and generation time.

The multi-objective optimization effectively evaluates 10,000 designs in just 12 hours using 50 CPU cores, fully optimizing each design for maximum performance.

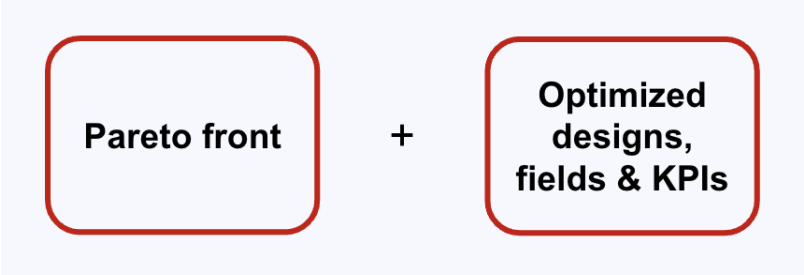

Fig. 2
Optimization outcomes

Leveraging physics-informed neural networks: An introductory guideline for problem-solving across various physical domains

Lucas Schmeing, Fabian Pioch, Jan Hauke Harmening (Westphalian University)

1 Summary

Physics-informed deep learning is a powerful tool for surrogate modeling, reconstruction of sparse data, and inverse problems in all fields of computational physics. Physics-informed neural networks are trained by embedding the governing equations, boundary conditions, and labeled data in a combined loss function. When exploring applications of physics-informed deep learning, appropriate choices of crucial elements such as model architecture, training strategies, and other hyperparameters can be challenging. To assist researchers and practitioners in leveraging physics-informed deep learning in their domains, we present and explain the method and provide a best practice guideline. Initially, we provide a brief introduction to the integration of physical principles into a neural network and its training to satisfy governing equations. We further show a variety of exemplary applications in fluid dynamics, structural mechanics, and electrodynamics. Subsequently, advantages and disadvantages of physics-informed deep learning are discussed in comparison to traditional simulation and machine learning methods. Moreover, we present a guideline for researchers and practitioners, identifying the essential steps to prepare and successfully train a physics-informed neural network. To showcase the guideline, we apply it to a use case from the field of electrodynamics. Our contribution aims to provide the knowledge required to effectively utilize physics-informed neural networks across various physical domains.

2 Introduction

Physics-informed neural networks (PINNs) have emerged as a powerful tool in computational physics. They were first presented by Lagaris et al. [1] and Raissi et al. [2], who demonstrated the ability of PINNs to solve various partial differential equations. Since then, a growing number of studies concerning PINNs have been published, showcasing their applications in a variety of fields of computational physics. As physics-informed deep learning is a relatively novel method, the capabilities, pitfalls, limitations, and best practices of PINNs are not clear at first appearance. In this work, we give a short overview of how PINNs work, what they can be used for, where they have been applied yet, and present a guideline for beginners that is showcased using a surrogate modeling example from the field of electromagnetism.

PINNs are neural networks (NNs) that are trained to satisfy given equations. The method is not limited to specific network architectures and, hence, various networks can be applied such as feedforward neural networks (FNNs) or convolutional neural networks (CNNs), among others. Satisfaction of the given equations is trained by using a composed loss function which is the pivotal part of a PINN. The composed loss function adds several sub-losses that correspond to the underlying equations, boundary conditions, or labeled training data. Like a traditional numerical solver, a PINN is designed to predict the dependent variable or solution field with respect to the independent variable or spatial coordinates. Hence, traditionally, a PINN receives a set of coordinates as inputs and then gives back a number of output variables. During training, the weights and biases of the network are adjusted so that the predictions satisfy the governing equations and boundary conditions and, hence, the optimization (training) process of the network is utilized to solve the computational problem. Fig. 1 exhibits an example of a feedforward PINN and the composed loss function.

Typical applications of PINNs comprise reconstruction of sparse experimental data, forward problems, surrogate modeling, or inverse problems, among others. A comprehensive review of the state of the art of PINNs is given by Cuomo et al. [3]. In the following, an overview of applications of PINNs in fluid dynamics, solid mechanics, and electrodynamics is given.

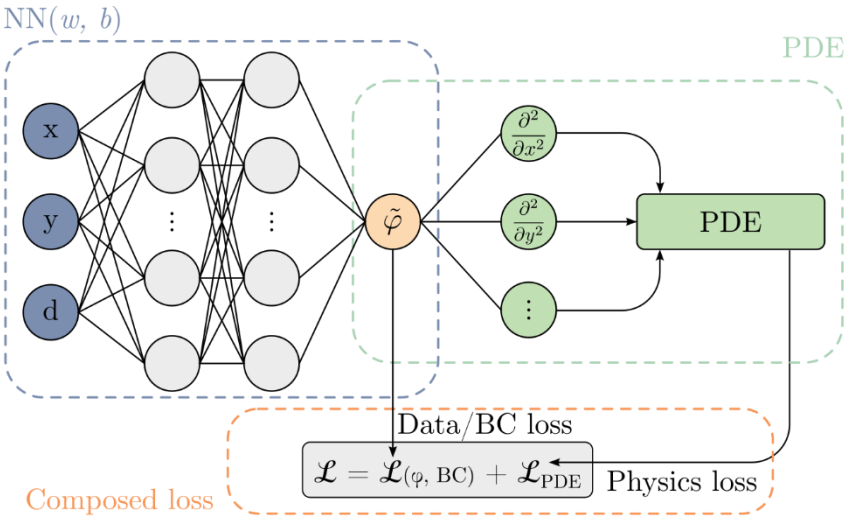

Fig. 1
Example of the architecture of a physics-informed neural network.

3 State-of-the-art and fields of applications of PINNs

3.1 Fluid dynamics

Most studies on the application of PINNs in fluid dynamics primarily address Reynolds numbers below 1,000 (e.g. [4–6]), with notable exceptions such as Eivazi et al. [7] handling up to 200,000, Harmening et al. [8] reaching 1,000,000, and Pioch [9] extending to 5,800,000. Research initially concentrated on simple 2D flow domains such as cylinder flow and its wake [10; 11], with an evolving interest towards more complex scenarios like airfoils [8] or hemodynamics [12; 13]. While initial applications of unsupervised learning with PINNs were restricted to simpler geometries, incorporating measurement or simulation data has enabled these models to tackle more complex flow phenomena. Consequently, PINNs are proving to be valuable to refine low-resolution data from simulations [14] or measurements [15] as well as interpolating results to form surrogate models [8; 16]. For a comprehensive overview of PINNs in fluid mechanics, see Cai et al. and Faroughi et al. [17–19].

3.2 Solid mechanics

In the field of solid mechanics, a majority of studies applied PINNs to predict displacements and stress fields of geometrically simple domains. An application to a two-dimensional square with a hole under consideration of linear elasticity has been done by Henkes et al. [20], while Bai et al. [21] developed a PINN-based method to also solve several geometric nonlinear two- and three-dimensional problems. Similarly, Abueidda et al. [22] used a PINN to predict the stress and deformation of a three-dimensional cantilever for elasticity and also extended the method to hyperelasticity. Various studies covered more specialized problems, such as an investigation by Yang et al. [23], who applied PINNs to composites by utilizing generative adversarial networks (GANs). Another example is a study of Rao et al. [24], who used a mixed-variable network and hard boundary constraints to solve the elastodynamic propagation of a wave without labeled data. Furthermore, an extension of the PINN method to solve the displacement and stress field of shell models has been presented by Bastek and Kochmann [25]. PINNs were also applied to inverse problems to infer geometric shapes or material parameters. Under consideration of elasticity as well as elastoplasticity, Haghighat et al. [26] applied parallel networks trained with simulated reference data to infer material parameters and stresses. The PINN method has also been used to infer geometric shapes and material parameters of voids and inclusions inside a rectangular domain by Zhang et al. [27], who also used labeled training data. For further literature reviews, the reader is referred to the comprehensive studies of Faroughi et al. [18] and Jin et al. [28].

3.3 Electrodynamics

PINNs have been utilized in various domains of electrodynamics to predict different quantities of interest. They have been applied to both forward magnetostatic problems, predicting the magnetic vector potential, and inverse problems, such as predicting the magnetic flux density from a given magnetization distribution, as done by Kovacs et al. [29]. It was demonstrated by Khan and Lowther [30] that they can be used for electromagnetics in an unsupervised as well as a supervised manner. Additionally, research has shown the effectiveness of PINNs in learning the magnetic field response of an EI-core as a function of design parameters [31]. This approach has been adopted by Baldan et al. [32] to develop a magnetostatic coil model. The latter also introduced hypernetworks [33] into PINNs for a real-time field

solver. Recently, there have been initial use cases of PINNs for modeling complex electromagnetic problems, as Son et al. [34] have shown on the example of a permanent-magnet synchronous motor. By Brendel et al. [35], further variations of the PINN architecture were successfully used and compared for predicting the inductances and coupling of axisymmetric transformers.

3.4 State of the method and comparison of PINNs with traditional solvers

PINNs feature a variety of traits useful in computational physics. Firstly, no computational grid needs to be designed, as the networks can be trained on randomly distributed training points. This is an advantage over traditional numerical approaches that require a time-consuming generation of finite element, finite volume, or finite difference meshes. Secondly, to calculate the losses of the governing partial differential equations, no discretization scheme needs to be applied, as the derivations are calculated exactly via backpropagation. Consequently, no diffusive or dispersive numerical errors affect the predicted solution fields. Thirdly, PINNs can be used for simultaneous training to learn solution fields as a function of additional parameters. One example of such an application is demonstrated in the following sections of this work. This is another advantage over traditional solvers that can only be used to calculate a single solution field, depending on a single discrete setting of additional parameters.

On the other hand, the multidimensional optimization problem of the network in combination with the traits of the governing equation imposes challenges in attempting useful solution fields in some cases. For applications of PINNs to real-life problems, this is a major concern. As described above, at the moment, most studies cover simple computational tasks. For more complex applications, PINNs often fail to yield predictions that are in close agreement with reference numerical solution fields. Hence, there is a growing number of studies focusing on methodological improvements of PINNs that include distributed PINNs, novel weight initialization methods, and adaptive loss weighting, among others [36].

4 Workflow

The following chapter introduces a guideline that supports users in maneuvering the workflow to utilize a PINN for their own simulation tasks. Before building the network itself, preprocessing must be done, which is depicted as a flowchart in Fig. 2. The first relevant question is the objective of the study. This may include a reconstruction task, a surrogate model, solving an inverse problem, or using a PINN as a solver for a forward problem. When selecting a model type, the availability and suitability of data must be taken into consideration. For instance, if the objective is a reconstruction from a given dataset, the availability of data is crucial; however, when using a PINN as a solver, data is optional, but its implementation should be considered. It is also important to determine whether classical solvers, such as finite element, finite volume, or finite difference solvers, may be a more appropriate choice in terms of computational resources and accuracy.

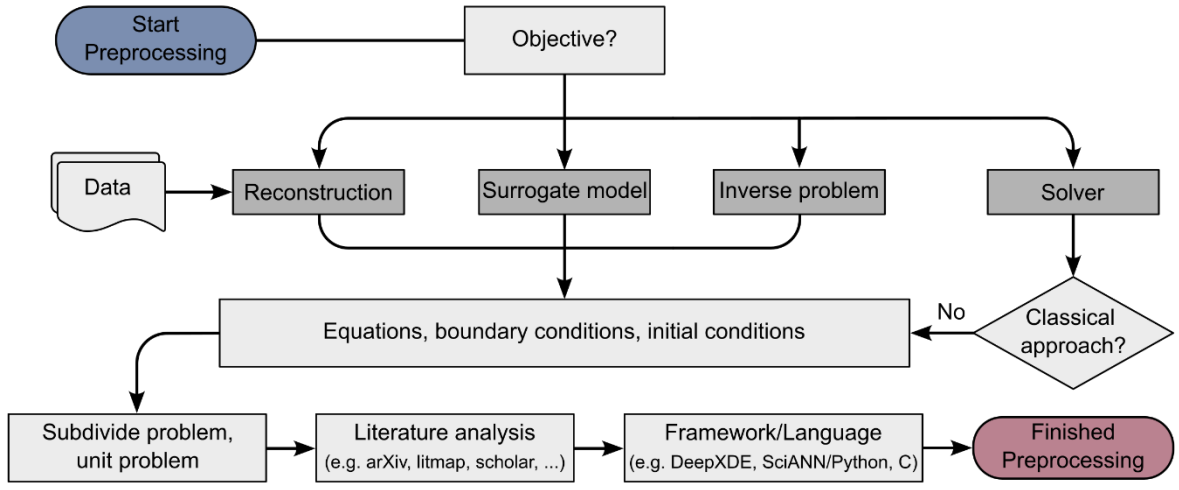

Fig. 2
Flowchart preprocessing for physics-informed deep learning.

Subsequently, the systems governing equations, boundary conditions, and initial conditions must be formulated. Once this is done, the problem should be subdivided into smaller problems or even unit problems to better control the deep learning application process by managing the complexity; this may also include simplification of equations, boundary conditions, and geometries. The level of detail can then be increased incrementally. In a following literature review, it can be ascertained if a similar issue

has been solved before and if the published methods could be leveraged to solve the own problem. When this has been accomplished, a programming language and a framework must be chosen, with Python being recommended here, as it is relatively straightforward to learn and offers a wide range of libraries and frameworks. Afterward, the equations, boundary conditions, loss functions, and network architecture must be converted into code.

If this stage has been completed, preprocessing is concluded, and the main setup begins. This includes defining the network architecture, training strategy, and placement of training points, as depicted in Fig. 3. Regarding the network architecture, first the type of network must be specified. Basic types of neural networks, such as convolutional neural networks and feedforward neural networks, may serve as a suitable foundation for a PINN, with the potential for adaptation to meet the specific needs of the given task. From here on, an initial architecture in terms of the number of input neurons, output neurons, hidden layers, and neurons per layer must be specified. Further on, a decision has to be made whether to use a fully or not-fully connected network and which activation function to choose. The number of input and output neurons is determined by the number of input and output variables that a model should have. For most models, it is also best practice to use a fully connected neural network and the hyperbolic tangent (tanh) as an activation function. For all the aforementioned points as well as the training strategy and distribution of training points, the information obtained from the literature review should be utilized.

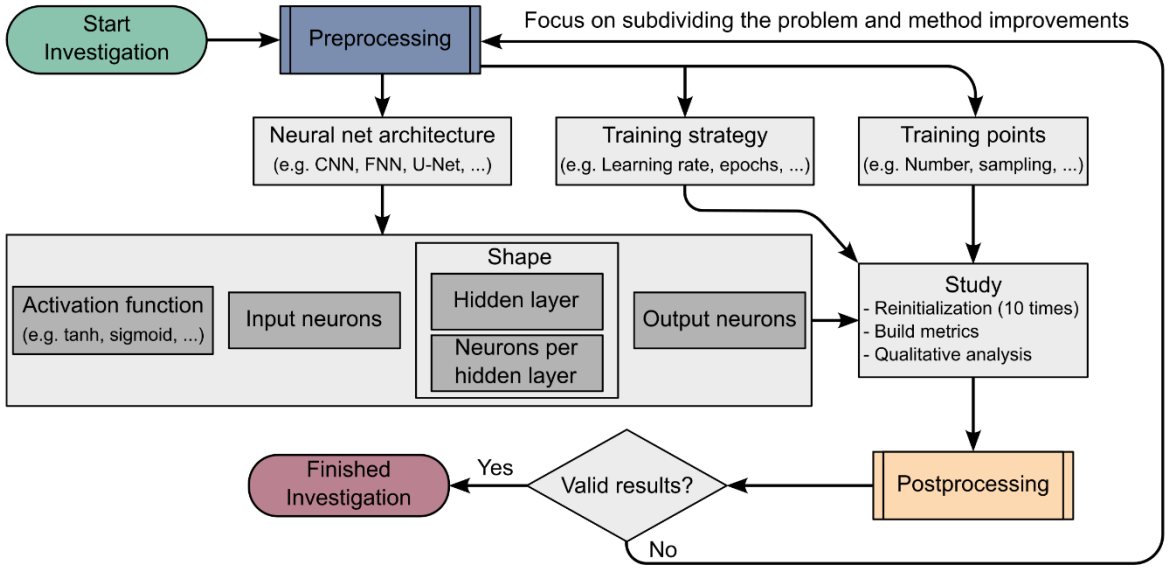

Fig. 3
Flowchart main setup of a physics-informed neural network.

When the network is built, a study must be conducted, to evaluate the most suitable network architecture by reviewing the chosen metrics. The training should be reinitialized at least ten times, and the models' predictions reviewed based on the chosen metrics and its qualitative output. The latter is part of the postprocessing, as illustrated in Fig. 4. This includes saving the model and testing if it can be opened again, as well as visualizing the predictions and metrics appropriately.

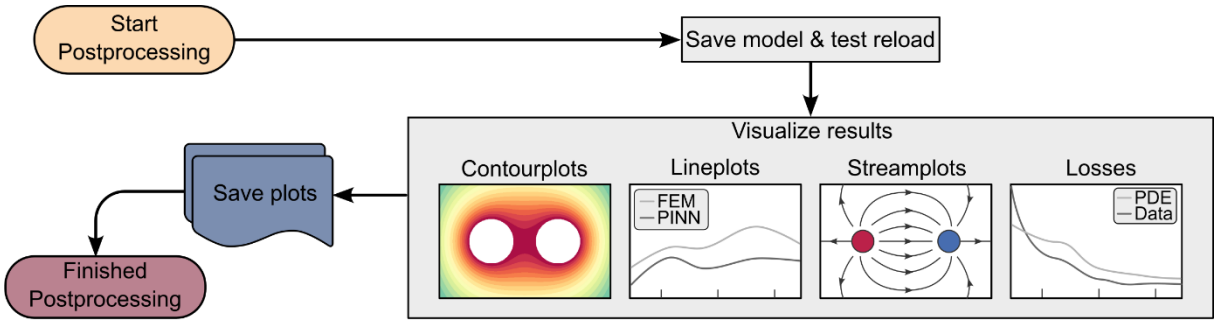

Fig. 4
Flowchart postprocessing for physics-informed deep learning.

After the study and the postprocessing have been conducted, the decision must be made, whether the results are valid and satisfying. If that is not the case, one should focus on subdividing the problem even

further and improve the chosen methods. Therefore, a more in depth preprocessing with further research may be necessary. Otherwise, if the results are valid and satisfying, the investigation is finished, and the PINN was successfully built and trained.

5 Use case

The following chapter presents an example of the application of the guideline to train a PINN. The first step comprises the preprocessing and the question about the objective. Here, we aim to apply a PINN as a surrogate model to predict the electric potential in a two-dimensional domain. The system's governing equation is Laplace's equation, which can be written as $\Delta\varphi = 0$. The domain is a square with two circular cutouts at a distance d from each other. The applied Dirichlet boundary conditions are $\varphi_e = 0$ on the outer edges of the square and $\varphi_h = 1$ on the edges of the holes. In this case, a further subdivision of the problem is not necessary. In a literature review, a comparable study could be found, in which an electromagnetic case without any cutouts in the domain was investigated [30]. For this work, the framework DeepXDE was chosen. In order to train the PINN, a third dimension was employed to integrate the distance between the holes into the training. Consequently, a hypercube was created, whose third dimension represents the distance d. The domain and the boundary conditions can be seen in Fig. 5.

After the preprocessing, the main process was conducted. Based on the literature review, the PINN was built as a feedforward neural network. It was trained for 20,000 epochs with an Adam optimizer and a learning rate of $1e^{-3}$ initially and an L-BFGS-B optimizer subsequently. For the training, 1,000 training points were randomly distributed in the xy-plane of the domain, with another 1,000 points on the edges of the square and 1,000 on the edges of the holes. In the d-axis, distances of 0.6, 1.0, and 1.4 were included in the training. As inputs, the three dimensions x, y, and d of the hypercube were used, and the output is the electric potential φ. No additional data was incorporated, thus the training was unsupervised. To evaluate an appropriate network architecture, a preliminary screening study was conducted with nine distinctive network architectures, ranging from two hidden layers and eight neurons up to eight hidden layers and 32 neurons. To provide a reference solution, the problem was solved using the finite element method (FEM). For this, the 2×2 domain was discretized with approximately 1,500 triangular elements with second-order shape functions.

In the postprocessing, the predictions and metrics are visualized. Fig. 5 illustrates the predictions of a PINN for two hidden layers and eight neurons per layer on the left, eight hidden layers and 32 neurons per layer in the middle, and the reference results from the FEM on the right. In each case, the distances 0.6 and 1.4 are displayed. The network with two layers and eight neurons is unable to accurately represent the electric potential, whereas the larger network shows very close resemblance with the FEM results for distances of 0.6 and 1.4.

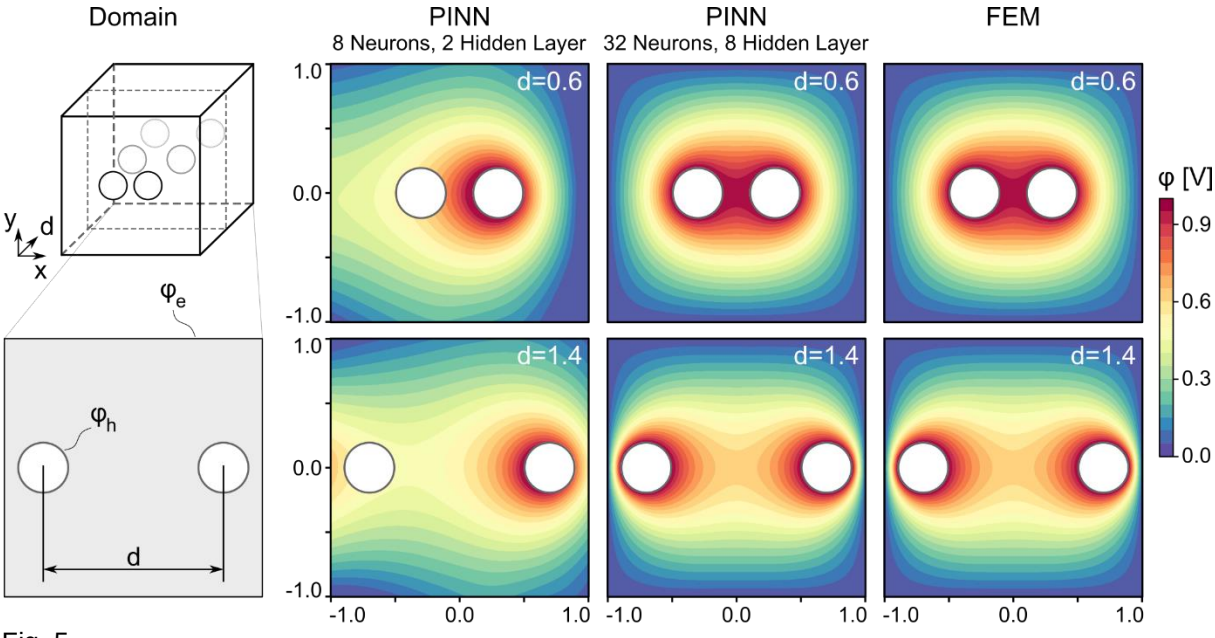

Fig. 5
Computational domain and predicted electric potential from PINN and FEM for distances 0.6 and 1.4.

A comprehensive overview of the results of the screening study is shown in Fig. 6, which displays the accuracy of different architectures. For the evaluation, the mean squared error (MSE) for each architecture was calculated using the FEM results as ground truth. It can be observed that the error declines as the number of hidden layers and neurons increases. However, not only the overall number of neurons in the network is important, but also their distribution over the hidden layers.

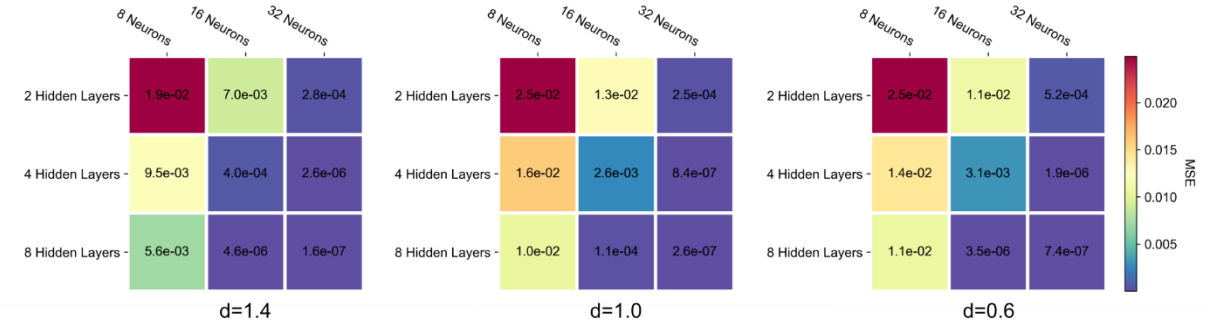

Fig. 6
Mean squared errors for different network architectures and values of d.

The before mentioned results show that the network architecture with eight hidden layers and 32 neurons per layer yields valid solution fields and can be used for simultaneous surrogate modeling. For the presented use case, the potential distribution in a two-dimensional domain was successfully trained for three variations of the geometric parameter d. In a single training run, the potential for the three geometries was learned at once, a possibility a classical numerical solver cannot provide. Moreover, the trained model can be used to interpolate the potential distribution for values of d not included in the training. The results also underline the importance of a screening study to determine a suitable network architecture.

6 References

[1] Lagaris I. E., Likas A., Fotiadis D. I.: "Artificial neural networks for solving ordinary and partial differential equations", IEEE transactions on neural networks, 1998

[2] Raissi M., Perdikaris P., Karniadakis G. E.: "Physics-informed neural networks: A deep learning framework for solving forward and inverse problems involving nonlinear partial differential equations", Journal of Computational Physics, 2019

[3] Cuomo S., Di Cola V. Schiano, Giampaolo F., Rozza G., Raissi M., Piccialli F.: "Scientific Machine Learning Through Physics–Informed Neural Networks: Where we are and What's Next", Journal of Scientific Computing, 2022

[4] Ryno Laubscher, Pieter Rousseau: "Application of mixed-variable physics-informed neural networks to solve normalised momentum and energy transport equations for 2D internal convective flow", Unpublished, 2021

[5] Wandel N., Weinmann M., Klein R.: "Teaching the incompressible Navier–Stokes equations to fast neural surrogate models in three dimensions", Physics of Fluids, 2021

[6] Xu S., Sun Z., Huang R., Guo D., Yang G., Ju S.: "A practical approach to flow field reconstruction with sparse or incomplete data through physics informed neural network", Acta Mechanica Sinica, 2023

[7] Eivazi H., Tahani M., Schlatter P., Vinuesa R.: "Physics-informed neural networks for solving Reynolds-averaged Navier–Stokes equations", Physics of Fluids, 2022

[8] Harmening J. Hauke, Pioch F., Fuhrig L., Peitzmann F.-J., Schramm D., el Moctar O.: "Data-Assisted Training of a Physics-Informed Neural Network to Predict the Reynolds-Averaged Turbulent Flow Field around a Stalled Airfoil under Variable Angles of Attack", 2023

[9] Pioch F.: "Echtzeitfähige digitale Zwillinge auf Basis Physik-informierter neuronaler Netze für die Strömungsvorhersage in und um Stallungen", 2024

[10] Ma H., Zhang Y., Thuerey N., null X. Hu, Haidn O. J.: "Physics-Driven Learning of the Steady Navier-Stokes Equations using Deep Convolutional Neural Networks", Communications in Computational Physics, 2022

[11] Xu H., Zhang W., Wang Y.: "Explore missing flow dynamics by physics-informed deep learning: The parameterized governing systems", Physics of Fluids, 2021

[12] Arthurs C. J., King A. P.: "Active training of physics-informed neural networks to aggregate and interpolate parametric solutions to the Navier-Stokes equations", Journal of Computational Physics, 2021

[13] Arzani A., Wang J.-X., D'Souza R. M.: "Uncovering near-wall blood flow from sparse data with physics-informed neural networks", Physics of Fluids, 2021

[14] Pioch F., Harmening J. Hauke, Müller A. Maximilian, Peitzmann F.-J., Schramm D., el Moctar O.: "Turbulence Modeling for Physics-Informed Neural Networks: Comparison of Different RANS Models for the Backward-Facing Step Flow", Fluids, 2023

[15] Hasanuzzaman G., Eivazi H., Merbold S., Egbers C., Vinuesa R.: "Enhancement of PIV measurements via physics-informed neural networks", Measurement Science and Technology, 2023

[16] Sun L., Gao H., Pan S., Wang J.-X.: "Surrogate modeling for fluid flows based on physics-constrained deep learning without simulation data", Computer Methods in Applied Mechanics and Engineering, 2020

[17] Cai S., Mao Z., Wang Z., Yin M., Karniadakis G. Em: "Physics-informed neural networks (PINNs) for fluid mechanics: a review", Acta Mechanica Sinica, 2021

[18] Faroughi S. A., Pawar N. M., Fernandes C., Raissi M., Das S., Kalantari N. K., Kourosh Mahjour S.: "Physics-Guided, Physics-Informed, and Physics-Encoded Neural Networks and Operators in Scientific Computing: Fluid and Solid Mechanics", Journal of Computing and Information Science in Engineering, 2024

[19] Cai S., Wang Z., Wang S., Perdikaris P., Karniadakis G. Em: "Physics-Informed Neural Networks for Heat Transfer Problems", Journal of Heat Transfer, 2021

[20] Henkes A., Wessels H., Mahnken R.: "Physics informed neural networks for continuum micromechanics", PAMM, 2021

[21] Bai J., Rabczuk T., Gupta A., Alzubaidi L., Gu Y.: "A physics-informed neural network technique based on a modified loss function for computational 2D and 3D solid mechanics", Computational Mechanics, 2023

[22] Abueidda D. W., Lu Q., Koric S.: "Meshless physics-informed deep learning method for three-dimensional solid mechanics", International Journal for Numerical Methods in Engineering, 2021

[23] Yang Z., Yu C.-H., Buehler M. J.: "Deep learning model to predict complex stress and strain fields in hierarchical composites", Science advances, 2021

[24] Rao C., Sun H., Liu Y.: "Physics informed deep learning for computational elastodynamics without labeled data", 10.06.2020

[25] Bastek J.-H., Kochmann D. M.: "Physics-Informed Neural Networks for shell structures", European Journal of Mechanics - A/Solids, 2023

[26] Haghighat E., Raissi M., Moure A., Gomez H., Juanes R.: "A physics-informed deep learning framework for inversion and surrogate modeling in solid mechanics", Computer Methods in Applied Mechanics and Engineering, 2021

[27] Zhang E., Dao M., Karniadakis G. Em, Suresh S.: "Analyses of internal structures and defects in materials using physics-informed neural networks", Science advances, 2022

[28] Jin H., Zhang E., Espinosa H. D.: "Recent Advances and Applications of Machine Learning in Experimental Solid Mechanics: A Review", Applied Mechanics Reviews, 2023

[29] Kovacs A., Exl L., Kornell A., Fischbacher J., Hovorka M., Gusenbauer M., Breth L., Oezelt H., Praetorius D., Suess D., Schrefl T.: "Magnetostatics and micromagnetics with physics informed neural networks", Journal of Magnetism and Magnetic Materials, 2022

[30] Khan A., Lowther D. A.: "Physics Informed Neural Networks for Electromagnetic Analysis", IEEE Transactions on Magnetics, 2022

[31] Beltran-Pulido A., Bilionis I., Aliprantis D.: "Physics-Informed Neural Networks for Solving Parametric Magnetostatic Problems", IEEE Transactions on Energy Conversion, 2022

[32] Baldan M., Di Barba P., Lowther D. A.: "Physics-Informed Neural Networks for Inverse Electromagnetic Problems", IEEE Transactions on Magnetics, 2023

[33] Ha D., Dai A., Le Q. V.: "HyperNetworks", arXiv, 2016

[34] Son S., Lee H., Jeong D., Oh K.-Y., Ho Sun K.: "A novel physics-informed neural network for modeling electromagnetism of a permanent magnet synchronous motor", Advanced Engineering Informatics, 2023

[35] Brendel P., Medvedev V., Rosskopf A.: "Physics-Informed Neural Networks for Magnetostatic Problems on Axisymmetric Transformer Geometries", IEEE Journal of Emerging and Selected Topics in Industrial Electronics, 2023

[36] Wang S., Sankaran S., Wang H., Perdikaris P.: "An Expert's Guide to Training Physics-informed Neural Networks", 16.08.2023

Hydrogen storage 3D architecture automated generation with AI

Jean-Pierre Roux (Dessia Technologies) - Hugues Massé (OP Mobility)

OP Mobility (ex Plastic Omnium) positions itself as a global leader in hydrogen mobility, the group directs its strategic vision in this field around a comprehensive and competitive offering covering the entire hydrogen value chain. This includes hydrogen tanks, fuel cells, and integrated hydrogen systems.

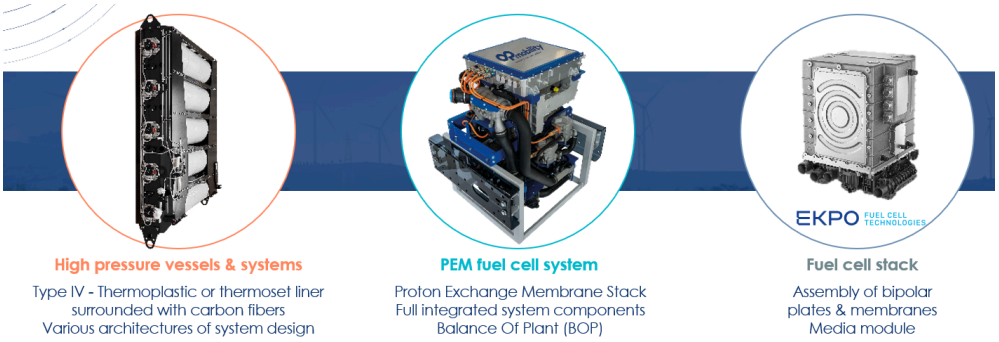

Fig1: OP Mobility H2 Product Range

Hydrogen storage in the form of compressed gas is a crucial challenge for the development of hydrogen as an energy vector in the automotive sector. Hydrogen storage is more complex and costly than that of other gases due to its very low density, thus requiring high pressures, typically 700 bars. Type IV tanks (with polymer liner) have improved these storage conditions. They separately manage the tightness and mechanical resistance to pressure, allowing the use of lighter materials while maintaining safety. However, these tanks are constrained in their shape to minimize stresses in the material due to pressure, and this shape does not allow optimal use of the available space in the vehicle.

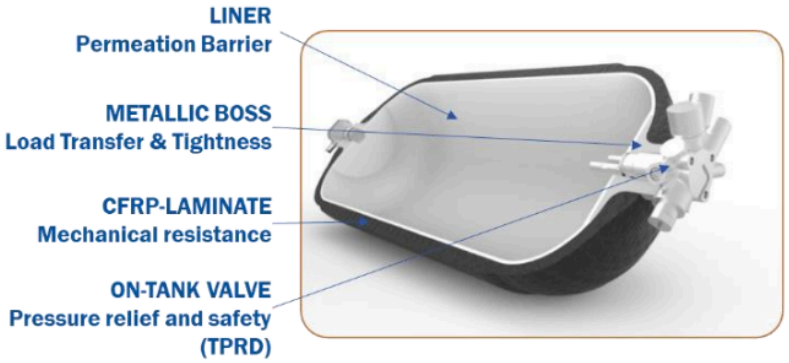

Fig2: Type IV high pressure vessel design

Therefore, a software solution for optimizing storage architecture within the vehicle brings clear commercial interest, whether to reliably and quickly respond to RFQ or to optimize the cost-to-quantity ratio of onboard hydrogen, which is a fundamental element of storage system sizing.

Fig3: H2 Storage system

This dedicated software solution has been developed using Dessia Technologies' process automation software platform. Leveraging the libraries of the platform, it's possible to describe a system through object-oriented modeling and associate attributes and methods such as 3D CAD generation or solution generation using AI algorithms.

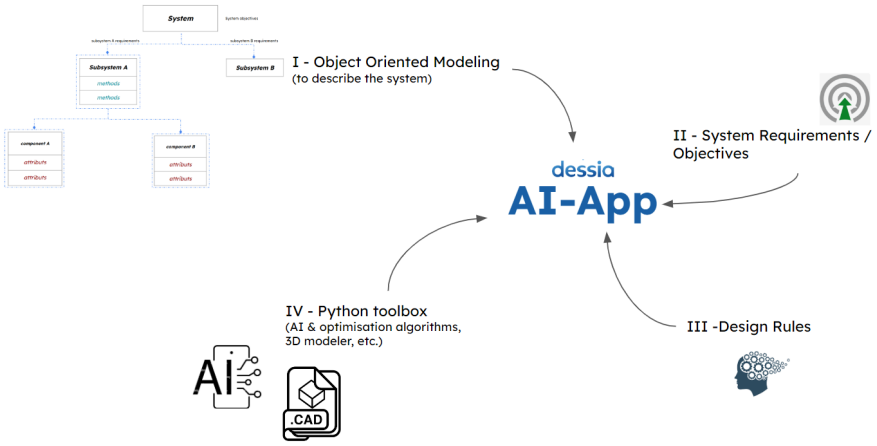

Fig4: Object Oriented System Modeling connected with AI, rules and requirements

Different types of AI algorithms are used depending on the purpose of the software application to be developed

- Generative algorithms from the symbolic or Explainable AI family are used, for instance, decision trees with pruning strategies to generate data from knowledge.
- Statistical Artificial Intelligence algorithms are used in situations where a large amount of data is available.

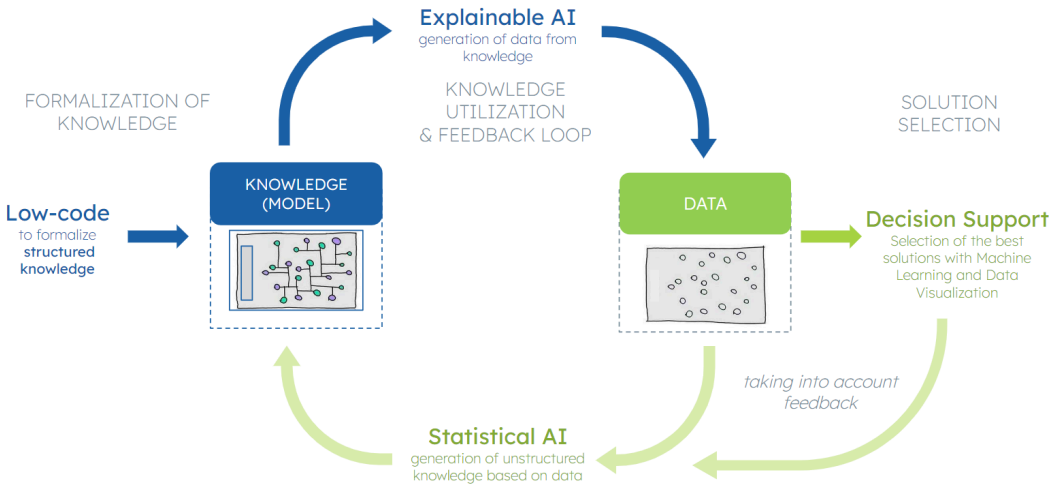

Fig5: Explainable versus Statistical AI

This software application for optimizing hydrogen storage architecture uses generative algorithms to automatically generate

- all possible solutions for integrating tanks within a given functional volume, starting from a catalog containing all possible tank models.
- the pipes routing that connect the tanks to a hydraulic collector.

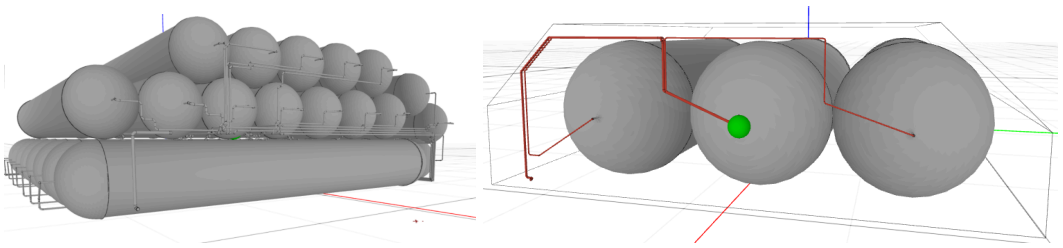

Fig6: Example of H2 Storage solution generated by the Application

- Clustering algorithms to organize the solutions into architecture families, facilitating assistance in selection and decision-making. This approach also enables the exploitation of results to quickly identify the most functionally and economically efficient solutions.

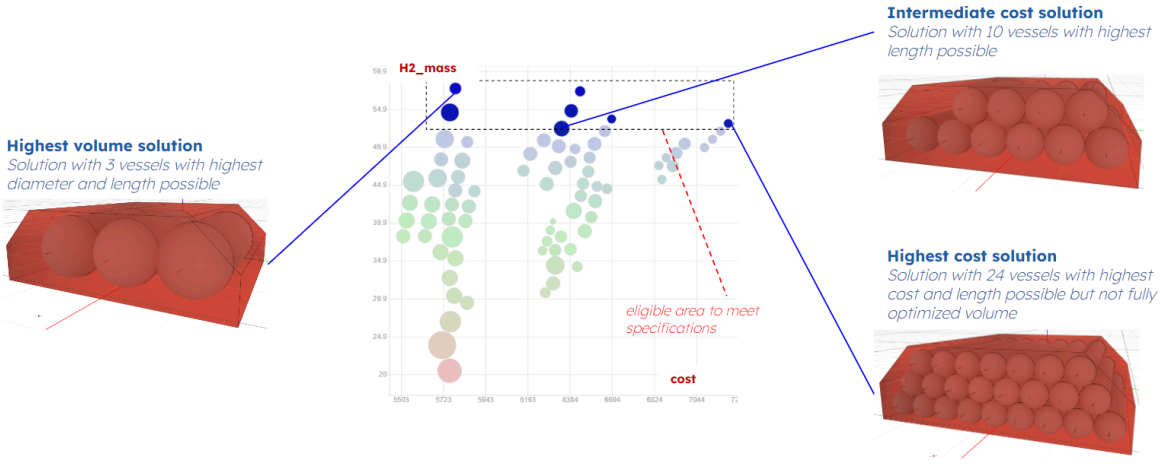

Fig7: Data driven Design Solution selection

Conclusion:

A software application combining knowledge and rules with explainable and statistical AI algorithms has been developed; it opens the capacity to explore automatically the field of all 3D architecture solutions in a few minutes where a manual process takes days to come up with a good design.
Trade-off & impact studies can be performed amongst the various solutions, and informed design decisions are taken.

Collaboration and SPDM

Michael Schlenkrich

Director Product Management HMI Design & Engineering

(Hexagon)

In today's complex product development landscape, effective collaboration across disciplines is paramount. This paper explores the crucial role of collaboration within the context of a mature Simulation Process and Data Management (SPDM) solution. We will delve into the distinct functionalities of two key systems: the System of Record (SoR) and the System of Engagement (SoE).

The SoR acts as the central repository, ensuring data integrity and serving as the single source of truth for all simulation data. Conversely, the SoE fosters real-time interaction and knowledge sharing among stakeholders. We will analyse the optimal positioning of these systems within the SPDM ecosystem, highlighting how they work in tandem to empower collaboration.

By promoting seamless data exchange and fostering communication channels, a mature SPDM solution facilitates a collaborative environment. This, in turn, drives innovation, streamlines workflows, and ultimately accelerates product development success.

Accelerating AI Adoption in CAE with cloud-native SPDM

Richard Szöeke-Schuller (SimScale), Jon Wilder (SimScale), Dr. Naghman Khan (SimScale)

1 Summary

AI tools are being trialed across the engineering industry with all sectors looking at how adoption of machine learning can help streamline product development. Early adopters however, have encountered one major obstacle, this being data integrity and compatibility. Most data repositories are a mix of disorganized distributed files and require significant investment in data hygiene to become useful. Adopters of AI are often forced to generate entirely new data sets, costing time and money. In this paper we ask the question - what if we could create training data sets while also saving time and cost in the overall product development process. The solution can be found in cloud-native engineering simulation with intrinsic SPDM capabilities [1].

2 A Traditional CAE Design Workflow

Figure 1 shows a typical standard simulation workflow, a loop that starts and ends with PLM where most aspects of the process are centralized. PLM data is effective for managing CAD models and tracking changes to them. Simulation reports are almost certainly stored alongside these CAD models making it easy to see what results apply to which model. This process however, means that engineering teams are likely to be using multiple software tools both desktop/legacy and cloud, and are creating simulation data in various formats, spread across multiple sites, offices and machines. The challenge we face is to streamline these workflows and behaviors to allow the rapid adoption of AI, which demands quality and quantity of data, neatly collated in a way not previously seen.

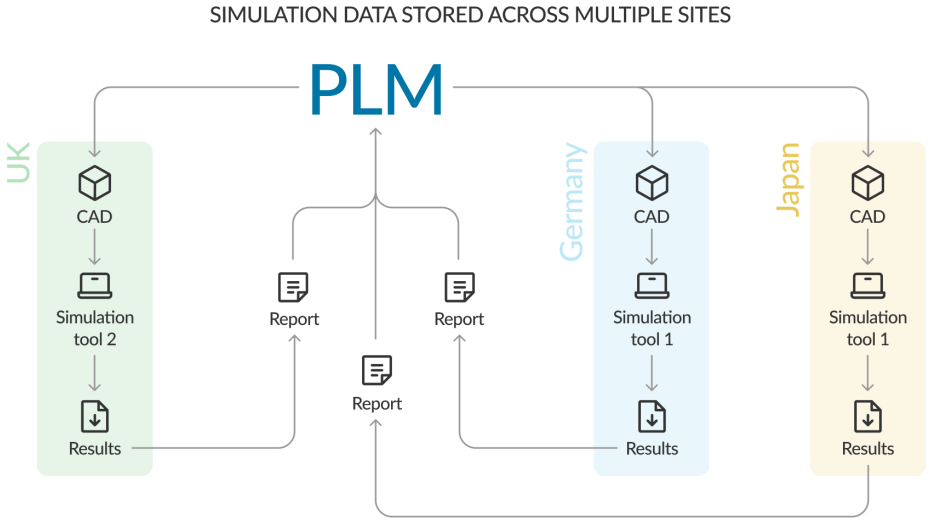

Figure 1; Traditional workflow. PLM keeps CAD centralized. Simulation quickly becomes decentralized with results from different tools distributed across the globe.

3 What is Cloud-Native CAE and Where Does AI Fit in

Engineering simulation has long been a fundamental tool for refining and validating designs. Burdened with hardware, computational, and software limitations, CAE simulation has had convoluted bottlenecks such as the basic lack of access to a license, inoperable license servers, scalability, accuracy-to-speed trade-offs, long simulation cycle times, and, more critically today, long simulation lead times. With the

advent of cloud computing, cloud-native simulation has empowered organizations to not only resolve these bottlenecks but also eliminate them altogether. Furthermore, running simulations online has also allowed organizations to overcome the data silos between teams, enabling them to collaborate on simulation projects in real time by simply sharing the projects at a click of a button, thus facilitating the company-wide deployment of simulation. Supporting AI with simulation data helps optimize business decision-making and overcome the common challenge of real-world data scarcity by providing a data-rich simulated environment for synthetic data generation and reinforcement learning.

SimScale has launched a fully capable AI simulation feature, powered by NAVASTO, that sits side by side with its physics solvers [2]. This means the simulation data is naturally always building up, in preparation for AI. We foresee all data from simulation to be used for AI training and inference, to accelerate rapid design convergence in the cloud. Simulation projects would benefit from AI's capabilities to increase the speed of executing complex simulations or fill gaps in CAE and simulation models using generative AI. Today, only a cloud-native simulation infrastructure can benefit from the full advantage of AI, as all simulations are immediately ready for AI training on GPUs hosted in the cloud. As new data is added, retraining of AI models is straightforward, automatic even. On SimScale's cloud-native platform, for example, AI CAE models are deployed next to CFD simulations, with AI results used for near-instantaneous evaluations and CFD for the final validation (Figure 2).

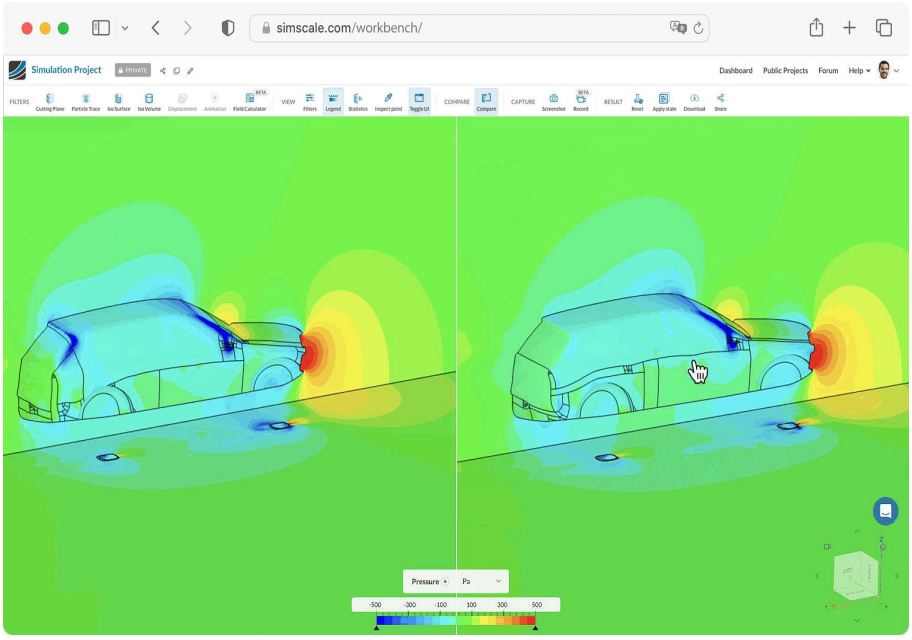

Figure 2: Parallel simulations in SimScale showing the PDE results (left) and the near instantaneous AI-assisted simulation results (right) on the same workbench

4 Why is Cloud-Native so Important for SPDM

Emphasizing flexibility, cloud-native approaches should never enforce a specific Computer-Aided Design (CAD) authoring or SPDM strategy. This technical agnosticism allows for a seamless SPDM deployment, catering to diverse engineering needs. Our approach offers a flexible and integrated framework for user, data, and process management, focusing on SimScale's data, while offering API access for third-party data integration.
We explore the transformative potential of cloud-native technology in creating and enhancing seamless SPDM integration by constructing an architecture from 'first principles' and with AI capabilities at its core. This presentation will show a case study of how AI trained model data is used in the product development process of a large engineering team and the SPDM features that emerge from it. By integrating advanced features like user management, real-time collaboration, and comprehensive data handling, it establishes a robust framework for future-oriented simulation practices in the cloud.

5 A Better Workflow Using Cloud-Native SPDM and AI

If the simulation tool is fully cloud-based, all data could be in one place. In this scenario the teams are still working across borders but, like CAD within PLM, all of their simulation data is stored together (Figure 3).

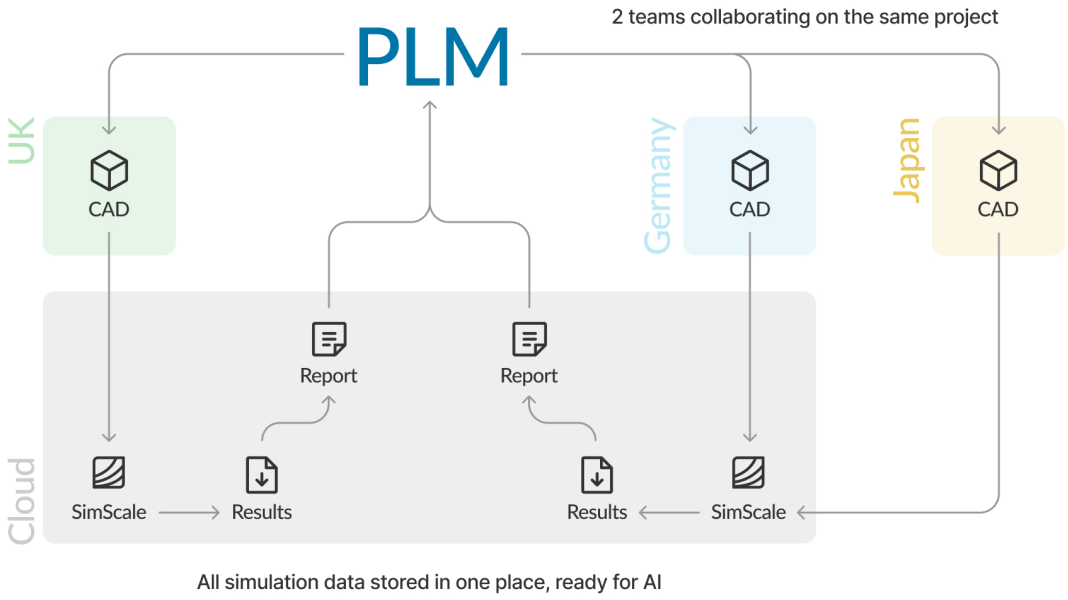

Figure 3; In a Cloud native workflow, simulation is now centralized. Results from different locations are stored together online.

Templated workflows (Figure 4) add to this enhanced process and are essentially fully automated, removing anything between CAD and reporting, while still building a repository to power AI. This is the same as the above but is triggered as part of an SPDM sequence. As soon as a CAD model is updated, the template is reused and the report produced and added back into PLM. AI is finally and easily adopted into the standard process and becomes a part of the same workflow, faster and much cheaper. The real engineering advantage from AI is that results can be updated at a fraction of the cost of the standard workflow.

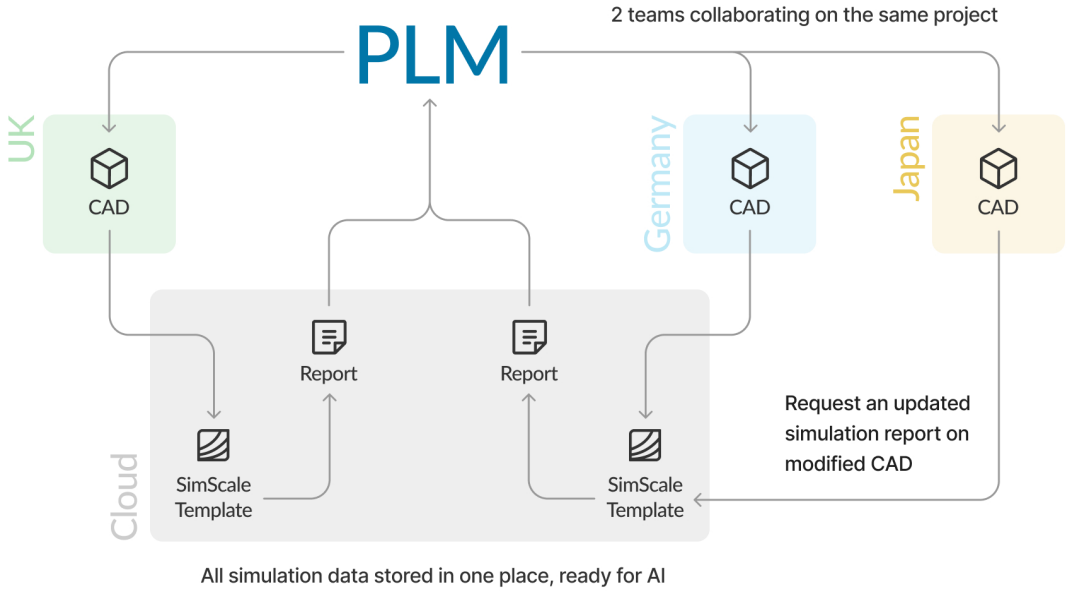

Figure 4: AI enabled cloud native workflow with Templates.

With results now centralized, the data can now easily be leveraged for AI driven SPDM

6 References

[1] SimScale 2024; The Convergence of Emerging Technologies, URL

[2] World Congress Experience, Society of Automotive Engineers (SAE) presentation on 18 April 2024; Real-Time Automotive Design via a Unified Simulation, Data, and Physics AI Solution – A Case Study. Heiny, D (2024)

Managing key parameters from simulation inputs and results

Leonel Garategaray, Hernan Giagnorio,

Fatouma Doucouré (Inensia)

Summary

In the realm of modern engineering practices, the effective management of parameters within the Simulation Process and Data Management (SPDM) framework stands as a critical challenge. Today, organizations are faced with different and often disconnected parameter management approaches, hindering the flow of information in the simulation process. In this context, this paper delineates a strategic initiative to redefine parameter management within the SPDM paradigm. Presenting a comprehensive methodology, we aim to close existing gaps and improve parameter management in simulation activities. We believe this is essential to achieve a more agile, efficient, and integrated approach to recurring engineering and optimization techniques..

An integral aspect is how SPDM facilitates parameter management within the context of Model-Based Systems Engineering (MBSE), and its architectural model, where variables are commonly parameterized. Integrating these parameterized variables into SPDM introduces flexibility and adaptability, allowing for adjustments to analyze their holistic impact on the system, such as modifying attributes like size, weight, or performance.

This capability enables the evaluation of diverse system scenarios or configurations without the need to overhaul the entire model. By adjusting these parameters, the specific effects of changes on system performance or functionalities come to light, empowering engineers with informed decision-making throughout the project's lifecycle.

When we talk about parameters, we refer to input parameters, necessary to perform any simulation, and output parameters, obtained from simulation results which could be compared with product requirements. These parameters could be extracted from file content, consolidating them in a singular repository for traceability and offering a holistic view to assess design efficacy.

In a typical Development Lifecycle, design process begins with an envelope and requirements, and then models that fulfill the needs. Then the simulation tth CAD designs, accompanied by design parameters, boundary conditions, and materials properties, all interpreted as Input parameters. Afterwards, the simulation process, which consists of interlinked simulation activities with various simulation branches, yield results or reports containing key information like performance values, all these are considered as Output parameters.

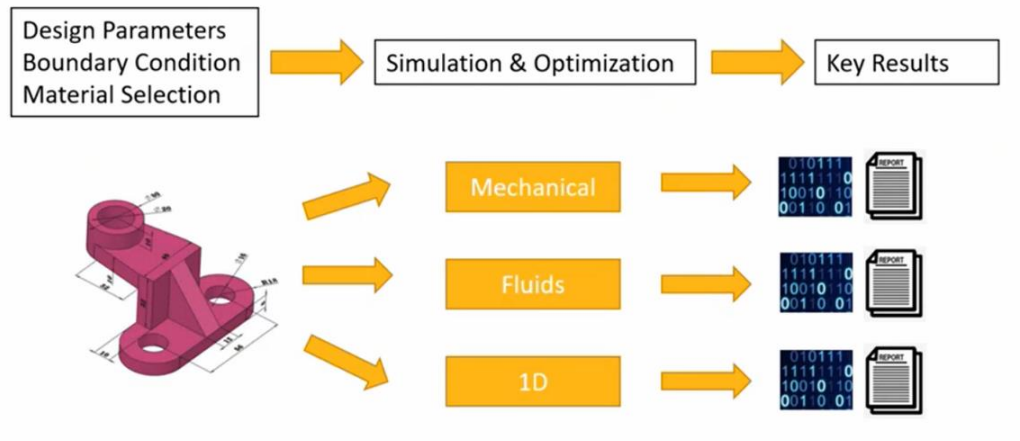

The challenge lies in this flow, since the information is usually disconnected, due to its nature of being documentation-based, which prevents a more pragmatic use to interpret the quality of the design.

The objective of this paper will be to:

- Demonstrate how an SPDM platform streamlines parameter extraction and programmatic management from various files.
- Emphasize the dual centralization of both simulation data and parameters, ensuring traceability and change control.
- Illustrate how this approach accelerates analysts' understanding of designs and results, fostering a more efficient workflow.
- Exemplify, through a practical use case, the creation of parameter repositories from an organized files repository.
- Highlight how this initiative ensures a Single Source of Truth for simulation data, promoting clarity and reliability.

We conclude that harmonizing simulation inputs and outputs through streamlined parameter management in the SPDM platform, enhance the efficiency and reliability of decision-making.

Managing Key Parameters in SPDM

Fatouma Doucouré - Inensia

AGENDA

1. Who we are?
2. Introduction to Use Case
3. Parameter Management in SPDM
4. Implementation Details
5. Conclusion

INENSIA

Transform the way our clients imagine, make and operate their products by providing high quality Business & IT services, delivered by continuously trained teams and powered by cutting edge technologies.

1 | Our playground - Digital Industry

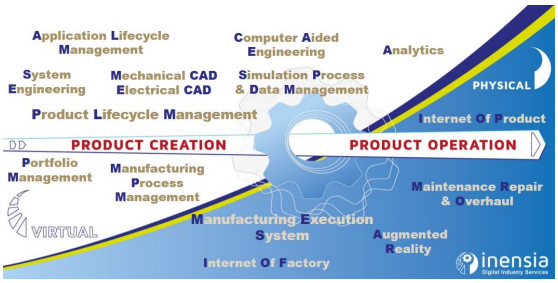

2 | Our Services/ expertise as Ansys Minerva Partners

3 | On the SPDM Arena

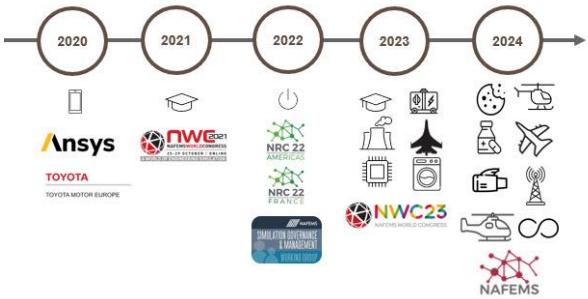

4 | Our team – 110+ motivated experts

inensia Digital Industry Services

Representative Customer Use case To-Be status

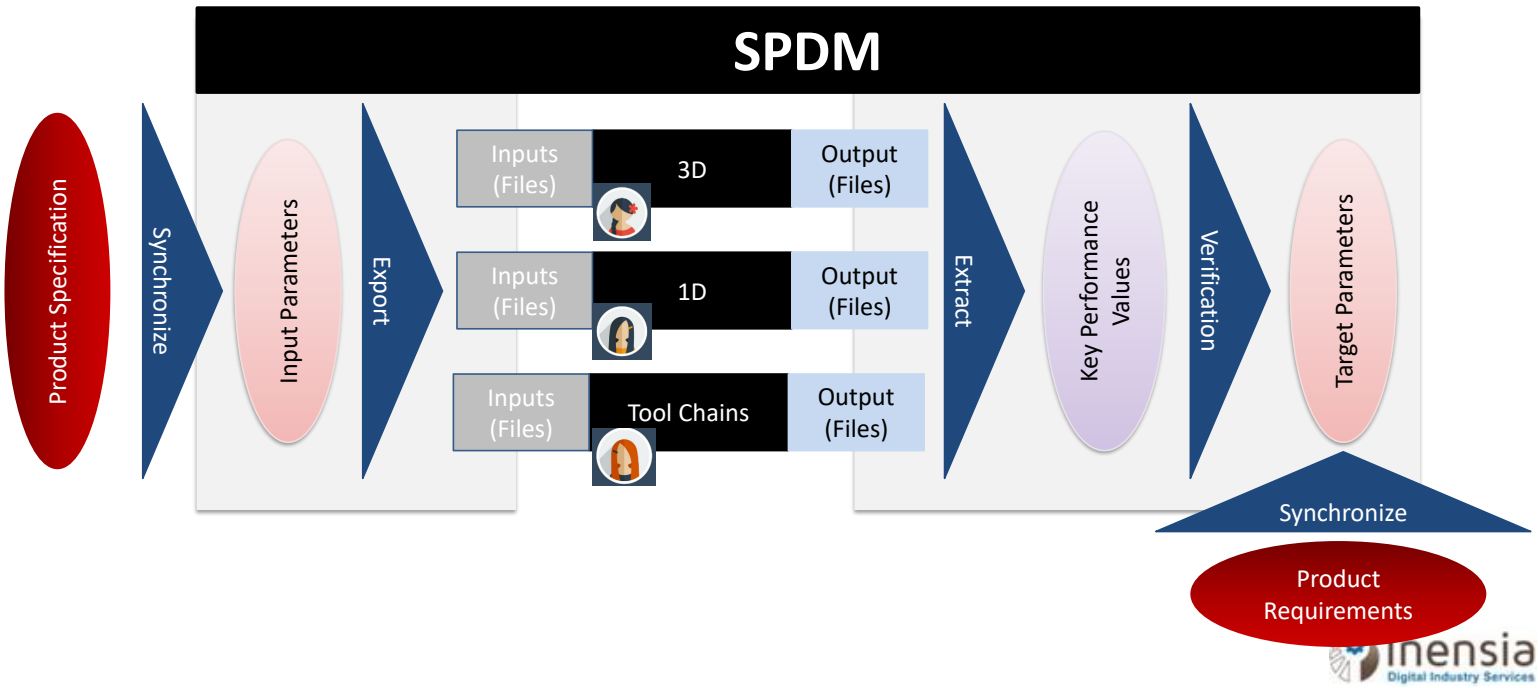

inensia Digital Industry Services

Representative Customer Use case As-is Status

Design Parameters
Boundary Condition
Material Selection

→ Simulation & Optimization → Key Results

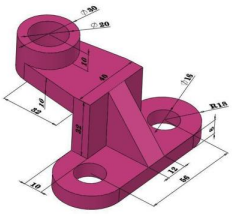

→ Mechanical
→ Fluids
→ 1D

→ Information is **Disconnected** and **Document based**

SPDM yesterday/today: File Focused

Inputs (Files) | Simulation Model | Output (Files)

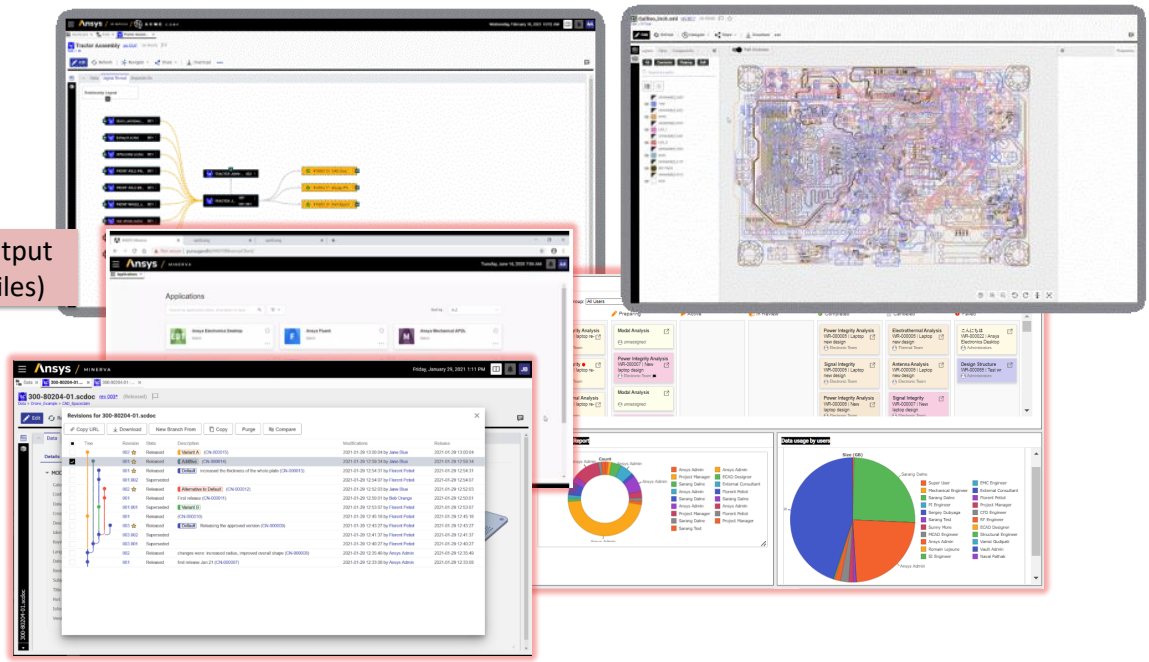

Parameter Management in SPDM

Basic Requirements

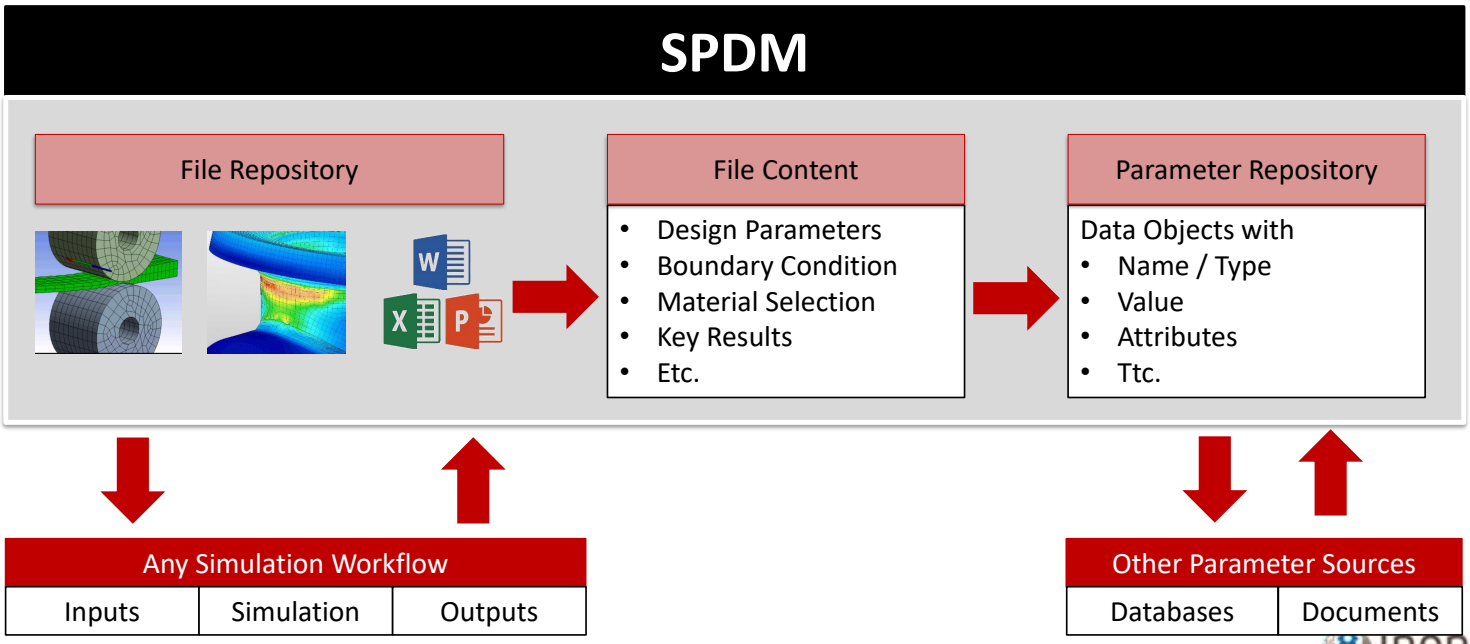

Parameter Management in SPDM

Advanced Requirement

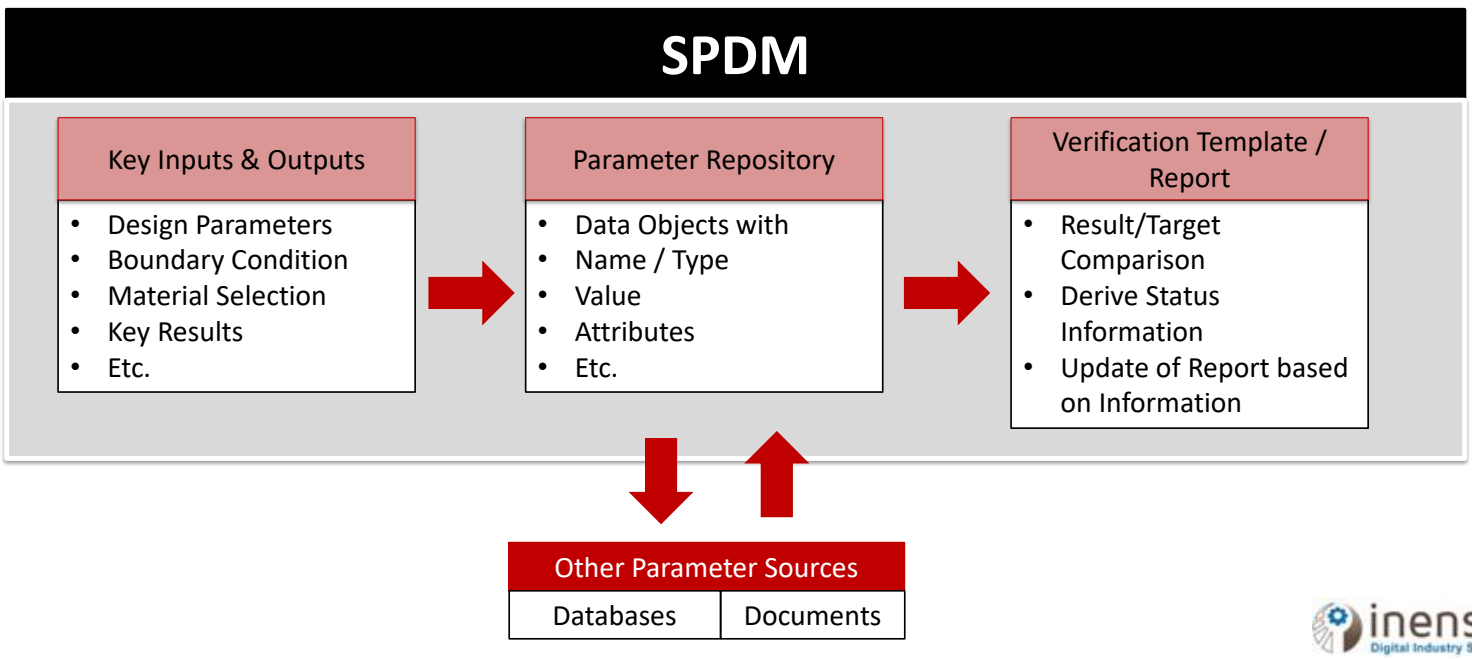

Parameter Management in SPDM

Verification Report: Idea

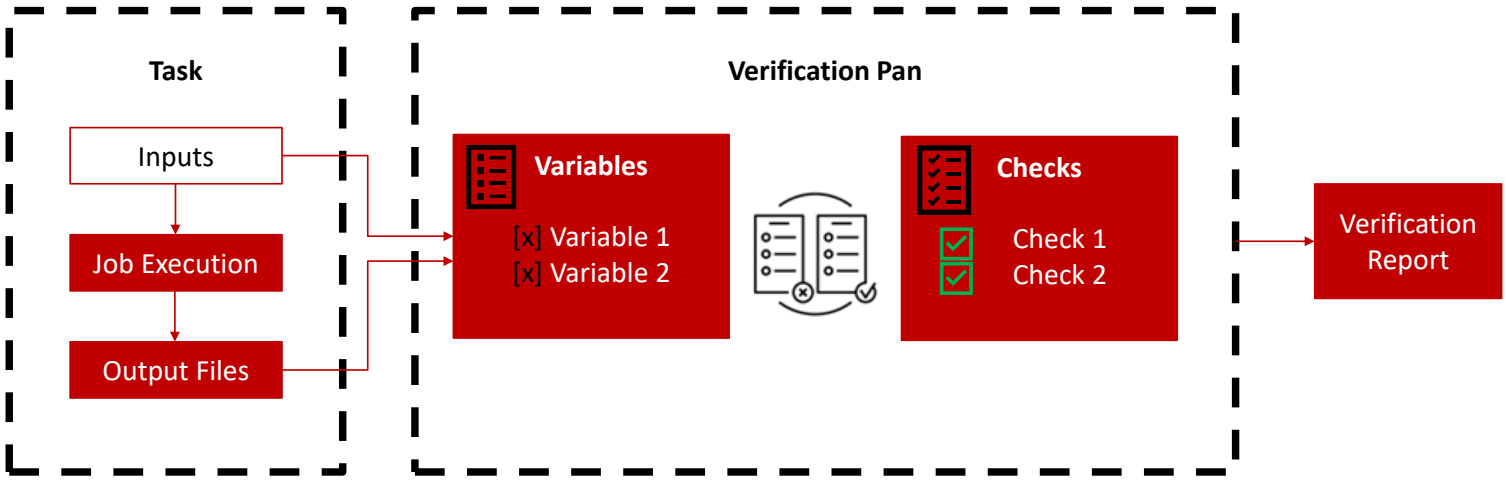

Parameter Management in SPDM

Verification Report: Representative Scenarios

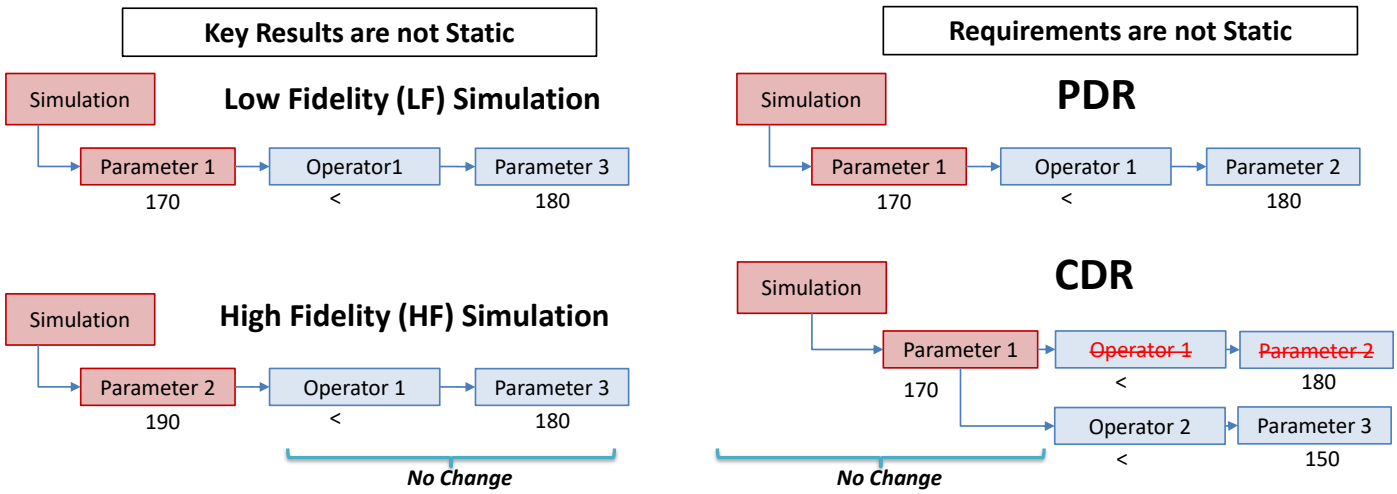

Type	Result	Requirement	Checks
LF	170 (P1)	< 180 (P3)	Pass
HF	190 (P2)	<180 (P3)	Fail

Phase	Result	Requirement	Checks
PDR	170 (P1)	< 180 (P2)	Pass
CDR	170 (P1)	<150 (P3)	Fail

Implementation Details

Driving Criteria for SPDM tool selection

- SPDM Core Features
- Application integration for Desktop / Remote / HPC execution
- Readiness for Parameter Management
- Flexibility and Open for configuration

Implementation Details

Consuming Parameters / Files from SPDM

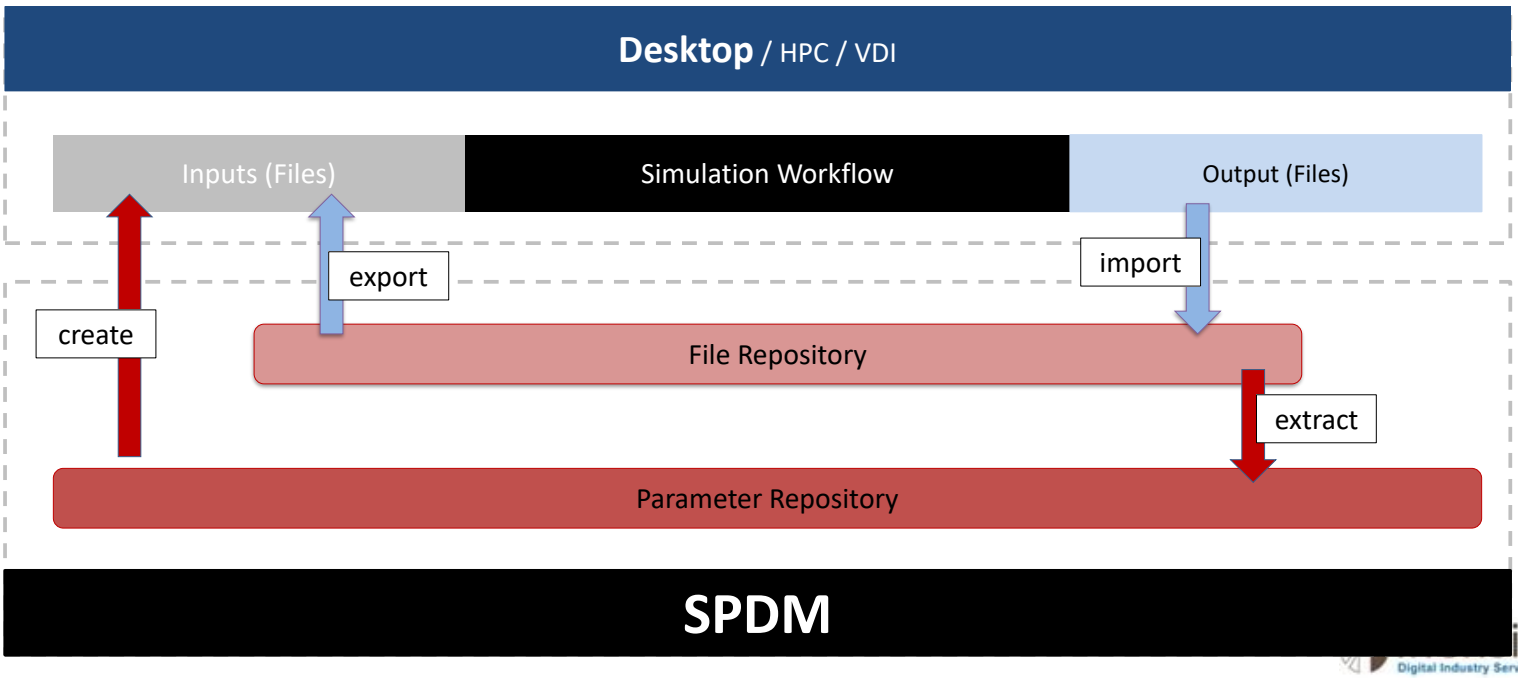

NAFEMS DACH Konferenz 2024: Konferenz für Berechnung & Simulation im Engineering, 10. – 12. Juni 2024, Bamberg, D

Implementation Details

Organizing and Creating Parameters

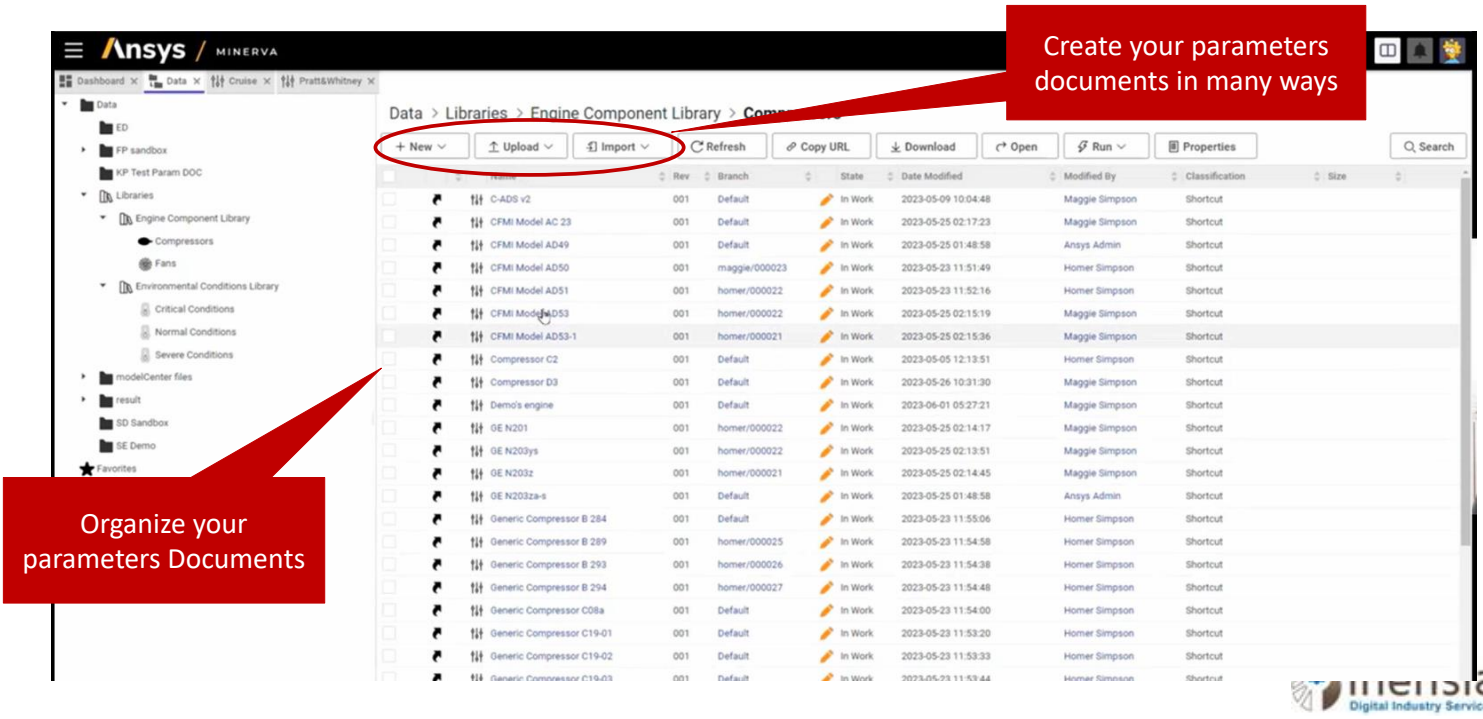

Implementation Details

Updating and revisioning Parameters

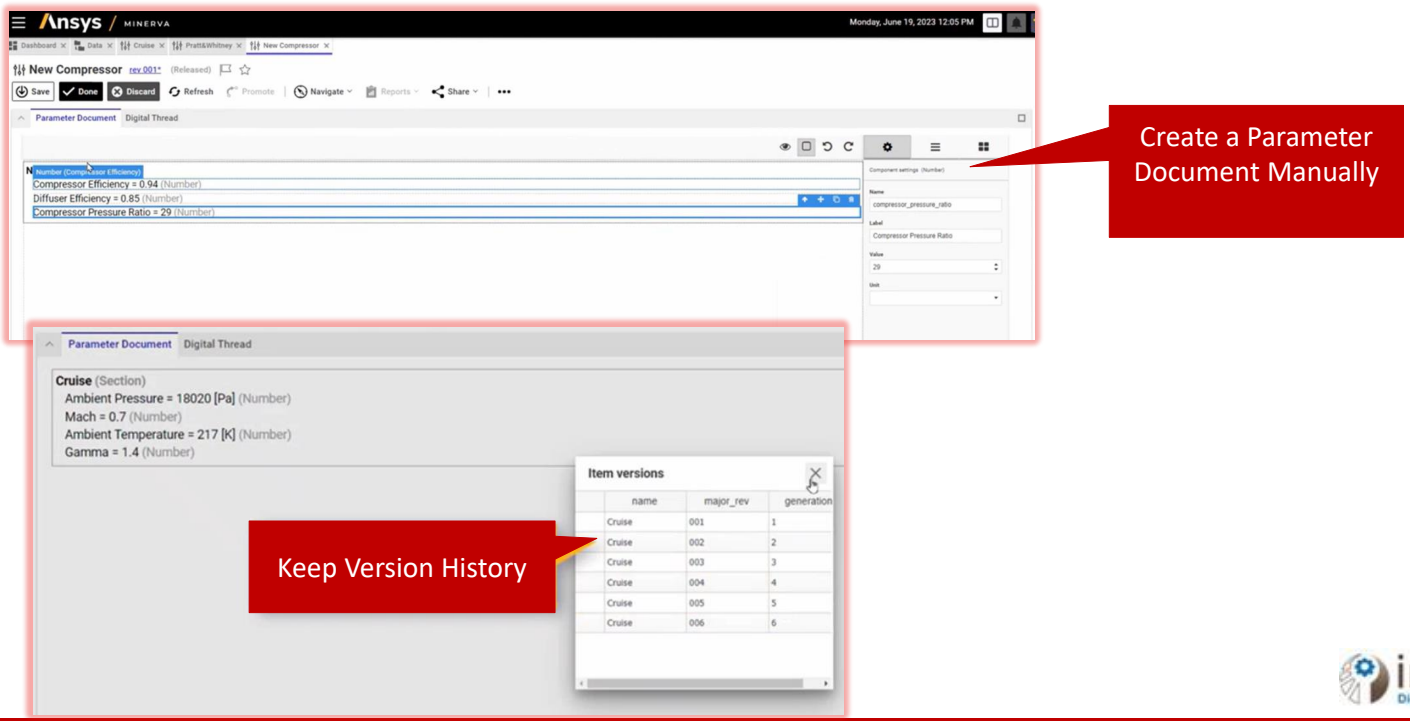

Implementation Details

Using Parameters in Applications

- Launch you application on HPC or Locally, consuming parametesr and files from your SPDM

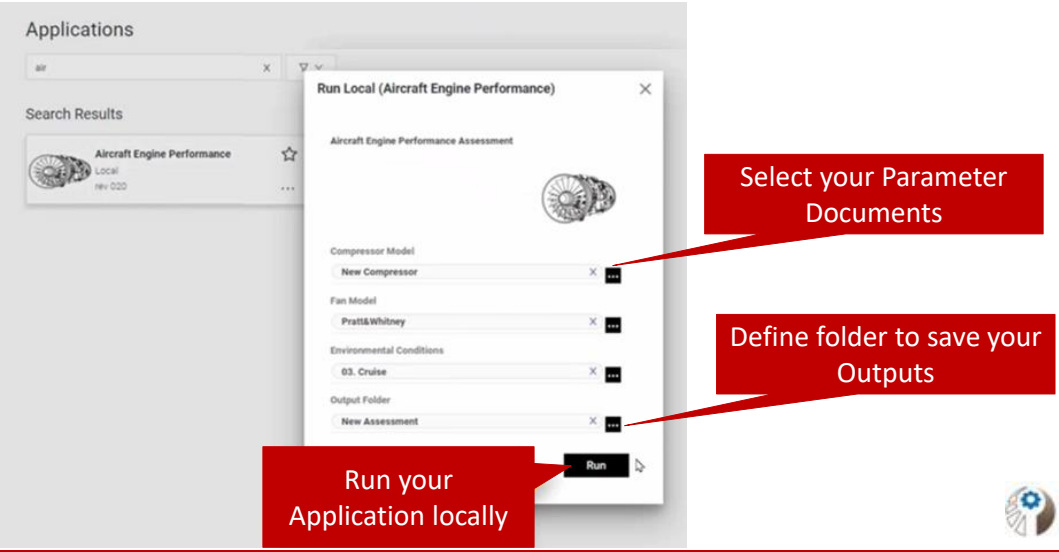

Implementation Details

Parameter Dependencies

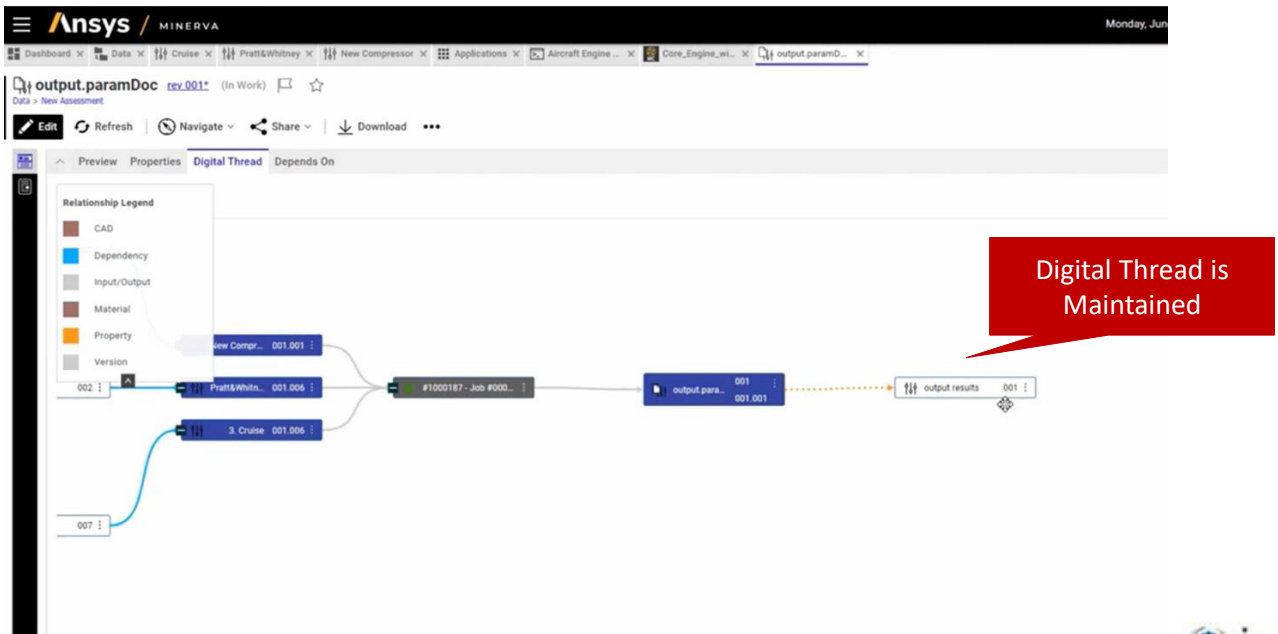

Implementation Details

Verification Plan

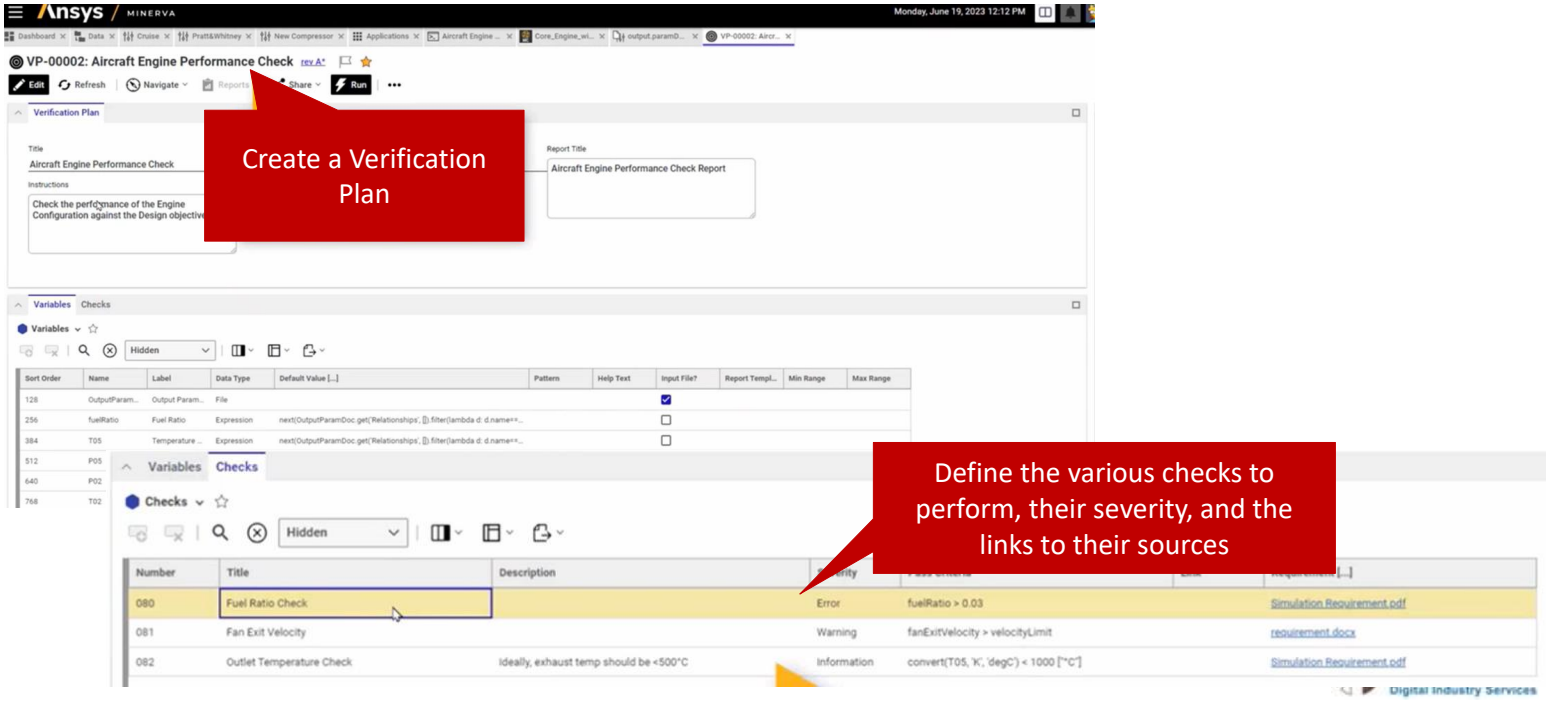

Implementation Details

Verification Report

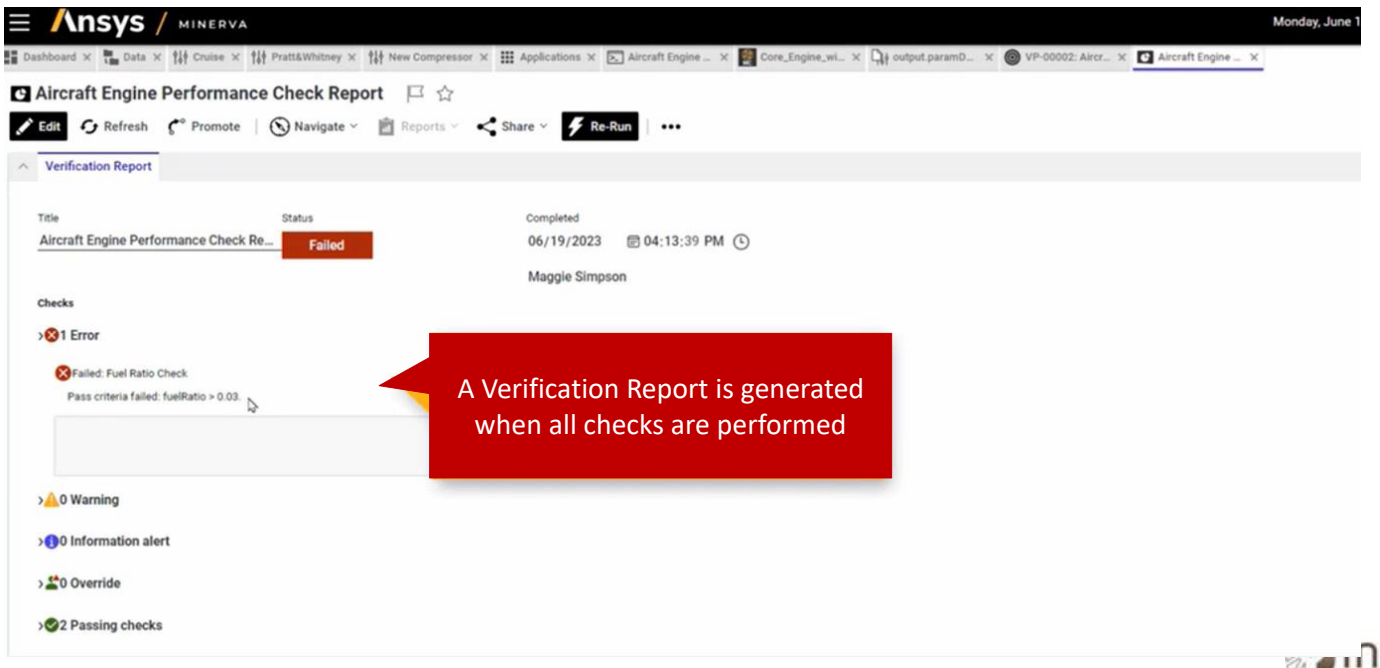

Conclusion & Outlook

Achievements

- Utilization of SPDM to have all relevant simulation data in a single source of truth
- Extracting information from the file content and store them as individual parameters
- Parameters documents approach, simplifies the organization & classification of parameters
- Managing parameters from inputs and results enable connecting simulation product specification and requirements

Future Activities

- Import of Parameters from SPDM external sources
- Refinement of dependency tracking across multiple sources of information
- Enriching parameter dependencies, e. g. by considering correlation and sensitivity information

Managing Key Parameters in SPDM

Fatouma Doucouré
fatouma.doucoure@inensia.com
Leonel Garategaray
leonel.garategaray@inensia.com
Hernan Giagnorio
hernan.giagnorio@inensia.com

NAFEMS DACH Konferenz 2024: Konferenz für Berechnung & Simulation im Engineering, 10. – 12. Juni 2024, Bamberg, D

Unlocking the Potential of Simulation Results inside SPDM: "Smart Simulation Results Management" within SPDM

Prasad Mandava

(Visual Collaboration Technologies Inc.)

Introduction
The manufacturing industry is undergoing a paradigm shift from traditional physical testing to Digital Testing, driven by the need for faster product development cycles, reduced costs, and improved product quality. This transformation necessitates the adoption of innovative tools and methodologies, such as Simulation Process and Data Management (SPDM) and Rapid Results Review (RRR), to effectively manage and leverage the wealth of simulation data generated throughout the product development lifecycle.

The Critical Role of SPDM in the Digital Testing Era
SPDM serves as the central repository for simulation data, processes, and best practices, enabling engineers and stakeholders to efficiently access, analyze, and utilize simulation data. By providing a structured framework for data management, SPDM enhances collaboration, ensures traceability, and streamlines workflows, ultimately leading to better-informed design decisions and accelerated innovation.

Rapid Results Review (RRR): A Game-Changer for SPDM
The integration of RRR solutions within the SPDM framework marks a significant advancement in simulation data management. RRR empowers users with intuitive, web-based 3D visualization and interaction capabilities, allowing for in-depth analysis and collaborative review of simulation results. "Rapid Results Review" provides the ability to quickly extract and visualize analysis results from a broad range of multi-physics solvers, skipping the time-consuming manual post-processing process as we know it today.

RRR allows engineers to go directly from analysis to design decision through high fidelity & efficient multi-format graphic displays to be used for design review meetings, also allowing ease of sharing graphical results data with the engineering teams.

This interactive approach fosters a deeper understanding of complex simulation behaviors, facilitates knowledge sharing across teams, and expedites decision-making processes. Furthermore, RRR's intelligent data extraction capabilities significantly reduce the size of simulation result files without compromising data integrity. This not only optimizes storage and resource utilization but also enables seamless sharing and long-term archiving of simulation insights within SPDM.

Transforming Simulation Data into Actionable Simulation Insights
Rapid Results Review systems offer a comprehensive suite of tools for smart post-processing, seamless integration of multi-physics data, automated CAE reporting, and generation of rapid results reviews. By leveraging these advanced capabilities, engineers can transcend the limitations of traditional, manual post-processing and reporting methods. RRR enables the extraction of meaningful insights from complex multi-physics simulation datasets, the identification of trends, and ultimately, the ability to make data-driven design decisions.
A key innovation of RRR is the generation of high-fidelity Digital Slides, which serve as fundamental building blocks for the Digital Thread. These Digital Slides preserve simulation information in its most accurate form, eliminating inefficiencies associated with reviewing low-fidelity representations. By

bridging the gap between simulation and real-world outcomes, RRR empowers organizations to mitigate risks, optimize designs, and deliver superior products to market.

Real-World Applications and Case Studies
The integration of RRR solutions into leading SPDM platforms has proven instrumental in addressing critical challenges faced by engineering enterprises. VCollab's RRR is being adapted by many manufacturing companies to cut development time because of the vast process efficiency it brings. Case studies from various industries demonstrate how RRR empowers organizations to streamline workflows, improve collaboration, reduce time-to-market, and enhance product performance. These real-world examples underscore the tangible benefits of integrating RRR into the SPDM ecosystem.

The Future of Simulation Data Management
As the manufacturing industry continues to embrace Digital Testing, the role of SPDM and RRR will become increasingly vital. The ongoing development of advanced visualization techniques, artificial intelligence, and machine learning algorithms promises to further enhance the capabilities of RRR systems, enabling engineers to unlock even deeper insights from simulation data and drive innovation to new heights.

Conclusion
The convergence of SPDM and Rapid Results Review technologies represents a paradigm shift in simulation data management. By leveraging the power of RRR within the SPDM framework, engineering enterprises can transform raw simulation data into actionable insights, accelerate product development cycles, improve collaboration, and ultimately gain a competitive edge in the rapidly evolving landscape of modern manufacturing.

Unlocking the Potential of Simulation Results inside SPDM

Prasad Mandava
Founder and CEO
VCollab

Historic Turning Point in Simulation

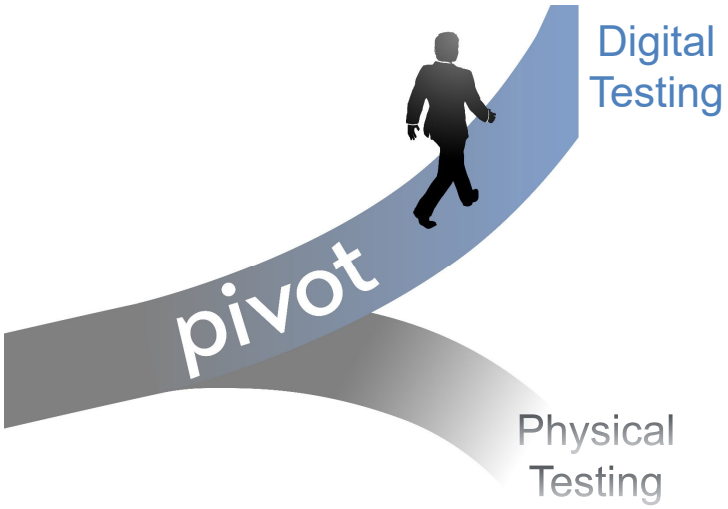

NAFEMS DACH Konferenz 2024: Konferenz für Berechnung & Simulation im Engineering, 10. – 12. Juni 2024, Bamberg, D

As Companies Move Away from Expensive, Time-Consuming Physical Testing

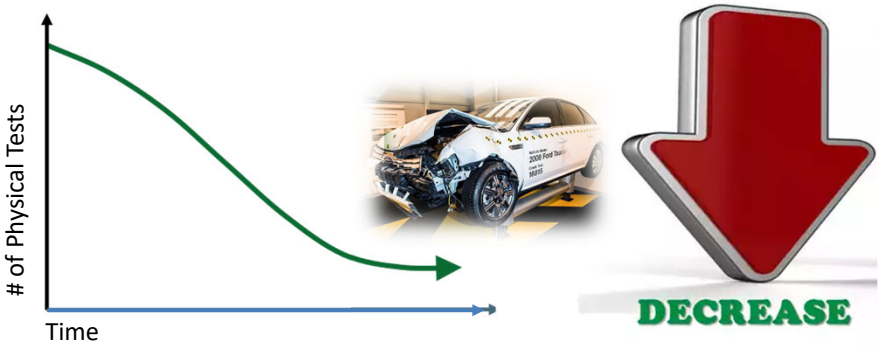

Simulation Becomes the Key Critical Path Item for Design Confidence

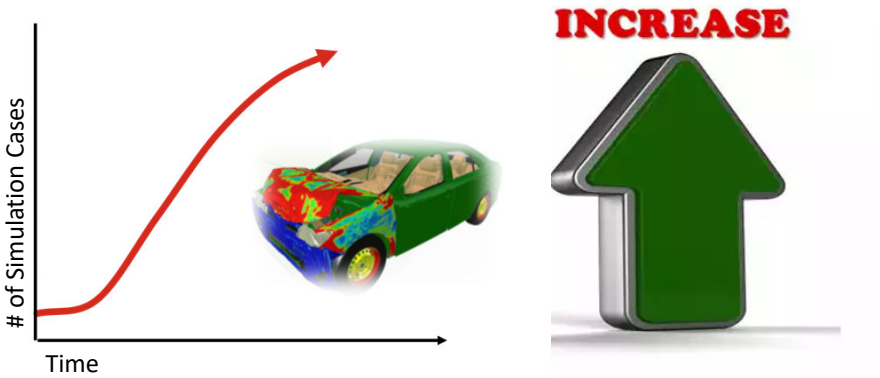

The Shift Towards Simulation

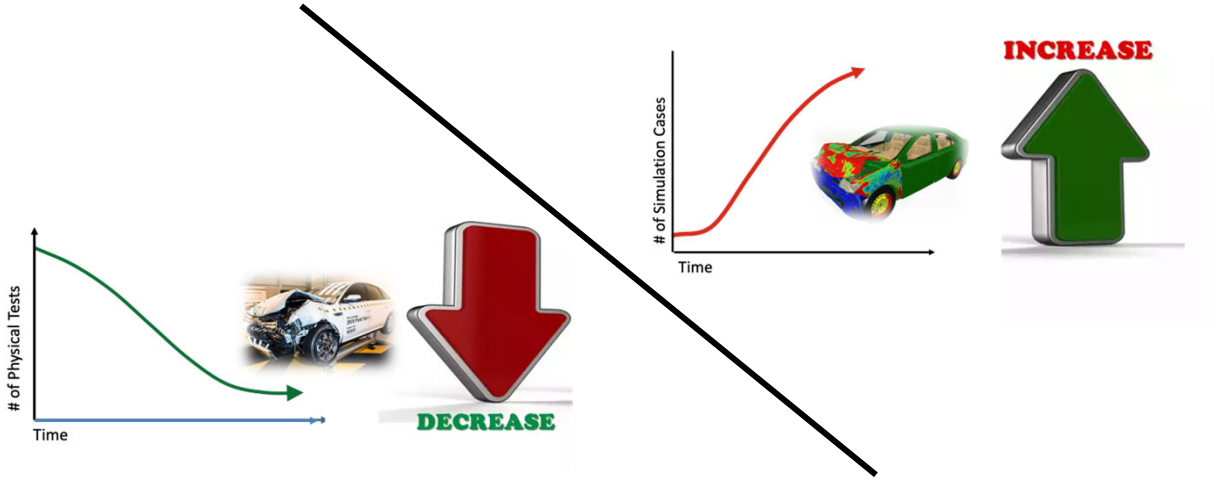

The Auto Industry Strategy

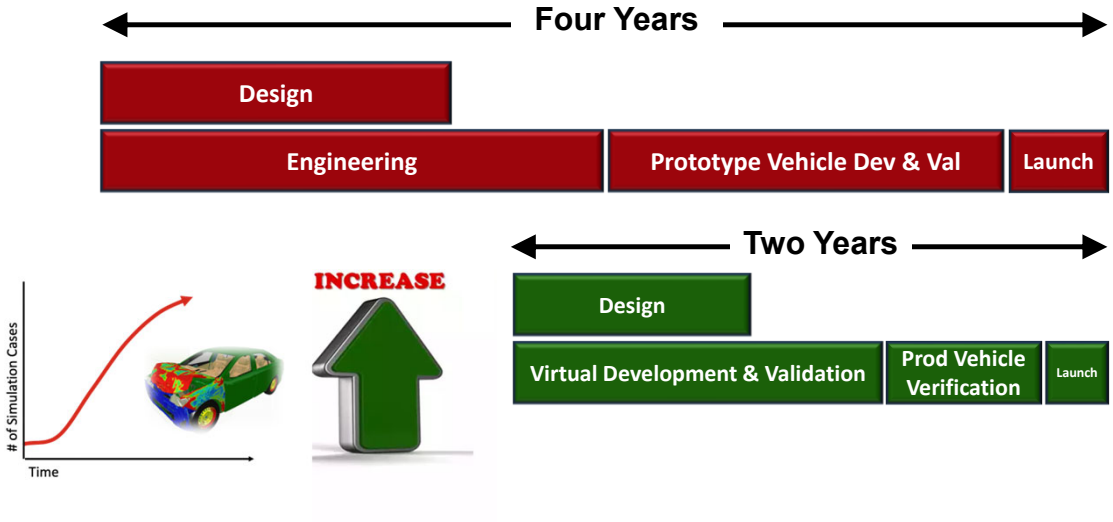

Implications of These Trends

- No Physical Testing = Lot more simulation studies to provide the engineering insight previously provided by physical testing. **Need for more results reviews exploded exponentially.**
- Find ways to reduce the risk of "No Physical Testing".

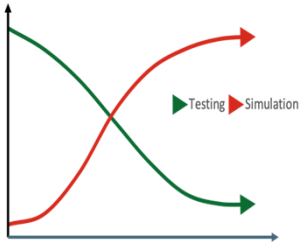

- Current simulation **processes have to be more efficient** to meet the volume and timing needed to support accelerated development times.
- Additional resources and **new class of tools & training** to meet this increased volume of required studies are not available.
- **Using old processes = Missed or skipped gates** in order to meet timeline.
- **Bypassing critical steps in product development** may result in:
  - **The late and expensive discovery of problems**
  - **Product warranty issues**
  - **Recalls**

Extremely High Stress on the CAE Teams

What we hear from smart customers:

Simulation Automation…*Maximizing Process Efficiencies*

- Reduction / Elimination of CAE model preparation (Pre-processing)
  - Use of auto meshing/no mesh technologies – FEA, CFD, …
- **Elimination of time consuming and inefficient manual Post-processing & reporting process.**
- **Improving results review process.**
  - Full implementation of interactive graphical visualization software for **"Rapid Results Review"**
    - ✓ **Critical for driving immediate actions in Design Review meetings**
    - ✓ **Quick and efficient for sharing digital results with engineering teams**
    - ✓ **Automated Report Archiving**
- **Democratization of CAE** tools/methods/**results** for broad application among all engineers

New Class of Tools Required

REF: "Digital Transformation of the Vehicle Design Cycle"
Mario J. Felice

New Tools

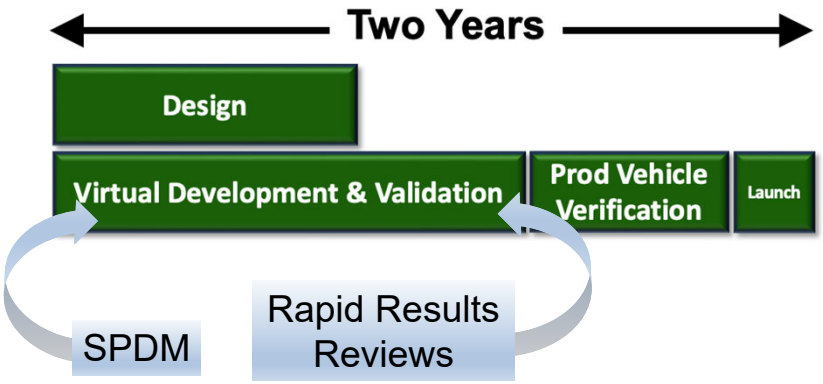

Simulation Process & Data Mgmt.

Management, analysis, and application of simulation data throughout the product development lifecycle

The Case for SPDM

SPDM Benefits

- Increase Analyst Capacity
- Increase number of simulations
- Automate simulation processes
- Manage simulation results
- Institutionalize simulation methods

SPDM Challenges

- Different users with different requirements
- Multiple, multidisciplinary CAE applications
- Storing & Sharing Simulation Results
- Interpreting complex results data
- Visualization of results
- Difficult deployment

While Many Solutions have Automated Model Preparation, None have Focused on Results

- Model Preparation
- Post Processing
- Presenting & Reviewing Results
- Reporting
- Results Sharing with stake holders

While Many Solutions have Automated Model Preparation, None have Focused on Results to Design Decision workflow

- Model Preparation
- Post Processing
- Presenting
- Reviewing and Reporting
- Results Sharing

Where decision-making occurs

RRR Address this Critical Need For Rapid, Accurate Decision-making

- Model Preparation
- Post Processing
- Presenting & Reviewing
- Reporting
- Results Sharing

Rapid Results Review Solution

RRR Increases the Value of SPDM

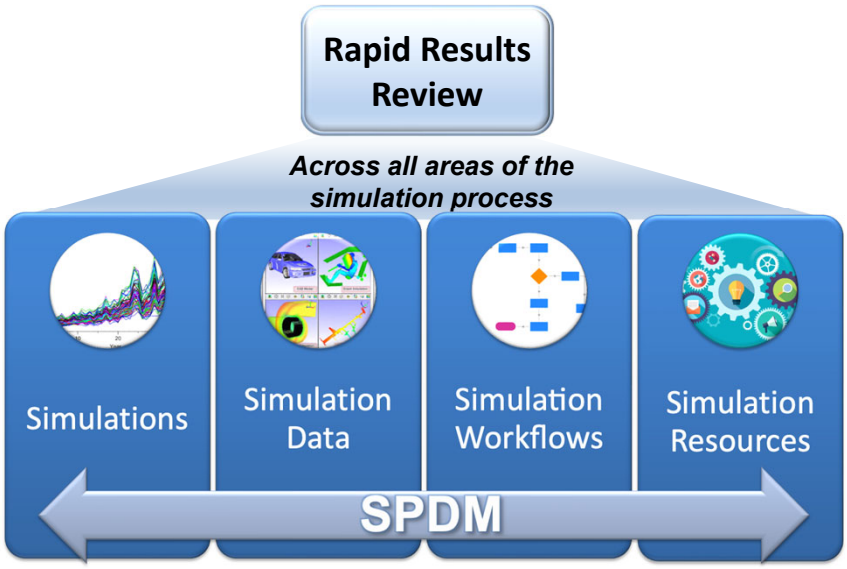

RRR Increases the Value of SPDM

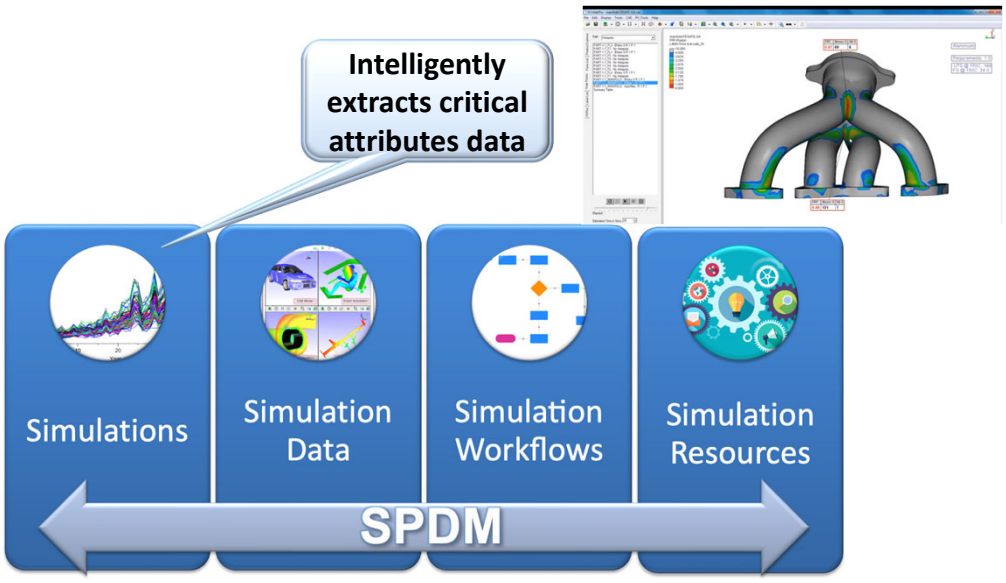

NAFEMS DACH Konferenz 2024: Konferenz für Berechnung & Simulation im Engineering, 10. – 12. Juni 2024, Bamberg, D

RRR Increases the Value of SPDM

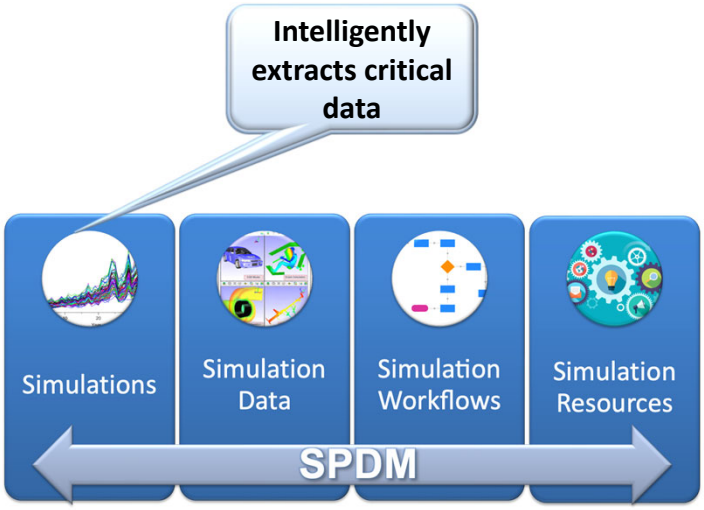

RRR Increases the Value of SPDM

[Durability Digital Slide]

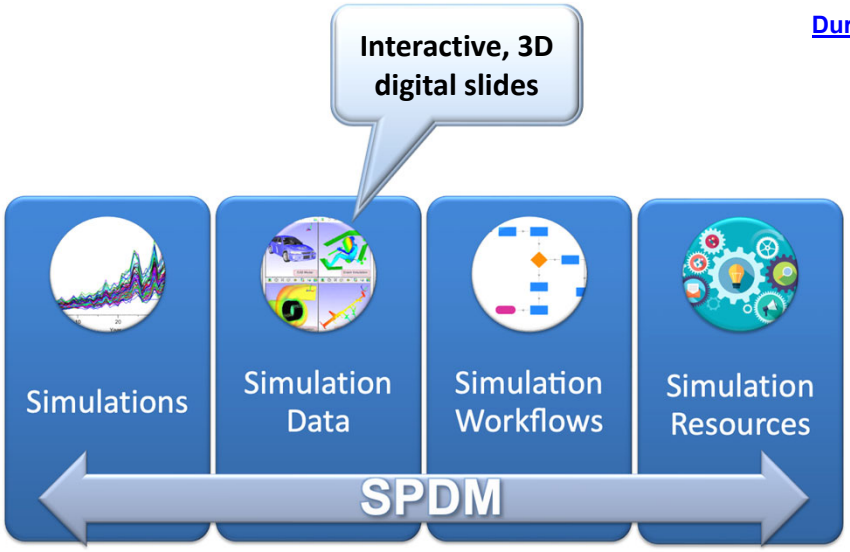

NAFEMS DACH Konferenz 2024: Konferenz für Berechnung & Simulation im Engineering, 10. – 12. Juni 2024, Bamberg, D

RRR Increases the Value of SPDM

Mode Shape Digital Slide

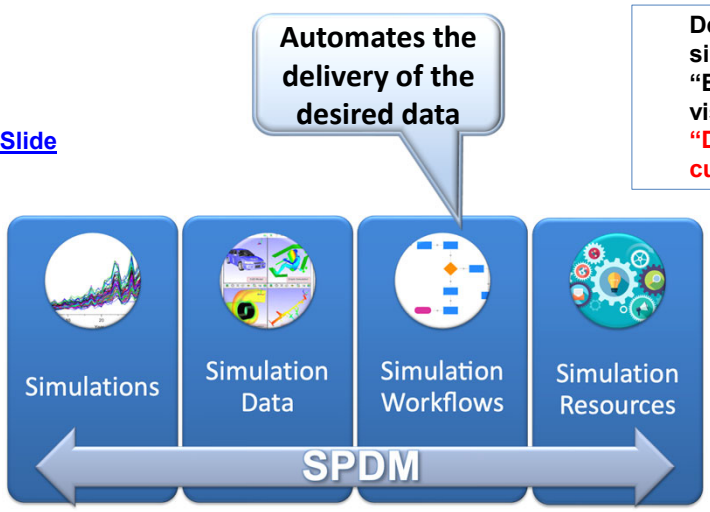

Democratize the simulation results with "Browser-based 3D visualization" : Share "Digital Slides" with customers

There are no plug-ins to be installed.

RRR Increases the Value of SPDM

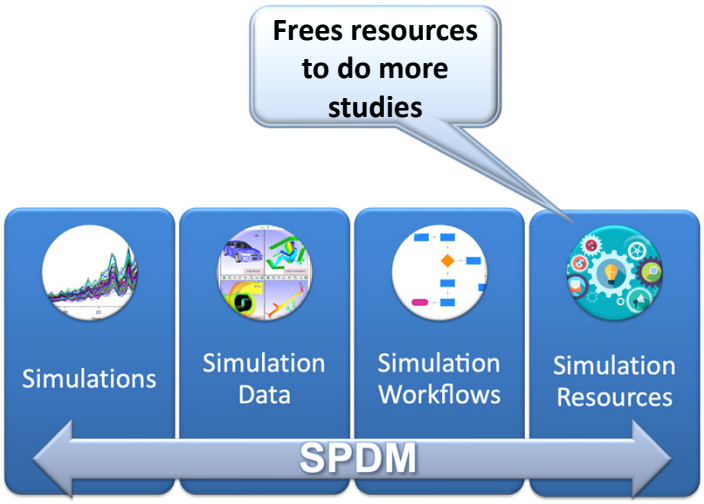

NAFEMS DACH Konferenz 2024: Konferenz für Berechnung & Simulation im Engineering, 10. – 12. Juni 2024, Bamberg, D

A Few Rapid Results Review Capabilities

- Advanced Capabilities for:
  - Multi-physics data integration
  - Solver independent format to store key multi physics attributes
  - Smart Results processing
  - Digital CAE Slides/Reporting
  - Rapid Results Reviews
  - Web-based results visualization
  - Simulation data analytics

Value of "Rapid Results Review" Solution

- **Streamlines the "results to the design decision" process**.
  - **Efficiency - Dramatically reduced time for post processing and report/information creation.**
  - **Reduces CAE analyst stress by eliminating the boring processes while still allowing him to post process Digital Slides and to manage the final outcome/reporting.**
  - **Eliminate human errors & never miss a hotspot.**
  - **Facilitate Analysis Reviews among global CAE teams : Rich 3D visualization in the Digital Slides to Rapidly Review Results & gain faster and greater understanding of simulation results.**
  - **Improved Visual Collaboration: Extend the visibility of CAE data to the Design Stakeholders of the enterprise**
  - **Faster delivery of simulation results/information to meet accelerated development schedules.**

=

More simulations studies with the available resources and within the stipulated time

NAFEMS DACH Konferenz 2024: Konferenz für Berechnung & Simulation im Engineering, 10. – 12. Juni 2024, Bamberg, D

SPDM + “Rapid Results Review” Integration

From CAD to 3D Digital Decisions

NAFEMS DACH Konferenz 2024: Konferenz für Berechnung & Simulation im Engineering, 10. – 12. Juni 2024, Bamberg, D

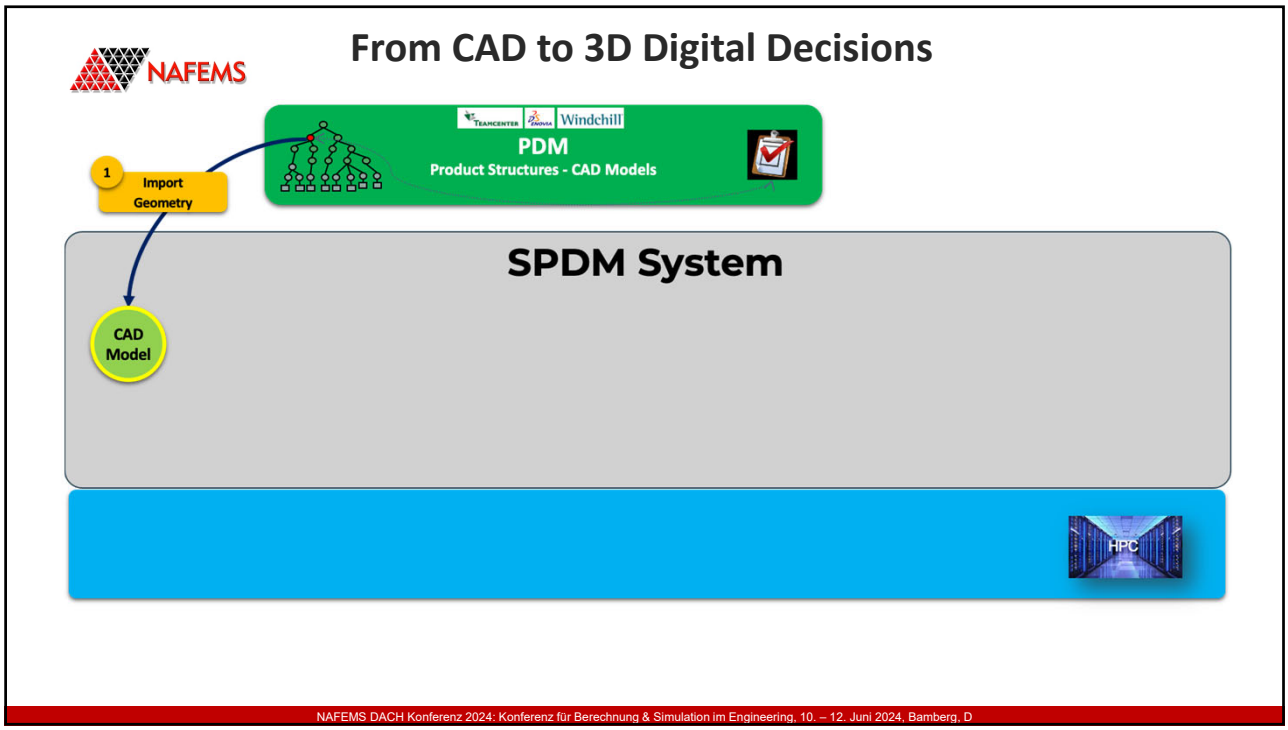
From CAD to 3D Digital Decisions
NAFEMS
Windchill
PDM
Product Structures - CAD Models
1
Import Geometry
SPDM System
CAD Model
HPC

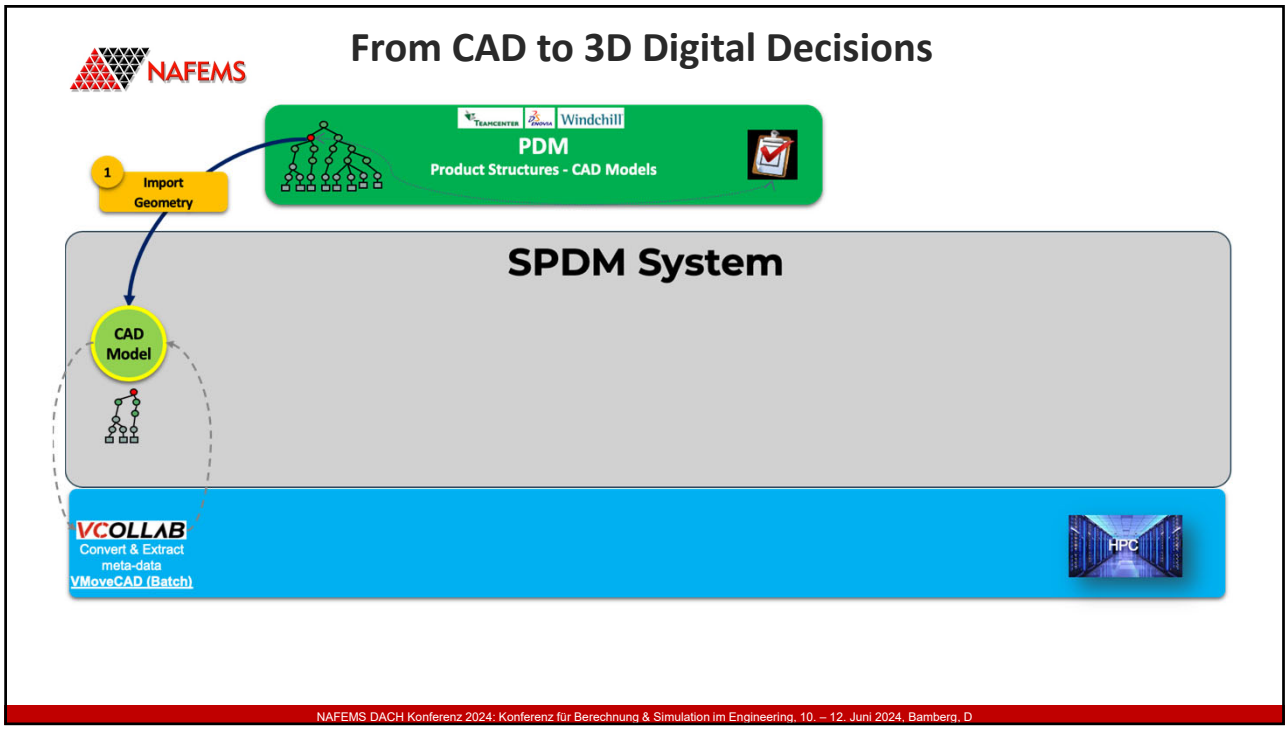
From CAD to 3D Digital Decisions
NAFEMS
Windchill
PDM
Product Structures - CAD Models
1
Import Geometry
SPDM System
CAD Model
VCOLLAB
Convert & Extract meta-data
VMoveCAD (Batch)
HPC

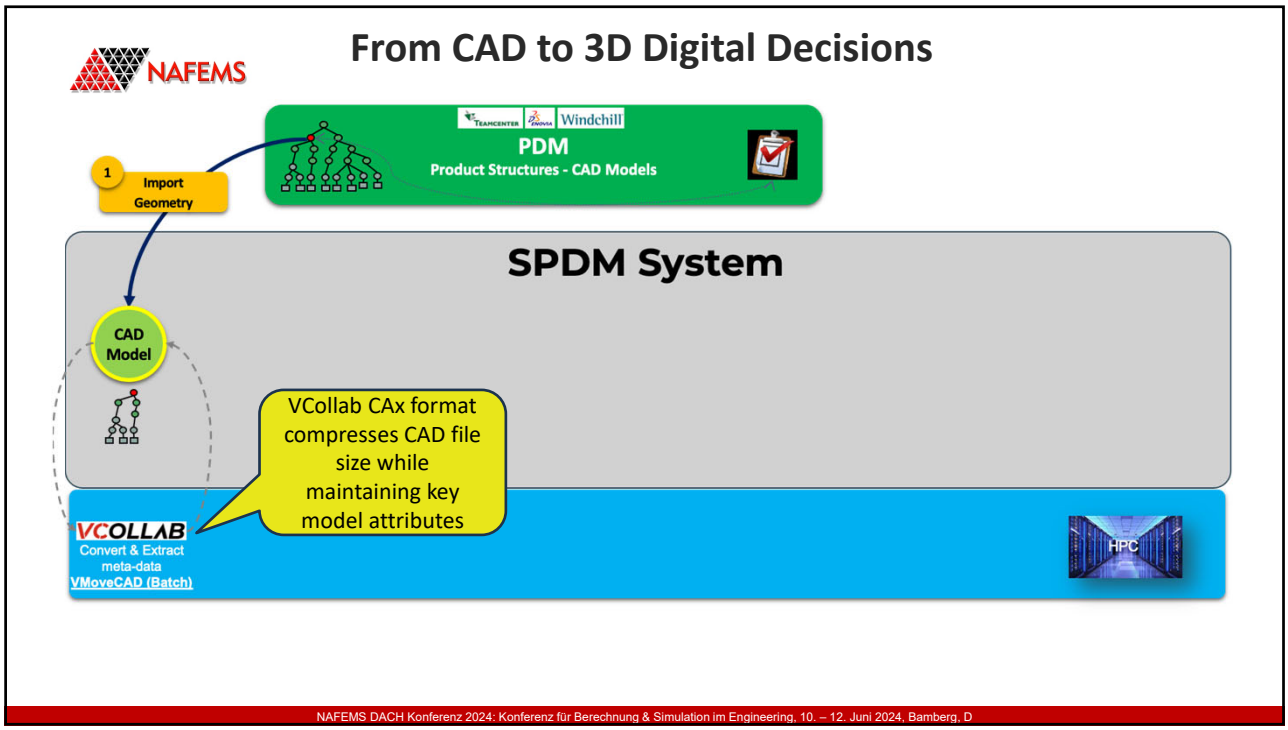
From CAD to 3D Digital Decisions
NAFEMS
Windchill
PDM
Product Structures - CAD Models
1
Import Geometry
SPDM System
CAD Model
VCollab CAx format compresses CAD file size while maintaining key model attributes
VCOLLAB
Convert & Extract meta-data
VMoveCAD (Batch)
HPC
NAFEMS DACH Konferenz 2024: Konferenz für Berechnung & Simulation im Engineering, 10. – 12. Juni 2024, Bamberg, D

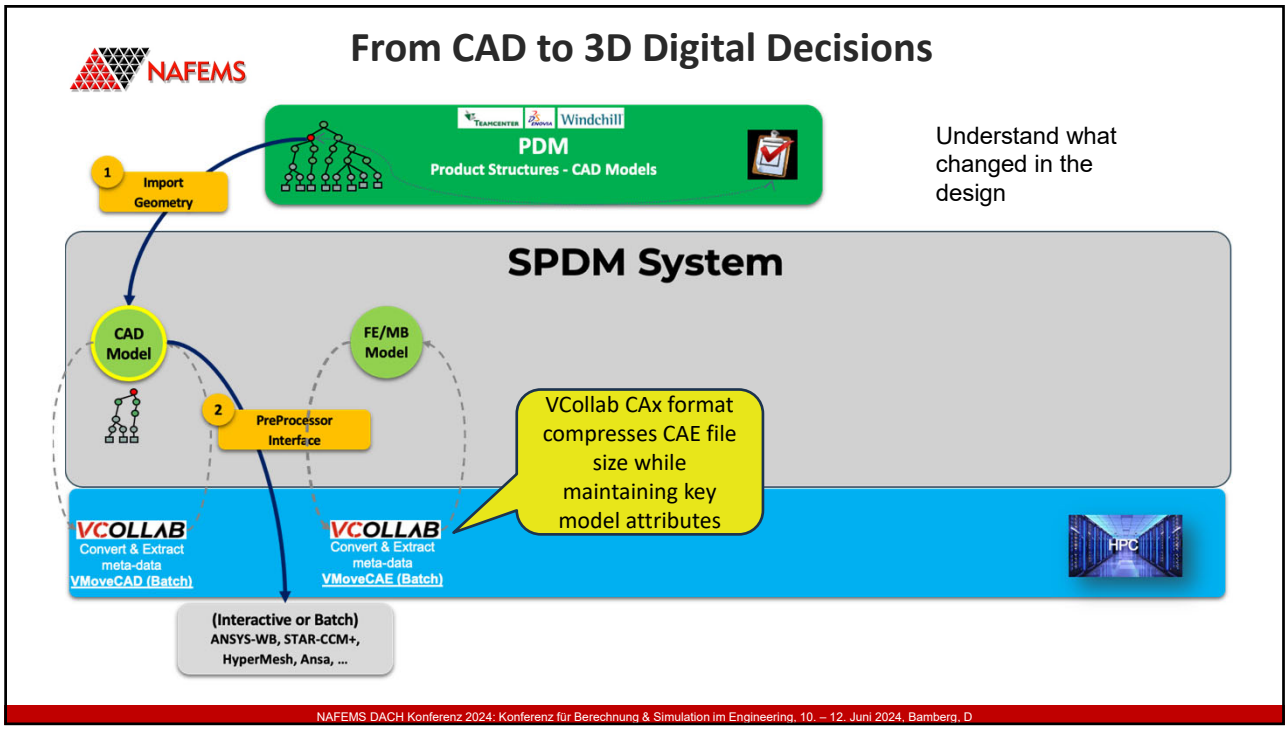
From CAD to 3D Digital Decisions
NAFEMS
Windchill
PDM
Product Structures - CAD Models
1
Import Geometry
Understand what changed in the design
SPDM System
CAD Model
FE/MB Model
2
PreProcessor Interface
VCollab CAx format compresses CAE file size while maintaining key model attributes
VCOLLAB
Convert & Extract meta-data
VMoveCAD (Batch)
VCOLLAB
Convert & Extract meta-data
VMoveCAE (Batch)
HPC
(Interactive or Batch)
ANSYS-WB, STAR-CCM+, HyperMesh, Ansa, ...
NAFEMS DACH Konferenz 2024: Konferenz für Berechnung & Simulation im Engineering, 10. – 12. Juni 2024, Bamberg, D

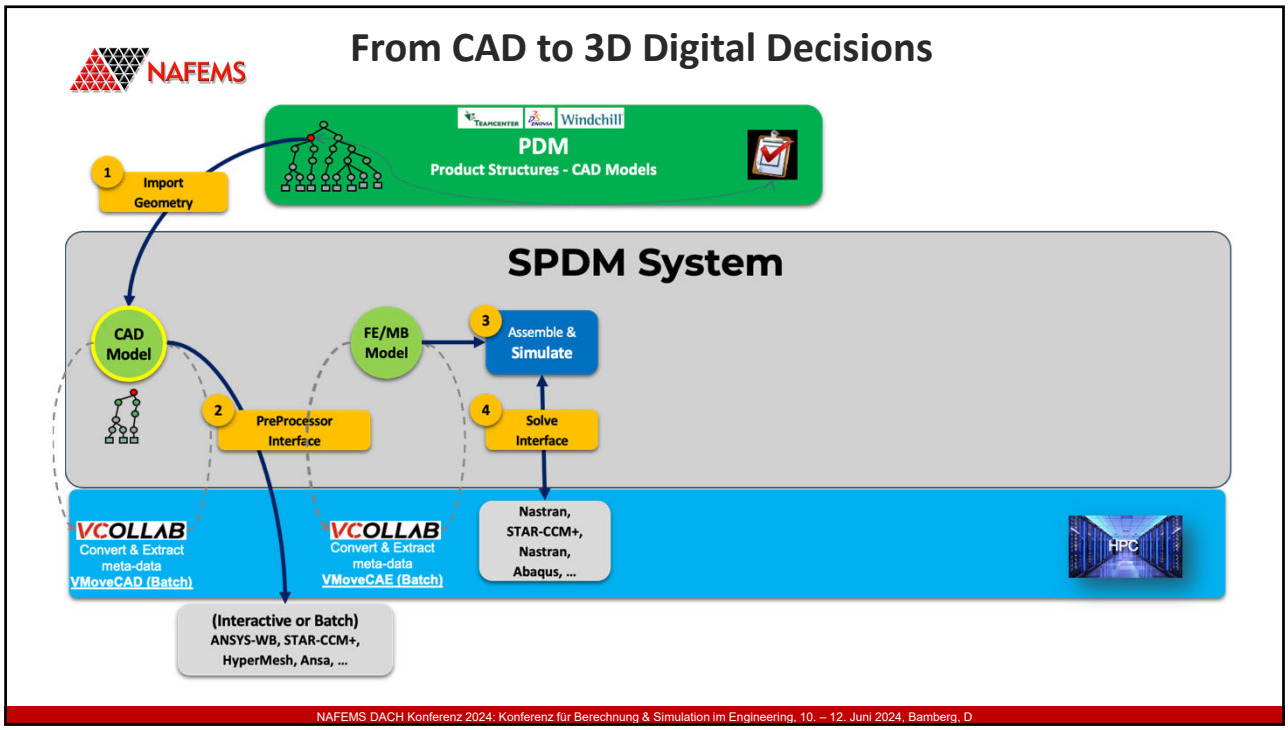
From CAD to 3D Digital Decisions
NAFEMS
Windchill
PDM
Product Structures - CAD Models
1
Import Geometry
SPDM System
CAD Model
FE/MB Model
3
Assemble & Simulate
2
PreProcessor Interface
4
Solve Interface
VCOLLAB
Convert & Extract meta-data
VMoveCAD (Batch)
VCOLLAB
Convert & Extract meta-data
VMoveCAE (Batch)
Nastran, STAR-CCM+, Nastran, Abaqus, ...
HPC
(Interactive or Batch)
ANSYS-WB, STAR-CCM+, HyperMesh, Ansa, ...
NAFEMS DACH Konferenz 2024: Konferenz für Berechnung & Simulation im Engineering, 10. – 12. Juni 2024, Bamberg, D

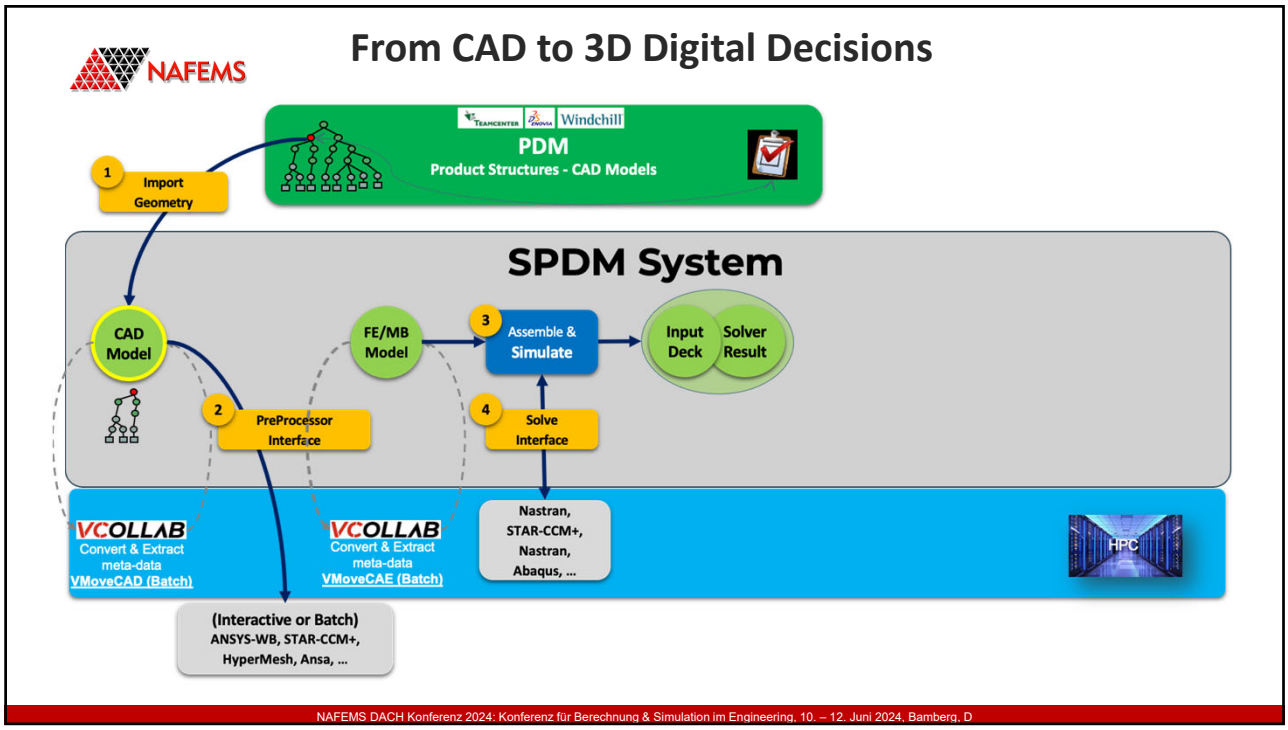
From CAD to 3D Digital Decisions
NAFEMS
Windchill
PDM
Product Structures - CAD Models
1
Import Geometry
SPDM System
CAD Model
FE/MB Model
3
Assemble & Simulate
Input Deck
Solver Result
2
PreProcessor Interface
4
Solve Interface
VCOLLAB
Convert & Extract meta-data
VMoveCAD (Batch)
VCOLLAB
Convert & Extract meta-data
VMoveCAE (Batch)
Nastran, STAR-CCM+, Nastran, Abaqus, ...
HPC
(Interactive or Batch)
ANSYS-WB, STAR-CCM+, HyperMesh, Ansa, ...
NAFEMS DACH Konferenz 2024: Konferenz für Berechnung & Simulation im Engineering, 10. – 12. Juni 2024, Bamberg, D

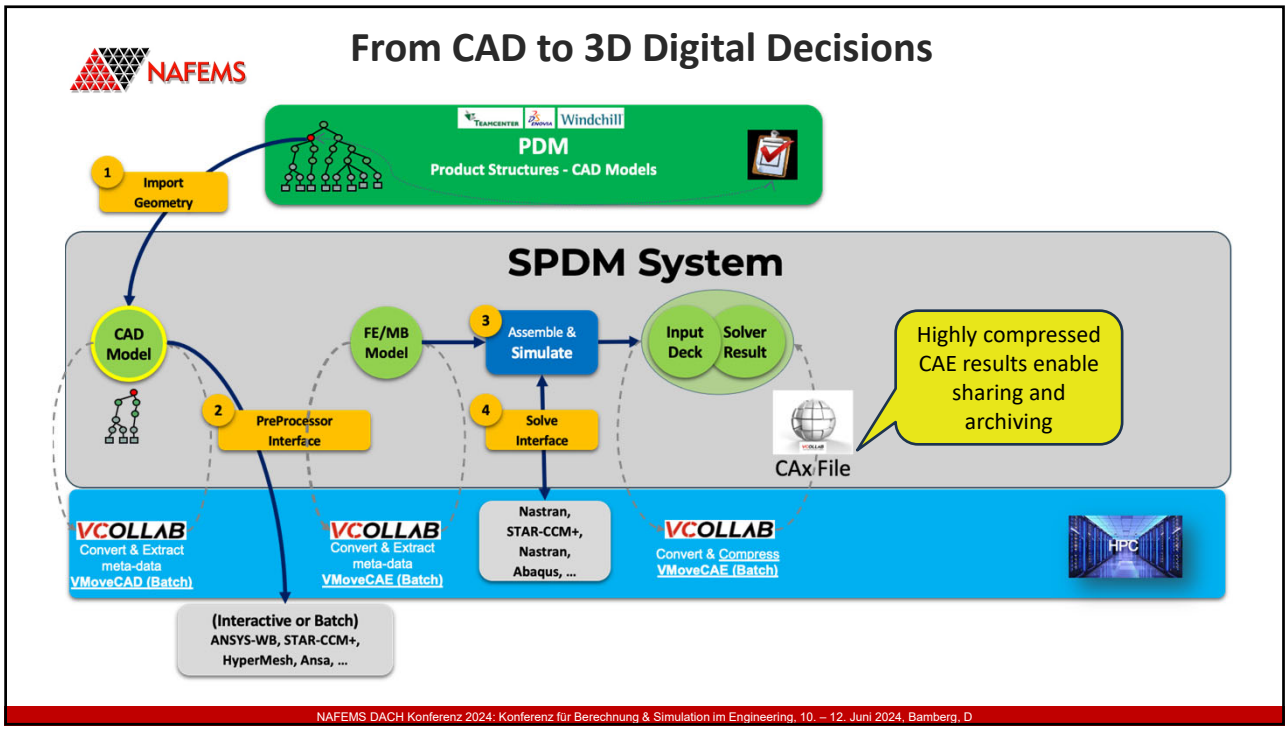
From CAD to 3D Digital Decisions
NAFEMS
Windchill
PDM
Product Structures - CAD Models
1
Import Geometry
SPDM System
CAD Model
FE/MB Model
3
Assemble & Simulate
Input Deck
Solver Result
2
PreProcessor Interface
4
Solve Interface
Highly compressed CAE results enable sharing and archiving
CAx File
VCOLLAB
Convert & Extract meta-data
VMoveCAD (Batch)
VCOLLAB
Convert & Extract meta-data
VMoveCAE (Batch)
Nastran, STAR-CCM+, Nastran, Abaqus, ...
VCOLLAB
Convert & Compress
VMoveCAE (Batch)
HPC
(Interactive or Batch)
ANSYS-WB, STAR-CCM+, HyperMesh, Ansa, ...
NAFEMS DACH Konferenz 2024: Konferenz für Berechnung & Simulation im Engineering, 10. – 12. Juni 2024, Bamberg, D

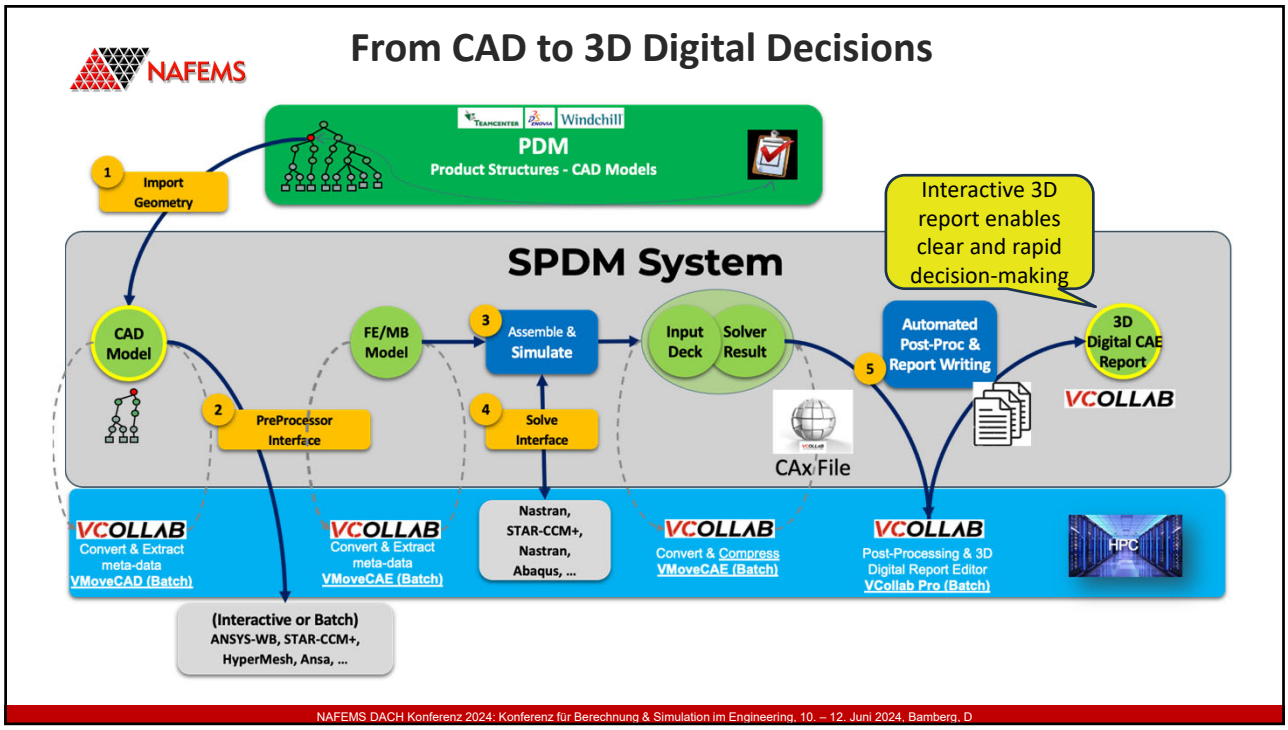
From CAD to 3D Digital Decisions
NAFEMS
Windchill
PDM
Product Structures - CAD Models
1
Import Geometry
Interactive 3D report enables clear and rapid decision-making
SPDM System
CAD Model
FE/MB Model
3
Assemble & Simulate
Input Deck
Solver Result
5
Automated Post-Proc & Report Writing
3D Digital CAE Report
VCOLLAB
2
PreProcessor Interface
4
Solve Interface
CAx File
VCOLLAB
Convert & Extract meta-data
VMoveCAD (Batch)
VCOLLAB
Convert & Extract meta-data
VMoveCAE (Batch)
Nastran, STAR-CCM+, Nastran, Abaqus, ...
VCOLLAB
Convert & Compress
VMoveCAE (Batch)
VCOLLAB
Post-Processing & 3D Digital Report Editor
VCollab Pro (Batch)
HPC
(Interactive or Batch)
ANSYS-WB, STAR-CCM+, HyperMesh, Ansa, ...
NAFEMS DACH Konferenz 2024: Konferenz für Berechnung & Simulation im Engineering, 10. – 12. Juni 2024, Bamberg, D

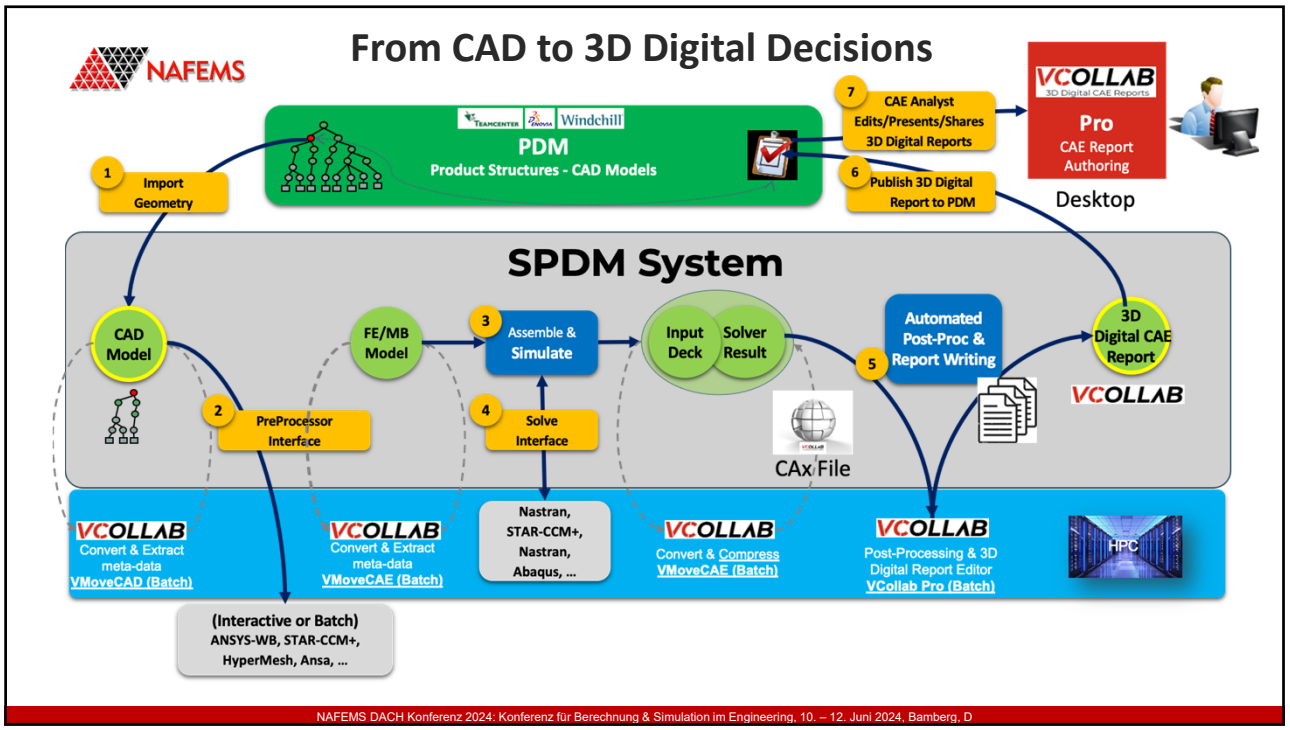
From CAD to 3D Digital Decisions
NAFEMS
PDM
Product Structures - CAD Models
1 Import Geometry
7 CAE Analyst Edits/Presents/Shares 3D Digital Reports
6 Publish 3D Digital Report to PDM
VCOLLAB
3D Digital CAE Reports
Pro
CAE Report Authoring
Desktop
SPDM System
CAD Model
2 PreProcessor Interface
FE/MB Model
3 Assemble & Simulate
4 Solve Interface
Input Deck
Solver Result
5 Automated Post-Proc & Report Writing
3D Digital CAE Report
CAx File
VCOLLAB
Convert & Extract meta-data VMoveCAD (Batch)
VCOLLAB
Convert & Extract meta-data VMoveCAE (Batch)
Nastran, STAR-CCM+, Nastran, Abaqus, ...
VCOLLAB
Convert & Compress VMoveCAE (Batch)
VCOLLAB
Post-Processing & 3D Digital Report Editor VCollab Pro (Batch)
HPC
(Interactive or Batch)
ANSYS-WB, STAR-CCM+, HyperMesh, Ansa, ...
NAFEMS DACH Konferenz 2024: Konferenz für Berechnung & Simulation im Engineering, 10. – 12. Juni 2024, Bamberg, D

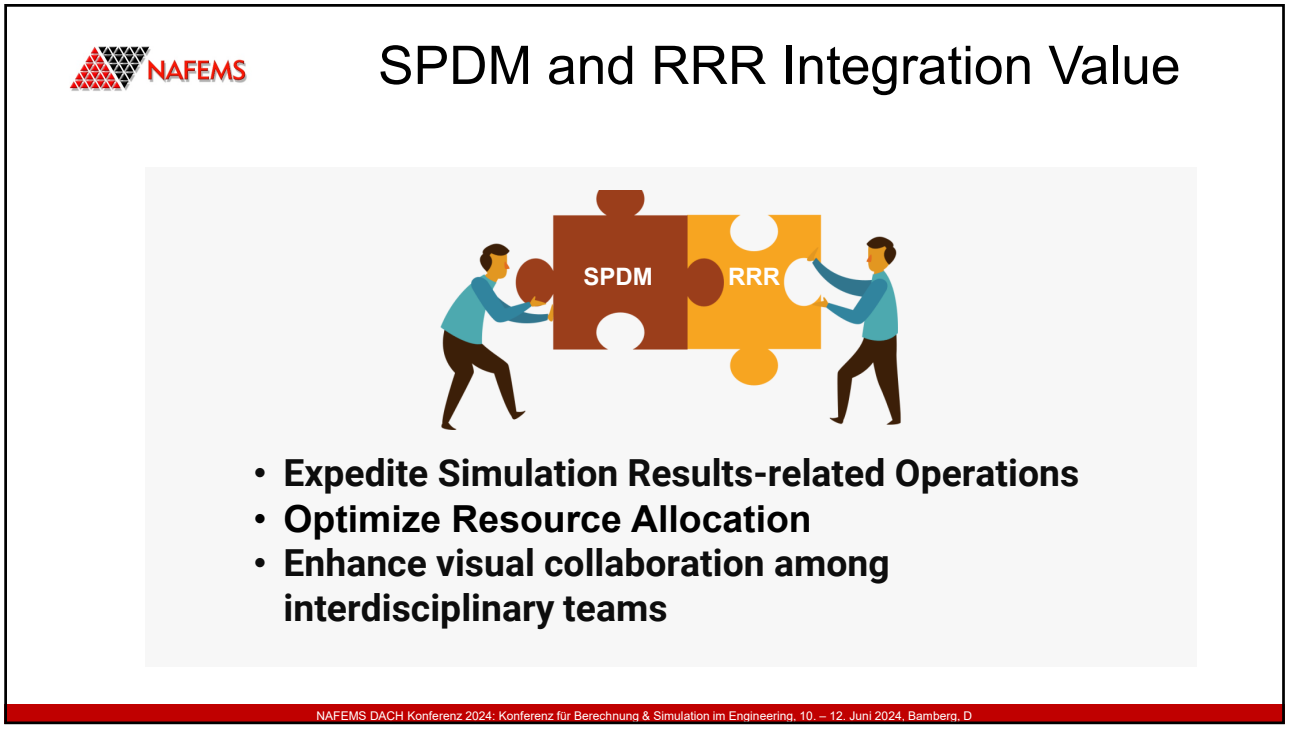
NAFEMS
SPDM and RRR Integration Value
SPDM
RRR
• Expedite Simulation Results-related Operations
• Optimize Resource Allocation
• Enhance visual collaboration among interdisciplinary teams
NAFEMS DACH Konferenz 2024: Konferenz für Berechnung & Simulation im Engineering, 10. – 12. Juni 2024, Bamberg, D

SPDM and RRR Integration Value

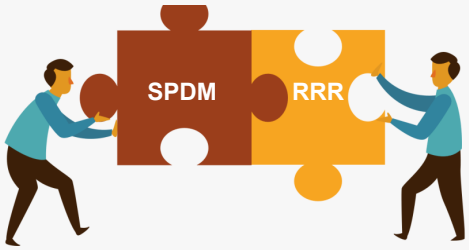

- Expedite Simulation Results-related Operations
- Optimize Resource Allocation
- Enhance Collaboration among interdisciplinary teams

Increased Production and Rapid Product Launches

An Integral Part of an SPDM Strategy

SPDM System

Manages the Simulation Process & Data for Performing Analysis

- Manage simulation Related files
- Search the data
- Manage/automate simulation workflows
- Provides data & process traceability
- BOM Management

VCOLLAB

Automates & Enhances the Process for Interpreting the Analysis Results

- Common format for singular viewing of multi-CAE results
- Automate post-processing and reporting
- 3D digital slides enables presenting, reviewing, sharing and reporting CAE results
- **Faster & Informed Design Decisions**

NAFEMS DACH Konferenz 2024: Konferenz für Berechnung & Simulation im Engineering, 10. – 12. Juni 2024, Bamberg, D

The Impact of “Rapid Results Review” in SPDM

THANKS

prasad@vcollab.com

NAFEMS DACH Konferenz 2024: Konferenz für Berechnung & Simulation im Engineering, 10. – 12. Juni 2024, Bamberg, D

Guard Rails for Simulation Credibility Standards and Recommendation

Hans-Martin Heinkel, Muhammed Atak (Robert Bosch GmbH)

Martin Geissen (Unity)

Virtualization and digitalization are becoming increasingly important in development. This means that decisions and releases will be based much more on simulation results. The prostep SmartSE project has been working for more than 10 years on the necessary building blocks for collaborative development and validation of complex products through simulation.

In this presentation we will start with showing the challenges from using simulation locally to the usage of simulation in cooperation with partners.

In the main part we will give an overview of the, in the in April 2024 from prostep SmartSE, published white paper Guard Rails for Simulation Credibility Standards and Recommendation.

This white paper aims to describe a process framework for embedding numerical engineering simulations in the decision-making process of complex technical products and systems and thus to lay the foundations and guidelines for a Simulation Credibility Standard and Recommendation yet to be created.

This is intended to create a further basis for joint discussions with international standardization bodies and future standardization activities with regards to Simulation Credibility Standards and Recommendation.

NAFEMS DACH CONFERENCE

Guard Rails for “Simulation Credibility Standards and Recommendation”

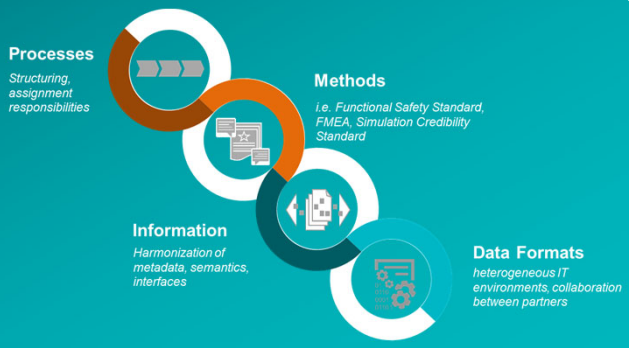

Bamberg 11 June 2024
Hans-Martin Heinkel, Bosch
Muhammed Atak, Bosch
Martin Geissen, Unity

1. Simulation based Cooperation between Partners
2. Prostep ivip SmartSE Project
3. White paper Guard Rails for “Simulation Credibility Standards and Recommendation”.
4. Conclusions – Next steps

Prostep Smart Systems Engineering (SmartSE)
Building Blocks for Simulation based Cooperation between Partners

Metaverse	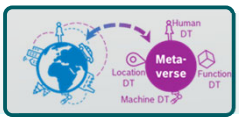	*Floating transition between real and virtual world*
Collaboration Networks	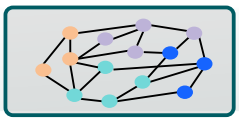	*Heterogeneous changing networks, collaboration models*
Company internal Digitalization, Virtualization	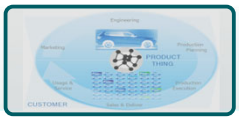	*Continuous use, enrichment of information, knowledge evaluation*
Simulation supported Development	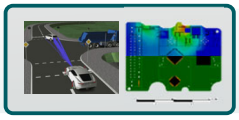	*Alignment with reality, prediction of reality basis for virtualization*
Real Products, Components		*Development of reliable and sustainable components and products*

From Digitalization to Virtualization
From Documentation to Prediction

What does virtualization mean
- We make prediction, statements about properties, behavior based on simulation, models and their parameterization.
- These statements can have far-reaching consequences
- We must be able to trust them

Prostep Smart Systems Engineering (SmartSE)
Building Blocks for Simulation based Cooperation between Partners

Metaverse	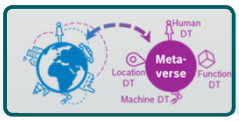	*Floating transition between real and virtual world*
Collaboration Networks	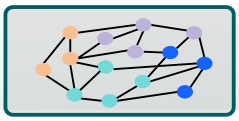	*Heterogeneous changing networks, collaboration models*
Company internal Digitalization, Virtualization	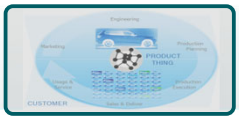	*Continuous use, enrichment of information, knowledge evaluation*
Simulation supported Development	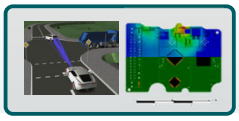	*Alignment with reality, prediction of reality basis for virtualization*
Real Products, Components		*Development of reliable and sustainable components and products*

Strong involvement, interaction with users (people)

Availability of Information in heterogeneous IT environments,

Traceability, Simulation Credibility

Verification Validation of Models, Parameters, Simulation

Reduced number of real prototypes

We need Building blocks to support these challenges

Prostep Smart Systems Engineering (SmartSE)

Building Blocks for Simulation based Cooperation between Partners

Metaverse	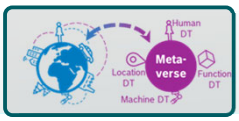	*Floating transition between real and virtual world*
Collaboration Networks	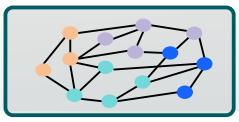	*Heterogeneous changing networks, collaboration models*
Company internal Digitalization, Virtualization	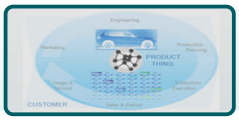	*Continuous use, enrichment of information, knowledge evaluation*
Simulation supported Development	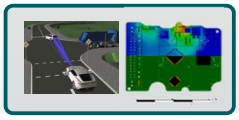	*Alignment with reality, prediction of reality basis for virtualization*
Real Products, Components		*Development of reliable and sustainable components and products*

Not possible — **Prerequisite**

Feedback, recursions with human experts decreasing

Automatization of workflows processes increasing

Fast, efficient but limited to human resources, experts

Efficiency, quality

We need the experts for establish and maintain the automatization (Expert knowledge within workflows)

Prostep Smart Systems Engineering (SmartSE)

Building Blocks for Simulation based Cooperation between Partners

Metaverse		*Floating transition between real and virtual world*
Collaboration Networks	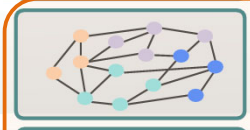	*Heterogeneous changing networks, collaboration models*
Company internal Digitalization, Virtualization	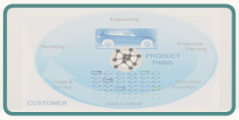	*Continuous use, enrichment of information, knowledge evaluation*
Simulation supported Development	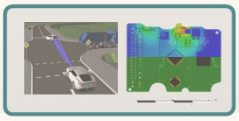	*Alignment with reality, prediction of reality basis for virtualization*
Real Products, Components		*Development of reliable and sustainable components and products*

Focus of prostep Smart SE project

Strong involvement, interaction with users (people)

Availability of Information in heterogeneous IT environments,

Traceability, Simulation Credibility

Verification Validation of Models, Parameters, Simulation

Reduced number of real prototypes

We need Building blocks to support these challenges

Smart Systems Engineering - SmartSE
Building Blocks for cross-company simulation-based engineering

prostep ivip

25+ project participants

Mission Phase 5 (2022-2024)

Enabling collaborative development and validation of complex products by simulation along a multi-tier supply chain.

SmartSE Project Organization

- *Simulation Credibility & Traceability*
- *Dealing with Abstraction & Modeling*
- *SE and Agile Methods*
- *New V Model*
- *Standardization & Industrialization*
- *Demonstrators & Show Cases*

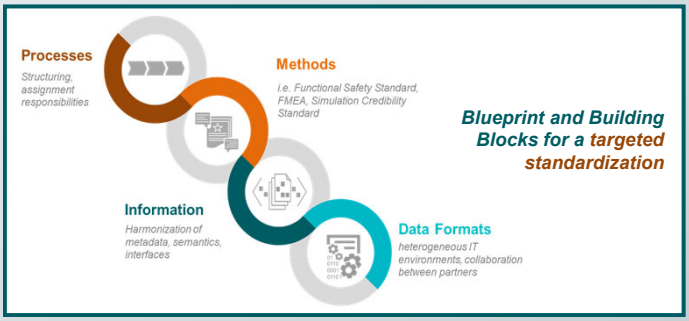

Blueprint and Building Blocks for a targeted standardization

The initiation, development and industrialization of standards in the field of model-based and cross-company development is an important part of the work of the SmartSE project group.

Motivation Smart Systems Engineering (SmartSE)
Collaborative Simulation-based Engineering

prostep ivip

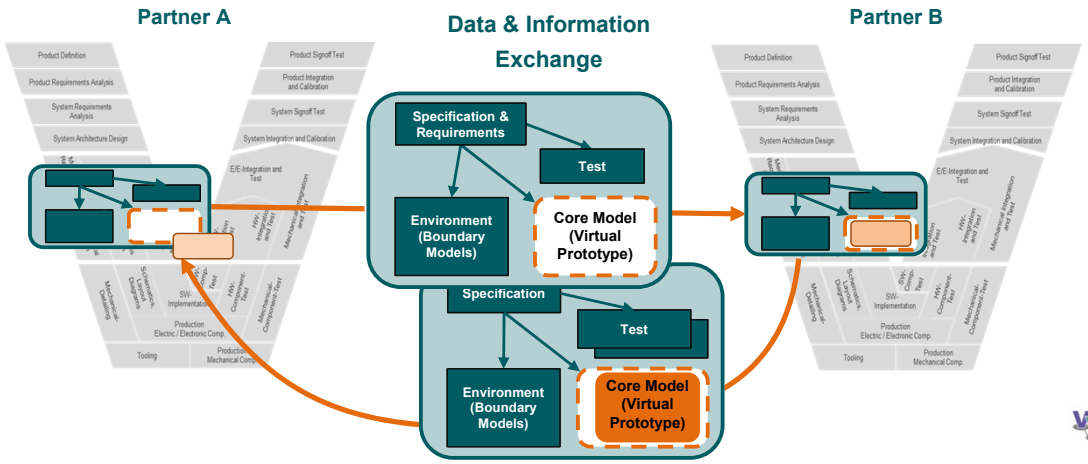

In Scope: Exchange of all artefacts required for an efficient, cross-company simulation-based engineering like specifications, requirements, test cases, simulation models and model meta data.

Building Blocks for Simulation based Cooperation
Agenda

Guard rails for Simulation credibility standards and recommendations
General approach

Focus on *"Guard Rails for a Recommendation"* (not Standardization) for reasons of feasibility and limited resources in SmartSE project. Implementation by a body still to be defined.

*Defining a final **"Simulation Credibility" Recommendation** or Standard is to be carried out by a standardization committee with international and cross-industry authority, which is yet to be identified.*

What do we understand by "Guard Rails"?
Rough concept paper in addition to white paper "Simulation-based decision making" describing the solution space for an international, cross-industry recommendation (kind of specifications for the recommendation itself).

Guard rails for Simulation credibility standards and recommendations
Core elements of the technical paper

Overall Process Framework

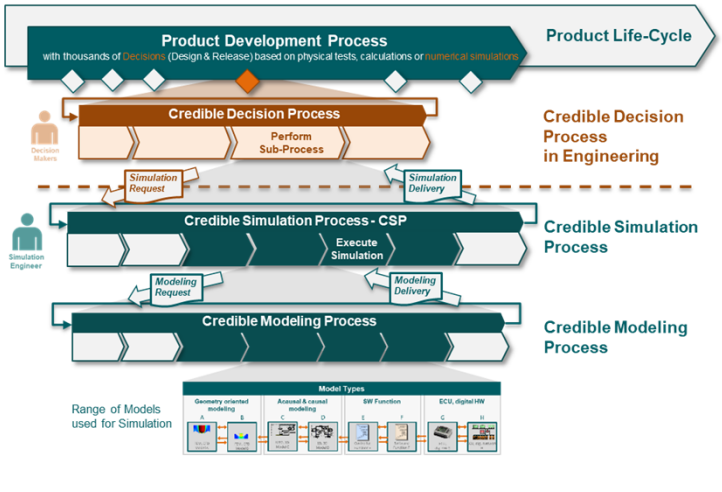

Top 15+ Terms and Definitions

- Simulation-based Decisions
- Simulation-informed Decisions
- Fidelity
- Credibility of a simulation
- Quality of a Simulation
- Fidelity of a Simulation
- Criticality of a simulation
- Verification
- Validation
- Engineering Simulation
- Credible Decision Process (in Engineering) - CDP
- Credible Simulation Process (CSP)
- Credible Modeling Process (CMP)
- Simulation Taks
- Decision Makers
- Simulation Engineer

Technical Paper "Simulation Credibility"
Embedding of the simulation in the higher-level product development process

Credible Decision Process

*At least part of the decision is based on results of **numerical / computational simulations**. However, the decision does not have to be based entirely on simulation results.*

For the decisons can be used:

- *Expert judgement*
- *Calculation*
- *physical tests*
- *descriptive models (testing for (logical) correctness, completeness)*
- *Credibility is enhanced by learned patterns across projects*

Relates to product (independent of simulation)

Relates to simulation solution

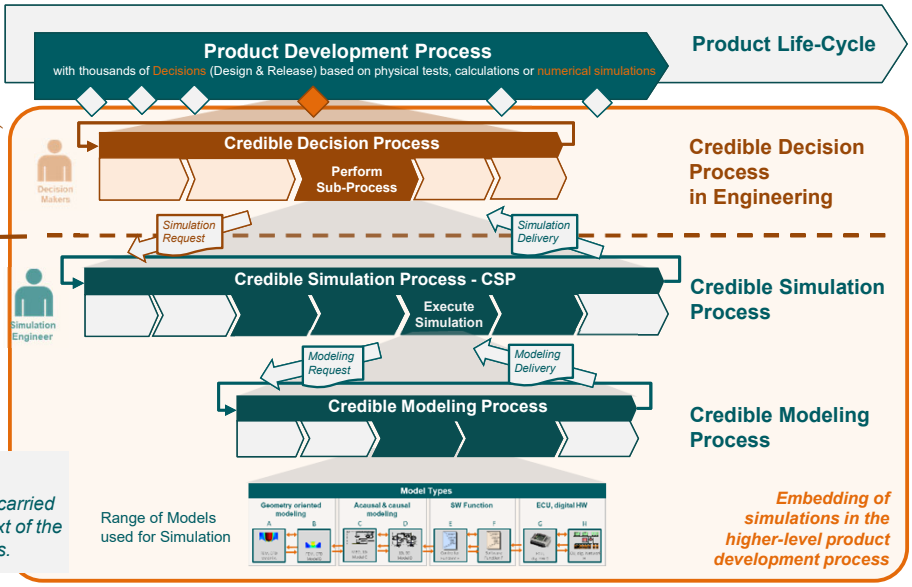

General Scope:

Numerical Engineering Simulations carried out for decision-making in the context of the overall product development process.

Guard rails for Simulation credibility standards and recommendations
First draft version was available July 2023

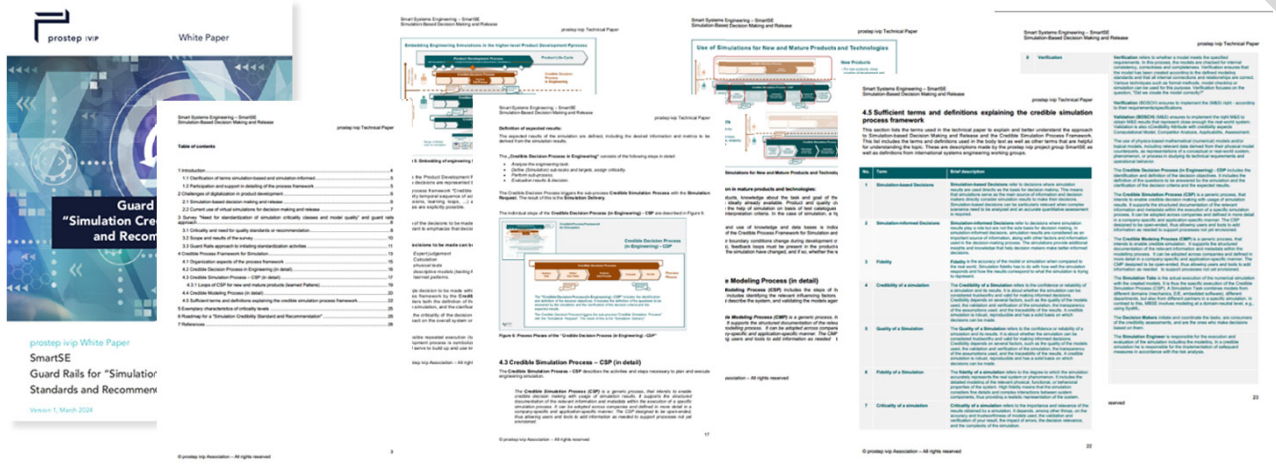

First draft version of the technical paper was available (80 % version) July 2023.
This version was created with the kind support of ASME / INCOSE and NAFEMS.

Guard rails for Simulation credibility standards and recommendations
What happened since begin 2023

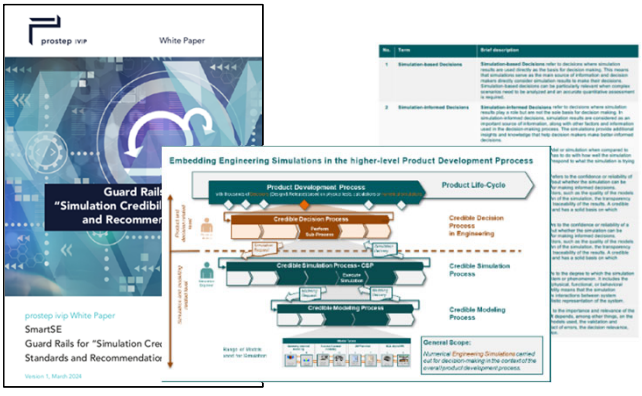

smart Systems Engineering *with the assistance of:* INCOSE ASME NAFEMS

- ***Very intensive discussions with experts from ASME / NAFEMS /INCOSE to finalize the process framework in Q1 and Q2 2023.***
- ***A draft version of the technical paper was completed to about 80% by the end of July 2023 and distributed for review.***
- ***An endorsement regarding participation by ASME / INCOSE /NAFEMS was sought. However, official endorsement couldn't be achived.***
- ***Therefore, this paper is a purely prostep ivip publication.***
- ***Publication White paper in March 2024***

White paper "Guard rails for Simulation credibility standards and recommendations" is publicly available
https://www.prostep.org/fileadmin/prod-download/TechnicalPaper_Simulation-Credibility_2024_V8.1_v2.pdf

“Simulation Credibility (Quick)-Check / Assessment”

Data Formats for Exchange: Heterogeneous IT Environments, Collaboration

Topic		Status
Guard Rails for a “Simulation Credibility“ Recommendation		*First version of White paper will be available End of 2023*
“Simulation Credibility“ Standard (s)	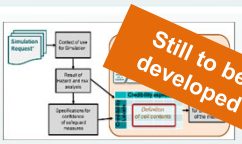	*Up to now open point, which organization will drive the development and when it will be available*
“Simulation Credibility (Quick)-Check” (long-term ➔ Assessment)		*Assessment are (partly) in use, but no alignment, harmonization up to now in industry*
“Simulation Credibility“ Methods		*Methods, trainings available and known, used in varying forms in industry*

We need all theses levels

To close the gaps, we should also make a bottom-up approach

Cross-Company Standardization in Credibility of Simulation

We want to establish M&S credibility together

NAFEMS

smart Systems Engineering

INCOSE

ASME SETTING THE STANDARD

ASSESS ANALYSIS, SIMULATION AND SYSTEMS ENGINEERING SOFTWARE STRATEGIES

Goal: Developing an international and cross-industry standard for “Modeling and Simulation Credibility” with standardization bodies

Credibility and Traceability of Simulation as an Enabler for Virtualization
What happens next?

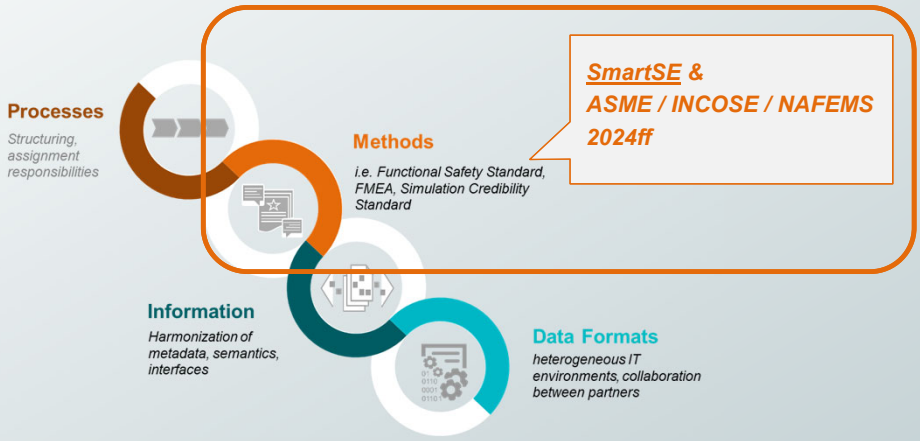

Credibility and Traceability of Simulation as an Enabler for Virtualization
What happens next?

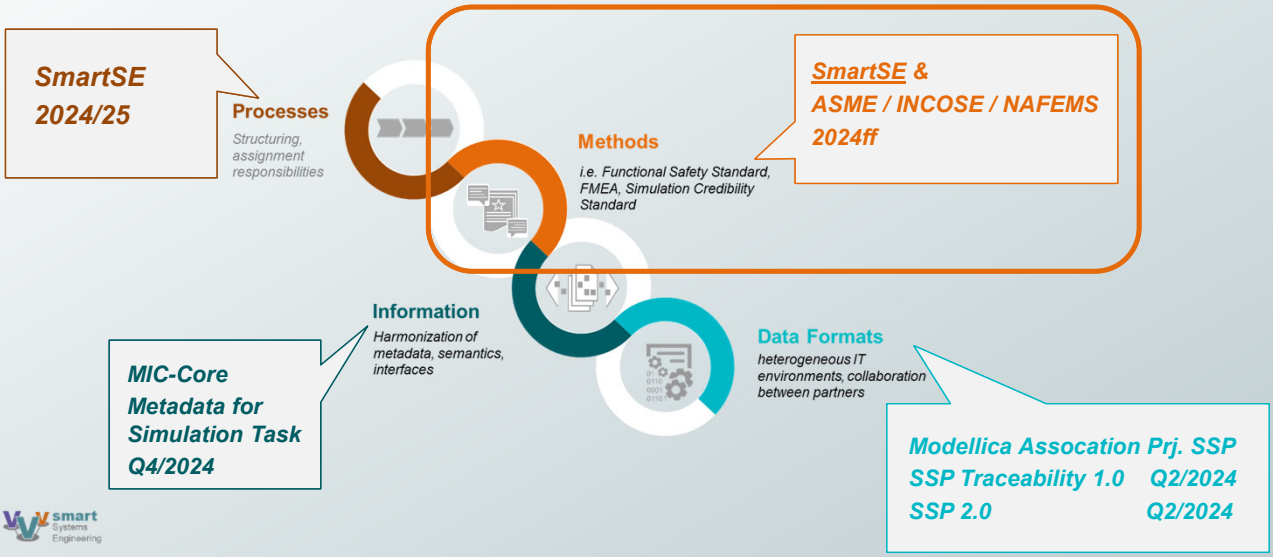

Credibility and Traceability of Simulation as an Enabler for Virtualization

prostep ivip SmartSE Phase V

Mission Phase 5
(2022-2024)

Enabling collaborative development and validation of complex products by simulation along a multi tier supply chain.

If you are interested in these topics
Get in contact and join the SmartSE project group

Contact
Melanie Kluge, melanie.kluge@b-h-c.de
Tel.: +49 7031 2050002

Discussion

Thank you

for your attention

Risk Based Decision and Approach for Credibility Assessment / Check

Hans-Martin Heinkel, Alexander Filimon, Muhammed Atak (Robert Bosch GmbH)

Martin Geissen (Unity)

The presentation Guard Rails for "Simulation Credibility Standards and Recommendation" provided an overview of the white paper published in April 2024.

In this presentation, we will first take a closer look at the influencing factor of risk in a decision

- Determining the risk of a decision
- Determination acceptable residual risk
- Fixing of necessary simulation credibility

Currently we develop and implement a credibility framework at Bosch. It is strongly influenced by the work of NAFEMS and ASME

We will use an example to show how credibility can be determined and communicated.
We also want to present the tool support based on open standards

NAFEMS DACH CONFERENCE

Risk based Decision and approach for Credibility Assessment / Check

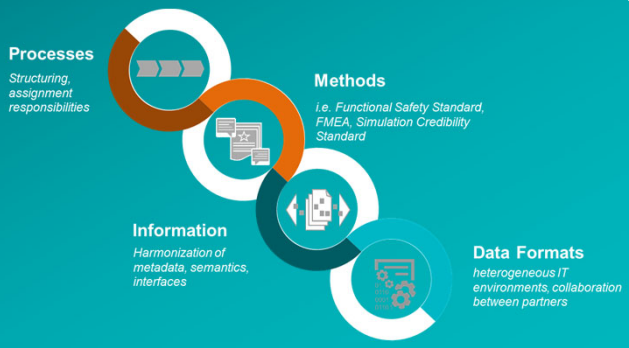

Bamberg 11 June 2024
Hans-Martin Heinkel, Bosch
Alexander Filimon, Bosch
Muhammed Atak, Bosch
Martin Geissen, Unity

Agenda

1. Prostep ivip SmartSE Project
2. Risk analysis and derive simulation credibility requirements
3. Example and tool-support
4. Conclusions – Next steps

Smart Systems Engineering - SmartSE
Building Blocks for cross-company simulation-based engineering

prostep IVIP

25+ project participants

Mission Phase 5 (2022-2024)

Enabling collaborative development and validation of complex products by simulation along a multi-tier supply chain.

SmartSE Project Organization

- *Simulation Credibility & Traceability*
- *Dealing with Abstraction & Modeling*
- *SE and Agile Methods*
- *New V Model*
- *Standardization & Industrialization*
- *Demonstrators & Show Cases*

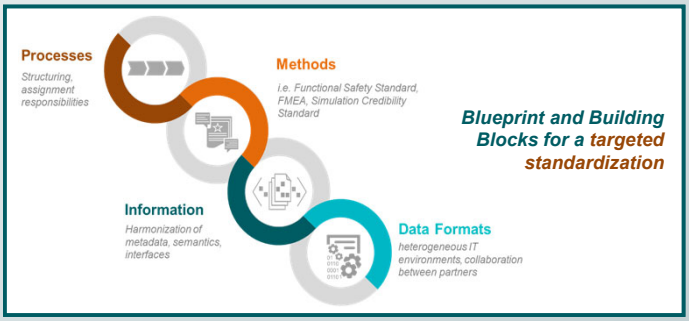

Blueprint and Building Blocks for a targeted standardization

The initiation, development and industrialization of standards in the field of model-based and cross-company development is an important part of the work of the SmartSE project group.

Building Blocks for Simulation-based Collaboration
Levels of consideration for successful standardization

prostep IVIP

Processes

Structuring, assignment responsibilities

Methods

i.e. Functional Safety Standard, FMEA, Simulation Credibility Standard

Information

Harmonization of metadata, semantics, interfaces

Data Formats

heterogeneous IT environments, collaboration between partners

smart Systems Engineering

Building Blocks for Simulation based Cooperation
Process framework for Simulation Credibility

Process hierarchy with clear information structuring

- ***Sub-processes can be integrated into specific company processes***
- ***Clear assignment of responsibilities***

Meetings for alignment "Big Picture and core terms"

as basis for domain specific credibility standards.

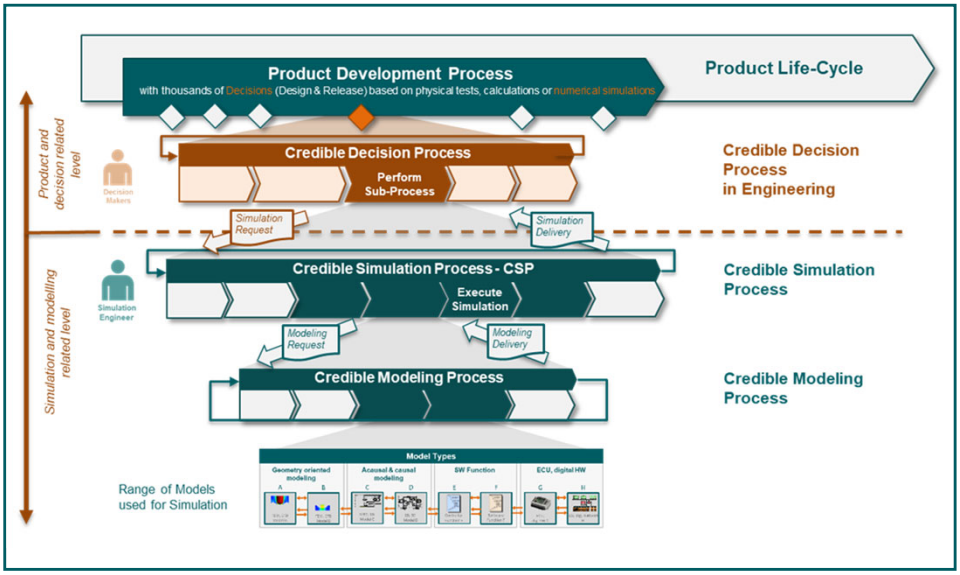

Building Blocks for Simulation based Cooperation
Process framework for Simulation Credibility

Clear separation between responsibilities and tasks:

Output of
"Fixing of necessary simulation credibility"

Is input for
"Determination of simulation credibility"

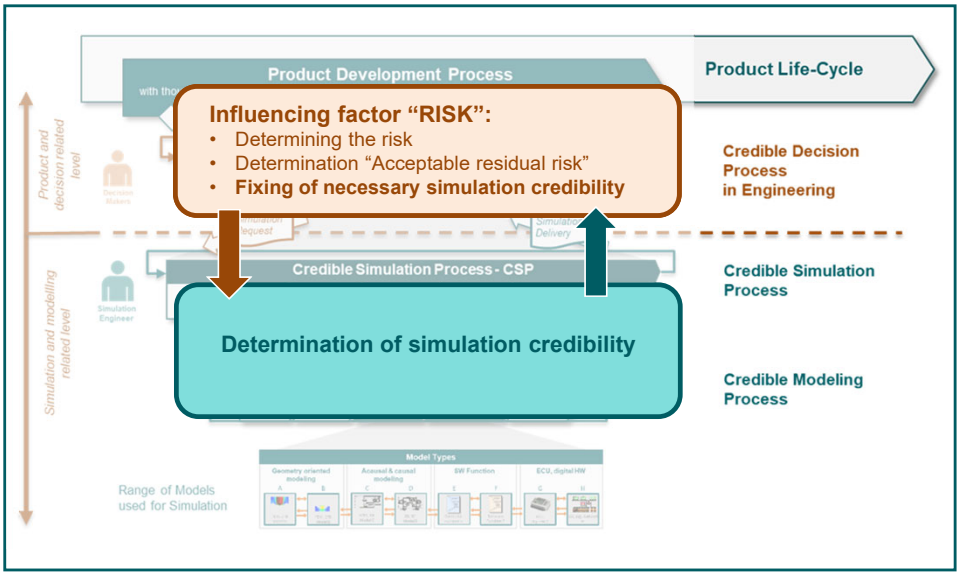

Building Blocks for Simulation based Cooperation
Process framework for Simulation Credibility

Correlation between the influencing factor "risk" of a decision

and the

"credibility of the simulation".

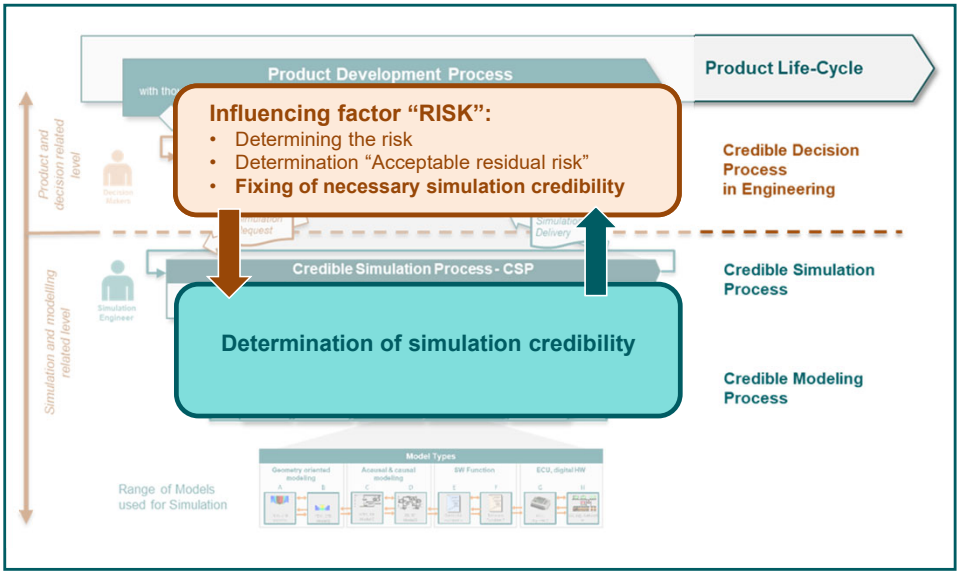

Influencing factor "RISK" on decision making
The Three Layers

Human beings are key for decisions as they evaluate the risks and eventually make a decision. The evaluation of the risk is not unique as human beings are complex beings which are influenced by many factors (e.g. emotions). Thus, the decisions at a given situation with given risks may differ completely.

Risk is the potential for performance shortfalls which may be faced in the future. Thus, risks play a a central role as a further influencing factor in the decision-making process.

Data are the fundamental driving force for informed decisions. MBE methods (simulation, real testing, calculation) support the meaningful data generation.

A simulation-based decision should provide a transparent, comprehensible link between the underlying data, the *potential risk* and the decision made.

Key Enabler: Connecting Risks with Data
The Nature of Risks

Scenarios
What can happen?

Captured by risk identification and description

Likelihood
How likely is it to happen?

Represented by probability of occurrence

Consequence
What is the impact if it did happen?

Described by impacts on performance shortfalls

Risk **is operationally defined as a set of triplets.**

Key Enabler: Connecting Risks with Data
Aspects of Performance Shortfalls

Safety	from **inconsequential** to **permanent disability or death**
Technical	from **no effect** to **severely degraded to none**
Cost	from **no effect** to **severe cost overruns**
Schedule	from **no effect** to **SOP missed**

Performance shortfalls **may be related to one or more of the following domains.**

Key Enabler: Connecting Risks with Data
Modeling the Decision Consequences

- Safety
- Technical
- Cost
- Schedule

Categorizing decision consequences according to the criticality

neglible — minor — moderate — significant — catastrophic

The qualifying terms are situationally dependent

Decision consequences **reflect the performance shortfalls and can be generalized and categorized.**

Key Enabler: Connecting Risks with Data
Modeling the Data Influence

- Data Influence

Categorizing decision consequences according to the impact

neglible — minor — moderate — significant — catastrophic

The qualifying terms are situationally dependent

The role of data **depend on the degree to which data impact a decision under consideration and can be related to.**

Data Layer
Credibility Requirements

The credibility of data *depend on the decision consequence and the data influence.*

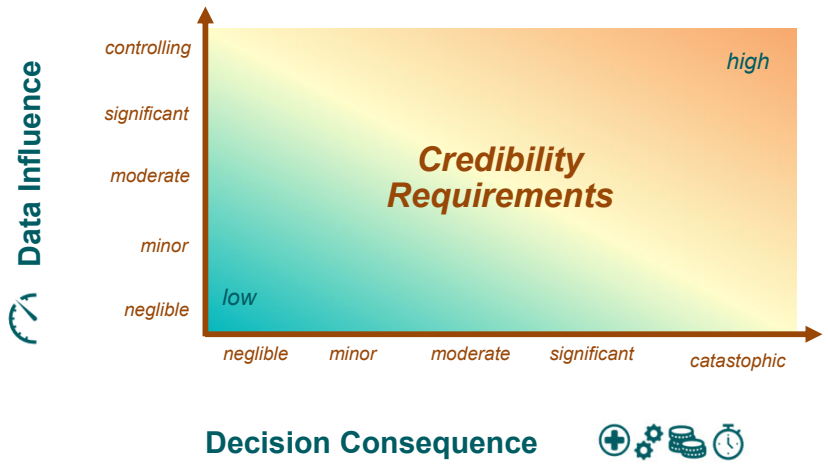

Credibility Attributes
Definition and "the Why"

M&S Credibility

Know-how and experience *must be available to the extent that a* ***credible statement*** *can be made about the residual risk.*

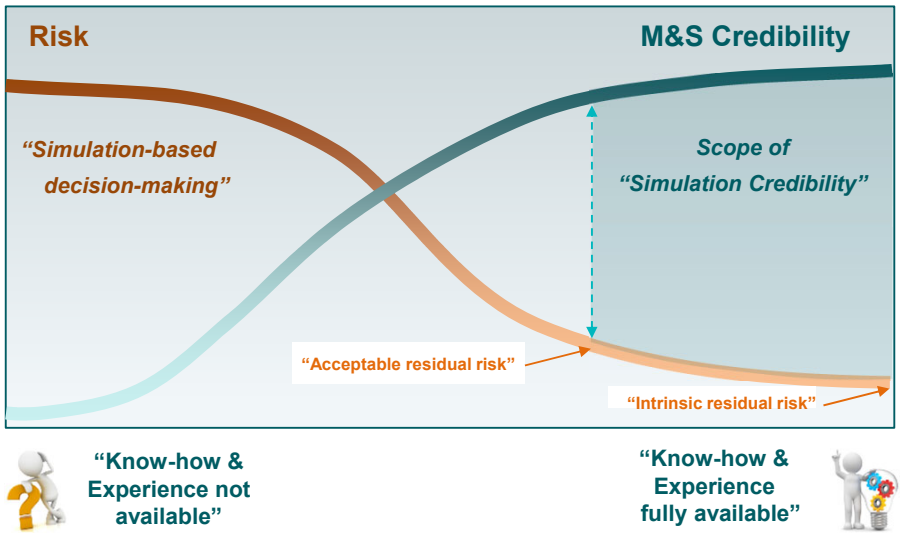

Building Blocks for Simulation based Cooperation
Standards and Recommendations for Simulation Credibility

Approach for Credible Decision:
Clear separation between responsibilities and tasks:

Output of
"Fixing of necessary simulation credibility"

Is input for
"Determination of simulation credibility"

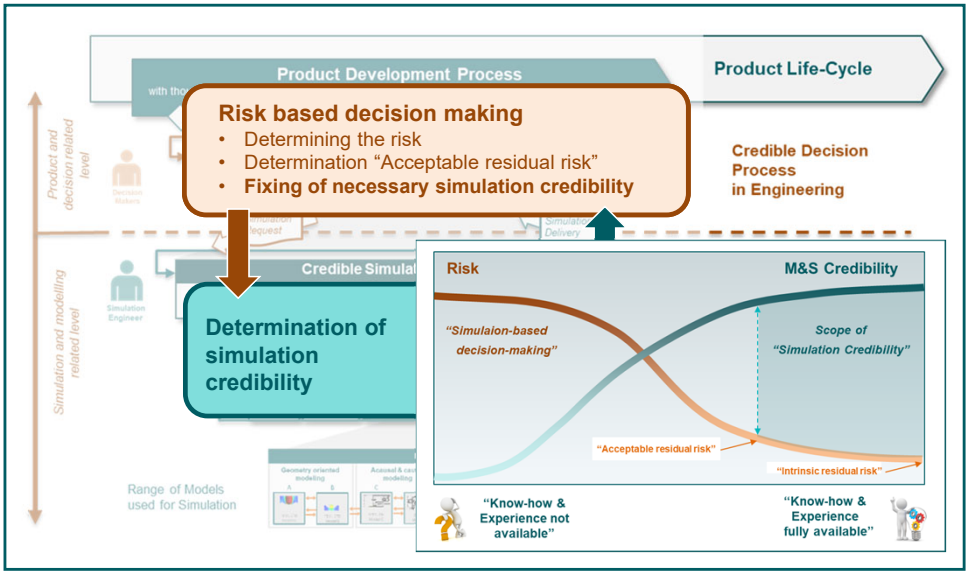

Credibility and Traceability of Simulation as an
Enabler for Virtualization

Part of the presentation was already shown and discussed on the NAFEMS World Congress 2023

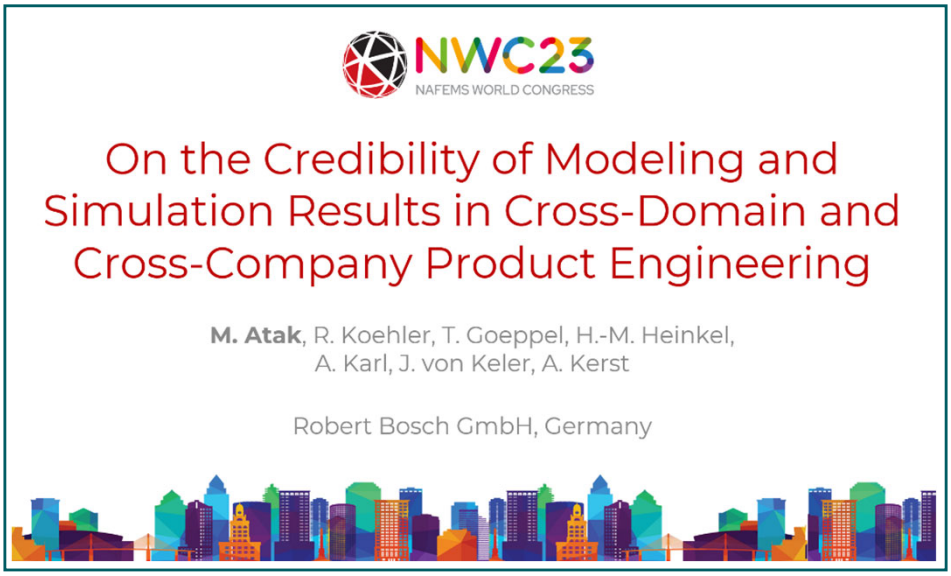

Virtual Validation of Vibration

E-Machine
on a shaker

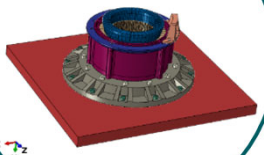

Question of Interest
What loads are generated at the design elements of an e-machine by external excitations?

Simulation Goal
Determine transfer functions to convert external excitations into internal loads at design elements using M&S.

Transfer Function
for reliability analysis

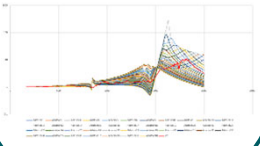

Sensitivity Analysis & Uncertainty Propagation

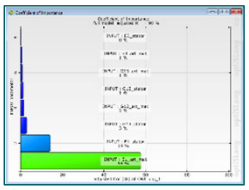

Model Fitting & Validation

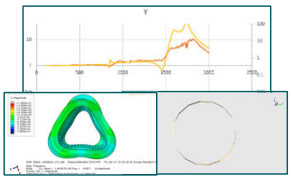

How to assess & communicate the credibility of the transfer functions determined by M&S?

Credibility Attributes

The framework consists of the following *4 Credibility Attributes*

Verification

Did we implement the M&S right?
Were the models implemented correctly, per their requirements/specifications?

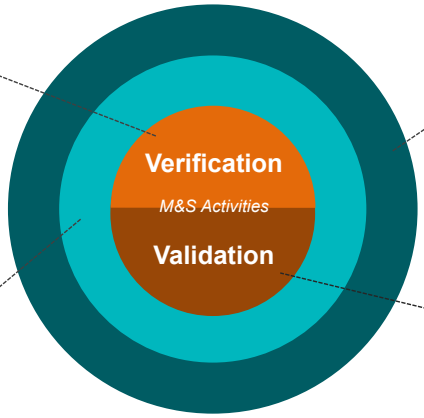

Organizational Capability

Did we consider the required and available qualifications, experiences and processes?

M&S Error Management

Did we consider error handling mechanisms? This can contribute to a target- and economical-oriented choice of V&V (verification & validation) activities.

Validation & UQ

Did we implement the right M&S?
Did the M&S results compare favorably to the referent data,
and how close is the referent to the real-world system?

Each credibility attribute contains further credibility aspects and credibility activities
They are used to concretize and to evaluate the credibility attributes

Assessing & Establishing the Credibility

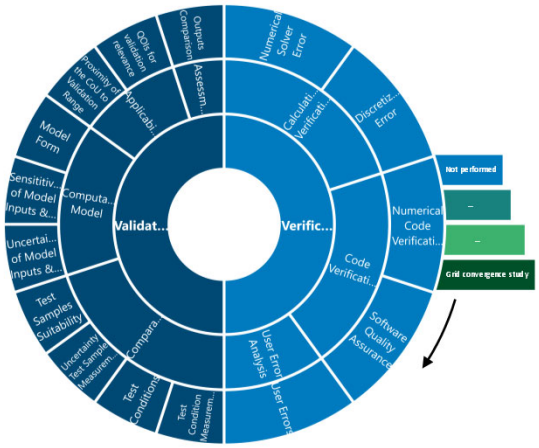

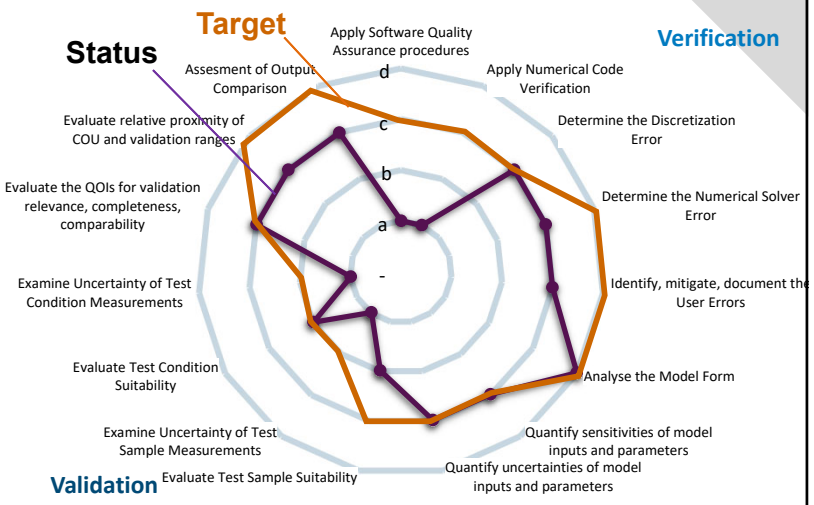

Credibility Evaluation Checklist establishes a fundament to make the credibility of the simulation models and results transparent and comprehensible

Assessing & Establishing the Credibility
Tooling

COSTA
(Credible Of Simulation Tool Assistant)

Chapters to navigate

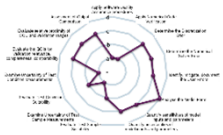

Credibility spider is generated by tool

Assessing & Establishing the Credibility
Tooling

COSTA (Credible Of Simulation Tool Assistant)

Chapter

Explanation

Textual description of activities by user

Check boxes for selecting status level and target level

3.1 Code Verification

The objective is to identify and to remove errors in the source code and numerical algorithms of the computational software.

The goals of code verification are to identify and remove errors in the source code and numerical algorithms of the computational software...

3.1.1 Software Quality Assurance

Apply Software Quality Assurance (SQA) procedures and document the results to ensure that the software is functioning correctly and produces repeatable results on a specified computer resource in a specified software environment.

The objective of SQA is to ensure that the software is functioning correctly and produces repeatable results on a specified computer resource in a specified software environment....

Documentation

`Describe your executed activities`

Status Level

- a: No SQA procedures are documented.
- b: SQA procedures from the vendor are referenced.
- c: An audit is conducted with the vendor to confirm that quality procedures are conducted and documented during the software development process.
- d: Benchmark verification test cases, provided by the vendor, are run on the user's computer platform. The results are compared to vendor results and documented.

Target Level

- a: No SQA procedures are documented.
- b: SQA procedures from the vendor are referenced.
- c: An audit is conducted with the vendor to confirm that quality procedures are conducted and documented during the software development process.
- d: Benchmark verification test cases, provided by the vendor, are run on the user's computer platform. The results are compared to vendor results and documented.

Example of checklist structure

Credibility and Traceability of Simulation as an Enabler for Virtualization
Harmonizing “Simulation Credibility (Quick)-Check / Assessment”

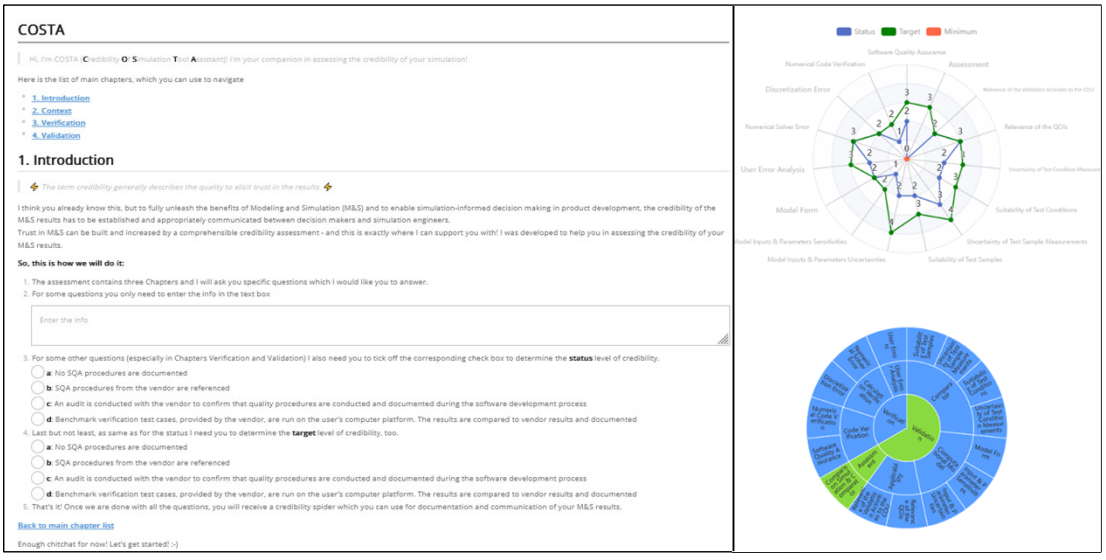

Implementation Tooling

- Use of Plain Markdown
- Markdown is directly supported by many tools e.g. Git

→ easy portability

Credibility and Traceability of Simulation as an Enabler for Virtualization
Harmonizing "Simulation Credibility (Quick)-Check / Assessment"

Status:

- Large overlap of methods which are used in principle (methods from SW development, methods NAFEMS, ASME,...)
- Heterogeneous approaches for the validation of simulation results in the companies
- Currently no overarching approaches, proposals for simulation credibility assessments

"Simulation Credibility" Methods

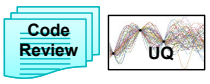

Proposal for Bottom-Up Harmonization of Simulation Credibility Assessment / Quick Check:

- Collection of best practice and experiences
  - *How is it made?*
  - *Criteria for acceptance for users: what is applicable?*
- Bosch brings in SmartSE project its current status for the Credibility Evaluation Checklist as a basis

"Simulation Credibility (Quick)-Check" (long-term → Assessment)

Goal: **Use harmonization for in-house applications, no contractual consequences. When harmonization has stabilized and is applicable, can be "official" basis for collaboration or standardization**

Open Standards for Simulation at Bosch
Usage and Piloting in simuLAB

Building Blocks for cross-company simulation-based engineering

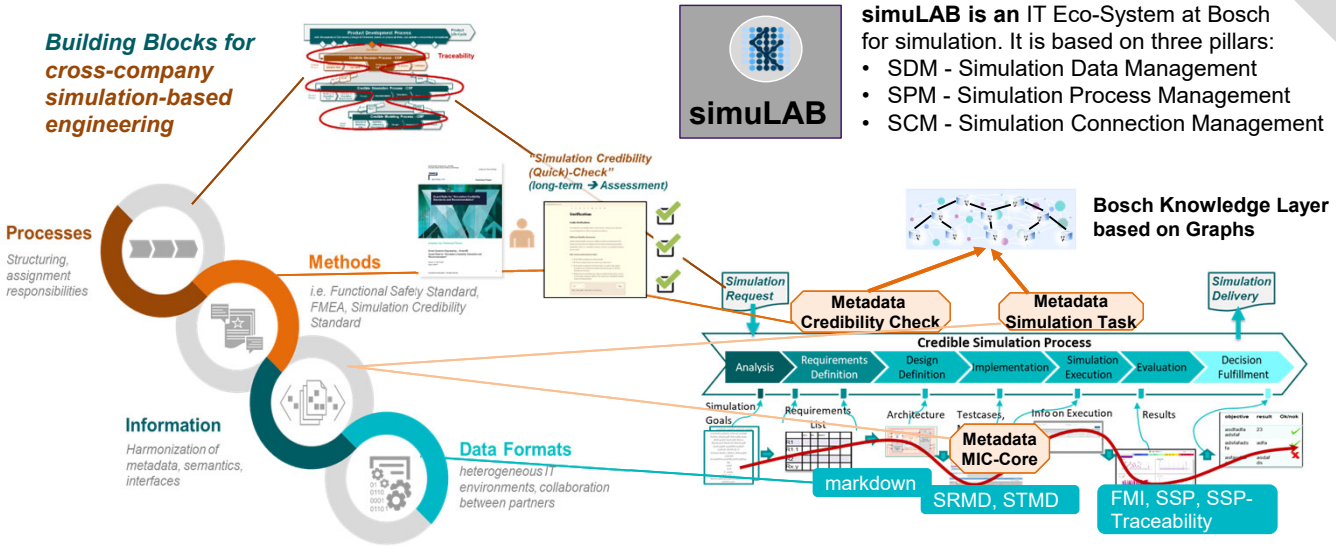

simuLAB is an IT Eco-System at Bosch for simulation. It is based on three pillars:

- SDM - Simulation Data Management
- SPM - Simulation Process Management
- SCM - Simulation Connection Management

Bosch Knowledge Layer based on Graphs

Credibility and Traceability of Simulation as an Enabler for Virtualization

prostep ivip SmartSE Phase V

Mission Phase 5
(2022-2024)

Enabling collaborative development and validation of complex products by simulation along a multi tier supply chain.

If you are interested in these topics
Get in contact and join the SmartSE project group

Contact
Melanie Kluge, melanie.kluge@b-h-c.de
Tel.: +49 7031 2050002

Discussion

Thank you

for your attention

30 years of excellence

Estimation of material parameter uncertainties using probabilistic and interval approaches

Thomas Most (Bauhaus-Universität Weimar, Germany)

1 Introduction

Within the calibration of material models, often the numerical results of a simulation model **y** are compared with the experimental measurements **y***. Usually, the differences between measurements and simulation are minimized using least squares approaches including global and local optimization techniques. In this paper, the resulting scatter or uncertainty of the identified material parameters **p** are investigated by assuming the measurement curves as non-deterministic. Based on classical probabilistic approaches as the Markov estimator or the Bayesian updating procedure, the scatter of the identified parameters can be estimated as a multi-variate probability density function. Both procedures require a sufficient accurate knowledge or estimate of the scatter of the measurement points, often modeled by a Gaussian covariance matrix.
In this paper, we present a different idea by assuming the scatter of the measurements not as correlated random numbers but just as individual intervals with known minimum and maximum values. The corresponding possible minimum and maximum values for each input parameter can be obtained for this assumption using a constrained optimization approach. However, the identification of the whole possible parameter domain for the given measurement bounds is not straight forward. Therefore, we introduce an efficient line-search method, where not only the bounds itself but also the shape of the feasible parameter domain can be identified. This enables the quantification of the interaction and the uniqueness of the input parameters. As a numerical example, we identify the fracture parameters of plain concrete with respect to a wedge splitting test, where five unknown material parameters could be identified.

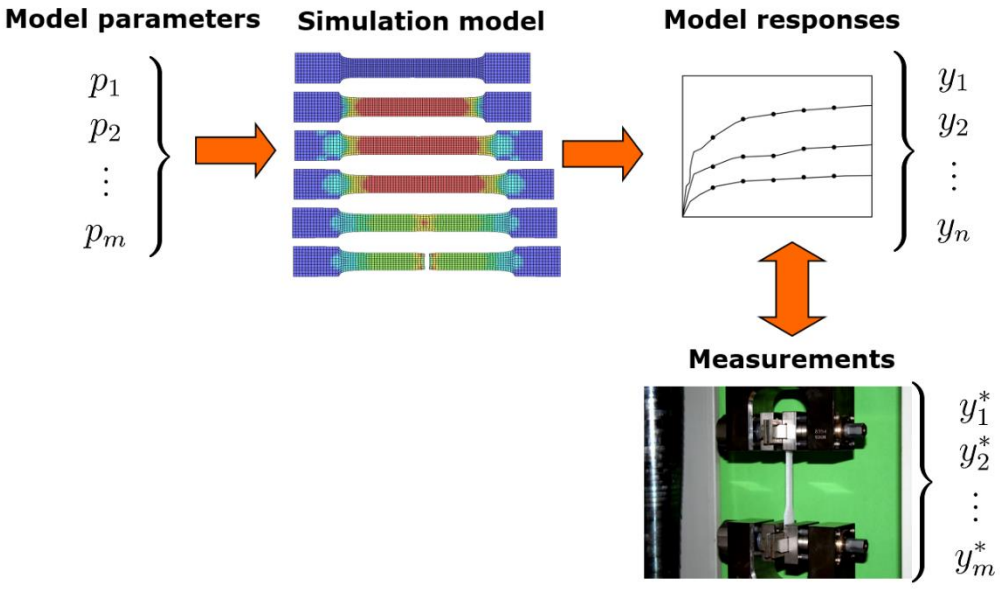

Fig. 1: Comparison of the results of a simulation model **y** by using a given parameter set **p** with measurement observation **y***

2 Probabilistic approaches

2.1 Maximum likelihood approach

In the calibration task, usually a simulation model is used to estimate unknown parameters by minimizing the deviation between the model responses and measurement observations. In the maximum likelihood approach [1,2] it is assumed that the simulation model can represent the physical phenomena perfectly and thus the resulting difference between measurements and simulation response are caused only by measurement uncertainties. Generally, a joint normal distribution is assumed for the measurement scatter

$$P(\mathbf{y}^* - \mathbf{y}) = \frac{1}{\sqrt{(2\pi)^m |\mathbf{C_{yy}}|}} \exp\left[-\frac{1}{2}(\mathbf{y}^* - \mathbf{y})^T \mathbf{C_{yy}^{-1}} (\mathbf{y}^* - \mathbf{y})\right]$$

where $\mathbf{C_{yy}}$ is the covariance matrix of the measurement uncertainty. If the likelihood of the parameters is maximized, we obtained the following objective function, which has to be minimized

$$J = (\mathbf{y}^* - \mathbf{y})^T \, \mathbf{C_{yy}^{-1}} \, (\mathbf{y}^* - \mathbf{y}) \rightarrow \min$$

By linearizing this objective, we obtain the following updating scheme

$$\Delta \mathbf{p} = \left(\mathbf{A}^T \mathbf{C_{yy}^{-1}} \mathbf{A}\right)^{-1} \mathbf{A}^T \mathbf{C_{yy}^{-1}} \Delta \mathbf{y}, \quad \mathbf{A} = \frac{\partial \mathbf{y}}{\partial \mathbf{p}}$$

where **A** is the local sensitivity matrix containing the derivatives of the individual response values **y** w.r.t. the model parameters **p**.

2.2 Markov estimator

Assuming, that the optimal parameter set $\mathbf{p_{opt}}$ has been found by e.g. a combination of a global and local optimization approaches, we can calculate the sensitivity matrix at the optimal parameter set and estimate the covariance matrix of the parameters [2]

$$\mathbf{C_{pp}} = \left(\mathbf{A}_{opt}^T \mathbf{C_{yy}^{-1}} \mathbf{A}_{opt}\right)^{-1}$$

This covariance matrix $\mathbf{C_{pp}}$ contains the necessary information about the scatter of the individual parameters as well as possible pairwise correlations. The distribution of the parameters is normal as assumed for the measurements. The estimated scatter and correlations are a very useful information to judge about the accuracy and uniqueness of the identified parameters in a calibration process. This method can be interpreted as an inverse first order second moment method: assuming a linear relation between parameters and measurements and a joint normal distribution of the measurements, we can directly estimate the joint normal covariance of the parameters. However, the application of this linearization scheme requires an accurate estimate of the optimal parameter set by a previous least squares minimization.

2.3 Bayesian updating

Another probabilistic method is the Bayesian updating approach [1], which considers nonlinear relations between the parameters and the responses but requires much more numerical effort to obtain the statistical estimates. In this approach the unknown conditional distribution of the parameters w.r.t. to the given measurements is formulated using the Bayes' theorem as

$$P(\mathbf{p}|\mathbf{y}^*) = \frac{P(\mathbf{y}^*|\mathbf{p}) \cdot P(\mathbf{p})}{P(\mathbf{y}^*)}$$

where the likelihood function can be formulated as multi-normal probability density function similar to the Markov estimator

$$P(\mathbf{y}^*|\mathbf{p}) = \frac{1}{\sqrt{(2\pi)^m |\mathbf{C_{yy}}|}} \exp\left[-\frac{1}{2}(\mathbf{y}^* - \mathbf{y})^T \mathbf{C_{yy}^{-1}} (\mathbf{y}^* - \mathbf{y})\right]$$

Since the normalization term $P(\mathbf{y^*})$ is usually not known, the posterior parameter distribution $P(\mathbf{p}|\mathbf{y^*})$ is obtained by sampling procedures such as the Metropolis-Hastings algorithm [3]. The prior distribution

P(**p**) can be assumed either from previous information or as uniform distribution within assumed parameter bounds. Further details on this procedure can be found e.g. in [4].

The challenge in both probabilistic approaches is the estimate of the covariance matrix of the measurement uncertainty $\mathbf{C_{yy}}$. If a measurement procedure is repeated very often, this matrix can be estimated directly from measurement statistics. However, this is often not possible. A valid estimate could be to assume the measurement errors to be independent. The resulting covariance matrix is then diagonal, where at least the scatter of the individual measurement points has to be estimated. From a small number of measurement repetitions this can be estimated straight forward. If even such information is not available, the measurement error can be assumed to be constant for each output value

$$\mathbf{C_{yy}} = \sigma_y^2 \mathbf{I} \qquad \mathbf{C_{pp}} = \sigma_y^2 \left(\mathbf{A}_{opt}^T \mathbf{A}_{opt} \right)^{-1}$$

In this case, the estimated covariances of the parameters is directly scaled by the assumed measurement scatter. In case, that only a single measurement curve is available for the investigated responses, the misfit of the calibration process can be used for a rough estimate. Assuming the measurement errors to be constant and independent, we obtained the well-known least squares formulation.

3 Interval line-search approach

Instead of modeling the measurement points as correlated random numbers, which requires the estimate of the full covariance matrix, we can assume, that each measurement output is an interval number with known minimum and maximum bounds as shown in figure 2.

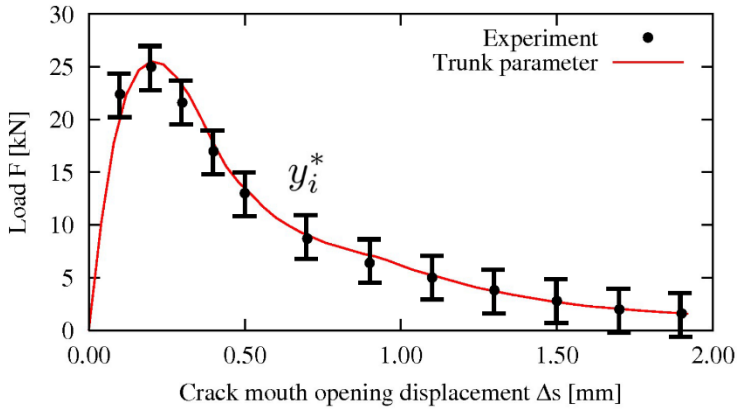

Fig. 2: Assuming the uncertain measurement data as interval numbers for the identification of the input parameter bounds

In the classical interval optimization approach, usually the interval of an uncertain response is obtained from the known interval of the input parameters by several forward optimization steps. This is the so-called α-level optimization [6] and is shown in principle in figure 3: the most probable value is assumed for each input parameter with the maximum α-level and a linear descent to zero at the lower and upper bounds. The α-level optimization will then detect the shape of the corresponding α-levels of the unknown outputs. In the inverse approach, we now search for the possible minimum and maximum values of the input parameters **p** within the given level, while each of the response value **y** is constrained to the corresponding interval. This can be solved for each input parameter and each α-level individually by a constrained optimization run with all unknown input parameters as optimization design variables.
This optimization, which searches for the bounds of each input parameter separately cannot investigate the interactions or correlations between the possible input parameter combinations. Therefore, we suggest a new interval-search approach, which investigates the whole joint domain of the input parameters. Based on the optimal parameter set $\mathbf{p_{opt}}$, found by a previous deterministic calibration, the input parameter space is discretized by a given number of uniformly distributed circular search directions as shown in fig 4. For each of these directions a line-search is applied to find the boundary of the feasible parameter domain w.r.t. to the given interval bounds of the measurement points. This approach is similar to the directional sampling method known from the reliability analysis [7,8].

In order to extend this method to more than two input parameters, the search directions have to be discretized on a 3D- or higher dimensional (hyper-) sphere. One very efficient discretization method to generate such direction vectors on the hyper-sphere are the so-called Fekete points [8], which are generated using a minimum potential energy criterion. This results in very equally distributed points as shown in fig 4. This optimized discretization will require a significant smaller number of model evaluations to obtain a suitable representation of the parameter domain boundary. For each of the search directions then a line-search is performed to obtain the boundary of the feasible parameter domain. Since this is an independent one-dimensional search for every direction point on the hyper-sphere is can be efficiently computed. The final points on the boundary can be used to obtain a discretized shape of the feasible parameter domain. If more than two or three parameters are investigated, the visualization of the parameter domain can only be displayed in a subspace.

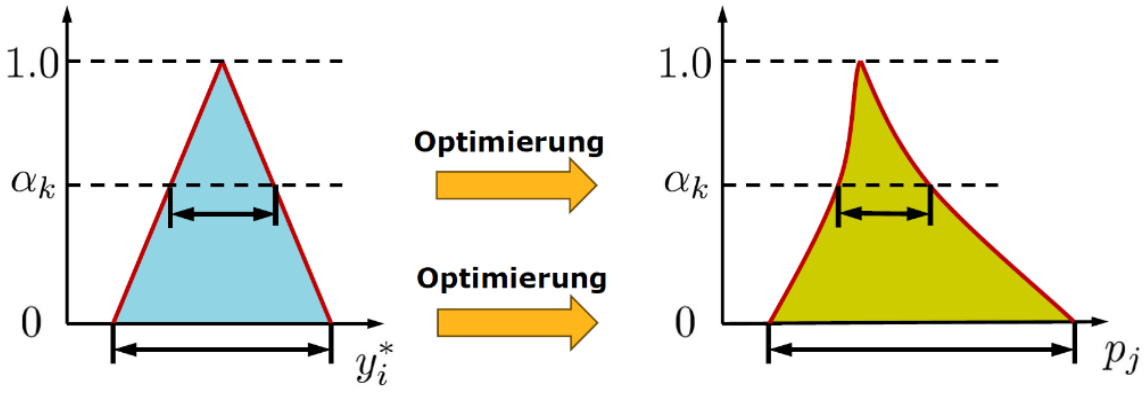

Fig. 3: Interval optimization applied to the inverse identification of minimum and maximum parameter bounds based on given measurement intervals

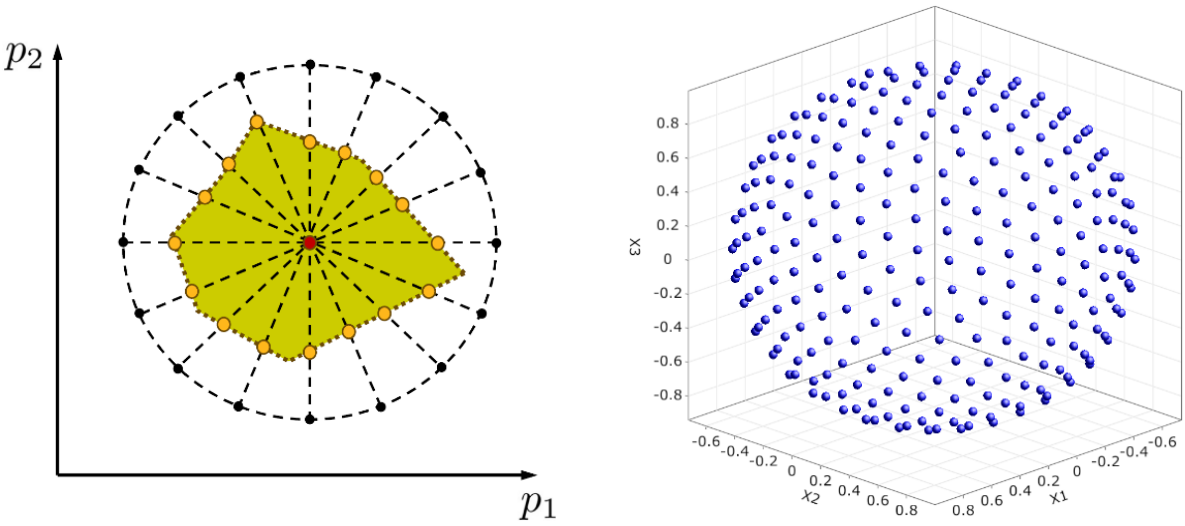

Fig. 4: Identification of the feasible input parameter domain using the interval line-search approach in two dimensions (left) and using Fekete points on the hyper-sphere in higher dimensions (right)

4 Numerical example

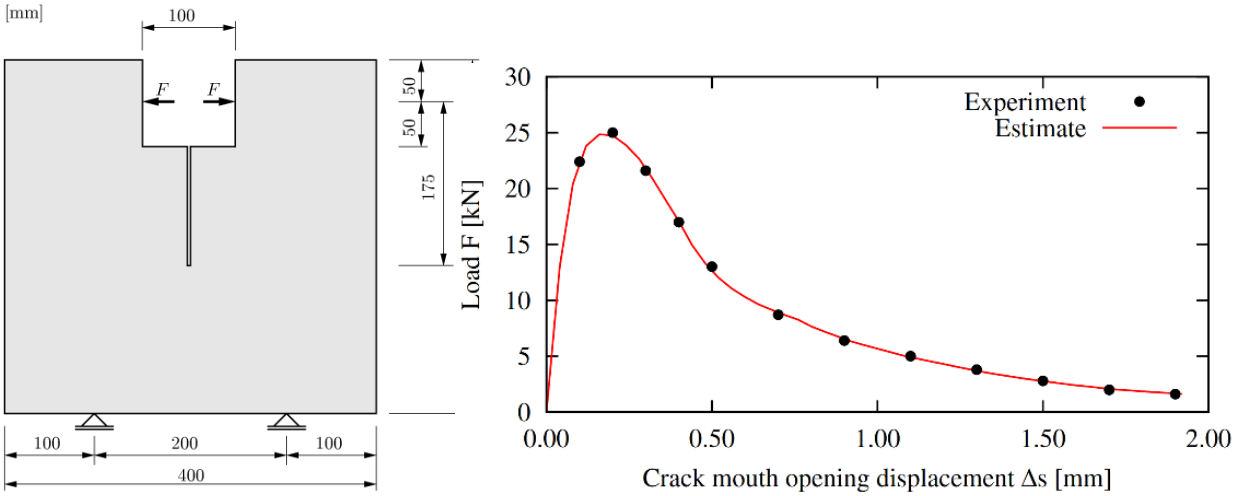

Fig. 5: Investigated wedge-splitting test setup according to [9] (left), comparison of measurements and calibrated simulation model (right)

By means of this numerical example the material parameter of plain concrete are identified using the measurement results of a wedge splitting test published in [9]. Six unknown parameters are investigated as the Young's modulus *Emod*, the Poisson's ratio *nue*, the tensile strength *fct*, the Mode-I fracture energy *Gf* and the two shape parameters *alpha_ft* und *alpha_wc* of a bilinear softening law. The geometry of the investigated concrete specimen is shown in figure 5. The structure is discretized by 2D finite elements and a predefined straight crack and the softening curve is obtained by a displacement-controlled simulation. Further details about the simulation model can be found in [10]. In a first step using a forward sensitivity analysis [5] it was observed, that the Poisson's ratio does not have any influence on the simulation curve. Therefore, it cannot be identified with the given experimental setup and is not considered in the following investigations.

In a second step the remaining five parameters are calibrated with a global and local optimization run using a least squares formulation with constant measurement errors for the objective function. The simulation curve of the optimal parameter set is compared to the measurement points in figure 5. The corresponding Root-Mean-Square-Error (RMSE) is 151 N, which is approximately 0.6% of the maximum force.

In a third step this RMSE is used to estimate a diagonal measurement covariance matrix as the standard deviation for all measurement points. Based on the covariance matrix of the measurements, the covariance matrix of the input parameters is estimated by the Markov estimator assuming a normal distribution for all parameters. In figure 6 the generated samples of the multi-variate Gaussian probability density are shown for two subspaces. The figure indicates, that a significant correlation between the identified Young's modulus and the tensile strength can be observed, meanwhile the fracture energy is almost uncorrelated w.r.t. the tensile strength. Additionally, to the Markov estimator, we apply the Bayesian updating procedure using the same measurement covariance matrix. In figure 6 the samples obtained by the Metropolis-Hastings algorithm are shown. The figure indicates, that the distribution of the Young's modulus and the tensile strength is not symmetric as assumed by the Markov estimator.

Finally, the introduced interval search algorithm is applied in this example. In a first step only the Young's modulus and the tensile strength are considered as uncertain parameters meanwhile the remaining parameters are kept constant. The resulting two-dimensional search points are shown for different sizes of the measurement intervals in figure 7. The figure clearly indicates, that the obtained parameter domain boundary is not symmetric as assumed by the Markov estimator. The assumed interval size of +/- 500 N corresponds 3.3 times the RMSE, which is equivalent to the 99.9% confidence interval. In a second step all five parameters are considered in the interval search. The identified points on the boundary are shown additionally in figure 7 in the same subspace as used in the previous investigation. The identified boundary of the input parameters in the five-dimensional case is slightly extended for small values of the Young's modulus compared to the 2D analysis.

As a result of the presented investigations, we can summarize, that all approaches provide in general similar results. The Markov estimator is most efficient but assumes normally distributed input parameters. The presented interval search approach does not require any knowledge on the measurement covariance matrix but requires much more model evaluations similar as the Bayesian updating approach.

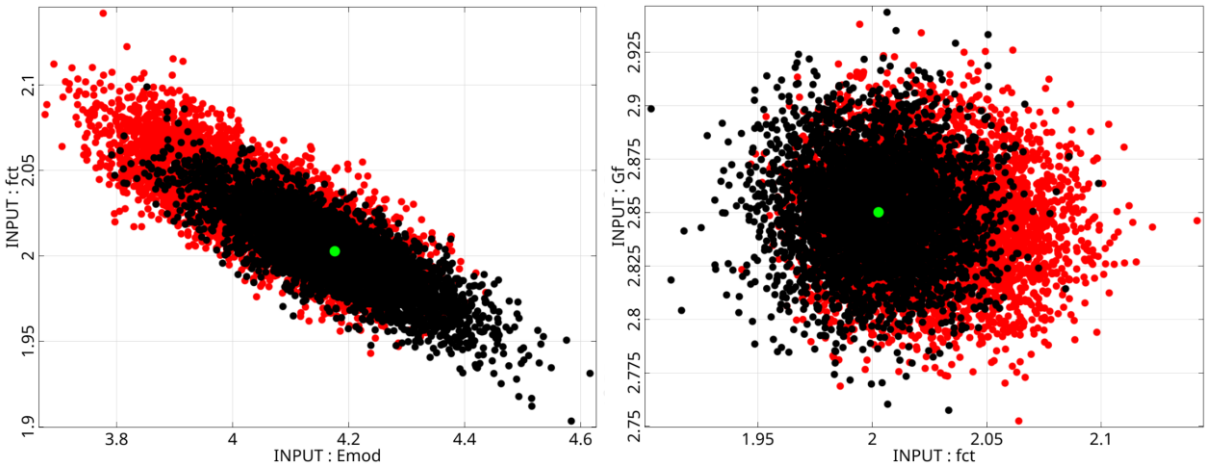

Fig. 6: Estimated parameter scatter and correlations for the Young's modulus (Emod), the tensile strength (fct) and the specific fracture energy (Gf) using the Markov estimator (black) and the Bayesian updating approach (red)

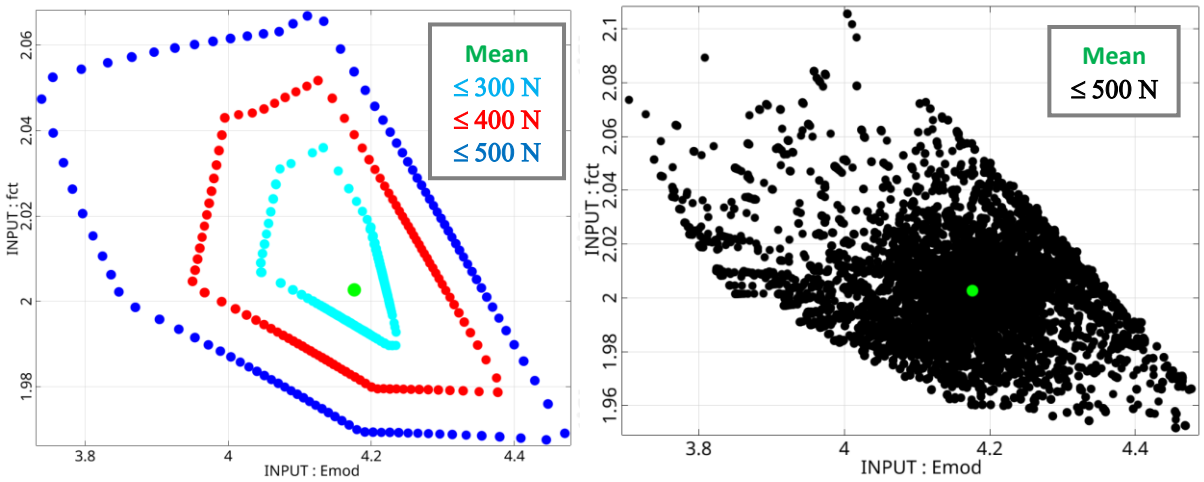

Fig. 7: Estimated α-level bounds in the subspace of the Young's modulus and the tensile strength considering only the two parameters in the line-search (left) and considering all five parameters (right)

5 References

[1] Beck, J. V. and K. Arnold (1977). *Parameter estimation in engineering and science.* New York: Wiley Interscience

[2] Ledesma, A., A. Gens, and E. E. Alonso (1996). *Estimation of parameters in geotechnical backanalysis – I. Maximum likelihood approach.* Computers and Geotechnics 18, 1–27.

[3] Hastings, W. (1970). *Monte Carlo sampling methods using Markov chains and their applications.* Biometrika 57, 97–109.

[4] Most, T. (2010). *Identification of the parameters of complex constitutive models: Least squares minimization vs. Bayesian updating*. IFIP Working Group Conference, München, 2010

[5] Most, T.; Kallmeyer, R.; Niemeier, R. (2019). *Estimate of Material Parameter Uncertainties in calibrated Simulation Models.*, NAFEMS World Congress, Quebeq, Kanada, 2019

[6] Möller, B.; Beer, M. (2000). *Fuzzy structural analysis using α-level optimization.* Computational Mechanics, 26:547-565

[7] Bucher, C. (2009). *Computational analysis of randomness in structural mechanics.* Structures and infrastructures book series, Vol. 3. CRC Press.

[8] Nie, J.; Ellingwood, B.R. (2000). *Directional methods for structural reliability analysis.* Structural Safety 22, 233-249

[9] Trunk, B. (1999). *Einfluss der Bauteilgrösse auf die Bruchenergie von Beton.* Dissertation, Eidgenössische Technische Hochschule, Zürich

[10] Most, T. (2005). *Stochastic crack growth simulation in reinforced concrete structures by means of coupled finite element and meshless methods,* Dissertation, Bauhaus-Universität Weimar

Hierarchical VVUQ Strategy for the Development and Credibility Assessment of a Biodegradable Pulmonary Heart Valve

Nils Götzen (4RealSim Services BV), Malte Rolf-Pissarczyk (TU-Graz), Mikel Isasi (Leartiker), Tahir Turgut (4RealSim Services BV), Omar Zahalka (4RealSim Services BV), Vincent Bouwman (4RealSim Services BV), Mohammad J. Mirzaali (TU-Delft), Matthias Pierlink (TU-Delft), Rick van Tunen (TU-Delft)

1 Summary

Within the EU-funded SimInSitu project [1], we implemented a hierarchical VVUQ approach to develop a credible patient-specific in-silico FEM model for biodegradable heart valves. This approach encompasses seven levels of complexity, beginning with material modelling and concluding in the actual in-silico patient-specific platform. We hereby report on the development progress of a Pulmonary Heart Valve, which is made from a biodegradable scaffold. This scaffold gradually dissolves in the human body, simultaneously promoting the formation of new native tissue.
The modelling process thus far encompasses three levels: Material Characterization and Constitutive Modelling, Device Component, and Complete Device. For each of the levels, we systematically carried out verification, validation, and uncertainty quantification activities. At the material level, we also engaged in calibration efforts to account for various sources of uncertainty related to material behaviour and experimental characterization. The hierarchical approach allowed us to propagate the uncertainty from the lower complexity levels to the higher one, while also identifying the significant factors and parameters. All modelling activities and simulations were conducted and executed with Abaqus Standard/Explicit including UMAT/VUMAT programming. All automation and UQ tasks including meta-modelling were conducted with Isight. Experimental validation tests were designed and conducted to specifically evaluate the functions of the device's conduit and leaflets independently. While the model realistically captured the behaviour of the leaflets, the structural response of the conduit exhibited significant discrepancies when compared to the experimental data. A subsequent, detailed root-cause-analysis identified a mismatch in the mechanical behaviour between the test coupons of the conduit and the actual conduit itself. After adjusting, conducting additional characterization, and recalibration, the validation was successfully repeated with positive results.
The hierarchal approach requires substantial work at all levels of development and complexity but is particularly useful in establishing model credibility.

2 Device Description

The Pulmonary Valve (PV) is a surgical heart-valve substitute device, comprising a conduit and three leaflets that are positioned centrally within a sinus region. Both components, conduit and leaflets, are manufactured from two individual scaffold materials, respectively, which are produced through a dedicated electro-spinning process. This process yields a very porous scaffold structure, which is facilitation the biodegradation and restauration process of the native tissue (Fig. 1).

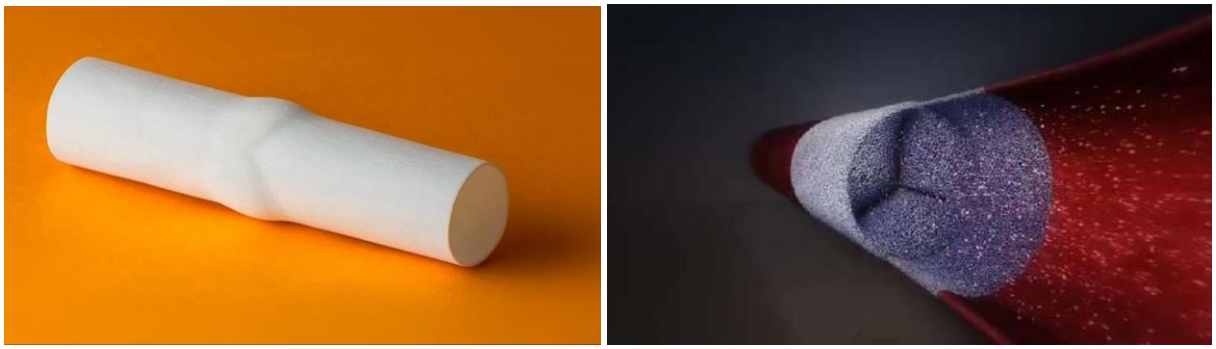

Fig. 1: Pulmonary Valve made form biodegradable scaffold (left) and the animated biodegradation and tissues restauration process (right) [2]

3 Hierarchical Modelling and VVUQ Approach

We used a hierarchical modelling and VVUQ approach [6] to build the FEM model bottom-up (Fig. 2). Three complexity levels are present in the model: material model level, component level, and assembly level. At each complexity level verification, validation, and uncertainty quantification activities were conducted. At the material model level, also calibration activities were conducted. Uncertainty factors that were identified as significant at a lower level were propagated to the higher complexity level and were considered at that stage in the UQ assessment as well. We followed the well-established ASME V&V standards [3][4][5].

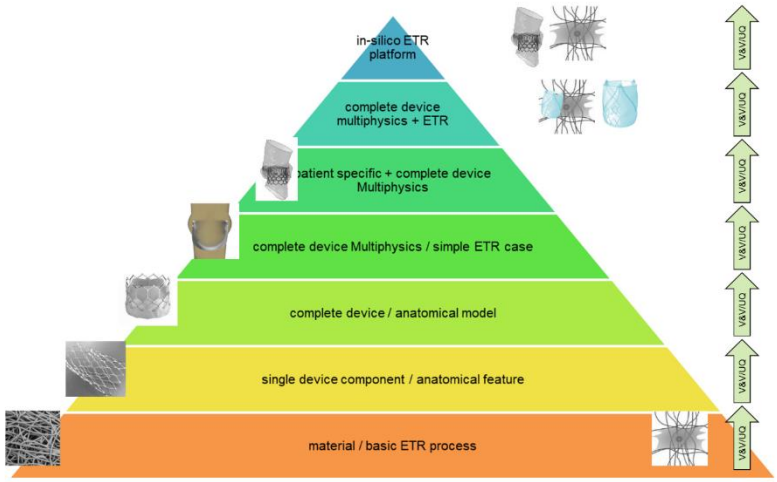

Fig. 2: Hierarchical VVUQ strategy to establish credibility for in-silico ETR platform.

4 Material Level

The VVUQ pyramid starts at the bottom with the material model level. For the PV model, two material models needed to be developed and calibrated: the leaflet and the conduit scaffold materials. Both materials are similar in their general composition and overall mechanical behaviour, while these are tuned according to performance and safety related requirements.

4.1 Material Characterization

The two scaffold materials (for leaflets and conduit) were characterized by means of uniaxial and biaxial tensile cyclic increased loading and by uniaxial stress relaxation. Material coupons were manufactured from sheets (5 samples per scaffold material and test mode) of cylindrical scaffold types following the circumferential and axial direction. Obtained stress-strain (& time) data confirm the hyperelastic, anisotropic, and viscoelastic nature of the behaviour in addition to the well pronounced Mullin's effect and plastic set point (Fig. 3). Additionally, the uniaxial and biaxial tests were conducted at several laboratories within the SimInSitu consortium as part of a Round Robin study, to assess the uncertainty originating from experimental test execution.

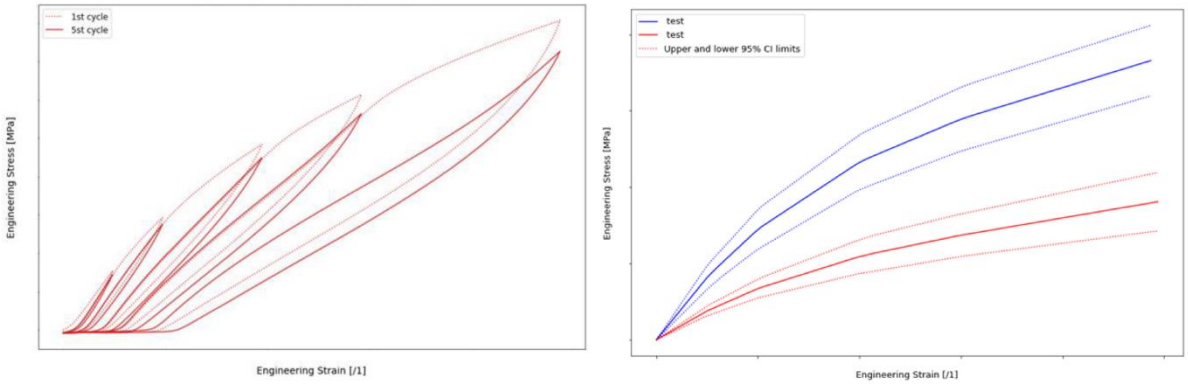

Fig. 3: Representative (filtered and averaged) experimental stress-strain curves for the scaffold material showing the characteristic material properties.

4.2 Constitutive Modelling

The hyperelastic anisotropic response of the scaffold material model is introduced by a polyconvex function expressed by the invariants of second-order structural tensors. Inelastic effects, including stress softening and permanent deformation, are expressed through a pseudo-elastic function, combined with a finite strain viscoelastic model. Moreover, the developed scaffold material model was successfully implemented in Abaqus standard user-subroutine UMAT and Abaqus explicit user-subroutine VUMAT (Fig. 4).

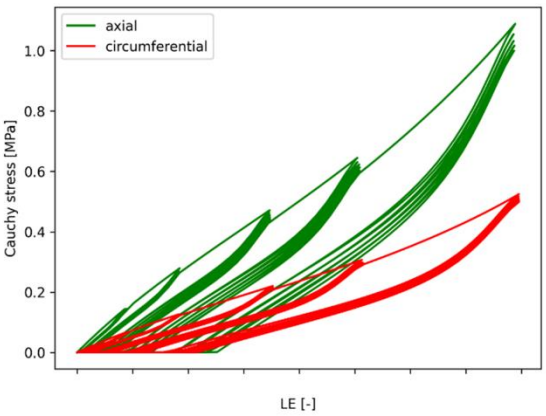

Fig. 4: representative numerical stress-strain curve for a calibrated scaffold material in axial and circumferential direction

4.3 Code and Calculation Verification

With two numerical examples, a biaxial tensile and a simple shear test, we compared the numerical solutions of Abaqus with an analytical solution of the constitutive framework. Then, a third numerical example, the so-called Cook's membrane problem, was chosen for the calculation verification to investigate the convergence of the numerical solution by using different element formulations during several mesh refinement steps. In summary, we were able to successfully carry out the planned verification activities.

4.4 Material Calibration

The parameter identification and uncertainty quantification were successfully implemented utilising a probabilistic approach, specifically through Bayesian inference. Overall, the results demonstrated good qualitative agreement between experiments and theoretical predictions, even considering the large variability in the experimental results. The model was capable of approximating various inelastic effects globally; note that, however, the quantitative agreement locally depended on the chosen calibrated stretch regime as well, as we have shown. In addition, to incorporate the uncertainties in the experimental setup, the Round Robin data were considered in the calibration.

4.5 Model Validation

For the model validation, we conducted an experimental test: the parallel plate test (Fig. 5), using five samples for each of the three types of scaffold materials. Each sample was tube-shaped, measuring either 6mm or 23mm in diameter. Additionally, we developed and implemented a computational model to simulate the parallel plate test in Abaqus. Based on the output of the computational model, a comprehensive global sensitivity analysis and uncertainty quantification was performed to identify influential parameters. Based on the results from the comparator and the computational model, we conducted a validation assessment for different sets of material parameters identified to different strain regimes: small and large strain. We achieved satisfactory validation results, although shortcomings were identified. A qualitative agreement was particularly noticeable for the larger diameter of 23 mm.

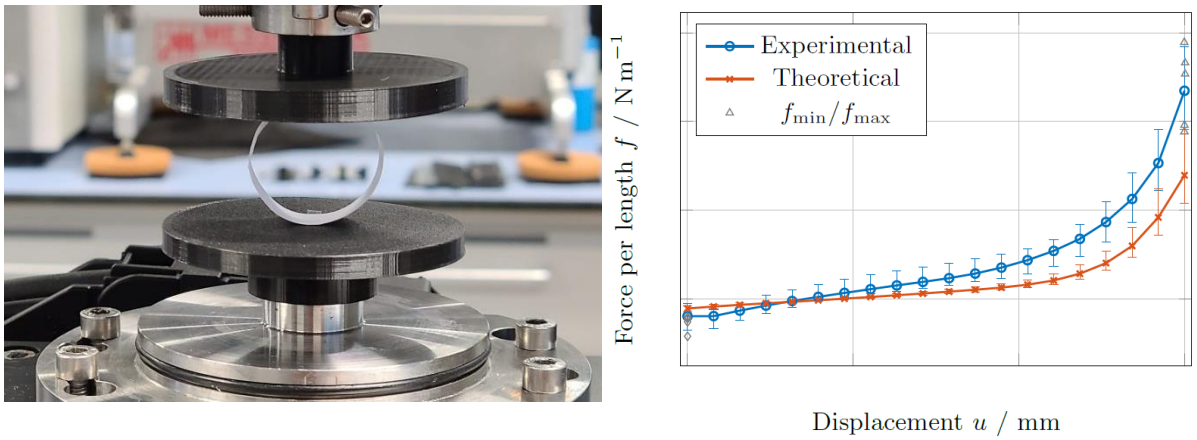

Fig. 5: Parallel Plate material validation test (left) and representative comparison between numerical and experimental force-displacement curves for a 23.0mm tube segment.

5 Device Component Level

The PV device was modelled in three relevant sizes (16/18/20mm). Both device components, conduit and leaflet, were modelled fully parametric to incorporate the needed degree of parameter flexibility. For instance, the positioning and alignment of the individual leaflets with the conduit was modelled through various positioning parameters. Likewise, the trim-position and angles were defined for the proximal and distal position. Thickness distribution and principal material direction were implemented individually through continuous field functions. The sinus shape of the conduit was introduced into the model by means of a virtual manufacturing step, where the individual leaflets imprint the final shape from the inside. All components were meshed with three-dimensional continuum elements (Fig. 6).

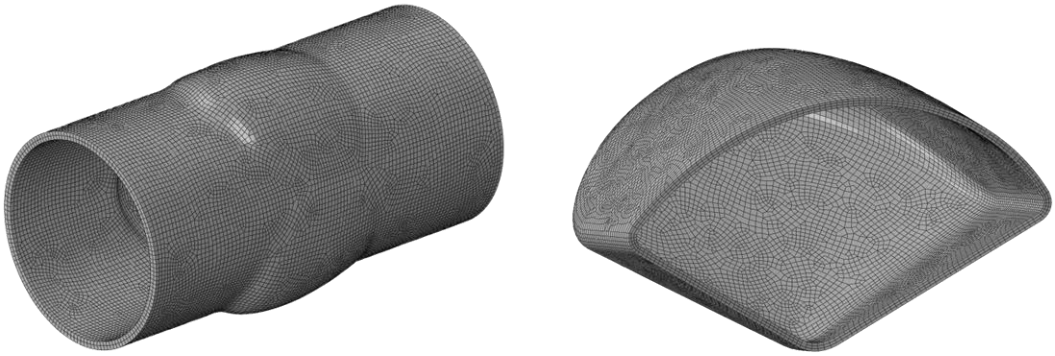

Fig. 6: FEM model of the PV-conduit comprising the sinus region (left); FEM model of one PV-leaflet (right).

5.1 Verification

Verification activities were conducted on a component level and covered all relevant credibility factors, such as code verification, discretization error (spacial and temporal), and solver error. Stress and strain development was the relevant model output and a relative error around or smaller 1% was achieved.

5.2 Validation and Uncertainty Quantification

Due the intrinsic manufacturing process of the PV, it was not possible to conduct any meaningful experimental test with the individual components. Therefore, validation and uncertainty quantification activities were conducted at the assembly level with the entire PV device.

6 Device Assembly Level

The leaflets and conduit were connected by means of tie-constraints (Fig. 7). The interface between the individual leaflets and the conduit was defined as frictionless penalty contact. Self-contact for all components was included as well. Because the PV model will be used in a later project stage within a patient-specific model of the right-heart (right ventricle outflow tract and pulmonary artery), the free end of the conduit will be connected to the corresponding native counterparts. Also, the in-vivo loading will be modelled through Fluid-Structure-Interaction with the pulsatile blood flow. At the current stage of the project, the device is considered as a stand-alone model. Therefore, the free ends of the conduit are displacement-constrained in the axial and circumferential direction. In-vivo loads are applied by means of transient pressure loads at the right-ventricle side and pulmonary outflow side. All simulations were conducted with Abaqus Explicit.

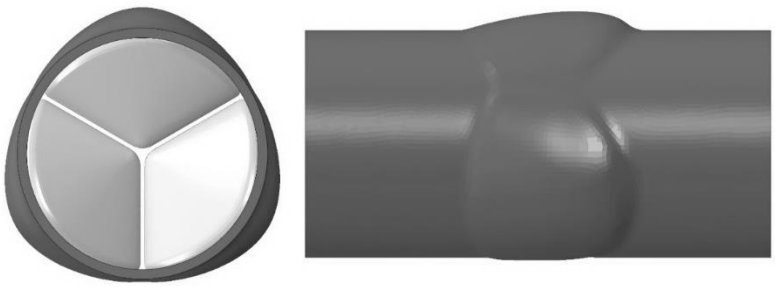

Fig. 7: The entire PV model comprising the conduit with well pronounced sinus region and the three centrally aligned leaflets.

6.1 Verification

For the assembly level verification, additional time-discretization and solver error (for example: contact parameters, mass scaling, bulk viscosity or viscous pressure) were investigated (Fig. 8) and chosen to introduce a relative error smaller than 1%.

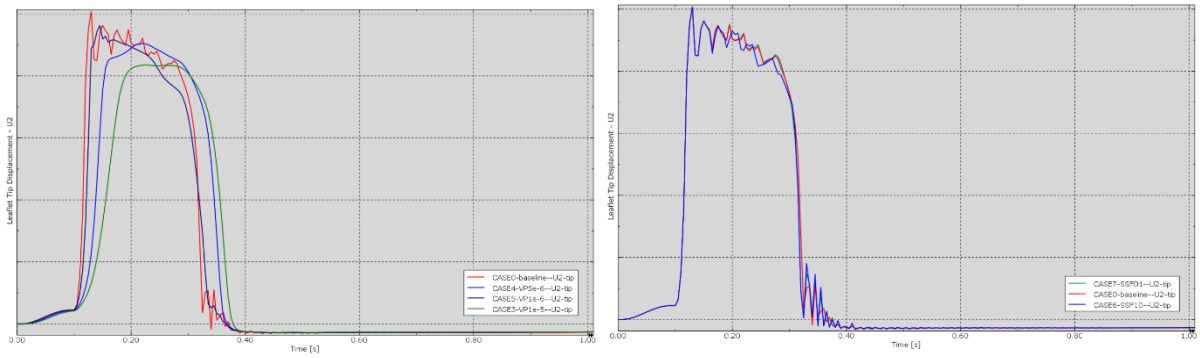

Fig. 8: transient leaflet motion (radial position: 0.0 = centre position) of a leaflet-tip as a result of varying degree of viscous pressure (left) and contact stiffness (right).

6.2 Model Validation and Uncertainty Quantification

Two comparators were defined to validate the structural response of the PV model with regards to the functions of the components. For the leaflet the opening resistance was chosen as a surrogate for Pressure Gradient, and for the conduit the parallel-plate compression stiffness as used as an indicator for the crush-resistance (Fig. 9).
Uncertainty quantification was considered in both cases and was initiated through an in-depth review-process considering all relevant uncertainty parameters (device dimensions, material properties, loading condition, etc). For each of the validation cases, meta-models (response surfaces) were constructed for the simulation output from a sufficient number of sample points and were used in subsequent Monte-Carlo-Simulations to compute the propagated output uncertainty. Obtained data points were used to assess the global probabilistic sensitivity factors as well.

6.2.1 Leaflet Opening Resistance

The opening resistance was determined by pushing a smooth cylindrical rod into the device and opening the leaflets, thereby recording the axial reaction force (Fig. 10). This was done with the FEM model and corresponding experimental tests. Tests were conducted for all three sizes with n=5 samples/tests per size. Uncertainty quantification was conducted by also considering sample alignment deviations. Experimental and simulation Cumulative Distribution Functions (CDFs) were compared by means of normalized area metric [3]. For the peak resistance force we obtained area metric values of 24.3%, 29.3% and 26.8%, for device size 16, 18, and 20, respectively (Fig. 11). These values were higher than our targeted value (10%) and are mainly driven by the difference in distribution width – the simulation CDFs have consistently a higher scatter.

6.2.2 Parallel-Plate Compression

This test was conducted by placing the PV device between two parallel plates and compressing it by a predefined amount while recording the vertical reaction force (Fig. 9). The compression resistance was measured at a given compression level (Fig. 10). Likewise, to the leaflet-test, 5 samples were tested for each device size and experimental uncertainty factors (e.g. rotational placement) were considered in the validation. For this validation we obtained area metric values for the three sizes, ranging between 51 – 63% (Fig. 11), which was unacceptably high.

6.2.3 Recalibration and Revalidation

As a consequence of this large discrepancy, an extensive root-cause analysis following the hierarchical approach from-top-to-bottom, was initiated to identify possible reasons for this deviation. The scaffold test-coupons were identified as the main source for the deviation. While the test samples were produced through a very similar manufacturing process (electro-spinning), the scaffold behaviour of the final device conduit showed a significantly different material behaviour than the coupons. After recalibration of the corresponding material models, all validation simulations were repeated and obtained validation metrices improved to an acceptable level.

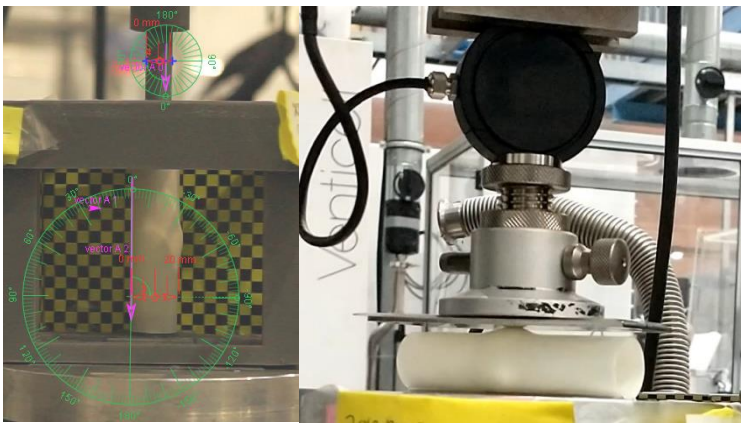

Fig. 9: Leaflet Opening Resistance Test (left) and Parallel-Plate Compression Test (right).

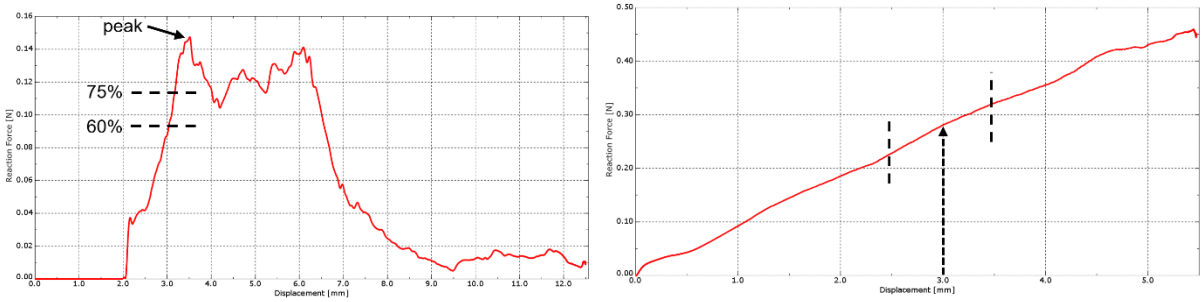

Fig. 10: exemplary reaction forces as simulated for the leaflet opening resistance (left) and parallel-plate compression (right). Dashed lines indicate the evaluation region.

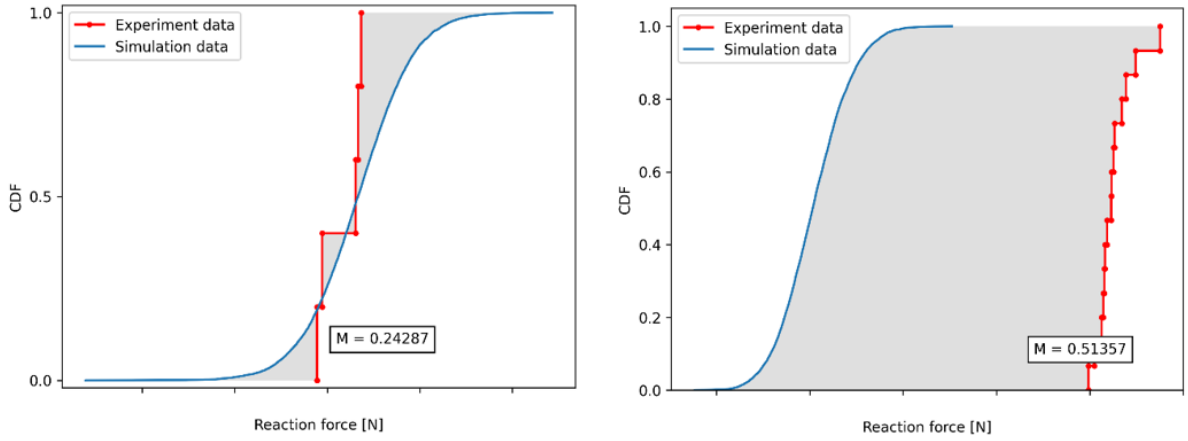

Fig. 11: Leaflet Peak Resistance (left) and Conduit Compression Resistance (right) showing the area metric as the grey are between the simulation and experimental CDF, respectively.

7 Conclusions

Within the SimInSitu project we implement a hierarchical VVUQ approach to develop an in-silico platform to simulate the heart valve performance in a virtual patient environment while also considering the biodegradation & restauration process of in-situ tissue engineered heart valve devices. The presented data represent the development-stages up the complexity level-3 and we show that VVUQ process, though demanding and tedious, is helping to establish a thorough model credibility and supports a structured root-cause analysis and identification.

8 References

[1] EU Project: SimInSitu, GA No. 101017523
[2] Xeltis BV
[3] ASME V&V-10 2019
[4] ASME V&V-20 2009
[5] ASME V&V-40 2018
[6] Oberkampf & Roy, Verification and Validation in Scientific Computing. ISBN 9781139813761

Konsolidierung von Materialkarten für die FEM-Simulation mit unterschiedlichen CAE-Systemen

Uwe Diekmann, Constantin Bunge (Matplus GmbH)

Thies Marwitz (Matplus GmbH)

Alex Miron (Matplus GmbH

1 Zusammenfassung

In großen Unternehmen mit verteilten Entwicklungs- und Fertigungsprozessen existiert eine Vielfalt von Systemlandschaften für Computer-Aided Engineering (CAE). Diese Diversität führt oft zu heterogenen Werkstoffbezeichnungen und Standards, was die interdisziplinäre Zusammenarbeit und den effizienten Datenaustausch erheblich erschwert. Ein einheitliches Verständnis und die Nutzung von Werkstoffdaten ist oft begrenzt, sodass die Prozesseffizienz in der Produktentwicklung beeinträchtigt wird.

Lösungsansatz ist die Schaffung eines übergeordneten "Material Master", der die Herausforderungen heterogener Systemlandschaften und Werkstoffstandards überwinden soll. Dieser zentrale Datensatz soll standortübergreifend konsistente und umfassende Informationen zu jedem Werkstoff bereitstellen. Aus diesem Master-Datensatz können dann die spezifischen Materialkarten für die individuellen CAE-Systeme generiert werden. Ein Schritt dabei ist die Harmonisierung von Einheitensystemen, Benennungen und Modellen. Der Fokus liegt auf der Schaffung einer systemneutralen Basis, die eine effiziente Parametrisierung und das Modellierung ermöglicht.

Anhand eines praktischen Beispiels wird gezeigt, wie Materialkarten aus LS-Dyna in ein systemneutrales Format importiert und für die Verwendung in Pamcrash aufbereitet werden können. Dieser Prozess umfasst die Abbildung der Materialmodelle durch konstitutive Gleichungen, die eine flexible Anwendung über verschiedene CAE-Systeme hinweg ermöglichen. Die Kommunikation erfolgt dabei durch offene REST-Schnittstellen, die auch von übergeordneten Pre-Prozessoren genutzt werden können. Das Multi-CAE Roundtripping von Materialkarten kann die Übertragbarkeit und Kompatibilität von Materialdaten zwischen unterschiedlichen Simulationsumgebungen signifikant verbessern.

Die Konsolidierung von Materialkarten für die FEM-Simulation stellt einen effektiven Weg dar, um die Herausforderungen heterogener CAE-Systemlandschaften und Werkstoffstandards in großen Unternehmen zu adressieren: Aufwände für die Erstellung von Materialkarten können reduziert und gleichzeitig Fehlerquellen minimiert werden. Zudem können Werkstoffauswahlprozesse durch Visualisierung der Modelle und Kurven optimiert werden. Der dargestellte Lösungsbaustein ist Teil eines umfassenderen Gesamtsystems für ein unternehmensweites Wissensmanagement für Werkstoffe.

Dieses System umfasst neben der Konsolidierung von Materialkarten weitere Themenfelder wie Stammdatenmanagement, Werkstoffsimulation, Integration und Auswertung von Werkstoffqualifikationsprojekten.

2 Problemstellung und Zielsetzung

2.1 Heterogenität in der Systemlandschaft

In multinationalen Unternehmen variieren die verwendeten CAE-Systeme oft von Standort zu Standort. Diese Unterschiedlichkeit resultiert in einer fragmentierten Datenhaltung und inkompatiblen Prozessen zur Werkstoffauswahl,-anwendung und -berechnung.

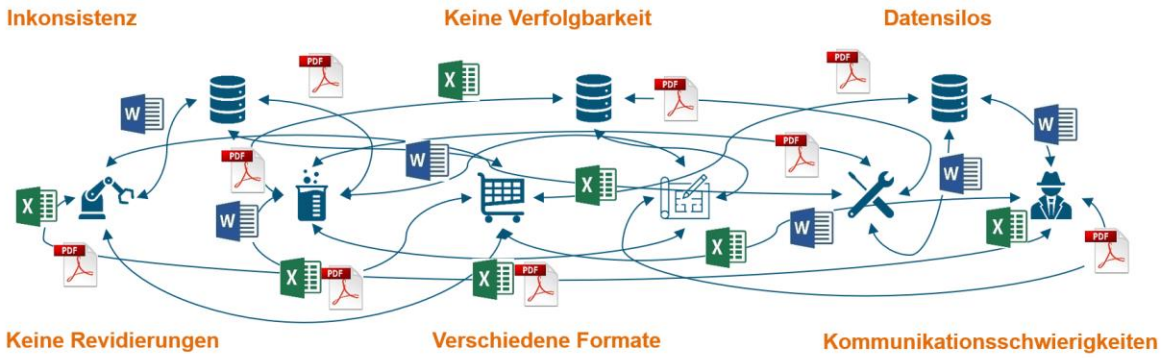

Abb. 1
Datenvielfalt in Unternehmen

2.2 Herausforderungen in der Werkstoffstandardisierung

Die unterschiedlichen Bezeichnungen und Standards für Materialien verhindern eine einheitliche Datenverwaltung und -nutzung. Diese Problematik führt zu ineffizienten Prozessen, erhöhtem Aufwand bei der Datenpflege und potenziellen Fehlern in der Materialauswahl.

2.3 Anforderungen an eine integrierte Lösung

Die Lösung muss:

- Einen einheitlichen und systemübergreifenden Datensatz für Werkstoffe bereitstellen.
- Die Konvertierung und Nutzung von Materialdaten zwischen verschiedenen CAE-Systemen ermöglichen.
- Flexibel genug sein, um Anpassungen an spezifische Unternehmensbedürfnisse zu erlauben.
- Eine offene und erweiterbare Architektur bieten, die die Integration neuer Materialdaten und Standards unterstützt.

Das Hauptziel unserer Arbeit ist die Entwicklung eines "CAE-Materialdatenpools" in der Matplus EDA®-Umgebung, der als zentrale Datenquelle für alle Materialinformationen dient und von allen CAE-Systemen im Unternehmen genutzt werden kann. Dieser Master soll:

- Standortübergreifende Konsistenz in den Materialbezeichnungen und -eigenschaften gewährleisten.
- Die Erstellung und Pflege von Materialkarten standardisieren und vereinfachen.

Die Prozesseffizienz durch verbesserte Werkstoffauswahl und -anwendung steigern.

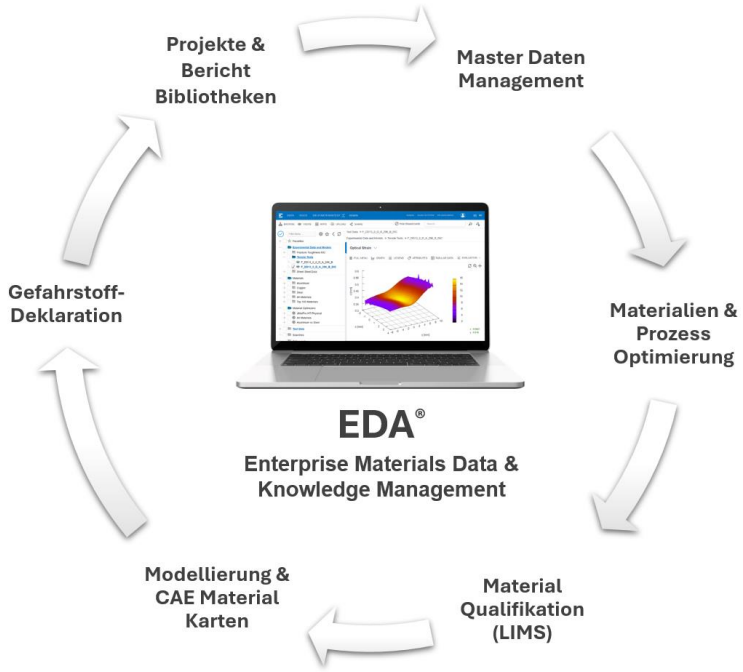

Abb. 2
Materialdaten und Wissensmanagement mit Matplus EDA®

3 Lösungsansatz und Implementierung

Der CAE-Materialdatenpool wird als systemneutrale Struktur auf Basis von Matplus EDA® entwickelt. Das von Anwendern erweiterbare System basiert auf ausgereiften FOSS (Free and Open Source Software) Komponenten, wie MongoDB, Python, Django.

JSON (JavaScript Object Notation) ist das grundlegende interne Datenformat. Die Vorteile von JSON sind:

- **Leichtgewichtig und flexibel**: JSON ist ein textbasiertes Format, das weniger Speicherplatz benötigt als andere Formate wie XML. Es ist leicht zu lesen und zu schreiben, sowohl für Menschen als auch für Maschinen.
- **Interoperabilität**: Da JSON von den meisten Programmiersprachen und Plattformen nativ unterstützt wird, erleichtert es die Datenintegration über verschiedene Systeme und Technologien hinweg.
- **Erweiterbarkeit**: JSON-Strukturen können einfach erweitert werden, um neue Datenfelder oder komplexe Datentypen ohne Unterbrechung der bestehenden Systeme zu integrieren.

Speziell für CAE-Anwendungen und Materialkarten sind Fließkurven von großem Interesse. Diese lassen sich in Form von parametrischen Arrays innerhalb des JSON-Formats speichern:

- **Kompakte Speicherung**: Parametrische Darstellung von Fließkurven reduziert den benötigten Speicherplatz, indem nur wesentliche Parameter statt kompletter Datensätze gespeichert werden.
- **Einfache Anpassung und Skalierung**: Die parametrischen Modelle in EDA® ermöglichen es, Materialverhalten unter verschiedenen Bedingungen leicht zu simulieren und zu analysieren, indem Parameter dynamisch angepasst werden.

Eine Mapping-Engine ermöglicht es, die Attribute und Einheiten zwischen den verschiedenen CAE-Systemen automatisch zu mappen. Diese Engine verwendet das JSON-Format und das Metadaten-Verzeichnis, um festzustellen, welche Attribute und Einheiten konvertiert werden müssen und tut dies automatisch, um Kompatibilität zu gewährleisten. Die Mapping-Engine beinhaltet Funktionen zur automatisierten Konversion und Synchronisation von Materialdaten zwischen den Systemen. Dadurch wird sichergestellt, dass alle Systeme Zugriff auf die neuesten und korrekt konvertierten Daten haben.

Die flexible Implementierung des Systems ermöglicht Anpassungen an spezifische Unternehmensbedürfnisse und technologische Entwicklungen. Die JSON-Objekte und das Metadaten-Verzeichnis sind leicht erweiterbar, um neue Attribute, Einheiten und CAE-Systeme integrieren zu können.
Die Integration erfolgt über offene REST-Schnittstellen, die eine flexible Anbindung an verschiedene CAE-Systeme ermöglichen. Dies unterstützt den reibungslosen Austausch von Materialdaten und fördert die Kollaboration zwischen den Teams.

Die Visualisierung und Analyse der Materialdaten ist entscheidend für die effektive Nutzung des Material Masters. Die Verwendung von SciPy und Vega für diese Aufgaben bietet mehrere Vorteile:

- **SciPy**: Diese Python-basierte Bibliothek bietet robuste Funktionen zur numerischen Integration, Optimierung und statistischen Analyse. SciPy ist ideal für die Bearbeitung und Analyse von parametrischen Daten der Materialmodelle, insbesondere für die Anpassung und Auswertung von Fließkurven.
- **Vega**: Als deklarative Sprache zur Erstellung, Speicherung und Freigabe interaktiver Visualisierungen ermöglicht Vega die effiziente Darstellung komplexer Materialdaten. Die Visualisierungen können leicht in Webanwendungen integriert werden, was die Zugänglichkeit und Nutzbarkeit der Daten verbessert.

3.1 Praktisches Beispiel: Implementierung in LS-Dyna und Pamcrash

An einem praktischen Beispiel wird die Umsetzung des Material Masters demonstriert, indem Materialkarten aus LS-Dyna in ein systemneutrales Format konvertiert und für die Verwendung in Pamcrash aufbereitet werden. Dieses Beispiel illustriert die Übertragbarkeit und Anwendbarkeit des Material Masters über verschiedene Simulationssysteme hinweg.

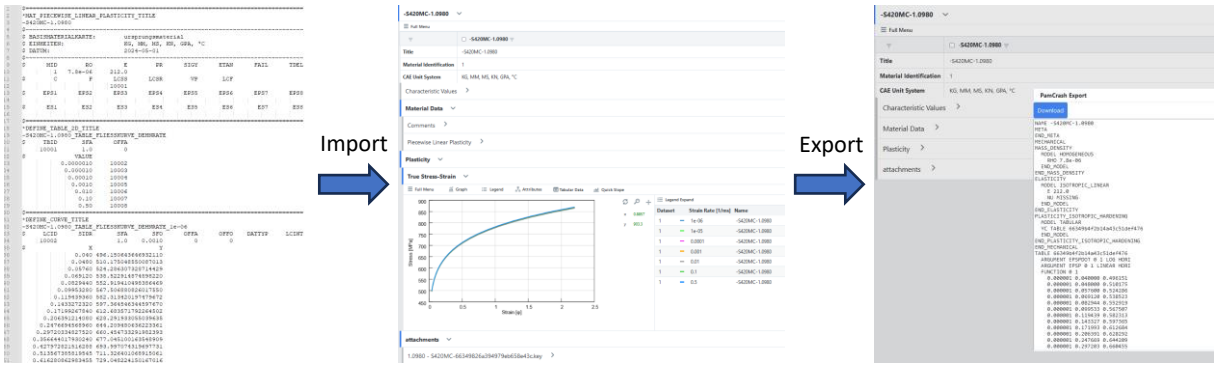

Abb. 3
Anwendung des Material Masters für verschiedene Simulationssysteme

4 Schlussfolgerung und Ausblick

Die Implementierung eines CAE-Materialdatenpools unter Nutzung von JSON, parametrischen Arrays und fortschrittlichen Visualisierungs- und Analysetools stellt eine umfassende Lösung dar, die nicht nur die Herausforderungen heterogener CAE-Systemlandschaften adressiert, sondern auch die Grundlage für weiterführende Innovationen im Bereich der Materialwissenschaft und Fertigungstechnik legt. Zukünftige Entwicklungen könnten die Integration zusätzlicher Datenquellen, die Erweiterung der Analysefunktionen und die Verbesserung der Benutzerinteraktion umfassen, um die globale Zusammenarbeit und Effizienz in multinationalen Unternehmen weiter zu steigern.

5 Referenzen

[1] U. Diekmann, A. Miron, and I. Alperovich, “Towards integration of advanced material models of steels into digital product development,” presented at the Steels in Cars and Trucks, Mailand: VDEh, Jan. 2021
[2] U. Diekmann, A. Miron, and A. Trasca, “Hybrid Modeling of Materials Properties for Improved CAE-Simulations,” in Materials Science Forum, Trans Tech Publ, 2016, pp. 163–166

[3] U. Diekmann, “Werkstoffdaten als Klaviatur der Technologie,” IT&Production, Marburg, Feb. 03, 2022. Accessed: Mar. 08, 2022. [Online]. Available: https://www.it-production.com/onlinefachbeitrag/werkstoffdaten-als-klaviatur-der-technologie/
[4] U. Diekmann, “Integration and processing of material property data to create material cards,” presented at the NAFEMS World Congress 2021, Salzburg, Oct. 27, 2021

Integrating of Carbon Footprint into Material Selection within the CAE Simulation Chain

Daniel Trost, Prof. Dr. Viktor Pocajt, Total Materia AG, Zürich, Switzerland

1 Summary

This paper describes the implementation of integration of carbon footprint calculation into the material selection process in the context of CAE simulations and product design. By analyzing the carbon footprint of various ferrous and non-ferrous alloys, the research underscores the critical role of chemical composition in understanding and mitigating environmental impacts. Moreover, the study emphasizes the need for informed materials selection to identify alternatives with lower carbon footprints while maintaining necessary structural requirements, mechanical and physical properties. It explores possibilities for selecting greener alternatives, both in the early design phase and in replacing the existing materials. Results also indicated significant variations in carbon emissions based on factors such as manufacturing routes, recycled content, location and transport type. Overall, the article underscores the importance of integrating environmental considerations into CAE simulations and product design to achieve sustainability goals.

2 Introduction

According to Green Deal [1], the EU has taken an ambitious goal of reducing greenhouse gas (GHG) emissions by at least 50% by 2030, whilst Germany set a yet more aggressive goal of reducing GHG emissions by 65% [2]. This has been supported by a set of new regulations, such as The Corporate Sustainability Reporting Directive (CSRD) [3], which introduces mandatory sustainability reporting for all enterprises, and the Carbon Border Adjustment Mechanism (CBAM) [4], aimed to stop carbon leakage and put a fair price on the carbon emitted during the production of carbon-intensive goods that are entering the EU. Complete supply chains, regardless of the location of participants, will therefore need to adapt their activities quickly to these regulations, starting from the initial conceptualization and design of a product till the end of its life.

On the other hand, materials with their production and processing represent a major contributor to GHG emissions, with an increase of 120% from 5 billion metric tons CO2-equivalent (GtCO2e) in 1995 to 11Gt in 2015, raising their share of the global total from 15 to 23%, with forecasted further increase. In most cases, materials are by far the biggest contributor to the product's carbon footprint, at least until the product has been produced [5].

The importance of accurate and optimal material selection in the early phases of product design and CAE (Computer Aided Engineering) simulations can never be overstated. Besides classical engineering considerations such as mechanical performance and cost, new aspects need to include carbon footprint (CF) and environmental impact, as well as lightweight optimization, compliance with regulations, and optimizing sourcing and supply chain, in order to optimize related emissions.

Therefore, the sustainable product design incorporates Life Cycle Assessment (LCA) of materials using selected indicator(s) providing environmental impact to materials selection, e.g. in automotive industry ranking (c) is often calculated as $c = 0.4 \cdot mass + 0.2 \cdot cost + 0.4 \cdot CF$ [6].

Other more complex decision-making models for materials selection are proposed [7], making the need for reliable and simplified calculation of CF value for thousands of diversified structural materials from carbon and stainless steel, to special alloys, nonferrous metals and polymers, considering their manufacturing routes, processing, finish and transport. A full LCA study is demanding in terms of both data collection efforts and user expertise requirements, while streamlined LCA often uses generic data related to the materials production, energy used for their processing and transportation [8]. Typically, streamlined LCA uses only a fraction of the inputs to estimate carbon footprint compared to the full LCA inventory [9].

This paper presents recent developments designed to help engineers in the CAE simulation field to cope with these challenges.

3 Streamlined LCA Methodology

There are numerous simplification approaches in LCA, whereby here will be described approach that combines the composition of alloys with carbon footprint values of base metal and alloying elements production [10-12]. The LCA tool described in the current study (Figure 1) can cover a variety of ferrous and non-ferrous alloys due to the use of:

- chemical compositions from a large database containing structural material properties (Total Materia Horizon [13]) which comprises more than 500,000 materials, and
- country, manufacturing route, processing, and transport-specific life cycle inventory (LCI) collected from Ecoinvent v3.10 [14], along with relevant data from scientific articles.

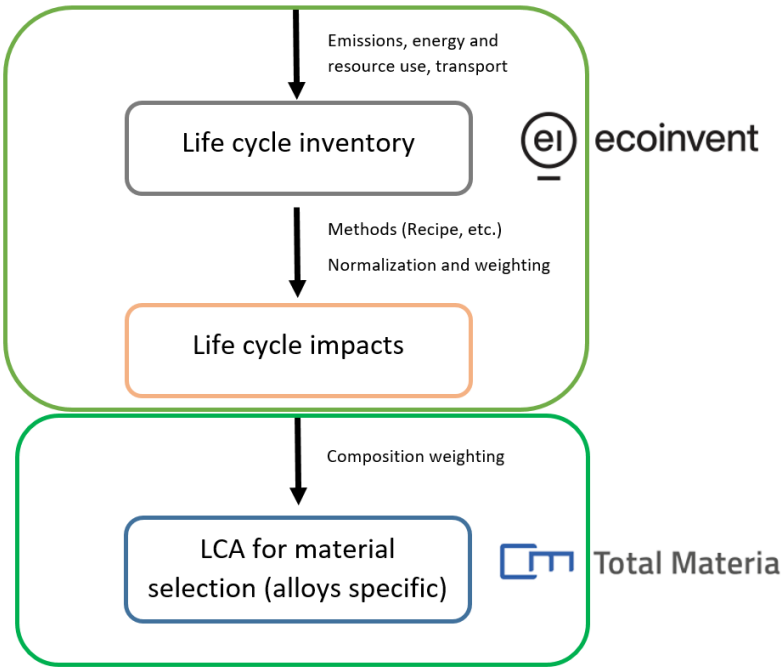

Fig 1. LCIA assessment approach.

3.1 Goal, Scope, Functional unit and System boundaries

The aim of this LCA is to quantify the impact of steel and various non-ferrous alloys (Al, Cu, Mg, Ni and Ti based) according to ISO 14040 standards [15], analyzing the influence of the composition on the carbon footprint.

The functional unit has been defined as 1 kg of produced material, considering the country of manufacturing and processing as well as transport to the buyer's gate.

The scope of this research, as shown in Figure 2, is to estimate the environmental impact of the production and the transport of materials (cradle to gate), accounting for raw materials extraction, manufacturing, and processing.

3.2 Inventory data and impact category

Ecoinvent's Life Cycle Inventory Assessment (LCIA) datasets if available, were used where possible including:

- Datasets for base metals
- Datasets for alloying elements, utilized in the manufacturing calculation through chemical composition weighting
- Datasets for processing, quantified in kg CO2-eq per kg of material, per kg of removed material, or per m^2, varying with the type of processing
- Datasets for the energy mix, allowing country-specific calculation
- Datasets for transport, covering a wide range of transport routes

Calculations are based on the Allocation at the Point of Substitution (APOS) system model, the IPCC 2021 no LT LCIA method, and the Climate change – Global Warming Potential (GWP100) indicator. A simplified calculation example is given in Figure 3 as an illustration of the applied method.

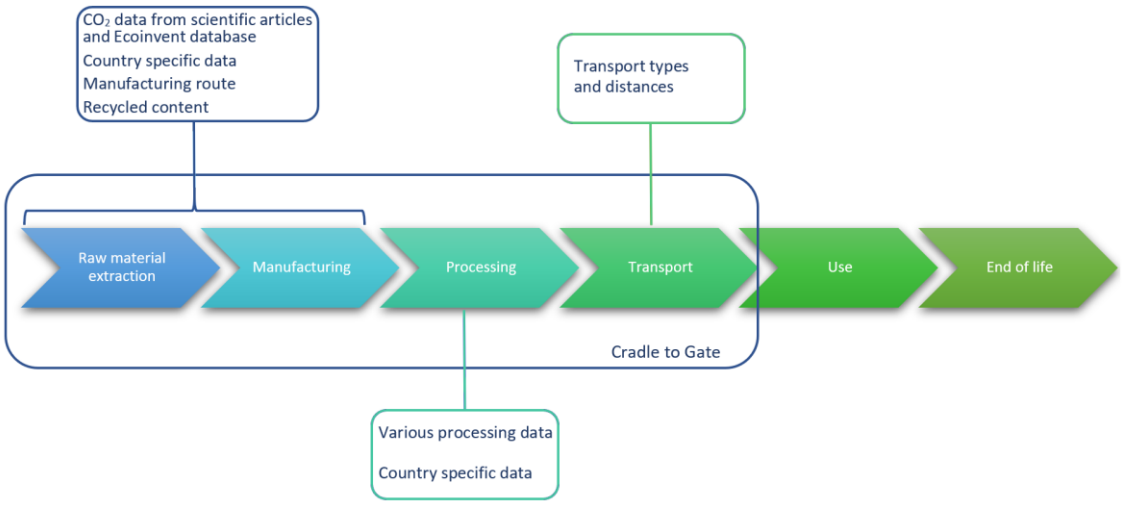

Fig 2. System boundaries.

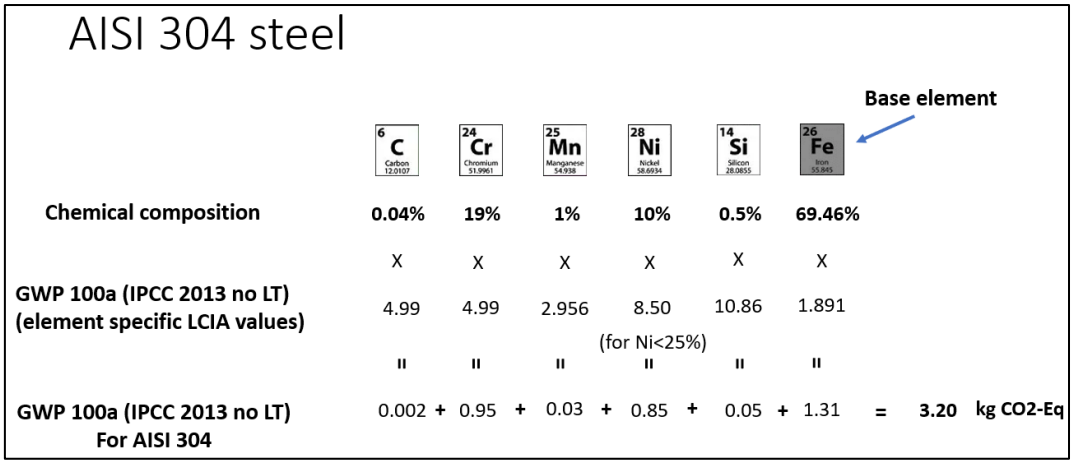

Fig 3. An example of CF calculation based on LCIA data for 304 steel.

Additional sources were used from scientific literature [16-18] for data not available in Ecoinvent, expanding the calculation scope with:

- Scrap content adjustment
- Manufacturing contributions from various countries/regions
- Contributions from different manufacturing routes
- Various processes in different countries/regions

For intensive electricity-consuming processes such as hot rolling, cold rolling, and stamping, electricity consumption data (measured in MJ/kg or kWh/kg) has been collected. This data, combined with the energy mix information from Ecoinvent, contributes to the final calculation.

The final CO2-eq score is the cumulative sum of contributions from material production (manufacturing), processing, and transport.

4 Analysis CF Results

In this work, six different alloys that are commonly used have been selected for the carbon footprint analysis. The chemical composition of alloys is defined by specific standard, while details on studied alloys production are presented in Figure 4.

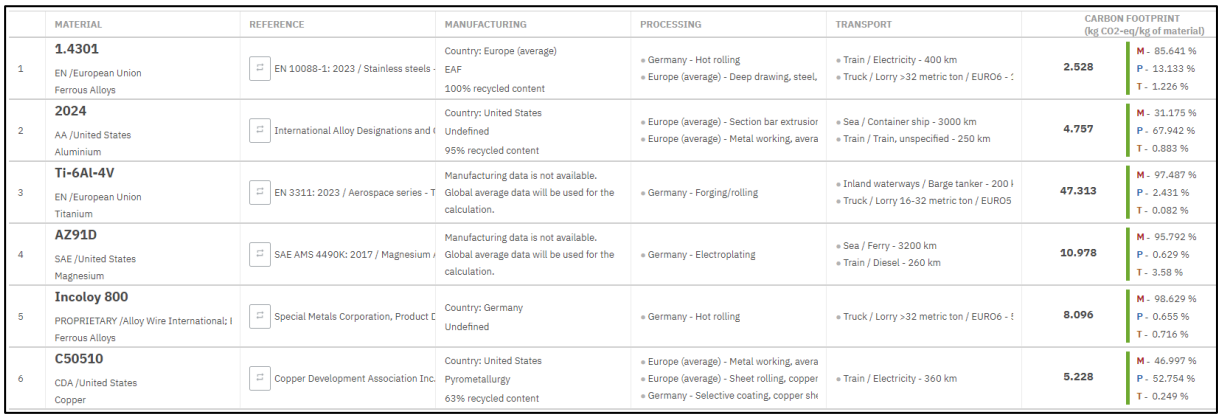

	MATERIAL	REFERENCE	MANUFACTURING	PROCESSING	TRANSPORT	CARBON FOOTPRINT (kg CO2-eq/kg of material)	
1	**1.4301** EN /European Union Ferrous Alloys	EN 10088-1: 2023 / Stainless steels -	Country: Europe (average) EAF 100% recycled content	• Germany - Hot rolling • Europe (average) - Deep drawing, steel,	• Train / Electricity - 400 km • Truck / Lorry >32 metric ton / EURO6 -	**2.528**	M - 85.641 % P - 13.133 % T - 1.226 %
2	**2024** AA /United States Aluminium	International Alloy Designations and	Country: United States Undefined 95% recycled content	• Europe (average) - Section bar extrusion • Europe (average) - Metal working, avera	• Sea / Container ship - 3000 km • Train / Train, unspecified - 250 km	**4.757**	M - 31.175 % P - 67.942 % T - 0.883 %
3	**Ti-6Al-4V** EN /European Union Titanium	EN 3311: 2023 / Aerospace series - T	Manufacturing data is not available. Global average data will be used for the calculation.	• Germany - Forging/rolling	• Inland waterways / Barge tanker - 200 • Truck / Lorry 16-32 metric ton / EURO5	**47.313**	M - 97.487 % P - 2.431 % T - 0.082 %
4	**AZ91D** SAE /United States Magnesium	SAE AMS 4490K: 2017 / Magnesium /	Manufacturing data is not available. Global average data will be used for the calculation.	• Germany - Electroplating	• Sea / Ferry - 3200 km • Train / Diesel - 260 km	**10.978**	M - 95.792 % P - 0.629 % T - 3.58 %
5	**Incoloy 800** PROPRIETARY /Alloy Wire International; Ferrous Alloys	Special Metals Corporation, Product D	Country: Germany Undefined	• Germany - Hot rolling	• Truck / Lorry >32 metric ton / EURO6 -	**8.096**	M - 98.629 % P - 0.655 % T - 0.716 %
6	**C50510** CDA /United States Copper	Copper Development Association Inc.	Country: United States Pyrometallurgy 63% recycled content	• Europe (average) - Metal working, avera • Europe (average) - Sheet rolling, copper • Germany - Selective coating, copper sh	• Train / Electricity - 360 km	**5.228**	M - 46.997 % P - 52.754 % T - 0.249 %

Fig 4. Result of CF calculation for selected alloys.

After specifying details on manufacturing (country, method, and recycled content), processing (country and processing applied), and transport (type and distance), the values of Carbon Footprint are determined for each alloy (Figure 4), providing the contribution of each stage of analysis.

The lowest environmental impact of all studied alloys has steel 1.4301 with a value of 2.5 kg CO2-eq/kg. As a manufacturing route for 1.4301 alloy is selected EAF (Electric Arc Furnace) with 100% recycled content, where electricity is used to melt scrap steel and produce new steel, in contrast to BF-BOF (Blast Furnace-Basic Oxygen Furnace) where extraction of iron ore is needed and relies heavily on coal or coke as a fuel source for the blast furnace, which emits significant amounts of CO2 during combustion. Although numerous factors or variables play a role in determining the environmental impacts of metal production, one of the most significant parameters is recycled content.

Titanium alloy has the highest environmental impact of all studied alloys: emits up to 47.3 kg CO2-eq/kg of material. Ti-6Al-4V alloy is selected for this study even though it is very expensive and has a high energy consumption of production in the long and demanding Kroll process, because it is one of the most popular joint implant materials due to its biocompatibility, low density, and strength.

Although Al, Cu, and Fe-Ni-based alloys have similar CF values (4.7 to 8 kg CO2-eq/kg), it can be observed that in the case of aluminum and copper alloys, the most significant contribution comes from the processing of those alloys (52 to 68%) unlike Incoloy which processing contribute with modest 0.72%. It can be seen that the CF value for Incoloy 800 is three times greater than 1.4301 alloy. The high environmental impact of Incoloy 800 is mainly caused by nickel content (max. 10% in 1.4301 alloy, while max. 35% in Incoloy 800) and very high carbon footprint values for nickel itself. And this is proof of why chemical composition cannot be neglected.

The effect of transportation is very small with a contribution of up to 3.6% in Figure 4 for the selected transport parameters. However, it can have a much higher relative contribution for low-impact alloys, especially for long distances. Figure 5 shows the effect of different transport types and it can be seen that the selection of air transport can double the carbon footprint value of the material compared to sea transport (for the same manufacturing and processing parameters).

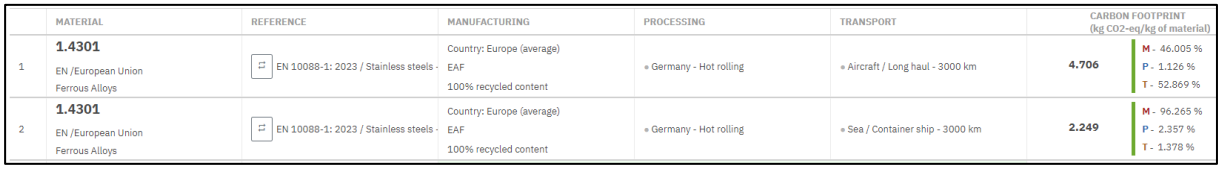

	MATERIAL	REFERENCE	MANUFACTURING	PROCESSING	TRANSPORT	CARBON FOOTPRINT (kg CO2-eq/kg of material)	
1	**1.4301** EN /European Union Ferrous Alloys	EN 10088-1: 2023 / Stainless steels -	Country: Europe (average) EAF 100% recycled content	• Germany - Hot rolling	• Aircraft / Long haul - 3000 km	**4.706**	M - 46.005 % P - 1.126 % T - 52.869 %
2	**1.4301** EN /European Union Ferrous Alloys	EN 10088-1: 2023 / Stainless steels -	Country: Europe (average) EAF 100% recycled content	• Germany - Hot rolling	• Sea / Container ship - 3000 km	**2.249**	M - 96.265 % P - 2.357 % T - 1.378 %

Fig 5. Effect of different transport types.

Further contribution analysis can be made for each alloy giving the detailed contribution for manufacturing, and each processing step as well as transportation type, as shown in Figure 6 for the 1.4301 steel. Results show that deep drawing increases CF with factor of 5 in comparison with hot rolling, which suggests that this and similar processes should be performed on locations having energy supplied from renewable sources.

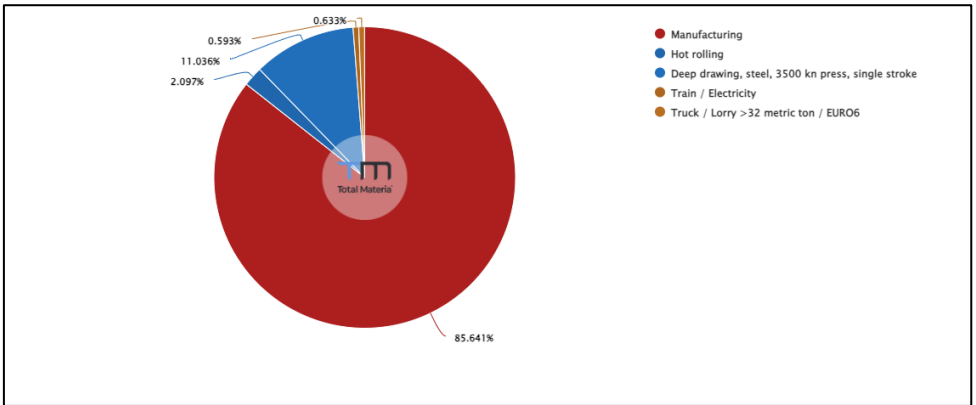

CONTRIBUTIONS	KG CO2-EQ/KG OF MATERIAL	% OF TOTAL CONTRIBUTION
Manufacturing - Europe (average); EAF; 100% Recycled content	2.165	85.641
Processing (2)	0.332	13.133
Germany - Hot rolling	0.053	2.097
Europe (average) - Deep drawing, steel, 3500 kn press, single stroke	0.279	11.036
Transport (2)	0.031	1.226
Train / Electricity - 400 km	0.015	0.593
Truck / Lorry >32 metric ton / EURO6 - 150 km	0.016	0.633

Fig 6. Detailed contribution analysis for 1.4301 steel.

5 Material selection and looking for a greener alternative

Besides finding more environmentally sustainable manufacturing processes (different manufacturing routes, higher scrap content, different locations), lower energy demand additional processing and greener transportation alternatives, another approach in reducing the Carbon Footprint is to find alternative materials (different chemical composition), but having similar mechanical and physical properties.

Although the selection of alternative materials must take into consideration various factors related to the availability, supply chain, etc., from the environmental point of view the decision can be facilitated by using a proper cross-reference system that simultaneously suggests alternatives based on various criteria. There are two scenarios for material selection:

1) In the early design phase when the material is still not selected and when certain mechanical and physical requirements should be fulfilled;
2) When certain material already in use should be replaced with greener alternative, but keep the same characteristics.

In the first case, Total Materia Advanced Search can be used, where the user can simply set up the needed criteria and obtain the list of materials that fulfill the requirements, Figure 7.

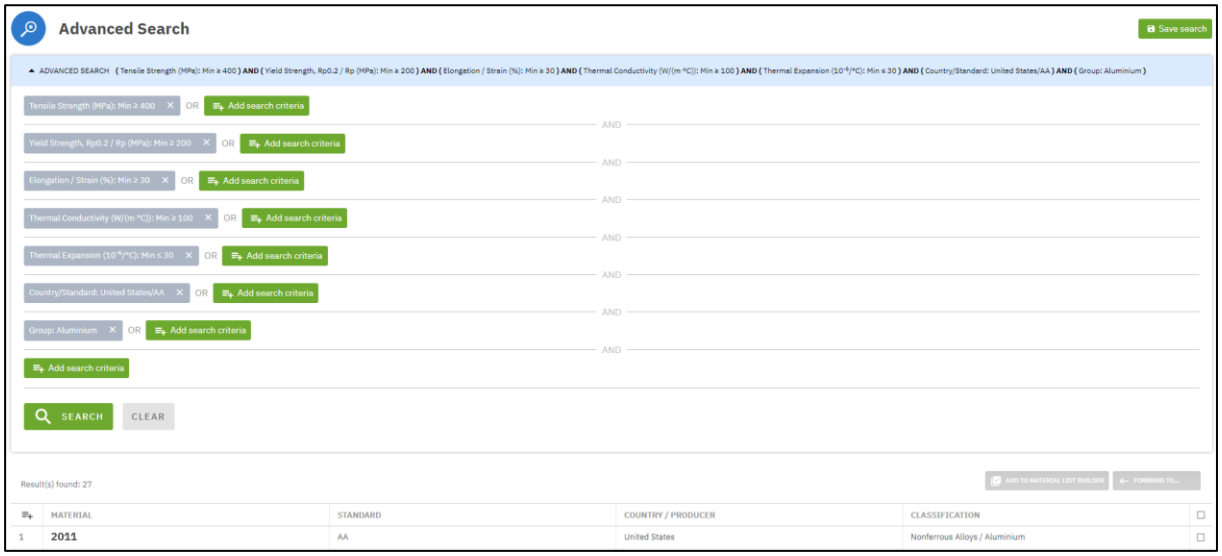

Fig 7. Setting desired parameters for search

Furthermore, the obtained list of materials should be forwarded to Total Materia Carbon Footprint, a specialized product where the user can easily calculate the environmental impact of selected materials, compare the CF values, and find the best option. In the example from Figure 7, the resulting 27 aluminum materials are forwarded to Carbon Footprint, and their CF values are calculated without any processing and transport, while for manufacturing are used global average data. This is done in order to find the material with the lowest CF value based on chemical composition. Among these 27 materials, CF values varied from 6.0 to 6.8 kg CO2-eq/kg, and the material with the lowest value of 6.0 kg CO2-eq/kg was selected.

In the second case, when the material is already in use, finding an alternative material with a lower CF value is possible in Total Materia Carbon Footprint module through the cross-reference option. The system offers alternatives based on various criteria. As an example for this case, 1.4301 alloy is used with all set-up parameters from Figures 4 and 6 (with CF value of 2.528 kg CO2-eq/kg). In Figure 8 it can be seen that this analysis suggests 921 alternative materials ordered by CF value in ascending order. In this view user can add additional columns with mechanical and physical properties to ensure that the material also fulfills the required characteristics. In this example, material NSSC 2120 meets the required mechanical and physical criteria, and the carbon footprint value is reduced from 2.5 to 2.2 kg CO2-eq/kg (which is a reduction of 12%) compared to the initially selected material 1.4301.

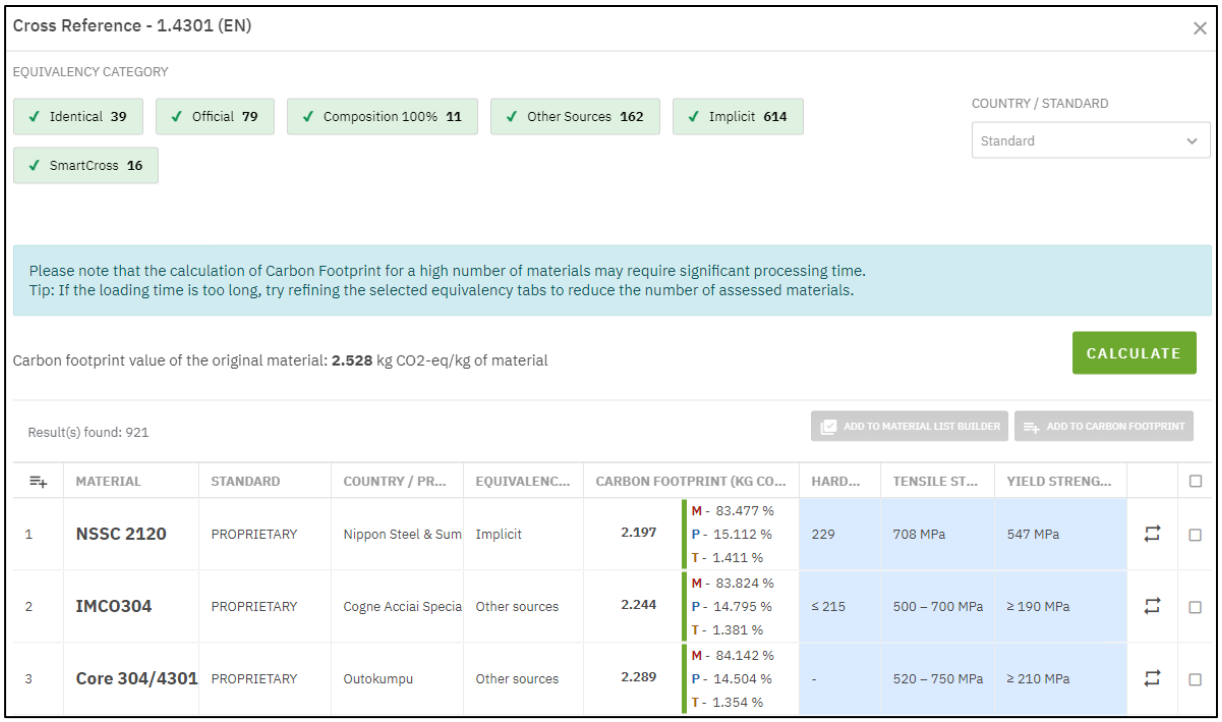

Fig 8. Alternatives to 1.4301 steel based on cross reference.

6 Conclusions

This work describes the approach of using the material composition and relevant processes, in order to accurately assess the environmental impact of ferrous and non-ferrous alloys, on the example of carbon footprint. This enables engineers not just to compare these alloys solely on cost or mechanical/physical attributes but also to evaluate carbon footprint, and thereby making more informed choice concerning the material selection. The described approach also provides the possibility to find more environmentally friendlier manufacturing processes (different manufacturing routes, higher scrap content, different locations), lower energy demand additional processing, and greener transportation alternatives in the early phases of product design, thus enabling industries to identify greener alternatives and align with sustainability objectives while ensuring product quality and performance.

There are multiple possibilities for further research and enhancements of the described approach. One direction is to further enlarge the number of datasets for additional material processing. Another is to add different, more specific manufacturing routes, especially for certain non-ferrous alloys, as well as to increase the number of countries/regions of manufacturing, in order to take into account regional specifics such as energy mix. These enhancements will provide more specific data and emission factors and therefore more accurate results of carbon footprint assessment.

7 References

[1] The European Green Deal: https://eur-lex.europa.eu/legal-content/EN/TXT/?uri=COM:2019:640:FIN, accessed April 2024

[2] Federal Climate Protection Act: https://www.bmuv.de/gesetz/bundes-klimaschutzgesetz, accessed April 2024

[3] The Corporate Sustainability Reporting Directive (CSRD): https://eur-lex.europa.eu/legal-content/EN/TXT/?uri=CELEX:32022L2464, accessed April 2024

[4] Carbon Border Adjustment Mechanism (CBAM): https://eur-lex.europa.eu/legal-content/EN/TXT/?uri=CELEX:32023R0956, accessed April 2024

[5] Hertwich E.G., Increased carbon footprint of materials production driven by rise in investments, Nature Geoscience 14 (2021) 151–155

[6] Ermolaeva N.S., Castro M.B.G., Kandachar P.V., Materials selection for an automotive structure by integrating structural optimization with environmental impact assessment, Materials and Design 25 (2004) 689–698

[7] Ic Y.T., Hamzaoğlu B.M., Yurdakul M., A Robust Aluminum Material Selection Process in the Aviation Industry: A Linear Discrete System Stability Test Perspective for Fuzzy Multicriteria Decision-Making, Arabian Journal for Science and Engineering (2024)

[8] Tasala Gradin, K., Simplified Life Cycle Assessment Approaches and Potential Impact Shifts, Doctoral Thesis, KTH Royal Institute of Technology, Stockholm, Sweden (2020)

[9] Treloar G., Love P., Smith J., Streamlined life cycle assessment: a method for considering environmental impact of road construction. In: Hughes, W (Ed.), 15th Annual ARCOM Conference, 15-17 September 1999, Liverpool John Moores University. Association of Researchers in Construction Management, Vol. 2, 753-62

[10] Gómez P., Elduque D., Sarasa J., Pina C., Javierre C., Influence of Composition on the Environmental Impact of a Cast Aluminum Alloy, Materials 9 (2016) 412

[11] Gutiérrez I.G., Elduque D., Pina C., Tobajas R., Javierre C., Influence of the Composition on the Environmental Impact of a Casting Magnesium Alloy, Sustainability 12 (2020) 10494

[12] Gutiérrez I.G., Elduque D., Pina C., Tobajas R., Javierre C., Excel tool to assess the environmental impact of steels based on the composition, 9th International Workshop on Simulation for Energy, Sustainable Development & Environment, ISSN 2724-0061 (2021)

[13] Total Materia AG: www.totalmateria.com, accessed April 2024

[14] Wernet G., Bauer C., Steubing B., Reinhard J., Moreno-Ruiz E., Weidema B., The ecoinvent database version 3 (part I): overview and methodology, The International Journal of Life Cycle Assessment, 21(9) (2016) 1218-1230; Version 3.10 (2023)

[15] International Standard ISO 14040 (2006) Environmental Management—Life Cycle Assessment—Principle and Framework

[16] Broadbent C., Steel's recyclability: demonstrating the benefits of recycling steel to achieve a circular economy, The International Journal of Life Cycle Assessment 21 (2016) 1658-1665

[17] Norgate T.E., Jahanshahi S., Rankin W.J., Assessing the environmental impact of metal production processes, Journal of Cleaner Production 15 (2007) 838-848

[18] Nilsson A.E., Aragonés M.M., Torralvo F.A., Dunon V., Angel H., Komnitsas K., Willquist K., A Review of the Carbon Footprint of Cu and Zn Production from Primary and Secondary Sources, Minerals 7 (2017) 168

Mechanical testing and material modeling of short glass fiber reinforced plastics - fossil and bio-based

Felix Dillenberger, Georg Stoll (Fraunhofer Institute for Structural Durability and System Reliability LBF)
Markus Fornoff (SIMCON kunststofftechnische Software GmbH)

1 Summary

Lightweight structural components made from plastics play an important role in achieving decarbonization targets in technical applications. Due to cost advantages and design freedom, short-fiber-reinforced plastics processed by injection molding represent an important material class here. To improve sustainability, traditional fossil-based plastics are increasingly being replaced by recyclates and plastics with biological components. For reliable component design using structural simulations, the mechanical properties must be known and adequately represented in the simulation model. The static and dynamic behavior of injection-molded components, and thus their load-bearing capacity and service life, depends on fiber volume content, as well as the fiber orientation and length distribution, which are influenced by the manufacturing process. Thus, for an efficient component design, the corresponding anisotropic mechanical properties must be considered. This paper presents the results of mechanical tests on petrochemical-based glass fiber-reinforced plastics (PA6-GF30) and bio-based alternatives (PA610-GF40). Furthermore, the process of material modeling for the structural simulation using ANSYS is discussed, including the mapping of the fiber orientation results from upstream process simulations. Adjusted material models are introduced, to optimize the simulative representation of the experimental test data. Finally, the results of the structural simulation at sample level are presented and discussed. On this basis, the article provides relevant insights on the representation of the described plastic materials in structural mechanics simulation with ANSYS.

2 Experimental Work

Two short fiber reinforced thermoplastics were selected for the study. The reference material consists of a standard PA6-GF30 grade (refPAGF), with 30 weight-% glass fibers, that is frequently applied in automotive applications at project partner Boge. As possible substitute for the reference material project partner Tecnaro developed a biobased PA610-GF40 (bioPAGF). The polyamide matrix is obtained from linseed oil and optimized for durability and 40 weight-% glass fibers are added to increase the load bearing capacity.

Different specimens were produced by injection molding. These consisted of standard 1A type tensile bars according to DIN EN ISO 527, as well as plates of the geometry 80 mm x 80 mm x 2 mm. BZ12 tensile bars with a parallel length of 12 mm were extracted from the plates by milling in the orientations 0°, 90° and 45°, in reference to the main injection molding direction, compare [1]. The geometry is depicted in Fig. 1.

To determine mechanical properties, quasi-static tensile tests were conducted at a temperature of 23°C and relative humidity of 50%. The tests were performed at equivalent nominal strain rates, by applying a test speed of 1 mm/min for the BZ12 samples and a speed of 6.67 mm/min for the 1A specimen.

The straining of the specimens was determined locally by using digital image correlation. Therefore, the specimen surfaces were spray painted by a grey scale pattern, the deformation of which was filmed during the tests by a 2D camera system. Subsequently, the local surface strain field was determined by digital image correlation Software VIC2D from Correlated Solutions. Scalar logarithmic Hencky strain values in longitudinal and lateral direction were extracted by averaging the strain field in the parallel region of the specimens (corresponding to the grey area in Fig. 1).

Fig. 2 plots the experimental results from the tensile tests. In comparison to bioPAGF, refPAGF shows a higher stiffness and a significantly lower fracture strain. These differences between the refPAGF and bioPAGF materials occur due to strongly differing fiber orientation distributions. Fig. 3 and Fig. 4 show the analysis of the principal components of the fiber orientation tensor in through thickness direction, in the center of the respective samples. These were evaluated by micro-computed tomography by the method developed by [2]. Fig. 3 depicts the orientation in injection molded plates from which the BZ12 were extracted. The orientation in the 1A specimens is plotted in Fig. 4. The refPAGF exhibits a significantly higher orientation in the longitudinal 2-direction (loading direction) for all samples.

Differing fiber orientations also lead to the difference between the stress-strain results of the 1A and BZ12 samples. The fibers in the BZ12 samples, which were extracted from plates, show a characteristic skin-core configuration through the thickness. Most fibers are oriented in inflow direction in the skin section, whilst the fibers in the core section are mostly oriented in crossflow direction. Such a fiber orientation distribution is characteristic for injection molded plates. The 1A specimen does not show such a pronounced core configuration. Thus, the number of fibers oriented in injection molding direction is higher, leading to a higher strength of the specimens. For bioPAGF the fiber orientation in the 1A sample is much lower than for refPAGF.

The anisotropic nature of the short fiber reinforced materials is evident, when comparing the tensile behavior in 0°, 90°, and 45° in Fig.2. Based on the higher fiber orientation in the refPAGF plates, the differences between the 0° and 90° loading directions are more pronounced for this material. Overall, the refPAGF material shows higher stiffness and strength at the tested conditions.

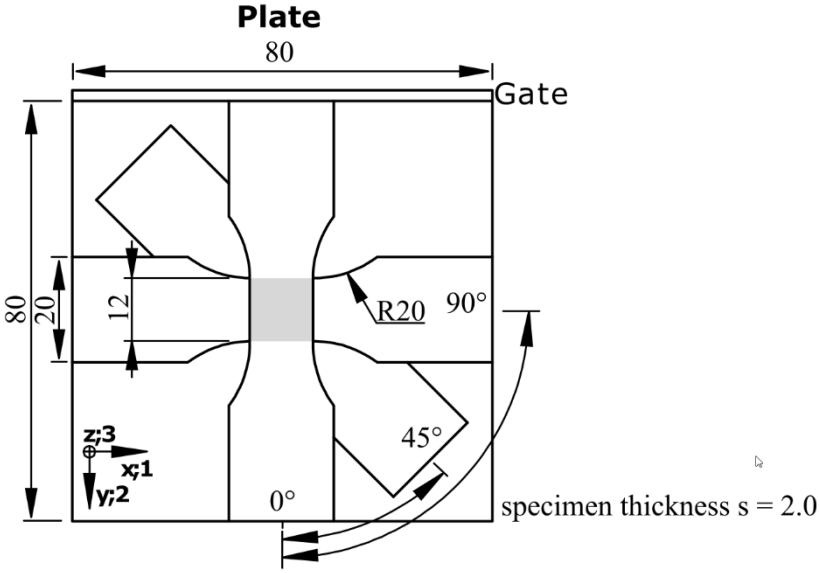

Fig. 1
Geometry of BZ12 tensile specimen and extraction angles from injection molded plate. The grey area depicts the strain averaging region for digital image correlation.

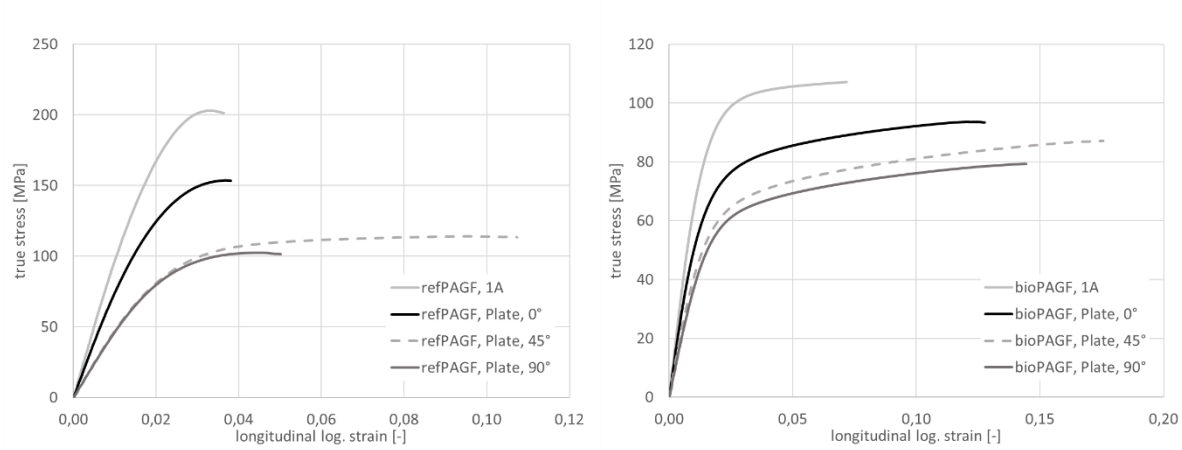

Fig. 2
Stress-strain diagrams from quasistatic tensile testing of different specimens and different loading orientations; left: refPAGF, right: bioPAGF

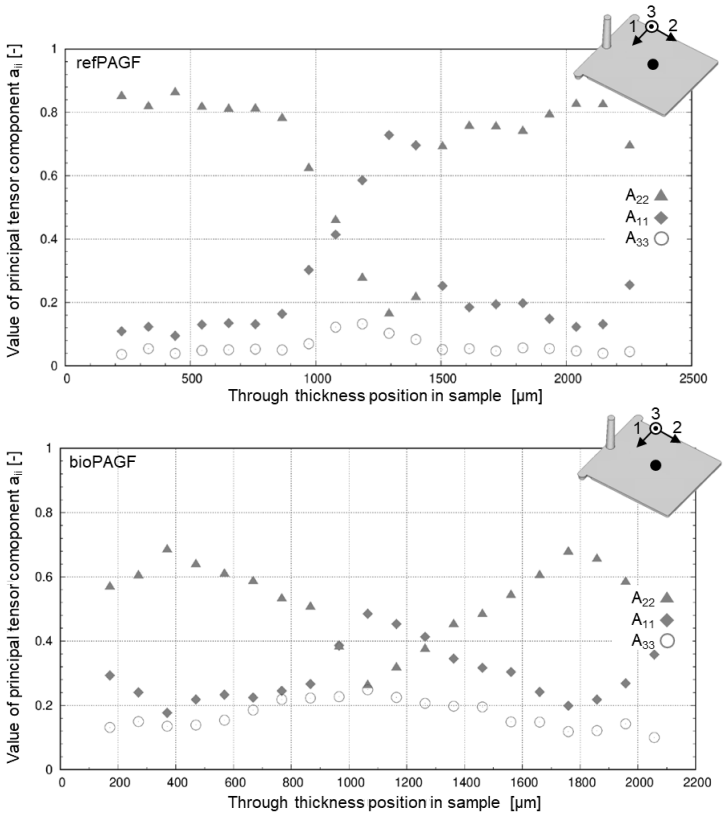

Fig. 3
Comparison of the principal components of the orientation tensor in through thickness direction, in the center of the injection molded plates (evaluated by micro-computed tomography); top: refPAGF, bottom: bioPAGF

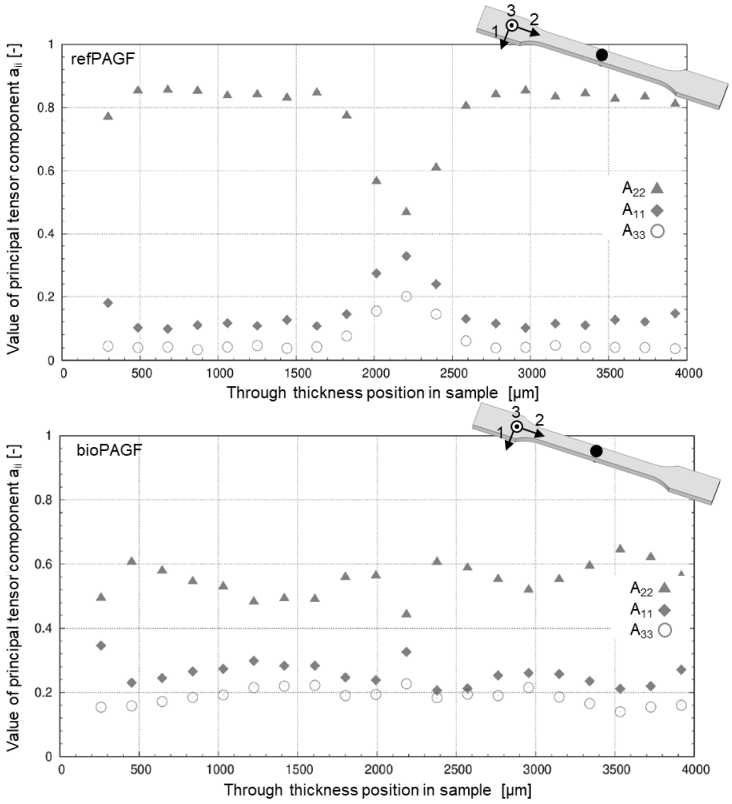

Fig. 4
Comparison of the principal components of the orientation tensor in through thickness direction, in the center of the injection molded 1A specimens (evaluated by micro-computed tomography); top: refPAGF, bottom: bioPAGF

3 Material Modelling and Structural Simulation

3.1 Injection Molding Simulation

The injection molding process of the refPAGF and the bioPAGF plates and 1A specimens was simulated via CADMOULD software by SIMCON. For the bioPAGF material a new material card was created, based on pressure and temperature depended specific volume measurement (pvT), thermal and viscosity measurements. For the refPAGF material existing data from the CADMOULD database was applied. The calculated fiber orientations were exported for further use in the structural simulation. For this the second order orientation tensor description was used, [3].

3.2 Material modelling

To generate a material description that accounts for the anisotropic behavior of the short fiber reinforced materials, the Software ANSYS Material Designer 2023 R1 was applied [4]. The stiffness and plastic deformation curves from the 0° and 90° BZ12 test specimen were input to the software and related to an orientation tensor. The orientation tensor was derived from the injection molding simulation results.

An elasto-plastic material model was generated to account for the non-linear deformation of the test specimens. The approach in the Material Designer Software is closely related to a methodology developed by [1]. The material model is based on the combination of three sub-models, [4]:

1. A linear-elastic model based on a micromechanics approach as developed by Mori-Tanaka ([5], [6]), which is widely applied for short fiber reinforced plastics:
   The model is fitted to the experimental data by setting fiber modulus and fiber volume fraction to defined values, while iteratively adjusting matrix modulus and fiber aspect ratio. The results are extracted as orthotropic stiffness matrices for different orientation tensor definitions.
2. A yield criterion based on an orthotropic Hill plasticity definition [7]:
   The R-Values of the Hill criterion are fitted to the experimental data and extracted for different orientation tensor definitions based on a phenomenological criterion as developed by [8]. In this approach, the R-Values are scaled to different orientation tensor values.
3. A non-linear plastic hardening model:
   The inverse polynomial model suggested by [1] is applied to fit the non-linear behavior of the experimental data. The hardening behavior is then scaled to different orientation distributions based on the respective R-Values of the underlying Hill plasticity model.

The material model is passed to the structural simulation in form of tabulated orthotropic stiffness parameters, tabulated R-values for a Hill yield surface, each sampled over 10 possible orientation distributions, as well as a non-linear hardening curve.

3.3 Structural Simulation of Specimens

The mechanical behavior of the test specimens was simulated in the structural simulation using ANSYS 2023 R1 software. The workflow in ANSYS Workbench for coupling the structural simulation with the fiber orientation results from the injection molding simulation and the material model from ANSYS material designer is depicted in Fig.5.

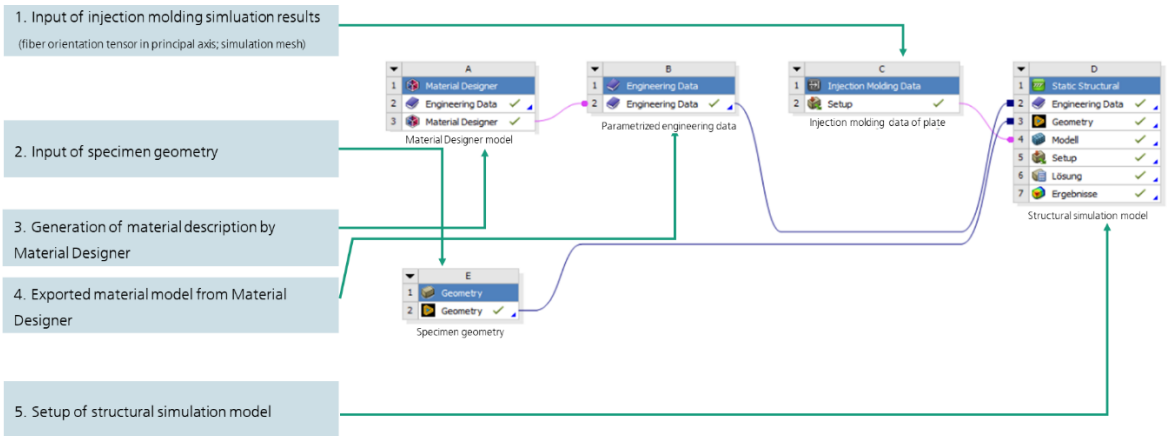

Fig. 5
Workflow representation in ANSYS Workbench for the integrated simulation of the test specimens

First, the fiber orientation data and the injection molding simulation mesh from CADMOULD were imported into the Injection Molding Data module. Next, the CAD file of the specimen geometry was imported. In this step, it is important to ensure that the specimen geometry is properly aligned with the injection molding simulation mesh. This requires the spatial position and orientation to be set as they were in the real specimens milled from the injection molded samples. The information from the injection molding simulation was transferred to the structural mesh by the ANSYS mapping algorithms. The mapping algorithm first computes elements orientations which correspond to the principal coordinate systems of the averaged orientation tensor in each element. In addition, for each element, the principal components of the orientation tensor are transferred to the structural mesh. These results are shown in Fig. 6 for the tensile specimen. By applying this information, the appropriate orthotropic material model is assigned to each element during the structural simulation.

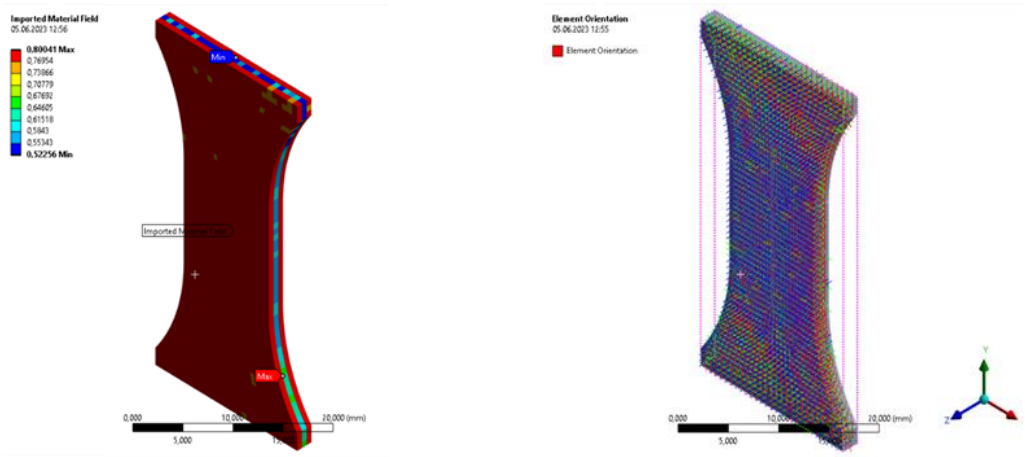

Fig. 6
Left: Fringe plot of the first principal orientation tensor component, mapped to the specimen mesh
Right: Element orientation designated by the orientation tensor principal axis system, mapped to the specimen mesh.

To validate the model, a quasi-static tensile test of the specimen was simulated. The specimens were modeled with three solid quadratic elements in through the thickness direction, thus the elements had an average element length of 0.7 mm. One side of the mesh was fixed, and the opposite side was subjected to a displacement boundary condition. The evaluation of the simulation results was done in correspondence to the mechanical experiments. The resulting stress was computed from the reaction force of the specimen and correlated with the average strain in the parallel section of the specimen surface.

The left side of Fig. 7 depicts the results for refPAGF in comparison to the experimental data of the BZ12 specimens extracted from the plates in different orientations. The simulated curves closely correlate to the experimental data. The right side of Fig. 7 compares the results for bioPAGF. Up to a strain of 0.05 the results of the simulation match the results from the experiments. However, due to convergence issues the simulation fails at higher deformations.

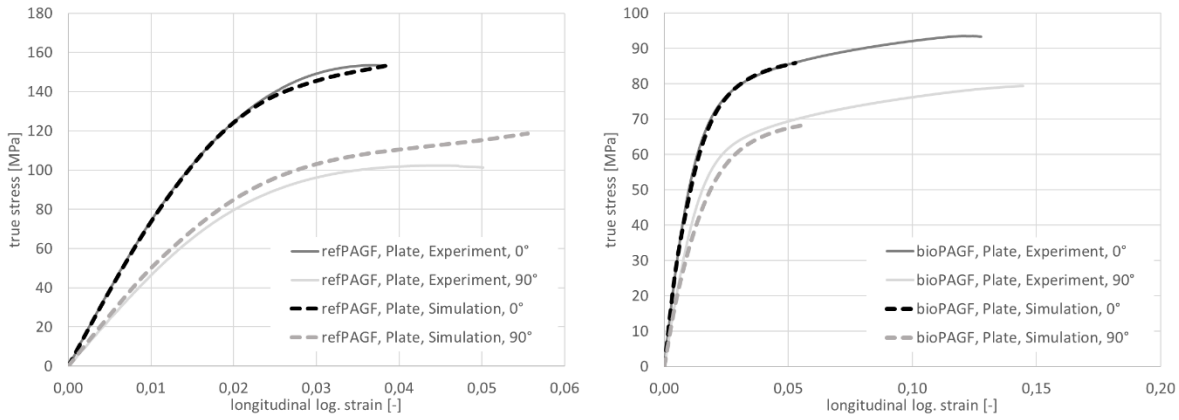

Fig. 7
Comparison of the experimental stress strain behavior of the specimens extracted from the injection molded plates to the simulated results; left: refPAGF, right: bioPAGF

3.4 Adjustment of the hardening curve

The convergence issues during the simulation of the bioPAGF occur due to the hardening curve of the material model. The applied inverse polynomial form leads to constant stress values at high deformation values. Due to the missing gradient of the hardening curve at higher deformation values instabilities occur, which lead to convergence issues in the structural simulation. The original form of the inverse polynomial hardening model was developed by [1] to model short fiber reinforced plastics with minimal non-linear behavior. Such a material behavior can be seen for refPAGF. However, the biobased bioPAGF shows much higher non-linearities.

To account for the extended non-linear behavior of biobased materials, an adjustment of the inverse hardening model is suggested. Thus, the inverse hardening model of [1] is extended by an additional quadratic term $c\,(\varepsilon^{pl})^2$. This corresponds to suggestions made for inverse polynomials in [8]:

$$\sigma\left(\varepsilon^{pl}\right) = \varepsilon^{pl}\left(\frac{1}{\sigma_{\max}-\sigma_{\mathrm{Y}}}\varepsilon^{pl} - \frac{2}{E-\frac{\sigma_{\mathrm{Y}}}{a}} - c\left(\varepsilon^{pl}\right)^2\right)^{-1} + \sigma_{\mathrm{Y}} \qquad \text{(Eq. 1)}$$

with
ε^{pl}: plastic strain (variable)
σ_{Y}: yield stress
E: Youngs modulus
a: fitting parameter for the hardening model
c: fitting parameter for the hardening model, controlling the quadratic term
$\sigma_{\max}$: fitting parameter for the hardening model (corresponds to asymptotic maximum for $c = 0$).

By adding term c, non-linear behavior can be included for high values of ε^{pl}. This allows an extended adaptability of the model. [1] suggests an adaptation of the hardening curve to different orientation distributions by adjustment of the parameters $\sigma_{\mathrm{Y}}, \sigma_{\max}, E$. However, in material designer the adaptation to different orientation distributions is implemented by keeping all parameters constant and scaling the entire curve $\sigma(\varepsilon^{pl})$ via the Hill R-values of the respective orientation state. Thus, the equation can be simplified to:

$$\sigma(\varepsilon^{pl}) = \varepsilon^{pl}(m\varepsilon^{pl} + b - c\,(\varepsilon^{pl})^2)^{-1} + \sigma_{\mathrm{Y}} \qquad \text{(Eq. 2)}$$

with
b: fitting parameter for the hardening model
m: fitting parameter for the hardening model

With regard to the denominator from Eq. 2, a definition gap arises at the strain $\varepsilon_{1,2}^{asymp}$, when

$$m\varepsilon_{1,2}^{asymp} + b - c\left(\varepsilon_{1,2}^{asymp}\right)^2 = 0. \qquad \text{(Eq. 3)}$$

$1/b$ corresponds to the initial slope of the hardening curve (compare [1]). Therefore, $b > 0$ applies. Furthermore, $\sigma_{\max} > \sigma_{\mathrm{Y}}$ leads to $m > 0$. In the area of the definition gap, the stress values run asymptotically towards infinity. To obtain an admissible model equation for mapping experimental curves, the definition gap must not lie in the area of the curve. For this to be fulfilled, it must apply that $\varepsilon_1^{asymp} < 0$ and $\varepsilon_2^{asymp} \gg \varepsilon_F^{pl} > 0$, with ε_F^{pl} depicting the plastic failure strain. Using these considerations, the parameter c can be expressed as

$$c = \frac{m\varepsilon_2^{asymp}+b}{\left(\varepsilon_2^{asymp}\right)^2} > 0. \qquad \text{(Eq. 4)}$$

For $\varepsilon_2^{asymp} \to \infty$ the equation leads to $c = 0$. In this case, the original model from [1] is obtained, which converges to a constant stress value at $\sigma_{\max}$ for high plastic strains.

Setting c to positive values, makes it possible to adjust the non-linear behavior of the hardening curve at high plastic strains. Fig. 8 presents the results of the simulation of the bioPAGF specimen with the adjusted hardening curve. The quadratic inverse polynomial hardening model was parametrized to include an increasing gradient at higher strains. The simulation results could be obtained for the entire deformation range without convergence issues.

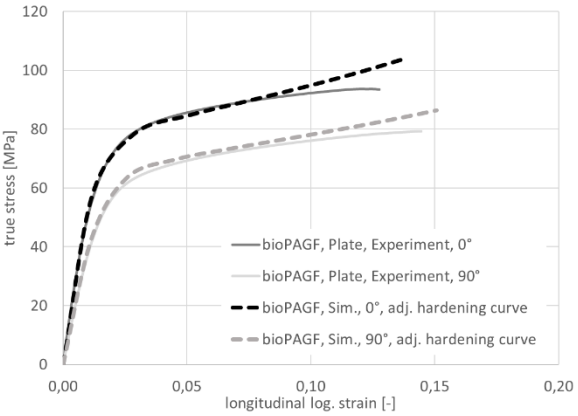

Fig. 8
Comparison of the experimental stress strain behavior of the bioPAGF specimens extracted from the injection molded plates to the simulated results. The inverse quadratic polynomial hardening curve was applied.

4 Conclusions

The presented results show that the behavior of short fiber reinforced thermoplastic can be predicted by simulation, applying a micromechanical approach combined with a phenomenological approach as was recently implemented in ANSYS Material designer. It was shown that the inverse hardening curve suggested by [1], leads to reasonable results for traditional materials such as the tested refPAGF. However, biobased materials with increased non-linear behavior cannot be accurately predicted with this approach. The suggested expansion of the hardening model with an additional quadratic term makes it possible to simulate the behavior at high deformations. By applying the novel hardening model, the non-linear behavior of bio-based materials can be more accurately simulated.

5 Acknowledgements

This work was supported by the German Federal Ministry of Economic Affairs and Climate Action (BMWK) under the TTP-Leichtbau programme as part of the project COOPERATE (Grant No. 03LB3036E)..

6 References

[1] F. Dillenberger, On the anisotropic plastic behaviour of short fibre reinforced thermoplastics and its description by phenomenological material modelling, Mechanik, Werkstoffe und Konstruktion im Bauwesen 53, Springer, 2020
[3] R. Glöckner, S. Kolling, C. Heiliger: A Monte-Carlo Algorithm for 3D Fibre Detection from Microcomputer Tomography, in: Journal of Computational Engineering vol. 2016, pp. 1–9.
[4] S. G. Advani, C. L. Tucker: The use of tensors to describe and predict fiber orientation in short fiber composites, in: Journal of Rheology vol. 31.8, pp. 751–784, 1987
[5] Material Designer User's Guide, ANSYS, Inc. Release 2023 R1, Southpointe, January 2023
[6] T. Mori, K. Tanaka, Average stress in matrix and average elastic energy of materials with misfitting inclusions, Acta Metallurgica 1973; 21: 571-574.
[7] Y. Beneviste, A new approach to the application of mori-tanaka's theory in composite materials. Mechanics of Materials. 1987; 6(2): 147-157.
[8] R. Hill, The Mathematical Theory of Plasticity. New York: Oxford University Press, 1983
[9] A. Launay, M.H. Maitournam, Y. Marco, & I. Raoult, Multiaxial fatigue models for short glass fiber reinforced polyamide – Part I: Nonlinear anisotropic constitutive behavior for cyclic response. International Journal of Fatigue. (47), 382-389, 2013
[9] NELDER, J. A. (1966): Inverse Polynomials, a Useful Group of Multi-Factor Response Functions, Biometrics vol. 22.1, pp. 128–141.

Entwicklung eines Vorgehens zur automatisierten Auslegung zyklisch belasteter, endlosfaserverstärkter Bauteile

Marc Gadinger, Christoph Bode, Sandro Wartzack (Friedrich-Alexander-Universität Erlangen-Nürnberg, KTmfk)

1 Motivation

Leichtbau und effizienter Materialeinsatz gewinnen in verschiedenen Wirtschaftssektoren zunehmend an Bedeutung. Dies zeigen auch anstehende Leitinitiativen und gesetzliche Vorgaben im Kontext der Klimaziele und des Übergangs zu einer ressourceneffizienteren Wirtschaft. Vor diesem Hintergrund finden Bauteile aus Faserverbundwerkstoffen verstärkt als wichtige Strukturbauteile im Serieneinsatz Verwendung. Dort sind sie häufig zyklischen Belastungen ausgesetzt, die mit steigender Zyklenzahl zu einer Verschlechterung bzw. Degradation der Werkstoffeigenschaften führen. Bisherige Auslegungsansätze und Optimierungsroutinen berücksichtigen die Betriebsfestigkeit jedoch kaum. Vielmehr erfolgt meist eine Überdimensionierung nach empirischen Kriterien. Um das volle Leichtbaupotential eines Bauteils auszuschöpfen, ist jedoch eine gezielte Auslegung auf eine definierte Lebensdauer zielführend.

2 Stand der Technik

Faser-Kunststoff-Verbunde (FKV) bieten zwar ein erhebliches Potential für Leichtbauanwendungen, weisen aber auch ein sehr komplexes Ermüdungsverhalten auf. Bei Ermüdungsprozessen in FKV entsteht eine spezifische Kombination von Schädigungen, die sowohl die Fasern, die Matrix als auch die Grenzflächen betreffen. Zusätzlich treten lokale Ablösungen und großflächige Delaminationen auf. Dieses Zusammenspiel verschiedener Faktoren führt zu einem sehr komplexen Schädigungsmuster.

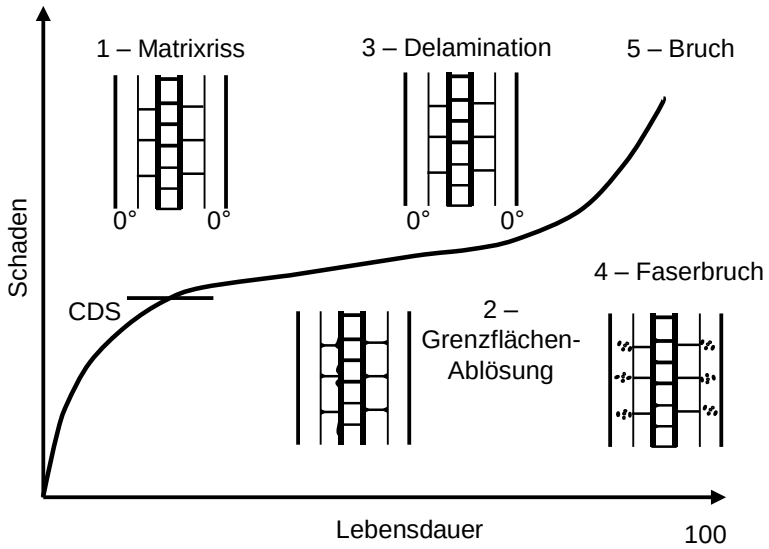

Abbildung 1: Fortschritt des Ermüdungsschadens in FKV nach [1].

Über die Lebensdauer von FKV führen diese Effekte zu einem Steifigkeitsverlust, der häufig über einen Schadensfaktor quantifiziert wird. Der Steifigkeitsverlust ist in Abbildung 1 dargestellt und kann in drei Phasen unterteilt werden. Die erste Phase ist durch eine starke Verringerung der Materialsteifigkeit infolge von Rissbildung in der Matrix gekennzeichnet. In der zweiten Phase nimmt das Ausmaß der Schädigung stetig zu, jedoch langsamer als in Phase eins. In der letzten Phase steigt die Schädigung

durch lokale Ausfälle infolge von Faserbrüchen oder vollständiger Delamination der Grenzflächen erneut stark an [1, 2].
Grundlage für das Verständnis des Ermüdungsverhaltens von FKV sind experimentell ermittelte Wöhlerkurven [3, 4]. Dazu werden Probekörper zyklisch bei konstantem Lastverhältnis bis zum Versagen belastet. Gleichung 1 beschreibt den Verlauf einer derartigen Ermüdungskurve. So lässt sich mit Hilfe des Steigungsparameters b und des Festigkeitsparameters σ die maximal ertragbare Spannung σ_{res} für eine bestimmte Schwingspielzahl N bestimmen.

$$\sigma_{res} = \sigma \cdot N^{b} \tag{1}$$

3 Problemstellung und Zielsetzung

Die dynamische Belastung endlosfaserverstärkter Bauteile und deren Einfluss auf das Langzeitverhalten sind von großer Bedeutung. Der traditionelle Ansatz zur Auslegung dynamisch belasteter Strukturen besteht darin, einen sogenannten Knock-Out-Faktor in eine ansonsten statische Auslegung einzubeziehen, um eine Sicherheitsmarge für die schwingende Beanspruchung zu gewährleisten. Diese Herangehensweise wird jedoch dem komplexen Ermüdungsverhalten von FKV nicht gerecht und ist in Bezug auf das resultierende Bauteilgewicht äußerst ineffizient.
Um diese Lücke zur gezielten Betriebsfestigkeitsauslegung von Faserverbundbauteilen zu schließen, soll eine neue Auslegungsmethode zur Berücksichtigung des Ermüdungsverhaltens von faserverstärkten Kunststoffen entwickelt werden. Ziel ist dabei die lokale Verstärkung eines Basislaminats, um sicherzustellen, dass der FKV eine geforderte, minimale Schwingspielzahl erreicht. In dieser Arbeit wird daher eine Methode entwickelt und untersucht, welche ein dynamisch belastetes Bauteil simulativ mithilfe von Fiber-Patch-Placement (FPP) gegen eine anliegende Schwingung optimiert.

4 Methodik und Vorgehensweise

4.1 Ablauf der Optimierungsroutine

Der grundlegende Ablauf der Optimierungsmethode ist in Abbildung 2 dargestellt. Das Gütekriterium für die Optimierung besteht darin, für jedes Element und jede Schicht im Modell sicherzustellen, dass die kritische Schwingspielzahl N_{krit} erreicht wird. Diese Größe wird zu Beginn durch die Produktentwickler vorgegeben. Als Hauptregelgröße dient das Aufbringen neuer Lagen in Form von Patches auf das Grundlaminat. Während der Optimierung werden zudem die Faserorientierungen der Hauptlagen verfeinert, indem sie an die Hauptrichtung der größten Spannungen angepasst werden. Diese Anpassung erfolgt jedoch unabhängig vom Qualitätskriterium und stellt nur eine Nebenbedingung dar.

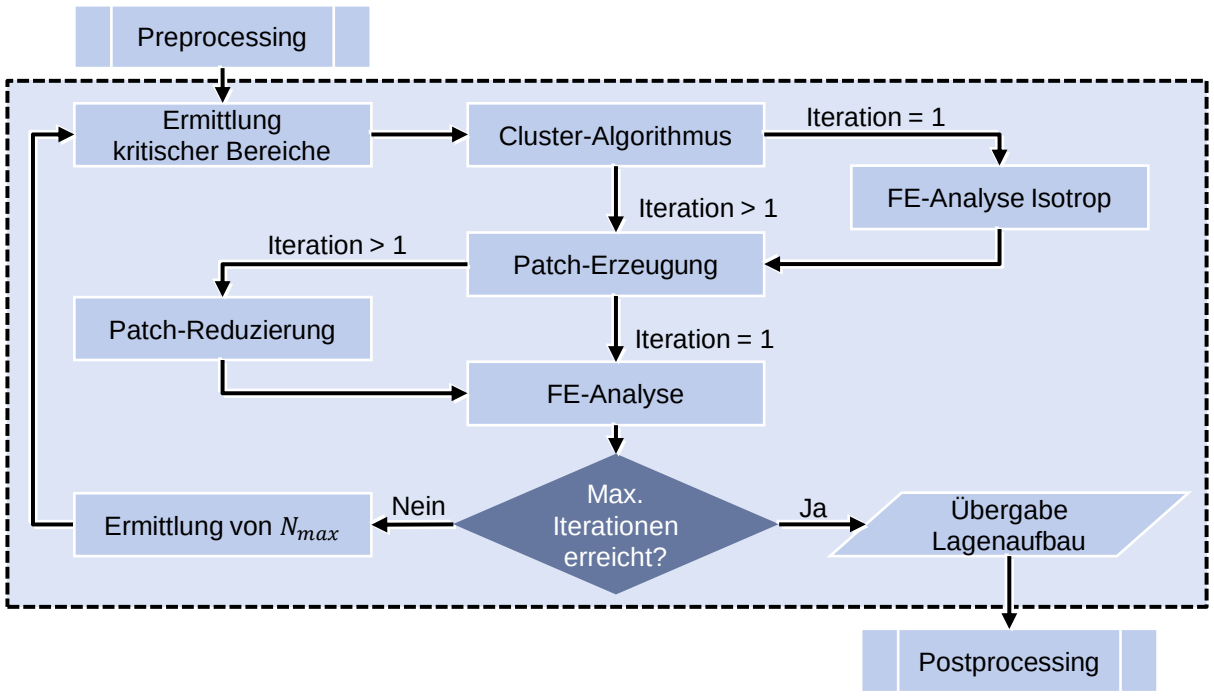

Abbildung 2: Ablauf der Optimierungsmethode.

Zunächst wird das FE-Modell des zu untersuchenden Bauteils mit den dazugehörigen Randbedingungen und Lastfällen eingelesen. Der nächste Schritt im Preprocessing ist die Berechnung der maximal ertragbaren Schwingspielzahl für jede Schicht in jedem Element. Die Ergebnisse aus dem Preprocessing werden nur für den ersten Iterationsdurchlauf benötigt. Anschließend werden die Schwingspielzahlen laufend - basierend auf den sich durch die Optimierung ergebenden Änderungen - neu berechnet. Die Vorgehensweise zur Berechnung der Schwingspielzahlen ist in Abschnitt 4.2 ausführlicher dargestellt.

Jeder Iterationsdurchlauf der Optimierung beginnt mit der Identifizierung der kritischen Bereiche. Hierzu wird jede Schicht in jedem Element auf die Einhaltung des Gütekriteriums ($N_{max} > N_{krit}$) überprüft. Der Algorithmus speichert dabei die Elemente, deren berechnete Schwingspielzahl kleiner als der geforderte Mindestwert ist. Die Clusterfunktion verwendet im anschließenden Schritt den Spannungszustand der kritischen Elemente, um die Hauptrichtungen der Spannungen zu bestimmen. Die folgende Patch-Erzeugung benötigt sowohl die Informationen aus der FE-Analyse als auch dem Clustering. Sie konvertiert die Cluster in entsprechende Patches und weist entsprechend der Richtung der größten Hauptspannung innerhalb des Clusters dem Patch eine Faserorientierung zu. Abschließend folgt nun der Punkt der sogenannten Patch-Reduzierung. Bei der Patch-basierten Optimierung von FKV-Bauteilen wirken sich Patches in bestimmten Regionen über die Steifigkeitsmatrix auf das gesamte Bauteil aus. Schwache Bereiche können somit auch ohne eigene Patch-Lagen verstärkt werden. Daher werden nun die Elemente geprüft, die durch Patches verstärkt wurden, jedoch möglicherweise stabil genug sind, um auf die Verstärkung zu verzichten.

Abschließend werden die in der Optimierung berechneten Patches in fertigungsgerechte, unidirektionale Streifen für das FPP-Verfahren umgewandelt. Dazu wird ein Ablegealgorithmus nach Voelkl et al. verwendet [5]. Dieser betrachtet jeden der ermittelten Patches und erzeugt daraus einen rechteckigen Streifen mit einer vom Benutzer vorgegebenen Breite und einer an die Patch-Größe angepassten Länge. Auf diese Weise entstehen Tape-Streifen, die den zuvor ermittelten Patch vollständig umschließen.

4.2 Ermittlung der maximal ertragbaren Schwingspielzahl

Ein zentraler Bestandteil des Optimierungsverfahrens ist die Berechnung der bis zum Versagen ertragbaren Schwingspielzahl. Hierzu werden die im Bauteil wirkenden Spannungen und Dehnungen mittels einer Finiten-Elemente-Analyse ermittelt und örtlich aufgelöst pro Schicht und Element mit Hilfe eines modifizierten Versagenskriteriums betrachtet. Ein weit verbreitetes mathematisches Modell zur Beschreibung des Versagensverhaltens von FKV ist das Tsai-Hill-Kriterium. Es kombiniert die Komponenten des lokalen Spannungstensors zu einer Funktion, die bei Erreichen eines Schwellwertes Versagen anzeigt [6]. Andere vergleichbare Kriterien sind das Tsai-Wu-Kriterium oder das Puck-Kriterium, wobei letzteres Informationen über die Versagensart liefern kann. Das Tsai-Hill-Kriterium ist aus dem Fließkriterium nach Hill [7] abgeleitet, das bei transversal isotropen Werkstoffen vereinfacht werden kann:

$$\left(\frac{\sigma_{\parallel}}{\sigma_{\parallel,f}}\right)^2 + \left(\frac{\sigma_{\perp}}{\sigma_{\perp,f}}\right)^2 + \left(\frac{\tau_{\parallel\perp}}{\tau_{\parallel\perp,f}}\right)^2 - \left(\frac{\sigma_{\parallel}\sigma_{\perp}}{\sigma_{\parallel,f}^2}\right) = 1 \tag{2}$$

Die Werte der Konstanten $\sigma_{\parallel,f}$, $\sigma_{\perp,f}$ und $\tau_{\parallel\perp,f}$ müssen experimentell an Couponproben bestimmt werden. Sie stehen für die Festigkeit des Materials unter Zug- bzw. Druckbelastung. Die Festigkeit in Faserrichtung wird durch $\sigma_{\parallel,f}$, die senkrechte Festigkeit durch $\sigma_{\perp,f}$ und die Scherfestigkeit durch $\tau_{\parallel\perp,f}$ ausgedrückt [6]. Werden die statischen Festigkeiten in Gleichung 2 durch die entsprechenden Wöhlergleichungen ersetzt, kann die maximal ertragbare Schwingspielzahl für einen bestimmten Spannungszustand nach Gleichung 3 bestimmt werden. Die dafür notwendigen Erkenntnisse über das anisotrope Festigkeitsverhalten liefern zyklische Versuche an unidirektionalen Probekörpern.

$$N_{max}(\sigma_{\parallel}, \sigma_{\perp}, \tau_{\parallel\perp}) = \left[\left(\frac{\sigma_{\parallel}}{\sigma_{\parallel,f}}\right)^2 + \left(\frac{\sigma_{\perp}}{\sigma_{\perp,f}}\right)^2 + \left(\frac{\tau_{\parallel\perp}}{\tau_{\parallel\perp,f}}\right)^2 - \left(\frac{\sigma_{\parallel}}{\sigma_{\parallel,f}^2}\right)\right]^{\frac{1}{2b}} \tag{3}$$

5 Optimierung eines gewölbten Bauteils unter zyklischer Belastung

Im Folgenden wird die vorgestellte Optimierungsmethode auf ein Bauteil mit industrieller Komplexität angewendet. Es handelt sich um ein Schubfeld mit komplexen Formen, wie beispielsweise einer doppelten Krümmung. Die Geometrie des untersuchten Schubfeldes ist zusammen mit den definierten Randbedingungen in Abbildung 3 dargestellt. Das Bauteil wird über die unteren vier Bohrungen fest eingespannt, während die mittleren Bohrungen mit 4000 N und die oberen Bohrungen mit 8000 N belastet werden. Hierdurch entstehen Zug-, Druck- und Schubspannungen im Bauteil. Für die Simulation wurde als Material unidirektionales kohlenstofffaserverstärktes Epoxidharz mit einem symmetrischen Lagenaufbau von $[45, 90, -45, 0]_s$ verwendet. Die Lagenstärke beträgt dabei 0,2 mm. Sowohl die Sicken als auch die Einspannung sind mit einem dickeren Material versehen.

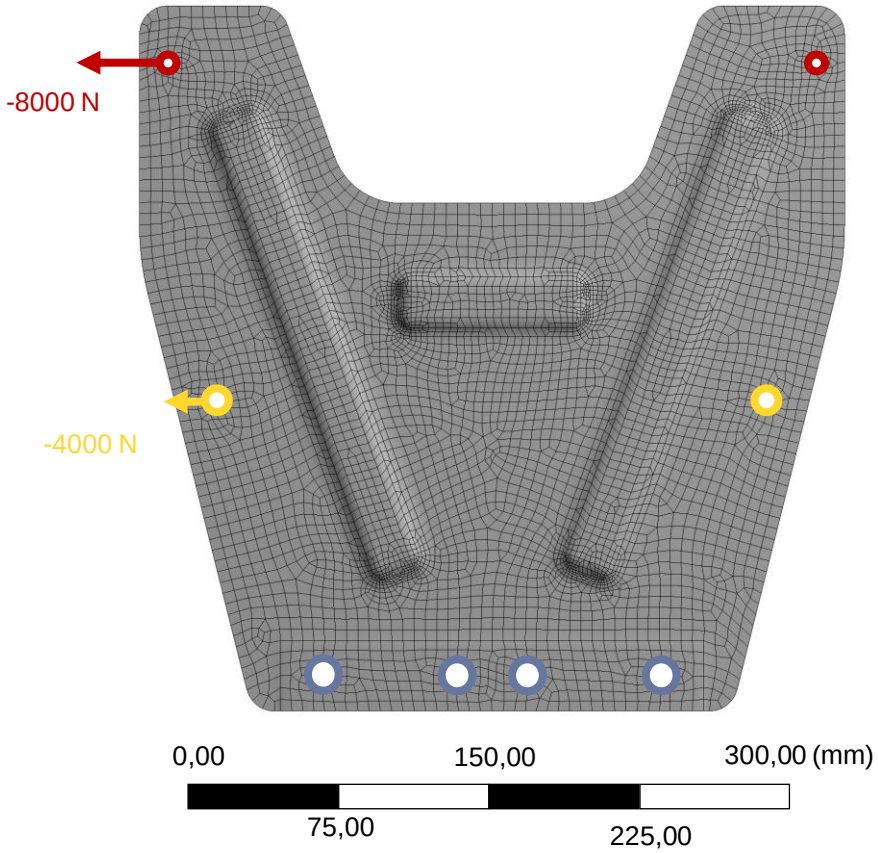

Abbildung 3: Darstellung der Geometrie und der Randbedingungen des zu optimierenden Bauteils.

Der Wert für die kritische Schwingspielzahl N_{krit} liegt bei 100 000 Schwingungen. Die zulässige Winkeldifferenz zwischen den Hauptrichtungen zweier Patches beträgt 20° und die Breite der Tapes ist auf 50 mm festgelegt. Die Patch-Stärke beläuft sich auf 0,6 mm.

Abbildung 4 fasst den Optimierungsprozess in Form von Diagrammen zusammen. Das erste Diagramm (a) zeigt die maximal ertragbare Schwingspielzahl des schwächsten Elements im Bauteil. Dies ist der wichtigste Werte für die Optimierung. Hier sind starke Schwankungen der Werte zu erkennen. Es ist zu vermuten, dass diese durch die komplexen Spannungszustände im Bauteil hervorgerufen werden. Der Versuch der Optimierung, sich dem kritischen Wert langsam von oben zu nähern, sobald dieser überschritten wird, ist gut zu erkennen. Die relative Gewichtszunahme (b) zeigt, dass bereits ab der zehnten Iteration kaum noch Patches hinzugefügt werden. Dies ist an der relativ konstanten Gewichtsänderung ab der zehnten Iteration zu erkennen. Die Schwankungen in (a) werden also nur von einem kleinen Anteil der Elemente erzeugt. Die mediane Schwingspielzahl der kritischen Elemente (c) zeigt diese Schwankungen ebenfalls, jedoch mit einem deutlichen Anstiegstrend.

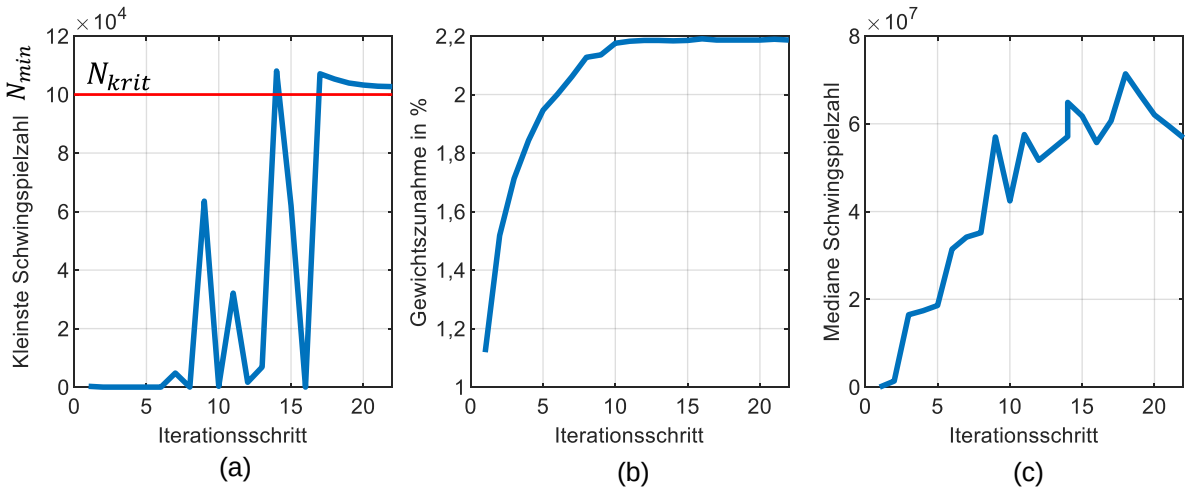

Abbildung 4: (a) Verlauf der kleinsten Schwingspielzahl N_{min} des Bauteils; (b) Verlauf der Gewichtszunahme in %; (c) Verlauf der medianen Schwingspielzahl aller kritischen Elemente der jeweiligen Iteration.

Im Anschluss an die Optimierung wird das Postprocessing durchgeführt, das den Ablegealgorithmus beinhaltet. Das Ergebnis ist in Abbildung 5 dargestellt. Die Mittelachsen der einzelnen Patches sind durch die roten Streifen gekennzeichnet. Die maximale Lagenanzahl ist 19 (8 Basislagen + 11 Patches). Die linke Einspannungsbohrung und die Spitze der rechten Sicke wurden besonders stark durch Tapes verstärkt. Die rechte Bohrung zur Befestigung wurde ebenfalls verstärkt. Aufgrund der Schubbelastung entsteht ein Moment im Bauteil. Da die beiden inneren Bohrungen näher an der neutralen Faser dieses Moments liegen, sind sie weniger stark belastet und wurden daher nicht verstärkt. Es sind viele relativ lange Tape-Streifen zu erkennen, die meist diagonal angeordnet sind. Allerdings sind in diesem Modell auch einige sehr kurze Streifen zu erkennen, die in der realen Fertigung zu Problemen führen können. Dies könnte durch Anpassungen am Ablegealgorithmus adressiert werden. Insgesamt zeigt sich, dass die Schwingfestigkeit des Demonstrators ohne große Veränderungen am Bauteil optimiert werden konnte. Dabei bleibt ein Großteil des Bauteils unverändert, indem sich die Methode auf die kritischen Bereiche begrenzt.

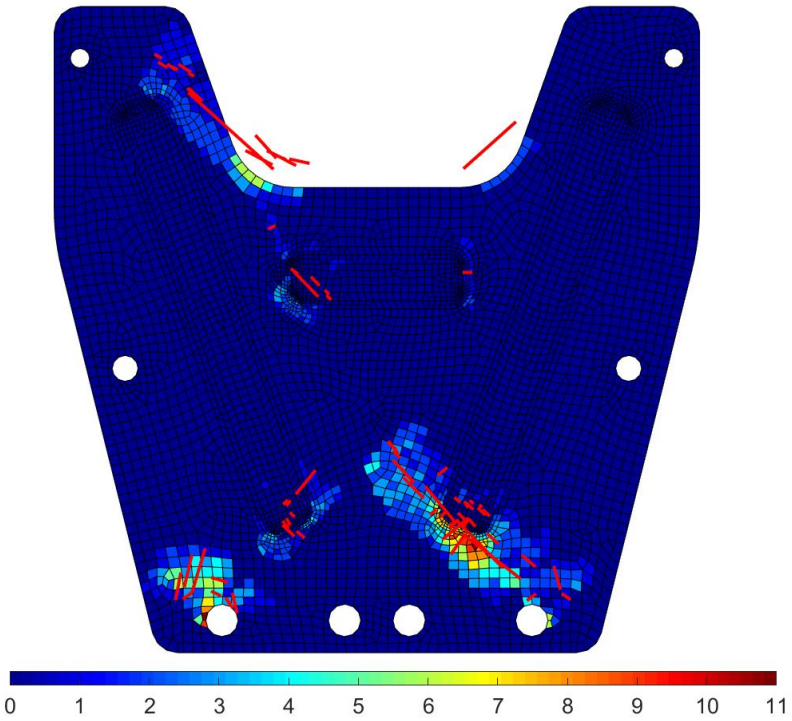

Abbildung 5: Anzahl der Patch-Lagen nach dem Postprocessing und Mittelachsen der UD-Tapes.

6 Zusammenfassung

Das Ermüdungsverhalten von Faserverbundwerkstoffen ist ein komplexer Vorgang, der von einer Vielzahl von Faktoren beeinflusst wird. Gleichzeitig sind Bauteile aus Faserverbundwerkstoffen in zunehmendem Maße als wichtige strukturelle Komponenten in Serienanwendungen im Einsatz. In diesem Einsatzbereich unterliegen sie häufig zyklischen Belastungen, die mit steigender Zyklenzahl die Werkstoffeigenschaften verschlechtern. Bisherige Auslegungsansätze berücksichtigen dabei jedoch nicht die Berechnung von Materialermüdung, sondern legen statisch gegen ein oder mehrere Versagenskriterien aus. Bei Berücksichtigung von Materialermüdung durch zyklische Beanspruchung lässt sich durch die Verringerung nötiger Sicherheitsfaktoren jedoch noch weiteres Leichtbaupotential erschließen.
Daher wurde ein Optimierungsverfahren zur Zeitfestigkeitsauslegung von Faserverbundbauteilen vorgestellt. Dabei werden auf Basis experimentell ermittelter Wöhlerkurven und mathematischen Versagensmodellen die maximale Lebensdauer aller Elemente bestimmt und kritische Bereiche identifiziert. Durch die lokale Verstärkung des Basislaminats stellt die Optimierung das Erreichen einer geforderten, minimalen Schwingspielzahl sicher. Anschließend werden die Ergebnisse der Optimierung in fertigungsgerechte Patches umgesetzt, die beispielsweise über das Fiber-Patch-Placement an das Bauteil angebracht werden können. Der Einsatz der Methode wurde in einem Benchmark an einem industrienahen Bauteil verdeutlicht. Die Ergebnisse zeigen, dass FKV-Bauteile automatisiert gegen eine Schwingungsbeanspruchung optimiert werden können. Zukünftige Arbeiten werden sich mit der weiteren Verbesserung der Herstellbarkeit der entstehenden Patch-Lagen beschäftigen. Hier besteht ein großes Potential, z. B. durch die Umwandlung kleinerer Patches in größere bzw. deren Zusammenlegung.

Autorenbeiträge

Konzeptionierung, C.B.; Methodik, C.B. und MG; Software, C.B.; Validierung, C.B. und M.G.; Formale Analyse, C.B und M.G.; Untersuchungen, C.B und M.G.; Ressourcen, C.B. und M.G.; Datenkuration, C.B. und MG; Erstellung des Originalentwurfs, M.G.; Überprüfung und Bearbeitung, M.G und S.W.; Visualisierung, M.G.; Betreuung, S.W.; Projektadministration, M.G. and S.W.; Fördermittelakquise, S.W. Alle Autoren haben die veröffentlichte Fassung des Manuskripts gelesen und sind damit einverstanden.

7 Literaturverzeichnis

[1] Wu F., Yao W.: “A fatigue damage model of composite materials”, Int. J. Fatigue, 32 (2010) Nr. 1, S. 134–138. https://doi.org/10.1016/j.ijfatigue.2009.02.027.

[2] Carraro P. A., Maragoni L., Quaresimin M.: "Prediction of the crack density evolution in multidirectional laminates under fatigue loadings", Composites Science and Technology, (2017), S. 24–39. https://doi.org/10.1016/j.compscitech.2017.03.013.

[3] Haibach E.: „Betriebsfestigkeit : Verfahren und Daten zur Bauteilberechnung“. 3., korrigierte und ergänzte Auflage. Berlin, Heidelberg: Springer, 2006. https://doi.org/10.1007/3-540-29364-7.

[4] Radaj D., Vormwald M.: "Ermüdungsfestigkeit, Grundlagen für Ingenieure", Springer, Berlin, Heidelberg, 2007. https://doi.org/10.1007/978-3-540-71459-0.

[5] Voelkl H., Kiesskalt A, Wartzack S.: “Design for Composites: Derivation of Manufacturable Geometries for Unidirectional Tape Laying”, In: Proceedings of the Design Society: International Conference on Engineering Design 1 (2019), Nr.1, S. 2687-2696

[6] Nutini M, Vitali M.: “Interactive failure criteria for glass fibre reinforced polypropylene: validation on an industrial part”. Int. J. Crashworthiness 2017;24(1): 24–38. https://doi.org/10.1080/13588265.2017.1389629.

[7] Hill R.: “The mathematical theory of plasticity”. Oxford: Clarendon Press; 1998.

Enhancing ML-Based VRU Injury Prediction with High-Fidelity Crash Simulation Data and Domain Knowledge

Niranjan Ballal, Thomas Soot, Dr. Michael Dlugosch (Fraunhofer Institute for High-Speed Dynamics,)

1 Summary

In the domain of automotive safety engineering, the utilization of machine learning (ML) techniques is emerging as a pivotal tool for predicting crash dynamics in (near) real time. The effectiveness of an ML model heavily relies on suitable model architectures, underscoring the importance of quality data for training. Given the challenges and limitations of using existing real-world crash data for this prediction, there's a dependence on reliable synthetic data sources such as FE crash simulation data. Crash simulation data, despite expensive to obtain, offers unparalleled fidelity and the information about the underlying physics that is not always available from real-world crash data. Simple ML architectures often rely only on scenario parameters like impact velocity from crash simulation data to directly predict crash dynamics such as intrusion or injury. But the wealth of information within crash simulation data enables a more nuanced approach to prediction, one that leverages domain expertise in combination with all the details of the underlying physical phenomena. Our proposed method capitalizes on domain knowledge to dissect the problem domain into smaller, more homogeneous sub-domains based on specific physical phenomena, thereby reducing degrees of freedom (DoF) within a ML model. By doing so, we unlock the latent insights embedded within the simulation data and pave the way for more accurate injury predictions with less samples because of reduction of DoF. Central to our approach is the construction of model trees that are guided by domain expertise, delineating the problem domain into distinct sub-domains. Data from each sub-domain is then used to train a unique ML model tailored to its specific simulation traits, rather than relying on a single complex ML model to capture the varied simulation response. This strategy optimizes data utilization, enhances prediction accuracy, and minimizes reliance on one-size-fits-all models. Through comprehensive evaluation, we compare the performance of our methodology against traditional prediction models, emphasizing its effectiveness in capturing intricate simulation dynamics and improving prediction performance.

Fraunhofer EMI

Fraunhofer-Institut für Kurzzeit-dynamik, Ernst-Mach-Institut, EMI

Niranjan Ballal, Thomas Soot, Dr. Michael Dlugosch

Enhancing ML-Based VRU Injury Prediction with High-Fidelity Crash Simulation Data and Domain Knowledge

Fraunhofer-Gesellschaft and Fraunhofer Ernst-Mach-Institut

EMI is one of the 76 institutes that are a part of Fraunhofer-Gesellschaft

Fraunhofer-Gesellschaft

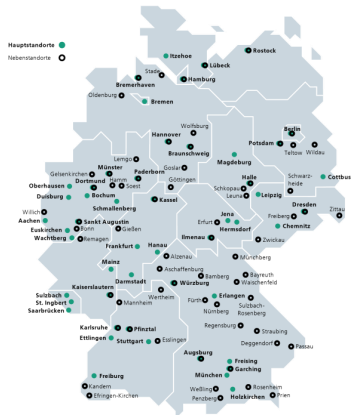

- > 30,000 employees
- 76 Institutes and research units

Fraunhofer Ernst-Mach-Institut

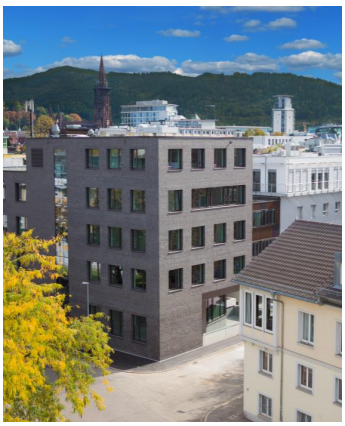

- ~ 360 employees
- 3 locations

Defense | Security | Automotive | Space | Aviation

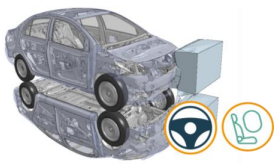

- Crash center with X-ray Car Crash tech
- Analytics and data-driven engineering
- AD and multi-modal traffic simulation
- Battery and H2 safety
- Materials characterization and modelling

Fraunhofer EMI

Motivation

Data-driven prediction of injury risks can benefit decision making in multi-modal traffic safety

Vulnerable Road Users (VRUs) have the largest share of deaths in urban traffic

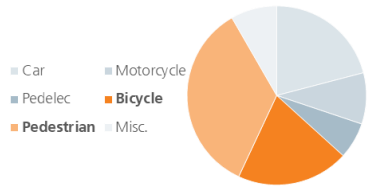

Overproportionate share and increasing severity of injuries in VRUs

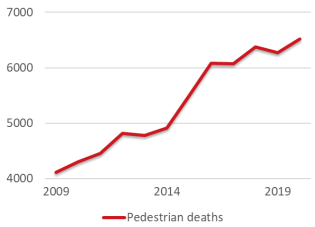

Mitigate injury severity

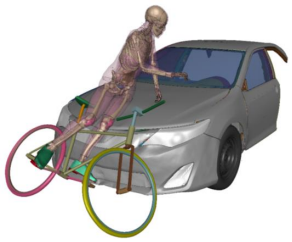

ML-based injury mitigation in project ATTENTION*

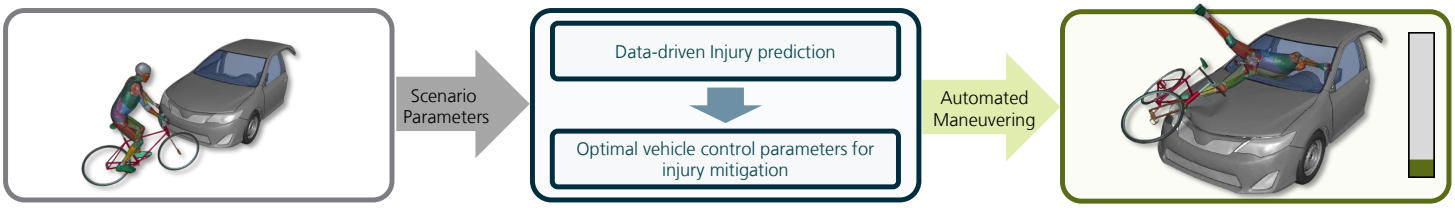

*The project ATTENTION is funded by the German Federal Ministry for Economic Affairs and Climate Action

Fraunhofer EMI

Challenges for Real-time Injury Prediction with ML

Opportunity to leverage underlying physics present in high-fidelity FE simulation

Global Modeling

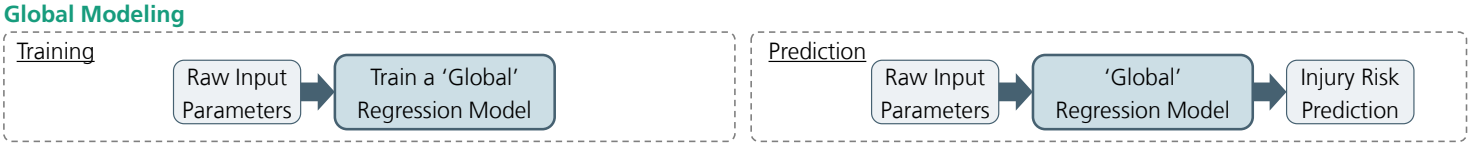

But,

- Limited or no availability of training data
- Higher complexity and DoFs in the Regression Model
- High computational cost of high-fidelity Finite Element simulations → Expert-augmented methods to leverage dense information present in each simulation

Fraunhofer EMI

Proposed Approach for Real-time Injury Prediction with ML

Decomposing the Problem Domain Using »Hierarchical Model-Tree« Approach

Model Training – »Hierarchical Model-Tree« Approach

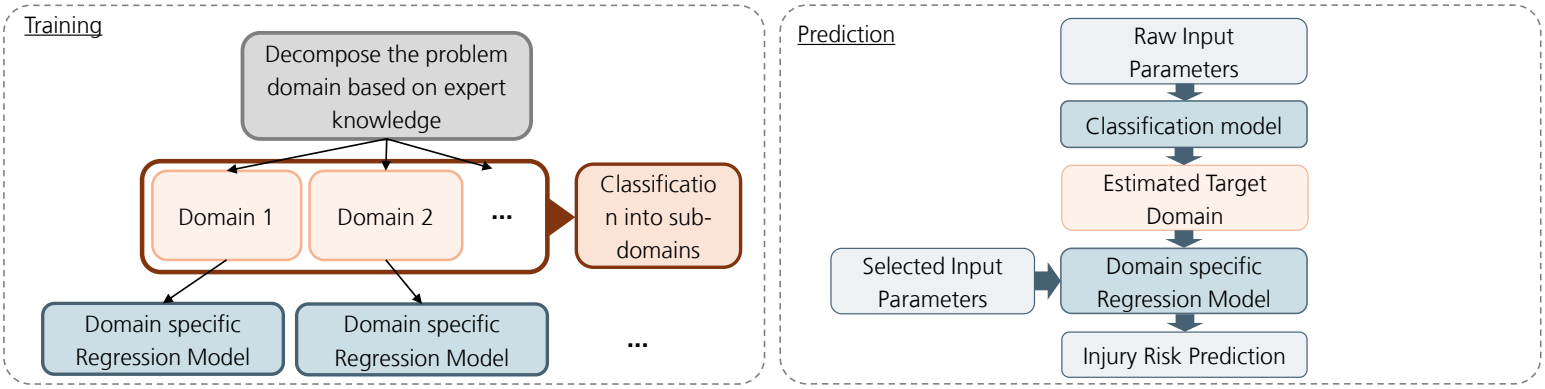

Fraunhofer EMI

Standard Global Modeling Approach to Mitigate Injury Risk

One ML model to predict all injuries or individual ML models to predict individual injuries

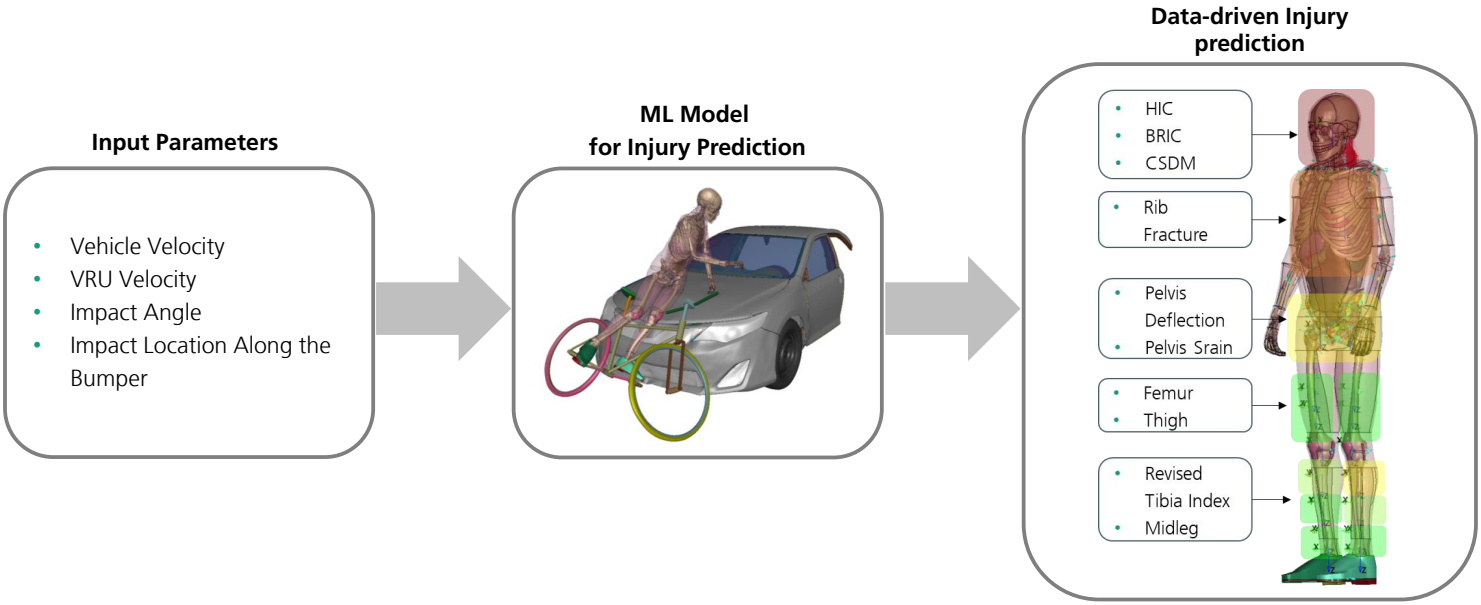

Fraunhofer EMI

Our Proposed Approach to Mitigate Injury Risk

Delineate the problem domain into distinct sub-domains

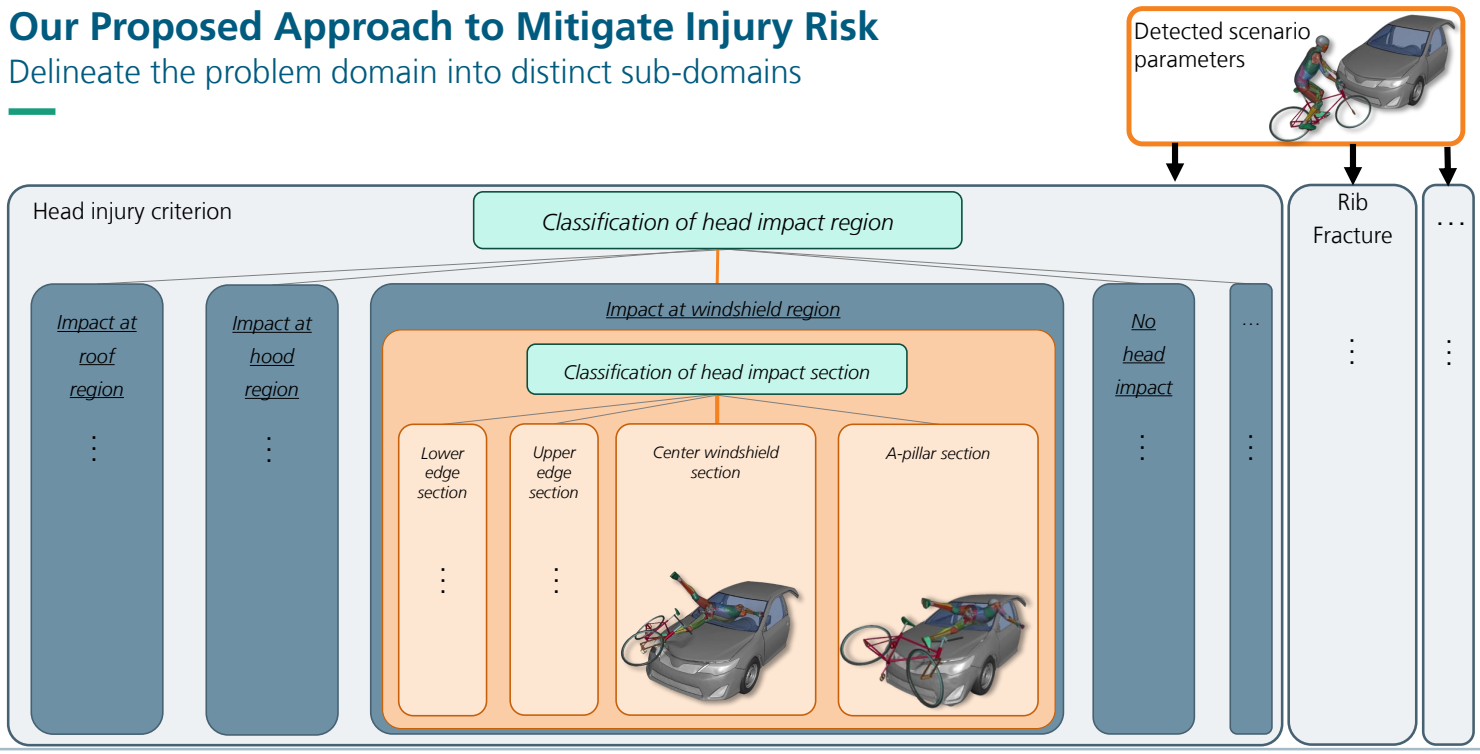

Fraunhofer EMI

Comparison of Results for Head Impact at Windshield Region

»Hierarchical Model-Tree« approach outperforms Global Modeling

Global Modeling

	R2 Test Score
All simulations with first contact with Windshield	0.478

»Hierarchical Model-Tree« Approach

Section	R2 Test Score
WS Center	0.904
A-Pillar	0.803
Transition	0.519

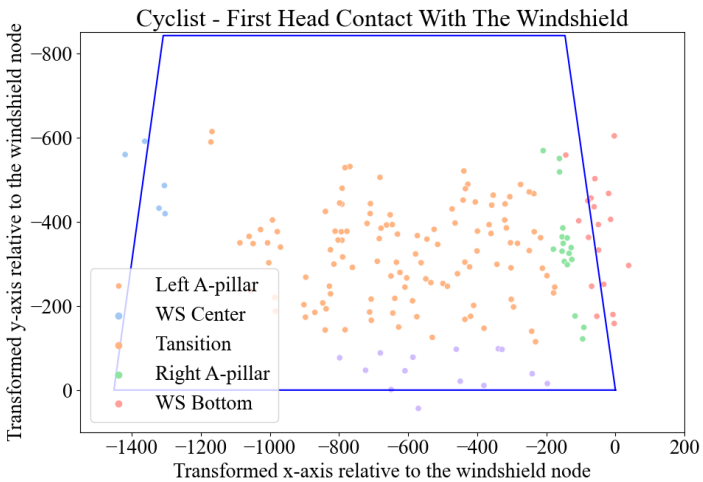

Fraunhofer EMI

Thank You

Fraunhofer EMI

Niranjan Ballal
Digital Engineering
Fraunhofer EMI
Phone: +49 761/2714-358
Niranjan.Ballal@emi.fraunhofer.de
http://www.emi.fraunhofer.de

Scan me to know more about DE ☺

Digital Engineering

Structured representation of the relationship between model changes and findings from the simulation results analysis using an explorative ML-based approach

D. Steffes-lai[1], R. Iza-Teran[1], M. Pathare[1], T. N. Klein[1], J. Garcke[1]

[1] Fraunhofer SCAI, Schloss Birlinghoven 1, 53757 Sankt Augustin

1 Summary

In any CAE crashworthiness development project, many model changes are made to fulfill design criteria and regulations for crash safety. All the resulting simulations have to be analyzed. Recently we have developed a methodology for an automated comparison of multiple simulation results, with the aim of automatically detecting similar simulation results as well as unexpected deformation behavior or distribution of mesh functions, called events. However, bringing the applied model changes into relation with the detected events is still a major challenge. The overall goal is to automatically find correlations between model changes and effects in order to learn from these relationships for future projects. Several steps are necessary to support this kind of analysis. First, a structured representation of all model changes across multiple iterations is required. Second, the simulation results must be present in the same structured way. Third, these two already complex analyses need to be combined in a structured way to enable correlation analysis. To address this, we have investigated a machine learning approach for the data from model changes to obtain a structured representation of all model changes over several iterations with respect to a reference model. This approach considers several categories of model changes, among them thickness changes, material changes, as well as geometrical changes. On the other hand, we have significantly enhanced our software tool SimExplore to allow the access to parametrized model changes in the resulting structured representation of simulation results. This is a first step to process changes in simulation results together with underlying model changes for the first time and thus simplify the detection of possible correlations. We demonstrate our developed explorative ML-based approach on a frontal crash scenario.

2 Introduction

Numerical simulations play an important role in the automotive product development process. Particularly in the CAE-based crashworthiness analysis process, the large number of design possibilities combined with increasing requirements and regulations for crash safety lead to large so-called development trees. These reflect the many undertaken design measures and corresponding simulation runs performed until given design criteria are satisfied. A key challenge is to learn useful designs from a set of model changes and corresponding simulation results, for example to mitigate undesired deformations. The complex and diverse data to be studied suggests the use of AI approaches to handle the complexity of the evaluation. Specifically machine learning has gotten impressive results for image recognition as well as for learning complicated tasks using data. Methods that can learn from existing data and then make predictions for related, but new situations are indeed very attractive for product development. However, most existing machine learning methods are not directly applicable to the analysis of CAE data. On the one hand, they require large amounts of training data, which are not available because simulations are computationally intensive, and on the other hand, the data are high-dimensional, where the dimensionality is given by the size of the finite element meshes. Until now engineers are limited to investigate key values for the simulation outcomes and scalar values for input changes automatically. However geometrical changes play a major role in the product development. We have developed approaches specifically adapted to CAE simulations that overcome these limitations. Specifically, we employ our own approaches to provide an overview of many simulation results, in particular to analyze similarities or exceptions in deformations and mesh functions, called events. Moreover, the investigation of the similarity propagation over time is a powerful means to support the engineer in the complex and highly important task of load path detection to understand the energy absorption in the crash load case. However, bringing the applied model changes, called measures, into relation with the detected events is still a major challenge. The overall goal is to automatically find correlations between model changes and effects in order to learn from these relationships for future projects.

In addition to the simulation outputs, the design measures as input to the simulations are very heterogeneous, including changes in geometry, in material parameters, or in welds. Thus, representing measure information as features for machine learning algorithms is still a challenge. To address this, we have investigated a machine learning approach for the data from model changes to obtain a structured representation of all model changes over several iterations with respect to a reference model. Assuming the simulation results are present in the same structured way, these two already complex analyses need to be combined in a structured way to enable correlation analysis.
Bringing our representation approaches for model changes as input and simulation results as output together can significantly improve the CAE-based product design process. The combined representation of model changes and results allows to set the model changes into context with the insights from simulation results analysis. This provides a fundamental basis for further post processing of results, like sensitivity and correlation analysis, and thus, is the key to the envisioned future development of AI based assistant systems to support the engineer in decision making in the crashworthiness development process.

3 Automatic detection and structural representation of model changes

Design measures include changes in geometry, in material parameters, or in welds. For example a modification of the B-Pillar might include a geometrical change of a structural member, e.g., a cut or extension, which could require changes in the weld connections or of material thickness. To appropriately deal with all these changes we have developed and implemented a corresponding structured digital representation in our software ModelCompare [6]. Each model can be compared with respect to the respective predecessor or a reference model. A special challenge is the parametrization of geometrical changes to be used with machine learning algorithms which is one of our currently ongoing research topics. A simple way to parametrize geometrical changes is by using a mapping to the reference and comparing the differences as a mesh function. To provide an overview of model changes across several iterations, the results of the comparison of many models can be saved in a (graph) database keeping track of model information using parts and their connections. Furthermore, the database can be queried easily to summarize changes or to search for specific measures applied. Ongoing work is to further extend the semantics of this representation, including components as groups of parts, and on making it available for filtering and searching (semantic) design measures.

4 Similarity analysis of many simulation results

A similarity analysis of many simulation results is one way to get a quick overview of the impact of design variations. With this, simulations behaving similarly are grouped together in clusters whereas different single ones will be located outside of it, called outliers. The advantage to only outlier detection is that we can compare how far the outliers are away from the clusters to rank their severity, and distinguish e.g., transition zones between two behavioural modes. The workflow for similarity analysis is made of two main phases. First, a longer running off-line batch-process, which can run at the simulation cluster where the raw data is available, and a second interactive exploring phase, which can run on a client computer and where in particular the raw data does not need to be available. The results of the first phase are a list of most affected components and the so called shape features necessary for the interactive representation at the second phase. The results of the second phase contain the cluster and outlier information per component, time step, and mesh function together with some scores, e.g., indicating particular components or simulations deviating strongly from other simulations. Furthermore, the existing results can be updated easily with a new simulation. In this case, an event indicator will show if the new simulation belongs to or is between existing behaviour modes. This helps the engineer to interpret the result and to evaluate the model change as useful or not.

4.1 Geometric Fourier approach

We employ suitable similarity concepts to arrange the simulation results in an overview diagram, e.g., to reflect the different deformation modes. In particular, we use a dimensionality reduction approach based on the spectral decomposition of the Laplace-Beltrami (LB) operator on the surface. This can be thought of as a „Fourier-decomposition for geometries", which allows a clustering of many simulations based on their crash behavior using these "geometry-aware Fourier-modes". Formally, for any mesh function f of a simulation result corresponding projection coefficients α_j into the spectral basis are computed. This allows to write f as a linear combination of eigenvectors ϕ_j:

$$f = \sum_{j=1}^{N} \alpha_j \phi_j \, , \alpha_j = \langle f, \phi_j \rangle$$

where N is a chosen number of coefficients, up to the number of grid nodes. Note that usually only a few coefficients in this surface-aware decomposition are needed to represent relevant variations, resulting in a dimensionality reduction. These coefficients have proved useful as low-dimensional coordinates to cluster, for example, deformation changes. The geometric features can be calculated for all components of interest, where a component consists of one or more parts defined in the FE-model.

4.2 Clustering in latent space and interactive exploration

For visualization purposes the number of coefficients is limited to three. Using the geometric features, an optimization algorithm will select three coefficients per component and time step that show the best overall separation into clusters. A density-based clustering algorithm is then applied to identify clusters, i.e., simulations that behave similarly, and outliers, i.e., simulations that behave significantly differently. Furthermore, cluster representatives provide a quick overview of different general deformation modes or functional behavior.
A 3D visualization of the coefficients of the shape features allows a seamless interactive and easy-to-use exploration and analysis of different components, together with selected mesh functions. It provides an intuitive overview of the similarities and exceptions in the simulation results with respect to the selected functions. Clusters and outliers can be easily investigated in this representation by accessing additional information. For example, by selecting in the visualization a point representing a simulation, one can quickly see the corresponding mesh function in a 3D viewer, or other relevant data from the selected simulation run. For outliers it will be possible to investigate connections to design measures easily, based on the introduced structured data representation.

4.3 Identify the simulations or components with the largest deviations

To further automate the process, an outlier score is computed per function, component, and simulation. The outlier score is mainly based on the distance of the simulation from the cluster means, with respect to the deformations or other selected mesh functions. After an aggregation over all time steps and a normalization the outlier score allows a ranking of the simulations with respect to their deviations from the other analyzed simulations. Highly ranked simulations are outliers and most often worthwhile to investigate in more detail.
In addition to a score per simulation, we developed a component score that helps to find patterns in the deviations per component across all simulations and all time steps. The component score is based on the difference between the component of the outlier simulations and the simulations within clusters. Several suitable metrics and methods are available for distance calculation and aggregation. We provide a score which reflects real distances in the used function, e.g. deformations in [mm], so that the score is interpretable by the user. The aim of the analysis is to see if there are components in the group of outlier simulations that always show large deviations compared to the simulations within clusters. These components could be a good starting point to improve or stabilize the crash behavior of the model.

5 Ability for correlation analysis between measures and simulation results

The most important basic step to set model changes into context with the insights from the simulation result analysis is a structured, parametrized representation of all model changes as well as the same structured representation of simulation results. With our developments for measures described in section 3 and the representation of simulation results described in section 4.1 we have achieved such a common representation. Fig. 5 illustrates that by selecting a point representing a simulation in the visualization, the corresponding model changes can be displayed immediately. Based on the parametrized measures, a state-of-the art correlation method, like basic Pearson correlation values, can be evaluated. It is important to emphasize that the connection of the information between changes and simulation outcomes is possible due to the features computed in section 4.1 that allows the parametrization and corresponding representation of geometric information.

6 Experimental Results for a Toyota Yaris frontal crash analysis

We demonstrate our developed explorative ML-based approach on a frontal crash scenario. Our study is based on the Toyota Yaris study for a Euro NCAP front crash with a velocity of 56 km/h against a rigid wall which was set up and presented in [4, 5]. The study is restricted to the body in white parts of the vehicle, see Fig. 1. Changes are applied to main structural beams adding beads as well as changing the position of them, whereas weight reduction is obtained by reducing the thickness of 4 main structural members, see [4]. Our analysis uses only a subset of in total 10 simulations for illustration purposes.

6.1 Overview of Model Changes

ModelCompare runs over all models with respect to the reference model and detects all applied changes and categorizes them into the two groups thickness changes and geometrical changes. Then we run a graph database server and feed the compare results into it to get an overview of all changes as

described in section 3 and [7]. The obtained summary is given in a plotly dash web interface. Fig. 1 shows the corresponding graph presentation of all parts in the model as points colorized with all model changes in the dataset in different categories. To get a full overview about all changes in a specific category in the entire dataset the changes need to be parametrized accordingly. Scalar changes, for example, all thickness changes, can be represented in a diagram using a dimensional reduction method like principal component analysis. An example for the left structural beams varied is given in Fig. 2. With our research on parametrizing also geometrical changes in a similar way, a full overview would be provided which builds the basis for the connection of changes and resulting simulation behavior.

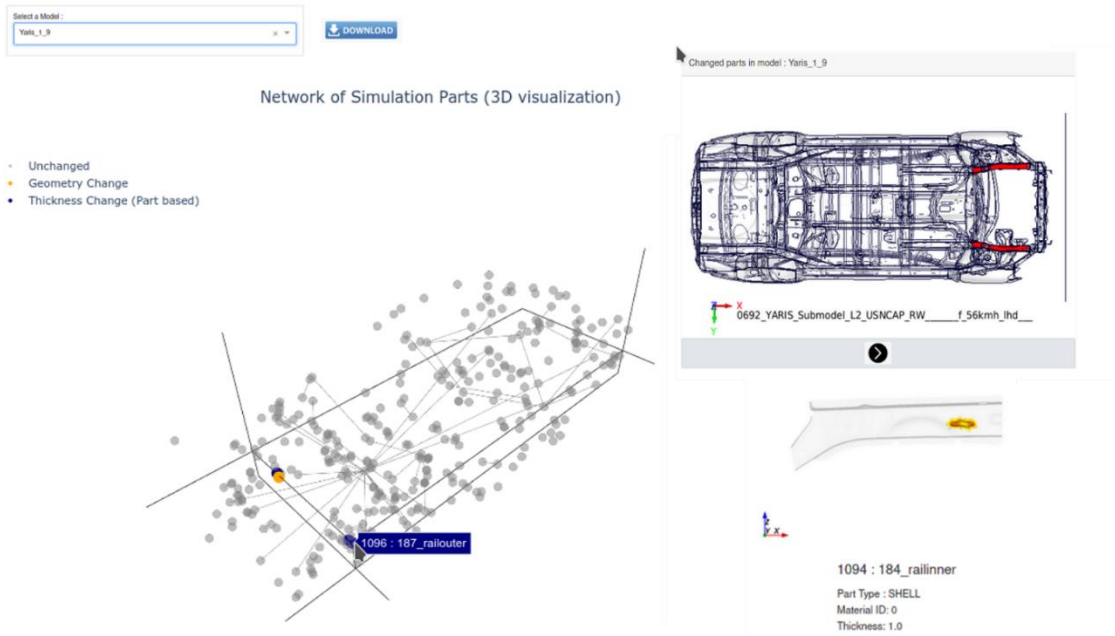

Fig. 1
Graph presentation of all parts in the model to easily navigate through all the model changes. Left: Each point is one single part of the model colorized with its change for the selected model. Right above: the changed parts in the model are highlighted in red, right below: Click on a part (point) in the graph view shows the corresponding part together with its change, in this case a bead position was changed.

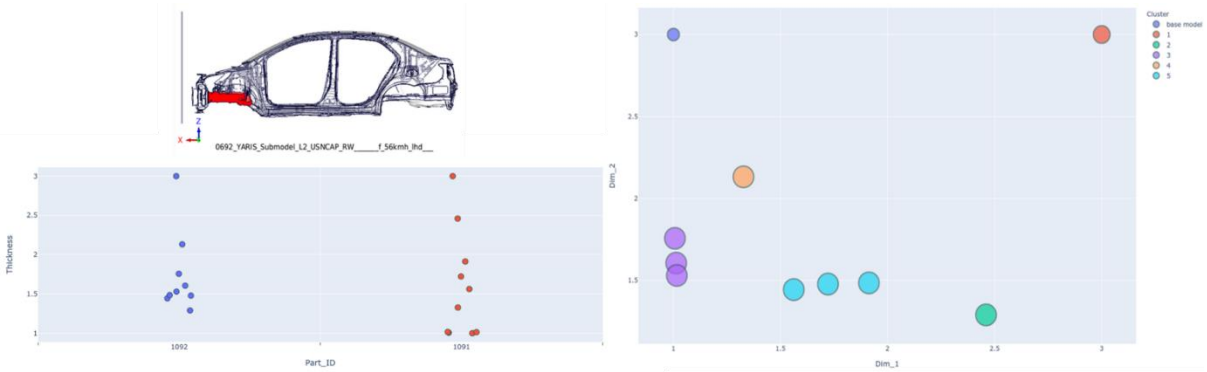

Fig. 2
Overview of all thickness changes in the dataset applied to the left structural beams “inner rail, pid 1092” and “outer rail, pid 1091”. Left: The thicknesses of these two parts are varied in [1,3] mm, each point corresponds to one model. Right: the models are arranged in a diagram based on the similarity of applied thickness change using a dimension reduction method.

6.2 Similarity analysis of simulation results

The next step is the analysis of corresponding simulation results, for example, the resulting deformations. The outlier score identifies two simulations behaving very differently compared to the others in the dataset. The component score identifies few parts with the main deviations between the several simulations. Fig. 3 shows the deformation clusters in low dimensional coordinates exemplary for the firewall. The mesh together with the deformation values are reconstructed on the fly with the geometry-aware Fourier-modes.

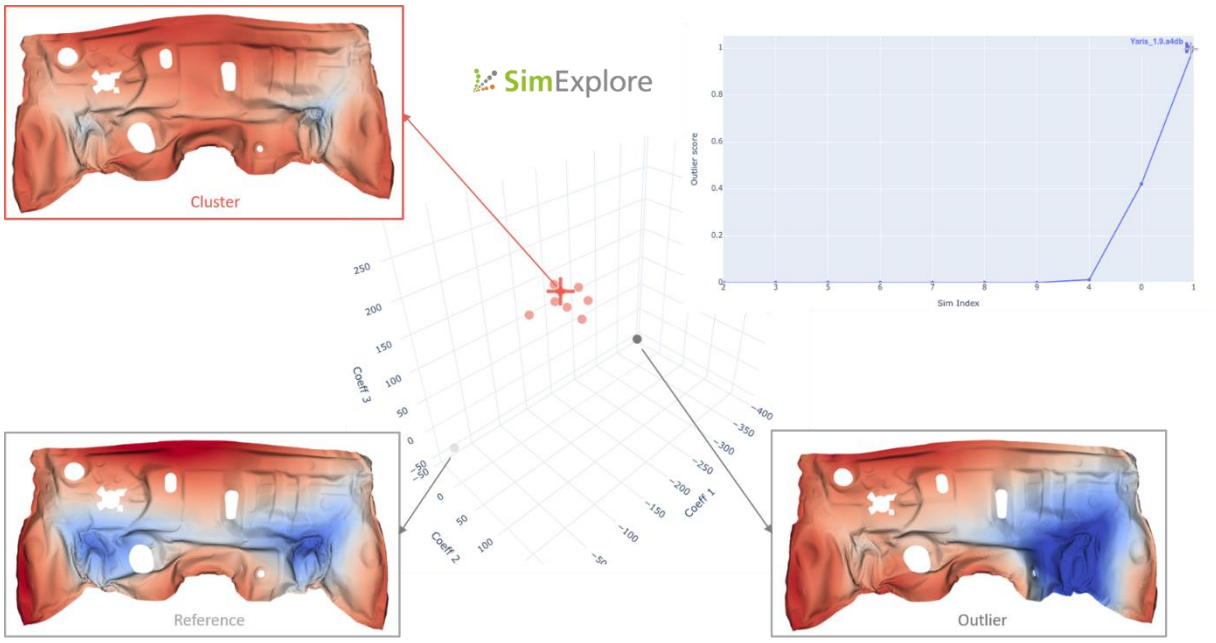

Fig. 3
The simulations are arranged in a diagram due to their similarity based on the deformations of the firewall. Our approach could identify two simulations, marked as outliers (grey points), which behave differently compared to the ones in the red cluster, and which are detected with the outlier score.

6.3 Correlations between model changes and events

The underlying data structure and parametrization of input changes and simulation results allows to set the model changes into context with the deformation patterns of the parts. As a first example, we investigate the linear Pearson correlation between the applied thickness changes and the deformation

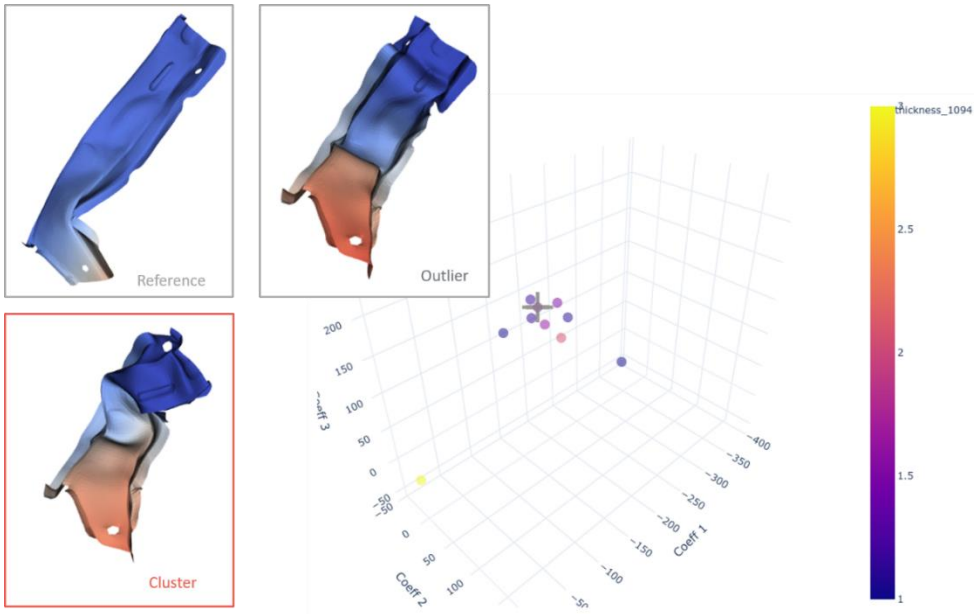

modes of the firewall in Fig. 4. Additionally, by clicking on the simulation (point) in the diagram all corresponding model changes compared to its predecessor are accessed and displayed as in Fig. 5 to get a full overview.

Fig. 4
A Pearson correlation analysis with the thickness changes applied in the dataset show a correlation with the thickness of the left inner rail colorized in the embedding. The reconstructed part and its deformation in the three selected points from Fig. 3 is shown.

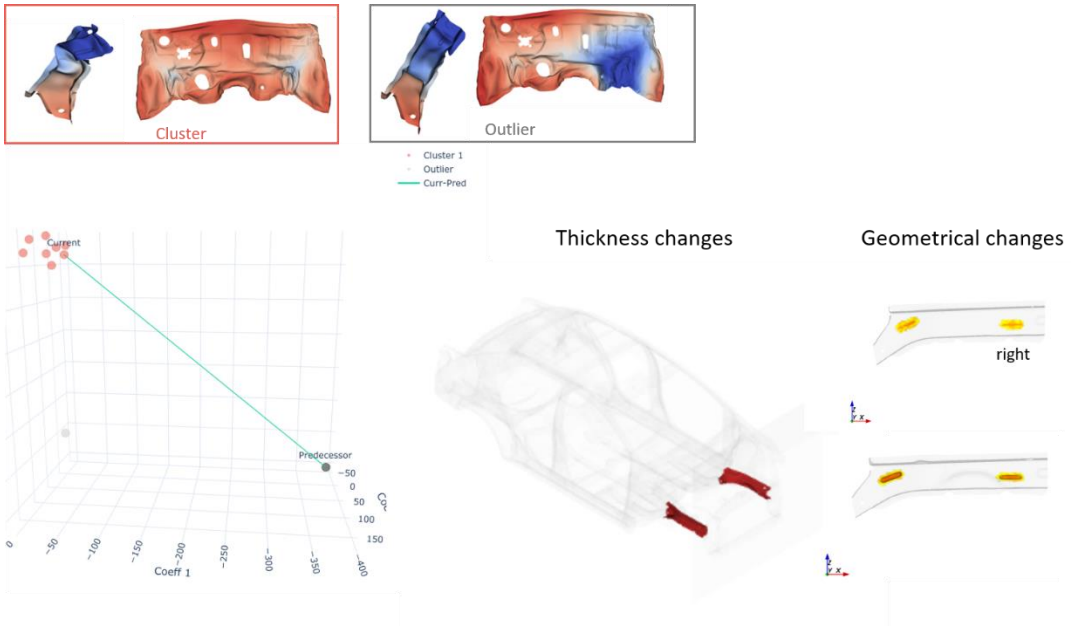

Fig. 5
A comparison of the current simulation with its predecessor and all applied changes detected with ModelCompare become possible.

6.4 Load path detection using the component score

The developed component score provides a ranking of the components with respect to their amount of differences in the changes in deformation behavior. A fringe plot of the component score can be useful to understand changes in the load path during the crash due to model changes. Fig. 6 shows the component scores on the reference simulation in different time steps. The changes in deformation start at the right side of the car and continue over the firewall to the left side.

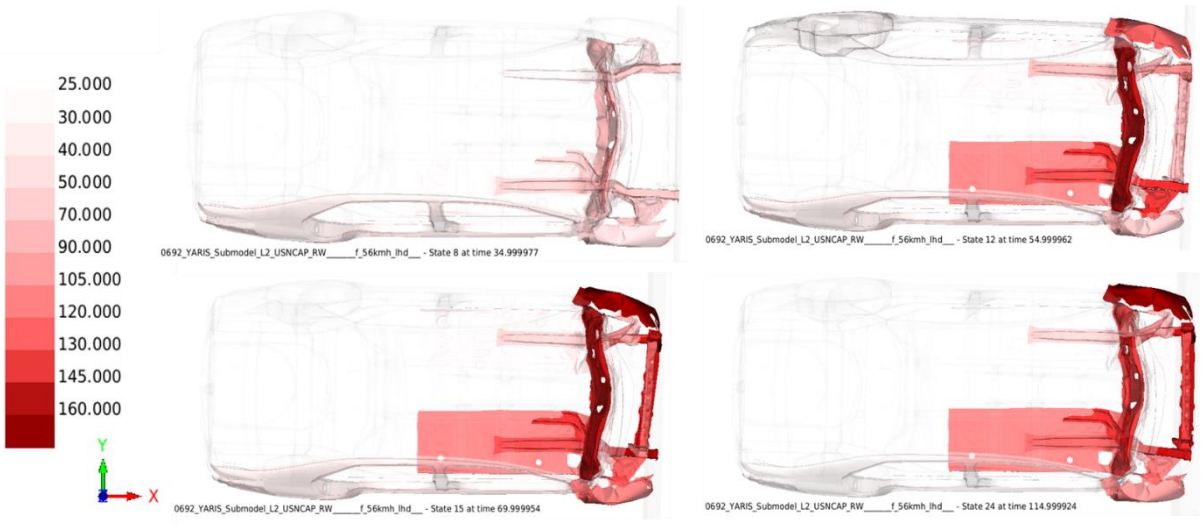

Fig. 6
A fringe plot of the component score over time can indicate changes in the load path during the crash due to model changes. The component score is visualized on the reference simulation. The deviation in deformations starts (state 8, 35 ms) at the right side of the car in the structural beams changed and continues over the firewall (state 12, 55 ms) to the left side (state15, 70 ms).

7 Conclusions

The described LB-shape feature approach, as well as the clustering and scoring, are included in SCAI's SimExplore software tool. It supports CAE engineers in their simulation data analysis workflow by providing a browsable overview of many crash simulation results, e.g., in terms of clusters and outliers based on deformations and mesh functions. In particular, SimExplore provides a web-based application for interactive visualization.
The capabilities of the LB-shape feature approach have been investigated using industrial data, for example in [2], [3]. Therein, we examine simulation data from a robustness analysis of a vehicle front-end crash load case where the wall thicknesses of several selected components have been varied. The simulation results are analysed to identify similarities as well as outliers in the deformation behavior.
Overall, this novel and patented LB-shape feature approach enables not only automatic classification of simulation behavior, but also an adequate parametrization of geometric information which enables a representation of the information such that changes can be mapped to outcomes. This type of analysis as available in SimExplore, represents a breakthrough towards an automatic event detection for car crash simulations within the overall crashworthiness data analysis process.

8 References

[1] Iza-Teran R., and Garcke J.: "A geometrical method for low-dimensional representations of simulations". SIAM/ASA Journal on Uncertainty Quantification, 7(2):472–496, 2019

[2] Steffes-lai D., Pathare M., and Garcke J.: "Towards a Framework for Automatic Event Detection for Car Crash Simulations". In NAFEMS World Congress 2021, 2021

[3] Garcke J., Iza-Teran R., Pathare M., Schwanitz P., Steffes-lai D.: „Identifying similarities and exceptions in deformations and mesh functions comparing many simulation results automatically". SIMVEC Kongress, Baden-Baden 2022, VDI Berichte 2407:277-288, ISBN: 978-3-18-092407-6, 2022

[4] Singh H., Schumacher A., et.al.: „Hierarchical Multi-Level-Optimization of crashworthy structures using automatic generated submodels". In 11th European LS-DYNA Conference 2017, Salzburg, Austria, 2017

[5] Falconi D. C.J., Walser A.F., Singh H., Schumacher A.: "Automatic Generation, Validation and Correlation of the Submodels for the Use in the Optimization of Crashworthy Structures". In: Schumacher A., Vietor T., Fiebig S., Bletzinger KU., Maute K. (eds): Advances in Structural and Multidisciplinary Optimization. WCSMO 2017. Springer, Cham., https://doi.org/10.1007/978-3-319-67988-4_117, 2018.

[6] Garcke J., Pathare M., and Prabakaran. N.: "ModelCompare", In Griebel M., Schüller A., and Schweitzer M.A., editors, Scientific Computing and Algorithms in Industrial Simulations: Projects and Products of Fraunhofer SCAI, pages 199–205. Springer International Publishing, Cham, 2017.

[7] Thakur S.: "Modelling and Analysis of Automobile Simulations using Knowledge Graphs", Master of Science Thesis, Computer Science, University of Bonn, 2021.

Machine Learning Optimization and Quick Verification of an Electric Vehicle Rocker Design

Dipl.-Ing. C. Chatzigeorgiadou, Dipl.-Ing. A. Papadopoulos,
MSc Dipl.-Ing D. Drougkas, Dipl.-Ing. Dipl.-Wirt.Ing. Athanasios Fassas

(BETA CAE Systems, Greece)

Abstract

Prior to their market debut, all prototypes of vehicles undergo validation for their crashworthiness. Achieving compliance with safety standards, while simultaneously avoiding compromises in other crucial design aspects, demands a highly detailed engineering simulation approach during the product design phase. These processes become even more complicated, and time-consuming, with electric vehicles, such as Lithium-ion battery-powered cars. In many cases to accomplish the safety aims during product design, while also meeting time limitations and deadlines, sophisticated simulation tools need to be employed. Such tools are those that enable optimization studies and that take advantage of Machine Learning capabilities.

In this study, an optimization and a quick verification of an electric vehicle rocker design were performed with the aid of an Optimization tool and Machine Learning methods.

This Optimization tool employs Design Experiments and a Machine Learning predictive model (referred to as a "Predictor") to approach optimal design parameters for a given objective and constraints. This extends to quick verification of new designs, enabling rapid testing of modifications without re-solving the model. To enhance efficiency, a macroscopic battery model is used, allowing the ML Predictor to consider electromagnetic phenomena in damaged batteries without increasing solution time in side-crash simulations.

All in all, using the Machine Learning based Optimization tool, and the Transfer Learning related functionality, an already trained predictive model was able to estimate the optimal design of the vehicle with updated components and verified the updated designs without having to re-run the complete optimization and solution processes.

1. Optimization Method and Model Description

The current study focuses on the crash simulation of a Li-ion battery-powered EV module platform which is imposed to a side collision with a rigid pillar at 60 km/h. For the battery modeling of the li-ion batteries located inside the platform, the macroscopic battery model “BatMac” based on the equivalent Randles circuit was used. For the investigation of an internal battery short, LS-DYNA provides a keyword that triggers the short when the criteria defined inside the function are me. In the current case, the shorting conditions are based on the stress values applied to each cell. When the stress exceeds a particular value, an internal battery short occurs.

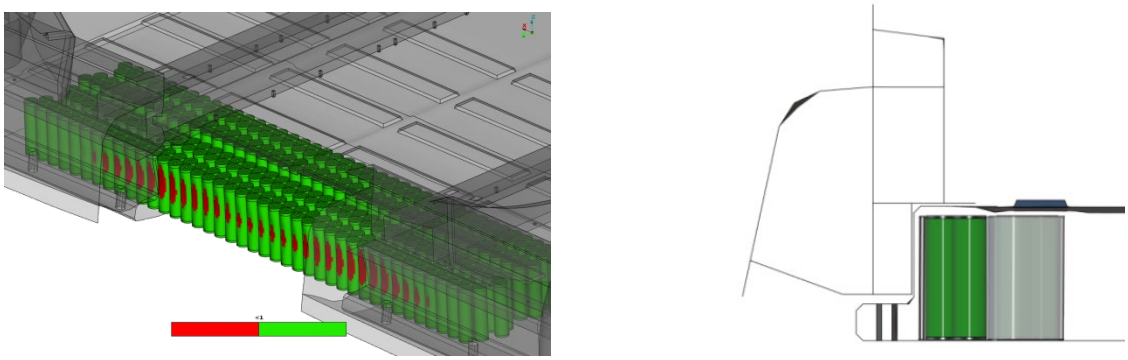

Figure 1: Side-crash simulation model of the electric vehicle

Regarding the optimization workflow, a set of pre- and post-processing functionalities were used, accelerating the optimization process of an electric car platform design, using the embedded Machine Learning Optimization tool. Specifically, the process consists of setting up an Optimization Task which embeds the Design of Experiment method to produce several DOE studies. The design parameters whose value varies from study to study, are referred to as Design Variables, and the dependent critical results as Responses. Based on these datasets, an ML Predictor is trained using the Response Surface Model. Then, the objective and constraints of the Optimization Study are defined, and finally, by utilizing the predictive model of the Predictor, the Optimizer returns the optimal solution. In the studied optimization scenario, the objective is to minimize the number of damaged batteries without increasing the rocker’s mass, and hence, the corresponding values were assigned as Responses. The defined Design Variables are the rocker plates’ thickness and location variation along the y-axis.

2. Predictive Model and Optimization Results

The values of the design variables are obtained by the Uniform Latin Hypercube DOE generation algorithm. For each iteration, the generated experiments with the different DV values are solved and post-processed as assigned in the Optimization Task workflow. This way, a file repository occurs, containing all the necessary data to train a predictor. In this case, 100 DOEs were solved.

To evaluate the quality of this dataset, information can be retrieved from the Correlation Matrix and the Pair Plot of the DVs versus the Responses, as well as the Power Predictive score. In the following matrix, the correlation is described through a factor that fluctuates between -1 and 1. Values close to 0 mean that there is not any relationship between the DVs and responses, and values closer to 1 and -1 mean that there is a strong correlation. In this case, it is highlighted that the mass is mainly affected by thicknesses 1 and 2 and the number of damaged cells is affected mostly by Plate Location and Thickness 2. The positive and negative signs imply that the variables are proportional and reversely proportional, respectively.

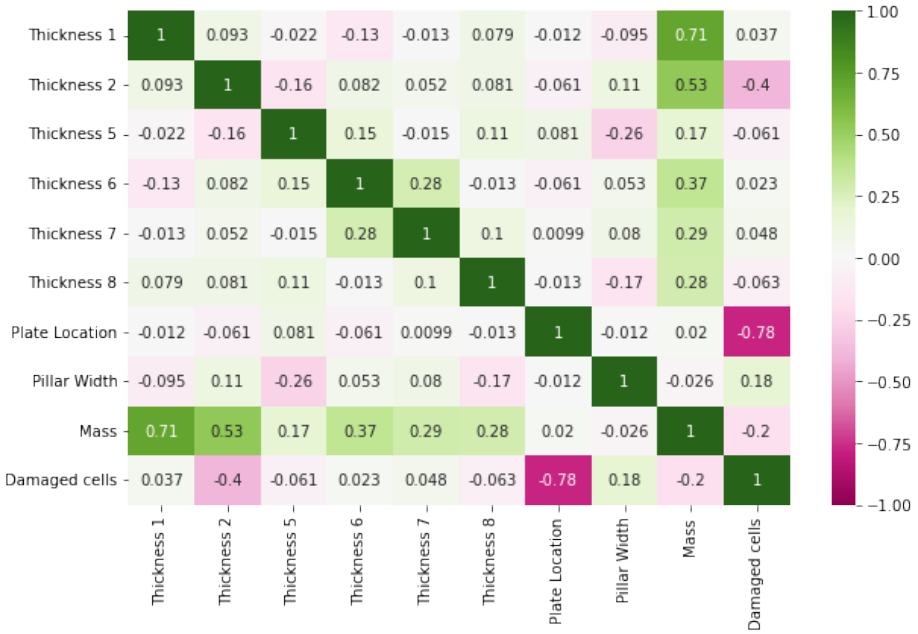

Figure 2: Correlation Matrix

In the following pair plots, each DV's values are depicted versus the corresponding response value. In the plots where patterns are noted e.g., in thickness 1 vs mass or Plate Location vs Num. of damaged cells, it is safe to assume that there is a linear correlation between the corresponding variables.

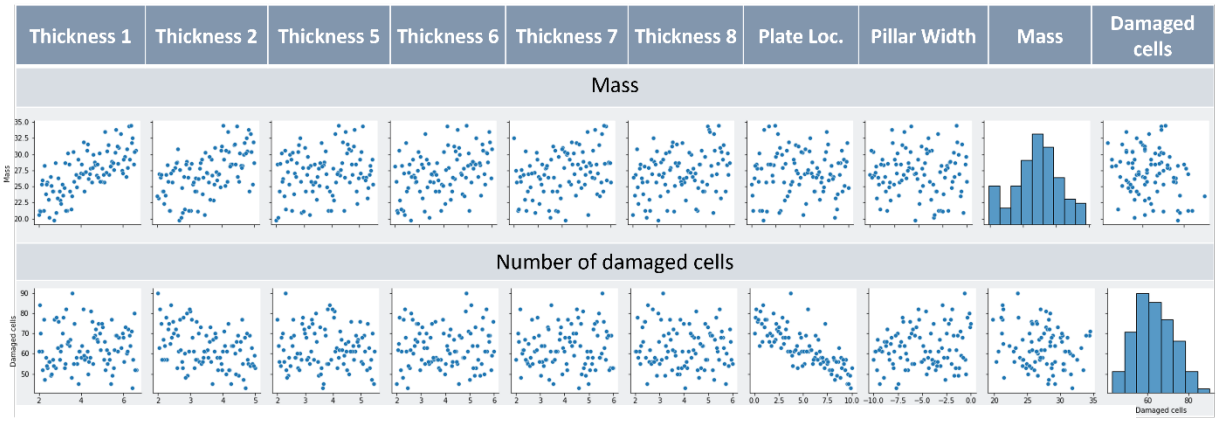

Figure 3: Pair Plots of the Responses vs. DVs

Lastly, the predictive power score (PPS) is an asymmetric, data-type-agnostic score that can detect linear or non-linear relationships between two columns. The score takes values between 0 (which means no predictive power) and 1 (which means perfect predictive power). For the Mass, the PPS is 0.98 whilst for the Number of Damaged Cells is 0.64.

The occurring calculated predictive model calculates the relationship between the Design Variables and the Responses using a Regression method. Once the predictor is trained, graphs are reported giving information about the quality of the Predictor. The shown bar chart sorts the design variables according to their importance in the optimization process. As shown, the number of damaged cells is mostly affected by the plate location, whilst the mass mostly depends on the thickness of plate 1. Then, from the variance estimation graph, the predictions with their confidence bounds are indicated. The Minimum Average Error of Variance is the minimum error of the confidence bounds for each

prediction and the Accuracy is the percentage of the configuration bounds that correctly include the ground truth value.

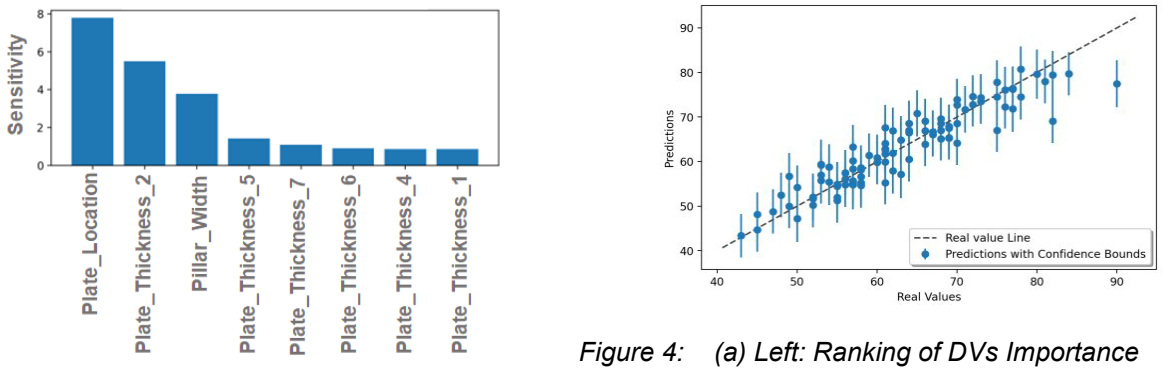

Figure 4: (a) Left: Ranking of DVs Importance regarding the number of damaged cells. (b) Right: Variance Estimation graph.

Finally, using the Differential Evolution method, the Optimization Study is run resulting in the optimal solution. As shown below, all the studies explored by the Optimizer do not exceed the Mass constraint of 36 kg. The optimal solution is the last study which suggests that the predicted mass is at 24.5 kg whilst the predicted damaged batteries are 37.

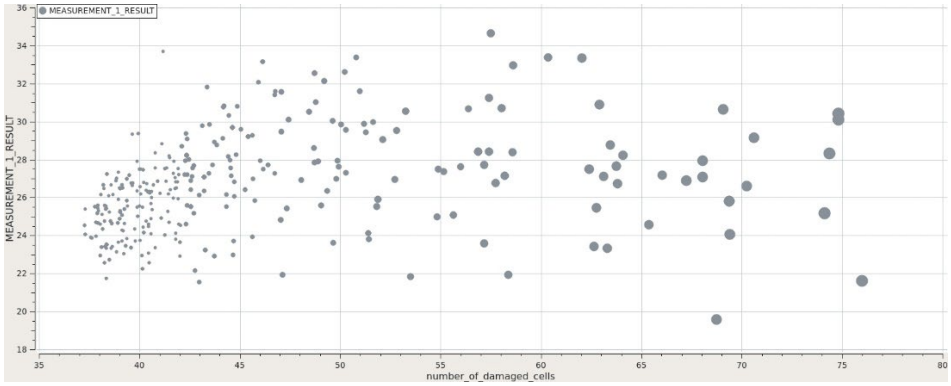

Figure 5: Optimization Studies: Mass vs Number of Damaged Cells

Moreover, the optimized model is solved conventionally to validate the optimization process, while also the optimization results are evaluated overall.

Response	Initial Model	Predicted Optimal	Validated Model
Mass [kg]	37.56	24.57	24.39
Num. of damaged cells	68	37	46

Table 1: Evaluation of Optimization Results

3. Quick Verification of the Modified EV Model

The predictive model trained previously can be used in cases where the initial model has been slightly modified on areas affected by the design variables and they have a relatively high similarity factor among the parameters of the baseline model. The response values can be quickly predicted without requiring solving the model. So, this way, the changes in the geometry can be quickly evaluated. Again, the results were validated and they highlight that the particular change in the plate's thickness will worsen the crash behavior of the vehicle. This way, the designers can save a significant amount of time during the early design stages, as they are prevented from following the wrong design direction without requiring solving numerous design scenarios.

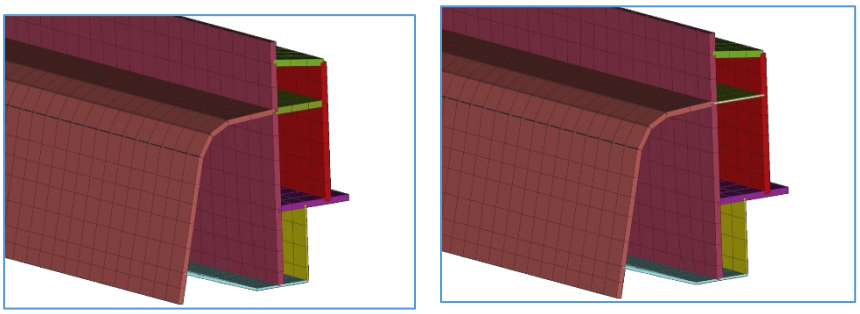

Figure 6: (a) Left: Initial rocker design, (b) Right: Modified rocker design

Response	Initial Model	Predicted	Real Modified
Mass [kg]	37.56	35.8	35.82
Num. of damaged cells	68	72	73

Table 2: Evaluation of Quick Verification Results

4. Conclusions

To conclude, the ML Optimization process discussed in this study introduces a semi-automated way: (a) to produce the required data to train an ML Predictor, (b) to estimate the optimal design of an EV using the trained Predictor and (c) to quickly evaluate potential relatively small modifications to the Baseline Model without demanding training a new predictive model. Lastly, the embedded plotting functionalities facilitate the visualization of the ML-related results, allowing the inspection of the Predictor accuracy as well as to evaluate the whole Optimization process.

Multidisciplinary Design Optimization for Additive Manufacturing Repair

Talal Akkaoui, Michela Turrin[1], Stijn Brancart[2], Babak Gholami[3]

[1]Design Informatics, Department of Architectural Engineering and Technology, Faculty of Architecture and the Built Environment, Delft University of Technology, Julianalaan 134, 2628 BL Delft, The Netherlands; M.Turrin@tudelft.nl

[2]Structural Design and Mechanics, Department of Architectural Engineering and Technology, Faculty of Architecture and the Built Environment, Delft University of Technology, Julianalaan 134, 2628 BL Delft, The Netherlands; S.Brancart@tudelft.nl

[3]Product Owner: Generative Design, Functional Development and Data Management division, BMW Group; Babak.Gholami@bmw.de

Abstract:

The circular economy proposes recovery strategies that extend the service life of technical nutrients at their end-of-life (EoL) to create more sustainable consumption and production patterns. Current hardware component development overlooks EoL strategies in the conceptual design stage, and postpones them to later stages of development, this often results in unsustainable EoL scenarios such as landfilling. With the aim of implementing an EoL strategy in the conceptual design process, a computational workflow is developed that implements an additive manufacturing (AM) repair strategy into a component's conceptual design using multidisciplinary design optimization. The optimization is multi-objective as it aims to minimize both material consumption of the initial design and filament consumption of the future AM repair process. To do so, the developed method integrates the parametric design of the component with a damage simulation and an AM simulation. A wall panel is used as a case study where including a AM repair considerations in the design, not over dimensioning the design, and maintaining good aesthetic performance are considered as design priorities. The resulting pareto front reveals geometry data, damage behavior, AM repair cost, aesthetic performance, and material footprint of different design options. The optimum design space achieves a geometry's volume reduction of up to 44.28% and reduction of the AM repair filament consumption of up to 43.41%. Four main conclusions were revealed. First, the method supports the generation and exploration of design options and provides performance information to the designer making it a useful conceptual design tool. Second, the possibility of independent analysis of each process is useful when abstracting the task to find the essential problems. Third, the proposed method requires investment in time and resources in the early design stages, changing the perception of the design process and making it highly dependent on the user-experience of the dedicated software. Finally, damage modes, severity, probability, and detection number highly influence the prioritization between design variables in the conceptual design process.

Keywords: Multidisciplinary Design Optimization, Additive Manufacturing, Repair, Circular Economy, Damage Simulation

1 Introduction

The industrial revolution dating back to the late 18th century brought unprecedented advancements in technology which initiated a “Make-Use-Dispose” industrial model. These unsustainable activities caused a rapid transition towards a destructive production system that pollutes air, water and soil, poorly manages valuable materials, causes diseases, and erodes biodiversity and cultural practices around the world. The circular economy proposes recovery strategies that extend the service life of technical nutrients at their end-of-life (EoL) to create more sustainable production and consumption patterns. The main phases of a product’s development process are task clarification, conceptual design, embodiment design and detail design. The conceptual design phase involves incorporating pre-defined task clarifications into conceptual alternatives which are then compared based on preliminary analysis to select viable concepts for further development in the embodiment and detail design phases [**1**]. Current product development processes overlook EoL recovery strategies in the conceptual design stage, where 80% of a product’s environmental impact is determined, this often results in unsustainable EoL scenarios such as landfilling. With the aim of implementing an EoL recovery strategy in the conceptual design process, a computational workflow is developed that implements an additive manufacturing (AM) repair strategy into a component’s conceptual design using multidisciplinary design optimization. A wall panel is used as a case study and the pre-defined design priorities are to include AM repair considerations in the design, not over dimensioning the design, and maintaining good aesthetic performance.

1.1 Literature Study / Related work

A literature study reveals different methods of implementing design optimization for additive manufacturing for EoL recovery strategies. The methods differ between non-algorithmic, topology optimization, lifecycle costing and artificial intelligence approaches. Research by Wits et al. [**2**] investigate a non-algorithmic optimization of AM for maintenance, repair, and overhaul strategies. The designs are compared in terms of design time, print time and material usage. Executing a topology optimization approach, Liu et al. [**3**] develop a methodology to upgrade and repair existing designs for structural applications. The process itself involves topology optimization on an additive and subtractive manufacturing domain. Three case studies are developed. The first optimizes the design to adapt to a new structural load case which represents its new function. The second remanufactures a damaged part by reinstating its original structural performance. The third optimizes an already topologically optimized part, to a new structural function.

There is a considerable amount of research that employs a lifecycle costing approach. Research by Al Handawi et al. [**4**] integrate repair and replacement cost via a lifecycle cost model into a two-objective optimization of an aeroengine turbine rear structure. First a bi-objective optimization problem is formulated related to structural considerations, then a single objective lifecycle cost model is formulated to obtain a single design that minimizes the lifecycle cost. Al Handawi et al. [**5**] investigate further a set-based design methodology to obtain scalable optimal solutions that can satisfy changing requirements through remanufacturing. In this remanufacturing approach, a stiffener is added to the turbine rear structure by direct energy deposition to support higher loading requirements, from which a thermo-mechanical analysis is caried out and optimization is used to maximize the safety factor. A feasible design set is deducted as the intersection of all constraint sets which includes designs that meet all design requirements. Lawand et al. [**6**] develops a model that accounts for component lifecycle cost when considering alternative remanufacturing and/or repair solutions early in the design process. Firstly, design variables and parameters critical to the AM process are identified. A system dynamics model is developed to identify relationships between the component’s lifespan and service life costs, and therefore evaluate different EoL scenarios using lifecycle cost as the key performance indicator. Finally, an optimization problem is solved to minimize lifecycle cost with respect to design variables. Lawand et al. [**7**] developed a method to integrate a dynamic life cycle costing model with a nested optimization approach to assess alternative mean-of-life extension using AM to adapt component geometry during operations. First the required component lifespan range is selected based on historical data and customer preferences. The selected range is input to a bi-objective optimization problem that minimizes the lifecycle cost and maximizes the performance, using the safety factor developed in [**5**]. The latter determines a pareto set of design alternatives. A second outer optimization is used to minimize the distance between the utopia point and the pareto front points, and therefore find the design option closest to the utopia point.

Finally, there are artificial intelligence-based approaches. Habeeb et al. [**8**] researched a fuzzy-genetic approach to improve the decision making in repair and restoration of a turbocharger with AM. The fuzzy logic system determines if the turbocharger is repairable, if yes, then a genetic algorithm is used to minimize the cost of the repairing process. Habeeb et al. [**9**] develop an artificial neural network that predicts the suitable method to compensate the geometry of the deformed part. Four sets of training

data are used. The first corresponds to the changes in each geometric parameter. The second corresponds to the AM process parameters to simulate the AM process. Third, a series of failure modes and causes corresponds are used to decide where corrective actions need to be taken and to determine what actions need to be performed and when. The fourth set utilizes mean squared error as the loss function to estimate the difference between the input and output and is used to train the ANN.

Current methods in literature optimize the AM repair of an existing design that is already at its EoL. None of them include a simulation of the EoL scenario such as a damage analysis. Integrating a damage analysis within a design optimization workflow for AM repair can highlight the pros and cons of this method. It would also investigate the possibility of optimizing a design for their AM repair, subject to a pre-defined EoL scenario.

2 Methodology

This research aims to implement a foundational design optimization workflow for additive manufacturing repair that implements a damage analysis into the conceptual design. To do so, a process integration and design optimization program is used. An automated experiment is developed to simulate an AM repair scenario, which outputs data that is used in the optimization of a parametric geometry. The first step is the definition of the design's geometry with parameters. The second step uses the defined geometry to simulate a damage using finite element analysis (FEA). Third, a broken geometry is deducted from the FEA analysis, to do so a z-axis nodal displacement threshold is defined where nodes that have undergone a larger displacement than the defined threshold will constitute the damaged geometry. Finally, the damaged geometry serves as input for an AM simulation. (Figure 1)

The four steps described above are integrated using macro programs and operating system commands to form an automated experiment that is ready for optimization. Due to the multidisciplinary nature of the integrated process, each optimization experiment generates geometry data, structural damage behavior and AM repair cost as numerical and visual data.

A single objective optimization would result in over-dimensioning the geometry to minimize the inflicted damage. To avoid that, a bi-objective optimization is defined. A hybrid algorithm is used that combines a differential evolution algorithm and a normal boundary intersection gradient algorithm. The first objective is to minimize the volume of the geometry, and therefore, the material consumption of the initial design. The second objective, to minimize the filament consumption of the future AM repair process. (Figure 2)

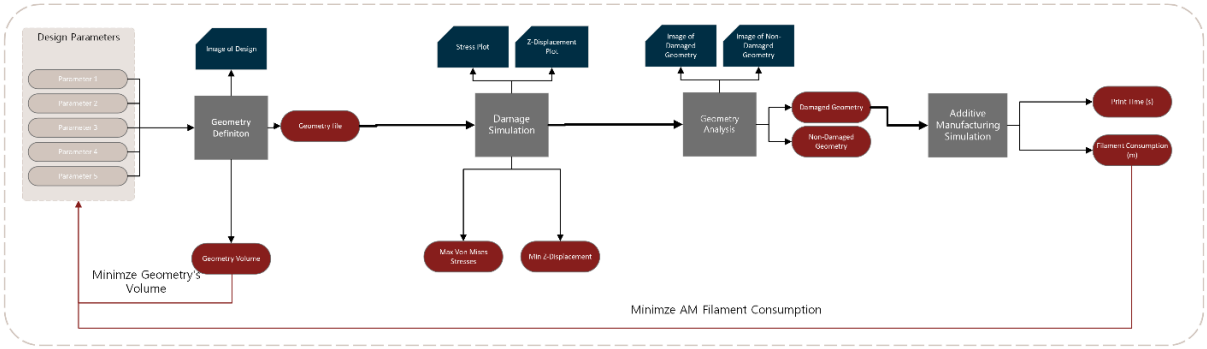

Fig. 1
Multidisciplinary Design Optimization Workflow for Additive Manufacturing Repair

2.1 Assumptions:

This research aims to create a foundational workflow that integrates a damage simulation in a design optimization for AM repair. Multiple assumptions are therefore made and serve as groundwork for future research. Firstly, in a design for repair process, it is necessary to carry out a design failure mode and effect analysis (DFMEA) to predict damage modes, severity, probability, and detection number to make design decisions. Damage prediction analyses are outside the scope of this research. For simplicity, a predefined misuse impact damage example is used to deduct the geometry of the damaged part. Additionally, in practice, failure analysis usually accounts for non-linearities in the material behavior, large strain rates and are often solved using explicit solvers. The dynamic non-linear nature of these assessments usually makes them computationally heavy. To minimize computational cost and complexities related to material plastic deformations, a quasi-static implicit FEA is defined, and a nodal displacement threshold in the z-direction is used to differentiate the damaged from the non-damaged

geometry. Finally, in-situ additive manufacturing requires collision, material, temperature, contact and robotic tool path planning considerations. All robotic, thermodynamic and collision matters are outside of the scope of research and an existing fused deposition molding AM slicer is used for simplicity.

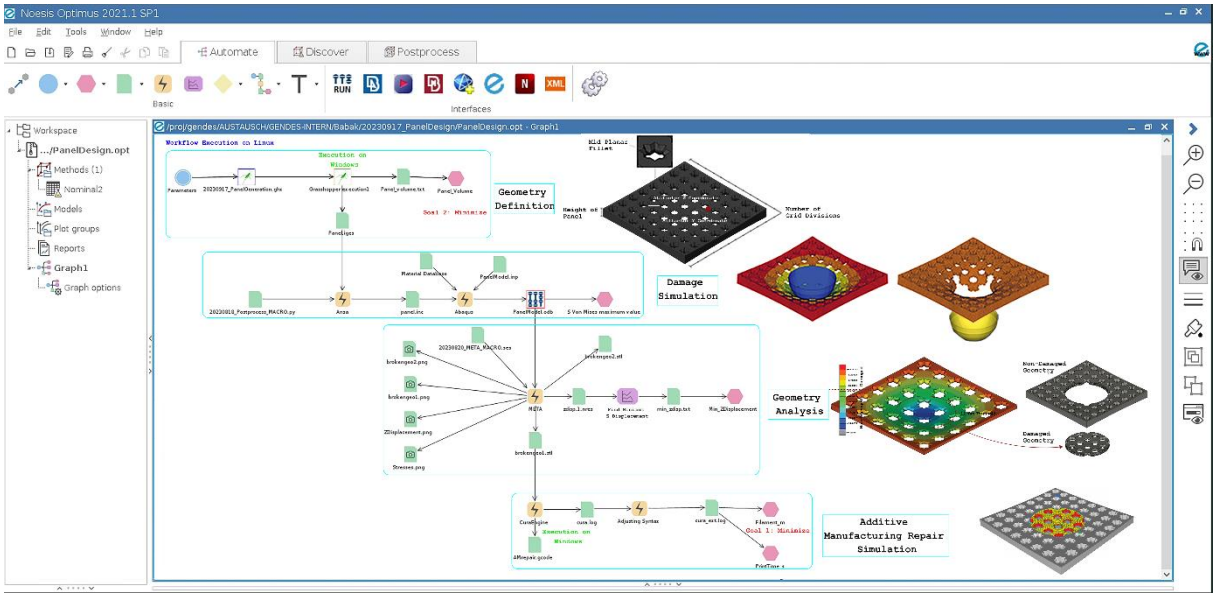

Fig. 2
Multidisciplinary Design Optimization workflow on the Optimus canvas

3 Results / Findings

The goal of this research is to investigate a workflow that implements an AM repair strategy into a component's conceptual design using multidisciplinary design optimization. The results are examined in terms of their usability within a conceptual design process and achievement of the pre-defined design objectives. The optimization converges after 40 experiments with a success rate of 90% taking approximately 20 hours and 22 minutes (73350s). The resulting pareto front (Figure 3) reveals five optimum solutions with conflicting objectives weights. Experiment 26 has a weight of 1 to minimize the panel volume and a weight of 0 to minimize the AM repair filament consumption. It therefore is the design option with smallest volume, but subsequently the one with the largest AM repair filament consumption, due to undergoing greater damage. On the other hand, experiment 1 has a weight of 1 to minimize the AM repair filament and a wight of 0 to minimize the geometry volume. Experiment 34 is the design option closest to the utopia point and is the closest to an equal weight objective. The optimum solution space ranges from a panel volume of 4729500 mm^3 to 2635300 mm^3 which corresponds to a 44.28% decrease. The AM repair filament consumption ranges from 36.21 to 20.49 corresponding to a 43.41% decrease. The pareto front plot helps the designer visualize different experiments and their performance with respect to the two objectives defined.

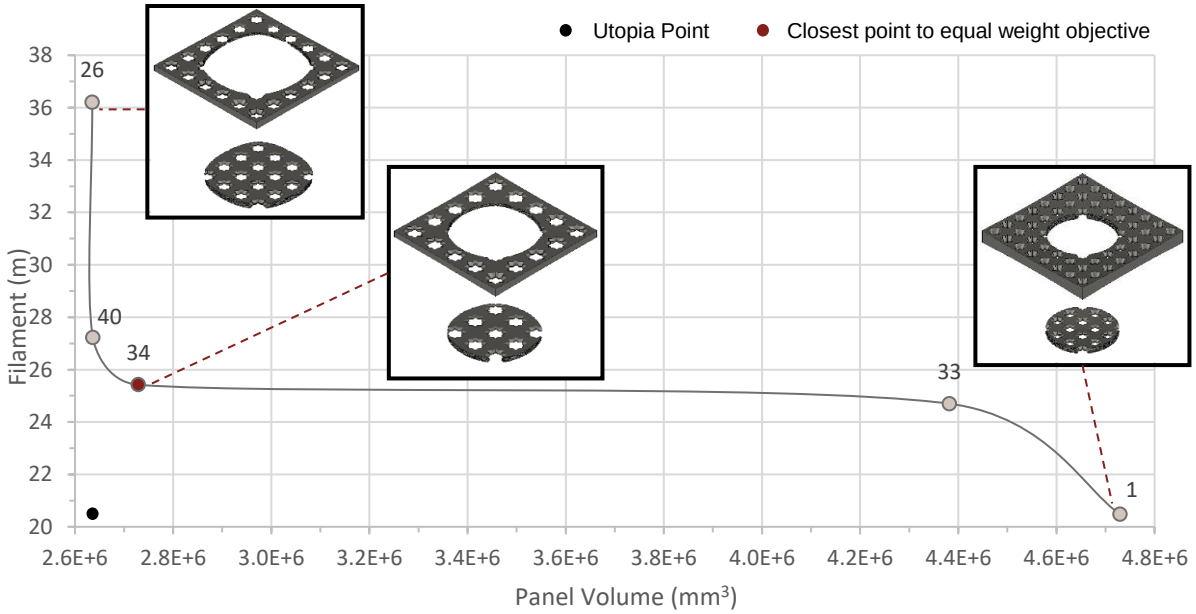

Fig. 3
Pareto Optimum Solutions

The workflow outputs von-mises stress and z-displacement plots which allow the designer to visualize the structural performance of each design option. When the geometry is constituted of an even grid, the 8-point star motif is located at the center of the panel, where the impact occurs (Figure 4). On the other hand, an uneven grid results in a different geometry at the point impact. Due to the varying geometries at the point of impact, the stress distribution on the material varies for each design option. Additionally, it can be observed that thickness and number of grid divisions also play a big role in the structural performance of the design. Structural performance plots are therefore important to make visual relationships between structural performance and geometry during the conceptual design.

The workflow also outputs an image of the damaged and non-damaged geometry for each design option. This feature is important to visualize the damaged geometry which can indicate the need for further assessment. More importantly, the images of the non-damaged geometry can be used to evaluate the aesthetic performance of the design options, which is one of the pre-defined design objectives and is therefore major consideration during the conceptual design.

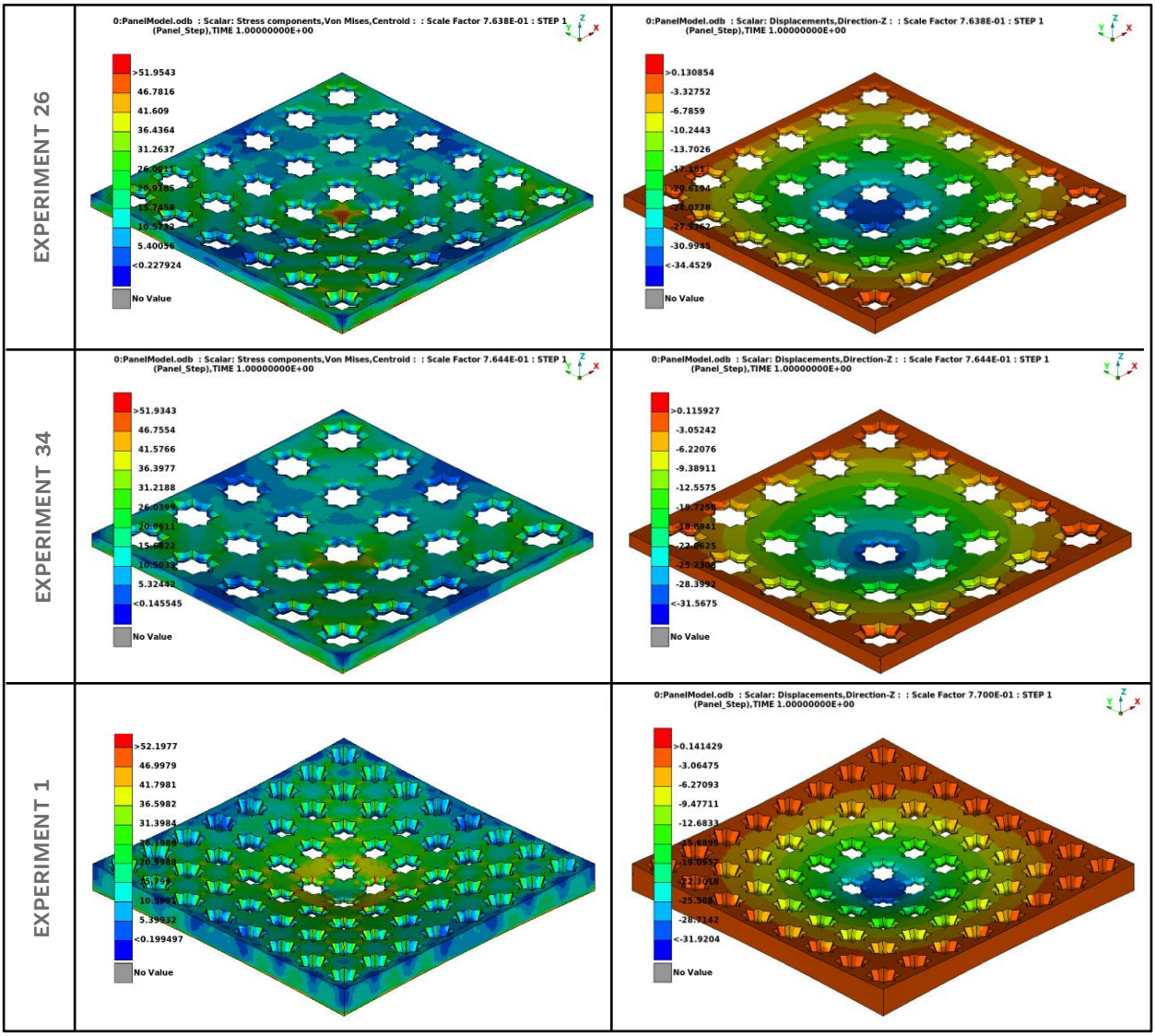

Fig. 4
Damage Simulation Results

The results can also be interpreted for further analysis. To compare the material footprint of a repair compared to a replace EoL scenario, a material flow analysis is carried out (Figure 4). The material flow analysis considers the production material input, the EoL material input and the material output. The production material input, in the case of both a repair and replace scenario, corresponds to the material weight of the initial geometry. The EoL material input, in the case of a repair scenario, corresponds to the material weight of the AM repair process. On the other hand, in the case of a replace scenario, it corresponds to the material weight of the initial geometry, as it will be fully produced again. Finally, the material output in the case of a repair scenario corresponds to the material weight of the damaged geometry, which is discarded in this case. In contrast, material output of a replace scenario corresponds

to the material weight of the initial geometry, as the part is totally discarded with no repair. It is observed that experiment 40 has the lowest material footprint for a repair EoL scenario. Experiment 26 results in the lowest material footprint for a replace EoL scenario. Experiment 1 corresponds to the largest reduction of material footprint between a repair and replace EoL scenario at 64.82%. It is also the experiment with the largest volume. Experiment 26, with the lowest volume corresponds to a 60.82% reduction in material footprint between a repair and replace EoL scenario. A repair EoL scenario is therefore exponentially more impactful in minimizing the material footprint of designs the larger the volume. Material footprint is an important consideration in the conceptual design process to inform the designer of the environmental impact of different design options.

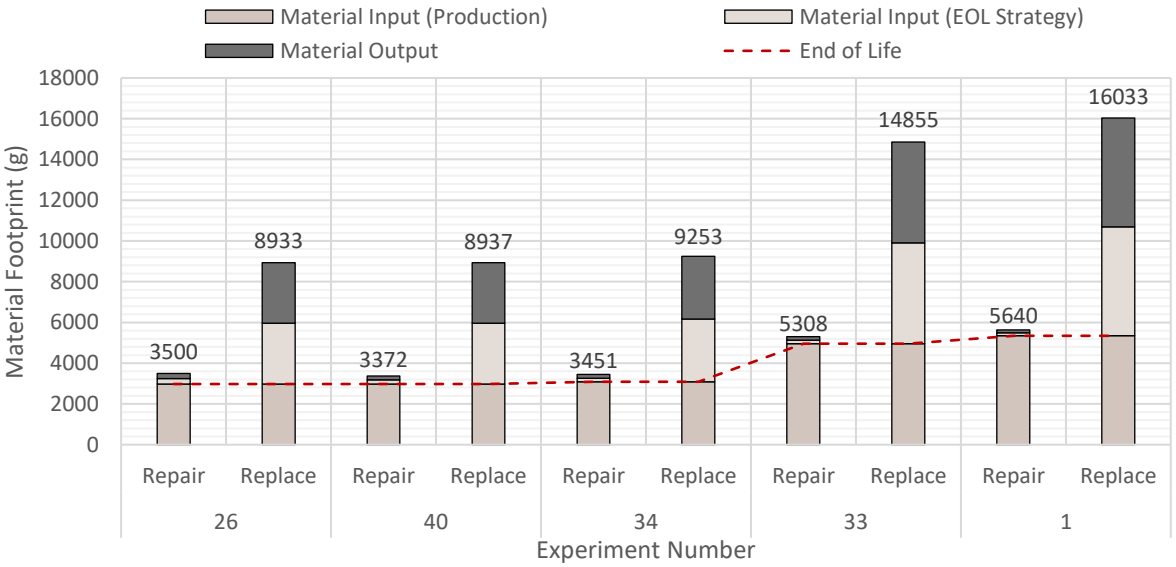

Fig. 5
Material Flow Analysis

4 Conclusions

This paper integrates a foundational design optimization workflow for additive manufacturing repair that implements a damage analysis into the conceptual design. A wall panel is used as a case study. An automated experiment constituted of various integrated processes is used to simulate an AM repair scenario. The output data is used to optimize the parameters of the design. To do so, a geometry definition, damage simulation, geometry analysis and AM simulation are first developed individually, then macro programs and operating system commands are used to integrate the processes and automate the experiment. The automated experiment is used to optimize the geometry's parameters to minimize the panel volume and the filament consumption of the AM repair. The results are investigated based on their use in the conceptual design stage. The optimization results in five pareto optimum solutions, structural performance plots and images of the different design options. The volume of design options and the filament consumption of the AM repair process is also provided which is used for a material flow analysis comparing a repair and a replace EoL scenario. The following conclusions can be drawn:

- The method supports the generation and exploration of design options which can inspire the designer by proposing spontaneous design options and allows sorting them using performance information.

- The workflow's setup using a series of integrated processes allows for the analysis of each process independently and brings added flexibility in its reformulation. This feature is useful when abstracting the task to find the essential problems in the conceptual design phase.

- The proposed method requires investment in time and resources in the early design stages of development, which causes changes in the way the design process is conceived. The design process becomes highly dependent on the user-experience of the software and the resources used. Flexibility in the post-processing of the results and process is a potential solution to this problem.

- Design failure mode and effect analysis (DFMEA) considerations such as damage modes, severity, probability, and detection number highly influence the prioritization between design variables in the conceptual design process.

In conclusion, the developed method has potential of being a valuable conceptual design tool that would encourage sustainable strategies in the conceptual design process but requires further developments to provide more reliable performance information to the designer.

4.1 Future Work:

Due to the multidisciplinary and foundational nature of this method, several future directions are possible. Firstly, future work is possible in addressing the assumptions made. A possible direction is implementing failure mode and effect analysis (DFMEA) predictions. This can be done by training a Gaussian regression machine learning model on a data set and extracting a probability density function of all admissible functions that fit the data. A Monte Carlo method can then be used to predict the most probable damage scenarios of the component. Additionally, research can be done to account for non-linear material degradation in the damage simulation, stiffness degradation and maximum damage initiation criterions can be used to identify the damaged geometry with more accuracy. It is important to address the computational cost of these analyses within an optimization loop in this case. Furthermore, research can explore detailed in-situ AM repair considerations, and designs can be optimized to minimize collisions of the repair process. Additionally, future work is also possible in investigating different circular economy EoL recovery strategies such as reuse, refurbish, remanufacturing and repurpose where new processes would need to be developed to fit the definition of each strategy. Finally, additional research can extend the material flow analysis to a lifecycle analysis by incorporating the embodied energy and carbon footprint for each design option.

5 References

1. G. Pahl, W. Beitz, J. Feldhusen and K. H. Grote, *Engineering design: A systematic approach*, Springer London2007.
2. W. W. Wits, J. R. R. García and J. M. J. Becker, *How additive manufacturing enables more sustainable end-user maintenance, repair and overhaul (mro) strategies*, Procedia CIRP **40** (2016), 693-698.
3. J. Liu, Y. Zheng, Y. Ma, A. Qureshi and R. Ahmad, *A topology optimization method for hybrid subtractive–additive remanufacturing*, International Journal of Precision Engineering and Manufacturing-Green Technology **7** (2020), no. 5, 939-953.
4. K. Al Handawi, L. Lawand, P. Andersson, R. Brommesson, O. Isaksson and M. Kokkolaras, *Integrating additive manufacturing and repair strategies of aeroengine components in the computational multidisciplinary engineering design process*, Proceedings of NordDesign: Design in the Era of Digitalization, NordDesign 20182018.
5. K. Al Handawi, P. Andersson, M. Panarotto, O. Isaksson and M. Kokkolaras, *Scalable set-based design optimization and remanufacturing for meeting changing requirements*, Journal of Mechanical Design, Transactions of the ASME **143** (2021), no. 2.
6. L. Lawand, K. Al Handawi, M. Panarotto, P. Andersson, O. Isaksson and M. Kokkolaras, *A lifecycle cost-driven system dynamics approach for considering additive re-manufacturing or repair in aero-engine component design*, Proceedings of the Design Society: International Conference on Engineering Design **1** (2019), no. 1, 1343-1352.
7. L. Lawand, M. Panarotto, P. Andersson, O. Isaksson and M. Kokkolaras, *Dynamic lifecycle cost modeling for adaptable design optimization of additively remanufactured aeroengine components*, Aerospace **7** (2020), no. 8, 110.
8. H. A. Habeeb, D. Abd Wahab, A. H. Azman and M. R. Alkahari, *Fuzzy-genetic based approach in decision making for repair of turbochargers using additive manufacturing*, Jurnal Kejuruteraan **35 (5)** (2023), 1153-1164.
9. H. A. Habeeb, D. Abd Wahab, A. H. Azman and M. R. Alkahari, *Design optimization of components for additive manufacturing-repair: An exploration of artificial neural network requirements and application*, International Journal of Integrated Engineering **15** (2023), no. 5, 189-197.

Analyzing the Structure of an Aircraft Wing

Dr. Ceyhun Sahin (Noesis Solutions)

Summary

In this article, we discuss how nvision, an AI-powered surrogate modelling tool by Noesis Solutions, enables to generate insights from historical simulation design data to be exploited in optimization processes in Optimus and to create competitive products for the future, while saving time and resources.

Structural analysis plays a crucial role in aircraft engineering as it has a direct impact on safety. For each new product going on the market, several impact tests are done to ensure the robustness of the design creating a vast amount of simulation data. Studying the damage curves from an older design helps engineering designers to make data-led decisions from the beginning of their design journey.

How does nvision enable GKN Fokker Aerospace BV, a leading aircrafts part manufacturing company, to use the full potential of this historical simulation data, to make effective analysis of an optimized aircraft wing structure? How does the recycling of the dormant know-how of a company and training of surrogate models with simulation data that has already consumed time and resources used to serve for a safer and a more competitive product? How can these surrogate models replace the simulations in an Optimus workflow dedicated to optimization and reduce the usage of resources and time?

1 Introduction

In the realm of engineering and scientific discovery, time and knowledge is money. With the rise of sophisticated technologies and complex simulations, the demand for quicker, trustworthy, and efficient insights is paramount. In this fast-evolving digital engineering era, engineers rely on automation and optimization tools to generate a trustworthy simulation database.

The case study to be discussed in this article is based on aircraft wing structural analysis. The airworthiness specifications put high emphasis on bird strike tests. Due to the potential to cause severe structural damage to the wing leading edge, engine nacelles, and cockpit windows, bird strikes represent a significant threat to aircraft safety. To mitigate this risk, manufacturers must go through complex and resource-intensive analysis which includes tests as well as impact simulations which most of the time require expert personnel to be prepared and analyzed. This could be a burden when optimization is introduced in the picture.

We have used Optimus, an automation and optimization tool by Noesis Solutions, for creating an engineering case focused on optimizing an aircraft wing leading edge to withstand bird strikes at different conditions. Optimizing any aircraft piece necessitates hundreds of simulations. Optimus helps in creating a trusted simulation database. However, the demanding constraints and objectives of airworthiness can require unpredictable numbers of iterations, especially for fresh designs.

Such demanding iteration processes can be handled much easier thanks to the surrogate model technologies. The trusted simulation database created by Optimus can be turned into a surrogate model in nvision, the AI-powered reduced order modeling tool of Noesis Solutions. Once a reliable surrogate model is available for the bird strike analysis of an aircraft wing, the users will expect direct access to this model in the automated optimization environment. With the new update of Optimus 2023.2, the tool offers a direct access to nvision models, which allows the user to integrate real-time predictions into an Optimus workflow. With this feature, the arduous simulation process is streamlined, enabling engineers to explore a wide range of design variables swiftly and effectively. This will result in faster innovation cycles, quicker validation, and accelerated product development.

2 The Case Study – Leading Edge Structural Analysis

The target of the case study is replacing structural finite element analysis (FEA) with real-time predictions especially for the iterative part of an optimization process.

2.1 Model training

Any surrogate model requires a trustworthy training data set as a starting point. In this case study, Abaqus is used as the FEA tool to simulate the responses of wing leading edges with different thicknesses to sudden impact at different speeds. The Optimus workflow generating a database of Abaqus input and output files can be seen in Fig. 1. The Adaptive DOE method in Optimus is used to efficiently sample the design space of different shell thicknesses and relative speeds. The input and output database for Abaqus simulations is saved in the Optimus project Datastore.

The training data set out of Optimus is imported in nvision and a surrogate model for the impact of shell thickness and relative bird strike speed on structural deformation is trained using the tool (Fig. 2).

Running 20 different Abaqus cases took approximately 2.5 hours.	Training the surrogate model in nvision took about 25 minutes

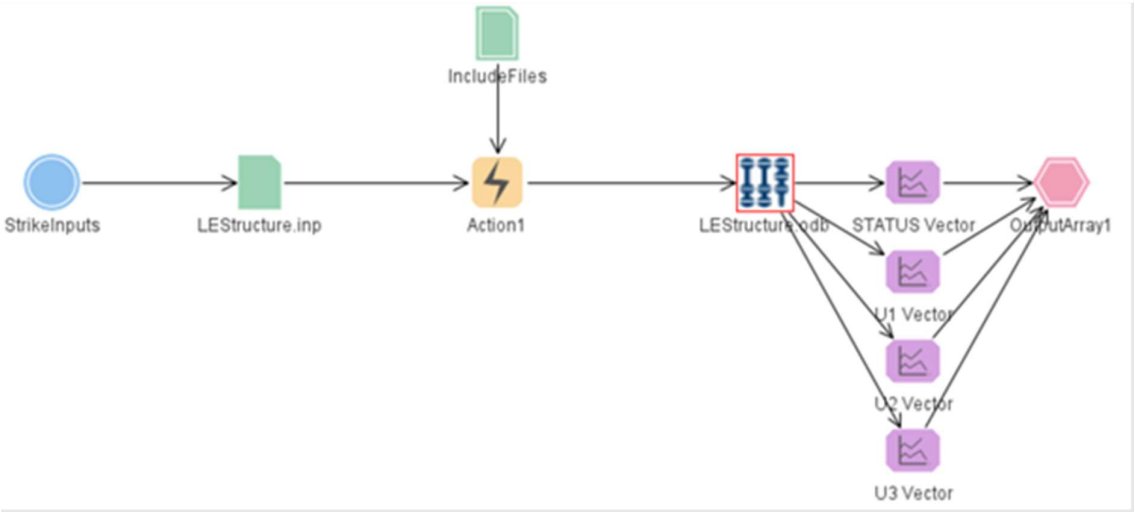

Fig. 1 Optimus workflow for automated Abaqus simulations.

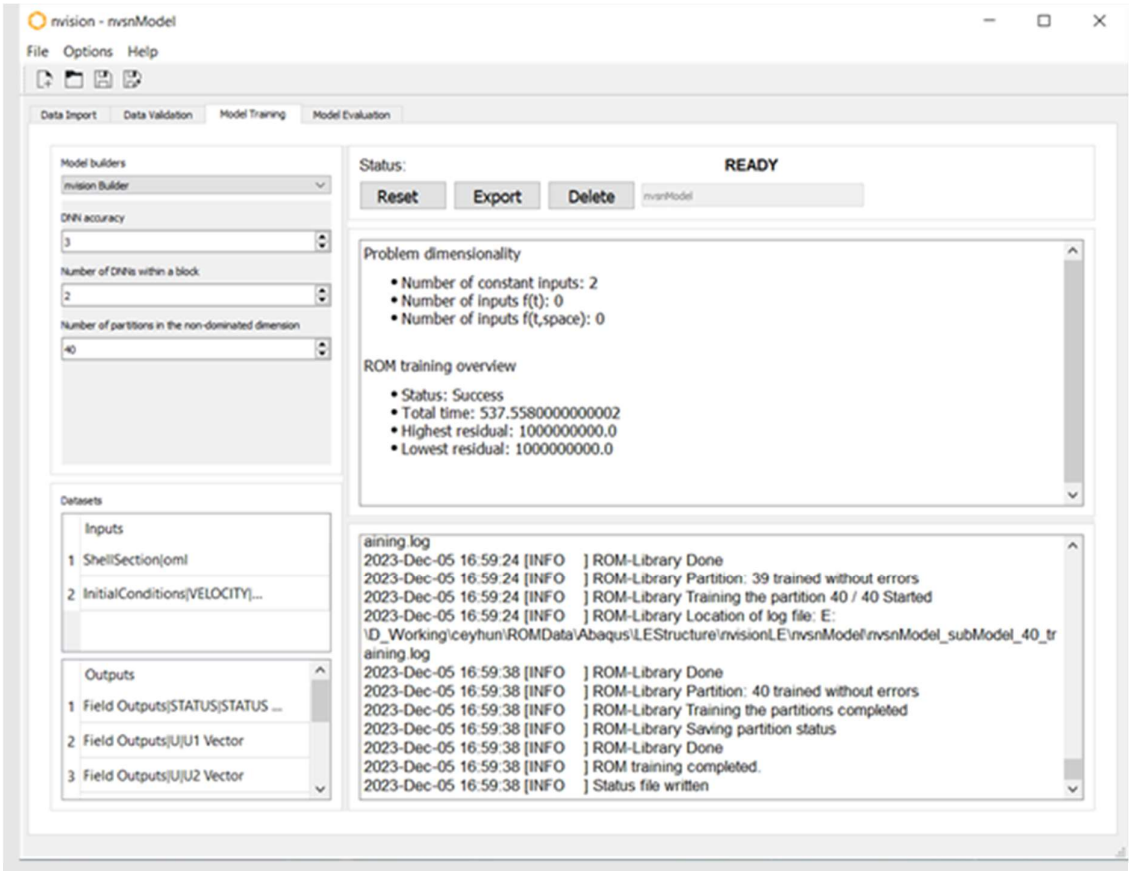

Fig. 2 nvision model to predict deformations for different shell thicknesses and bird speeds ready.

2.2 Challenging the nvision model with synchronized simulations

Using a surrogate model always starts with assessing the accuracy of the model predictions. A model to replace a high-fidelity simulation should be able to predict the deformation of nodes which represent high risk for the structural integrity of the wing.

In that sense, the criteria are set on the direct impact region on the leading edge, and the comparison is set between the maximum deformation as an outcome of the Abaqus simulation, and the deformation predicted by nvision for the exact same location. The nvision interface and parallel execution functionality in Optimus allow to evaluate and to simulate new design points via the nvision model and in Abaqus, respectively, in a single Optimus workflow. The workflow is designed to calculate the normalized error on the node going under the largest deformation, to run in parallel both for nvision and Abaqus executions.

The workflow with two parallel branches, running a simulation and evaluating the nvision model for the same exact scenario is shown in Fig. 3. This workflow provides one-to-one comparison of predictions and high-fidelity simulations.

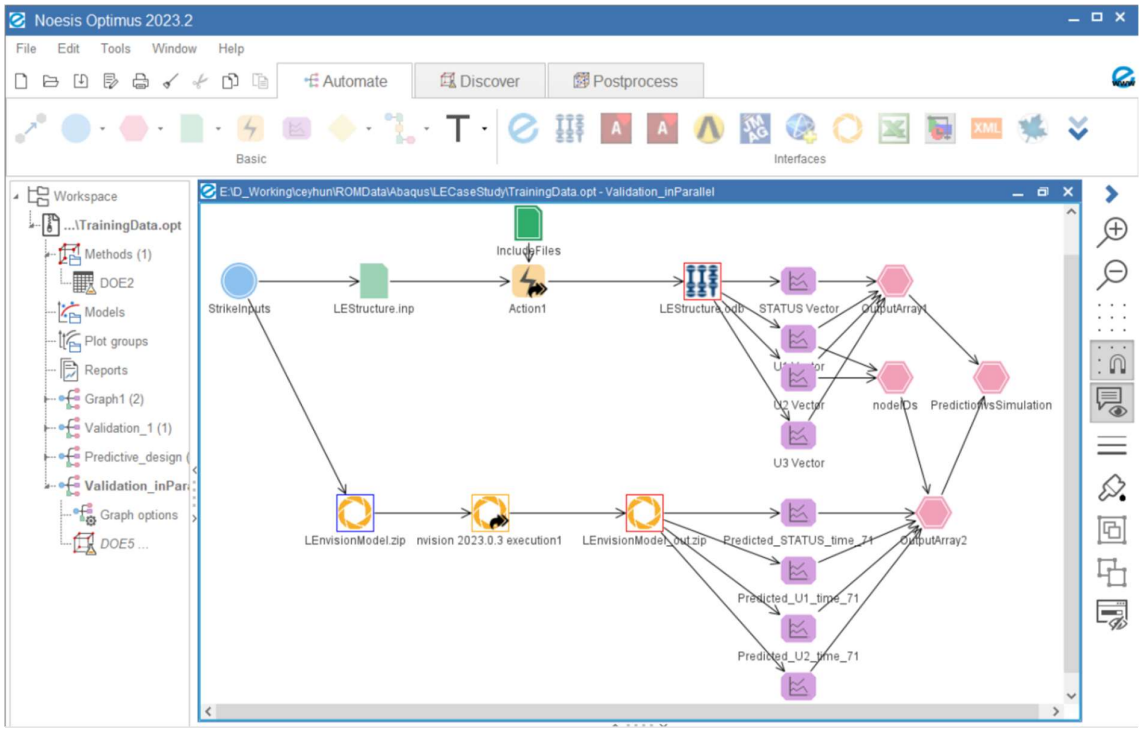

Fig. 3 Optimus Workflow to quantify the nvision model quality and the advantage in process time.

2.2.1 The Essence of Time: Reducing Simulation Duration:

Thanks to the parallel execution functionality of Optimus, the time the user gains by running only the nvision branch is also evident. The transient deformation of 15 new designs were predicted by nvision by the time 3 of them could be simulated in Abaqus, enabling a quick turn-around time for engineers.

2.2.2 The model quality:

The distribution of maximum deformation out of an Abaqus simulation with respect to the predicted deformation for the same node is presented in Fig. 4. The green line represents the perfect match. The correlation coefficients calculated automatically by Optimus indicate a model quality of 90%.

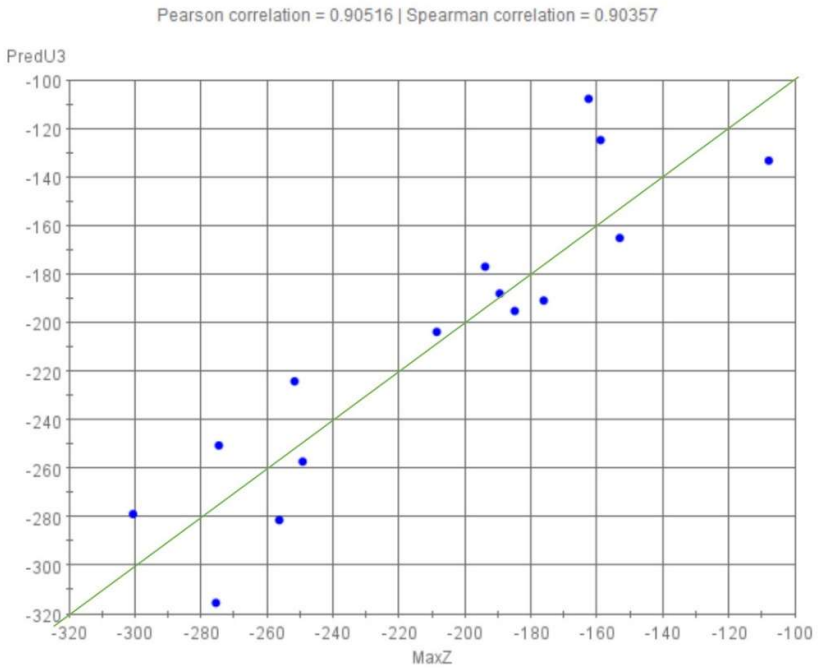

Fig. 4 Comparison of deformation as an output of Abaqus simulations and nvision predictions

Next step will be relying only on the nvision model and getting the results for previously unthinkable designs will be a matter of seconds.

2.3 Optimizing with an nvision model:

From this stage on, engineers can move to real time predictions with the available model. An Optimus workflow does not require a branch anymore to run the Abaqus simulations in parallel to nvision predictions (Fig. 5).

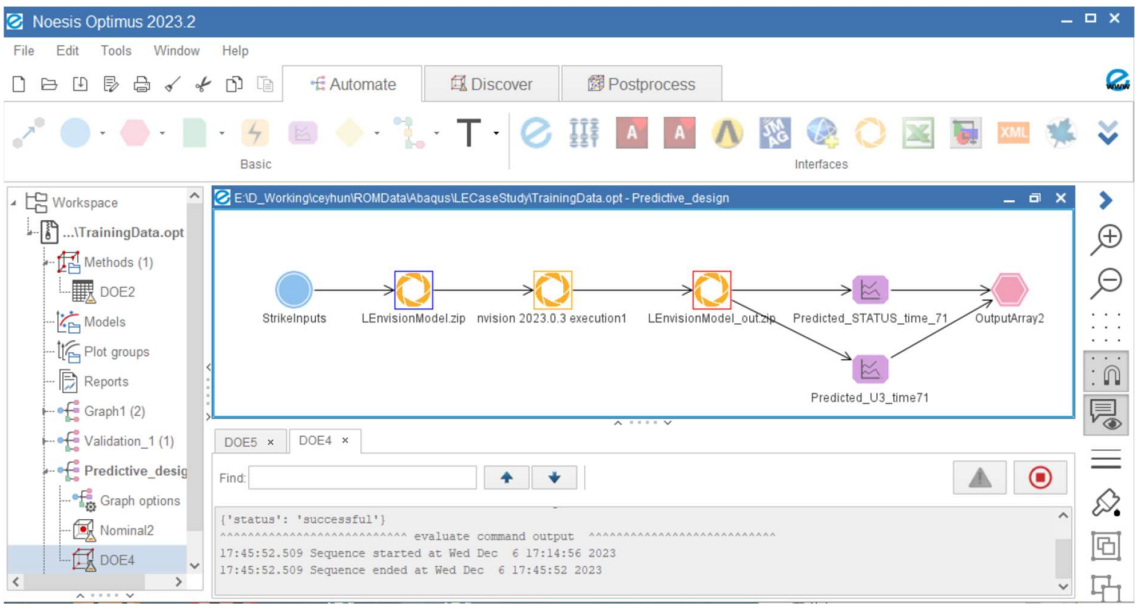

Fig. 5 Optimus workflow for automated real-time predictions with nvision.

While working on innovative designs thanks to the available nvision model, a new model can be retrained by appending the Abaqus files generated in the validation process to the initial training data set. We have already observed that nvision takes more or less 1/6th and 1/5th of the overall simulation time to train a new model and to evaluate new data points on the model, respectively. From this stage on, the model quality will only get better and reliable predictions for new designs will be served in the blink of an eye.

3 Conclusions

In conclusion, thanks to the Noesis Solutions products, GKN Fokker Aerospace BV was not only able to address the time-consuming nature of generating simulation databases but also empowered their engineers and designers to make educated decisions at the inception of their projects with the integration of reduced order modelling, exemplified by nvision. By recycling the wealth of knowledge encapsulated in previous and recent simulations, nvision provided a multidimensional map for their designers to navigate, allowing them to anticipate potential failure points in the future projects. This seamless integration with optimization tools like Optimus streamlines the entire process of model deployment. As we move forward, relying on nvision models unlocks the potential for engineers to explore design possibilities that were once deemed impractical or expensive.

References

[1] **nvision software**; www.noesissolutions.com/our-products/nvision; Noesis Solutions, April 2024

[2] **Optimus software**; www.noesissolutions.com/our-products/optimus; Noesis Solutions, January 2024.

Non-parametric Optimized E-Machine in Dynamic Noise and Vibration Simulation

Yi ZHOU (Dassault Systèmes), Christian KREMERS (Dassault Systèmes)

Michael PÖSCHL (Dassault Systèmes), Max QUIRING (Dassault Systèmes)

Timo BARUTH (Dassault Systèmes)

1 Introduction

With the development of new technologies such as artificial intelligence, the automotive industry has ushered in more rapid and technological innovation. While the vehicle comfort, as the most basic requirement from consumer, is not ignorable. Noise and Vibration (NV) performance is therefore one of the important influencing factors. Moreover, due to vehicle electrification, the focus of studying and improving NV performance has gradually shifted from traditional combustion engine to electric drive systems, especially on electrical machines.

Despite the shift of focus, Computer-Aided Engineering (CAE) is nonetheless an effective tool to investigate the causes of NV problems and provide improvement suggestions through optimization. By means of CAE simulation, we can find the optimal design even before manufacturing the first prototype, which can shorten the time to market, save the cost and ultimately ensures a better vehicle comfort performance. Advanced electrical machine optimization and accurate NV simulation will be two crucial aspects to achieve this goal.

In this work, we will firstly introduce advanced ways to optimize the electrical machine and furthermore encapsulate its behavior in a surrogate model. Secondly, we will compare three general approaches to achieve an accurate and efficient NV simulation. In the end, we will utilize the above-mentioned methods to optimize a practical electric drive train and compare the results.

2 Electrical machine optimization and its corresponding surrogate model

Finding the best design of an electrical machine is a challenging task due to both multiple constraints and goals from different physical domains as well as huge design spaces and the non-linear nature of the electrical machine. An optimization should guarantee a machine design, as light, small and cheap as possible, but at the same time fulfilling challenging torque, power and efficiency requirements. In addition, the drive should withstand harsh conditions and the passengers comfort should be taken into account as well. As shown in Fig. 1, parametric optimization and non-parametric optimization are two common approaches.

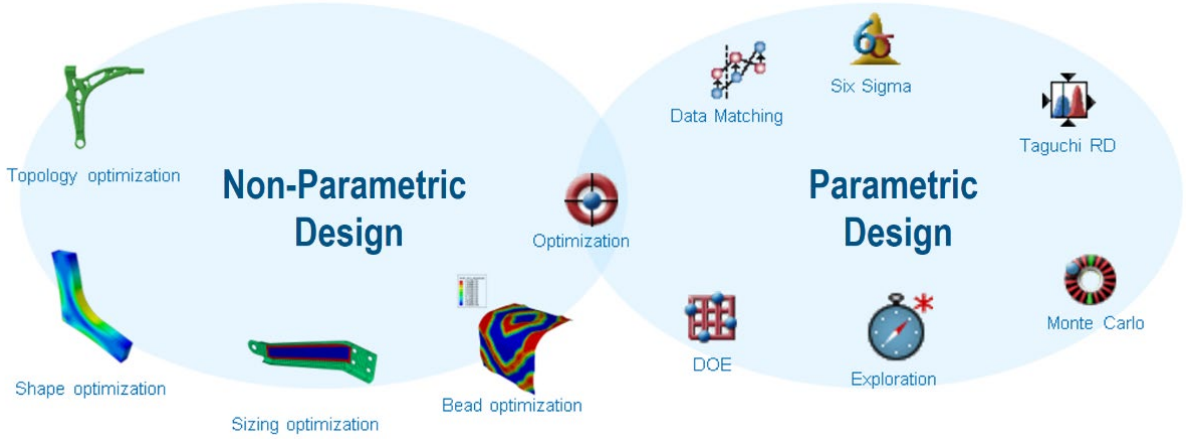

Fig. 1
Non-parametric and parametric optimization

Both approaches can be realized within SIMULIA CST Studio Suite® [1] or additionally with SIMULIA TOSCA® [2]. Both tools are tightly coupled to ensure ease of use. Compared with traditional parametric approaches, non-parametric optimization schemes enable engineers to find novel designs and push machine performance to its farther limit with much faster convergence. Based on different optimization purposes, as shown in Fig. 2 and Fig. 3, there are topology optimization and shape optimization.

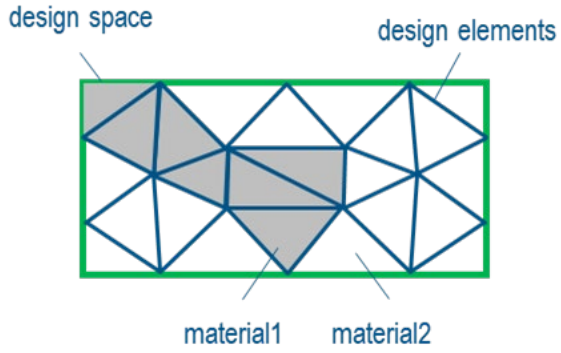

Fig. 2
Topology optimization

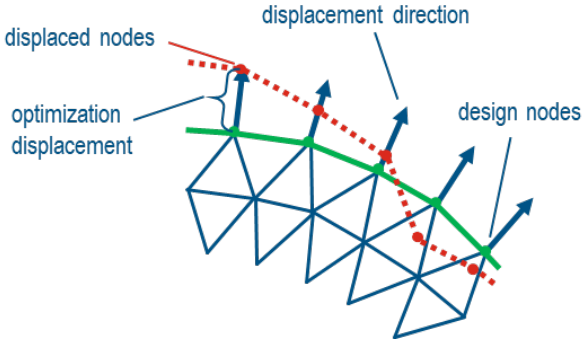

Fig. 3
Shape optimization

- Topology optimization is usually used for conceptual design. After optimization, the mesh elements will consist of either the original material or the material specified for filling. For example, we can use minimizing the weight as design goal and maintaining the mean torque as design constraint.

- Shape optimization is usually used for fine-tuning through moving mesh nodes on selected material surfaces. For example, we can chose to minimize selected radial spatial force orders (design goal) and reducing torque ripple under a specified value (design constraint).

After obtaining the optimal design, one has to encapsulate its behavior, including higher torque harmonics and lumped forces, to system and / or NV simulation domains. A surrogate model, like the Reduced Order Model (ROM) [3] that we provide in CST Studio Suite®, will be sufficient in this case. This technique tailors for constructing physical equivalent and energy conserved compact models in order to realize an abstract imprint on a system level [4]. Combined with a system level simulator, we could achieve the results as accurate as with the finite element method (FEM) but with a considerable reduced computational time.

3 NV simulation of electric drive train

Regarding to electric drive train NV simulation, there are generally two approaches.

- Static structural simulation, like through SIMULIA Abaqus®, is a quick way to investigate NV performance.

- Dynamic multibody simulation, like through SIMPACK® [5], will predict more accurate performance prediction when we need to consider the effects like from roller bearings, gearing contacts, flexible shafts and so on.

In this work, we will use the dynamic multibody simulation to incorporate dynamic effects of the whole drive trains.

An accurate and easy-to-use description of machine electromagnetic (EM) forces is important for the precise and efficient NV simulation of an electrical drive train. As shown in Fig. 4, there are three different approaches in SIMPACK® to incorporate force excitations from the electromagnetic FEM of an electric machine.

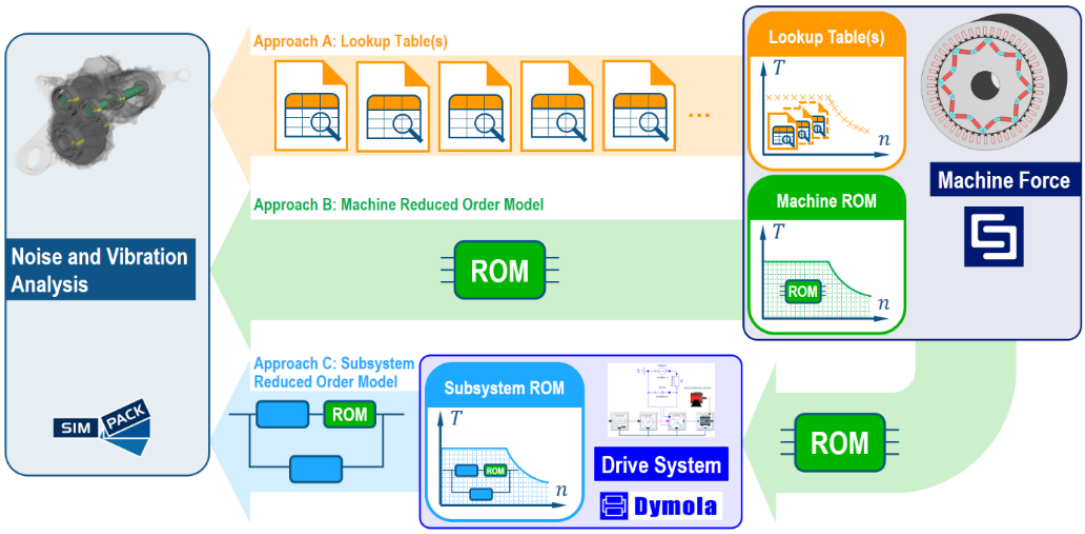

Fig. 4
Approaches for dynamic NV simulation

- The first approach consists of look-up table(s), which can describe a single operating point (OP) or a single valued torque speed trajectory - T(n) through discrete points. However, this approach has some limitations. Firstly, the number of discrete points is important. Too many increase complexity. Too few lead to inaccurate results. Secondly, a new EM simulation is required for operating point(s) beyond pre-calculated T(n) trajectory. Thirdly, this look-up table approach is inadequate for e.g. torque ramp or profile at fixed speed, since torque cannot be expressed as a function of rotor speed anymore.

- In order to overcome the above-mentioned limitations, machine ROM approach can be used, which uses only one file to achieve a similar fidelity as finite element simulation over the complete operating range (T-n) enabling the user to investigate any kind of drive scenarios.

- In addition, to study multiphysics effects (e.g. inverter, thermal, etc.) on the NV behavior, Subsystem ROM (SROM) approach can be utilized, which is created by a system simulator (like Dassault Systèmes Dymola® [6]), and includes not only the above-mentioned machine ROM, but also e.g. switch-mode inverter models with corresponding control unit as well as thermal models into one file. Therefore, a SROM describes EM forces as arbitrary profiles of full T-n range as well as includes e.g. inverter harmonics and control algorithm effects.

4 NV performance comparison between an initial and optimized electric drive train

We use the following electric drive train as shown in Fig. 5 for demonstration. It contains a Permanent Magnet Synchronous Machine (PMSM) with 4 pole pairs and 48 slots as well as a two-stage reduction gearbox supported by roller bearings. As NV performance indicator, acceleration is measured on the flexible Housing structure.

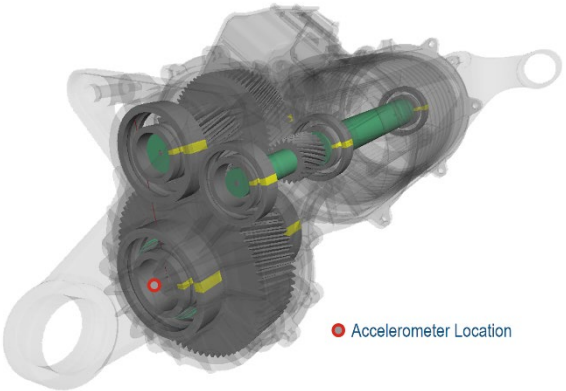

Fig. 5
Exemplar electric drive train

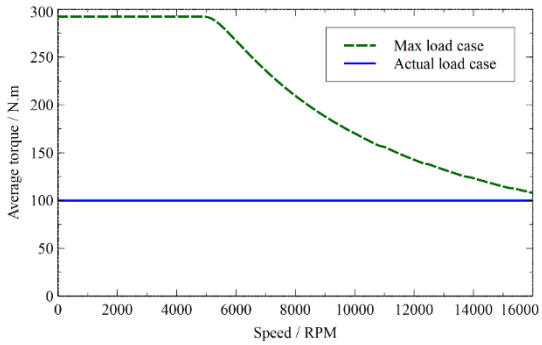

Fig. 6
Maximum and actual load case

In the test case as shown in Fig. 6, the exemplar drive train does not run at maximum torque, but constant at 100 N.m. The torque does therefore not change during the entire speed run up from 0 to 16000 RPM. Since we use the ROM approach for dynamic NV simulation, even if we switch load case from max to 100 N.m, we do not have to simulate again to get electromagnetic force excitation. This is easily possible as the ROM includes the completely machine-operating regime.

The measurement signal on the accelerometer shown in Fig. 5 is visualized in the Campbell plot shown in Fig. 7. It shows a quite strong acceleration magnitude on a single point with around 2000 RPM at a frequency corresponding to the 48th mechanical order. The broad horizontal line of high acceleration around the 24th mechanical order is not only coming from the electric machine but also from the gearbox whose noise reduction is not in the scope of this work.

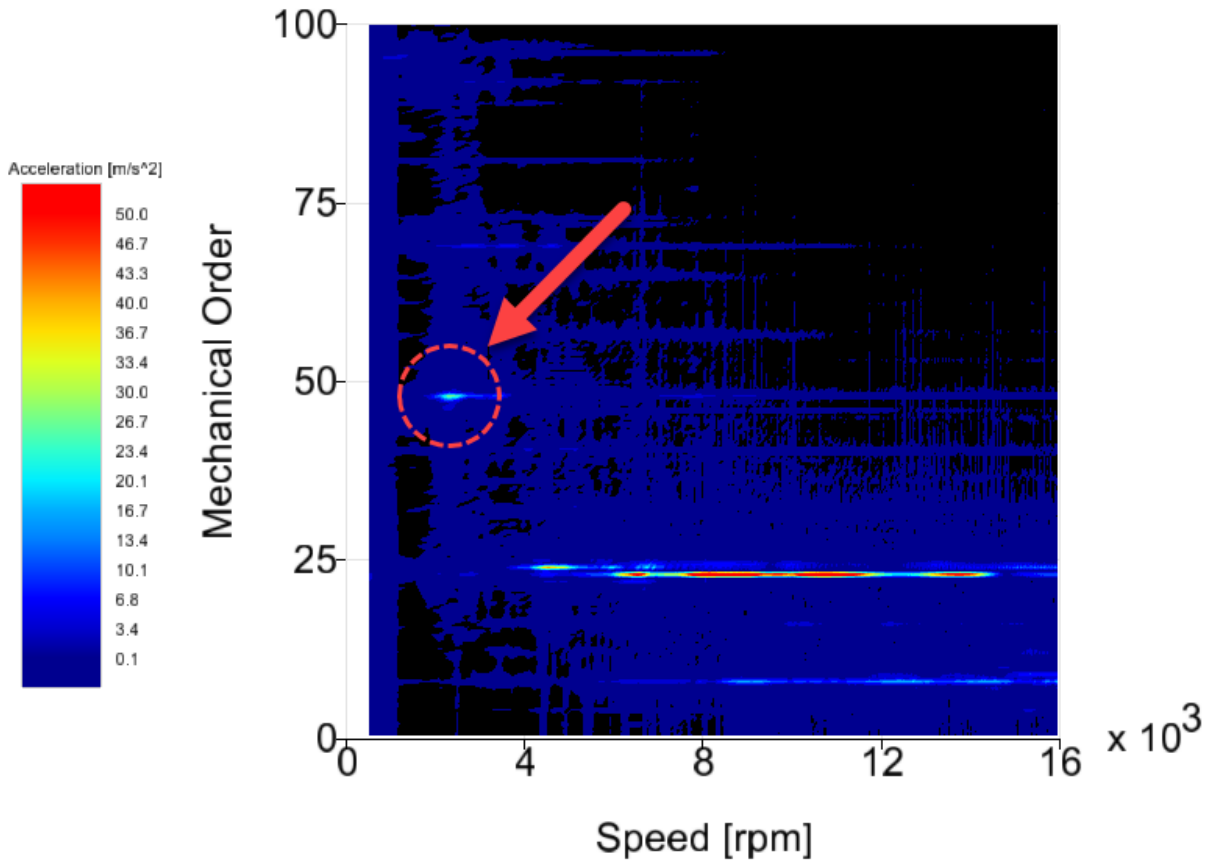

Fig. 7
Campbell plot of initial electric drive train

Since the 48th torque order seems to be the main reason causing the hot spot and we do not want to make major changes to the original design of the current electrical machine, we can use non-parametric shape optimization to suppress the 48th torque order on 2000 RPM and 100 N.m average torque. We can also add some additional constraints for mean torque and torque ripple if required. For example, mean torque should be at least bigger than 95% from initial value and torque ripple should be at least less than 95% from initial value.

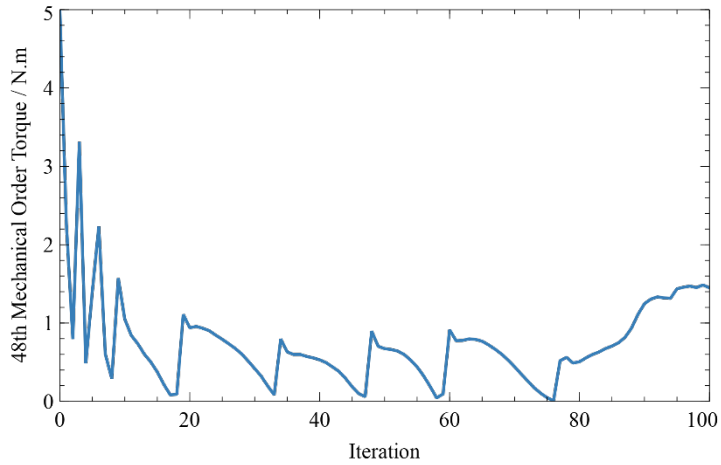

Fig. 8
Convergence curve of non-parametric shape optimization

After completing 100 optimization steps with 48th harmonic of the torque as shown in Fig. 8, we found the best design at optimization step 76 with around 99.83% reduction in the 48th torque order (from 4.996 N.m to 0.008 N.m). It also fulfills the constraints on the mean torque and the torque ripple according to Fig. 9.

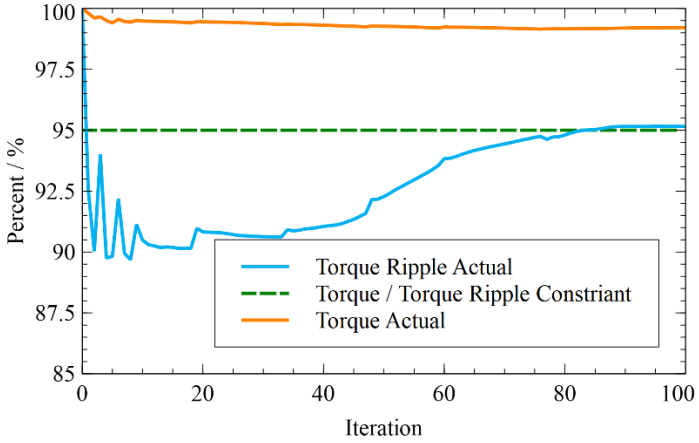

Fig. 9
Constraints curve of non-parametric shape optimization

Next, we generate a new ROM from the FEM model of the best design candidate (iteration 76). Replacing with this the original ROM and rerunning simulation, we obtain the Campbell plot in Fig. 10 on the optimized electric drive train. We can observe that the hot spot on 48th order with 2000 RPM disappears almost.

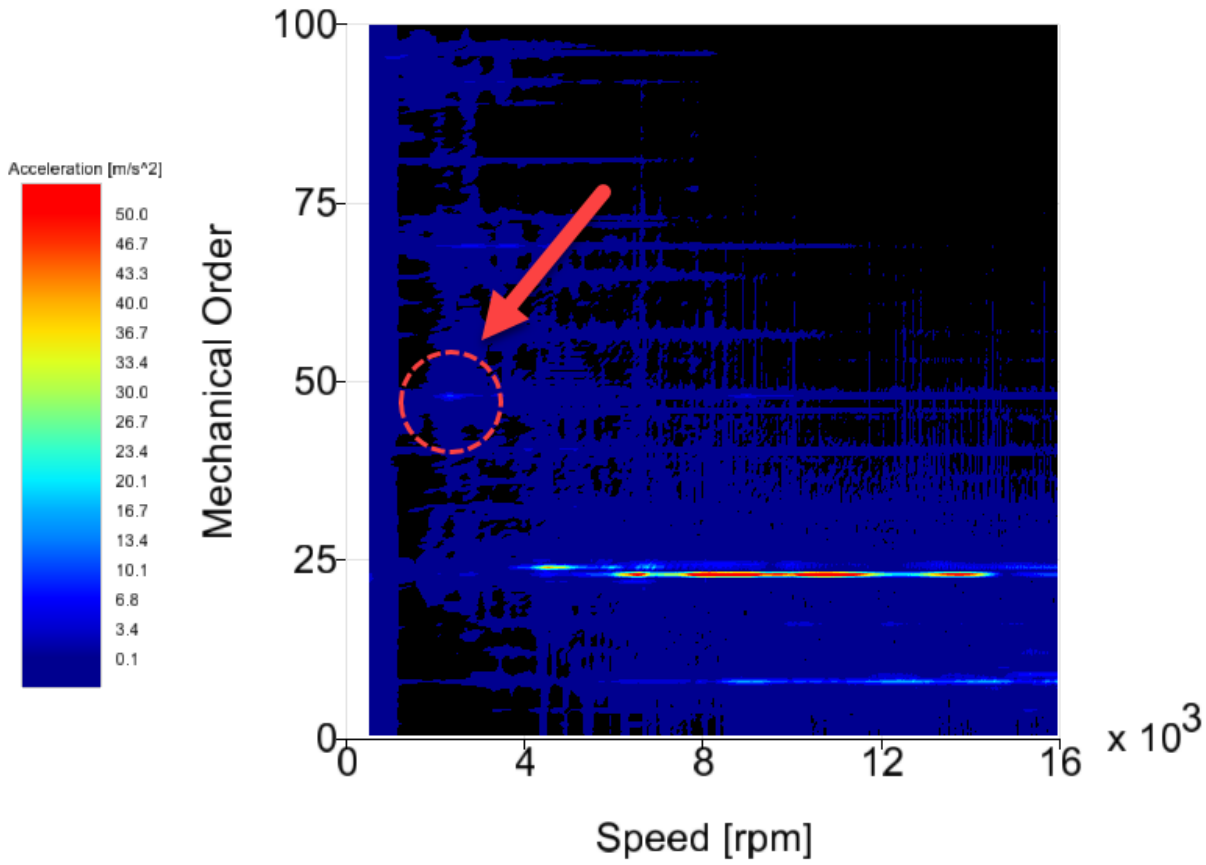

Fig. 10
Campbell plot of optimized electric drive train

5 Conclusions and outlook

In this work, we especially introduced shape optimization of non-linear optimization. In addition, through the combination of ROM and SIMPACK®, we can efficiently and accurately obtain the dynamic NV performance under any load case. According to the test electric drive train, we can find that through non-linear shape optimization, a particular harmonic component in the torque can be suppressed without affecting negatively other aspects of the machine design, thereby achieving better NV performance and thus improving the vehicle comfort.

In the current work, sinusoidal current excitations are assumed when the ROM is created. As outlined in the beginning, one could replace the ROM with the subsystem ROM (SROM) to take into account effects of the controller, inverter if needed. With respect to the optimization, one could additionally include multiple operating points as well as KPI's from the structural domain like for example maximum displacement or stress at maximum rotational speed as additional constraints.

6 References

[1] Dassault Systèmes: "CST Studio Suite 2024", https://www.3ds.com/products/simulia/cst-studio-suite, 2024-May-02
[2] Dassault Systèmes: "TOSCA 2024", https://www.3ds.com/products/simulia/tosca, 2024-May-02
[3] Christian K.: "https://blog.3ds.com/brands/simulia/comparison-reduced-order-model-approaches-rom-electrical-machines/", 2024-May-02
[4] Weber, N., et al.: "Combined Field/System Simulations of Low-Frequency Devices in Time Domain based on Adaptive Nonlinear Reduced Order Models", 2019 International Conference on Electromagnetics in Advanced Applications (ICEAA). IEEE, 2019.
[5] Dassault Systèmes: "SIMPACK 2024", https://www.3ds.com/products/simulia/simpack, 2024-May-02
[6] Dassault Systèmes: "Dymola 2024", https://www.3ds.com/products/catia/dymola, 2024-May-02

Automatisierte CFD-Auslegungstools am Beispiel der Wärmebehandlung von Titanbauteilen

Ulrich Heck, Martin Becker, DHCAE Tools GmbH

1 Zusammenfassung

Während CFD-Methoden für einfachere Strömungszustände bereits Einzug in die Produkt- und Prozessentwicklung gehalten haben, ist bei komplexen Problemstellungen wie Mehrphasen- oder Multiphysikanwendungen häufig noch eine intensive Modellvalidierung und aufgrund der meist hohen Rechenzeiten eine Modelloptimierung erforderlich. Eine Möglichkeit, dem Entwickler für diese anspruchsvolleren CFD-Aufgaben ein Entwurfswerkzeug zur Verfügung zu stellen, ist die Erstellung eines automatisierten CFD-Design Tool für einen konkreten Prozess, das für die Anwendung validiert und optimiert ist. Am Beispiel der Modellierung des Abkühlverhaltens von Titanbauteilen bei der Wärmebehandlung wird die Erstellung und Anwendung eines solchen Tools zur Reduzierung von Kriechvorgängen beim Abkühlen demonstriert. Dabei werden natürliche Konvektion, Wärmeleitung, Strahlungsaustausch und Energiefreisetzung durch Gefügeumwandlung in einer instationären konjugierten Wärmetransportanalyse berücksichtigt. Das CFD-Modell wurde in OpenFOAM erstellt, durch zahlreiche Experimente validiert und rechenzeitoptimiert. Der CFD-Modellaufbau und der Simulationsablauf wurden vollständig automatisiert. Eine Schnittstelle zu Abaqus zur Nutzung der transienten Temperaturfelder in der Kriechanalyse wurde implementiert. Das Tool wird beim Endanwender zur Optimierung der Abkühlbedingungen für Titanbauteile in der Vorentwurfsphase eingesetzt.

2 Vorgehensweise

Die Umsetzung des Prozesses in ein automatisiertes CFD-Tool erfolgt in mehreren Schritten:

- Zunächst muss eine CFD-gerechte Implementierung gefunden und die geeigneten Simulationsmodelle z.B. für die verschiedenen Transportmechanismen gefunden werden.
- Dieses Modell muss für verschiedene Bauteilgeometrien implementiert und insbesondere für komplexe Prozesse validiert werden.
- Wenn die Modelle die physikalischen Sachverhalte abbilden und validiert sind, ist es bei wiederkehrenden Aufgabenstellungen sinnvoll, das Modell zu optimieren. Hierbei wird in der Regel die erforderliche Modellgröße überprüft und Maßnahmen zur Reduzierung der Rechenzeit getroffen.
- Der nächste Schritt ist die Automatisierung des Modells. Dazu werden die notwendigen Eingangsdaten (Geometrieimport und -varianten, Randbedingungen und Betriebsparameter) definiert und in einem automatisierten Workflow für das Modell umgesetzt. Das automatisierte CFD-Tool kann entweder für den Inhouse-Einsatz oder über ein Browser-Interface in Verbindung mit Cloud-Ressourcen genutzt werden.
- Schließlich kann das Modell vom Endanwender zur Prozessauslegung verwendet werden.

3 CFD-Modellierung

Das umzusetzende Modell für die Strömungsanalyse besteht aus einem Titanbauteil, das auf Stützen gelagert ist. Die Stützen wiederum sind auf einem Gitterrost montiert. Betrachtet wird die Abkühlung bei ruhender Luft und bei erzwungener Konvektion.
Es wird eine konjugierte CFD-Analyse mit der CFD-Toolbox OpenFOAM durchgeführt. Dabei werden sowohl das eigentliche Bauteil als auch die Stützen und der Rost als Festkörper berücksichtigt (s. Abb. 1).

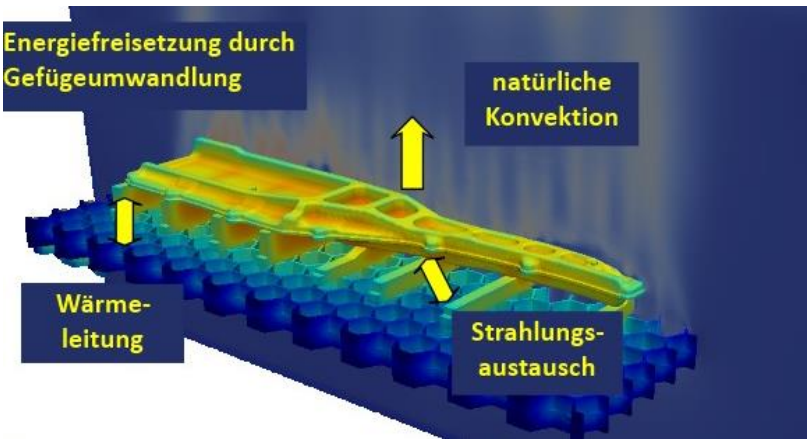

Abbildung 1: CHT Modell in der CFD-Analyse.

Die Analyse erfolgt instationär mit einer RANS-Turbulenzmodellierung (k-Omega SST). Als Wärmetransportmechanismen sind natürliche Konvektion, Strahlung (modelliert mit einem fvDOM-Ansatz) und Wärmeleitung zu berücksichtigen, wobei im Titanbauteil zusätzlich eine Gefügeumwandlung stattfindet, bei der ebenfalls Energie freigesetzt wird. Die Energiefreisetzung durch die Gefügeumwandlung wird durch ein vereinfachtes Modell in temperaturabhängige cp-Werte umgesetzt. In Abhängigkeit von den Abkühlbedingungen werden folgende Ansätze verwendet:

3.1 Abkühlung an ruhender Luft

Bei der Abkühlung an ruhender Luft wird in der Realität das Bauteil auf einem Rost aus dem Ofen gefahren und in der Werkshalle abgekühlt. Eine Schwierigkeit bei der CFD-Modellierung ist hier die Zeitskala, auf der die transiente Abkühlung zu berücksichtigen ist: Typischerweise sind Abkühlzeiten von ca. 15 Minuten zu berücksichtigen, wobei ein stabiler Zeitschritt in der Simulation in der Regel bei wenigen Millisekunden liegt. Hier kommen insbesondere adaptive Zeitschrittweiten und Optimierungen in den Lösungsverfahren zum Einsatz. Zur Entwicklung und Optimierung der Verfahren wurden Messungen an verschiedenen Bauteilen an unterschiedlichen Positionen durchgeführt, um die Berechnungsverfahren zu validieren.
Abbildung 2 zeigt den normierten Temperaturverlauf und die Abkühlrate einiger Vergleichspositionen. Im Allgemeinen wird eine gute Übereinstimmung zwischen Simulation und Experiment erzielt. Die Darstellung der Abkühlraten zeigt, dass die Anfangsphase des Abkühlprozesses durch eine Energiefreisetzung bei der Gefügeumwandlung gekennzeichnet ist.

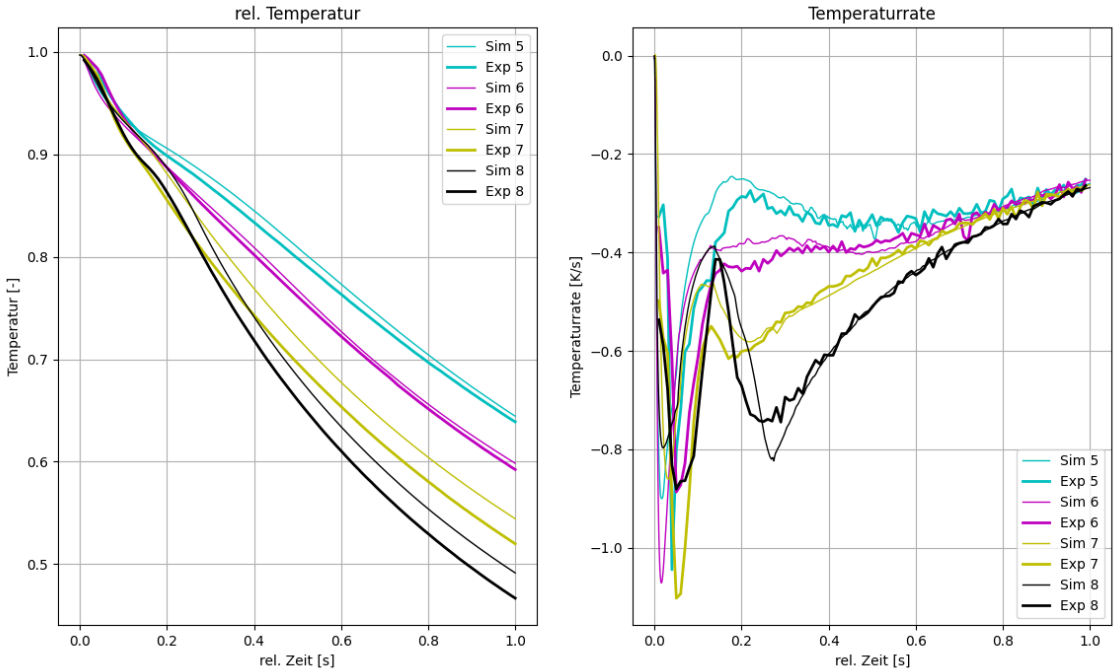

Abbildung 2: Dimensionslose Temperaturverläufe, Vergleich Simulation/Experiment für Abkühlung an ruhender Luft.

3.2 Abkühlung in einer Luftschnellkühlkammer.

Für die Abkühlung in der Luftschnellkühlkammer muss in der Geometrie zusätzlich die Kammer mit den einzelnen Düsenfeldern und den Rostauflagen modelliert werden. Die Mechanismen des Wärmetransports bei der Luftschnellkühlung unterscheiden sich deutlich von der Abkühlung in ruhender Luft: Während die Abkühlung in ruhender Luft durch Strahlung dominiert wird, wird die Abkühlung in der Luftschnellkühlkammer durch die erzwungene Konvektion im Düsenfeld dominiert. Dies erfordert eine andere Strategie bei der Modellierung des Wärmetransports. Da die Gasgeschwindigkeit aus dem Düsenfeld konstant ist, kann hier ein sogenannter Frozen-Flow-Ansatz verwendet werden. Dabei wird das Strömungsfeld stationär berechnet und in der anschließenden transienten Simulation nur die Energiegleichung mit Strahlung, Leitung, Strukturumwandlung und Konvektion im konstanten Geschwindigkeitsfeld gelöst. Hierbei müssen jedoch verschiedene Phasen in den Randbedingungen berücksichtigt werden, wie z.B. die Transportphase, in der das Bauteil aus dem Ofen in die Schnellkühlkammer transportiert wird. Abbildung 3 zeigt auch hier einen Vergleich zwischen Simulation und Experiment für einige Messpositionen. Die Übereinstimmung ist zufriedenstellend, aber nicht ganz so gut wie bei der Abkühlung an ruhender Luft. Als mögliche Ursache wurde die Positionierung des

Düsenfeldes identifiziert. Durch eine detaillierte Analyse der Temperaturdaten aus der Strömungsanalyse konnte gezeigt werden, dass zwischen einem Staupunkt unter einer Düse und der Zwischenposition zwischen zwei Düsen ein Temperaturunterschied von 50 K auftreten kann. Im Vergleich zwischen Simulation und Experiment bleibt dies als Unsicherheit bestehen, da hier keine Übereinstimmung in der Positionierung des Bauteils zwischen Simulation und Experiment möglich ist.

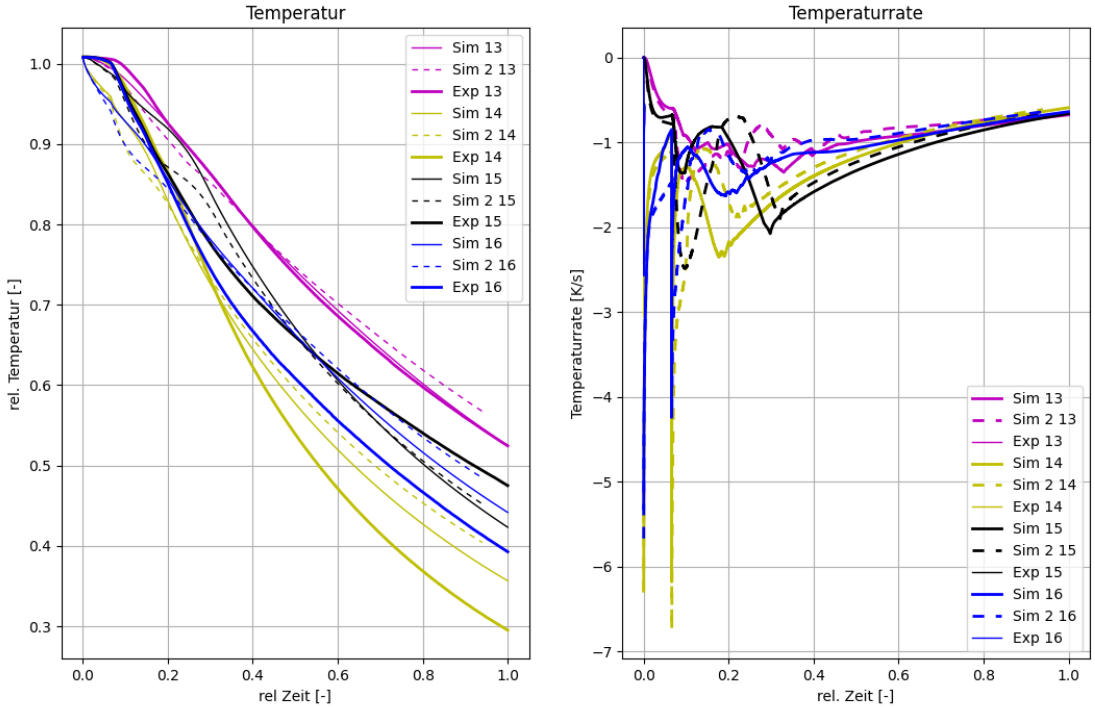

Abbildung 3: Dimensionslose Temperaturverläufe, Vergleich Simulation/Experiment für Abkühlung in der Luftschnellkühlkammer.

4 Optimierung des CFD-Modells

Das Modell soll als Entwurfswerkzeug in der Entwicklung eingesetzt werden. Daher ist eine Vielzahl von Berechnungen mit dem Werkzeug vorgesehen. Andererseits sind die Rechenzeiten bei instationärer Abkühlung relativ hoch. Eine Optimierung hinsichtlich der Rechenzeit ist daher im Hinblick auf den späteren Einsatz unabdingbar. Dazu werden weitere Varianten durchgeführt, bei denen insbesondere die Lösungseinstellungen während des Rechenlaufs angepasst werden. Dies gilt insbesondere für die Zeitschrittweite, bei der aus Stabilitäts- und Genauigkeitsgründen mit kleinen Zeitschritten begonnen werden muss (z.B. um die Energiefreisetzung bei der Gefügeumwandlung abzubilden), später aber die Zeitschrittweite erhöht werden kann. Durch diese Maßnahmen kann die Rechenzeit typischerweise um einen Faktor 2-3 reduziert werden.

5 Schnittstelle zur Kopplung FEM

Es wird eine unidirektionale Kopplungsschnittstelle zum strukturmechanischen Solver Abaqus realisiert, um die transienten Temperaturfelder für eine nachgeschaltete Kriechanalyse zu verwenden. Über die Samplingfunktion in OpenFOAM werden die Temperaturen zu den jeweiligen Zeitpunkten auf die separat exportierten Knoten des FE-Netzes gemappt. Über die von Abaqus bereitgestellten Fortran-Schnittstellen werden die Daten aufbereitet und die Temperaturen als Lasten für die thermische Dehnungs- und Kriechmodellierung in der Strukturanalyse verwendet [1]. In diesem Fall muss nur das Titanbauteil modelliert werden. Die Auflager können im Kontakt im dem Titanbauteil als Starrkörper modelliert werden.

6 Automatisierung

Der CFD-Workflow ist vollständig automatisiert (s. Abbildung 4). Als Eingabe dient die im STL-Format exportierte Geometrie für Rost, Stützen und Bauteil. Mit einer Parameterdatei für die individuellen Randbedingungen wird der Fall über ein Python- und Shell-Scripting automatisiert vernetzt, mit Randbedingungen versehen und berechnet. Für die Vernetzung wird der OpenFOAM-interne Vernetzer SnappyHexMesh verwendet, der ein hexaederdominantes Polyedergitter erzeugt. Die Vernetzung und

Simulation erfolgen auf einem Server unter Linux. Ein Monitoringtool ermöglicht die Kontrolle des Simulationsfortschritts von einem Windows-Desktop aus. Das Mapping der Temperaturdaten nach Abaqus erfolgt schließlich ebenfalls über das Monitoringtool.
Neben der aktuellen Nutzung beim Endanwender über eine Eingabedatei und unter Nutzung firmeninterner Server für die Simulation wurde das System in eine Cloud-basierte Umgebung mit Webinterface zur Eingabe der Parameter integriert [2]. Dies ermöglicht die Berechnung für andere Nutzer für ähnliche Abkühlprozesse durch Strahlung und Konvektion in Kombination mit Wärmeleitung in Festkörpern. Die Parameter werden über einen Browser in ein Webinterface eingegeben. Die Simulation wird dann automatisiert auf Basis der hochgeladenen Geometrie und der vorgegebenen Parameter unter Verwendung von Cloud-Ressourcen durchgeführt.

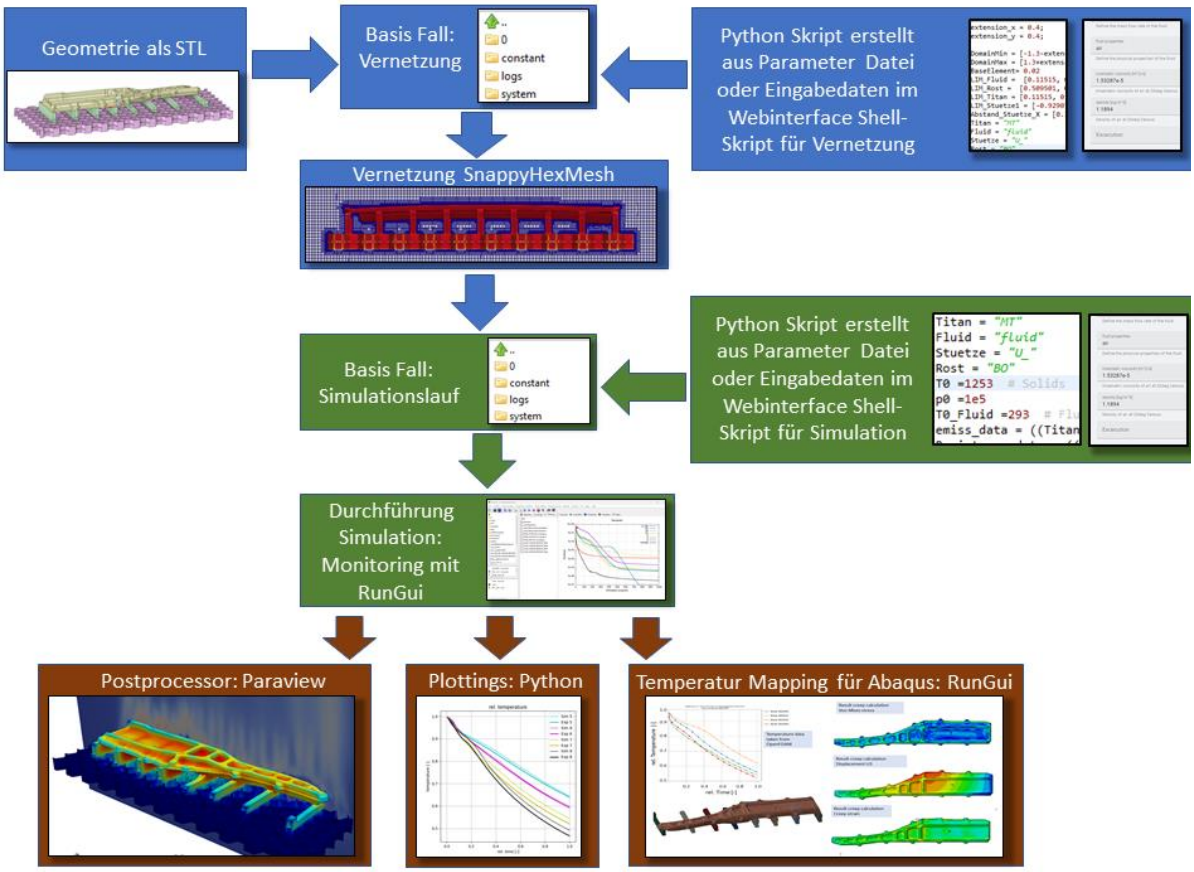

Abbildung 4:Umsetzung des automatisierten CFD-Workflows.

7 Anwendung

Das CFD-Werkzeug wird in der Entwicklung zur Optimierung der Abkühlbedingungen als Auslegungstool eingesetzt. Es konnte gezeigt werden, dass das Kriechen des Bauteils deutlich reduziert werden kann, wenn keine signifikante Temperaturdifferenz zwischen Ober- und Unterseite des Bauteils auftritt. Die Abkühlung im bisherigen Prozess kühlt die Unterseite langsamer ab, da der darunterliegende Rost die Wärme länger speichert. In der Simulation können zu diesem Zweck z.B. einfach zusätzliche Reflektoren installiert werden. Es kann dann für die spezifischen Bauteile analysiert werden, ob die Abkühlung sowohl gleichmäßig als auch mit den erforderlichen Abkühlraten erfolgt. Insgesamt kann daher bereits aus der reinen CFD-Wärmetransportanalyse eine Optimierung des Abkühlprozesses erfolgen, die durch eine nachgeschaltete Strukturanalyse auch in den Verformungen des realen Bauteils quantifiziert werden kann (s. Abbildung 5).

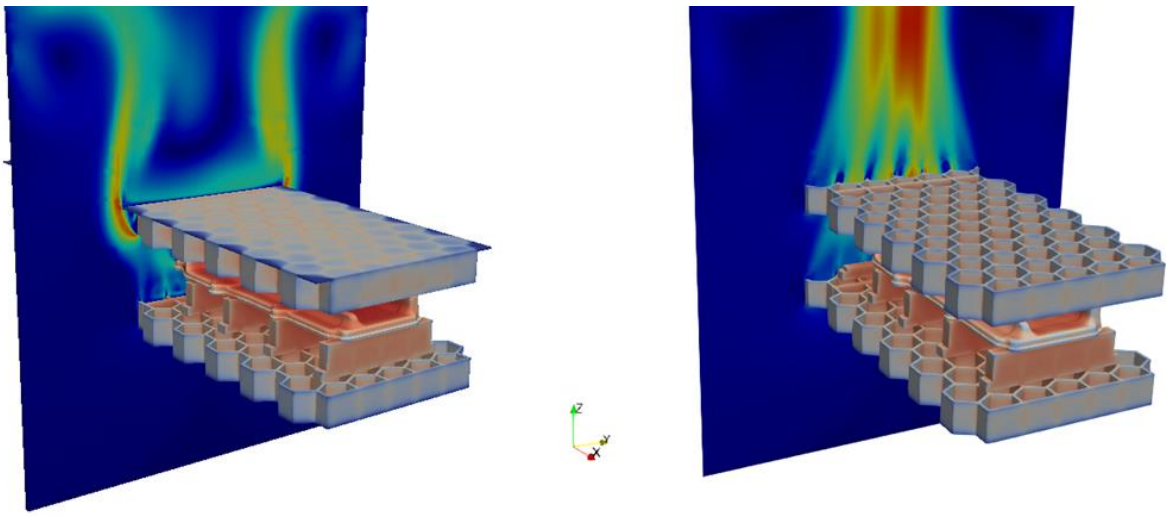

Abbildung 5: Optimierung des Abkühlungsverhalten mit dem automatisierten CFD-Werkzeug.

8 Danksagung

Das Projekt wurde vom Bundesministerium für Wirtschaft und Klimaschutz auf der Grundlage eines Beschlusses des Deutschen Bundestages gefördert.

9 Referenzen

[1] Ulrich Heck, Martin Becker, Ralf Paßmann, Volker Hardenacke
A coupled flow, heat and structural analysis tool to reduce creep during heat treatment of titanium components, Conference Proceedings, Nafems Multiphysics Conference, Munich 14-15 Nov. 2023

[2] Automatisierte CFD-Workflows www.cfdtools.com

Kontakt:
Dr. Ulrich Heck
DHCAE-Tools GmbH
Friedrich-Ebert-Str. 368
47800 Krefeld
Phone + 49 2151 9490201
www.dhcae-tools.de

CFD-Simulation von rotierenden Vakuumverdrängerpumpen: Möglichkeiten und Herausforderungen

Dr. Andreas Spille (CFX Berlin Software GmbH)

Summary

Rotationsverdränger wie Schraubenverdichter, Scrollverdichter, Drehschieberpumpe oder Roots-Gebläse werden außer zur Verdichtung von Prozessgasen auch als Vakuumpumpen zur Erzeugung von Unterdrücken eingesetzt. Hierbei werden einige Anpassungen vorgenommen:

- Aufgrund der niedrigen Massenströme ist eine effiziente Kühlung von Gehäuse und Rotoren notwendig.
- Die Spaltmaße (Radial-, Axial- und Profileingriffsspalte) sind oft deutlich kleiner.
- Drehkolbenpumpen werden oft in einem Gehäuse mehrstufig ausgeführt, um tiefere Drücke erreichen zu können.
- Schrauben-Vakuumpumpen haben im Unterschied zu Schraubenverdichtern kantige Profile und oft variable und kleinere Steigungen.

Diese Anpassungen stellen auch erhöhte Anforderungen an die Strömungssimulation dar, die einfachere Methoden wie Overset Meshes oder Remeshing schwer nutzbar machen, sondern konturangepasste Hexaeder-/Prismengitter erfordern.
Dieser Vortrag erläutert für eine mehrstufige Drehkolbenvakuumpumpe und für eine Schraubenvakuumpumpe, wie bei der Gittererstellung, der Umsetzung der Kammerdeformationen und dem Aufsetzen der Vakuumpumpe auf diese Anforderungen reagiert wird. Hierbei wird auch auf die Grenzen des Kontinuumsansatzes und die Möglichkeit eingegangen, mit einer Slip-Randbedingung für Geschwindigkeiten und Temperaturen den Anwendungsbereich bis in die Gleitströmung bei Knudsenzahl <0.1 zu erweitern.

CFD-Simulation von rotierenden Vakuumverdrängerpumpen: Möglichkeiten und Herausforderungen

Dr. Andreas Spille

CFX Berlin Software GmbH, Berlin, Germany

NAFEMS DACH CONFERENCE

10-12 June 2024 | Bamberg, Germany

1

Inhalt

- Einführung
  - Vakuum und Vakuumpumpen
  - Beispiele Scroll-, Roots-, Schraubenpumpe
  - Kontinuumsansatz, Knudsen-Zahl
- CFD-Simulation von Schraubenpumpen
  - Setup in TwinMesh und Ansys CFX
  - Bestimmung des Saugvermögens
  - Gleitströmung mit Slip-Randbedingung
  - Simulation der Rotor-Erwärmung
- Zusammenfassung und Ausblick

2

Vakuum und Vakuumpumpen

CFX BERLIN

Was ist Vakuum?

- Vakuum ist Unterdruck unter 300 mbar (Druck auf Mount Everest)
- Gas (meist Luft) wird aus einem Raum entfernt → Vakuumpumpe
- Ideales Vakuum (keine Atome) nicht realisierbar

Einordnung anhand der Druckbereiche

Druckbereich	Druck		Moleküldichte[a)]
Normaldruck	101,325 kPa	1013,25 mbar	$2{,}7 \cdot 10^{19}$ cm^{-3}
Grobvakuum[b)]	…100 Pa	…1 mbar	…10^{16} cm^{-3}
Feinvakuum	100 Pa…100 mPa	1…10^{-3} mbar	10^{16}…10^{13} cm^{-3}
Hochvakuum (HV)	100 mPa…1 µPa	10^{-3}…10^{-8} mbar	10^{13}…10^{8} cm^{-3}
Ultrahochvakuum (UHV)[c)]	1 µPa…1 nPa	10^{-8}…10^{-11} mbar	10^{8}…10^{5} cm^{-3}
extrem hohes Vakuum (XHV)[c)]	< 1 nPa	< 10^{-11} mbar	< 10^{5} cm^{-3}
Ideales Vakuum (IV)[d)]	0 Pa	0 mbar	0 cm^{-3}

Anwendungen:
- Hebetechnik, Verpackung, Entgasen
- Gefriertrocknung, Vakuummetallurgie
- Teilchen-Beschleuniger, Elektronenstrahlanlagen

https://de.wikipedia.org/wiki/Vakuum

3

Vakuum und Vakuumpumpen

CFX BERLIN

- Vakuumpumpen zum Absaugen des Gases:
  - Verdichtung von p_{Vakuum} auf p=1 atm
  - Saugvermögen als Funktion(p_{Vakuum}) in m^3/h oder l/s
  - Enddruck der Pumpe: Saugvermögen → 0
- (Vor-) Pumpen für Grobvakuum:
  - Oszillationsverdränger: Hubkolbenpumpe, Membranpumpe
  - Rotationsverdränger: Drehschieberpumpe, Scrollpumpe, Roots-Pumpe, Schraubenpumpe
  - Treibmittelstrahlpumpe

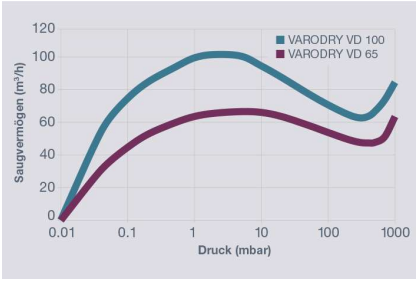

Quelle Bild:
https://www.leyboldproducts.de/produkte/trockenverdichtende-vakuumpumpen/varodry/pumpen/3020/varodry-vd65

- Hochvakuum / Ultrahochvakuum durch vorgeschaltete weitere Pumpe(n):
  - Turbomolekularpumpe
  - Diffusionspumpe
  - Kryopumpe, Getterpumpe, Sublimationspumpe (gasbindend)

4

Scrollpumpe

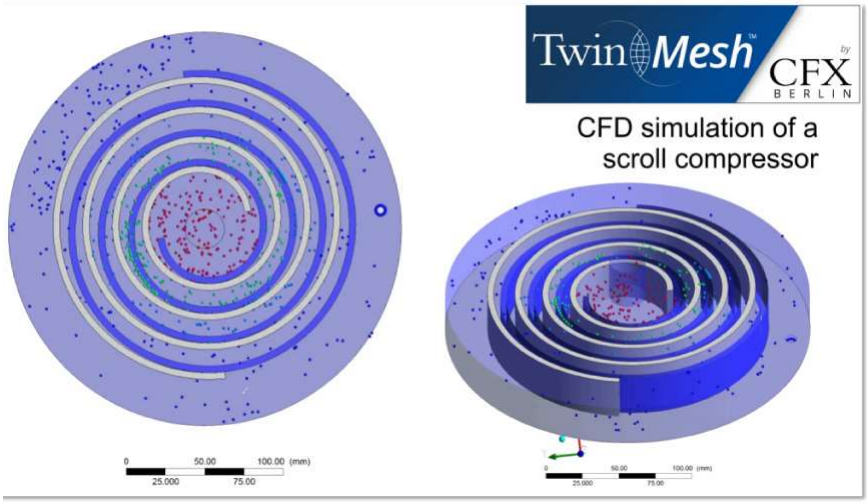

Scrollpumpe:

- Graue Spirale orbitiert um blaue Spirale
- innere Verdichtung
- Luft von 0.17 bar, 20°C auf 0.95 bar
- Wände bei 60°C
- 1704 U/min

NAFEMS DACH 2024 Seite 5

5

Roots-Pumpe / Wälzkolbenpumpe

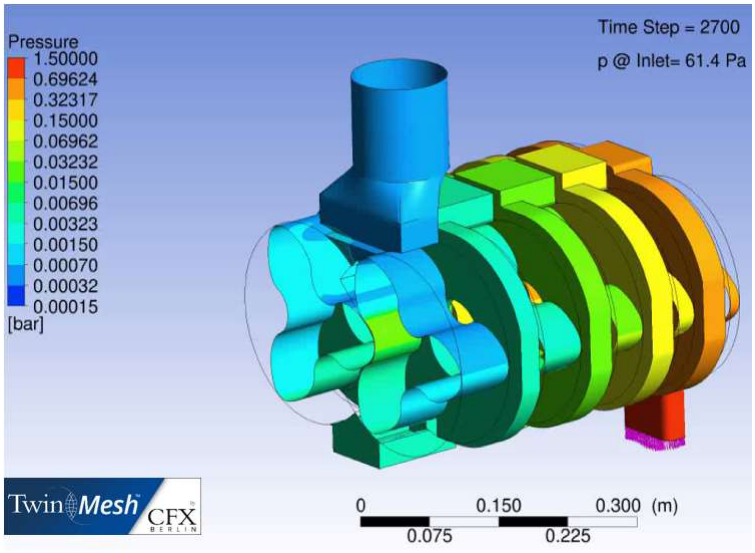

Roots-Pumpe:

- 2- oder 3-flüglige gegensinnig drehende Rotoren
- keine innere Verdichtung
- 5 Stufen
- Luft von 50 Pa, 20°C auf 1 bar
- Wände bei 20°C
- 5400 U/min

lot vacuum Leader Of Technology Vacuum

NAFEMS DACH 2024 Seite 6

6

Schraubenpumpe

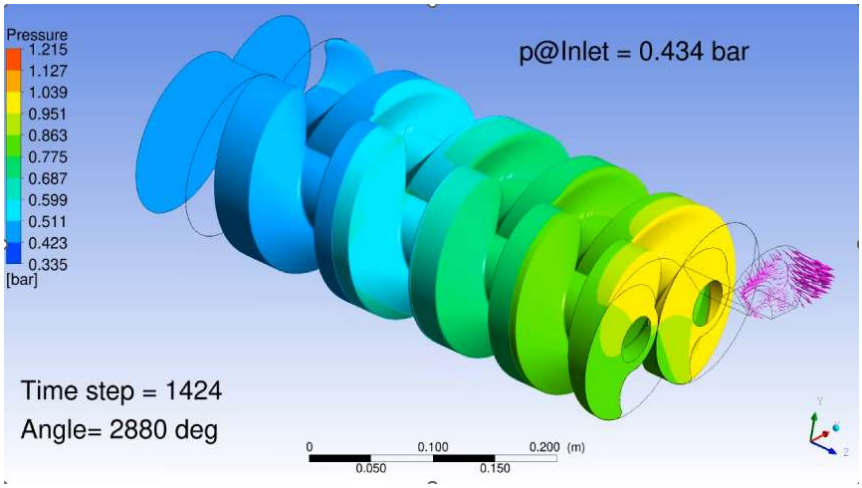

Schraubenpumpe:

- gegensinnig drehende Rotoren
- innere Verdichtung
- Luft auf 1 bar
- Wände bei 20°C
- 3000 U/min
- Einlass geschlossen, initialisiert auf 1 bar

7

Kontinuumsansatz

- CFD-Löser basiert auf Navier-Stokes-Gleichungen für makroskopische Größen wie Dichte, Druck, Geschwindigkeit, Temperatur
- Kontinuumsansatz statt Betrachtung einzelner Moleküle
- Voraussetzung: Teilchen-Teilchen-Stöße >> Teilchen-Wand-Stöße
  → mittlere freie Weglänge $\lambda = \frac{1}{n \cdot \sigma}$

Einordnung anhand der Druckbereiche

Druckbereich	Druck		Moleküldichte[a)]	mittlere freie Weglänge[a)]
Normaldruck	101,325 kPa	1013,25 mbar	$2{,}7 \cdot 10^{19}$ cm^{-3}	68 nm
Grobvakuum[b)]	…100 Pa	…1 mbar	…10^{16} cm^{-3}	0,1…100 µm
Feinvakuum	100 Pa…100 mPa	1…10^{-3} mbar	10^{16}…10^{13} cm^{-3}	0,1…100 mm
Hochvakuum (HV)	100 mPa…1 µPa	10^{-3}…10^{-8} mbar	10^{13}…10^{8} cm^{-3}	100 mm…10 km
Ultrahochvakuum (UHV)[c)]	1 µPa…1 nPa	10^{-8}…10^{-11} mbar	10^{8}…10^{5} cm^{-3}	10…10^{4} km
extrem hohes Vakuum (XHV)[c)]	< 1 nPa	< 10^{-11} mbar	< 10^{5} cm^{-3}	> 10^{4} km
Ideales Vakuum (IV)[d)]	0 Pa	0 mbar	0 cm^{-3}	∞

https://de.wikipedia.org/wiki/Vakuum

8

Knudsen-Zahl

Knudsen-Zahl: Kn=λ/L mit mittlerer freier Weglänge λ, Längenmaß L

- Kn>10: freie Molekularströmung
- 0.1 < Kn < 10: Übergangsströmung
- 0.01 < Kn < 0.1: Gleitströmung
- Kn < 0.01: Kontinuumsströmung, viskose Strömung ➔ L>100 λ

Einordnung anhand der Druckbereiche

Druckbereich	Druck		Moleküldichte[a)]	mittlere freie Weglänge[a)]
Normaldruck	101,325 kPa	1013,25 mbar	$2{,}7 \cdot 10^{19}$ cm^{-3}	68 nm
Grobvakuum[b)]	…100 Pa	…1 mbar	…10^{16} cm^{-3}	0,1…100 µm
Feinvakuum	100 Pa…100 mPa	1…10^{-3} mbar	10^{16}…10^{13} cm^{-3}	0,1…100 mm
Hochvakuum (HV)	100 mPa…1 µPa	10^{-3}…10^{-8} mbar	10^{13}…10^{8} cm^{-3}	100 mm…10 km
Ultrahochvakuum (UHV)[c)]	1 µPa…1 nPa	10^{-8}…10^{-11} mbar	10^{8}…10^{5} cm^{-3}	10…10^{4} km
extrem hohes Vakuum (XHV)[c)]	< 1 nPa	< 10^{-11} mbar	< 10^{5} cm^{-3}	> 10^{4} km
Ideales Vakuum (IV)[d)]	0 Pa	0 mbar	0 cm^{-3}	∞

https://de.wikipedia.org/wiki/Vakuum

CFD-Simulation von Schraubenpumpen

3D-CFD-Simulation einer Schraubenpumpe:

- Geometrie:
  - Zwei gleiche Rotoren mit Außenradius 70 mm und Achsabstand 100 mm
  - Länge 400 mm mit 4 bis 6 Windungen
  - Radialspalte Rotor-Gehäuse 50 µm
  - Axialspalte 100 µm
- Randbedingungen:
  - Fluid: Luft als ideales Gas
  - 20°C Einlass- und Wandtemperatur
  - Drehzahl 3000 U/min
  - Zeitauflösung: 0.112 ms (2.02°)
- Zielgrößen:
  - Saugvermögen
  - Leistung

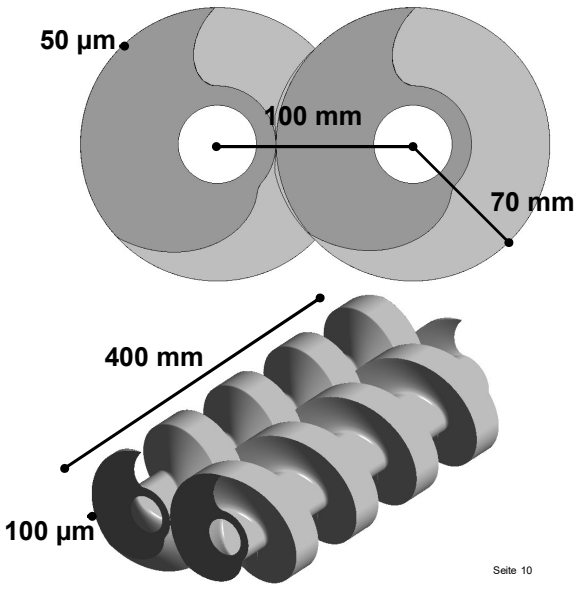

Setup in TwinMesh und Ansys CFX

CFX BERLIN

CAD

↓

TwinMesh

1. Rotorgeometrie importieren
2. Parameter definieren
3. Interfaces erstellen
4. Gittereinstellungen
5. 2D-Gitter erstellen
6. Qualität überprüfen
7. Randbedingungen setzen
8. 3D-Gitter exportieren

↓

ANSYS

1. Preprocessing-Skript ausführen
2. Weitere Gitter zur Laufzeit einlesen

Setup in TwinMesh und Ansys CFX

CFX BERLIN

CAD

↓

TwinMesh

1. Rotorgeometrie importieren
2. Parameter definieren
3. Interfaces erstellen
4. Gittereinstellungen
5. 2D-Gitter erstellen
6. Qualität überprüfen
7. Randbedingungen setzen
8. 3D-Gitter exportieren

↓

ANSYS

1. Preprocessing-Skript ausführen
2. Weitere Gitter zur Laufzeit einlesen

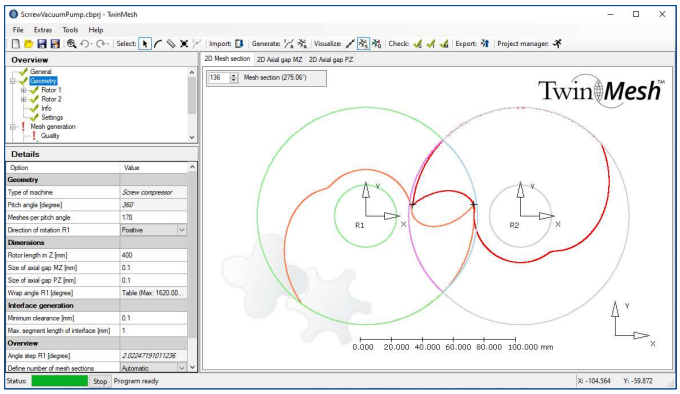

Setup in TwinMesh und Ansys CFX

CFX BERLIN

CAD

↓

TwinMesh

1. Rotorgeometrie importieren
2. Parameter definieren
3. Interfaces erstellen
4. Gittereinstellungen
5. 2D-Gitter erstellen
6. Qualität überprüfen
7. Randbedingungen setzen
8. 3D-Gitter exportieren

↓

ANSYS

1. Preprocessing-Skript ausführen
2. Weitere Gitter zur Laufzeit einlesen

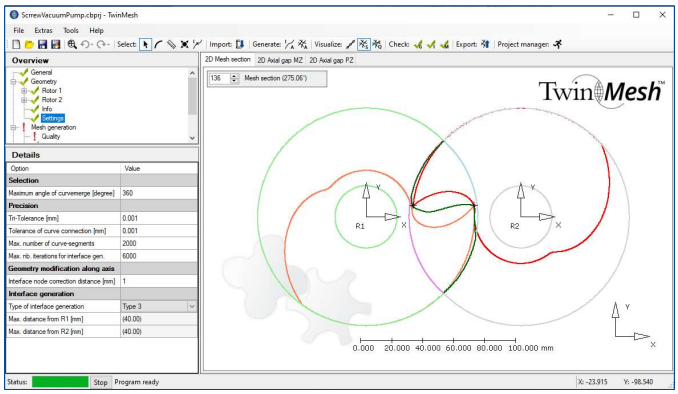

13

Setup in TwinMesh und Ansys CFX

CFX BERLIN

CAD

↓

TwinMesh

1. Rotorgeometrie importieren
2. Parameter definieren
3. Interfaces erstellen
4. Gittereinstellungen
5. 2D-Gitter erstellen
6. Qualität überprüfen
7. Randbedingungen setzen
8. 3D-Gitter exportieren

↓

ANSYS

1. Preprocessing-Skript ausführen
2. Weitere Gitter zur Laufzeit einlesen

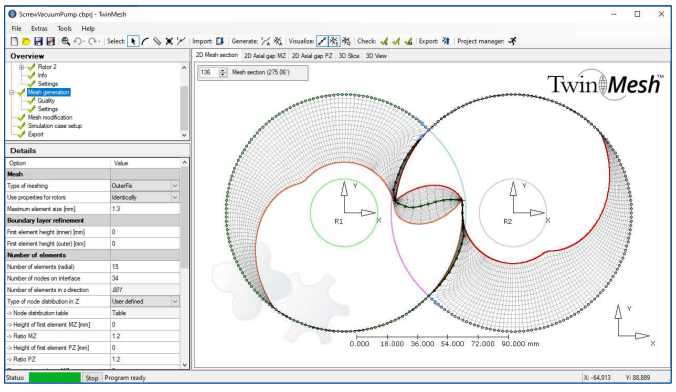

14

Setup in TwinMesh und Ansys CFX

CAD

↓

1. Rotorgeometrie importieren
2. Parameter definieren
3. Interfaces erstellen
4. Gittereinstellungen
5. 2D-Gitter erstellen
6. Qualität überprüfen
7. Randbedingungen setzen
8. 3D-Gitter exportieren

↓

1. Preprocessing-Skript ausführen
2. Weitere Gitter zur Laufzeit einlesen

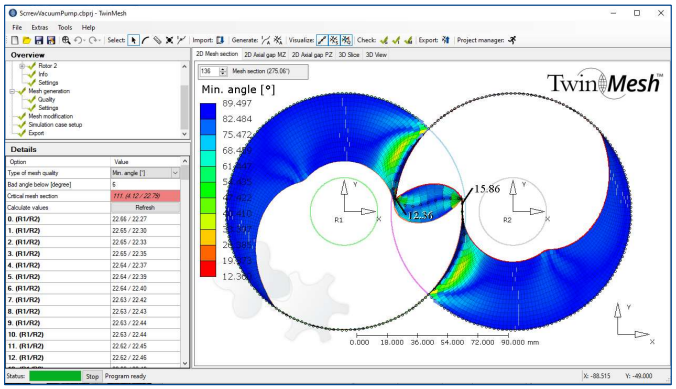

Setup in TwinMesh und Ansys CFX

CAD

↓

1. Rotorgeometrie importieren
2. Parameter definieren
3. Interfaces erstellen
4. Gittereinstellungen
5. 2D-Gitter erstellen
6. Qualität überprüfen
7. Randbedingungen setzen
8. 3D-Gitter exportieren

↓

1. Preprocessing-Skript ausführen
2. Weitere Gitter zur Laufzeit einlesen

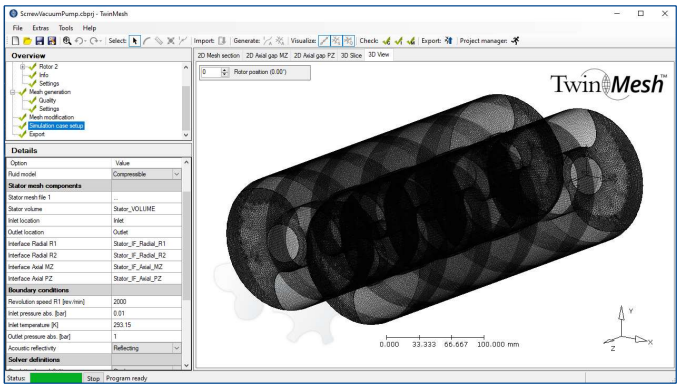

Setup in TwinMesh und Ansys CFX

CFX BERLIN

CAD

↓

TwinMesh

1. Rotorgeometrie importieren
2. Parameter definieren
3. Interfaces erstellen
4. Gittereinstellungen
5. 2D-Gitter erstellen
6. Qualität überprüfen
7. 3D-Gitter exportieren
8. Skripte schreiben

↓

ANSYS

1. Preprocessing-Skript ausführen
2. Weitere Gitter zur Laufzeit einlesen

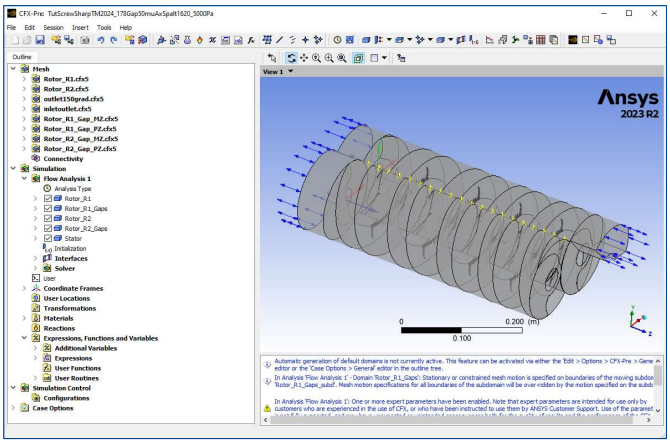

Setup in TwinMesh und Ansys CFX

CFX BERLIN

CAD

↓

TwinMesh

1. Rotorgeometrie importieren
2. Parameter definieren
3. Interfaces erstellen
4. Gittereinstellungen
5. 2D-Gitter erstellen
6. Qualität überprüfen
7. 3D-Gitter exportieren
8. Skripte schreiben

↓

ANSYS

1. Preprocessing-Skript ausführen
2. Weitere Gitter zur Laufzeit einlesen

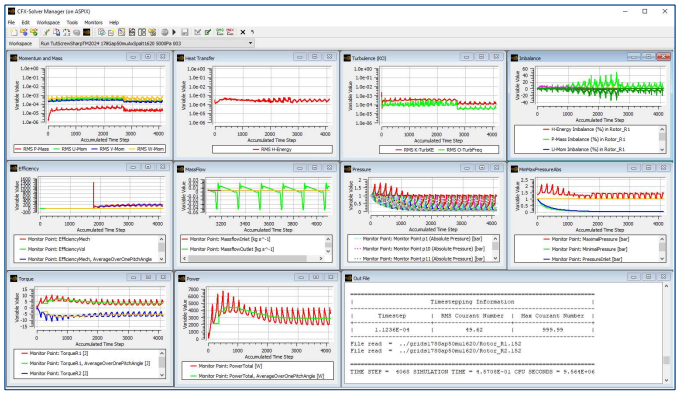

Bestimmung des Saugvermögens

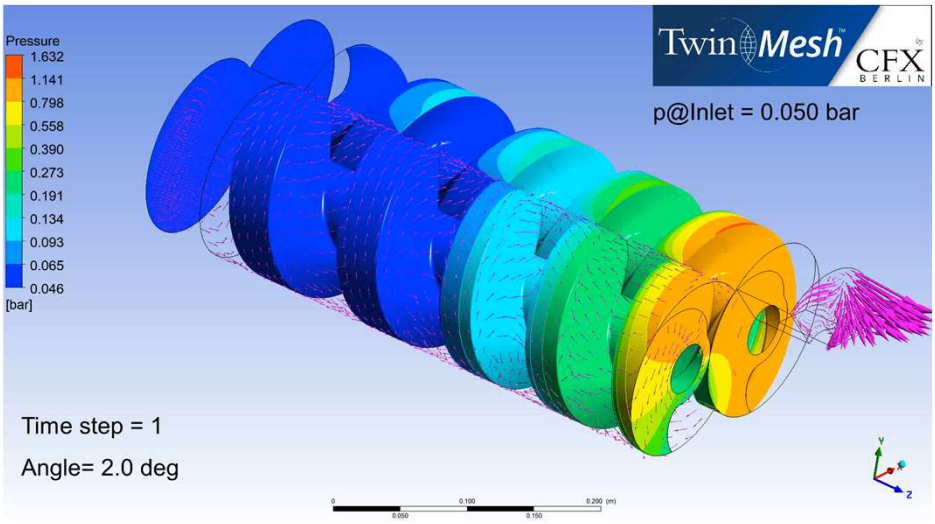

Parameter:

- Radialspalt 50 µm
- 3000 U/min
- Einlass auf 5000 Pa = 0.05 bar
- Auslass auf 1 bar
- Wände auf 20°C

➢ Massenstrom 2.89 g/s
➢ Saugvermögen 175 m^3/h
➢ Leistung 2810 W

19

Bestimmung des Saugvermögens

Abhängigkeit des Saugvermögens von

- Drehzahl (3000 U/min)
- Wandtemperatur (20°C)
- Spaltmaßen (50 µm)
- **Vakuumdruck**

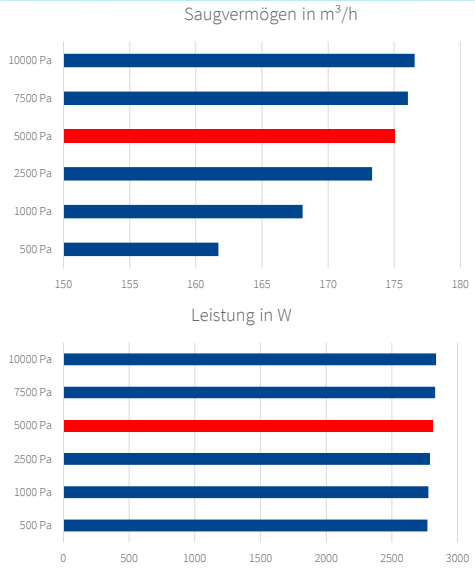

20

Bestimmung des Saugvermögens

CFX BERLIN

Abhängigkeit des Saugvermögens von

- Drehzahl (3000 U/min)
- Wandtemperatur (20°C)
- Spaltmaßen (50 µm)
- Vakuumdruck (5000 Pa)
- **Schraubensteigung**

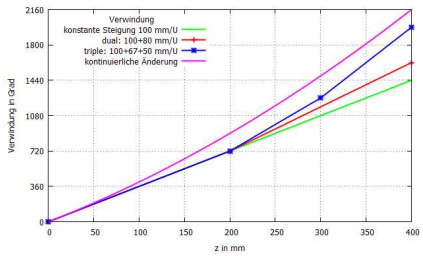

2160°
1980°
1620°
1440°

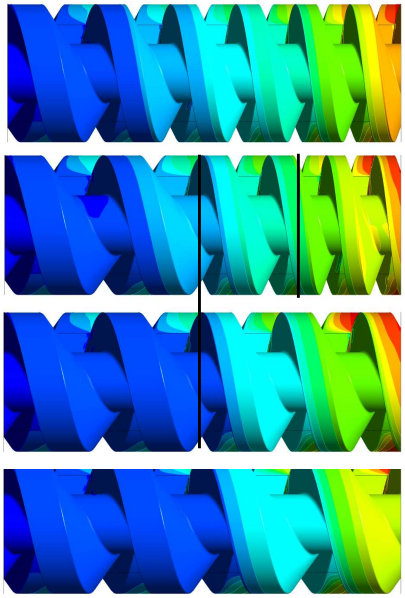

kontin.
2160°

triple
1980°

dual
1620°

konstant
1440°

21

Bestimmung des Saugvermögens

CFX BERLIN

Abhängigkeit des Saugvermögens von

- Drehzahl (3000 U/min)
- Wandtemperatur (20°C)
- Spaltmaßen (50 µm)
- Vakuumdruck (5000 Pa)
- **Schraubensteigung**

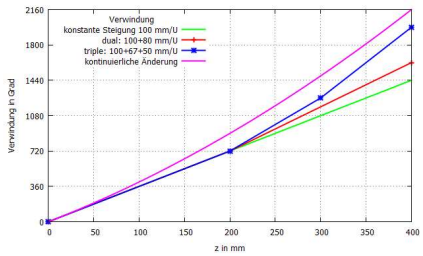

2160°
1980°
1620°
1440°

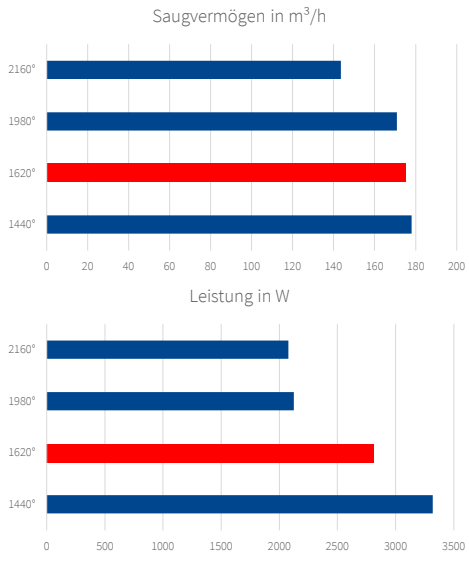

22

Bestimmung des Saugvermögens

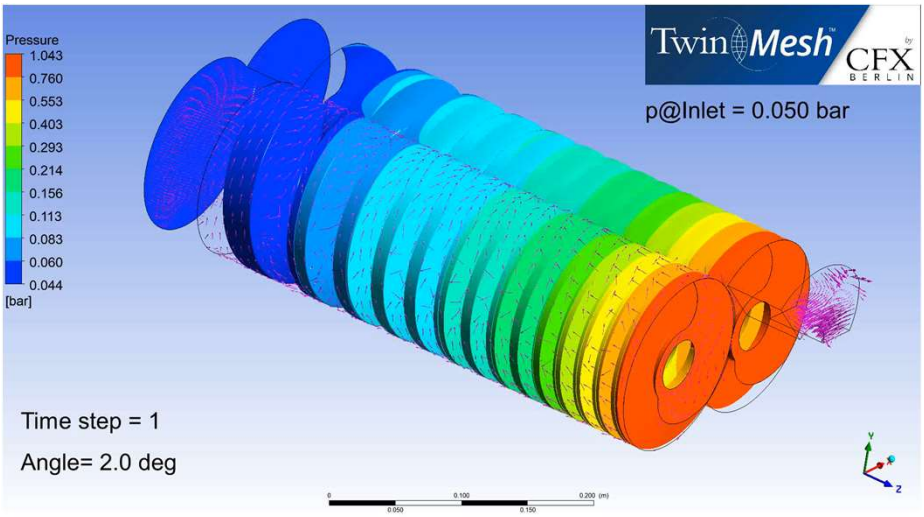

Parameter:

- Radialspalt 50 µm
- 3000 U/min
- Einlass auf 5000 Pa = 0.05 bar
- Auslass auf 1 bar
- Wände auf 20°C
- **6x innere Kompression: 5040°=14 U**

➢ Saugvermögen 85 m^3/h (175)
➢ Leistung 970 W (2810 W)

Gleitströmung mit Slip-Randbedingung

- Erweiterung des Anwendungsbereichs der Navier-Stokes-Gleichungen in den Bereich der Gleitströmung:
  - Slip-Bedingung statt Haftbedingung:

$$U_{wall} - U_{gas} = \frac{2-\alpha_v}{\alpha_v}\lambda\frac{\partial U}{\partial n} + \frac{3}{4}\frac{\mu}{\rho T}\frac{\partial T}{\partial tan}$$

  - Temperatursprungbedingung:

$$T_{wall} - T_{gas} = 2\frac{2-\alpha_T}{\alpha_T}\lambda\frac{\partial T}{\partial n}$$

  - mit den Akkomodationskoeffizienten (thermisch und Impuls-):

Gas	Oberfläche	α_T	α_v
Luft	Aluminium	0,87-0,97	0,87-0,97
He	Aluminium	0,073	—
Luft	Eisen	0,87-0,96	0,87-0,97
H2	Eisen	0,31 - 0,55	—
Luft	Bronze	—	0,88-0,95

Earle H. Kennard: Kinetic Theory of Gases 1938

- Quelle: Bachelorarbeit „CFD-Simulation einer verdünnten Strömung am Beispiel einer Drehschieberpumpe“, Simon Galap, TU Berlin, 2017

Gleitströmung mit Slip-Randbedingung

CFX BERLIN

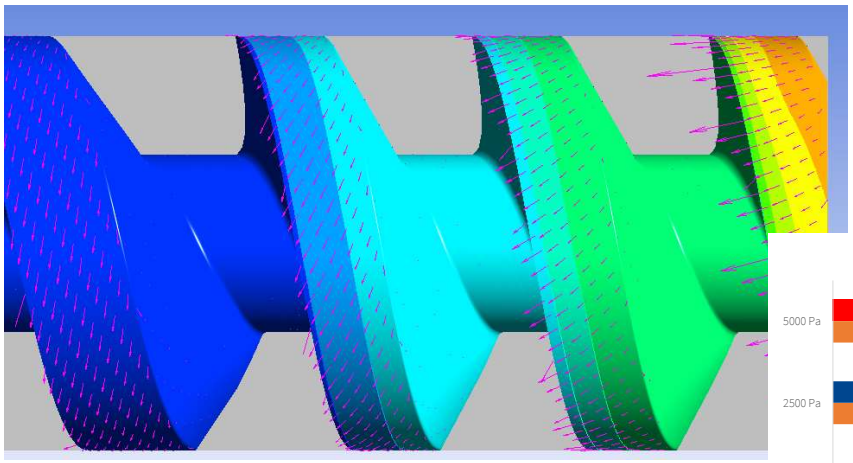

Darstellung von
$U_{Slip} = U_{Gas} - U_{wall}$

Effekt ist klein:
$U_{slip} \approx 0.5$ m/s @ 5000 Pa
$U_{wall} \approx 22$ m/s

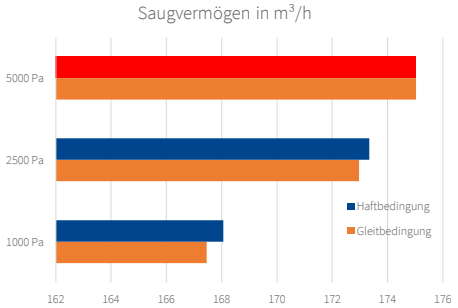

NAFEMS DACH 2024 Seite 25

25

Simulation der Rotor-Erwärmung

CFX BERLIN

Motivation:

- Vakuumpumpen haben einen hohen Druckaufbau (0.05 bar→1 bar: Faktor 20)
- Starke Gaserwärmung durch Kompression (adiabat=Faktor 2,35)
- Geringe Durchflussraten
- Kühlung der Festkörper (Rotoren + Gehäuse) notwendig
- Annahme von 20°C Wandtemperatur idealisiert

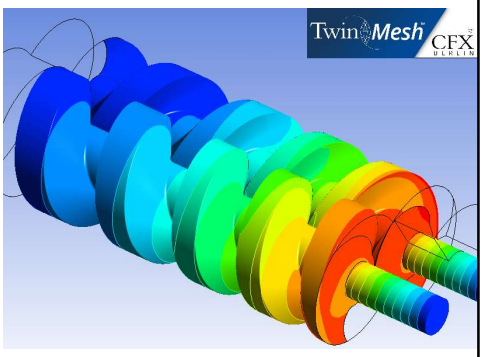

Simulation der Rotor-Erwärmung:

- Einfügen der Rotoren als Festkörper (Edelstahl)
- Wärmeübergang zwischen Gas und Festkörper (CHT)
- Erwärmung der Festkörper (unterschiedliche Zeitskalen!)
- Eingeschwungener, periodischer Zustand nach ca. 50 Umdrehungen

NAFEMS DACH 2024 Seite 26

26

Simulation der Rotor-Erwärmung

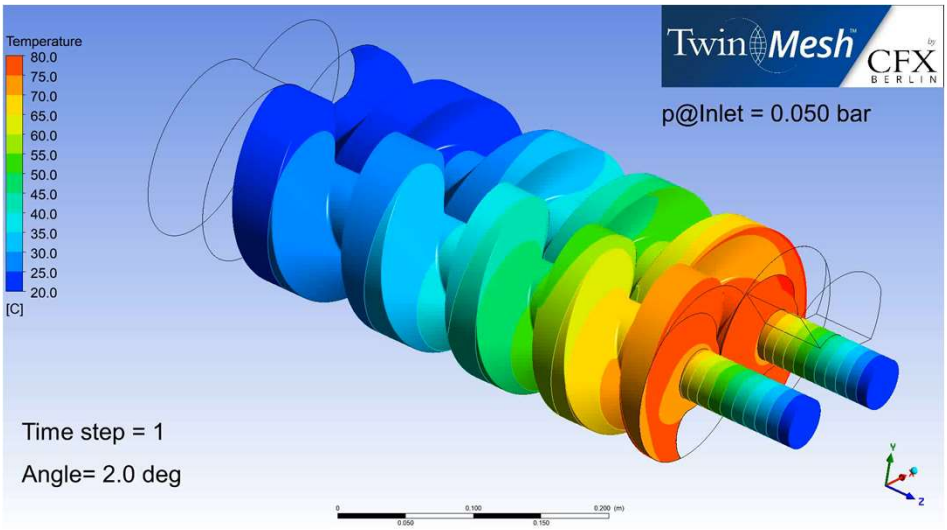

Parameter:

- Radialspalt 50 µm
- 3000 U/min
- Einlass auf 5000 Pa = 0.05 bar
- Auslass auf 1 bar
- Gehäusewände auf 20°C
- **Einseitig gelagerte Rotoren, Wellenenden auf 20°C**

➢ Saugvermögen 165 m^3/h (175)

➢ Leistung 2940 W (2810 W)

27

Zusammenfassung und Ausblick

CFD-Simulation von rotierenden Vakuumverdrängerpumpen möglich:

- TwinMesh vereinfacht Simulationsprozess mit Vernetzung, Setup, Simulation, Postprocessing
- Einbindung komplexerer Modelle
  - Slip-Randbedingung für Gleitströmung
  - Erwärmung der Rotoren
- Variation von Parametern (Spaltmaße, Steigung, Drehzahl,…)
- Bestimmung von Saugvermögen und Enddruck der Vakuumpumpen

Ausblick:

- Gesamte Kühlung der Pumpe
- Einfluss von Verzug auf Spaltmaße
- Mehrstufige Pumpen

28

MESHFREE Simulations for Industrial Applications

Fabian Castelli, Isabel Michel, Jörg Kuhnert (Fraunhofer-Institute for Industrial Mathematics ITWM)

1 Introduction

Numerical simulations have become an indispensable tool for industrial research and development processes. Despite recent advances in numerical methods, software and hardware, the simulation of industrial applications is computationally challenging. Classical discretization methods, such as the finite element or finite volume method, are mesh-based and face crucial challenges for example in case of complex model geometries, large deformations, or free surfaces. Meshfree approaches overcome the expensive meshing step for classical methods.
At Fraunhofer ITWM and Fraunhofer SCAI, we develop and implement the MESHFREE software [1] providing a simulation tool for industrial applications. The discretization is based on a Generalized Finite Difference Method (GFDM). The method is purely meshfree and suited for fluid as well as continuum mechanical processes. Examples include water management of vehicles or metal cutting processes.
In this talk, we present our software MESHFREE. We emphasize its advantages over mesh-based methods. We give an insight into the mathematical modeling providing the key idea of MESHFREE and demonstrate the many possible areas of application.

2 Mathematical Modeling

The conservation equations for modeling fluid mechanics problems are the basis for many of our application problems. The typical conservation equations in Lagrangian form are the mass, momentum, and energy balance:

$$\frac{\mathrm{d}}{\mathrm{dt}}\rho + \rho \cdot \nabla \mathbf{v} = 0$$
$$\frac{\mathrm{d}}{\mathrm{dt}}(\rho \mathbf{v}) + (\rho \mathbf{v}) \cdot \nabla \mathbf{v} = \nabla \mathbf{S} - \nabla \mathrm{p} + \rho \cdot \mathbf{g}$$
$$\frac{\mathrm{d}}{\mathrm{dt}}(\rho \mathrm{E}) + (\rho \mathrm{E}) \cdot \nabla \mathbf{v} = \nabla(\mathrm{S} \cdot \mathbf{v}) - \nabla(\mathrm{p} \cdot \mathbf{v}) + (\rho \cdot \mathrm{g} \cdot \mathbf{v}) + \nabla(\mathrm{k} \cdot \nabla \mathrm{T})$$

Due to a splitting of the tensor S into a solid and a viscous part, we are able to implement various solid and fluid mechanics material models like Vogel-Fulcher-Tammann (VFT), Carreau or Johnson-Cook, Drucker-Prager.
Subject to appropriate initial and boundary conditions, we solve the set of partial differential equations with the GFDM. As basis for the discretization, MESHFREE uses a point cloud instead of a mesh. The point cloud has no directly connected points but relies on indirect neighborhood information depending on a discretization parameter called the interaction radius. A sophisticated point cloud engine manages the quality of the discretization. Visualized in Fig. 1, the point cloud engine allows adaptive refinement. This technique increases the accuracy of the simulation results and keeps the number of points low. For more details in the mathematical treatment, we refer to previous works [2-5].

Fig. 1
The adaptive refinement of the point cloud allows the resolution of vortices and keeps the number of discretization points in less turbulent regions low.

3 Industrial Applications

In the past, MESHFREE has established its position as a numerical tool for industrial applications not only in automotive, hydro power, manufacturing, and chemical engineering. In Fig. 2, we see four snapshots of a dynamic mixing and stirring process. Classical mesh-based methods encounter the difficult handling of the free surface and the moving geometry of the stirring rods. MESHFREE easily overcomes these challenges due to its mesh-free implementation. During the talk we give more examples of industrial applications.

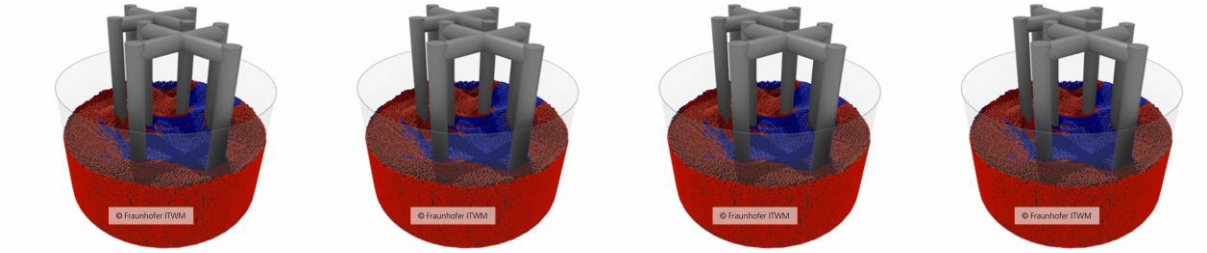

Fig. 2
Example of a dynamic mixing and stirring process from chemical engineering.

4 Conclusions

Our software MESHFREE implements the GFDM and solves real-world industrial problems efficiently. It is robust, flexible, and scales well for large problems. MESHFREE easily handles free surfaces, moving geometries, phase boundaries, or fluid-structure interaction. In particular, it avoids the costly generation and usage of a mesh completely. Successfully implemented industrial applications – for example in the automotive, hydro power, manufacturing engineering, and food industries – demonstrate the wide range of capabilities of MESHFREE. Further applications are listed on our website https://www.meshfree.eu.

5 References

[1] MESHFREE Team
MESHFREE software
Fraunhofer ITWM & SCAI, 2024, URL: https://www.meshfree.eu/.

[2] I. Michel, T. Seifarth, J. Kuhnert, P. Suchde
“A meshfree generalized finite difference method for solution mining processes”
In: Computational Particle Mechanics, 8(3), pages 561-574, 2021.

[3] P. Suchde, J. Kuhnert, S. Tiwari
“On Meshfree GFDM Solvers for the Incompressible Navier-Stokes Equations”
In: Computers & Fluids, 165, pages 1-12, 2018.

[4] P. Suchde, J. Kuhnert
“Point cloud movement for fully Lagrangian meshfree methods”
In: Journal of Computational and Applied Mathematics, 340, pages 89-100, 2018.

[5] A. Jefferies, J. Kuhnert, L. Aschenbrenner, U. Giffhorn
“Finite pointset method for the simulation of a vehicle travelling through a body of water”
In: M. Griebel, A. M. Schweitzer, editors, Meshfree Methods for Partial Differential Equations VII, pages 205-221. Cham Springer International Publishing, 2015.

Modeling High-Pressure, High-Temperature Diamond Crystal Growth

Marc Hainke, Magdalena Lang, Christian Kranert, Jochen Friedrich (Fraunhofer Institute for Integrated Systems and Device Technology IISB, Germany)

Ilya Ponomarev (Euclid Beamlabs, USA)

Boris N. Feigelson (U.S. Naval Research Laboratory, USA)

Scott S. Dossa, Jeffrey J. Derby (Department of Chemical Engineering and Materials Science, University of Minnesota, USA)

1 Introduction

Diamond exhibits a unique combination of certain physical properties like wide band gap, high thermal conductivity, low thermal expansion and low x-ray absorptivity. The properties make single crystalline diamond attractive for various high-tech applications, like detectors for high energy particles, power electronic devices, optics for high power lasers & x-rays and quantum sensors and computers. [1]

The High-Pressure, High-Temperature (HPHT) crystal growth system has the capability to grow diamonds of the highest crystalline quality by replicating the conditions of natural growth deep inside the earth. Thus, this near-equilibrium process is carried out under extreme conditions, where diamond single crystals are grown from a molten metal solvent. Since there are no available diagnostics to directly monitor crystal growth in the HPHT cell, faithful models are needed to connect experimental outcomes to system design and process conditions. A computational model was developed to describe the growth characteristics of single-crystal diamond in the HPHT process. [1, 2]

The principle of the process is schematically depicted in Fig. 1. A temperature gradient ($T_2 > T_1$) is applied to the growth cell. The carbon source dissolves into a liquid flux and diffuses to the seed at T_1. Supersaturation at the seed surface leads to diamond growth. The growth continues as long as $\omega_0(T_2) > \omega_0(T_1)$.

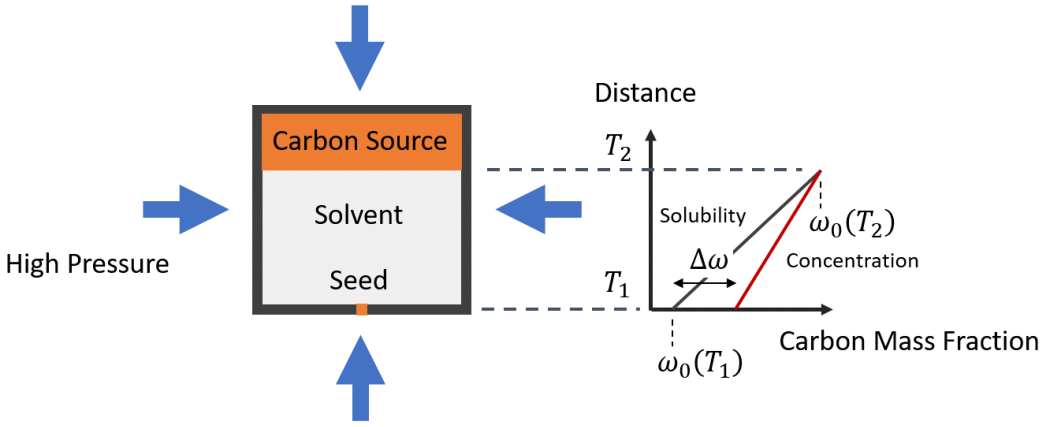

Fig. 1: Schematic illustration of the principle of crystal growth of diamonds with the HPHT process.

2 Diamond Growth Model

In the simulations a fixed geometry is assumed and process analysis is performed for a certain crystal size (height h). The model includes buoyancy-driven flow in the solvent and heat transport in all domains of the system. Carbon transport is considered by diffusion and convection. The carbon source is at equilibrium, i.e. $\omega_0(T_2)$. The solution growth model from [1] is implemented in the Ansys Fluent software

utilizing the UDF functionality. User defined extensions of the Fluent software are necessary to model the aspects of the macroscopic growth of the faceted crystal. Species transport across the growth interfaces is modelled with a nonlinear flux condition

$$\mathbf{n} \cdot \nabla\omega = \frac{1}{\rho D}\rho_c \beta_k \frac{\omega - \omega_0}{\omega_0}(1 - \omega)$$

with the kinetic coefficient β_k, the density of the crystal ρ_c and of the liquid solution ρ, the diffusion coefficient D. The macroscopic growth velocity of the crystal v_g is assumed to be proportional to the local supersaturation at the crystal surface

$$v_g = \beta_k \frac{\omega - \omega_0}{\omega_0}$$

The influence of the kinetic coefficient on the species transport through the solvent and the resulting growth rate is systematically analyzed in [1].

3 Parametrized Process Models in Ansys Workbench

A global model for the resistance heating systems was developed via the Ansys Workbench 2023. Joule heating from the applied alternating current is simulated by a quasi-steady, harmonic electric analysis and employed with a heat transfer analysis to predict the temperature field of the system. The temperature values at the growth cell are used as boundary conditions for detailed simulations of the species transport and crystal growth in the growth cell. The model setup in Ansys Workbench is shown in Fig. 2. The model is fully parametrized which allows an efficient variation and analysis of different model configurations. This includes geometry parameters like the diamond size (A), material properties (B) and process parameters of the HPHT-process (C). As an exemplary application, the numerical model enables the systematic analysis of the effects of flow, carbon transport, and temperature distributions on growth rate, which favorably compare to experimental data [3].

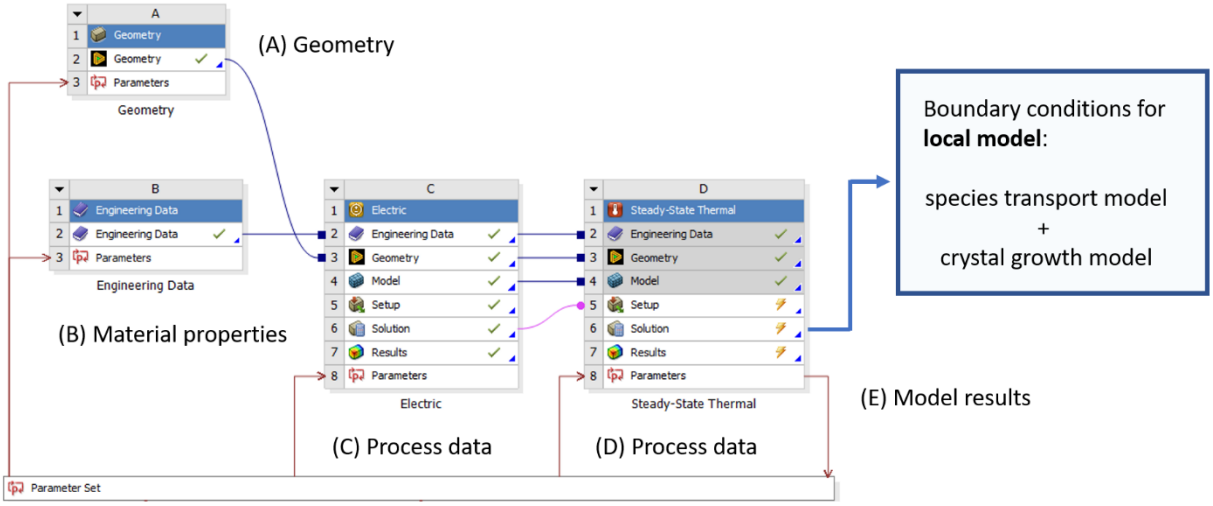

Fig. 2: Fully parametrized model of the HPHT-single process as implemented in Ansys Workbench.

4 Conclusion

Numerical simulation yields important insights on the behavior of single-crystal diamond growth in a HPHT system. The fully parameterized model in Ansys Workbench enables efficient parameter studies of the influence of process and material parameters.

5 References

[1] Dossa, Scott S.; et al.: Analysis of the High-Pressure High-Temperature (HPHT) growth of single crystal diamond, J. Cryst. Growth, 609, 2023

[2] Derby, J.; et al.: Understanding Transport and Kinetic Effects during High-Pressure, High-Temperature (HPHT) Growth of Single-Crystal Diamond, iCCGE20, Int. Conf. Cryst. Growth and Epitaxy, Napels, Italy, 2023

[3] Babich, Y.V.; et al.: Nitrogen aggregation and linear growth rate in HPHT synthetic diamonds, Diamonds and Related Materials, 13, 1802-1806, 2004

Beitrag zum Stand der Simulation der Induktiven Erwärmung

Ralf Paßmann (systemworkx AG)

1 Summary

Die Induktive Erwärmung gehört zu den direkten Erwärmungsverfahren. Das wechselnde magnetische Feld eines stromdurchflossenen Leiters erzeugt – kontaktlos - einen Wirbelstrom in dem zu erwärmenden Bauteil.
Auf der Basis einer (konventionellen) Literaturstudie sollen in diesem Beitrag die auftretenden physikalischen Bedingungen und deren Abbildung in numerischen Simulationen vorgestellt werden. Hier zeigt sich eine Konzentration auf statische bzw. nur langsam ablaufende Prozesse. An einem einfachen Beispiel wird das Vorgehen in der Simulation detailliert erläutert. In schnell ablaufenden und mehrstufigen Verfahren treten Kopplungseffekte zwischen Elektro-Magnetismus, Wärmetransport und Strukturmechanik auf. So soll abschließend ein Ausblich auf die Abbildung schnell ablaufender Prozesse unter Berücksichtigung multi-physikalischer Effekte in der Simulation gegeben werden.

2 Induktive Erwärmung

2.1 Verfahren

Die Induktive Erwärmung gehört zu den direkten Erwärmungsverfahren. Typische Anwendungen in der Metallindustrie sind die Erwärmung zur Umformung und die Wärmebehandlung zur Steigerung der Güte und Festigkeit von Produkten. Durch die aktuelle Energiepolitik ergibt sich ein weiterer Fokus auf das mit Strom betriebene Verfahren. Eine ausführliche Beschreibung verschiedener Verfahren findet sich in [10].

Ein Strom durchflossener Leiter (Induktor) erzeugt ein wechselndes magnetisches Feld, welches in Abhängigkeit der Stromstärke und der Frequenz des Wechselstromes in einem elektrischen Leiter, das Bauteil, einen elektrischen Strom (Wirbelstrom – eddy current) induziert. Dieser elektrische Strom führt zu einer Erwärmung des Bauteils.

Nach [1] erlaubt die Induktive Erwärmung eine örtlich genaue und schnelle Erwärmung von elektrisch leitfähigen Materialien. Es können nicht zuletzt fossile Brennstoffe für Prozesse der Wärmebehandlung und der Erwärmung vor Warm-Umformprozessen mehr und mehr ersetzt werden. In [2] werden die Anwendungen in die Bereiche der Industrie, des Haushaltes und der Medizin unterteilt. Insbesondere die Fortschritte in der Medizin sind erst in den letzten Jahren erzielt worden.

Nach [1] sind folgende physikalische Effekte zu berücksichtigen:

- Gesetz der elektro-magnetischen Induktion (Maxwell) zur Beschreibung der Erzeugung eines elektrischen Stromes (Foucault's current/Wirbelstromes/eddy current) in einer Probe durch ein alternierendes magnetisches Feld
- Joule Effekt zur Beschreibung der Verluste eines elektrischen (Wirbel-) Stromes und der Erwärmung der Probe
- Oberflächen-, Abstands- und Ring-Effekte zur Beschreibung nicht gleichmäßiger elektrischer Ströme und Wärmequellen
- Beschreibung des Wärme-Transportes innerhalb der Probe und des Wärme-Austauschs zwischen Körpern.

Der Induktor hat je nach Einsatzzweck verschiedene Formen, [1]. So ermöglicht eine umschließende Spirale die durchgehende Erwärmung eines Stabes, wie im Bild 1 dargestellt. Hierbei ist (a) der Induktor, (b) das zu erwärmende Bauteil und (c) das erzeugte magnetische Feld.

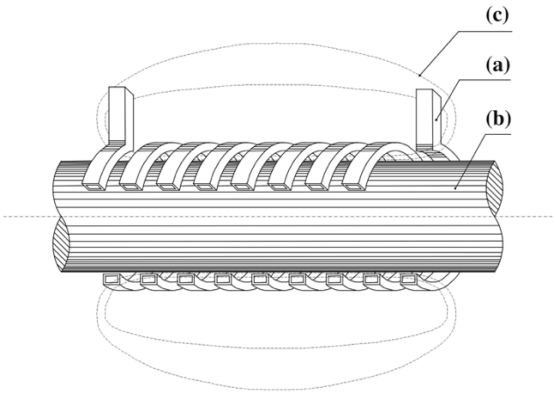

Bild 1: Magnetisches Feld nach [1]

Eine Aufstellung der wesentlichen Größen des Elektro-Magnetismus ist in Bild 2 dargestellt.

Table 1: Basic quantities in electromagnetism.

Derived quantity	**Symbol**	**SI unit**	**SI base unit**
Electric field intensity	$\mathbf{E}$	$\mathrm{V/m}$	$\mathrm{m\,kg\,s^{-3}\,A^{-1}}$
Electric flux density	$\mathbf{D}$	$\mathrm{C/m^2}$	$\mathrm{m^{-2}\,s\,A}$
Magnetic field intensity	$\mathbf{H}$	$\mathrm{A/m}$	$\mathrm{m^{-1}\,A}$
Magnetic flux density	$\mathbf{B}$	T	$\mathrm{m^2\,kg\,s^{-2}\,A^{-1}}$
Current Density	$\mathbf{J}$	$\mathrm{A/m^2}$	$\mathrm{m^{-2}\,A}$
Magnetic flux	ϕ	Wb	$\mathrm{m^2\,kg\,s^{-2}\,A^{-1}}$
Permeability	μ	$\mathrm{H/m}$	$\mathrm{m\,kg\,s^{-2}\,A^{-2}}$
Permittivity	ε	$\mathrm{F/m}$	$\mathrm{m^{-3}\,kg^{-1}s^4\,A^2}$
Volume charge density	ρ	$\mathrm{C/m^3}$	$\mathrm{m^{-3}\,s\,A}$
Conductivity	σ	$\mathrm{S/m}$	$\mathrm{m^{-1}kg^{-1}s^3A^2}$
Resistivity	ρ_c	$\Omega\mathrm{m}$	$\mathrm{m^3\,kg\,s^{-3}A^{-2}}$

Bild 2: Wesentliche Größen aus [3]

2.2 Zu beschreibende Effekte

2.2.1 Skin Depth

Die Eindringtiefe, Skin Depth, ist nach [3] abhängig von der elektrischen Leitfähigkeit des Materials, der Frequenz des elektro-magnetischen Feldes und den magnetischen Eigenschaften des Materials.
In [6] findet sich eine Formel für die Skin Depth:

$$\delta = \sqrt{\frac{1}{\pi f \sigma \mu}}$$

Mit δ gleich der Eindringtiefe, σ gleich der elektrischen Leitfähigkeit, f der Frequenz und μ gleich der magnetischen Permeabilität. Hieraus resultiert für den Anwendungsfall Stahl eine Eindringtiefe von 3 mm bei einer Frequenz von 50 Hz und 0,04 mm bei 10^5 Hz.

2.2.2 Hysterese-Effekt

In [3], siehe auch Bild 3, wird auf den Hysterese Effekt hingewiesen. Wird ein, nicht magnetisiertes, ferromagnetisches Material einem Magnetfeld ausgesetzt so hängt die magnetische Flussdichte (B) nicht linear von dem Magnetfeld (H) ab. Wird das äußere Magnetfeld reduziert, so bleibt das Material magnetisiert und wird erst bei Erreichen der Koerzitivkraft entmagnetisiert. Es bildet sich eine Hysterese. Durch das Durchlaufen der Hysterese im wechselnden Magnetfeld entsteht eine zusätzliche Erwärmung der Probe von bis zu 7%.

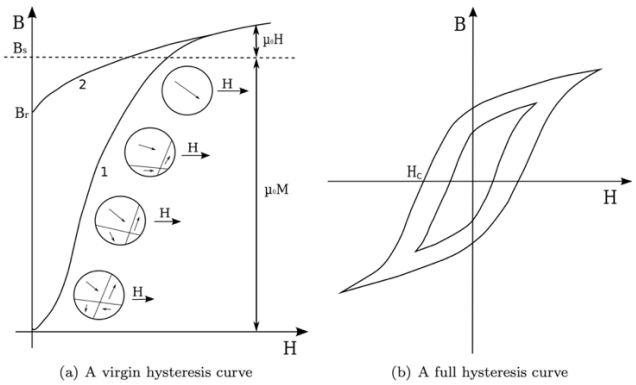

Bild 3: Hystereseffekt aus [3]

In [3] wird die Curie Temperatur als die Temperatur beschrieben, wenn ein ferromagnetisches Material paramagnetisch wird. Bei Eisen ist das z.B. bei 768 Grad. Die Curie Temperatur fällt mit einem Peak der spezifischen Wärmekapazität zusammen. Die oben beschriebene Hysterese wird zu einer Geraden. Häufig wird die Beschreibung der Hysterese nach Frölich verwendet.

2.2.3 Relaxation der Ladungsdichte

In [3] wird zudem auf die Relaxation der Ladungsdichte hingewiesen. Die sehr schnelle Relaxation führt zu dazu, daß die Ladung in einem Punkt im Innern der Probe recht schnell verschwindet und an der Oberfläche auftaucht.

2.2.4 Poynting Vektor

In [3] wird auch der Poynting Vektor erwähnt. Er beschreibt eine Beziehung für die gespeicherte Energie-Rate im elektrischen Feld und dem Energie Fluss. Der Realteil beschreibt den Teil, welcher in Wärme umgewandelt wird.

2.2.5 Frequenzbereich des Induktors

Für den Induktor wird nach [1] und [2] ein Frequenzbereich zwischen 50 Hz und 1MHz bei einer Leistung von bis zu 3 MW angegeben, von welchem ein Großteil in Wärme umgesetzt werden kann.

2.2.6 Temperaturabhängigkeit

In allen Quellen wird auf die Abhängigkeit der meisten Materialparameter von der Temperatur hingewiesen.

2.3 Simulationsbeispiele

Wie auch in [13] beschrieben finden sich in der Literatur zumeist Beispiele mit einfacher Geometrie, mit durch Symmetrien reduzierte Modellgrößen oder mit der Vernachlässigung ferromagnetischer Materialien. Es finden sich Beispiele, welche sowohl mit kommerziellen Software-Systemen als auch eigenen Codes simuliert werden. Soweit erkennbar wird, im Gegensatz zu strukturmechanischen Simulationen, immer mit einem Finite Element Netz für alle Komponenten gearbeitet. Durch die Temperaturabhängigkeit der Materialparameter findet sich auch häufig eine Kopplung der elektro-magnetischen Simulation mit der Simulation des Wärmetransportes in der Probe.

In [6] wird eine Lösung mittels FEM für den axialsymmetrischen Fall vorgestellt. Es gilt geeignete Randbedingungen an den Rändern des Modells zu verwenden, um artifizielle Reflektionen an den Rändern des Modells zu vermeiden. Der Einfluss einer sich durch die Induktoren bewegende Probe wurde durch die Bewegung des Induktors dargestellt. Hierbei wurde die Bewegung durch wechselnde Eigenschaften (von Luft zu Induktor zu Luft) der Elemente abgebildet. Die elektro-magnetische Simulation wird mit thermisch-mechanischen Simulation gekoppelt.

In [9] wird darauf hingewiesen, daß wegen der Temperaturabhängigkeit der wesentlichen Materialparameter eine gekoppelte Analyse von Elektro-Magnetismus und Wärmetransport notwendig ist. In dieser Arbeit wird vorausgesetzt, daß das Magnetfeld in einer Sinus-Funktion von der Zeit abhängt, das Problem zweidimensional ist und die magnetische Permeabilität nicht von dem magnetischen Feld abhängt. Es wird auch vorausgesetzt, daß der Einfluss der elektro-magnetischen Strahlung vernachlässigt werden kann (quasi-statische Approximation). Es wird wie auch in anderen Beiträgen darauf hingewiesen, daß der Zeitschritt der elektro-magnetischen Simulation deutlich kleiner ist als der der Berechnung des Wärmetransportes.

In [11] wird für ein Verfahren zur direkten Erzeugung von endlosen Blechen, auf Coils gewickelt, zur Zwischenerwärmung vor weiteren Walzschritten beschrieben. Es wird insbesondere auf der höheren elektrischen Flussdichte an den Kanten und Maßnahmen zur Beeinflussung durch magnetische Isolatoren eingegangen.

3 Beispiel mit Abaqus/Standard

In Abaqus/CAE wurde ein einfaches, 3-dimensionales, Modell aufgebaut. Symmetrien wurden nicht verwendet, um ein Gefühl für notwendige Rechenzeiten zu gewinnen und um weitere Verwendungen zu ermöglichen. Ein zylindrischer Stab, siehe Bild 4, wird von einem Induktor erwärmt.

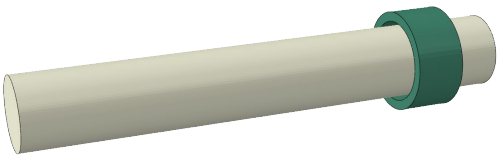

Bild 4: Modell zur Berechnung der Induktiven Erwärmung

Hierbei wurde der Induktor sowohl als Spirale als auch als Hohlzylinder, wie im Bild 4, modelliert. Die umschließende Luft wird ebenso vernetzt. Im Schnitt kann man das durchgängige Netz gut erkennen, Bild 5.

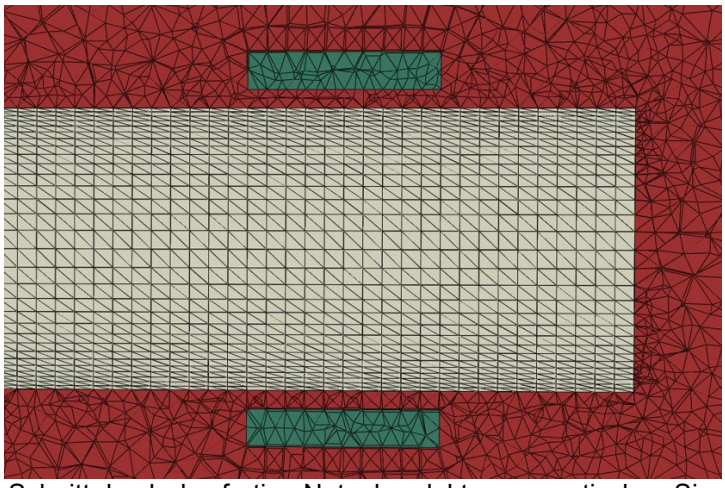

Bild 5: Schnitt durch das fertige Netz der elektro-magnetischen Simulation

Die Materialdaten, verwendet wird das SI-System, wurden der Literatur und den Abaqus Benchmarks entnommen. Eine Abhängigkeit der Materialparameter von der Temperatur wurde hier noch nicht verwendet. Der Aufbau des Modells der elektro-magnetischen Simulation enthält als Last den Strom im Induktor sowie Randbedingungen auf den Außenflächen des Modells (der Luft). Das Modell für die Simulation der Wärmetransportes enthält nur den zylindrischen Stab. In diesem Beispiel wird nur die Wärmeleitung im Stab berücksichtigt. In beiden Modellen hat der Stab eine Anfangsbedingung für die Temperatur.

Die Kopplung erfolgt über die in Abaqus enthaltene Co-Simulation. Der Benutzer muss nur vorgeben, für welche Bauteile welche Variablen übergeben werden sollen. In diesem Fall wird für den Stab die Temperatur und der Wärmestrom aufgrund des Joule Effektes übergeben.

Der zylindrische Stab wird im Bereich des Induktors erwärmt.

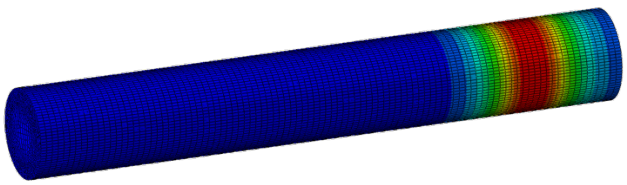

Bild 6: Erwärmung des Stabes in der gekoppelten Simulation

4 Conclusions

Die physikalischen Grundlagen der induktiven Erwärmung sind weitestgehend untersucht und beschrieben. In der Literatur finden sich viele Beispiele zur Simulation der Induktiven Erwärmung. Meist beschränken die Simulationen sich aber auf einfache Geometrien und statische oder langsam ablaufende Prozesse. Hier scheint auch der Modellaufbau ein Hindernis darzustellen.

Das dargestellte Beispiel ist als Ausgangspunkt weiterer Untersuchungen zu verstehen. Ziel ist es, mittelfristig schnell ablaufende Prozesse numerische beschreiben zu können.

5 References

[1] Lupi, S., 2017, "Induction Heating," *Fundamentals of Electroheat*, Springer International Publishing, Cham, pp. 353–524.

[2] Lucia, O., Maussion, P., Dede, E. J., and Burdio, J. M., 2014, "Induction Heating Technology and Its Applications: Past Developments, Current Technology, and Future Challenges," IEEE Trans. Ind. Electron., **61**(5), pp. 2509–2520.

[3] Fisk, M., 2008, "Simulation of Induction Heating in Manufacturing," Luleå University of Technology.

[4] 2023, "Wikipedia:Hauptseite," Die freie Enzyklopädie.

[5] "Dassault Systèmes User Assistance" [Online]. Available: https://help.3ds.com/HelpProductsDS.aspx. [Accessed: 06-Jun-2023].

[6] Bay, F., Labbe, V., Favennec, Y., and Chenot, J. L., 2003, "A Numerical Model for Induction Heating Processes Coupling Electromagnetism and Thermomechanics," Int. J. Numer. Meth. Engng., **58**(6), pp. 839–867.

[7] Rudnev, Valery, 2011, "Computer Modeling of Induction Heating: Things to Be Aware of, Things to Avoid."

[8] Rudnev, V., 2013, "Unique Computer Modeling Approaches for Simulation of Induction Heating and Heat-Treating Processes," J. of Materi Eng and Perform, **22**(7), pp. 1899–1906.

[9] Ter Maten, E. J. W., and Melissen, J. B. M., 1992, "Simulation of Inductive Heating," IEEE Trans. Magn., **28**(2), pp. 1287–1290.

[10] Nacke, B., and Baake, E., eds., 2014, *Induktives Erwärmen: Wärmen, Härten, Glühen, Löten, Schweißen*, Vulkan Verlag, Essen.

[11] Peng, W., Chen, X., Zhang, L., Li, X., Sun, J., and Zhang, D., 2021, "Finite Element Analysis of Temperature Uniformity in Transverse Induction Heating Process in ESP Rolling," Int J Adv Manuf Technol, **115**(11–12), pp. 3423–3439.

[12] Areitioaurtena, M., Segurajauregi, U., Fisk, M., Cabello, M. J., and Ukar, E., 2022, "Numerical and Experimental Investigation on the Residual Stresses Generated by Scanning Induction Hardening," Procedia CIRP, **108**, pp. 827–832.

[13] Areitioaurtena, M., Segurajauregi, U., Akujärvi, V., Fisk, M., Urresti, I., and Ukar, E., 2021, "A Semi-Analytical Coupled Simulation Approach for Induction Heating," Adv. Model. and Simul. in Eng. Sci., **8**(1), p. 14.

[14] Plumed, E., Lope, I., and Acero, J., 2022, "Modeling and Design of Cookware for Induction Heating Technology With Balanced Electromagnetic and Thermal Characteristics," IEEE Access, **10**, pp. 83793–83801.

[15] Samran, S., Thanaset, T., and Chanchai, T., 2013, "Thermal Analysis of Inductive Coils Array against Cylindrical Material Steel for Induction Heating Applications," AMM, **330**, pp. 754–759.

Modellierung des Laserschneidens von Glasröhren für pharmazeutische Anwendungen

Magdalena Lang, Marc Hainke (Ostbayerische Technische Hochschule Amberg-Weiden)

Doris Ruider, Steffen Fröhle, Bernhard Schmitt (Medical Systems, Gerresheimer Regensburg)

1 Einleitung

Glaskörper für Glasspritzen oder Glasampullen für pharmazeutische Anwendungen unterliegen sehr engen Fertigungstoleranzen, was hohe Anforderungen an den Produktionsprozess stellt (siehe Fig. 1). Die Bestimmung der optimalen Prozessparameter kann durch Simulationsmodelle unterstützt werden, die Umsetzung der Modelle erfolgt in der Ansys Workbench 2024 R1. In dieser Arbeit wird der Schneidvorgang zum Abtrennen der Glasröhren auf eine bestimmte Länge betrachtet. Axialsymmetrische Modelle benötigen die kürzeste Rechenzeit und sind demnach für Parameterstudien besonders geeignet. Das entwickelte Modell ist vollständig parametriert, um effizient Parameteranalysen und Sensitivitätsanalysen durchführen zu können.

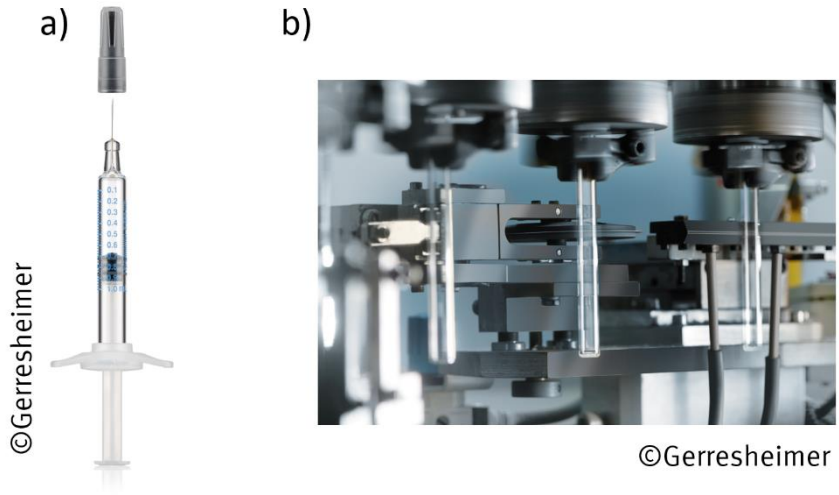

Fig. 1: a) Spritze und b) der Fertigungsprozess zur Trennung der Glasröhren.

Der Schneidvorgang von Gläsern wird in der Literatur sowohl durch experimentelle Arbeiten als auch in theoretischen Analysen betrachtet. So wurde z.B. in einer frühen Arbeit ein analytisches Modell zu den thermischen Verhältnissen beim Schneidvorgang unter Berücksichtigung der Dickenabnahme beim Trennvorgang vorgestellt [1]. Ein in Ansys implementiertes Simulationsmodell wird ausführlich in [2] diskutiert. Ein Überblick zu der Modellierung und Simulationsansätzen kann in [3, 4] gefunden werden. Der Einfluss der Laserparameter auf die Qualität der Trennfläche wird experimentell in [5] untersucht. Die Möglichkeiten von Neuronalen Netzen zur Vorhersage der thermomechanischen Spannungen wurden bereits in [6] betrachtet.

2 Mathematische Modellierung

Das Simulationsmodell zur numerischen Berechnung der thermomechanischen Spannungen beim Trennvorgang ist in der Ansys Workbench 2024 R1 umgesetzt. In Zylinderkoordinaten kann die Wärmeübertragung im Glas mit der Beziehung [7]

$$\frac{\partial}{\partial t}\left(\rho c_{\mathrm{p}} T\right) = \frac{1}{r}\frac{\partial}{\partial r}\left(r\lambda\frac{\partial T}{\partial r}\right) + \frac{\partial}{\partial z}\left(\lambda\frac{\partial T}{\partial z}\right) + q_{\mathrm{T}}$$

beschrieben werden, mit der Dichte ρ, der spezifischen Wärmekapazität c_{p}, der Temperatur T und der Wärmeleitfähigkeit λ des Glases. Der axiale Verlauf der Energiedichte im Laser q_{T} wird entsprechend einer Gaußverteilung angenommen [2, 4]

$$f(z) = \frac{1}{\kappa\sqrt{2\pi}} \cdot e^{-\frac{1}{2}\left(\frac{z}{\kappa}\right)^2}$$

Der Wärmeeintrag wird in den Studien als Oberflächenquelle angenommen. Die Eindringtiefe δ der Laserleistung auch in das Volumen des Materials wird in der Literatur beispielsweise durch einen Ansatz der Form [nach 2]

$$\delta(r) = \beta e^{-\beta(R-r)}(1 - a_r)$$

beschrieben, mit dem Absorptionskoeffizienten β und dem Reflexionskoeffizienten a_r. In diesem Fall muss die Laserleistung als Volumenquelle in der Simulation berücksichtigt werden, was eine entsprechende Auflösung mit dem Gitter erfordert. Die thermomechanischen Spannungen σ ergeben sich aus der Lösung in der Cauchy-Gleichungen in Ansys Mechanical. Die einfache Abschätzung [2]

$$\sigma \approx \frac{1}{2}\alpha E \Delta T$$

mit dem thermischen Ausdehnungskoeffizienten α und dem Elastizitätsmodul E zeigt, dass die Spannungen mit zunehmender lokaler Temperaturdifferenz ΔT im Trennbereich ansteigen. Eine Abschätzung zur kritischen Spannung im Material ist gegeben mit [8]

$$\sigma_{\text{crit}} = 10^{-3} E$$

Der schematische Modellaufbau ist in der folgenden Abbildung Fig. 2 dargestellt. Im Brennfleck des Lasers wird die Wärmemenge $P(t)$ eingetragen, wobei aufgrund der angenommenen Symmetrie die Leistung über den Umfang gemittelt wird. An den restlichen Flächen der Glasröhre wird Energie durch Wärmestrahlung $q_{\text{rad}} = h_{\text{rad}} \cdot (T - T_0)$ an die Umgebung abgegeben. Die Temperaturverteilung in der Glasröhre ist Eingangsgröße für die Berechnung der thermomechanischen Spannungen. Zur Bewertung der Prozessparameter werden in den Simulationen die Temperaturen und Spannungen entlang der gekennzeichneten Linie für die gesamte Prozesszeit ausgewertet.

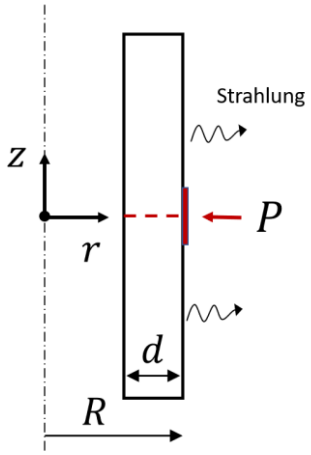

Fig. 2: Axialsymmetrisches Modell der Glasröhre für die Berechnung der Erwärmung beim Trennvorgang.

3 Parametrierte Modelle in der Ansys Workbench

Die Modelle zur Berechnung der thermomechanischen Spannung beim Schneidprozess sind in der Ansys Workbench 2024 R1 umgesetzt. Die Randbedingungen zur Modellierung der Laserleistung entsprechend einer Gaußverteilung wurden mit Hilfe eines APDL-Codes implementiert. Die Rechenzeit für einen Schneidprozess beträgt wenige Minuten, so dass mit dem Modell umfangreiche Parameter-variationen durchgeführt werden können. Das Modell ist vollständig parametriert um effizient Parameteranalysen und Sensitivitätsanalysen durchführen zu können (Fig. 3):

- A: Materialparameter
- B: Geometrieparameter (verschiedene Glasröhrendurchmesser)
- C: thermische Randbedingungen (Laserparameter, Wärmestrahlung)
- D: Mechanische Analyse
- E: Parametervorgabe mit dem Design Explorer

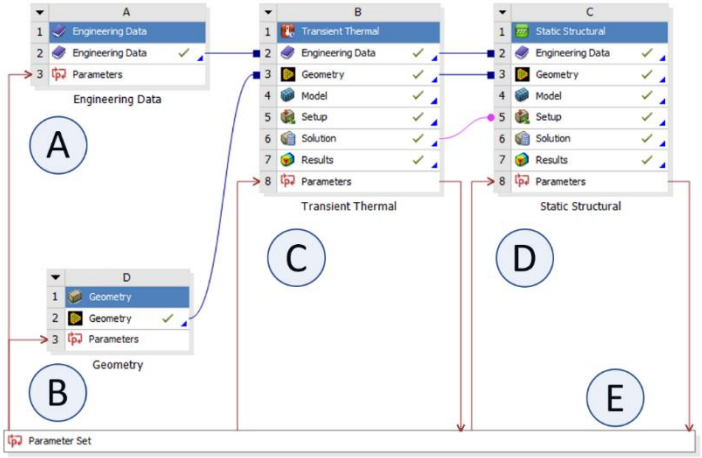

Fig. 3: Umsetzung des Berechnungsmodells in der Ansys Workbench.

Zwei exemplarische Parametervariationen werden im Folgenden dargestellt. Zur Überprüfung der numerischen Vorhersagen werden die Ergebnisse mit einfachen analytischen Abschätzungen verglichen. Die mittlere Erwärmung der Glasröhre im Bereich des Lasers kann beispielsweise abgeschätzt werden mit [7]

$$\Delta T = \frac{P}{A}\frac{1}{\sqrt{\lambda c_\mathrm{p} \rho}}\frac{2}{\pi}\sqrt{t}$$

mit der Leistung P, der Umfangsfläche $A = 2\pi R$, dem Radius der Glasröhre R und der Dauer des Energieeintrags mit dem Laser t. Bei höheren Laserleistungen kommt es aufgrund der Erwärmung der Glasröhre zu Abweichungen von der analytischen Abschätzung.

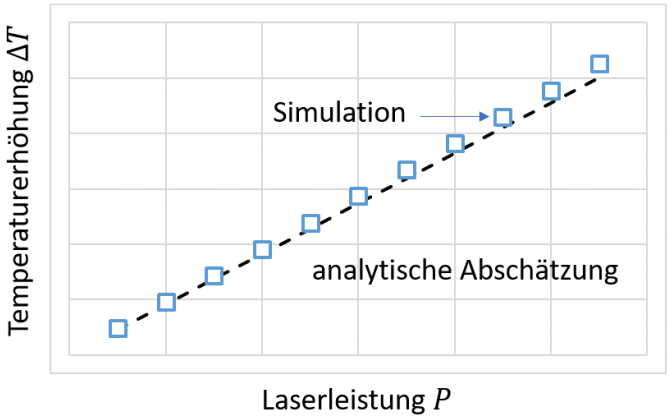

Fig. 4: Mittlere Erwärmung der Glasröhre entsprechend einer analytischen Abschätzung (Linie) und numerisch ermittelte Werte (Symbole).

Mit zunehmender Laserleistung nehmen die Temperaturdifferenzen im Material zu und die mechanischen Spannungen steigen an (Fig. 5).

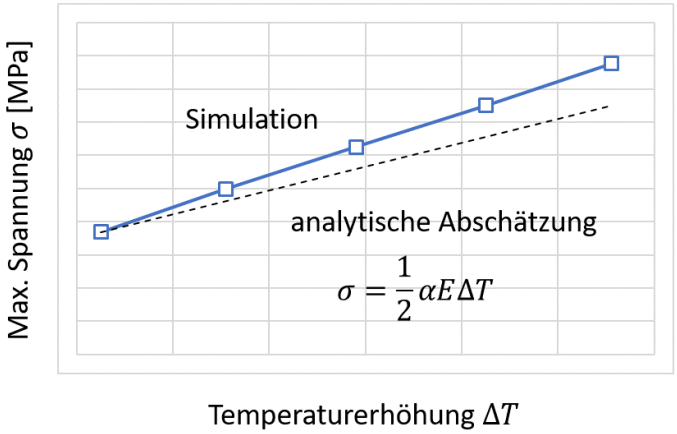

Fig. 5: Exemplarische Studie zur Abhängigkeit der kritischen Spannungen von der Temperaturerhöhung der Glasröhre aufgrund unterschiedlicher Laserleistungen.

4 Fazit

In der Ansys Workbench wurde ein axialsymmetrisches Modell zur Berechnung der thermo-mechanischen Spannungen bei Laserschneiden implementiert. Das Modell ist hinsichtlich vieler Eingangsgrößen parametriert, was die effiziente Durchführung von Parameterstudien ermöglicht. Die aktuelle Umsetzung soll aufgrund der Vielzahl der Designparameter zukünftig an das Tool optiSLang angebunden werden.

5 Literatur

[1] Atanasov, P.A.; Gendjov, S.I.: Laser cutting of glass tubing – a theoretical model, J. Phys. D: Appl. Phys., 20, 597-601, 1986
[2] Loch, H.; Krause, D.: Mathematical simulation in glass technology, Springer, 2002
[3] Kagiri, C.M.; Ikua, B.W.; Keraita, J.N.; Gituku, E.W.: Overview of the modeling and simulation of laser machining of glass, Mech. Eng. Conf. Sustainable Research and Innovation, 151-154, 2012
[4] Parandoush, P.; Hossain, A.: A review of modeling and simulation of laser beam machining, Int. J. Machine Tools and Manufacture, 85, 135-145, 2014
[5] Rave, H.; Heiming, H.; Szumny, P.; Kaiser, M.; Kleiner, J.; Flamm, D.: Glass tube cutting with aberration-corrected non-diffracting ultrashort laser pulses, Soc. Photo-Optical Instr. Eng. (SPIE), 2021
[6] Kadri, M.B.; Nisar, S.; Khan, S.Z.; Khan, W.A.: Comparison of ANN and finite element model for the prediction of thermal stresses in diode laser cutting of float glass, Optik, 126, 1959-1964, 2015
[7] Baehr, H.D.; Stephan, K.: Wärme- und Stoffübertragung, Springer, 1998
[8] Coelho, J.M.P.; Alves, D.C.; Abreu, M.A.: Laser cutting of glass tubes, Mat. Sci. Forum, Vols. 514-516, 729-733, 2006

Robust Quality Measures for the Assessment of Machine Learning Models

Thomas Most, Lars Gräning (Ansys Germany GmbH)

Sebastian Wolff (Ansys Austria GmbH)

1 Introduction

The application of mathematical surrogate models in computer aided design and safety assessment has become a general standard procedure nowadays. Since the assessment of the prediction quality of these mathematical models is quite important for a successful integration into the virtual product development workflow, reliable measures to estimate the prediction quality are required. One common measure is the Coefficient of Prognosis (CoP) [1] which quantifies the explained variation of the surrogate model of a specific response. With help of this measure, different model types can be assessed and the most suitable can be selected for a specific application. In this paper we discuss the robustness of the CoP as well as the quality of the statistical estimator by means of an analytical and an application example.

2 Measures for goodness of fit

Let us assume a simulation model with a certain number of scalar outputs. Each of these outputs can be represented as an arbitrary function of a given number of inputs

$$y(\mathbf{x}) = f(x_1, x_2, \ldots, x_m). \tag{1}$$

If these output functions are approximated by a mathematical surrogate model, such as polynomial regression [2], Kriging [3], Moving Least Squares [4] or artificial neural networks [5], we obtain an approximation of the true function

$$\hat{y}(\mathbf{x}) = \hat{f}(x_1, x_2, \ldots, x_m). \tag{2}$$

If the approximation model is build or trained based on a given number of support points *n*, we can calculate the residuals for each of the support points and estimate different error measures to quantify the goodness of fit

$$\epsilon_i = y(\mathbf{x}_i) - \hat{y}(\mathbf{x}_i) = y_i - \hat{y}_i. \tag{3}$$

One well known measure is the root mean squared error (RMSE)

$$RMSE = \sqrt{\frac{1}{n}\sum_{i=1}^{n}(y_i - \hat{y}_i)^2}, \tag{4}$$

which has the same unit as the output itself and can be interpreted as the standard deviation of the approximation error. Another well-known measure is the unitless Coefficient of Determination (CoD)

$$CoD = 1 - \frac{SS_E}{SS_T}, \quad 0 \leq CoD \leq 1, \tag{5}$$

which measures the ratio of the explained vs. the original variation of the investigated response, where SS_T is equivalent to the total variation of the response and SS_E quantifies the unexplained variation

$$SS_T = \sum_{i=1}^{n}(y_i - \mu_Y)^2, \quad \mu_Y = \frac{1}{n}\sum_{i=1}^{n} y_i, \quad SS_E = \sum_{i=1}^{n}(y_i - \hat{y}_i)^2. \tag{6}$$

Both are measures for the goodness of fit, which quantify the deviation between the support point values used for the training and the approximation values at these points. Unfortunately, this will not give us any information of the prediction quality of the surrogate model for unknown data points. In figure 1 an interpolation function of the distorted data of a quadratic function is shown. The CoD would indicate a perfect match between the data and the interpolation model, although the original function was not represented well.

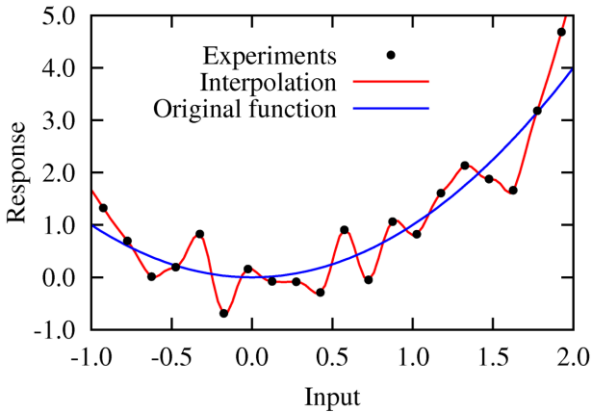

Fig. 1: Interpolation of distorted data points of a smooth function with an interpolation model with perfect goodness of fit

3 Measures for the prognosis quality

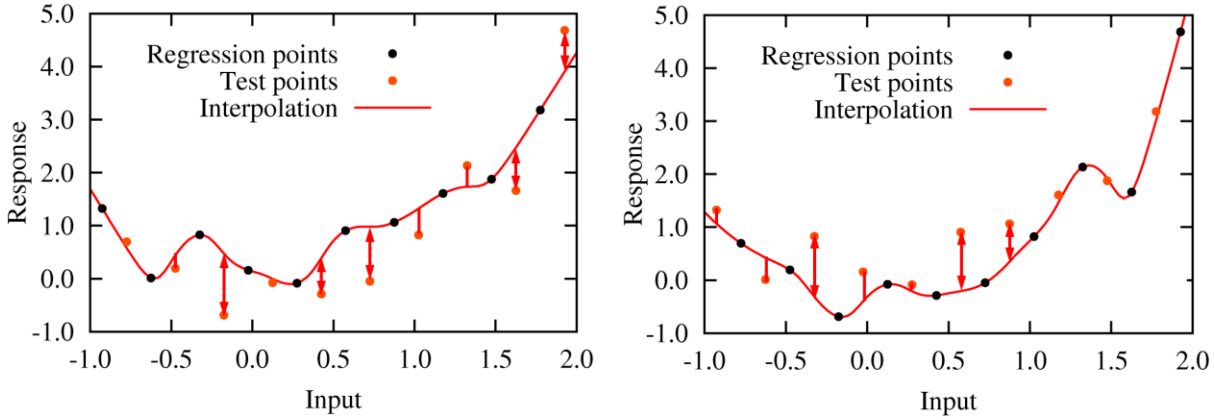

Fig. 2: Basic idea of the cross validation procedure for splitting the data set in two subsets: Using set one for training and set two for prediction (left) and set two for training and set one for prediction (right)

In order to estimate the prediction error of a mathematical surrogate model, we can split the data set e.g. in two data sets of same size and use set number one for the training and set number two for the testing the approximation by means of unused data. In a second step this procedure is applied by using data set two for the training and data set one for the estimation. This procedure as shown in figure 2 is called cross validation and is explained in more detail in [6]. We can subdivide the original data set in *q* subsets of almost equal size, where the points in each subset should be selected in that way that they cover the investigated space of the input variables almost uniformly. Each of the *n* support points is mapped to one subset

$$\zeta : \{1, \ldots, n\} \rightarrow \{1, \ldots, q\}. \tag{7}$$

Once, the *q* individual cross validation models have been trained, we use their approximation values to evaluate the prediction residuals for each of the available data points

$$\hat{y}^{cv}(\mathbf{x}_i) = \hat{f}_{\sim\zeta(i)}(\mathbf{x}_i), \tag{8}$$

Where $\hat{f}_{\sim\zeta(i)}(\cdot)$ is the approximation model built by using all cross-validation subsets except the one set belonging to the support point *i*. The corresponding residuals of the cross-validation prediction errors can be estimated as

$$\epsilon_i^{cv} = y(\mathbf{x}_i) - \hat{y}^{cv}(\mathbf{x}_i) = y_i - \hat{y}_i^{cv}. \tag{9}$$

The residuals of the goodness of fit in equation 3 and of the cross-validation residuals can be displayed in a so-called residual plot as shown in figure 3. If a large deviation of the residuals from the fit and the prediction can be observed, we can assume that the applied surrogate model tends to over-fitting.

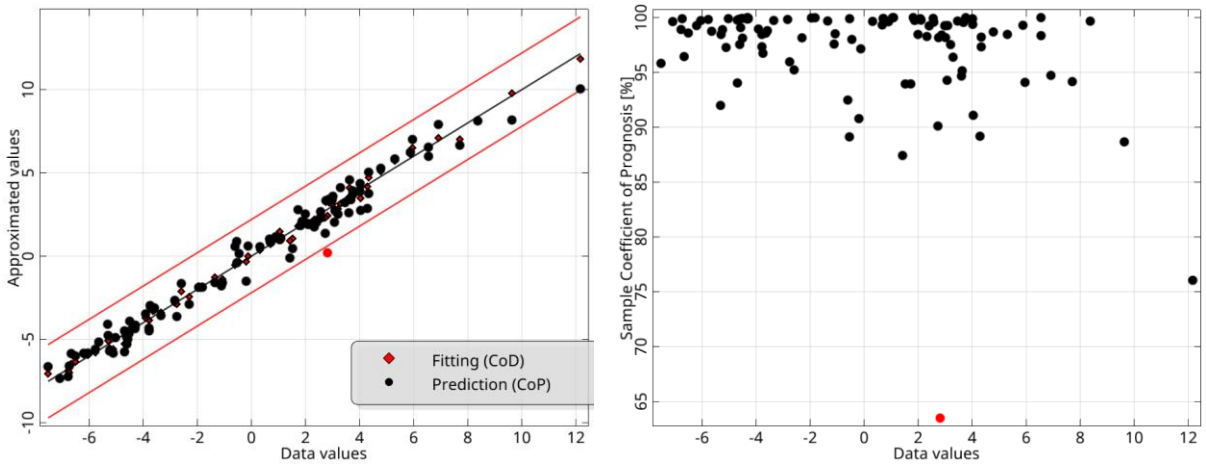

Fig. 3: Residual plot with the fitting and prediction residuals (left) and sample CoP, which quantifies the contribution of each sample to the CoP (right). One possible outlier is indicated in red.

Based on the prediction residuals we can estimate the root mean squared error

$$RMSE^{cv} = \sqrt{\frac{1}{n}\sum_{i=1}^{n}(y_i - \hat{y}_i^{cv})^2}, \tag{10}$$

and the Coefficient of Prognosis [1]

$$CoP = 1 - \frac{SS_E^{cv}}{SS_T}, \quad SS_E^{cv} = \sum_{i=1}^{n}(y_i - \hat{y}_i^{cv})^2. \tag{11}$$

The estimated RMSE in equation 10 can be used to identify possible outliers. Since the RMSE can be understood as the standard deviation of the approximation error, we can assume a boundary of about $\pm 3 \times RMSE^{cv}$ to check for possible outliers. In the residual plot in figure 3, this is indicated as the two red lines.

Usually, 5-10 subsets are used within the cross-validation procedure to obtain stable estimators [6]. This procedure is usually called *k*-fold cross validation. Since some mathematical surrogate models provide closed form solutions for a *n*-fold cross validation, where each set belongs just to a single sample, this so-called leave-one-out (LOO) cross-validation is very attractive from the computational point of view. However, in our examples we will show that the LOO cross-validation may be too optimistic as an error estimator and the *k*-fold cross validation gives more reliable results.

In order to get an estimate, how the residuals of an individual support point $\boldsymbol{x}_i$ contribute to the CoP, we can further formulate the sample CoP as follows

$$CoP_{\mathbf{x}_i} = 1 - \frac{(y_i - \hat{y}_i^{cv})^2}{SS_T}, \tag{12}$$

which is shown additionally in figure 3. The figure clearly indicates that the sample CoP may help to detect outliers more clearly by using a different scaling. The mean value of all individual sample CoPs is consequently the global CoP value introduced in equation 11.

4 Analytical benchmark function

In a first example, we investigate an analytical benchmark function with 20 inputs

$$\begin{aligned} y(\mathbf{x}) =& 0.5 \cdot x_1 + x_2 + 0.5 \cdot x_1 x_2 + 5.0 \cdot \sin(x_3) + 0.5 \cdot x_4 + 0.5 \cdot x_4^2 + 0.1 \cdot x_5 \\ &+ \sum_{i=6}^{20} 0.01 \cdot x_i + 0.5 \cdot \mathcal{N}(0,1), \quad -\pi \leq x_i \leq \pi. \end{aligned}$$

where *N(0,1)* is a standard normal noise term. This benchmark function consists of additive linear and non-linear terms and one coupling term. Furthermore, the inputs x_5 to x_{20} have minor importance.

We investigate this example by generating 100 support points by Latin-Hypercube Sampling (LHS) within the given input bounds. An isotropic Kriging approximation model according to [6] is trained by using these support points and a k-fold and LOO cross-validation is performed to estimate the prediction errors. Unimportant inputs are removed automatically from the approximation model using the Metamodel of Optimal Prognosis approach [1]. 500 additional test samples are generated by an independent LHS and are evaluated with the benchmark function. These samples are used to compare the estimated prediction errors from the cross-validation procedure with the errors in unknown data. For this purpose, the prediction sum of squares SS_E is evaluated for the cross-validation residuals and for the additional test data according to equation 11.
In order to quantify the statistical scatter of the prediction error estimates, we generate 50 independent data sets for the support points and perform the model training and error estimation and compare these estimates with the prediction error of a fixed test data set. Since the SS_T itself varies for each support point set, we compare not directly the estimated CoP from the cross-validation with the CoD of the test data. Instead, we scale the SS_E from the cross-validation with the SS_T of the test data as follows

$$\Delta SS_E^{cv} = \frac{\frac{1}{n} SS_E^{cv} - \frac{1}{n_T} SS_E^{test}}{\frac{1}{n_T} SS_T^{test}},$$

where the normalization with the number of supports n and the number of test data points n_T is necessary due to the different number of samples in both sets. In figure 6 the obtained ΔSS_E is shown for the 50 investigated runs by using either LOO or k-fold-cross-validation as error estimator. The figure indicates that in case of LOO the number of runs, where the SS_E is over-estimated is similar as the number of cases where the SS_E is under-estimated. If the k-fold-cross-validation is used, the estimated SS_E is mostly larger as in the test data, which means that the CoP estimate is in the most cases conservative and does not over-estimate the prediction quality of the investigated surrogate model.

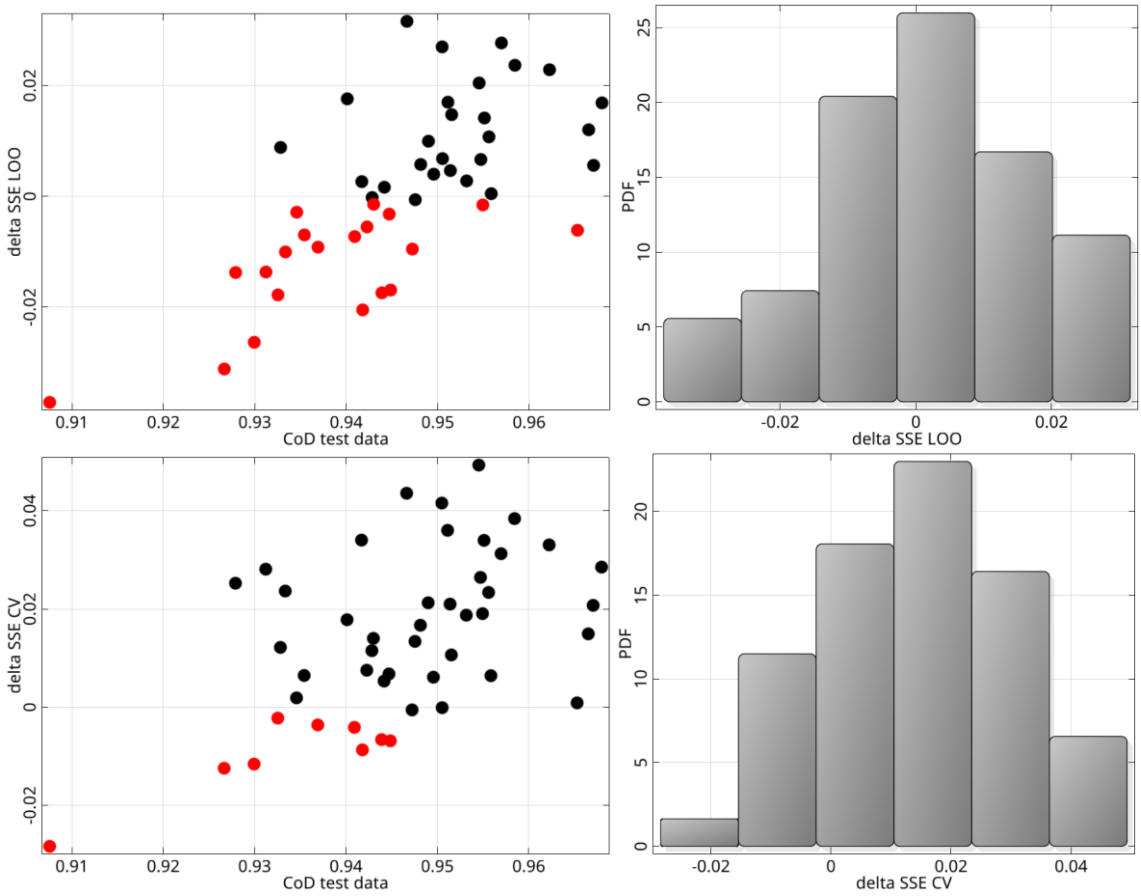

Fig. 4: Statistical evaluation of the prediction errors of the analytical test function by using 100 support points and 500 test points with LOO-cross-validation (top) and k-fold-cross-validation (bottom)

5 Application example

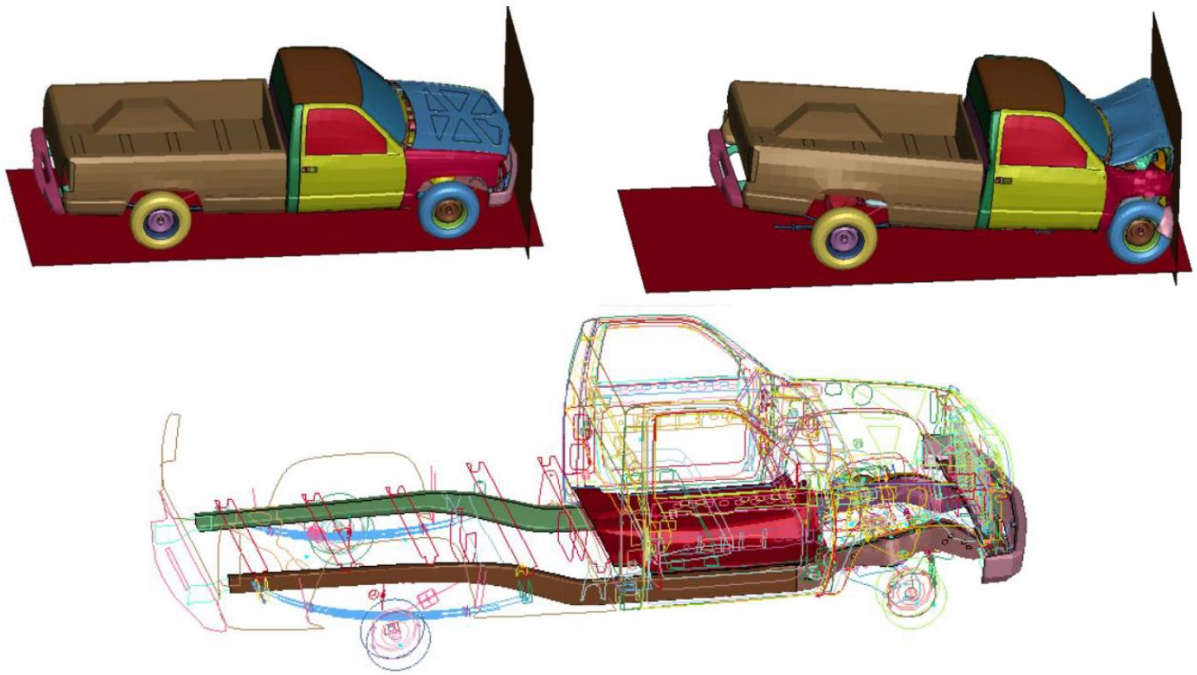

Fig. 5: Investigated front crash example according to [7] considering 22 varying inputs in a LS-Dyna simulation model

In the second example we investigate the presented error measures for a highly non-linear application, where the intrusions and pulses of a truck impact example are analyzed with the LS-Dyna finite element solver. The pulses are acceleration related quantities computed over two-time-intervals of the crash event. 22 input variables have been considered in the analysis which belong to the metal sheet thicknesses and the material properties of specific parts of the car body. Further details on this example can be found in [7].
For this example, different data sets of 100, 200 and 400 Latin Hypercube samples have been used for the model training and a single test data set of 1200 samples for the validation of the estimated prediction errors. In figure 6 the estimated CoPs are shown for the approximated scalar outputs by using 100 and 400 support points. Additionally, the residual plots are shown for one selected response, which indicate, that the fitting and the prediction residuals from k-fold-cross-validation agree very well. Figure 6 indicates that the most important inputs can be identified already with 100 support points.
In table 1 the CoP estimates are compared to the calculated CoD of the test data. The table indicates a very good agreement for the almost all investigated responses. For the HIC value, a suitable approximation seems not possible. In the other cases, the CoP seems to be a very robust measure to quantify the prediction quality of a surrogate model independent of the model type.

	100 samples			200 samples			400 samples		
	Model	CoP	CoD Test	Model	CoP	CoD Test	Model	CoP	CoD Test
N1_disp	Polynomial	74,8%	76,0%	Kriging	81,1%	80,4%	Kriging	82,8%	82,5%
N2_disp	Kriging	81,4%	78,1%	Kriging	83,2%	83,9%	Kriging	85,1%	85,2%
Stage1_pulse	Kriging	99,1%	98,9%	Kriging	99,2%	99,4%	Polynomial	99,1%	99,1%
Stage2_pulse	Polynomial	94,6%	90,8%	Kriging	95,9%	93,2%	Kriging	96,4%	95,3%
HIC	MLS	7,1%	0,0%	Kriging	43,5%	0,0%	Kriging	0,8%	0,0%
total_mass	Polynomial	100,0%	100,0%	Polynomial	100,0%	100,0%	Polynomial	100,0%	100,0%

Table 1: Estimated prediction quality of the surrogate models of specific simulation outputs for the front crash example for different support sample sizes and calculated errors for the verification test data

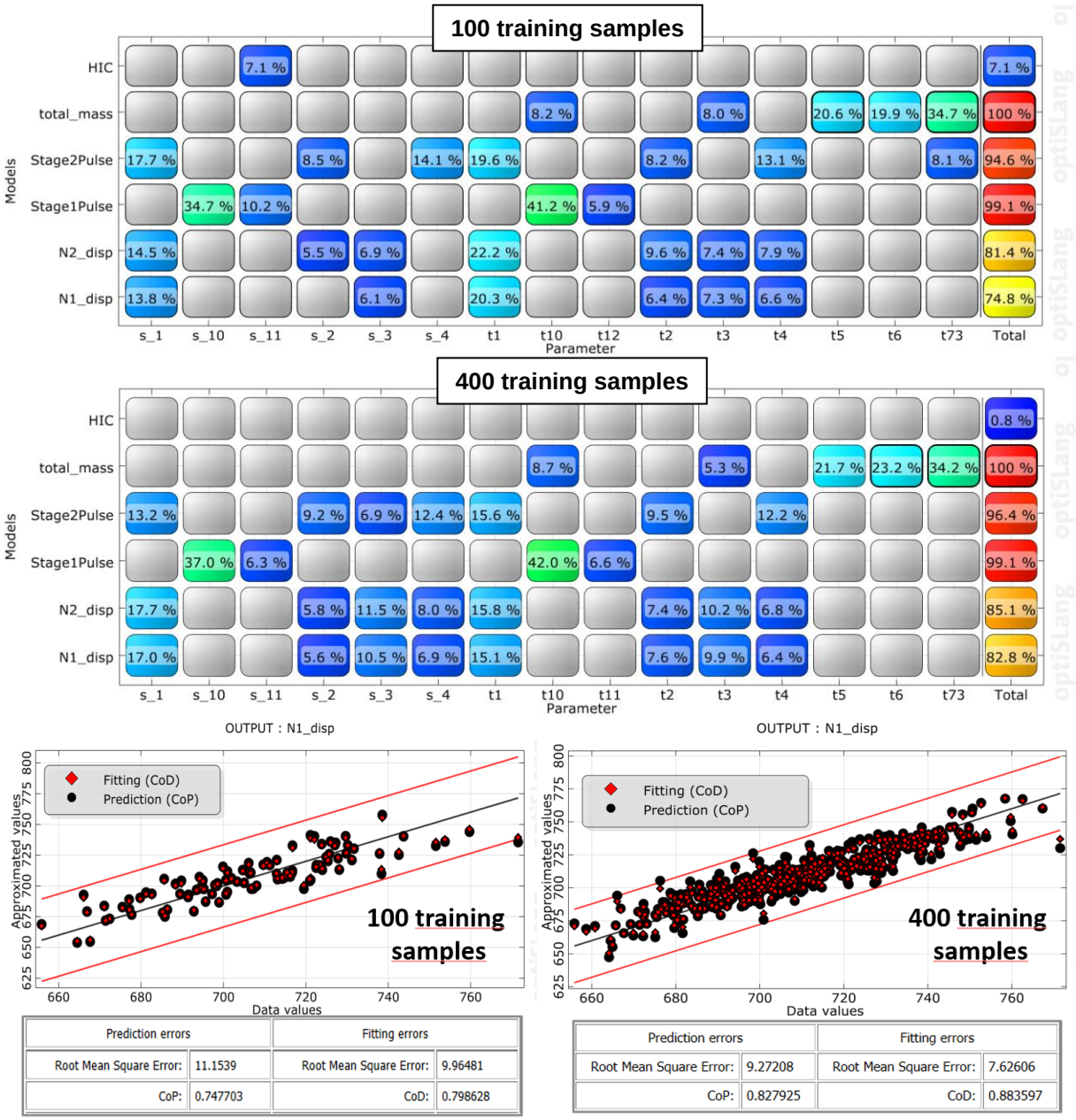

Fig. 6: Estimated CoPs and input sensitivities for the simulation model responses of the truck front crash example by using 100 support points (top) and 400 support points (middle) and the residual plot with the fitting and prediction residuals for one selected simulation response output (bottom)

6 References

[1] Most, T., and Will, J., 2011, “Sensitivity analysis using the Metamodel of Optimal Prognosis,” In Weimarer Optimierungs- und Stochastiktage 8.0, Weimar, Germany.

[2] Montgomery, D. C., and Runger, G. C., 2003, Applied Statistics and Probability for Engineers, third ed. John Wiley & Sons.

[3] Krige, D., 1951, “A statistical approach to some basic mine valuation problems on the Witwatersrand,” Journal of the Chemical, Metallurgical and Mining Society of South Africa, 52, pp. 119–139.

[4] Lancaster, P., and Salkauskas, K., 1981, “Surface generated by moving least squares methods,” Mathematics of Computation, 37, pp. 141–158.

[5] Hagan, M. T., Demuth, H. B., and Beale, M., 1996, Neural Network Design PWS Publishing Company.

[6] Forrester, A., Sobester, A., and Keane, A., 2008, Engineering design via surrogate modelling: a practical guide John Wiley & Sons.

[7] Stander, N., Basudhar, A., Gandikota, I. et al., 2021, “LS-OPT Status Update”, 13th European LS-DYNA Conference 2021, Ulm, Germany

Interaktives 3D Design und Simulation basierend auf Neuronalen Netzwerken

Thomas Emmel[1], Andreas Fellmeth[1], Jing Bi[2], Victor Oancea[2]

[1]Dassault Systemes Deutschland GmbH, Aachen, Germany
[2]Dassault Systemes SIMULIA, Johnston, United States

Summary:

Simulationen realer Vorgänge decken unterschiedliche physikalische Bereiche ab und werden in verschiedenen Maßstäben durchgeführt. Kontinuumssimulationen im Makromaßstab auf Teile- und Baugruppenebene, bei denen in der Regel herkömmliche numerische Verfahren wie 3D-Finite Elemente oder Finite Volumen zum Einsatz kommen, werden aufgrund ihres hohen Vorhersagewerts häufig in der Produktentwicklung verwendet. Allerdings sind diese Simulationen oft sehr rechen-, zeit, - und ressourcenintensiv. Surrogat- oder Ersatzmodelle, die von diesen rechenintensiven 3D-Modellen abgeleitet werden, reduzieren die Ausführungszeiten massiv auf Sekunden (oder interaktive Zeiten) und ermöglichen eine große Anzahl von Parameterauswertungen im Designraum.
Diese Ersatzmodelle sind jedoch oft von geringerer Genauigkeit und liefern nur begrenzte Informationen durch einige wenige Indikatoren, wie z. B. maximale Spannung, maximaler Druck, maximale Intrusion usw. Um die Reichhaltigkeit von 3D-Simulationsergebnissen zu erhalten und gleichzeitig die Ausführungszeit erheblich zu reduzieren, wird in diesem Beitrag ein auf neuronalen Netzen basierender Ansatz vorgestellt, der letztendlich eine quasi-interaktive 3D-Entwurfsexploration ermöglichen soll.
Als Ausgangspunkt werden traditionelle Multiphysik-Multiskalen-Simulationen verwendet: FEA-Analysen der Strukturstatik, Dynamik, Fertigung, Verpackung und Sicherheit sowie CFD- oder Elektromagnetische Analysen werden per Design of Experiments (DOEs) erstellt, um die parametrischen Designdaten zu generieren. Die Daten werden verarbeitet und zum Trainieren schnell laufender neuronaler Netze als 3D-Ersatzmodell verwendet. Die Wahl der Algorithmen und Architekturen neuronaler Netze hängt von der Art der Physik und der Fragestellung ab. Die trainierten neuronalen Netze können für interaktive Entwurfsexplorationen eingesetzt werden, wobei ein Schwerpunkt auf der Güte und Zuverlässigkeit der fertigen Netze gelegt wird. Der vorgeschlagene Ansatz erweitert herkömmliche Ersatzmodelle, um sowohl transiente physikalische Reaktionen als auch 3D-Felder abzudecken, was zu einer informationsreichen und wesentlich produktiveren Umgebung für die Produktentwicklung führen und die Modelle außerhalb der Simulationsabteilungen verbreiten kann.

Keywords:

Design, Simulation, Neural Networks, Surrogate Model, 3D, DOE, FEA, FEM, Machine Learning

1 Einordnung und Definitionen

Die Verwendung sogenannter Surrogatmodelle (Ersatzmodelle) hat in der Simulation physikalischer Vorgänge und Strukturen eine lange Tradition, schon allein da die Modellierung der realen Zustände aus Gründen der Komplexität oder Größe der Modelle nicht möglich war oder immer noch ist. So kann man auch Materialmodelle oder Modale Superposition in diese Kategorie aufnehmen, was üblicherweise allerdings nicht erfolgt, da diese zum Standardwerkzeug einer jeden Modellierung gehören.
Im Kontext des Vortrags unterscheiden wir daher „Reduced Order Modelle“ (ROM) von „Machine Learning Modellen“ (ML). Erstere gehören in der Mehrzahl zu den „intrusiven“ Methoden, da diese Eingriffe in die Modellierung selbst, d.h. in die Berechnungsmethode und schließlich in die Software notwendig machen, beispielsweise POD-Methoden („Proper Orthogonal Decomposition) wie Craig-Bampton (lineare Dynamik), TPWL – Trajectory PieceWise Linearizations u.a., oder PGD-Methoden („Proper Generalized Decomposition“), die jeweils als ausgereifte Methoden in den bekannten Werkzeugen, wie Abaqus [1], zur Verfügung stehen.

Ergänzend dazu kann man die ML-Methoden einordnen, die üblicherweise zu den „nicht intrusiven“ Methoden zählen, da hierbei nur der Eingang der Parameter, also das Ausgangsmodell und die daraus erzielten Ergebnisse betrachtet werden, ohne den Weg zu berücksichtigen, wie diese Ergebnisse erzielt wurden. Der Begriff „Machine Learning“ (ML) mag hier irreführend sein, denn in diesem Kontext werden auch Modelle verwendet, die auch außerhalb der künstlichen Intelligenz schon seit langer Zeit Anwendung finden (z.B. Kriging, Gauss‘sche Prozesse (stochastisch), Polynomial Response Surfaces etc.).
Dabei handelt es sich meist um erprobte Methoden, die sich ebenfalls schon in den bekannten Werkzeugen Verwendung finden (beispielsweise für eine DOE) [2]. Relativ neu sind die Neuronalen Netzwerke (ANN, RNN, FFN...), deren Verwendung viele neue Möglichkeiten zeigt, aber mindestens ebenso viele neue Fragen aufwirft.

Ziel und größter Vorteil solcher Methoden und Modelle ist der wesentlich reduzierte Bedarf an Ressourcen wie Rechenzeit, Speicher und CPU gegenüber einer vollständigen Modellierung des eigentlichen Problems. Gleichzeitig können externe Quellen wie Testdaten aus Experimenten als Eingangsgröße für solche Modelle dienen.

Die Erstellung präziser Surrogatmodelle bleibt im Allgemeinen eine Kunst, die Komplexität variiert stark, vor allem, da sich durch die neuen Methoden eine Erweiterung von 0D/1D-Modellen auf die 3D-Modellierung, inklusive dynamischer Probleme, erschließt. Ebenso kann bisher nicht beantwortet werden, inwiefern sich alle Fragestellungen der Simulation mit hinreichender Genauigkeit mit den bisher existierenden Neuronalen Netzwerken und deren Erstellung beantworten lassen. So sind z.B. scheinbar einfache Lösungen zur Bestimmung von Eigenfrequenzen und Eigenmoden noch nicht ausgereift, befinden sich aber in der Erprobung.

2 Untersuchte Fragestellungen

In der Präsentation werden einige Beispiele gezeigt, die die Anwendbarkeit Neuronaler Netzwerke in verschiedenen Disziplinen (Abbildung 1 und 2) verdeutlichen.

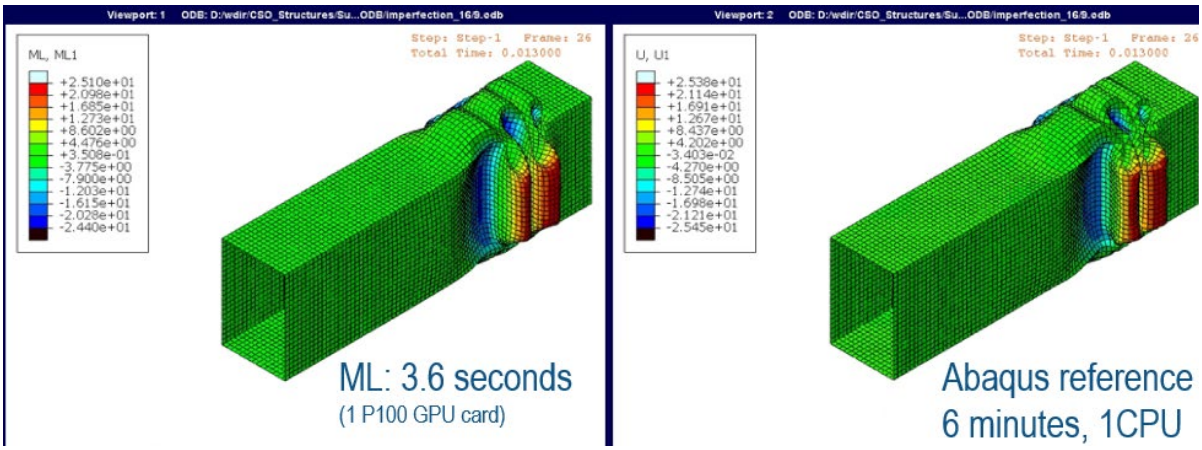

Abb. 1: Aluminium Crushing Column – links Machine Learning, rechts Referenz

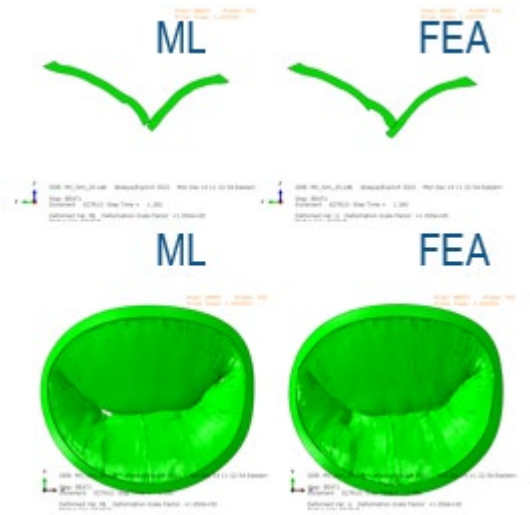

Abb. 2: Mitralklappe (menschliches Herz) Co-Simulation

Es wird der Vergleich der durch Machine Learning erzeugten mit den dazu gehörenden Referenzergebnissen (volle Simulation) gezeigt, sowie die verwendete Zahl der Trainingsmodelle und der Fehler diskutiert. Die Frage einer optimalen oder notwendigen Zahl von Trainingsmodellen und Trainingsläufen kann bisher noch nicht abschließend beantwortet werden.
Eine einfache Illustration der möglichen Unsicherheit bei begrenzter Datenlage in Abbildung 3 verdeutlicht die Problematik: Letztlich gilt es bewerten, ob das Neuronale Netzwerk ein „Over-Sampling“ der Basisdaten erzeugt, und somit in der Abbildung nur der Streuung der Test- oder Simulationsdaten folgt, oder ob es sich hierbei um einen relevanten – möglicherweise aber lokalen – Zustand des Modells handelt.

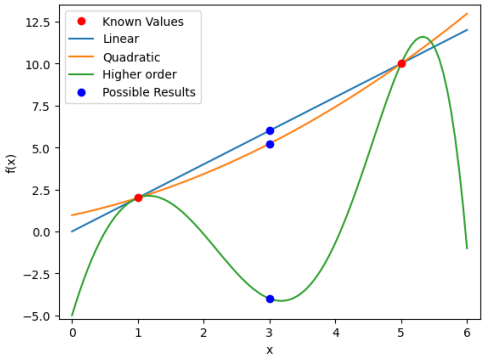

Abb. 3: Generelle Unsicherheit von Interpolationsmethoden bei begrenzten Eingangsdaten

Wie weit man die trainierten Modelle verwenden kann und darf, muss – wie bei bewährten Verfahren (DOE etc.) – genau untersucht und definiert werden. Dabei spielen Anzahl der Parameter (soweit vorhanden) und der Komplexität eine große Rolle, ebenso wie die Sensitivität der einzelnen Modellierung.

So ist möglicherweise eine kleine Parametervariation Grund für den Wechsel eine laminaren zu einer turbulenten Strömung und die Frage des Mappings der Ergebnisse zur Visualisierung stellt ein nicht unerhebliches Problem dar.
Grundlegend gibt es bereits Möglichkeiten via „Genauigkeit“ und „Verlust“ während des Trainings erste Erkenntnisse zu gewinnen (vgl. Abbildung 4), wie akkurat ein trainiertes Netzwerk arbeiten wird und welche Grenzen existieren. Aktuell werden verschiedene Validierungsverfahren untersucht . Zudem existieren bereits sinnvolle Methoden zur Vermeidung des beschriebenen „Over-Samplings“.

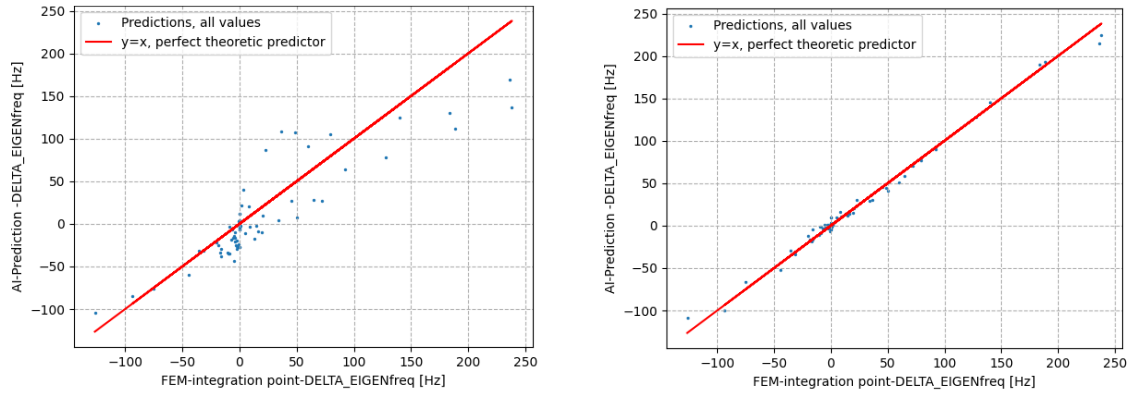

Abb. 4: Vorhersagegenauigkeit abhängig von der Wahl der Trainingsdaten/Validierungsdaten

Insofern bereits vorhanden, werden erste Ergebnisse bei sehr diskontinuierlichen Fragestellungen präsentiert, wie beispielsweise Modalanalysen.

3 Ausblick

Das Interesse an den vorgestellten neuen Verfahren und Modellen ist sehr groß und wird weiterwachsen, getrieben von allgemeinen Diskussionen zu Künstlicher Intelligenz (KI/AI). Allerdings bleibt abzuwarten, ob alle Erwartungen erfüllt werden können, solange grundlegende Fragen, z.B. der allgemeinen Anwendung der verschiedenen Neuronalen Netzwerke, in diesem Kontext noch nicht geklärt wurden. Mit steigender Komplexität der Probleme steigen auch die Anforderungen, allerdings auch die Gefahr des „Over/Underfitting“ und damit der Fehlinterpretation der erzeugten Ergebnisse. Eine finale Überprüfung der Vorhersagen mittels Tests und Simulation bleibt weiterhin zentrales Mittel, um die Ergebnisse bewerten zu können.
Dies ist vor allem bei nicht-kontinuierlichen Problemen notwendig, um die Aussagefähigkeit eines Neuronalen Netzwerkes zu beurteilen.

4 Literatur

[1] Dassault Systèmes: "ABAQUS – User‘s Guide, *Theory Guide*", 2024
[2] Dassault Systèmes; „ISight – User‘s Guide, *Kriging Model*“, 2024

Leveraging Machine Learning (ML) for Optimal Seal Design in Automotive Connectors

Rajesh Kumar, TE Connectivity Germany GmbH

1 Summary

This study introduces an approach to assist seal design processes in automotive connectors by analytics and machine learning (ML). The digitization of various seal data not only helps in automatic comparison between measurement and simulation, but also enables analytics and ML.

The results have already demonstrated that comparing simulation with measurement can significantly contribute to virtual validation. Currently, the ML model overestimated both the maximum insertion force and contact pressure. This could be because of limited size of the dataset and complex nature of seal materials (hyper-elastic).

A developed digitized pipeline will continuously collect data with each seal design and measurement. This will help in training ML models on large datasets and incorporating additional seal parameters such as aging and deformed seal images.

2 About TE Connectivity (TE)

TE Connectivity is a global industrial technology leader creating a safer, sustainable, productive, and connected future. The broad range of connectivity and sensor solutions enable the distribution of power, signal and data to advance next-generation transportation, renewable energy, automated factories, data centers, medical technology and more. With more than 85,000 employees, including 8,000 engineers, working alongside customers in approximately 140 countries, TE ensures that EVERY CONNECTION COUNTS.

3 Introduction

The fundamental purpose of an electrical connector (Figure 1) is to establish a reliable connection between electrical components, allowing the flow of power or signal.

Figure 1: Electrical connector.

In automotive applications, where connectors are exposed to harsh conditions including moisture, road debris, and chemicals from road treatments, seals are essential to prevent corrosion, short circuits, and other damage that could compromise the electrical system's integrity.

Common seals in automotive electrical connectors include single wire (SWS), radial, face, and family seals (Figure 2). Each has a unique function, but all aim to protect the connector from external elements. SWS seals guard individual wires, radial seals shield the circumference, face seals protect mating interfaces, and family seals accommodate various wire sizes. Together, they ensure connector durability and reliability in challenging environments.

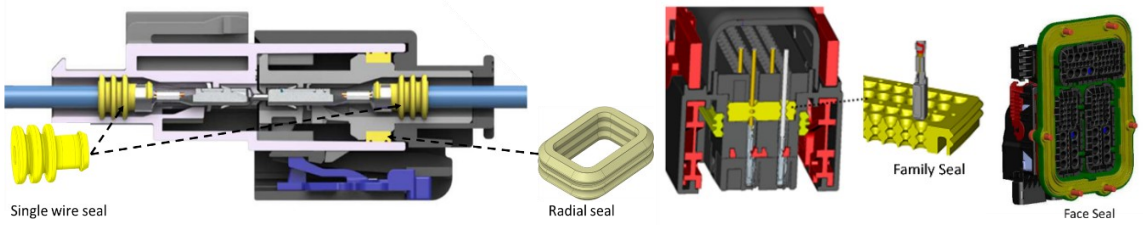

Figure 2: Commonly used seals in electrical connectors.

Radial and SWS seals are considered in this work (Figure 3). Each seal type could have different profile and a different number of seal lips. The radial seal could be rectangular, oval, and round.

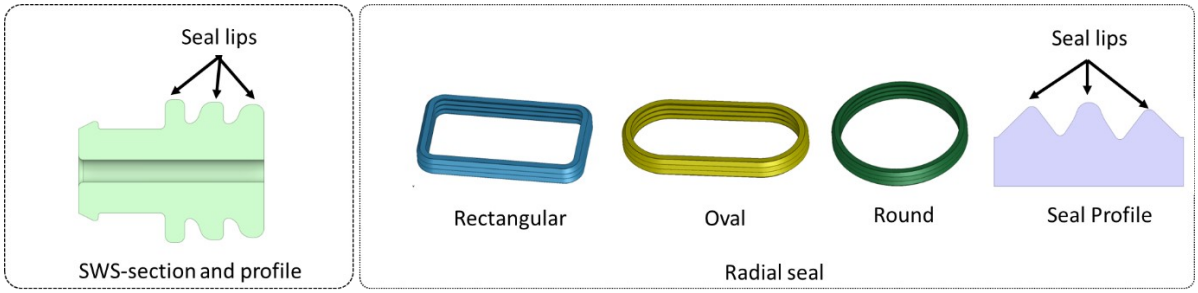

Figure 3: SWS and Radial seal illustrations.

4 Challenges and motivations for seal data digitization and ML integration

The challenges and motivations for seal digitization and the use of ML in this context are multifaceted. They are described below:

Complex Environmental Conditions: Electrical connectors undergo rigorous environmental testing, including aging at high temperatures, temperature shocks, and pressure cycles. Seals play a pivotal role in maintaining connector integrity under such conditions. However, accurately predicting seal performance in both new and aged conditions during the design phase remains a significant challenge.

Material Properties: Rubber possesses an impressive ability to undergo substantial deformation and effortlessly revert to its original, nearly undeformed shape once the load is lifted. Its hyperelastic deformation characteristics and near-incompressibility distinguish it from other materials. While it's feasible to extract simulation parameters from tests like uniaxial, biaxial, and planar tests, conducting such tests for each material at varying temperatures can be prohibitively costly. As a result, there's often a scarcity of physical testing data available for simulation inputs.

Design Optimization: Designers struggle with ensuring seals meet tightness, compression, and insertion force criteria, compounded by limited digitized data availability. Seal failures during measurement incur high costs for design changes, often necessitating expensive tooling adjustments, leading to production delays.

To address the above challenges, digitization efforts are centered around gathering a wide array of seal-related data. Seal data digitization facilitates analytics and ML, offering significant potential to aid in the early stages of the design process. This ultimately drives the development of more robust, fast, and efficient seal designs.

5 Methodology

Initially, stakeholders are convinced about the beneficial impacts of digitization. Upon obtaining their buy-in, tailored templates are prepared to capture essential data, encompassing project details, product information, geometry, material, simulation outcomes, and measurements.

The data primarily consists of text, floating-point values, and images. An approach is devised to maintain seamless connectivity between various data sources (product information, simulation data, and measurements). Designers and simulation engineers undergo training to use the templates.

The digitized data is centralized within a CAE database, and stored in diverse formats (.csv, .pickle, and .json). This repository serves as a foundation for seamless integration into dashboards and utilization in ML. Furthermore, the data architecture is structured to facilitate interoperability with other software systems within TE.

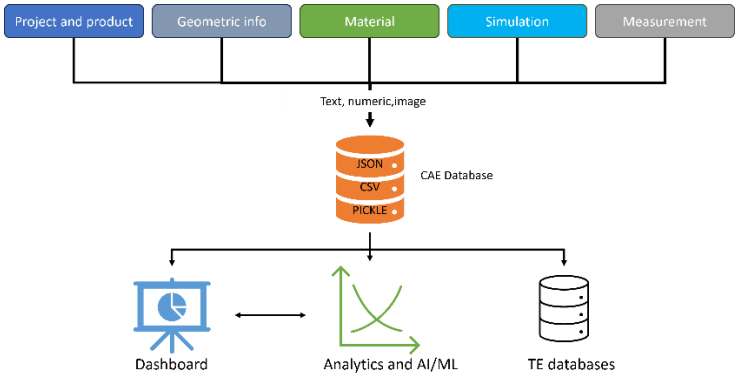

Figure 4: Digitization pipeline of seal design.

6 Result and Discussion

6.1 Simulation result validation

The simulation model (Figure 5) showing both the open and assembled states. Seal is flexible and other parts are rigid. Simulation is performed for new conditions.

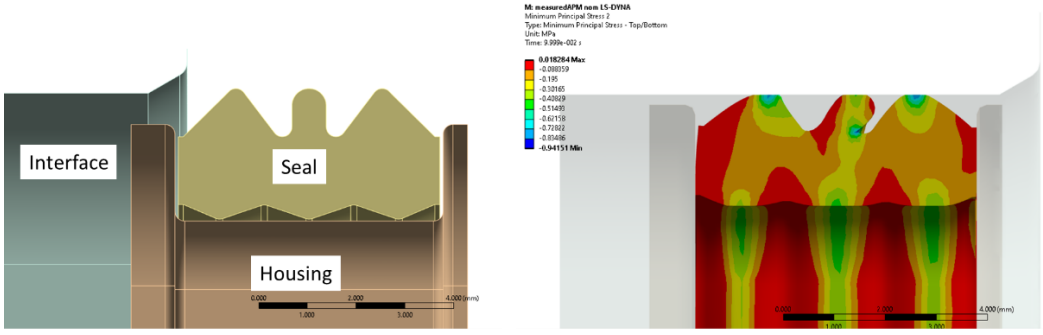

Figure 5: Simulation model in open and assembled state.

The Figure 6, illustrates that the simulated deformed model closely resembles the computed tomography (CT) scan model, and the insertion force curve aligns well with the measurement data. Despite the complexity of seals and the absence of high-quality material data, the measurements and simulations remain remarkably close. Digitization will help in collecting and comparing simulation and measurement data. Consequently, it will not only bridge the gap between simulation and measurement but also enhance accuracy, quality, and increase trust in the virtual validation of seals.

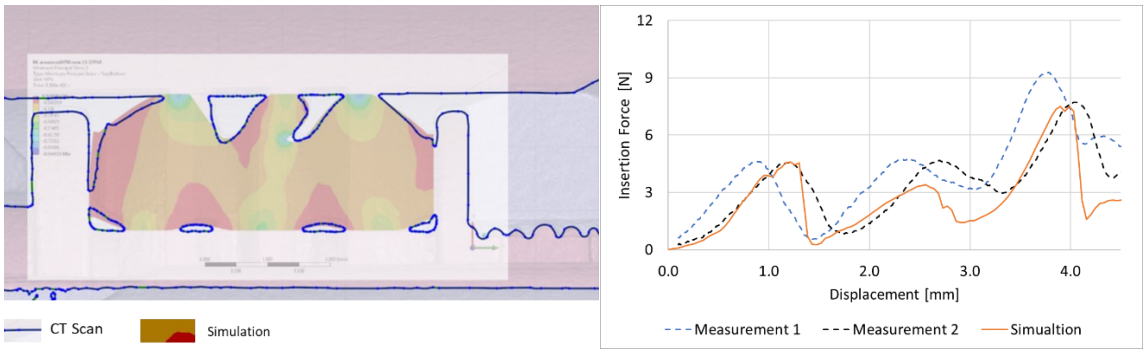

Figure 6: Left: Overlay of CT scan vs. simulation model in assembled state. Right: Insertion force comparison between simulation and measurement.

6.2 ML model

An AI software is used to train and validate data. Currently, the input for the AI model is limited to geometric and material parameters, while the output comprises of two parameters: maximum insertion force and contact pressure between the seal and its counterparts. To validate predictions, the ML inputs used are from already validated simulation and measurement data (see Figure 6).

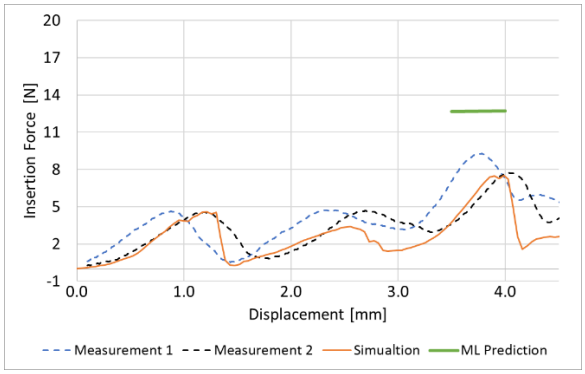

	Max insertion force [N]	Contact Pressure [MPa]
Simualtion	7.50	0.47
ML Prediction	12.70	0.81
% difference	69%	73%

Figure 7: ML model prediction.

The ML prediction (Figure 7) value is higher than the simulated values. High deviation is understandable due to the small dataset for training and complex nature of hyperplastic materials. Although ML predictions deviate, it still provide a quick and rough estimate at early design phase, a process that would otherwise takes weeks of simulation.

7 Conclusion and limitation

This study shows the benefits of digitization and data connectivity across diverse sources. It enables automatic comparison between measurement and simulation data. Thus, it helps to improve and enhances the accuracy of virtual validation processes. Furthermore, analytics and ML help to predict some aspect of seal (compression ratio, insertion forces). Although, the current model has limitations as it shows prediction deviation more than 50% from simulation. It may be due to small data set, few parameters and complex nature of hyperplastic materials.

In the future, ML models will be enhanced to include additional seal parameters, including aging effects, and incorporate deformed images. These improvements aim to provide a more comprehensive analysis to distinguish between good and bad designs.

8 Acknowledgement

I express my heartfelt gratitude to our colleagues (all from TE Connectivity) Carlo L'Abbate, Volker Heid, Rainer Bachmann for their invaluable support, particularly in providing assistance with actual parts and CT scan data.

Kerbspannungsnachweis von Schweißnähten mit Unterstützung von neuronalen Netzen

Prof. Dr.-Ing. W. Feickert, Dipl.-Ing. (FH) Tim Kirchhoff

(ihf Ingenieurgesellschaft mbH)

1 Zusammenfassung

Beim Schweißnahtnachweis mit dem Kerbspannungsverfahren (notch stress) müssen drei Spannungskomponenten richtungsgetreu und örtlich bestimmt werden. Hierzu gehören an allen Nachweisstellen die Spannungen normal und parallel zur Schweißnaht. Bezüglich der Spannungen parallel der Naht sind die Nennspannungen im Nachweis zu verwenden. Da die örtlichen Spannungen parallel der Naht durch die Behinderung der Querkontraktion gegenüber der Nennspannung erhöht sind, müssen die Spannungen anderweitig ermittelt werden. Hierzu wurden erste Konzepte entwickelt und vorgestellt: Extrapolation der Spannungen und Nutzung des örtlichen Spannungsgradienten. Diese Konzepte erlauben eine Verbesserung des Nachweises, sind aber mit Streuungen und Fehlern behaftet. In diesem Beitrag wird der Einsatz eines neuronalen Netzes zur besseren Ermittlung einer Nennspannung aus den örtlichen Spannungen vorgestellt. Das Konzept besteht darin, zunächst typische Schweißnahtdetails, die den Normkatalogen entsprechen, zu untersuchen. Für diese Konfigurationen ist die Nennspannung bekannt. Das neuronale Netz wird dabei mit hunderten von Ergebnissen an verschiedenen örtlichen Stellen der Naht trainiert. Zur Überprüfung des Modells werden anschließend mit dem trainierten neuronalen Netz unbekannte Schweißnahtdetails untersucht und die so erhaltenen Ergebnisse mit bekannten Ergebnissen verglichen. In dem vorliegenden Beitrag werden Untersuchungen an T-Stößen, Kreuzstößen und Stumpfstößen vorgestellt und diskutiert. Die Einsatzmöglichkeiten des Verfahrens und die Vorteile für die Bewertung der Schweißnaht werden aufgezeigt.

2 Einleitung

Schweißnähte sind eines der wichtigsten Verbindungsmittel in der Technik. Bei wechselnder Belastung (Verkehrslasten, wechselnde Betriebslasten, Unwucht, Schwingungen, etc.) sind sie in den meisten Fällen auch die versagenskritischen Schwachstellen. Bei der Auslegung eines Produktes müssen sie folglich im Hinblick auf statische Beanspruchung und Ermüdungsfestigkeit ausgelegt werden. Der Nachweis erfolgt nach Regelwerken, wie z.B. den IIW Recommendations [1], der FKM-Richtlinie [2], dem Eurocode 3 und 9 [3] oder anderen nationalen Regelwerken, wie DS 952 [4], DVS 1612 [5] und DIN 13001 [6], je nach Einsatz der Schweißnaht (Maschinenbau, Druckbehälter, Offshore-Anwendung, Stahlbau, Kranbau, etc.).
Schweißnähte versagen typischerweise vom Nahtübergang ins Innere hinein oder von der Schweißnahtwurzel nach außen (siehe Bild 1).

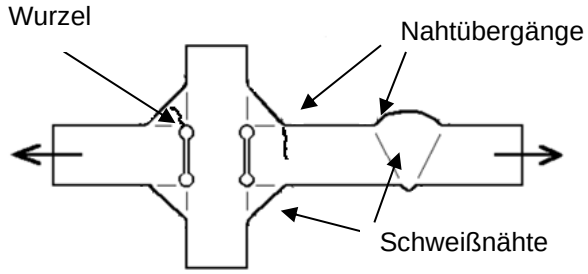

Bild 1: Schweißnahtversagen am Kreuzstoß

Die Bewertung von Schweißnähten ist, auch in der modernen simulationsgetriebenen Produktentwicklung, eine Herausforderung. Aufgrund der besonderen Eigenschaften der Schweißnähte

(z.B. scharfe und recht unregelmäßige Kerben) sind häufig aufwändige Methoden zur Spannungsermittlung für den Nachweis erforderlich.
Mit Verbreitung der rechnergestützten virtuellen Produktsimulation (Finite-Elemente-Methode, FEM) haben sich Verfahren, die auf Strukturspannungen oder Kerbspannungen basieren, zum Stand der Technik entwickelt. Mit diesen Verfahren lassen sich nun die Beanspruchungen am Nahtübergang oder in der Wurzel - also an den Versagensorten - für fast beliebige Schweißnähte direkt ermitteln und nachweisen. Insbesondere auch für Schweißnähte, die mit dem klassischen Nennspannungskonzept gar nicht bewertet werden können.
Beim Kerbspannungsverfahren wird ein fiktiver Kerbradius von 1mm, 0,3mm oder 0,05mm am Schweißnahtübergang und in der Schweißnahtwurzel in das Simulationsmodell eingeführt (siehe Bild 2). Die Schweißnaht und der Kerbradius müssen im Simulationsmodell geometrisch abgebildet werden. Für eine Schweißnahtwurzel stellt dieses Verfahren zurzeit den Stand der Technik dar.

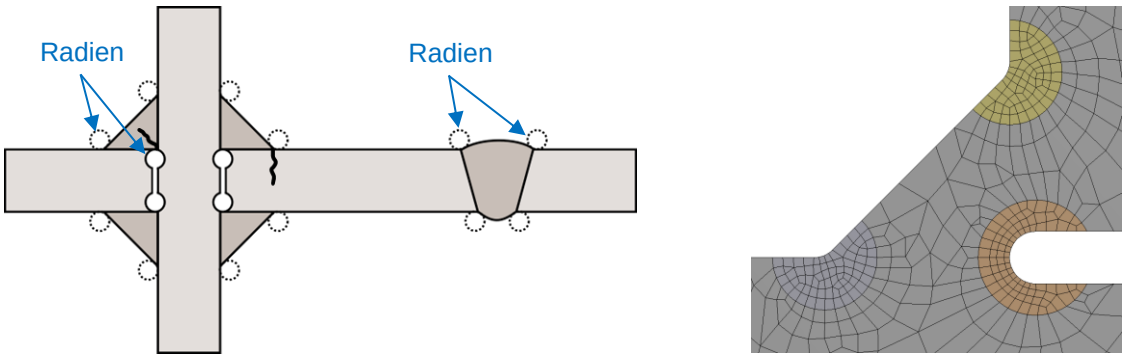

Bild 2: Kerbspannungsverfahren: Modellierung von Radien (links), Vernetzungsbeispiel (rechts)

Der Aufwand für die Berechnung ist ohne speziell auf das Nachweisverfahren zugeschnittene Software sehr hoch. Insbesondere die Ermittlung der lokalen Spannungen an den Schweißnähten und deren Bewertung ist bei vielen Nähten ohne spezielle Software wirtschaftlich nicht möglich.
Beim Nachweis der lokalen Spannungen am Schweißnahtübergang und in der Schweißnahtwurzel mit dem Kerbspannungsverfahren (notch stress) müssen drei Spannungskomponenten richtungsgetreu und örtlich bestimmt werden. Hierzu müssen an allen Nachweisstellen die Richtungen normal zur Schweißnaht und parallel der Schweißnaht ermittelt werden.
Bezüglich der Spannungen parallel der Naht sind entsprechend der FKM-Richtlinie die Nennspannungen im Nachweis zu verwenden. Die örtlichen Spannungen längs der Naht entsprechen aber aufgrund der Behinderung der Querkontraktion, verursacht durch die Spannung senkrecht zur Naht, nicht der Nennspannung. Die Überhöhung der parallelen Spannung ist dabei abhängig vom Kerbradius (der Kerbschärfe).
Die lokalen Spannungen werden im Allgemeinen mit Hilfe einer FE-Analyse ermittelt. Die Nennspannungen müssen dann anderweitig ermittelt werden und können nicht anschaulich festgelegt werden.
Im Beitrag „Korrektur der Spannungen parallel der Schweißnaht“ [7] wurden zwei Konzepte vorgestellt, um eine Nennspannung aus der örtlichen Kerbspannung abzuschätzen: Extrapolation der Spannungen und Nutzung des örtlichen Spannungsgradienten. Diese Konzepte erlauben eine Verbesserung des Nachweises, sind aber noch mit Streuungen und Fehlern behaftet. In diesem Beitrag wird der Einsatz eines neuronalen Netzes zur besseren Ermittlung einer Nennspannung aus den örtlichen Spannungen untersucht, mit dem Ziel, die Abschätzung einer korrekten parallelen Nennspannung weiter zu verbessern.

3 Spannungen parallel zur Schweißnaht

Für die Schweißnahtbewertung nach dem Kerbspannungskonzept müssen die Spannungen parallel zur Schweißnaht als Nennspannungen erfasst und mit einer Nennspannungs-FAT-Klasse bewertet werden. Wenn in einer FEM-Simulation örtliche Kerbspannungen ermittelt wurden, stellt sich folgende Frage: Wie können aus den örtlichen Spannungen Nennspannungen abgeleitet werden? Prinzipiell könnte man einen Integrationsbereich festlegen, in diesem Bereich die Kräftesumme parallel zur Naht bestimmen und durch Gewichtung mit der Integrationsfläche eine Nennspannung ermitteln. Hier treffen aber in dem Bewertungsverfahren zwei völlig verschiedene Konzepte aufeinander, die nicht einfach verheiratet werden können. Im Allgemeinen ist das Nennspannungsverfahren, mit dem über Querschnitte einfache Spannungsverläufe ermittelt werden können, auf einfache Querschnitte beschränkt. Wird ein örtliches

Verfahren eingesetzt, sind die Strukturen und die Spannungsverläufe in der Regel wesentlich komplexer. Querschnitte lassen sich meist gar nicht definieren. Unter dem Ansatz, dass sich die bestimmenden maximalen Spannungen auf der Bauteiloberfläche und in der Kerbe manifestieren, kann die Nennspannung parallel zur Naht durch die Kerbspannung aber sicher nach oben abgeschätzt werden.

Wie entsteht die Spannungskomponente parallel zur Naht?
Natürlich erzeugen lokale Kräfte längs der Naht eine entsprechende Spannungskomponente parallel zur Naht, die entsprechend zu bewerten ist. Daneben entsteht aber, bedingt durch das Kerbspannungsverfahren, in der Kerbe eine „artifizielle“, in der Größe nicht zu vernachlässigende, Spannung parallel zur Naht.

Am Schweißnahtübergang bzw. in der Kerbe treten im Allgemeinen hohe Spannungen normal zur Schweißnaht bzw. in Umfangsrichtung des Kerbradius auf. Diese Spannungskomponente hat eine hohe Querkontraktion in Richtung parallel zur Schweißnaht zur Folge. Ins Innere des Bauteils hinein fällt die Spannung normal zur Schweißnaht rasch ab. Dort treten entsprechend kaum Querkontraktionen, initiiert durch diese Spannungskomponente, auf. Dies führt dazu, dass die Querkontraktion auf der Bauteiloberfläche durch das Material im Bauteilinneren behindert wird. Diese Behinderung der Querkontraktion hat eine „artifizielle“ Spannungskomponente parallel zur Naht zur Folge. Die Querkontraktion wird im Materialgesetz mit der Querkontraktionszahl ν beschrieben. Bei vollständiger Behinderung der Querkontraktion ergibt sich daraus eine Spannung parallel zur Naht in der Größe ν mal Spannung normal zur Naht (siehe Bild 3).

Beim Kerbspannungsverfahren sind je nach Blechdicke verschiedene Kerbradien zur Abbildung des Nahtüberganges bzw. der Nahtwurzel normativ zulässig. Die lokale Kerbspannung ist wiederum vom Kerbradius abhängig. Dies führt dazu, dass die „artifizielle“ Spannung parallel zur Naht vom gewählten Kerbradius bestimmt wird. Die lokal ermittelten Spannungen parallel zur Naht sind damit überhöht und führen im Nachweis zu deutlich zu hohen Auslastungsgraden.

Die Spannung parallel zur Naht muss also in Abhängigkeit vom Kerbradius korrigiert werden.

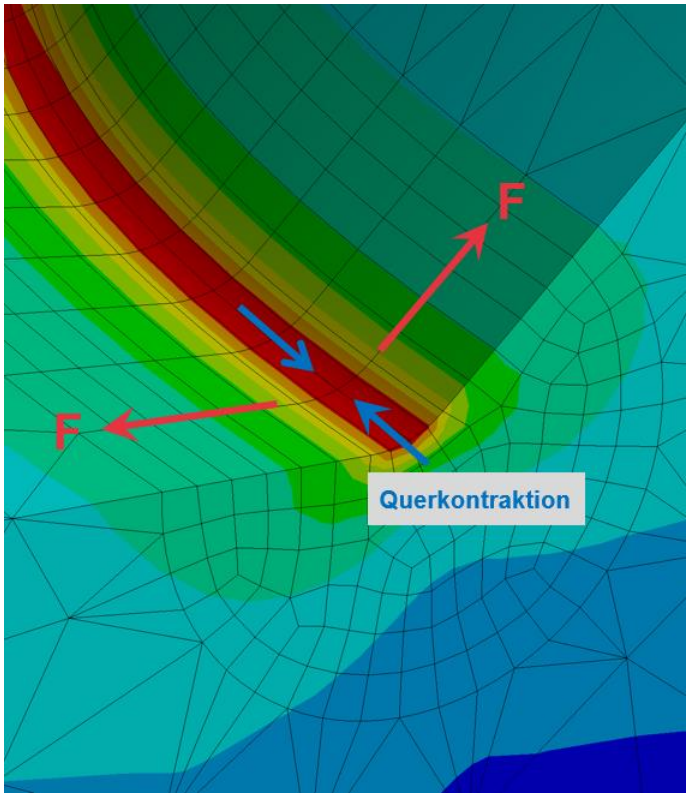

Bild 3: Entstehung der „artifiziellen“ Spannung parallel zur Schweißnaht

3.1 Korrektur der parallelen Spannung mit einem neuronalen Netz

Angesetzt wird, dass die Spannungskomponente parallel zur Schweißnaht infolge der Behinderung der Querkontraktion örtlich sehr begrenzt ist und in ihrer Größe und Ausbreitung vom Spannungsverlauf ins Bauteil abhängt. Der Spannungsverlauf ins Bauteilinnere wiederrum wird von mehreren Größen beeinflusst, zum Beispiel dem Kerbradius, dem Kerböffnungswinkel und der lokalen Geometrie.
Im Beitrag [7] konnte ein grundlegender Zusammenhang zwischen der Überhöhung der Spannungskomponente parallel zur Schweißnaht und dem Spannungsverlauf ins Bauteilinnere gezeigt werden. Aufgrund der vielfältigen Einflussfaktoren ist es jedoch schwierig, eine allgemeingültige Regel aufzustellen, mit der dieser „artifizielle“ Anteil der parallelen Spannungskomponente möglichst genau abgeschätzt werden kann. Diese Abschätzung soll mit Unterstützung eines neuronalen Netzes verbessert werden.

Das Konzept besteht darin, zunächst typische Schweißnahtdetails, die den Normkatalogen entsprechen, zu untersuchen. Für diese Konfigurationen ist die Nennspannung parallel zur Naht bekannt. Wenn die gesuchte Nennspannung bekannt ist, kann der „artifizielle“ Anteil der parallelen Spannung durch die Behinderung der Querkontraktion an jedem Auswertepunkt errechnet werden:

$$Artifizielle\ Spannung_{\parallel} = Lokale\ Spannung_{\parallel} - Nennspannung_{\parallel}$$

Der maximal mögliche Wert für den „artifiziellen“ Anteil der parallelen Spannung, bei maximaler Behinderung der Querkontraktion, ergibt sich aus der lokalen Spannung senkrecht zur Naht, multipliziert mit der Querkontraktionszahl des verwendeten Materialgesetzes. Für das Training des neuronalen Netzes wird daraus ein Sollwert festgelegt mit:

$$Sollwert = \frac{Artifizielle\ Spannung_{\parallel}}{Lokale\ Spannung_{\perp} \cdot Querkontraktionszahl}$$

Der Sollwert gibt für einen Auswertepunkt an wie stark die Querkontraktion an dieser Stelle behindert wird. Das neuronale Netz wird mit hunderten von Ergebnissen an verschiedenen örtlichen Stellen der Kerbradien entlang der Naht darauf trainiert, den Sollwert aus dem Spannungsverlauf in das Bauteilinnere heraus abzuschätzen. Dazu wird der lokale Spannungsverlauf ins Bauteilinnere an allen Auswertepunkten der verwendeten Simulationsmodelle ermittelt und als Eingangsgröße für das Training verwendet. Als Zielwert für das neuronale Netz wird der oben definierte Sollwert verwendet.

Zur Überprüfung des neuronalen Netzes werden anschließend mit dem trainierten neuronalen Netz unbekannte Testmodelle untersucht und die so erhaltenen Istwerte mit den Sollwerten für diese Modelle verglichen.
Damit wird zunächst gezielt untersucht, ob das trainierte neuronale Netz auf Modelle mit anderen Konfigurationen, wie zum Beispiel anderen Radien, Öffnungswinkeln oder Lasten, anwendbar ist.

In den folgenden Abbildungen werden die Istwerte aus einer Abschätzung durch das trainierte neuronale Netz an den Auswertepunkten eines Testmodelles mit den bekannten Sollwerten verglichen. Stimmen Soll- und Istwert genau überein, liegt der entsprechende Punkt genau auf der durch die grüne Linie dargestellten Diagonale.

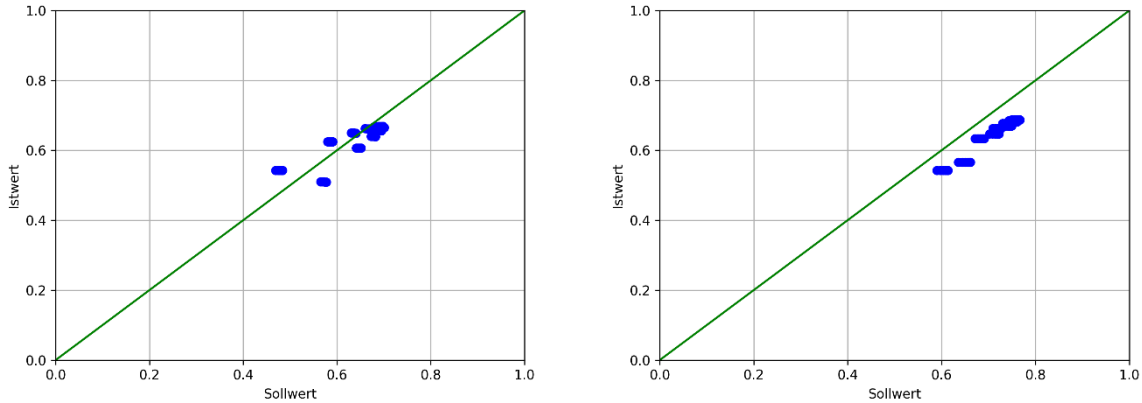

Bild 4: Vergleich der Ist- und Sollwerte bei zwei Testmodellen „Kreuzstoß mit 120 Grad Öffnungswinkel“

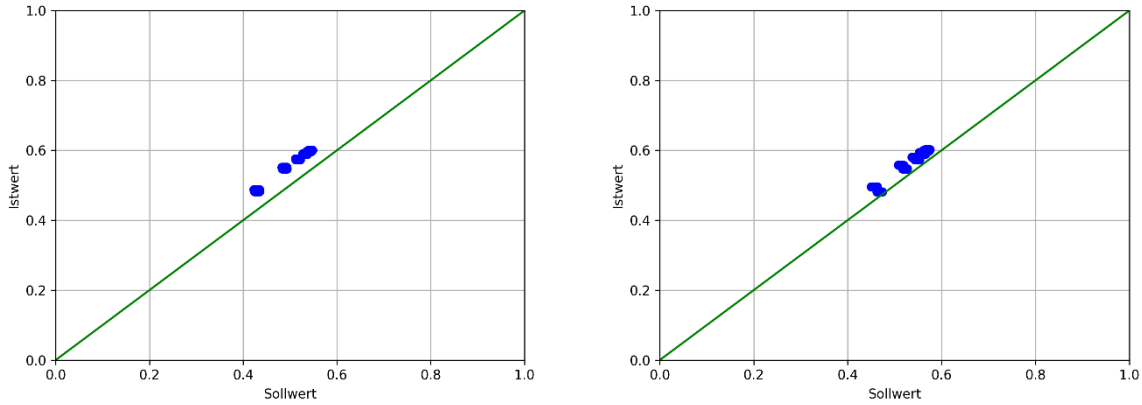

Bild 5: Vergleich der Ist- und Sollwerte bei zwei Testmodellen „Kreuzstoß mit 150 Grad Öffnungswinkel“

In den gezeigten Testmodellen ergibt sich eine gute Übereinstimmung zwischen Soll- und Istwerten. Es ist aber zu erwarten, dass die Abweichungen größer werden, wenn die Eigenschaften der Modelle stärker von Trainingsdatensatz unterscheiden.

Aus den gewonnenen Istwerten kann der „artifizielle“ Anteil der Spannungskomponente parallel zur Naht abgeschätzt werden, um so die gesuchte Nennspannung parallel zur Naht zu ermitteln.

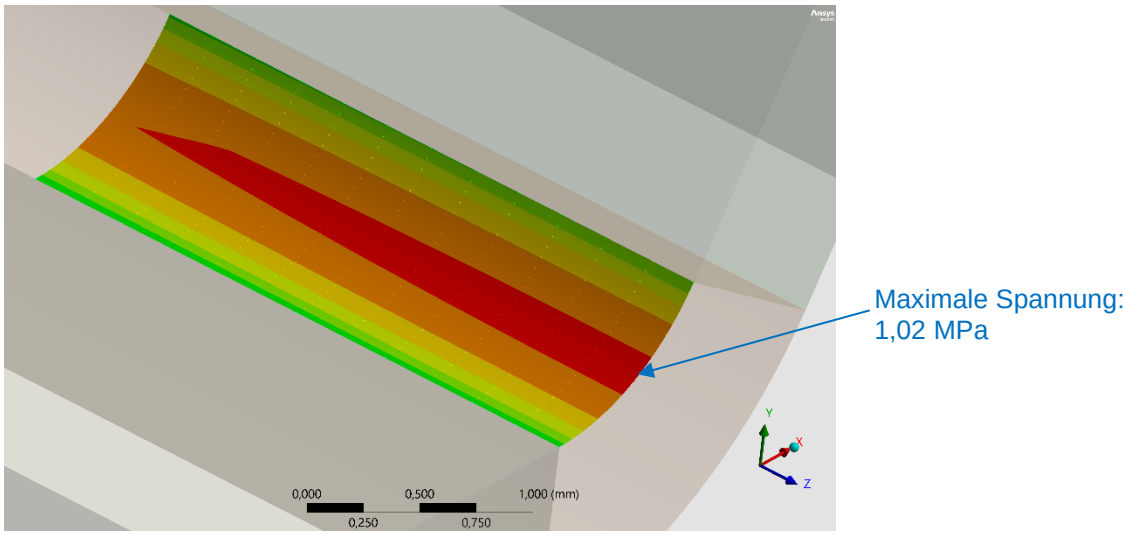

Bild 6: Lokale Spannung parallel zur Naht im Modell „Kreuzstoß mit 120 Grad Öffnungswinkel (rechts)“

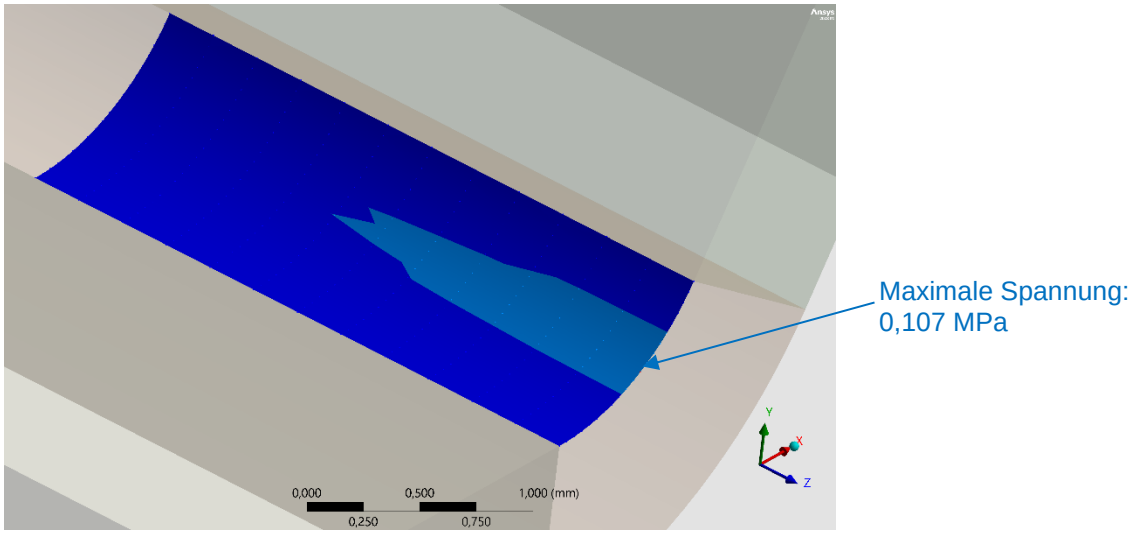

Bild 7: Korrigierte Spannung parallel im Modell „Kreuzstoß mit 120 Grad Öffnungswinkel (rechts)“

In den Bildern 6 und 7 wird beispielhaft für ein Testmodell „Kreuzstoß mit 120 Grad Öffnungswinkel“ die lokale Spannung parallel zur Naht sowie die korrigierte Spannung parallel zur Naht gezeigt, bei gleicher Skalierung der Werte. Die Soll- und Istwerte zu diesem Modell sind in Bild 4 (rechts) dargestellt. Die Berechnung der Spannungen an der Schweißnaht wurde mit der Software AutoWeld [8] durchgeführt.

Die korrigierten Werte der parallelen Spannung liegen deutlich näher an der für dieses Modell richtigen Nennspannung von 0 MPa. Die maximale Überhöhung der parallelen Spannung konnte durch den Einsatz des neuronalen Netzes von 1,02 MPa auf 0,107 MPa und damit um knapp 90% reduziert werden.
Die Abschätzung mit dem neuronalen Netz liefert in den bisher untersuchten Testmodellen, auch in den Bereichen mit geringeren Spannungen, sinnvolle Werte.

4 Fazit

Beim Nachweis der lokalen Spannungen am Schweißnahtübergang und in der Schweißnahtwurzel mit dem Kerbspannungsverfahren müssen die Spannungen normal und parallel zur Schweißnaht ermittelt werden. Bezüglich der Spannungen parallel zur Naht sind entsprechend der FKM-Richtlinie die Nennspannungen im Nachweis zu verwenden. Da die örtlichen Spannungen parallel zur Naht durch die Behinderung der Querkontraktion einen großen „artifiziellen“ Anteil abhängig vom Kerbradius (Kerbschärfe) enthalten, muss diese Spannungskomponente korrigiert werden. Die lokal ermittelten Spannungen parallel zur Naht sind ansonsten erheblich überhöht und führen im Nachweis zu deutlich zu hohen Auslastungsgraden und damit zu konservativen Ergebnissen.
In diesem Beitrag wird ein Verfahren vorgeschlagen, mit dem im örtlichen Nachweis mit einer FE-Analyse die Spannungen parallel zur Naht mit Hilfe eines neuronalen Netzes korrigiert werden können. Gegenüber den im Beitrag „Korrektur der Spannungen parallel der Schweißnaht“ [7] vorgestellten Verfahren zeigen die ersten Testmodelle eine bessere Korrektur der maximalen Spannungsüberhöhung. Vor allem ist aber die bessere Abschätzung der Spannungen in geringer belasteten Bereichen der Kerbradien vielversprechend, bei denen die bisherigen Verfahren Schwächen zeigen.
In den bislang untersuchten Testmodellen ergibt sich eine gute Übereinstimmung zwischen Soll- und Istwerten, jedoch deckt die Varianz der Modelle im Trainingsdatensatz noch nicht die in der Praxis vorliegende Vielfalt an Nahtkonfigurationen ab.
Ziel für weitere Arbeiten ist daher, den Trainingsdatensatz signifikant zu vergrößern und die Übertragbarkeit auf andere Nahtkonfigurationen durch eine hinreichende Varianz bei den Vergleichsmodellen zu überprüfen.

5 Literatur

[1] Guideline IIW „Recommendations for fatigue design of welded joints and components“, Hobbacher, Springer Nature, 2016

[2] Rennert, R.; Kullig, E.; Vormwald, M.; Esderts, A.; Siegele, D.: FKM-Richtlinie Rechnerischer Festigkeitsnachweis für Maschinenbauteile, VDMA Verlag, 6. überarbeitete Auflage, 2012

[3] DIN EN 1999-1-3: Eurocode 3: Bemessung und Konstruktion von Stahlbauten – Teil 1-9: Ermüdung; Deutsche Fassung EN 1993-1-9:2005 + AC:2009; Beuth Verlag GmbH, Berlin; Ausgabe Dezember 2010 und DIN EN 1993-1-9: Eurocode 9: Bemessung und Konstruktion von Aluminiumtragwerken – Teil 1-3: Ermüdungsbeanspruchte Tragwerke; Deutsche Fassung EN 1999-1-3:2007 + A1:2011; Beuth Verlag GmbH, Berlin; Ausgabe Dezember 2010

[4] DS 952 “Vorschrift für das Schweißen metallischer Werkstoffe in Privatwerken. Anhang II: Richtlinie für die Berechnung der Schweißverbindungen.“, 1977

[5] Guideline DVS 1612 “Gestaltung und Dauerfestigkeitsbewertung von Schweißverbindungen an Stählen im Schienenfahrzeugbau”, Deutscher Verband für Schweißen und verwandte Verfahren, 2014-08

[6] DIN EN 13001-3-1: Krane – Konstruktion allgemein – Teil 3-1: Grenzzustände und Sicherheitsnachweis von Stahltragwerken; Deutsche Fassung EN 13001-3-1:2012+A1:2013; Beuth Verlag GmbH, Berlin; Ausgabe Dezember 2013

[7] W. Feickert, T. Kirchhoff, T. Schlitzer: Verfahren zur Korrektur der Spannungen parallel der Schweißnaht, NAFEMS DACH Regionalkonferenz 2022

[8] ihf Ingenieurgesellschaft: Software AutoWeld, https://ihf-ffm.de/software/autoweld

Digital Twins at Rolls-Royce

Akin Keskin

(Rolls-Royce Group)

Today's Simulation & Modelling capability has reached a high level of accuracy, providing a tool for engineers to perform design and analysis tasks for complex products.

The next level is to merge physics based data with simulation data and create virtual products that can be used to analyse product attributes in the computer or to predict how a physical product will behave in the future.

This concept is referred to "Digital Twins" and is a significant building block in commercial enterprises to increase product understanding during design, improve service offerings in the aftermarket, and tailor products to customer needs.

The presentation will show how the Digital Twin concept is used at Rolls-Royce and how this technology is influencing business decisions.

Vereinfachte Verhaltensmodelle zur Bewertung der thermomechanischen Zuverlässigkeit leistungselektronischer Baugruppen

Ralf Döring, Rainer Dudek, Sven Rzepka (Fraunhofer ENAS)
Christian Walbrecker-Baar (Siemens AG, T ICE ELI-DE, München),
Pauline Langbehn (iPoint-systems gmbH Hamburg)

Fraunhofer ENAS, Focus Team Reliability
Technologie-Campus 3, 09126 Chemnitz, Germany
Phone: +49 371 45001 410, e-mail: ralf.doering@enas.fraunhofer.de

1 Zusammenfassung

Diese Präsentation beinhaltet die Vorstellung einer Methodik zur Bewertung der thermomechanischen Zuverlässigkeit leistungselektronischer Baugruppen. Besonders im Fokus steht dabei eine Methodik zur Ermittlung und Bewertung von Schwachstellen der Aufbau- und Verbindungstechnik. Ziele sind einerseits die Prognostizierung des Ausfallverhaltens dieser Baugruppen als auch die Bereitstellung dieses Expertenwissens für Produktentwickler in Form von vereinfachten Verhaltensmodellen.
Die Methodik wird an einem Beispiel exemplarisch demonstriert.
Perspektivisch sollen dieses Verhaltensmodell durch Einbeziehung der realen Belastungshistorie und Einsatzbedingungen in einen digitalen Zwilling überführt werden, welcher das Ausfallverhalten eines spezifischen Moduls prognostiziert und durch Einbindung in eine übergeordnete Systemsimulationen diese in die Lage versetzen soll, auf drohende Ausfälle rechtzeitig zu reagieren.

2 Motivation

In den nächsten Jahren werden durch Trends wie Industrie 4.0, Elektromobilität oder der zunehmende Einsatz dezentraler Anlagen für erneuerbare Energien die Leistungselektronik und additive Fertigungsmethoden zu den weltweit größten Wachstumsmärkten gehören. Leistungselektronik wird für das Wandeln von elektrischen Strömen, Spannungen und Frequenzen eingesetzt und stellt ein Bindeglied zwischen dem Energieerzeuger und dem Energieverbraucher dar.
Speziell beim Einsatz in sicherheitsrelevanten Umgebungen (z.B. autonomes Fahren) ist die Entwicklung ausfallsicherer Module von höchstem Interesse.
Die Sicherstellung der thermomechanischen Zuverlässigkeit während des Einsatzes derartiger Module ist Expertenwissen, welches bei Entwicklern nicht unbedingt vorausgesetzt werden kann. Um die Entwickler dennoch in die Lage zu versetzen, dieses Wissen bereits in der Designphase zu berücksichtigen ist es sinnvoll, sie mit Werkzeugen auszustatten, welches ihnen dieses know how bereitstellt, ohne dass man die genutzten Methoden genau kennen muss. Dieses vereinfachte Verhaltensmodell ist zudem Voraussetzung für die Entwicklung eines digitalen Zwillings, welcher den Zustand eines einzelnen Leistungsmoduls im Einsatz überwacht und bewertet.

3 Methodik

Leistungsmodule weisen Schalt- und Durchlassverluste auf. Dabei wird der größte Teil der elektrischen Energie in thermische Energie umgewandelt, was zu einer Erwärmung der Baugruppe während des Betriebs führt. Die Folgen sind nicht nur hohe Aufwendungen für eine effiziente Kühlung, sondern unmittelbar daraus resultierend auch signifikante Herausforderungen an die thermo-mechanische Zuverlässigkeit der genutzten Aufbau- und Verbindungstechnik derartiger Module.

3.1 Herausforderungen

Alle Aspekte der Aufbau- und Verbindungstechnik (AVT) haben die Aufgabe, die Funktionalität der Leistungsmodule unter den gegebenen Bedingungen sicherzustellen. Von dominanter Bedeutung ist hierbei die Einhaltung der vom Hersteller der Leistungsbausteine definierten Junction-Temperatur [Tj] bei möglichst großer Leistungsausbeute sowie die Sicherstellung der Stromlastfähigkeit über die Lebensdauer der Module.
Wesentliche Einflussgrößen sind hierbei die eingebrachte Leistung, die Kühlbedingungen, die Materialien im Kühlpfad sowie ein geringer elektrischer Widerstand in Durchflussrichtung.

3.1.1 Untersuchungsobjekt

Exemplarisch beschrieben wird die entwickelte Methodik an einem Konzeptdemonstrator, welcher im Verbundprojekt „KoLibri“ entwickelt und genutzt wurde. Der Demonstrator ist eine klassische Halbbrücke, bei der die Leistungsdioden auf ein DCB-Substrat gelötet (SAC-Lot) und mittels Dickdrahtbonds kontaktiert sind (Fig. 1).

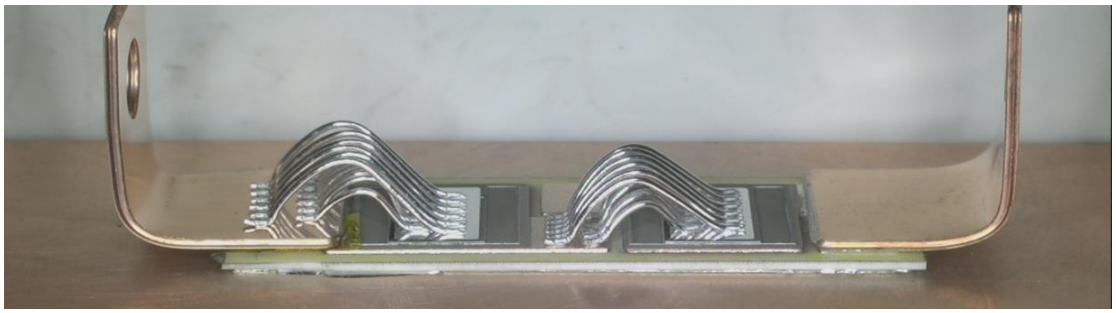

Fig. 1
Konzeptdemonstrator (Projekt „KoLibri“)

3.1.2 Schwachstellenermittlung

Zur Ermittlung von Schwachstellen in der AVT werden Leistungselektronik-Baugruppen standardisierten Tests unterzogen. Dabei werden sie unter gleichbleibenden Testbedingungen zeitlich konstant ein- und ausgeschaltet (z.B. 3s T_{on} / 6s T_{off}), wobei sich um die Leistungsbauelemente herum durch die generierte Verlustleistung periodisch ein Temperaturfeld ausbildet. Der dadurch generierte thermische Mismatch stresst die Komponenten der AVT im unmittelbaren Umfeld der Leistungsbauelemente und führt zum allmählichen Versagen.
Typische Schwachstellen für den betrachteten Aufbau sind Die-Attach-Versagen und Wirebond-Versagen (Abheber).
Die-Attach-Versagen wird durch den thermisch induzierten Mismatch zwischen Substrat und Chip (Die) verursacht. Dieser Mismatch bewirkt eine allmähliche Zerrüttung des Attach-Materials und damit eine Reduzierung der effektiven wärmeleitenden Fläche. Im Test äußert sich dies durch die allmähliche Erhöhung Junction Temperatur Tj (Fig. 2 blaue Linie).
Wirebond-Versagen wird durch den thermisch induzierten Mismatch zwischen Wirebond und der Die-Metallisierung verursacht. Dieses bewirkt eine fortschreitende Rissbildung im Bondfuß-Interface.
Ermittelt wird dieser Schadensmode über die sprunghafte Erhöhung elektrischen Widerstandes in Durchflussrichtung (Fig. 2 orangene Linie).

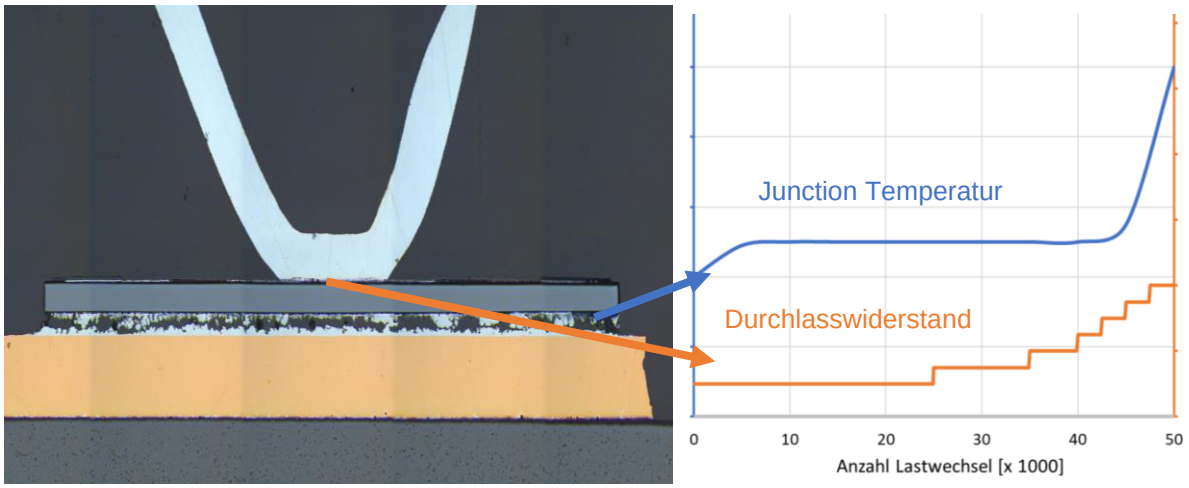

Fig. 2
Typische Versagensmodi drahtgebondeter Leistungsaufbauten und deren Ermittlung im Test

Die Schädigungsentwicklung für beide Schadensmodi ist dabei nicht linear über den Testverlauf, sondern exponentiell zum Ende hin steigend. Man erhält somit erst eine messbare Abweichung von den Soll-Messwerten, wenn das Leistungsmodul bereits kurz vor dem Versagen steht. Für den Praxiseinsatz ist dies ungenügend.
Die Herausforderung war somit, eine Methodik zu entwickeln, welche eine deutlich genauere Abschätzung der Restlebensdauer unter definierten Lastbedingungen erlaubt.

3.2 Prinzipielle Vorgehensweise

Grundlage der verwendeten Methodik ist zunächst die Simulation des thermischen und des thermomechanischen Verhaltens des Leistungsmoduls. Dabei kommt eine langjährig bewährte kombinierte experimentelle-simulative Methode zum Einsatz, mit deren Hilfe die numerischen Simulationen experimentell überprüft und somit vertrauenswürdig gemacht werden. Dieser Schritt ist unerlässlich, da die Simulationen viele potentielle Fehlerquellen enthalten (notwendige geometrische Vereinfachungen, hochgradig nichtlineares Materialverhalten, Bewertungsmethodik).
Im zweiten Schritt können weitere, für den Designprozess wichtige Bewertungskriterien hinzugezogen werden. Das vereinfachte Verhaltensmodell wird mittels Parametervariation für einen definierten Parameterraum erzeugt und mittels standardisierter Schnittstelle zur externen Nutzung zur Verfügung gestellt. Zusammengefasst sind diese Schritte in Fig. 3.

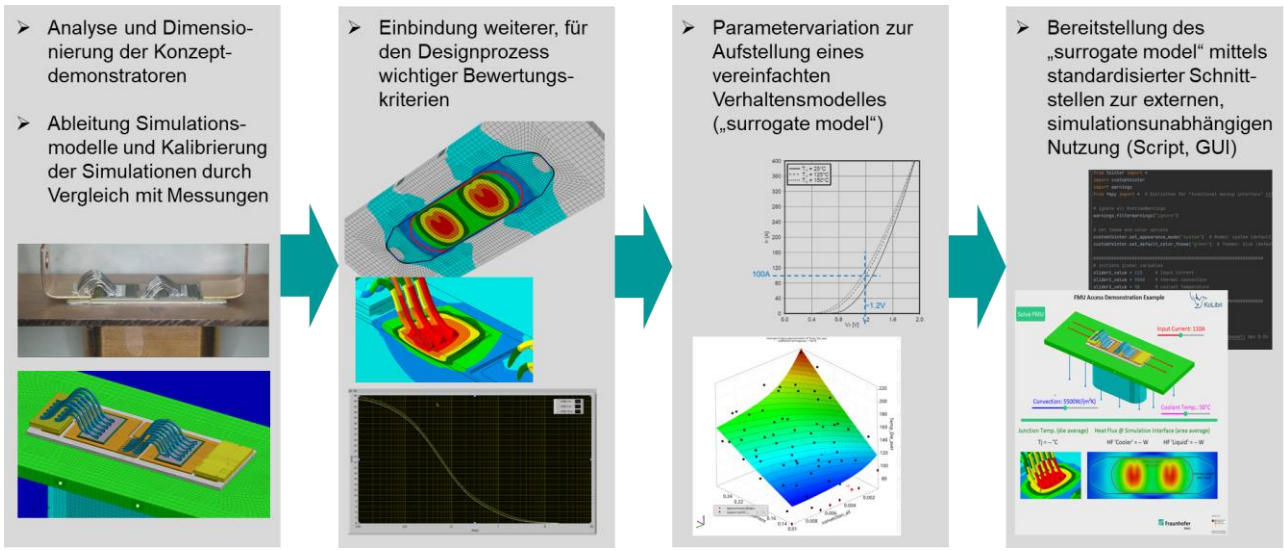

Fig. 3
Wesentliche Schritte zur Aufstellung eines vereinfachten Verhaltensmodelles

3.2.1 Bewertung der thermo-mechanischen Zuverlässigkeit

Der prinzipielle Ablauf der simulativen Ermittlung der thermo-mechanischen Zuverlässigkeit ist in Fig. 4 dargestellt.

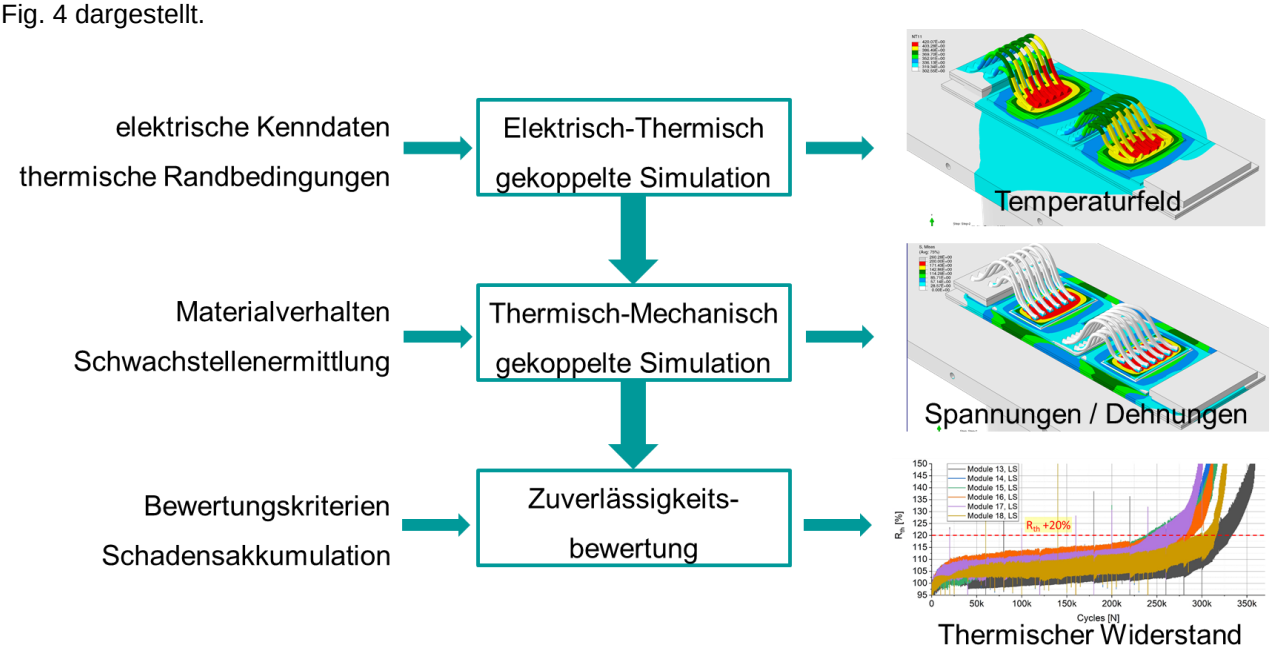

Fig. 4
Ablauf der Bewertung der thermo-mechanischen Zuverlässigkeit

Zunächst erfolgt eine elektro-thermisch gekoppelte Simulation, um das sich ausbildende Temperaturfeld örtlich und zeitlich ausreichend genau zu bestimmen. Dieses Temperaturfeld wird in die thermo-mechanische Simulation eingekoppelt, und die zur Schadensbewertung notwendigen physikalischen Parameter zu ermitteln. Im letzten Schritt müssen die Schädigungsmodi mittels geeigneter Modelle zur Abschätzung der Lebensdauer bewertet werden.
Exemplarisch wird dies hier am Beispiel des Die-Attach-Versagens dargestellt (Fig. 5).
Die Lebensdauer wird anhand von Temperatur-Zyklen Nf angegeben, welche mittels Manson-Coffin-Beziehungen aus der akkumulierten Kriechdehnung und Kriechenergiedichte für SAC ermittelt werden. Da Weichlot ein zeitabhängiges, kriechendes Materialverhalten aufweist, variieren die Manson-Coffin-Koeffizienten in Abhängigkeit von den Belastungsbedingungen. Diese müssen in aufwändigen Versuchsreihen ermittelt werden und sind für die schnellen Temperaturtests noch Gegenstand der Forschung.

SAC 378/305

Manson-Coffin/ Morrow

$$N_f = c_1(\Delta\varepsilon_{cr})^{-c_2}$$

$$N_f = c_3(\Delta Wcr)^{-c_4}$$

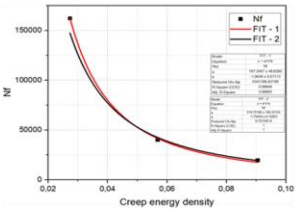

c_1	c2	c3	c4	
4.5	1.295	345	1.02	Standard TST
0.055	2.3	200	1.86	APC, preliminary

Fig. 5
Ermittlung der Lebensdauer eines Die-Attach-Verbundes mit SAC-Lot

3.2.2 Einbindung weiterer, für den Designprozess wichtiger Bewertungskriterien

Neben der thermischen Performance und der thermo-mechanische Zuverlässigkeit der Leistungsmodule können während des Designprozesses noch weitere Bewertungskriterien berücksichtigt werden. Ein Beispiel dafür ist die Ermittlung der Umweltbilanz für Herstellung, Betrieb und Entsorgung von Produkten, welche in zunehmendem Maße gefordert werden. Im KoLibri-Projekt wird dies exemplarisch am Beispiel der Substitution der Kupfer-Baseplate durch Schaum-Werkstoffe untersucht (Fig. 6).

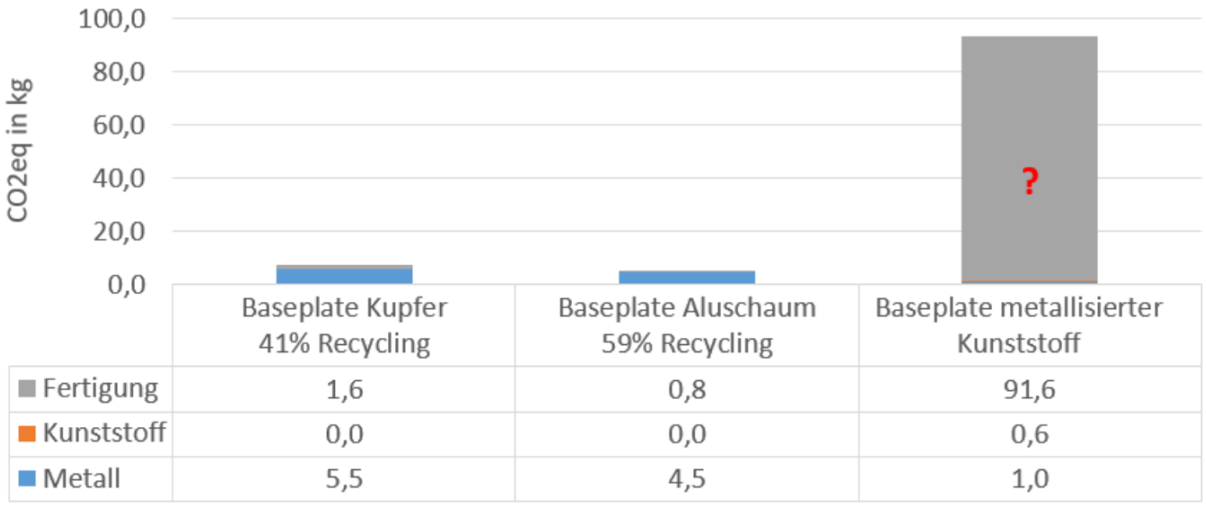

	Baseplate Kupfer 41% Recycling	Baseplate Aluschaum 59% Recycling	Baseplate metallisierter Kunststoff
Fertigung	1,6	0,8	91,6
Kunststoff	0,0	0,0	0,6
Metall	5,5	4,5	1,0

Fig. 6
Vergleich der Treibhausgasemissionen bei äquivalenter Kühlleistung und 1 kg Ausgangsmasse „cradle to grave“ (Quelle: Berechnungen der TU Dresden, Institut für Leichtbau und Kunststtofftechnik)

4 Exemplarische Umsetzung

Das vereinfachte Verhaltensmodell wird mittels Parametervariation unter Nutzung der Response-Surface-Methode erzeugt. Um das darin gebündelte Fachwissen den Entwicklern zur Verfügung stellen zu können, muss das Modell mittels einer standardisierten Schnittstelle ansprechbar sein.
Hierfür wurde das „Functional Mockup Interface“ (FMI) genutzt. FMI ist ein freier Standard, der einen Container und eine Schnittstelle für den Austausch von dynamischen Simulationsmodellen mit einer Kombination aus XML-Dateien, Binärdateien und C-Code definiert. Er wird von über 170 Tools unterstützt und als „Modelica Association Project“ gepflegt.
In Fig. 7 ist exemplarisch die Einbindung des im Kolibri-Projekt erstellten vereinfachten Verhaltensmodells in Form einer „Functional Mockup Unit“ in eine Python-GUI dargestellt.

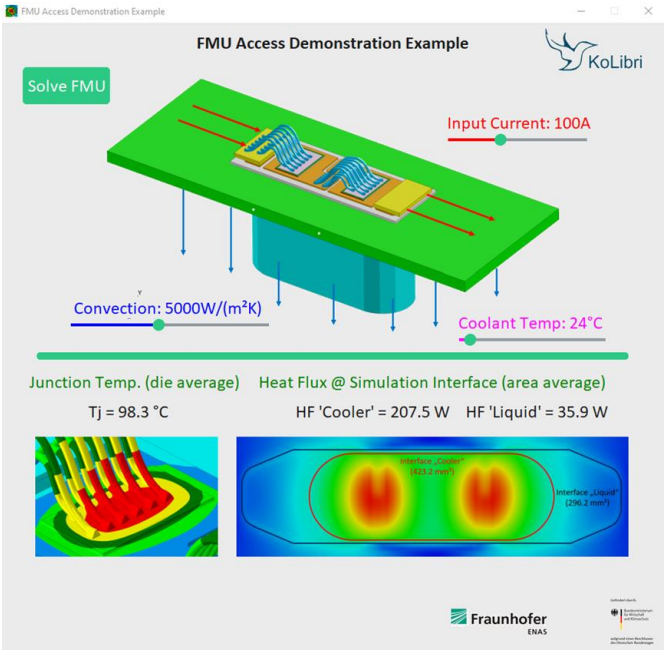

Fig. 7
Einbindung des vereinfachten Verhaltensmodells in eine GUI

5 Schlussfolgerungen und Ausblick

Die vorgestellte Methodik gewährleistet neben der Bewertung der thermischen Performance auch die Beurteilung der thermomechanischen Zuverlässigkeit von Leistungsmodulen. Gerade der zweite Punkt ist eine notwendige Ergänzung, welche bisher noch wenig berücksichtigt werden konnte. Die Möglichkeit, weitere Bewertungskriterien einzubinden und die Ergebnisse in Form vereinfachter Verhaltensmodelle zur Verfügung zu stellen, komplettieren die Methodik.
Es ist jedoch festzustellen, dass die Entwicklung der Methodik keinesfalls abgeschlossen ist. Sie beinhaltet ein breites Spektrum an Expertenwissen, welches einer ständigen Neubewertung bedarf.
Perspektivisch soll die Methodik bei der Entwicklung digitaler Zwillinge zum Einsatz kommen.

6 Referenzen

[1] Rainer Dudek, Ralf Döring, Anu Mathew, Sven Rzepka, “Modelling thermal fatigue in power electronics based on strength- and damage criteria”, 8th European Expert Workshop on Reliability of Electronics and Smart Systems, Berlin Oct. 13 - Oct. 14, 2021

7 Danksagung

Die hier vorgestellten Arbeiten wurden zum großen Teil im Rahmen des durch das Bundesministerium für Wirtschaft und Energie geförderten Projekts „KoLibri“ FKZ 03LB3039F (Komplexe Leichtbaustrukturen für elektronische Anwendungen innerhalb der Mobilität) durchgeführt.
Mein Dank gilt allen Projektteilnehmer, die durch ihre Zuarbeit diese Arbeiten ermöglicht haben, insbesondere jedoch Christian Walbrecker-Baar von der Siemens AG München und Pauline Langbehn von der iPoint-systems gmbH Hamburg.

Beispiele zur Demokratisierung der Simulation

Ralf Paßmann (systemworkx AG)

1 Summary (Überschrift 1)

Die Simulation - d.h. die digitale Darstellung der Herstellung, des Gebrauchs und des Betriebs von Produkten in der Struktur-, der Fluidmechanik oder des Elektro-Magnetismus - hat eine hohe Bedeutung in der Produktentwicklung. Der Einsatz der Simulation wächst besonders in den letzten Jahren rasant. Ein wesentlicher Teil dieser Simulationen wird durch speziell geschulte Berechnungs-Ingenieure erbracht. Heutzutage wächst die Kritik an dem bestehenden System der Trennung von Konstruktion und Simulation. So wird die getrennte Abarbeitung als zeitraubend und für die Lösungsfindung störend empfunden.
Aufbauend auf der NAFEMS Definition zur Demokratisierung der Simulation und einer kurzen Darstellung bestehender Lösungen will dieser Beitrag Konzepte einer Demokratisierung vorstellen und diskutieren. Als Beispiele wurden das generative Design und der geführte Berechnungsprozeß ausgewählt. Beide Beispiele werden mittels der 3DEXPERIENCE Plattform der Dassault Systèmes erstellt. Es sollen so mögliche Wege zur Demokratisierung der Simulation und der zukünftigen Rolle des Berechnungs-Ingenieurs aufgezeigt werden.

2 Demokratisierung der Simulation

2.1 Einleitung

In diesem Beitrag wird vorausgesetzt, daß die Simulation (z.B. der Mechanik, der Fluiddynamik, des Elektro-Magnetismus) ein wesentlicher und nützlicher Bestandteil des Produktentwicklungsprozesses ist.

Zur Demokratisierung der Simulation finden sich in der Literatur viele verschiedene Begriffe, wie z.B.:

- Demokratisierung
- Konstruktions-integrierte Simulation
- Simulation-Driven Design
- CAD-integrierte Werkzeuge
- template-based customizations/apps
- designer-driven analysis
- Simulation-Based Design
- simulation-driven product development.

Gemeint ist damit fast immer die Durchführung von Simulationen direkt durch den Konstrukteur. Eine konstruktions-integrierte Simulation gibt es bereits seit den 1980er Jahren. Werkzeuge wie CATIA oder SolidWorks haben schon seit vielen Jahren eine Simulation integriert, siehe auch [1] und [2]. Innerhalb von SolidWorks greift man ebenso auf eine recht leistungsfähige Fluid-Simulation zurück. Bei diesen Lösungen wurden oft Beschränkungen verwendet, wie z.B.

- Vereinfachte Bauteil-Verbindungen
- Lineares Materialverhalten
- Beschränkung auf kleine Bewegungen und Verformungen
- Reduzierte Steuerung der Simulation.

Diese Beschränkungen erforderten in vielen Fällen eine differenzierte Betrachtung durch einen Berechnungs-Ingenieur. Die Zusammenarbeit verschiedener Abteilungen für die Konstruktion und die Simulation wird in der Literatur heute oft negativ beschrieben.

Nach [3] ist es wichtig, daß der „schöpferische und kreative“ Konstruktionsprozeß nicht unterbrochen wird. Dies geschah in der Vergangenheit durch das Warten auf Versuche oder das Warten auf die Simulation. In [4] wird die Simulations-Abteilung als ‚bottleneck‘ im Entwicklungsprozeß bezeichnet. In [5] führt der sequentielle Arbeitsablauf von Konstruktion-Simulation-Konstruktion zu ineffektiven Entwicklungsprozessen.

In den letzten Jahren gab es durch die Entwicklung der Software Systeme für die Simulation eine deutliche Verbesserung der Werkzeuge für die Simulation. Wesentliche Punkte sind dabei:

- Verbesserte Geometrie-Aufbereitung
- Automatische Vernetzung auch “schlechter” Geometrien
- Verbessertes Konvergenz-Verhalten der impliziten Solver
- Einsatz expliziter Solver für statische Problemstellungen
- Einsatz des automatischen Kontaktes zwischen Bauteilen
- Beseitigung der Schnittstellen bei Multi-Physics Anwendungen.

In [4] werden die Vorteile der konstruktions-integrierten Simulation für die Industrie anhand von Umfrage-Ergebnissen dargelegt. Hierbei wird zwischen innovativ führenden Firmen (Best-in-Class) und dem „Rest“ (All Others) unterschieden. Betont wird das „Left Shifting“, eine frühe Verifikation und Optimierung des Produktes. Ein Wechsel hin zur konstruktions-integrierten Simulation wird von vielen Firmen angestrebt. Hierdurch konnten die Firmen die Kosten und die Dauer der Entwicklungsprozesse deutlich reduzieren.

So wird nach [3] der Einsatz von Simulation im Konstruktionsprozeß deswegen besonders wichtig, da der Wechsel von einer erfahrungsbasierten zu einer wissensbasierten Entscheidung in der Konstruktion erfolgen muss. In [6] werden die Vorteile einer Konstruktions-integrierten Simulation dargestellt. Die Anforderungen an die Konstruktionsprozesse sind in einer schwierigeren Umgebung stark gestiegen. Hier ist die Konstruktions-integrierte Simulation ein Problemlöser.

Zusammenfassend werden viele Gründe für eine Demokratisierung der Simulation und somit einer Integration der Simulation in die Konstruktion genannt. Viele dieser Gründe wurden bereits vor vielen Jahren für den Aufbau von Simulations-Abteilungen verwendet. So zum Beispiel:

- Schnelleres Auffinden der optimalen Konstruktion
- Hohe Innovationsleistung durch die Betrachtung viel mehr möglicher Lösungen
- Frühere Design Entscheidungen
- Reduktion von Fehlern und Unterbrechungen
- Verkürzung von Entwicklungszeiten
- Reduktion von Entwicklungskosten.

Für viele Berechnungs-Ingenieure stellt die Nafems Ltd. [7] eine für Ihre Arbeit wichtige Organisation dar. So findet sich hier in [8] folgende Definition:

„Democratisation: A solution delivery approach which enables individuals who are not simulation specialists to execute simulations and obtain valid results within specified ranges of parameters in a managed, traceable environment, built by a simulation engineer who is responsible for the results obtained.“.

„Demokratisierung: Ein Lösungsansatz, der es Personen, die keine Simulationsspezialisten sind, ermöglicht, Simulationen durchzuführen und gültige Ergebnisse innerhalb bestimmter Parameterbereiche in einer verwalteten, nachvollziehbaren Umgebung zu erhalten, die von einem Simulationsingenieur aufgebaut wird, der für die erzielten Ergebnisse verantwortlich ist."

Als Lösung der Demokratisierung wird folglich ein geführter Prozess vorgeschlagen. Dieser Prozess wird von einem Berechnungs-Ingenieur verantwortet. Nach [9] finden sich neben diesem ‚template-based customizations/apps‘-Ansatz auch neuere Ansätze, welche folgende Anforderungen erfüllen sollen:

- die Software benötigt keine Spezialkenntnisse
- Modellaufbau sowie Simulation laufen schnell ab
- Große Toleranz gegenüber ‚schlechten‘ Geometrien
- Qualität der Simulation ist gut.

Man kann also unterscheiden in

- Automatisierte Berechnungsprozesse
- Geführte Berechnungsprozesse.

2.2 Automatisierte Berechnungsprozesse

In [10] wird das Produkt SimSolid von der Firma Altair beschrieben, Bild 1. Hier handelt es sich, zum Zeitpunkt der Verfassung dieses Textes, um ein Produkt zur Simulation der linearen und nicht-linearen Statik. Als wesentliche Vorteile werden hervorgehoben:

- Keine Geometrie-Vereinfachung durch den Verwender notwendig
- Kein Meshing durch den Verwender notwendig
- Berücksichtigung von Baugruppen, Verbindungstechnik und Kontakt
- Ergebnisse in Sekunden

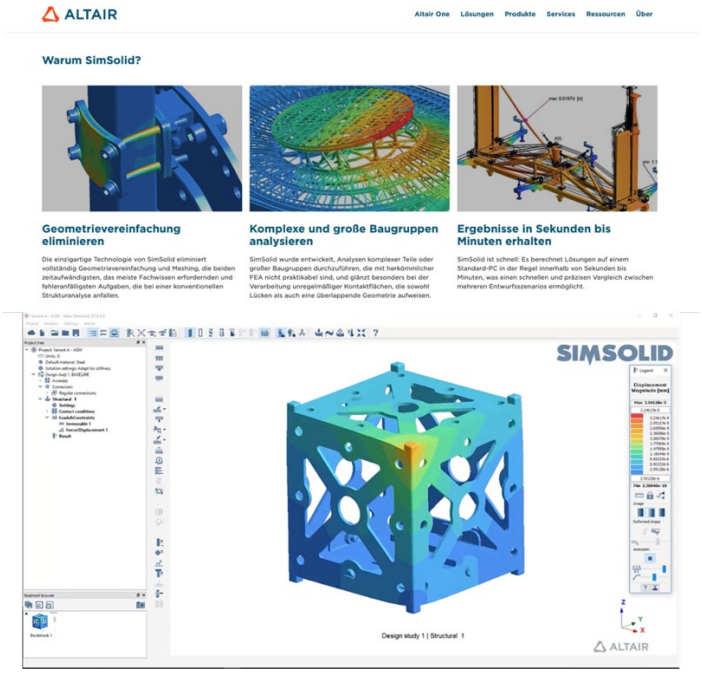

Bild 1: SimSolid aus [10]

In [9] werden verschiedene lineare Testfälle (NAFEMS Benchmarks) mit der Software SimSolid berechnet. Hierbei gibt es nur geringe Abweichungen gegenüber den Referenzlösungen.

In [11] wird die Software ANSYS Discovery vorgestellt, Bild 2. Hier werden ähnliche Vorteile, wie der Entfall der Geometrie-Vereinfachung und des Meshings genannt. Ebenso können Baugruppen, Verbindungs-technik und Kontakt berücksichtigt werden. Der Solver umfasst neben der Strukturmechanik auch die Fluidmechanik, die Berechnung des Wärmetransportes sowie gekoppelte Analysen. Die Durchführung der Simulation wird als „Live“ bezeichnet.

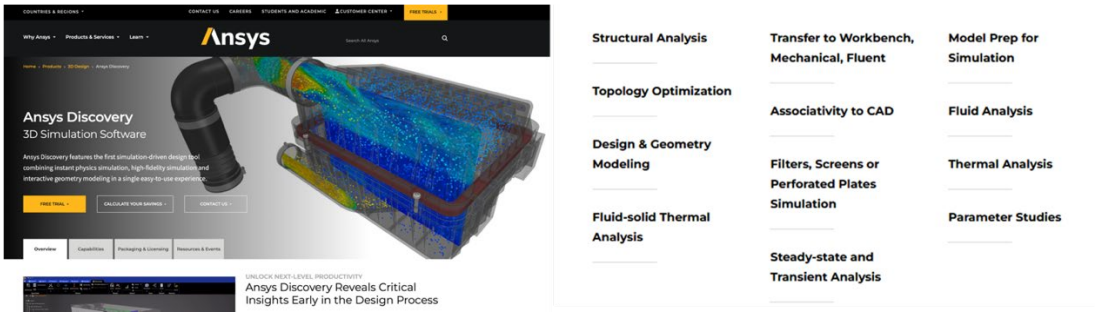

Bild 2: Ansys Discovery aus [11]

Ein ausführliche Beschreibung der Verwendung von Ansys Discovery findet sich in [3].

2.3 Geführte Berechnungsprozesse

Dassault Systèmes hat in den letzten Jahren sehr viel in die konstruktions-integrierte Simulation investiert. In [12] wird der MODSIM Ansatz von Dassault Systèmes beschrieben. MODSIM ist ein auf der 3DEXPERIENCE Plattform integrierter Ansatz, die Demokratisierung der Simulation im Sinne der

obigen NAFEMS Definition zu realisieren. Die Vorteile innovativerer Produkte in kürzeren Entwicklungszeiten sollen so leicht zu realisieren sein.
Es handelt sich hierbei aber nicht ausschließlich um geführte Prozesse, da die zur Verfügung gestellten Werkzeuge ebenso ohne Führung verwendet werden können. Dann wird aber sehr viel mehr Aufwand betrieben werden müssen. Der große Vorteil der 3DEXPERIENCE Plattform liegt in der Integration verschiedener Disziplinen, wie CAD, CAE und CAM und der Verwendung des gleichen Modells (Model Based Engineering). In dem Rahmen dieses Beitrages beschränken wir uns auf eine kurze Erläuterung. So kann im Rahmen von MODSIM der Berechnungs-Ingenieur ein Best Practice Vorgehen im Rahmen eines Templates festgehalten werden, Bild unten links. Dieses Template wird von dem Konstrukteur für die Auslegung des Produktes verwendet, Bild 3.

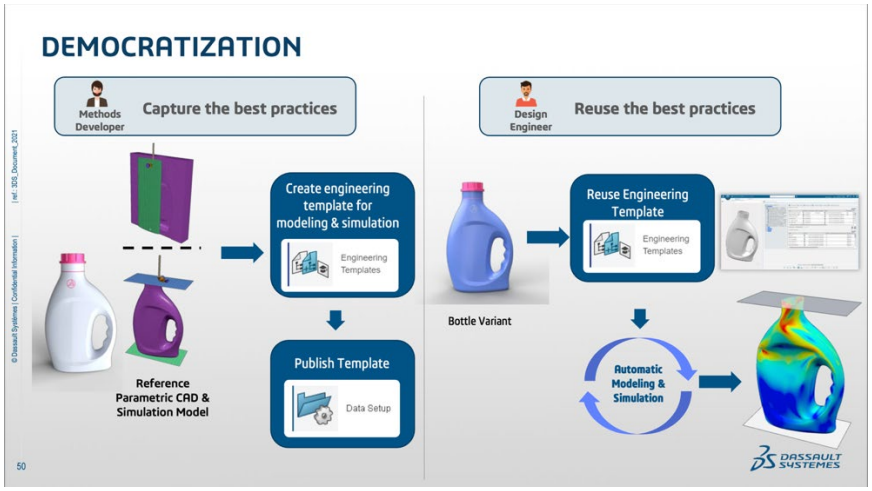

Bild 3: Demokratisierung nach [12]

Grundlage für den Ablauf von solchen Templates ist der Process Composer, mit welchem auch aufeinander aufbauende Simulationen definiert werden können, Bild unten links. Ebenso werden dem Konstrukteur die Analyse der Ergebnisse erleichtert, Bild 4.

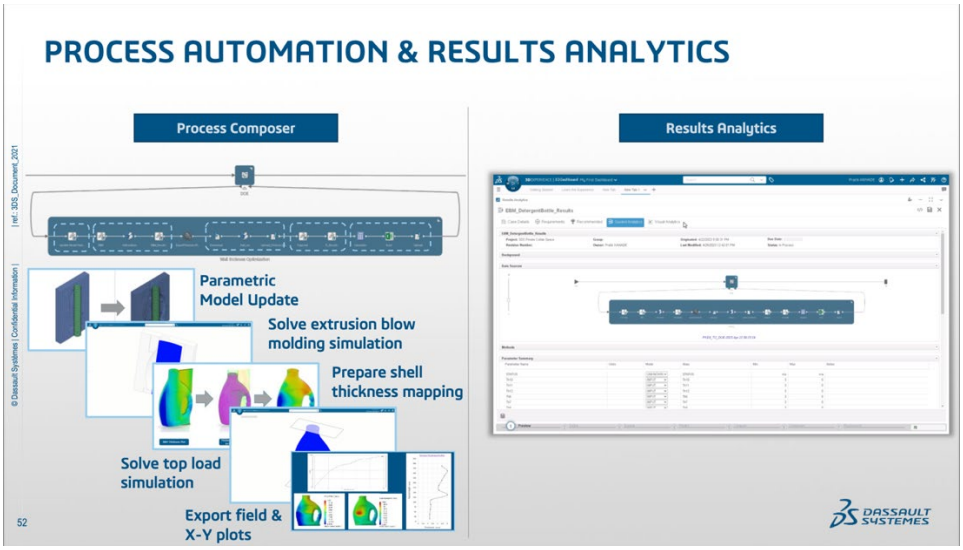

Bild 4: Geführte Prozesse nach [12]

Das Generative Design für die Strukturmechanik und die Fluidmechanik stellt eine Ergänzung dieser Idee dar. Hier sind die Simulationsprozesse zur bestmöglichen Nutzung eines vorgegebenen Bauraumes bereits voll in die Arbeit des Konstrukteurs integriert, Bild 5.

Bild 5: Generative Design für die Fluidmechanik nach [12]

3 Beispiel

Als Beispiel wird hier eine einfache Simulation eines Pumpengehäuses verwendet. Dieses Beispiel findet sich in den Schulungsunterlagen der Dassault Systèmes.

Die fertige Konstruktion eines Pumpengehäuses besteht hier aus den Komponenten Gehäuse (pump housing), Deckel (pump cover) und Dichtung (gasket), Bild 6. Es soll eine einfache lineare Analyse des Verhaltens unter Innendruck durchgeführt werden. Hierzu wird die App ‚Linear Structural Validation' verwendet.

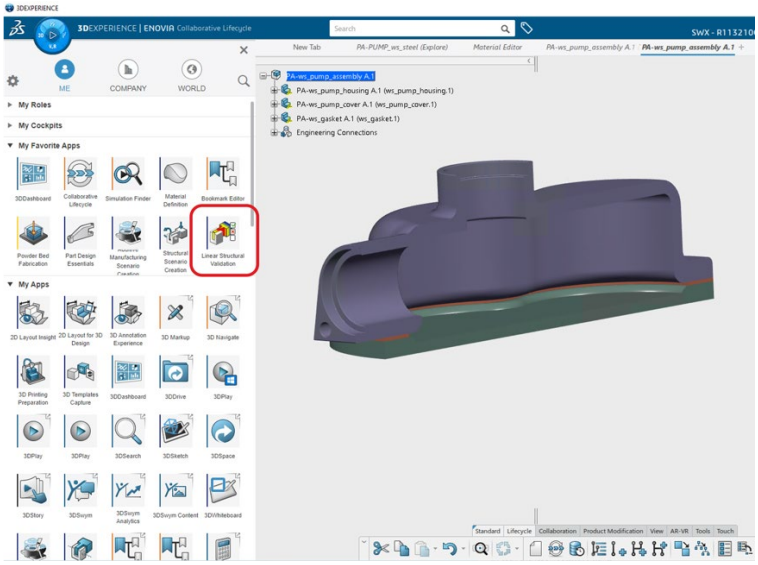

Bild 6: Fertige Konstruktion eines Pumpengehäuses

Bei Starten der App entscheidet der Benutzer, welche Art von Analyse er durchführen will. Zur Auswahl stehen eine Struktur-, eine Beul-, eine Frequenz- und eine thermische Analyse, Bild 7.

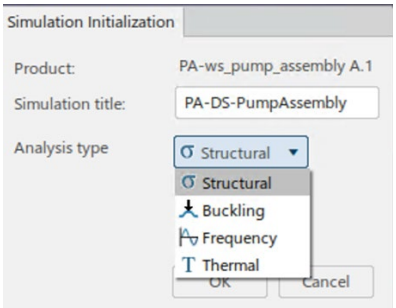

Bild 7: Auswahl der Analyse

Beim Öffnen der App erscheint ein Assistent zur weiteren Bearbeitung, Bild 8. Die Übernahme der CAD Daten für die einzelnen Parts und deren Positionierung erfolgt automatisch. Die mit einem roten Kreis markierten Punkte müssen bearbeitet werden. Die Definition von Kontakt und Verbindungstechnik ist optional, bei diesem Beispiel mit mehreren Bauteilen aber notwendig. Die mit einem roten,

durchgestrichenen, Kreis markierten Punkte können erst bearbeitet werden, wenn die vorherigen Punkte erfolgreich abgeschlossen wurden.

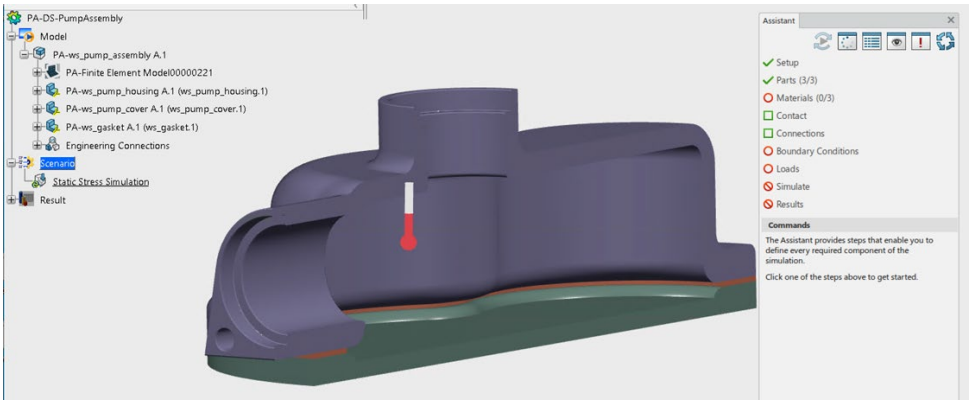

Bild 8: Assistent für die Durchführung der Simulation

Wählt man einen Arbeitspunkt an, so erscheinen im unteren Teilbild verschiedene Commands, welche die Bearbeitung des Punktes erleichtern. In dem Bild 9 ist die Zuteilung von Materialien für die einzelnen Komponenten dargestellt.

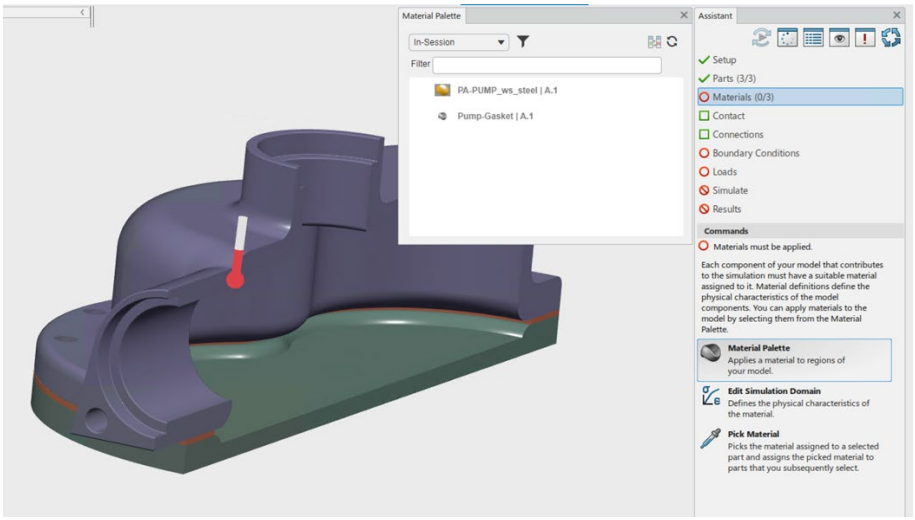

Bild 9: Aufgaben für die einzelnen Arbeitspunkte

Am Ende des Prozesses steht die Durchführung der Simulation und die Auswertung der Ergebnisse, Bild 10.

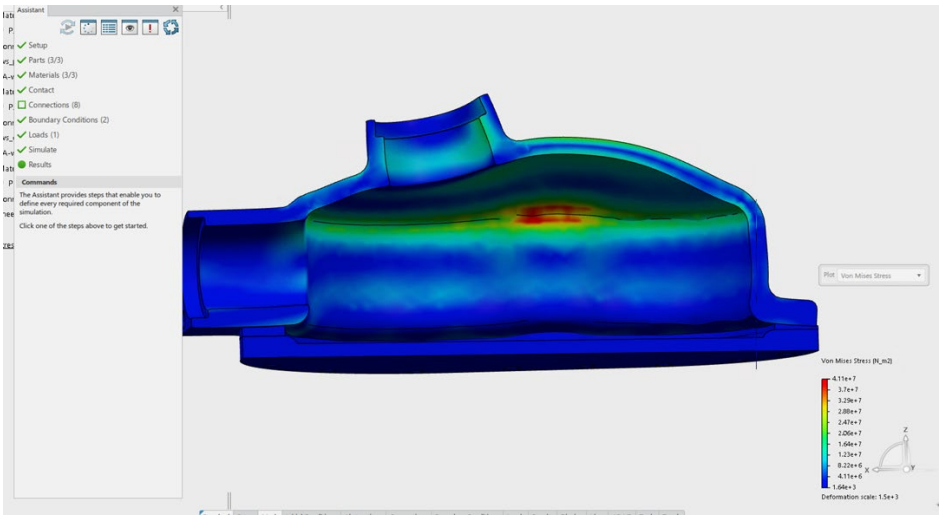

Bild 10: Von Mises Spannungen bei Belastung

4 Conclusions

In der Literatur finden sich genügend Argumente für eine deutliche Stärkung der konstruktionsintegrierten Simulation. Die Demokratisierung der Simulation führt zu besseren Produkten in kürzeren Entwicklungsprozessen.

Die Software-Hersteller stellen dafür die notwendigen Werkzeuge bereit, wobei zwischen geführten und neueren/automatisierten Berechnungsprozessen unterschieden werden kann.

5 References (Überschrift 1)

[1] "CATIA™ V5 Portfolio - Dassault Systèmes® 3D Software" [Online]. Available: https://www.3ds.com/products-services/catia/products/v5/portfolio/. [Accessed: 18-Jun-2023].

[2] Dassault Systèmes SOLIDWORKS, 2018, *AUSSAGEKRÄFTIGE SIMULATIONEN VERBESSERN DIE PRODUKTENTWICKLUNG*, Dassault Systèmes.

[3] Brand, M., Baur, K., Brunner, S., and Gebhardt, C., 2020, *Physik begreifen – besser konstruieren*, Springer Berlin Heidelberg, Berlin, Heidelberg.

[4] Cline, G., 2017, *THE BENEFITS OF SIMULATION-DRIVEN DESIGN*, ABERDEEN GROUP.

[5] Karlsson, L., Pahkamaa, A., Karlberg, M., Löfstrand, M., Goldak, J., and Pavasson, J., 2011, "Mechanics of Materials and Structures: A Simulation-Driven Design Approach," J. Mech. Mater. Struct., **6**(1–4), pp. 277–301.

[6] Jackson, C., *The Four Benefits of Simulation-Driven Design*, Lifecycle Insights.

[7] Nafems Ltd., "NAFEMS Engineering Modelling, Analysis, Simulation Community," NAFEMS [Online]. Available: https://www.nafems.org/. [Accessed: 23-Sep-2023].

[8] "NAFEMS - Glossary Terms D-I" [Online]. Available: https://www.nafems.org/publications/glossary/terms_d-i/. [Accessed: 28-Jun-2023].

[9] Symington, I., 2020, "Designer Oriented Software - Is It Accurtae? Part 1," NAFEMS Benchmark Magazine, (Januar 2020).

[10] "Strukturanalyse Für Schnelle Designiterationen | Altair SimSolid" [Online]. Available: https://www.altair.de/simsolid/. [Accessed: 28-Jun-2023].

[11] "Ansys Discovery | 3D Product Simulation Software" [Online]. Available: https://www.ansys.com/products/3d-design/ansys-discovery. [Accessed: 28-Jun-2023].

[12] Popielas, F., 2022, "Introduction TO MODSIM."

[13] systemworkx AG, "Home - PLM Blog & Knowledge Center - Simulation, etc.," PLM Blog & Knowledge Center [Online]. Available: https://plm.systemworkx.de/. [Accessed: 01-Oct-2023].

„Was ist es, was die Welt (der Simulation) im Innersten zusammenhält?“

– der Medici-Effekt in der Simulation

Dipl.-Ing. Maydi Stuhlmann–El Sharif, Dr.-Ing. Martin Küssner

TECHNIA GmbH

1 Zusammenfassung

Es gibt nicht den „einen“ digitalen Zwilling in der Simulation. Die Zwillinge innerhalb der „Simulationsfamilie“ unterscheiden sich durch die Art der Abstraktion und der Physik, die sie repräsentieren. Faszinierend sind die neuen Möglichkeiten, diese verschiedenartigen digitalen Zwillinge assoziativ zu verbinden – und somit eine automatisierte Ansatzraumerkundung über die verschiedenen Abstraktionsarten und -stufen hinweg zu ermöglichen. Der als „Medici-Effekt“ bezeichnete Ansatz beschreibt ganz allgemein das riesige Potenzial für neue innovative Ideen beim Aufeinandertreffen von unterschiedlichen Disziplinen und Kulturen. Es wird gezeigt, wie ein sorgfältig gesponnen digitaler Faden zwischen den verschiedenen digitalen Zwillingen den „Medici-Effekt“ in der Simulation ermöglicht.

2 Einführung

Die Familie Medici stammt aus Florenz, ihr Wohlstand gründete sich auf Textilhandel und später auf das Bankenwesen. Ihre einflussreiche Dynastie währte vom fünfzehnten bis zum achtzehnten Jahrhundert, aus ihr gingen unter anderem drei Päpste, zwei französische Königinnen und viele toskanische Großherzöge hervor.

Uns bleiben die Medicis aber hauptsächlich durch ihre Prägung der Kulturepoche der Renaissance präsent. Doch wie muss man sich diese Prägung vorstellen? Baute Cosimo de‘ Medici eigenhändig den Palazzo Medici Riccardi?

Fig. 1
Der Palazzo Medici Riccardi,
erbaut 1444-1458
Quelle: Wikipedia

Natürlich nicht – die Medicis gaben aber Geld, damit Künstler unterschiedlicher Hintergründe gemeinsam Neues erschaffen konnten. Der Schlüsselwörter des Erfolgs der Medicis sind hier also „*unterschiedliche Hintergründe*“ und „*gemeinsam Neues*“.

Diese Schlüsselwörter aufgreifend veröffentliche Frans Johannson im Jahr zweitausendvier ein Buch, das eines der Standardwerke der Innovationskultur und deren Verankerung in Unternehmen und Organisationen werden sollte: „The Medici Effect“ [1]. Der Autor erklärt, wie innovative Ideen genau dann entstehen, wenn Fachleute *unterschiedlicher Hintergründe gemeinsam* an einer Problemlösung arbeiten. Und weil die Medicis bereits vor sechshundert Jahren diesem Prinzip gefolgt sind, nannte Johannson es den „Medici-Effekt“.

Welche Unternehmenskultur führt zu einem „Medici-Effekt“ in der digitalen Wertschöpfung und welche Rolle spielt die Simulation hier?

3 Die Rolle der Simulation bei der digitalen Wertschöpfung

Auf numerischer Mathematik basierende Simulationswerkzeuge werden seit mehr als einem halben Jahrhundert produktiv in der Wertschöpfungskette eingesetzt. Selbstredend passiert dies mit wachsender Genauigkeit, stets mit sich ausbreitenden Anwendungsgebieten und Methoden und einer Akzeptanz, deren Grenzen noch nicht absehbar sind. Waren bei Ray W. Clough, dem „Vater“ der Finiten Elemente, in den sechziger Jahren noch strukturmechanische Probleme im Vordergrund, sind heute Simulationen im Bereich Fluide, Akustik, Elektromagnetismus und vielem mehr möglich.

In diesem Zusammenhang wird oft der Begriff „Digitaler Zwilling“ verwendet. Bei der Breite der Anwendungen der Simulation ist klar, dass es nicht nur den „einen“ digitalen Zwilling gibt. Beim Finite-Elemente-Spannungs-Zwilling wird das Deformationsverhalten auf einer "Lego-Stein-Ebene" ermittelt und das globale Ergebnis aus der Gesamtheit der Lego-Stein-Ergebnisse abgeleitet. Ein Mehrkörper-Dynamik-Zwilling wird durch meist ideal starre Teile abgebildet, die wiederum durch Gelenke verbunden sind. Ganz anders der System-Simulations-Zwilling: Hier werden Systeme und Subsysteme nur durch ihr Verhalten und nicht durch ihre 3D-Repräsentierung abgebildet. Auch die Skalen haben sich erweitert – Simulationen gibt es nicht mehr nur auf der Makroskala, auch auf Meso- und Mikroskalen wird simuliert, selbst Simulationen auf atomarer Ebene sind möglich. Zwillinge, soweit das Simulationsauge reicht…

Soweit bekannt und seit Jahren in der Praxis erfolgreich praktiziert, für alle wesentlichen Bereiche gibt es Erkenntnisse, die auf Simulationen beruhen. Eigentlich großartig – sind wir also in Sachen Simulationstechnik am Ziel? Trotz all der Fortschritte noch lange nicht, es fehlt oft noch die Verbindung der Zwillinge, die Assoziativität zwischen Disziplinen und Abstraktionsebenen und die Einbindung in den Kontext der gesamten Wertschöpfung.

4 Simulation im Kontext

Das Aufgabengebiet der „Simulanten“ hat sich mit der Einführung der durchgehenden digitalen Wertschöpfung verändert. Früher waren die Simulationsexperten wie Schrankenwärter – wenn die Spannungen unterhalb eines kritischen Limits waren, wurde das Modell als genehmigt durchgewunken. Waren die Spannungen oberhalb des erlaubten Grenzwerts, blieben die Schranken unten, und der Entwurf wurde an die Konstruktion zurücküberwiesen.

Heute ist die Simulation fest verwoben mit der Konstruktion und im Zentrum der digitalen Wertschöpfung. Auch Simulationen, die früh in der Konstruktionsphase zur Anwendung kommen und daher vielleicht nur qualitative statt quantitative Aussagekraft besitzen, sind ein wichtiger Teil der digitalen Wertschöpfung. Bei der TECHNIA nennen wir dies „Simulation im Kontext“, was bedeutet: Simulation ist keine isolierte Disziplin mehr! „Simulation im Kontext“ impliziert aber nicht nur die Integration der Simulation in die Konstruktion, sondern auch die Integration des Simulationsprozesses in die Wertschöpfungskette, inklusive der Nachverfolgbarkeit der Ergebnisse.

Beispiel: Was ist der Wert eines Spannungsplots, wenn er nicht im Kontext der Problemstellung abgelegt ist, die diese Spannungen hervorgerufen haben? Was ist der Wert, wenn die zugeordneten Lasten, Randbedingungen oder Materialien nicht mehr nachträglich ermittelt werden können? Man kann diesen Spannungsplot mit einer Krankenakte vergleichen – die Ergebnisse aller medizinischen Tests sind detailliert vermerkt, aber der Wert ist nichtig, wenn der Name des Patienten fehlt …. Ein Spannungsplot, der nicht eindeutig der Problemstellung und Variante zuzuordnen ist, ist so wertvoll wie eine Krankenakte ohne Namen. Die Simulation in einer Schrankenwärterfunktion brauchte die Nachverfolgbarkeit noch nicht, für die Simulation im Kontext der digitalen Wertschöpfung ist die Nachverfolgbarkeit zwingend notwendig.

5 „It is all about the process'' – Wertschöpfung auf einer Business Platform

Kommen wir zurück zu den Medicis: Damals engagierten sie Maler und Architekten – aber nicht, damit der Maler ein Bild malt oder dass der Architekt ein Haus baut, sondern dass der Maler und Architekt zusammen ein Haus bauen, um *gemeinsam Neues* zu schaffen.

Zurück zum Heute: Wie wird ein Smartphone entwickelt? Für den Anwender ist ein Telefon ein Computer mit Hard- und Software, für die Entwickler aber ist es u.a. ein Struktur-, ein Wärmeleitungs-, ein Batterieladungs-, ein Brandschutzproblem. Zudem gibt es Herausforderungen hinsichtlich der elektromagnetischen Verträglichkeit, des Recyclings, der Kosten, der Produktion, der Regularien und vielem, vielem mehr.

Um ein Smartphone marktfähig zu entwickeln, müssen verschiedene Expertenteams zusammenarbeiten – um *gemeinsam Neues* am „Kunstwerk Smartphone" zu schaffen. Ganz im Sinne von Johannson kann man sagen, dass Innovation aus der Synergie verschiedener Disziplinen entsteht. Jedes Strukturdetail eines Smartphones hat Einfluss auf die strukturelle Integrität, aber auch auf den Wärmehaushalt, auf die elektromagnetische Abstrahlung und auf die Kosten usw. „Die Vernetzung mit allen Beteiligten – von der Ideenfindung über die Konstruktion bis hin zur Fertigung und darüber hinaus – ist unabdingbar" [2]. Nur durch ein disziplinübergreifendes *Gemeinsam* entsteht *Neues. Alleine* verweilen wir im Verbessern.

Die Vernetzung aller Beteiligten und aller Disziplinen erfordert ein Format, das erlaubt, assoziativ und in Echtzeit im Team *gemeinsam* an einer digitalen Wertschöpfung zu arbeiten. Es erfordert eine Business Plattform, die als „Betriebssystem" der digitalen Wertschöpfung agiert, und die die Entwickler zum „Gemeinsam" führt, aus dessen Synergie Neues ersteht. „3DEXPERIENCE von Dassault Systémes ist eine Unternehmens- und Innovationsplattform, die Unternehmen eine ganzheitliche Echtzeitansicht ihrer Geschäftsprozesse und des gesamten Ökosystems bietet. Sie verbindet Menschen, Ideen, Daten und Lösungen in einer einzigen kollaborativen Umgebung und bietet Unternehmen – von Start-ups bis zu großen Unternehmen – völlig neue Möglichkeiten für Innovation, Produktion und Handel." [3].

Eine Business Plattform ist also nicht auf die Simulation beschränkt, es geht auch um Konstruktion, Anforderungsmanagement, Produktion, Dokumentenmanagement und alles andere, was wir bisher als Silos aus der Produktentwicklung kennen – diesmal eben nur in einer einheitlichen, assoziativen Plattform integriert. Konkret heißt das Arbeiten auf einer Business Plattform, dass alle an der Entwicklung Beteiligten auf das gleiche Datenmodell zugreifen können – die „single source of truth", Rückgriff auf die eine Wahrheit des jeweiligen Entwicklungsstands.

Die Suche nach der Wahrheit war auch dem Doktor Faust aus Goethes Hauptwerk ein Anliegen – so sehr, dass er einen Pakt mit dem Teufel schloss, um herauszufinden, „was die Welt im Innersten zusammenhält". Wir müssen heute keinen Pakt mit dem Teufel schließen, um herauszufinden, was die Welt der Simulationen im Innersten zusammenhält – alles, was man heute braucht, ist eine Business Plattform für die digitale Wertschöpfung. Dort sind alle Informationen assoziativ mit dem Datenmodell (der „Wahrheit") verbunden, sodass automatisch jede Änderung auf alle abgeleiteten Modelle kaskadiert.

Natürlich will der Strukturmechaniker das Smartphone besonders widerstandsfähig machen, der Elektrotechniker die ungewollte elektromagnetische Emission am liebsten ganz unterdrücken und der Controller die Kosten halbieren. Gefragt ist hier eine Mehrzieloptimierung, ein Abwägen zwischen den unterschiedlichen Zielen. Diese Mehrzieloptimierung kann – sofern man auf einer Business Plattform arbeitet und keinen Bruch in der Datenkette braucht – auch automatisiert erfolgen. Eine vollumfängliche Erkundung des Ansatzraums mit der Berechnung der Sensitivitäten der beteiligten Eingabegrößen sind heute schon auf einer Business Plattform Stand der Technik.

6 Der Medici-Effekt: Mensch und Technik

Ein Smartphone als „Gesamtkunstwerk“ zu entwickeln, um bei dem Beispiel der Medicis zu bleiben, braucht also das Zusammenspiel von drei Faktoren

- exzellente Simulationswerkzeuge in den jeweiligen Disziplinen und notwendigen Abstraktionsstufen
- eine Business Plattform zur Zusammenführung aller Disziplinen wie Konstruktion, Simulation, Produktionsplanung und vielem mehr
- und Menschen, die bereit sind, im Team zu arbeiten.

Jedes dieser Faktoren ist essenziell wichtig für den Erfolg – aber im Zentrum eines jeden Erfolgs stehen die daran beteiligten Menschen. In einem erfolgreichen Prozess der digitalen Wertschöpfung kann es nur noch Teamplayer geben. Vorbei sind die „Berechnungssilos“ der Schrankenwärter, vorbei sind aber auch die abgekapselten Teams – „Digitalisierung“ kann man mit Recht als einen Prozess bezeichnen, der in allererster eine Frage der Haltung aller Beteiligten ist, bevor wir überhaupt von der technischen Umsetzung reden [4].

7 Zusammenfassung

Die Digitalisierung ist in aller Munde – sie wird zurecht als Epoche prägend bezeichnet, ähnlich der Elektrifizierung in der Mitte des vorvergangenen Jahrhunderts. Auch damals gab es Skeptiker – Industriemagnaten, die mit Kohle großen Wohlstand erwirtschaftet hatten und die mit Skepsis auf die Elektrizität als Ersatz blickten. Die Firmen dieser Skeptiker sind im ausgehenden vorvergangenen Jahrhundert geradezu implodiert.

Ähnlichkeit zu heute: Firmen, die den Wert einer Datenkette ohne Brüche nicht wertschätzen, werden es schwer haben wie die Firmen der Kohle-Barone im neunzehnten Jahrhundert. Die Digitalisierung wird alle Bereiche unseres Lebens durchdringen – und es ist nur verständlich, dass dies von manchen auch mit Sorge betrachtet wird. Umso wichtiger ist es, dass alle an dem Wertschöpfungsprozess Beteiligten sich aktiv für eine positive Ausgestaltung der Digitalisierung in ihrem Bereich einsetzen. Wer nicht selbst gestaltet, dem wird etwas vorgegeben.

Noch nie war die Disziplin der Simulation so spannend wie heute: Die mit der Digitalisierung verbundenen Durchgängigkeit auf einer Business Plattform bietet eine große Chance: Eine Chance, *gemeinsam Neues* zu schaffen. Ganz im Sinne der alten Medicis ….

8 Quellen

[1] Johansson, F.: "The Medici Effect", Harvard Business School Press, 2004, ISBN159-1-39-1865

[2] TECHNIA, Whitepaper “Der PLM Guide 2024”

[3] Dassault Systèmes, “The 3DEXPERIENCE Platform”, 2024, www.3ds.com

[4] Sippel, H., Küssner, M.: “Predictive Lifecycle Assessment”, 2012, ISBN 978-3-00-038577-3

Development and Credibility Assessment of a TAVI Heart-Valve FSI-Model

Nils Götzen (4RealSim Services BV), Tahir Turgut (4RealSim Services BV), Omar Zahalka (4RealSim Services BV), Vincent Bouwman (4RealSim Services BV)

1 Summary

TAVI heart valves have evolved to a standard treatment, especially for elderly patients, to improve the blood flow by replacing an aortic valve that does not open fully. It is a minimally invasive process where the device is placed into the living heart using a catheter-approach. Within the SimInSitu project [1], we have developed a detailed FSI-model of a Sapien-3 TAVI Heart Valve using a tiered modelling and VVUQ approach, able to simulate the in-vitro hemodynamic performance of the device.
All relevant device components, such as stent-frame, skirt, and the three leaflets are modelled, while the implantation procedure using balloon inflation is also considered. The entire heart-valve model is virtually placed into a simplified in-vitro test-setup and the fluid-structure interaction is implemented using a SPH solution.
The model underwent an extensive verification and validation program considering available structural and hemodynamic test data coming from various publications. A thorough uncertainty quantification & propagation was conducted for the structural and hemodynamic behaviour using various forms of Monte-Carlo-Simulations. Due to the complexity of the model, meta-modelling was partially necessary.
The VVUQ activities confirmed a particularly good agreement between experimental and simulation data for the structural behaviour of the stent frame, while the leaflet mechanics, structurally and hemodynamically, showed initially an insufficient agreement. This was associated with the lack-of-data about the device specifications we were confronted with and was corrected by introducing minor changes in the material properties and leaflet dimensions.
The heart-valve FSI-model is currently being implemented in a patient-specific model of the left ventricle / aortic root / aortic arch to simulate the deployment process and device performance in an in-vivo setup.

2 Device Description

The Edwards Lifesciences Sapien 3 ULTRA is a balloon-expandable transcatheter heart valve that is used for treating patients whose aortic heart valve fails to function properly (Fig. 1). There are 3 design sizes with different nominal valve diameters, 23-, 26-, and 29-mm available. The S3 ULTRA THV is composed of a stent frame, a tri-leaflet valve, and a fabric skirt. The stent frame is made from cobalt-chromium material, the valve is a processed bovine pericardial tissue, and the skirt is made from polyethylene terephthalate (PET) material. The leaflets and the skirt are sutured to the stent frame.

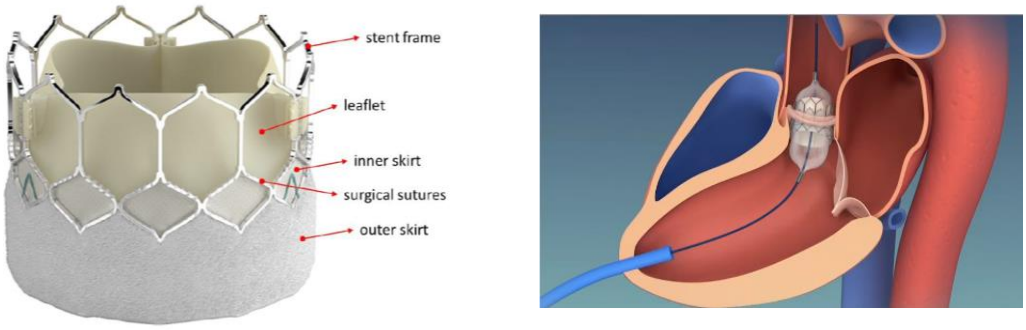

Fig. 1: Sapine-3 TAVI Heart Valve Device (left) and idealized device transcatheter deployment through the ventricular apex of the human heart (right)

3 Hierarchical Modelling and VVUQ Approach

We used a hierarchical modelling and VVUQ approach [5] to build the FSI model bottom-up (Fig. 1). Four complexity levels are present in the model: material model level, device component level, complete device level, multi-physics device level. At each hierarchy level verification, validation, and uncertainty quantification activities were conducted. Significant uncertainty factors were propagated from lower to higher complexity levels. We followed the well-established ASME V&V standards [2][3][4] for the credibility assessment.

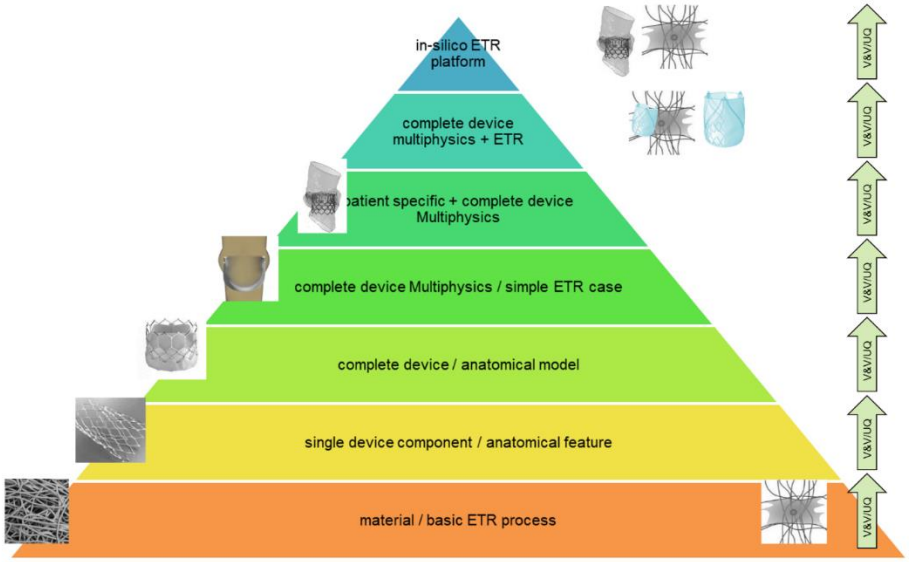

Fig. 2: Hierarchical VVUQ strategy for in-silico ETR platform of the SimInSitu project [1].

4 Structural FEM Model

The TAVI device model was developed fully parametric (scriptable) in two sizes, ND23 and ND26, while it comprises the stent frame (beam-elements with coupled surface elements), the three leaflets (shell elements), and the skirt (continuum elements). Accompanying to the TAVI device model is a balloon delivery system (shell elements), which comes in corresponding sizes (Fig. 3).

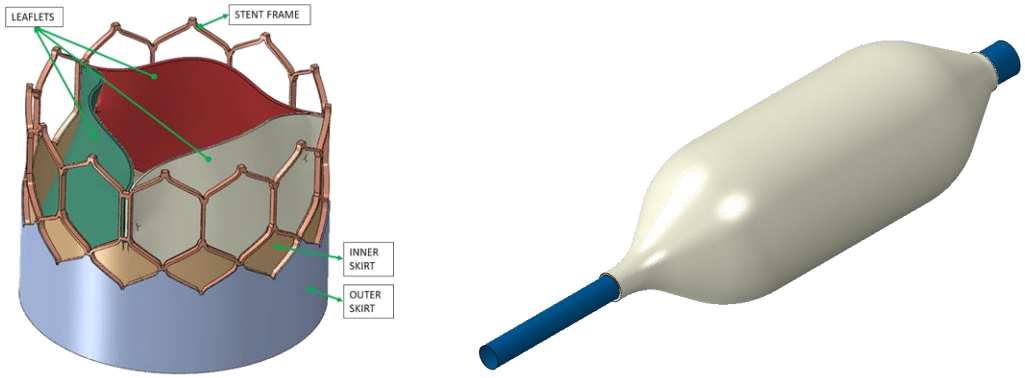

Fig. 3: FEM Model of the TAVI device (left) and the balloon delivery system (right)

The individual material models for the individual components (stent-frame: CoCr as Johnson-Cook plasticity; leaflets: bovine tissue as HGO anisotropic hyperelasticity; skirt: PET as isotropic hyperelastic; balloon: polymer as isotropic hyperelastic) were calibrated based on available technical device document and literature. The various, often inconsistent literature sources were also used to assess the associated uncertainty, considering aleatory and epistemic contributions. Component were assembled using various tie-constraints and cohesive contact definitions.

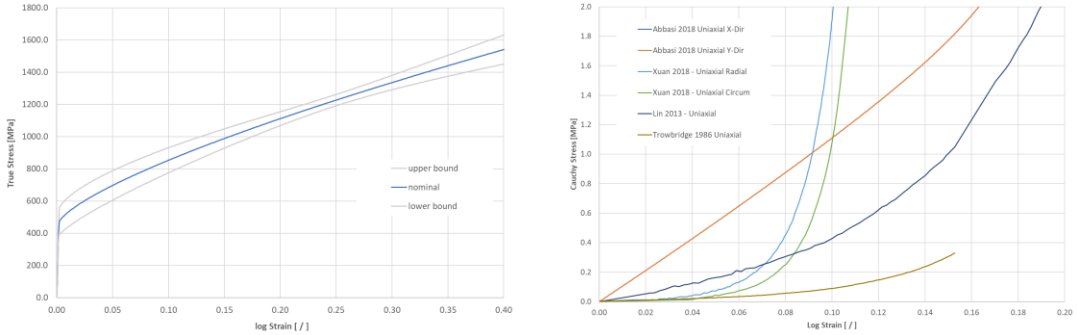

Fig. 4: Calibrated material models for the stent-frame (left) and bovine leaflets (right) illustrating the observed variance.

All individual model components, the full device assembly, and the device-balloon system underwent an exhaustive verification program, which included code-verification, discretization error assessments (spacial and temporal), and solver error assessments (e.g. viscous pressure, contact stiffness, mass-scaling) through a multitude of quasistatic and transient analysis related to the intended purpose and question-of-interest of the heart-valve model.

5 Fluid-Structure-Interaction SPH Model

Fluid-Structure-Interaction (FSI) was introduced by means of Smoothed-Particle Hydrodynamics (SPH). Therefore, the FEM model was placed into a virtual test-chamber, like they are used typically for in-vitro device testing of hydrodynamic performance according to ISO 5840. Due to technical limitations of the currently available SPH technology, the entire fluid domain needed to be made available as particles prior to the actual FSI simulation. Therefore, additional fluid chambers were introduced representing the left-ventricle inlet side and aortic outlet side (Fig. 5). The objective of the FSI analysis was to compute the pressure gradient of the valve (during the systolic phase) and the flow regurgitation (during the diastolic phase). Therefore, a dedicated hybrid pressure-velocity inlet boundary-condition was developed in implemented (Fig. 5).

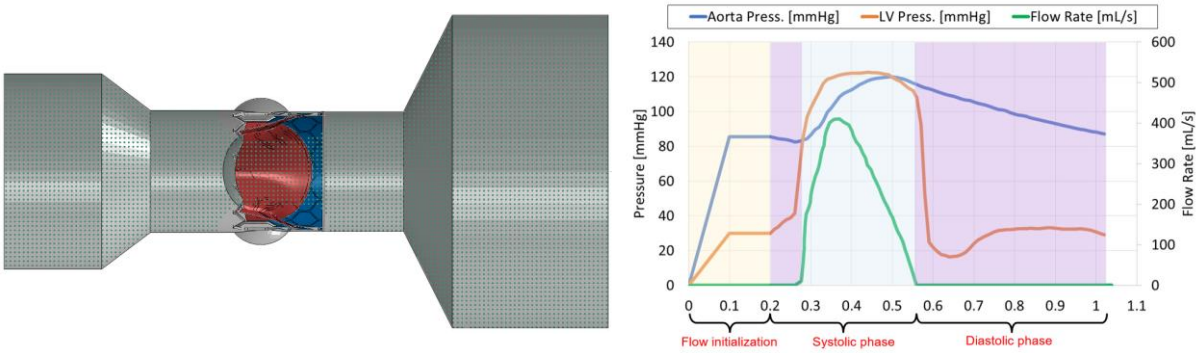

Fig. 5: TAVI FEM model placed into the virtual in-vitro flow-chamber with connected inlet- and outlet fluid-particle chambers (left) and applied hybrid pressure-velocity boundary conditions (right).

Likewise, to the FEM model, thorough verification and debugging activities were conducted, which focused predominantly on the interplay between FEM-element size, SPH-particle-size, and flow bulk viscosity and their impact on the device performance parameters.

6 Model Validation and Uncertainty Quantification

The validation of the device model followed closely the risk-based framework as described in ASME V&V-40 [4] and included an uncertainty quantification approach, which incorporated a segregated assessment of aleatory and epistemic uncertainty (mixed-UQ / second order probability). Due to the numerical complexity of the models and computational demand to conduct full-cardiac cycle analyses, a direct Monte-Carlo Simulation was not possible. Instead, a (global) surrogate-modelling strategy (higher order response surfaces or radial basis functions) was used for the UQ in the Structural Models and a local sensitivity approximation was used for the UQ in the FSI model.

6.1 Structural Performance

The structural FEM model was validated independently for stent-frame and the leaflets since they have individual functions. All experimental data were obtained from various literature sources leading to substantial lack-of-knowledge, which was treated as additional epistemic uncertainty.

The mechanical behaviour of the stent-frame was validated by comparing the expansion diameter after balloon dilatation and elastic recoil. MicroCT measurements were available in the literature [6] for three planes within the stent-frame (Fig. 6), which were compared with corresponding simulation results. Obtained normalized area metric ranged between 0.7% and 10.4% depending on the plane, which is an excellent result, while the influence of the epistemic uncertainty was higher than for the aleatory uncertainty.

The quasi-static mechanical behaviour of the leaflets was validated by comparing the vertical deformation under quasi-static pressure loading (Fig. 7), for which also a literature source was used to provide experimental data [7]. The obtained area metric showed an unacceptable large discrepancy which could be explained by the lack-of-knowledge associated with the device specification, leaflet-material properties, and experimental measurement setting. Based on computed sensitivity-factors, leaflet dimensions and material stiffness were adjusted, and the validation simulation were repeated which led to a significantly improved area-metric ranging between 21% – 43%.

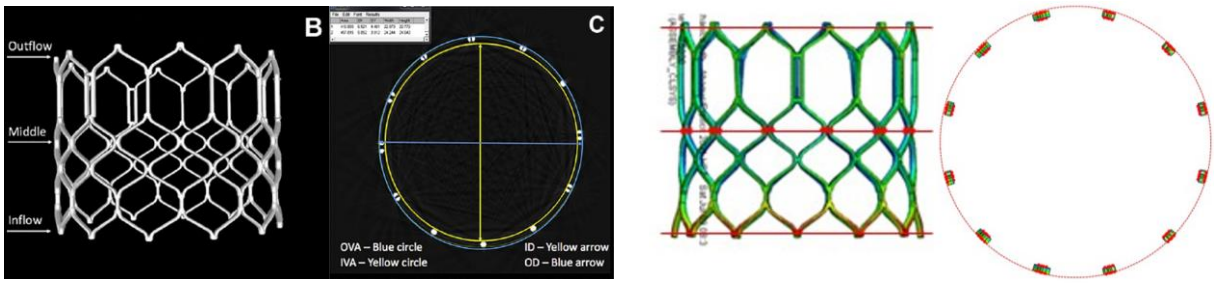

Fig. 6: stent-frame expansion after ballon dilatation and elastic recoil (left: exp [6]; right: sim)

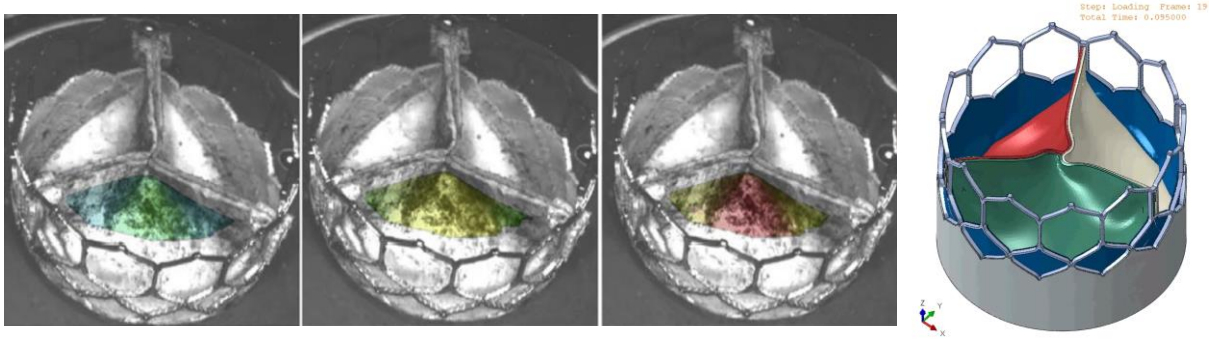

Fig. 7: leaflet deformation under quasistatic pressure loading (left: exp [7]; right: sim)

6.2 Haemodynamic Performance

For the FSI model validation, several clinical device parameters were compared. Depending on the availability in the literature [6], these were: Mean Pressure Gradient, Geometrical Orifice Area (Fig. 8); Effective Orifice Area, Regurgitant Fraction, Regurgitant Volume, Leaflet Restriction, and Coaptation Defect. As a result of a large discrepancy between computational and experimental results, additional model adjustments in the leaflet geometry were necessary, which lead to a very good area-metric: Effective Orifice Area: 0.03; Mean Pressure Gradient: 0.06; and Regurgitation Fraction Output: 0.36.

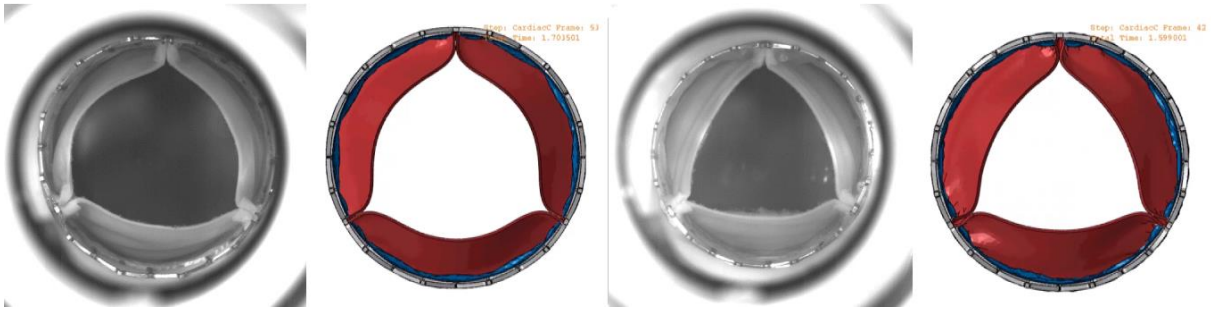

Fig. 8: Maximum valve opening (Geometrical Orifice Area) during systolic phase (left: ND26; right ND23; [6])

7 Conclusions

This study shows that SPH can be successfully used to model and predict hydrodynamic valve behaviour if limited to performance and leaflet kinematics. The hierarchical VVUQ concept facilitated the development and credibility assessment of the model. The limited access to reliable device specifications, material properties, and experimental date caused on several occasions a significant discrepancy between simulation and experiment, but could be overcome by model adjustments.

8 References

[1] EU Project: SimInSitu, GA No. 101017523
[2] ASME V&V-10 (2019)
[3] ASME V&V-20 (2009)
[4] ASME V&V-40 (2018)
[5] Oberkampf & Roy, Verification and Validation in Scientific Computing. ISBN 9781139813761
[6] Abbasi et al (2018) doi.org/10.1016/j.jbiomech.2018.05.020
[7] Sathananthan et al (2018) doi.org/10.1016/j.jcin.2018.06.027

CFD-Simulation der Fluid-Struktur-Interaktion in der Pumpenkonstruktion

Brandon Arthur Lobo

(Cascate GmbH)

Diese Studie präsentiert eine CFD-Simulation der Fluid-Struktur-Interaktion (FSI) einer Pumpe. Die Pumpe verfügt über eine Membran, die zwei Kammern trennt: die obere Kammer enthält ein Gas, in der unteren Kammer befindet sich ein Kolben mit Einlass- und Auslassöffnungen. Der Status der Gaskammer als Einlass oder Auslass wechselt je nach Kolbenbewegung und gewährleistet so eine effiziente Steuerung des Flüssigkeitsstroms.

Das Ziel dieses Vortrages ist es zu zeigen, wie sich eine solche Aufgabenstellung durch die Kopplung von Fluid und Struktur einfach und effizient in einem gemeinsamen Simulations-modell lösen lässt ohne die Notwendigkeit einer Kopplung mit einem externen Tool.

Analysiert wird das Verhalten der Membran einschließlich ihrer Wechselwirkung mit den Kammerwänden. Speziell beobachten wir, dass die Membran genau an der Wand anliegt und eine robuste Kopplung zwischen den festen und fluiden Bereichen ermöglicht.

Diese Arbeit hebt die Fähigkeiten von CFD-Simulationen bei der Modellierung komplexer FSI-Phänomene hervor und bietet Einblicke in die Leistung und Optimierung von Pumpen. Obwohl quantitative Ergebnisse nicht präsentiert werden, liegt unser Fokus darauf, die aktuellsten Fähigkeiten zu demonstrieren. Durch die nahtlose Integration von FSI-Simulationen in einem einzigen modernen CFD-Code wird die Notwendigkeit einer externen Toolkopplung beseitigt. Dies vereinfacht nicht nur den Workflow, sondern reduziert auch potenzielle Fehler oder Diskrepanzen. Der gekoppelte Solver berücksichtigt umfassend die Wechselwirkungen zwischen Fluid und Struktur und erfasst dynamische Effekte, die in sequentiellen Simulationen oft übersehen werden. Letztendlich gewährleistet dieser Ansatz eine genauere Darstellung realer Szenarien und fördert eine robuste und aufschlussreiche Ingenieursanalyse.

CFD-Simulation der Fluid-Struktur-Interaktion in der Pumpenkonstruktion

Dr.-Ing. Brandon Arthur Lobo
Cascate GmbH

Outline

- Fluid-Structure Interaction
  - Significance and challenges
- Diaphragm Pump
  - Setup and analysis
- Summary and conclusions

FLUID-STRUCTURE INTERACTION

What is Fluid-Structure Interaction (FSI)?

- Situations where the state of the fluid domain depends on the state of the solid domain and vice-versa
- Coupling can be either mechanical, thermal or a combination
- Typically
  - Fluid-Structure interaction (FSI): Mechanical coupling
  - Conjugate heat transfer (CHT): Thermal coupling

Why FSI?

- Predict and understand Fluid-Structure Interaction
  - Compute fluid loads on structures to reduce conservative manufacture
  - Analyze coupled systems to prevent failure
- Explore design variants early in the development process
  - Optimize component topology
  - Reduce material costs
  - Maximise component lifecycle

Why FSI

Tacoma Narrows Bridge (1940)

Triangle of Continuum Mechanics

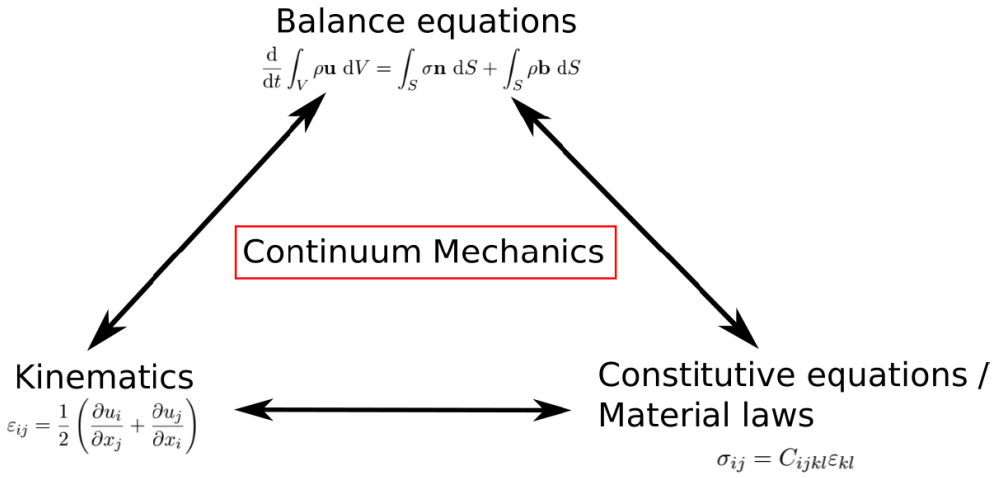

FSI Coupling Within a Simulation

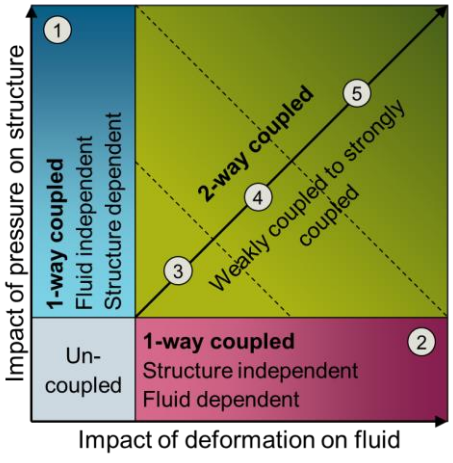

1. Fluid not affected by the strucutre: Eg. Bridge
2. Structure not affected by the fluid: Eg. Peristaltic pump
3. Static Equilibrium: Eg. Opened valve under steady flow
4. Weakly coupled: Eg. Diaphragm pump
5. Strongly coupled: Eg. Blood flow through a heart valve

FSI with Mechanical Contact

- Modeling of mechanical contacts between solid and elastic bodies (membranes)
- One- and two-way coupling between fluid and solid
- Mesh re-generation between iterations if necessary

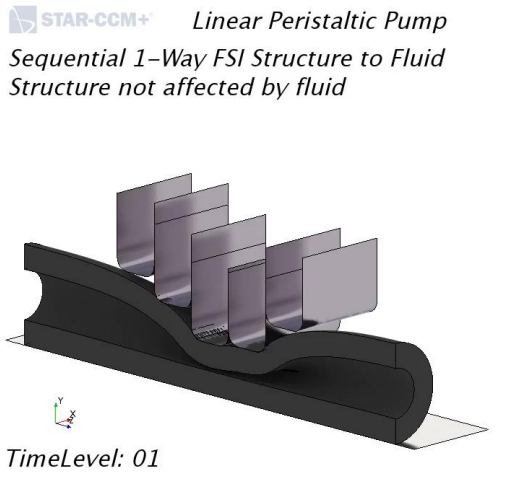

Courtesy of Siemens ©

MEMBRANE PUMP

Geometry + Mesh

- Grey: Piston
- Blue: Gas
- Yellow: Membrane
- Orange: Water
- Cylinders: Gas (left) and Water (right)

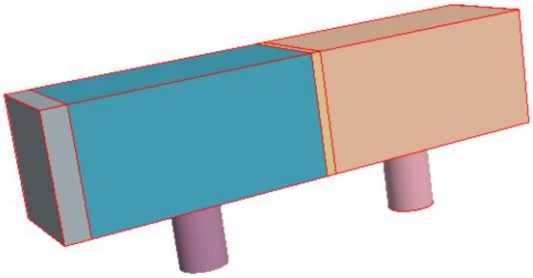

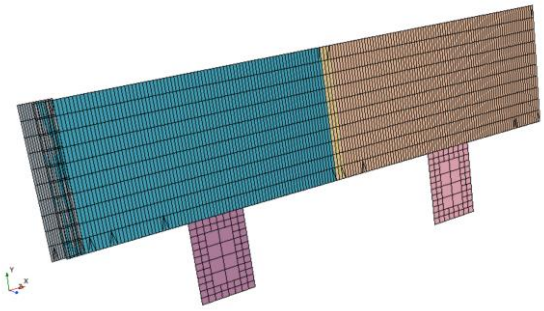

Simulation Animation

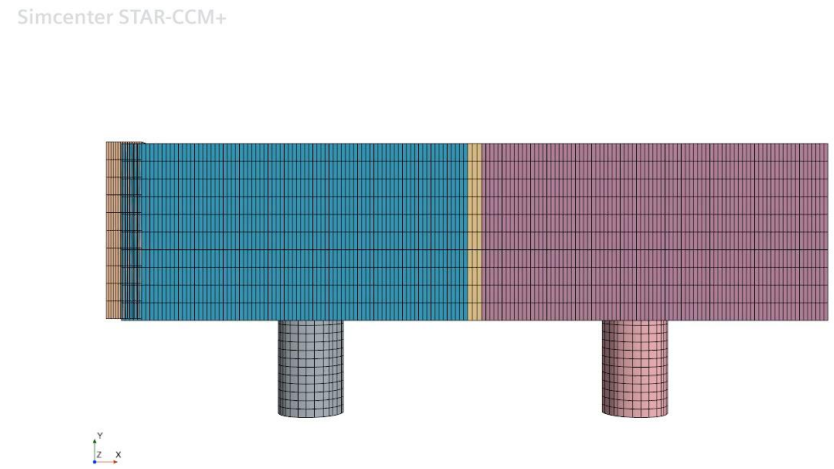

Results

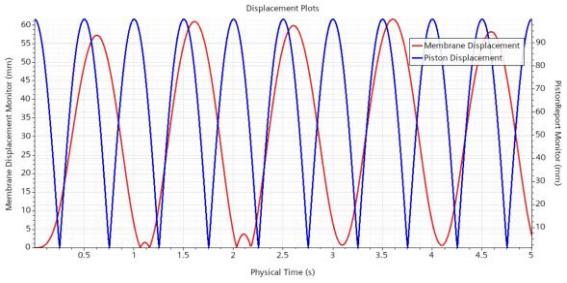

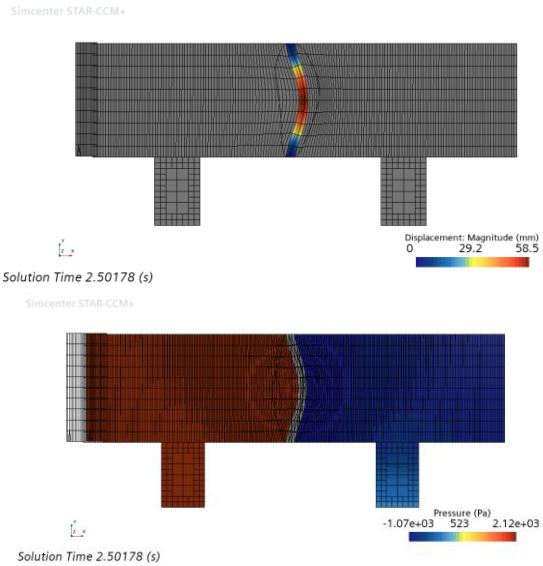

FSI: Weak and Strong Coupling

Weak Coupling

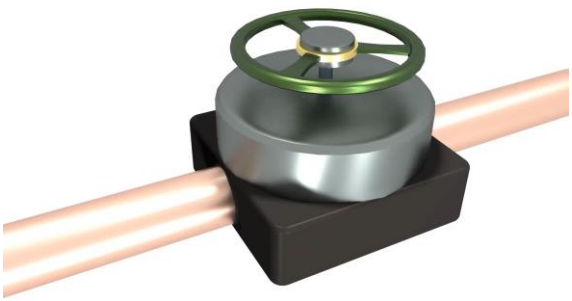

Courtesy of Siemens ©

Strong Coupling

Courtesy of Siemens ©

SUMMARY AND CONCLUSIONS

Summary and Conclusions

- FSI simulations within a single tool
  - Faster simulations
  - Easier workflow
  - Robust and efficient
  - Increased accuracy
- Benefits of FSI-Simulations
  - Predictive maintenance
  - Cost-saving
  - Faster time to market
  - Improved product performance

Ansprechpartner

Brandon A. Lobo
brandon.lobo@cascate.de
+49 (0) 711 99 88 51 27

CASCATE GmbH
info@cascate.de
Industriestraße 2
70565 Stuttgart

Vielen Dank für Ihre Aufmerksamkeit.

HABEN SIE NOCH FRAGEN?

Data-Driven Modelling of Particle-Induced Turbulence in Sediment Transport

Yvonne Stöcker

(TU Wien)

The aim of this work is to improve the turbulence modelling in low-fidelity, cost-efficient RANS simulations for particle-laden flows. Based on high-fidelity data from DNS studies, the model-form errors of the Boussinesq assumption and the modelled turbulence transport equations are extracted.

They serve as target data for a data-driven machine learning process, called SpaRTA (Sparse Regression of Turbulent Stress Anisotropy). It employs deterministic symbolic regression techniques to infer corrective algebraic models written as tensor polynomials, while promoting sparsity. The models are constructed from a predefined library of candidate functions built from the mean strainrate-and rotation-rate tensor of the fluid. In the present work, the algorithm is extended so that additional values can be taken into account. Moreover, a new modelling approach is introduced, in which the models can be expressed as a scalar polynomial.

The learnt models are implemented in a CFD solver for cross-validation to assess their predictive performance. This study shows the applicability of the SpaRTA algorithm to multi-phase flows and the relevance of incorporating sediment-related quantities to the library of functions from which the models are assembled. An average improvement of ca. thirty percent on various flow values is achieved, compared to the standard turbulence models.

This work was later expanded and published as a Journal article:
Stöcker, Y., Golla, C., Jain, R. *et al.* DNS-Based Turbulent Closures for Sediment Transport Using Symbolic Regression. *Flow Turbulence Combust* **112**, 217–241 (2024). https://doi.org/10.1007/s10494-023-00482-7

GPU-beschleunigte automatische Kontakterkennung

Stephanie Ferreira, Tristan Schulz, Sebastian Besler, Johannes Mueller-Roemer, Daniel Weber
(Fraunhofer IGD & TU Darmstadt)

1 Zusammenfassung

Bei der Simulation von Baugruppen im Computer Aided Engineering (CAE) spielt das Behandeln von Kontakt eine wichtige Rolle. Um Kontakt modellieren zu können, müssen Bereiche identifiziert werden, die in Kontakt sind oder innerhalb des nächsten Simulationsschrittes potenziell in Kontakt kommen können. Oft muss der Benutzer vorgeben, welche Bereiche als Kontaktflächen modelliert werden sollen. Für komplexere Baugruppen kann dies jedoch sehr aufwendig sein. Alternativ können solche Kontaktbereiche über Abstandsberechnungen automatisch identifiziert werden. Für die korrekte Simulation von Kontakt werden Abstandsinformationen der diskretisierten Geometrie benötigt, um diesen genau abzubilden. Diese Informationen zu generieren kann, je komplexer die Geometrie beziehungsweise, je mehr Freiheitsgrade die diskretisierte Geometrie hat, sehr zeitaufwendig sein.
In der Computergrafik ist die effiziente Abstandsberechnung insbesondere auch bei der Behandlung von Kollision in der Computeranimation ein etabliertes Forschungsfeld. Ein beliebter Ansatz sind räumliche Beschleunigungsstrukturen, wie zum Beispiel die „Bounding Volume Hierarchy“ (BVH, dt. Hierarchie von Hüllkörpern). Diese unterteilt den betrachteten Raum, beziehungsweise die betrachteten Objekte, hierarchisch in Teilvolumen, mit Hilfe derer effizient räumlich nahe Teilgebiete identifiziert werden können (siehe Abbildung 1). Des Weiteren ist der Einsatz von Grafikprozessoren (engl. graphics processing unit - GPU) etabliert. Diese ermöglichen es, große Mengen an Daten parallel zu verarbeiten. Wir untersuchen, wie BVHs gepaart mit einem GPU-basierten Kontakterkennungsalgorithmus in der statischen Kontaktsimulation eingesetzt und die Berechnungen beschleunigt werden können.

2 Methoden aus der Computergrafik

In der Computergrafik wird physikalische Simulation vor Allem im Bereich der Animation eingesetzt. Damit Szenen in Animationsfilmen oder Computerspielen möglichst realistisch wirken, muss die Welt so detailgetreu wie möglich, aber nur mit so wenig Rechenzeit und -aufwand wie nötig abgebildet werden. Besonders in Computerspielen sind kurze Rechenzeiten wichtig, um in Echtzeit auf die Benutzerinteraktion reagieren zu können.
Die Behandlung von Kontakt in einer dynamischen Szene ist dementsprechend ein etabliertes und immer noch aktuelles Forschungsgebiet in der Computergrafik ([1], [2]).
In dieser Arbeit liegt der Fokus auf Kontakterkennungsmethoden, die gepaart mit Algorithmen zur Kontaktbehandlung eingesetzt werden können. Mit Kontakterkennung ist hierbei die Identifikation von Bereichen (zum Beispiel in Form von Primitiven des diskretisierten Netzes) gemeint, die innerhalb eines Simulationsschrittes potenziell in Kontakt kommen können.

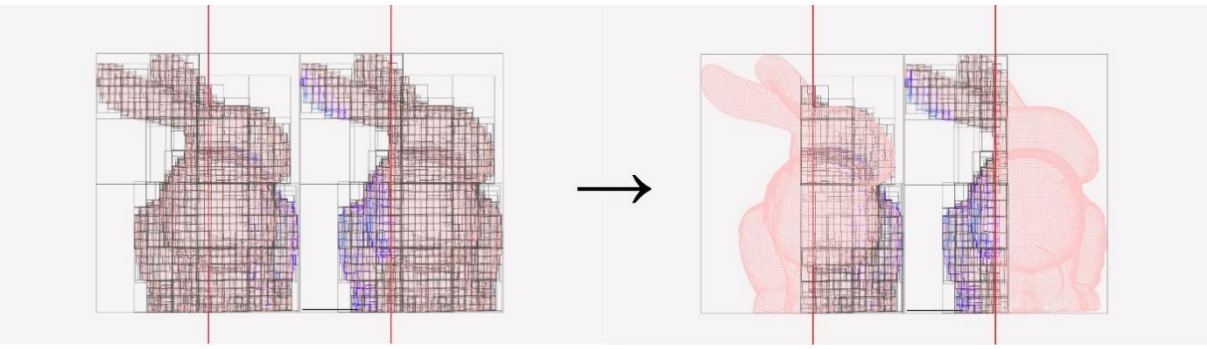

Abbildung 1: Nutzen einer Bounding Volume Hierarchy pro Objekt, um schnell Bereiche zu identifizieren, die sich nahe sind.

2.1 GPU-beschleunigte Kontakterkennung

GPUs wurden ursprünglich für die Bildgenerierung entwickelt, hierbei werden gleichzeitig Berechnungen durchgeführt um den Farbwert jedes Pixels zu bestimmen. Diese Fähigkeit parallel Berechnungen durchzuführen, wird mittlerweile in vielen Bereichen eingesetzt. Getrieben von der Computerspieleindustrie und mittlerweile auch von KI-Anwendungen werden GPUs immer weiterentwickelt. Sie vereinen mittlerweile tausende Kerne auf einem Chip und ermöglichen aktuell bis zu 83 Billionen Rechenoperation pro Sekunde [3]. Um diese Fähigkeiten optimal zu nutzen ist es notwendig spezielle Datenstrukturen und Algorithmen zu entwickeln, die für die spezielle Architektur von GPUs ausgelegt sind.

2.2 Bounding Volume Hierarchies

BVHs sind Beschleunigungsstrukturen, die genutzt werden, um eine effizientere Durchführung von geometrischen Abfragen zu ermöglichen, z.B. Abstandsberechnungen. Einsatzgebiete sind neben der Kollisionserkennung vor Allem Ray Tracing (dt. Strahlverfolgung), bei der Schnittberechnungen von Objekten mit Millionen bis Milliarden von Strahlen durchgeführt werden, um fotorealistische Bilder zu erzeugen [4]. Eine BVH unterteilt eine Geometrie hierarchisch in immer kleiner werdende Hüllkörper, das Ergebnis ist eine Baumstruktur, wie in Abbildung 2 gezeigt. Als Hüllkörper können zum Beispiel Kugeln oder quaderförmige Begrenzungsboxen verwendet werden.
BVHs ermöglichen Abstandsabfragen für die Kontakterkennung in einer Laufzeit von $O(n\log(n))$ statt $O(n^2)$. Teilbereiche, die für die Kontakterkennung uninteressant sind, da sie weit auseinander liegen, können schnell verworfen werden, dadurch wird die Anzahl der tatsächlich notwendigen Abstandsberechnungen deutlich reduziert. Das Aufstellen der BVH benötigt jedoch zusätzlichen Aufwand, darüber hinaus muss die BVH aktualisiert werden, wenn sich Knotenpositionen verändern. Die Generierung der BVH ist parallelisierbar, in dieser Arbeit wurde der GPU-basierte Ansatz von Lauterbach et al. [5] genutzt.

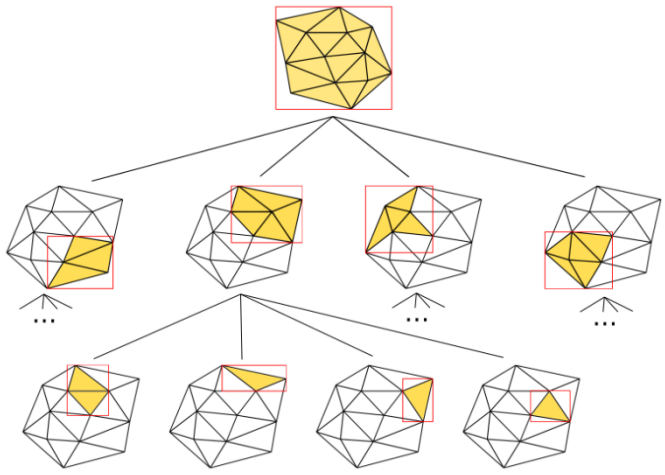

Abbildung 2: Beispielhafte Darstellung der Baumstruktur einer BVH. Jedem Knoten des Baums sind Dreiecke des Netzes zugeordnet (gelb eingefärbt). Die zugehörige Begrenzungsbox ist in Rot dargestellt.

2.3 Continuous Collision Detection

Eine weitere verbreitete Technologie in der Computergrafik ist „Continuous Collision Detection“ (CCD, dt. kontinuierliche Kollisionserkennung), welche auch in Kombination mit BVHs eingesetzt werden kann [6]. Hierbei werden Bewegungsinformationen genutzt, um Kollisionen bzw. Kontaktstellen entlang der aktuellen Bewegung zu identifizieren. In dynamischen Szenen kann hierzu das Wissen über Geschwindigkeit und Beschleunigung genutzt werden. Besonders bei hohen Geschwindigkeiten oder großen Zeitschritten wird mit diesem Ansatz vermieden, dass Kollisionen unentdeckt bleiben, da die Kollisionserkennung entlang des gesamten Bewegungspfades durchgeführt wird. Konkret kann der Bewegungspfad für jedes Primitiv (Dreieck, Kante, Knoten) im FE-Netz betrachtet werden. Für jedes Primitiv-Paar kann nun geprüft werden, ob sich deren Bewegungspfade während des Simulationsschrittes gekreuzt haben. Wenn die Bewegung als lineare Bewegung approximiert wird, ist hierfür das Lösen einer skalarwertigen kubischen Gleichung notwendig. Im Kontext der dynamischen Simulation ist die Kontakterkennung über CCD genauer, benötigt jedoch mehr Rechenzeit.
Im Kontext der statischen Struktursimulation könnte dieser Ansatz genutzt werden, um sicherzustellen, dass keine unvorhergesehenen und deshalb unbehandelten Kontakte aufgetreten sind. Hierfür ist es

notwendig einen Simulationsschritt durchzuführen. Anhand der resultierenden Deformation können die Bewegungspfade aus dem Initialzustand hin zur Gleichgewichtslage betrachtet werden. Treten Pfadkreuzungen auf kann diese Information genutzt werden, um die Kontaktnebenbedingungen anzupassen. Darüber hinaus bietet es sich an, diesen Ansatz gepaart mit einem Simulationsalgorithmus mit Pseudo-Zeitschritten einzusetzen.

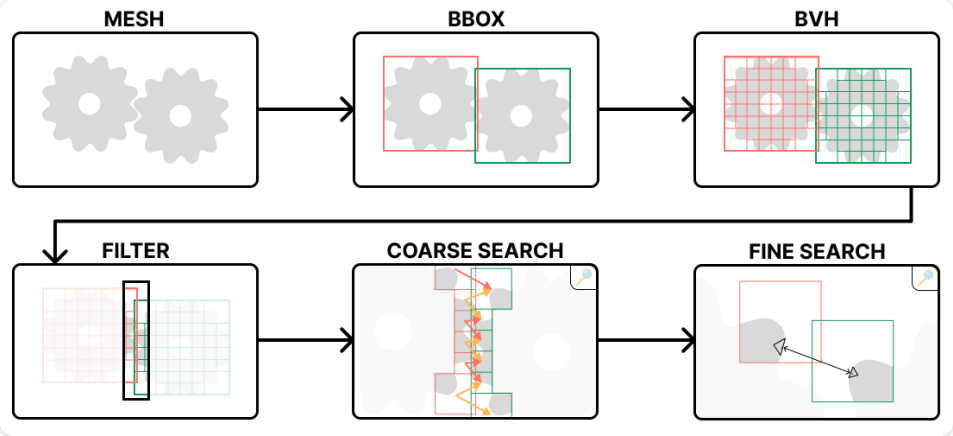

Abbildung 3: Pipeline des implementierten Kontakterkennungsalgorithmus.

3 Methode und Ergebnisse

Der hier entwickelte Ansatz dient der Identifikation von Kontaktpaaren auf Tetraedernetzen mit linearen Ansatzfunktionen, konkret Knoten-Dreieck und Kante-Kante Paaren, die potenziell im nächsten Simulationsschritt in Kontakt kommen könnten. Dies beruht hier rein auf Abstandsberechnungen, das heißt, ist der Abstand, zum Beispiel zwischen einem Knoten und Dreieck der Oberflächennetze der finite Elemente Netze, kleiner als ein netzgrößenabhängiger Schwellenwert, wird dieser als Kontaktpaar gespeichert und für die Kontaktberechnung in Betracht gezogen.
In Abbildung 3 ist eine Übersicht der Komponenten des implementierten Ansatzes gezeigt. Im ersten Schritt werden für jedes FE-Netz der Objekte eine Begrenzungsbox (engl. bounding box) berechnet. Hier nutzen wir eine an den Koordinatenachsen ausgerichtete Begrenzungsbox (engl. Axis-Aligned Bounding Box, AABB). Daran kann in einem ersten Schritt entschieden werden, welche Objekte sich nahe sind und für die weitere, detailliertere Kontakterkennung verwendet werden sollen. Anschließend wird für jedes Netz eine BVH unter Einsatz eines GPU-beschleunigter Algorithmus aufgebaut. Im nächsten Schritt werden Knoten der BVH-Bäume identifiziert, die sich nahe sind (siehe Abbildung 1). Sind sich zwei BVH-Knoten nahe muss für diese eine feine Suche durchgeführt werden. Hierbei werden alle Primitive des einen BVH-Knoten mit den Primitiven des anderen verglichen und überprüft, ob deren Abstände kleiner als der vorgegebene Schwellenwert sind.

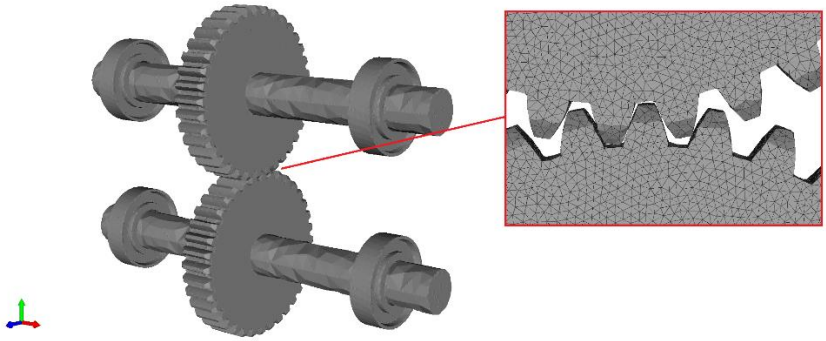

Abbildung 4: Testszenario mit höchster Auflösung von 2.2 Millionen FE-Knoten, wovon ca. 370 Tausend auf der Oberfläche liegen.

3.1 Ergebnisse

Alle vorgestellten Schritte sind speziell für die Durchführung auf einer GPU entwickelt. Um den Algorithmus zu evaluieren, wurden verschieden hoch aufgelöste FE-Netze eines Zahnrades betrachtet, die wie in Abbildung 4 dargestellt angeordnet sind. Je feiner die Netze aufgelöst sind, desto mehr Vergleiche von Abständen müssen durchgeführt werden. Die Tests wurden auf einer Workstation mit Intel i9-13900K Prozessor und einer NVIDIA GeForce RTX 4090 GPU durchgeführt. Wie in Abbildung 5 zu sehen, skaliert der Ansatz sehr gut mit der Größe der Netze. Das in diesem Test am feinsten aufgelöste FE-Netz mit 2,2 Millionen Freiheitsgraden und ca. 370 Tausend Knoten auf dem Oberflächennetz, benötigt die Kontakterkennung nur knapp über 25 ms. Hierbei wird in etwa die Hälfte der Laufzeit für die Generierung der BVH benötigt und die andere Hälfte für die paarweise Abstandsberechnung für Primitive in den identifizierten sich nahegelegenen BVH Knoten.

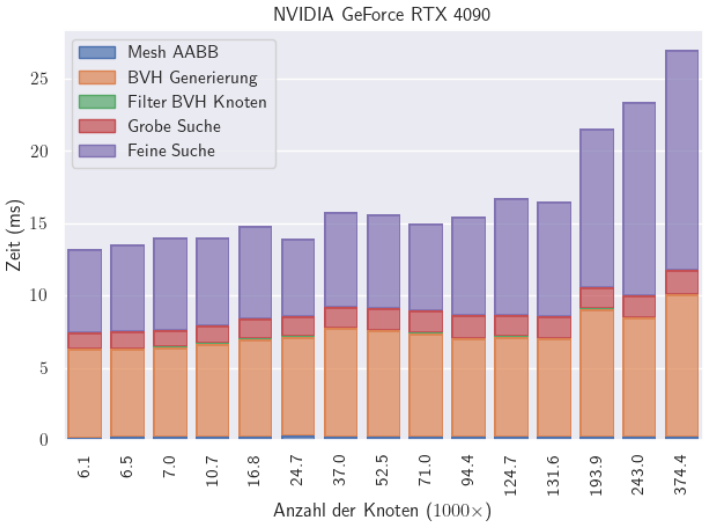

Abbildung 5: Darstellung der Laufzeiten in Abhängigkeit der Anzahl der Knoten des Oberflächennetzes für verschieden fein aufgelöste Modelle.

4 Fazit und Ausblick

Grafikkarten bieten enormes Potenzial, Berechnungen zu beschleunigen. Wir konnten durch den Einsatz eines GPU-beschleunigten Algorithmus die Kontakterkennung mittels Abstandsberechnung für ein hochaufgelöstes Modell in unter 30 ms erreichen. Aktuell werden die generierten Kontaktinformationen als Eingabe für eine Kontaktsimulation genutzt. In einem nächsten Schritt könnten die Algorithmen so angepasst werden, dass sie auch innerhalb einer Kontaktsimulation eingesetzt werden können. Zum Beispiel in einem CCD-ähnlichem Ansatz, bei dem durch mehrfaches Durchführen von Simulationen die Kontaktinformationen iterativ angepasst werden, sodass ein möglichst genaues Ergebnis der Kontaktsimulation berechnet wird. Der vorgestellte Ansatz bietet gepaart mit einem GPU-basierten Löser [7] das Potenzial Kontaktsimulationen erheblich zu beschleunigen.

5 Danksagung

Diese Arbeit wurde finanziert vom Bundesministerium für Bildung und Forschung unter dem Förderkennzeichen 01IS17047 als Teil des Software Campus Projekts „GPU-QP“ und dem Bundeministerium für Wirtschaft und Klimaschutz unter dem Förderkennzeichen 01MF21006C als Teil des Mittelstand-Digital Zentrum Darmstadt.

6 Referenzen

[1] M. Li, „Reliable Contact Simulation With IPC“, *IEEE Comput. Graph. Appl.*, Bd. 42, Nr. 3, S. 108–114, Mai 2022, doi: 10.1109/MCG.2022.3161841.

[2] R. Bridson, R. Fedkiw, und J. Anderson, „Robust treatment of collisions, contact and friction for cloth animation“, *ACM Trans. Graph.*, Bd. 21, Nr. 3, S. 594–603, Juli 2002, doi: 10.1145/566654.566623.

[3] NVIDIA, „GeForce RTX 4090“. Zugegriffen: 3. Mai 2024. [Online]. Verfügbar unter: https://www.nvidia.com/de-de/geforce/graphics-cards/40-series/rtx-4090/

[4] D. Meister, S. Ogaki, C. Benthin, M. J. Doyle, M. Guthe, und J. Bittner, „A Survey on Bounding Volume Hierarchies for Ray Tracing“, *Comput. Graph. Forum*, Bd. 40, Nr. 2, S. 683–712, Mai 2021, doi: 10.1111/cgf.142662.

[5] C. Lauterbach, M. Garland, S. Sengupta, D. Luebke, und D. Manocha, „Fast BVH Construction on GPUs“, *Comput. Graph. Forum*, Bd. 28, Nr. 2, S. 375–384, Apr. 2009, doi: 10.1111/j.1467-8659.2009.01377.x.

[6] B. Wang, Z. Ferguson, T. Schneider, X. Jiang, M. Attene, und D. Panozzo, „A Large-scale Benchmark and an Inclusion-based Algorithm for Continuous Collision Detection“, *ACM Trans. Graph.*, Bd. 40, Nr. 5, S. 1–16, Okt. 2021, doi: 10.1145/3460775.

[7] D. Weber, T. Grasser, J. Mueller-Roemer, und A. Stork, „Rapid Interactive Structural Analysis“, gehalten auf der NAFEMS DACH conference, 2020.

Nonlinear Dynamic Analysis Using Harmonic Balance Method

M. Klein, R. Helfrich, T. Willerding; INTES GmbH

1 Summary

There is for sure a high demand for nonlinear structural dynamics in implicit Finite Element Analysis (FEA). Although such methods are available, there are severe obstacles to use them daily. One is their extreme and not predictable computation time, which makes it often impossible to get results in time. Another point is the restriction of the methods to the time domain, which is in many cases in contrary to the usual design rules based on frequency domain results.

The Harmonic Balance Method (HBM) is a solution for at least an important sub-class of analysis cases, which resolves the two mentioned obstacles. As a starting point, we define HBM as a frequency response analysis with nonlinear elements like springs, dampers, or control elements. This allows to solve contact problems or mounting problems with nonlinear force-deflection curves. In fact, the HBM is a method in frequency domain, but an alternating use of frequency domain and time domain is necessary to cope with the nonlinearities. The primary results are in frequency domain. For all calculated frequencies, a solution in time domain is also available for a periodic response.

The paper will use a simplified radiator as industrial example to demonstrate the HBM. To prove the validity of the HBM procedure, a comparison with a linear frequency response analysis is performed, which shows same results. Then, rubber bushes and contact are added to the model as nonlinearities. Sufficient damping is applied to avoid multiple solutions for any frequency in the observed frequency range. Then, key results of stress and fatigue are presented. Finally, the computation times are analyzed to demonstrate the feasibility of the described process for practical applications in research and industry.

All simulations are performed with the FEA software PERMAS, which contains the HBM among other analysis methods in structural dynamics.

2 Introduction

The theoretical basis of the HBM (see also [1,2,3,4,5,6] is an extension of the linear formulation as for a frequency response analysis by a nonlinear term:

$$M\ddot{u} + C\dot{u} + Ku + f_{nl}(\dot{u}, u) = f_{ext}(t) \qquad (1)$$

with time-periodic excitation

$$f_{ext}(t) = f_{ext}(t+T),\ T = \frac{2\pi}{\omega} \qquad (2)$$

Typically, a truncated Fourier series is used for the excitation

$$f_{ext}(t) \approx f_0 + \sum_{k=1}^{r} (f_c^k \cos k\omega t + f_s^k \sin k\omega t) \qquad (3)$$

and for the displacement result:

$$u(t) \approx u_0 + \sum_{k=1}^{r} (u_c^k \cos k\omega t + u_s^k \sin k\omega t) \qquad (4)$$

In FEA, the nonlinear term in (1) is modeled by nonlinear elements like nonlinear spring elements for the stiffness, where the force-deflection relationship is nonlinear. Where necessary, the damping can be modeled by nonlinear damping elements as well.

3 Example Model

The following example of a simple radiator in Fig. 1 is used to demonstrate the use of the HBM.

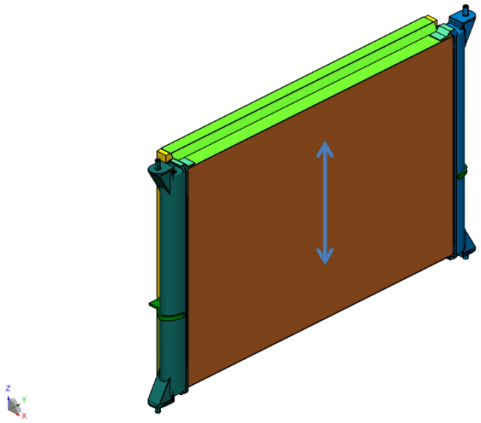

Fig. 1
Example of a radiator. The dynamic loading is a sine function using the self-weight in Z direction. The model has about 400k nodes and 750k solid elements.

In order to compare results for the same node, a reference node has been selected as depicted in Fig. 2.

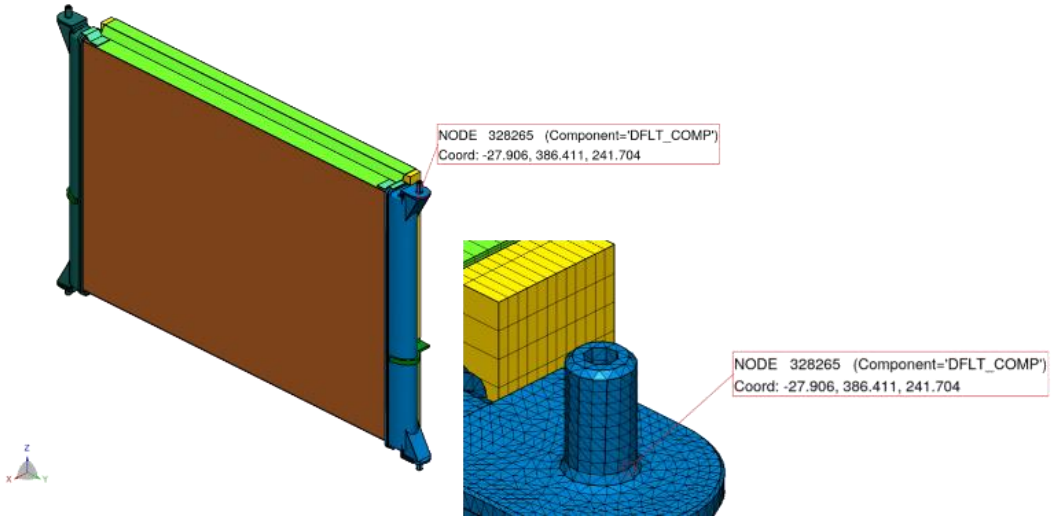

Fig. 2
The node 328265 is used as reference node to compare the results.at the right upper mounting pin of the radiator.

The mounting of the radiator has two components for each of the four pins. One component is a rubber mount and the other component is the contact between the pin and the rubber. A first analysis will show the effect of the rubber and a second analysis will show the results of both rubber and contact. The shape of the rubber mounts and the position of the rubber mounts is shown in Fig. 4.

Due to a different shape in XY plane compared to XZ and YZ plane, we have different force-deflection characteristics of the rubber mount in XY plane (see Fig 4) compared to Z direction (see Fig. 5). The characteristics were found by a nonlinear analysis using a reduced polynomial strain energy potential for the rubber. Of course, test results of the force-deflection characteristics could also be used. Then, a fitting is used to find nonlinear polynomials for the force deflection curves. These polynomials are used to define the behavior of nonlinear spring elements.

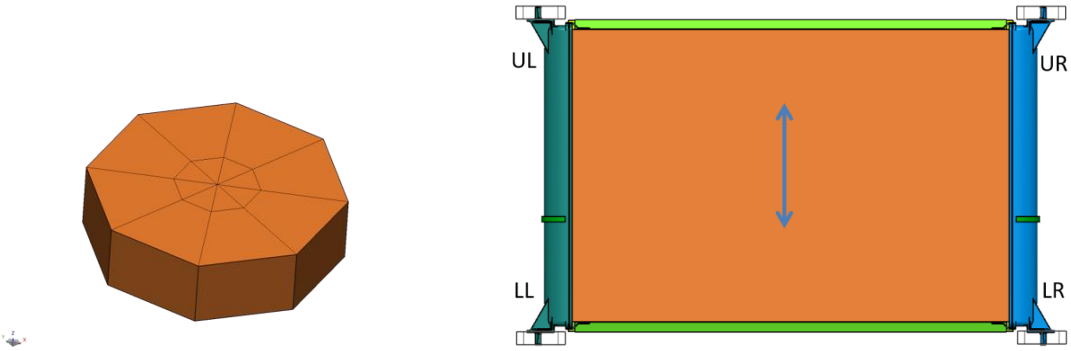

Fig. 3
The rubber mounts have a circular shape in XY plain and are like a plate in Z direction. The rubber mounts are applied at the upper left (UL), upper right (UR), lower left (LL), and lower right (LR) pin of the radiator.

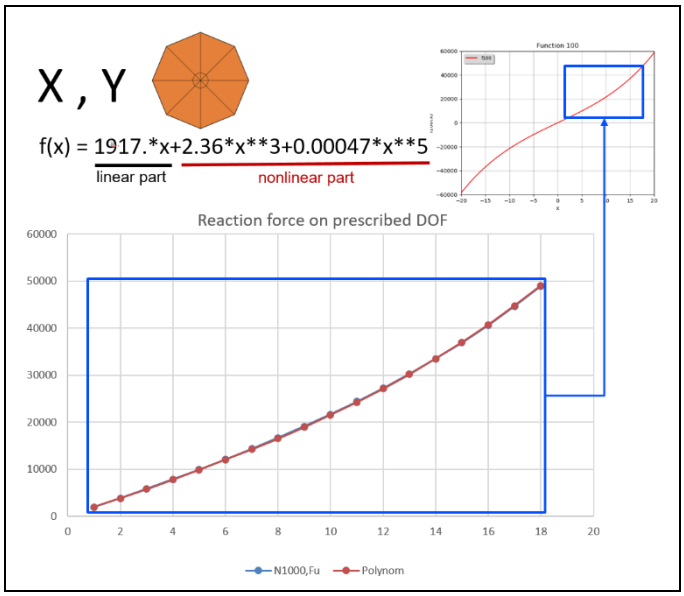

Fig. 4
The calculated rubber mount force-deflection curve in XY plane with the fitted polynomial of 5th order.

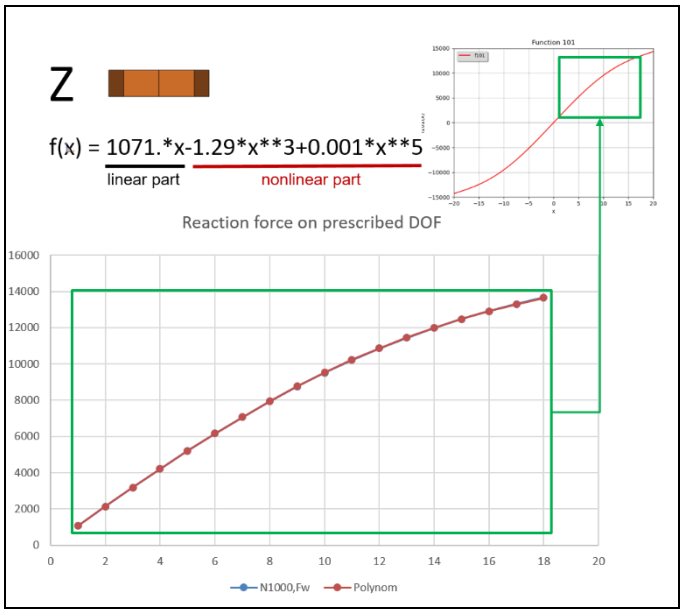

Fig. 5
The calculated rubber mount force-deflection curve in Z direction with the fitted polynomial of 5th order.

4 First Analysis: Rubber Mounts Only

Our first study will be made with the rubber mounts only neglecting the effect of contact between pin and rubber mount. Fig. 6 shows the modeling of one spring-damper system, which represents a rubber mount. The force-deflection curves of the nonlinear spring are taken from Figs. 4 and 5 respectively. Such spring-damper systems have to be created for all directions at all four mounting pins. While the springs behave nonlinear, we decided to use a linear function for all dampers in order to make it easier for the reader to understand the results.

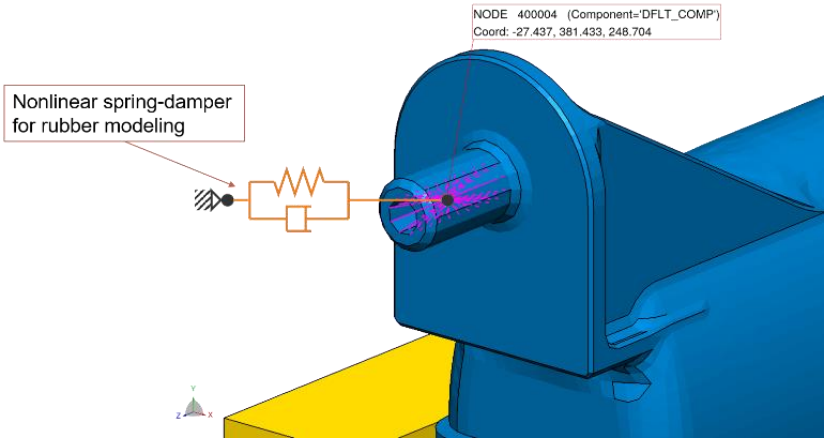

Fig. 6
The modeling of a rubber mount by a spring-damper system. This system has to be duplicated for all directions at all four pins. The two end-nodes of the spring-damper system have the same position in space. One is connected to a center node of the pin, while the other is fixed.

4.1 The Linear Solution

If one uses the HBM with linear springs, we expect that the result is identical to the result of a frequency response analysis (in the following denoted as FRF). To this end, we do not use the nonlinear functions of Fig. 4 and 5, but only the linear part of the polynomials as depicted in the same figures. The damping is linear with a coefficient of 0.02. Fig. 7 shows the comparison of HBM and FRF, which allows the conclusion that both results are identical as expected.

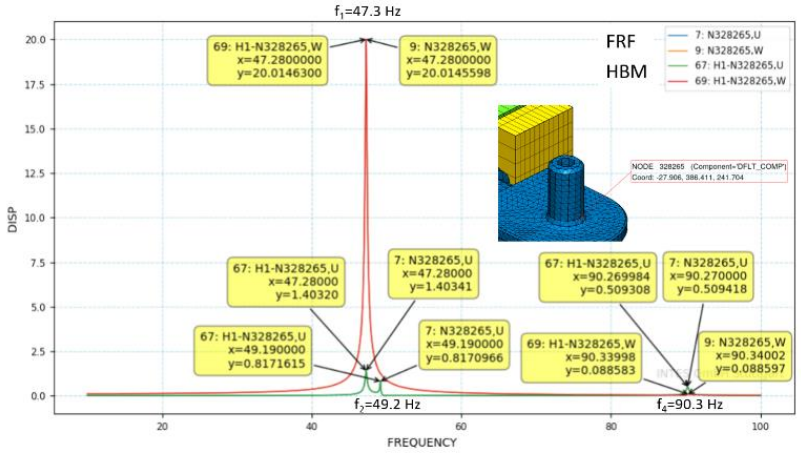

Fig. 7
For the reference node 328265, the FRF and HBM results are shown simultaneously for DOF U and W. The mentioned frequencies f1, f2, and f4 are the eigenfrequencies in Z and X direction as well as rotation around the Y axis.

4.2 The Nonlinear Solution

Using the nonlinear functions from Figs. 5 and 6, the result is shown in Fig. 8 with damping coefficient 0.02. Very typical for nonlinear solutions in frequency domain, one can see multiple solutions for the same frequency.

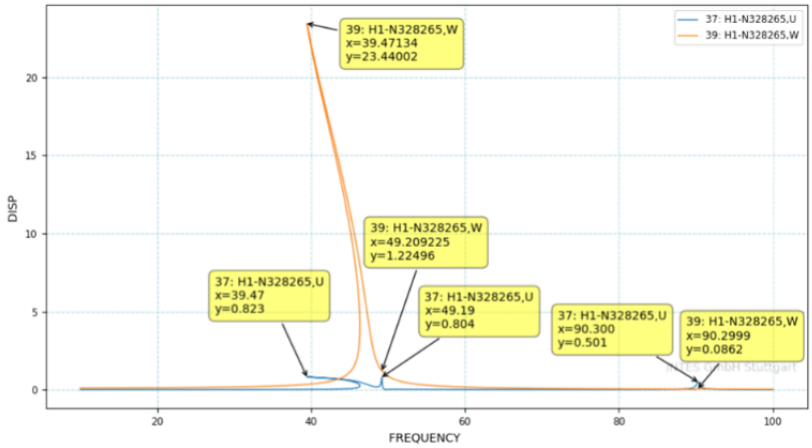

Fig. 8
For the reference node 328265, nonlinear HBM results are shown simultaneously for DOF U and W.

A comparison of linear and nonlinear solution is shown in Fig. 9, where the nonlinear solution shows lower peak frequency and higher amplitude.

Multiple solutions for one frequency could indicate instabilities. Technical products should avoid instabilities and therefore also multiple solutions. This can be achieved by increasing the damping of the rubber mount. Of course, the used rubber material should be able to provide this higher damping. By increasing the damping coefficient from 0.02 to 0.08, all multiple solutions can be avoided. Fig. 10 shows the comparison of the response curves for both damping coefficients.

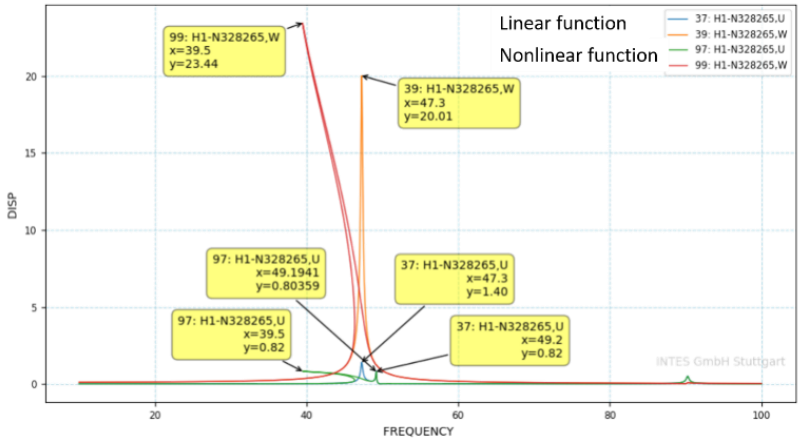

Fig. 9
For the reference node 328265, linear and nonlinear HBM results are shown simultaneously for DOF U and W with same damping coefficient 0.02.

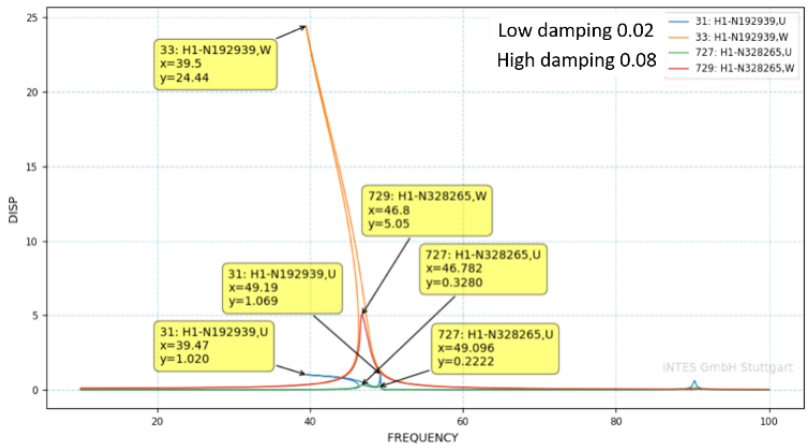

Fig. 10
For the reference node 328265, nonlinear HBM results for damping coefficients 0.02 and 0.08 are shown simultaneously for DOF U and W. The response with higher damping coefficient does not show any multiple solutions at same frequency anymore.

5 Second Analysis: Rubber Mounts with Contact

Our second study will be made with the rubber mounts and contact between pin and rubber mount. Fig. 11 shows the modeling with the rubber mount as in Fig. 6 and another nonlinear spring for contact.

We expect that the mounting of the radiator is made without any initial gap, so the radiator is not loose but properly fixed in the rubber mounts. Then, all initial gap widths are set to Zero. This implies that relative motions between pins and rubber mounts are (almost) not possible. Hence, any frictional damping will not take place. So, additional damping has to come from the rubber mounts only. Fig. 12 shows the characteristic of the contact, where the function indicates a linear behavior in case of a closed contact and no contact force in case of an open contact.

Fig. 13 shows the nonlinear response curve when taking contacts into account and with a damping coefficient of 0.08. There are again multiple solutions at some frequencies.

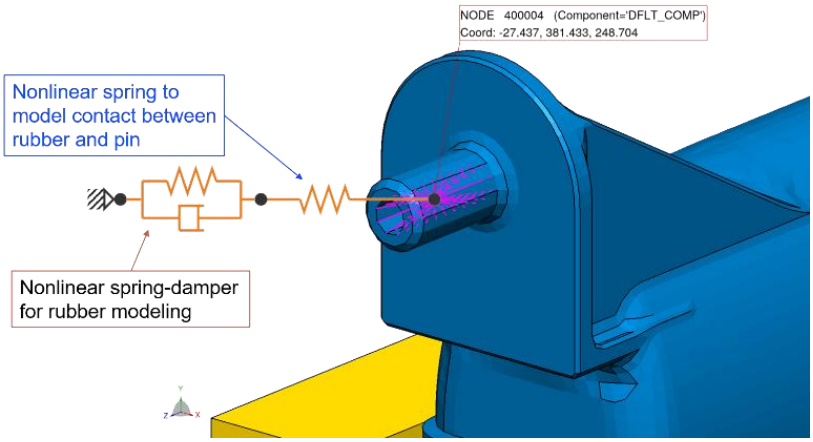

Fig. 21
The modeling of a rubber mount by a spring-damper system as in Fig. 6. In addition, a nonlinear spring is added to model the contact. This system has to be duplicated for all directions at all four pins. The three nodes of the spring-damper system and the contact have the same position in space. The node connected to the pin is connected to a center node of the pin, the node between rubber mount and contact is free in one direction, and the end-node of the rubber mount is fixed as in Fig. 6.

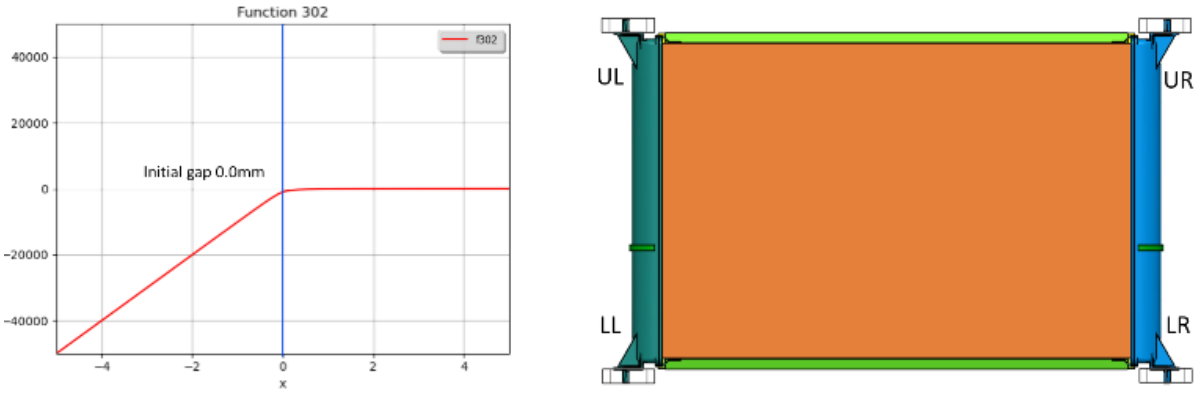

Fig. 32
The nonlinear function to model the contact is characterized by a linear behavior in case of a closed contact and no contact force in case on of an open contact.

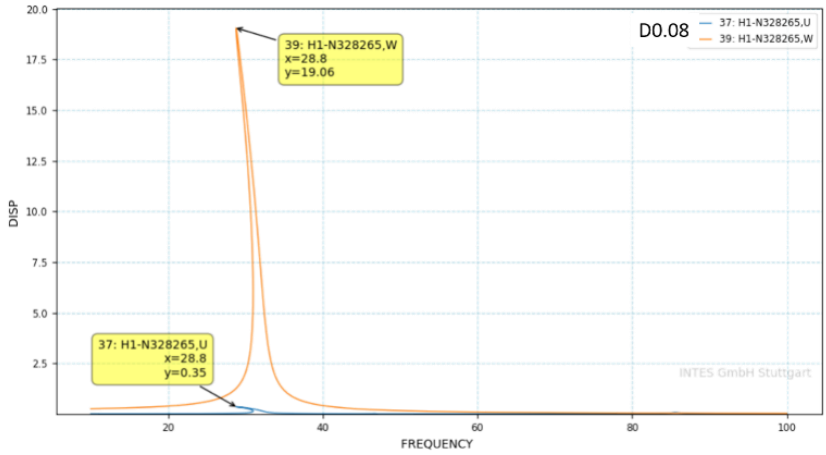

Fig. 43
For the reference node 328265, nonlinear HBM results with rubber mount and contact are shown simultaneously for DOF U and W.

In order to avoid multiple solutions at any frequency the damping coefficient of the rubber mounts has to be increased from 0.08 to 0.2. This is still in the range of possible rubber damping values (≤ 0.3). By increasing the damping coefficient from 0.08 to 0.2, all multiple solutions can be avoided. Fig. 14 shows the comparison of the response curves for both damping coefficients.

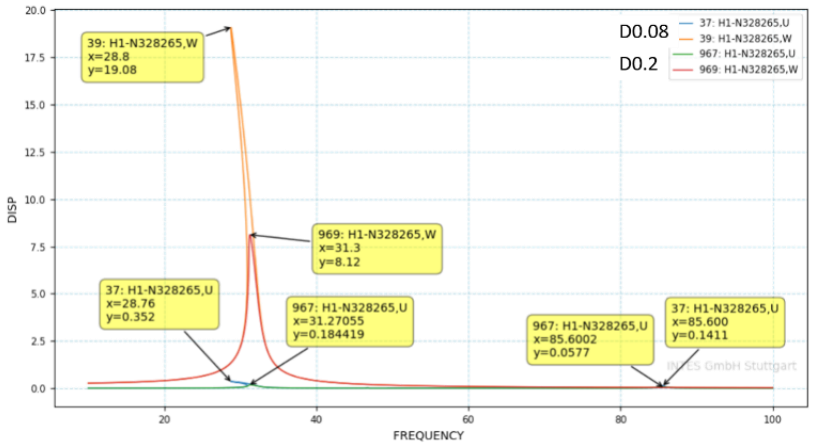

Fig. 14
For the reference node 328265, nonlinear HBM results for damping coefficients 0.08 and 0.2 are shown simultaneously for DOF U and W. The response with higher damping coefficient does not show any multiple solutions at same frequency anymore.

In addition, Fig. 15 shows the comparison of the response curves with and without contact, where the damping coefficient is 0.2 for both curves. The main resonance peak is now at 31.3 Hz with contact and at 47.2 Hz without contact. The maximum amplitude is 8 mm with contact and 2 mm without contact. If the mounting cannot avoid contact, the contact case is more critical.

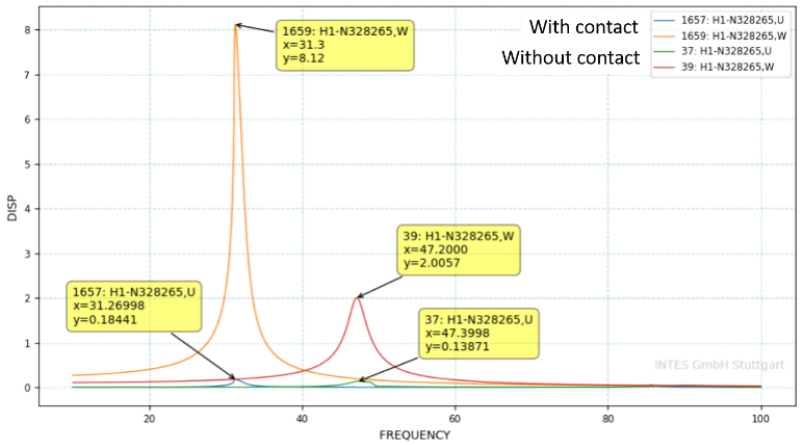

Fig. 55
For the reference node 328265, nonlinear HBM results for damping coefficient 0.2 are shown simultaneously for DOF U and W with and without contact.

6 Transformation to Time Domain

After solving with HBM, we have a solution in frequency domain. Using all calculated harmonics, a transformation to time domain is available. To this end, a frequency out of the HBM analysis is selected together with a timestep and a number of loops.

Taking the frequency of the highest resonance peak at 31.3 Hz (see Fig. 16) and using 100 loops, the timestep is

$$\Delta t = \frac{1.}{100.* 31.3} = 0.0003195$$

With these numbers, one gets two sine waves at 31.3 Hz with 200 timesteps. Now, we can check the spring element forces for rubber and contact.

Fig. 16 shows the rubber displacement and forces during the vertical motion of the radiator. The effect of contact is clearly visible. If upper contact is closed, the lower contact is open, and vice versa.

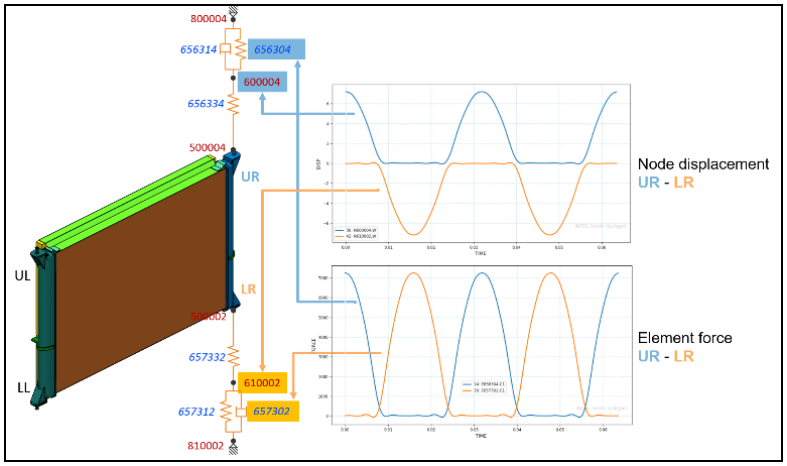

Fig. 66
During the vertical vibration of the radiator, the contact at the upper pin is closed while the contact at the lower pin is open and vice versa.

Fig. 17 shows the contact displacement and forces during the vertical motion of the radiator. The input of the contact is freely vibrating, the output shows the typical contact behavior

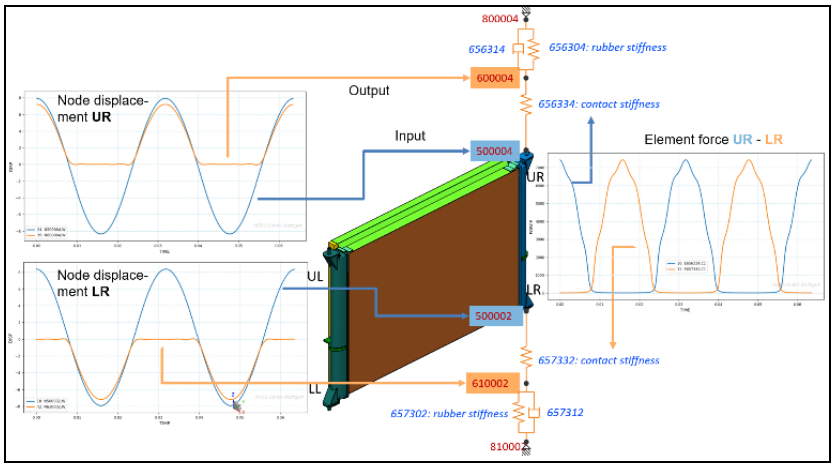

Fig. 77
During the vertical vibration of the radiator, the contact input is freely vibrating while the output of the contact cuts any penetration. This behavior is alternating at the upper and lower pin.

7 Fatigue Damage in Frequency Domain

After transformation to time-domain we perform a fatigue damage analysis for a subset of frequencies from 29.9 Hz to 34.9 Hz. Outside this frequency range, the fatigue damage is very close to Zero. Then, a fatigue damage is calculated for these frequencies with a timestep of 1/(100*f) and 200 timesteps. Fig. 18 shows the SN-curve of the tank material and the fatigue damage distribution over the used frequencies (here with the displacement response at node 357683). In addition, Fig. 19 shows the upper part of the right tank with the calculated fatigue damage and the highest damage at 31.36 Hz.

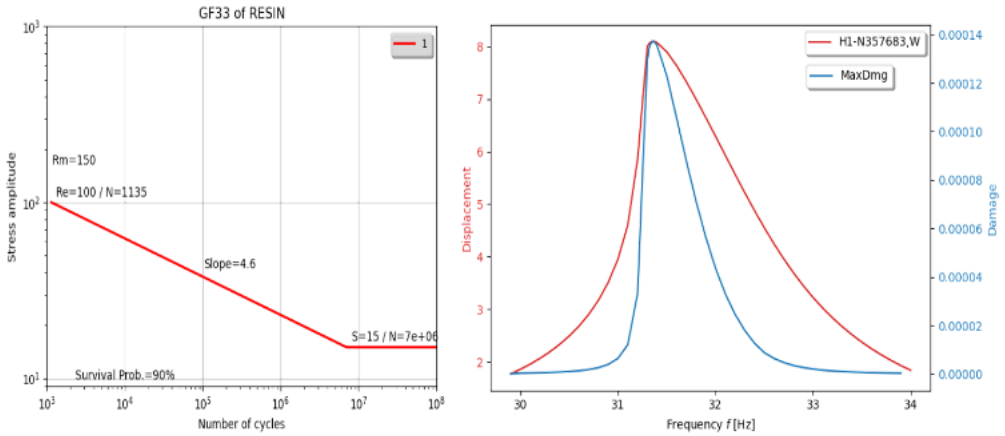

Fig. 88
SN curve of the tank material on the left. On the right, the damage is shown over the frequency (in blue) and the displacement response (in red). Maximum damage and displacement are at 31.36 Hz, 8.1 mm displacement, 1.37E-04 damage. This corresponds to a life time of 465 s (2/(dmg*f)) at this frequency.

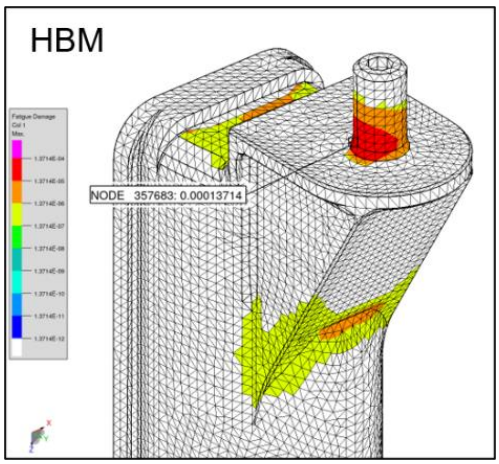

Fig. 19
Maximum damage 1.37E-04 at node 357683 for frequency 31.36 Hz.

The remaining point is now to check the maximum damage value by a time-history analysis using the same model with its nonlinear rubber mounts and contacts. A modal time-history analysis with the excitation function at 31.36 Hz is made. We need the steady-state results avoiding any non-periodic response. Therefore, we take 20000 timesteps and derive the fatigue damage for the last 200 timesteps as for the HBM. Fig. 20 shows the time history. Fig. 21 shows the fatigue damage in the right upper tank. The difference between HBM and TH (Time-History) result is

$$\frac{(TH - HBM)}{TH} = \frac{(0.00013795 - 0.00013714)}{0.00013795} = 0.00587 < 0.6\%$$

The damage is the same for HBM and time-history analysis, but runtime is much different. The elapsed run time on 28 cores is 1.5 hours for the time-history analysis compared to about 3 minutes with HBM for the same frequency.

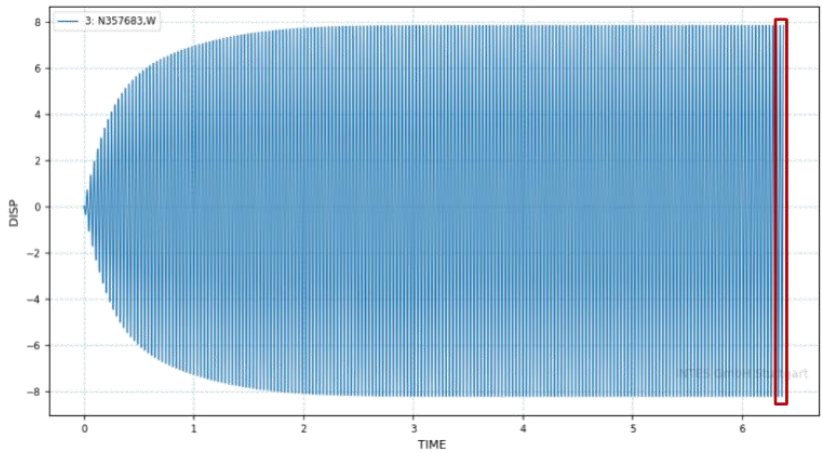

Fig. 20
Modal time-history analysis with fatigue damage calculation for the last 200 timesteps (red box).

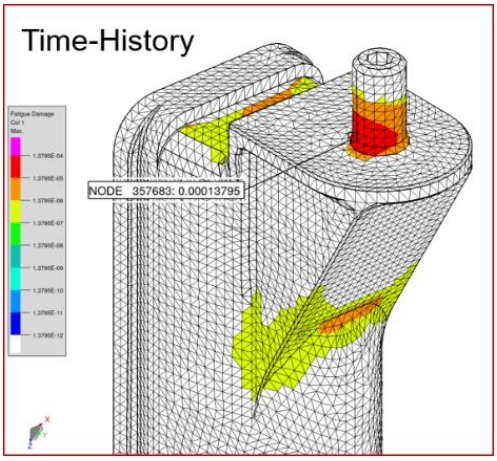

Fig. 21
Maximum damage 1.38E-04 from a modal time history analysis at node 357683 for frequency 31.36 Hz.

8 Conclusions

HBM is used to solve nonlinear dynamic problems in frequency domain. Nonlinearities used for the mounting of a radiator-like structure are rubber mounts and contacts at the 4 fixation pins. The force-deflection curve of rubber is made by a separate model, but could also come from a test result.

HBM results show multiple solutions for same frequency, which was cured by sufficient damping provided by the rubber mounts in order to avoid instabilities.

HBM results are transformed to time domain and followed by a fatigue analysis providing fatigue damage in frequency domain. For the frequency with the highest fatigue damage, a modal time-history analysis has been made giving the same fatigue damage.

HBM, time-history and fatigue analysis are all integrated in PERMAS, which allows one single job for all three analyses (with a run time of about 3 minutes per frequency).

9 References

[1] Cameron, T.M., Griffin, J.H.: An alternating frequency/time domain method for calculating the steady-state response of nonlinear dynamic systems, Journal of Applied Mechanics, Vol. 56, (1989), pp. 149—154 https://doi.org/10.1115/1.3176036

[2] Saunders, B.E., Vasconella, R., Kuether, R.J., Abdelkefi, A.: Insights on the continuous representation of piecewise-smooth nonlinear systems: limits of applicability and effectiveness, Nonlinear Dynamics, https://doi.org/10.1007/s11071-021-06436-w

[3] Mahmoodi, A., Ahmadian, H.: Forced Response Vibration Analysis of the Turbine Blade with Coupling between the Normal and Tangential Direction, Vol. 2022, https://doi.org/10.1155/2022/2413022

[4] Lentz, L., von Wagner, U.: Avoidance of artifacts in harmonic balance solutions for nonlinear dynamical systems, Journal of Theoretical and Applied Mechanics 2020; 58(2): pp. 307–316, https://doi.org/10.15632/jtam-pl/118161

[5] Martinelli, C., Coraddu, A. & Cammarano, A.: Approximating piecewise nonlinearities in dynamic systems with sigmoid functions: advantages and limitations, Nonlinear Dyn (2023), https://link.springer.com/article/10.1007/s11071-023-08293-1

[6] PERMAS Examples Manual, INTES Publication No. 550, Stuttgart, 2022

10 Contact Information

For questions and more information, please contact Michael Klein by e-mail Michael.klein@intes.de.

Managing technical parameters to setup virtual tests

Hardy Krappe, Alexander Mahl (PDTec AG)

1 Summary

In today's complex engineering environments, managing technical input parameters and simulation results is a crucial task. Beside managing those data, the full traceability from input data such as technical parameter to test results becomes increasingly important. In order to reach this goal, technical parameters needs to be represented in an “machine understandable” way. Collecting the required input data is often a time consuming task for simulation engineers. This could be significant reduced by providing a central, intelligent data hub which could be a main source for any Engineer.

This paper describes concepts how technical parameters could be collected, managed and used efficiently by Engineers. The paper suggests a “request” and “delivery” process for collecting the technical parameters. Due to amount of data it is important to provide comprehensive overview to users responsible for delivery and consumer.

Full traceability of all input data including technical parameters, simulation models and output data is required from a simulation process and data management system (SPDM). This ensures that all relevant input data is properly documented and stored, so all simulation results can be accurately tracked and reported. This enables the Engineer detect differences in input data (e.g. technical parameters) for given simulations.

2 Concept for managing technical parameters

In the context of this paper, the term “technical parameters” or “technology data” describes characteristics of a product (E.g., car, wheel loader), components (E.g, axis) or systems (E.g., brake system). Examples for technical parameters are mass of a component or product , mass inertia, motor characteristics, bushing curves of an axis etc. In case of automotive industry examples would be bushing curves on front axis, weight of axis etc. This could be several hundred for one car. There are various technical parameters which are input for simulations.

They need to be collected by the simulation Engineer in order to setup its installation. The process of collection the “correct” data may be time consuming. Typically there is no “unified” naming for the technical parameters and no unified data format. Sometimes the relevant information needs be taken from pdf file, excel file or text from an e-mail.

Managing technical parameters in an central IT system and common format would be very beneficial for simulation engineers: Data would be easily accessible by the engineer and would save time to manually collect the information. Storing the technical parameters in machine readable format enables automatization capabilities.

2.1 Representation of technical parameters in a management system

In order to manage technical parameters in an IT system in structured way, a proper representation is required. There could be multiple “data types” of technical parameters identified – such as curves (real and complex values), single values, data tables or 3D data grids etc.

As stated above, there are many technical (product) parameters required to be handled. Those depend strongly on the product(s) to be described and may be extended over the time. Therefore a flexible approach is required. We suggest a “catalogue” which describes all available technical parameters. In our approach, the catalogue defines catalog elements which relate to data set definitions that in turn describe a set of data item definitions that represent the physical representation of the technical parameters.

A “Dataset Definition” groups technical parameters of a product, component or system. Examples for a dataset definition would be “vehicle parameters” or “Bushing of front axle”. The dataset bushing of front axle may consists of technical parameters like translation stiffness in x, y and z direction (type=curves). Each data item represents a technical parameter and is from one of the defined data types (single value, curve etc.). Here also aspects like axis name, unit etc. needs to be considered.

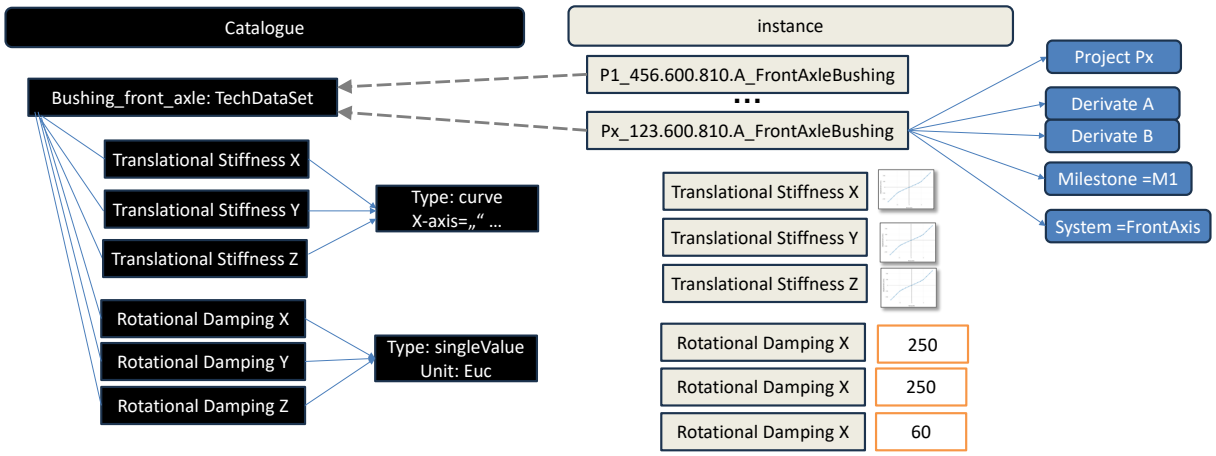

Figure 1: Representation of technical parameters based on catalogue

Moreover there might be many “product variants” (derivates) which adds additional complexity. This is handled by intelligent advanced mechanism.

2.2 Support process for collecting technical parameters

Proving a management system for technology data is one important pillar of the solution. Another also very important pillar is the process of delivering all relevant data to the management system. Here we have consider one very important aspect: In many cases users who “provide” the technical parameters are not the consumer. That means it is an additional

effort for the individual person. Of course, the entire company benefits from that but to be successful the process of providing the data must be as convenient (and user friendly) as possible.

Typically technical parameters are required at least for each design milestone of a development project. But also continuous managing the data is required to support simulation tasks between milestones.

Thanks to standardization reached by catalogue mechanism, an Engineer can request the data needed to accomplish the simulation (or testing) task – which may be milestone driven or not. The process itself needs to be established by the company itself and it may highly vary between companies. This is due to diversity of companies (E.g. OEM, suppliers (first tier, second tier) or engineering service providers) and their boundary conditions.

In order to support this with a standard software, this “flexibility” needs to be taken in account. The approach suggested in this paper is to provide a “process library” which provides the relevant process step (E.g., “define request”, “validate request”, “deliver request”). Those steps could be assigned to roles which are “build-in” or defined by customer. Based on these bricks the process could be assembled.

3 Setup virtual tests and keep full traceability

Beside CAD, technical parameters are one of the main sources for the simulation Engineer to prepare the input models for a simulation. Without support by software it is a manual task to populate the solver models with the corresponding data. Thanks to standardized storage of the technical parameters, this process step could be automated. This depends on solver an methodology how simulation engineer builds its solver models. Therefore a “plugin interface” for executing custom logic is suggested.

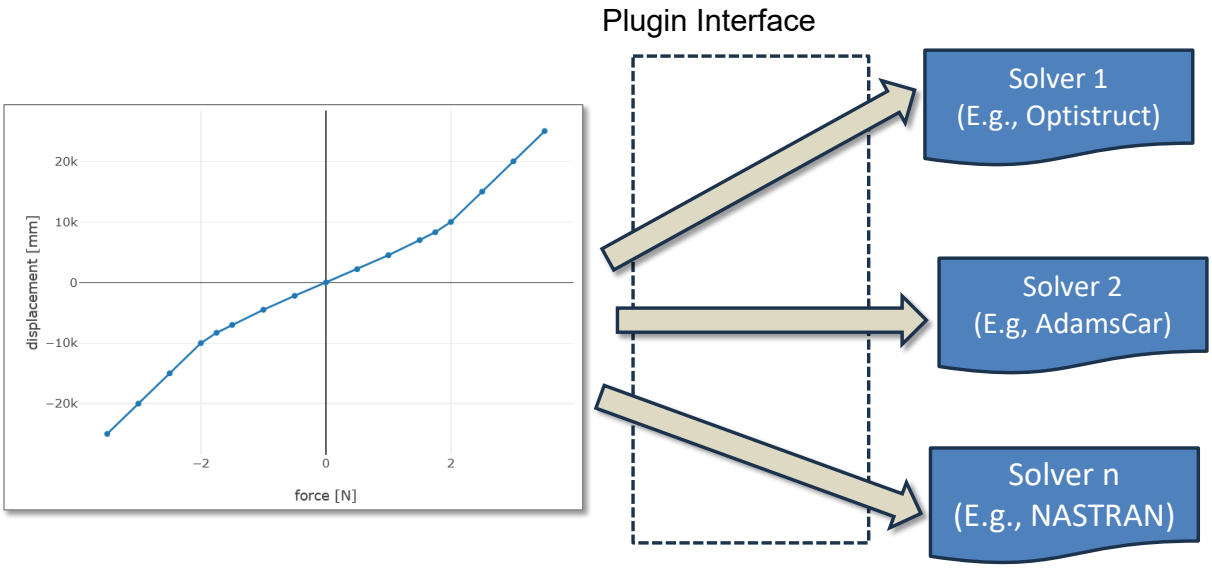

Figure 2: Propagate technical parameters into solver specific models automatically

Looking at the entire CAE process, preparing the input models is first step. After that simulation will be setup and solving will be executed. The results will be analyzed by the engineer and rated against target criteria.

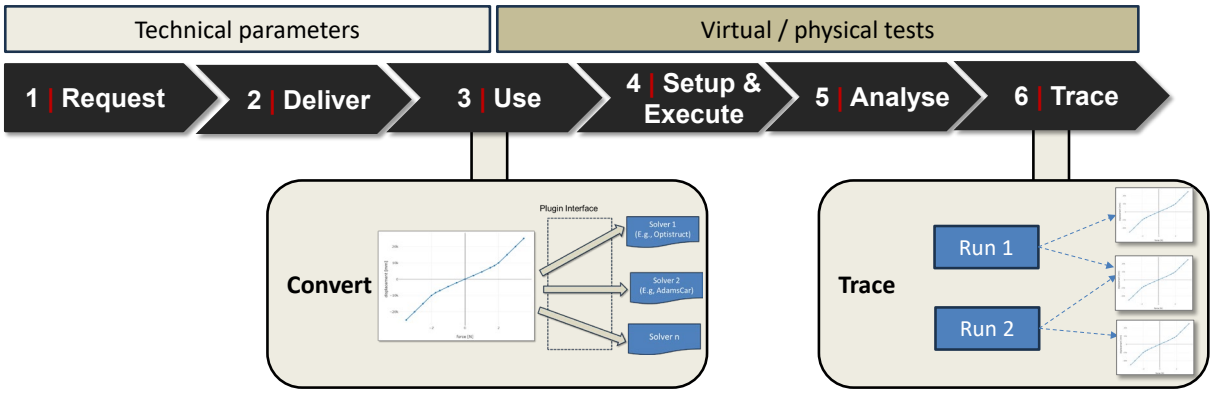

Figure 3: CAE process connected with technical parameter management

Tracing technical parameters as input for the simulation is another requirements to be handled by management system. As an additional benefit, It could be detected if two simulations base on different technical parameters even different solvers or even different domains. For example a FEM simulation (E.g., Optistruct or NASTRAN) and a MBS simulation (E.g. AdamsCar) could be checked if they base on same technical parameters.

The concepts described in this paper were implemented in SimData Manager representing one technical solution. Here the traceability is visualized by a graph with boxes which represents a set of objects.

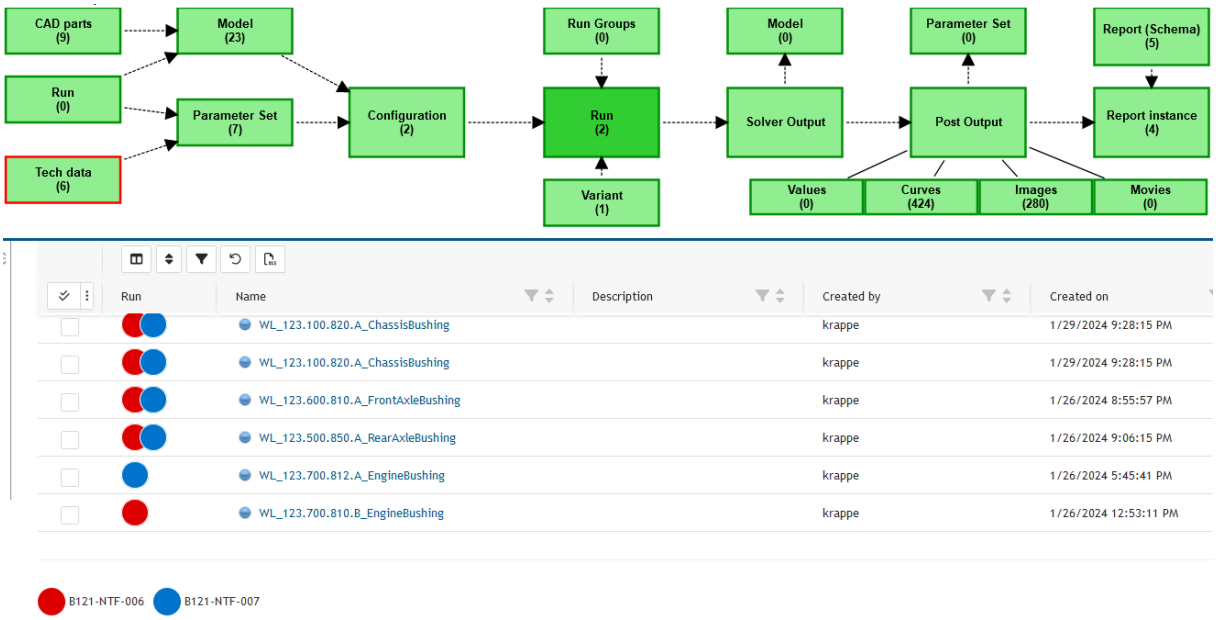

In this case we trace two simulations (runs). The grpah shows all input data and output data of those simulations. The box “Tech data” contains the technical data used as input for the

simulations to be traced. The column “run” indicates which technical data is used in which simulation. This is one possible way of visualizing common usages and differences.

4 Conclusions

The paper describes concepts in the context of handling technology data and the efficient usage as base for virtual and physical test. Due to diversity of technical parameters, a catalogue mechanism was suggested. This could be setup according to the needs of the company their products and processes. A customizable request and order process may be put in place to populate the management system with technology data to be used by simulation Engineers as single source of truth. Storing technical parameters in machine readable format and a generic plugin interface is an enabler for automated converting the technical parameters into solver specific models. This reduces significantly the time for collecting the input data and setup of solver models.

Tracing technical parameters used in a simulation is one of the key benefits using management systems such as SimData Manager for handling technology data and simulation data.

Automatische, baugruppenbasierte Modellierung und Simulation

Alexandru Dadalau (Meshparts GmbH)

1 Zusammenfassung

Die Baugruppenbasierte Modellierung ist seit vielen Dekaden ein Standard in der CAD-Modellierung. Nur so lassen sich komplexe Baugruppen wirtschaftlich realisieren.
Seit nun mehr als 10 Jahren wurde dieser Modellierungsansatz durch Meshparts in die Welt der FE (Finite-Elemente)-Modellierung übertragen.
Bald steht in steht in der Meshparts-Software auch PERMAS als Solver zur Verfügung.
Wir zeigen, welche Vorteile die neue Kombination aus Pre-, Postprozessor und Solver mit sich bringt.

1.1 CAD-Zwilling

Den FE-Modellierungsansatz von Meshparts bezeichnen wir als CAD-Zwilling (CAD Twin). Ein CAD-Zwilling ist ein FE-Modell mit identischer Modell- und Dateistruktur verglichen mit einem CAD-Modell. Das bedeutet, dass ein CAD-Zwilling 100% einer CAD-Baugruppe entspricht, wobei man gedanklich die CAD-Komponenten durch FE-Komponenten ersetzen sollte.

Beim Aktualisieren einer FE-Baugruppe (eines CAD-Zwillings) wird für jedes einzelne FE-Teil geprüft, ob das entsprechende CAD-Teil geändert wurde. Geänderte CAD-Teile werden wieder importiert und neu vernetzt. Auf dieser Weise lassen sich FE-Modelländerungen deutlich schneller und praktisch unabhängig von der Baugruppenkomplexität durchführen.

2 FE-Modellbibliothek

Darüber hinaus, der CAD-Zwilling erlaubt die direkte Integration einer FE-Modellbibliothek. Insbesondere im Maschinenbau (aber nicht nur) werden Baugruppen entwickelt, die auf wiederkehrende Teile basieren. Beispiele dafür sind Linearführungen, Wälzlager, Kupplungen, Schrauben, Servoantriebe, Kugelgewindetriebe usw. Ein FE-Bibliotheksteil kann aber auch ein eigenes FE-Modell oder -Baugruppe sein, die oft in den entwickelten Produkten vorkommt. Jedenfalls erlaubt die FE-Modellbibliothek eine signifikante Verkürzung der FE-Modellierungszeit. Gleichzeitig ergibt sich dadurch eine Reduktion der Fehlerwahrscheinlichkeit, weil die Komponenten nach der Erprobung unverändert in neue Modelle übernommen werden. Die Anwender benötigen dank der Standardisierung weniger Expertenwissen, um komplexe und detaillierte FE-Modelle aufzubauen.

3 Automatisierung der Modellierungsprozesse

Die oben eingeführten zwei Grundbausteine (CAD-Zwilling und FE-Modellbibliothek) der FE-Modellierung mit Meshparts erlauben die Automatisierung von FE-Modellierungsprozessen. Mit Blick auf die Schwierigkeiten bei der Automatisierung sind die FE-Modellierung von Zukaufteilen und die automatische und korrekte Kontaktdefinition zu nennen.

Die FE-Modellierung der Zukaufteile, die sonst ein manueller Prozess ist, wird in Meshparts durch die sogenannten Part-Mappings. Dies sind Tabellen, die Namen von CAD-Komponenten zu FE-Komponenten aus der FE-Modellbibliothek mappen. Bei einem neuen CAD-Import werden CAD-Teile, in der Mapping-Tabelle vorhanden sind, automatisch durch entsprechende FE-Modelle aus der Bibliothek ersetzt. Dadurch wird der erste Teil der Automatisierung „on-the-fly“ erledigt.

Bei der automatischen und korrekten Kontaktdefinition besteht die Schwierigkeit automatisch zu erkennen, welche Kontaktpaare bspw. Reib- oder Verbundkontakte sein sollen. Unser Ansatz besteht aus einer farbbasierten Definition auf CAD-Teil-Ebene von Kontaktflächen. Rote Flächen bspw. sind Reibkontakte, blaue Flächen dagegen Verbundkontakte. Die manuelle Definition der Kontakte verlagert sich also von der FE-Software in die CAD-Software. Die Vorteile bei dem Ansatz sind, dass der Konstrukteur die Definition der Kontakte ohne FE-Spezialwissen vornehmen kann und dass die

Definition in der Regel nur einmal gemacht werden muss. Bei neuen Versionen des gleichen CAD-Teils bleiben die Farben in der Regel erhalten.

4 Fazit

Meshparts ist ein Pre- und Post-Prozessor für die FE-Modellierung und -Ergebnisvisualisierung. Das eigentliche Lösen der FE-Modelle erfolgt mit externen FE-Solvern, derzeit PERMAS, ANSYS, ABAQUS, CALCULIX und RISTRA. Der Anbindung des PERMAS-Solvers ist noch in der Entwicklung jedoch zeigt sich jetzt schon, dass dieser Solver bedeutende Vorteile hinsichtlich der Rechenperformance mit sich bringt. Des Weiteren erreichen wir durch die enge Zusammenarbeit mit der Firma INTES aus Stuttgart eine bessere Integration des Solvers in Meshparts. Wir blicken daher gespannt auf das baldige offizielle Release der Meshparts-PERMAS-Kombination.

meshparts

Automatic, assembly-based modellingmodelling and simulation

NAFEMS DACH Users Conference, Bamberg

2024.06.12

1

meshparts
einfach – präzise – simulieren

Overview

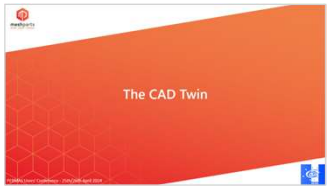

PERMAS Users' Conference - 25th/26th April 2024

2

What is Meshparts?

PERMAS Users' Conference - 25th/26th April 2024

3

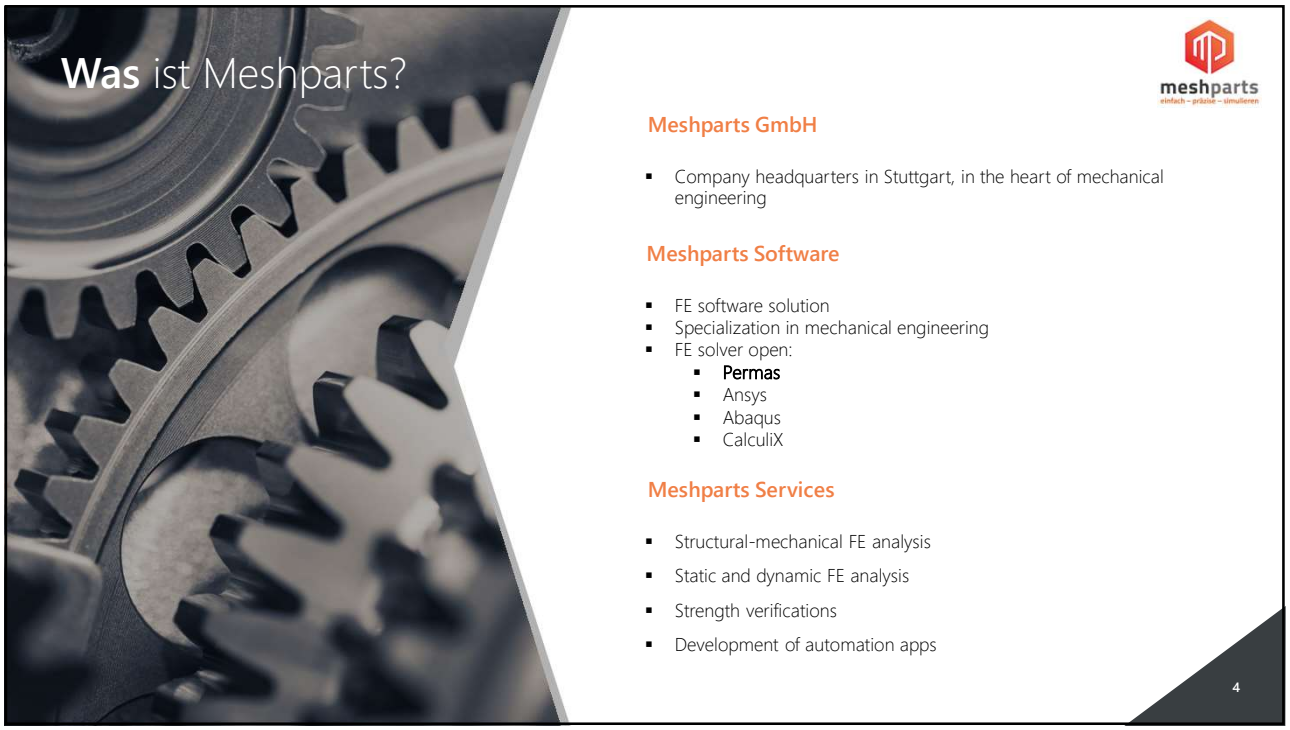

4

How does Meshparts and Permas work together?

5

Simulation process between Meshparts and Permas

Meshing & Modelling with Meshparts → Generation of Abaqus Input File for Permas (including UCI) → Solving with Permas → Postprocessing with Meshparts

6

Currently supported computations with Permas Solver

- Static, modal and transient analysis
- Linear tied connections
- Nonlinear friction contact
- Non-linear springs

7

Future developments of the interface to Permas Solver

- Pretension joints
- Non-linear materials
- Connection to Permas topology optimization

8

The CAD Twin

PERMAS Users' Conference - 25th/26th April 2024

9

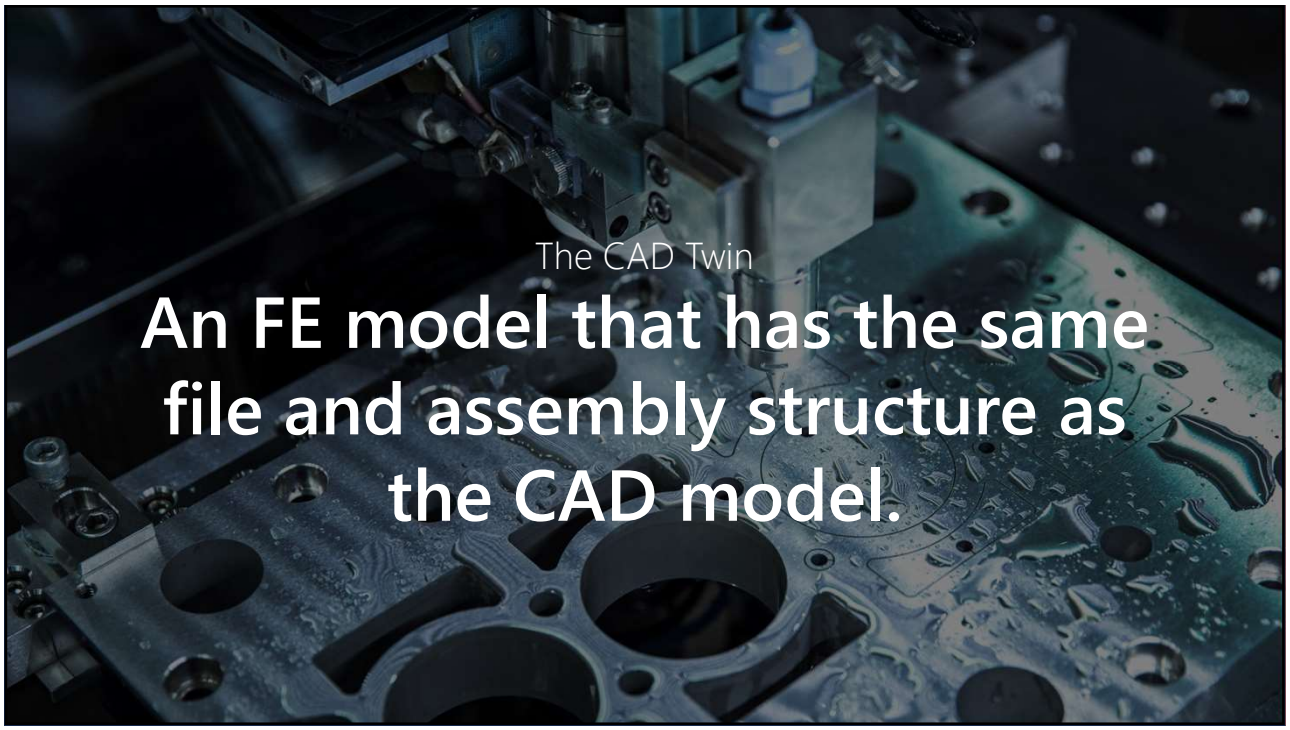

10

File structure in Meshparts

Name	Typ
Fraeseinheit_1.mpasm	MPASM-Datei
Maschine_1.mpasm	MPASM-Datei
PortalBG_1.mpasm	MPASM-Datei
XAchse_1.mpasm	MPASM-Datei
XAntriebsstrang.mpasm	MPASM-Datei
XZAchsen_1.mpasm	MPASM-Datei
ZAchse_1.mpasm	MPASM-Datei
ZAntriebsstrang.mpasm	MPASM-Datei
ZKupplung_1.mpasm	MPASM-Datei
1 MR W 35-A-G0-V1-R1-CN-S10-LN.inp.mpprt	MPPRT-Datei
1 MR W 35-C-G0-V1-R1-CN-S10-LN.inp.mpprt	MPPRT-Datei
1502-3-4086_f_s_77_01.inp.mpprt	MPPRT-Datei
900114-006_T1~0_1_1.inp.mpprt	MPPRT-Datei
900114-006_T2~0_1_1.inp.mpprt	MPPRT-Datei
Fraesspindel_1.inp.mpprt	MPPRT-Datei
Fraesspindelaufnahme_1.inp.mpprt	MPPRT-Datei
MS2N06-EXXXN-AXUH0-XNXNN-NN.inp.mpprt	MPPRT-Datei
Portal_1.inp.mpprt	MPPRT-Datei
Spacer_ZWagen_1.inp.mpprt	MPPRT-Datei
XLoslagerhalter_1.inp.mpprt	MPPRT-Datei
XMesskopf.inp.mpprt	MPPRT-Datei

9 assemblies

12 parts

File structure in CAD

Name	Typ
Fraeseinheit_1.sldasm	SOLIDWORKS Assembly Document
Maschine_1.SLDASM	SOLIDWORKS Assembly Document
PortalBG_1.sldasm	SOLIDWORKS Assembly Document
XAchse_1.sldasm	SOLIDWORKS Assembly Document
XAntriebsstrang.sldasm	SOLIDWORKS Assembly Document
XZAchsen_1.sldasm	SOLIDWORKS Assembly Document
ZAchse_1.sldasm	SOLIDWORKS Assembly Document
ZAntriebsstrang.sldasm	SOLIDWORKS Assembly Document
ZKupplung_1.sldasm	SOLIDWORKS Assembly Document
1 MR W 35-A-G0-V1-R1-CN-S10-LN.sldprt	SOLIDWORKS Part Document
1 MR W 35-C-G0-V1-R1-CN-S10-LN.sldprt	SOLIDWORKS Part Document
1502-3-4086_f_s_77_01.sldprt	SOLIDWORKS Part Document
900114-006_T1~0_1_1.sldprt	SOLIDWORKS Part Document
900114-006_T2~0_1_1.sldprt	SOLIDWORKS Part Document
Fraesspindel_1.sldprt	SOLIDWORKS Part Document
Fraesspindelaufnahme_1.sldprt	SOLIDWORKS Part Document
MS2N06-EXXXN-AXUH0-XNXNN-NN.sldprt	SOLIDWORKS Part Document
Portal_1.sldprt	SOLIDWORKS Part Document
Spacer_ZWagen_1.sldprt	SOLIDWORKS Part Document
XLoslagerhalter_1.sldprt	SOLIDWORKS Part Document
XMesskopf.sldprt	SOLIDWORKS Part Document

11

Model structure in Meshparts

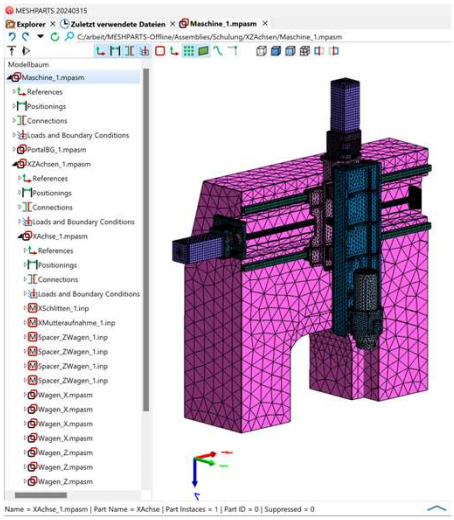

Model structure in CAD

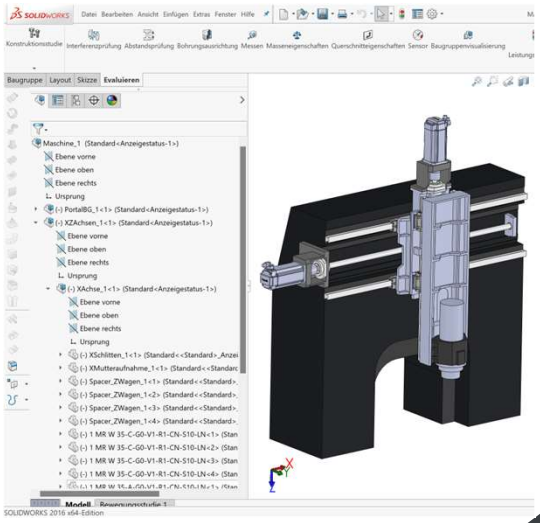

12

1. Original part in CAD

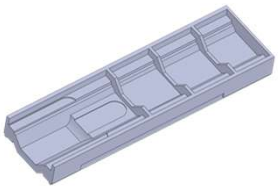

2. Modified part in CAD

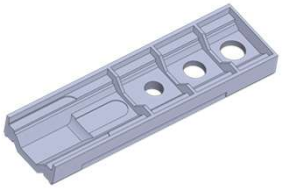

3. Updated part in the FE assembly

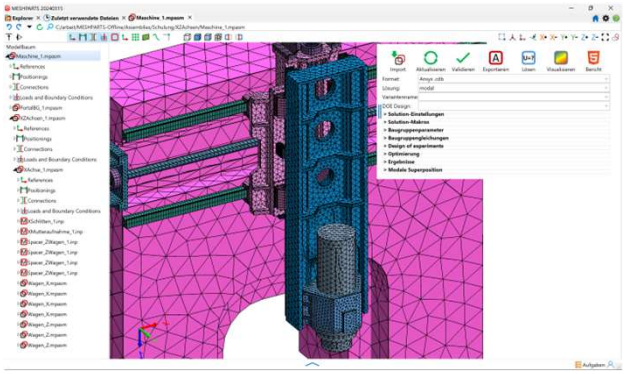

- When updating the FE assembly, for each individual FE part the corresponding CAD part is checked for modification.
- Modified CAD parts are re-imported and re-meshed.

13

Demo video

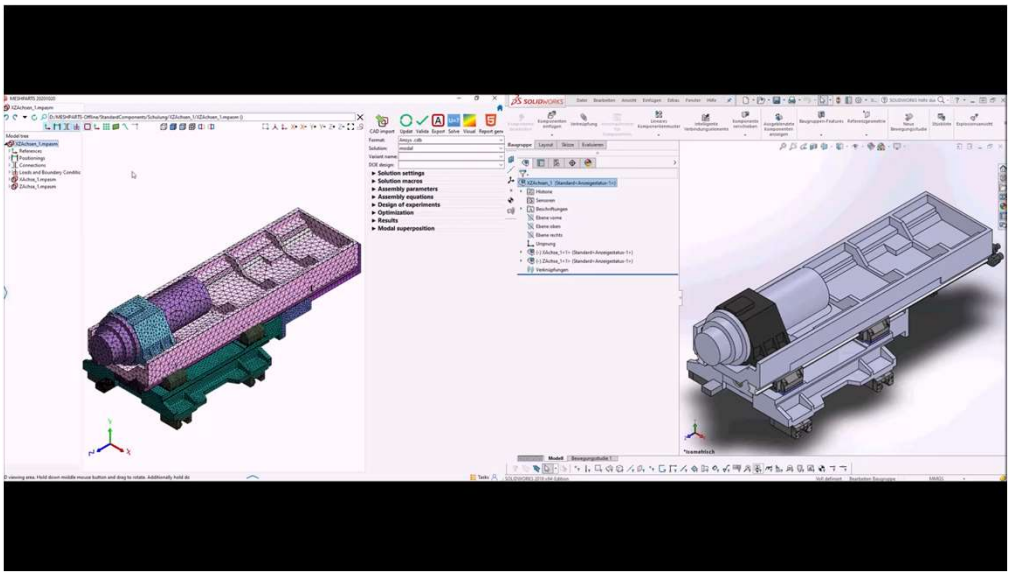

14

The FE Model Library

15

FE Model Library

- A collection of finished FE models
  - FE parts
  - FE assemblies
- Typically, these are purchased parts
  - Rolling bearings
  - Linear guides
  - Ball screw drives
  - Servo motors
  - Couplings
  - Gearboxes
  - etc.
- Your own specific libraries are also possible

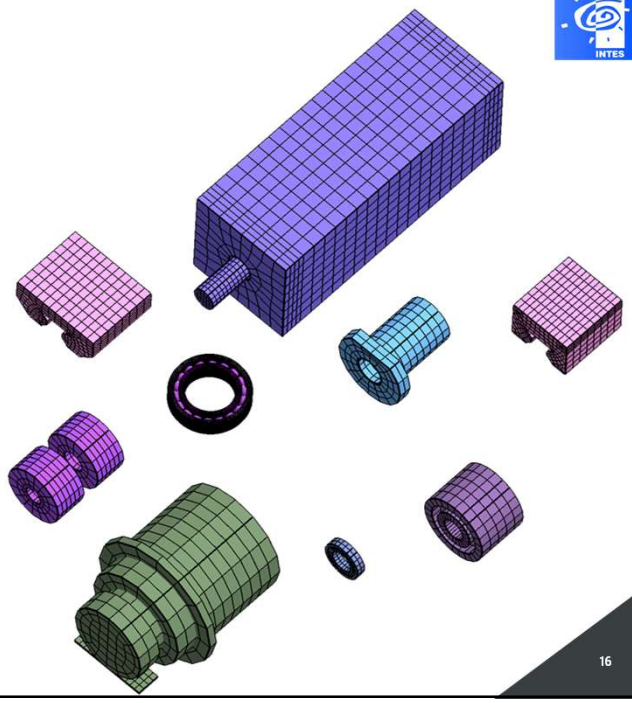

16

FE Model Library

- The models contain all the necessary physical properties:
  - Mass, Inertia
  - Stiffness
  - Kinematic transmission
  - Damping

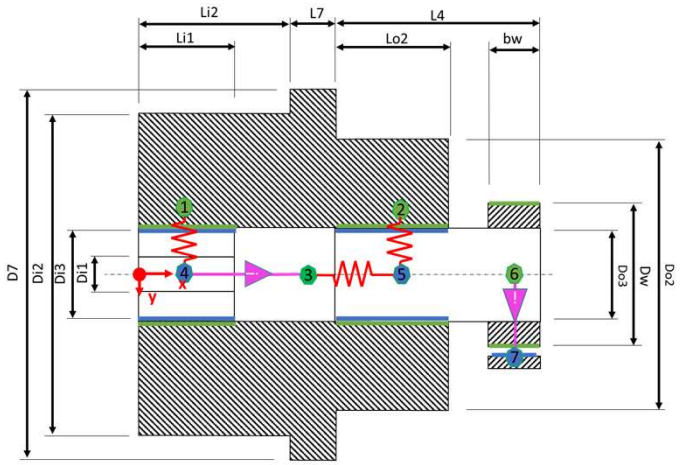

17

CAD single part

- Mass is usually incorrect because internal details are filled in
- Stiffness is greatly overestimated because rolling elements, gears etc. are not shown
- Kinematic transmission not represented (gearbox, ball screw nut)

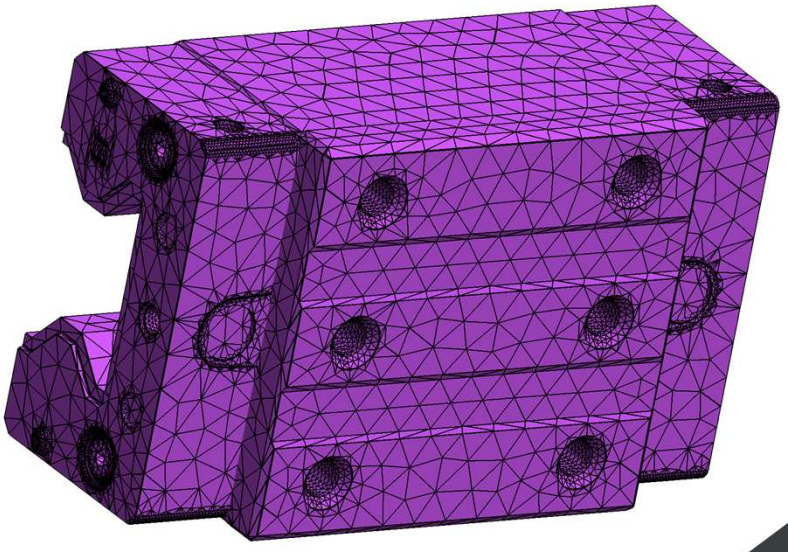

18

FE Part

- Mass is modeled correctly via point masses or equivalent density
- Stiffness is modeled correctly using equivalent springs
- Kinematic transmission is modeled via coupling equations (gearbox, ball screw nut)

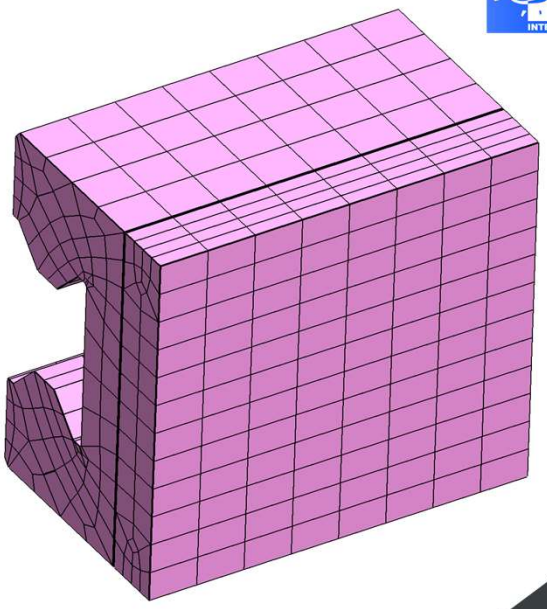

19

First step

- Select CAD part to be replaced
- Call replace function

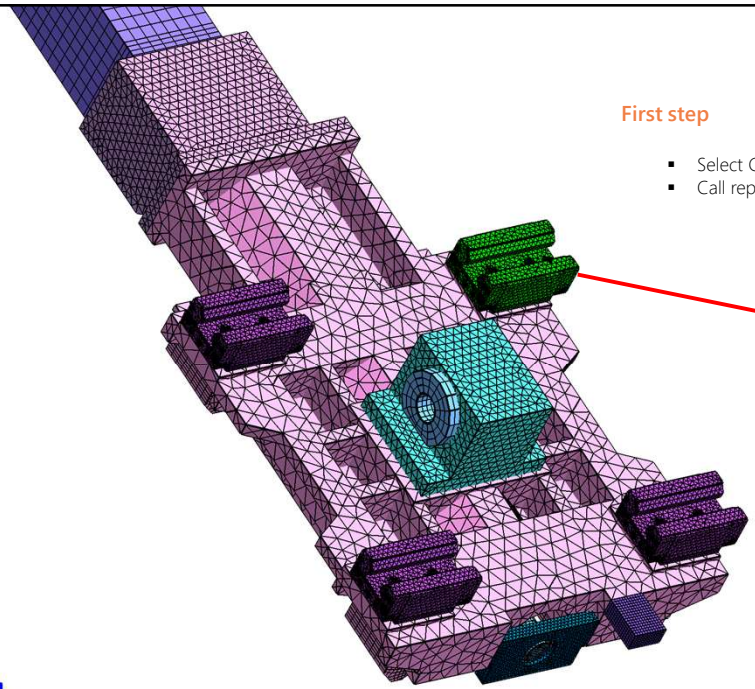

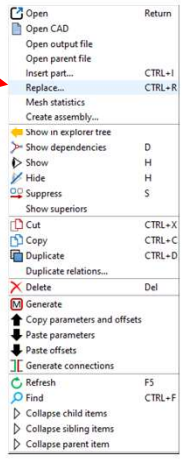

20

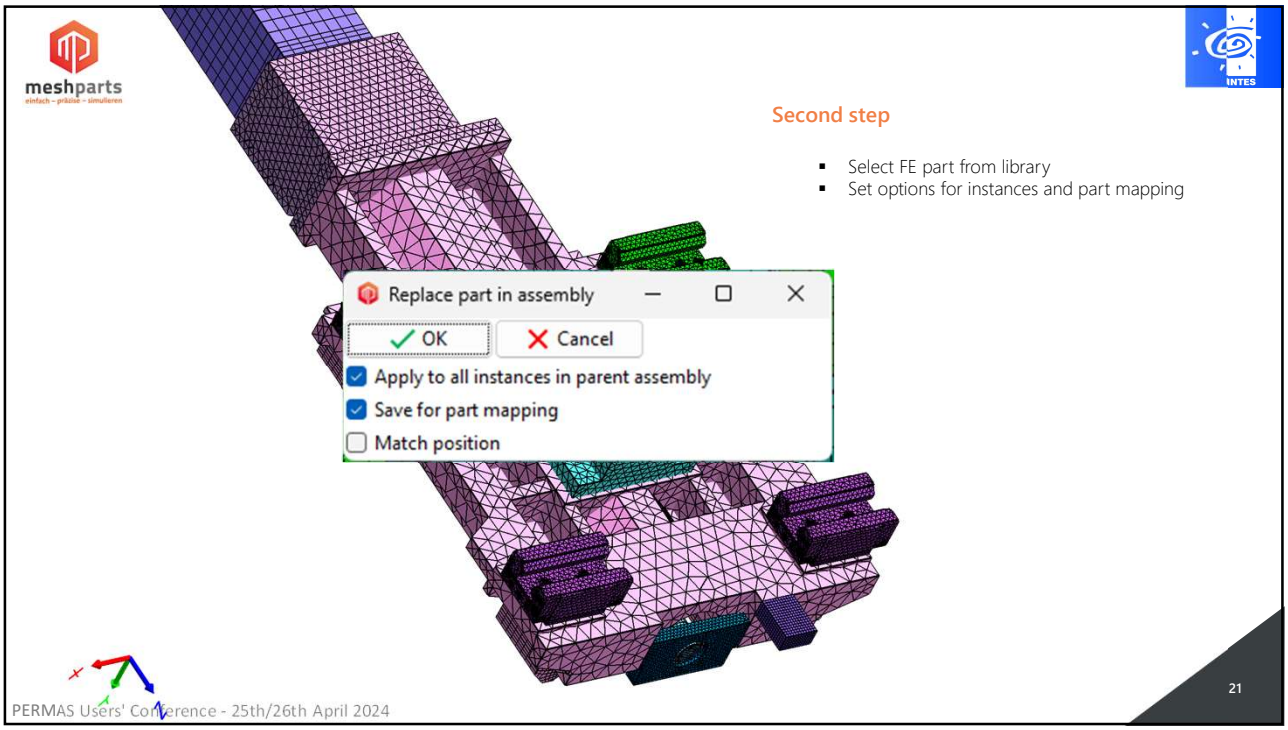
meshparts
einfach – präzise – simulieren
INTES
Second step
Select FE part from library
Set options for instances and part mapping
Replace part in assembly
OK
Cancel
Apply to all instances in parent assembly
Save for part mapping
Match position
PERMAS Users' Conference - 25th/26th April 2024
21

21

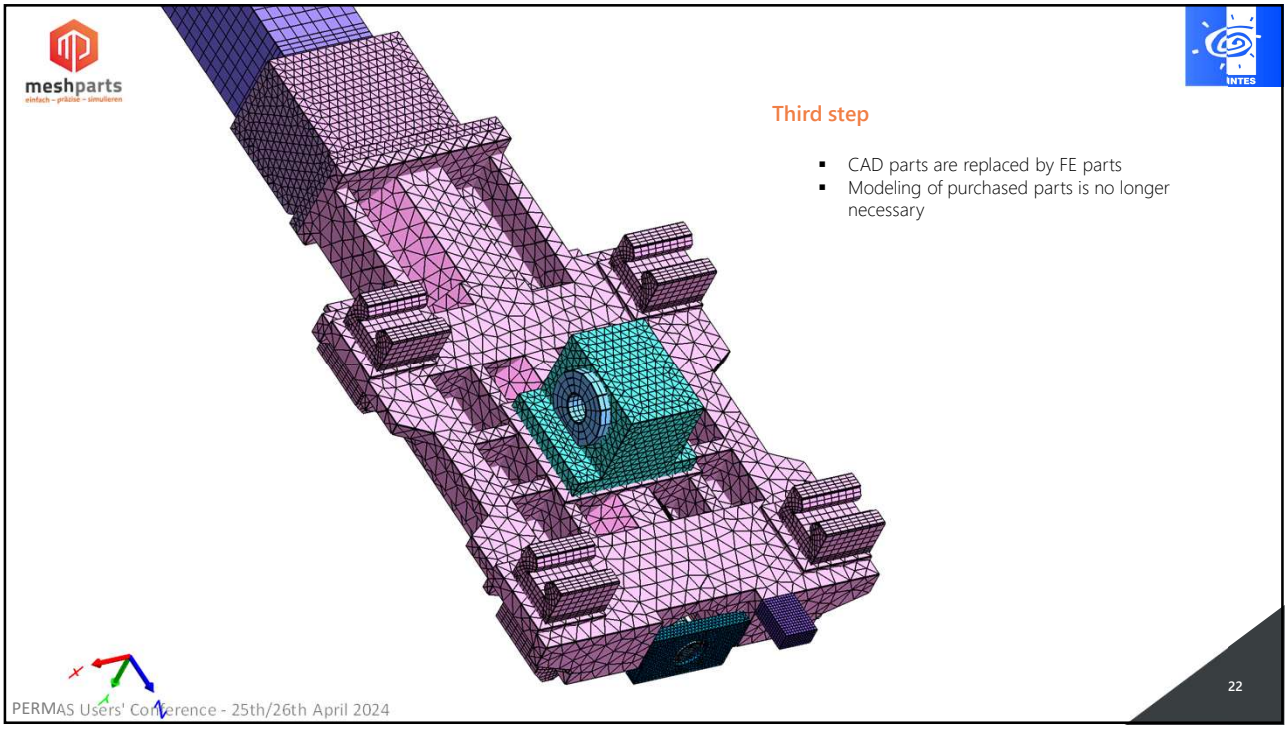
meshparts
einfach – präzise – simulieren
INTES
Third step
CAD parts are replaced by FE parts
Modeling of purchased parts is no longer necessary
PERMAS Users' Conference - 25th/26th April 2024
22

22

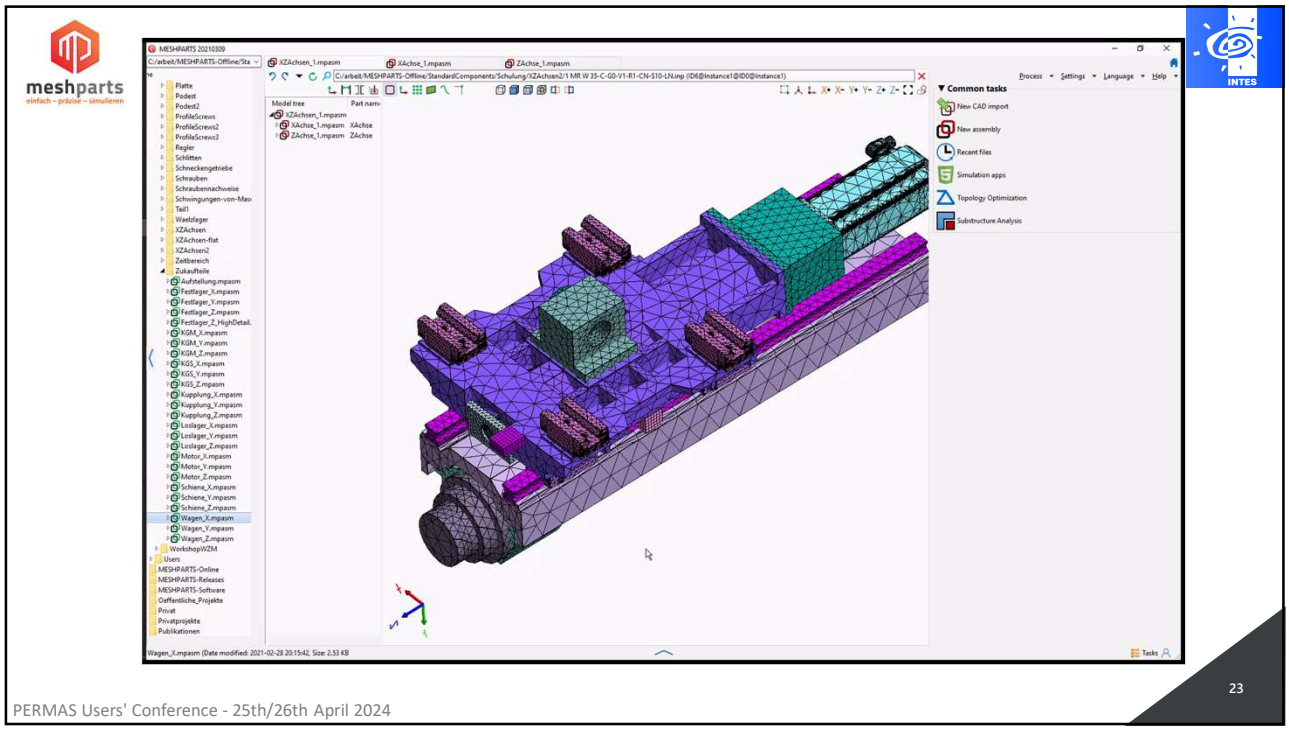
meshparts
einfach – präzise – simulieren
INTES
Common tasks
New CAD import
New assembly
Recent files
Simulation apps
Topology Optimization
Substructure Analysis
PERMAS Users' Conference - 25th/26th April 2024
23

23

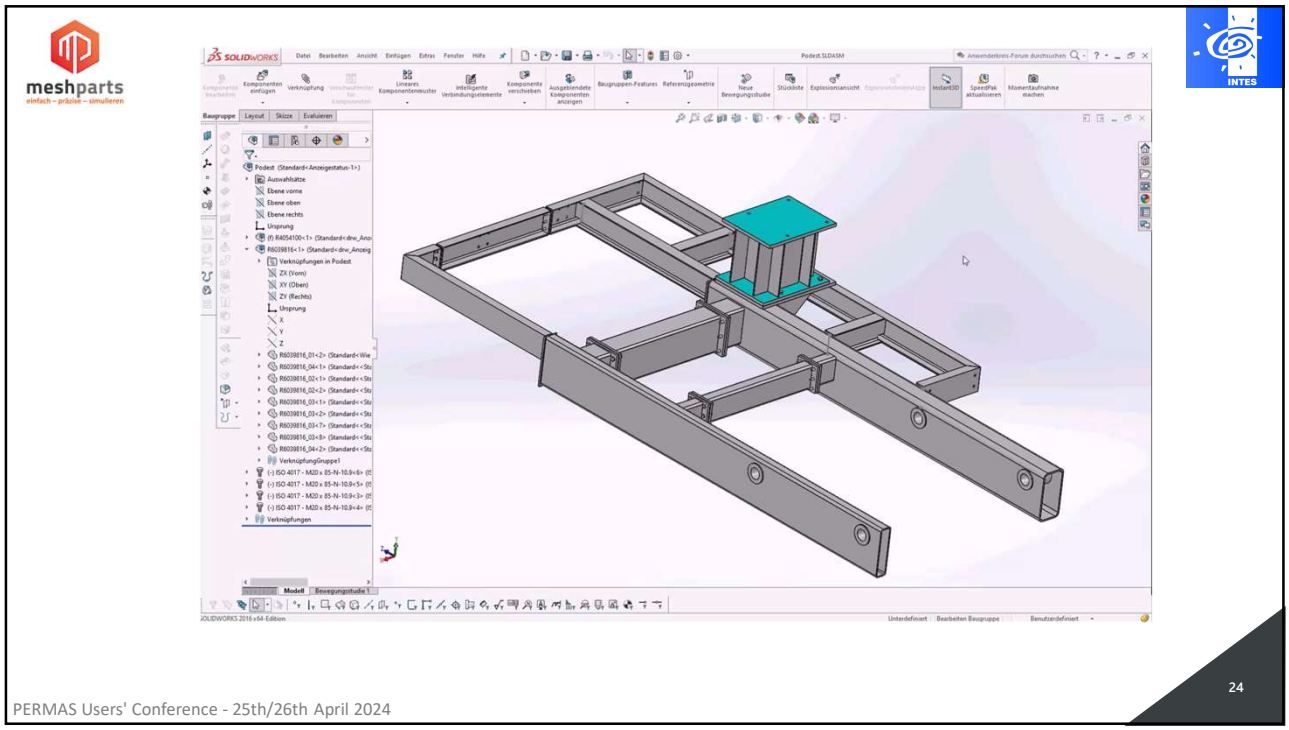
meshparts
einfach – präzise – simulieren
INTES
PERMAS Users' Conference - 25th/26th April 2024
24

24


meshparts
einfach – präzise – simulieren
Automatic Purchased Parts
PERMAS Users' Conference - 25th/26th April 2024
INTES

25

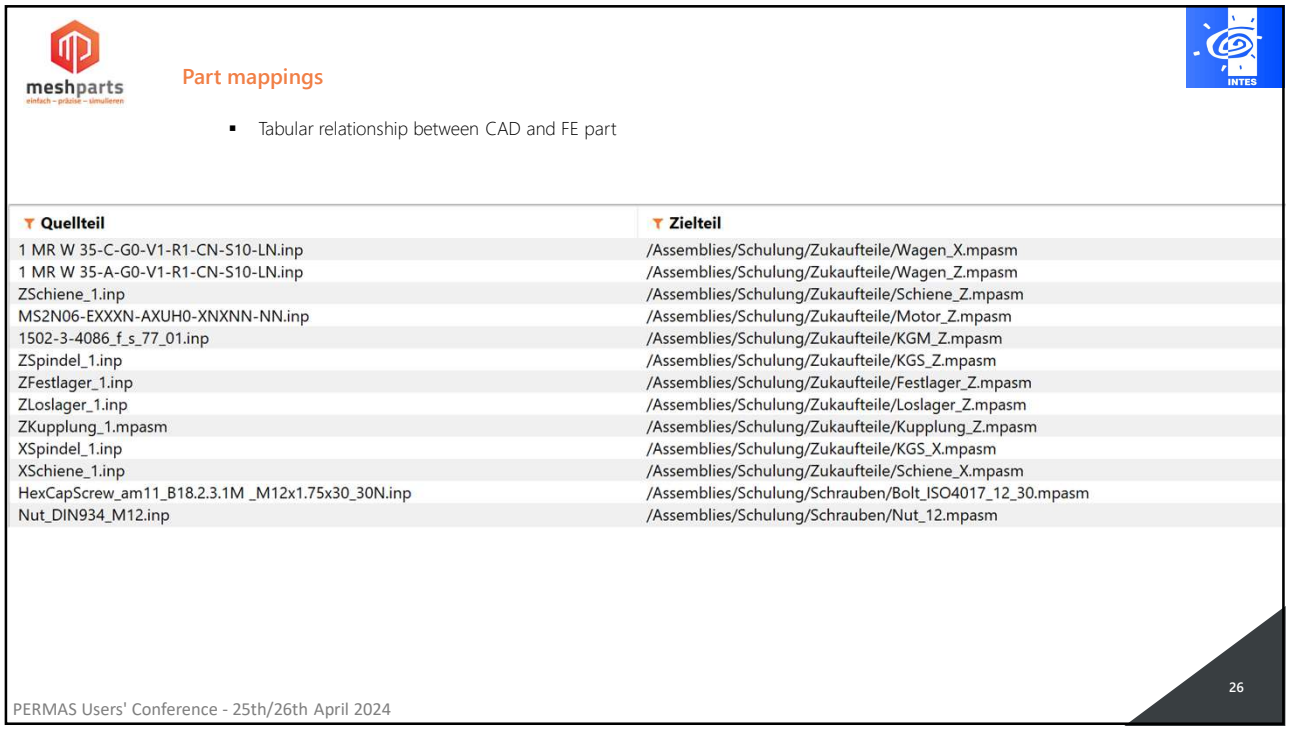
meshparts
einfach – präzise – simulieren
INTES
Part mappings
Tabular relationship between CAD and FE part
Quellteil
Zielteil
1 MR W 35-C-G0-V1-R1-CN-S10-LN.inp
/Assemblies/Schulung/Zukaufteile/Wagen_X.mpasm
1 MR W 35-A-G0-V1-R1-CN-S10-LN.inp
/Assemblies/Schulung/Zukaufteile/Wagen_Z.mpasm
ZSchiene_1.inp
/Assemblies/Schulung/Zukaufteile/Schiene_Z.mpasm
MS2N06-EXXXN-AXUH0-XNXNN-NN.inp
/Assemblies/Schulung/Zukaufteile/Motor_Z.mpasm
1502-3-4086_f_s_77_01.inp
/Assemblies/Schulung/Zukaufteile/KGM_Z.mpasm
ZSpindel_1.inp
/Assemblies/Schulung/Zukaufteile/KGS_Z.mpasm
ZFestlager_1.inp
/Assemblies/Schulung/Zukaufteile/Festlager_Z.mpasm
ZLoslager_1.inp
/Assemblies/Schulung/Zukaufteile/Loslager_Z.mpasm
ZKupplung_1.mpasm
/Assemblies/Schulung/Zukaufteile/Kupplung_Z.mpasm
XSpindel_1.inp
/Assemblies/Schulung/Zukaufteile/KGS_X.mpasm
XSchiene_1.inp
/Assemblies/Schulung/Zukaufteile/Schiene_X.mpasm
HexCapScrew_am11_B18.2.3.1M _M12x1.75x30_30N.inp
/Assemblies/Schulung/Schrauben/Bolt_ISO4017_12_30.mpasm
Nut_DIN934_M12.inp
/Assemblies/Schulung/Schrauben/Nut_12.mpasm
26
PERMAS Users' Conference - 25th/26th April 2024

26

Part mappings

- CAD parts are replaced by corresponding FE parts immediately after a CAD assembly is imported.
- There is no need for meshing and further modeling of these CAD parts.

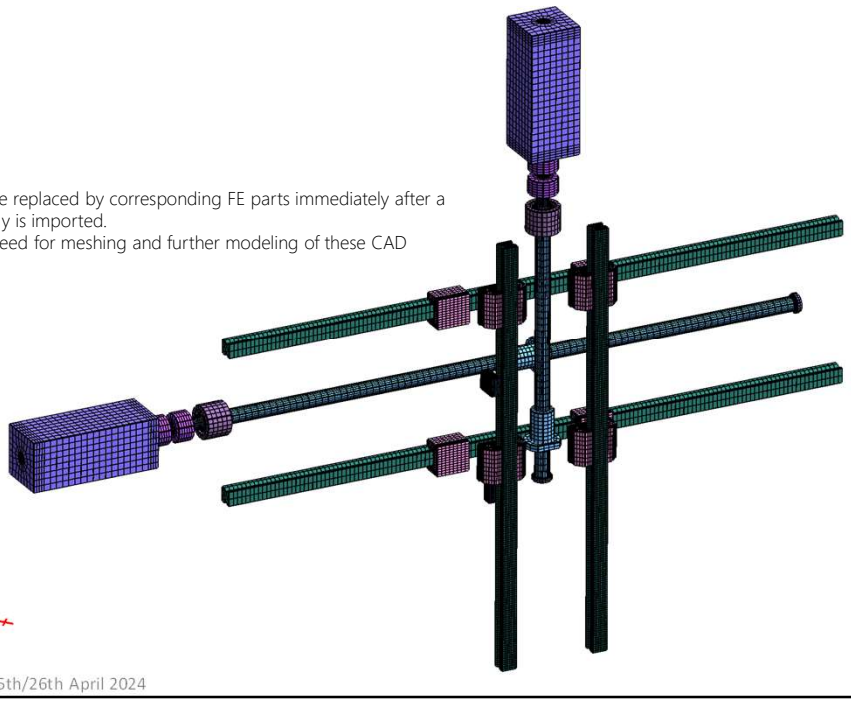

27

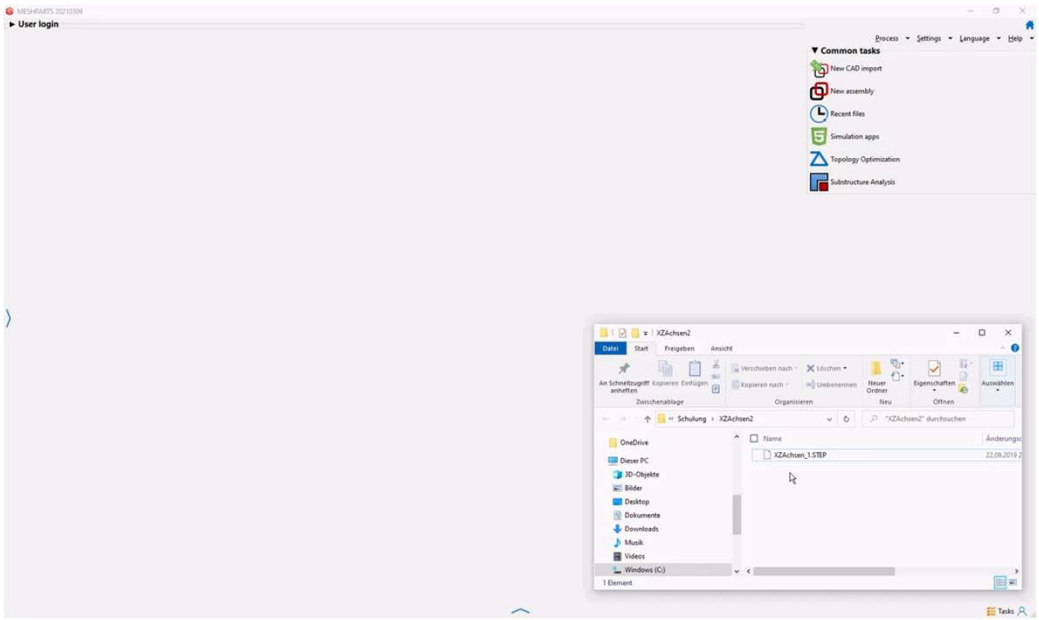

28

Automatic Connections

29

Target:

- Automatic definition of connections (contacts) between individual parts
- Differentiation between:
  - frictional contact
  - bonded contact
  - sliding contact (no separation)

Implementation:

- Color coding of functional surfaces in CAD:
  - Frictional contact: red
  - Bonded contact: blue
  - Sliding contact (no separation): green
- Corresponding options and functions in Meshparts ensure automatic contact definition

30

Geometry type	Color	Meaning	RGB code
Surface	Red	Friction contact	255,0,0
Surface	Blue	Bonded contact	0,0,255
Surface	Green	Sliding contact (simplification friction contact)	0,255,0
Surface	Yellow	Hydraulic pressure surface	255,255,0
Surface	Purple	Ignore	128,0,128
Part	Purple	Suppressed	128,0,128

31

Cooperation with the company Römheld:

- https://www.roemheld.de/de/services/serviceleistungen/FE-Simulationen
- Römheld creates thousands of CAD models of clamping elements with predefined connection points
- This enables fast and cost-effective FE analysis of clamping fixtures, a service for Römheld customers

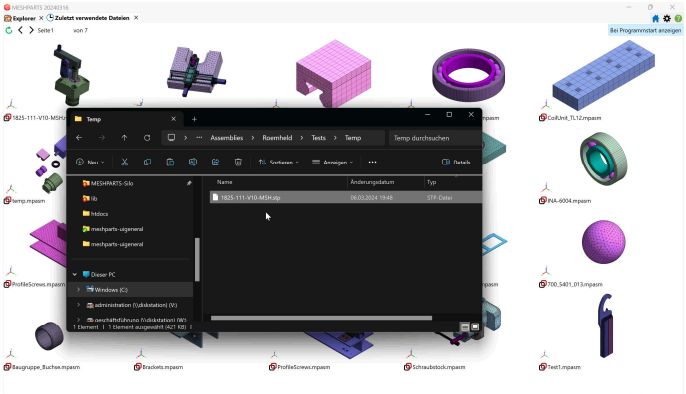

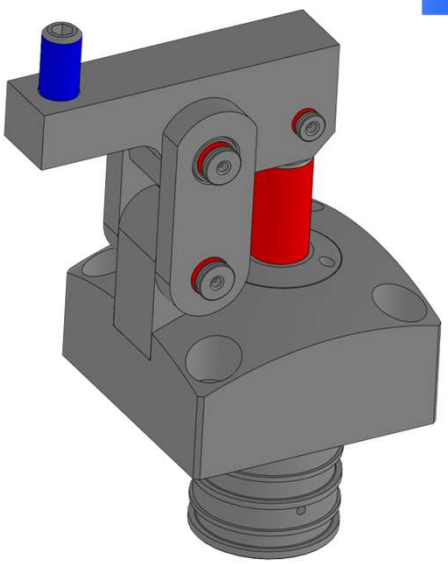

32

Automatically defined connections

- 27 Connections
- 12 Bonded contacts
- 15 Friction contacts

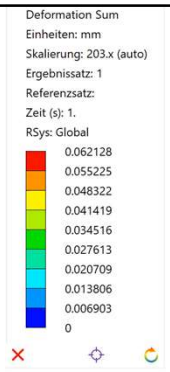

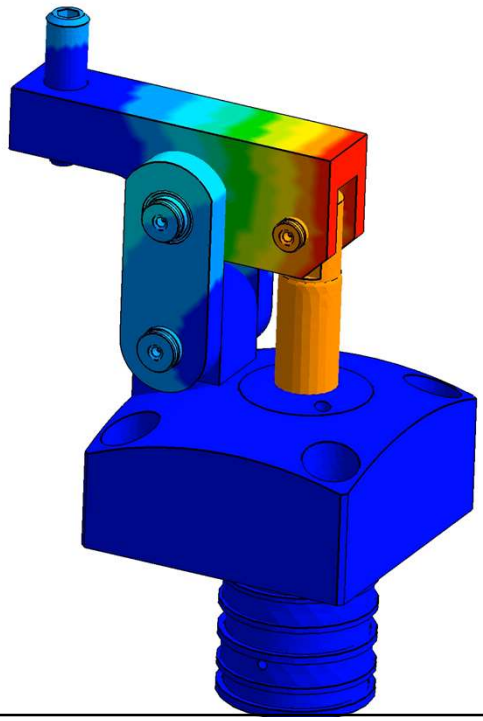

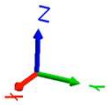

33

Automatic Strength Calculations

34

Automatic bolt safety according to VDI 2230

- 100% automated thanks to the FE model library

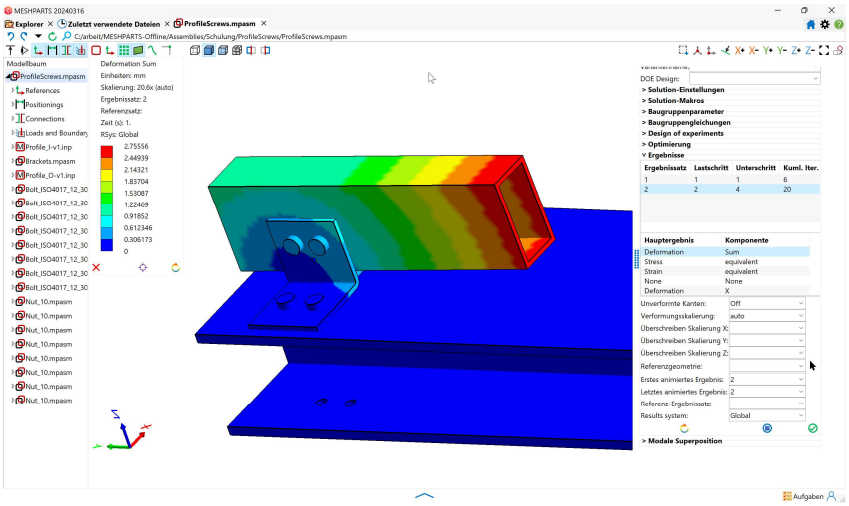

35

Strength according to FKM guideline

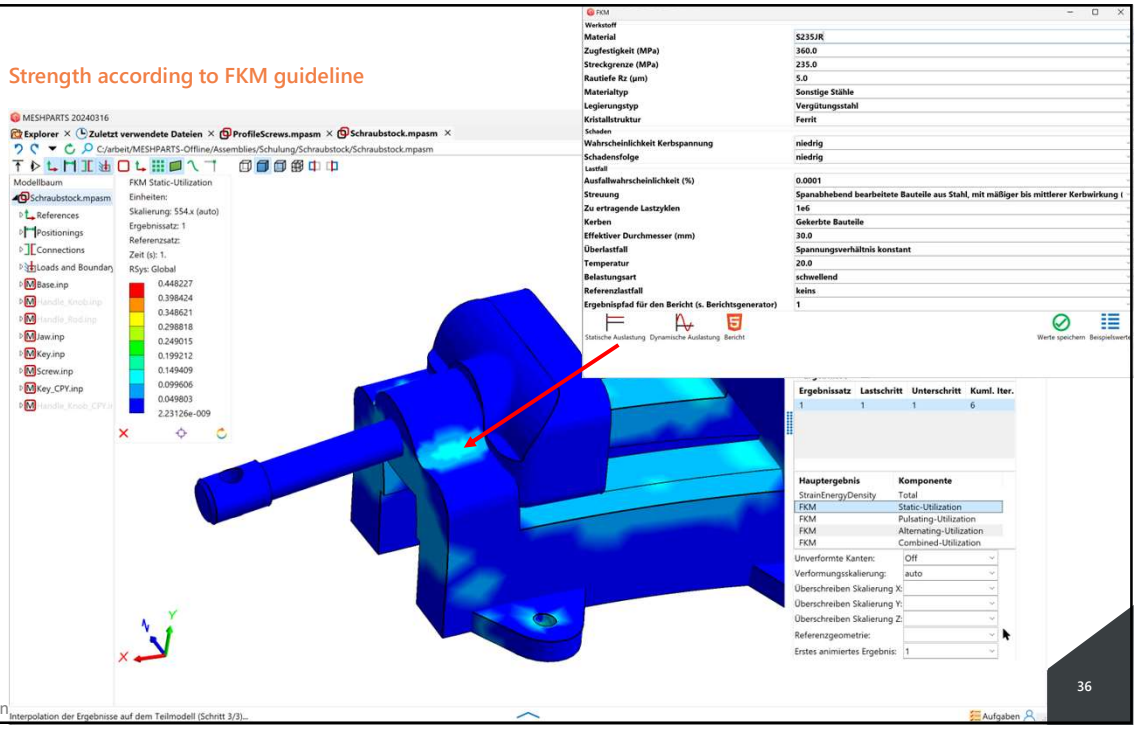

36

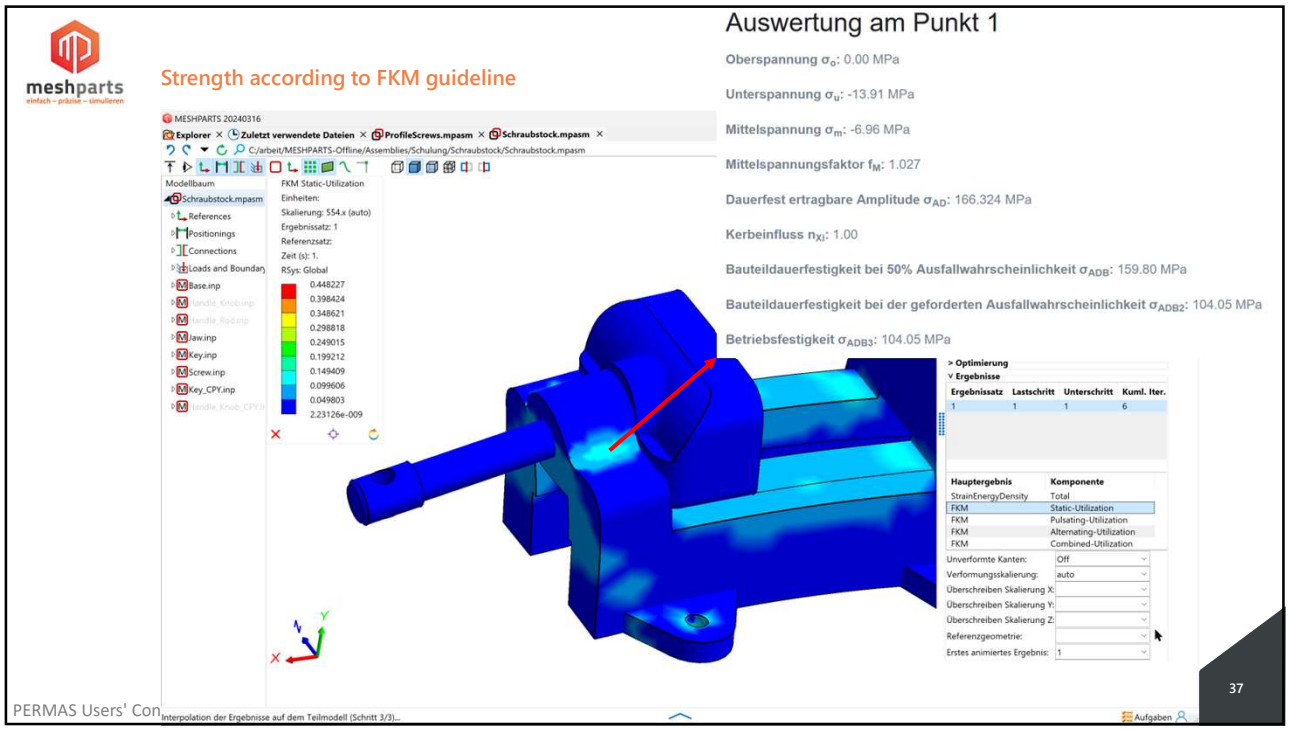
meshparts
einfach – präzise – simulieren
Strength according to FKM guideline
Auswertung am Punkt 1
Oberspannung σ_o: 0.00 MPa
Unterspannung σ_u: -13.91 MPa
Mittelspannung σ_m: -6.96 MPa
Mittelspannungsfaktor f_M: 1.027
Dauerfest ertragbare Amplitude σ_{AD}: 166.324 MPa
Kerbeinfluss n_{Xi}: 1.00
Bauteildauerfestigkeit bei 50% Ausfallwahrscheinlichkeit σ_{ADB}: 159.80 MPa
Bauteildauerfestigkeit bei der geforderten Ausfallwahrscheinlichkeit σ_{ADB2}: 104.05 MPa
Betriebsfestigkeit σ_{ADB3}: 104.05 MPa
MESHPARTS 20240316
Explorer
Zuletzt verwendete Dateien
ProfileScrews.mpasm
Schraubstock.mpasm
C:/arbeit/MESHPARTS-Offline/Assemblies/Schulung/Schraubstock/Schraubstock.mpasm
Modellbaum
Schraubstock.mpasm
References
Positionings
Connections
Loads and Boundary
Base.inp
Jaw.inp
Key.inp
Screw.inp
Key_CPY.inp
FKM Static-Utilization
Einheiten:
Skalierung: 554.x (auto)
Ergebnissatz: 1
Referenzsatz:
Zeit (s): 1.
RSys: Global
0.448227
0.398424
0.348621
0.298818
0.249015
0.199212
0.149409
0.099606
0.049803
2.23126e-009
> Optimierung
v Ergebnisse
Ergebnissatz
Lastschritt
Unterschritt
Kuml. Iter.
Hauptergebnis
Komponente
StrainEnergyDensity
Total
FKM
Static-Utilization
Pulsating-Utilization
Alternating-Utilization
Combined-Utilization
Unverformte Kanten:
Verformungsskalierung:
Überschreiben Skalierung X:
Überschreiben Skalierung Y:
Überschreiben Skalierung Z:
Referenzgeometrie:
Erstes animiertes Ergebnis:
Interpolation der Ergebnisse auf dem Teilmodell (Schritt 3/3)...
Aufgaben
PERMAS Users' Con
37

37


meshparts
einfach – präzise – simulieren
The Chain Analysis
PERMAS Users' Conference - 25th/26th April 2024

38

Chain analysis for machine tools

- Chain analysis is used to determine the static and dynamic contributions of individual components and sub-assemblies for complex assemblies such as machine tools in a simulated and automated process.
- Historically, chain analysis arose from a practical problem: If only complete assemblies are simulated, then the static and dynamic deformations result from a complex interaction of coupled, mutually influencing effects.

39

Stage 1 of the chain: Spindle

40

Stage 2 of the chain: Z carrier

41

Stage 3 of the chain: Z guides + Z Ball screw nut

42

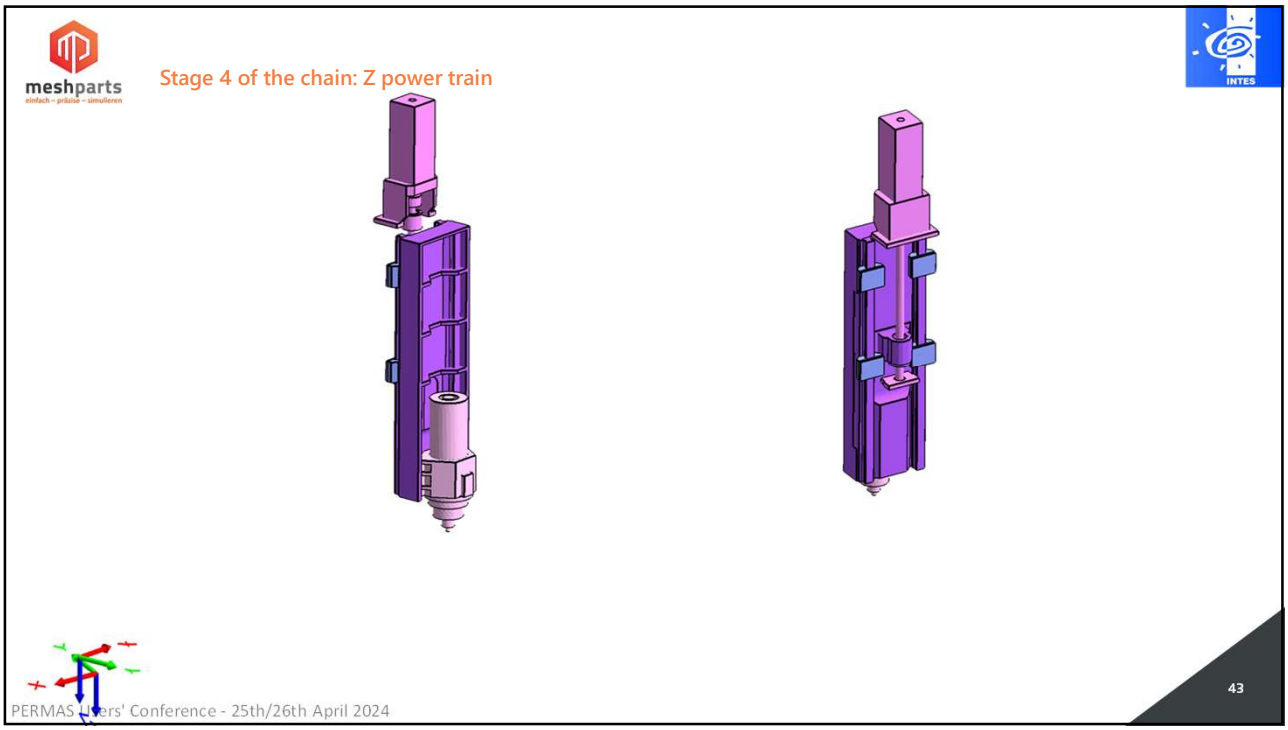
meshparts
einfach – präzise – simulieren
Stage 4 of the chain: Z power train
INTES
PERMAS Users' Conference - 25th/26th April 2024
43

43

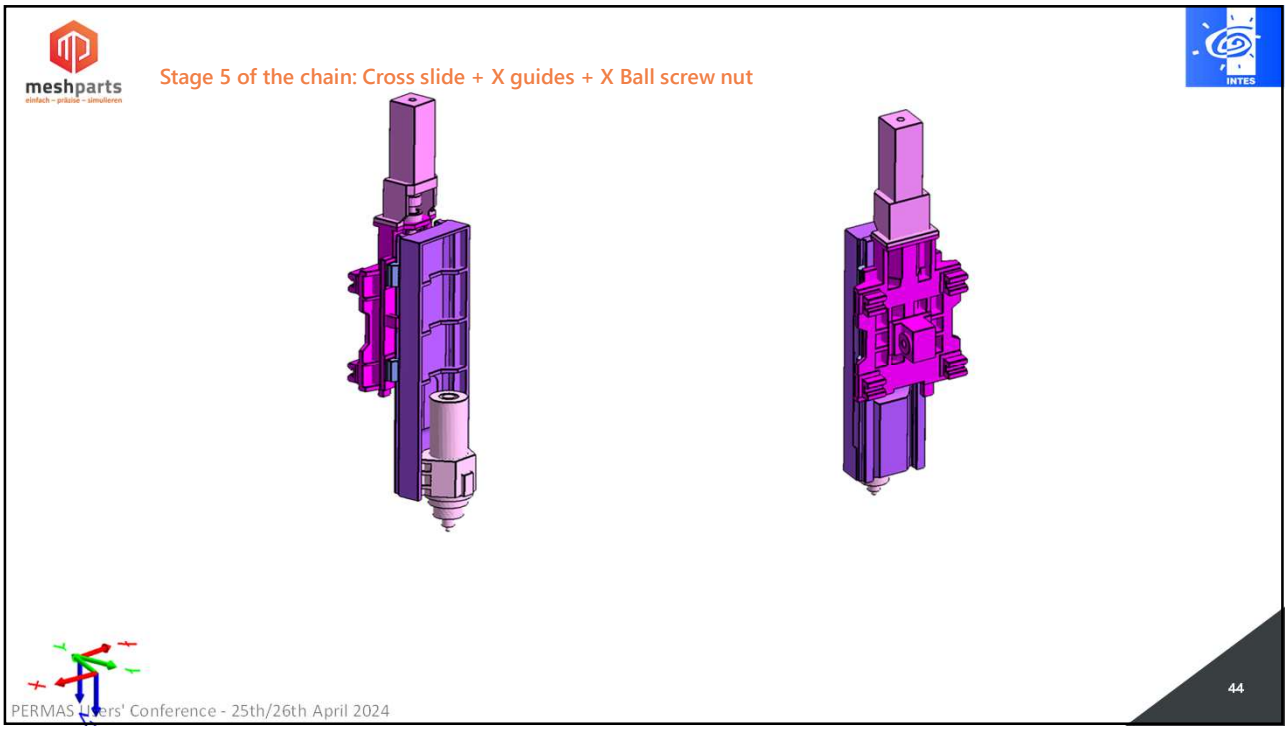
meshparts
einfach – präzise – simulieren
Stage 5 of the chain: Cross slide + X guides + X Ball screw nut
INTES
PERMAS Users' Conference - 25th/26th April 2024
44

44

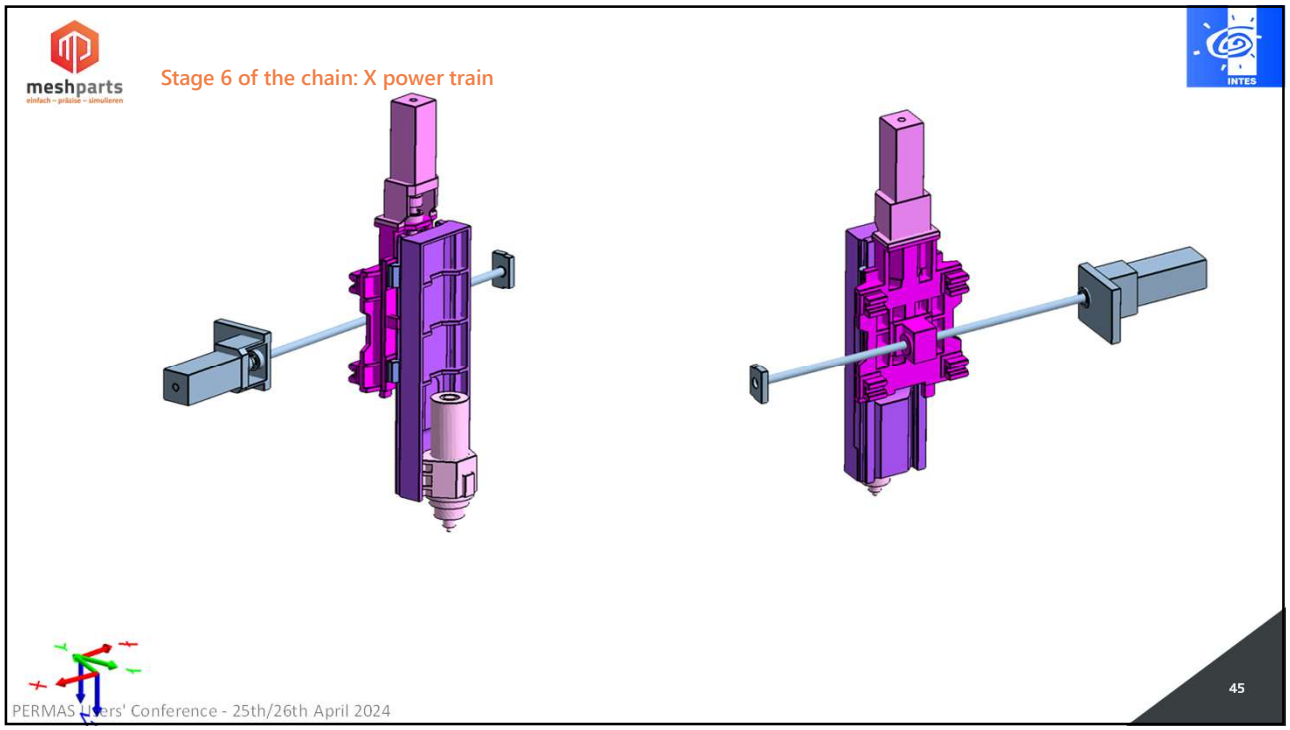
meshparts
einfach – präzise – simulieren
Stage 6 of the chain: X power train
INTES
PERMAS Users' Conference - 25th/26th April 2024
45

45

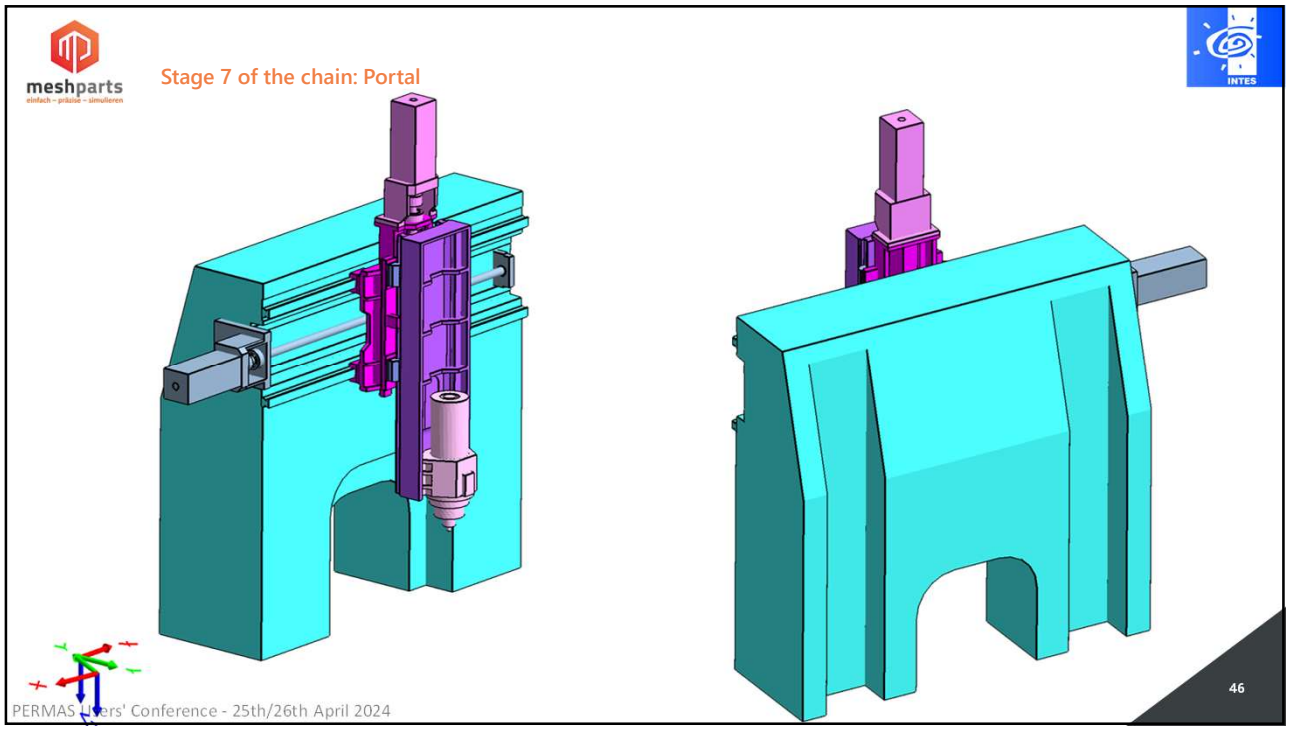
meshparts
einfach – präzise – simulieren
Stage 7 of the chain: Portal
INTES
PERMAS Users' Conference - 25th/26th April 2024
46

46

Solve and evaluate

- Thanks to automation, the cost of a chain analysis is practically the same as the cost of a single dynamic FE analysis of an entire machine.

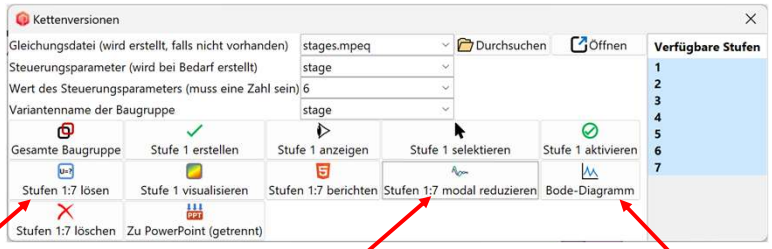

Solve all stages

Modal reduce all stages

Display and compare all frequency responses

47

Input: 2, Output: 2, Dämpfung: 0.03, Eingangsskalierung: 1.0, Amplitudeneinheiten: µm

Stage 3 of the chain: Compliance frequency response

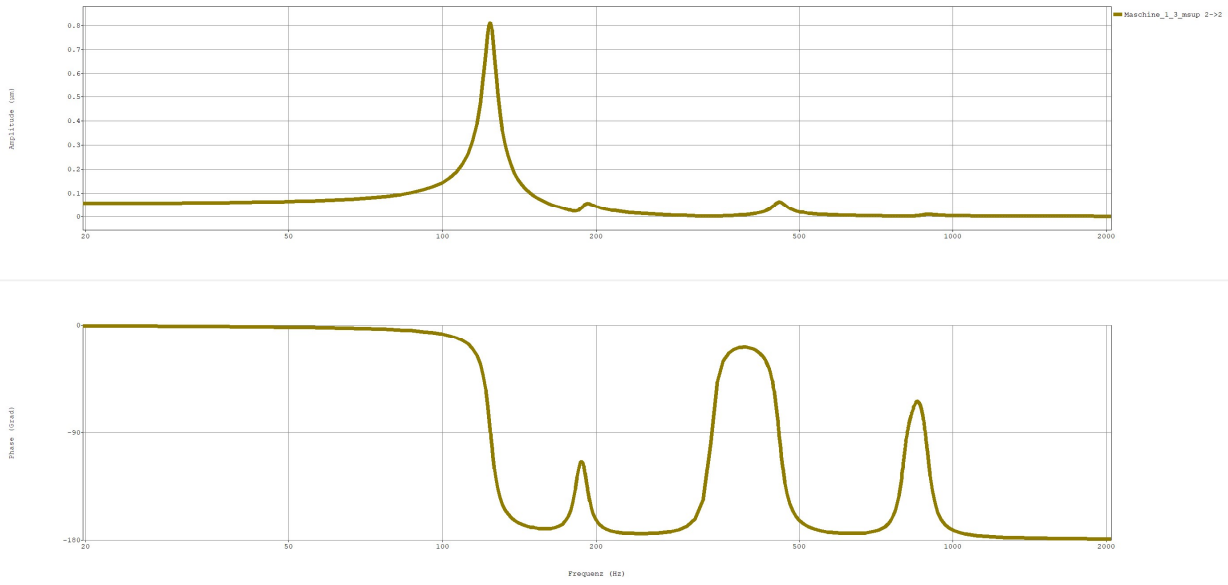

48

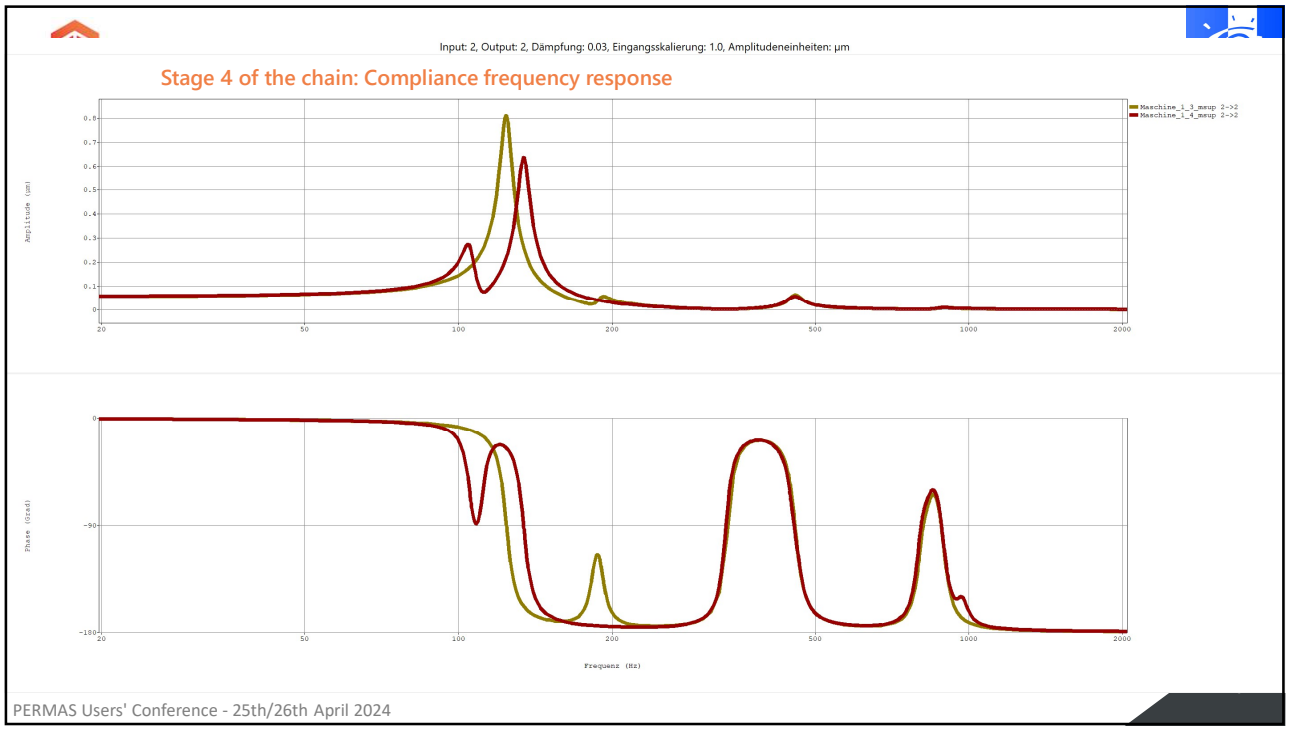
Input: 2, Output: 2, Dämpfung: 0.03, Eingangsskalierung: 1.0, Amplitudeneinheiten: µm
Stage 4 of the chain: Compliance frequency response
Maschine_i_3_msup 2->2
Maschine_i_4_msup 2->2
Amplitude (cm)
Phase (Grad)
Frequenz (Hz)
PERMAS Users' Conference - 25th/26th April 2024

49

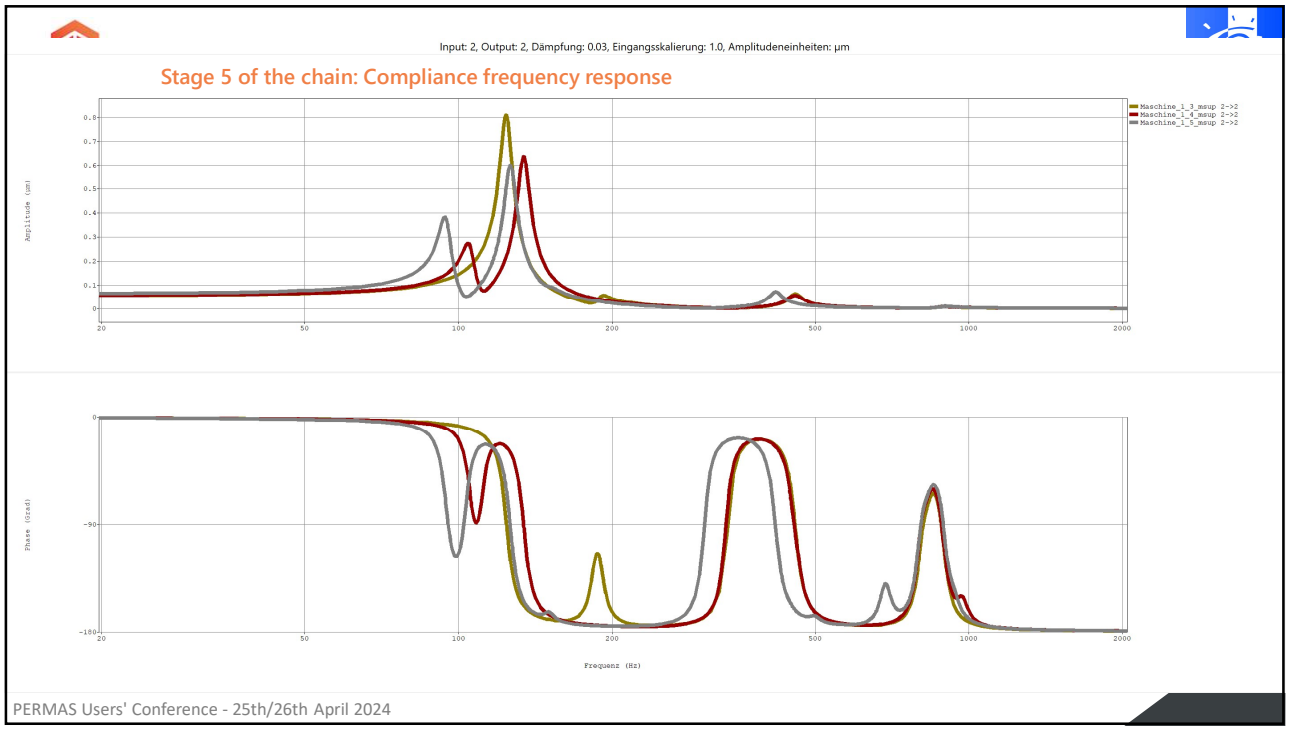
Input: 2, Output: 2, Dämpfung: 0.03, Eingangsskalierung: 1.0, Amplitudeneinheiten: µm
Stage 5 of the chain: Compliance frequency response
Maschine_i_3_msup 2->2
Maschine_i_4_msup 2->2
Maschine_i_5_msup 2->2
Amplitude (cm)
Phase (Grad)
Frequenz (Hz)
PERMAS Users' Conference - 25th/26th April 2024

50

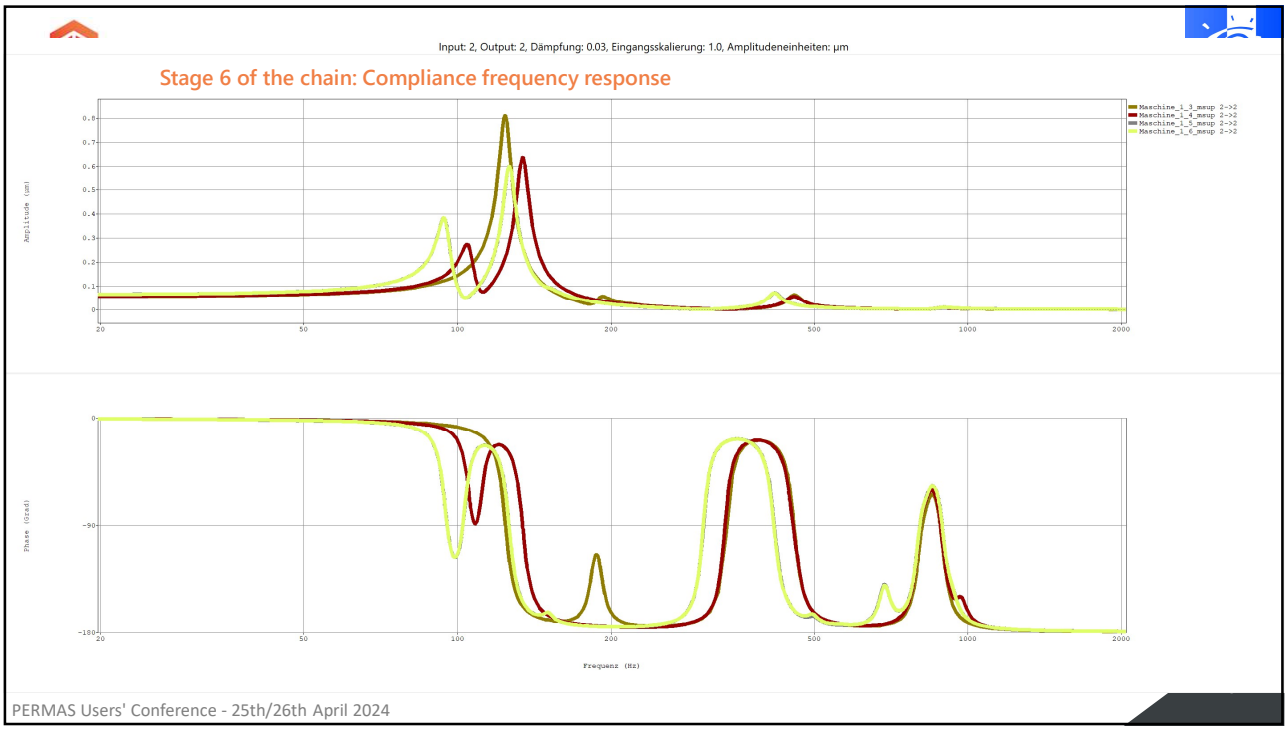
Input: 2, Output: 2, Dämpfung: 0.03, Eingangsskalierung: 1.0, Amplitudeneinheiten: µm
Stage 6 of the chain: Compliance frequency response
Amplitude (cm)
Phase (Grad)
Frequenz (Hz)
PERMAS Users' Conference - 25th/26th April 2024

51

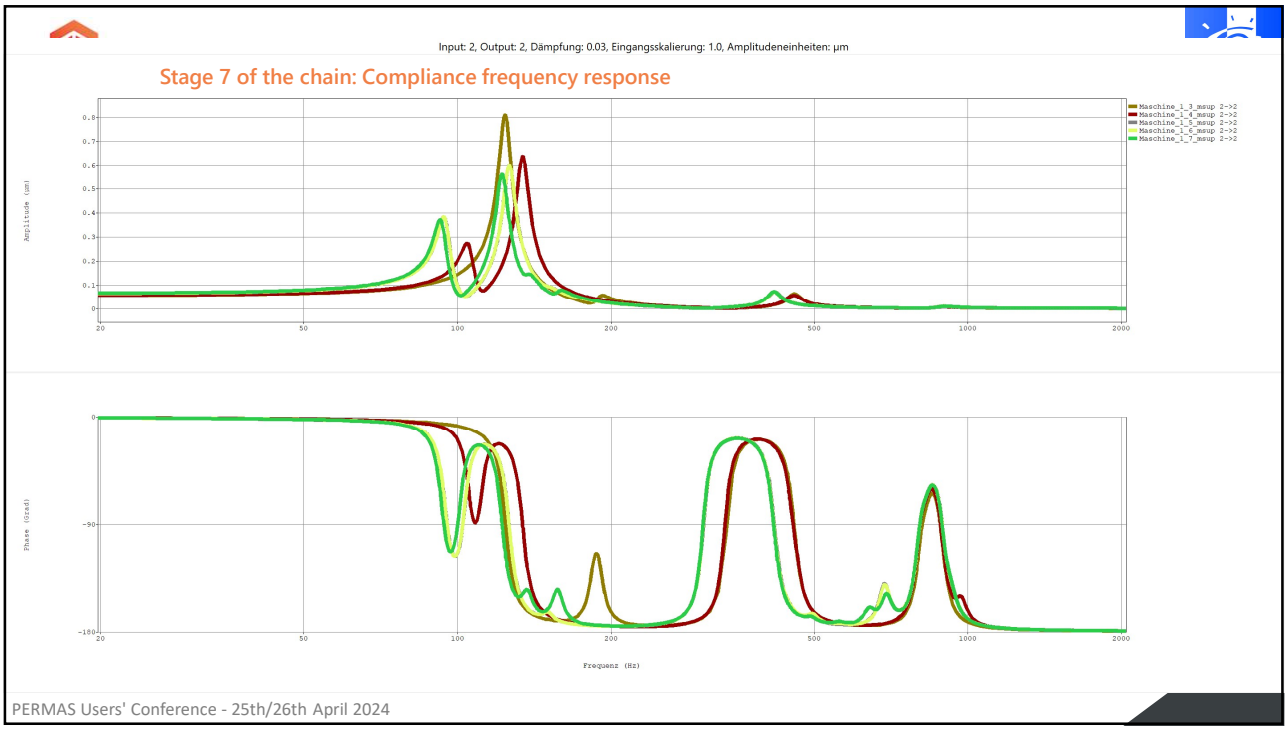
Input: 2, Output: 2, Dämpfung: 0.03, Eingangsskalierung: 1.0, Amplitudeneinheiten: µm
Stage 7 of the chain: Compliance frequency response
Amplitude (cm)
Phase (Grad)
Frequenz (Hz)
PERMAS Users' Conference - 25th/26th April 2024

52

Fingerprint of the machine

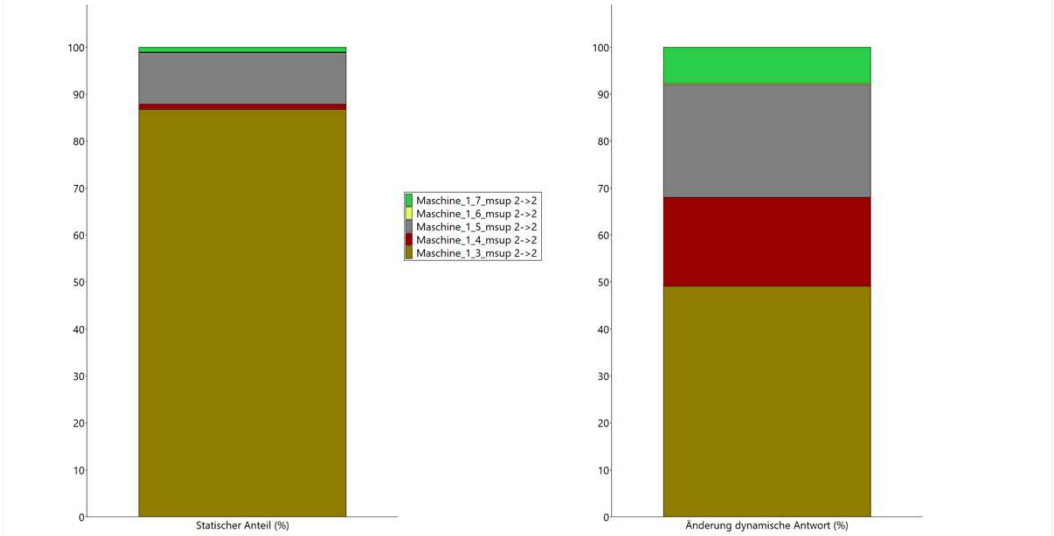

53

Conclusion

54

Conclusion

- The combination of pre- and post-processor Meshparts and the solver **Permas** enables structural-mechanical tasks to be solved efficiently.
- The assembly-oriented working method facilitates the handling of large assemblies.
- The integrated FE model library reduces the modeling effort.

Questions?

+49 711 9958 7001 | alexandru.dadalau@meshparts.de

Die Verbindung von Workflow Management Systemen und Cloud Computing

Dr.-Ing. Robert D. Bitsche (Rescale)

1 Cloud Computing für Simulationsanwendungen

Unter Cloud Computing versteht man die Bereitstellung von Computing-Ressourcen durch sogenannte Cloud Service Provider als Dienste über das Internet. Unternehmen nutzen dabei einen virtuellen Pool von gemeinsam genutzten Ressourcen und bezahlen nur für die tatsächliche Nutzung. Dies ermöglicht es den Unternehmen, schneller und effizienter zu skalieren, ohne ihre eigenen physischen Rechenzentren betreiben zu müssen.

Cloud Computing hat in den vergangenen Jahren einen beispiellosen Boom erlebt. Der Jahresumsatz des größten Cloud Service Providers - AWS - ist in den 10 Jahren von 2013 bis 2023 von 3.1 Mrd. Dollar auf 90 Mrd. Dollar gewachsen (Quelle: Statistia).

Cloud Computing eignet sich in vielerlei Hinsicht ideal für Simulations-Anwendungen, da Lastspitzen problemlos abgedeckt werden können und sich die verwendete Hardware mühelos an die Erfordernisse der jeweiligen Simulations-Anwendung anpassen lässt. Die großen Cloud Service Provider bieten inzwischen leistungsstarke Cloud Infrastruktur an, die speziell für Simulations-Anwendungen entwickelt wurde. Es überrascht also nicht, dass immer mehr Unternehmen aufwändige Simulationsprozesse in die Cloud verlagern.

Ein weiterer Grund, weshalb Cloud Computing sich ideal für Simulations-Anwendungen eignet, sind die sogenannten Spotmärkte. Die großen Cloud Service Provider wie AWS oder Microsoft Azure bieten ihre Recheninfrastruktur auch auf einem Spotmarkt zu stark reduzierten Preisen an.
Das Prinzip der Elastizität der Cloud erfordert, dass zu jedem Zeitpunkt eine gewisse Menge von virtuellen Servern in Reserve gehalten wird. Es könnten schließlich jederzeit Kunden eine große Menge zusätzlicher Server anfordern, die dann innerhalb von wenigen Minuten zur Verfügung gestellt werden müssen. Diese Reserve kann zum Beispiel 20% der vorhandenen Ressourcen ausmachen.
Es wäre nun wirtschaftlich nicht sinnvoll, diese virtuellen Server einfach brachliegen zu lassen. Stattdessen werden diese Server zu sehr günstigen Preisen auf dem sogenannten Spotmarkt angeboten. Der Haken dabei ist, dass der Cloud Service Provider jederzeit das Recht hat, einen auf dem Spotmarkt gekauften Server wieder zurückzuziehen, wenn dieser auf dem regulären Markt benötigt wird. Die auf dem Server laufenden Prozesse werden dabei mit nur sehr kurzer Vorwarnung beendet.
Solche Server eigenen sich also offensichtlich nicht für den Betrieb von Anwendungen, die ständig zur Verfügung stehen müssen, wie zum Beispiel einem Webserver. Sie eignen sich aber durchaus für viele Arten von numerischer Simulation, die durch einen schrittweisen Simulationsfortschritt gekennzeichnet sind.
Viele Simulationsprogramme verfügen über die Möglichkeit, abgebrochene Simulationsprozesse an einem gewissen Haltepunkt fortzusetzen. Um dies zu ermöglichen, gibt es im Wesentlichen zwei Strategien: Eine Strategie besteht darin, dafür zu sorgen, dass die für eine Fortsetzung der Simulation erforderlichen Daten beim Rückzug der Hardware durch den Cloud Service Provider nicht verloren gehen. Eine zweite Strategie besteht darin, die Simulationsprozesse so zu gestalten, dass die einzelnen Prozessschritte hinreichend klein sind, und der gelegentliche Verlust eines Prozessschrittes verkraftbar ist und durch einfache Wiederholung kompensiert werden kann.

Bei der zweiten Strategie können Workflow Management Systeme mit Ihrer abstrakten Definition von Prozessen eine große Hilfe sein. Das System weiß, dass es einen Prozessschritt, der durch den Rückzug der Hardware durch den Cloud Service Provider gestört wurde, einfach nur zu wiederholen braucht.

2 Automatisierung komplexer Simulationsprozesse mit Workflow Management Systemen

Traditionell bestehen viele einfache Simulationsprozesse aus 3 Schritten: Der Erstellung eines mathematischen Modells (Preprocessing), dem Lösen eines Gleichungssystems (Solving) und dem Auswerten der Ergebnisse (Postprocessing). In den vergangenen Jahrzehnten haben sich aber auch

weit komplexere Prozesse entwickelt, bei denen zum Beispiel die Ergebnisse einfacherer Simulationsprozesse als Eingabedaten für weitere Simulationsprozesse dienen. Dabei kommt auch oft Software verschiedener Anbieter zum Einsatz, die über gewisse Schnittstellen miteinander kommunizieren.
So wird zum Beispiel die im Rahmen einer Strömungssimulation ermittelte Druckverteilung auf einem Flügel als Eingabedaten für eine strukturmechanische Simulation des Flügels benutzt. Umgekehrt werden auch die im Rahmen einer strukturmechanischen Simulation ermittelten Deformationen eines Flügels als Eingabedaten für eine Strömungssimulation verwendet.

Es ist generell wünschenswert, dass Simulationsergebnisse reproduzierbar sind. Die Simulationsergebnisse sollen also zum Beispiel nicht von der Person abhängen, die die Simulation durchgeführt hat. Diese Reproduzierbarkeit kommt besonders dann eine große Bedeutung zu, wenn wichtige Design-Entscheidungen auf Basis von Simulationsergebnissen getroffen werden, oder gar die Sicherheit eines Produkts von diesen Simulationsergebnissen abhängt. Außerdem ermöglicht es nur ein hohes Maß an Reproduzierbarkeit, aus vergangenen Fehlern für die Zukunft zu lernen.

Um das Ziel möglichst reproduzierbarer Simulationsergebnisse zu erreichen, müssen Simulationsprozesse stark automatisiert werden. Außerdem ist es wichtig alle Faktoren, die die Ergebnisse beeinflussen zu erfassen und zu dokumentieren. Dabei spielt das sogenannte Simulationsdatenmanagement eine zentrale Rolle.

Traditionell erfolgt diese Automatisierung von Simulationsprozessen durch Skripte, die meist nicht von Programmierern, sondern von Ingenieuren oder Wissenschaftlern der entsprechenden Fachrichtung geschrieben werden. Im Fall von komplexen Simulationsprozessen stoßen diese Skripte oft an ihre Grenzen - zum Beispiel dann, wenn der Berechnungsfortschritt nicht linear ist, sondern sich in verschiedene parallele Prozesse verzweigt. Abbildung 1 zeigt ein Beispiel für einen solchen Prozess. In diesem Beispiel stellt jede Box eine Strömungssimulation dar, die von den Parametern p1 und p2 abhängt. Die Ergebnisse einer Simulation werden als Eingabedaten (Initiale Lösung) anderer Simulationen benutzt. Man spricht dabei von einem gerichteten azyklischen Graphen (englisch DAG, directed acyclic graph). Es ist im Voraus nicht klar, in welcher zeitlichen Reihenfolge die einzelnen Simulationen ablaufen und wie viele Simulationsprozesse zu einem gegebenen Zeitpunkt parallel laufen. Dementsprechend schwierig ist es, diesen Prozess in einem einfachen Skript abzubilden und die erforderlichen Ressourcen für einen solchen Simulationsprozess kostengünstig bereitzustellen.

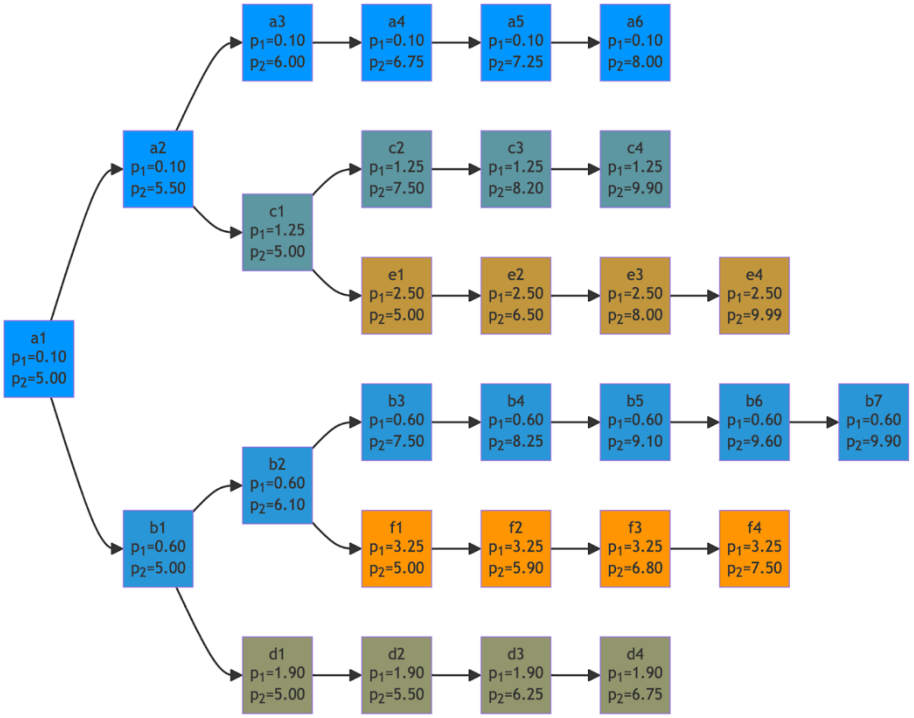

Abbildung 1: Komplexer Simulationsprozess

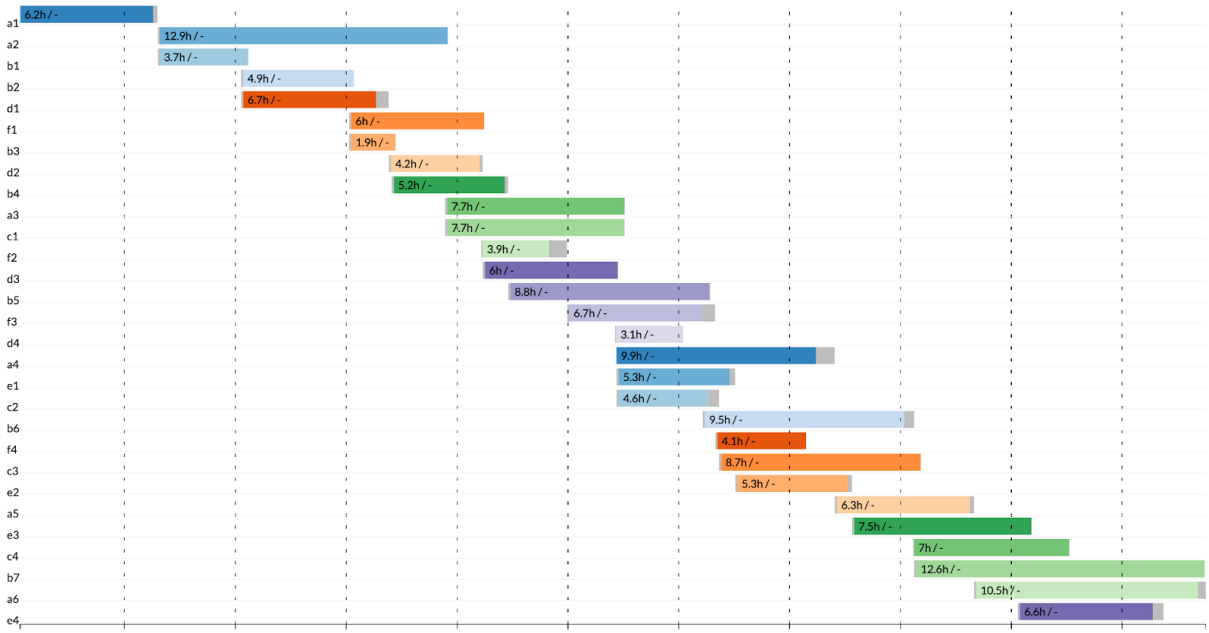

Abbildung 2: Prozess-Zeitachse zu Workflow in Abbildung 1

Wo Skripte an ihre Grenzen stoßen, kommen inzwischen vermehrt wissenschaftliche Workflow Management Systeme zum Einsatz, die das Zusammenspiel verschiedener Software- und Hardware-Ressourcen effizient orchestrieren. Es gibt eine große Auswahl an solchen Systemen. Wir wollen hier das Open Source Workflow Management System Nextflow [1] näher beschreiben.
Nextflow ist ein von Seqera Labs [2] betreutes Open-Source-Projekt und kann im Rahmen der Apache 2.0-Lizenz kostenfrei genutzt werden. Nextflow wird traditionell hauptsächlich im Bereich der Bioinformatik eingesetzt, aber eignet sich auch hervorragend für andere Simulationsprozesse, wie wir im Folgenden zeigen werden.

In Nextflow werden Simulationsprozesse mit Hilfe von sogenannten Prozessen und Workflows beschrieben. Abbildung 3 zeigt ein Beispiel für die Definition eines Prozesses. Der Prozess “run_abaqus” definiert zwei Input Channels: “inputfile_template” (die parametrisierte Abaqus Input Datei) und “cof” (coefficient of friction). Außerdem wird ein Output Channel “all” definiert, der alle vom Prozess erzeugten Dateien ausgibt. Der Prozess selbst ersetzt den Platzhalter “<cof>” in der Abaqus Input Datei mit dem cof Wert und ruft den Abaqus Solver auf.

```
process run_abaqus {
  input:
    path inputfile_template
    val cof
  output:
    path '*', emit: all
  script:
    """
    cp $inputfile_template model.inp
    sed -i 's/<cof>/$cof/g' model.inp
    abaqus job=model.inp interactive
    """
}
```

Abbildung 3: Definition eines einfachen Prozesses in Nextflow

```
workflow {
  input_template=file('bearing_template.inp')
  run_abaqus(input_template, 0.3)
  run_abaqus_restart_1(input_template, 0.35, run_abaqus.out.all)
  run_abaqus_restart_2(input_template, 0.40, run_abaqus.out.all)
  run_abaqus_restart_3(input_template, 0.45, run_abaqus.out.all)
}
```

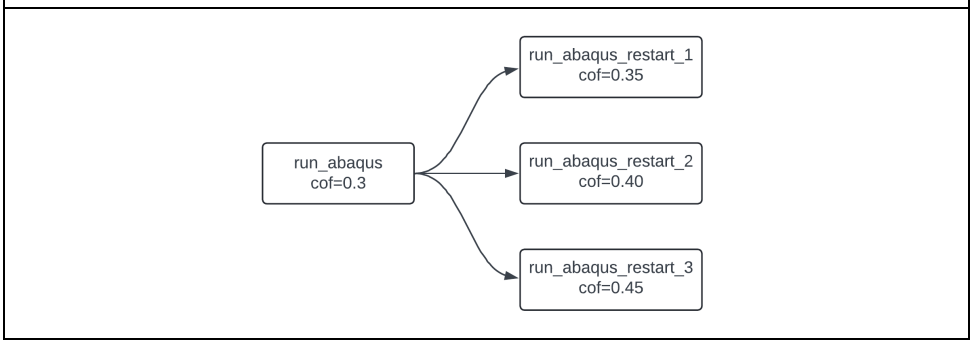

Abbildung 4: Definition eines einfachen Workflows in Nextflow

Im Rahmen des in Abbildung 4 dargestellten Workflows werden die verschiedenen Prozesse aufgerufen wie Funktionen. Es ist aber wichtig zu verstehen, dass die Reihenfolge der Ausführung dieser Prozesse nicht dadurch bestimmt wird, dass “run_abaqus_restart_1” in Abbildung 4 nach “run_abaqus” aufgerufen wird. (Diese beiden Prozesse hätten auch in umgekehrter Reihenfolge aufgerufen werden können.) Die Reihenfolge der Ausführung wird vielmehr dadurch bestimmt, dass ein Output Channel des “run_abaqus” Prozesses (run_abaqus.out.all) als Input des “run_abaqus_restart_1” Prozesses benutzt wird.
Diese Herangehensweise macht es einfach, komplexe Workflows zu beschreiben, die keinen linearen Berechnungsfortschritt aufweisen, sondern sich in verschiedene parallele Prozesse verzweigen.

Ein weiteres wichtiges Konzept in Nextflow ist der sogenannte Executor. Der Executor ist jene Komponente, die bestimmt, in welcher Umgebung ein Workflow ausgeführt wird. Dieses Konzept ermöglicht es, die Logik der Prozesse und Workflows unabhängig von der tatsächlichen Umgebung zu schreiben, in der der Workflow läuft. Ein Workflow kann also nahezu unverändert auf einem lokalen Computer, einem Cluster-Ressourcen-Manager oder in der Cloud ausgeführt werden.

Auf der Rescale Plattform [3] ist seit kurzem ein Nextflow Executor verfügbar, der Nextflow Prozesse als Rescale Jobs ausführen kann. Dieses Konzept bringt für den Anwender eine ganze Reihe von Vorteilen:

- Komplexe Simulationsprozesse lassen sich mit geringem Aufwand beschreiben.
- Das sogenannte “License Queuing” ermöglicht eine intelligente Nutzung eines verfügbaren Software-Lizenz-Pools.
- Hardware-Ressourcen werden optimal eingesetzt, weil zu jedem Zeitpunkt nur so viele Ressourcen in der Cloud gestartet werden, wie gerade erforderlich sind.
- Die Aufteilung von Prozessen in einzelne - kürzer laufende - Rescale Jobs ermöglicht es oft, von den günstigen Preisen der Cloud Spotmärkte zu profitieren. Bei Rückzug der Hardware durch den Cloud Service Provider wird der entsprechende Prozessschritt einfach automatisch wiederholt.

Abbildung 5 zeigt wie ein Nextflow „Control Job“ auf Rescale mit Hilfe des Nextflow Executors zwei parallel laufende Abaqus „Worker Jobs“ startet.

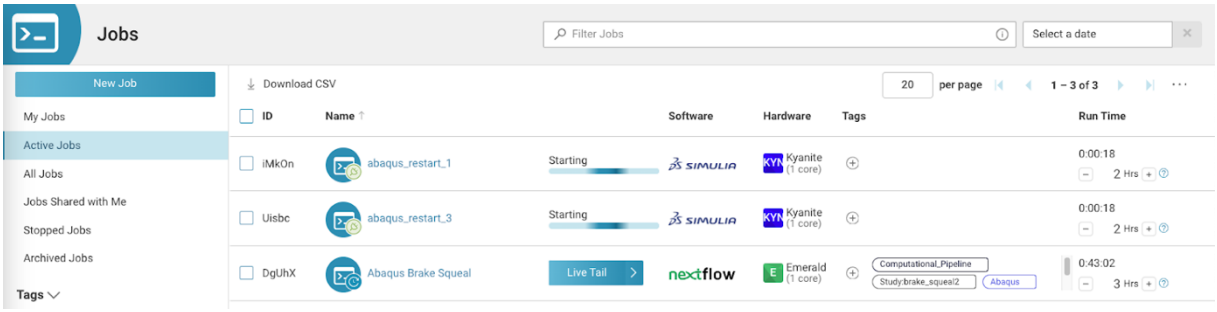

Abbildung 5: Ein „Control Job“ startet „Worker Jobs“ mit Hilfe des Nextflow Executors auf Rescale.

3 Workflows mit automatischer Auswahl von Cloud Hardware

Auf einer Cloud-Plattform wie Rescale kann der User aus einer langen Liste von Hardware-Konfigurationen wählen, die von verschiedenen Cloud Service Providern zur Verfügung gestellt werden. Die konkrete Wahl der Hardware basiert meist auf dem in Benchmark-Studien ermittelten Preis-Leistungs-Verhältnis. Mit einem Workflow Management System wie Nextflow ist es aber auch leicht möglich, die Wahl der Hardware dynamisch durchzuführen, indem sie von den Ergebnissen eines vorangegangenen Prozesses abhängig gemacht wird.

Abbildung 6 zeigt ein Beispiel für einen solchen Workflow, der eine Erweiterung des Workflows in Abbildung 4 darstellt. In einem ersten Prozessschritt wird ein sogenannter “Datacheck” mit der Software Abaqus durchgeführt. Dadurch wird unter anderem der Hauptspeicherbedarf des Abaqus-Modells ermittelt. In einem weiteren Prozessschritt wird automatisch eine Hardware-Konfiguration ermittelt, die ausreichend Hauptspeicher zur Verfügung stellt, und gleichzeitig möglichst hohe Rechenleistung bei möglichst geringen Kosten erwarten lässt. Außerdem wird basierend auf einer Analyse der Abaqus Input Datei automatisch Hardware mit GPU (graphics processing unit) Unterstützung gewählt, wenn sich davon ein Vorteil hinsichtlich der Rechenleistung und Lizenznutzung erwarten lässt.

Jeder der in Abbildung 6 durch eine Box dargestellten Prozesse läuft mit Hilfe des Nextflow Executors als eigener Rescale Job, mit Ausnahme des “select hardware” Prozesses, dessen geringe Ansprüche an die Hardware keinen eigenen Job rechtfertigen.

Ein detailliertes Tutorial zu diesem Workflow ist unter
https://github.com/rescale-labs/Tutorial_Computational_Pipelines verfügbar.

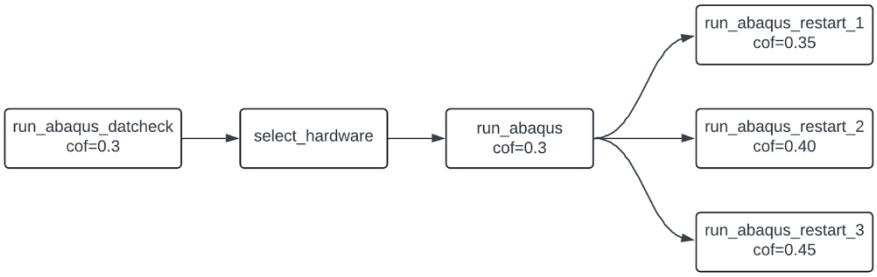

Abbildung 6: Nextflow Workflow mit automatischer Hardware-Auswahl

4 Workflows mit bedingten Prozessen

In Abbildung 7 (links) stellt jede Box eine Strömungssimulation dar. Die Ergebnisse einer Simulation werden als Eingabedaten (Initiale Lösung) anderer Simulationen benutzt. Dieser Workflow ist sequenziell in dem Sinn, dass jeder Prozess die Ergebnisse eines fest vorgegebenen anderen Prozesses verarbeitet. Der Prozess a4 wird zum Beispiel stets mit den Ergebnissen des Prozess a3 initialisiert.

Ein Workflow kann aber auch bedingte Prozesse enthalten. So kann zum Beispiel der Wunsch bestehen am Ende eines Prozesses (einer Strömungssimulation) zu prüfen, ob der Solver “konvergiert ist”, also ob eine ausreichend genaue mathematische Näherungslösung gefunden wurde. Wenn das der Fall ist, setzt der Workflow wie bisher mit dem nächsten Prozess fort. Wenn das nicht der Fall ist, soll ein zweiter Versuch unternommen werden (“fallback”), bei dem die Strömungssimulation mit den Ergebnissen eines anderen vorausgegangenen Strömungssimulation initialisiert wird. Ein Beispiel für einen solchen Prozess ist in Abbildung 7 (rechts) dargestellt. Wenn der Prozess “a3“ konvergiert, wird der Prozess “a3 fallback” gar nicht ausgeführt. Wenn der Prozess “a3“ nicht konvergiert, wird der Prozess “a3 fallback” ausgeführt, der mit „a3“ identisch ist, aber mit den Ergebnissen von “a1” (statt “a2”) initialisiert wird. Der Prozess a4 verarbeitet schließlich die Ergebnisse des Prozesses “a3” oder “a3 fallback”.

Solche Workflows mit bedingten Prozessen können in Nextflow ohne weiteres umgesetzt werden. Da die Ausführung von Prozessen in Nextflow aber auf dem Konzept von Channels basiert, kann die Beschreibung nicht mit Hilfe der gewohnten bedingten Anweisungen (if/else) erfolgen. Stattdessen kommen spezielle Channels und Operatoren zum Einsatz. Die Seite https://nextflow-io.github.io/patterns/ beinhaltet zahlreiche hilfreiche Beispiele, um solche Workflows mit Nextflow umzusetzen.

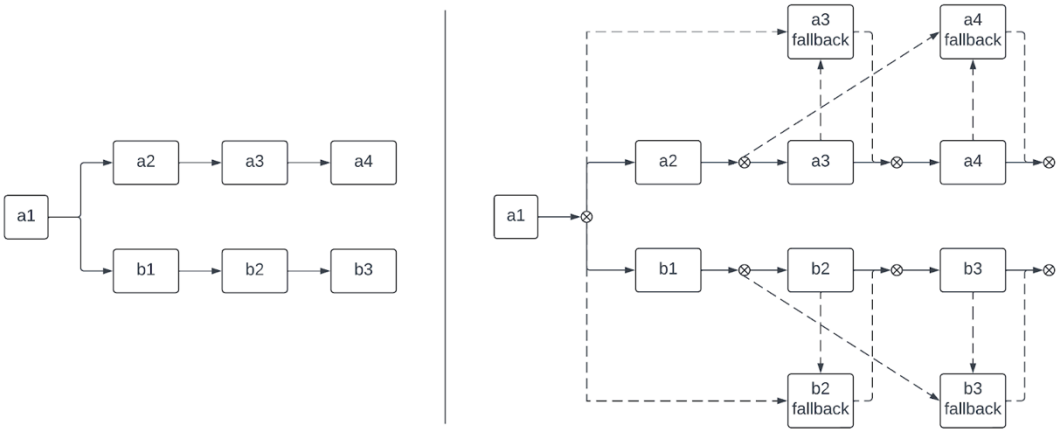

Abbildung 7: Sequenzieller Workflow (links) und Workflow mit bedingten Prozessen (rechts)

5 Zusammenfassung

Wir haben anhand von Nextflow [1] gezeigt, wie wissenschaftliche Workflow Management Systeme das Zusammenspiel verschiedener Software- und Hardware-Ressourcen effizient orchestrieren können. Speziell im Zusammenspiel mit Cloud Computing ergeben sich dabei zahlreiche Vorteile. Durch die Automatisierung komplexer Simulationsprozesse kann Arbeitszeit eingespart und die Zusammenarbeit verschiedener Teams und Fachrichtungen verbessert werden. Außerdem ergeben sich Möglichkeiten durch die Nutzung der Cloud Spot Märkten Kosten zu sparen, durch die dynamische Anpassung der eingesetzten Hardware an den jeweiligen Prozessschritt die Rechenleistung zu steigern, und durch massive Parallelisierung Projekte schneller abzuschließen.

6 Quellenverzeichnis

[1] Nextflow: https://www.nextflow.io

[2] Seqera Labs: https://seqera.io

[3] Rescale: https://rescale.com

Das Projekt EuroCC

Henry Strauss, Dr. Andreas Wierse, (SICOS BW GmbH)

1 Ein Überblick

EuroCC ist ein „Meta-Projekt“ der EU im Bereich HPC+.

Ziel ist dabei nicht die Förderung eines einzelnen Vorhabens, Themas oder Produkts, sondern es geht um die Etablierung von nationalen Kompetenzzentren (National Comptence Centres = NCCs) für HPC (High Performance Computing), HPDA (High Performance Data Analytics) und KI (Künstliche Intelligenz), kurz HPC+.
Diese NCCs werden in allen 32 beteiligten europäischen Staaten als erste und zentrale Anlaufstellen zu den genannten Themen für die Industrie (dabei liegt ein besonderer Schwerpunkt auf kleinen und mittelständischen Unternehmen), den akademischen Bereich und die öffentliche Verwaltung dienen. Hierzu tragen die NCCs die vorhandenen Kompetenzen und die verfügbaren Services von HPC-Zentren zusammen und bereiten sie so auf, dass Interessenten sehr schnell die für sie relevanten Angebote identifizieren können.
Ein Beispiel sind hierbei Simulations-Workflows und wie sie einschließlich Vor- und Nachbearbeitung mittels HPC und KI schneller, in besserer Qualität und möglicherweise auch für komplexere Fragestellungen durchgeführt werden können.

2 Die Services

Die SICOS BW GmbH hat in der zweiten Phase des EuroCC-Projekts die Leitung der Tasks/Unterprojekte „Services to and Interaction with Industry“ und „Service Portfolio and Competence Management“ übernommen.

2.1 Task: Services to and Interaction with Industry

In diesem Task wird zurzeit am Aufbau einer „Customer Acquisition Group“ gearbeitet. Darüber hinaus werden in einer Arbeitsgruppe die „Needs of Industry“ untersucht bzw. definiert. Als besondere Herausforderung stellt sich dabei (paradoxerweise) heraus, dass in Deutschland bereits ein stark entwickeltes HPC-Ökosystem existiert: es gibt zum Beispiel eine Vielzahl von HPC-Rechenzentren, die „unter einen Hut gebracht“ werden müssen, d.h. die Angebote, die an die Industrie gemacht werden, sollten auch über die verschiedenen HPC-Rechenzentren hinweg koordiniert und aufeinander abgestimmt sein.

2.2 Task: Service Portfolio and Competence Management

In der zweiten genannten Task liegt ein Schwerpunkt aktuell auf dem Aufbau des deutschen „LinkHPC“, einer Art Internet-Marktplatzes, auf dem die Services des NCC Deutschlands angeboten werden, ganz im Sinne eines „Single Point of Contact“. Zu den angebotenen Services gehören beispielsweise die HPC-Beratung für Anfänger:innen, Proofs of Concept, Simulationsberatung, Hilfe bei der Softwareoptimierung, -portierung, -parallelisierung und Visualisierung, Beratung und Anwendungsunterstützung von HPDA, KI und Visualisierung, Beratung zum Aufbau und Betrieb eigener Clustersysteme und Cloud Computing.

3 Kooperation und Erfolgsgeschichten

Im Vortrag wird auch auf die Zusammenhänge mit anderen EU-Projekten im Bereich HPC+, wie z.B. die Centres of Excellence (CoEs) eingegangen sowie exemplarisch eine Erfolgsgeschichte dargestellt. Es wird aufgezeigt, wie insbesondere Engineering-Unternehmen vom NCC Deutschland oder vom NCC Österreich profitieren können und welche von der EU und dem BMBF geförderten Unterstützungsangebote in diesem Kontext verfügbar sind. Das schließt auch die neuen großen Systeme in der EU ein, die vom EuroHPC Joint Undertaking gemeinsam mit den Mitgliedsstaaten beschafft wurden, wie z.B. Lumi in Finnland (#5 der Top500), Leonardo in Italien (#6) und Mare Nostrum in Spanien (#8).
Aber auch bei den kommenden Systemen, vor allem dem ersten europäischen Exascale-Computer, JUPITER, der noch in diesem Jahr verfügbar sein soll, werden die EuroCC-Kompetenzen Interessenten dabei helfen, sich deren Leistung zunutze zu machen.

EURO²

NAFEMS DACH Konferenz, Bamberg, 11. Juni 2024

1

Das EuroCC-Projekt

Henry Strauß, SICOS BW GmbH

EURO²

Überblick

- SICOS BW GmbH – Wir vermitteln Höchstleistung.
- EuroCC(2) – Ein Meta-Projekt der EU im Bereich HPC+
- Projektstruktur WP2
- Zahlen
- Centres of Excellence
- HPC/Simulation Workflows
- Success Story

2

SICOS BW GmbH

Wir vermitteln Höchstleistung.

Fokus Mittelstand: Unterstützung bei der Einführung und dem Einsatz von HPC-, HPDA- und KI-Technologien, insbesondere für KMUs

- SICOS: Simulation, Computing und Storage
- BW: Grundfinanzierung durch MWK Baden-Württemberg und Gesellschafter
- GmbH: non-profit!, gegründet 2011, aktuell 12 Mitarbeiter
- Gesellschafter: KIT/SCC & Universität Stuttgart/HLRS
- Solution Center: asc(s, SDSC-BW, MSC-BW, CASE4Med
- „Mediator“, Aufzeigen von Fördermöglichkeiten
- regelmäßig Beteiligung an Förderprojekten

SICOS
Wir vermitteln Höchstleistung.

3

EuroCC(2)

Ein Meta-Projekt der EU im Bereich HPC+

Ziel: Etablierung von NCCs (National Competence Centres) für HPC+ in jedem der beteiligten 32 Staaten im Rahmen von Digital Europe

- HPC+: HPC, HPDA & KI
- Single Point of Contact für Industrie, Forschung und öffentliche Verwaltung
- Meta:
  - keine Projektförderung im klassischen Sinne
  - Vielzahl der beteiligten Staaten über Arbeitspakete (WP)
- EuroCC: RIA = Research and Innovation Action
- Begleitprojekt CASTIEL: CSA = Coordination and Support Action

4

Zahlen

- Budget: ~€62M
- 50% von EuroHPC JU
- 50% von den beteiligten Staaten
- Dauer:
- 1. Projektphase: September ’20 bis August/Dezember ’22
- 2. Projektphase: Januar ’23 bis Dezember ’25 (WP2: 261,5 PMs)

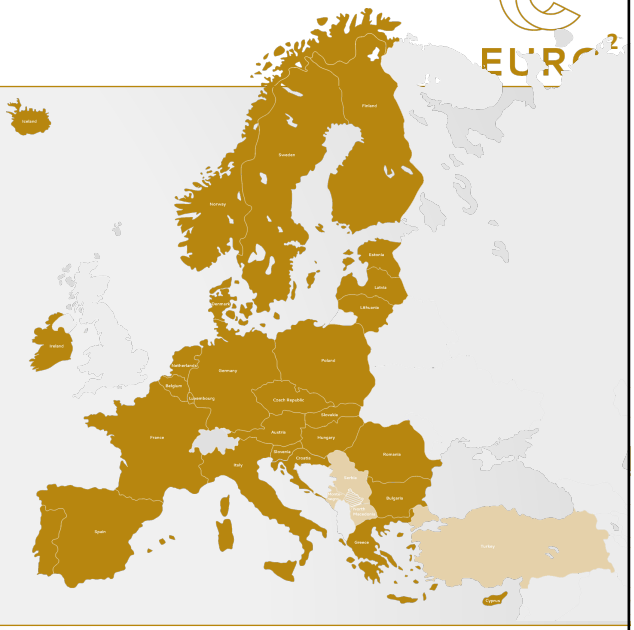

5

Projektstruktur NCC Deutschland

3 Partner (GCS):

- Uni Stuttgart/HLRS
  WP1 (Projektleitung) + WP2
- SICOS BW GmbH)
- FZJ/JSC
- (LRZ)

Kooperation mit Gauß-Allianz & Verein NHR (Nationales Hochleistungsrechnen)

7 Tasks:

- 2.1: NCC Management
- 2.2: Training and Skills Development
- **2.3: Services to and Interaction with Industry**
- 2.4: Services to and Interaction with Academia and Public Administration
- **2.5: Service Portfolio and Competence Management**
- 2.6: Collaboration
- 2.7: Awareness Creation and Communication

6

Task 2.3

Services to and Interaction with Industry

Verständnis der Bedürfnisse der Industrie und Aufbau eines passenden Angebots von Services

- Customer Acquisition Group
- Arbeitsgruppe „Needs of Industry“
- Konzeption geeigneter Angebote
- Entwicklung neuer Services (u.a. HPC-Beratung, Proofs of Concept, Softwareoptimierung, -portierung, -parallelisierung, Visualisierung, ...)
- Unterstützung bei der Umsetzung

7

Task 2.5

Service Portfolio and Competence Management

Schwerpunkt zurzeit: Aufbau des deutschen LinkHPC (MarketPlace)

Services:

- Koordination aller Services (Industrie T2.3, Forschung und öffentliche Verwaltung T2.4)
- Erfassung aller Kompetenzen und Erstellung einer „Competence Map“
- Integration geeigneter Services in ein europäisches Angebot
- Aufbau einer Datenbank und Erstellung eines deutschen Marktplatzes
- Kooperation mit anderen deutschen Kompetenzträgern in HPC+

8

Centres of Excellence (CoEs) für HPC
Auftrag, Zielsetzung, Nutzen, Zielgruppe

Europäische CoEs für HPC: Von der Großskalierung zur Exascale-Innovation
Ausgewählt im Rahmen von Ausschreibungen für europäische Forschungsinfrastrukturen

- **Auftrag**: Förderung des Exascale Computing, Überbrückung der Qualifikationslücke
- **Zielsetzung:** Spezialisierte Ausbildung, Wissensintegration, Co-Design-Aktivitäten
- **Nutzen**: Verbesserte Leistung, Kompetenzentwicklung, kollaborative Fortschritte
- **Zielgruppe**: Hochschulen, Industrie, Forschungsinstitutionen, Staatliche Agenturen, Europäische HPC-Gemeinschaft

9

Centres of Excellence (CoEs) für HPC
Liste

- **POP - PERFORMANCE OPTIMISATION AND PRODUCTIVITY**
- **COEC - ADVANCED TECHNOLOGY FOR COMBUSTION SIMULATION**
- **EOCOE - ENERGY ORIENTED COE FOR COMPUTER APPLICATIONS**
- **EXCELLERAT - European CoE for Engineering Applications**
- **RAISE - RESEARCH ON AI- AND SIMULATION-BASED ENGINEERING AT EXASCALE**
- BIOEXCEL - COE FOR BIOMOLECULAR RESEARCH
- COMPBIOMED - COE IN COMPUTATIONAL BIOMEDICINE
- PERMEDCOE - HPC TO TREAT DISEASE AT INDIVIDUAL LEVEL
- CHEESE - COE FOR EXASCALE IN SOLID EARTH
- ESIWACE - EXCELLENCE IN SIMULATION OF WEATHER AND CLIMATE IN EUROPE
- HIDALGO - HPC AND BIG DATA TECHNOLOGIES FOR GLOBAL CHALLENGES
- MAX - MATERIALS DESIGN AT THE EXASCALE
- NOMAD - NOVEL MATERIALS DISCOVERY
- TREX - TARGETING REAL CHEMICAL ACCURACY AT THE EXASCALE

10

HPC-Workflow

einfache Version

EURO²

Preprocessing

- Beschaffung eines HPC-Accounts (optional)
- Aufbereitung/Bereitstellung/Übertragung der Input-Daten

Berechnung

- Erstellung einer Batchdatei
- Abschicken des Jobs mithilfe eines Batchsystems

Postprocessing

- Übertragung der Output-Daten
- Visualisierung (optional)

11

HPC/Simulation Workflow

EURO²

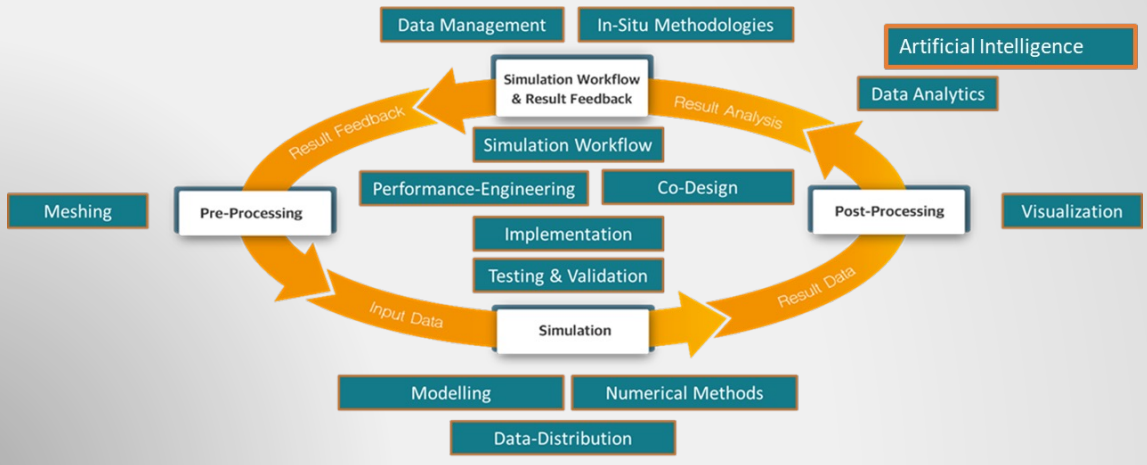

12

Success Story

Optima Pharma

- 550 employees
- Filling and packaging technology
- Simulation of air flow in clean room environments
- OpenFOAM-based solution established
- in co-operation with HLRS
- Uses the HLRS 3D-Virtual-Reality-Environment

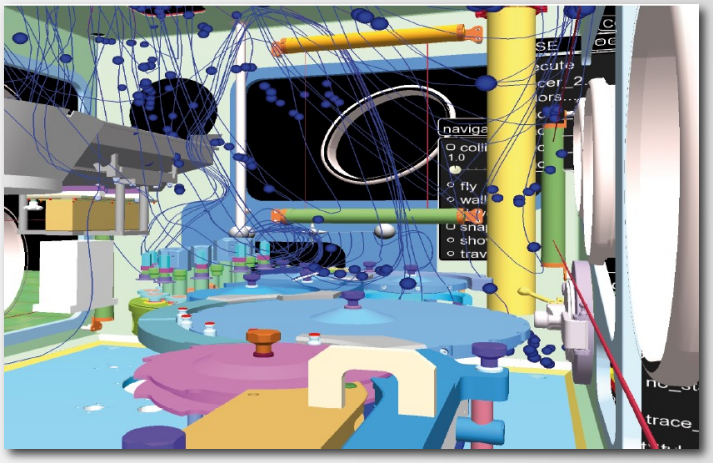

13

EuroHPC Access Calls

https://eurohpc-ju.europa.eu/access-our-supercomputers/eurohpc-access-calls_en

z.Zt. offen:

- CALL FOR PROPOSALS FOR AI AND DATA-INTENSIVE APPLICATIONS ACCESS MODE
- CALL FOR PROPOSALS FOR REGULAR ACCESS MODE
- CALL FOR PROPOSALS FOR EXTREME SCALE ACCESS MODE
- CALL FOR PROPOSALS FOR BENCHMARK ACCESS MODE
- CALL FOR PROPOSALS FOR DEVELOPMENT ACCESS MODE

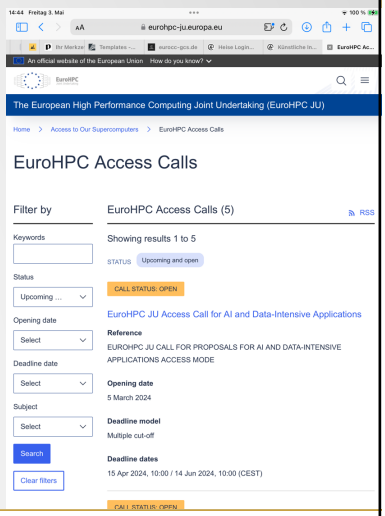

14

https://youtu.be/HB9JUH0mPqI?si=YmidDcTy1Wf4puu9

15

Thanks!

This project has received funding from the European High-Performance Computing Joint Undertaking (JU) under grant agreement No 101101903. The JU receives support from the Digital Europe Programme and Germany, Bulgaria, Austria, Croatia, Cyprus, Czech Republic, Denmark, Estonia, Finland, Greece, Hungary, Ireland, Italy, Lithuania, Latvia, Poland, Portugal, Romania, Slovenia, Spain, Sweden, France, Netherlands, Belgium, Luxembourg, Slovakia, Norway, Türkiye, Republic of North Macedonia, Iceland, Montenegro, Serbia

16

Interoperability of CAD and CAE for Enhanced Car Component Design and Optimization in Crash Scenarios

Zafeiria Kanellia, Michael Tryfonidis (Beta CAE Systems)

1 Summary

Achieving optimum performance for car components in crash scenarios necessitates a meticulous examination of various design aspects, particularly component geometry. This paper presents a methodology employed by simulation engineers to efficiently address this challenge. By identifying key parameters transferred from Computer-Aided Design (CAD) files to simulation models and employing Design of Experiment (DOE) techniques to vary them, engineers can iteratively refine component designs. However, the transfer of these design parameters from the Finite Element (FE) environment back to CAD software poses a significant hurdle. To streamline this process, an automated workflow has been developed to ensure seamless interoperability across different operating systems. Additionally, advancements in Computer-Aided Engineering (CAE) tools, such as ANSA morphing, provide engineers with valuable insights into how geometric variations impact crash performance. Despite these advancements, communication barriers between CAD and CAE departments persist, hindering collaborative efforts. In this context, this work describes how these challenges can be addressed by these challenges by outlining a scenario wherein CAE functions are enhanced through geometrical manipulation, particularly focusing on frontal rails. Optimization studies are conducted to analyze the impact of shape variations on component performance. Furthermore, an automated process is proposed to facilitate the transfer and update of design parameters between CAD and simulation environments, ultimately expediting design updates and reducing associated time and costs. The presented methodology, demonstrates the feasibility and benefits of integrating CAD parameters directly into the optimization workflow, paving the way for more efficient and effective component development in the automotive industry.

2 Introduction - Challenges

In the ever-evolving landscape of automotive engineering, ensuring the safety and performance of vehicle components, particularly in crash scenarios, stands as a paramount concern. Central to this endeavor is the comprehensive analysis and evaluation of crashworthiness, a task primarily handled through sophisticated computational methods collectively known as CAE. These methods, while immensely powerful, rely heavily on the accurate representation of geometric features within the simulated models. However, effective collaboration between CAD and CAE departments remains a challenge due to differences in processes, tools, and objectives. As complex systems undergo review, CAE engineers must engage in mutual interaction to assess outcomes and discuss potential issues.

CAD, as Computer-Aided Design, is a technology that empowers designers to craft, adjust, and enhance digital models of architectural structures. It facilitates meticulous drafting and visualization of projects, offering a visual depiction of the final design. By amalgamating geometric computations, algorithms, and user inputs, CAD software generates and manipulates designs.

CAE, short for Computer-Aided Engineering, supplements CAD by simulating how structures behave under diverse circumstances. It aids engineers in scrutinizing the structural integrity, functionality, and safety of designs. CAE encompasses techniques such as, finite element analysis (FEA), computational fluid dynamics (CFD), and structural optimization. CAE tools offer insights into stress distribution, energy usage, and potential shortcomings, helping engineers to refine their designs and make informed decisions.

The design process encompasses several stages, ranging from conceptualization to the creation of traditional blueprints and the development of both 2D construction plans and 3D models. CAD simplifies this process, minimizing errors and facilitating efficient collaboration. On the other hand, CAE software serves the purpose of simulating and evaluating the performance of systems and

structures. Through virtual simulations and tests, engineers can detect potential issues and enhance the design for optimal performance and efficiency, ultimately saving time and resources.

Together, CAD and CAE software provides engineers with a robust toolkit for collaboration and the creation of aesthetically pleasing and structurally sound designs. Integrating CAD designs with CAE simulations allows teams to identify potential issues early in the design phase, mitigating the risk of costly errors and delays later on.

2.1 Background

In recent years, advancements in pre-processing capabilities, such as ANSA morphing, have provided CAE engineers with powerful tools to explore geometric variations and their impact on crash performance. One of the most advanced tools developed to meet the needs for fast model modifications is the Morphing Tool. It expands the reusability of existing models by allowing the versatile procession of alternative variations. Morphing operations are performed on FE or geometry models. Applications include fields such as optimisation processes and sensitivity analysis. Furthermore, numerous software features, including the Morphing Tool, the scripting and the process automation, can be combined to offer versatile coupling with optimizations codes. These tools enable engineers to conduct optimization studies aimed at uncovering the most effective design changes to enhance CAE function. By conducting rigorous optimization studies, engineers can unravel the complex relationships between geometric variations and performance metrics, thereby paving the way for informed design decisions.

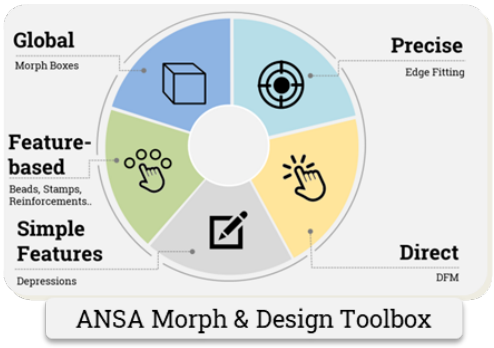

Fig. 1
Ansa Morph and Design Toolbox

2.2 Challenges in CAD-CAE Collaboration

Computer-Aided Design (CAD) and Computer-Aided Engineering (CAE) stand as indispensable tools in the process of designing and innovating new products. CAD facilitates the efficient design of new products, while CAE systems are employed to anticipate and evaluate the prospective functionalities, such as durability and structural strength. Typically, these systems operate autonomously, but their interdependence is a subject of interest for researchers.

Despite the availability of sophisticated pre-processing tools, CAD and CAE departments often face communication barriers. The inherent differences in their workflows and objectives can lead to misunderstandings and inefficiencies in the design process. Bridging this gap and fostering seamless collaboration between these departments is imperative for realizing the full potential of CAE-driven design improvements.

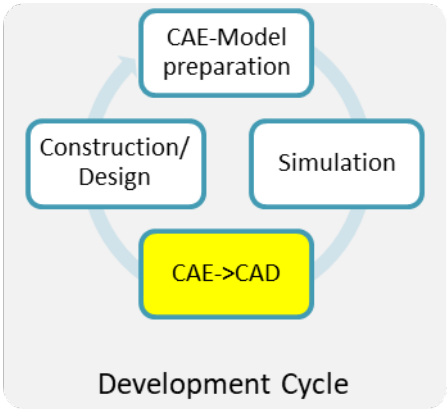

Fig. 2
Development Cycle

3 Approach

The concept at hand revolves around ensuring the preservation of crucial information and seamless adaptation to geometric changes throughout the optimization process. The challenge stemmed from discrepancies between the desired geometries communicated by the CAE specialist and what was actually delivered by the CAD team, necessitating iterative refinement and coordination with the design team.

To address this, the approach involved leveraging the original CAD file, the foundation of the meshing process, and parameterizing it to accommodate any specified geometric adjustments. This parameterization facilitated a secondary optimization iteration aimed at precisely fine-tuning the identified parameters, thereby arriving at the desired final geometric configurations.

To streamline this complex process, an automation service was essential. However, it had to be versatile enough to navigate different software platforms, considering the specific requirements of tools such as,Catia. Scalability is another critical factor; the solution must be able to serve the orders for multiple users.

Moreover, seamless integrated into ANSA, the optimization tool in use, was imperative. The goal was to avoid loading users with a further burden through unfamiliar interfaces with unfamiliar interfaces but rather to seamlessly integrate these functionalities into the existing toolkit, ensuring a smooth transition and maximizing user efficiency.

4 Implementation

The starting point for this process involves the Parametrized CAD-Design of the specific component in question, alongside the Crash Simulation Scenario. Through this process, the outcome is an optimized CAD-file, meticulously adjusted to incorporate parameters that yield optimal performance within our Crash Simulation Scenario.

We established our optimization framework, in the optimization tool of ANSA each line delineates a distinct experiment or design variant for comparison. Our infrastructure relies on the SPDRM Workflow Manager, serving as our pre-programmed automation service capable of executing ordered processes, such as generating specific geometries or meshes. For each experiment, the workflow is called, the order delivery lands in our workflow manager. The CAD update happens within the CAD software. FE update is done within ansa on different machines, simulation runs and post processing happens. When all experiments are delivered and executed, the results are pushed ANSA‘s optimization tool in order to proceed with the optimization.

On the one side, we have the input parameters. We begin with a parameterized CAD file and a simulation-ready model, along with key performance metrics defining our optimization goals.

Conversely, on the results side, our aim is to attain the optimized shape. What needs to be noticed here is the slight modification in the stamp, achieved by obtaining the optimized CAD file, retaining all pertinent information in a fully-fledged Catia format, ensuring no loss of data, and enhancing the behavior as per our optimization objectives.

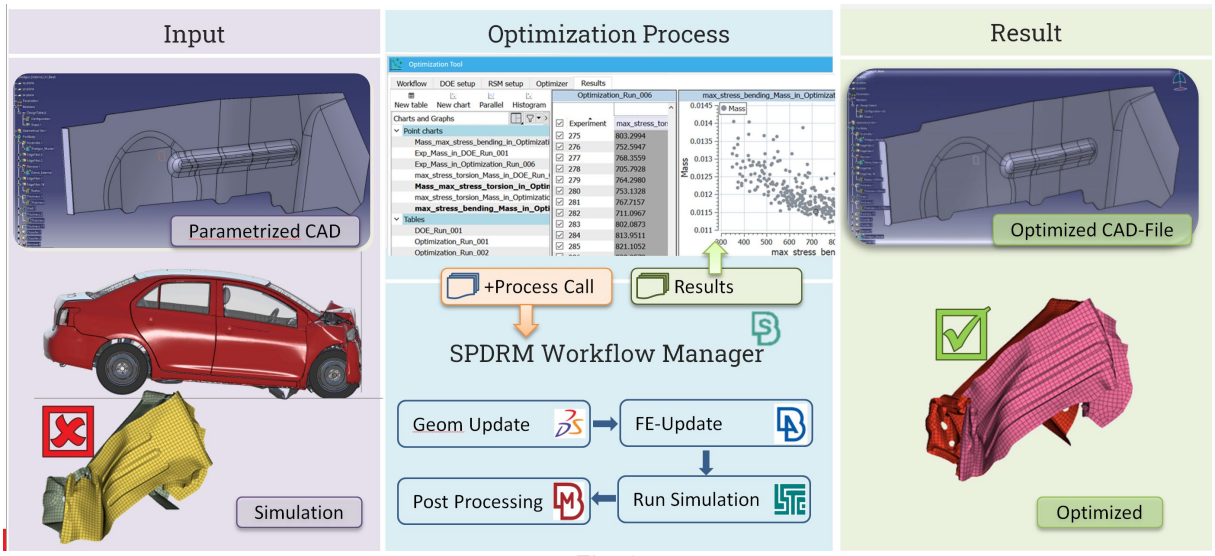

Fig. 3
Implementation of the process

Two automated procedures were meticulously crafted: one for extracting CAD parameters, utilizing both Catia and NX, and the other for the FE update process. The former, spearheaded by SPDRM, orchestrates the initiation of Catia on a remote system, accesses the CAD file, scrutinizes its contents, and transmits the design parameters back to ANSA. These parameters seamlessly integrate into the model browser, empowering users to generate design variables effortlessly. The latter scenario involves Catia's geometry update functionality, seamlessly interfacing with ANSA to mesh the updated geometry. This cohesive workflow streamlines the experiment generation process, with Catia handling geometry alterations while ANSA seamlessly executes the subsequent batch meshing steps, including mid-surfacing meshing.

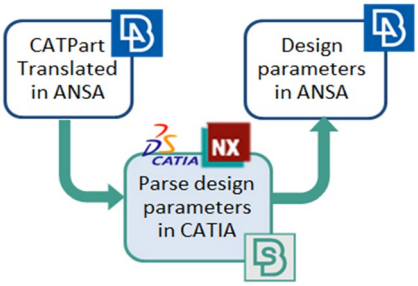

Fig. 4
Use Case 1: Parse CAD-parameters

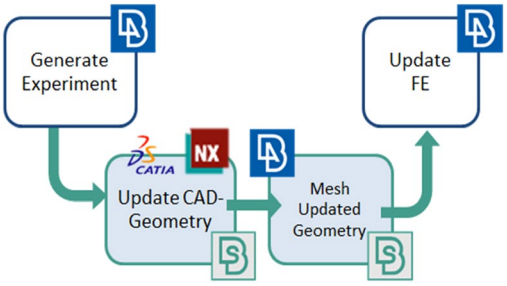

Fig. 5
Use Case 2: Update FE

5 Case Study

To illustrate the challenges and opportunities in CAD-CAE collaboration, we present a detailed case study focused on enhancing the CAE function of car components, specifically frontal rails, through geometric manipulation. The study involves conducting optimization runs to analyze the effects of geometric variations on crash performance and translating these findings into actionable design changes. This refers to the public Yaris front crash simulation case, where a decision was made to implement optimization, including the design optimization through CAD software. We applied this design exploration on this particular part, the front rail and the design space exploration includes the modification of some beads and a cross section.

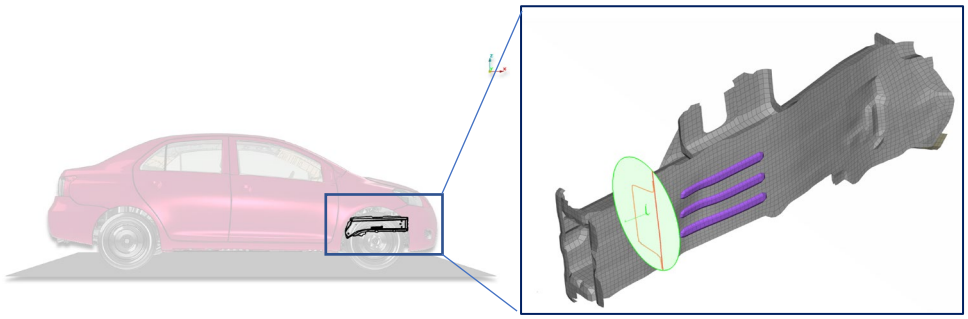

Fig. 6
Design Exploration Space: Modification of beads and cross section

5.1 Design Space Exploration with FE-Based Optimization

The approach entails a systematic multi-step procedure, commencing with the structuring based on modular run management principles. Subsequently, the focus shifts to pinpointing crucial design parameters influencing CAE functionality. ANSA morphing tools are utilized to explore geometric variations and their impact on crash performance through simulation and optimization studies. Mesh morphing allows to avoid these drawbacks suggesting the users to work on the finite element mesh directly reducing time taken to go back to update the geometry. This approach is FE based. We introduced five parameters, thus design variables. After running the doe, 20 experiments and visualizing the results in META postprocessor, some of the distribution and scatter plots, help in finding some linearities and understanding if there is a way to influence the key result by the design variables. Diving deeper, we take the characteristic line that describes the deformation pattern of this part. This is like a section cut on this cross section part.

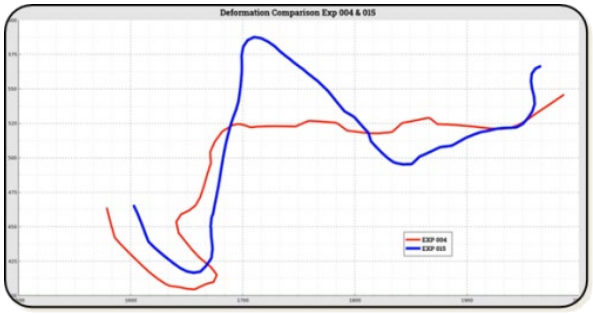

Fig. 7
The characteristic line and its deformation

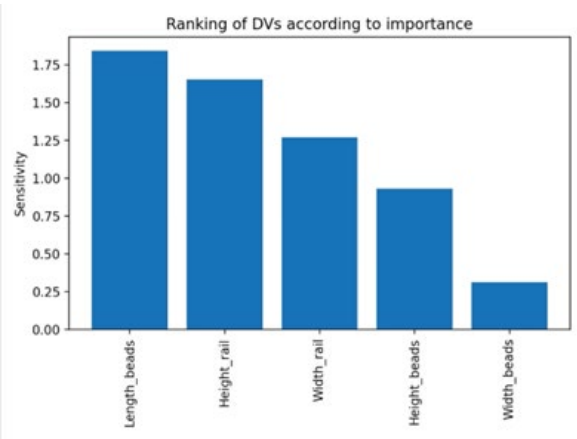

Fig. 8
Ranking of design variables first optimization run

From all the design variables, the one that defines the length of the beads, it was the most decisive one. This is the parameter that is going to be asked from the designing team. And then, the resulting CAD designs will be equipped with native parameters for further manipulation and optimization.

5.2 2nd optimization cycle including CAD-Design Parameters

As the second optimization run initiates, a streamlined automated workflow is developed to facilitate the transfer and update of design parameters from CAD to ANSA. This automated process ensures interoperability between different operating systems, making the exchange of design information efficient and seamless. In order to scale up an engineering team to achieve fast progress on complex products it is essential that team members can share their product data they are working with. Upon parsing the geometry, we observe the design parameters displayed in ansa.

The process initiates by sending the file in Catia, and SPDRM seamlessly takes charge, launching Catia on a remote machine, accessing the CAD file, scrutinizing its contents, and then relaying the design parameters back to ANSA. These parameters become visible within ANSA, shielding the user from the complexities associated with interfacing with Catia. With a simple click of a button, the user can proceed without grappling with the intricacies of invoking Catia or similar processes.

The user then proceeds to define their design variables, incorporating them into the optimization tool, and advancing to the subsequent phase. Then the next step is the experiment generation with Catia and the corresponding batch meshing step that takes over of mid surfacing meshing. The final step is the part replacement to get the new mesh and proceed with the simulation, participated in the model and fire up the simulation.

The second optimization run, revealed that the impact of thickness is not as important as the Limit Forward. We commence by investigating the Design Variable (DV) Limit_Fwd and how the change of its value affects the pair part. The length of the beads was the most decisive design variable in the first optimization run, and the Limit_Fwd, which is the distance of the bead from the front side of the rail seems to be the most decisive for pair part cases in the second optimization run.

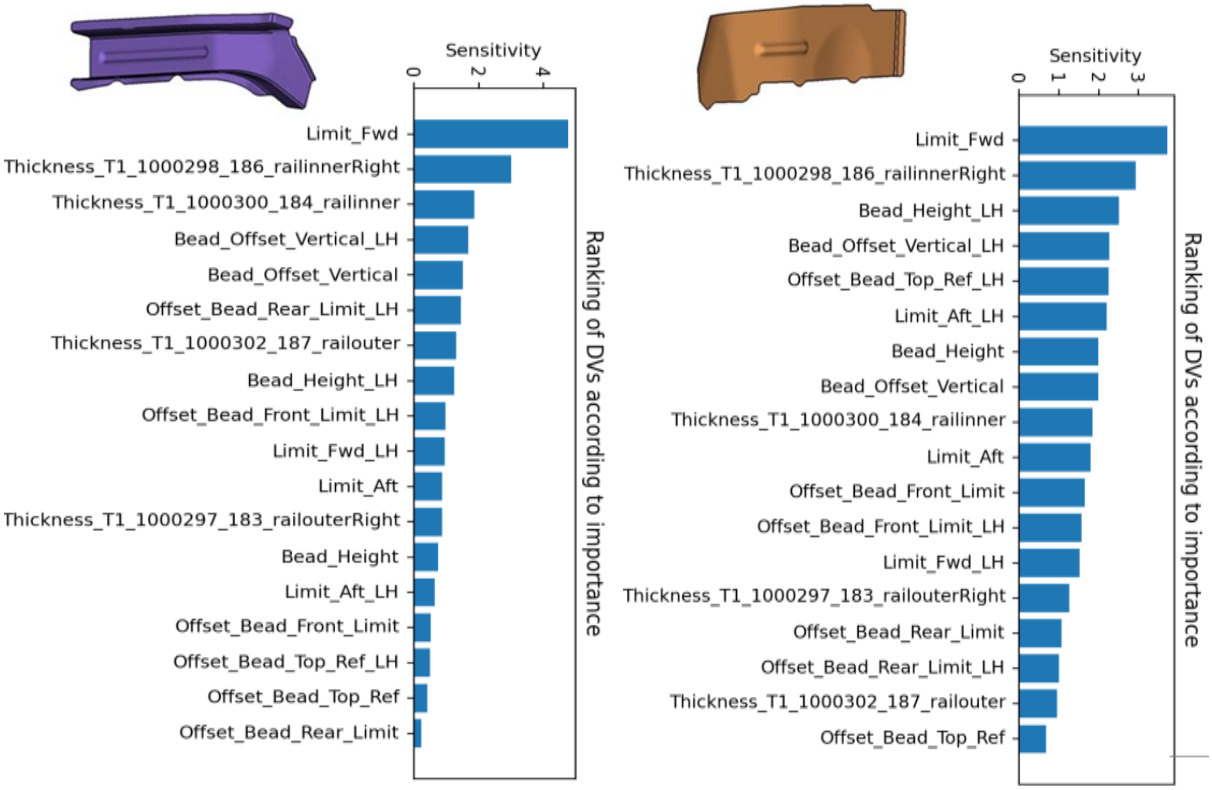

Fig. 9
Ranking of design variables second optimization run for the front rails pair on the left side

5.3 Conclusions of the Case Study

Preliminary results from our optimization studies underscore the transformative potential of geometric manipulation in augmenting CAE function. By iteratively refining design parameters based on simulation feedback, we have observed tangible improvements in crash performance metrics, promising enhanced safety and reliability for automotive components. Moreover, the streamlined automated workflow has proven instrumental in expediting the design iteration process, significantly reducing time-to-market and unlocking cost efficiencies.

6 Conclusions

In conclusion, the seamless integration of CAD and CAE workflows holds immense promise for revolutionizing the design and development of automotive components. By harnessing advanced pre-processing capabilities and fostering collaborative synergy between disparate departments, automotive manufacturers can unlock new frontiers in safety, performance, and efficiency. Addressing communication barriers and embracing automation will be pivotal in navigating the complexities of modern engineering challenges and propelling the automotive industry towards a future defined by innovation and excellence.

7 Acknowledgements

We extend our heartfelt appreciation to a multide of teams within our organization whose invaluable contributions made this research possible.

Firstly, we express gratitude to the Optimization Team for their pivotal role in defining and detailing the experiments generation step. Their expertise and dedication greatly enriched the methodology of our study.

Special recognition is due to the CATIA Design and Automation Team for their unwavering patience and commitment in generating designs that precisely met our requirements. Their meticulous efforts significantly enhanced the quality of our work.

We also acknowledge the META Post Processing Team for their collaborative spirit and innovative insights, which enabled us to effectively express the functions we aimed to improve. Their partnership was instrumental in achieving our research objectives.

The indispensable support of the Machine Learning Team deserves sincere acknowledgment for their assistance in creating the necessary prediction models. Their expertise in machine learning greatly bolstered the analytical framework of our study.

Furthermore, we are indebted to the SPDRM-Team for their instrumental role in designing the workflow, which streamlined our processes and encapsulated a complex task into a single-button solution. Their contributions revolutionized our approach and efficiency.

In conclusion, we express our deepest gratitude to all the teams involved, whose collective efforts and expertise were integral to the success of this endeavor.

8 References

[1] Proceedings from 9th Before Reality BETA CAE Systems conference, Closing the Optimization cycle: incorporating CAD-design parameters, Michail Tryfonidis, Zafeiria Kanellia, Spyros Tzamtzis, BETA CAE Systems

Fatigue Strength Assessment of Injection-Molded Fiber-Reinforced Plastic Components for Electric Vehicles

M. Stojek, S.Pazour (PART Engineering),
V. Mortazavian (Ascend Performance Materials)

1 Motivation

The use of plastic components in technical applications, especially in the automotive sector, has always required developers to evaluate the service life under oscillating loads. With the increasing substitution of metals, this requirement is growing. At the same time, the number of available material types is increasing due to optimized properties, adapted to special requirements. The measurement of characteristic values for the fatigue strength (SN-curves) is expensive and time consuming, not least because of the relatively low permissible frequencies for plastics under vibrating loads due to their self-heating.

An *anisotropic* fatigue assessment increases the necessary amount for measurement data considerably due to the directional dependency, making anisotropic SN-curves a rare resource. Therefore, estimating or simplifying methods are very helpful for fatigue assessment and are often the only option for a simulation driven design.

2 Approach

Ascend has developed a group of fiber reinforced PA66 grades with particularly good damping properties. While improving the components performance, higher damping in general reduces the allowable testing frequency even more.

A special test component has been tested in static and cyclic loading conditions. (although investigated, NVH and acoustics are not covered here). Figure 1 shows the test component used in the structure for vibrational stress.

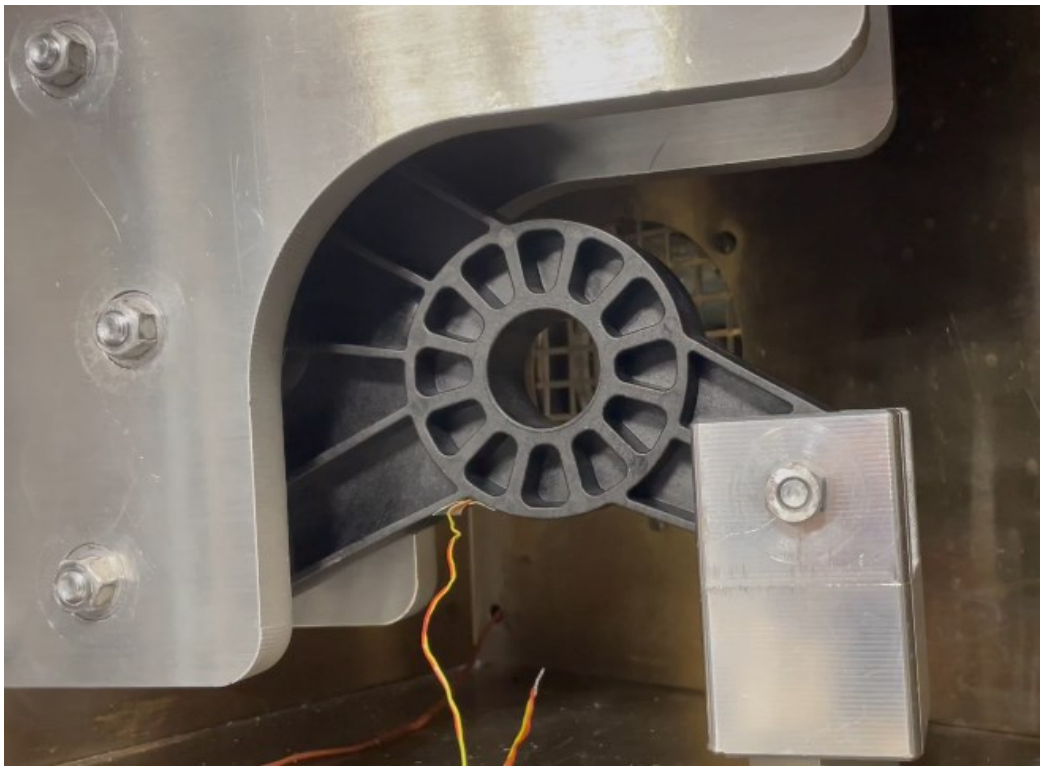

Figure 1 Test Component Under Cyclic Loading

In a first approach, a fatigue assessment is presented based on an isotropic simulation and the Oberbach method [1]. Generic Wöhler curves are generated based on short-term tensile tests (see Fig. 2) and local utilization ratios are calculated. In an additional step, an anisotropic procedure based on these generic SN curves is discussed. This includes an anisotropic material model for the stress calculation and the components stiffness.

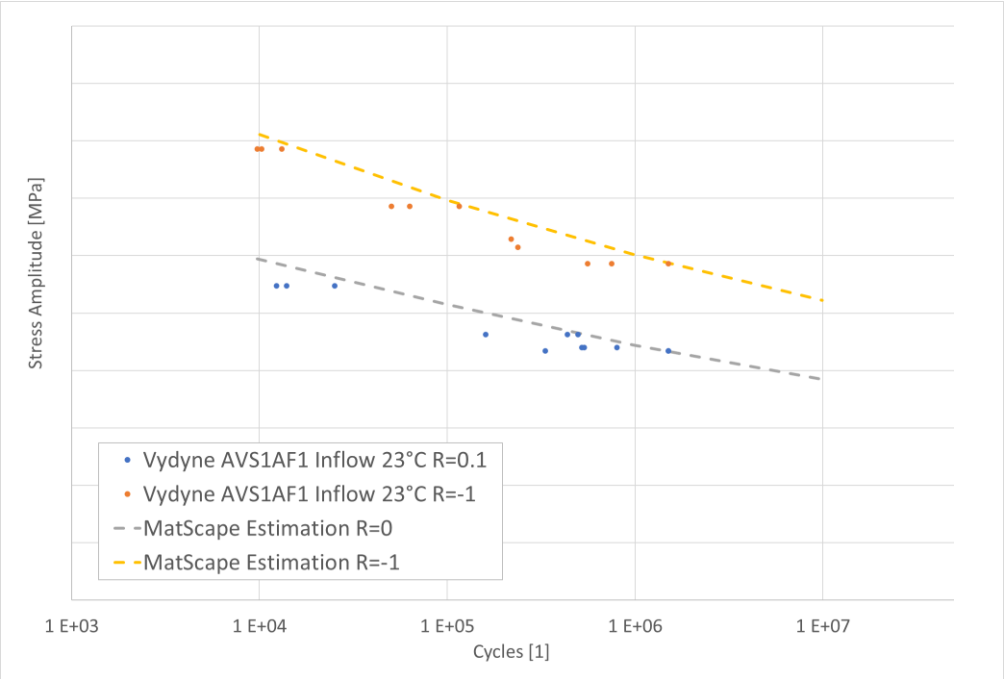

Figure 2 Comparison Between Measured Data and Generic SN-Curves

All calculation results are compared with the real test data.

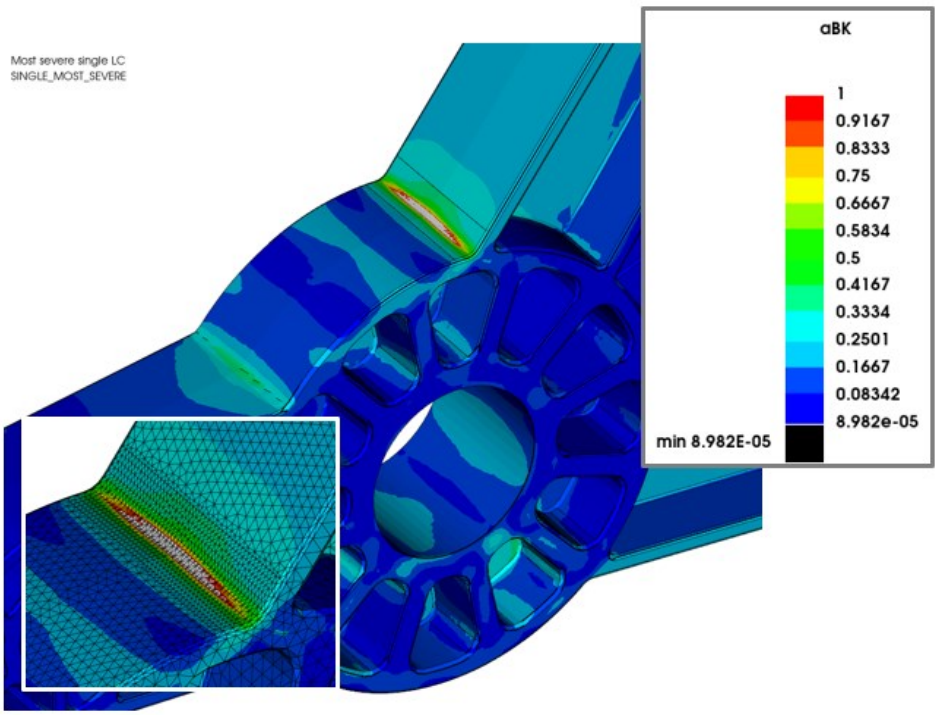

Figure 3 Result of a Fatigue Assessment with S-Life Plastics

3 References

[1] Reprint (10/2020): Allowable Strength Limits, Kunststoffe, Oberbach, www.partengineering.com

Cracking the Code of Welded Shaft Reliability in e-Axle Motors

Hirubaakaran Moorthy, Andrea Marchi (Valeo Automotive Germany GmbH)

1 Abstract

In the world of engineering and manufacturing, where reliability and durability are key, this paper dive into the study of a welded shaft in an e-Axle motor. This critical component faced a major challenge during bench testing when it failed at the weld joint. This incident raised important questions about its safety and the accuracy of typical simulation methods in predicting such failures. The complexity of the situation deepens when the intricate changes in material properties considered during welding, the shift from isotropic to anisotropic characteristics layer by layer throughout the weld thickness. Thermomechanical effects and variations in geometry add further layers of complexity. This comprehensive assessment blends welding and structural simulations with life assessment methodologies.

Initial part of the study involved detailed welding process simulation using SIMUFACT. Essential factors like weld speed, energy, and torch dimensions were considered and also took into account material behavior, welding distortions, residual stresses, and variations in hardness within the heat-affected zone. These factors were used as starting conditions for the following static structural analysis. We then assessed the structural integrity of the shaft under real-world conditions in ANSYS by introducing loads like speed, torque, interference, and bearing misalignment. These loads played a key role in evaluating how the shaft performed in practical situations.

As the shaft experiences cyclical stresses due to rotation- N-code was used for crucial fatigue assessment, with the combined results from the static structural analysis & Process simulation. Material mapping in the weld region considered hardness variations across thickness and width. Comprehensive approach, encompassing welding and structural simulations, as well as various loads and parameters, provides deep insights into the shaft's behavior in real-world conditions. The strong alignment between simulation results and actual testing outcomes demonstrates the effectiveness of this methodology. At the end , failure was precisely predicted in simulation.

This study underscores the importance of precise life assessment in engineering, where even minor changes in material properties, geometry, and welding processes can significantly impact component integrity and the overall system's reliability. With ongoing research and the refinement of simulation methods, this paper contributes to the continuous enhancement of structural analysis and fatigue assessment, ultimately enhancing the safety and efficiency of engineering systems.

2 Problem statement:

1. The study focuses on a critical issue within engineering and manufacturing, where a welded shaft in an e-Axle motor experienced a significant failure during bench testing at the weld joint.This incident has raised questions about the safety and accuracy of conventional simulation methods in predicting such failures. The problem necessitates a comprehensive assessment that combines welding and structural simulations with life assessment methodologies.

3 Product Architecture and validation

The shaft is fabricated into 2 parts and welded together using seam weld for the e-Axle motor. Shaft was tested in bench setup with a speed duty cycle, It failed in the test at weld joint. To predict this welding failure with the existing simulation method it was observed that the shaft is safe for the given test bench speed & torque duty cycle. In order to predict the **weld joint life** due to the complex change in material microstructure (Material changes from isotropic to anisotropic, layer by layer throughout weld thickness as shown in below image), thermomechanical effects and geometric variations which induce stress concentration during the welding process, this study of Weld joint life assessment is conducted which includes the above mentioned factors which are closer to reality. The assessment explained in this paper is upto the stage where cracking of material is about of happen.

Welding + Structural + Life simulation

In **SIMUFACT** weld process simulation is conducted by using the input parameter such as weld speed, weld energy, and weld torch dimensions and also by considering the elastoplastic behaviour, welding distortion, residual stresses, hardness value changes in heat affected zone (HAZ) are mapped in the welding location as initial condition for static structural analysis.

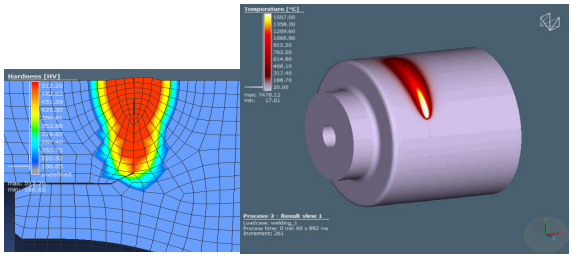

Fig. 1: Manufacturing Process in simulaiton

In addition to this initial stress state, loads such as speed, torque, interference between shaft and rotor, bearing misalignment load (steady state loads) are used for Structural evaluation in **ANSYS**.The shaft undergoes changes in stress state due to the cycles of rotation which is captured via changing the direction of bearing misalignment load. The weld fatigue simulation with ncode is conducted using results from static structural analysis (ie combination of process simulation and steady state loads). The material mapping in the weld region is based on the hardness distribution in weld region (ie. Along the thickness and width hardness changes included for evaluation)

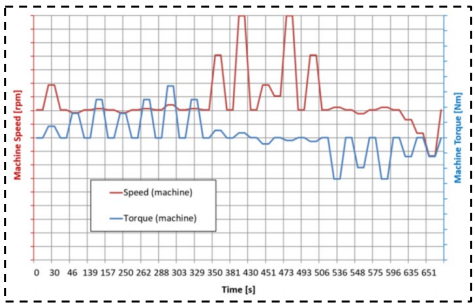

Fig. 2: Load cycle profile

4 Conclusion

The maximum damage value observed at 40% cycle time . The weld life is estimated through interpolation for unit Damage (Miner's rule) occurs at 34 % cycle time which is close to the range where failure is observed during testing. It is suspected that deviation from simulation and testing is due to not taking account of crack propagation time. Prediction from simulation exactly matches with the crack observed in the failed sample.

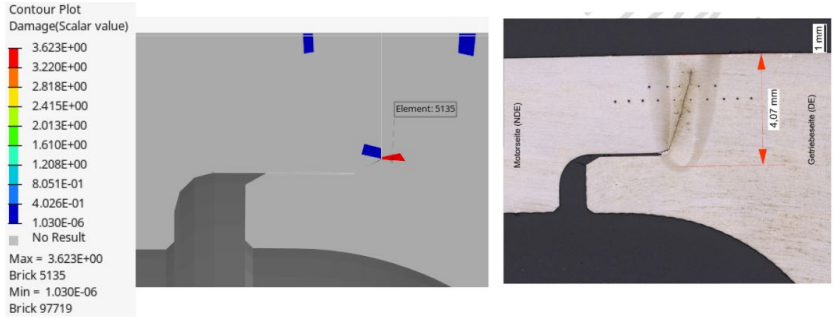

Fig. 2:Failure due to crack propagation in shaft welding region

The present work can be expanded further by studying the soldering process and its effect on fatigue. In addition to that crack growth study is planned to be conducted using LEFM theory based on the testing data about initial crack size.

Nonlinear modeling of a flat flexible body in multibody dynamics by a 2D segmentation approach

Dr. Tobias Ulmer (Airbus Operations GmbH).

1 Summary

For integration tests of flap actuation systems, Airbus at Bremen performs physical tests on test benches as well as virtual tests based on flexible multibody simulation.
In the case under consideration, the focus lies on the determination of relative motions between two flaps under different system states and environmental conditions.
For aerodynamic reasons, the two flaps are connected by a rubber sealplate. Relative motion between the flaps leads to deformation of the plate. This leads to reaction forces influencing the motion between the flaps. In consequence, the seal plate has to be considered in the multibody simulation model. Due to nonlinearities (shear buckling, sagging) the usual approach of a linear modal representation of the flexible sealplate (Craig-Bampton Transformation) is deemed to be non applicable. Co-simulation between multibody simulation and nonlinear FEM is possible but shall be avoided because of the expected high computational cost.
Consequently, alternative approaches are investigated.
To approximate geometric nonlinearities, good results have been achieved by splitting flexible bodies into segments.
The segments are modeled as usual by a linear, modal representation, whilst the segments' rigid body motions are considered fully nonlinear.
Satisfactory results can be achieved for relatively low numbers of segments (<5) for slender bodies (e.g. wind turbine blades or wings of aircraft). However, the approach is quasi one dimensional as the splitting is performed only in spanwise direction.
Hence, the splitting approach is experimentally extended to two dimensions. The seal plate is segmented in two directions. The segments are modeled linearly-elastically and connected in the multibody model by joints. Both, the generation of flexible segments and the integration in the MBS model are performed parametrically and script-based. This is necessary as even small numbers of segments lead to considerable numbers of connecting joints.
First results show qualitatively correct capturing of the expected nonlinear effects at acceptable computational cost.

2 Introduction

The geometry of the wing of an aircraft (A/C) is optimized for the conditions in cruise flight, i.e. high speeds and altitudes.
To provide acceptable low speed performance, enabling takeoff and landing at acceptable speeds for given runway lengths, the wing geometry has to be adapted to the specific conditions during takeoff and landing. This is achieved by high lift devices at the leading edge (slats) and trailing edge (flaps) of the wing. Deployment of slats at the leading edge generally allows it to fly at higher angles of attack before stall occurs, hence allowing it to produce sufficient lift at lower speeds. Deployment of flaps at the trailing edge of the wing generally increases the surface and/or the curvature of the wing with the same result: lift increases at lower speeds.
The high lift actuation system consists of the components which are required to position the high lift devices during flight and to perform the monitoring of the system's state. These are central motors converting hydraulic or electric power into mechanical power (Power Control Units, PCUs), a transmission system consisting of shafts, bearings and gearboxes which is powered by the PCUs, brakes, sensors, controllers (Slat Flap Control Computers, SFCCs), which are controlling and monitoring the system as well as the flaps lever in the cockpit for pilot interaction with the system.
Development tests for all new Airbus A/C high lift systems are conducted in Bremen. For the conduction of the development test program, the Airbus Test Center Bremen uses physical testing on test benches (test rigs), which are extended and complemented by computer simulation based tests (virtual test, VT). Mainly, these virtual tests are based on multibody simulations. Due to the properties of the high lift components and the boundary conditions acting on them, some of the components have to be modeled as flexible bodies. Generally, the combination of properties and load conditions are such that the resulting deformations can be considered as linear elastic. In consequence, the flexible bodies are

modeled by a linear elastic, modal-based super-element approach (modal neutral file, (.mnf) resulting from a Craig-Bampton transformation [1]).
In particular cases, e.g. the measurement of the relative displacements between the inboard and the outboard flap of one wing, the linear approach can be inacceptable. In the case under consideration, the two flaps are connected for aerodynamic reasons by a rubber sealplate which closes the gap between the flaps at the lower cover. The following figure 1 shows the interflap area and the interflap sealplate colored in blue.

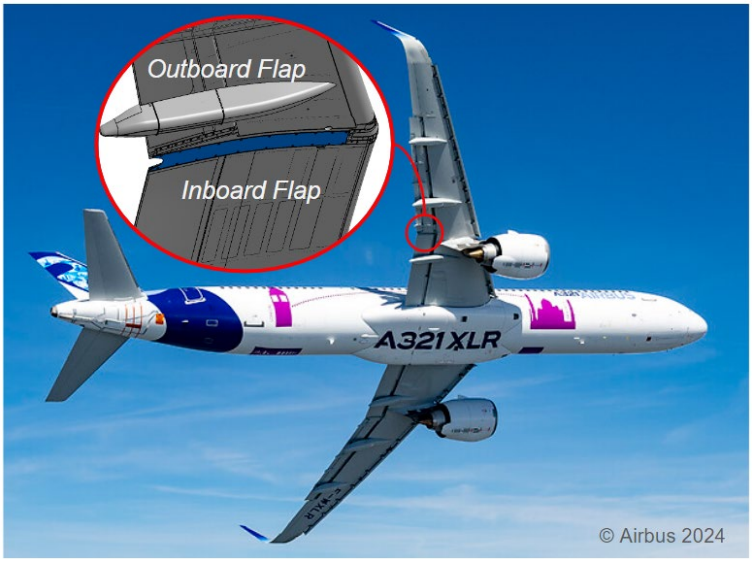

Fig. 1
Interflap area and sealplate (colored in blue).

Depending on the boundary conditions acting on the mechanism (aerodynamic forces acting on the flaps as well as enforced displacements resulting from aerodynamic forces acting on the wing) and the system condition, the relative displacements lead to deformations of the sealplate, which in turn lead to reaction forces generated by the plate, acting on the flaps and feeding back on the motion of the flaps. The deformation of the plate can be such that nonlinear effects are observed:

- Whilst an increasing distance between the flaps in spanwise direction leads to tension forces in the plate, the plate does not produce pressure forces if the flaps are approximating each other. It shows sagging instead.
- Shear buckling occurs for shear loading resulting from position offsets of the flaps in direction of flight (respectively chordwise direction).
- Besides these geometric effects, one can expect that the material of the sealplate shows nonlinear behavior (hyperelasticity).

As the described effects cannot be covered by a linear elastic modal approach, alternative approaches are investigated.

3 Modeling Approaches

An obvious self evident approach consists of a co-simulation between nonlinear (N/L) finite element analysis (FEA) and multibody simulation (MBS). The MBS analysis delivers the boundary conditions to the N/L FEA, which feeds back sealplate reaction forces to the MBS. By closing the loop and performing a coupled simulation, it is expected to achieve an adequate representation of reality. The advantage of this approach is that the N/L FEA is able to consider both material and geometric nonlinearities. However, the expected computational effort is considerable. N/L FEA is generally expensive. Furthermore, for the described force-displacement-coupling small coupling step sizes are to be expected in order to achieve convergence and consistency of the states of the two coupled models.
Hence a N/L FEA of the sealplate is planned to be performed as a reference solution for selected cases, whereas for larger simulation activities, including parameter variations for uncertainty assessment, coupled simulations are to be avoided.
That is why until now, the sealplate is discretized in direction of flight (chordwise direction) and represented by approximately 10 pairs of forces. For each pair, one force represents the pure shear force for displacements in chordwise direction. A nonlinear law for computation of the force's magnitude can be used optionally to model shear buckling (shear force collapses if buckling occurs for displacements exceeding a given threshold). The second force represents the tension forces in the sealplate. This force is defined by a line-of-sight approach. This means that the orientation of the forces

adopts to the instantaneous position of the ends of the sealplate. This includes a force component for large displacements in chordwise direction acting as a shear force component. Also steps between the flaps leading to an increase of distance in diagonal direction are covered. Due to the discretization in chordwise direction, varying distances in chordwise direction (cleavage) are considered, too. With a nonlinear law for calculation of the forces' magnitudes, nonlinear material behavior as well as the half sided contact (tension for increasing distance, no pressure for closing in) can be considered.
The challenge of the approach is the selection of parameters, namely the related stiffness values and the buckling displacement threshold for shear force deactivation.
In the past, good results for modeling geometric nonlinearity have been achieved by splitting flexible bodies into segments. The segments are modeled "classically" by the linear elastic modal approach. Connection of the segments in the multibody simulation by fixed joints and treatment of each segment as a dedicated body, hence enabling a full nonlinear consideration of its rigid body motion, results in a fairly good approximation of the geometric nonlinearity. Experience has shown that even for comparably small numbers of segments (<5) an acceptable correlation with nonlinear FE analyses can be obtained. However, till to date, the approach was used in a quasi one dimensional way, splitting long, slender bodies, e.g. a wing, into segments along one direction (spanwise). The sealplate, being a flat, quasi two-dimensional body, needs to be segmented in two directions, enabling e.g. the possibility of observing buckling.

4 2D Segmentation Approach

The sealplate is discretized in two directions, chordwise and spanwise. The resulting segments are modeled by linear elastic finite element models. Different approaches have been investigated: modeling the segments by multiple finite elements (sub-discretization) andmodeling a segment by one finite element only. Besides that, modeling by 2D shell elements as well as modeling by 3D solid elements have been investigated.
For modelling, the sealplate geometry is defined by two end curves, which are in turn defined by a set of points on the two end ribs. The discretization in chordwise direction is performed along these two end curves, splitting the curves by separation points in a chosen number *ny* of equally sized segments. The discretization in spanwise direction is performed by splitting the spanwise connections between adjacent separations points into a chosen number *nx* of equally sized segments. The following figure 2 shows exemplarily the two endribs, the sealplate's end curves defined by nine points each and a discretization of the sealplate into *nx*=5 chordwise respectively *ny*=10 spanwise segments. The segments each consist of one single CQUAD4 element.

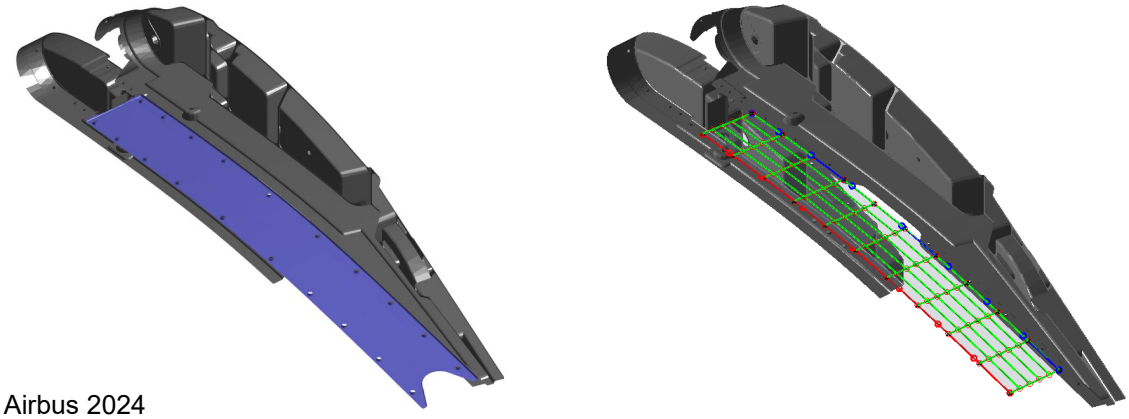

Fig. 2
End ribs and sealplate, seen from below, discretized with 10 × 5 segments.

Sub-discretization yields the potential advantage of lower numbers of segments. Whereas in this case problems arise from the connection of the segments by joints in the multibody simulation environment. Basically each contact node at the intersection of two segments needs to be connected to its neighbor by a fixed joint. This results in unmanageable high numbers of joints. Furthermore, the connection nodes strictly speaking have to be interface nodes of the flexible bodies, leading to an unreasonable high number of constraint modes in the related flexible bodies. The standard FE approach of using rigid body elements to attach multiple points to one connection point is not an option: RBE2 elements would introduce unrealistic rigidifications, RBE3 elements are deemed to be theoretically possible. But although different connection patterns have been investigated, the approach led to numerical problems. Omitting connection points and stitching only a subset of interface points, e.g. the corners of segments,

is not an option either as this leads to slits in the sealplate, significantly affecting the stiffness of the body. The following figure gives an overview on the different connection options and the associated problems.

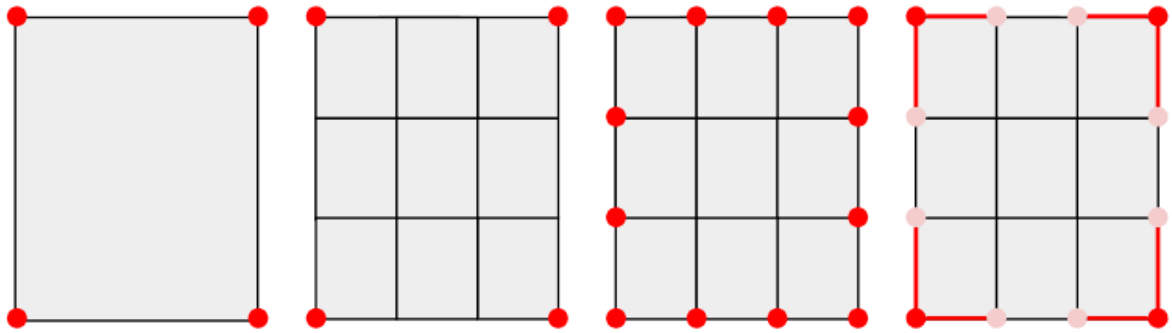

(1) Single Element per Segment. *Connection at corners* *OK*	*(2) Subdiscretization* *Connection at corners* *KO: slits opening under load*	*(3) Subdiscretization* *Connection at all grids on edges* *KO: too many interface nodes in .mnf* *too many joints in MBS*	*(4) Subdiscretization* *Connection via Rigid Body elements* *KO: RBE2s lead to rigidifications* *RBE3s lead to numerical problems*

Fig. 3
Connection options for segments with and without subdiscretization.

Accordingly, each segment is modeled by a single CQUAD4 element. An ASET card is defined at each corner node resulting in an interface node for connection of the segments. The parameter K6ROT is used to introduce a penalty stiffness to be added to the normal rotation of the CQUAD4 element, enabling an interface which allows introduction of loads in all six degrees of freedom, although for shell elements the normal rotation has no physical meaning and in general should be ignored. The penalty stiffness removes the singularity in the normal rotation [2].
The resulting flexible segment is degraded to some extent, as it shows flexibility only in tension, shear and twist. It does not have any bending stiffness, respectively degrees of freedom. This is why the connection of the segments in the multibody simulation environment is realized by bushings instead of fixed joints. The bushings have high (dummy) stiffnesses in translational direction, as these degrees of freedom are covered by the plate segments' flexibility. However low stiffness values are used for the bending degrees of freedom around the chordwise and spanwise direction. This is deemed to be correct as the quasi two-dimensional sealplate shows very low bending stiffness around the related axes. Only the normal rotation respectively in plane bending stiffness is set to a high value, which avoids overlapping respectively intersecting of the sealplate segments under load. Besides that, the bushings might be used to approximate nonlinear material behavior in case of need.
To enable the testing of different discretization settings, the creation of the $nx \times ny$ FEM models is done by script execution. Depending on discretization and connection settings, the script produces the resulting bulk data files, the related solution decks (SOL103 with .mnf file generation) as well as a set of .bat files for job execution. By distributing the $nx \times ny$ Nastran jobs into multiple .bat files which are executed simultaneously, a simple but effective approach of parallelization is implemented.
In the case of the sealplate, the two defining end curves are fairly parallel and have almost the same length. This results in almost exactly congruent sealplate segments. In consequence, instead of creating dedicated .mnf files for each segment, optionally only one common .mnf file can be created. This reduces significantly the number of .mnf file generations needed. In the MBS environment, each segment is represented by the common .mnf file and positioned at its required location by a rigid body transformation. The transformation information (translation and rotation) is also calculated by the script for flexible body generation.
In order to achieve a connection between the segments in all required directions whilst avoiding redundant constraints, the connection pattern shown in figure 3 is applied. Specific bushings are suppressed as they would result in redundant constraints on the collocated connection points. Note that the connection points are actually colocated, for separability they are drawn at different locations in the schematics.

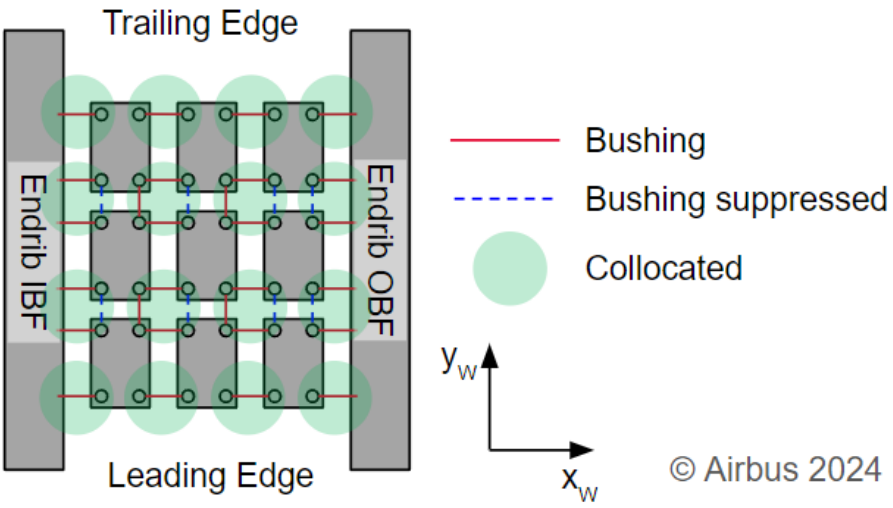

Fig. 3
Connection pattern for sealplate segments.

As mentioned above, the connection of the segments in the MBS environment leads to a considerable number of joints. For example, the discretization introduced above with 5 × 10 = 50 segments results in a sealplate model with 156 bushings for segment connection. This is why the MBS model creation of the sealplate is also done by script execution. In this case, the model is defined in a table, which is read by a python script that uses the pre-processors API to perform the defined modeling steps (creation of parts, import and assignment of flexible bodies (respectively application of rigid body transformation as described above if one common .mnf is used) and creation of the connecting bushings.
The related code has been integrated into an existing model creation script [3] and the specification of the tabular model definition has been extended accordingly. Thanks to this approach the definition of the sealplate model is done by a limited number of parameters (discretization *nx*, *ny*, .mnf file naming pattern, modal damping and bushing stiffness properties) in one single line of the model definition table. This reduces significantly the manual effort needed for integration of the model and increases the resulting quality of the model as it avoids slips during model setup.

5 Results, Conclusions and Outlook

Different discretization settings have been tested for the following three load cases:

- pure tension,
- pure shear,
- pure compression.

For all cases one end rib was fixed to ground and a displacement of 50mm was applied on the other end rib in direction x (tension and compression) respectively y (shear). Reaction forces at the attachment point were measured (joint reaction forces).
The results show qualitatively for all discretization settings the expected results. For the compression load case, the sealplate sags as can be seen on the following figure on the left (examples for a seal plate discretization of 35x7).

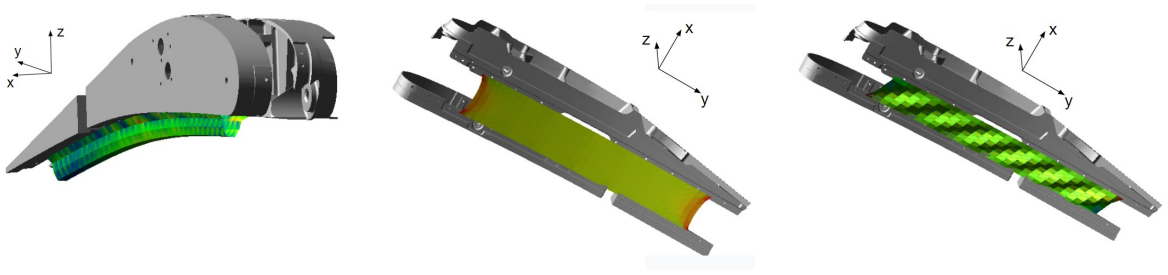

Fig. 4
Sealplate (discretized 35x7) under compression load, tension load and shear load (left to right)

For the tension load case, the seal plate narrows at its ends and for the shear load case, the sealplate shows characteristic shear buckling.

For all load cases and discretization settings, the computation times are acceptable.Calculation was performed by a dynamic analysis with the Gstiff integrator after an initial static solution. Quasi static calculations were performed as well but failed in the shear load case at the occurrence of buckling.

The quantitative assessment shows for the tension load case no observable dependency on the discretization settings. The following figure shows the normalized reaction forces for three different settings (10×5, 20×5 and 35×7). The reaction force F_x in direction of the applied displacement behaves fairly linear. As expected, for the tension loadcase, the observed reaction force F_y perpendicular to the displacement is close to zero.

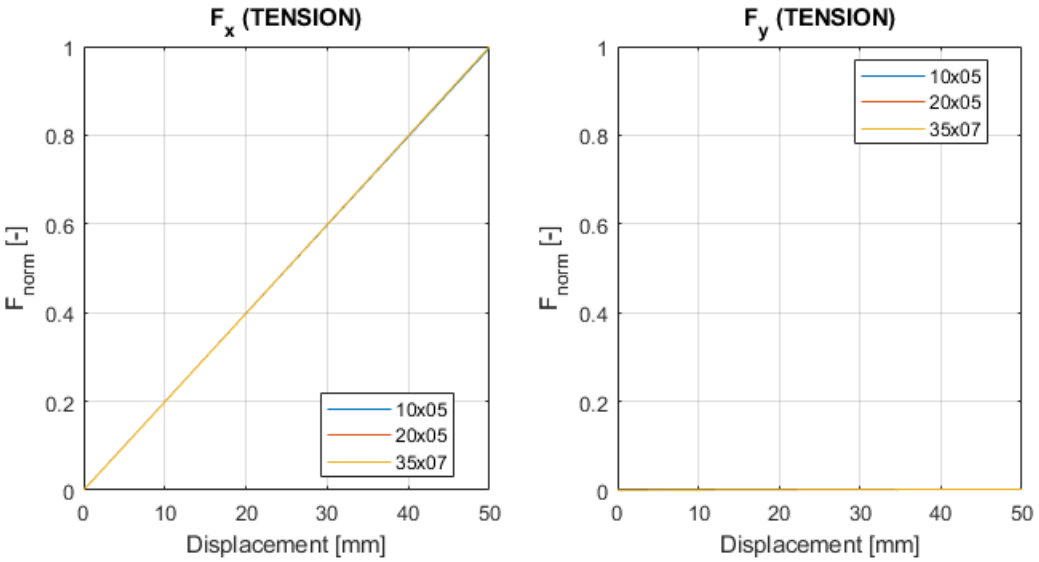

Fig. 5
Tension load case, reaction forces in directions x and y.

The shear load case shown in the following figure produces expectedly reaction forces in both directions (x / perpendicular to the applied displacement and y / parallel to the applied displacement).

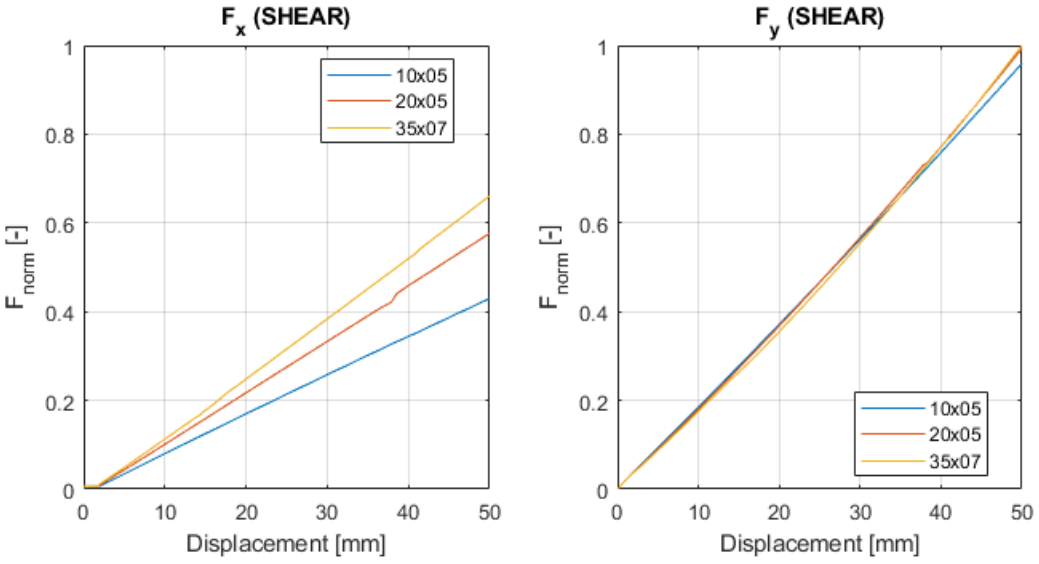

Fig. 6
Shear load case, reaction forces in directions x and y.

The force in x-direction starts to build up at a displacement of approximately 2mm which corresponds to the moment when the sealplate starts to buckle. In case of the 20×5 discretization setting, a step in the reaction force F_x can be observed near 38mm, corresponding to the moment when an additional buckle occurs in the plate. For the 35×7 discretization setting the same effect can be observed (less dominant) near 41mm of displacement. The force in x-direction visibly depends on the discretization

settings. For the considered settings no convergence was observed yet. The force parallel to the applied displacement (y-direction) behaves similarly for all considered settings. Apparently the force converges, since the difference between the settings 20×5 and 35×7 is hardly visible. Especially the two settings with finer discretization show a certain nonlinear behavior. This is explained by the tension component, which contributes increasingly to the shear reaction force for increasing displacement (lateral tension).
In summary, for the given material and geometry parameters (Young's modulus, Poisson's ratio, shell thickness and dimensions of the plate) the sealplate behaves fairly linear for tension and shear. Shear buckling can be visually observed, whereas in regards to the reaction forces no significant nonlinearities can be observed.
In conclusion, the 2D splitting approach demonstrates the capability of replicating the expected effects with acceptable computational effort for both, preprocessing and solving. The study performed to date also indicates that, depending on the sealplate's properties, an FE based consideration might not even be necessary. In consequence, for further analysis, the MBS results produced by the splitting approach will be compared with results obtained from related nonlinear FE calculations. These calculations will permit further assessments of the approach and will enable the decision, in which cases the splitted approach is suitable, or, alternatively a simple modeling by pairs of forces (see chapter 3) is sufficient or, to the contrary, a full nonlinear FE analysis is required. This might be the case especially if nonlinear material behavior, which is currently neglected, shows to play a governing role.
In general, it can be said that the results available to date are promising, leading to the conclusion that the 2D splitting approach seems to be applicable and provides an attractive ratio between computational cost and achievable accuracy. Nevertheless, further investigation is recommended to finally conclude if the approach is adequate, unnecessarily complex or not complex enough. Another point, which requires further consideration, is the test of applicability in more complex, flexible multibody simulation models than the relatively simple model that was used throughout this first analysis.

6 References

[1] Young, J. T., Haile, W. B..: "PRIMER ON THE CRAIG-BAMPTON METHOD", National Aeronautics and Space Administration (NASA) , 2000

[2] MSC.Software Corporation: "MSC Nastran 2013.1 Quick Reference Guide", MSC.Software Corporation, 2013

[3] Ulmer, T., Lopez Parras, R.: "Virtual Testing for High Lift Systems - Script-Based Processes for Efficient and Traceable Model Creation", NAFEMS, NWC19

Multi-body simulation of the switching processes within an innovative ankle foot orthosis mechanics

Patrick Steck, David Scherb, Jörg Miehling, Sandro Wartzack (Lehrstuhl für Konstruktionstechnik Friedrich-Alexander-Universität Erlangen-Nürnberg)

1 Introduction and motivation

The shifting demographics worldwide signal a looming challenge: an increasingly aging population. Alongside this demographic transformation comes a surge in age-related health concerns, among which neurological afflictions such as strokes loom. Figure 1 illustrates how the probability of suffering a stroke increases with age [1].

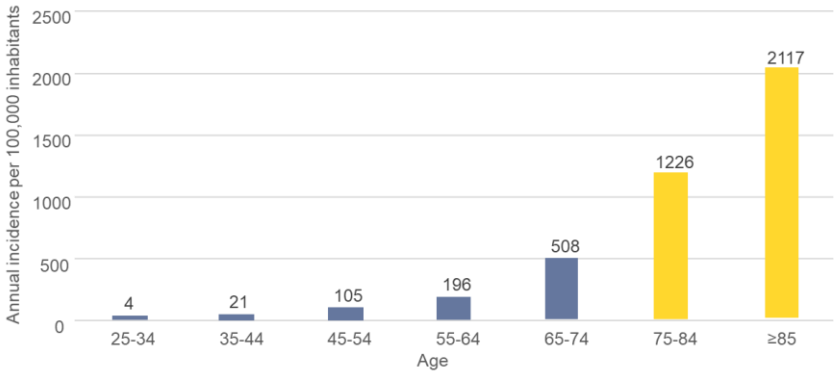

Figure 1 Annual stroke incidence per 100,000 inhabitants [1].

Patients who suffering on such diseases often have a so-called plantar and dorsal weakness, i.e. a reduction in lifting and lowering the foot during gait. The resulting gait abnormalities not only compromise mobility but also significantly elevate the risk of falls and associated injuries. An established treatment method is the use of so-called active or passive ankle foot orthoses (AFO) [2]. While active AFOs offer dynamic support through external energy sources, passive AFOs are more reliable because of the use of their inherent stiffness or the energy generated by the wearer itself [3]. Despite their potential benefits, current passive AFOs predominantly focus on supporting dorsiflexion [4]. Research into the passively support of plantar flexion is still at the beginning and is now to be significantly expanded by the innovative mechanism presented in this contribution [5].

2 Methods

The basic premise for a "normal" gait pattern is, that the calf and shin muscles (plantar and dorsiflexors) can be activated to such an extent that the desired angular moments can be provided. In order to ensure that an AFO can provide a supporting moment, an appropriate database must first be created for the design process. After that, a reliable energy saving orthosis mechanism can methodically be developed. As the ankle joint angle and moment follow an anticyclical curse, it must be possible to switch the mechanism on and off at certain times. To test the principal functionality, an integration into a multi body simulation software (MBS) is needed.

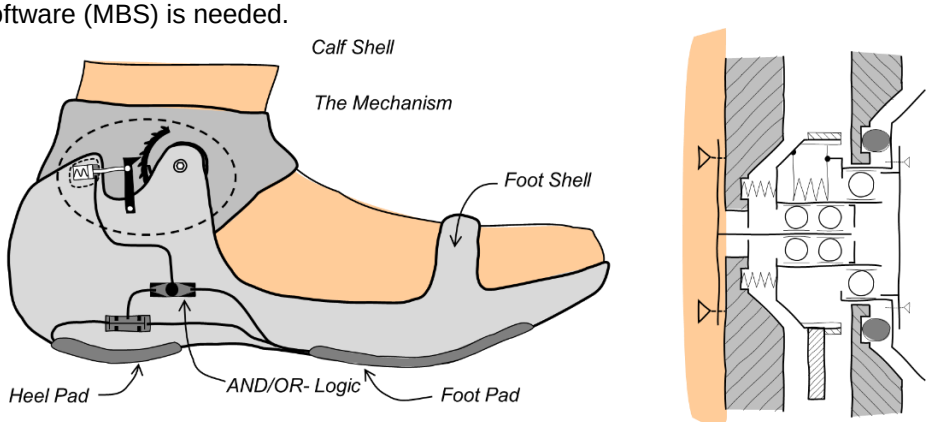

Figure 2 Conceptual draft of the orthosis and the mechanism

In this contribution a weakened torque curve of one test subject with medium gait speed and 50% plantar weakening (50% residual activity) into the Ansys Motion simulation environment was set. The corresponding activation points for the angle and moment curse are transferred directly as a Heaviside function. In order to be able to optimally scale the storage medium for the energy, 15 different design points were used.

3 Results

In the approach described in this contribution, the mechanism stored the required energy for the support in torsion springs. Furthermore, a OR/AND logic was developed to control the mechanism, which was first designed separately from the mechanism, then simulatively tested with Matlab Simulink and finally experimentally validated on a scaled model. As a closed system, this logic is able to transmit corresponding signals to the mechanism with so-called control pads that are placed on the heel and ball of the foot at the defined support times.

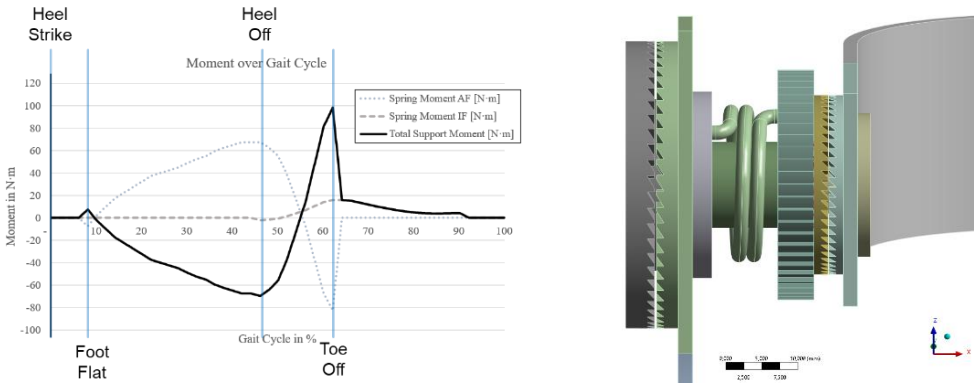

Figure 3 Support course of the supporting torsion spring.

The greatest moment due to the plantar flexion from a test subject occurs at the heel off (HO) with 99 Nm. The maximum torque provided by the mechanism during the HO was 79 Nm. The design points of the torsion springs were 3 Nm/° for plantar flexion and 0.4 Nm/° for dorsiflexion. The torque that could be applied by the residual muscle activity (50 Nm) was therefore increased by 58%.

4 Discussion and Conclusion

The developed mechanism for supporting the entire gait cycle, including plantar flexion, showed very promising results in an initial simulation. Simulations demonstrated that simple torsion springs can provide the necessary support for weakened patients. Furthermore, a simple logic was used to simulatively and experimentally prove that by using just two sensor points on the sole of the foot, a mechanism can be controlled which supports the entire gait cycle. However, since a calculation required approx. 11 minutes of computing time and many further simulations must be carried out for a general formulation of the mechanism, a model order reduction with static condensation or a trained model should be considered. In future work, the logic will also be integrated directly into the simulation model in order to directly investigate its effects and interactions with the mechanism and the gait behavior.

5 References

[1] S. Fiebiger, „Schlaganfall - Zahlen, Daten, Fakten“, Schlaganfallbegleitung. Zugegriffen: 3. Mai 2024. [Online]. Verfügbar unter: https://schlaganfallbegleitung.de/wissen/schlaganfall-fakten

[2] K. K. Chui, M. Jorge, S.-C. Yen, und M. M. Lusardi, Hrsg., *Orthotics and prosthetics in rehabilitation*, Fourth edition. St. Louis, Missouri: Elsevier, 2020.

[3] P. Steck, D. Scherb, J. Miehling, und S. Wartzack, „On the Influence of Incorrect Idealized Joint Axes to the Design Process of Orthoses“, in *Computer Methods in Biomechanics and Biomedical Engineering II*, W. Skalli, S. Laporte, und A. Benoit, Hrsg., Cham: Springer Nature Switzerland, 2024, S. 187–194. doi: 10.1007/978-3-031-55315-8_21.

[4] P. Steck, D. Scherb, J. Miehling, H. Völkl, und S. Wartzack, „Synthesis of passive lightweight orthoses considering humanmachine interaction“, in *Proceedings of the 33rd Symposium Design for X*, in 119, vol. 119. 2022, S. 1–10. doi: 10.35199/dfx2022.11.

[5] P. Steck, D. Scherb, C. Witzgall, J. Miehling, und S. Wartzack, „Design and Additive Manufacturing of a Passive Ankle–Foot Orthosis Incorporating Material Characterization for Fiber-Reinforced PETG-CF15“, *Materials*, Bd. 16, Nr. 9, Art. Nr. 9, Jan. 2023, doi: 10.3390/ma16093503.

Mehrkörpersimulation einer Sprunggelenkorthesenmechanik

P. Steck, D. Scherb, J. Miehling, S. Wartzack

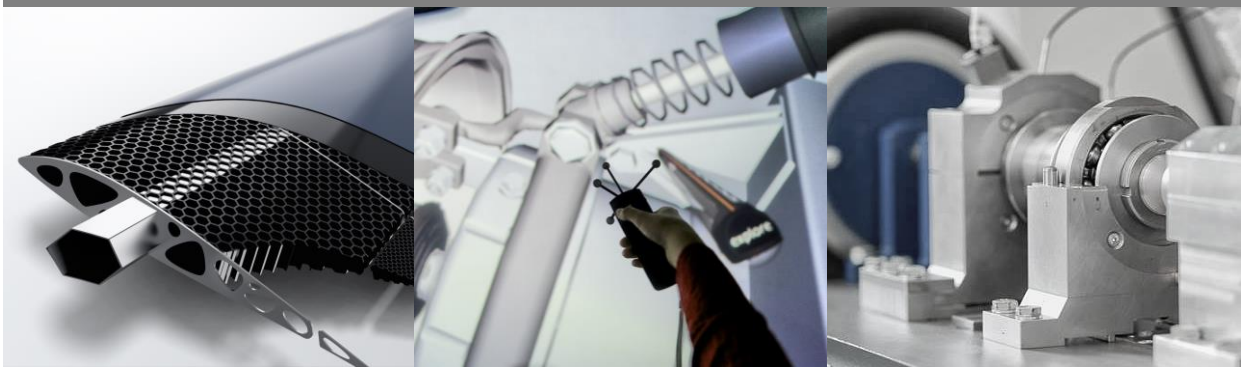

Friedrich-Alexander-Universität
Technische Fakultät

Lehrstuhl für
Konstruktionstechnik
Prof. Dr.-Ing. Sandro Wartzack

Gliederung

- Was sind passive Orthesen und wofür werden sie verwendet?
- Vorarbeiten, Inputparameter und weitere Randbedingungen
- Eine Lösung für vollfunktionale, passive Sprunggelenkorthesen
- Zusammenfassung

Eine passive Sprunggelenkorthese für den gesamten Gangzyklus

Beispiele orthetischer Anwendungsbereiche

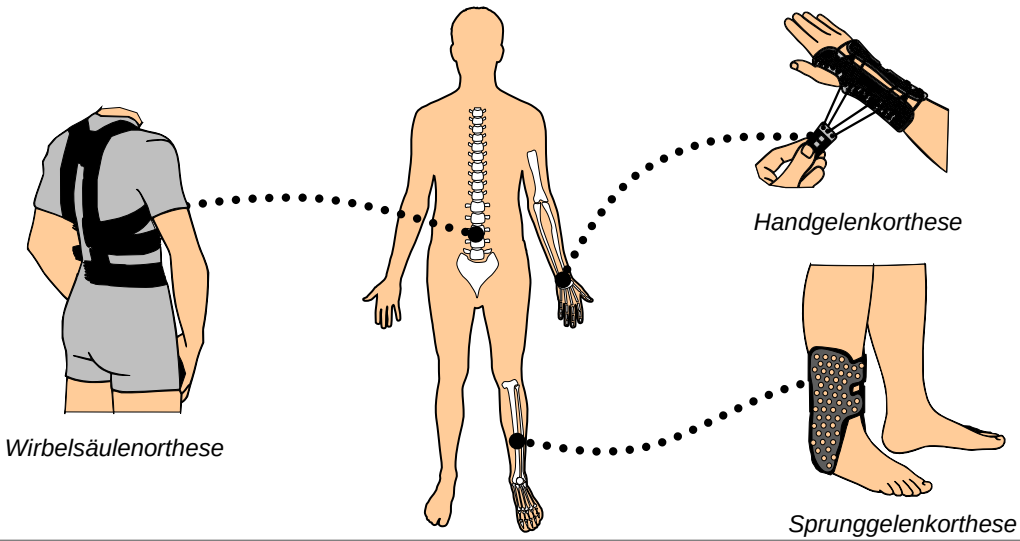

Mehrkörpersimulation einer Sprunggelenkorthesenmechanik

Vor- und Nachteile von aktiven und passiven Orthesen

„Eine **Orthese** ist ein medizinisches Hilfsmittel zur Behandlung von neuromuskularen und skelettalen Beeinträchtigungen des Körpers."

Specht, 2008, Technische Orthopädie: Orthesen und Schuhzuwerk

Aktive Orthesen	Passive Orthesen
+ Steuer- und regelbar	+ **Gute mobile Einsetzbarkeit**
– Nicht-triviale Realisierung der Energieversorgung	+ **Leichte kompakte Bauweise**
– **Eingeschränkt mobil einsetzbar**	+ **Gutes Fail-Safe Verhalten**
– **Höheres Gewicht**	– Konservative Orthesen auf Dorsalflexion beschränkt → Folge: abnormaler Gang (Fehlbelastung, Atrophie, etc.)
– **Kein Fail-Safe Verhalten**	

Quelle:
Colins et al.; Reducing the energy cost of human walking using an unpowered exoskeleton; Nature; 2015

Eine passive Sprunggelenkorthese für den gesamten Gangzyklus

Behandlungsdiagnose: Sprunggelenkorthese

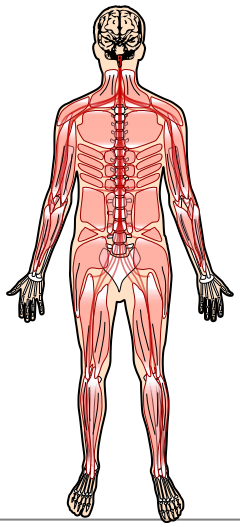

- *Schlaganfälle*
- *Krebs*
- *Andere nervliche Entzündungen, wie z. B.*
  - *Kompression des Rückenmarks zwischen L4 und L5*
  - *Amyotrophe Lateralsklerose (ALS)*
  - *…*

→ *Hebe- und Senkschwäche des Fußes*

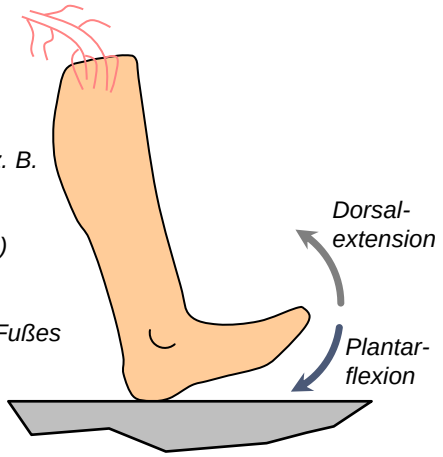

Mehrkörpersimulation einer Sprunggelenkorthesenmechanik

Kurzfilm: High Steppage Gait

Quelle:
https://www.youtube.com/watch?v=jzJIpY6vRLo

Gliederung

- Was sind passive Orthesen und wofür werden sie verwendet?
- Vorarbeiten, Inputparameter und weitere Randbedingungen
- Eine Lösung für vollfunktionale, passive Sprunggelenkorthesen
- Zusammenfassung

Mehrkörpersimulation einer Sprunggelenkorthesenmechanik
Entwurf des Mechanismus

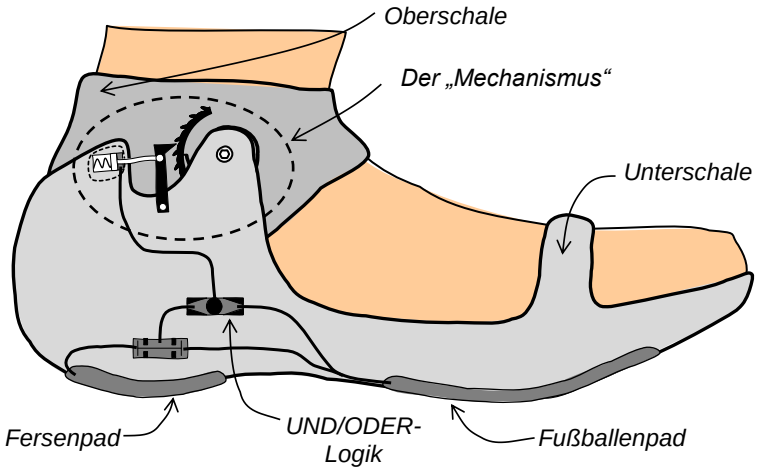

Mehrkörpersimulation einer Sprunggelenkorthesenmechanik
Datenerhebung

Bewegungsstudie mit
15 Probanden

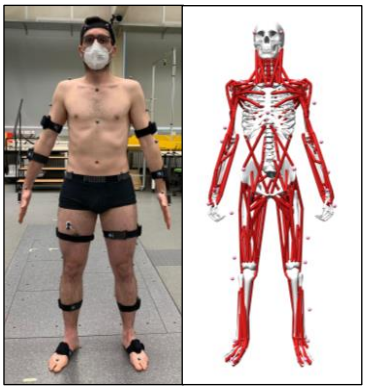

Muskuloskelettale Simulation mit 3 versch. Ganggeschwindigkeiten
und 5 versch. Schwächungszustände

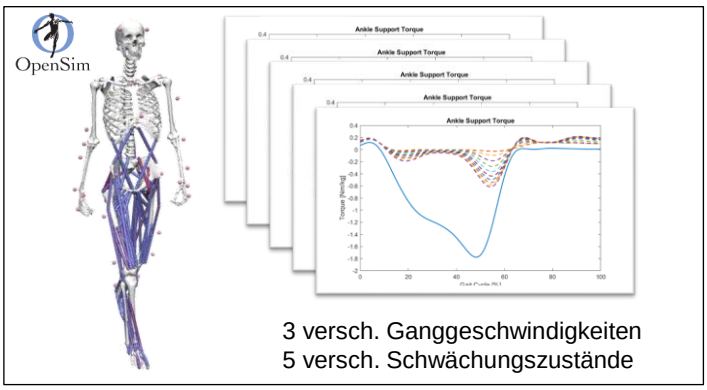

3 versch. Ganggeschwindigkeiten
5 versch. Schwächungszustände

Mehrkörpersimulation einer Sprunggelenkorthesenmechanik
Datenerhebung

Scans von Fußabformungen zur
Generierung individueller Bauräume

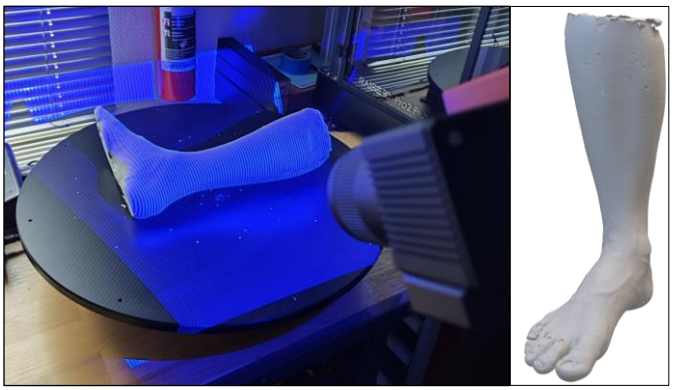

Überführung in B-Rep und
Vereinfachung des Bauraumes

Gliederung

- Was sind passive Orthesen und wofür werden sie verwendet?
- Vorarbeiten, Inputparameter und weitere Randbedingungen
- Eine Lösung für vollfunktionale, passive Sprunggelenkorthesen
- Zusammenfassung

Mehrkörpersimulation einer Sprunggelenkorthesenmechanik
Entwurf des Mechanismus

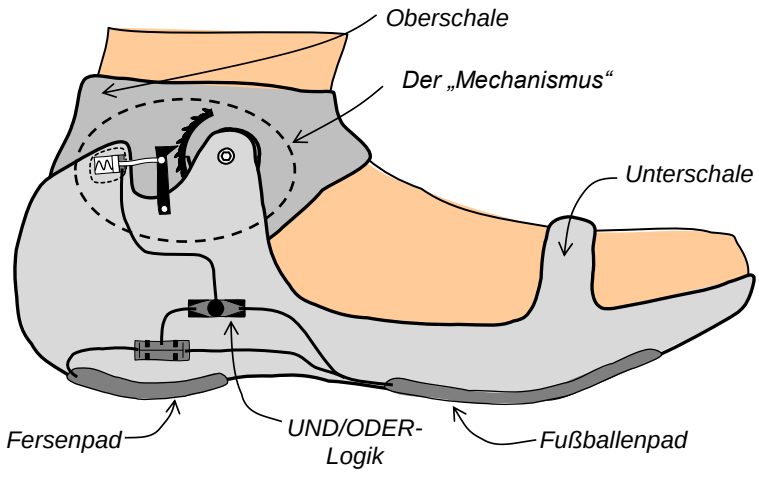

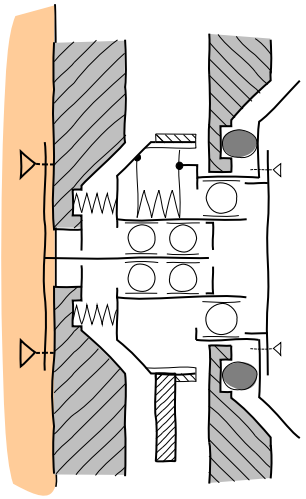

Mehrkörpersimulation einer Sprunggelenkorthesenmechanik
Einteilung der Gangphasen und der Unterstützungszeitpunkte

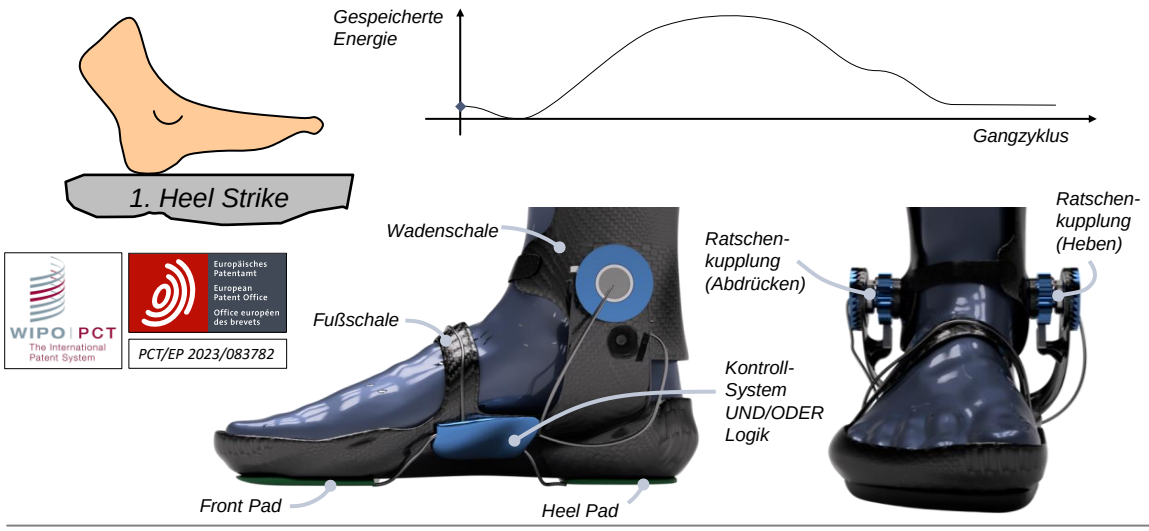

Mehrkörpersimulation einer Sprunggelenkorthesenmechanik
Einteilung der Gangphasen und der Unterstützungszeitpunkte

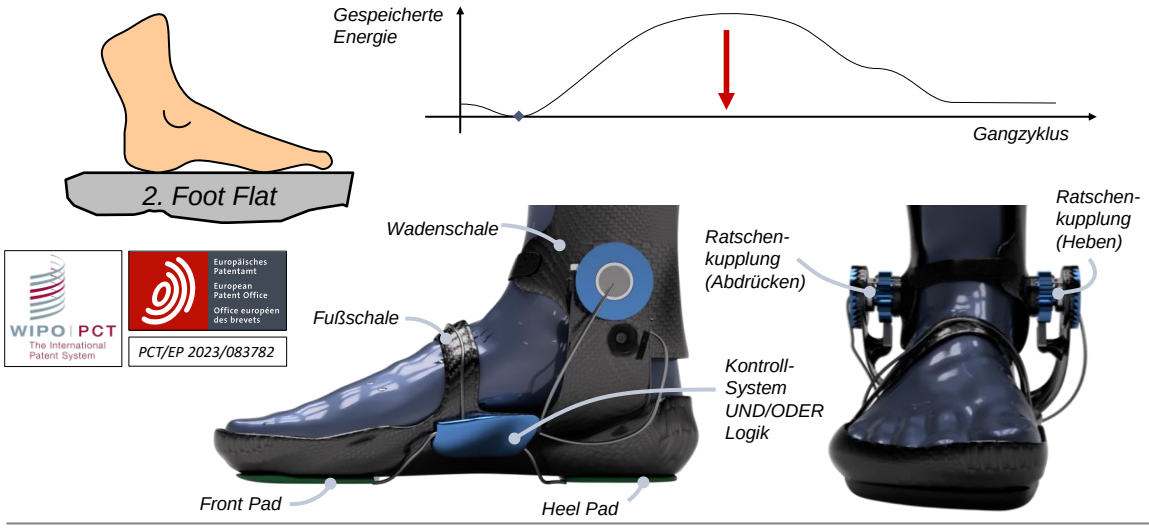

Mehrkörpersimulation einer Sprunggelenkorthesenmechanik
Einteilung der Gangphasen und der Unterstützungszeitpunkte

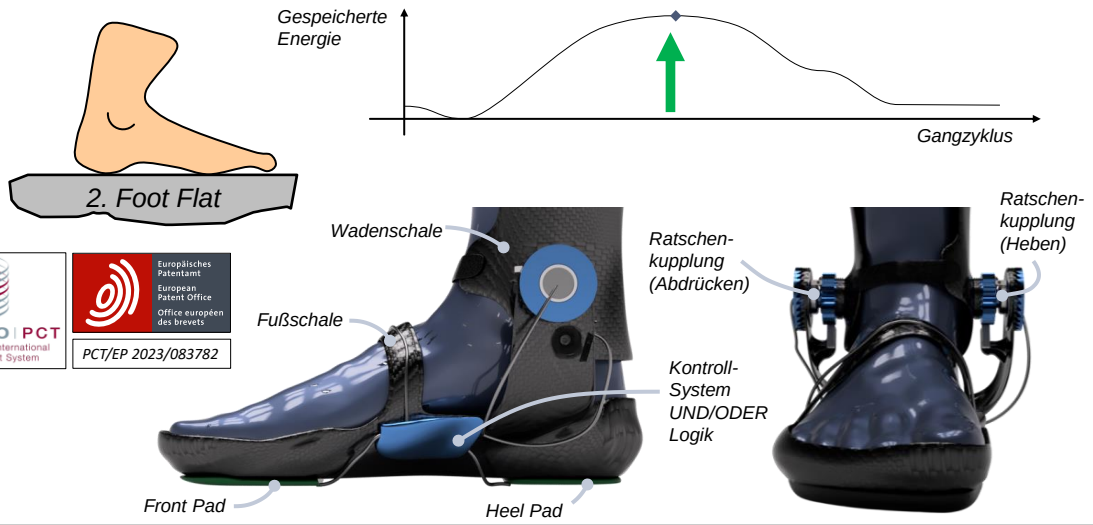

Mehrkörpersimulation einer Sprunggelenkorthesenmechanik
Einteilung der Gangphasen und der Unterstützungszeitpunkte

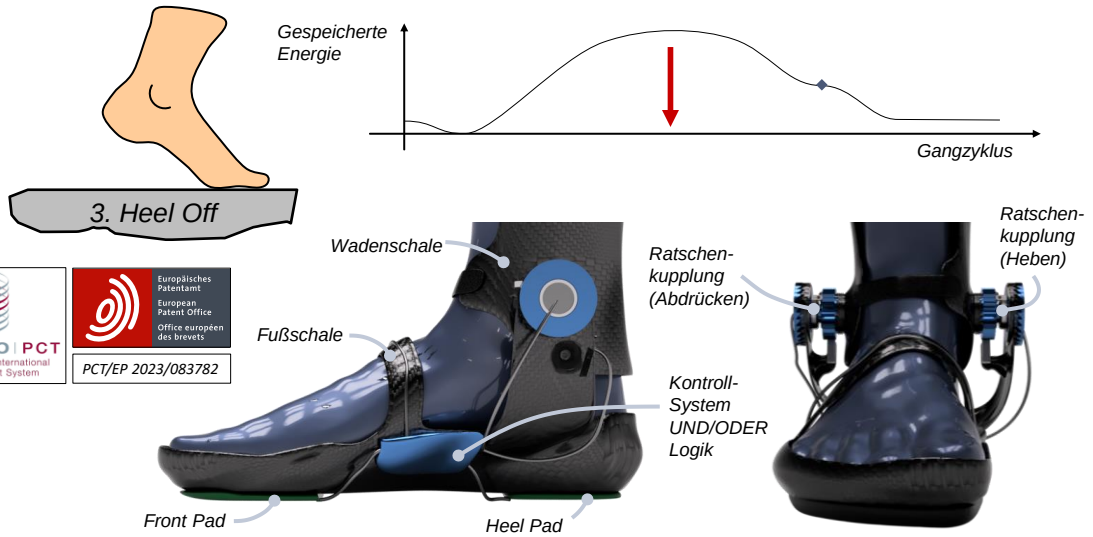

© LEHRSTUHL FÜR KONSTRUKTIONSTECHNIK
Friedrich-Alexander-Universität Erlangen-Nürnberg
Prof. Dr.-Ing. Sandro Wartzack

Mehrkörpersimulation einer Sprunggelenkorthesenmechanik
Einteilung der Gangphasen und der Unterstützungszeitpunkte

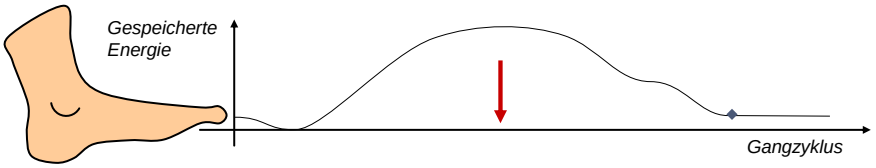

4. Toe Off

Mehrkörpersimulation einer Sprunggelenkorthesenmechanik
Einteilung der Gangphasen und der Unterstützungszeitpunkte

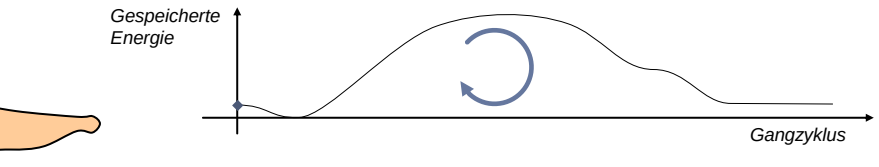

1. Heel Strike

© LEHRSTUHL FÜR KONSTRUKTIONSTECHNIK
Friedrich-Alexander-Universität Erlangen-Nürnberg
Prof. Dr.-Ing. Sandro Wartzack

Mehrkörpersimulation einer Sprunggelenkorthesenmechanik

Entwurf der Schaltlogik

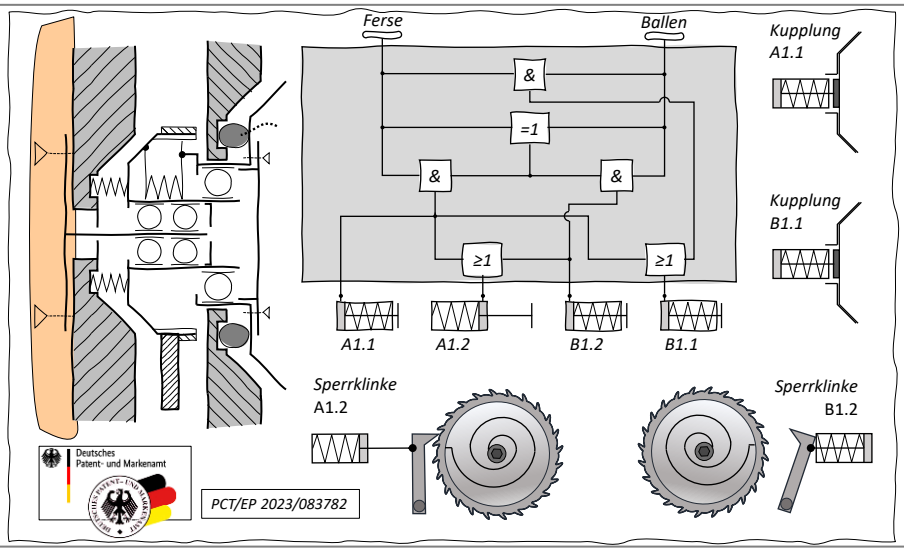

Friedrich-Alexander-Universität Erlangen-Nürnberg
Prof. Dr.-Ing. Sandro Wartzack

Mehrkörpersimulation einer Sprunggelenkorthesenmechanik

Simulationsaufbau

1) Simplifizierte Baugruppe

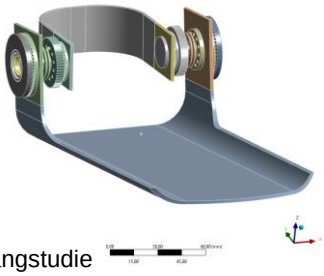

2) Freiheitsgraddefinition (Federn)

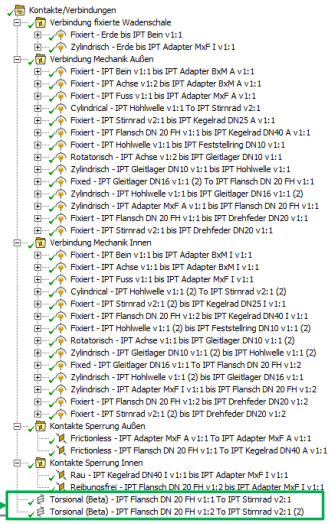

3) Input Bewegungsdaten aus Gangstudie

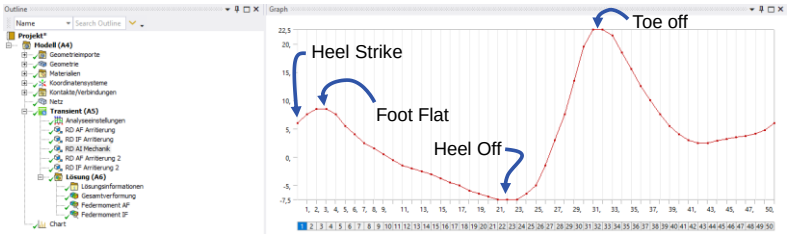

Friedrich-Alexander-Universität Erlangen-Nürnberg
Prof. Dr.-Ing. Sandro Wartzack

Mehrkörpersimulation einer Sprunggelenkorthesenmechanik
Randbedingungen

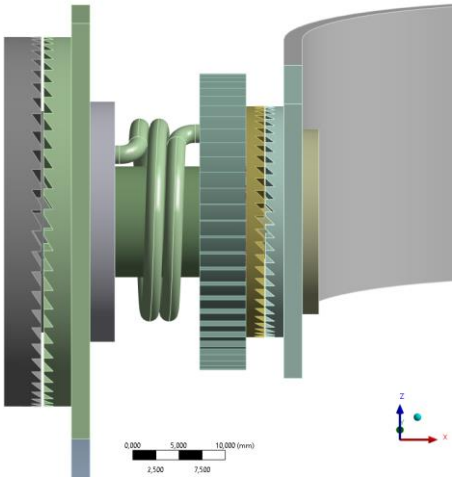

- Materialien: bis auf Kunststoffschalen alles Stahl

→ Gewicht ca. 300g

- Zeit-Integration: Runge-Kutta 4 Ordnung
- Zeitschritte: 50
- Auflösung Zeitschritt: 0,01s
- Anzahl Gelenke: 79
- Freiheitsgrade: 54

- Materialien: bis auf Kunststoffschalen alles Stahl
- Federsteifigkeit: initial angenommen 3Nm/° und 0,4Nm/°

Mehrkörpersimulation einer Sprunggelenkorthesenmechanik
Funktionstest

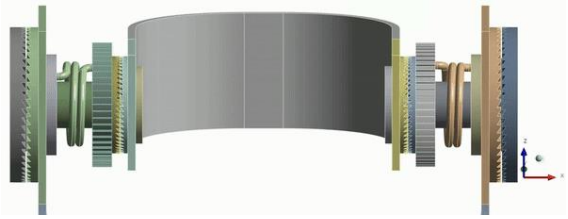

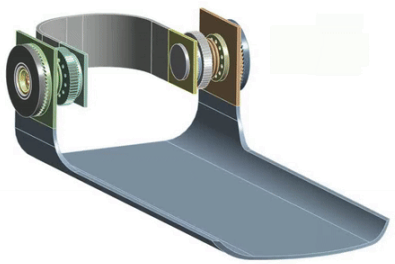

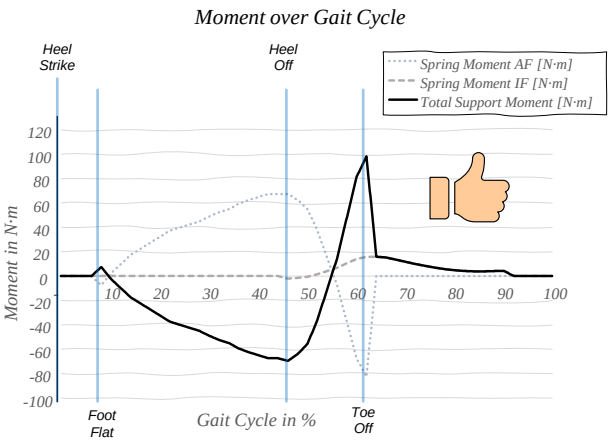

Mehrkörpersimulation einer Sprunggelenkorthesenmechanik
Work-in-Progress

1. Contact Step Control zur Steuerung der Schaltmomente und Energieübertragung der einzelnen Federn
2. Implementierung einer Moderordnungsreduktion zur schnelleren Berechnung
3. Integration mithilfe von pyAnsys in eine Co-Simulation mit OpenSim
4. Hinzufügen von weiteren Modulen um z. B. den erforderlichen Druck aus der Schaltung zu ermitteln

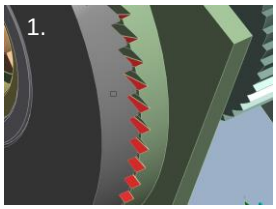

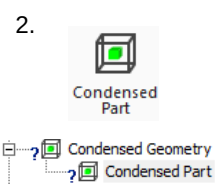

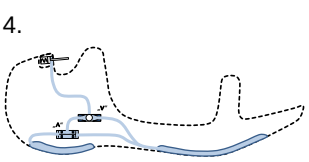

Zusammenfassung

- Medizinischen Nutzen von passiven Sprunggelenkorthesen identifiziert.
- Datenerhebung aus Bewegungsstudie und Körperscans
- Vorstellung einer passiven Sprunggelenkorthesen mit Ratschenkupplung und Drehfeder
- Simulation des Unterstützungsmoments durch Bewegungseingangsdaten

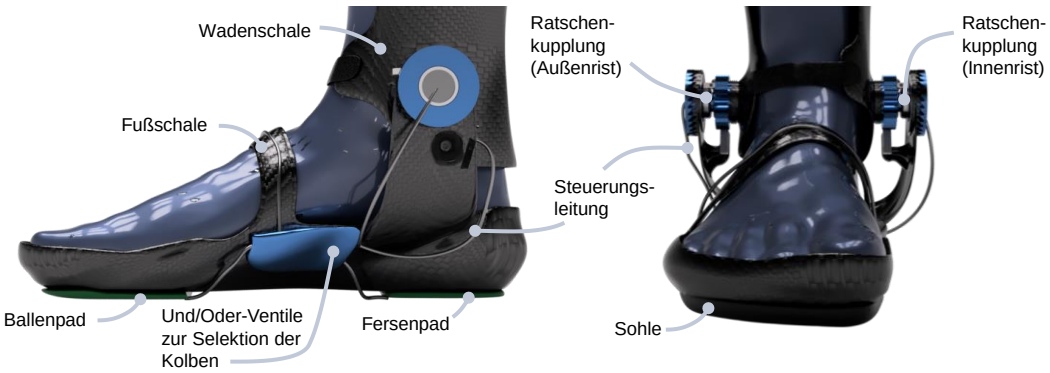

Vielen Dank für Ihre Aufmerksamkeit!

Elastische Mehrkörpersimulation von Wälzlagern

Tobias Baumann[1,*], Bodo Hahn[2], Stephan Tremmel[1]

[1]Lehrstuhl für Konstruktionslehre und CAD, Universität Bayreuth, Deutschland
[2]Schaeffler Technologies AG & Co. KG, Herzogenaurach, Deutschland
*E-Mail: tobias.baumann@uni-bayreuth.de

Kurzfassung: Transiente Vorgänge in Wälzlagern, insbesondere bei Wechselwirkungen mit der Lagerumgebung, lassen sich im Detail nur mit Dynamiksimulationen analysieren. Schaeffler nutzt hierfür die selbst entwickelte Mehrkörpersimulationssoftware Caba3D. Neben der klassischen Modellierung der Lagerkomponenten als dreidimensionale Starrkörper mit wälzlagerspezifischen Kontaktmodellen steht auch ein elastisches Käfigmodell zur Verfügung. Die Modellierung der Lagerringe als Starrkörper ist gerechtfertigt, wenn die Anschlusskonstruktion ausreichend steif ist. Für Großwälzlager, wie sie beispielsweise in Windenergieanlagen eingesetzt werden, trifft diese Forderung nicht zu, da mit zunehmender Lagergröße die Umgebungssteifigkeit im Verhältnis zu den Kontaktsteifigkeiten abnimmt. Weiterhin führen auch bei kleineren Lagern Leichtbaumaßnahmen zu nachgiebigeren Umgebungen, sodass die Lastübertragung im Lager beeinflusst wird und die Nachgiebigkeit der Umgebung berücksichtigt werden muss. Dieser Beitrag stellt einen Ansatz zur Integration der Umgebungssteifigkeit in die Mehrkörpersimulation von Wälzlagern vor. Der Lösungsansatz basiert auf der Reduktion eines Finite Elemente Modells von der Lagerumgebung durch einen erweiterten Fourier-Polynom-Verschiebungsansatz. Während der Mehrkörpersimulation werden die Verschiebungsmoden mit den unverformten Kontaktflächen zu den verformten Kontaktflächen superponiert, welche anschließend in der wälzlagerspezifischen Kontaktberechnung verwendet werden. Neben der Simulationsmethode wird der Computer Aided Engineering Prozess zur Integration der elastischen Lagerumgebung beschrieben und das Potential der Methode anhand eines Kugel- und eines Rollenlagers aufgezeigt.

Stichwörter: Wälzlagerdynamiksimulation, Elastische Mehrkörpersimulation, Finite Elemente Analyse, Finite Elemente Modellreduktion

1 Einleitung

Wälzlager haben die Aufgabe, relativ zueinander rotierende oder schwenkende Bauteile zu führen und Kräfte zwischen diesen Bauteilen zu übertragen. Ihre grundlegende Berechnung ist mit einfachen, analytischen Berechnungsverfahren, wie beispielsweise die Abschätzung der Lebensdauer nach DIN ISO 281 [1], möglich. Für detaillierte Analysen des Wälzlagers, beispielsweise bezüglich Reibung, Temperaturentwicklung oder Schwingungen, sind zwingend numerische Berechnungsverfahren notwendig [2-4], sodass sich transiente Vorgänge im Wälzlager, insbesondere bei Wechselwirkungen mit der Lagerumgebung, nur mit Dynamiksimulationen untersuchen lassen.
Schaeffler nutzt für die Mehrkörpersimulation von Wälzlagern die firmeneigene Simulationssoftware Caba3D. Alle Lagerkomponenten werden als dreidimensionale Starrkörper mit drei translatorischen und drei rotatorischen Freiheitsgraden modelliert. Zusätzlich steht ein elastisches Käfigmodell, welches insbesondere für Wälzlageranwendungen im hohen Drehzahlbereich relevant ist, zur Verfügung [5, 6]. Da für realistische Ergebnisse die wälzlagerspezifischen Kontakte korrekt abgebildet werden müssen, sind in Caba3D spezielle Kontaktmodelle integriert. DIN 26281 [7] schreibt für die Wälzkörper von Rollenlagern eine Unterteilung in Scheiben vor, sodass die Kontaktberechnung in Caba3D ebenfalls auf einem Scheibenmodell basiert [8].
Die Modellierung der Lagerringe als Starrkörper ist gerechtfertigt, wenn die Anschlusskonstruktion (Gehäuse, Radkörper, Welle etc.) sehr steif ist, da Lagerringe häufig eine geringe Wandstärke haben und deswegen eine sichere Kraftübertragung nur bei ausreichender Unterstützung durch die Lagerumgebung gewährleistet ist [2]. Bei vielen Anwendungen ist eine steife Lagerumgebung konstruktiv sichergestellt, die Lagerumgebung von Großwälzlagern ist dagegen aufgrund von Bauraumbegrenzungen relativ nachgiebig: Mit zunehmender Lagergröße nimmt also die Umgebungssteifigkeit im Verhältnis zu den Kontaktsteifigkeiten ab [2]. Weiterhin führen Leichtbaumaßnahmen auch bei kleineren Lagern zu nachgiebigeren Umgebungen, sodass die konventionelle Forderung nach möglichst steifen Wälzlagerumgebungen nicht immer erfüllt ist und der Einfluss der Umgebungssteifigkeit auf die Lastübertragung im Lager berücksichtigt werden muss [2, 4].
Dieser Beitrag stellt in Kapitel 2 einen recheneffizienten Ansatz zur Integration der Umgebungssteifigkeit in die Mehrkörpersimulation von Wälzlagern vor. In Kapitel 3 wird der dafür notwendige Computer Aided Engineering (CAE) Prozess beschrieben und abschließend in Kapitel 4 die Ergebnisse zur Validierung der Methode vorgestellt.

2 Methode zur Integration der elastischen Lagerumgebung

Die hier präsentierte Methode zur Integration der elastischen Lagerumgebung basiert auf der Reduktion eines Finite Elemente (FE) Modells der Lagerumgebung durch einen erweiterten Fourier-Polynom-Verschiebungsansatz. Für die Kontaktmodellierung in der Mehrkörpersimulation werden die Verschiebungsmoden mit den unverformten Kontaktflächen als Linearkombination zu den verformten Kontaktflächen überlagert. Im Folgenden wird der Kontakt zwischen den starren Wälzkörpern und den nachgiebigen Laufbahnen eines Rillenkugel- und eines Zylinderrollenlagers beschrieben.
Die starren/unverformten Laufbahnflächen eines Rillenkugel- und eines Zylinderrollenlagers ohne Profilierung entsprechen einem Torus- bzw. einem Zylindersegment (vgl. Abbildung 1 und Symbolverzeichnis am Ende dieses Beitrags).

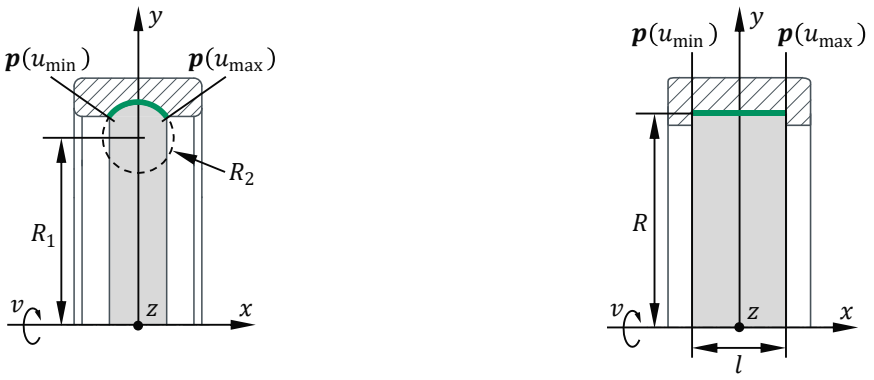

Abbildung 1: Unverformte Laufbahngeometrie eines Rillenkugellagers (a) und Zylinderrollenlagers (b).

Das zweidimensionale Laufbahnprofil $\boldsymbol{p}(u)$ mit dem Laufbahnparameter u lässt sich allgemein parametrisieren als

$$\boldsymbol{p}(u) = \begin{bmatrix} p_x(u) \\ p_y(u) \end{bmatrix}, u \in [u_{\min}, u_{\max}]. \tag{1}$$

Die Grenzen des Laufbahnprofils liegen an den Stellen $\boldsymbol{p}(u_{\min})$ und $\boldsymbol{p}(u_{\max})$. Durch Rotation des Laufbahnprofils $\boldsymbol{p}(u)$ um die axiale Achse des Lagerrings mit dem zweiten Laufbahnparameter v ergibt sich die unverformte Laufbahnfläche

$$\boldsymbol{q}_0(u,v) = \begin{bmatrix} q_{0,x}(u) \\ q_{0,y}(u,v) \\ q_{0,z}(u,v) \end{bmatrix} = \begin{bmatrix} p_x(u) \\ p_y(u)\cos(2\pi v) \\ p_y(u)\sin(2\pi v) \end{bmatrix}, u \in [u_{\min}, u_{\max}], v \in [0,1]. \tag{2}$$

In Anlehnung an Wensing [9] werden die Statikmoden des Craig-Bampton-Reduktionsverfahrens [10] um den globalen Verschiebungsansatz

$$\boldsymbol{u}_k(x,r,\varphi) = \sum_{n=0}^{N_k}\sum_{m=0}^{M_k}\sum_{l=0}^{L_k} a_{k,n,m,l}\cos(n\varphi)\,T_m(x)T_l(r) + \sum_{n=1}^{N_k}\sum_{m=0}^{M_k}\sum_{l=0}^{L_k} b_{k,n,m,l}\sin(n\varphi)\,T_m(x)T_l(r) \tag{3}$$

adaptiert. Der Index k kennzeichnet die axiale, radiale und tangentiale Richtung ($k \in [x,r,t]$). Die Positionsabhängigkeit der FE-Knoten wird in Umfangsrichtung φ über Fourier-Polynome und in axialer sowie radialer Richtung x bzw. r über Tschebyschow-Polynome T_m bzw. T_l berücksichtigt. Die Parameter N_k, M_k und L_k steuern die Ordnung der Fourier- und Tschebyschow-Polynome.
Der wesentliche Vorteil dieses Reduktionsansatzes gegenüber dem Verfahren nach Craig-Bampton ist, dass das Verschiebungsfeld der Laufbahn kontinuierlich über die glatte, analytische Funktion (3) statt diskret über die einzelnen Verschiebungen der FE-Knoten beschrieben wird. Nach Umformulierung des Verschiebungsansatzes (3) in Parameterform ist schließlich die verformte Laufbahnfläche $\boldsymbol{q}_1$ die Summe aus der unverformten Fläche $\boldsymbol{q}_0(u,v)$ und den elastischen Verschiebungsanteilen $\boldsymbol{u}(u,v)$:

$$\boldsymbol{q}_1(u,v) = \boldsymbol{q}_0(u,v) + \boldsymbol{u}(u,v). \tag{4}$$

Die starren Wälzkörper werden, wie in Abbildung 2 skizziert, in eine endliche Anzahl an Scheiben N_s unterteilt. Während der Kontaktsuche wird jede Scheibe auf Durchdringung mit der verformten Laufbahnfläche (4) überprüft. Dazu wird ein restringiertes Optimierungsproblem mit der Langrange-Newton-Iteration gelöst. Bei vorhandener Durchdringung folgt die Berechnung der Kontaktkraft in Normalenrichtung $\boldsymbol{n}_i$ nach der Hertzschen Theorie und anschließend die Berechnung der Reibungs- und Dämpfungskraft [8].

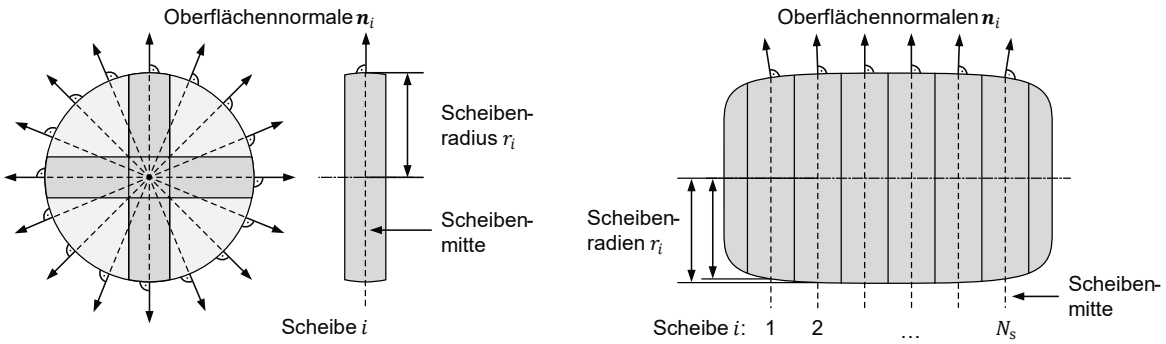

(a) (b)

Abbildung 2: Scheibenmodell des Wälzkörpers für eine Kugel (a) und Rolle (b).

3 CAE-Prozess zur Integration der elastischen Lagerumgebung

Abbildung 3 visualisiert den CAE-Prozess zur Integration der elastischen Lagerumgebung in Caba3D. Die Lagerringgeometrie ist in einer initialen CAD-Datenbank hinterlegt. Damit wird das Voll-FE-Modell (nicht reduziertes FE-Modell) der Lagerringe inklusive der Anschlusskonstruktion aufgebaut. Da eine recheneffiziente Reduktion mit dem Ansatz nach Gleichung (3) in den Standard-FE-Programmen (Abaqus, Ansys, Nastran etc.) nicht möglich ist, wird das Voll-FE-Modell erst im folgenden Präprozessor reduziert. Zwischenergebnis der Finite Elemente Analyse (FEA) sind die FE-Strukturinformationen, die Steifigkeits- und Massenmatrix des Voll-FE-Modells und die Craig-Bampton-Transformationsmatrix. Der Präprozessor modifiziert die Transformationsmatrix entsprechend dem Reduktionsansatz nach Gleichung (3) und führt die Reduktion mit der neuen Transformationsmatrix durch. Schließlich wird in Caba3D der reduzierte elastische Körper dem Lagerring zugewiesen und die Mehrkörpersimulation unter Berücksichtigung der elastischen Lagerumgebung gestartet.

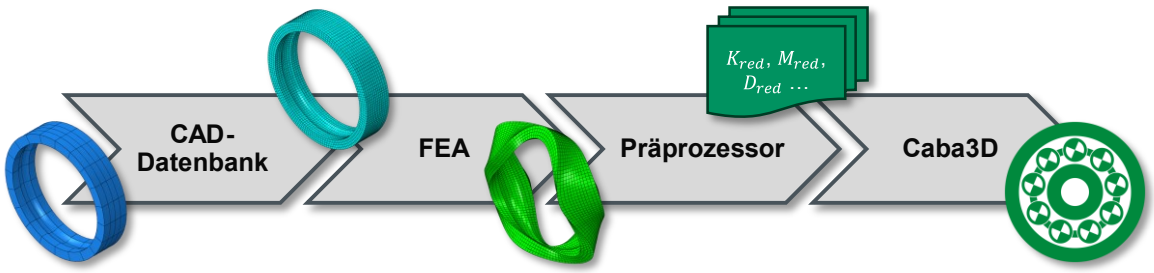

Abbildung 3: CAE-Prozess zur Integration der elastischen Lagerumgebung in Caba3D.

4 Validierung und Ergebnisse

In diesem Kapitel werden exemplarisch die Ergebnisse für das Rillenkugellager 6209 und das vollrollige Zylinderrollenlager SL192332 präsentiert. Bei beiden Lagern sind die Außenringe ohne zusätzliche Anschlusskonstruktionen elastisch modelliert. Die übrigen Lagerkomponenten sind Starrkörper.
Die wichtigsten Validierungsgrößen sind die Lastverteilung zwischen den Wälzkörpern und elastischem Außenring sowie die Kinematik der Wälzkörper. Während eine korrekte Lastverteilung im Lager eine richtige Berücksichtigung der Lagerringsteifigkeit voraussetzt, ist für die Kinematik der Wälzkörper ein sauberes Abrollen über die verformte Laufbahn erforderlich. Zur Beurteilung der Lastverteilung wird die Kontaktkraft in Normalenrichtung ausgewertet. Die Kinematik der Wälzkörper wird anhand der Wälzkörperdrehzahl untersucht.
In den folgenden Diagrammen sind die Normalkraft auf die maximale Normalkraft und die Wälzkörperdrehzahl auf die kinematische Drehzahl normiert – jeweils bei starrer Modellierung des Außenrings.

4.1 Einzelkontakt

Die Vorgänge im Wälzlager sind aufgrund der hohen Anzahl an Lagerkomponenten und den gegenseitigen Wechselwirkungen sehr komplex. Um den Wälzkörper-Laufbahnkontakt isoliert beurteilen zu können, wird daher zunächst ein einzelner, stehender Wälzkörper mit einer Radialkraft in den drehenden, elastischen Außenring gedrückt. Die externe Kraft führt zu einer Verformung des Rings und zusammen mit der Rotation des Rings und der Reibung im Kontakt zur Beschleunigung des Wälzkörpers. Als erste Referenz für die radiale Ringaufweitung an der Wälzkörperposition wird eine analytische Lösung von Harris [4], welche auf gekrümmten Timoshenko-Balken basiert, und als zweite Referenz das Ergebnis einer statischen FEA des nicht reduzierten FE-Modells herangezogen.
Abbildung 4 zeigt, dass beim Rillenkugellager die radiale Ringaufweitung in Caba3D mit steigendem Ansatz für N gegen die Referenzlösungen konvergiert. Ab N = 4 liegt der relative Fehler unter 5 %. Voraussetzung ist die Wahl von M = 1 und L = 1. Bei starren Laufbahnquerschnitten (M = 0 und L = 0) liegt der relative Fehler über 50 %. Die Drehzahl n_{WK} des Wälzkörpers pendelt sich nach dem Einschwingen des elastischen Lagerrings auf einen konstanten Wert ein, sodass der Wälzkörper sauber über den verformten Lagerring abrollt.

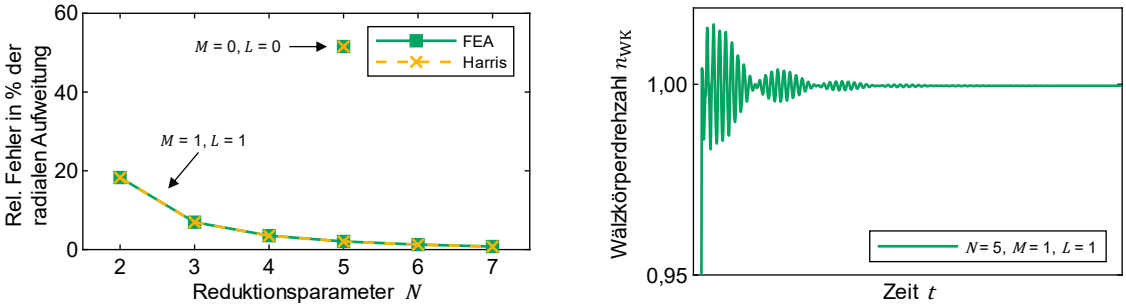

Abbildung 4: (a) relativer Fehler der radialen Ringaufweitung an der Wälzkörperposition und (b) Wälzkörperdrehzahl n_{WK} des Rillenkugellagers.

Beim Zylinderrollenlager weicht die radiale Ringaufweitung in Caba3D ab einem ausreichend hohen Ansatz für N nur geringfügig von den Referenzlösungen ab (vgl. Abbildung 5). Die Unterschiede in den Referenzlösungen sind auf den komplexen Lagerringquerschnitt mit Borden und einer dadurch ungenaueren Lösung des Timoshenko-Balken-Ansatzes von Harris [4] zurückzuführen. Die Auswertung der Drehzahl n_{WK} zeigt nach dem Einschwingen des Lagerrings erneut ein sauberes Abrollen des Wälzkörpers.

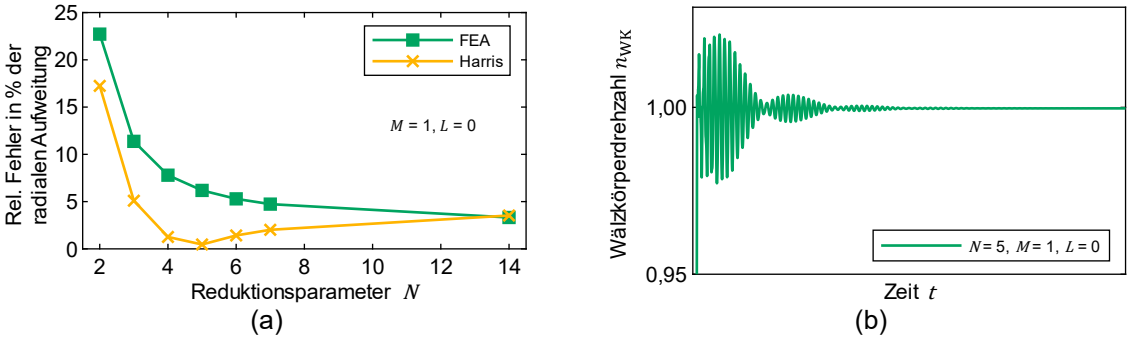

Abbildung 5: (a) relativer Fehler der radialen Ringaufweitung an der Wälzkörperposition und (b) Wälzkörperdrehzahl n_{WK} des Zylinderrollenlagers.

4.2 Vollmodell: (Quasi-)Statisch

Nach dem Einzelkontakt wird das komplette Lager bei nicht rotierendem Innen- und Außenring untersucht. Auf den Innenring wirkt eine Radialkraft, die über die Wälzkörper auf den Außenring übertragen wird, und zur Verformung des Außenrings führt. Als Referenz für die Lastverteilung dient die Lösung des (quasi-)statischen Berechnungsprogramms Bearinx, welches ebenfalls von Schaeffler entwickelt wird [2].
Die Caba3D-Ergebnisse für die Normalkraft F_{n} konvergieren mit steigendem N gegen die Referenzlösung (vgl. Abbildung 6). Beim Rillenkugellager liegen die Abweichungen ab N = 3 unter 10 % und ab N = 5 unter 5 %. Beim Zylinderrollenlager sind für Abweichungen unter 10 % ein Ansatz von

$N \geq 4$ und für unter 5 % ein Ansatz von $N \geq 5$ erforderlich. Für die folgenden Untersuchungen wird daher der Ansatz $N = 5$ für beide Lager gewählt.

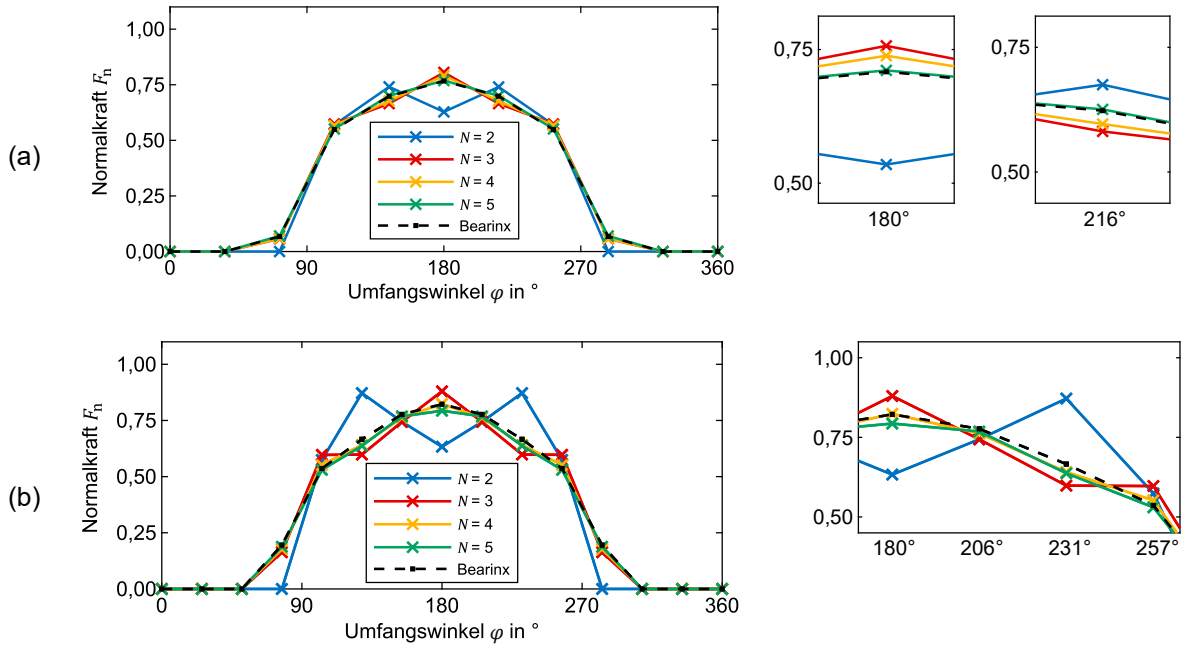

Abbildung 6: Einfluss des Parameters N auf die Lastverteilung beim (a) Rillenkugellager ($M = 1$, $L = 1$) und (b) Zylinderrollenlager ($M = 1$, $L = 0$).

Je Lager werden vier Betriebszustände mit variierender Radialkraft F_r betrachtet. Die Radialkraft F_r liegt bei 25 %, 50 %, 75 % und 100 % der statischen Tragzahl C_{0r} unter Berücksichtigung der statischen Tragsicherheit S_0. Es wird ein normaler, ruhiger und vibrationsfreier Lauf angenommen, sodass die statische Tragsicherheit $S_0 = 1{,}0$ (Rillenkugellager) bzw. $S_0 = 1{,}5$ (Zylinderrollenlager) beträgt [2]. In Abbildung 7 sind die Lastverteilungen für die verschiedenen Betriebszustände visualisiert. Sowohl beim Rillenkugel- als auch beim Zylinderrollenlager weichen die Normalkräfte F_n um weniger als 5 % ab.

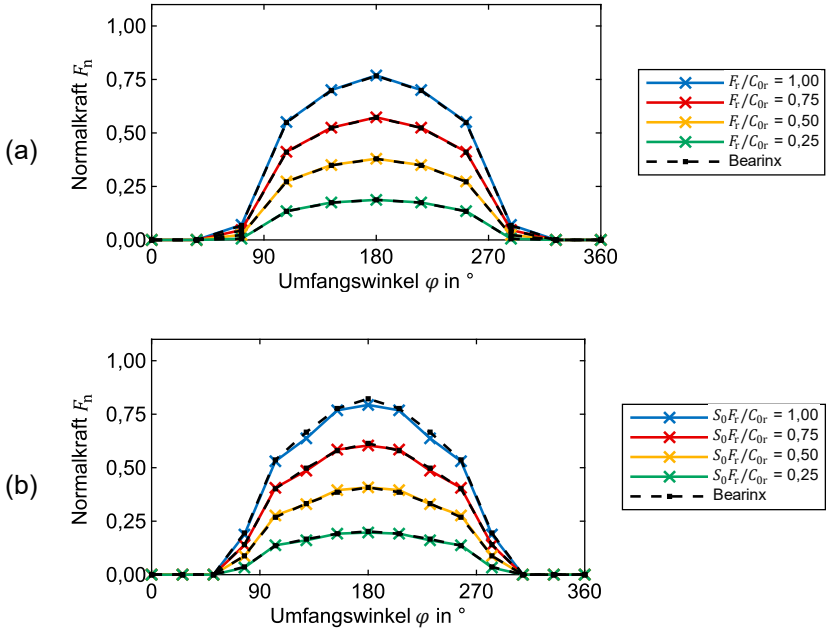

Abbildung 7: Lastverteilung für verschiedene Betriebszustände mit variierender Radialkraft F_r für (a) Rillenkugellager ($N = 5$, $M = 1$, $L = 1$) und (b) Zylinderrollenlager ($N = 5$, $M = 1$, $L = 0$).

4.3 Vollmodell: Dynamisch

Abschließend wird das komplette Lager mit rotierendem Innenring unter Radiallast untersucht. Als Referenz für die Lastverteilung dient erneut die Lösung von Bearinx. In Abbildung 8 sind die Lastverteilung und Wälzkörperdrehzahl n_{WK} für eine komplette Umdrehung des Wälzkörpersatzes dargestellt. Um den Einfluss der elastischen Modellierung zu beurteilen, sind zusätzlich die Ergebnisse für den starren Außenring abgebildet.
Die Normalkraft F_{n} weicht beim Rillenkugellager weniger als 3 % und beim Zylinderrollenlager weniger als 5 % ab. Bei elastischer Modellierung des Außenrings stellen sich im Vergleich zum starren Außenring breitere Lastzonen ein. Ferner sind die maximalen Wälzkörperkräfte um 25 % beim Rillenkugellager und um 20 % beim Zylinderrollenlager geringer.
Innerhalb einer Umdrehung des Wälzkörpersatzes variiert die Wälzkörperdrehzahl. Mit Eintritt der Wälzkörper in die Lastzone werden diese ungefähr auf die kinematische Drehzahl beschleunigt und bewegen sich danach mit konstanter Drehzahl weiter. Einzig beim starren Rillenkugellager bildet sich im Drehzahlverlauf kein Plateau aus, da das Rillenkugellager kleiner als das Zylinderrollenlager ist und zudem schneller dreht, sodass sich die Wälzkörper kürzer in der Lastzone befinden. Beim elastischen Rillenkugellager zeigt sich aufgrund der breiteren Lastzone wiederum ein Bereich konstanter Drehzahl. Zum Ende der Lastzone werden die Wälzkörper durch das entgegenwirkende Reibungsmoment und ihr Eigengewicht abgebremst. Außerhalb der Lastzone verlieren die Wälzkörper den Kontakt zum Innenring, sodass der Innenring die Wälzkörper nicht mehr antreibt, und bereits leichte Wälzkörper-Käfig-Kontakte beim Rillenkugellager und Wälzkörper-Wälzkörper-Kontakte beim Zylinderrollenlager sprunghafte Drehzahländerungen verursachen. Da die Lastzone beim elastischen Ring breiter als beim starren Ring ist, werden die Wälzkörper früher beschleunigt und später abgebremst. Insgesamt rollen die Wälzkörper auch beim rotierenden Lager sauber ab, weil alle Schwankungen im Drehzahlverlauf der Wälzkörper physikalisch bedingt sind.

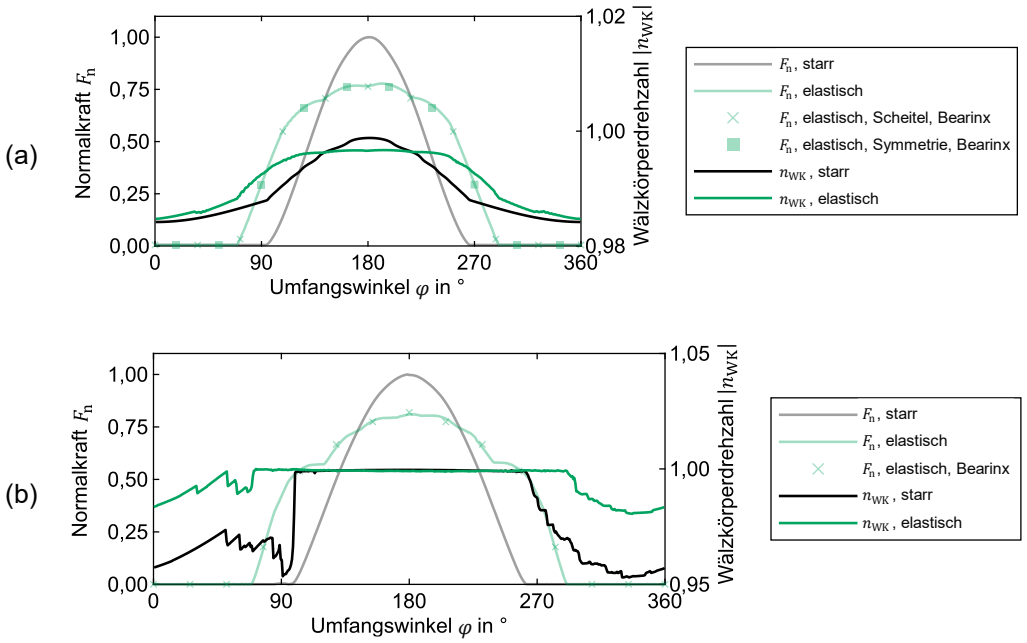

Abbildung 8: Lastverteilung und Wälzkörperdrehzahl n_{WK} bei starrem und elastischem Außenring für (a) Rillenkugellager (N = 5, M = 1, L = 1) und (b) Zylinderrollenlager (N = 5, M = 1, L = 0).

5 Zusammenfassung

Dieser Beitrag stellt einen Ansatz zur Integration der elastischen Lagerumgebung in die Mehrkörpersimulation von Wälzlagern vor. Begründet ist die Berücksichtigung der Umgebungssteifigkeit durch zunehmend nachgiebigere Lagerumgebungen. Die Methode basiert auf der Reduktion eines FE-Modells durch einen erweiterten Fourier-Polynom-Verschiebungsansatz. In der anschließenden Mehrkörpersimulation wird die Verformung der Laufbahn recheneffizient in den wälzlagerspezifischen Kontaktmodellen berücksichtigt. Die Validierung der Methode für ein Rillenkugel- und ein Zylinderrollenlager mit elastischen Außenringen zeigt einen signifikanten Einfluss auf die Lastverteilung und die Wälzkörperkinematik im Vergleich zur starren Modellierung des Außenrings.

6 Literaturverzeichnis

[1] DIN ISO 281: 2010-10. *Wälzlager - Dynamische Tragzahlen und nominelle Lebensdauer*

[2] SCHAEFFLER TECHNOLOGIES AG & CO. KG (Hrsg.): *Wälzlagerpraxis* : *Handbuch zur Gestaltung und Berechnung von Wälzlagerungen*. 5. Aufl. Mainz : Vereinigte Fachverlage GmbH, 2019

[3] HARRIS, Tedric A. ; KOTZALAS, Michael N.: *Essential concepts of bearing technology*. 5. Aufl. Boca Raton : CRC Press, 2007

[4] HARRIS, Tedric A. ; KOTZALAS, Michael N.: *Advanced Concepts of Bearing Technology*. 5. Aufl. Boca Raton : CRC Press, 2007

[5] VLASENKO, Dmitry ; HAHN, Bodo: Modeling of Elastic Cages in the Rolling Bearing Multi-Body Tool CABA3D. In: KECSKEMÉTHY, Andrés; GEU FLORES, Francisco (Hrsg.): *Multibody Dynamics 2019* : *Proceedings of the 9th ECCOMAS Thematic Conference on Multibody Dynamics*. Cham : Springer, 2020 (Computational Methods in Applied Sciences, 53), S. 96–103

[6] SEILER, K. ; TREMMEL, S. ; WARTZACK, S. ; HAHN, B. ; PLOGMANN, M. ; GRAF-GOLLER, O.: *Dynamics simulation of rolling element bearings considering elastohydrodynamic cage contacts*. In: *Bearing World Journal* (2016), Nr. 1, S. 75–85

[7] DIN 26281: 2010-11. *Wälzlager - Dynamische Tragzahlen und nominelle Lebensdauer-Berechnung der modifizierten nominellen Referenz-Lebensdauer für Wälzlager*

[8] VESSELINOV, Vladimir: *Dreidimensionale Simulation der Dynamik von Wälzlagern* : *Threedimensional Simulation of Bearing Dynamics*. Universität Karlsruhe. Dissertation. 2003

[9] WENSING, Jeroen Anton: *On the dynamics of ball bearings*. Universität Twente. Dissertation. 1998

[10] CRAIG, Roy R. ; BAMPTON, Mervyn C. C.: *Coupling of substructures for dynamic analyses*. In: *AIAA Journal* 6 (1968), Nr. 7, S. 1313–1319

7 Symbolverzeichnis

Symbol	Beschreibung
x	Skalar
$\boldsymbol{x}$	Vektor
a, b	Fourier-Koeffizienten
$C_{0\mathrm{r}}$	Statische Tragzahl
F_{n}	Normierte Normalkraft zwischen Wälzkörper und Laufbahn
F_{r}	Radialkraft (auf den Innenring)
l	Länge des Zylinders
$\boldsymbol{n}_i$	Oberflächennormale der Scheibe i
N_{S}	Anzahl der Scheiben
n_{WK}	Normierte Wälzkörperdrehzahl
$\boldsymbol{p}$	Laufbahnprofil
$\boldsymbol{q}_0$	Unverformte Laufbahnfläche
$\boldsymbol{q}_1$	Verformte Laufbahnfläche
r	Radialkomponente der Zylinderkoordinaten
R	Radius des Zylinders
R_1	Radius der Kreislinie des Torus
R_2	Radius des rotierenden Kreises des Torus
S_0	Statische Tragsicherheit
T_m, T_l	Tschebyschow-Polynome
$\boldsymbol{u}$	Verschiebungen der Laufbahnfläche
u	Erster Laufbahnparameter
$u_{\min}$, $u_{\max}$	Minimum und Maximum des Laufbahnparameters u, Werte sind abhängig von der Form der Laufbahnfläche
v	Zweiter Laufbahnparameter
x	Axialkomponente der Zylinderkoordinaten
φ	Winkelkomponente der Zylinderkoordinaten

NAFEMS REGIONAL CONFERENCES 2024

Weltweit finden im Frühjahr und Herbst 2024 weitere NAFEMS Regionalkonferenzen statt:

www.nafems.org/nrc24

NWC25

NAFEMS WORLD CONGRESS

19-22 MAY 2025 | SALZBURG | AUSTRIA

A WORLD OF ENGINEERING SIMULATION

Safe the date!

Abstract submission deadline voraussichtlich Mitte November 2024

www.nafems.org/congress

NAFEMS

NAFEMS Deutschland, Österreich, Schweiz GmbH
Griesstr. 20, 85567 Grafing b. M.
Tel.: +49 176 217 984 01
Fax: +49 3 22 11 08 99 13 41
E-mail: info@nafems.de
www.nafems.org